Scientific Program and Book of Abstracts

17th International Conference on Crystal Growth and Epitaxy

Scientific Program and Book of Abstracts: 17th International Conference on Crystal Growth and Epitaxy

Published July 2013, ISBN 83-89585-36-7

Disclaimer

The Organisers and the Publisher have made every effort to provide accurate and complete information in this Book. However, further changes or corrections may still be necessary and may be made without notice after the date of publication. To ensure that you receive the most up-to-date information, please check the Corrigenda, if issued.

Status of the program as on July 31st, 2013.
Revision: 130.8.5, 2013-07-31 16:04 GMT

Table of Contents

Welcome

17th International Conference on Crystal Growth and Epitaxy - ICCGE-17

University of Warsaw,
Warsaw (Poland)
11th – 16th August, 2013

Dear attendee,

Welcome to the 17th International Conference on Crystal Growth and Epitaxy (ICCGE-17). The conference will take place in the wonderful campus of the University of Warsaw, located very close to the old town, the most charming part of Poland's capital. We hope that all participants will enjoy the stay in Warsaw and feel the warm hospitality of its inhabitants.

For the first time since this series of international crystal growth conferences was initiated, the name has been modified with the addition of "Epitaxy". This was made in order to apply the decision taken by the Council of the International Organization for Crystal Growth during the last meeting in Beijing. But aside from formalities, the adoption of the new name wants to underline the unifying spirit of crystal growth as the discipline which provides the theoretical and experimental tools for developing crystalline materials, independently of their size and shape.

The mixture of traditional and new approaches is well apparent from the exciting technical program that you will find in the next pages. We wish to thank the Program Chairs Zbigniew R. Zytkiewicz and Jochen Friedrich and the entire Program Committee for their terrific work. It is worth mentioning that, in the spirit of strengthening the cooperation with other scientific societies, four sessions were jointly organized with representatives of the Commission of Crystal Growth and Materials Characterization of the Intern. Union of Crystallography.

The organization of ICCGE-17 was possible thanks to the concerted efforts of the International Organization on Crystal Growth (IOCG), and Polish and German Crystal Growth Societies, but especially thanks to the tireless work of the Local Organizing Committee and the great support of the co-organizing institutions: Institute of High Pressure Physics and Institute of Physics of the Polish Academy of Sciences, University of Warsaw, and Institute of Electronics Materials Technology. It is our pleasure to express wholehearted thanks to all members of the above mentioned bodies and institutions for their efforts and generous help in the whole process of organization of the Conference.

ICCGE-17 benefited from financial support by Poland's Ministry of Science and Education and International Union on Crystallography (IUCr) . Elsevier Ltd accepted to publish the Conference Proceedings in Journal of Crystal Growth but also contributed directly with a financial support. All these supporting actions are gratefully acknowledged.

We hope you will enjoy the scientific sessions as well as the social program and we look forward to meeting you in person at ICCGE-17 in Warsaw.

Warsaw, 21 July 2013

Stanislaw Krukowski and Roberto Fornari

Co-chairs of ICCGE-17

Prizes of International Organization for Crystal Growth

Since 1989 at ICCG-9 (Sendai), the International Organization for Crystal Growth (IOCG) has sponsored two triennial prizes, the Frank Prize and the Laudise Prize. Beginning in 2004 at ICCG-14 (Grenoble), there was a new triennial IOCG prize, the Schieber Prize, sponsored by the Journal of Crystal Growth. These prizes consist of a commemorative item plus an invitation and financial support to present the work, which is the subject of the award, at the ICCG meeting at which the award takes place. The 2013 winners will deliver invited talks during the ICCGE-17 in Warszawa.

2013 Frank Prize for Prof. K. Tsukamoto (Tohoku University, Sendai)

The International Organization for Crystal Growth (IOCG) has awarded the 2013 Frank prize to Prof. Katsuo Tsukamoto of Tohoku University in Sendai, Japan. The Frank prize is warded for significant fundamental contributions to the field of crystal growth and Prof. Tsukamoto receives this prize for his foundational discoveries in the physics of solution-based crystallization achieved through his pioneering work in developing phase-shift interferometry for in-situ investigations of crystal growth mechanism of both inorganic and organic materials. He has lead the development of phase-shift interferometry to increasing levels of sophistication, allowing real-time imaging of mono-molecular step motion and miniaturizing such set-ups to open up new applications. Prof. Tsukamoto has in particular used this technique for fundamental studies under microgravity conditions, but has also done experiments under conditions deep in the earth.

Prof. Katsuo Tsukamoto (born in 1948) studied mineralogy at the Tohoku University in Sendai and obtained his PhD in 1982 with Prof. Sunagawa as supervisor. He has visited many institutions during his career, including two years as invited researcher in The Netherlands in the group of Prof. Bennema. He is the (co-)author of more than 290 scientific publications.

2013 Laudise Prize for Prof. C.T. Chen (Beijing)

The International Organization for Crystal Growth (IOCG) has awarded the 2013 Laudise prize to Prof. Chuang-Tian Chen of the Beijing Centre for Crystal Research and Development in the Technical Institute of Physics and Chemistry of the Chinese Academy of Sciences. The Laudise prize is awarded for significant technological contributions to the field of crystal growth and Prof. Chen receives this prize for his seminal contributions to the discovery and development of new non-linear optical crystals. First he proposed and developed a theoretical model for understanding the relationship between the structures of these crystals and their non-linear optical properties. On the basis of this theoretical understanding he and his group discovered and developed a series of new borate non-linear optical crystals, such as BaB_2O_4 (BBO), LiB_3O_5 (LBO), and $KBe_2BO_3F_2$ (KBBF). Such crystals, grown by a newly developed flux method, now find widespread use for making UV and deep-UV radiation through second harmonic generation.

Prof. Chen (born in 1937) studied physics at the University of Beijing, is a member of the Chinese Academy of Sciences and is currently director of the Bejing Center for Crystal Research & Development. He is (co-)author of more than 150 scientific papers and has been awarded a large number of patents, both in China and in the USA.

2013 Schieber Prize for Prof. Y. Kimura (Tohoku University, Sendai)

The International Organization for Crystal Growth (IOCG) has awarded the 2013 Schieber prize to Prof. Yuki Kimura of Tohoku University in Sendai, Japan. The Schieber Prize recognizes a young author for his or her outstanding scientific publications in the field of Crystal Growth. Prof. Kimura receives this prize for his innovative work on the nucleation and growth of cosmic nano-minerals based on size effects of nanoparticle. Through innovative experimental approaches, Prof. Kimura has developed a new understanding of the initial formation of materials within space which has extensions to the modern synthesis of nanomaterials He has published over 100 papers in a wide cross-section of disciplinary journals. A graduate of Ritsumeikan University, Prof. Kimura had been awarded a fellowship from the Japan Society for the Promotion of Science to work at the US NASA Goddard Space Center as well as fellowship in the Institute of Low Temperature Science in Japan. He has received the Young Scientist Prize of National Conference on Crystal Growth in Japan and the Japanese Society for Planetary Sciences Outstanding Young Scientist Award.

Organisers

Polish Society for Crystal Growth (PTWK)

German Association for Crystal Growth (DGKK)

University of Warsaw (UW)

Institute of High Pressure Physics of the Polish Academy of Sciences (IHPP PAS)

Institute of Physics of the Polish Academy of Sciences (IP PAS)

Institute of Electronic Materials Technology (ITME)

Organizing Committee

ICCGE-17 Chairmen

- Stanislaw Krukowski (Poland)
- Roberto Fornari (Germany)

Program Chairmen

- Zbigniew R. Zytkiewicz (Poland)
- Jochen Friedrich (Germany)

Proceedings

- Keshra Sangwal (Poland)
- Ewa Talik (Poland)
- Peter Gille (Germany)
- Wolfram Miller (Germany)

Secretary

- Dorota A. Pawlak (Poland)
- Konrad Sakowski (Poland)

Treasurer

- Boleslaw Lucznik (Poland)

Local Committee

Chairman

- Roman Stępniewski (Poland)

Tenders

- Beata Brejniak (Poland)
- Katarzyna Kurdybacha (Poland)

Exhibition

- Marcin Sarzynski (Poland)

Sponsorship

- Michal Leszczynski (Poland)

Social Program

- Agnieszka Grabias (Poland)

Book of abstracts

- Marta Sobanska (Poland)

Website

- Konrad Sakowski (Poland)

Local staff coordination

- Pawel Kempisty (Poland)
- Pawel Strak (Poland)

Transportation

- Mirosław Wróblewski (Poland)

International Advisory Committee

Horia Alexandru (Romania)
Wolfgang Assmus (Germany)
Chuangtian Chen (China)
Alex A. Chernov (USA)
Mitch M. C. Chou (Taiwan)
Florinda M. Costa (Portugal)
Hanna Dabkowska (Canada)
Jim De Yoreo (USA)
Jeffrey Derby (USA)
Thierry Duffar (France)
Roberto Fornari (Germany)
Charles Thomas Bayley Foxon (GB)
Hiroshi Fujioka (Japan)
Juan M. Garcia-Ruiz (Spain)
Brian Glennon (Ireland)
Nicolas Grandjean (Switzerland)
Michael Heuken (Germany)

Alain Ibanez (France)
Koichi Kakimoto (Japan)
Zdenek Kozisek (Czech Rep.)
Stanislaw Krukowski (Poland)
Thomas Kuech (USA)
Janaki Kumar (India)
Chung-Wen Lan (Taiwan)
Abel Moreno (Mexico)
Yusuke Mori (Japan)
Wang Mu (China)
Manfred Muehlberg (Germany)
Tadashi Ohachi (Japan)
Vyacheslav V. Osiko (Russia)
Gordon M. Parkinson (Australia)
Katalin Polgar Lassanyi (Hungary)
Vyacheslav Puzikov (Ukraine)
Kevin Roberts (GB)
Michael L. Roth (Israel)
Marco Rubbo (Italy)
Peter Rudolph (Germany)
Wojciech Sadowski (Poland)
Stefano Sanguinetti (Italy)
Keshra Sangwal (Poland)
James Speck (USA)
G.B. Stringfellow (USA)
Olavo Ferreira Sukarno (Brazil)
Yoshikazu Takeda (Japan)
Ewa Talik (Poland)
Katsuo Tsukamoto (Japan)
Elias Vlieg (Netherlands)
Alexey Voloshin (Russia)
Jiyang Wang (China)
Rositza Yakimova (Sweden)
Kader Zaidat (France)

Program Committee

Jacek M. Baranowski (Poland)
Torsten Boeck (Germany)
Kullaiah Byrappa (India)
Helmut Coelfen (Germany)
Arne Croell (Germany)
Hanna Dabkowska (Canada)
Andreas Danilewsky (Germany)
Bruno Daudin (France)
Govindhan Dhanaraj (USA)
Michael Dudley (USA)
Thierry Duffar (France)
Partha Dutta (USA)
Michael Fiederle (Germany)
Jochen Friedrich (Germany) – Program Chair
Marek Godlewski (Poland)
Izabella Grzegory (Poland)
Jeffrey J. Derby (USA)
Dariusz Kaczorowski (Poland)
Koichi Kakimoto (Japan)
Maria Kaminska (Poland)
Michal Leszczynski (Poland)
Jacek Majewski (Poland)
Fumihiro Matsukura (Japan)
Thomas Michely (Germany)
Abel Moreno (Mexico)
Yoshichika Onuki (Japan)
Alexandar Ostrogrosky (USA)
Jolanta Prywer (Poland)
Vyacheslav Puzikov (Ukraine)
Joan Redwing (USA)
Kevin Roberts (UK)
Maciej Sawicki (Poland)
Ferdinand Scholz (Germany)
Albrecht Seidl (Germany)
Marek Skowronski (USA)
Gunther Springholz (Austria)
Sudhir B. Trivedi (USA)
Shiro Tsukamoto (Japan)
Elias Vlieg (The Netherlands)
Deren Yang (China)
Thomas Zettler (Germany)
Zbigniew R. Zytkiewicz (Poland) – Program Chair

Sponsors

- Polish Ministry of Science and Higher Education
- International Union of Crystallography
- Elsevier Inc
- Aixtron SE
- CrystAl-N GmbH
- EU 7th Framework Programme, grant REGPOT-CT-2013-316014 (EAgLE)
- K-Space Associates, Inc.

Frame program

Plenary Sessions (Mickiewicz Hall, Auditorium Maximum):

1. Monday, August 12th	9:00 – 10:20 (including Opening ceremony)
2. Tuesday, August 13th	8:30 – 9:50
3. Wednesday, August 14th	8:30 – 9:50
4. Thursday, August 15th	8:30 – 9:50 (IOCG Prize Lectures)
5. Friday, August 16th	13:30 – 14:00 Closing ceremony

Poster Sessions (2nd and 3rd floor, Old Library):

1. Monday, August 12th	17:00 – 18:30
2. Wednesday, August 14th	16:00 – 17:30

Sessions:

G01	Hall 16, Old Library	Fundamentals and Modeling
G02	Room A, Auditorium Maximum	Bulk crystal growth
G03	Room B, Auditorium Maximum	Biological and Biogenic Crystallization
G04	Room B, Auditorium Maximum	Industrial crystallization
G05	Room D Auditorium Maximum	Characterization
G06	Hall 16, Old Library	In situ monitoring, new equipment and technologies
G07	Room D, Auditorium Maximum	Defect formation/elimination
G08	Room D, Auditorium Maximum	Nanomaterials and low dimensional structures
G09	Hall 16, Old Library	Surfaces and interfaces
G10	Room C, Auditorium Maximum	Thin film and epitaxial growth
T01	Mickiewicz Hall, Auditorium Maximum	Intermetalic and highly correlated electron materials
T02	Mickiewicz Hall, Auditorium Maximum	Materials for spintronics
T03	Room C, Auditorium Maximum	Wide bandgap semiconductors
T04	Room C, Auditorium Maximum	Compound semiconductors
T05	Room A, Auditorium Maximum	Si/Ge for microelectronics and photovoltaics
T06	Mickiewicz Hall, Auditorium Maximum	Oxides and halides including laser and nonlinear optical applications
T07	Room B, Auditorium Maximum	Novel materials and structures
T08	Room A, Auditorium Maximum	External fields, microgravity
T09	Old Library, 2nd - 3rd floor	Late news

Registration:

Please note that the Registration office will be open in Auditorium Maximum according to the timetable below:

Sunday, August 11th	15:00 – 19:00
Monday, August 12th	7:30 – 18:00
Tuesday, August 13th	8:00 – 15:00
Wednesday, August 14th	8:00 – 18:00
Thursday, August 15th	8:00 – 18:00
Friday, August 16th	8:00 – 14:00

Exhibition:

Monday, August 12th	9:00 – 18:00
Tuesday, August 13th	9:00 – 15:00
Wednesday, August 14th	9:00 – 18:00
Thursday, August 15th	9:00 – 18:00

The following companies will present their offer during ICCGE-17:

1. Ammono SA http://ammono.com
2. Aixtron SE http://www.aixtron.com
3. CrystAl-N GmbH http://www.crystal-n.com
4. Dr Eberl MBE-komponenten GmbH http://www.mbe-komponenten.de
5. Elsevier Inc http://www.elsevier.com
6. WEP Control http://www.wepcontrol.com
7. Juropol Sp.z.o.o. http://www.juropol.pl
8. MV Laboratories Inc. http://www.mvlaboratories.com
9. K-Space Associates, Inc. http://www.k-space.com
10. QWED Sp.z.o.o. http://www.qwed.eu
11. PANalytical B.V. http://www.panalytical.com
12. PW-WIM http://www.inmat.pw.edu.pl
13. Scientific Instruments Dresden GmbH http://www.scidre.de
14. EFG GmbH Berlin http://www.scidre.de
15. Rigaku Corp http://www.rigaku.com
16. STR Group Inc. http://www.semitech.us
17. TopGaN Sp.z.o.o. http://www.topganlasers.com
18. Vacuum Barrier Systems http://www.vbseurope.com
19. Heraeus Holding GmbH http://www.heraeus.com

Programme

Plenary Session

Programme

Sunday, 11 August

Registration
Sunday afternoon, 11 August, 15:00

Welcome party
Sunday afternoon, 11 August, 17:00

Monday, 12 August

Opening ceremony
Monday morning, 12 August, 9:00

Plenary 1
Monday morning, 12 August, 9:40
Mickiewicz Hall, Auditorium Maximum

9:40 Plenary Lecture

Jan Czochralski and historical development of the Czochralski method - part 1

Anna Pajaczkowska[1], Reinhard Uecker[2]

1. *Institute of Electronic Materials Technology (ITME), Wólczyńska 133, Warszawa 01-919, Poland* **2.** *Leibniz Institute for Crystal Growth (IKZ), Max-Born-Str 2, Berlin 12489, Germany*

e-mail: apajaczkowska@gmail.com

A brief summary of the life and scientific achievements of the worldwide known metallurgist and inventor of the new crystal growth method, hereafter named Czochralski method (CZ method), is presented. Czochralski was born on October 23rd 1885 in Kcynia, a small town belonging then to the German Empire, now in central part of Poland, close to Torun, the city of Copernicus. First part of his life he spent in Berlin, Germany, where he studied, worked to become a well known specialist in metallurgy, the career finally crowned by founding and heading of the German Metallurgical Society. In this period, in 1916 he made his most outstanding discovery of the method of growing single crystals during investigations of growth velocities of metals. He obtained single crystals of metals a few mm in diameter and length up to 150 mm. The CZ method, originally invented for metals, was improved and cited from its very beginning (1918). Later on, the method was extended to other substances with most notable success in semiconductors, since germanium and silicon transistors were discovered. By invitation of the President of Poland, he returned to then reemerged Poland in 1928 and since then he continued his research at the Technical University in Warsaw. After the Second World War, he was forced to come back to Kcynia. He died in Poznan and was buried in 1953 in Kcynia. During his entire professional life he was a very active and competent scientist, able to identify most important aspects of physical problems to understand them, and finally to find successful application of the conceived ideas. He used several methods for characterization of metals and alloys. He was an author of large number of papers and patents which can be easily found in Chemical Abstracts. He was active in German and Polish Materials Sciences Societies.

Still in the lifetime of Czochralski the crystal growth method named after him gained tremendously in importance for the growth of materials applied in electronics technology. Initiated by the invention of the first transistor (based on Ge) in 1947, germanium and silicon were the first semiconductor crystals grown by the Czochralski method on industrial scale. In the middle of the fifties the crystal diameter reached already 6 and 4 inch, respectively. The availability of the Czochralski method also contributed substantially to the rapid development of compound semiconductors invented in the early fifties with GaAs as most important representative. In 1960 the first - ruby - laser was operated. This event triggered a huge demand worldwide for bulk crystals for optical applications. Henceforward a rapidly increasing number of oxide and fluoride crystals were grown by the Czochralski method. The first oxide crystal was $CaWO_4$ in 1960, and the first fluoride CaF_2 in 1961, both grown at Bell Telephone Laboratories, the same potent US-company which has been the first commercial producer of Ge and Si Czochralski crystals. The early spread of the Czochralski method into other countries strongly depended on their economic potential after the Second World War. However, whereas the importance of the Czochralski method for silicon dropped in favour of the floating zone technique until the mid of the 70`s, it had become well established for other compounds, e.g. for oxide crystals by the mid of the sixties. At that time a boom started in the commercial production and utilisation of single crystals in different fields. To make the Czochralski method applicable for this wide spectrum of materials an increasing number of international research groups made several important modifications during the following decade. These included measures which suppress melt evaporation, influence the fluid flow in the melt and allow a precise diameter control of the growing crystal. Nowadays, the Czochralski technique is the highest developed method with regard to the technical level and the process automation and therefore the method of choice for the growth and production of high perfect bulk single crystals, among them silicon as well as a multitude of oxides, fluorides and multicomponent compounds.

From the perspective of almost the passed century the common opinion of the scientific community recognized him as a great scientist and investigator who has laid the foundation for the development of the global electronics. For recognition of his scientific achievements the Polish Parliament adopted a resolution declaring 2013 as the Year of Jan Czochralski.

10:00 Plenary Lecture

Jan Czochralski and historical development of the Czochralski method - part 2

Reinhard Uecker[1], Anna Pajaczkowska[2]

1. *Leibniz Institute for Crystal Growth (IKZ), Max-Born-Str 2, Berlin 12489, Germany* **2.** *Institute of Electronic Materials Technology (ITME), Wólczyńska 133, Warszawa 01-919, Poland*

e-mail: reinhard.uecker@ikz-berlin.de

A brief summary of the life and scientific achievements of the worldwide known metallurgist and inventor of the new crystal growth method, hereafter named Czochralski method (CZ method), is presented. Czochralski was born on October 23rd 1885 in Kcynia, a small town belonging then to the German Empire, now in central part of Poland, close to Torun, the city of Copernicus. First part of his life he spent in Berlin, Germany, where he studied, worked to become a

well known specialist in metallurgy, the career finally crowned by founding and heading of the German Metallurgical Society. In this period, in 1916 he made his most outstanding discovery of the method of growing single crystals during investigations of growth velocities of metals. He obtained single crystals of metals a few mm in diameter and length up to 150 mm. The CZ method, originally invented for metals, was improved and cited from its very beginning (1918). Later on, the method was extended to other substances with most notable success in semiconductors, since germanium and silicon transistors were discovered. By invitation of the President of Poland, he returned to then reemerged Poland in 1928 and since then he continued his research at the Technical University in Warsaw. After the Second World War, he was forced to come back to Kcynia. He died in Poznan and was buried in 1953 in Kcynia. During his entire professional life he was a very active and competent scientist, able to identify most important aspects of physical problems to understand them, and finally to find successful application of the conceived ideas. He used several methods for characterization of metals and alloys. He was an author of large number of papers and patents which can be easily found in Chemical Abstracts. He was active in German and Polish Materials Sciences Societies.

Still in the lifetime of Czochralski the crystal growth method named after him gained tremendously in importance for the growth of materials applied in electronics technology. Initiated by the invention of the first transistor (based on Ge) in 1947, germanium and silicon were the first semiconductor crystals grown by the Czochralski method on industrial scale. In the middle of the fifties the crystal diameter reached already 6 and 4 inch, respectively. The availability of the Czochralski method also contributed substantially to the rapid development of compound semiconductors invented in the early fifties with GaAs as most important representative. In 1960 the first - ruby - laser was operated. This event triggered a huge demand worldwide for bulk crystals for optical applications. Henceforward a rapidly increasing number of oxide and fluoride crystals were grown by the Czochralski method. The first oxide crystal was $CaWO_4$ in 1960, and the first fluoride CaF_2 in 1961, both grown at Bell Telephone Laboratories, the same potent US-company which has been the first commercial producer of Ge and Si Czochralski crystals. The early spread of the Czochralski method into other countries strongly depended on their economic potential after the Second World War. However, whereas the importance of the Czochralski method for silicon dropped in favour of the floating zone technique until the mid of the 70`s, it had become well established for other compounds, e.g. for oxide crystals by the mid of the sixties. At that time a boom started in the commercial production and utilisation of single crystals in different fields. To make the Czochralski method applicable for this wide spectrum of materials an increasing number of international research groups made several important modifications during the following decade. These included measures which suppress melt evaporation, influence the fluid flow in the melt and allow a precise diameter control of the growing crystal. Nowadays, the Czochralski technique is the highest developed method with regard to the technical level and the process automation and therefore the method of choice for the growth and production of high perfect bulk single crystals, among them silicon as well as a multitude of oxides, fluorides and multicomponent compounds.

From the perspective of almost the passed century the common opinion of the scientific community recognized him as a great scientist and investigator who has laid the foundation for the development of the global electronics. For recognition of his scientific achievements the Polish Parliament adopted a resolution declaring 2013 as the Year of Jan Czochralski.

Coffee
Monday morning, 12 August, 10:20

Sessions
G01, G02, G03, G08, G10, T06
Monday morning, 12 August, 11:00

Lunch (JCG Editors meeting)
Monday afternoon, 12 August, 13:00

Sessions
G01, G02, G03, G08, G10, T06
Monday afternoon, 12 August, 15:00

Posters - MoP
G01, G02, G03, G05, G10, T02, T06
Monday afternoon, 12 August, 17:00

Break
Monday evening, 12 August, 18:30

PTWK assembly
Monday evening, 12 August, 19:00

Tuesday, 13 August

Plenary 2
Tuesday morning, 13 August, 8:30
Mickiewicz Hall, Auditorium Maximum

8:30 Plenary Lecture

In situ TEM investigations of particle-mediated crystal growth

James J. De Yoreo[1], Dongsheng Li[1], Michael H. Nielsen[2], David Kisailus[3]

1. *Pacific Northwest National Laboratories (PNNL), PO Box 999, Richland, WA 99352, United States* **2.** *University of California, Berkeley, CA 94720, United States* **3.** *University of California, Riverside, CA 92521, United States*

e-mail: james.deyoreo@pnnl.gov

Assembly of molecular clusters and nanoparticles in solution is now recognized as an important mechanism of crystal growth in many materials, yet the assembly process and attachment mechanisms are poorly understood. To achieve this understanding we are investigating nucleation and assembly of iron oxide, titanium oxide and calcium carbonate nanoprticles. TEM analysis shows that the TiO_2 nanowire branching occurs through attachment of anatase nanoparticles to rutile wires on a specific crystallographic plane for which the anatase-to-rutile transformation leads to creation of a twin plane. Using an *in-situ* heating stage on an aberration corrected microscope, we follow the

transformation of anatase nanoparticles into single crystal rutile both through heating and by attachment to larger anatase particles. We document the atomic reorganization and appearance of intermediate structures that lead to formation of a final co-aligned single crystal. *In-situ* TEM using a custom-designed holder and fluid cell to obtain sub-nanometer resolution shows that, in the iron oxide system, primary particles of ferrihydrite interact with one another through translational and rotational diffusion until a near-perfect lattice match is obtained either with true crystallographic alignment or across a twin plane. Oriented attachment (OA) then occurs through a sudden jump-to-contact, after which the interface expands through ion-by-ion attachment at a curvature-dependent rate. Analysis of the acceleration during the attachment process indicates that OA it is driven by an electrostatic attraction with about one unit of charge on each particle driving the event.

Plenary 3
Tuesday morning, 13 August, 9:10
Mickiewicz Hall, Auditorium Maximum

9:10 Plenary Lecture

Growth and Laser Performance of Rare-earth Vanadate Family Crystals

Jiyang Wang

Institue of Crystal Materials, Shandong University, Jinan 250100, China

e-mail: jywang@sdu.edu.cn

All-solid state lasers have been developed since the successfully manufacture of laser diode in last two decades. The most popular laser crystals are Nd:YAG, Nd:YVO_4 and $TiAl_2O_3$. Among these, Nd:YVO_4 is widely used in mid- and low- power output all-solid lasers. Since 1990's, a series of rare-earth vanadate crystals have been grown including Nd-, Yb, Tm, Cr- doped and Cr-,Nd- codoped vanadate crystals. $GdVO_4$, $LuVO_4$ and their mixture crystals with different dopants were also grown. The basic properties of these crystals have been determined. Laser performances and passive Q-switch for these series crystals were described in detail.

Coffee
Tuesday morning, 13 August, 9:50

Sessions
G01, G02, G04, G08, G10, T06
Tuesday morning, 13 August, 10:20

Lunch (IOCG Exec. Com. meeting)
Tuesday afternoon, 13 August, 12:20

Sessions
G01, G02, G04, G05, G10, T06
Tuesday afternoon, 13 August, 14:00

Break
Tuesday afternoon, 13 August, 15:30

Excursion
Tuesday afternoon, 13 August, 16:00

Wednesday, 14 August

Plenary 4
Wednesday morning, 14 August, 8:30
Mickiewicz Hall, Auditorium Maximum

8:30 Plenary Lecture

Diluted magnetic semiconductors – from bulk crystals to low dimensional structures

Jacek Kossut

Polish Academy of Sciences, Institute of Physics, al. Lotników 32/46, Warszawa 02-668, Poland

e-mail: kossut@ifpan.edu.pl

After a brief historical introduction to the physics of diluted magnetic semiconductors (DMSs) I shall describe some aspects of their physics that make the prospective applications in spintronics potentially possible. In particular, I shall mention those properties of bulk crystals, as well as low dimensional structures (quantum wells, nanowires and quantum dots) incorporating various members of the DMS family that focus on their unique properties that are related to exchange interaction between valence and/or conduction band electrons with localized magnetic moments present in those materials. I will talk about methods of fabrication and growth of these materials. Finally, I will introduce several concepts of useful devices put so far forward and I discuss feasibility of their realization.

Plenary 5
Wednesday morning, 14 August, 9:10
Mickiewicz Room, Auditorium Maximum

9:10 Plenary Lecture

Growth of GaN on Si – an overview

Alois Krost

Otto-von-Guericke-Universität Magdeburg, Institut für Experimentelle Physik, Universitätsplatz 2, Magdeburg 39106, Germany

e-mail: alois.krost@ovgu.de

Growth of GaN on various silicon surfaces by MOVPE is reviewed. Currently, GaN-on-Si(111) is considered to be the most promising material for high power electronic applications. Another major application for GaN-on-Si(111) will be high-power LEDs for general lighting. First high power white LEDs suitable for general lighting are already in production now. Several groups have already demonstrated that high quality GaN on Si can be grown by MOVPE on 150 mm diameter substrates and that growth is easier than on large diameter sapphire. Using in-situ curvature measurement technique we observed the strain state of group-III-nitride layers during growth and established a process for growing thick, crack-free GaN layers with a quality comparable to that on sapphire. Growth on Si(100), (110), and semipolar GaN on Si(11h) surfaces will be reported, too.

Coffee
Wednesday morning, 14 August, 9:50

Sessions
G01, G02, G03, G05, G10, T06
Wednesday morning, 14 August, 10:20

Lunch (IOCG Council meeting)
Wednesday afternoon, 14 August, 12:20

Sessions
G01, G02, G03, G07, T03, T06
Wednesday afternoon, 14 August, 14:00

Posters - WeP
G04, G06, G07, G08, G09, T01, T03, T04, T05, T07, T08, T09
Wednesday afternoon, 14 August, 16:00

IOCG assembly
Wednesday afternoon, 14 August, 17:30

Break
Wednesday evening, 14 August, 18:30

Conference Dinner
Wednesday evening, 14 August, 20:00

Thursday, 15 August

Frank Prize Lecture
Thursday morning, 15 August, 8:30
Mickiewicz Hall, Auditorium Maximum

8:30 Plenary Lecture

In-Situ Observation of Crystal Growth: in the past and in the future

Katsuo Tsukamoto

Graduate school of Scienece, Tohoku University, Sendai 980-8578, Japan

e-mail: ktsuka@m.tohoku.ac.jp

It was during the banquet of ICCG-4 (1974) in Tokyo when I met Professor Frank. I was a master course student who attended international conference for the first time. I knew his name for spiral growth theory. I wanted to have his signature on a small square wooden cup for Japanese rice wine. The organizer at the banquet presented the cup to us. Although I was very much hesitated to ask him, he kindly wrote his signature on my wooden cup. I still keep this cup in my office for the memory of my start of crystal growth study, so that it was my biggest honor to receive the award that bears the name of Frank.

In the lecture, I want to discuss why in-situ observation of crystal growth from solution phase was necessary in those days, followed by the recent development together with the applications and then possible future of in-situ observation.

Ichiro Sunagawa was my first professor who introduced me to the world of crystal growth by showing beautiful spiral patterns on various minerals that were grown mainly from vapor phases. It was a shock for me not only because of the beautiful spiral patterns but also because of the ability of optical phase-contrast microscopy, which could reveal mono-molecular growth steps with the height of a few Angstrom.

He often showed me a work of Bennema in the Netherlands who had been investigating the growth mechanism of aqueous solution grown crystals by measuring the growth rate vs supersaturation. His thesis was to verify the applicability of spiral growth theory to aqueous solution grown crystals. Professor Sunagawa then invited Professor Bennema to Tohoku University, where we had a good time for discussion on crystal growth. After he came back to the Netherlands, he invited me to his laboratory in 1977-1979.

I leaned from Sunagawa to observe crystal surface by phase-sensitive optical microscopy to understand the growth history of the crystal. However the surface pattern, which could be observed, were already “dead”. While, in the lab of Bennema, I learned how to measure extremely slow growth rate of crystals by measuring the weight increase or the size increase and how to apply crystal growth theories to real crystal growth. However I was not satisfied with their methods because of two reasons: it takes several weeks to finish a measurement of growth rate vs supersaturation, and we could not see, during experiment, the crystal surfaces that should posses the information about the growth mechanism.

In order to overcome these difficulties, I started to couple the surface observation method with the crystal growth rate measurement by developing various optical in-situ observation methods for crystal growth.

These in-situ observation methods have been applied to crystal growth not only to investigate crystal growth mechanisms for fundamental sciences but also to crystal growth in earth and in astronomical environments for the understand of nature and the history. These new and successful studies could be achieved thanks to the efforts of my colleagues, students and companies.

The topics for Frank Prize Award Lecture will be selected from the following categories:

1. Development of High Resolution Optical In-Situ Observation Methods and the Application to Fundamental Crystal Growth Studies

Before 1980s, if one wants to investigate growth mechanism from solution, the measure the growth rate vs supersaturation by weighing method developed by Bennema was the only way. However, it took more than a few weeks to complete all of the measurements and the analysis on growth mechanism was indirect. We developed in-situ observation method directly to observe mono-molecular spiral steps on crystal faces by advanced optical microscopies during crystal growth in well-controlled conditions (1983). This made us possible also to understand the effect of defects and flows in crystals on the growth of kinetics of inorganic crystals (1988) and of proteins (1989).

The in-situ surface observation was later coupled with interferometer to visualize the concentration/temperature fields over the surface together with the observation of monomolecular growth steps, to study the effect of flow and the inhomogeneity of concentration around the crystals (1988). The high temperature in-situ observation method was applied to study the natural crystallization from magma, LiNibO3 and GaAs from the melt phase.

Ultra-high resolution interferometry (Real-Time Phase-Shift Interferometry, RPSI) for crystal growth studies was developed in 1994. This interferometer showed two-order of magnitude higher resolution than conventional interferometry and thus pioneered some new research fields, in which crystal growth/dissolution rate is extremely slow like in earth sciences, in environmental sciences or in carbon sequestration. The interferometry has further been developed to posesse the capability of 3D observation (2010) and ultra-high speed (10,000 frame/s) for the study of mass and heat transfer in nucleation process as well (unpublished).

2. Utilization in Other Fields:

(1) Application to Space Experiments

Numerous growth experiments have been conducted under microgravity in space shuttles, rockets and so on. However the method to study the growth mechanism of crystals was a simple way as follows: to grow crystal in space followed by the transport of these materials to the ground for the characterization on the ground. We did not like this indirect way of studies and for the first time successfully used interferometer for in-situ studies of crystal growth mechanism under microgravity (1991). The in-situ method was later applied in NASA and ESA projects for mainly to the studies of protein crystal growth mechanism using space shuttles.

Everybody believed that growth rate of protein crystals under microgravity would be smaller than that in gravity because buoyancy driven convection and flows could be suppressed in space. However the growth rate of protein crystals measred in a Russian satellite in 2007 and in the International Space Sation in 2011 by in-situ method was sometimes larger than that in gravity.

Simultaneously with this velocity increase in microgravity, appearance of the sharp corner of the elementary step was observed even in impure soluiotns. That sharpning was identified as impurity controlled. These two findings (the velocity measurements and morphology change) suggest that lack of convection allows self- purification of the growing crystal via absorbing impurities from the surrounding mother liquor. That may be solution of the long standing problem on why protein crystals sometimes grow more perfect in microgravity.

(2) Application to environmental sciences and engineers

Application of in-situ observation to natural slow phenomena was started to measure the solubility and reaction kinetics of insoluble minerals (1991). The ultra-slow growth rate of giant gypsum crystals, ~11 m long in Mexico was measured with collaboration of Garcia Ruiz et al. (2012) to be 10-5nm/s (<1μm/year) by newly developed white beam phase-shift interferometry (PSI). This was the champion data of the slowest crystal growth rate which has been mesed so far.

The PSI had practically been applied to nuclear waste studies in Japan (1993). The waste will be stored in the glass state with surrounding barrier of clay minerals under the ground for 100,000 years but reacts with ground water. However, so far there is not suitable method to measure the dissolution rate of the clay minerals exactly. The meased growth rate is the order of 10-5 nm/s.

The in-situ observation was also useful to the study of "Carbon Sequestration" or "CCS" in which how the dissolved CO2 in water could be sealed and trapped in the cap rocks is the key.

(3) Crystallization 4.6 billion years ago: rapid crystallization in space

Combination of in-situ observation of crystal growth with experience under microgravity made a new progress in space sciences (1998, 2006). Chondrules are silicate spheres with a few mm size formed from melt droplets 4.6 billion years ago in the primitive solar system. These spheres are often found in meteorites and regarded as the result of very slow cooling and growth rate in many years time. However, levitating these melt droplets experimentally showed that the crystallization of the melts has to be finished in a few seconds at the supercooling of several hundreds K or more in the hypercooling regime (2010).

(4) Structures of the solution at the crystal surface

Recently, we have successfully used newly developed frequency-modulate AFM (FM-AFM) with atomic resolution to reveal atomic configuration of the crystal surface during crystal growth from solution (2012). Since this FM-AFM is very sensitive, we also succeeded to visualize the hydrated structures in-situ at the crystal surface and even at the step front. Notwithstanding that the growth rate of solution grown crystals is controlled by the dehydration process, we know litte about the hydrated structure at the surface and steps.

Laudise Prize Lecture

Thursday morning, 15 August, 9:00
Mickiewicz Room, Auditorium Maximum

9:00 Plenary Lecture

Super nonlinear optical crystal-$KBe_2BO_3F_2$

Chuantiang T. Chen

Technical Institute of Physics and Chemistry, CAS, Beijing 100190, China

e-mail: cct@mail.ipc.ac.cn

In this paper, the $KBe_2BO_3F_2$(KBBF) crystal has been demonstrated to be a super nonlinear optical crystal. Firstly, KBBF has excellent nonlinear optical properties including a widest phase-matching wavelength region, a widest temperature bandwidth and highest damage threshold in all nonlinear optical crystals. Secondly it has superior capability to produce deep-UV second harmonic generation. For example, it can produce 153nm with 0.5mW output power, 120mW 177.3nm as well as 191nm cw laser at mW level. Finally, some important applications are introduced especially in the advanced deep-UV laser angle- and spin- resolved photoemission spectrometers and deep-UV laser photon-electronic emission microscope et. al.

Schieber Prize Lecture

Thursday morning, 15 August, 9:30
Mickiewicz Room, Auditorium Maximum

9:30 Plenary Lecture

Nucleation and growth of cosmic nanominerals based on size effects in mesoscale

Yuki Kimura

Graduate school of Scienece, Tohoku University, Sendai 980-8578, Japan

e-mail: ykimura@m.tohoku.ac.jp

Meteorites contain many kinds of microscopic particles of minerals such as metals, silicates, sulfides, carbides, and oxides. Most of these were formed when the Solar system was still a nebula, 4.6 billion years ago. Some, known as presolar grains, are even older than this and were formed in a gas outflow of earlier dying stars. It is important to understand the process of formation of nanometer-sized minerals, because cosmic minerals are the smallest building blocks of planetary systems and they operate as substrates for the formation of molecules in space.

Despite extensive studies over a long time, the processes by which solar and presolar minerals were formed remain largely unknown. We have assumed that there are two keys to achieving an understanding of these processes; one is the size effect, and the other is the formation of cosmic minerals under conditions of microgravity.

Many studies on nanometer-sized solid particles were initiated following Kubo's seminal theoretical study that showed that extremely small metallic particles have physical properties that differ from those of the bulk material as a result of their discrete electronic states [R. Kubo, J. Phys. Soc. Jpn. 17 (1962) 975]; this has come to be known as the Kubo effect. Later studies on nanometer-sized particles have confirmed and progressed that their physical properties differ markedly from those of the bulk materials. For example, the existence of extremely large diffusion coefficients results in the anomalous phenomenon of spontaneous alloying [e.g., H. Yasuda and H. Mori, Phys. Rev. Lett. 69 (1992) 3747]. We have also reported the occurrence of spontaneous mixing of ions in alkali halide nanocrystals [Y. Kimura et al. Phys. Low-Dim. Struct. 1/2 (2000) L1; Physica E 13 (2002) 11].

Because the actual size of cosmic nanomineral particles is of the order of 100 nm or less, I would expect that the singular physical properties and related phenomena that appear on the nanoscale will have to be taken into account if we are to understand the process of formation of nanominerals in the universe. Indeed, we have been able to duplicate in the laboratory several features of cosmic nanominerals, such as the formation of carbonaceous hollow particles [M. Saito & Y. Kimura Astrophys. J. Lett. 703 (2009) 147], the low-temperature crystallization of forsterite [Y. Kimura et al. Astrophys. J. Lett. 680 (2008) 89], the formation of composite particles with a titanium carbide core and a carbon mantle through decomposition of carbon monoxide gas [Y. Kimura et al. Meteorit. & Planet. Sci. 41 (2006) 673], the formation of pyrrhotite by a solid–solid reaction [Y. Kimura et al. ICARUS 177 (2005) 280], and the existence of fullerenes around evolved stars [Y. Kimura et al. Astrophys. J. Lett. 632 (2005) 159], and we have suggested processes for the formation of such nanominerals that are based on crystallization in the mesoscale. I do not claim that all of these minerals were formed by processes identical to those used in the laboratory experiments, but our studies confirm that a knowledge of the significant physical properties of nanoparticles is necessary if we are to understand the life cycles of cosmic minerals.

We recently began a project on homogeneous nucleation that incorporates studies on physical properties of nanoparticles with the aim of achieving a better understanding of the process of formation of nanoparticles and evaluating nucleation theories. Nucleation theory can be used to predict the nucleation temperatures, phase, sizes, size distributions, and number densities of products. Unfortunately, it has become apparent that nucleation rates that are determined experimentally or by means of molecular dynamics simulations always differ by several orders of magnitude from those of classical nucleation theory. Generally, this difference can be considered to be a limitation of nucleation theory. However, on the basis of our experimental results, we have adopted the idea of coalescence growth, which is a process for the growth of nanoparticles, to provide a partial explanation for this discrepancy. We have shown that tiny nuclei can fuse together to form larger particles, thereby reducing their number density by a few orders of magnitude [Y. Kimura et al. J. Crystal Growth 316 (2011) 196; Cryst. Growth & Des. 12 (2012) 3278].

Although cosmic minerals are formed under conditions of microgravity, existing speculations as to mechanisms for their formation have generally been based on experiences on the Earth, where crystallization inevitably involves effects of buoyancy-driven convection and heterogeneous nucleation. When we perform experiments in the laboratory, mineral samples are kept in containers, which form sites for heterogeneous nucleation, and buoyancy-driven convection generates inhomogeneities in the environment for particle formation. We have therefore started a new project that incorporates experiments on homogeneous nucleation under conditions of microgravity and we recently performed such experiments on the sounding rocket S-520-28, launched on December 17th, 2012. I believe that further experiments based on this concept will clarify not only the process of formation of cosmic nanominerals, but also the nucleation process itself.

Coffee
Thursday morning, 15 August, 9:50

Sessions
G01, G04, G07, T03, T06, T08
Thursday morning, 15 August, 10:20

Lunch (EMCG meeting)
Thursday afternoon, 15 August, 12:20

Sessions
G04, G06, G07, T01, T03, T08
Thursday afternoon, 15 August, 14:00

Coffee
Thursday afternoon, 15 August, 16:00

Sessions
G06, G07, T01, T03, T05, T07
Thursday afternoon, 15 August, 16:30

End of Sessions
Thursday evening, 15 August, 18:30

Friday, 16 August

Sessions
G09, T02, T04, T05, T07
Friday morning, 16 August, 8:30

Coffee
Friday morning, 16 August, 10:30

Sessions
G09, T02, T04, T05, T07
Friday morning, 16 August, 11:00

Coffee
Friday afternoon, 16 August, 13:00

Closing ceremony
Friday afternoon, 16 August, 13:30

Posters

Monday, 12 August

Posters - MoP

G01, G02, G03, G05, G10, T02, T06
Monday afternoon, 12 August, 17:00

Wednesday, 14 August

Posters - WeP

G04, G06, G07, G08, G09, T01, T03, T04, T05, T07, T08, T09
Wednesday afternoon, 14 August, 16:00

General Session 1

Fundamentals and Modeling

Session Coordinators

Koichi Kakimoto (Japan) *kakimoto@riam.kyushu-u.ac.jp*

Jeffrey J. Derby (USA) *derby@umn.edu*

Programme

Monday, 12 August

MoO1

G01:Fundamentals and Modeling
Monday morning, 12 August, 11:00
Hall 16, Old Library

11:00 Invited oral

Step patterns induced by a line source of adatoms

Makio Uwaha[1], Masashi Kawaguchi[1], Shinji Kondo[1], Hitoshi Miura[2], Masahide Sato[3]

1. *Nagoya University, Department of Physics (NU), Furo-cho, Chikusa-ku, Nagoya 464-8602, Japan* **2.** *Nagoya City University, Nagoya 467-8601, Japan* **3.** *Kanazawa University, Kakuma-machi, Kanazawa 9201192, Japan*

e-mail: uwaha@nagoya-u.jp

Being motivated by a comb-like step pattern observed during Ga deposition on Si(111) surfaces[1], we theoretically study growth of a step which is guided by a line adatom source moving in front of the step. The pattern formation in a lattice model[2] and in a phase-field model is discussed.

The line source of adatoms located initially next to a straight step moves at a constant speed V_p away from the step. It releases adatoms of the density c =1/2, and makes the step grow. Many intrusions are soon formed by Mullins-Sekerka instability. In growth towards [11] direction, the comb-like step pattern appears with small V_p after coarsening of the pattern via competition of the intrusions. Periodic tips of the comb-like pattern follow the source steadily. With large V_p, a fractal pattern is formed by noise.

For the comb pattern, the structure becomes finer with increasing V_p. The period of initial intrusions is given by the capillary length d_0 and the diffusion length $l_D=D_s/V_p$ as $(d_0 l_D)^{1/2}$. The period λ of the steady comb-like pattern is controlled by the noise strength F_u. The period becomes logarithmically shorter with increasing the noise: $\lambda \sim (d_0 l_D)^{1/2} |\ln F_u|$. Such noise dependence suggests a peculiar mechanism to terminate the coarsening.

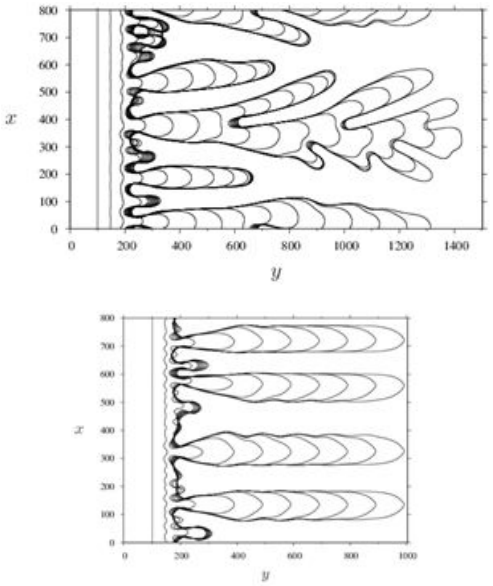

Fig.1: Time evolution of an irregular step pattern(upper) and a periodic comb-like pattern(lower).

[1] H. Hibino, H. Kageshima and M. Uwaha: Surf. Sci., **602** (2008) 2421.

[2] S. Kondo, M. Sato, M. Uwaha and H. Hibino: Phys. Rev. B **84**, 045420 (2011).

11:30 Oral

On the Energetics and Structural Behavior of some Si_n Clusters: Molecular Dynamics Simulations

Lynda Amirouche[1], Malika Bouaziz[1], Sakir Erkoc[2]

1. *Laboratoire de Physique Théorique, Faculté de Physqiue, U.S.T.H.B., Alger 16311, Algeria* **2.** *Middle East Technical University (METU), Inonu Bulvari, Ankara 06531, Turkey*

e-mail: lynda.amirouche@polytechnique.edu

We investigate, by molecular dynamics simulations, the structural behavior of silicon nanoparticles of sizes N ranging from 4 to 20 atoms. The interaction between silicon atoms is modeled by the EDIP potential (Environment Dependant interatomic Potential) which takes into account the tetravalent character of silicon as well as the covalent type of its chemical binding. EDIP potential is well known for its reliability in reproducing correctly the bulk silicon properties. In the present contribution, we use it for silicon nanoparticles of relatively small sizes, in the aim to estimate the deviations with regard to its approach for a nanoscopic system. Two sets of simulations have been carried out, for the whole range of sizes, starting each one from a different atomic initial configuration: (i) fragment of the diamond structure since silicon crystallises in this structure and (ii) atomic closed shells. The energy curves reveal that for N<9, the second initial configuration produces more stable structures than the first one. On the other hand, a dominant tendency to icosahedral structures is observed, above a certain size, for all the nanoparticles resulting from the two initial configurations. A third set of simulations is carried out by starting, for each size, from the most stable configuration resulting from the two previous sets of simulations. In this set, a simulated annealing followed by a quenching to the temperature of 1K is performed in order to approach the global minimum structures (optimization algorithm). Thus, the latter set of simulations is supposed to generate the most stable structures. However, some exceptions have been found out for some

particular sizes (N=5, 6, 11, 15, 16, 17 and 20). Our finding are compared to both experimental and computational results available in the literature for the same nanoparticles.

11:45 Oral

Molecular Assembly and Crystal Nucleation: How Molecular Dynamics Simulations Enhance Our Understanding

Dimitrios Toroz, Kevin J. Roberts, Robert B. Hammond

University of Leeds (SPEME), Leeds LS2-9JT, United Kingdom

e-mail: d.toroz@leeds.ac.uk

Molecular dynamics simulations are employed to elucidate the structure, lifetime and relative stability of putative assemblies of the fundamental growth-units of crystals. In the present study simulations carried out for the organic molecule para-aminobenzoic acid (PABA). PABA is an enantiotropic system which has two known polymorphic forms alpha stable above 13.8C° and beta stable below this transition temperature. Simulations were used to investigate the stability of clusters of solute molecules for PABA as a function of solution supersaturation and temperature. Of particular interest is the stability of carboxylic acid dimers, both singularly and when assembled into larger clusters, as these dimers are manifested in the solid-state packing of the alpha polymorph alone. Elucidating the energy landscape of solute clusters in supersaturated solutions is the key to understand how particular polymorphs are selected via solution crystallisation according to factors such as solvent choice, de-supersaturation profile and temperature.

The lifetime and stability of solute clusters was investigated with the objective of estimating the critical cluster-size, as a function of index of supersaturation, in a solvent environment based on the probability for cluster dissolution. Particularly interesting is the solvent effects of the molecular self-assembly of solute molecules in solution. MD simulations enable free-energy changes associated with the solvation of both monomers and dimers of PABA to be calculated, at temperatures above and below the transition temperature, by which a link to the relative thermodynamic stability of the polymorphs in the bulk might be made.

Key Words: Nucleation, Homogeneous, Heterogeneous, Crystal, Polymorphism, Molecular Assembly, Solution Structure, Molecular Dynamics, Molecular Clusters, Atomistic Potentials, Charge Models, Para-aminobenzoic Acid.

12:00 Oral

Polymorph prediction by nucleation modeling

Rita Bylsma[1], Hugo Meekes[1], Elias Vlieg[2], Joop Horst' ter[3], Niek Klerk' de[1]

1. *Radboud university Nijmegen, Solid State Chemistry (RU/SSC), Heyendaalseweg 135, Nijmegen 6525AJ, Netherlands* **2.** *Radboud University Nijmegen, Heyendaalseweg 135, Nijmegen 6525AJ, Netherlands* **3.** *Delft University of Technology, Process and Energy Laboratory (TUD/PE), Leeghwaterstraat 44, Delft 2628CA, Netherlands*

e-mail: R.Bylsma@science.ru.nl

Most organic compounds are polymorphic, i.e. they can crystallize in more than one crystal structure. This explains why crystals of the same compound can exhibit different solubility and effectiveness as a drug.

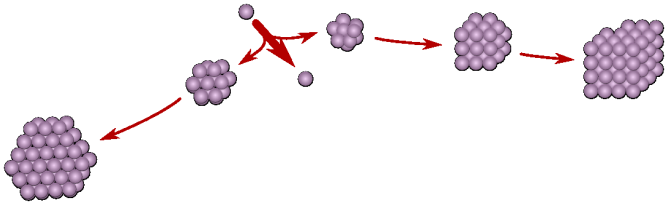

Conventional polymorph prediction routines are based on thermodynamic stability and predict that only one form would exist, the `stable' form. However, due to nucleation kinetics, a thermodynamically unstable form may crystallize and prevent the stable form from crystallizing (Ostwald's rule of stages). Thermodynamics predicts subsequent conversion to the stable form, but as conversion in the crystalline phase is often very slow, unstable polymorphic forms do actually exist over extended periods of time. Therefore, unstable polymorphic forms cannot be ignored in industry and they can even be of use. To be able to predict their formation, we are developing a kinetic polymorph predictor that simulates the nucleation process using a Monte Carlo algorithm.[1]

To ensure computability, our kinetic polymorph predictor uses crystal graphs: abstract descriptions of molecular structure, which contain all the important aspects that determine nucleation. We have been using the molecular mechanics program Cerius to compute crystal graphs from crystallographic data. In order to be independent of crystallographic data and to be more accurate, we started using the open source ab initio DFT program Siesta in combination with JuNoLo that adds a vdW-DF-functional. Together they function as a sophisticated energy-based polymorph prediction routine, generating many possible polymorphic structures. We added the functionality of representing them as crystal graphs.

Our kinetic polymorph predictor is highly automated and efficient, making decisions by root-finding methods rather than using grid methods. Thus, it is feasible to compare several hundreds of crystal graphs that result from the energy-based polymorph prediction routine.

Nucleation would be strongly influenced by the existence of precursor clusters in solution. We therefore added the possibility of simulating nucleation from all possible precursor clusters.

We will show results for some polymorphic drugs.

12:15 Oral

Analyzing Capture Zone Distributions (CZD) in Growth: Theory and Applications

Theodore L. Einstein[1], Alberto Pimpinelli[1,2], Diego Luis Gonzalez[1,3], Rajesh Sathiyanarayanan[1,4]

1. *University of Maryland, College Park, MD, United States* **2.** *Rice University, 6100 Main St., Houston, TX 77005, United States* **3.** *Universidad del Valle, Departimento de Fisica, Cali AA 25360, Colombia* **4.** *IBM Seimconductor Research and Development, Bangalore 560045, India*

e-mail: einstein@umd.edu

In submonolayer epitaxial island growth, it is fruitful to consider the distribution of the area of capture zones [BM96,ETB06,PE07], i.e. Voronoi (proximity) cells constructed from the island centers. For random nucleation centers (Poisson Voronoi diagrams) the CZD is expected to follow a Gamma distribution [K66,FN07], but more generally we have argued [PE07], drawing from experiences analyzing the terrace-width distributions of vicinal surfaces [EP99], that the CZD is better described by the single-parameter generalized Wigner distri-

bution (GWD): $P(s) = as^{\beta} \exp(-bs^2)$, where s is the CZ area divided by its average value; a and b are beta-dependent constants that assure normalization and unit mean of P(s). Painstaking simulations by Amar's [SSA09] and Evans's [LHE10] groups showed inadequacies in our mean field Fokker-Planck argument relating β to the critical nucleus size (conventionally called i+1), i.e. the size of the smallest cluster assumed not to decay. We refine our derivation to retrieve their finding that β is nearly $i + 2$ [PE10]. While the GWD describes the CZD in the regime in which there is significant data in experiments ($0.5 < s < 2$), it has shortcomings in the tails at both high and low s [LHE10,OA11]. For large s, $P(s)$ may decay exponentially rather than in gaussian fashion. We discuss several treatments of this issue, emphasizing the fragmentation model we developed [GE11], which depends on two physically motivated scaling exponents (one of which changes values around $s = 1.7$).

We discuss applications of this formula and methodology to experiments involving Ge/Si(001), various organics on SiO_2, and para-hexaphenyl (6P) films on amorphous mica [PTW11,TW12]. We report a series of studies by Fanfoni et al. of InAs quantum dots on GaAs [FP07,FA12] and very recent applications to metallic droplets [NM12], also on GaAs. (The former [FA12] also shows that the more-often-probed island-size distribution [ISD,ETB06] is comparable to the CZD at lower temperatures but not at higher temperatures when detachment--and consequent coarsening--becomes important.) At Maryland, for small admixtures of pentacenequinone (PnQ) with pentacene, our experimental colleagues and we studied the CZD at 0.3 ML coverage on SiO_2 [CG08]. As the fraction of PnQ was increased, the value of β dropped from 6.7 below 1% to 5.0 above 1%, indicative of the poorer packing possible when PnQ was present. For thick 50 ML films, this sudden change around 1% is reflected in a sudden decrease grain size and a consequent decrease in linear mobility. We also found for C_{60} on ultrathin SiO_2 that β varies nonmonotonically with temperature, increasing from 2 at room temperature, peaking near 3 around 375K, then declining; other evidence suggests that surface defects are responsible for this behavior. We have also used the GWD framework to elucidate kinetic Monte Carlo studies of homoepitaxial growth on Cu(100) with codeposited impurities of different sorts [HSPE11]. Finally, we have applied this approach to the distribution of metro stations in Paris [GE11] and of the areas of French districts (arrondissements) [GE11,S09,LCD93], counties in southeastern US states [S09], and other such secondary administrative units such as Polish powiaty and gminy [S09].

*Supported by UMD NSF-MRSEC Grant DMR 05-20471, NSF-CHE Grant 07-50334, and the Condensed Matter Theory Center, with ancillary support from CNAM (Center for Nanophysics and Advanced Materials).

[BM96] J. A. Blackman and P. A. Mulheran, Phys. Rev. B 54, 11681 (1996); P. A. Mulheran and J. A. Blackman, Philos. Mag. Lett. 72, 55 (1995); Phys. Rev. B 53, 10261 (1996).

[CG08] B. R. Conrad, E. Gomar-Nadal, W.G. Cullen, A. Pimpinelli, T. L. Einstein, E. D. Williams, Phys. Rev. B 77, 205338 (2008).

[CG12] M. Groce, B.R. Conrad, W.G. Cullen, A. Pimpinelli, E.D. Williams, and T. L. Einstein, Surface Sci. 606, 53 (2012).

[EP99] T. L. Einstein and O. Pierre-Louis, Surface Sci. 424, L299 (1999); T. L. Einstein, Appl. Phys. A 87, 375 (2007).

[ETB06] J.W. Evans, P. A. Thiel, and M. C. Bartelt, Surf. Sci. Rep. 61, 1 (2006).

[FA12] M. Fanfoni, F. Arciprete, C. Tirabassi, D. Del Gaudio, A. Filabozzi, A. Balzarotti, F. Patella, and E. Placidi, Phys. Rev. E 86, 061605 (2012).

[FN07] J.-S. Ferenc and Z. N´eda, Physica A 385, 518 (2007).

[FP07] M. Fanfoni, E. Placidi, F. Arciprete, E. Orsini, F. Patella, and A. Balzarotti, Phys. Rev. B 75, 245312 (2007)

[GE11] Diego Luis González and T. L. Einstein, Phys. Rev. E 84, 051135 (2011).

[GPE11] Diego Luis González, A. Pimpinelli, and T. L. Einstein, Phys. Rev. E 84, 011601 (2011).

[HSPE11] Ajmi BH. Hamouda, Rajesh Sathiyanarayanan, A. Pimpinelli, and T. L. Einstein, Phys. Rev. B 83, 035423 (2011); Rajesh Sathiyanarayanan, Ajmi BH. Hamouda, A. Pimpinelli, and T. L. Einstein, Phys. Rev. B 83, 035424 (2011).

[ISD] M.C. Bartelt and J.W. Evans, Phys. Rev. B 46, 12 675 (1992); C. Ratsch, A. Zangwill, P. Smilauer, and D.D. Vvedensky, Phys. Rev. Lett. 72, 3194 (1994); J.G. Amar, F. Family, and P.M. Lam, Phys. Rev. B 50, 8781 (1994).

[K66] T. Kiang, Z. Astrophysik 64, 433 (1966).

[LCD93] G. Le Ca¨er and R. Delannay, J. Phys. I (France) 3, 1777 (1993).

[LHE10] M. Li, Y. Han, and J. W. Evans, Phys. Rev. Lett. 104, 149601 (2010).

[NM12] D.M. Nothern & J.M. Millunchick, J. Vac. Sci. Tech. B 30, 060603 (2007)

[OA11] T. J. Oliveira and F. D. A. Aar˜ao Reis, Phys. Rev. B 83, 201405 (2011).

[PE07] A. Pimpinelli and T. L. Einstein, Phys. Rev. Lett. 99, 226102 (2007).

[PE10] A. Pimpinelli and T. L. Einstein, Phys. Rev. Lett. 104, 149602 (2010).

[PTW11] T. Potocar, G. Lorbek, D. Nabok, Q. Shen, L. Tumbek, G. Hlawacek, P. Puschnig, C. Ambrosch-Draxl, C. Teichert, and A. Winkler, Phys. Rev. B 83, 075423 (2011); S. Lorbek, G. Hlawacek, and C. Teichert, Eur. Phys. J. Appl. Phys. 55, 23902 (2011).

[S09] Rajesh Sathiyanarayanan, Ph.D. thesis, U. of Maryland, College Park, 2009; R. Sathiyanarayanan et al., preprint.

[SSA09] F. Shi, Y. Shim, and J. G. Amar, Phys. Rev. E 79, 011602 (2009).

[TW12] L. Tumbek and A. Winkler, Surface Sci. 606, L55 (2012).

12:30 Oral

Nucleation and growth of fluoride crystals by agglomeration of the nanoparticles

Pavel Fedorov[1], Vjatcheslav V. Osiko[1], Sergey V. Kuznetsov[1], Oleg V. Uvarov[1], Mariya Maykova[1], Darya S. Yasirkina[1], Anna Ovsaynnikova[1], Valerii V. Voronov[1], Vladimir K. Ivanov[2]

1. *General Physics Institute, Vavilov Str. 38, Moscow 117942, Russian Federation* **2.** *Kurnakov Institute of General and Inorganic Chemistry RAS (IGIC), Leninsky prospect, 31, Moscow 119991, Russian Federation*

e-mail: ppfedorov@yandex.ru

Classic theory of crystal growth states that all crystals grow by adding new building units (i.e., atoms, ions, molecules or their complexes) to their surfaces from solution, melt, vapor or another solid phase [1]. However, there is another theory of the alternative mechanism of the crystal growth – micro-block mechanism – that suggests that the crystal growth occurs by the intergrowth of the independently grown smaller crystals that made a contact in the course of their size increase. The latter approach, initially developed by P. Goubert as early as in the 19-th century, was actively pursued and developed by E. S. Fedorov, A. Traube, M. P. Shaskolskaya, A. V. Schubnikov, N. N. Sheftal, D. Balarev, N. P. Yushkin [2], A. M. Askhabov, I. V. Melikhov and other. The propriety of the micro-block mechanism has been confirmed by scanning (SEM) and transmission (TEM) electron microscopy as well as other experimental nano-methods [3-5]. In our presentation, we would like to report our novel results related to the formation of nano-

powders in the course of their co-precipitation from aqueous solutions. Our data confirm the aforementioned micro-block mechanism of crystal growth for the obtained fluoride nanopowders (TEM measurements were carried out at the Center of mutual use of equipment at Prokhorov General Physics Institute). Specifically, we would like to emphasize the following features of the observed processes: 1. The formed primary particles are not X-ray amorphous, they are nanocrystals. 2. Nanoparticles can mutually orient each other in colloid solutions as well as in solid-state phases. 3. Usually, the first step of crystal formation is not the particle merge to an existing large single crystal; instead, it includes primary merging of already formed nanoparticles. 4. Crystallization has a step-wise hierarchical nature with the periods of rapid nanoparticle growth changing to the relaxation periods; the latter periods include processes of imperfection decrease and stress elimination. 5. The above transformations occur at the temperatures much lower than the melting temperature (i. e., the so-called Tammann temperature T < 0.6*Tmelt). 6. In aqueous media, the aforementioned processes are typical for the crystal growth of the substances with low solubility. We consider that the driving force of the observed non-classical micro-block crystallization is the thermodynamic tendency to minimize the system free energy in the course of crystal growth. Describing the dynamics of the nanoparticle formation, one may name this force as "orientation ordering force" for convenience purpose.

References [1] L.N. Rashkovich, J.J. De Yoreo, C.A. Orme, and A.A.Chernov. Crystallography Reports, 51(6), (2006), pp. 1063-1074. [2] N.P. Yushkin. Theory of micro-block crystal growth in natural heterogeneous solutions. Syktyvkar, 1971 (in Russian). [3] P.P. Fedorov, A.A. Luginina, S.V. Kuznetsov, and V.V. Osiko. J. Fluorine Chemistry. Vol.132. (2011) pp.1012-1039. [4] P. P. Fedorov, M. N. Mayakova, S. V. Kuznetsov, V. V. Voronov, V. V. Osiko, R. P. Ermakov, I. V. Gontar', A. A. Timofeev, and L. D. Iskhakova. Nanotechnologies in Russia. Vol.6. (2011) pp. 203–210. [5] P.P. Fedorov, V.K. Ivanov. Doklady Physics. Vol.56. (2011) pp. 205-207.

12:45 Oral

Analytical and numerical study of nanoisland spectrum evolution

Maxim Nazarenko[1,2], Nickolay V. Sibirev[1,2,3], Maxim Kazansky[1], Vladimir G. Dubrovskii[1,2]

1. *St Petersburg Academic University, Khlopina Str 8/3, S.Petersburg 194021, Russian Federation* **2.** *Ioffe Physico-Technical Institute (Ioffe), Polytechnicheskaya, 26, Saint-Petersburg 194021, Russian Federation* **3.** *Saint-Petersburg State University, Saint-Petersburg, Russian Federation*

e-mail: NazarenkoMV@gmail.com

Introduction

Classical nucleation-condensation theory is based on the kinetic Zeldovich equation in partial derivatives of the second order for the distribution of nanoparticles over sizes [1-4]. This equation is obtained as a continuous approximation of finite-difference master equations in the monomer limit, where the growth-evaporation rates are related via the detailed balance with the known minimum work of nanoparticle formation [5]. Since the growth equation contains unknown supersaturation of a metastable phase, one should also consider the material balance [2-4]. In an open system with pumping, the supersaturation changes in time due to the monomer consumption by the growing nanoparticles and the material influx into the system [1-3]. Analytical or numerical studies of a particular condensing system therefore requires a solution of two connected equations for the time-dependent size distribution and the supersaturation: the differential Zeldovich equation and the integral equation of material balance [2,3]. Steep exponential dependence of nucleation rate on the supersaturation [1,2] makes the whole system strongly non-linear. The non-linearity of the equations, the fluctuation-induced effects and many other factors make the nucleation-condensation theory rather complex for the analysis. Such analysis is of great importance however in connection with thin films and surface islands [1,4], semiconductor quantum dots (QDs), freestanding nanowires and many other applications.

Green function and dispersion increase

Below we study the case of homogeneous nucleation in the monomer approximation with the growth-evaporation processes (i)+(1)⇔(i+1), where (i) denotes the embryo containing i monomers and (1) is the monomer in a metastable mother phase. The corresponding growth rate W_i^+ is assumed to be of quite general form [1-4]:

$W_i^+=m(\zeta+1)i^{(m-1)/m}/\tau$,

where W_i^+ is growth rate of nanoparticle containing i monomers, ζ is the supersaturation of the mother phase, τ is characteristic microscopic time of nanoparticle growth, and m is the growth index that depends on the space dimensions of the nanoparticle and the metastable environment and nanoparticle growth regime. m normally lies between 1 and 3, for condensation of 2D GaAs nanoislands from adatom sea m=2 corresponds to ballistic regime and m=1 to diffusion regime.

Following Kuni [2], we define invariant size ρ as $\rho=i^{1/m}$, so that $d\rho/dt=\zeta/\tau$. A new time-dependent variable $z(t)$ is defined as the most representative invariant nanoparticle size at time t. The Zeldovich equation for the nanoparticle distribution function $f(\rho,z)$ in supercritical region can be written as

$$\partial_z f(\rho,z)=-\partial_\rho f(\rho,z)+\partial_\rho[\varphi(z)/(m\rho^{m-1})\partial_\rho f(\rho,z)], \quad (1)$$

where ∂_z is partial derivative with respect to z, ∂_ρ is partial derivative with respect to ρ, and $\varphi=1/2+1/\zeta$. The first right hand side term in (1) is well-known regular growth rate and the second one is responsible for fluctuation-induced spreading of size distribution.

During the growth stage, Green function $g(\rho,z)$ of the Zeldovich equation (1) can be asymptotically found in the form of Gaussian with z-dependent dispersion $\psi(z)$:

$g(\rho,z)=(2\pi\psi(z))^{-1/2}\exp[-(\rho-z)^2/(2\psi(z))]$

In this asymptotic case under the constant material flux the Zeldovich equation (1) leads the following equation for $\psi(z)$:

$\partial\psi/\partial z=2\varphi(z)/(mz^{m-1})$.

Solving this equation we can obtain the Green function and, consequently, solution of the Zeldovich equation for any initial condition. As an illustration, we calculate spectrum shape evolution of 2D GaAs nanoislands growing from the adatom sea in ballistic (m=2) and diffusion (m=1) regimes (cf. Fig. 1 and 2). It is easy to see that broadening of the size distribution is almost negligible for the ballistic regime (m=2), while for the diffusion regime (m=1) the diffusion-induced spreading is huge.

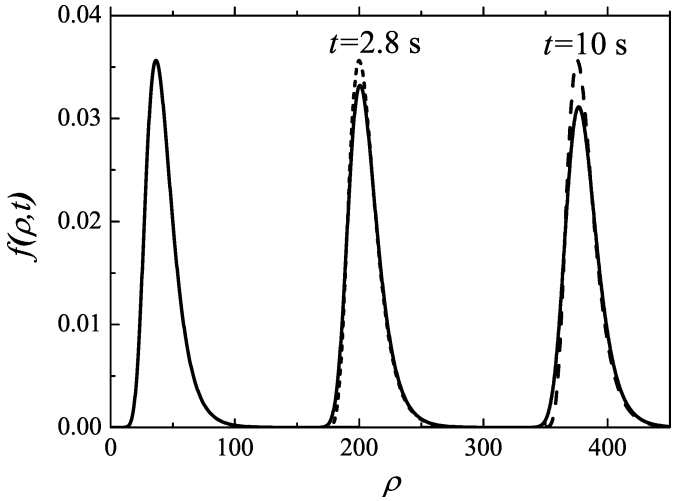

Figure 1. Time evolution of 2D nanoislands size spectrum in m=2 case. Dashed line show time-invariant spectrum.

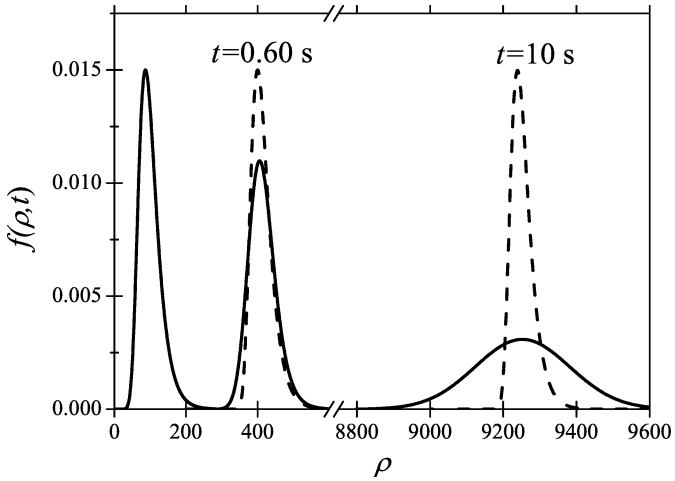

Figure 2. Time evolution of 2D nanoislands size spectrum in m=1 case. Dashed line show time-invariant spectrum.

Direct numerical simulations

Numerical simulation allows us to consider critical size, absent in the Zeldovich equation (1). Following Ref. [7] we introduce U as $U=(\rho/\rho_c)^{m/d}$, ρ_c being the critical size and d being the nanoparticle dimension. Assuming $(1-U)\ln(\zeta+1)\ll 1$ we can arrive at the following equation for the nanoparticle distribution function

$$\partial_t f(\rho,t)=-\partial_\rho[\zeta(1-U)f(\rho,t)/\tau]+\partial_\rho\{[2+\zeta(1+U)]\partial_\rho[f(\rho,t)/(m\rho^{m-1})]/(2\tau)\}, \quad (2)$$

with ∂_t being partial derivative with respect to time t.

By solving equation (2) with the appropriate boundary conditions numerically we are able to compute the spectrum dispersion D. The results are presented in Figure 3. The parameters used correspond to GaAs nanoisland formation. While the simplified analytical approximation and the numerical results agree qualitatively, the subcritical nanoparticles do change the quantitative results.

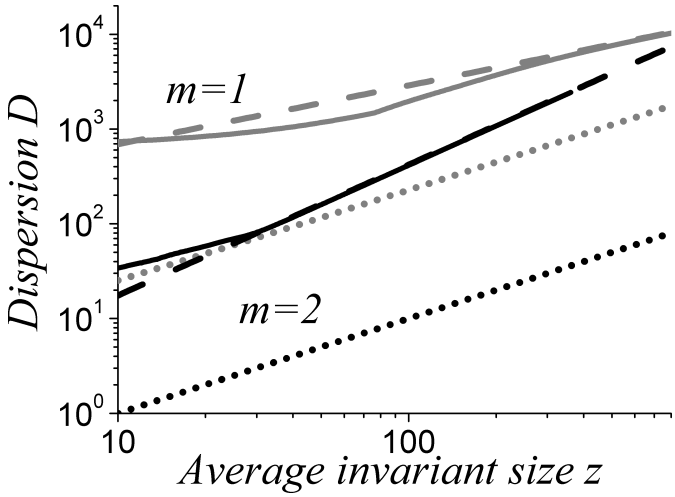

Figure 3. The dispersion of supercritical nanoislands D against the average invariant size z for d=2 and different m: gray – m=1, black – m=2. Dotted lines correspond to analytical asymptotic expressions, solid lines – numeric results, dashed – numeric asymptotics.

Ostwald ripening

The OR process onsets when the critical size reaches the pre-existing size distribution, and larger embryos start growing at the expense of smaller ones. This effect has a major impact on the size spectrum: the number of particles is no longer conserved and the dispersion increases much faster than at the growth stage.

By the very nature of the OR stage, its analysis require one to consider large time intervals, so direct numerical simulation we use above becomes infeasible. Therefore, we apply the explicit scheme of the Crank-Nicolson finite difference method [8] on a regular grid, which allows us to study times up to 10^6 s. We compare our result to those predicted by Lifshits and Slezov (LS) [9] using the standard LS notation:

$f(\rho,t)=\rho_c^{-m-1}F(x), \quad x=\rho/\rho_c(t)$

The results obtained are presented in Figures 4 (m=2) and 5 (m=1). While the spectra of the system with m=2 seem to collapse to a slightly different shape, the integral discrepancy is rather small.

Conclusions

To sum up, we present both analytical and numerical study of nanoparticle size spectrum evolution. The Green function for the second order Zeldovich equation allows us to find size spectrum at the growth stage accounting for the dispersion increase. Direct numerical calculation enable us to consider the critical size influence and to perform an independent check of the previous analytical results. Moreover, a slightly different numerical technique allows us to consider OR stage at times up to 10^6 s.

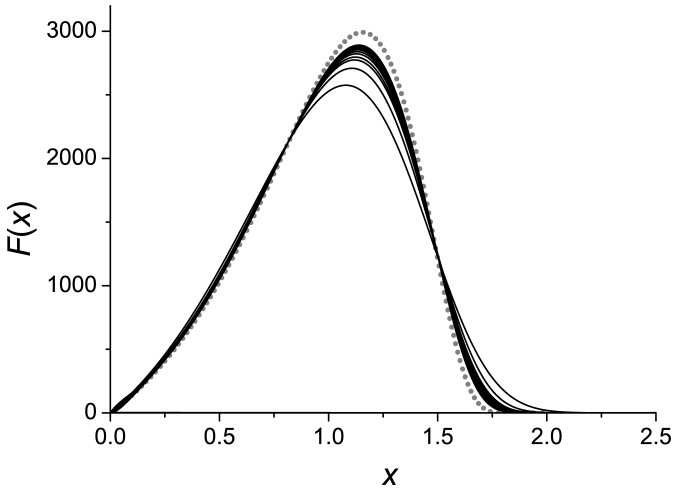

Figure 5. Numerical distributions at the late OR stage for the system with m=2, time t varying from 0 to 10^6 s. (solid), compared to the LS spectrum (dots).

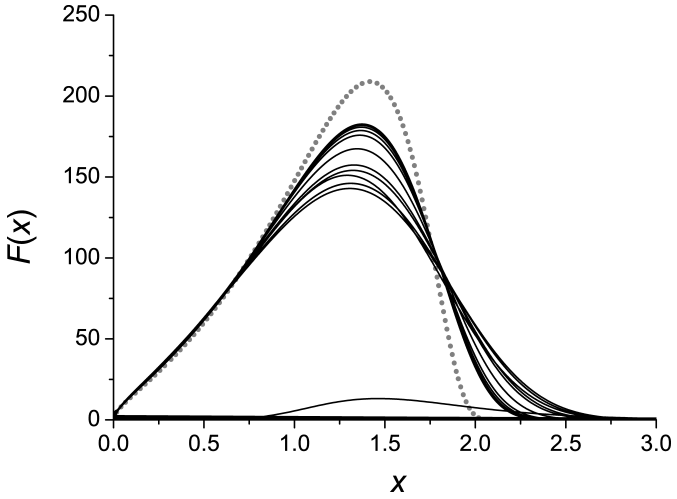

Figure 6. Numerical distributions at the late OR stage for the system with m=1, time t varying from 0 to 10^6 s. (solid), compared to the LS spectrum (dots).

Acknowledgments. This work was partially supported by different grants of RFBR.

References

1. D.Kashchiev, *Nucleation: Basic Theory with Applications* (Oxford: Butterworth Heinemann), 2000.
2. F.M. Kuni, *Colloid J.* **46**, 791 (1984).
3. V.G. Dubrovskii, *J. Chem. Phys.* **131**, 164514 (2009).
4. S.A. Kukushkin, and A.V. Osipov, *Prog. Surf. Sci.* **51**, 1 (1996).
5. D. Kashchiev, *J. Chem. Phys.* **129**, 164701 (2008).
6. V.G. Dubrovskii, *J. Chem. Phys.* **131**, 164514 (2009).
7. N.V. Sibirev, M.V. Nazarenko and V.G. Dubrovskii, *Tech. Phys. Lett.* **37(7)**, 596 (2011).
8. J. Crank, P. Nicolson, *Proc. Camb. Phil. Soc.* **43**, 50 (1947).
9. I.M. Lifshitz and V.V. Slezov, *Sov. Phys. JETP* **8**, 331 (1959).

Lunch (JCG Editors meeting)

Monday afternoon, 12 August, 13:00

MoO2

G01:Fundamentals and Modeling
Monday afternoon, 12 August, 15:00
Hall 16, Old Library

15:00 Invited oral

Step bunching and meandering processes in the crystal growth dynamics

Magdalena A. Zaluska-Kotur

Polish Academy of Sciences, Institute of Physics, al. Lotników 32/46, Warszawa 02-668, Poland Cardinal Stefan Wyszynski University, Faculty of Mathematics and Natural Sciences, Dewajtis 5, Warszawa 01815, Poland

e-mail: zalum@ifpan.edu.pl

Formation of various geometric patterns during crystal growth remains a subject of continuous interests of many researchers. It is important as an interesting example of far from equilibrium, stationary process and because of practical applications in the crystal growth technology. Kinetic Monte Carlo simulation method of analysis is based on a simple model of particles jumping between well-defined crystal site positions. The main task in the extended kinetic Monte Carlo (kMC) study is to find proper parameters of the model, i.e. coupling constants between particles, energy barriers for each type of particle jump such that describe main characteristics of the studied system. When correctness of the model is already verified by comparison with experimental data it can be used in further investigations. The simplicity of the model and small number of control parameters allows studying systems of large number of particles, performing long time simulations and examining the system behavior in various conditions. The kMC simulation results for two different systems are compared : GaN(0001) surface model in N-rich conditions represented by lattice of Ga atoms only and full, two component model of 4H SiC(0001). Within certain parameters steps move uniformly and stay straight during growth or sublimation processes of both simulated crystals. However within a wide parameter range different instability phenomena are observed. Step bunching and step meandering are the most characteristic ones. Both processes were studied as a function of time, temperature and misorientation angle. Detailed analysis of the character of structures and their evolution dependence on the growth parameters was done. For some parameters step bunching happens rapidly and as a result single bunch of all steps is formed. For other range of parameters two, four step arrangements develop or step train structure is observed. Phase diagram for all observed structure was found. The comparison of the kMC results with simple analytic models of step dynamics confirms that bunching and meandering instabilities are caused by the step movement during the process of crystal growth or sublimation. All surface patterns, emerging in the simulations, have their corresponding cases in the experimental results. The numerical models allow to observe how they develop and to study their time evolution.

15:30 Oral

Numerical analysis of multi-phase flow in the sublimation growth of SiC crystal by a 2-D incompressible kinetic model

Yuan Li, Xuejiang Chen, Juan Su

School of Energy and Power Engineering, Xi'an Jiaotong University, Xi'an 710049, China

e-mail: yuanli@stu.xjtu.edu.cn

Wide-band gap silicon carbide (SiC) is a promising semiconductor material for electronic and optoelectronic devices working in many extreme conditions, such as high temperature, high frequency, high power and intensive radiation environments. The physical vapor transport (PVT) method has been one of the most successful and common method for growth of bulk SiC crystals. During the process of SiC crystal growth by PVT, primary particles in the crucible transport from SiC powder surface to crystal growth surface and grow the SiC crystal, which is very important control process of the crystal growth. So it is necessary to study the multi-phase flow and particle transport inside the crucible for growing SiC crystal with large-size and high-quality.

In present paper, a two-dimensional incompressible growth kinetic model is developed to optimize the growth process and design the growth furnace for large-size SiC crystals. In this model, flow coupling between argon gas and vapor species, Stefan effect and buoyancy effect are considered. The gas flow and species concentration in the crucible are simulated by this model, and then based on the species concentration, the growth rate is also obtained. Firstly, the effect of three main vapor species in the crucible, namely Si, Si2C and SiC2 on growth rate at different growth temperatures is investigated. It is found that the effect of Si2C on growth rate is significant when growth temperature is below 2600 K, while the effect is weakened as the growth temperature continue to increase. Therefore, we can conclude that the effect of Si2C on growth rate can not be neglected in numerical models, as the growth temperature is below 2600 K, while it can be neglected completely as the growth temperature is beyond 2680 K. Furthermore, the flow patterns of convection and diffusion in the growth furnace at different total pressures and growth temperatures is also analyzed. As the results shown, the effects of convection on transport of vapor species are significant at high growth temperature and low total pressure, so it should be considered in numerical models. The results of this study may lead to the development of effective methods for producing SiC single crystals with large-size and high-quality.

15:45 Oral

Numerical simulation of the dissolution process of silicon into germanium melt

Farid Mechighel[1,3,4], Dost Sadik[2], Mahfoud Kadja[3]

1. *Université de BADJI-MOKHTAR, BP 12, Sidi Amar, Annaba 23000, Algeria* **2.** *University of Victoria, Victoria V8W3P6, Canada* **3.** *Constantine University (LMDM), Ain El Bey Road, Constantine 25014, Algeria* **4.** *Laboratoire Science des Procédés Céramiques et de Traitements de Surface - UMR 6638 CNRS - ENSCI, 47 avenue Albert Thomas, Limoges 87065, France*

e-mail: f_mechighel@etu.unilim.fr

The dissolution behaviour of silicon in a germanium melt has been numerically investigated. The numerical simulations were carried out using an axisymmetry model.

The effect of free surface on mixing was examined. The effect, while slight, did show a tendency of higher mixing with a free surface on the melt. The effect of the direction of gravity was also examined. One set of numerical experiments placed the silicon dissolution interface on top of the melt and the others the bottom of the melt. The chosen orientation with respect to gravity had a significant effect on dissolution. Far more dissolution was realized with the dissolution interface at the bottom of the melt. Silicon transport was aided by its buoyancy in the germanium melt. The melt, in these cases, remained inhomogeneous. This is likely due to very fast dissolution and strong convective flows.

The numerical results indicate that careful consideration of system geometry is needed when silicon is to be dissolved into germanium melt. Silicon dissolution from the surface of the melt will be limited by diffusion time scales. Silicon dissolution from the bottom of the melt will occur much faster but be subject to instability and melt inhomogeneity.

16:00 Oral

Formation of regular polyicosahedral and defected crystalline structures in growing Lennard-Jones clusters

Wiesław Polak

Lublin University of Technology, Department of Applied Physics (LUT), Nadbystrzycka 38, Lublin 20-618, Poland

e-mail: w.polak@pollub.pl

Formation of solid structure and its subsequent enlargement have been the main problems to be solved in simulated nucleus/cluster growth from vapour using the two-temperature-region cluster growth model [1]. Simulations were done for unsupported heavy rare-gas (Ar, Ne, Kr, Xe) clusters using Lennard-Jones (LJ) interaction potential. Four series of the Monte Carlo simulations, carried out for constant temperature T^* = 0.25, 0.30, 0.35 and 0.40 in reduced units (T = 30.3 K, 36.3 K, 42.4 K and 48.4 K for argon, respectively), were started from LJ_{13} icosahedral cluster used as a seed in a supersaturated LJ vapour. Evolution of cluster structure during growth was examined using structural analysis based on the Coordination Polyhedron method [2] accompanied with visualisation of the cluster structure, if necessary.

In the first simulation stage, growth was stopped when clusters achieved the final size N = 900-1000 atoms. In this way, every simulation series produces over 100 final clusters as well as much more clusters of intermediate size during growth. The structural analysis revealed that the clusters at all analysed temperatures are initially liquid and then transform to solid ones. The solidification is caused solely by a growing number of cluster atoms and occurs in the range from 160 to 900 atoms. Irregular non-crystalline structures prevail in the coldest final clusters, but many hotter clusters show regular non-crystalline or regular crystalline structure; regular structure is observed in 10%, 29%, 41% and 58% of cluster population for T^* = 0.25, 0.30, 0.35 and 0.40, respectively. Regular non-crystalline structures, mainly in the form of regular polyicosahedral (r-PIC) and rarely as defected decahedral (d-Dh) structure, are formed, respectively, in 9%, 25%, 27% and 44% of clusters, while regular crystalline structure in 1%, 4%, 14% and 15%. Regular crystalline clusters are classified as layered (L) ones with a few sandwiched parallel fcc and hcp close-packed layers and as defected layered (dL) or tetrahedral fcc core (t-FCC) clusters. This occurs as a result of kinetic trapping of nonparallel hcp surface planes on curved fcc cluster surface. All mentioned types of cluster structure were found recently in LJ clusters solidified during simulated cooling [3].

In order to analyse the growth of solid cluster structure, in the second simulation stage practically all the obtained clusters were grown until

N = 3300 was reached. Finally, in the third stage many selected clusters characterised by the regular internal structure of the types: r-PIC, d-Dh, L, dL or t-FCC were grown in simulations from N = 3300 up to N = 10 000 in the final clusters. Structural analysis revealed that the layered structure maintains layered fcc-hcp character by the addition of new atoms at the end of existing layers, keeping flat interface and its width constant during growth along the layers. The cluster growth in the perpendicular direction occurs by formation of new dense-packed layers by island formation mechanism. The r-PIC structure, characterised by regularly located icosahedral units, fcc tetrahedral regions and linear chains of decahedral units forming edges of regular tetrahedrons (see Fig. 1), initially keeps the structure during the growth, but its subsequent growth leads to the formation of disordered regions. The same occurs finally with d-Dh and t-FCC clusters, since they all evolve to r-PIC clusters during growth forming the long decahedral chains. The disturbed growth of r-PIC clusters is explained by structural misfit of tetrahedral fcc regions leading to internal tensions and formation of defects in growing clusters.

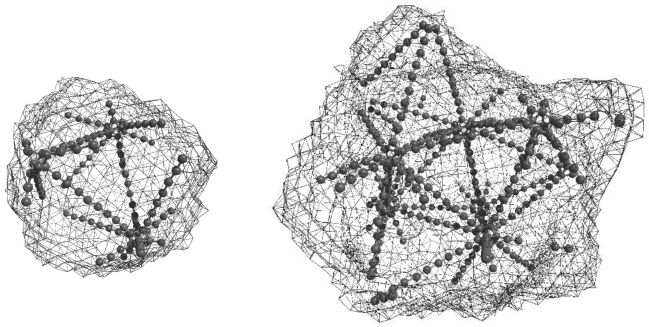

(a) (b)

Fig. 1. Formation of regular structure of decahedral chains during growth of r-PIC cluster from: (a) N = 3300 to (b) N = 10000 atoms.

[1] W. Polak, Phys. Rev. B 71 (2005) 235413.

[2] W. Polak, A. Patrykiejew, Phys. Rev. B 67 (2003)
[3] W. Polak, Phys. Rev. E 77 (2008) 031404.

16:15 Oral

Nucleation of crystals when the nucleation rate does not exist

Richard Sear

University of Surrey, Guildford Surrey GU27XH, United Kingdom

e-mail: r.sear@surrey.ac.uk

Recent experimental results for the nucleation of both aspirin crystals in solution [1], and the freezing of water droplets [2], are not consistent with a nucleation rate that is in the thermodynamic limit. Essentially, what is happenining is that although each crystallising droplet has a well defined nucleation rate, this rate varies by orders of magnitude from one nominally identical droplet to another. Then there is no well defined rate for a set of droplets at a given temperature and supersaturation. This highly variable rate is caused by heterogeneous nucleation on impurities that vary from one droplet to the next. I show how to diagnose an undefined nucleation rate, and how to model the probability of nucleation as a function of time [3]. The simplest way to observe an undefined nucleation rate is to plot the fraction of a set of droplets that have crystallised - deviations from an exponential function of time indicate an undefined rate. Then it may often be possible to fit to the data what is called the Weibull distribution of extreme-value statistics. If so then this fit can be used to determine the scaling of the median time to nucleation with volume [3]. I will show that, generically, the larger the deviations from exponential behaviour, the slower the time to nucleation varies with solution volume. [1] Y. Diao et al., J. Am. Chem. Soc. 133 (2011) 3756. [2] B.J. Murray e al., Atmos. Chem. Phys. 11 (2011) 11, 4191. [3] R. P. Sear, Cryst. Growth Design 13 (2013) 1329.

16:30 Oral

Growth Mechanism of Lysozyme Crystals in The International Space Station Based on The Analysis of In-Situ Interferometric Observation

Katsuo Tsukamoto[1], Izumi Yoshizaki[2], Yoshihisa Suzuki[3], Hitoshi Miura[4], Gen Sazaki[5], Masaru Tachibana[6], Kenta Murayama[1], Kentarou Oshi[1], Juan Manuel Garcia-Ruiz[7]

1. *Graduate school of Scienece, Tohoku University, Sendai 980-8578, Japan* **2.** *JAXA, Tsukuba 3058505, Japan* **3.** *Institute of Technology and Science, The University of Tokushima, 2-1 Minamijosanjima, Tokushima, Tokushima 770-8506, Japan* **4.** *Nagoya City University, Aichi 4678501, Japan* **5.** *Institute of Low Temperature Science, Hokkaido University (ILTS), N19-W8, Kita-ku, Sapporo 060-0819, Japan* **6.** *Yokohama City University, Yokohama, Japan* **7.** *Instituto Andaluz de Ciencias de la Tierra, CSIC-UGR (LEC-IACT), Avda. Las Palmeras, n° 4, Granada 18100, Spain*

e-mail: ktsuka@m.tohoku.ac.jp

So many protein crystals have been grown under microgravity condition to improve the quality of the crystals. However no one has clear answers why the quality is improved or at least is believed to be improved. To answer this question, we have for the first time measured growth rate vs supersaturation and the slope of spiral hillocks of lysozyme crystals from 3 different solutions with respect to concentration by Michelson Interferometry under microgravity condition in the international space station from August to December 2012.

Growth rates from two different solutions with different purity, 99.99% and 98.5% under microgravity were found to be the same, notwithstanding that growth rate under normal gravity differs a lot at relatively low supersaturation, <80%. It was also surprising to notice the disappearance of “dead zone” in all solutions near the equilibrium condition, where the growth rate becomes zero because of the pinning effect of impurities. When the growth rate under microgravity was compared with the rate in gravity, the rate was found to be similar or even larger than that in gravity. This is the same tendency as obtained from our ex-situ measurements of growth rate in the Foton-M3 recovery satellite.

The shape of growth hillocks is known as largely influenced by the purity of solution. When the solution is purer, the growth hillocks are more elongated in shape. This is the general tendency in laboratories and thus this morphological change would be a good criterion for the impurity effects on growth. The interferometry clearly demonstrated that the shape of spiral hillocks of crystals growing in impure solution were more elongated as if the crystals grew in a very pure solution.

These two findings, the growth rate measurements and morphology change of hillocks suggest that lack of convection allows self-purification of the growing crystal via absorbing impurities from the surrounding solutions. That may be solution of the long-standing problem on why protein crystals sometimes grow more perfect under microgravity.

The growth mechanism was discussed based on the growth rate vs supersaturation relationship. The interfacial tension for 2D homogeneous nucleation growth under microgravity was calculated to be ~0.5 mJ/m^2 and thus the same value as obtained in gravity. However 2D heterogeneous nucleation growth, which is dominant in gravity, did

not operate under microgravity. This finding also supports the above-mentioned conclusion from a kinetic point of view.

16:45 Oral

Ordering of Brownian Particles from Walls Due to an External Force

Masahide Sato[1], Hiroyasu Katsuno[2], Yoshihisa Suzuki[3]

1. *Kanazawa University, Kakuma-machi, Kanazawa 9201192, Japan* **2.** *Gakushuin University, 1-5-1 Mejiro,Toshima-ku, Tokyo 171-8588, Japan* **3.** *The University of Tokushima,Institute of Technology and Science,Department of life system, 2-1, Minamijosanjima, Tokushima, Tokushima 770-8506, Japan*

e-mail: sato@cs.s.kanazawa-u.ac.jp

Colloidal crystals are three-dimensional regular structures formed by colloidal particles with submicron size.The formation of colloidal crystals has received much attention for their application as photonic crystals.With regard to the distance between particles, the colloidal crystals are classified under two types.When the distance between particles is as large as the diameter of particles, i.e the particles are packed tightly,the crystals are called close-packed colloidal crystals. They are now the focus of attention as templates for inverse opals with three-dimensional photonic bandgaps.

From now on, many groups have tried to create a close-packed colloidal crystal by some techniques, e.g. using a template with a regularrarray of pyramidal pits [1], and sedimentation by gravitation [2]. However, the colloidal crystals formed in those studies [1,2] are thin or narrowly columnar. In order to use a templates for inverse opals, it has been necessary to increase the size of the grain of colloidal crystals.

Recently, Suzuki and co-workers[3,4] used a centrifugation method and succeed in creating a three-dimensional colloidal crystal with large grain size.In one of their experiments[4], they controlled the direction of the centrifugal force. When the direction of the force is tilted from the normal direction of the wall of a container,
the grain size is larger than that with an external force perpendicular to a wall.

Keeping their experiment[4] in mind, we carry out a simulation of Brownian dynamics, and study how ordering of particles with short ranged repulsion interaction changes by the direction and the strength of a uniform external force. When the external force is added to particles with a uniform density, the particles move to the direction to the force. Two-dimensional ordering of particles occurs on walls. Then, three-dimensional ordering starts from the walls. The density of particles on the walls increases all at once when the direction of external force is perpendicular to the walls, so that the positions of the particles attached on the walls do not move easily and ordering on the walls is law. On the other hands, the density of particles increases from an edge with a tilted force, so that ordering of particles, which proceeds from the edge, is high.
The difference in ordering on walls affects on the grain size of colloidal crystal. In bulk, both grains with the face-centered cubic structure and those with the hexagonal close-packed structure are formed. Irrespective of the type of structure, a lot of large grains are formed with a tilted external force.

References

[1] Y. Yin, Z. Li, and Y. Xia, Langmuir **19**, 622 (2003).

[2] K. E. Davis, W. B. Russel, and W. J. Glantschnig, Science **245**, 507 (1983).

[3] Y. Suzuki, T. Sawada, and K. Tamura, J. Cryst. Growth **318**, 780 (2011).

[4] K. Hashimoto, A. Mori, K. Tamura, and Y. Suzuki, Jpn. J. Appl. Phys. **52**, 030201 (2013).

MoP-G01
Monday afternoon, 12 August, 17:00
Room 105, Old Library

Break
Monday evening, 12 August, 18:30

Tuesday, 13 August

TuO1

G01:Fundamentals and Modeling
Tuesday morning, 13 August, 10:20
Hall 16, Old Library

10:20 Invited oral

Accurate simulation of aqueous crystal growth - solutions and challenges

Paolo Raiteri[1], Raffaella Demichelis[1], Julian D. Gale[1], Andrew G. Stack[2], Adam F. Wallace[3], James J. De Yoreo[3]

1. *Curtin University, Perth 6845, Australia* **2.** *Oak Ridge National Laboratory (ORNL), One bethel Valley Road, Oak Ridge, TN 37932, United States* **3.** *Lawrence Berkeley National Laboratory (LBNL), 1 Cyclotron Road, Berkeley, CA 94720, United States*

e-mail: J.Gale@curtin.edu.au

Computer simulation can be a valuable complement to experiment, especially for probing the atomic scale detail during crystal growth. However, this is contingent on being able to address several key challenges, namely length-scale, time-scale and the accuracy of the underlying potential energy landscape. The aim of this presentation will be to describe some of the approaches available for tackling these challenges for crystal growth of minerals from aqueous solution. In particular, the case of calcium carbonate formation will be examined. Here the process of nucleation and growth is made more intriguing by the presence of prenucleation species, both liquid and solid amorphous phases, in addition to the question of polymorphism.

In this work the derivation and application of an accurate force field for describing aqueous calcium carbonate systems will be discussed. In contrast to previous models, considerable emphasis has been placed on the accurate reproduction of the thermodynamics of the system, rather than just structural or mechanical properties [1]. By fitting the properties of both the hydrated ions and two of the bulk mineral phases, calcite and aragonite, the simulation model is able to reproduce the solubility and key relative polymorph energetics. Based on this, several questions regarding the growth of calcium carbonate from aqueous solution have been addressed:

1) What is the nature of prenucleation species in calcium carbonate solution?

Gebauer *et al* [2] have concluded that stable species exist in solutions of calcium and carbonate ions prior to nucleation. Subsequently, Pouget *et al* [3] identified nm-sized clusters using cryo-TEM. Given the diffi-

culty of directly characterising the structure and dynamics of these species in situ by experiment, this represents an ideal opportunity for simulation. Here molecular dynamics indicates that the initial association of ions is in the form of an ionic supramolecular polymer that is dynamically changing [4]. As the concentration increases, enhanced sampling techniques show that this transforms to more compact structures that remain significantly hydrated [5]. Significantly, no minimum is observed in the free energy landscape that would give rise to a preferred cluster size.

2) How do organics influence the nucleation of calcium carbonate?

During biomineralisation organic molecules clearly have a strong influence on the growth and assembly of calcium carbonate. This raises the question of how much of this influence occurs prior or subsequent to nucleation? Here the interaction of three simple carboxylate-containing molecules with various calcium carbonate species will be discussed along with the implications for the broader impact of organics on nucleation/growth [6].

3) Why does amorphous calcium carbonate appear as a precursor to crystalline phases?

Under certain conditions amorphous calcium carbonate (ACC) is observed to occur as a precursor to formation of crystalline polymorphs. One explanation for this might be that nucleation of the amorphous phase is faster and so this is just a matter of kinetic control. Simulations of the thermodynamics of nanoparticles of ACC and calcite indicate that below a size of approximately 4 nm the former material is actually the thermodynamically stable species [7]. Therefore under homogeneous conditions it appears likely that both thermodynamics and kinetics will favour initial formation of ACC. Furthermore, the ACC nanoparticles are able to lower their free energy by incorporating more water as the size of the particle increases. Under kinetically controlled growth conditions this would therefore lead to a heterogeneous distribution of water through out the nanoparticle, consistent with the proposed structure of ACC from Goodwin *et al* [8].

4) How do ions attach to calcite during growth?

Growth of calcite from solution is well known to occur via attachment of ions to steps/kinks on the dominant (104) surface. A subtle question is whether ions attach directly from solution or whether they first coordinate to the flat surface and then diffuse to the more reactive growth sites? Due to the presence of two strongly ordered water layers above this surface, which is observed by X-ray reflectivity and well described by the present simulation model (at least in terms of the water structure) [9], it appears that neither Ca^{2+} or CO_3^{2-} ions are able to coordinate directly to the (104) facet. Using an approach previously demonstrated for barite [10], that is able to yield quantitative rate constants for multistep growth processes, we are beginning to explore both the thermodynamics and kinetics of ion attachment to calcite.

[1] P. Raiteri *et al*, *J. Phys. Chem. C*, **114**, 5997-6010 (2010)

[2] D. Gebauer *et al*, *Science*, **322**, 1819-1822 (2008)

[3] E. Pouget *et al*, *Science*, **323**, 1455-1458 (2009)

[4] R. Demichelis *et al*, *Nature Comm.*, **2**, 590 (2011)

[5] A.F. Wallace *et al* (submitted)

[6] P. Raiteri *et al*, *Faraday Discussions*, **159**, 61-85 (2012)

[7] P. Raiteri and J.D. Gale, *J. Am. Chem. Soc.*, **132**, 17623-17634 (2010)

[8] A.L. Goodwin *et al*, *Chem. Mater.*, **22**, 3197-3205 (2010)

[9] P. Fenter *et al*, *J. Phys. Chem. C.*, **117**, 5028-5042 (2013)

[10] A.G. Stack *et al*, J. Am. Chem. Soc., 134, 11-14 (2012)

10:50 Oral

Numerical Calculation Method of Solution Growth and the Main Effect of Fluid Flow

Hiromoto Susawa

Home, Aichi 489-0888, Japan

e-mail: automobile_21@yahoo.co.jp

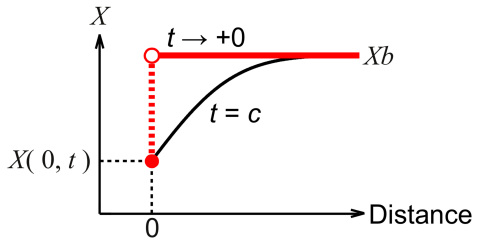

Fig. 1. A parameter varies abruptly. *X* denotes the parameter. *t* denotes a time. At $t \rightarrow +0$, it is difficult to treat the phenomenon. At $t = c$, the phenomenon moderates and we can treat the phenomenon within the tolerance of parameter. In this presentation, the distance : the distance from the growth interface, *t* : a growth time, *X* : the mole fraction of a component in the liquid phase, *Xb* : *X* just before the growth, *X*(0, *t*) : *X* that is in an equilibrium state with the solid phase.

1. Introduction

We reviews author's previous reports on solution growth.

Conventionally, we calculate phase diagram to predict experimental conditions in solution growth. However, we cannot grow the solid just in the calculated conditions. More than twenty years ago, the speed of computer was slow. A phase diagram could be computed only few times. More extended calculation was impossible. The materials we could grow were limited by the phase diagrams. Nowadays, a home computer has the speed of supercomputer in those days. We can compute a phase diagram many times, and take into account supersaturation and the other effect on the growth. We can also compute fluid flow in the liquid solution. The fluid flow has lately attracted considerable attention because it supplies poorly soluble solutes to the growth interface. For example, ammonothermal method is succeeding using fluid flow. GaN growth from sodium solution also uses fluid flow. We begin to overcome the limit of the phase diagram. Thus, it is important to understand the effect of fluid flow on solution growth.

Unfortunately, the properties of the hot materials are unknown. Then, this presentation deals with a well-known material to investigate the main effect of fluid flow on segregation. We deal with the case where the mass transfer through the growth interface is limited by the diffusion of each solute.

The calculation of segregation is delicate because the boundary condition does not have fixed values on the growth interface. In many calculations of crystal growth, the mole fractions have fixed values on the growth interface, while in the calculation of segregation, not fixed values. Moreover, boundary layer thicknesses of solute mole fractions are thin in the initial stage of growth. In conventional calculations, the results are buried under the errors [1]. We have to simplify the model to avoid introducing the errors.

Liquid solution is supersaturated prior to growth. Temperature is uniform and constant during growth. The mole fraction of each solute in the liquid solution is much smaller than the mole fraction of its component in the solid phase. We take into account that each component has a different diffusion coefficient from those of the other components in the liquid solution. We neglect moving boundary conditions, e.g., the movement of the position where a solid grows.

Ref. 2 is inquired about many times from the world. This reference dealt with an ideal case without fluid flow. This presentation reviews it first. This is the simplest model, but includes the common phenomenon (Fig. 1) in many fields such as crystal growth, phase-field model, fluid dynamics, chemical engineering, mechanical engineering, electromagnetism, etc. Next, the results without fluid flow are applied to the cases with fluid flow. We will know the mechanism to understand the main effect of fluid flow on solution growth.

2. An ideal case without fluid flow [2]

This section deals with the case without fluid flow. The size of liquid solution is sufficiently larger than the boundary layer thicknesses of solute mole fractions. One reason why we select this simplest case is that we have already known the analytic solutions for the model. The basic equations are the diffusion equations of solutes in the liquid solution. They are similar to the equation of heat conduction in the thermal engineering. We utilize the results in this field.

We deal with a ternary system. XL, XM : the mole fractions of component L, M in the liquid phase, respectively. YL, YM : the mole fractions of component L, M in the solid phase, respectively. XLb, XMb : XL, XM just before growth, respectively. DL, DM : the diffusion coefficient for component L, M in the liquid solution, respectively. $DL > DM$. The z-axis is defined to be in the direction perpendicular to the growth interface. The origin is defined to be on the growth interface. $XL(z, t)$, $XM(z, t)$: XL and XM at z and t, respectively. pL, pM : $\partial XL / z$, $\partial XM / z$ at the growth interface, respectively. r denotes the ratio of volume per unit atom in the liquid to that in the solid. Mass transfer through the growth interface is as follows:

$$DM (pM) / DL / pL = [r (YM) - XM(0, t)] / [r (YL) - XL(0, t)]. \quad (1)$$

When we numerically solve the diffusion equations for the mole fractions of solutes, we use the finite difference method. ΔzdL and ΔzdM : the mesh sizes in the z direction to solve the diffusion equations for component L and M, respectively. The above derivatives are approximated as follows:

$$pL \approx (XL(\Delta zdL, t) - XL(0, t)) / \Delta zdL, \quad (2)$$

$$pM \approx (XM(\Delta zdM, t) - XM(0, t)) / \Delta zdM. \quad (3)$$

We approximate Eq. 1 as follows:

$$(DM / DL) (XM(\Delta zdM, t) - XM(0, t)) (\Delta zdL) / \Delta zdM / (XL(\Delta zdL, t) - XL(0, t)) \approx [r (YM) - XM(0, t)] / [r (YL) - XL(0, t)]. \quad (4)$$

The mole fractions vary abruptly at the growth interface (Fig. 1). The finite difference method cannot express it. We derive the condition at $t \rightarrow +0$, that is, initial condition. If we could obtain the limit of Eq. 4 when $\Delta zdL \rightarrow 0$ and $\Delta zdM \rightarrow 0$, we obtained the initial condition. In Eq. 4, we previously made the mistake that $\Delta zdL / \Delta zdM$ was set to one. If we consider only Eq. 4 and do not consider the physical background, we have to make ΔzdL approach zero independently of ΔzdM, and it makes the limit of $\Delta zdL / \Delta zdM$ indeterminate. That is, we cannot calculate initial mole fractions from Eq. 4. Then, we use analytic solutions of derivatives as follows:

$$pL = (XLb - XL(0, t)) / \mathrm{sqrt}(\pi (DL) t), \quad (5)$$

$$pM = (XMb - XM(0, t)) / \mathrm{sqrt}(\pi (DM) t). \quad (6)$$

Here, sqrt denotes square root function. We derive the following initial condition by substituting Eqs. 5, 6 for the derivatives in Eq. 1. $XL0$, $XM0$, $YL0$ and $YM0$, respectively, denote the mole fractions of component L, M in the liquid phase and component L, M in the solid phase on the growth interface when the growth just started.

$$\mathrm{sqrt}(DM / DL) (XMb - XM0) / (XLb - XL0) = [r (YM) - XM0] / [r (YL) - XL0]. \quad (7)$$

The physical meaning of this derivation is based on that the boundary layer thickness develops with time so that it is proportional to sqrt((diffusion coefficient) (growth time)). We can calculate mole fractions in the solid phase using the initial condition for short growth times because mole fractions are constant on the growth interface. We do not need any more calculations for this ideal case.

In the calculation only with the above initial condition, the mole fractions except for the growth interface are not numerically calculated in the liquid solution. We establish a numerical calculation method in this internal region to apply it to the cases with the fluid flow. The mole fractions are calculated with the finite difference method. We consider the basic equation of mass transfer through the growth interface. In this equation, the largest computational errors are generated at the derivatives. These errors decrease with time because the abrupt spatial profiles of mole fractions moderate (Fig. 1). We calculate these derivatives so that the relative discretization error of these derivatives is within the tolerance of these derivatives from a certain growth time. c : this certain growth time. $e1$: this relative error. $o1$: this tolerance. We estimate the discretization error using the analytic solution of mole fractions in the liquid phase. The tolerance of these derivatives is derived from the tolerance of mole fractions in the solid phase using Eq. 1. As a result, we obtain the following conditions for the mesh size.

$$e1 = 1 - \mathrm{sqrt}(\pi (\kappa)) \mathrm{erf}(0.5 / \mathrm{sqrt}(\kappa)) < o1,$$

$$\Delta zdM = \mathrm{sqrt}((DM) c / \kappa).$$

Here, κ denotes a dimensionless parameter characterizing the mesh size. We verify this method using the mole fractions obtained the initial condition because mole fractions are constant on the growth interface for short growth times. We confirm that the relative errors of the mole fractions obtained numerically are within the tolerance after the growth time c.

3. Cases with fluid flow [3-7]

This section deals with fluid flow in the liquid solution. The top of the liquid solution is flat. The slip condition is applied at this boundary. At the other boundaries, the no-slip condition is applied. It is assumed that the velocity perpendicular to the boundaries is zero. The basic equations of fluid flow are the conservation of mass and the conservation of momentum. We deal with the case where the fluid flow is independent of situation on mole fractions of solutes. The velocity of fluid flow is computed with computational fluid dynamics.

The boundary condition at the growth interface is the mass transfer and phase diagram. This condition is implicitly solved with the method derived in the case without the fluid flow.

The convection-diffusion equations of solute are explicitly solved with the finite difference method.

A one-dimensional (1-D) model takes into account only the fluid flow parallel to the growth interface. The fluid flow transports the liquid solution retaining the initial supersaturated state to the boundary layers of solute mole fractions. We can understand the most main effect of the fluid flow on the growth. The fluid flow enhances the growth. The mole fraction of solute that has the largest diffusion coefficient increases most largely because its boundary layer thickness is largest. Then, the mole fraction of this solute increases on the growth interface. The equilibrium state varies on the growth interface. That is, segregation varies. The fluid flow makes the lager boundary layer thickness of a solute approach the less boundary layer thickness of another solute. Namely, the fluid flow makes the phenomena independent of the properties of materials.

Two-dimensional (2-D) model takes into account the velocity of fluid flow perpendicular to the growth interface. When the liquid solution flows from the growth interface to the internal region of liquid solution, the fluid flow transports a dilute liquid solution whose solutes are consumed by the growth to the boundary layers of solute mole fractions. This fluid flow inhibits the growth. This case is opposite to the case of the above 1-D model. The mole fraction of solute that has the largest diffusion coefficient decreases most largely. This effect propagates to the growth interface. Then, on the growth interface, the mole fraction of this solute decreases. Segregation varies in the direction opposite to the above 1-D model. If we did not know this mechan-

ism, we may think the calculation failed because we think fluid flow always enhances the growth from the conventional knowledge. This presentation names a model full-2-D model. In this model, segregation is calculated over the entire growth interface. As an approximation of the full-2-D model, this presentation defines a quasi-2-D model. In the quasi-2-D model, segregation is calculated only at the center of growth interface; and the values at the center are substituted for the values at the other points on the growth interface. At the center, the time dependencies of mole fractions in the quasi-2-D model are similar to those in the full-2-D model. The variations with time in the full-2-D model are larger than those in the quasi-2-D model. Some characteristic properties in the quasi-2-D model deviates from those in the full-2-D model. The quasi-2-D model saves the computational time when the phase diagram has not been calculated yet. The full-2-D model can show the spatial variation of segregation. We find when a vortex exists in the liquid solution, the mode of effect on the growth varies from enhancement to inhibition at the place where the vortex contacts with the growth interface. We have to more carefully deal with mean values such as mean velocity in turbulence model, compared with other fields such as thermal engineering.

References

[1] H. Susawa, Proc. 7th Int. Workshop Model. Crtst. Growth, Dep. Chem. Eng., Natl. Taiwan Univ., (2011) 39-40.
[2] H. Susawa *et al*., Initial Condition and Calculation Method for the Numerical Simulation of LPE, J. Chem. Eng. Jpn. 40 (2007) 928-938.
[3] H. Susawa *et al*., Theor. Appl. Mech. Jpn. 55 (2006) 279-284.
[4] H. Susawa *et al*., DOI: "http://dx.doi.org/10.2197/ipsjdc.3.114".
[5] H. Susawa, 16th Int. Conf. Cryst. Growth (2010) Sess.: 01.Fundam. Cryst. Growth, Aug. 11.
[6] H. Susawa, Leibniz Inst. Cryst. Growth (IKZ), abstract book 5th Int. Workshop Cryst. Growth Technol., Berlin, (2011) 61-62.
[7] H. Susawa, Proc. 7th Int. Workshop Model. Cyst. Growth, Dep. Chem. Eng., Natl. Taiwan Univ., (2011) 103-104.

11:05 Oral

A model for impurities segregation in crystallization

Fengkai Ma, Lihe Zheng, Liangbi Su, Xiaodong Xu, Huili Tang, Jingya Wang, Jun Xu

Shanghai Institute of Ceramics, Chinese Academy of Sciences, 1295 Dingxi Road, Shanghai 200050, China

e-mail: hkai80@gmail.com

A model of impurity distribution based on tolerance degree of crystals was performed, expressions of cases like one kind of ions on one certain kind of lattice sites, one kind of species on more than one kind of sites and two or more kinds of ions on one kind of sites were delivered in premise of no crystal structural change and keeping high quality of crystal, no matter what growth conditions were. It also provides a method of improving concentrations of needed doping ions in crystals. Accordingly we have calculated maximum concentration of Ti^{3+} in sapphire to be $1.75\times10^{19}/cm^3$, in right trends of magnitudes with experiment data.

11:20 Oral

Role of impurity on oscillatory growth of crystals

Hitoshi Miura[1], Katsuo Tsukamoto[2]

1. *Nagoya City University, Aichi 4678501, Japan* **2.** *Tohoku University, Sendai, Japan*

e-mail: miurah@m.tohoku.ac.jp

Crystals characterized by oscillatory zoning show a quasi-cyclic alternation in the chemical composition in the growth direction, from a few tens of nanometers to several tens of micrometers in thickness. Such mineral zoning is a common phenomenon in magmatic rocks, hydrothermally altered rocks, mineralized rocks, and carbonate sequences [1]. Oscillatory zoning may originate from an intrinsic mechanism —complex diffusion-attachment processes at the solution-crystal interface— even under stable growth conditions. An important factor that affects the crystal growth kinetics is impurity, which is known to inhibit crystal growth. Pinning is a well-known effect of impurities on the kinetics of crystal growth in solution [2-4]. The pinning mechanism has been discussed successfully for various crystallizing systems with different impurities. However, the role of impurities on oscillatory growth has not been modeled on a physical basis to date.

We consider the adsorption and desorption of the impurities on the growing crystal surface along with the pinning mechanism. If the steps barely pass beyond a certain area on the crystal surface, the adsorption and desorption of impurities reach an equilibrium state (Langmuir isotherm). In contrast, repeated passage of steps shortens the exposure time of adsorption sites for impurities, and this tends to decrease the density of the adsorbed impurities [5]. Assuming for simplicity that once the step has passed beyond this area, the impurities adsorb in the crystal and do not seriously obstruct the advance of subsequent steps [2]. Frequent step passages will result in less impurities at the surface, as if the crystal surface is swept by the advancing steps. Because of impurity sweeping coupled with pinning, there is a potential feedback on the change in the step velocity through the change in the impurity density. The feedback loop causes periodic oscillation of the step velocity.

We formulated these two mechanisms, pinning mechanism and impurity sweeping, as relations between the adsorbed impurity density θ and the step velocity V. We found steady solutions that satisfy both of two relations simultaneously when the supersaturation at interface σ is larger than a critical value (see Fig. 1). The steady solution is unique when σ is large enough. There are, however, two different steady solutions for intermediate σ. One of the solutions suggests a steady growth with large step velocity under less effect of impurity. Another is an unstable solution that would not appear in actual systems. The multiple-valued feature may result in oscillatory behavior as suggested previously [6-8].

The nature of the oscillatory growth in this system is as follows. We assume that the system is at point A in Fig. 1 at the beginning. As the crystal grows, s decreases because of solute depletion in the solution, resulting in a decrease in V along the solid curve. If solute transportation is inefficient, σ and V continue to decrease, and finally, V jumps from point B to point C because of the positive feedback between the decrease in V and the increase in θ. At point C, the impurity adsorption reaches equilibrium, and step advancement does not occur because of the pinning mechanism. The suppression of crystal growth leads to an increase in σ by solute transportation. At point D, step advancement resumes, and then, the system jumps to point A because of the positive feedback between the increase in V and the decrease in θ, completing one cycle.

Refs. [1] Shore & Fowler 1996, Can. Miner. 34, 1111-1126. [2] Cabrera & Vermilyea 1958, in Growth and Perfection of Crystals, Proceedings, pp. 393-410. [3] Burton et al. 1951, Phil. Trans. Roy. Soc. London, 243, pp. 299-358. [4] Kubota & Mullin 1995, JCG 152, 203-208. [5] van Driessche et al. 2009, Crys. Growth Des. 9, 3062-3071. [6] Haase et al. 1980, Science 209, 272-274. [7] Ortoleva 1990, Earth Sci. Rev. 29, 3-8. [8] Kalischewski et al. 2007, Phys. Rev. E 75, 021601.

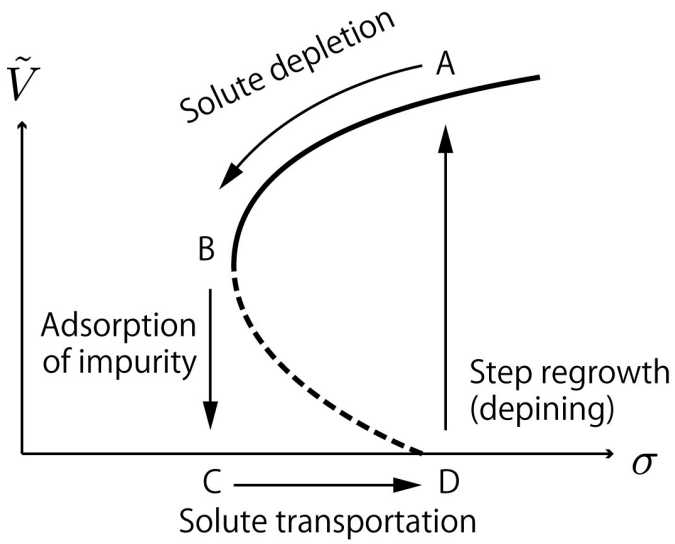

Fig. 1: Steady solution that satisfies both of two relationships: pinning mechanism and impurity sweeping by step advancement. The horizontal axis is the supersaturation at crystal-liquid interface and the vertical one is the normalized step velocity.

11:35 Oral

Effect of magnesium ions on the structure of amorphous calcium carbonate

Hidekazu Tomono, Hiroki Nada

National Institute of Advanced Industrial Science and Technology (AIST), Tsukuba 305-8569, Japan

e-mail: hiroki.nada@aist.go.jp

The nucleation of$CaCO_3$ crystals has been an important research subject in the field of crystal growth, physics, chemistry, mineralogy and biomineralization from long ago. Especially, the effect of Mg^{2+} ions on the nucleation of $CaCO_3$crystals has attracted great interest, because Mg^{2+} ions affect $CaCO_3$ polymorphism [1]. That is, normally, the nucleation of vaterite or calcite occurs. However, the nucleation of other polymorphs, such as aragonite and monohydrocalcite, occurs if Mg^{2+} ions exist. The cause of the polymorphism in the presence of Mg^{2+} ions still remains unclear.

Recently, several experimental studies have reported amorphous $CaCO_3$ (ACC) precursors formed in solution, and the nucleation of $CaCO_3$ crystals from the precursors [2]. It has been proposed that the structure of ACC precursors may determine which $CaCO_3$ crystal structure is formed preferentially. Hence, the changes in the atomic-scale structure ib ACC precursors by adding Mg^{2+} ions is particularly relevant to $CaCO_3$ polymorphism in the presence of Mg^{2+} ions.

In this study, molecular dynamics simulations were conducted to elucidate the effect of Mg^{2+} ions on the structure of ACC [3]. Simulation results indicated that although ACC did not have a long-range ordered structure, it did have a weakly ordered local structure resembling the local structure of a $CaCO_3$ crystal. The local structure of pure ACC resembled that of vaterite. However, the formation of the vaterite-like local structure was hindered by Mg^{2+} ions. Moreover, when the fraction of water molecules in ACC was high, the formation of a monohydrocalcite-like local structure was promoted by Mg^{2+} ions.

The effects of Mg^{2+} ions on the structure of ACC were verified using the size of Mg^{2+} ions, and the interaction among Mg^{2+} ions, H_2O and $CaCO_3$. The simulated structure of ACC obtained in the simulation was compared with the structure of $CaCO_3$ crystals nucleated from ACC precursors in real systems. At the presentation, we will discuss the role of Mg^{2+} ions in $CaCO_3$ polymorphism.

References

[1] E. Loste, R. M. Wilson, R. Seshadri, and F. C. Meldrum, J. Cryst. Growth 254 (2003) 206.

[2] E. M. Pouget, P. H. H. Bomans, J. A. C. M. Goos, P. M. Frederik, G. de With, and N. A. J. M. Sommerdijk, Science 323(2009) 1455.

[3] H. Tomono, H. Nada, F. Zhu, T. Sakamoto, T. Nishimura, and T. Kato, to be published.

11:50 Oral

The effect of boron concentration on facet formation in in-situ doping silicon selective epitaxial growth

Wonseok Yoo

SAMSUNG ELECTRONICS CO. LTD., Hwasung 445-701, Korea, South

e-mail: wonseok.yoo@samsung.com

The effect of boron concentration on sidewall facet formation at SiO_2/Si interface during in-situ doping silicon selective epitaxial growth was investigated using a standard production Chemical Vapor Doposition(CVD) reactor. Cross sectional SEM analysis revealed that films grown through oxide contacts with (110) sidewall orientations exhibit not any facets in case of high boron concentration($>1e^{20}/cm^3$), but typically (111) facets are well defined at low boron concentration($<1e^{19}/cm^3$). In order to find the cristical limits of process conditions degrading crystalline quality, B_2H_6 gas flow rate, HCl gas flow rate and temperature were varied. Consequently degradation of crystalline quality must be because of boron dopants which impede the growth of the epitaxial layer and facilitate the formation of extended defects.

12:05 Oral

Combined-Convection Segregation Coefficient and Diffusion Coefficients of Impurities in Si Melt

Aleksandar G. Ostrogorsky

Illinois Institute of Technology, 10 West 33rd Street, Chicago, Il 60616, United States

e-mail: AOstrogo@IIT.edu

In the Burton, Prim and Slichter's BPS formula, the effective segregation coefficient k_{eff} is a function the stagnant film thickness δ. During the past decades, the shortcomings of the BPS model have been recognized and several new models film-thickness based models have been proposed.

The film-thickness models are revisited. A new effective segregation coefficient, were Nusselt numbers are used to quantify convection, is presented. This combined-convection coefficient is presented in dimensionless form, k_{CC} (Nu_{FC} , Nu_{NC} , Pe), where Nu_{FC} and Nu_{NC} are Nusselt numbers for forced and natural convection and Pe is Peclet number for convection due to freezing. In contrast to BPS, the "combined-convection" segregation coefficient k_{CC} accounts for both forced and buoyancy-induced convection. The proposed segregation coefficient is used to recalculate the diffusivity values of impurities in Si. The presently accepted values have been calculated using the BPS formula (which ignores buoyancy-induced convection), and thus are inflated.

Lunch (IOCG Exec. Com. meeting)

Tuesday afternoon, 13 August, 12:20

TuO2

G01:Fundamentals and Modeling
Tuesday afternoon, 13 August, 14:00
Hall 16, Old Library

14:00 Invited oral

The role of liquid ordering in solution growth

Elias Vlieg

Radboud University Nijmegen, Heyendaalseweg 135, Nijmegen 6525AJ, Netherlands

e-mail: e.vlieg@science.ru.nl

When growing a crystal from solution, the role of the solvent can be more than just a transport medium. It is well-known that the habit of a crystal can be very different for different solvents; for example NaCl crystals have {100} facets when growing from aqueous solution, but have {111} facets in water-formamide solutions. Another case is formed by protein crystals that are only stable when they contain large inclusions of (disordered) water. In order to unravel the role of such solvents at the molecular/atomic level, we have used X-ray diffraction (using synchrotron radiation sources) to determine the structure of various crystal-solution interfaces and in particular the ordering properties of the solution in contact with the crystal surface. We find that typically three layers are quite strongly ordered perpendicular to the surface ('layering') and that the first layer often shows significant lateral ordering as well.

A few examples will be discussed. When growing InP nanowires using the so-called vapour-solid-liquid (VLS) method, often the wurzite crystallographic structure is formed instead of the zinc-blende that is the most stable structure in the bulk. We found that the position of the solution atoms hampers the zinc-blende growth and thus provides a possible explanation for this [1]. At the interface of liquid In with Si(111), the In is found to have a higher density than in the bulk liquid, which seems to be caused by the mismatch between the surface lattice and the size of the In atoms [2]. In the case of wet chemical etching ('negative growth') of Si(111) in alkaline solutions, the solution provides not only the reactants but also the H-atoms to keep the surface stable. The H-terminated, hydrophobic surface leads to only weak ordering of the liquid.

[1] R.E. Algra et al., Nano Lett. 11 (2011) 1259.

[2] V. Vonk et al., unpublished.

[3] I.A. Shah et al., Surf. Sci. 605 (2011) 1027.

14:30 Oral

Thermodynamic stabilities of two types of quasi-liquid layers on basal faces of ice crystals

Harutoshi Asakawa, Gen Sazaki, Ken Nagashima, Shunichi Nakatubo, Yoshinori Furukawa

e-mail: h.asakawa@lowtem.hokudai.ac.jp

Recently, we have succeeded in the directly observing 0.37-nm-thick elementary steps and their dynamic behavior on ice crystal surfaces[1], by laser confocal microscopy combined with differential interference contrast microscopy (LCM-DIM) [2]. By LCM-DIM, we found that two types of quasai-liquid layer (QLL) phases, which respectively exhibit a liquid-drop shape (α-QLLs) and a thin-layer shape (β-QLLs), appear on basal faces of ice crystals just below the melting temperature (0°C)[3]. The different morphologies of α- and β-QLLs strongly suggest that α- and β-QLLs have different structures. In this study, to reveal the differences in α- and β-QLLs, we examined thermodynamic stabilities of α- and β-QLLs.

Sample ice crystals for the observation and other ice crystals for the supply of water vapor were prepared in an air-tight observation chamber. The temperatures of the sample and source ice crystals were controlled separately. The temperature of the sample ice determined the growth temperature T_{sample} of the sample ice and water vapor pressure P_e formed by the evaporation of the sample ice. The temperature of the source ice, whose volume was significantly larger than that of the sample ice, controlled water vapor pressure P_{H2O} inside the observation chamber.

We directly observed the lateral growth of elementary steps on basal faces, and then determined equilibrium ice-vapor pressure at which step velocity became zero. Plots of $V_{step} = 0$ (open circles) in Fig.1 represent the results. We also measured the temporal changes in the sizes of α- and β-QLLs, and then determined the critical water vapor pressures of α- and β-QLLs at which their size remained constant. Plots of α- and β-QLLs (open squares and rhombus) in Fig.1 respectively summarized the results. As shown in Fig.1, the critical pressures of both QLLs are significantly higher than the equilibrium pressure between ice and vapor. This result clearly demonstrates that both QLLs are thermodynamically less stable than solid ice. Hence, we concluded that the appearances of both QLLs are due to the condensation of supersaturated water molecules on basal faces rather than the melt of most stable ice crystals. The picture of QLLs obtained in this study is quite different from the long-standing conventional picture in which a QLL phase has been considered as a thermodynamically stable phase[4].

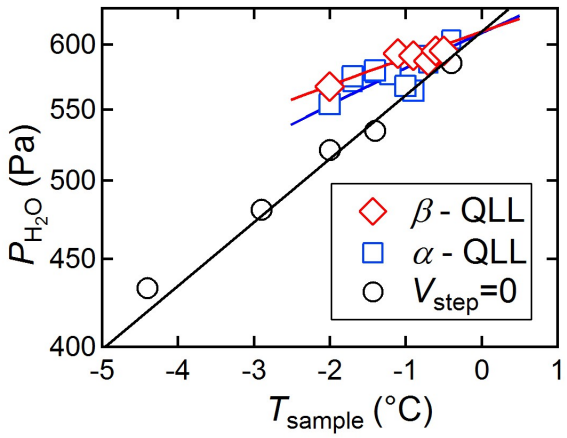

Fig. 1. Apparent phase diagram of α- and β-QLLs.

Reference

1. Sazaki, G. *etal*., *Proc. Natl. Acad. Sci. USA***2010**, 107, 19702-19707.

2. Sazaki, G. *etal*., *J.Cryst.Growth.***2004**, 262, 536-542.

3. Sazaki, G. *etal*., *Proc. Natl. Acad. Sci. USA***2012**, 109, 1052-1055.

4. Kuroda, T. & Lacmann, R. *J. CrystGrowth*, **1982**, 56 189-205.

14:45 Oral

Crystal nucleation kinetics of polyethylene on active centers

Zdeněk Kožíšek, Pavel Demo, Alexey Sveshnikov

Institute of Physics AS CR, Cukrovarnická 10, Prague CZ-16200, Czech Republic

e-mail: kozisek@fzu.cz

Nucleation agent was added to the supercooled polymer melt to increase the number of formed folded chain polyethylene crystalline nuclei. Kinetic model of nucleation on active centers is modified to include exhaustion of the active centers via modified boundary condition in contrast to the standard Avrami model, where addition equation describing such a process is needed [1, 2].

The basic characteristics of nucleation process (the size distribution of nuclei, the total number of nuclei, and nucleation rate) were determined by numerical solution of kinetic equations and compared with measured data. It seems that the total number of nuclei, Z_i, greater than some detectable size i increases after some time delay linearly with time. However nucleation rate, $J_i = dZ_i/dt$, after reaching some maximum, which is lower than stationary nucleation rate J^S, decreases with time and as a consequence Z_i is not linear in time (Fig. 1). It is caused by exhaustion of active centers during phase transition.

This work was supported by the Czech Science Foundation (Grant No. P108/12/0891).

[1] Z. Kožíšek, M. Hikosaka, K. Okada, and P. Demo, J. Chem. Phys. 134, 114904 (2011).

[2] Z. Kožíšek, M. Hikosaka, K. Okada, and P. Demo, J. Chem. Phys. 136, 164506 (2012).

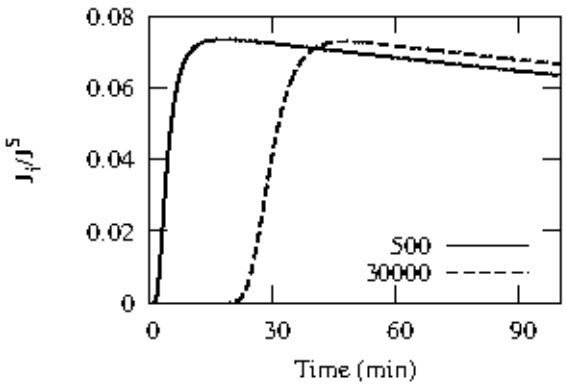

Fig. 1. Dimensionless nucleation rate, J_i/J^S, for nucleus size i = 500 (full line) and 30000 (dashed line) as a function of time.

15:00 Oral

The Effect of the Shear Flow on Particle Growth in the Undercooled Melt

Mingwen Chen, Xiaojian Ji, Yahong Zheng, Ping Qian, Zidong Wang

University of Science and Technology Beijing, Lihua Building 214, Xueyuan Rd 30, haidian district, Beijing, Beijing 100083, China

e-mail: chenmw@ustb.edu.cn

Convection effects are of fundamental importance in controlling pattern formation of interface microstructures. A great number of experimental and simulation works have shown the effect of solute convection, external forced flows on interface microstructures[1-3]. The external forced flow imposed in the undercooled melt will strongly change the solidification dynamics and then pattern formation of interface microstructures. The upstream flow imposed on the growing crystal enhances the growth velocity of the interface growing in the opposite direction to the flow[4]. The uniform streaming flow results in higher local growth rate near the surface where the flow is incoming[5]. Due to the melt convection, the crystal directly nucleates from the convective undercooled melt and grows up to a large scale[6]. In the uniform streaming flow, an initially spherical particle evolve into a peach-like shape[7]. Lan *et al.*[8,9] experimentally and numerically investigated the convective effects driven by accelerated crucible rotation on the segregation, interface shape, and morphological instability during crystal growth. Jung *et al.*[10] investigated the effect of an external time-dependent flow to simulate the industrial Czochralski process for growing silicon crystals. In recent years, these phase selection and grain refinement have been investigated for the perspective of applications. It has provided strong motivation for the direct calculation of interface morphologies and evolution of particle growth. In the paper, we study the effect of the shear flow on particle growth in the undercooled melt[11]. When a flow is exerted on the melt, the fully coupled problem of the heat transfer and the fluid flow is hard to solve with numerical and analytical approaches accurately. However, the fluid velocity near the particle can be decomposed into the superposition of the uniform streaming flow and the linear flow. By using the multi-variable expansion method, we find the asymptotic solution temperature field and shape of the particle in the fully coupled problem. With the analytical solution, we show the temperature field, interface evolution and growth of the particle. We calculate the interface shape of iron particles in Cu-Fe alloys in convective solidification, and the result shows that the shear flow significantly deforms the interface of the particle. Due to the competition between the shear flow effect and the anisotropy effect of surface tension, the particle rapidly splits into more fine particles and refines the interface microstructure. The result is in good agreement with the experimental results.

References

[1] D. Medvedev, T. Fischaleck, K. Kassner, Journal of Crystal Growth **303**, 69(2007).

[2] C. W. Lan, M. H. Lee, M. H. Chuang, C. J. Shih, Journal of Crystal Growth **295**, 202(2006).

[3] M. Asta, C. Beckermann, A. Karma, W. Kurz, R. Napolitano, M. Plapp, G. Purdy, M. Rappaz, R. Trivedi, Acta Materialia **57** 941(2009).

[4] P. K. Galenko, O. Funke, J. Wang, D. M. Herlach, Materials Science and Engineering A **375–377**, 488(2004).

[5] D. S. Noh, Y. Koh, I. S. Kang, Journal of Crystal Growth, **183**, 427 (1998).

[6] T. Li, X. Lin, W. D. Huang, Acta Materialia **54**, 4815(2006).

[7] M. W. Chen, Y. L. Wang, H. Zhang, L. Y. Wu and Z. D. Wang, Journal of Applied Physics **109**, 103517 (2011).

[8] Y. C. Liu, B. Roux, C. W. Lan, Journal of Crystal Growth **304**, 236 (2007).

[9] L. C. Wang, Y. C. Liu, W. C. Yu, B. Roux, T. P. Lyubimova, C. W. Lan, Journal of Crystal Growth **311**, 684(2009).

[10] T. Jung, J. Seebeck, J. Friedrich, Journal of Crystal Growth **368**, 72(2013).

[11] Z. D. Wang, X. W. Wang, Q. S. Wang, I. Shih, J. J. Xu, Nanotechnology **20**, 075605(2009).

15:15 Oral

Degenerate dendrtite - between order and chaos

Andrey G. Borisov

Physico-Technological Institute of Metals and Alloys (PTIMA), Vernadskogo av. 34, Kiev 03680, Ukraine

e-mail: wwwrogneda@ukr.net

In experiments connected with the study of rheocasting methods for Al-Si alloy (A356) besides "classic dendrites" (Fig. 1a) were fined morphologies demonstrating more or less splitting of structure elements (Fig. 1 b – d).

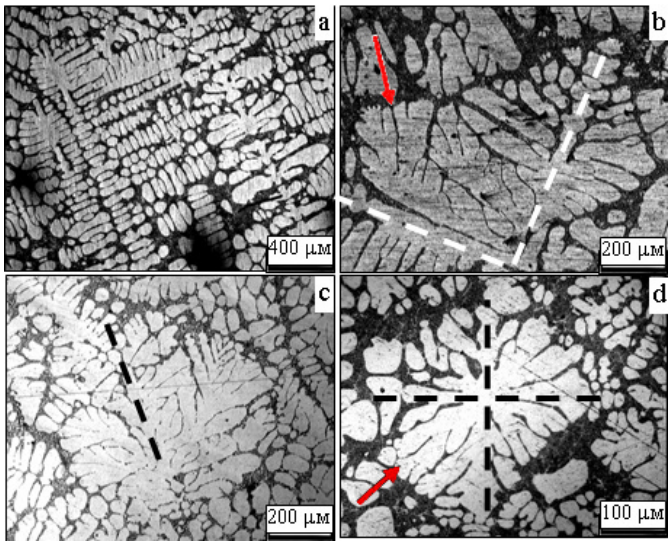

Fig.1. a) – classic dendrite, b) - d) – splitting patterns. Dashed lines marks "dendrite stems". Arrows on b) and d) indicate splitting elements for comparison with Fig. 6 d), h)

Such structure retains some "dendrite features", therefore we entitled them as degenerate dendrites. Possible reasons for its appearance are discussed further.

It is known that regular dendrites forms spontaneously by growth in preferential direction (<100> for cubic symmetry), that reflects crystallographic anisotropy. For growth in other directions anisotropy had be "overcome" due to some circumstances. It seems that such circumstances can be reduction of anisotropy, transition processes and forced conditions.

Reduction of anisotropy

Formation of splitting patterns in absence of anisotropy was demonstrated widely in numerical modeling. As concerns Al-based alloy [1] declare the possibility of splitting pattern formation in consequence of alteration of preferential growth direction due to increase of Zn content for Al-Zn alloy. For verification such ability for Al-Si alloy, the experiments on crystal growth in concentration gradient were performed. Complex cylindrical sample from two parts – pure Al and Al-Si eutectic was fabricated. Sample in crucible was melted fully and then directional crystallization took place, so Al dendrites grow in eutectic region, Fig. 2.

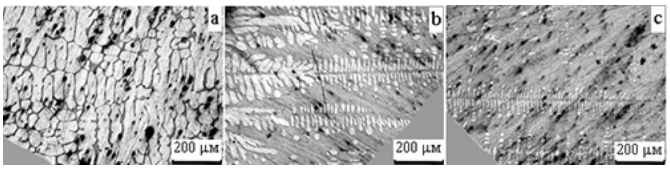

Fig. 2. Al dendrites grow in eutectic region. a) – Al region, b) – transitory region, c) – eutectic region

As it can be seen from the figure, dendrites continuously grow through the whole sample, and no changes of preferential growth direction or splitting were observed.

Transition processes

Relatively transition processes it must be noted that in real casting growing crystal is surrounded with neighboring, so transition processes from one stationary growth state to another can be not completed and structure of casting will fix just transition stage. Concerning possibility of splitting morphology formation as the result of such processes, we take into account two moments.

At first, in [2] appearance of non-dendrite splitting patterns associates with two stage crystallization – formation of dendrites, which partially melted, and final structure is the result of loss of stability and further growth of fragments of different shares. To verify this hypothesis experiments with partial melting and further growth of camphene-10 wt.% salol alloy were carried out, Fig. 3

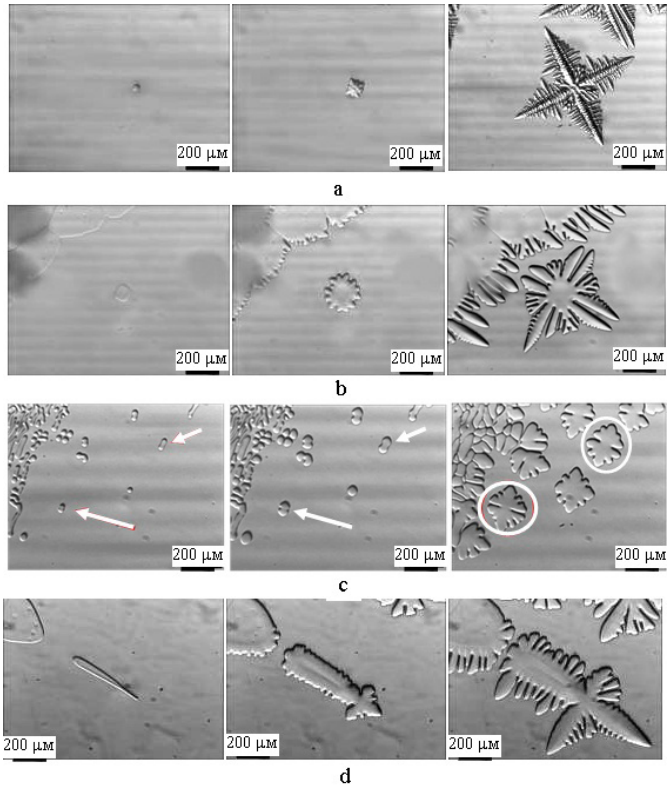

Fig. 3 Consequence stages of the growth of fragments. Row a) – seed crystal less than critical size, row b) – rounded seed crystal a little more than critical size. See the duplex dendrite structure. Row c) – small elongated seed crystal. See dumbbell-like structure. Row d) – large elongated seed crystal

During the melting of initial dendrite different types of fragments were formed. Depending on shape and size of fragments further growth formed different but regular dendrite structures.

At second, one of the possible reason for formation of irregular splitting morphology can be deceleration of the growth. Background for such suggestion are results of Trivedi [3]. It was pointed out that at least for directional solidification abrupt reduction of growth rate resulted in transient process accompanied with splitting of the pattern, see Fig 4 b), c).

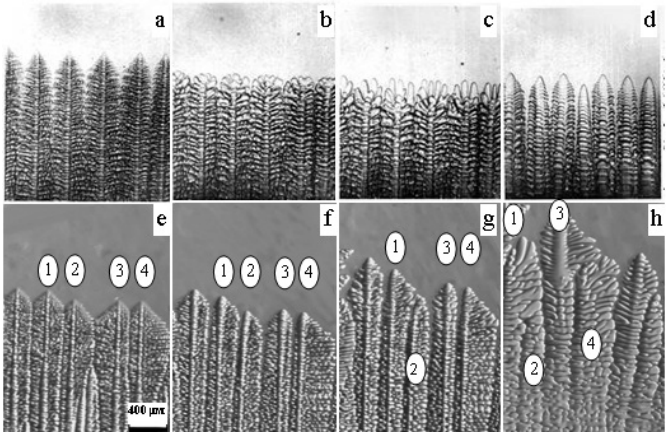

Fig. 4 Changes of growth morphology due to reduction of growth rate. a) – d) – data from [1]. Directional solidification of SCN-based alloy. e) – h) – reduction of supercooling from 2,2 ^{0}C to 0,6 ^{0}C. Camphene-based alloy.

We made experiments with reduction of growth rate by abrupt reduction of supercooling from 2,2 ^{0} C to 0,6 ^{0}C. As shown Fig. 4 e) – h), no splitting took place during transition. "Thickening" of dendrites took place by suppression of neighbors. Multiple dendrites are the result of large size of seed crystal, see Fig. 3 d).

Forced conditions

Relatively forced conditions, "constrains" crystal to grow in non preferential direction, growth of succinonitrile – 2 wt. acetone alloy was studied in thin gap (20 µm) between parallel glass slides as well as its directional solidification with different orientation of seed crystal relatively direction of thermal gradient.

As shown Fig. 5 c), d) as dendrite as splitting patterns can exist depending on orientation of seed crystal relatively plane of the slide. The last pattern looks like rather as result of percolation than crystal growth.

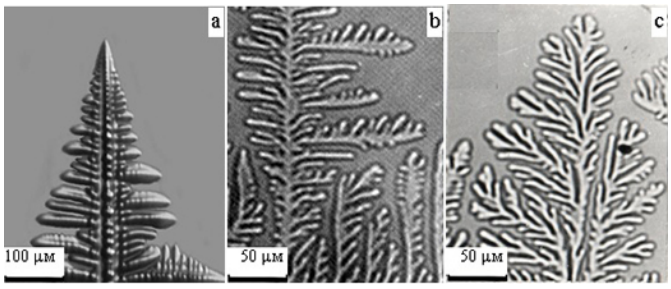

Fig. 5 Various morphologies. a) unconstrained dendrite growth, b) dendrite pattern in the gap, c) splitting pattern in the gap.

For growing of crystals in non preferential direction installation for directional solidification was used, that permits to rotate cuvette with seed crystal relatively direction of imposed thermal gradient, which was 40 ^{0}C/sm. It was found that for rate 6 µm/s, Fig. 6 e) – h), structure elements (dendrites) were growing in preferential direction <100> independently from orientation of seed crystal, while for rate 3 µm/s structure elements tilted to thermal gradient direction and formed splitting patterns similar to those for degenerate dendrites (compare marked with red arrows structures on Fig. 6 c), d) and Fig. 1 b), d)).

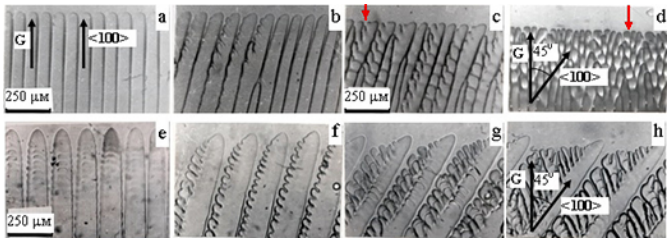

Fig. 6 Directional solidification. G – direction of thermal gradient. Angle between G and <100> direction is 0^0 for a), e) ; 15^0 for b), f); 30^0 for c), g) and 45^0 for d), h). Rate of growth is 3 µm/s for a) – d) and 6 µm/s for e) – h). Arrows on c) and d) indicates splitting element to compare with Fig. 1.

So analogy in morphologies put forward the question relatively analogy of "forced conditions" in both cases. Back to the rheocasting process (producing of degenerate dendrites) it must be noted that its essential feature is intensive shearing of the melt. Thereby it seems that flow incoming on solid-liquid interface generate some gradient. Due to this locally crystal is growing along this gradient (not in preferential direction) and some "directional solidification" take place.

References

1. Orientation selection in dendrite evolution / *T. Haxhimali, A. Karma, F. Gonzales, M. Rappaz* // Nature Materials.- **5**, 660-664 (9 July 2006) doi:10.1038/nmat1693 Article

2. *Flemings M. C., Yurko J.A., Martines R.A.* Semi-solid forming – our understanding today and its implications for improved processes // Symposium in Honor of Wilfred Kurz, Charlotte, NC, USA, March 14-18, 2004.- P. 3-14.

3. *Somboonsuk K., Trivedi R.* Dynamic studies of dendritic growth // Acta metallurgicaю- 1985.- Vol. 33.- № 6.- P. 1051-1060.

Break
Tuesday afternoon, 13 August, 15:30

Wednesday, 14 August

WeO1

G01:Fundamentals and Modeling
Wednesday morning, 14 August, 10:20
Hall 16, Old Library

10:20 Invited oral

Concave-corner-mediated self-organized crystal growth

Mu Wang

National Laboratory of Solid State Microstructures, Department of Physics, Nanjing University (NJU), Hankou Road 22#, Nanjing 210093, China

e-mail: muwang@nju.edu.cn

In lateral growth of a crystalline layer on a foreign substrate, by successive nucleation at the concave corner of crystal facet and substrate, consecutive rotation of crystallographic orientation of the crystalline layer can be observed. Such a consecutive rotation of crystallographic

orientation may lead to a number of effects, such as the spatial periodic faceting-roughening transitions and regular zigzag growth (Consecutive rotation of crystallographic orientation in lateral growth, Phys. Rev. Lett. 94, 125505 (2005); Fractal aggregations at low driving force with strong anisotropy, Phys. Rev. Lett. 80, 3089 (1998); Nucleation-mediated lateral growth on foreign substrate, J. Phys. Chem. C, 111, 1071-1075 (2007)). The physical origin of these effects is the imbalance of surface/interface tensions at the concave corner, which deforms the embryo of nucleus at the concave corner and changes the crystallographic orientation layer-by-layer. A theoretical model is provided, which predicts a criterion to observe such an effect in the nucleation-mediated lateral growth. The theoretical expectations are consistent with the experimental observations. The corner-mediated growth may also contribute to the unexpected pattern formation of hierarchical windmill structure of ZnO (Microscopic view of the role of repeated polytypism in self-organization of hierarchical nanostructures, Phys. Rev. B87, 085306 (2013)). This effect can be applied further to generate regular nanosized metallic wire arrays (Creating in-plane metallic-nanowire arrays by corner-mediated electrodeposition, Adv. Mater.,21, 3576 (2009)).

10:50 Oral

Characteristic IR radiation under crystallization, sublimation, and condensation (PeTa effect).

Vitali A. Tatartchenko

Shanghai CEC Zhenhua Crystal Technology Co., Ltd. (CECCG), Building 50, 1000 Zhangheng Road, Shanghai 201210, China

e-mail: vitali.tatartchenko@orange.fr

The paper presents a new physical phenomenon - infrared characteristic radiation under phase transitions of the first order: crystallization from melts as well as vapors deposition and condensation. In the paper [1] this phenomenon was named the Perel'man – Tatartchenko effect. Thus, to clarify a subject, in this paper and the later, the phenomenon will be titled the PeTa (Perel'man – Tatartchenko) effect. The PeTa effect was theoretically predicted by M. Perel'man [2, 3] and for the first time was experimentally investigated by V. Tatartchenko [4 – 6]. Here, the new theoretical results are analyzed as well as the experimental ones concerning crystallization from the melt of some substances and condensation of water vapor. A background of the PeTa effect is an assertion that, during phase transition from metastable higher energetic level (in a melt or in a vapor) to the main stable condensed lower level (in a crystal or in a liquid), the particle emits transient radiation. The radiation carries away the latent heat by characteristic frequencies photons generated under this transition. With respect to our model, the transient radiation results a "recombination" of the multi-pole and its virtual "mirror reflection" in medium. The estimated ratio of radiated energy of evaporation to the temperature boiling confirms and proves the empirical Trouton's rule applicable to many simple substances [7]. It allows an estimation of critical parameters interrelation for corresponding substances. It is postulated an appearance of transparency window for the characteristic radiation in the substances where first order phase transitions take place as well as a possibility of new effects in quantum electronics: amplification of certain frequency infrared beams in supersaturated vapors or super cooled melts. The radiation has to be taken into account during modeling of processes of crystallization and condensation. It is possible to imagine numeral applications of this phenomenon in different fields. For instance, new types of crystallization process regulation; crystallization stimulated by the characteristic radiation; an infra-red laser based on the condensation of water vapor, or crystallization of lithium fluoride or sapphire. Formation of hailstorm clouds in the atmosphere should be accompanied intensive characteristic infra-red radiation that could be detected for process characterization and meteorological warnings.

References:

1. Ravilious, K., 2010, 27 November. Cloud power. New Scientist, 38 – 41.

2. Perel'man M. E., 1971. Phase transitions caused by the opening of new channels in electron–photon interactions, Physics Letters A 37, 411- 412.

3. Perel'man, M.E., Tatartchenko,V.A., 2008. Phase transitions of the first kind as radiation processes. Physics Letters A 372, 2480–2483.

4. Tatarchenko, V.A., 1979. Appearance of distinguishing features in emission spectra during crystallization of substances transparent in the IR region. Soviet Physics - Crystallography 24, 238-239.

5. Tatarchenko, V.A., Umarov, L.M., 1980. Infrared radiation accompanying the crystallization of sapphire. Soviet Physics - Crystallography 25, 748-749.

6. Umarov L.M., Tatarchenko V.A., 1984. Differential spectra of crystallization radiation of alkali-metal halides, Soviet Physics - Crystallography 29, 670-673.

7. Trouton F.T., 1884, On Molecular Latent Heat, Phil. Mag. 18, 54 – 57.

11:05 Oral

Numerical design of induction heating in the PVT growth of SiC crystal

Juan Su, Xuejiang Chen, Li Yuan

School of Energy and Power Engineering, Xi'an Jiaotong University, Xi'an 710049, China

e-mail: xjchen@mail.xjtu.edu.cn

A wide application of SiC in high-power, high-temperature, high-frequency and strong-radiation electronics is determined by its excellent physical properties. Although physical vapor transport (PVT) method has been widely used to produce SiC bulk crystals since 1970s, several issues such as reducing thermal stress and increasing growth rate remain unsolved. In PVT method, radio frequency induction heating is adopted to generate enough required heat for crucible in order to obtain a proper temperature distribution inside the crucible for higher growth rate, lower thermal stresses and lower energy consumption, etc. So it is very important to study the effects of parameters of induction heating, such as coil position and electrical frequency, on thermal field inside crucible.

In this study, a 2-D numerical global model is applied to investigate effects of induction heating system on silicon carbide crystal growth. Firstly, the coupled equations for electromagnetic field, conductive and radiative heat transfer are solved by a finite element method (FEM) to predict electromagnetic and thermal field, in which induction heating, heat conduction and radiative heat exchange are taken into account. Then based on the thermal field, the growth rate is calculated by solving Hertz-Knudsen equation and one-dimensional mass transfer equation. Further, models with several different radial coil positions and models with different electrical frequency are carried out to investigate the relationship between coil design and temperature distribution while the temperature of monitoring point is fixed at 2300K. The predicted growth rate along the substrate surface for each model is also compared and discussed.

The results show that the temperature distribution inside the crucible and the growth rate are affected by the radial coil position and frequency. Finally, based on the analysis of simulation results, one reas-

onable range of radial coil position and frequency to make compromise between higher growth rate, lower electrical power consuming, more stable operation of SiC powder and lower thermal stresses in grown crystal is obtained.

11:20 Oral

Solidification of multicrystalline silicon - phase field studies of micro-structures

Wolfram Miller[1], Alexandra Popescu[2]

1. *Leibniz Institute for Crystal Growth (IKZ), Max-Born-Str 2, Berlin 12489, Germany* **2.** *West University of Timisoara (UVT), Bd.V. Parvan nr.4, Timisoara 300223, Romania*

e-mail: wolfram.miller@ikz-berlin.de

We investigated the solidification of two grains with a special focus on the processes at the three-phase junction of the two grains and melt by means of a 2D phase-field simulation. The development of the local morphology is driven by both the interface energies and the growth kinetics. Thus, the choice of anisotropies in interface energy and growth kinetics is of great importance [2].
The results are discussed in the context of experiments with in-situ measurements [3,4], previous phase-field studies [5] and a recently introduced classification of grain boundaries [6].
[1] W. Miller, A. Popescu, G. Cantù, J. Crystal Growth http://dx.doi.org/10.1016/j.jcrysgro.2013.01.044
[2] G. Cantù, A. Popescu, W. Miller, Acta Mater. 60 (2012), 6755
[3] K. Fujiwara, Y. Obinata, T. Ujihara, N. Usami, G. Sazaki, K. Nakajima, J. Cryst. Growth 266 (2004), 441
[4] Kozo Fujiwara, Int. J. Photoenergy (2012), 169829
[5] P. Chen, Y. L. Tsai, C. W. Lan, Acta Mater. 56 (2008) 4114–4122
[6] Thierry Duffar, Amal Nadri, Scripta Mater. 62 (2010), 955
A. Popescu acknowledges the support by the project POSDRU 88/1.5/S/49516
co-financed by the European Social Fund through the Sectorial Operational Programme for Human Resources Development 2007-2013.

11:35 Oral

Revealing structural and thermodynamic details of calcium carbonate crystallization intermediates through ab initio methods

Raffaella Demichelis, Paolo Raiteri, Julian D. Gale

Nanochemistry Research Institute, Department of Chemistry, Curtin University, PO Box U1987, Perth 6845, Australia

e-mail: raffaella.demichelis@curtin.edu.au

Calcium carbonates ($CaCO_3$) play a significant role in the biochemistry of our body and in the geochemistry of our environment, where they are mostly present as a result of biomineralisation. The nucleation and crystal growth processes that lead to the formation of the final crystalline polymorphs have been recently shown to follow pathways alternative to the classical nucleation theory.[1] This has raised the interest in characterising the intermediate phases that appear during the various steps of the process, with the aim of understanding the mechanism itself and the factors driving to the final polymorph differentiation.

Computer simulation has the potential of providing useful information in this field, because it allows for an highly accurate exploration of the atomic details and the inter-atomic interactions that are peculiar of a given structure and responsible for its stability. In this respect, *ab initio* techniques have the advantage of providing the most accurate and transferable models. In fact, they explicitly account for electrons and are independent of empirical parameters, so that once the system is defined all its properties can be calculated straightforward. On the other hand, it is often necessary to find a compromise between accuracy and computing resources, while making sure that the model is realistic.

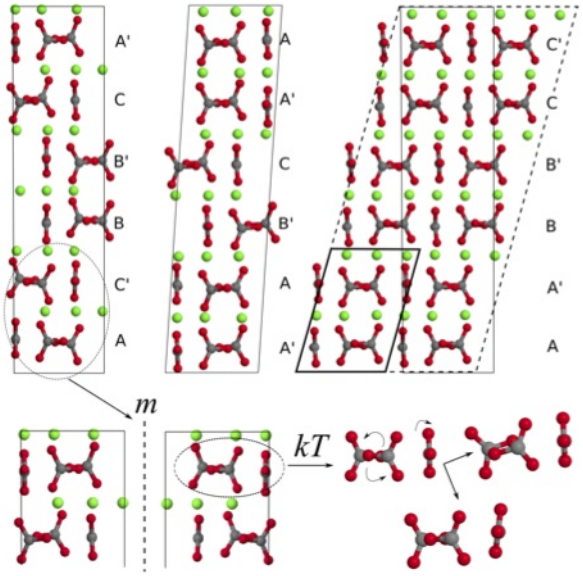

Figure 1: Graphical representation of three isoenergetic structures for vaterite. The different layer stacking sequence, the possible chirality and the rotational freedom of carbonate ions are shown (O, Ca and C atoms are coloured in red, green and grey, respectively).

Density Functional Theory (DFT) is arguably one of the most widely used method for the simulation of crystalline systems. It is implemented in most of the available solid state codes and usually allow to simulate realistic models with a reasonable amount of computing resources. The main disadvantage of DFT is that the exact formulation of the exchange-correlation term in the Hamiltonian is unknown, so that dispersion interactions are not properly accounted for. For this reason, approximations and corrections have to be introduced.[2]

Two recent studies that apply DFT to the investigation of the structural and thermodynamic properties of calcium carbonate hydrated and anhydrous phases will be presented, and success and failures will be discussed.

The former deals with the major advances that have been achieved through DFT methods in understanding the structure of vaterite.[3] Vaterite is a metastable $CaCO_3$ polymorph whose structure has puzzled scientists for more than half a century. A new model has been suggested, consisting of multiple structures, which establishes a link between the most recent models proposed in the literature.[3,4] The disorder of vaterite is here interpreted in terms of different orientations of the carbonate anions, different stacking sequences of the carbonate layers, and possible chiral forms. Hence, vaterite should be considered as a combination of different forms exhibiting similar average properties, rather than a single "disordered" structure (*Figure 1*). Furthermore, chirality represents a new and important direction for future investigation that may influence which of the possible vaterite structure is obtained.

The latter deals with the relative stability of the $CaCO_3$ anhydrous and hydrated polymorphs as obtained at the DFT level.[5] This study is currently at the limit of DFT capability, because it involves systems exhibiting a very different structure and characterized by different kinds of interactions. In particular, van der Waals interactions are

shown to play a non negligible role with respect to ionic and covalent contributions in all of the considered phases.

[1] Gebauer *et al.* (2008) *Science*, 322, 1819; Meldrum & Sear (2008) *Science*, 322, 1802; Demichelis *et al.* (2011) *Nat. Commun.*, 2, 590

[2] Grimme (2004) *J. Comput. Chem.*, 25, 1463; Becke & Johnson (2005) *J. Chem. Phys.*, 122, 154104

[3] Demichelis *et al.* (2012) CrystEngComm, 14, 44; Demichelis *et al.* (2013) *submitted* on February 22nd.

[4] Wang & Beker (2009) *Am. Mineral.*, 94, 380; Mugnaioli *et al.* (2012) *Angew. Chem. Int. Ed.*, 51, 7041

[5] Demichelis *et al.* (2013) *in preparation*

11:50 Oral

Two Pathways Determining Chirality in $NaClO_3$ Crystals Grown from Solution via Achiral Precursors

Hiromasa Niinomi[1], Hitoshi Miura[2], Yuki Kimura[2], Takahiro Kuribayashi[2], Makio Uwaha[3], Shunta Harada[1], Toru Ujihara[1], Katsuo Tsukamoto[2]

1. *Department of Materials Science and Engineering, Nagoya University, Furo-cho, Chikusaku, Nagoya 464-8603, Japan* **2.** *Tohoku University, Sendai, Japan* **3.** *Nagoya University, Department of Physics (NU), Furo-cho, Chikusa-ku, Nagoya 464-8602, Japan*

e-mail: niinomi@sic.numse.nagoya-u.ac.jp

Spontaneous chiral symmetry breaking during crystallization of sodium chlorate ($NaClO_3$) from aqueous solution has been of great interest. Each molecule of $NaClO_3$ is achiral, but they forms chiral cubic crystals (space group $P2_13$). Crystallization from a static solution by evaporation yields statistically equal numbers of L- and D-crystals because of equal thermodynamic stability of the two enentiomorphs. Nevertheless, if the solution is continuously stirred during crystallization, resulting crystals are almost all L or all D in each crystallization experiment [1]. This significant imbalance in chirality is referred to as chiral symmetry breaking. Mechanism of this spontaneous symmetry breaking is not fully understood yet.

Despite of many interpretations and implications of the symmetry breaking during early stage of crystallization, there have been few direct observations in the early stage of crystallization from the viewpoint of the chirality. Recently, we performed an *in-situ* observation of nucleation induced by droplet-evaporation with a polarized-light microscope, and we for the first time found that an unstable unknown crystalline phase nucleates prior to appearance of the chiral crystal [2]. However, owing to lack of information of the unknown phase, its role in the determination of chirality is unclear.

In this study, chirality and stability of the unknown phase were evaluated by a cryogenic single-crystal X-ray structure-analysis and solubility measurements respectively. Moreover, we also performed an in-situ observation of phase transition from the unknown phase into the chiral phase by using a polarized-light microscope. The microscope is capable to identify handedness of the chiral crystal.

As the result of the evaluation of the unknown phase, (1) Lattice constant, crystal system and space group were determined as follows: a = 8.42 (Å), b = 5.26 (Å), c = 6.70 (Å), β = 109.71(°), monoclinic, and $P2_1/a$, respectively. The space group $P2_1/a$ implies that the unknown phase is achiral. (2) Solubility was roughly determined to be 1.6 times higher than that of the chiral cubic phase in the range from 10 °C to 23 °C, meaning that the unknown phase is metastable phase. For (1), (2) and the fact that the metastable phase transforms into the chiral cubic phase, we concluded that the unknown phase plays the role of precursor of chiral crystals.

In addition, the in-situ observation showed that the phase transition is classified into two types according to transition rate. Fig. 1 (A) shows that a bright precursor rapidly changes into a dark chiral crystal with transition rate of ~2000 μm/s. In contrast, Fig. 1 (B) shows slow phase transition with transition rate of ~35 μm/s [Fig. 1 (B) (5)]. This large difference of the transition rate is considered to be due to difference of mechanism. Namely, the rapid transition should be structural phase transition governed by intracrystalline displacement of atoms, and the slow transition should be solution-mediated phase transition governed by dissolution/precipitation. Peculiarly, as shown in Fig. 1 (B) (3), the solution-mediated phase transition is induced by contact of a precursor with a chiral crystal. In this case, the precursor transforms into a chiral crystal with the same handedness as the contacted chiral crystal [Fig. 1 (B) (6)].

We concluded that the precursor transforms into chiral crystal by either solution-mediated phase transition or structural phase transition. If the precursor contacts with a chiral crystal, it transforms by the solution-mediated phase transition. Whereas handedness is determined randomly in the case of the structural phase transformation, handedness results in the same as that of contacted crystal in the case of solution-mediated phase transformation [Fig. 1 (C)].Beside the direct nucleation of the chiral crystal, the structural phase transition of the achiral precursor has a potential to bear the origin of handedness. Preferential choice of handedness seen in the solution-mediated phase transition may lead to chiral symmetry breaking.

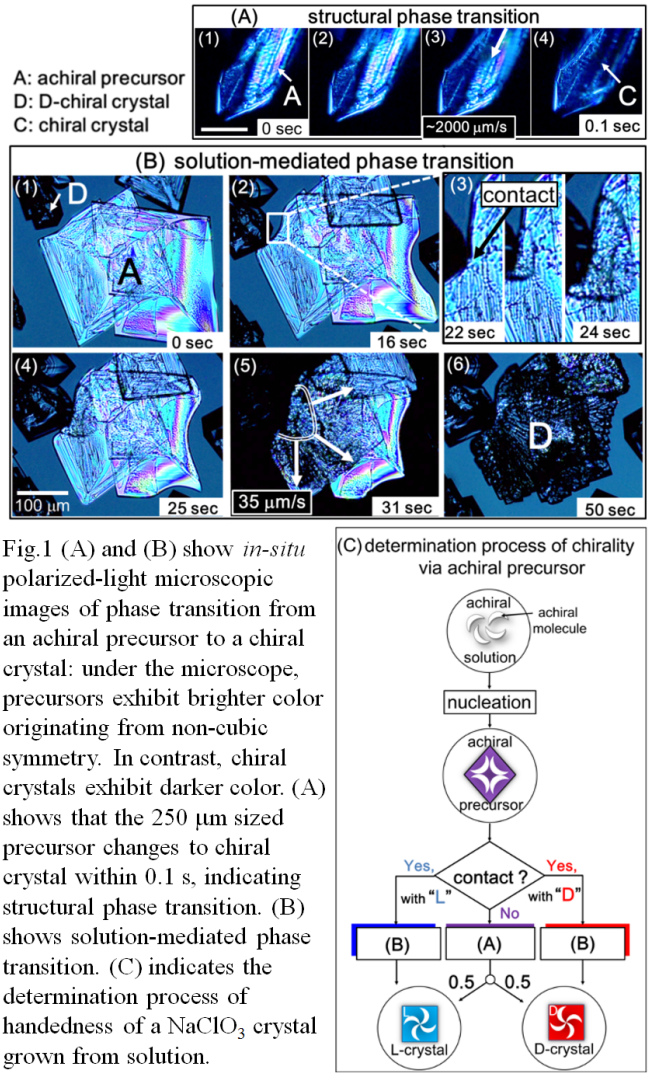

Fig.1 (A) and (B) show *in-situ* polarized-light microscopic images of phase transition from an achiral precursor to a chiral crystal: under the microscope, precursors exhibit brighter color originating from non-cubic symmetry. In contrast, chiral crystals exhibit darker color. (A) shows that the 250 μm sized precursor changes to chiral crystal within 0.1 s, indicating structural phase transition. (B) shows solution-mediated phase transition. (C) indicates the determination process of handedness of a $NaClO_3$ crystal grown from solution.

References
[1] D.K. Kondepudi, R.J. Kaufman, N. Singh, Science 1990, 250, 975-976. [2] H. Niinomi, K. Tsukamoto, M. Uwaha, H. Miura, Japan Geoscience Union Meeting 2010, MIS012-06.

12:05 Oral

Appearance of a homochiral state in crystallization by random fluctuation

Hiroyasu Katsuno[1], Makio Uwaha[2]

1. *Gakushuin University, 1-5-1 Mejiro,Toshima-ku, Tokyo 171-8588, Japan* **2.** *Nagoya University, Department of Physics (NU), Furocho, Chikusa-ku, Nagoya 464-8602, Japan*

e-mail: katsuno@sic.numse.nagoya-u.ac.jp

In 2005, Viedma found that, with grinding, chirality conversion of crystals occurs in this system[1]. A similar phenomenon has been found recently in organic systems[2,3]. In the latter case, a molecule has chirality, and the chirality of the minority molecules is converted to that of the majority. In order to understand the mechanism, several theoretical models have been proposed. In crystal growth[4,5], recombination of chiral clusters leads to the homochiral state deterministically and, in chemical reaction[6], random fluctuation also realizes a homochiral state eventually.

We studied the chirality conversion in crystal growth with a master equation based on a simple reaction model. With a stochastic crystallization process, although rate equation analysis provides no chiral symmetry breaking, random fluctuations drive the system to a homochiral state. The time necessary for the appearance of the homochiral state is proportional to the total number of molecules in the system[7].

In the present paper, We study a similar system with nucleation and recombination of chiral clusters. Although the system tends to become a racemic state, the chiral symmetry breaking occurs when the nucleation rate is small.

References:
[1] C. Viedma, Phys. Rev. Lett. 94 (2005) 065504.
[2] W. L. Noorduin, et al., Angew. Chem. 47 (2008) 6445.
[3] S. B. Tosogoeva et al., Angew. Chem. Int. Ed. 48 (2009) 590.
[4] M. Uwaha, J. Phys. Soc. Jpn. 73 (2004) 2601.
[5] Y. Saito and H. Hyuga, J. Cryst. Growth 318 (2011) 89.
[6] T. Sugimori et al., J. Phys. Soc. Jpn. 77 (2008) 064606.
[7] H. Katsuno and M. Uwaha, Phys. Rev. E 86 (2012) 051608.

Lunch (IOCG Council meeting)

Wednesday afternoon, 14 August, 12:20

WeO2

G01:Fundamentals and Modeling
Wednesday afternoon, 14 August, 14:00
Hall 16, Old Library

14:00 Invited oral

Modeling anisotropic shape evolution in Czochralski growth of oxide single crystals

Oleg Weinstein[1], Alexander Virozub[1], Wolfram Miller[2], Simon Brandon[1]

1. *Technion Israel Institute of Technology Dept. of Chemical Engineering, Technion City, Haifa 32000, Israel* **2.** *Leibniz Institute for Crystal Growth (IKZ), Max-Born-Str 2, Berlin 12489, Germany*

e-mail: cersbsb@technion.ac.il

Modeling anisotropic shape evolution in large scale melt growth systems has been reported in the literature over the past 10-15 years. However, in most cases relevant studies were concerned with interface attachment kinetics and associated faceting of melt/crystal interfaces in confined-growth (e.g. vertical Bridgman) systems (e.g. [1,2]). Very little attention has been given to Czocralski grown crystals which may exhibit anisotropy in the shape of both the melt/crystal and crystal/gas interfaces. Relevant studies include a two-dimensional capillary model used to analyze the cross-sectional shape of certain oxides [3], an axisymmetric thermal model linking shifts in the balance of heat transfer mechanisms with experimentally observed changes in morphology of sillenites [4], and most recently a three-dimensional analysis of the impact of interface-attachment kinetics on the cross-sectional shape of Bismuth Germanium Oxide (BGO) [5].

In this contribution we will present our efforts in developing and implementing efficient (e.g. Lattice-Boltzmann-Model based) algorithms for the three-dimensional numerical modeling of oxide single crystal growth *via* the CZ method. We will discuss the status of our algorithms with a specific emphasis on the application of appropriate boundary conditions at the partially faceted melt/crystal interface, at the melt/gas interface and along the three-phase contact line where melt, crystal and gas phases meet. Results to be presented include a discussion of the combined impact of interface attachment and growth angle anisotropy on the shape of the growing crystal.

This Research was supported by THE ISRAEL SCIENCE FOUNDATION founded by The Academy of Sciences and Humanities.

[1] O. Weinstein and S. Brandon, J. Crystal Growth **284**, 235 (2005).

[2] C.W. Lan and C.J. Chen, J. Crystal Growth **303**, 287 (2007).

[3] I.S. Pet'kov and B.S. Red'kin, J. Crystal Growth **131**, 598 (1993).

[4] J.C. Rojo, C. Marin, J.J. Derby and E. Diéguez, J. Crystal Growth **183**, 604 (1998).

[5] O. Weinstein and W. Miller, J. Crystal Growth **312**, 989 (2010).

14:30 Oral

Kinetics and Growth Efficiency of Tetragonal Crystals

Horia Alexandru

University of Bucharest, Faculty of Physics, Bucharest-Magurele p.o.box mg-11, Bucharest 76900, Romania

e-mail: horia@infim.ro

Peculiar aspects of crystal growth mechanism in solutions of KDP and ADP tetragonal crystals shall be presented using our published data and some new results. Fractional recrystallization procedure (in two or three steps) was used to improve the quality of the basic substance (H.V.Alexandru 2007). Double walled thermostated systems of 9 and 3 liters have been used and reversible rotation of the crystals tree sup-

port. Stirring rates ensured kinetic regime of the grown crystals. Linear (horizontal [001] and vertical [110]) crystals dimensions were registered in-situ versus the supersaturations. This way, pyramidal (011) and prismatic (100) faces, mean growth rate, were registered for the three crystals always grown in the same conditions. Arrhenius corrections of the growth rates, for our data and some literature data, were made for chosen growth temperature, using activation energy of growth.

Growths kinetic of KDP prismatic faces, more sensitive to Me^{3+} impurities, were registered in 9 liters solution volume of the crystallization chamber, up to one month. Growth kinetic in impure solutions was measured and analyzed. At higher supersaturations, ($\sigma > 8\%$) a dominant heterogeneous 2D-nucleation mechanism of growth was found, where the coverage of ad-molecules $q \sim 10^{-6}$ in the surface layer is about of the same order of magnitude as Fe^{3+} impurity concentration in solution. Using 2D-nucleation formalism introduced by Chernov we have found the edge free energy per growth unit $\gamma \approx 0.4\ k_BT$, in good agreement with the literature data. The lower limit of the adsorption energy 18 kcal/mol of this impurity was estimated on the prismatic faces of KDP, much higher than ~9.5 kcal/mol the activation energy for growth. The critical coverage $q^* \sim 10^{-3}$ at the limit of the "dead" growth zone, much higher than previous figure, suggest the segregation coefficient of this impurity increases dramatically towards the lower supersaturations (not published yet).

Macroscopic growth kinetic measurements were performed for pyramidal faces of KDP crystal. The three crystals were simultaneously grown in the same conditions, by temperature decreasing method. Arrhenius corrections were made for 40 ^{o}C growth temperature. Surface diffusion mechanism of growth appears as essential at small supersaturations, but several particular aspects dominate the growth. Pyramidal faces are less sensitive to impurities and show a large dispersion of the growth kinetic at s = 1÷5 %. There are distinct BCF curves fitting the experimental data on several ranges of supersaturation, corresponding to several efficiencies of growth. Bürgers vector and the linear dimension of the dominant centers of dislocations involved during growth shall be discussed.

Growth kinetic of pyramidal faces of ADP was studied at small supersaturations (s < 1 %.). There is a large dispersion of the kinetic data and apparently there is not a well defined relation between the growth rate and supersaturation, during a long run experiment. A special procedure was used to correlate the kinetic date with the efficiency of growth. The reverse of the estimated efficiencies versus the supersaturation, allowed estimating approximately the Burger's vector at several stages of growth and the edge free energy ratio γ/k_BT of the steps in the frame of the BCF dislocation mechanism of growth. Unexpected switching effect of efficiencies, found around 0.5 % supersaturations shall be discussed in relation with literature data (Vekilov, Kuznetsov 1992).

14:45 Oral

Morphological Prediction of the Polymorphic Forms of Para Amino-Benzoic Acid Based on Internal Crystallographic Structure and Crystallisation Environment

Ian Rosbottom, Kevin J. Roberts, Robert B. Hammond, Majeed Soufian

University of Leeds (SPEME), Leeds LS2-9JT, United Kingdom

e-mail: pmir@leeds.ac.uk

The shape of crystals is an important factor in processing crystalline products. Many industries including pharmaceuticals, fuels and fine chemicals process products using techniques such as filtering and milling where the morphology of the crystals is very important. The work presented forms part of the joint Critical Mass project between the University of Leeds and University of Manchester focused on understanding the process by which molecules cluster in solution, nucleate and grow to macroscopic crystals. In this case the morphology of para amino-benzoic acid (PABA) is predicted first in vacuum environment with analysis of the intermolecular 'intrinsic' synthons in the bulk structure and the unsaturated 'extrinsic' synthons at the surface. Using grid based search methods the solvent interactions at the habit faces are then analysed with respect to their effect on crystal morphology.

PABA has two known forms α and β[1]. The α polymorph crystallises is a needle like morphology whereas the β forms plate like crystals. HABIT 98[2] uses atomistic forcefields to calculate the strength of the intermolecular interactions within the crystal using the atom-atom approximation in a matter of seconds. The important morphological faces selected using the BFDH rule states that the morphological important faces will have the largest interplanar distance but does not account for chemical bonding. The attachment energy term pioneered by Bennema[3] et al takes into account the intermolecular forces within the crystal and is proportional to the growth rate of the faces and can also be calculated using HABIT for the user selected morphologically important habit faces using the following equations.
In addition to calculating the attachment energy the bulk intermolecular forces can be calculated and compared to the interactions at the surface. The orientation of the molecules and dangling unsaturated functional groups as predicted by perfect termination of the crystal provide valuable information about the surface chemistry at the crystal faces and can therefore allow predictions of how solvent will interact at crystal surfaces and effect the crystal morphology.

Further to the morphological prediction based on the internal structure in vacuum, solvent effects can be approximated using the grid based search SYSTSEARCH[4] developed at the University of Leeds. A probe solvent molecule is allowed to move around the crystal surface along user set grid points and change orientation to find the most energetically favourable position at the crystal surface. The intermolecular interaction between the probe molecule and the surface is calculated using the same atomistic forcefields as HABIT 98 and the whole process is possible in a matter of minutes. The interaction between the surface and the probe molecule can then be used to calculate a modified attachment energy and therefore a solvent induced morphology prediction.

Theoretical prediction of the morphology of PABA showed reasonable agreement using the attachment energy theory in HABIT. The intrinsic and extrinsic synthons were evaluated using HABIT. The SYSTSEARCH showed an improved prediction upon evaluation of the interactions at the surfaces and modified attachment energy. These results were also compared to other case studies undertaken within the group.

References

[1] Gracin, S.; Rasmuson, Å. C., Polymorphism and Crystallization of p-Aminobenzoic Acid. *Crystal Growth & Design*, 4 (2004) 1013-1023

[2] G. Clydesdale, R. Docherty, K.J. Roberts, HABIT - a program for predicting the morphology of molecular crystals, Computer Physics Communications, 64 (1991) 311-328.

[3] P. Hartman, P. Bennema, The attachment energy as a habit controlling factor: I. Theoretical considerations, Journal of Crystal Growth, 49 (1980) 145-156.

[4] R.B. Hammond, K. Pencheva, K.J. Roberts, Molecular modeling of crystal-crystal interactions between the alpha- and beta-polymorphic forms of L-glutamic acid using grid-based methods, Crystal Growth & Design, 7 (2007) 875-884.

15:00 Oral

Internal Radiation Effect on the Buoyancy-driven Flow pattern of Czochralski Oxide Melt

Reza Faiez[1], Yaser Abdollahpour[1], Farzad Najafi[2]

1. *SSL Research Group, School of Lasers and Optics, Tehran 11365-8486, Iran* **2.** *Research Institute of Petroleum Industry, Tehran 14665-137, Iran*

e-mail: rfaiez@gmail.com

The radiative heat transfer (RHT) through the melt and the crystal strongly couples with the buoyancy-driven flow during the Cz growth of oxide crystals. In the present modeling, a finite volume method was applied to compute quasi-steady and axisymmetric solutions to the fully coupled equations governing heat transfer and the melt hydrodynamics. As well, the discrete ordinate method was used to solve the RHT equation. Particular attention was paid to an undulating structure of the natural convection flow which appears in the optically thick oxide melt characterized by Pr = 4.69, Ra = O (10^6). The forced convection effect and the surface tension-driven flow were ignored. It was shown that, when the internal RHT is taken into account, the wavy structure of the flow and the convective distortion of the temperature field were smeared out, and consequently the secondary vortex located nearby the crucible bottom, disappeared. The shape and position of the vortex were studied in some detail. In the optically thick oxide melt of $2\times10^6 \leq Ra \leq 3\times10^6$, both the position of the vortex centroid, P, and its elliptical shape with the ratio of diameters AB/CD = 1.6 remains nearly unchanged while the area of the ellipse increases with Ra. At around the point P in the opaque melt, $(dT/dr)_{CD}$ found to be considerably (~40%) larger than $(dT/dz)_{AB}$. However, in the semitransparent melt, the ration between these local gradients equals to unity. This can be inferred that, in the opaque melt the local Richardson number, Ri_P might be smaller than ¼ as necessary criterion for instability. As well, the radial flow velocity profile along the vertical line including the vortex diameter, AB were compared for the two optically different cases. The Rayleigh-Fjørtoft instability condition found to be satisfied in the opaque melt. It was demonstrated that, the instability is suppressed by the stable stratification due to the internal RHT in the melt.

15:15 Oral

The application of PBC method to calculate the equilibrium form of sapphire crystals

Viktor N. Maslov, Sergey I. Bakholdin

A.F. Ioffe Physical-Technical Institute, Politekhnicheskaya 26, St-Petersburg 194021, Russian Federation

e-mail: maslov_vn@hotmail.com

The problems of theoretical calculation of the crystals forms are of great fundamental and practical importance. A number of publications are available now devoted to faceting of real crystals of corundum. Faceting sapphire single crystal rods grown by Stepanov method is described in deteil [1], giving the ratio of the size of faces on the side surface of cylindrical rod c {0001}> r{10-11}> a{11-20} as 8:4:1. There are, in eddition, reports calculat concerning on of theoretical faceting. Thus, [2] gives the result of quantum calculation, i.e. c {0001}> m{10-10}> R{10-12}> a{11-20}> r{10-11}. As in seen, the result of theoretical calculation does not agree with the data of the experiment.

M.D. Lubalinsuggested the mathematical tool for the theory of Periodic Bond Chain (PBC) to be applied in practice [3]. Here he introduces the parameters of bond unsaturation (H) and of atomic surface roughness (X). In the present work the parameters H and X for crystal lattice of α-Al_2O_3 are calculated. It is shown that energetically the most advantageous are c, r and a. The quantitative ratio of bond unsaturation (H) for the main faces is close to c> r> a as 4:3:2. Also shown is the difference in parameter H for negative and positive rhombohedrons. Thus, the result of calculation of corundum lattice according to the PBC theory describes to a good rather well the sequence of face display, although the quantitative values differ significantly.

It should be pointed out that on corundum crystals grown by flux method as well as on natural crystals there is observed quite different sequence of face sizes. This gives grounds to say that faceting of corundum crystals is influenced by the impurities of other atoms and the medium of crystal formation. On the other hand, the results on calculation by the PBC method best of all faceting of crystals of pure α-Al_2O_3 grown form reflect the melts in neutral atmosphere.

[1] Ю.Г. Носов, С.И. Бахолдин, В.М. Крымов Журнал технической физики, 2009, Т.79 №2, с. 76-82.

[2] I. Manassidis, M.J. Gillan. Journal American Ceramic Society, 1994, 77[2], p. 335-338

[3] М.Д. Любалин. Рост кристаллов в расплаве. Кристаллографический анализ и эксперимент. СПб.: Наука, 2008. 390с.

15:30 Oral

Morphology of Stripes Created in the (Zn) – Single Crystal

Waldemar Wołczyński

Polish Academy of Sciences, Institute of Metallurgy and Materials Sciences (IMIM PAN), Reymonta 25, Kraków 30-059, Poland

e-mail: w.wolczynski@imim.pl

Some experiments dealing with the (Zn)–hexagonal single crystal growth have been performed with the imposed positive thermal gradient and a set of the constant growth rates. Experiments were developed under stationary state created by means of the *Bridgman* system. The apparatus was equipped with a moving temperature field. A graphite crucible had a sophisticated geometry that the germs could be positioned within. The (Zn) – single crystal was doped by the small amount of titanium and copper. Titanium forms the $Zn_{16}Ti$ intermetallic compound with the zinc. Copper does not form any intermetallic compound but is solved in the zinc / titanium solid solution, (Zn).

Some eutectic stripes were generated periodically in the single crystal. The stripes consisted of strengthening inter-metallic compound, $Zn_{16}Ti$ and (Zn) – solid solution.

Three ranges of growth rates were distinguished in the (Zn) - single crystal formation: a/ at some low growth rates, the L – shape irregular eutectic structure appears, (with branches), b/ at some middle growth rates the regular lamellar structure is observed, c/ at some elevated growth rates the regular rod-like structure is the morphology which exists exclusively in the stripes.

Since the discussed single crystal growth occurs under stationary state the proper criterion which defines this state is to be applied. The thermodynamics of irreversible processes supposed that the only condition which describes the stationary state is the criterion of minimum entropy production.

Based on the mentioned criterion a **new procedure** of pattern selection has recently been formulated. According to the procedure this pattern is selected which exhibits the lower minimum entropy produc-

tion in the envisaged system. In the current model, the procedure will be applied to select the stripes morphology. Additionally, a growth rates range within which L-shape irregular rods were transforming continuously into the regular lamellae was observed. The progressive vanishing of branches occurs within the range. The formation of branches is referred to the creation of marginal stability in the system and continuous alteration of this stability into the stationary state. The existence of marginal stability is accompanied by the formation of a perturbation wave at the solid / liquid interface of the non-faceted (Zn) - eutectic phase which always appears in the stripes.

15:45 Oral

Nucleation statistics during the nanowire growth

Nickolay V. Sibirev[1,2], Maxim Nazarenko[1]

1. *St Petersburg Academic University, Khlopina Str 8/3, S.Petersburg 194021, Russian Federation* **2.** *Saint-Petersburg State University, Saint-Petersburg, Russian Federation*

e-mail: NickSibirev@yandex.ru

Nanowires (NWs) of III–V semiconductor compounds are promising building blocks for future nanophotonic and nanoelectronic devices and functional photonic circuits. III–V NWs are usually fabricated by different epitaxy techniques via the so-called vapor–liquid–solid mechanism activated by a metal (usually Au) catalyst. Nucleation process is of paramount importance in this case. These processes determined the NW crystal structure and therefore its physical properties.

This paper is devoted to study of nucleation during the NW growth. In our model we assume that growth proceeds in layer-by-layer regime in monocentric mode. Also we suggest that the time interval between two nucleation events is much larger than overgrowth time. Under these assumptions the nucleation statistics in nanowires with monocentric growth regime has been studied theoretically. It has been shown that the small size of droplet and its depletion cause anticorrelation of nucleation events and therefore suppress Poisson variation in the nanowire lengths. The dependence of the nanowire length dispersion on the growth rate and radius has been established. It has been shown that dispersion of nanowire length increase with increasing of evaporation rate from the droplet.

Thursday, 15 August

ThO1

G01:Fundamentals and Modeling
Thursday morning, 15 August, 10:20
Hall 16, Old Library

10:20 Invited oral

Metastable Epitaxial Alloys

Thomas F. Kuech[1], Kamran Forghani[1], Amita Anand[3], Yingxin Guan[2], Susan E. Babcock[2], Adam W. Wood[2], Luke J. Mawst[3], Tae Wan Kim[3], April Brown[4], Jincheng Li[4], Dane Morgan[2]

1. *University of Wisconsin-Madison, Department of Chemical and Biological Engineering, Madison, WI 53706, United States* **2.** *University of Wisconsin at Madison, Department of Materials Science and Engineering, 1509 University Avenue, Madison, WI 53706, United States* **3.** *University of Wisconsin-Madison, Department of Electrical and Computer Engineering, Madison, WI 53706, United States* **4.** *Electrical and Computer Engineering, Duke University, Durham, NC 27708, United States*

e-mail: kuech@engr.wisc.edu

Underlying most of our modern semiconductor devices, and hence optical and electronic systems, are semiconductor heterostructures composed of thin lattice-matched or pseudomorphic epitaxial layers. While some measure of lattice-mismatched derived strain can be accommodated within an epitaxial structure, the constraints of lattice-matching and thermodynamic stability of the alloy material have limited the choices of semiconductor alloy materials that can be used for structure design and device development. In order to increase the degrees of freedom within the design of devices, such as independent control over lattice parameter, band gap, band gap alignments, and electronic carrier transport characteristics, the chemical complexity of the epitaxial layer must increase through the incorporation of additional alloying elements. Unfortunately, most semiconductor alloys of arbitrary composition lie within a miscibility gap present in their respective phase diagrams. Epitaxial strain can be used to modify the phase relationships in epitaxial and pseudomorphic alloys. Alternatively, a variety of growth techniques have been used in attempts to form these thermodynamically immiscible materials as metastable phases. The formation of these potentially desirable alloys through epitaxial growth techniques that are characterized by being near thermodynamic equilibrium at the growth surface is generally impossible They can be formed, however, by suppressing those surface processes, such as surface mass transport, which lead to local phase separation during growth. Low growth temperature and chemical modification of the growth front can both be used to inhibit or suspend such surface transport processes and lead the formation of homogeneous alloys deep within a miscibility gap. Once formed, these alloys can be used in device applications since any subsequent phase separation would require some bulk diffusion, which is kinetically "frozen-out" under normal device operating conditions. This talk will discuss the thermodynamic relationships and kinetic processes that can be realized in a variety of alloy systems using established epitaxial growth techniques. Recent work on the formation of alloys which contain multiple anion substitutions in compound semiconductors and their extension to pentanary alloys will be presented as examples of the development of new materials that can open new areas of device design and technology.

10:50 Oral

A systematization of the structural stability in $A^N B^{8-N}$ compounds based on the bond-order potential

Tomonori Ito, Toru Akiyama, Kohji Nakamura

Mie University, 1577 Kurima-Machiya, Tsu 5148507, Japan

e-mail: tom@phen.mie-u.ac.jp

Wurtzite (WZ), zinc blende (ZB), and rocksalt (RS) structures are generally found in a number of binary octet $A^N B^{8-N}$ compounds, such as GaN (WZ), GaAs (ZB), and ZnSe (ZB), MgS (RS). To clarify why a given compound is formed in a certain structure, there has been some qualitative systematization of structural trends that have been accomplished using the dielectric model, pseudopotential orbital radii, and electrostatic interactions. Although these systematizations give successful interpretation in some aspects such as the separation of fourfold and sixfold-coordinated structures of $A^N B^{8-N}$ compounds, they cannot be applied to the structural stability for threefold-coordinated structure such as graphitic structure (G) crucial for nanotube and graphene. In this study, the bond-order potential (BOP) proposed by Abell [1] is employed to investigate the structural stability for $A^N B^{8-N}$ compounds in terms of bond length r_e and cohesive energy D_e on the basis of the previously reported ab initio results for ZB and RS in 26 compounds. To extract the crucial factor for the systematization, bond order p as a function of coordination number Z is also estimated within the framework of BOP using our ab initio calculations for G, ZB, and RS of C, BN, BeO, and Si. Moreover, simple energy formula of electrostatic interactions [2] is applied to determine the separation of threefold and fourfold-coordinated structures of $A^N B^{8-N}$compounds.

Figure 1 shows the calculated K_z+K_d for 26 compounds on the basis of the relationship in BOP assuming $p \propto Z^{-c}$ such as $r_e=K_z \ln(Z)+C_z$ and $r_e=K_d \ln(D_e/Z)+C_d$ where C, C_z, andC_d are the constants. Despite the values of K_z+K_d derived from the results of ZB and RS without G, this figure definitely reveals that the larger the K_z+K_d, the more stable the low-coordinated structures. Since large K_z+K_d is directly related to small r_e, small bond length is crucial for stabilizing low-coordinated structure such as G. In the range of $Z \leq 4$, however, the relation $p \propto Z^{-c}$ contradicts to ab initio results in Si obtained by Bazant and Kaxiras [3], who proposed $p \propto \exp(-bZ^2)$ instead of $p \propto Z^{-c}$. Thus we reasonably employ the formula of $p_{Z \geq 4}=(4/Z)^c$ at $Z \geq 4$ and $p_{Z \leq 4}=a\exp(-bZ^n)$ at $Z \leq 4$, where c, a, b, and n are the parameters adjusted to reproduce D_e for G, ZB, and RS with conditions of $d(p_{Z \geq 4})/dZ=d(p_{Z \leq 4})/dZ$ and $p=1$ at $Z=4$. The calculated bond order $p_{(3)}$ for Si ($p_{(3)}=1.09$) is favorably compared with the ab initio results ($p_{(3)}=1.05$) [3]. It is found that the values of $p_{(3)}$ of C, BN, and BeO are larger than those of Si consistent with the empirical Pauling relation $r_e \propto -\ln(p)$. Moreover, comparing the ionicity f_i for each material with critical iconicity for the separation of threefold and fourfold-coordinated structures $f_i^{c(3\text{-}4)}=3p_{(3)}^2/(3p_{(3)}^2+2Z_i^2)$ estimated by electrostatic interactions between bond charges p and between ionic charges Z_i, graphitic structure G is favored in C and BN because of their f_i (0 for C and 0.143 for BN) smaller than $f_i^{c(3\text{-}4)}$ (0.107 for C and 0.174 for BN) whereas WZ appears in BeO with its larger f_i (0.602) than $f_i^{c(3\text{-}4)}$ (0.316). This is consistent with experimental findings where G does not appear in $A^N B^{8-N}$ compounds with $N=2$. Consequently, bond length and ionicity are crucial for the structural stability of $A^N B^{8-N}$ compounds so that the threefold-coordinated structure does not appear in II-VI and I-VII compounds with large iconicity but limitedly appear in the compounds with small r_e introducing large $p_{(3)}$ and small f_i such as C and BN.

References

[1] G. C. Abell, Phys. Rev. B **31** (1985) 6184.

[2] T. Ito, Jpn. J. Appl. Phys. **37** (1998) L1217.

[3] M. Z. Bazant and E. Kaxiras, Phys. Rev. B **56** (1997) 8542.

11:05 Oral

Composition of a binary regular solid solution during its growth studied by the Monte Carlo simulation and the mean field approximation

Kiiko Matsumoto-Katsuno[1], Toshiharu Irisawa[2], Masao Kitamura[3]

1. *Seikei University, 3-3-1 Kichijoji-Kitamachi, Tokyo 180-8633, Japan* **2.** *Gakushuin University Computer Center, 1-5-1 Mejiro Toshima-ku, Tokyo 171-8588, Japan* **3.** *Graduate School of Science, Kyoto University, Kyoto 606-8502, Japan*

e-mail: kiiko@ejs.seikei.ac.jp

Predicting the composition of a sold solution (or alloy) during its growth has been one of the principle themes in the study of crystal growth. Recently, the epitaxial growth of semiconductor compounds, such as ternary alloys of AlGaN and GaAsSb, has also been extensively studied. On the other hand, the interface kinetics during the growth of a solid solution, especially a non-ideal solid solution, has not been fully understood and the theoretical study on the kinetics is still in progress.

The dependency of the distribution coefficients of a binary ideal solid solution growing from its vapor has been studied by using the Monte Carlo (MC) simulation and the mean field approximation [1, 2]. Our previous studies are then extended to the case of a binary non-ideal (regular) solid solution in the present study. The degree of the non-ideality is expressed by the value of $\Phi_{AB}-(\Phi_{AA}+\Phi_{BB})/2$, where Φ_{ij} is the bonds between i and j atoms.

The results of MC simulation show that the supersaturation range of lateral growth can be divided into three regions of (a, b, c). When the equilibrium distribution coefficient is smaller than 1, the composition of a solid approaches the equilibrium composition of terrace sites in (a), almost equals to the equilibrium composition of terrace in (b), and increases again in (c), as an increase of supersaturation. The behavior of the chemical composition of a solid can be explained by the relaxation processes on both terraces and terrace-tails, as in the case of ideal solid solution [2].

The introduction of the non-ideality changes the local atomic arrangements in a solid. These changes are clear in the case where a solid has the composition near A:B~1. Tiny clusters consisting of the ordered arrangement of AB is observed when $\Phi_{AB}>(\Phi_{AA}+\Phi_{BB})/2$ and clusters consisting of AA and BB when $\Phi_{AB}<(\Phi_{AA}+\Phi_{BB})/2$. The rate of the compositional change of a solid due to an increase of supersaturation is also affected by the non-ideality.

The mean field approximation model for ideal solid solution is extended for a non-ideal solid solution. The extended model explains the compositional changes in (a) obtained by the present MC simulation.

Reference

[1] K. Matsumoto, T. Irisawa, M. Kitamura, E. Yokoyama, Y. Kumagai, A. Koukitu, J. Crystal Growth 276 (2005) 635.

[2] K. Matumoto, T .Irisawa, M. Kitamura J. Crystal Growth 310 (2008) 646.

11:20 Oral

Creations of vacancy on growth interface during silicon melt growth by decreasing pulling rate

Takao Abe[1], Toru Takahashi[1], Koun Shirai[2]

1. *Shin-Etsu Handotai Co., Ltd. (SEH), Isobe RD Center 2-13-1 Isobe, Annaka 379-0196, Japan* **2.** *Institute of Scientific and Industrial Research, Osaka University, Osaka, Japan*

e-mail: takao.abe@seh.jp

1. Introduction

Almost people in the field of point defects research in silicon crystals have believed that both point defects coexist in growth interface. However, our following experimental results show that the growth interface is always filled with vacancies. On the other hand, interstitials are created far from the growth interface when and where the thermal gradient is increased.

2. Experiments

Since a 100 mm CZ crystal grown with 1.4 mm/min pulling rate was reached at stationary state, it was grown with gradually decreased pulling rate until 0.5 mm/min and finally it was detached from the melt and rapidly cooled. The crystal was cut parallel to growth direction with 1.0 mm in thickness and then annealed at 1000 ^{o}C, 16 hrs in dry O_2. Figure 1 is an x-ray topograph of the specimen.

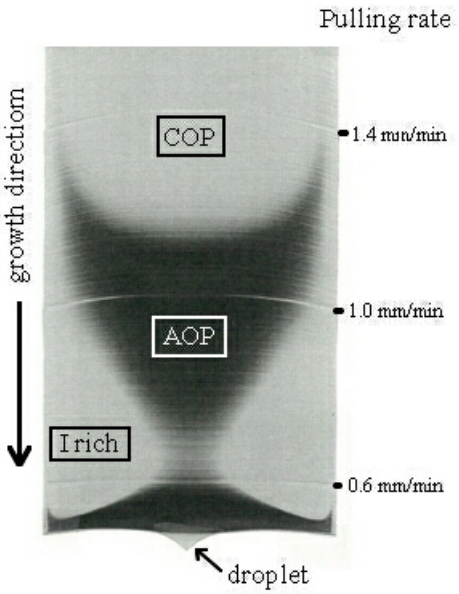

Fig. 1 X-ray topograph after AOP annealing of CZ crystal grown gradually decreased pulling rate and finally detached from melt.

The black contrast shows the strong x-ray diffraction intensity from oxygen precipitates (SiO_2). Such oxygen precipitation induced by one step annealing is called as the AOP (anomalous oxygen precipitation) [1] which presents that the existence of isolated vacancies before aggregation to produce a COP (crystal originated particle) [2] = void [3].

On the other hand, the existence of I is confirmed by using a WLT (wafer lifetime) method. Since the minority carriers induced by light are trapped by silicon dangling bonds which interstitial type dislocation loops have, the lifetime value is decreased. In both side regions under part of Fig. 2 the decreased WLT region is confirmed.

In Fig. 1 the three traces of growth interface shapes which are actually marked in the crystal by decreasing of crystal rotation rate for 30 second are seen. One is strong concave interface to a melt at 1.4 mm/min when decreasing pulling rate starts, second is weak concave shape at 1.0 mm/min and third is flat shape at 0.6 mm/min.

3. Results

In Fig. 1 the black contrast part like a wine glass shape is the V rich region which is formed by the AOP annealing. The upper white contrast part is the COP region which is produced by the aggregation of individual V. The lower both sides white regions are confirmed as I rich regions by the WLT map as seen in Fig. 2.

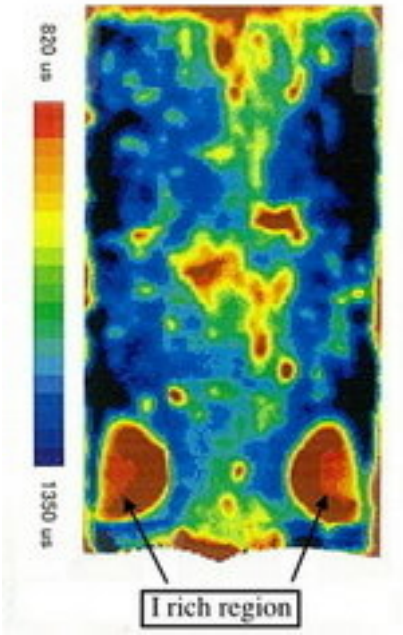

Fig. 2 WLT map of as grown crystal of Fig. 1.

Finally it is confirmed that the growth interface and neighbor grown region with the denser black color shows the high density V region.

According to the traditional Voronkov model [4], the growth interface should be the interstitial rich region with 0.6 mm/min pulling rate. However, even the growth interface with 0.5 mm/min pulling rate, the growth interface is filled with vacancy.

4. Conclusion

From the above results it is concluded that the growth interface is always filled with vacancy but interstitial is not existed. Interstitials are created far from the growth interface induced by a large thermal gradient.

References

[1] H. Harada, T. Abe, J. Chikawa, in: H.R. Huff, T. Abe, B.O. Kolbesen (Eds.) Semiconductor Silicon 1986, the Electrochem. Soc., Pennington, NJ, 1986, p. 76.

[2] J. Ryuta, E. Morita, T. Tanaka, Y. Shimanuki, Jpn. J. Appl. Phys. 29 (1991) L1947

[3] M. Itsumi, H. Akiya, T. Ueki, M. Yamawaki, J. Appl. Phys. 78 (1995) 5984.

[4] V.V. Voronkov, J. Cryst. Growth 59 (1982) 625.

11:35 Oral

Experimental investigation peculiarities of structural state aluminum melting on the base spectral fourier analysis acoustic emission

Vadim B. Vorontsov

Ural state university of transport, Ekaterinburg 02-935, Russian Federation

e-mail: VVorontsov@bgd.usurt.ru

This scientific work is devoted to the studying of the genetic connection structures of solid and liquid phases.

Fourier analysis of signals of acoustic emission (AE) accompanying melting high purity aluminum from the melting point up to t = 860 degrees Celsius was performed.

Based on the results of previous studies [1, 2] cluster formations in the melt – the micro-regions, those retain crystallinity (areas with short-range order of symmetry) were considered as the source of AE.

The experimental data allowed to follow the dynamics of disorder zones range order in the melt with increasing melt temperature up to their complete destruction.

The presented results of spectral analysis of the signals were analyzed from the standpoint of the theory of cluster melting metals.

1. Vorontsov V. B., Zhuravlev D. V., Vorontsov V. B., Zhuravlev D. V., "Cluster mechanism of solid phase forming at the example of growth of aluminium single-crystals of melt", Journal FOUNDRY PRODUCTION AND METALLURGY, 3 (57) ‘2010, p. 230;

2. Vorontsov V. B., Zhuravlev D. V., "Analysis of Acoustic Emission Signals Accompanying Growth of Single Aluminum Crystals: Experimental Results and Theoretical Model of the Cluster", Journal of Chemistry and Chemical Engineering, ISSN 1934-7375, USA, 6 (2012) 358-362;

11:50 Oral

Global theory for steady lamellar eutectic growth in directional solidification

Jian-Jun Xu[1], Xiang-Ming Li[2]

1. *McGill Unversity, 805 shebrooke street, west, Montreal H3A0B9, Canada* **2.** *School of Materials Science and Engineering, Kunming University of Science and technology, Kunming 650093, China*

e-mail: xu@math.mcgill.ca

The present paper is concerned with steady eutectic growth in the directional solidification of a binary mixture by using the two-dimensional model with the isotropic surface tension. We consider the case that Peclet number ε is small and the segregation coefficient κ is closed to the unit. The Peclet number ε is defined as the ratio of the half of primary spacing and mass diffusion length. By using multiple variable expansion and matched asymptotic method and exploring the singularity existing at the triple point, we obtain the global uniformly valid asymptotic solution for the steady state in the whole physical space. It is shown that the steady state solution contains two free parameters, the tilted angle parameter, which determines the orientation of the liquid open angle at the triple point and the Peclet number, which measures the primary spacing. Hence, given growth conditions the primary space may not be uniquely selected. The results show that the system has a boundary layer with the thickness of $O(\varepsilon^{1/2})$, where the slope and curvature of the interface are drastically large, hence the effect of isotropic surface tension pays a significant role and the interface has a noticeable non-uniform undercooling temperature. Our results lead to a self-consistent theory for steady lamellar eutectic growth, and raise the question on the validity of the hypothesis proposed by Jackson-Hunt, that the steady state with the minimum average undercooling at the interface is uniquely selected. The comparisons between the theoretical predictions and the available experimental observations have been made, which show quite good quantitative agreements.

12:05 Oral

Dynamics of Si island during evaporation

Yukio Saito[1], Olivier Pierre-Louis[2]

1. *Keio University, Faculty of Science and Technology (Keio), 3-14-1 Hiyoshi, Kouhokuku, Yokohama 2238522, Japan* **2.** *Université de Lyon, 43 Bd du 11 Novembre 1918 Villeurbanne, Lyon 69622, France*

e-mail: yukio@rk.phys.keio.ac.jp

When SOI wafer is kept at a high temperature, Si overlayer becomes unstable against dewetting and spontanesously agglomerates into islands. On further elevating the temperature, a Si atom reacts with an underlying SiO_2 molecule to produce two SiO molecules. Since SiO molecule is volatile, Si islands evaporate by leaving nano-pores in the dioxide layer.

In this paper, we study dynamical behavior of an evaporating island in terms of a simple solid-on-solid model with a two-dimensional adsorbate island on a one-dimensional substrate surface. The model is simulated with a kinetic Monte Carlo (KMC) method. Dynamics consists of five elementary processes: 1) Surface diffusion of adatoms A, 2) decomposition of a substrate atom S into A by emitting two oxygen atoms O, 3) reverse of 2), 4) interface diffusion of O, and 5) evaporation of A combined with O at the edge of an island.

Without decomposition, an adisland as a whole migrates on the substrate surface, and a means square displacement (MSD) of the island's center of mass increases linearly in time. The island diffusion constant Dc decreases as an island size R increases in a power law as $Dc \sim R^{-3}$. With decomposition and evaporation, the temporal behavior of an island MSD in general is classified in three stages: 1) Initially, MSD increases linearly in time, 2) then in an intermediate stage, MSD increases faster than a linear behavior due to the depinning of triple points, and 3) finally until the island disappears, MSD saturates since the island is trapped in a nano-pore it drilled.

In an early stage of evaporation, the interface between the island and the substrate has two dips near the edges of the island, because those O's produced close to edges can escape from the interface and the decomposition from S to A proceeds, whereas in the center of the island decomposition is balanced with the reverse reaction. Eventually, when the island becomes too small, it is trapped into one of the nano-pore that it drilled. The final shape of a drilled pore is deep when the evaporation rate is large.

Lunch (EMCG meeting)
Thursday afternoon, 15 August, 12:20

Posters

Monday, 12 August

MoP-G01
Monday afternoon, 12 August, 17:00
Room 105, Old Library

17:00 Poster Mo1

Creations of interstitial inside crystal during silicon melt growth by heating melt

Takao Abe[1], Toru Takahashi[1], Koun Shirai[2]

1. *Shin-Etsu Handotai Co., Ltd. (SEH), Isobe RD Center 2-13-1 Isobe, Annaka 379-0196, Japan* **2.** *Institute of Scientific and Industrial Research, Osaka University, Osaka, Japan*

e-mail: takao.abe@seh.jp

1. Introduction

Almost researchers in the field of point defects in silicon crystals have believed that both point defects coexist in growth interface. However, our following experimental results show that the growth interface is always filled with vacancy (V). On the other hand, interstitial (I) is created at a region to be long way from the growth interface, depending on increasing thermal gradient.

2. Experiments

Three 100 mm CZ crystals with 1.4 mm/min pulling rate were grown from the same melt in one crucible and then they were detached from the melt during growth and cooled rapidly. They were cut parallel to growth direction to obtain specimens with 1.0 mm in thickness and were annealed with 1000□, 16hrs in dry O_2. Their x-ray topographs were obtained as seen in Fig. 1, 2 and 3. Where the black contrast shows the strong intensity of x-ray diffraction from oxygen precipitates (SiO_2). Such oxygen precipitation induced by only one step annealing is called as the AOP (anomalous oxygen precipitation) [1], which presents that the existence of isolated vacancies before producing a COP (crystal originated particle) [2] = void [3] by aggregation.

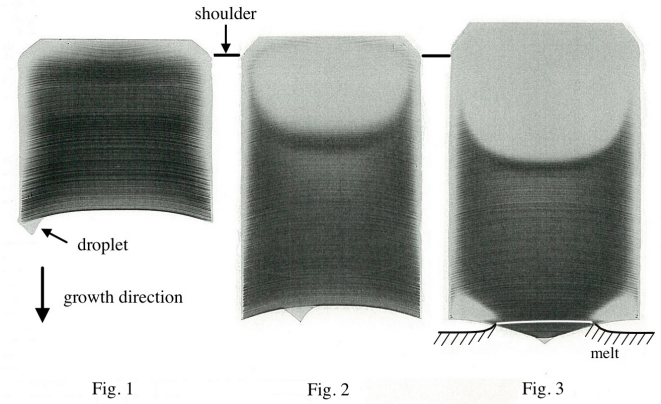

Fig. 1 Fig. 2 Fig. 3

Fig. 1 and 2 X-ray topographs after AOP annealing of mechanically detached CZ crystals at 50 mm from shoulder position and at 100 mm, respectively. Fig. 3 X-ray topograph after AOP annealing of partially detached CZ crystal by heating melt for 30 min and finally detached it mechanically. Schematic drawings of interface shape and meniscus of melt.

On the other hand, the existence of I is confirmed by using a WLT (wafer lifetime) method. Since the minority carriers induced by light are trapped by silicon dangling bonds of interstitial type dislocation loops, the lifetime value is decreased with increasing the density of the dislocation loop. In both side regions under part of Fig. 3, the decreased WLT region is confirmed.

3. Results and discussions

The first crystal as shown in Fig. 1 was detached from the melt at length of 100 mm from crystal shoulder. It is understood from the AOP distribution that almost whole crystal except surface area of the shoulder is V rich. The second crystal as shown in Fig. 2 was grown 50 mm in length and 36 min in period longer than those of the first crystal and was detached and cooled. During longer growth period the COP region is newly generated and spread 40 mm in depth from the shoulder level. This means that individual V in the AOP region aggregates to make a void. When the third crystal as seen in Fig. 3 was grown at the same length (150 mm) with the second crystal, instead of the mechanical detaching procedure the melt temperature was continuously increased for 30 min by increasing the input power. As the result both sides of peripheral area of the growth interface was separated from the melt but in the center area was grown continuously due to large cooling effect by pulling stop. The above explanations are recognized using a schematic line drawn along growth striations in Fig. 3. That is, the growth interface is deeply concave to the melt just at pulling stop but after that the interface shape becomes gradually deeply convex in center area. Finally the crystal was mechanically detached after 30 min from pulling stop. It is clear that the area where crystal contacts with the melt is always V rich but the both sides peripheral area where crystal does not contact with the melt are replaced by I rich region. The white contrast area in x-ray topograph in Fig. 3 corresponds to the low lifetime area where is the I rich region in WLT map in Fig. 4.

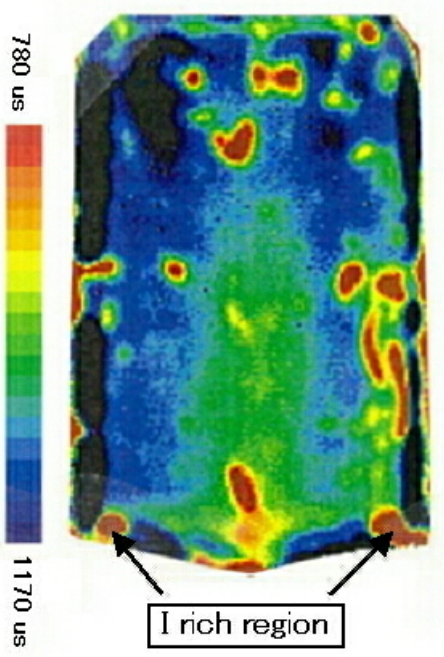

Fig. 4 WLT map of as grown crystal of Fig. 3

If the crystals which do not contact with the melt are heated up, the I is created. This fact was already reported by Roksnoer [4]. However, it is observed in our growing experiments that the V rich region converts into the I rich region in one crystal during growth. The third crystal was grown 30 min longer period than that of the second crystal so that the depth of the COP region elongated to 60 mm. It is recognized

that in standard crystal growth procedure the whole crystal becomes the COP crystal due to gradually cooling without detaching.

4. Conclusion

From the above results it is concluded that the growth interface is always filled with vacancy but interstitial is not existed. Interstitials are created far from the growth interface induced by a large thermal gradient.

References

[1] H. Harada, T. Abe, J. Chikawa, in: H.R. Huff, T. Abe, B.O. Kolbesen (Eds.) Semiconductor Silicon 1986, the Electrochem. Soc., Pennington, NJ, 1986, p. 76.

[2] J. Ryuta, E. Morita, T. Tanaka, Y. Shimanuki, Jpn. J. Appl. Phys. 29 (1991) L1947

[3] M. Itsumi, H. Akiya, T. Ueki, M. Yamawaki, J. Appl. Phys. 78 (1995) 5984.

[4] P.J. Roksnoer, J. Cryst. Growth 68 (1984) 596.

17:00 Poster Mo2

Numerical simulation of the crystal growth process of titanium doped sapphire fibers by the micro-pulling down technique

Hanane Azoui, Abdallah Laidoune, Djamel Haddad, Derradji Bahloul

Département de Science de la Matière, Faculté des Sciences, Université Hadj Lakhdar de Batna, 1 Avenue Boukhlouf Mohamed El Hadi, Batna 05000, Algeria

e-mail: bahloul@univ-batna.dz

In this work we present a numerical study of the solidification of crystalline fibers of titanium doped sapphire drawn by the micro-pulling down (μ-PD) growing technique. Our study emphasizes on the physical properties of the melting zone. The crystals of sapphire have many applications in lasers and in optoelectronics. In this study we have established a numerical, two-dimensional model in cylindrical coordinates with an axisymmetric configuration for a Newtonian and incompressible fluid, of a laminar flow based on the equations which are mainly those of derived from of the physical conservation laws. The flow, the thermal transfer and the mass transfer are modeled by the differential equations of conservation of the mass, of quantity of the movement, energy and the species. This problem, which takes into account the convection-diffusion coupling, is discretized using the Finite Volumes Method (FVM). Our model is in good agreement with experimental results. We have been able to show that the μ-PD method can gather the necessary conditions for optimization of the dopants concentration distribution for increasing the coupling between the laser wave and the ions of the doping agent in order to give the highest possible luminous power at the output of the laser. We found that, in the melt, Marangoni convection is dominant, and the buoyancy convection is negligible.

17:00 Poster Mo3

Transport and Interfacial Phenomena Modeling In Transient Vertical Bridgman Solidification of InSb

Paul C. Barvinschi[2], Floricica Barvinschi[1]

1. *Politehnica University of Timişoara, P-ţa Victoriei no. 2, Timisoara 300006, Romania* **2.** *West University of Timisoara (UVT), Bd.V. Parvan nr.4, Timisoara 300223, Romania*

e-mail: fbarvinschi@gmail.com

The vertical Bridgman technique is commonly used for the growth of III-V and II-VI semiconductors, halide and chalcogenide crystals, and a number of oxides for scintillation or laser applications. This technique has some drawbacks that are linked to the use of a crucible in intimate contact with the crystal. In order to solve these problems some variants based on capillary aspects have been proposed, such as full encapsulation or dewetting [1]. Modeling and simulation are very important for a better understanding of the phenomena involved in the crystal growth processes. In the specific case of the vertical Bridgman technique, it is useful to include in a single model the transport phenomena (energy, momentum, mass) and the interfacial phenomena at the melt-crystal-crucible and respectively melt-gas-crucible interfaces. We already made a stationary model and obtained some numerical results for the coupled heat transfer and fluid dynamics in the vertical Bridgman solidification of InSb [2]. In the present paper we extend our previous model by including the calculation of the energy, momentum and mass transport, plus the interfacial phenomena at the melt-gas-crucible interface, under normal gravity, while applying a time dependent step-type temperature distribution on the outer part of the crucible. The geometry of the model resemble that used in a vertical Bridgman configuration: a cylindrical silica crucible (90 mm in length, having a 5.5 mm inner radius and a 6.5 mm outer radius) contains the InSb charge. A slightly modified version of the model presented by Voller and Prakash [3] is used to account for solidification of the liquid phase, including convection and conduction heat transfer with mushy region phase change. In order to model the flow of two different, immiscible fluids, where the exact position of the interface is of interest, we have applied the phase-field (diffuse interface) method. All these new models were developed numerically by using the finite element software COMSOL Multiphysics. Using the actual models, the numerical calculation of the thermal field, velocity field, and interface shape gives qualitatively correct results (see Figure 1 for the shape of the interfaces). For developing better models numerical results must be compared with the experimental ones and this will be done in a next step of the study.

17:00 Poster Mo4

The influence of the heat exchange on the shape of sapphire profiles grown by the Stepanov method inside the zone of crystallization

Pavlo Bieliaiev

Institute for Single Crystals NAS of Ukraine (ISC), 60 Lenin Ave., Kharkov 61001, Ukraine

e-mail: Beljaev.Pavel.kr@gmail.com

It is very important to know the dependence of the shape of crystallization front on variations in technological parameters and heat exchange near this front along the boundary “shaper – melt” for optimize the process of sapphire profiles growing. The paper gives the mathematical model of the growing of sapphire profiles that considers the variations of thermal and hydrodynamic parameters with different rates of growing within the zone of crystallization. The model uses an adaptive mesh of finite elements for sampling inside the area of phase transfer. The used variation parameters are the rate of growing, the heat extraction of the crystal and inside the thermal zone. It is possible to obtain the distribution of temperature inside the zone of growth and also the shape of crystallization front for various configurations of the thermal zone and technological parameters of growing using the model. Parameters used for the sapphire profiles growing such as the configuration of thermal zone (the quantity and position of thermal screens), the design of shaper and the pulling rate can be defined using the calculation data by the model with sufficient accuracy. A period of

time which is needed for testing the configuration of thermal zone while changing cross-section types of the sapphire.

17:00 Poster Mo5

Kinetic anomalies of mixed crystals growth

Sergey N. Bocharov

Saint-Petersburg State University (SPBSU), 7/9 University emb., S.Petersburg 199034, Russian Federation

e-mail: bocharovsergei@mail.ru

Kinetic anomalies are oscillating nonmonotonous changes of growth rate with temperature. It was found in 1967 by V.Sipyagin and A.Chernov (Sipyagin, 1967; Sipyagin, Chernov, 1972) and now is known for dozens of water-soluble salts (Punin, Petrov, 1972; Kibalczyc, Kolasinski, 1977; Franke, 1986; Bocharov, 2004 etc). It was established that kinetic anomalies has influence on crystal morphology (Glikin et al, 2003) as well as chemical composition (Bocharov et al, 2009). So this phenomenon is important for industrial crystal growth from solution, mineralogical reconstruction and basic researches of crystal growth theory. Nevertheless this phenomenon is poorly known and not covered by monographs and articles. It is supposed that anomalies formation linked to structural transitions on molecular level (Bocharov, Glikin, 2008; Bocharov, 2011) at different parts of crystal-solution system (bulk of solution and adsorption layer). Comparison of kinetic anomalies features for different systems can give us information about anomalies nature as well as possibility to grow mixed crystals with precision control of chemical composition distribution.

From this point of view it is interesting to compare kinetic anomalies for matters with fixed chemical composition and matters with varying chemical composition (mixed crystals) as well as kinetic anomalies changes in chain of intermediate solution compositions between pure members. We investigated kinetic anomalies of mixed crystals growth for $NaClO_3$-$NaBrO_3$ system by traditional microcrystallization method and for Cu-Hg system by modified electrocrystallization method (Bocharov, Glikin, 2008). Kinetic anomalies for $NaClO_3$-$NaBrO_3$ system were investigated in temperature range 33 – 41 ^oC and compound ratio in solution which responds to alyotropic point of system ($NaClO_3$:$NaBrO_3$ = 20:1). For Cu-Hg system kinetic anomalies were investigated in temperature range 45-53 ^oC and compound ratio in solution from 1:50 to 1:500 (Cu:Hg). Extreme compound ratios correspond to pure members deposition since difference of electrochemical potentials for Cu and Hg exists.

Our investigations show that low deviation of solid phase chemical composition from end-member composition resulted in kinetic anomalies which are similar to anomalies of main phase as temperature position of peaks as well as peak intensity. As example kinetic anomalies of $Na(Cl,Br)O_3$ in the temperature range 33 – 41 ^oC are characterized by four maxima of growth rate. Three of these maxima correspond to maxima of pure sodium chlorate. Kinetic anomalies of Cu-amalgams deposited from solution with compound ratio 1:50 are characterized by seven maxima in the temperature range 47 – 52 ^oC. Five of them correspond to maxima of copper kinetic curve and two correspond to maxima of mercury kinetic curve. So, main difference of mixed crystal kinetic anomalies is existing additional peaks which relate to kinetic anomalies of opposite end-member. Changes in compound ratio result in complication of kinetic curves. It can be described as superposition of end-member kinetic curves plotted by maxima of growth rate.

Thus, on one hand, kinetic anomalies of mixed crystals growth are defined by initial ratio of compounds in solution. On other hand it is defined by kinetic curves of end-members. In some cases it can result in specific zone formation.

The reported study was partially supported by Russian Foundation for Basic Research, research project No. 12-05-00876-a.

17:00 Poster Mo6

Combined interface attachment kinetics and transport phenomena in large scale solution growth systems

Oren Bass[1], Alexander Virozub[1], Andrew Yeckel[2], Jeffrey J. Derby[2], Simon Brandon[1]

1. *Technion Israel Institute of Technology Dept. of Chemical Engineering, Technion City, Haifa 32000, Israel* **2.** *University of Minnesota, Chemical Engineering and Materials Science, 421 Washington Ave. S.E., Minneapolis, MN 55455, United States*

e-mail: cersbsb@technion.ac.il

Studies linking transport phenomena (e.g. [1]) to morphological stability and the formation of defects suggest that it may be possible to control the flow and resultant solute distribution near vicinal surfaces in a manner which will render these surfaces less susceptible to loss of stability and to the resultant formation of defects. Meso-scale analyses (e.g. [2]) of vicinal surfaces indicate that it may be useful to use flow modulation as a means to control interfacial stability. However, a macroscopic-view point of the same problem [2] demonstrated unexpected changes in morphology due to an interaction between periodically changing solute fields, step sources and moving steps. This motivated us in our efforts (presented in this contribution) to combine three-dimensional modeling of fluid flow and solute transport with non-trivial interface attachment kinetics as a means for investigating the impact of large scale dynamics of flow and solute transport on interfacial morphology.

We will discuss our modeling efforts which are specifically applied in the analysis of a potassium dihydrogen phosphate (KDP) growth system. This three-dimensional modeling project hinges on the CATS3D [3] finite element software developed at the University of Minnesota which, in this study, was modified to include interface motion consistent with interface attachment kinetic mechanisms such as rough, vicinal, screw-dislocation-driven and 2D-nucleation driven growth. Results to be presented will include analyses of different interactions between flow fields, supersaturation profiles and interfacial morphology.

This Research was supported by the U.S.-Israel Binational Science Foundation.

[1] A.A. Chernov, J. Crystal Growth **118**, 333 (1992).

[2] I. Rasin, S. Brandon and O. Weinstein, Int. J. Multiscale Comp. Eng. **6**, 585 (2008).

[3] A. Yeckel, Cats3D user manual (unpublished), University of Minnesota, USA (2009).

17:00 Poster Mo7

Crystallisation mechanism and kinetics from polythermal methods: methyl stearate from kerosene solutions

Diana M. Camacho Corzo[1], Kevin J. Roberts[1], Ken Lewtas[2], Iain More[2], Dimo Kashchiev[3]

1. *University of Leeds (SPEME), Leeds LS2-9JT, United Kingdom* **2.** *Infineum UK Ltd, Abingdom OX13 6BB, United Kingdom* **3.** *Institute of Physical Chemistry, Bulgarian Academy of Sciences, Sofia 1113, Bulgaria*

e-mail: pm07dmcc@leeds.ac.uk

A polythermal methodology to assess the mechanisms and the kinetics associated with solutions crystallisation is defined and analysed using the recently-derived KBHR model. This first principles approach yields crystallisation parameters that could otherwise only be obtained by the combined application of both isothermal and polythemal methods. The methodology is validated through assessment of experimental data measured for methyl stearate crystallising from kerosene solutions, revealing a progressive nucleation mechanism and interfacial tensions in the range of 1.64-1.79 with no obvious dependence on solution concentration in the range of 200 to 350 g/l, showing good agreement with values derived by isothermal methods. Sensitivity analysis reveals that a minimum of four different cooling rates separated by at least one order of magnitude together with at least five repeats for crystallisation temperature values at each cooling rate is appropriate.

17:00 Poster Mo8

Modeling of Particle Engulfment during the Growth of Multicrystalline Silicon for Solar Cells

Yutao Tao, Andrew Yeckel, Jeffrey J. Derby

University of Minnesota, Chemical Engineering and Materials Science, 421 Washington Ave. S.E., Minneapolis, MN 55455, United States

e-mail: derby@umn.edu

With a reasonable balance between cost and efficiency, multicrystalline silicon (mc-Si) has been a mainstream material for solar cells, and these cells make up approximately 50% of the market of today's photovoltaics industry. There are significant opportunities for increasing quality and reducing cost of the mc-Si substrate material via a better understanding of crystal growth processes. One challenge is the formation of silicon carbide and silicon nitride precipitates in the melt due to carbon and nitrogen impurities coupled with their relatively small segregation coefficients. These solid particles can be engulfed by the solidification front to form inclusions in the mc-Si solid. The presence of inclusions lowers cell efficiency and can lead to wafer breakage and sawing defects, even breakage of the wire saw.

To better understand the physical mechanisms responsible for these inclusions, we are applying finite-element, moving-boundary analyses to assess particle dynamics during engulfment via solidification fronts. Two-dimensional steady-state and dynamic models are developed using the Galerkin finite element method and elliptic mesh generation techniques. Such an approach is particularly well suited for rigorous and accurate representation of geometrical and interfacial interactions in this system, and we demonstrate how this model is able to represent very large deformations of the melt-solid interface during the process of engulfing a solid particle.

We discuss model formulation, implementation, validation, and its performance with respect to prior models of this process. We also present initial results to investigate various factors' influence on particle-solidification front dynamics, such as i) particle size, ii) different materials' densities and thermal conductivities, iii) interfacial premelting, iv) Gibbs-Thomson effects, v) temperature gradient, vi) gravity, and vii) the bulk flow caused by the density change upon solidification. Criteria to establish the all-important pushing/engulfing transition of a particle near a solid-melt interface are investigated via transient simulations. The significance of introducing a premelting film into the system is also discussed.

Supported in part by U.S. National Aeronautics and Space Administration, NNX10AR70G, the content of which does not necessarily reflect the position or policy of the United States Government, and no official endorsement should be inferred.

17:00 Poster Mo9

Thermocapillary Effect on the Pattern Transition of Czochralski Natural Convection of Oxide Melt

Reza Faiez[1], Yaser Abdollahpour[1], Farzad Najafi[2]

1. *Centre of Research And Application of Laser, Solid-State Lasers Department (CRAL-SSL), North Kargah, Tehran, Iran, Tehran 14689, Iran* **2.** *Research Institute of Petroleum Industry, Tehran 14665-137, Iran*

e-mail: rfaiez@gmail.com

Both steady-state and time-dependent simulations of the two-dimensional Navier-Stokes equations were performed to investigate the influence of surface tension-driven forces on the structure of convective flow in an open crucible Cz oxide melt with a stationary crystal dummy deflected into the fluid. The internal radiative heat transport was ignored and, for computational purposes, the coefficients and were allowed to vary within some reasonable ranges of values. The simulation results for were discussed in details.

For all cases with, the convective flow exhibits an undulating structure beyond the cold plume along the melt centerline and a small secondary vortex (RFV) nearby the crucible bottom. Increasing in slightly up to its threshold value i.e., the steady-state behavior of the melt changes suddenly for so that the wavy pattern of the flow and the secondary vortex both disappear. This can be shown that the effect is associated with a jump-discontinuity in the magnitude of stream function , and the jump is larger for a higher intensity of the natural convection.

In the interior of the melt, the buoyancy frequency, N as well as the frequency of disturbances and more strongly, the local Richardson number, Ri are decreasing with , so that for the wave-induced shear instability is satisfied for. The internal Froude number, increases exponentially with and equals to its critical value at for which the phase velocity, of the internal waves is equal to the mean flow velocity, i.e. independent of. For the subcritical state associated with shorter internal waves, changes abruptly to the super critical state with the waves of longer wavelength compared to the melt characteristic length [1]. In the critical state, the waves decay by a factor for. The factor found to be multiplied by $\sim 10^2$ for implying a strong modification of the flow under the influence of the longitudinal Marangoni waves.

The unsteady-state simulations with for the case display the effect of thermocapillary forces on (i) the dynamics of the Kirchhoff-type secondary vortex (RFV) and (ii) its development against the Hadley cell circulation (HCC). During the time, the RFV core area found to be highly (~3-4 times) increased. The ellipse orientation angle, meets its maximum value, at around when the HCC disappears. In the course of time, the up-going wavy streamlines are more and more flattened towards the crucible hot wall. This can be shown that, the equation , with and as the ratio of the ellipse semi-axes, is held at around for which [2]. The ratio between the straining part of the shear flow and the local vorticity (at the RFV center, found to be increasing with time at. However, the ratio remains smaller than unity suggesting that the fluid particles are entrained into the vertical region of coherent structure. The kinetic energy of the vortex ring found to be highly (~10 times) increased for a slight increment in during the first steps of this irreversible process.

References

[1] C.P. Lee, Phys. Fluids 10 (1998) 2765.

[2] S. Kida, J. Phys. Soc. Japan 50 (1981) 3517.

17:00 Poster Mo10

Forming of metal structures in dielectric CaF_2 crystals

Pavel Fedorov[1], Aleksandr Shcheulin[2], Alexander Angervaks[2], Alexander Ryskin[2], Radmir Gaynutdinov[3]

1. *General Physics Institute, Vavilov Str. 38, Moscow 117942, Russian Federation* **2.** *National Research University ITMO, St-Petersburg 197101, Russian Federation* **3.** *Shubnikiv Institut of crystallograhy Russian Academy of Sciences (ICRAS), Leninskii pr. 59, Moscow 119333, Russian Federation*

e-mail: ppfedorov@yandex.ru

Breaking the stoichiometric composition of calcium fluoride crystals under the impact of an ionizing radiation or at heating in the reduction atmosphere of metal vapors (so called "additive coloring" of crystal) results in color centers formation. In the process of additive coloring these centers arise due to recombination of anion vacancies and electrons which are produced on the heated crystal surface and diffuse into the crystal bulk. The centers are subdivided into "simple" (*F*, *M*, *R* and *N*) centers, which are composed of 1–4 anion vacancies, respectively, with an equal numbers of electrons and highly-aggregated centers. It was initially proposed that such centers are colloidal particles of calcium, which arise as a result of transformation of large accumulation of anion vacancies and electrons into metal inclusions [1,2]. Another type of highly-aggregated centers was found later, that is "quasi-colloidal" centers (see [3]). Their structure is unknown, it is likely that they are in an intermediate position between simple and colloidal center by the number of vacancies/electrons. Color centers have characteristic absorption bands. The most intensive absorption bands of simple centers are in the wavelength range of $l < 550$ nm, the absorption band of colloidal center is within the wavelength range of $l = 550–650$ nm, the bands of quasi-colloidal centers cover the wide spectral range of ~0.6–6 *m*m. As a rule, additively colored CaF_2 crystals contain predominantly simple and colloidal centers. Their ratio depends on the concentration of vacancies/electrons introduced into the crystal during its coloring, i.e. on the coloring mode. The stiffer the mode (the higher the calcium vapor pressure and the sample temperature) the larger the relative content of colloidal centers [4]. It was recently found that actually these centers are two-dimensional rounded or prolate metal islands with thickness of 1.3–1.4 nm and lateral size of 30–200 nm. Such islands occur at vacancies/electrons concentration of $\sim 10^{17}$ cm^{-3}[5]. When concentration increases up to $\sim 10^{18}$ cm^{-3} islands coalesce forming as it film fragments with pores of arbitrary shape and different size. Nevertheless the height of coalesced islands remains equal to 1.3–1.4 nm. Absorption spectrum of such crystals practically contains only the band of colloidal centers. That means the most of color centers are coalesced into "colloidal" particles scattered randomly over the crystal volume and only their small part form film fragments. These fragments are disposed in selected {111} planes; the crystal is cleaved exactly along these planes. Absorption spectrum of the crystals with even higher concentration of color centers changes drastically. The intensity of absorption band of "colloidal" centers decreases, and intense non-selective absorption arises typical for thin metal films. In such a crystal a majority of color centers are coalescent into fragments of such films. Under impact of the radiation resonant to absorption bands of particular color centers and the temperature the conversion of color centers occurs [6,7]. Their photochromic transformations underlie using CaF_2 crystals with color centers as highly-stable volume holographic media [8,9]. One should note that the specific diffusion-drift mechanism of hologram recording results in accumulation of color centers in the minima of fringe pattern; the larger the exposure the narrower are the regions of centers concentration [10,11]. This feature favors metal inclusion formation. Thus, recording holograms in additively colored CaF_2 crystal with sufficiently high concentration of anion vacancies/electrons can convert it into a metamaterial-like state.

1. H.V. Den Hartog, W. Tinbergen, W.G. Perdok, *Phys.Status Solidi A*, **2** (1970) 347-358.

2. W. Hayes, ed., *Crystals with the Fluorite Structure: Electronic, Vibrational, and Defect Properties* (Clarendon Press, Oxford, UK, 1974).

3. A.S. Shcheulin, *Thesis* (St.-Petersburg, 2008, in Russian).

4. A.S. Shcheulin, T.S. Semenova, L.F. Koryakina, M.A. Petrova, A.E. Angervaks, A.I. Ryskin, *Opt. Spectrosc.*, **110** (2011) 617-623.

5. A.E. Angervaks, A.S. Shcheulin, A.I. Ryskin, P.P. Fedorov, R.V. Gainutdinov, *Appl. Surf. Sci.*, **267** (2013) 112-114.

6. V.M. Orera, R. Alkala, *Solid State Commun.*, **27** (1978) 1109-1112.

7. N.E. Korolev, I.Yu. Mokienko, A.E. Poletimov, A.S. Shcheulin, *Opt. Spektrosk.*, **70** (1991) 1030-1034 (in Russian).

8. A.S. Shcheulin, A.K. Kupchikov, A.E. Angervaks, A.I. Ryskin, *Opt. Spectrosc.*, **103** (2007) 651-654.

9. A.S. Shcheulin, A.V. Veniaminov, Yu.L. Korzinin, A.E. Angervaks, A.I. Ryskin, *Opt. Spectrosc.*, **103** (2007) 655-659.

10. A.V. Veniaminov, A.S. Shcheulin, A.E. Angervaks, A.I. Ryskin, J. Opt. Soc. Am. B, **29** (2012) 335-339.

11. A.S. Shcheulin, A.E. Angervaks, A.V. Veniaminov, V.V. Zakharov, A.I. Ryskin, *Opt. Spectrosc.*, **113** (2012) 638-642.

17:00 Poster Mo11

Optimization of bottom heater parameters at growth of large BGO crystals by conventional Czochralski method

Evgeniy Galenin[1], Alexander Kolesnikov[1], Oleg Sidletskiy[1], Kiril Mazaev[2], Vladimir Kalaev[2]

1. *Institute for Scintillation Materials NAS of Ukraine (ISMA), Lenina ave., 60, Kharkov 61001, Ukraine* **2.** *STR Group, Inc., Engels av. 27, P.O. Box 89, St-Petersburg 194156, Russian Federation*

e-mail: galenin@isma.kharkov.ua

There are two existing methods of production of large-size $Bi_4Ge_3O_{12}$ (BGO) single crystals. The biggest known crystals now are produced by the low-thermal gradient Czochralski technology (LTG) [1]. At the same time, the conventional Czochralski method (Cz) has some advantages over LTG, such as lower Pt consumption for crucibles, higher yield of crystalline material due to cylinder shape of grown ingots, easy implementation on production-run equipment [2]. Therefore, optimization of BGO growth technology by Cz method is a topic of continuous interest.

One of existing drawbacks of the Cz method decreasing the production yield is a relatively big volume of the melt remaining in the crucible after growth. This is caused by heat transfer conditions in growth setups with induction heating [3], namely non-uniform crucible heating and BGO melt opacity. As a result, most of heat is released in side crucible walls, and crystallization interface (CI) is convex to the melt to the colder bottom crucible wall. This leads to contact of CI with crucible bottom and impossibility to crystallize about 40 % of the melt.

The present work is focused on solving this problem using the installation of additional passive heater. This heater is a metal disk installed under the crucible [4]. The disk is heated by the same induction coil as the crucible. Additional heating from below provides a higher temperature along the interface between the melt and the bottom crucible

wall. This helps to create heat conditions when CI shape is nearly flat. This allows one to crystallize sufficiently bigger fraction of the melt and, at the same time, avoid crystallization inside the crucible leading to crucible deformation and lowering its lifespan. Definitely, the simplicity of technical implementation is a serious advantage of this approach. Contrariwise, heat power releasing from the lower heater is directly depends on power incoming to the induction coil, hence, independent control of lower heater power is impossible. To skip this drawback, the dimensions and material of lower heater ensuring flat CI during growth process are determined using numerical modeling of global heat transfer in the growth setup.

Main goals of the current study are: (i) to reveal trends characterizing an influence of geometrical and physical parameters of the bottom heater on heat conditions of the BGO crystal growth; (ii) to determine optimal configuration of the parameters of the bottom heater, which allows one to receive nearly flat crystallization front through all growth stages.

Modeling is carried out by the Finite-Volume method using a CGSim program package [5]. The problem was solved in 2D axisymetrical approach using a quasistationary approximation. Convection patterns in melt are determined on the base of Navier-Stockes equation for incompressible liquid using the Boussinesq approach with RANS turbulence model. The effects of thermal and forced convection, as well as Marangoni effect at free melt surface are accounted for. Spectral absorptivity was approximated by a three-band model radiation heat transfer in the crystal, calculated by the discrete ordinates method. Calculation of radiofrequency (RF) was based on solving Maxwell equations in quasistationary approach for linear, isotropic, and inhomogeneous media.

In particular, we have found the optimal electric conductivity of the bottom heater and the optimal diameter of the bottom heater. The computation results are in satisfactory agreement with experiment implementing the bottom heater for CI shape optimization at growth of BGO crystals with the diameter up to 80 mm by Cz method in crucibles with 96 mm inner diameter. The demonstrated approach can be used in optimization of Cz growth technology for other materials with opaque melt.

1.Yu.A. Borovlev, N.V. Ivannikova, V.N. Shlegel, Ya.V. Vasiliev, V.A. Gusev, J. Cryst. Growth, 229 (2001), pp. 305-311.

2. http://www.ezan.ac.ru/products/crystalgrowth/nika3/

3. K. Mazaev, V. Kalaev, E. Galenin, S. Tkachenko, O. Sidletskiy, J. Cryst. Growth, 311 (2009), Iss. 15, pp. 3933-3937.

4. V. Bondar, E. Galenin, Ia. Gerasymov, V. Nagornyak, O. Sidlestkiy, S. Tkachenko, Patent of Ukraine №88579, Oct. 26, 2009

5. http://www.str-soft.com/products/CGSim/

17:00 Poster Mo12

Evaluation of kinetic coefficient for 111 facet of Ge

Vladimir D. Golyshev, Svetlana V. Bykova

CrystalsNord (CRYST), Oktiabrskaya 6 21, Aleksandrov 601654, Russian Federation

e-mail: vladimir.golyshev@CrystalsNord.ru

The formation of faceted melt/crystal (m/c) interfaces takes place at crystal growth of many technologically important semiconductor materials. As is shown, for example in work [1, 2], the faceted interfaces must be morphologically more stable than nonfaceted ones as interfacial kinetics exerts a strong influence on the stability of the growing interface. Thus, crystal growth by the faceted mechanism enables to obtain perfect single crystals with higher dopant concentration than it is allowed by rough growth. However, theoretically and experimentally, the problem of facet stability at high dopant concentration is insufficiently investigated. To investigate this phenomenon more accurately it is necessary to know a kinetic dependence for facet at a high dopant concentration.

So, the aim of this work is to find the kinetic dependence $V = V(dT)$, where V is crystal growth rate, dT is supercooling of singular facet 111 of Ge. To obtain data on $V = V(dT)$ it is necessary to find dTi values that took place at different Vi values. The experimental data on dT were obtained from data on visualization of shape of m/c interface after etching longitudinal section of grown Ge crystal as follows. For a known value of the temperature gradient in the melt, *gradTm*, the value of the supercooling can be calculated from expression: $dT = \Delta \times gradTm$, where Δ is the measured distance between the central part of the facet and the central part of the melting temperature isotherm as shown in Fig. 1. This approach of dT finding is based on fact that supercooling is negligible on nonfacetted regions of the interface.

Ge crystals were grown by AHP technique [3, 4]. The AHP method gives possibility to use a one dimensional model of a heat transfer to obtain data on V and *gradTm*. Thus, a set of data on dTi and correspond it data on Vi were obtained. Ge crystals were grown at 111 direction in 2 inch diameter graphite crucible. Accuracy of crystallography orientation was 1 minute. Crystals were doped by Sb and it's concentration in the melt was in the range of 9×10^{18} - 2×10^{20} cm^{-3}. The dislocation density was in the range of 10^4 – 10^5/ cm^2. Crystal growth rate, at which the dT value was found, was in the range of 5 – 25 mm/hour. To make more a facet size the growth rate was increased and the temperature gradient was reduced before m/c interface marking. M/c interface marking was made by the AHP heater translation up to contact with the melt-crystal interface. After this procedure, the AHP heater was returned to its initial position and it was again fixed relative to the growth setup casing. The single crystal of Ge which was grown in this manner was cut into plates in the longitudinal direction. To visualize the melt-crystal interface and structure of a crystal, the Ge plate was etched by the method of anode etching in a 0.1 mole Na_2SO_3 per liter of H_2O.

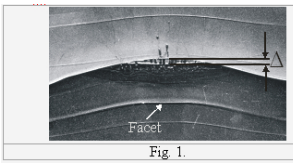

Fig. 1.

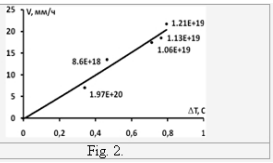

Fig. 2.

The obtained result on $V = V(dT)$ dependence is presented in Fig. 2. $V = V(dT)$ dependence has slightly squared relationship. This result corresponds to dislocations mechanisms of interfacial kinetic. One can see from Fig. 2 that as first approximation $V = V(dT)$ dependence is linear dependence and the kinetic coefficient, b^*, is constant for Sb concentration in the range of 9×10^{18} - 2×10^{20} cm^{-3} and the crystal growth rate in the range of 5 – 25 mm/hour. One can see that dT value is big enough in spite of big density of dislocations and it must be taken into consideration for crystal growth rate more then 25 mm/hour and at small temperature gradient.

1. Abbaschian, R.; Coriell, S.; Chernov, A. In Solidification1999;
2. Hofmeister, W. H., Rogers, J. R., Singh, et al., Eds.; TMS: Warrendale, PA, 1999;pp 219-228.
3. E. Balikci, A. Deal, R. Abbaschian, et al, Crystal Growth & Design, 2004, vol. 4, No 2, pp. 377-381.
4. S.V. Bykova, V.D. Golyshev, et al, Journal of Crystal Growth, 275 (2005) 229 - 236

17:00 Poster Mo13

The effect of pH on calcium carbonate polymorphs precipitated from aqueous solutions at 0°C

Yubin Hu[1], Gernot Nehrke[1], Mariëtte Wolthers[2,3], Gerhard Dieckmann[1], Dieter Wolf-Gladrow[1]

1. *Alfred Wegener Institute, Am Handelshafen 12, Bremerhaven 27570, Germany* **2.** *University College London, Department of Chemistry (UCL), Gordon Street, London WC1HOAJ, United Kingdom* **3.** *Department of Earth Sciences-Geochemistry, Utrecht University, 3508 TA, Utrecht 80021, Netherlands*

e-mail: Yubin.Hu@awi.de

Calcium carbonate ($CaCO_3$) has six different phases whose formation is affected strongly by precipitation conditions. Among them, pH is considered to be one of dominating factors controlling polymorphism during calcium carbonate precipitation. Furthermore, the Ca/CO_3 ratio in solution was recently shown to strongly affect $CaCO_3$ growth rate (e.g. Nehrke et al., 2007). However, the change of solution pH is at the same time associated with a change in hydrogen ion concentration (H^+) and the Ca/CO_3 ratio in solution, making it difficult to separate pH and solution stoichiometry effects. The objective of this study is to investigate whether the H^+ or Ca/CO_3 ratio has a control on calcium carbonate polymorphism.

Experiments were carried out at 0°C and two different pH conditions (pH = 12.6 and 9.0). Under each pH condition, different concentrations of $CaCl_2$ and $NaHCO_3$ were applied to achieve ratios of 1:1 and 10:1 for Ca/CO_3. $CaCl_2$ and $NaHCO_3$ solutions were pumped into different pH solutions with or without phosphate at different pumping rates. Results showed that, at high pH (pH = 12.6), only ikaite formed, independent of PO_4, pumping rate or the ratio of Ca/CO_3. At low pH (pH = 9.0), the precipitate was vaterite in the absence of PO_4 and ikiate in the presence of PO_4 regardless of the ratio of Ca/CO_3. These results indicate that at low temperature, the H^+ concentration determined which polymorph was precipitated (ikaite or vaterite) rather than Ca/CO_3 ratio.

17:00 Poster Mo14

Incorporation of divalent cations into surface sites and clusters of calcium carbonate

Jun Kawano[1], Hiroshi Sakuma[2], Takaya Nagai[3]

1. *Creative Research Institution, Hokkaido University, N21 W10, Kita-ku, Sapporo 001-0021, Japan* **2.** *Tokyo Institute of Technology, Tokyo 152-8551, Japan* **3.** *Hokkaido University, Sapporo 060-0810, Japan*

e-mail: j-kawano@mail.sci.hokudai.ac.jp

[Introduction]

Formation process of calcium carbonate polymorphs, calcite, aragonite and vaterite has been extensively investigated because of its importance in both geological and biological environments. In order to account for the formation of a particular polymorph, impurity effect has been proposed as controlling phenomena by many researchers, however incorporation mechanism of these impurities during crystal growth is poorly understood.

Here, we focused on the effect of alkaline earth cations (M^{2+}) other than Ca^{2+} as the impurities. In general, smaller divalent cations than Ca^{2+}, like Mg^{2+}, cannot form solid solution with aragonite, while larger cations like Ba^{2+} cannot be incorporated into the structure of calcite. However, the structure of a crystal surface or small cluster as an initial stage of crystal growth can be different from the bulk crystal because of its flexibility, and it can play an important role as the site for incorporation of ions which is unstable in the bulk structure and in the subsequent crystal growth. Therefore, in the present study, the stability of alkaline earth cation (1) on the surface and (2) in the cluster forming in an early stage of nucleation was investigated by the first-principles calculations based on the density functional theory, and the impurity effects on the formation of polymorphs were discussed.

[Mg^{2+} at a surface]

Recently, it has been pointed out that the surface energy difference among polymorphs could determine their stability field [1], so that it becomes more important to analyze in detail their surface structures and the incorporation process of ions and molecules into the surfaces. Here we focused on the case in which Mg^{2+} ion substitutes for Ca^{2+} site of aragonite (001) surface as an impurity. While Mg^{2+} is unstable in the nine-fold cation positions of aragonite and can hardly be incorporated into the bulk aragonite crystal, it is expected to be substituted for Ca^{2+} site at the surface. Our simulation results show that Mg^{2+} can be incorporated into the Ca^{2+} sites at the surface with lower substitution energy than that in the bulk. Furthermore, Mg^{2+} on the aragonite surface considerably affects the surface structure, especially on the arrangement of CO_3 groups, indicating that the presence of Mg^{2+} can change the surface stability of aragonite.

[Mg^{2+} in a cluster]

According to the concept of prenucleation cluster (e.g. Gebauer et al. [2]), stable small clusters of calcium carbonate form even in an undersaturated solution and play an important role for the formation of polymorphs. Tribello et al. [3] showed by using molecular dynamics simulations that, at an early stage of calcium carbonate growth, isolated ions disappear very quickly and charged clusters are rarely observed. It means that, Ca^{2+}/CO_3^{2-} pair forms first, and then larger clusters appear as the aggregation of these pairs.

Therefore, in order to understand the effect of impurities like Mg^{2+} on an early stage of $CaCO_3$ growth, we should discuss the incorporation process of these ions during the formation of Ca^{2+}/CO_3^{2-} pairs and their aggregation. In the present study, we calculated energies of (i) primary hydration shells of M^{2+}, (ii) M^{2+}/CO_3^{2-} pairs, and (iii) clusters including two M^{2+}/CO_3^{2-} pairs, and determined the stable arrangement of these clusters by the first-principles calculations.

The calculation results show that Mg^{2+} is easier to be incorporated into a small cluster and prefers to be at the center of the cluster, while the hydration energy of Mg^{2+} is higher than that of other divalent cations. This indicates that Mg^{2+} is difficult to be released from hydration shell, however, once released, it is easy to be incorporated into the clusters. Considering that thermal energy is needed to release Mg^{2+} ion from hydration shell, the effect of Mg^{2+} is expected to be more striking with increasing temperature.

[1] A. Navrotsky, PNAS 101 (2004) 12096, [2] D. Gebauer et al., Science 322 (2008) 1819, [3] G.A. Tribello et al., J. Phys. Chem.B 113 (2009) 11680.

17:00 Poster Mo15

Density Functional Theory (DFT) study of hydrogen on GaN (0001) surface

Pawel Kempisty[1], Pawel Strak[1], Stanisław Krukowski[1,2]

1. *Polish Academy of Sciences, Institute of High Pressure Physics (UNIPRESS), Sokolowska 29/37, Warszawa 01-142, Poland*
2. *University of Warsaw, Interdisciplinary Centre for Mathematical and Computational Modelling (ICM), Pawinskiego 5a, Warsaw 02-106, Poland*

e-mail: kempes@unipress.waw.pl

We present ab initio study within the framework of Density Functional Theory (DFT) on the behavior of hydrogen on the GaN (0001) surface depending on the surface coverage and the type of semiconductor doping. We show that the H_2 molecules are dissociatively adsorbed on bare GaN(0001) surface with adsorption energy in excess of 2 eV. The adsorption energy is determined by energy change of gallium surface state with respect to energy of bands states at the surface. For bare surface the Fermi level is pinned on surface states equidistant from the top of valence band which is bent at the surface respectively in opposite directions for n-GaN and p-GaN. Therefore, in this case the energy of adsorption does not change significantly and the small differences are due to the effect of the charge localization by different electric field. When surface coverage with hydrogen is about 75% of the monolayer the pinning on surface states disappears. In this situation the type of semiconductor and related Fermi level position is extremely important. We present the dependence of the adsorption energy as a function of hydrogen coverage, which shows a step change in value by about 2 eV when material was changing from n-type to p-type. For the surface coverage close to full monolayer the Fermi level becomes pinned again but in this case at the top of the valence band. Energy shift of the states associated with the adatoms relative to the Fermi level is also independent of the type of doping. Our results are consistent with the results of experiments of Ambacher et al. [1] and Wampler and Myers [2] and help to explain the differences between them.

[1] O. Ambacher et al., Phys. Status Solidi A 159, 105 (1997).
[2] W. Wampler and S. Myers, J. Appl. Phys. 94, 5682 (2003).

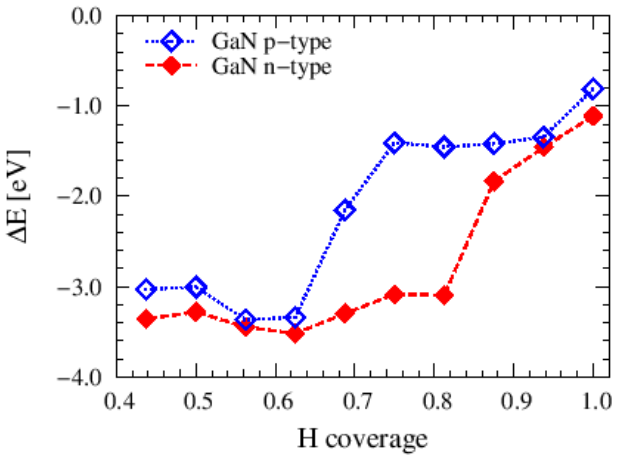

Adsorption energy of single H atom in function of GaN(0001) surface coverage for different type of GaN doping.

17:00 Poster Mo16

Adsorption of gallium on GaN(0001) surface in ammonia rich conditions - Density Functional Theory (DFT) study

Pawel Kempisty[1], Pawel Strak[1], Stanisław Krukowski[1,2]

1. *Polish Academy of Sciences, Institute of High Pressure Physics (UNIPRESS), Sokolowska 29/37, Warszawa 01-142, Poland*
2. *University of Warsaw, Interdisciplinary Centre for Mathematical and Computational Modelling (ICM), Pawinskiego 5a, Warsaw 02-106, Poland*

e-mail: kempes@unipress.waw.pl

Density Functional Theory (DFT) calculations were used to determine the adsorption energy of GaCl molecule on the GaN(0001) surface covered with mixture of NH_3 admolecules and NH_2 radicals. This corresponds to physical conditions during GaN growth by hydride vapor phase epitaxy method (HVPE). The average content of ammonia in the mixture of admolecules have been estimated to be in the range 25-32 percent. We present a series of adsorption curves for surface with various NH_3/NH_2 ratio. We show that the adsorption energy of GaCl molecule strongly depends on the composition of this mixture. Gallium chloride is strongly attached (with energy of about 6 eV) when the surface is covered mostly by NH_2 radicals. For comparison, we also show the adsorption of InCl molecule on the same surface. With the increase of ammonia content the adsorption energy of both species decreases significantly. Termination of the InCl adsorption occurs at lower NH_3/NH_2 ratio than termination of GaCl adsorption. That suggests the above factor contributing to the fact that InGaN growth requires different conditions than growth of pure GaN.

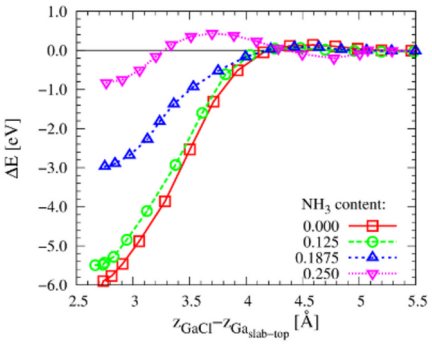

Adsorption energy of GaCl molecule on GaN(0001) surface covered with mixture of NH_3/NH_2 admolecules.

17:00 Poster Mo17

Quantitative analysis of morphology of polycrystalline precipitate received in temperature ranges of growth rate anomalies

Liubov A. Khazikova[1], Sergey N. Bocharov[2]

1. *Saint-Petersburg State University, Saint-Petersburg, Russian Federation* **2.** *Saint-Petersburg State University (SPBSU), 7/9 University emb., S.Petersburg 199034, Russian Federation*

e-mail: lubovkhazikova@gmail.com

Kinetic anomalies were discovered in 1967 and were found in all detailed measurements in randomly selected systems [3]. Anomalies represent the temperature ranges in which the growth rate undergoes sharp changes. It was subsequently shown that anomalies have a signi-

ficant influence on kinetic dependent properties of crystals such as chemical composition [1] and morphology [2]. Influence of kinetic anomalies on crystals morphology was investigated only for single crystals and at quality level. So the aim of this work is study of polycrystalline deposit morphology in the temperature range of kinetic anomalies.

Investigation of polycrystalline precipitate morphology in dependence on temperature was performed at copper electrocrystallization as example. The experiments were carried out in a temperature range of 46.0-51.0 ° C in solution of copper sulphate with a fixed concentration 15 g of the salt per 100 g of water. Kinetic curve for this temperature range and concentration was obtained earlier and it reproduces kinetic curve known from the reference [4]. Electrochemical copper precipitate obtained at different temperatures has been studied ex-situ by atomic force microscopy with quantitative analysis of received AFM images. Quantitative analysis consisted in statistical processing of images of the surface morphology in the NOVA program. We took the following characteristics as the main parameters that characterize morphology of the deposit: average roughness, scale height, ten point height, deviation from the mean height.

Statistical characteristics of copper precipitate morphology in dependence on temperature vary non monotonically. These variations have the same temperature positions but intensities are different that what we relate to the method of curves normalization. Quantitative characteristics of copper precipitate morphology reproduce kinetic curve of copper electrocrystallization in dependence on temperature. It confirms the data on kinetic anomalies influence on crystal morphology obtained for monocrystals case.

References:

[1] A.A. Chernov, V.V. Sipyagin, Current Topics in Materials Science, 5, p. 281 (1980).

[2] S. N. Bocharov, P. Gille, A. E. Glikin, Cryst. Res. Technol., 44, 1, p. 13 (2009).

[3]A.E. Glikin, S.N. Bocharov, E.V. Kir'yanova, V.V. Sipyagin, Zap. Vseross. Mineral. O–va, No. 2, p.99 (2003) [in Russian].

[4] S.N. Bocharov, A.E. Glikin, Crystallography Reports, Vol. 53, 1, p. 147 (2008).

17:00 Poster Mo18

Phase-field simulation of abnormal grain growth

Seong Gyoon Kim

Kunsan National University, Kunsan 573-701, Korea, South

e-mail: sgkim@kunsan.ac.kr

Grain growth in polycrystalline materials can proceed in two different modes: normal or abnormal mode. In the normal grain growth, most grain boundaries (GBs) migrate smoothly as time goes on. In the abnormal grain growth, some grains grow preferentially at the expense of their neighbor grains, whereas most boundaries between the matrix grains remain almost immobile by the pinning effect from the dispersed particles or grain boundary segregation. Notable among the characteristics of the AGG is the jerky motion (go-and-stop motion) of the grain boundaries surrounding the abnormally growing grains. This jerky motion has clearly been observed both in the in-situ and ex-situ experiments, and seems to be an natural consequence of the discontinuous interaction between GBs and the pinning particles (and/or segregated atoms). In this study we investigate the detailed process of the jerky motions of GBs in AGG by using a phase-field simulation. We show that the AGG takes place in a chain reaction like a series of collapsing dominoes. The jerky motion of GBs appears to be not a subsidiary result from AGG, but closely related with a key process in the fundamental mechanism of AGG

17:00 Poster Mo19

The study of temperature equilibrium of KDP, ADP crystals and solutions from their magnetic treatment

Sergey I. Kovalyov, Alexey E. Smirnov, Alexey E. Voloshin

A.V.Shubnikov Institute of Crystallography The Russian Academy of Sciences, Moscow, Russian Federation

e-mail: skovalev@crys.ras.ru

The effect of magnetic treatment of KDP and ADP crystals and solutions on their equilibrium temperature has been revealed and studied. The change in the temperature reaches a maximum immediately after the magnetization. Then, the effect decreases monotonically, and the equilibrium temperature approaches its equilibrium value for 5 h. It has been found that the observed decrease in the solubility depends on the impurity concentration, and it is maximum in magnetically treated KDP crystals with a chromium impurity; then, it decreases in the series: KDP crystal, KDP-ADP crystals in a KDP-ADP solution, KDP crystal in KDP-ADP solution, and KDP solution. For all five systems under study, the relaxation times have been determined. It has been revealed that the effect rapidly increases and reaches saturation at B = 0.02 T. The energy effects in the crystals and solutions have been estimated.

17:00 Poster Mo20

Kinetics of crystal growth of vivianite, $Fe_3(PO_4)_2,8H_2O$, from solution at 25, 35 and 45ºC

Hans Erik Lundager Madsen, Hans Christian Bruun Hansen

Faculty of Science (SCIENCE), Thorvaldsensvej 40, Frederiksberg C 1871, Denmark

e-mail: helm@life.ku.dk

Crystallization of the iron phosphate mineral vivianite, $Fe_3(PO_4)_2,8H_2O$, has been studied by simple precipitation from solutions of Mohr's salt, $Fe(NH_4)_2(SO_4)_2,6H_2O$, and a mixture of ammonium dihydrogen and monohydrogen phosphate, both 0.05 M. The vials were closed to the air, so that only initially dissolved oxygen was present. Initial pH of the solutions ranged from 4.5 to 7. Crystals of vivianite, which belong to the monoclinic prismatic class 2/m, were tabular with {010} as the dominating form and normally showed overgrowth of smaller crystals. The largest dimension was about 0.1 mm. At 25°C aggregates were common, but at higher temperatures single crystals were more frequent. In spite of high affinity towards oxidation, vivianite crystals were dominating in most precipitates, presumably because dissolved oxygen is consumed in the initial stage of the process as a result of fast precipitation of much less soluble, nanocrystalline strengite, $FePO_4,2H_2O$, following oxidation of iron(II) to iron(III). Crystal growth kinetics was determined from pH recording on solutions during 12 hours, and precipitate was examined in the microscope the following day. Results could be interpreted as spiral growth at low supersaturation and a combination of this mechanism with surface-nucleation growth at higher supersaturation. Edge free energies λ deduced from analyses of the latter mechanism did not show any significant dependence on temperature; most often they agreed with $\lambda = 27.4\pm0.5$ or 36.0 ± 0.4 pJ/m. Two experiments at 25ºC yielded values from the initial stage of the process as high as $\lambda = 80.4\pm4.5$ pJ/m. An abrupt decrease of slope of the graphs of growth rate versus supersaturation to a value in the usual range followed this stage. A few

experiments showed one or two pronounced minima in the graphs of growth rate versus supersaturation. This may be interpreted in terms of the Cabrera-Vermilyea theory of crystal growth inhibition, the inhibitor being most likely a minute amount of iron(III) from redissolved strengite.

17:00 Poster Mo21

Domain competition in deposition growth

Kenyu Osada[1], Hiroyasu Katsuno[1], Toshiharu Irisawa[1], Shintaro Suzuki[2], Yukio Saito[2]

1. *Gakushuin University Computer Center, 1-5-1 Mejiro Toshima-ku, Tokyo 171-8588, Japan* **2.** *Keio University, Faculty of Science and Technology (Keio), 3-14-1 Hiyoshi, Kouhokuku, Yokohama 2238522, Japan*

e-mail: 12141001@gakushuin.ac.jp

In heteroepitaxial growth, deposited adatoms start solidification by contacting with a substrate. Due to misfit or misorientations between the adsorbate and substrate, crystals started to grow from different contact points may be incoherent each other. We consider an extreme case that each contact point initiates separate crystal domain, and study their competition during deposition growth by kinetic Monte Carlo simulations of a lattice-gas system.
In a ballistic deposition (BD) model, a deposited adatom freezes at a position of a first contact with substrate or already crystallized adatoms. The number density of domains ρ decreases as the height h of the BD aggregate increases in a power law as $\rho \propto h^{-\gamma}$. The value of the exponent is $\gamma \cong 0.67$ in a two-dimensional BD model, and $\gamma \cong 1.1$ in a three-dimensional BD. The results agree with theoretical estimation that the exponent γ is inversely proportional to the dynamical exponent z of the d-dimensional BD growth front as $\gamma = (d-1)/z$. We study further the effect of surface diffusion on the exponent γ.

17:00 Poster Mo22

Simplified numerical approach for estimation of effective segregation coefficient at the melt/crystal interface

Anatoly I. Prostomolotov[1], Nataliya A. Verezub[2], Alexey E. Voloshin[3]

1. *Institute for Problems in Mechanics of RAS (IPMECH), Vernadskogo prospect 101, bl. 1, Moscow 119526, Russian Federation* **2.** *Institute for Problems in Mechanics RAS (IPMECH), Vernadskii prospect 101, bl. 1, Moscow 119526, Russian Federation* **3.** *Shubnikiv Institut of crystallograhy Russian Academy of Sciences (ICRAS), Leninskii pr. 59, Moscow 119333, Russian Federation*

e-mail: prosto@ipmnet.ru

The effective segregation coefficient – K_{eff} is an important parameter for the analysis of a dopant inhomogeneity in crystals grown from a melt. Its value depends on a structure and intensity of a melt flow, which substantially affect on a dopant flux from a melt into a crystal.

The estimations of K_{eff} value were done in many publications on the basis of two main approaches. The former of these approaches is quite simple, and therefore it is the most widely used in technological practice [1]. Its basis is the analytical expressions for calculation of K_{eff}, which is determined by the value of flow velocity near the melt/crystal interface, according to some analytical hydrodynamic formulas [2-3]. The second approach is based on the complete numerical simulation of crystallization process, requiring specialized program codes, large computational cost and high user qualification [4-6].

This work describes an intermediate approach for Bridgman GaSb(Te) crystal growth in microgravity [7]. For its implementation the numerical modeling is required, too. But it is much less costly than in second case. Its basis is a simplified model of convective heat and mass transfer in a melt on the assumption of a flat moving melt/crystal interface with taking into account of dopant flux from a melt into a crystal [8].

The crystallization process is considered for the constant velocity of the melt/crystal interface V_S in a flat melt layer of thickness D and length L at gravitational field g for following thermal conditions: T_S = 985 K (the melting point) and different values of T_w = 996 , 1057 K (Fig. 1), which determine the variation of longitudinal temperature gradient.

The equations of Navier-Stokes-Boussinesq and heat- and mass transfer in a melt may be written in the coordinate system associated with moving melt/crystal interface [8]. By solution of this system the velocity vector V, pressure P, temperature T, the dopant concentration C depending on the spatial coordinates and time are determined.

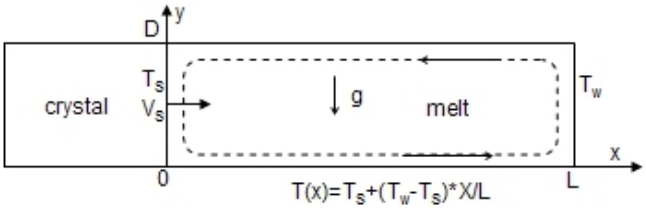

Fig. 1. Scheme of the simplified model: thermal boundary conditions, V_S − velocity of the melt/crystal interface, and the direction of melt flow (dashed line).

On the boundaries of a melt: V = 0 and T is defined as shown in Fig. 1. The initial concentration of dopant in a melt: C = Co. The boundary conditions for dopant concentration are following: $Dgrad(C) = (1 - K_o)V_S C$ – at the melt/crystal interface, and C = 0 – for all other boundaries in the case of a continuous crystallization for a whole ingot length.

For a GaSb (Te) melt the physical parameters were following: kinematic viscosity visc=0.0032 cm^2/s, thermal conductivity $1.02*10^6$ erg/cmKs, heat capacity $3.3*10^6$ erg/gK, thermal expansion coefficient $b=9.6*10^{-5}$ 1/K, tellurium diffusion coefficient $D = 5*10^{-5}$ cm^2/s, and equilibrium segregation coefficient $K_o = 0.37$. Crystallization rate was constant: $V_S = 3*10^{-4}$ cm/s, and microgravity was varied: $g/g_o = 1.6*10^{-5} - 2.2*10^{-3}$; $g_o = 980$ cm/s^2.

Desired value of the effective segregation coefficient is calculated by following formula: $K_{eff} = K_o\langle C\rangle/C_o$, where <C> is an average dopant concentration at the melt/crystal interface.

In this work the more simplified variant of the model was applied, which corresponds to the calculation of a discrete stage of crystallization (D = 1.5 cm, L = 4 cm), and the condition $C = C_o$ at x = L (Fig. 1). The parametric calculations were carried out with the use of widespread program code AnsysFluent [9], which was supplemented by the author subroutines in C++ taking into account of crystallization model [8].

Numerical results have been compared with those of analytical models [2,3] and data of semianalytic model [8], in which the equation for dopant concentration is solved numerically at the analytical velocity field in a melt:

$V_x(x,y) = (Gr/6)[1/4 - (y - 1/2)^2](y - 1/2)\{1 - e\text{-}\alpha x[\cos(\beta x) + (\alpha/\beta)\sin(\beta x)]\}$,

$V_y(x,y) = (Gr/24)[1/4 - (y - 1/2)^2]e\text{-}\alpha x(\alpha 2/\beta + \beta)\sin(\beta x)$.

Here: α=4.15, β=2.286, and Grashof's number $Gr=gb[(T_W-T_S)/L]D^4/visc^2$.

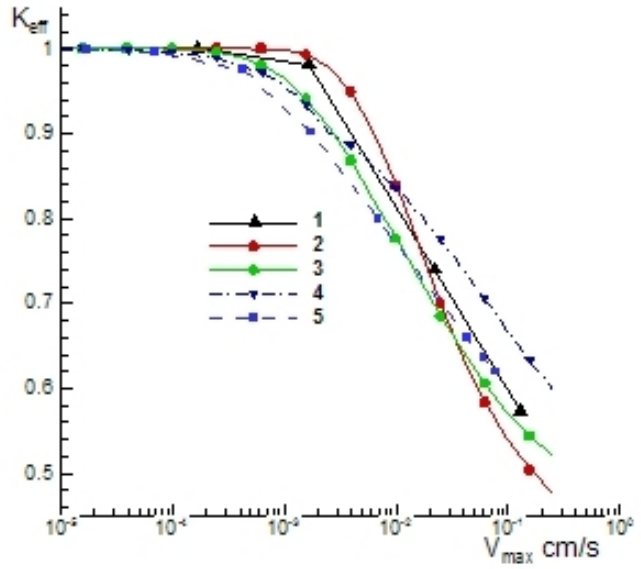

Fig. 2. The dependences of effective segregation coefficient K_{eff} upon maximum velocity V_{max} in a melt: 1 – the simplified model, 2 and 3 – the estimations by [2] with different formulas for the diffusion layer thickness, 4, 5 – the estimations by [3] and [8] respectively.

Fig. 2 illustrates the dependences of K_{eff} upon maximum velocity V_{max} in a melt as calculated by simplified model – 1, in accordance with [2] for the different formulas of the diffusion layer thickness – 2, 3, by formula [3] – 4, and with application of the analytical hydrodynamic model [8] – 5. May be noted the discrepancies of various analytical estimations of K_{eff} depending upon V_{max}. It is explained by an ambiguity at the choice of the formula for V_{max} in [2,3] and the approximate velocity field in [8], which corresponds to the thermal convection in a semi-infinite layer. By means of simplified approach (see 1 in Fig. 2) the best analytical model - 2 of [2] has been selected for the analysis of measured tellurium concentration [1] in GaSb crystal, grown in microgravity conditions [7].

ACKNOWLEDGMENTS

We thank the Russian Foundation for Basic Research for the support of projects: 11-08-00966, 12-02-01126.

References

[1] Voloshin A.E., Nishinaga T., Ge P. et al. Te distribution in space grown GaSb // J. Cryst. Growth. 2002. V. 234. P. 12-24.

[2] Burton J.A., Prim R.C., Slichter W.P. The distribution of solute in crystals grown from the melt. Part I. Theoretical // J. Chem. Phys. 1953. V. 21. N 11. P.1987-1991.

[3] Ostrogorsky A.G., Muller G. A model of effective segregation coefficient, accounting for convection in the solute layer at the growth interface // J. Cryst. Growth. 1992. V. 121. P. 587-598.

[4] Lan C.W., Lee I.F., Yeh B.C. Three-dimensional analysis of flow and segregation in vertical Bridgman crystal growth under axial and transversal magnetic fields // J. Cryst. Growth. 2003. V. 254. P. 503–515.

[5] Verezub N.A., Marchenko M.P., Nutsubidze M.N., Prostomolotov A.I. Inluence of convective

heat transfer on crystal-melt interface for Stockbarger method with step heater // Growth of Crystals. 1996. V. 20. New York: Consultants Bureau. P. 129-138.

[6] Strelov V.I., Zakharov B.G., Sidorov V.S. et al. Mathematical Modeling and Experimental Investigation of the Effect of Temperature Gradients on Crystallization Processes under Terrestrial and Space Conditions // Crystallography Reports. 2005. V. 50. N 3. P. 490-498.

[7]Ge P., Nishinaga T., Huo C. et al. Recrystallization of GaSb under microgravity during China returnable satellite No. 14 mission // Microgravity Q. 1993.V.3. N 2-4. P. 161-165.

[8] Polezhaev V.I., Bune A.V., Verezub N.A. et al. Mathematical Modeling of Convective Heat and Mass Transfer on the Basis of Navier–Stokes Equations. Moscow: Nauka. 1987. 272 p. [in Russian].

[9] ANSYS FLUENT Tutorial Guide: Release 14.0, ANSYS Inc. 2011.

17:00 Poster Mo23

Applications of synthonic Engineering Tools in Predicting Crystal Morphology as a function of Growth Environments

Kevin J. Roberts[1], Robert B. Hammond[1], Vasuki Ramachandran[1], Jonathan Pickering[1], Majeed Soufian[1], Thai H. Nguyen[1], Klimentina Pencheva[2], Robert Docherty[2]

1. *Institute of Particles Science and Engineering (IPSE), Clarendom Road, Leeds LS29JT, United Kingdom* **2.** *Pfizer, Sandwich CT13 9NJ, United Kingdom*

e-mail: v.ramachandran@leeds.ac.uk

There is a critical need in industry to get a desired morphology of a crystal in order to have control in downstream processing or flow properties and product yield. All crystalline products produce molecular analogues from side reactions and/or processing. These molecular analogues as additives/impurities and solvents may have an effect on the growth of the crystals leading to different physical and chemical properties which will in turn have an effect on the formulation behaviour. Therefore, the understanding of these crystal growth modifiers and their interactions with the host is critical in manipulating the host system to obtain a morphology that is most suitable for product formulation and processing requirements. VisualHABIT is a molecular modelling tool[1-4] routinely used to understand, predict and manipulate crystal growth morphology but with an added user-friendly graphical user interface. The morphology prediction is on the basis that the surface attachment energy of a particular crystal face is assumed to be proportional its relative growth. The attachment energy is the contribution from all the interactions that are normal to the growth surface (hkl). Thus, a quantitative analysis of the intermolecular forces (synthons) involved in the growth processes is provided by a systematic search approach within VisualHABIT. This knowledge of the strengths and contributions of intrinsic synthons (solute/solute) and extrinsic synthons (solute/solvent or solute/crystal growth modifiers) to the growth process enables the understanding and prediction of the effects of the crystallisation environment on crystal morphology.

This research was carried out as part of an EPSRC follow-on grant and it provides a molecular level understanding of industrial applications through case study examples. These case studies include the effects of different solvents on the morphology of an active pharmaceutical ingredient, solvent effect on the growth morphology of an ester, comparison of the effects of solvents on the growth morphology of hydrates and anhydrates and the effects of solvents on the crystal morphology of benzophenone.

References

1. G. Clydesdale, K. J. Roberts and D. R, *Journal of Crystal Growth*, 1996, **166**, 6.

2. G. Clydesdale, T. G. B, W. E. M, K. J. Roberts, M. P and R. Docherty, *Cryst. Growth and Des*, 2005, **5**, 9.

3. R. B. Hammond, K. Pencheva and K. J. Roberts, *Crystal Growth & Design*, 2006, **6**, 1324-1334.

4. R. B. Hammond, K. Pencheva, V. Ramachandran and K. J. Roberts, *Crystal Growth & Design*, 2007, **7**, 1571-1574.

17:00 Poster Mo24

Conformational Analysis of Para Aminobenzoic-Acid Using Gas-Phase and Solvent Continuum Calculations of Single Molecules and Clusters

Dimitrios Toroz, Ian Rosbottom, Robert B. Hammond, Kevin J. Roberts

University of Leeds (SPEME), Leeds LS2-9JT, United Kingdom

e-mail: pmir@leeds.ac.uk

The pre-ordering of molecules in the solution state is not fully understood with respect to the formation of crystal nuclei. Here we investigate the importance of the conformational stability in nucleation and subsequent growth of the two polymorphic forms of para-amino benzoic acid (PABA) and further to the examination of molecular pre-ordering of clusters in the solution state. Additionally solvent continuum calculations have proven effective in predicting solute-solvent interactions without the need of computationally expensive resources.

PABA is an enantiotropic system which has two known forms, α stable above 13.8C and β stable below this transition temperature. However crystallization experiments above or below the transition temperature almost always yield the α polymorph. Conformational analysis was performed for the single molecule of PABA in the gas phase with respect to the conformational preference in the crystal structure based on a hierarchical selection scheme using electronic structure theory methods. The conformational analysis showed that the β monomer is the most stable conformer which is a result of the pyramidal formation of the amino functional group of the β monomer compared to the planar conformation of the amino group of the α. Thus a scan of the dihedral angle that defines the amino group of PABA was explored to probe a potential energy barrier between the two polymorphs.

We then model the crystallization process through fundamental building blocks of increasing complexity (monomers, dimers, tetramer, octamers etc) to probe the transition state nucleation pathway from solvated molecules to their directed assembly at the crystal/solution interface into the solid state. All the building blocks were optimized within the COSMO solvent continuum model and the statistical thermodynamics COSMO-RS method was applied.

In agreement with the conformational analysis, the COSMO calculations showed that the β monomer is the most favoured conformer in solution. Comparison of dimers suggests that different building blocks favour different polymorphs in solution. When carboxylic acid dimers are present (which are only present in the α structure) these clusters are always favoured in solution, whereas alternate building blocks favour β beta in some solvents. Comparison of small clusters (up to 8 molecules) showed favourability to the α polymorph reflecting experimental data.

17:00 Poster Mo25

Hydrodynamical aspects of floating zone silicon crystal growth process

Kirils Surovovs, Andrejs Sabanskis, Andris Muiznieks

Faculty of Physics and Mathematics, University of Latvia, Zellu Street 8, Riga LV-1002, Latvia

e-mail: ks10172@lu.lv

Introduction

Although Floating Zone (FZ) process is widely known and has been developed for many years, it is necessary to improve numerical models of it. Computational resources allow considering many physical aspects of a system, for example, hydrodynamical (HD) processes in liquid silicon. In the present work HD approach is used for two purposes: obtaining more precise shape of phase boundaries and calculating radial resistivity profiles from dopant concentration field in melt. This allows to investigate influence of surface tension γ and its temperature coefficient $M = \partial\gamma/\partial T$ (i.e., Marangoni coefficient) on FZ process. It is essential for better understanding of modelling nuances because of Marangoni coefficient's strong dependence on oxygen content in atmosphere.

Description of the modelling software

The most important programs, which were used in the present study, are:

- *FZone*. This is a program for 2D axisymmetric modelling of FZ crystal growth. It performs iteratively coupled calculations of temperature field (HD in melt can be included) and thermal radiation (considering all surfaces as optically gray). High frequency 3D electromagnetic field, that induces current in thin silicon skin layer, is azimuthally averaged and then taken into account as a heat source distribution [1].
- *FZSiFOAM*. This is a program for 3D HD calculations in melt, based on *OpenFOAM* code library. 3D finite volume mesh is created on the base of shape of phase boundaries, which were obtained via *FZone*. *FZSiFOAM* considers non-stationary, incompressible, laminar, buoyancy driven flow; with Marangoni and EM tangential surface stresses. Dopant concentration, melt temperature and pressure fields are considered as well [2].

Results of the study

As an example characteristic 4" FZ system from ICG, Berlin is used. Crystal pulling rate is 3.4 mm/min and zone height is 34.87 mm. The current frequency was reduced from 3 MHz to 2.2 and 1.6 MHz in order to compare calculation results with experimental results [3]. Realistic shape of phase boundaries can be obtained with Marangoni coefficient equal to $-1.6 \cdot 10^{-4}$ N/(m·K) (see Fig. 1).

Then, it was investigated how does M influence radial resistivity distribution in single crystal. Wide range of M was examined – from 0.75 to $12 \cdot 10^{-4}$ N/(m·K), that correspond to strong variations of oxygen concentration [4]. At last, averaged resistivity profiles were obtained and compared with experimental data (few of them are shown in Fig. 2).

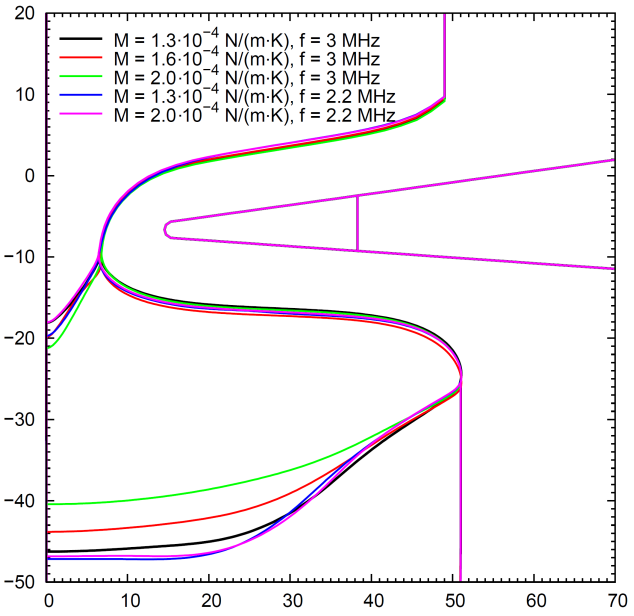

Figure 1. Shapes of phase boundaries obtained for 4" ICG system via *FZone*, using different values of Marangoni coefficient and inductor current frequency.

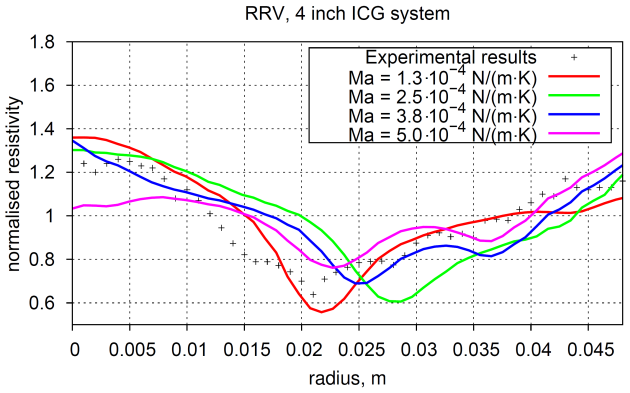

Figure 2. Averaged in time radial resistivity profiles. They are obtained from dopant concentration distribution on crystallization interface.

Acknowledgements

The present work is carried out at the University of Latvia and has been supported by the European Regional Development Fund, project contract No. 2011/0245/ 2DP/2.1.1.1.0/10/APIA/VIAA/114 and 2011/0002/2DP/2.1.1.1.0/10/APIA/VIAA/085.

References

[1] G. Ratnieks, A. Muiznieks, A. Muhlbauer, *Modelling of phase boundaries for large industrial FZ silicon crystal growth with the needle-eye technique*, JCG, 255, 227-240 (2003)
[2] A. Rudevics, K. Lacis, A. Muiznieks, N. Jekabsons, B. Nacke, *Using of open source code library OpenFOAM for 3D magnetohydrodynamic calculations in semiconductor crystal growth technologies*, Modelling for Electromagnetic Processing (2008)
[3] H.-J. Rost, R.Menzel, A.Luedge, H.Riemann, *Float-Zone silicon crystal growth at reduced RF frequencies*, JCG, 360, 43–46 (2012)
[4] Z. F. Yuan, K. Mukai, W. L. Huang, *Surface tension and its temperature coefficient of molten silicon at different oxygen potentials*, Langmuir, 18(6):2054-2062 (2002)

17:00 Poster Mo26

Time Dependency of Segregation in Numerical Simulation of Solution Growth

Hiromoto Susawa

Home, Aichi 489-0888, Japan

e-mail: automobile_21@yahoo.co.jp

Nomenclature

This abstract does not use superscript and subscript for symbols due to a printing reason. Then, some symbols deviate from the conventional nomenclature.

The presentation uses the conventional nomenclature, e.g., X_M^{s*}.

BM ($YM - YM0$) / $YM0$ (-)
c the growth time such that $e1(x, t) < o1(x, t)$ when $t < c$ (s)
DL, DM diffusion coefficients for component L, M in liquid solution
$e1$ the relative discretization error of pL and pM (-)
$e1(x, t)$ $e1$ at x and t (-)
h the length of liquid solution in the z direction (m)
L, M the most and less affected components by fluid flow
NL ($XL - XL0$) / ($XLb - XL0$) (-)
$NL(x, z, t)$, $NM(x, z, t)$ NL and NM at x, z, and t (-)
NM ($XM - XM0$) / ($XMb - XM0$) (-)
$o1$ the tolerance of $e1$ (-)
$o1(x, t)$ $o1$ at x and t (-)
pL, pM $\partial XL / \partial z$, $\partial XM / \partial z$ at growth interface (m^{-1})
r ratio of volume per unit atom in the liquid to that in the solid
sqrt(ξ) the square root of ξ (the square root of the unit of ξ)
t a growth time (s)
XL, XM mole fractions of component L, M in liquid phase
$XL(x, z, t)$, $XM(x, z, t)$ XL, XM at x, z, and t
$XL0$, $XM0$ XL, XM on growth interface when growth has just started
XLb, XMb XL, XM just before growth
YL, YM mole fractions of component L, M in solid phase
$YL0$, $YM0$ YL, YM when growth has just started
Δzd the mesh size in the z direction to solve the convection-diffusion equations of solutes (m)
δL, δM the boundary layer thicknesses of XL, XM (m)
κ a dimensionless parameter characterizing Δzd (-)

1. Introduction

We have understood the main behavior of computed results on segregation in numerical simulation of solution growth with fluid flow at the 7th Int. Workshop Model. Cyst. Growth [1]. The present presentation applies that discussion to understand changes in segregation with time. The time dependency had been showed in the 16th Int. Conf. Cryst. Growth [2]. That presentation was comprehensive. The present presentation simplifies the computational models to show the essential matters. The time dependency is discussed more in detail. We understand computed results, watching the fluid flow.

Conventionally, we cannot grow materials when poorly soluble solutes exist in the liquid solution. For example, we could not grow InGaAlP, which is a material for red LEDs. Aluminum is the poorly soluble solute. On the other hand, GaN grows from sodium solution [3]. In this growth, the fluid flow in the liquid solution plays an important role because it supplies the poorly soluble solute, nitrogen to the growth interface. Thus, it is important to understand the effect of the fluid flow on solution growth. It leads to designing new growth techniques.

The calculation of segregation is delicate. The boundary layers of solute mole fractions are thin at the initial stage of growth. The mole fractions do not have fixed values on the growth interface. It causes

the results to be buried under computational errors. On the other hand, all computed results include errors because the precision of arithmetic is not infinite on the computer, that is, we use finite resources. It is different from the traditional mathematics such as differential calculus. When we compare computed results with the experimental results, it is difficult to separate the error caused by flaws in the model from the error caused by the computation for the model. Moreover, the experimental results itself include errors. Then, we desire to consider the computed results theoretically.

2. Model and computational method

The x-axis is defined to be in the direction of the main flow. The z-axis is perpendicular to the growth interface. The origin is defined as the center of the growth interface. The computational domain is in the xz plane (Fig. 1a).

L and M denote components in the liquid solution. XL and XM denote the mole fractions of component L and M in the liquid phase, respectively. YL and YM denote the mole fractions of component L and M in the solid phase, respectively. $XL << YL$. $XM << YM$. The liquid solution is supersaturated before the growth. DL and DM denote the diffusion coefficients for component L and M in the liquid solution, respectively. $DL > DM$. The temperature is uniform and constant during the growth.

Concretely, we adopt a well-known material to facilitate the verification. We set parameters to approximate the previous experiment [4] (Appendix). The grown material is InGaP. Indium is the solvent of the liquid solution. L = P. M = Ga. $YL = 0.5$. XLb and XMb denote, respectively, XL and XM just before growth. $XLb = 2.8\times10^{-2}$. $XMb = 9.5\times10^{-3}$. The growth temperature is 1055 K.

2.1 Fluid flow

The fluid is molten indium and treated as an incompressible Newtonian fluid. The gravity and the change of fluid density dependent on solute mole fractions were neglected. That is, the fluid flow is independent of the situation on solute mole fractions. The basic equations of fluid flow are the conservation of mass and the conservation of momentum. The top of the liquid solution is flat. The slip condition was applied at this boundary. At the other boundaries, the no-slip condition was applied. It was assumed that the velocity perpendicular to the boundaries is zero. It is different from some vapor depositions.

Before the growth, the liquid solution was stationary and next, a velocity of 20 cm/s was applied on the bottom of the liquid solution for 0.25 s. Finally, this bottom stopped and the growth started. This boundary condition was modeled on the motion of sliding board in liquid phase epitaxy. Such a motion also appears in other techniques.

The velocities of the fluid flow were computed with SIMPLE [5], which is a computational method in computational fluid dynamics.

2.2 Transport phenomena of solutes

The diffusion of solutes limits the growth at the growth interface [6]. Convection-diffusion equations of solutes are explicitly solved with the finite difference method.

δL and δM denote the boundary layer thicknesses of XL and XM, respectively. h denotes the size of liquid solution in the z direction. $\delta M < \delta L << h$. $DM / DL = 0.56$ [4]. $DL = 1.6\times10^{-8}$ m^2/s [7].

t denotes a growth time. $XL(x, z, t)$ and $XM(x, z, t)$ denote XL and XM at x, z and t, respectively. pL and pM denote $\partial XL / \partial z$ and $\partial XM / \partial z$ at the growth interface, respectively. r denotes the ratio of the volume per unit atom in the liquid to that in the solid. Mass transfer through the growth interface is as follows:

$$DM(pM) / DL / pL = [r(YM) - XM(x, 0, t)] / [r(YL) - XL(x, 0, t)].$$

$XL0$ and $XM0$ denote, respectively, XL and XM on the growth interface when the growth has just started. $YL0$ and $YM0$ denote, respectively, YL and YM when the growth has just started. At the initial growth, the finite difference cannot express pL and pM. We use the analytic solutions of XL and XM. $XL0$, $XM0$ and $YM0$ were calculated with the method briefly described in Appendix. Ref. 8 provides detailed descriptions on the derivation of them and the meaning of them in the computation.

The time interval is set so that the results are obtained stably [9]. $e1$ denotes the relative discretization error of pL and pM. $o1$ denotes the tolerance of $e1$. It is estimated from the mass transfer through the growth interface. $e1(x, t)$ and $o1(x, t)$ denote $e1$ and $o1$ at x and t, respectively. c is defined as the growth time such that $e1(x, t) < o1(x, t)$ when $t < c$. Δzd denotes the mesh size in the z direction to solve the convection-diffusion equations of solutes. sqrt denotes square root function. It should be determined with the following equations [8] because the computational error does not retain the qualitative properties of the result [10].

$$1 - \mathrm{sqrt}(\pi(\kappa))\,\mathrm{erf}(0.5 / \mathrm{sqrt}(\kappa)) < o1.$$

$$\Delta zd = \mathrm{sqrt}((DM)\,c / \kappa).$$

Here, κ denotes a dimensionless parameter characterizing Δzd. BM is defined as $(YM - YM0) / YM0$. In the experiment, BM is of the order of 1×10^{-3}. As a result, for $c = 0.1$ s, the tolerance of $BM = 4\times10^{-5}$ and $o1 = 4\times10^{-5}$, Δzd becomes 20 times finer than the mesh size in the z direction to solve the basic equations of fluid flow. The mesh size in the z direction and time interval to compute XL and XM is much smaller than those to solve the basic equations of the fluid flow. Then, the velocities are interpolated with a cubic spline in the z direction and interpolated linearly in the time domain to obtain the velocities at the grid points for computing XL and XM.

The mole fractions on the growth interface were implicitly calculated to satisfy the mass transfer and phase diagram.

2.3 Quasi-model and full-model

Quasi-model [11] was defined as follows:

Mole fractions on the growth interface are calculated only at the origin. These calculated values are substituted for mole fractions at the other points on the growth interface.

This presentation adds a model and names this model full-model. In this model, the segregation is calculated over the entire growth interface.

2.4 The different conditions from the previous research

The model and methods are almost same as Ref. 11. The different conditions are as follows. The liquidus line and solidus line are approximated linearly by directly reading the phase diagram of Ref. 6 because we have found the non-linearity and absolute values in phase diagram are not essential matters from the discussions at the previous conferences [1, 2, 7, 10, 11, 12]. Liquidus line: $dXM / dXL < -6.5$. Solidus line: $dYL / dXL = 0$, $dYM / dXL < -8$.

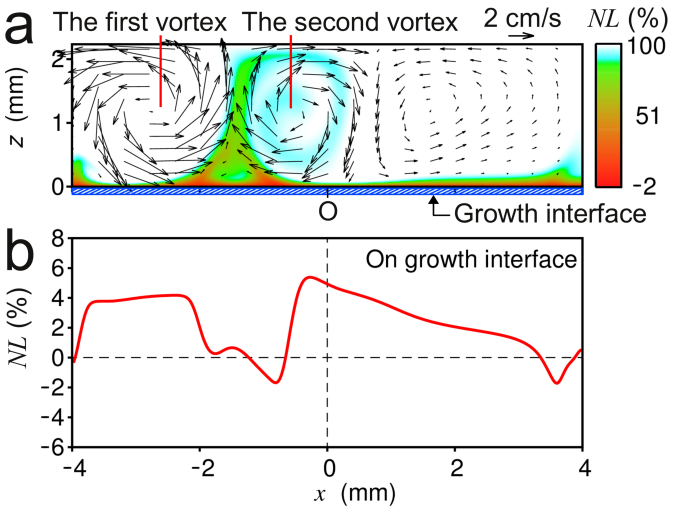

Fig. 1. Computed results at $t = 0.35$ s in the full-model: (a) flow pattern and normalized mole fraction of component L in the computational

domain, (b) normalized mole fraction of component L in the liquid phase on the growth interface.

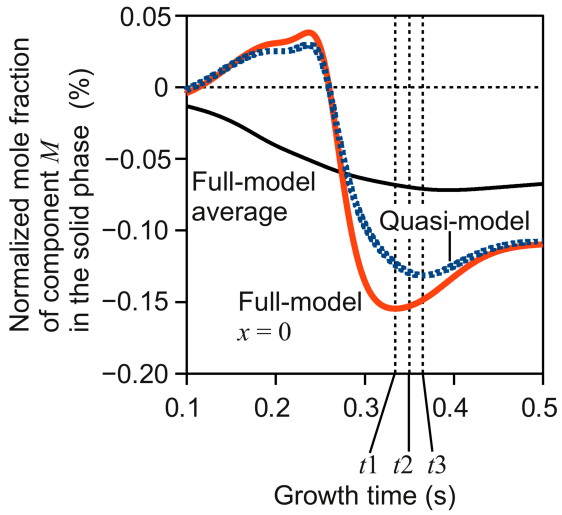

Fig. 2. Growth time vs. normalized mole fraction of component M in the solid phase.

3. Results and discussion

NL and NM are defined as follows:

$NL \equiv (XL - XL0) / (XLb - XL0)$,

$NM \equiv (XM - XM0) / (XMb - XM0)$.

The normalizations facilitate the understanding of results [1, 12]. The normalized values on the growth interface express the effect of fluid flow because they are zeros for short growth times without fluid flow.

Fig. 2 shows the time dependency of BM. The dashed curve is a result in the quasi-model. The solid curve similar to the dashed curve is a result at $x = 0$ in the full-model. The solid curve that shows $BM < 0$ at all the growth times is the average of BM over the entire growth interface in the full-model. Mainly, BM has lower values than the values without the fluid flow. It is coincident with a previous experiment [4] (Appendix). The variation in the full-model is larger than that in the quasi-model.

Around $t = 0.2$ s, BM increases at $x = 0$, because the fluid flow transports a dilute liquid solution consumed by the growth to the boundary layers of solute mole fractions. This interpretation was reported in the previous conferences [1, 2, 12]. The flow pattern at this time is reported in Ref. 11.

Around $t = 0.3$ s, BM decreases at $x = 0$. The reason was also discussed at the previous conferences. The summary is as follows. The fluid flow transports a liquid solution retaining the initial state to the boundary layers of solute mole fractions. Then, XL increases. XM increases not so much because $\delta M < \delta L$, that is, XM has almost the initial value and increases only slightly. Thus, the fluid flow affects component L most in the solutes. This effect of the fluid flow propagates into the internal region of solute mole fraction boundary layers. Then, on the growth interface, XL increases. XM decreases due to the liquidus line. Therefore, BM decreases.

$t1$ and $t3$ denote the growth times when the values of BM become minimum values in the full-model and quasi-model, respectively. Obviously, $t3$ is different from $t1$. The reason is as follows. $t2 = 0.35$ s. $t2$ is between $t1$ and $t3$. Fig. 1 shows the result of the full-model at $t2$. Fig. 1a shows the flow pattern and NL. In the shaded region, $NL < 0.9$. In the white region, NL almost retains the initial state. Fig. 1b shows NL on the growth interface at this time. At $x = 0$, near the growth interface, the liquid solution flows from the right to the left. In this direction, XL increases near the growth interface. The convection term in this direction has minus values. However, in the quasi-model, XL has the same value over the entire growth interface. Then, the convection term in this direction does not have such minus values. Therefore, BM continues to decrease at this time in the quasi-model. After this time, the momentum of the fluid flow is dissipated by the viscosity. Moreover, the second vortex moves to the left and a block of the fluid flow that has low velocities comes to the center of the growth interface. Then, BM begins to increase in the quasi-model.

4. Conclusion

We discussed the time dependencies of mole fractions in numerical simulations of solution growth. The temperature was uniform and constant during the growth. The effect of fluid flow was focused on. The computational domain was in a two-dimensional plane. In a quasi-model, mole fractions on the growth interface were calculated only at the center of growth interface. These calculated values were substituted for mole fractions at the other points on the growth interface. In a full-model, the segregation was calculated over the entire growth interface. The mole fraction in the solid phase varied with time. The outline of the variation in the quasi-model was similar to that in the full-model. The average behavior of the mole fraction in the solid phase was coincident with a previous experiment qualitatively. The variation in the full-model was larger than that in the quasi-model. In other words, the quasi-model is more stable than the full-model. It also saves the computational time when the phase diagram has not been calculated yet. Then, it is useful when the computational conditions are unknown. There was a difference of the growth times for a characteristic phenomenon between the quasi-model and full-model. The difference was caused by the approximation specific to the quasi-model, spatial variations of mole fractions on the growth interface and the flow pattern.

Appendix

Initial condition [8]

$XL0$, $XM0$ and $YM0$ are calculated with the following equation and phase diagram.

$\mathrm{sqrt}(DM / DL) (XMb - XM0) / (XLb - XL0)$

$= [r (YM) - XM0] / [r (YL) - XL0]$.

Previous experiment of solution growth

Ref. 4 reported an experiment of liquid phase epitaxy. The grown crystal is an InGaP. The solvent is indium. The solutes are phosphorus and gallium. In the present model, L = P and M = Ga. The substrate was separated from the liquid solution before the growth. After the liquid solution was supersaturated, the liquid solution slid to the substrate in order to start the growth. The composition in the solid phase was determined with X-ray diffraction. YM had low values when $t < 5$ s, compared with the values when $t > 5$ s.

References

[1] H. Susawa, Ideas to Interpret Computed Results without Floating-Point Arithmetic in Segregation with Fluid Flows, Proc. 7th Int. Workshop Model. Cyst. Growth, The Department of Chemical Engineering, National Taiwan University, (2011) 103-104.

[2] H. Susawa, Numerical simulation of compositional variation in liquid phase epitaxy focusing on the forced convection in the melt, 16th Int. Conf. Cryst. Growth (2010) Session: 01.Fundamental of Crystal Growth (Theory, Simulation, Modeling, Growth Mechanism, Surface and Interfaces) Aug. 11.

[3] F. Kawamura, M. Morishita, M. Tanpo, M. Imade, M. Yoshimura, Y. Kitaoka, Y. Mori, T. Sasaki, J. Cryst. Growth 310 (2008) 3946-3949.

[4] K. Hiramatsu, S. Tanaka, N. Sawaki, I. Akasaki, Analysis of Compositional Variation at Initial Transient Time in LPE Growth of InGaAsP/GaAs System, Jpn. J. Appl. Phys. 24 (1985) 1030–1035.

[5] S.V. Patankar, Numerical Heat Transfer and Fluid Flow, Hemisphere Publishing Corp., Washington, D.C. (1980).

[6] I. Crossley, M.B. Small, The Application of Numerical Methods to Simulate the Liquid Phase Epitaxial Growth of Ga1-xAlxAs from an Unstirred Solution, J. Cryst. Growth 15 (1972) 268–274.

[7] H. Susawa, T. Tsuji, K. Hiramatsu, T. Jimbo, T. Soga, Simulation of InGaP Liquid Phase Epitaxy Including Convection, Theor. Appl. Mech. Jpn. 55 (2006) 279-284.
[8] H. Susawa, T. Tsuji, T. Jimbo, T. Soga, Initial Condition and Calculation Method for the Numerical Simulation of LPE, J. Chem. Eng. Jpn. 40 (2007) 928-938.
[9] P. J. Roache, Computational Fluid Dynamics, Hermosa Publishers Inc., Albuquerque, N.M. (1976).
[10] H. Susawa, Computational Error by Singularity in Segregation from Supersaturated Liquid Solution with Fluid Flows, Proc. 7th Int. Workshop Model. Crtst. Growth, The Department of Chemical Engineering, National Taiwan University, (2011) 39-40.
[11] H. Susawa, T. Tsuji, K. Hiramatsu, T. Jimbo, T. Soga, Simulation of Compositional Variation in Liquid Phase Epitaxy InGaP Using a Two Dimensional Model, Inf. Process. Soc. Jpn. Trans. Math. Model. Appl. 48 No. SIG 2(TOM16) (2007) 147-157.
DOI http://dx.doi.org/10.2197/ipsjdc.3.114.
[12] H. Susawa, Leibniz Institute for Cryst. Growth (IKZ), abstract book of 5th Int. Workshop on Cryst. Growth Technol., Berlin, (2011) 61.

17:00 Poster Mo27

Theorems for Numerical Simulation of Solution Growth with Segregation and Fluid Flow

Hiromoto Susawa

Home, Aichi 489-0888, Japan

e-mail: automobile_21@yahoo.co.jp

1. Introduction

Solution growth contributes to mass production and is environment-friendly. The author originated light-emitting diodes (LEDs) made with Bragg reflectors constituted by semiconductor layers with metal organic vapor deposition [1, 2], which is a more dangerous technique than solution growth, and could enhance the light extraction efficiency, but the yield of product was limited because the thickness of each layer in a Bragg reflector required rigorous control all over a wafer. We needed more complicated structures with more layers to improve the yield [3]. On the other hand, a solid solution substrate offered a simple structure to enhance the light extraction efficiency. This substrate was transparent to light emitted from the active layer in LEDs. The electrode on the substrate could serve as a reflector. This solid solution substrate was produced with solution growth.

However, in solution growth, the mole fraction of each component in liquid phase is different from that of its component in solid phase. We find the mole fractions by experiment after repeated trial and error. Numerical simulation reduces these experiments. Moreover, it offers finer understanding and can propose new techniques.

When we grow a crystal on a substrate and do not dissolve the substrate on the initial growth, we supersaturate the liquid solution before the growth. When the growth has just started, the macroscopic model is singular. The liquid phase is in equilibrium with the solid phase on the growth interface, while mole fractions in the liquid phase have supersaturated values at the places except for the growth interface. The gradients of mole fractions at the growth interface are large for short growth times. This singularity causes a computational error. This error was recognized recently in an ideal case without fluid flow in the liquid solution [4].

In a technique of solution growth, to start growth, the entire liquid solution is put into contact with the substrate relatively. This motion induces a fluid flow in the liquid solution. The effect of this flow lasts for short growth times.

Moreover, the effect of fluid flow is important for short growth times. The growth lacks poorly soluble solutes rapidly. The fluid flow can supply them to the growth interface. For example, ammonothermal method is succeeding, utilizing fluid flow.

The main effect of fluid flow on solution growth was discussed [5-8]. A manuscript of proceedings for [9] was received a comment, "For the sake of clarity, the materials whose compositions are affected by forced convection should be named. Generally, your model should be applicable all mixed crystals i.e. solid mixtures of group IV elements (Si and Ge), group III-V compounds (GaAs and InAs etc.), and group II-VI compounds.". This presentation reflects this comment, generalizes those discussions and shows a solute affected by fluid flow most strongly. This is a key solute to verify the computed result. In the text, this solute is named *L*. This presentation also reflects the comments of the manuscript for the conference last year [9] so that the content is not misunderstood.

We recognized an open question whether a computed result should be verified with the experiment or the theory at the previous conference [10]. There is the following example of failure related to this question. A model was insufficient for the experiment, solved insufficiently and the computed result fit the experimental result but was against the mathematics. On the other hand, floating-point arithmetic causes errors due to the finite length of significand. Fore example, $A = 1.0 + 1.0\text{E}20$; $B = 1.0\text{E}20$; then, the result of $(A - B)$ is not 1.0 on the conventional computer. We cannot take complete measures against the errors. When we employ an experimental result for verifying a computation and do not use employ the experimental result for verifying the model, the experiment deviates from the original role. In this case, the experiment is employed as an analog computer. We have to have already known the property of each device in the analog computer. The circuit has to match the model. However, we usually do not expect it because we experiment for the phenomena that we have not known well. Therefore, we answer that question at the present time as follows. We can apply the experiment to verifying the model but it is better to theoretically verify the computation executed to solve the model than to apply the experimental result for verifying the computation. Then, this presentation shows theorems to interpret computed results qualitatively.

2. Nomenclature

Fig. 1a shows the coordinate system. The origin is defined to be at the center of the growth interface. The *x*-axis and *z*-axis are defined to be parallel and perpendicular to the growth interface, respectively.

In this abstract, some symbols deviate from the conventional nomenclature for the printing reason.

The presentation uses the conventional nomenclature, e.g., X_L^{1*}.

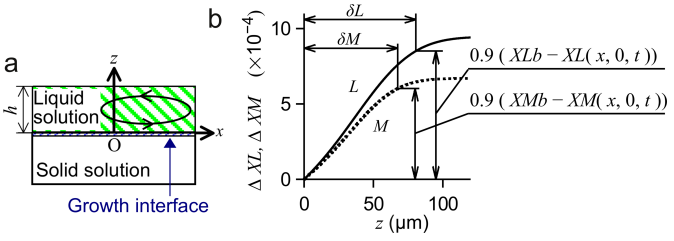

Fig. 1a. Coordinate system.
b. *ΔXL* and *ΔXM* in the boundary layers at enhancement of growth from inhibition of growth by fluid flows. The concrete model is the same as Ref. 6 except for the phase diagram approximated linearly by directly reading that in Ref. 11. This simulation was modeled on InGaP growth from indium melt. *L* = P. *M* = Ga. *x* = 0. *t* = 0.278 s.

DL, *DM* the diffusion coefficients for components *L* and *M* in the liquid solution, respectively (m^2/s)
h the length of liquid solution in the *z* direction (m)

L, M the most and less affected components by fluid flow, respectively (-)
NL ($XL - XL0$) / ($XLb - XL0$) (-)
$NL(x, z, t)$ NL at x, z, and t (-)
NM ($XM - XM0$) / ($XMb - XM0$) (-)
$NM(x, z, t)$ NM at x, z, and t (-)
pL, pM $\partial XL/\partial z$ and $\partial XM/\partial z$ at the growth interface, respectively
r ratio of volume per unit atom in the liquid to that in the solid
sqrt(ξ) the square root of ξ (the square root of the unit of ξ)
t a growth time (s)
u, w the x and z components of the fluid flow velocity, respectively
XL, XM the mole fractions of components L and M in the liquid phase, respectively (-)
$XL(x, z, t)$ XL at x, z, and t (-)
$XL0$, $XM0$ XL and XM when growth has just started, respectively
XLb, XMb XL and XM just before growth, respectively (-)
$XM(x, z, t)$ XM at x, z, and t (-)
YL, YM the mole fractions of components L and M in the solid phase, respectively (-)
$YL0$, $YM0$ YL and YM when growth has just started, respectively (-)
ΔXL $XL(x, z, t) - XL(x, 0, t)$ (-)
$\Delta XL(x, z, t)$ ΔXL at x, z and t (-)
ΔXM $XM(x, z, t) - XM(x, 0, t)$ (-)
$\Delta XM(x, z, t)$ ΔXM at x, z and t (-)
δL, δM the boundary layer thicknesses of XL and XM, respectively

3. The base of Model

We deal with the growth of a ternary solid solution from a liquid solution. We assume the growth interface is in an equilibrium state. During the growth, the temperature is uniform and constant, i.e., the phase diagram is fixed. $XL << YL$. $XM << YM$. $\delta L << h$. $\delta M << h$.

Mole fractions in liquid phase are the most important parameters to determine segregation. This presentation discusses only the effect of fluid flow on segregation.

It is assumed the solid solution grows only at $z = 0$.

4. Mass transfer through growth interface [12]

$$DL\,(pL) / DM / pM = [\,r\,(YL) - XL(x, 0, t)\,] / [\,r\,(YM) - XM(x, 0, t)\,]. \quad (1)$$

5. Known Theorem

We can approximate h to be infinite in order to use analytic solutions [13].

Theorem 1: Theorem 1 assumes that the solutes are transported only by diffusion in the liquid solution, the base of model and diffusion-limited model. Mole fractions are approximated to be constant on the growth interface.

6. The benefits of normalizations, NL and NM

- The normalized values on the growth interface express the effect of fluid flow. The reason is as follows: on the growth interface, the mole fractions approximately have the values when the growth has just started from Theorem 1; then, the normalized values are zeros on the growth interface without fluid flow.

- The normalized value of a component can be compared with that of another component based on the initial supersaturation state.

7. Assumptions related to fluid flow

The model is in the xz plane. $DL > DM$. The fluid flow traverses the boundary layers of mole fractions. Velocity perpendicular to the boundary of fluid flow is zero. Discussion starts with the mole fractions without the fluid flow.

8. Theorems by generalizing a series of these studies [5-9]

8.1 Enhancement of growth by fluid flow

Case 1: A liquid solution retaining the initial supersaturated state in an outer region of the boundary layers of XL and XM flows to their boundary layers.

Theorem 2: Theorem 2 deals with Case 1 and assumes the base of model and assumptions related to fluid flow.

Then, the fluid flow increases $XL(x, z, t)$ more than $XM(x, z, t)$ around the border between their boundary layers and the outer region of the boundary layers.

Reason:

Fig. 1b is an example to show the profiles of mole fractions in their boundary layers. Fig. 2 characterizes the boundary layers. This figure defines positions, e and f. Position e is in an outer region of the boundary layers. Position f is inside the boundary layer of XL and outside the boundary layer of XM. Suppose that a block of liquid solution retains the initial supersaturated state at Position e and $t = t1$, and comes to Position f at $t = t2$.

Fig. 2a illustrates how the fluid flow affects XL. The fluid flow transports a block of liquid solution in which XL has XLb to the boundary layer. $A1 = A2 + A3$. $XL(x$, Position f, $t2)$ increases by the amount proportional to Area $A2$.

Fig. 2b illustrates the effect on XM. The relation between Area $A4$, $A5$ and $A6$ is $A4 = A5 + A6$. The fluid flow increases $XM(x$, Position f, $t2)$ by the amount proportional to Area $A5$. The effect on XM is smaller than the effect on XL because the profile of XM was more saturated to its initial value than that of XL at $t1$.

Obviously, the above geometric discussion can be expanded to three-dimensional space. The upstream position and destination do not need to be along the z-axis.

The following becomes an index to verify the computed results. It is obvious form Fig. 2.

Theorem 3: Theorem 3 uses the assumptions and result of Theorem 2. The fluid flow decreases δL and δM.

From Theorem 3, this fluid flow enhances the growth.

The following is a preparation for the next theorem.

Proposition 1: The fluid flow increases XL and decreases XM on the growth interface.

Theorem 4: Theorem 4 uses the assumptions and results of Theorem 2 and 3. Theorem 4 assumes the result of Theorem 2 propagates to the growth interface and $dXM / dXL < 0$ on the liquidus line.

Proposition 1 is valid under Eq. 1.

Reason:

From Theorem 3, pL and pM increase. The increase of XM is less than that of XL in the vicinity of growth interface because the result of Theorem 2 propagates to the growth interface. The left hand side of Eq. 1 is greater than the right hand side if the equilibrium state remains constant. On the other hand, on the growth interface, XL and XM are on the liquidus line; then, when XL increases, XM decreases. The increase of XL on the growth interface contributes to the decrease of pL. The decrease of XM on the growth interface contributes to the increase of pM. That is, this change of equilibrium state contributes to the adjustment of the left hand side of Eq. 1 to the right hand side. Fig. 4a is examples of NL profiles in the boundary layers of XL. These profiles show how XL varies in z direction. Fig. 4b shows NL in the vicinity of growth interface. On the growth interface, "$dYL / dXL > 0$ or $dYM / dXM > 0$" is obvious. Suppose XL increases on the growth interface. Then, YL increases and YM decreases. $YL >> XL$. $YM >> XM$. Then, the right hand side in Eq. 1 increases. Therefore, the increase of XL on the growth interface decreases (the left hand side) - (the right hand side). At a certain value of XL on the growth interface, the left hand side balances with the right hand side. When suppose XL decreases on the growth interface, by repeating the similar consideration, we find Eq. 1 is not satisfied. That is, Proposition 1 is valid under Eq. 1.

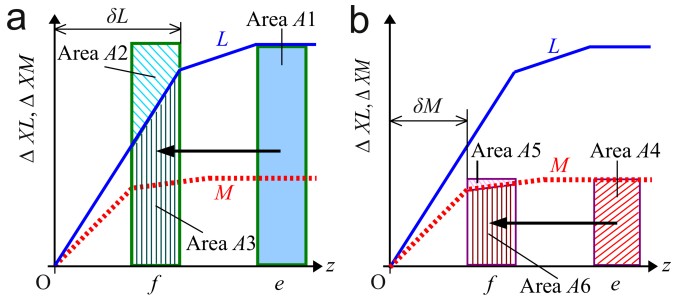

Fig. 2. Schematic illustration of the effect on the boundary layers by a fluid flow. Position *f* is inside the boundary layer of *XL* and outside that of *XM*. Suppose a liquid solution retaining the initial supersaturated state flows to Position *f* : (a) Effect on the boundary layer of *XL*, (b) Effect on the boundary layer of *XM*.

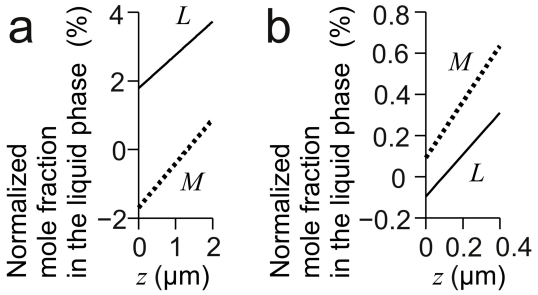

Fig. 3. Examples of normalized mole fractions in the liquid phase on the line, $x = 0$ near the growth interface Concrete model is the same as that in Fig. 1b. (a) The enhancement of growth by fluid flow at $t = 0.278$ s. (b) The inhibition of growth by fluid flow at $t = 0.12$ s.

8.2 Inhibition of growth by fluid flow

Case 2: The direction of a fluid flow is from the growth interface to an outer region of the boundary layers constituted by the mole fractions of solutes.

Case 2 is opposite to Case 1. We find out the reasons with the similar procedures. The fluid flow inhibits the growth. We move the control volumes form Position *f* to Position *e* in Fig. 2. The conclusions are opposite to those in Case 1.

Theorem 5: Theorem 5 deals with Case 2 and assumes the base of model and assumptions related to fluid flow.

Then, the fluid flow decreases $XL(x, z, t)$ more than $XM(x, z, t)$ around the border between their boundary layers and the outer region of the boundary layers.

Theorem 6: Theorem 6 uses the assumptions and result of Theorem 5. The fluid flow increases δL and δM.

Proposition 2: The fluid flow decreases *XL* and increases *XM* on the growth interface.

Theorem 7: Theorem 7 uses the assumptions and results of Theorem 5 and 6. Theorem 7 assumes the result of Theorem 5 propagates to the growth interface and $dXM / dXL < 0$ on the liquidus line.

Proposition 2 is valid under Eq. 1.

References

[1] H. Susawa, M. Hirotani, T. Kato, Surface Emitting LED with Reflector on GaAs, 1989 fall 50th meeting held by Jpn. Soc. Appl. Phys. 28 p-ZB-10 (in Japanese)

[2] T. Kato, H. Susawa, M. Hirotani, T. Saka, Y. Ohashi, E. Shichi and S. Shibata, J. Cryst. Growth, 107 (1991) 832.

[3] N. Yamauchi, T. Saka, M. Hirotani, T. Kato, and H. Susawa, European Patent Office, Patent Number: EP0483868B1 (Issue Date: January 22, 1997).

[4] H. Susawa, T. Tsuji, T. Jimbo, T. Soga, J. Chem. Eng. Jpn. 40 (2007) 928.

[5] H. Susawa, T. Tsuji, K. Hiramatsu, T. Jimbo, T. Soga, Simulation of InGaP Liquid Phase Epitaxy Including Convection, Theor. Appl. Mech. Jpn. 55 (2006) 279-284.

[6] H. Susawa, T. Tsuji, K. Hiramatsu, T. Jimbo, T. Soga, DOI http://dx.doi.org/10.2197/ipsjdc.3.114.

[7] H. Susawa, Numerical simulation of compositional variation in liquid phase epitaxy focusing on the forced convection in the melt, 16th Int. Conf. Cryst. Growth (2010) Sess.: 01 Aug. 11.

[8] H. Susawa, Leibniz Inst. Cryst. Growth (IKZ), abstract book 5th Int. Workshop Cryst. Growth Technol., Berlin, (2011) 61.

[9] H. Susawa, Proc. 7th Int. Workshop Model. Cyst. Growth, Dep. Chem. Eng., Natl. Taiwan Univ., (2011) 103.

[10] Panel discussion at the 55th Natl. Congr. Theor. Appl. Mech. in Kyoto Jpn. (2006).

[11] K. Hiramatsu, S. Tanaka, N. Sawaki, I. Akasaki, Jpn. J. Appl. Phys. 24 (1985) 1030.

[12] I. Crossley, M.B. Small, J. Cryst. Growth 15 (1972) 268.

[13] M. Feng, L.W. Cook, M.M. Tashima, G.E. Stillman, J. Electron. Mater. 9 (1980) 241.

17:00 Poster Mo28

The morphology features of salol crystal growth at the presence of nanoparticles I_2O_3

Taras Tsir

Physico-Technological Institute of Metals and Alloys, National Academy of Sciences of Ukraine (PTIMA), Vernadsky avenue, 34/1, Kyiv 03680, Ukraine

e-mail: jknd-t@ukr.net

Nowadays it is a widely interest to composites containing nanoparticles. But as it appears from our study nanoparticles can not only play the role as filler agent but affect directly on morphology during solidification. Thus it opens the possibility to make material with structure that impossible to get using conventional methods.

In present research impact of nanoparticles of I_2O_3 (d=20 nm) on the growth of salol crystals under different supercoolings ΔT (2, 5, 10, 32 ^{0}C) was studied. If was found difference as in morphology of crystal growth as in tendency of gas bubbles release from the melt. Fig. 1 shows growth of pure salol Figs. 1a-1d and salol with 10 wt.% nanoparticles Figs. 1e-1h.

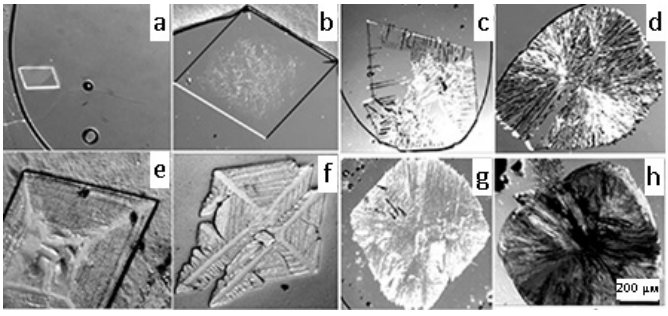

Fig. 1. The influence of nanoparticles on the growing structure (a), (e) ΔT=2 ^{0}C; (b), (f) ΔT=5 ^{0}C; (c), (g) ΔT=10 ^{0}C; (d), (h) ΔT=32 ^{0}C.

As it can be seen, for pure salol increasing of supercooling resulted in direct transition from faceted Figs. 1a, 1b, 1c to spherulite morphology Fig. 1d. For sample with nanoparticles intermediate (between faceted Fig. 1e and spherulite morphology Fig. 1h) dendrite stage took place Figs. 1f and 1g.

Relatively gas bubble release it must be noted that for pure salol intensive emission took place, followed by "classical" capturing – repulsion, Fig. 1c and 1d. For salol with nanoparticles another situation was observed. Gas bubbles appears occasionally, for $\Delta T < 22\ ^0C$ its interaction with interface is the same as for pure salol (see captured bubbles, Fig. 1g). For greater supercoolings gas bubble ahead the front "attract" sharp protuberance, Fig. 2a.

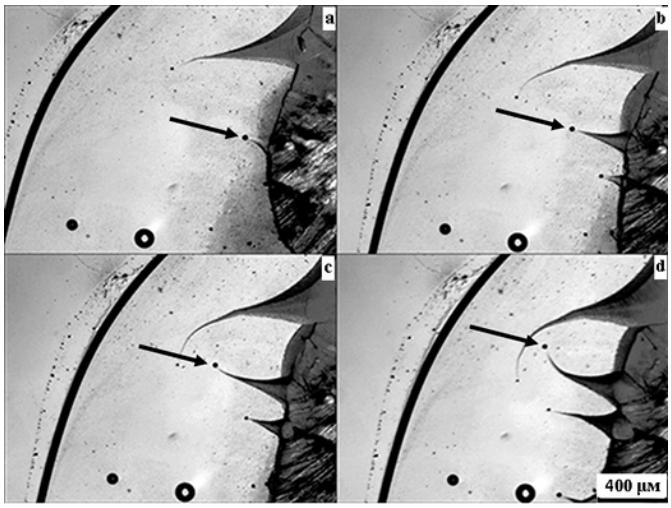

Fig. 2. Salol with nanoparticles, $\Delta T = 22\ ^0C$. Stages of growth, (a) t=o s, (b) t=15 s, (c) t=25 s, (d) t=40 s. Bubble is marked by arrow.

Than with the rate, essentially greater than rate of main crystal interface, this protuberance with bubble at the end propagates in the melt by rather arbitrary trajectory, Fig. 2b – 2d. It must be noted, that such behavior was not accidental and observed in all experiments with $\Delta T > 20\ ^0C$ (Fig. 1h is the stage of growth before meeting with bubble).

For pure salol such behavior was not observed in all interval of studied supercoolings.

17:00 Poster Mo29

The phenomenon of thermal unstability in Czochralski hydrodynamic model: physical and numerical simulation

Nataliya A. Verezub[1], Anatoly I. Prostomolotov[2], Vladimir S. Berdnikov[3]

1. *Institute for Problems in Mechanics RAS (IPMECH), Vernadskii prospect 101, bl. 1, Moscow 119526, Russian Federation* **2.** *Institute for Problems in Mechanics of RAS (IPMECH), Vernadskogo prospect 101, bl. 1, Moscow 119526, Russian Federation* **3.** *Kutateladze Institute Thermophysics SB RAS (ITP), Academician Lavrentev ave., Novosibirsk 630090, Russian Federation*

e-mail: verezub@ipmnet.ru

Formation of the microdefect's striations in crystals grown by Czochralski (Cz) method is connected with the instability of a melt flow, which causes the time-instability of liquid/solid interface and pulsating dopant flux from a melt into crystal. This problem is the subject of many experimental and theoretical papers that analyze the temperature fluctuations in a melt for concrete conditions of Cz crystal growth [1]. However, modern Cz numerical simulations use the multi-conjugated models, which are very complicated for detailed analysis of the flow instabilities in a melt. Their verification by means of experimental data obtained in complex technological conditions, in our opinion, gives only the qualitative notion about the correlation of calculated and experimental data.

In this paper the problem of flow instability is considered on the basis of Cz numerical hydrodynamic model. Its mathematical formulation fully corresponds to the laboratory experiment [2]. The study was carried out by using of modeling liquid (ethanol). The liquid fills the cylindrical crucible of the radius 0.1475 m till the height 0.1032 m. The disk of the radius 0.0536 m is located on the liquid surface coaxially with the crucible. Thermal conditions are following: the disk temperature T_s = 300 K, the crucible bottom is thermally insulated, and its lateral wall is heated to the temperature $T_w = T_s + \Delta T$. The flow structure is caused by the thermal gravitational convection and Marangoni convection under the action of thermocapillary forces on the free liquid surface. The transition to the hydrodynamic unstable flows is studied at variation of the temperature difference between the lateral crucible wall and the disc for the range ΔT = 1 ¸ 15 K.

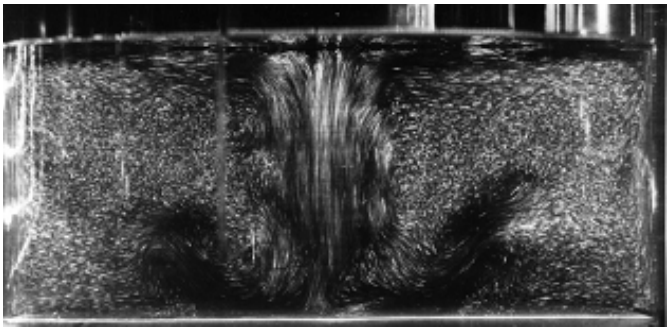

Fig. 1. The experimental picture of unstable flow structure.

The detailed description of the experiment is given in [2]. The according flow structure was visualized by finely dispersed aluminum particles (Fig. 1), and the temperature measurements were carried out by means of thermocouples located near the disk.

Numerical simulation was carried out by means of control volume method for a solution of Navier-Stokes and heat transfer equations in Boussinesq's approximation [3]. The axisymmetric and three-dimensional formulations of the problem were considered. The transitions of a steady flow and heat transfer to their unstable modes with the emergence and development of temperature fluctuations were investigated. The special subroutines of statistical treatment were applied for the calculation of average characteristics and a spectral power of velocity and temperature fluctuations.

In a clear graphic form an evolution of *thermic* was visualized: the formation, development and its tearing from the disk surface, the essence of which is as follows. In gravity field the inhomogeneity of temperature distribution in the crucible causes the melt motion under the action of gravitational thermal convection, which is amplified by the additional influence of thermocapillary forces at the free liquid surface. As a result, the liquid is heated and lifted up near the lateral crucible wall. Then it moves in the radial direction to the cold disk. Under this disc the cooled liquid drops to the bottom. The peculiarity of this flow is a presence of cooled liquid jet having the specific form in the crucible center (near the axis), which extends from the lower disk edge to the crucible bottom.

Under the disc the jet structures undergo the specific changes with increasing ΔT from 4 to 15 K. This jet steadily achieves the crucible bottom without losing its initial form at the small value of ΔT = 4 K. The essential radial changes of its shape become visible with removal down from the disk at the greater values of ΔT = 10 and 15 K. These spatial changes of downflow are time-dependent, too. At ΔT = 15 K the time dependence of temperature contours near the crucible bottom becomes clearly noticeable. It is accompanied by a radial turning of the jet from the axis to the lateral wall.

The experimental video shows that the pattern of instability in the flow structure according to the mechanism of formation, development and tearing of *thermics* from the disc is similar the formation of a liquid droplet on an icicle, and its periodic tearing from its surface. Similar experiments were carried out at some different geometry of the model and with using of silicone oil. Their data show a similar pattern of flow instability [4].

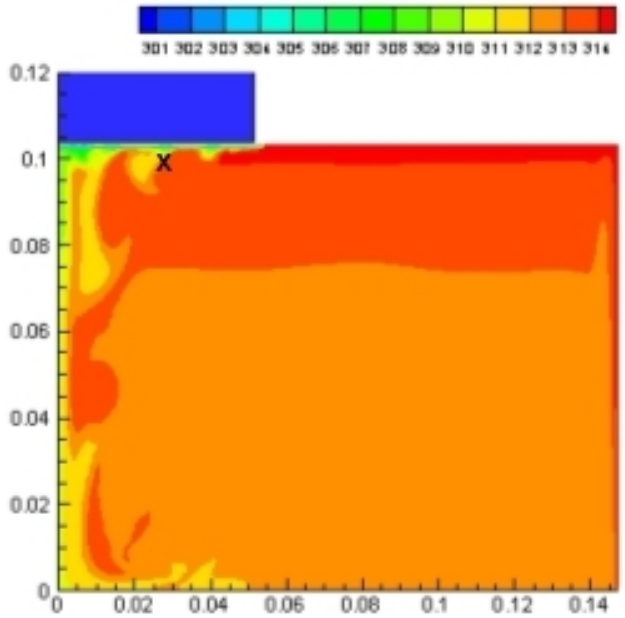

Fig. 2. The calculated instantaneous picture of temperature contours with its values atΔT = 15 K. Here:´is the location of "point-1" temperature sensor at r = 0.0268 m, z = 0.0982 m.

Fig. 2 shows the calculated instantaneous picture of temperature contours at ΔT = 15 K, at which the process of *thermics* development is clearly visible under the cold disk: *thermic's* formation near the disk edge, its increase towards the center and then its tearing from the disk near the central downflow.

The calculated spectral power of temperature fluctuations in "point-1" at ΔT = 15 K is shown in Fig. 3. This spectrum was plotted on basis of the records in "point-1" (see Fig. 2) of temperature fluctuations, which have been resulted from the axisymmetric and three-dimensional calculations. The spectrum of temperature fluctuations is noticeably discrete. In it the frequencies with the highest spectral power of temperature fluctuations are distinguished.

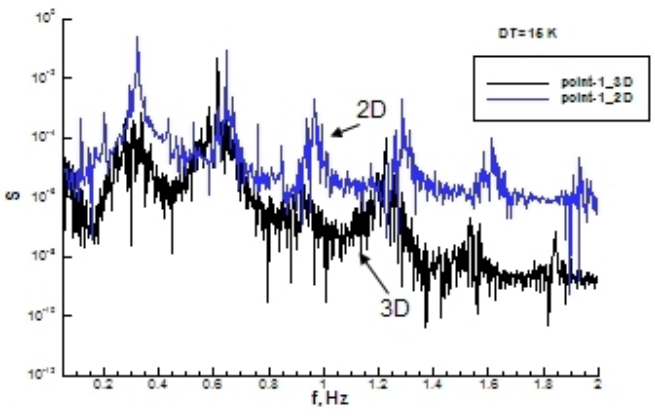

Fig. 3. The calculated spectral power of temperature fluctuations in "point-1" atΔT = 15 K. Here: 2D – axisymmetric and 3D – three-dimensional cases.

The experimental data (Fig. 4), corresponding to the discrete spectrum of laminar-turbulent transition, are in good agreement with these calculated results. In comparison with the calculated spectrum it may be noted a small shift of frequencies in experimental data. It may be explained by some difference of the location of "point-1" and the experimental sensor near the disk.

The experimental data (Fig. 4), corresponding to the discrete spectrum of laminar-turbulent transition, are in good agreement with these calculated results. In comparison with the calculated spectrum it may be noted a small shift of frequencies in experimental data. It may be explained by some difference of the location of "point-1" and the experimental sensor near the disk.

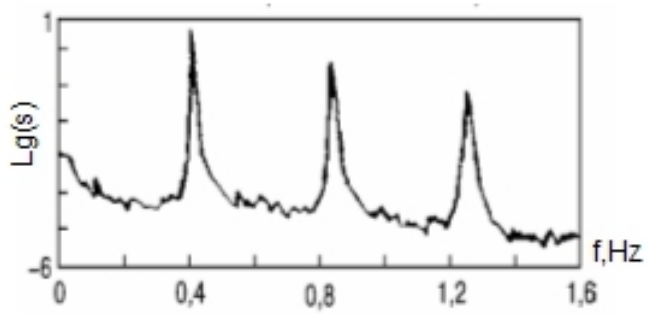

Fig. 4. The experimental spectral power of temperature fluctuations for unstable flow structure shown in Fig. 1.

The instantaneous three-dimensional picture for the process of formation and development of *thermics* may be illustrated by Fig. 5, which shows the discrete azimuthal distribution of *thermics* under the disc. Such distribution of *thermics* differs from their uniform azimuthal distribution for axially symmetric case.

Fig. 5. The spatial picture of thermics under the disk in 3D-calculation, which has been plotted as isothermal surface at T = 312 K.

The frequency distribution of the spectral power in axisymmetric case is approximately similar to three-dimensional one, but its power values are somewhat smaller in three-dimensional case (Fig. 3). This distinguishing feature of three-dimensional results is explained by the presence of azimuthal inhomogenity in distribution of *thermics*.

Acknowledgments

We thank the Russian Foundation for Basic Research for the financial support of projects: 11-08-00966, 12-02-01126.

References

[1] Miller W. Numerical simulation of bulk crystal growth on different scales: silicon and GeSi // Phys. Status Solidi B. 2010. V. 247. N 4. P. 885-869.

[2] Berdnikov V.S. Hydrodynamics and heat transfer during crystal pulling from a melt. Part 1. The experimental study of natural convection // Materials of Electronic Technics. 2007. N 4. P. 19-27 (in Russian).

[3] Devdariani M.T., Prostomolotov A.I., Fryazinov I.V. Finite difference method and program realization for solving three-dimensional Navier-Stokes equations in the cylinder // Proceedings of 1990 IMACS international conference "Mathematical Modeling and Applied Mathematics". Elsevier Science B.V. 1992. P. 119-132.

[4] Teitel M., Schwabe D., Gelfgat A.Yu. Experimental and computational study of flow instabilities in a model of Czochralski growth // J. Crystal Growth. 2008. V. 310. P. 1343-1348.

17:00 Poster Mo30

Effects of carboxylated ε-poly-L-lysine on crystallization of ice

Dmitry Vorontsov[1], Gen Sazaki[2], Suong-Hyu Hyon[3], Kazuaki Matsumura[4], Yoshinori Furukawa[2]

1. *Nizhny Novgorod State University, Nizhny Novgorod 603950, Russian Federation* **2.** *Institute of Low Temperature Science, Hokkaido University (ILTS), N19-W8, Kita-ku, Sapporo 060-0819, Japan* **3.** *Center for Fiber and Textile Science, Kyoto Institute of Technology, Kyoto 606-8585, Japan* **4.** *Japan Advanced Institute of Science and Technology, Ishikawa 923-1292, Japan*

e-mail: vorontsovda@mail.ru

The use of some biological agents gives a potential to control the crystallization processes of ice. Living organisms (polar fish, insects) produce anti-freeze proteins to survive in subfreezing environments. Some agents are used in medicine for preservation and transplantation of cells and tissues [1]. Carboxylated ε-poly-L-lysine (PLL) is a new cryoprotector which shows lower cytotoxicity [2].

In this study we have investigated the effects of carboxylated ε-poly-L-lysine as an impurity on crystallization of ice in supercooled water. Seed crystals of ice of hexagonal modification (space group $P6_3/mmc$) were created in a glass capillary and then were grown up in a growth cell filled with supercooled water with PLL concentrations 0-150 mg/ml H_2O. The accuracy of temperature control in the growth chamber was within ±0.02 °C. Measurements of growth rates R were performed by optical microscopy at supercoolings ΔT from 0 to 1.5°C. Images of growing crystal were captured at every fixed time interval by a video-system and processed by specially developed software. Ice crystal has a disk-like shape at small supercoolings (0.2-0.3°C) where the top and bottom planes are basal faces {0001}. Further increase in supercooling leads to formation of dendrites with branches parallel to the {0001} faces. The change to dendritic growth in the presence of PLL impurity occurs at lower supercoolings than in pure deionized water. An increase in PLL concentration inhibits growth rate of the faces of ice crystals at fixed supercooling. Growth rate sharply increases when supercooling reaches a certain critical value. Depression of melting point of ice has not been detected in water with PLL additions. Blocking effect of impurity is explained on the basis of Gibbs-Thomson law and under the assumption of Langmuir's dynamics of PLL adsorption. Retardation of ice growth in the presence of PLL occurs due to following factors: blocking of the surface by molecules of impurity and increase in the viscosity of solution with PLL addition. We used Punin's model for non-equilibrium adsorption [3] as a basis for theoretical description of the shape of kinetic curves $R(\Delta T)$ at different PLL concentrations. Calculated values for the growth rate correspond with the results of our experiments.

1. K. Matsumura, J.Y. Bae, S.H. Hyon. Cell Transplantation. 2010. V. 19. P. 691-699.
2. K. Matsumura, S.H. Hyon. Biomaterials. 2009. V. 30. P. 4842-4849.
3. Yu.O. Punin, O.I. Artamonova. Kristallographiya. 1989. V. 34. P. 1262-1266.

17:00 Poster Mo31

First-principles calculations of structural and electronic properties of GaN(0001)/Ga interface

Przemyslaw Witczak[1], Stanisław Krukowski[1,2]

1. *Polish Academy of Sciences, Institute of High Pressure Physics (UNIPRESS), Sokolowska 29/37, Warszawa 01-142, Poland* **2.** *University of Warsaw, Interdisciplinary Centre for Mathematical and Computational Modelling (ICM), Pawinskiego 5a, Warsaw 02-106, Poland*

e-mail: pfw@unipress.waw.pl

Ga-terminated GaN(0001) surface, covered with gallium metal is studied by density functional calculations within PBE version of GGA approximation, projector augmented waves method and periodic boundary conditions. Slab-vacuum model, rarely used for metal-semiconductor interface simulations, allowed us to vary electric field present in the semiconductor part by introduction of artificial acceptor state on the slab termination surface. We studied the system properties in function of the electric field, Fermi level or equivalently, the doping of the semiconductor bulk. The configurations used are 1x1 and 2x2 slabs with vacuum up to 30 Å to cancel the effect of periodicity. Metallic part of the structure was deposited and relaxed one by one Ga layers on top of GaN slab. The system is classical metal-semiconductor Schottky junction, but due to the low melting temperature of gallium, this work could be treated as the first step towards modelling of GaN and liquid phase of Ga interface. The work of Rosa and Nuegebauer [Phys. Rev. B 73, 205346 (2006)] where 1-2 gallium monolayer coverage of GaN was considered, is extended for several metal layers. The following structural and electronic parameters, customary used to describe metal-semiconductor interface, are calculated: structural parameters of Ga phase imposed by GaN (hexagonal ABAB with possible stacking faults) as compared to orthorhombic α-Ga phase, the most stable in the room temperature (few kelvins below melting point), interlayer distances of fully relaxed Ga bulk showing pronounced deviations (about 6.5%), Schottky barrier height (SBH, ~2.6 V for *p*-type or, adequately, ~0.8 V for *n*-type GaN), electric potential irregularities of Ga part (3-layer range order), projected density of states across the structure confirming fast fade-out of metallic states (two layers) inside the semiconductor, band edges of the semiconductor part, band structure projected onto interface plane (Γ-K-M). The possibility of emergence of the localized midgap states is discussed. The consequences of the obtained results are discussed, e.g., metallicity of the system (bandgap closure), linear dependence of SBH and energy levels on electric field. (The research supported by the EU within European Regional Development Fund, grant Innovative Economy POIG.01.01.02-00-008/08, and Polish National Science Center, Grant No. 2012/05/B/ST3/02516.)

17:00 Poster Mo32

The global theory of deep cellular growth in direcional solidification

Jian-Jun Xu[1], Yong-Qiang Chen[2]

1. *McGill Unversity, 805 shebrooke street, west, Montreal H3A0B9, Canada* **2.** *Tianjin Univesity of Urban Construction, Tianjin 300384, China*

e-mail: xu@math.mcgill.ca

The present paper elustrates the global theory of deep cellular growth in directional solidification. Especially the paper demonstrates the following issues: the multiple structure of steady state solutions, the presence of simle turning point singularty in the root region, the mechanism interface-closure; the global stabilities of the system and selection of steady states, the essence of the side-branching structure formed in oscillatory cellular growth.

17:00 Poster Mo33

Global stabilities and selection of lamellar eutectic growth in directional solidifation

Jian-Jun Xu[1], Xiang-Ming Li[2]

1. *McGill Unversity, 805 shebrooke street, west, Montreal H3A0B9, Canada* **2.** *School of Materials Science and Engineering, Kunming University of Science and technology, Kunming 650093, China*

e-mail: xu@math.mcgill.ca

The present paper is concerned with the global stability mechanisms of the steady state of lamellar eutectic growth in directional solidification, which depends on two free parameters the Peclect number ε and the tilted angle φ.

We perform the asymptotic analysis in the limit of Peclet number $\varepsilon \to 0$ and the segregation coefficient parameter $\kappa \to 1$ and find that the system involves two types of global instabilities: the low frequency (LF) instability and the oscillatory wave (OS) instabilities. Each of these stability mechanisms may have two types of modes, symmetric (S)-modes and anti-symmetric (A)-modes. The neutral LF modes yield the steady interface-patterns, while the neutral oscillatory wave modes yield the oscillatory interface-patterns. It appears that similar to the case of deep cellular growth, there is no selection in eutectic growth, neither for the steady state, nor for the oscillatory state. The neutral curves of these two types of global instability mechanisms on(φ,ε) - plane have the intersection, which determines the transition of the steady periodic pattern to the oscillatory pattern.

17:00 Poster Mo34

Form I/II binary crystal phase morphology of melt grown isotactic polybutene-1

Motoi Yamashita

Chiba Institute of Technology, 2-1-1 Shibazono, Narashino, Chiba 275-0023, Japan

e-mail: motoi.yamashita@it-chiba.ac.jp

Isotactic polybutene-1 (PB1) has outstanding mechanical properties. However, its applications are limited compared to those of the lighter olefin polymers such as polyethylene and polypropylene. One main reason is the complication introduced by crystal structure transformations. PB1 is polymorphous, with form I (trigonal form) and form II (tetragonal form) as the most common structures. Form I is stable and form II is metastable, but despite the metastability it is always form II which is obtained when PB1 crystallizes from the melt. The transformation to form I then takes place after cooling to room temperature, accompanied by strain of crystallized samples; several days are needed for it. Because of this transformation and strain, direct melt crystallization of PB1 form I has long been a big issue. In the 1990's, Kopp *et al.*[1] reported a breakthrough in forming form I. They successfully crystallized the form I in the melt via epitaxy on aromatic acids or salts, and demonstrated that the form I can grow in the melt even at atmospheric pressure if appropriate substrates are provided. We presented a new solution to this problem in our recent study[2]. Using solution-grown form I crystals as nuclei, we demonstrated that the form I crystals can grow in the melt via self-seeding at atmospheric pressure.

In the present work, we report the preliminary study of the morphology of PB1 form I single crystals coexisting with form II spherulites and form I single crystals in thin films. We are going to discuss briefly the influence of form II spherulite growth on the growth shape of melt crystallized PB1 forn I crystals grown by self-seeding.

[1] Kopp, S.; Wittmann, J.C.; Lotz, B, *Polymer***35**,*916*, 1994.

[2] Yamashita, M.; Hoshino, A.; Kato, M, *J. Polym. Sci. Part B: Polym. Phys.***45**, *684*, 2007.

17:00 Poster Mo35

Formation and melting of high pressure rotator phase of n-tridecane, pentadecane and heptadecane studied by FT-IR

Motoi Yamashita

Chiba Institute of Technology, 2-1-1 Shibazono, Narashino, Chiba 275-0023, Japan

e-mail: motoi.yamashita@it-chiba.ac.jp

The effect of pressure on the phase transition behavior of tridecane (C_{13}), pentadecane (C_{15}) and heptadecane (C_{17}) has been investigated up to 489, 220 and 387 MPa, respectively, using Fourier transform infrared spectroscopy at 25 °C. The transition between the high pressure ordered (HPO) and high pressure rotator (HPR) phase has been observed in the pressure ranges of 270–220, 106–95 and 152–181 MPa for C_{13}, C_{15} and C_{17}, respectively, and the transition between the HPR and liquid phase was observed in the pressure ranges of 171–112, 73–47 and 43–70 MPa for C_{13}, C_{15} and C_{17}, respectively. The P_1+P_3 band of the methylene rocking mode exhibits factor group splitting caused by intermolecular vibrational coupling. This was observed in both the HPO and HPR phases, while the P_1+P_3 band did not split in the liquid phase. The separation of the peaks in the P_1+P_3 band changed discontinuously at the HPO-HPR and HPR-liquid phase transitions, even though the separation is known to change continuously in the transition from the liquid to the high temperature rotator (HTR) phase. In the HPR phase, the ratio of the intensities of the higher and lower frequency components in the P_1+P_3 doublet is roughly unity independent of pressure, while it is known to be much less than unity in the HTR phase. The separation of the P_1+P_3 doublet in the HPR phase is found to be larger for longer alkanes. From the intensity ratio, a large proportion of alkane molecules is believed to participate in intermolecular vibrational coupling and possess herringbone-type short-range positional order in the HPR phase. Conversely, in the HTR phase only small proportion of alkane molecules participate in intermolecular vibrational coupling. From the pressure dependence of the separation of the doublet, intermolecular vibrational coupling and herringbone-type short-range positional order is considered to change discontinuously

at the HPR-liquid phase transition, while they are reported to change continuously at the HTR-liquid phase transition. The HPR-liquid phase transition is governed by the effect of molecular packing while the HTR-liquid phase transition is predominantly governed by the difference in entropy between the herringbone-type and parallel-type packing.

17:00 Poster Mo36

Regime transition of isotactic polybutene-1 form II crystal growth

Motoi Yamashita

Chiba Institute of Technology, 2-1-1 Shibazono, Narashino, Chiba 275-0023, Japan

e-mail: motoi.yamashita@it-chiba.ac.jp

For polymers and low-molecular-weight materials, crystallization mechanisms have been investigated through the morphology and growth rate of crystals. The nucleation theory of Hoffman[1] successfully explained the temperature dependence of polymer crystal growth rate by categorizing the growth mode into three distinct regimes, I, II and III, depending on the relative rates of formation of new surface nuclei on the growth front and the rate at which the nuclei once formed spread along the growth front. Regime I corresponds to single nucleation growth mode. At low supercoolings, the rate of spreading is so large compared with the rate of nucleation that a nucleus once formed spreads right across the growth front. Regime II is a growth mode of multiple nucleation. At higher supercoolings, several nuclei form and spread across the growth front together, the separation between them decreasing with increasing supercooling. Regime III corresponds to rough surface growth. At sufficient supercoolings, the separation is of the order of the molecular width and no more spreading takes place.

Between different growth regimes, transitions are observed in the temperature dependence of crystal growth rate. Regime I-II transition has been investigated in association with the morphological change of lateral growth shape of lamellar crystals. The most typical examples are change from lenticular shaped crystals into truncated-lozenge shaped ones reported for polyethylene by Toda et al[2]. Regime II-III transition corresponds to a change from multiple nucleation mode into rough surface growth mode, and one can naturally associate it with kinetic roughening transition of lateral growth shape. However, reports of morphological change of lamellar crystals in association with regime II-III transition are very few[3, 4].

We have investigated the melt crystal growth of isotactic polybutene-1 (PB1) form I (trigonal phase) and form II (tetragonal phase) in order to elucidate the mechanisms of polymer crystal growth and to explain growth kinetics consistently with morphology change of crystal growth shape[5,6]. Recently, PB1 is of growing interest because of its outstanding mechanical properties and its excellent thermal properties. Investigating PB1 crystal growth is also significant from a practical standpoint. In our previous work [5,6], we observed the kinetic roughening transition of PB1 form II crystals. In this work, we are going to make a preliminary report of regime II-III transition of form II crystals in association with kinetic roughening transition.

[1] Hoffman, J. D.; Miller, R. L. *Polymer***38**, *315*, 1997.

[2] Toda, A.; *Faraday Discuss. Chem. Soc*. **95,***129*, 1993.

[3] Abe, H.; Kikkawa, Y.; Inoue Y.; Doi, Y.; *Biomacromolecules***2**, *1007*, 2001.

[4] Abe, H.; Harigaya, M.; Kikkawa, Y.; Tsuge, T.; Doi, Y.; Biomacromolecules **6**, *457*, 2005.

[5] Yamashita, M.; Miyaji, H.; Hoshino A.; Izumi, K.; *Polymer J.*, **36**, *226*. 2004.

[6] Yamashita, M.; Miyaji, H.; Hoshino A.; Izumi, K.; *Polymer J.*, **41**, *1152*. 2009.

17:00 Poster Mo37

Growth behavior of monohydrocalcite crystals in silica rich alkaline solution

Gan Zhang, José Manuel Delgado López, Duane Choquesillo-Lazarte, Juan Manuel Garcia-Ruiz

Instituto Andaluz de Ciencias de la Tierra, CSIC-UGR (LEC-IACT), Avda. Las Palmeras, nº 4, Granada 18100, Spain

e-mail: ganzhang@ymail.com

Monohydrocalcite (MHC, $CaCO_3 \cdot H_2O$) is a metastable calcium carbonate crystalline phase, which can be rarely found in nature compared to other anhydrous crystalline phases such as calcite and aragonite or even vaterite.[1] In laboratory, most of the experiments reported that MHC has been synthesized by the reaction of Ca^{2+} and CO_3^{2-} in the presence of Mg^{2+} when the Mg/Ca ratio was higher than 1, the results suggesting that Mg^{2+} played a key role in MHC crystallization.[2] Although there were a few exceptions found that MHC can be synthesized without the presence of Mg^{2+}, the MHC crystal in these experiments behaved as an intermediated product and transformed into stable anhydrous calcium carbonate (calcite and aragonite) soon.[3, 4]

In this study, we show that the precipitation of calcium carbonate in silica rich alkaline solution by the counterdiffusion method results in the formation of spherical multi-layers structures made only of MHC crystals. The in situ analysis by X-ray diffraction (XRD) and Raman spectroscopy showed unequivocally that MHC is the only phase forming these structures and that the as formed MHC can be stabilized in the absence of Mg^{2+} at least for the duration of our experiments (months). Video optical microscopy showed that the MHC start growing as peanut-like crystals during the first week crystallization. Then, they develop into spherical structures with size of hundreds meters after 4 weeks growth. Further studies by field emission scanning electron microscopy (FESEM) and energy dispersive X-ray analysis (EDX) reveal that the multi-layers structure consisted of plenty of nano-rod and nano-sphere particles in different layers, the outer layer contains more silica than the former. These results suggested that silica played a key role in the formation of MHC multi-layer structure. The variation in time of pH and Ca^{2+} concentration during the crystallization was followed by pH microprobe and ICP-OE spectrometry, respectively. The time variation was correlated with the morphological evolution, as the crystallization of MHC can be divided into 4 stages according to the pH changes, namely: the initial MHC crystallization, the development from peanut-like structure to spherical structure, the formation of the multi-layers structure and the formation of silica outer skin.

According to our results, the formation of the multi-layers structure is thought to be driven by the different level of coupling between calcium carbonate and the coprecipitated silica in different stages of the crystallization, as well as the different silica content in nano-rod and nano-sphere particles. We propose that the precipitation of calcium carbonate decreased the local pH and thus triggered the coprecipitation of silica on the surface of the crystal. On the other hand, the precipitation of silica would increase the local pH again, which provoke the new nucleation and growth of calcium carbonate crystals. From the iteration of these two consecutive steps a multi-layer structure would result. Noticeably, we fail to get MHC precipitation in parallel experiments by either counter diffusion method without silica or classical mixing experiments with silica, which suggested: a) the key role of silica in

the formation of MHC and b) the importance of the supersaturation rate in $CaCO_3$ in selecting the precipitation of the MHC polymorph.

1. T. Kimura and N. Koga, The Journal of Physical Chemistry A, 2011, 115, 10491-10501.
2. F. Keisuke, M. Takashi, S. Minoru and Y. Shintaro, Sci. Tech. Adv. Mater., 2011, 12, 064702.
3. E. T. Stepkowska, J. Therm. Anal. Calorim., 2005, 80, 727-733.
4. C. Jiménez-López, E. Caballero, F. J. Huertas and C. S. Romanek, Geochim. Cosmochim. Acta, 2001, 65, 3219-3231.

General Session 2

Bulk crystal growth

Session Coordinators

Izabella Grzegory (Poland) *izabella@unipress.waw.pl*

Partha Dutta (USA) *duttap@rpi.edu*

Programme

Monday, 12 August

MoO1

G02: Bulk crystal growth
Monday morning, 12 August, 11:00
Room A, Auditorium Maximum

11:00 Invited oral

Germanium-doped Crystalline Silicon

Deren Yang

Zhejiang University, State Key Lab of Silicon Materials, 38 Zheda Road, Hangzhou 310027, China

e-mail: mseyang@dial.zju.edu.cn

Crystalline silicon is the major material used in both of microelectronic and photovoltaic industry. In the last decades, to lower the cost and improve the quality of crystalline silicon wafers has widely attracted research attention.

Germanium-doped crystalline silicon including both of Czochralski (CZ) silicon and multicrystalline (mc) has developed and intensively investigated by my group since 2002. It was reported that Ge-doping in CZ silicon could suppress void defects, increase oxygen precipitation, improve internal gettering and so on. Moreover, mechanical strength in CZ silicon is also increased by Ge-doping. Therefore, it is believed that Ge-doped CZ silicon should be benefit for integrated circuits (ICs). In fact, it has been used in IC industry last several years.

In this presentation, the behavior of Ge-doped crystalline silicon including both of the CZ silicon and mc silicon which are used for solar cells have been reported. It is believed that Ge-doping could increase the mechanical strength and decrease the breakage of silicon wafers. Meanwhile, the light induced degradation which is considered to be related to boron-oxygen complexes is suppressed in CZ silicon. Therefore, more power will be generated in the modules based on Ge-doped CZ silicon wafers. These findings suggest that Ge-doped crystallie silicon is a promising material for manufacturing the high-efficiency and low-cost solar cells.

11:30 Oral

2D simulation of transient CZ silicon crystal growth including process control

Andrejs Sabanskis, Kristaps Bergfelds, Andris Muiznieks

Faculty of Physics and Mathematics, University of Latvia, Zellu Street 8, Riga LV-1002, Latvia

e-mail: andrejs.sabanskis@gmail.com

The Czochralski (CZ) technique is widely used for the growth of monocrystalline ingots of semiconducting silicon (Si). Because the quality and physical properties (such as distribution of dopants) as well as the diameter of crystals have to be in a certain range, CZ puller has to be equipped with several mechanisms for the fine-tuning of the growth process. Typically, for the control of the flow in silicon melt, crucible and crystal rotation and an external magnetic field are used. Crystal diameter is traditionally controlled by two PID controllers, which adjust crystal pulling velocity and heater power.

The crystal is grown starting from a small seed crystal, which radius is carefully increased until the necessary crystal diameter value is reached. It is evident that effective mathematical and numerical methods are needed to capture the whole evolution of CZ process. Although this problem has already been addressed, see, e.g., [1, 2], there are still no publications in which the algorithm of handling the moving unstructured meshes is described and PID-based process control using crystal radius value is considered.

We present a non-stationary axisymmetric mathematical model of CZ Si growth, which is based on the transient model of floating zone process [3, 4]. A schematic view of the simplified CZ system is shown in Figure 1. Crystal-melt, melt-gas and crystal-gas interfaces are calculated in a transient way; the size of the mesh elements on the changing boundaries is automatically adjusted and unstructured finite element mesh is regenerated to fit the changing geometry. The non-stationary temperature field in crystal and melt is solved using the FEM. Only the main system components are modelled, e.g., while the heat transfer by thermal radiation is calculated with view factors, the influence of CZ puller walls is taken into account by the effective ambient temperature. The overall calculation algorithm of the develop computer program CZ-Trans is given in Figure 2.

For the control of crystal diameter, two PID-based controllers are considered, as shown in Figure 2. The output of the second controller is the change of heater power. For faster calculations, the temperature field in the heater is not solved explicitly; the change of heater temperature is related to the power change by using a simple integral model. Calculation example shown in Figure 3 demonstrates a successful simulation of CZ Si growth, which was started from a small seed crystal. To follow the considerable changes of the crystal geometry, the precise shape of crystal side surface is saved and used for the creation of a rougher mesh for temperature and radiation calculations.

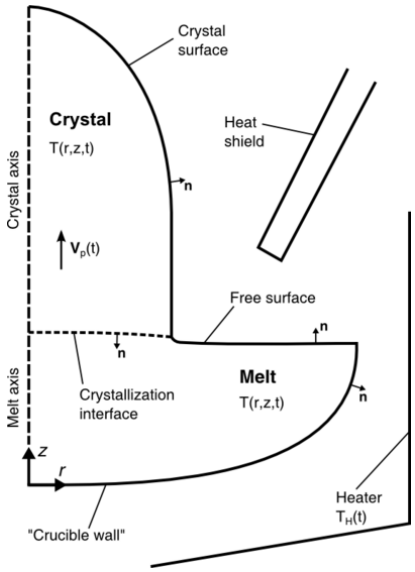

Figure 1.*An axisymmetric approximation of simplified Czochralski system.*

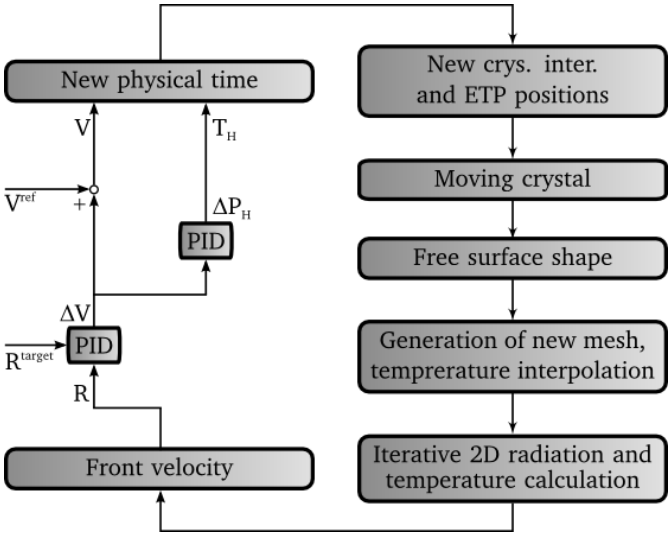

Figure 2.*A simplified calculation scheme. R is the crystal radius, V is the crystal pulling velocity, ΔP_H is the change of heater power. The change of heater temperature, T_H, is calculated using an integral model.*

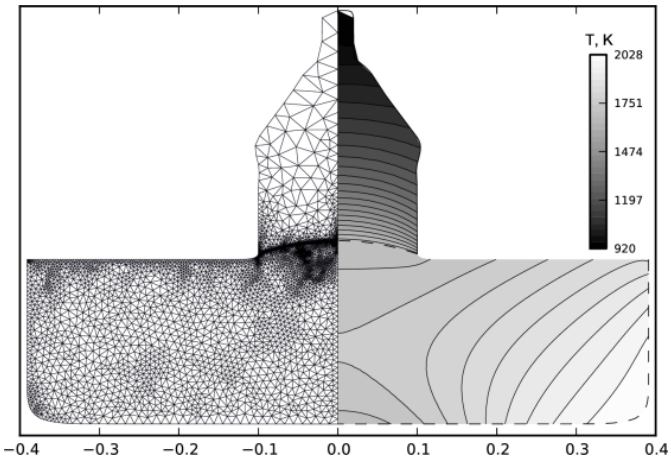

Figure 3.*Calculation example. Shown are the used finite element mesh, the calculated temperature field in crystal and melt, as well as the saved history of crystal shape.*

Acknowledgements

The present work is carried out at the University of Latvia and has been supported by the European Regional Development Fund, project contract No. 2011/0002/2DP/2.1.1.1.0/10/APIA/VIAA/085.

References

1. N. V. den Bogaert, F. Dupret, Dynamic global simulation of the Czochralski process I. Principles of the method. Journal of crystal growth 171(1-2):65-76, 1997.

2. F. Dupret, R. Rolinsky, L. Wu, F. Loix, A. De Potter, N. Van den Bogaert, V. Regnier, Global Simulation of CZ and FZ Bulk Crystal Growth: from Quasi-Dynamic and Dynamic Modelling to Process Control and Crystal Quality Optimization. ECS Transactions 18(1):935-943, 2009.

3. A. Rudevičs, A. Muižnieks, G. Ratnieks, A. Mühlbauer, Th. Wetzel, Numerical study of transient behaviour of molten zone during industrial FZ process for large silicon crystal growth. Journal of Crystal Growth 266(1-3):54-59, 2004.

4. A. Rudevics, A. Muiznieks, H. Riemann, A. Luedge, G. Ratnieks, W. von Ammon, Numerical study and comparisons with experimental data for transient behaviour of phase boundaries during industrial FZ process for silicon crystal growth. Journal of Crystal Growth 275(1-2): e561-e565, 2005.

11:45 Oral

Crystal growth of 50 cm square single crystal Si by directional solidification and its characterization

Yoshiji Miyamura[1], Hirofumi Harada[1], Karolin Jiptner[1], Jun Chen[1], Ronit R. Prakash[1,3], Takashi Sekiguchi[1,3], Satoshi Nakano[2], Bing Gao[2], Koichi Kakimoto[2]

1. *National Institute for Materials Science (NIMS), 1-1 Namiki, Tsukuba, Ibaraki, Tsukuba 305-0044, Japan* **2.** *Kyushu University, Fukuoka, Japan* **3.** *Tsukuba Univ., Tsukuba 305-8577, Japan*

e-mail: sekiguchi.takashi@nims.go.jp

It is necessary to achieve an efficiency of more than 20 % using low cost Si wafers. To meet this demand, growth method of single crystal Si by directional solidification, so called mono cast Si, has been proposed by BP solar [1,2]. Although a lot of efforts have been made to realize this technique, the mono-cast Si ingots of high quality have not yet appeared in the market due to several problems.

The first problem is to set a seed before growth. If we grow larger ingot, we need either to place the multiple seeds at the bottom of a cast crucible or conduct the crystal growth from a small seed. We have selected the latter choice and have partly succeeded in the growth of ingots of 50 cm square. The crystal growth condition was determined according to the result of numerical calculation [3]. The mushroom shaped interface is realized during the growth.

The second problem is to avoid light elements such as C, N, and O from the ingots. The reduction of C was realized by optimizing the gas flow condition.

The third problem is to reduce the residual strain and dislocations. By controlling the crystal growth and the following cooling history, the residual strain is reduced to the level without breakage. The dislocations/lineage and twins are also reduced by optimizing the growth procedure.

Now, the device performance of the mono-Si is going to be characterized to prove the advantage of this method.

Acknowledgement

This work was partly supported by the New Energy and Industrial Technology Development Organization (NEDO) under the Ministry of Economy, Trade and Industry (METI).

REFERENCES

[1] B. Wu, N. Stoddard, R. Ma, R. Clark, J. Cryst. Growth, 310 (2008) 2178.

[2] N. Stoddard, B. Wu, I. Witting, M. Wagner, Y. Park, G. Rozgonyi, R. Clark, Solid State Phenom, 131-133 (2008) 1.

[3] B. Gao, S. Nakano, H. Harada, Y. Miyamura, T. Sekiguchi, K. Kakimoto, J. Cryst. Growth, 352 (2012) 47.

12:00 Oral

Relationship between cooling flux direction and activation of slip systems of single -crystal silicon grown in [001] and [111] directions

Bing Gao[1], Satoshi Nakano[1], Hirofumi Harada[2], Yoshiji Miyamura[2], Koichi Kakimoto[1]

1. *Kyushu University, Fukuoka, Japan* **2.** *National Institute for Materials Science, Tsukuba 305-0047, Japan*

e-mail: gaobing@riam.kyushu-u.ac.jp

Dislocations in semiconductor crystals adversely affect the characteristic properties of semiconductors [1]. Dislocation-free or low-dislocation density bulk semiconductor crystals are required for substrates of high-performance electronic devices. To control and reduce the dislocation, the generation mechanism of dislocation has been broadly studied [2-4]. It is known that a dislocation can originate from several factors, such as agglomeration of point defects, surface damage, foreign particles or precipitates, chemical inhomogeneities, defective seeds, and thermal stress. Thermal stress is regarded as a primary reason for the presence of dislocations in as-grown crystals, and is mainly caused by the temperature gradient that exists during the crystal growth and cooling processes.

During crystal growth, the cooling rate must be controlled to a small value to grow high-quality crystals, and thus, the thermal stress is generally small; however, during cooling, the cooling rate is usually set to be high to decrease the production cost, and thus, the thermal stress is generally large. Therefore, a critical issue in reducing the dislocation density is how to control the cooling process.

Controlling the cooling process involves controlling both the radial cooling flux and the axial cooling flux. To determine the most effective method to reduce the dislocation density by adjusting the cooling flux, it is essential to determine the relationship between the activated slip system and its corresponding activation flux in the radial and axial directions (radial flux and axial flux). In this paper, we address this theoretical problem.

Results show that the effect of cooling flux on the activation of slip systems in single-crystal silicon is dependent on the directions of the cooling flux and crystal growth. For crystal growth in the [001] direction, the 12 slip directions can be divided into an 8-fold symmetric group A_{B2} and a 4-fold symmetric group B_{A1}. For crystal growth in the [111] direction, the 12 slip directions can be divided into three 3-fold symmetric groups C_{A2}, D_{A2}, and E_{A1}. Irrespective of the direction of crystal growth, radial flux only activates dislocation at the edges of slices and axial flux activates dislocation both in the interior and at the edges of slices.

For [001] growth, radial flux can activate both eight-fold symmetry (group A_{B2} at the edges of slices near both ends) and four-fold symmetry (group B_{A1} at the edges of slices between the ends); however, axial flux can only activate eight-fold symmetry (group A_{B2} in the interior of slices near both ends and at the edge of slices between the ends). For [111] growth, radial flux can only activate three-fold symmetry (group D_{A2} at the edges of slices); however, axial flux can activate both groups C_{A2} and E_{A1}, where group C_{A2} exists in the interior of slices near both ends and at the edges of slices between the ends, and group E_{A1} only exists in the interior of slices close to both ends.

For practical crystal growth, it is essential to reduce the radial cooling flux as much as possible for the reduction of dislocation density.

Reference

[1] G. Dhanaraj, K. Byrappa, V. Prasad, M. Dudley, “Handbook of Crystal Growth”, p1335-1378.

[2] J.P. Hirth, J. Lothe: Theory of Dislocations, Krieger, Malabar, 1992.

[3] H. Alexander: On dislocation generation in semi-conductor crystals, Radiat. Eff. Defects Solids 112(1/2), 1-12 (1989).

[4] W. Zulehner: Czochralski growth of silicon, J. Cryst. Growth 65 (1-3), 189-213 (1983).

12:15 Oral

Evaluation of numerical analysis of residual strain and dislocation density in a multicrystalline silicon for solar cells

Makoto Inoue[1], Satoshi Nakano[2], Karolin Jiptner[3,4], Bing Gao[2], Hirofumi Harada[3], Takashi Sekiguchi[3], Masayuki Fukuzawa[5], Koichi Kakimoto[1,2]

1. *Kyushu University, Fukuoka, Japan* **2.** *Kyushu University, Research Institute for Applied Mechanics, Kasuga 816-8580, Japan* **3.** *National Institute for Materials Science (NIMS), 1-1 Namiki, Tsukuba, Ibaraki, Tsukuba 305-0044, Japan* **4.** *Tsukuba Univ., Tsukuba 305-8577, Japan* **5.** *Kyoto Institute of Technology, Kyoto 606-8585, Japan*

e-mail: snaka@riam.kyushu-u.ac.jp

Multicrystalline sillicon using unidirectional solidification process is the most widely material for solar cells because of its cost-effectiveness and the mass productivity. However, dislocation density and residual stress are serious problems for solar cells because increasing of dislocation densities reduces the conversion efficiency of solar cells and increasing of residul stress causes the fracture of silicon ingot during the slicing process. It has been reported that dislocation densities rapidly increased during cooling process [1, 2]. Therefore, we have to optimize to temperature distribution in a silicon ingot during cooling process. We compared experimental and numerical results of residual strain, dislocation density and residual stress in a silicon ingot. Then, we evaluated the validity of numericalresults.

We investigated time-dependent dislocation multiplication in a silicon ingot. At first, thermal stress distribution in a silicon ingot was solved using temperature distribution in a silicon ingot. Then, we studied stress relaxation, creep deformation and the multiplication of the dislocations using Haasen-Alexander-Sumino model [3, 4].

We checked residual strain as a function of height from the bottom of the silicon ingot quantitatively. The numerical results show that a value of residual strain in a body of a crystal is order of 10^{-5}, and residual strain in the top and bottom areas of the silicon ingot is high (10^{-4}). This difference of residual strain between center area and edge area is due to outgoing thermal flux. Thermal flux in the top and bottom of the silicon ingot is large because conductive heat transfer in the bottom area and radiative heat transfer in the top area of the silicon ingot strongly affects to the residual strain. The value and distribution of residual strain obtained by numerical analysis are close to experimental

data. Then, we can analyze residual strain quantitatively using this simulation. However, dislocation density of numerical analysis is not close to experimental data because we assumed a crystal as isotropic, and took into account dislocation multiplication only based on increase rate of mobile dislocation density.

References

[1] M. M'Hamdi, E. A. Meese, E. J. Øvrelid and H. Laux, Proceedings 20th EUPVSEC (2005) 1236.

[2] D. Franke, T. Rettelbach, C. Häβler, W. Koch and A. Müller, Sol. Energy Mater. Sol. Cells 72 (2002) 83.

[3] H. Alexander and P. Haasen, Solid State Phys. 22 (1968) 27.

[4] M. Suezawa, K. Sumino and I. Yonenaga, J. Appl. Phys. 51 (1979) 217.

12:30 Oral

Numerical Simulation of Bulk Crystal Growth for Industrial Applications

François Dupret[1,2], Roman Rolinsky[2], Brieuc Delsaute[2], Rajesh Ramaya[2], Nathalie Van den Bogaert[2]

1. *Université Catholique de Louvain (UCL), Louvain-la-Neuve 1348, Belgium* **2.** *FEMAGSoft S.A., Avenue Jean Monnet 1, Louvain-la-Neuve B-1348, Belgium*

e-mail: francois.dupret@uclouvain.be

Bulk crystal growth has major high-tech applications among which three particularly important uses should be highlighted: (i) Integrated Circuit (IC) components such as DRAMs, transistors, etc., which all over fill our everyday life, are manufactured on mono-crystalline silicon or other semi-conductors; (ii) most solar cells are made on mono- or multi-crystalline silicon wafers; (iii) mono-crystalline sapphire is the key substrate of blue LEDs as devoted to completely replace traditional lighting in the near future. In general single- and multi-crystals represent strategic products to drive the progress of new and clean technologies for the forthcoming years.

Most of industrial bulk crystals are grown from the melt except in those peculiar cases where this technique is not applicable. In particular the Czochralski (Cz) process is principally used to grow mono-crystalline silicon boules for IC and solar applications. However the production of large diameter high quality wafers generally requires making use of rigid magnetic fields of various shapes (transverse or configured) to stabilize the melt flow. An alternative method to grow silicon single crystals is the Floating Zone (FZ) process, which is more expensive but whose use is needed to produce oxygen-free wafers for power devices. The Cz process may also be applied to grow sapphire single crystals in competition with alternative techniques such as the Heat Exchanger Method (HEM) or the Kyropoulos (Ky) technique. Finally the Directional Solidification System (DSS) is a rapidly developing process to produce silicon multi-crystals for solar applications. Nowadays, at a lower cost, the efficiency of DSS-produced cells almost reaches that of Cz-produced cells, especially when the mono-cast technique is used.

All the above examples may be used to illustrate the privileged interest of numerical simulation to optimize crystal growth and other forming processes. Using a trial and error approach the software user's objective is to perform so-called numerical experiments in order to investigate the effect of any change of the geometry (and especially the hot zone design), the selected material properties and the processing conditions (heater power, crystal growth and rotation rates, etc.) on the resulting crystal quality and process yield. To achieve this goal two requirements have to be fulfilled by the simulation tool: (i) the use of global and, if possible, time-dependent simulations is a need to predict the detail of the crystal and melt thermal evolution, the solidification front shape and the melt velocity field at any stage of the growth process; (ii) the software must have the ability to accurately predict crystal quality and any quantity measuring the process yield as resulting from these global calculations.

FEMAG*Soft* S.A. is a spin-off company of the Université catholique de Louvain (Belgium) whose activity is to develop crystal growth simulation software for industrial use. From its creation in 2003 most of the company research activity has borne on the development of physical models and numerical algorithms to simulate bulk crystal growth from the melt in collaboration with the university [1-5]. Accordingly, on the one hand, various programs have been developed to model the global heat transfer in the overall furnace, the melt and ambient gas flows and the solidification process in order to accurately predict the thermal, mechanical and geometrical evolution of the melt and crystal for Cz, FZ, DSS... processes. On the other hand, additional programs have been developed to predict the resulting crystal quality as measured by point- and micro-defect densities in the crystal (for mono-crystalline silicon or germanium), by thermal stresses and dislocation density (e.g. for mono-crystalline sapphire), and by the concentration of any species characterizing crystal stoichiometry or incorporated into the crystal during the growth process (dopants, impurities, oxygen in silicon growth, etc.). Improving the software prediction accuracy together with reducing the simulation time has constantly governed FEMAG*Soft*'s development strategy.

In general, numerical methods, programming techniques and computer hardware have experienced an accelerating progression rate during the last decades and this has driven a very steep increase of quality of the numerical tools used by the FEMAG family of products. In particular the development of a very efficient linear solver (in terms of computation cost and memory) together with the use of up-to-date numerical methods allow the FEMAG programs to provide well-resolved solutions to the user in a time not exceeding 1-2 days. However getting accurate results remains a complex and hard task in view of the high difficulty to model the involved physical phenomena. This holds true for both global heat transfer and crystal quality modeling. Correlating the resulting crystal quality and process yield to the furnace and process design nonetheless requires to have an accurate physical model at one's disposal. Therefore the current objective of FEMAG*Soft*'s R&D team is to improve the predictive capabilities of the FEMAG models wherever this is possible. This approach is illustrated by several examples in the following paragraphs.

A first application is provided by the growth of large diameter mono-crystalline silicon ingots under the effect of a strong transverse magnetic field [6]. Using this technique is mandatory in view of the very high crystal quality requirements imposed by IC technology. The numerical problem is solved by means of a combined FEM - spectral method with accurate resolution of the very thin Hartmann boundary layers. A key problem is to well-model the flow turbulence, which is rapidly weakened and becomes 2D without being completely cancelled out when the magnetic field is sufficiently strong. To this end a non-isotropic mixing length tensor is introduced in order to correctly model the momentum transfer resulting from the 2D turbulence.

A second application is provided by the growth of silicon multi-crystals by DSS process for the production of solar cells. Here again a combined FEM - spectral technique is applied to efficiently solve the 3D problem. Main issues are to model the growth transitions between columnar and equi-axial grain structures, and also to accurately predict the distribution of species (especially carbon and oxygen) in the crystal, taking into account the effects of the layered flow structure, of

Marangoni convection, of the gas flow and of segregation at the solid-liquid interface.

A last application is provided by the numerical modeling of FZ single crystal growth. Several difficult problems are posed. First, the high-frequency magnetic field has to be accurately calculated including its thermal and mechanical effects which are modeled as a heat flux, magnetic pressure and shear stress acting along the melt surface. This approach is favored to the equivalent but more expensive modeling of Joule heating and Lorentz force by use of refined boundary layer meshes in the melt [7, 8]. Secondly the open melting front is governed by complex physical effects since molten silicon flows along the feed-rod in the form of small droplets or as a non-uniform thin film whose material properties must be correctly averaged. Finally a main issue in FZ growth results from the absence of turbulent mixing. As an undesired technical consequence of this effect the distribution of dopants and of the associated resistivity in the crystal may be strongly segregated and various techniques are used to counteract this problem. These techniques generally result in a loss of the system axisymmetry or quasi-steadiness and hence require appropriate modeling.

References

[1] F. Dupret, P. Nicodème, Y. Ryckmans, P. Wouters, M.J. Crochet, *International Journal of Heat and Mass Transfer* 33 (1990), pp. 1849-1871.

[2] F. Dupret, N. Van den Bogaert, "Modelling Bridgman and Czochralski growth", Handbook of Crystal Growth, Chapter 15, Vol. 2, D.T.J. Hurle editor, Elsevier, 1994, pp. 875-1010.

[3, 4] N. Van den Bogaert, F. Dupret, *Journal of Crystal Growth*, 171 (1997), pp. 65-76, 77-93.

[5] T. Sinno, E. Dornberger, R.A. Brown, W. von Ammon, F. Dupret, "Defect engineering of Czochralski single-crystal silicon", *Materials Science and Engineering: R Reports*, 28 (2000), pp. 149-198.

[6] Y. Collet, O. Magotte, N. Van den Bogaert, R. Rolinsky, F. Loix, M. Jacot, V. Regnier, J.-M. Marchal, F. Dupret, to be published in *Journal ofCrystal Growth* (2012).

[7, 8] F. Bioul, F. Dupret, *IEEE Transactions on Magnetics*, 41 N° 9 (2005), pp. 2496-2505, 2506-2514.

12:45 Oral

Czochralski growth of 2" BaBrI crystals

Evgeniy Galenin, Sergey Gridin, Viktoriia V. Romanchuk, Sergey Vasyukov, Alexander Gektin

Institute for Scintillation Materials NAS of Ukraine (ISMA), Lenina ave., 60, Kharkov 61001, Ukraine

e-mail: galenin@isma.kharkov.ua

Modern need in equipment for prevention of radioactive terrorism is a driving force for development of scintillation detectors with improved characteristics, first of all, high light yield and energy resolution. BaBrI host is considered as one among the most promising for activation with Eu^{2+}. Recently, it has been demonstrated that BaBrI:Eu possesses a high light yield about 100000 ph/MeV and excellent energy resolution 2,55% (^{137}Cs), fast scintillation decay (~500 ns) relatively to other alkali earth halides [1]. The main problem limiting development and application of such materials is a high hygroscopicity. BaBrI is less hygroscopic relatively to $LaBr_3$, SrI_2, $CsBa_2I_5$ hosts.

BaBrI:Eu, as well as other alkaline earth halide crystals, are usually grown by Stockbarger method in evacuated ampoules in order to prevent oxidation. Crystals grown by this method are limited in diameter by ampoule size and normally do not exceed 1" - 1.5" in diameter. Absence of a seed does not guarantee growth orientation and structure perfection of grown crystals. They often crack due to adhesion to the material of ampoules.

This work is devoted to development of the Czochralski (CZ) growth technology of BaBrI. At current stage the growth conditions are optimized for 2" diameter ingots. A specific technique preventing raw material interaction with atmospheric air at uploading of raw material into the crucible was utilized.

Influence of radial temperature distribution in the crucible on the crystal-melt interface shape is studied. It is shown that the radial gradient of 15-20 K/cm leads to growth interface convexity and deterioration of crystal quality. Reduction of the radial gradient down to 5 K/cm leads to flattening of the crystallization interface and provides stable conditions of pulling for 2" diameter crystals (see fig.1.)

Figure 1. BaBrI 2" diameter CZ grown crystal.

Presence of oxygen-containing impurities was estimated by IR transmission measurements. The grown crystals have the absorption band at 880 cm^{-1} and 1410 cm^{-1} corresponding to CO_3^{2-}. The luminescence spectra demonstrate a set of bands ranging from 400 to 550 nm, which is in agreement with spectroscopic measurements made with undoped crystals obtained by the Stockbarger technique [2].

[1] E.D. Bourret-Courchesne, G. Bizarri, at al., Nuclear Instruments and Methods in Physics Research, A 613 (2010), 95–97.

[2] R. Hawrami, J. Glodo, E.V.D. van Loef, at al., IEEE Transactions on Nuclear Science, doi 10.1109/TNS.2013.2240696.

Lunch (JCG Editors meeting)

Monday afternoon, 12 August, 13:00

MoO2

G02: Bulk crystal growth
Monday afternoon, 12 August, 15:00
Room A, Auditorium Maximum

15:00 Invited oral

High-pressure synthesis of large high-quality single crystal diamonds

Hitoshi Sumiya

Sumitomo Electoric Industries (SEI), 1-1-1,Koyakita,Itami,Hyogo, Hyogo 664-0016, Japan

e-mail: sumiya@sei.co.jp

We have succeeded in synthesizing high-quality, large-size type IIa diamond crystals, measuring up to 12 mm in diameter or about 10 carats by the temperature gradient method under high pressure and high temperature (HPHT) of 5.5 GPa and 1300-1400 ^{o}C. The important points in the synthesis of the high-quality diamond crystals are the adequate selection and optimization of solvent metals and additives [1], the improvement of crystalline quality of seed crystal [2], and the high precious HPHT control over a prolonged time [3].

The derived high-quality diamond crystals have very few impurities (less than 0.1 ppm) and high crystalline quality (few crystal defects and little internal strain). X-ray topography found no crystal defects such as dislocations and stacking faults in the (001) growth sector of the large crystal grown on high-quality (001)-oriented seeds. Growth of crystals in which the (001) surface is dominant via advanced control of synthesis temperatures in the low-temperature region enabled us to produce diamond crystals free from crystal defects in large areas measuring 5 x 5 mm^2 or more [4]. The defect-free synthetic diamond will be valuable for a wide range of industrial and scientific applications such as optical windows, optical elements for synchrotron radiation, various high-sensitive detectors (sensors), substrates for high-quality CVD homoepitaxial diamonds, and so on. The excellent crystalline perfection of the high-quality synthetic diamond also permits us to comprehend the essential properties of diamond and to clarify the effects of the impurities and defects on the diamond properties.

REFERENCES

[1] H. Sumiya, S. Satoh, Diamond Relat. Mater., **5**, 1359 (1996).

[2] H. Sumiya, N. Toda, Y. Nishibayashi, S. Satoh, J. Crystal growth, **178**, 485 (1997).

[3] H. Sumiya, N. Toda, S. Satoh, J. Crystal Growth, **237-239**, 1281 (2002).

[4] H. Sumiya, K. Tamasaku, Jpn. J. Appl. Phys., **51**, 090102 (2012).

15:30 Oral

Ultra-high quality SiC crystal grown by solution method utilizing the conversion from threading dislocations to basal plane defects

Toru Ujihara, Yuji Yamamoto, Shunta Harada, Shiyu Xiao, Kazuaki Seki

Department of Materials Science and Engineering, Nagoya University, Furo-cho, Chikusaku, Nagoya 464-8603, Japan

e-mail: ujihara@numse.nagoya-u.ac.jp

Silicon carbide (SiC) is a promising material for next-generation power device. The performance of the SiC power device strongly depends on the crystal quality of SiC substrate. State of the art bulk growth of SiC crystals is carried out by the seeded sublimation growth method. In the early stage of the development, the unique macro-defect i.e. "micropipe," was a critical problem. 4 inch wafers are commercially available with almost zero micropipe density, today In current growth technology, however, crystals include the other extended defects (threading dislocations and basal plane dislocation) affecting the reliability.

Recently we have achieved the growth of ultra-high quality SiC crystal with top-seeded solution growth method utilizing the conversion phenomenon from threading dislocations to basal pane defects. For instance, the density of threading screw dislocation (TSD) in the crystal grown by the solution method (20-30 cm^{-2}) was much lower than that of the crystal produce by using conventional sublimation method (~1000 cm^{-2}). Moreover, it is easier to decrease the defect density in the short-term growth compared to the RAF (repeated *a*-face) method which is well-known as the specially modified sublimation method.

The key to high-quality crystal growth is to utilize the defect conversion due to the macrostep flow. Figure 1 shows the X-ray topographic images of 4H-SiC layer grown on vicinal (0001) Si-face taken at the same position before and after growth. Before the growth, we can observe many rice-shape images corresponding to TSDs. After the growth, most of the TSD images changes to line images extending towards the step-flow direction corresponding to the Frank-type plane defects on basal planes. The conversion phenomenon is induced by the macrostep flowing over the TSD on the surface, and the frequency of the conversion depends on the height of macrostep. In addition, the macrostep flowing leads to the conversion from threading edge dislocations (TEDs) to defects on basal planes as well. These conversion phenomena can improve the quality of SiC crystal. As shown in Fig. 2, the threading dislocations propagate to the grown layer, while the defects lying on basal planes are finally wiped out. Actually, we have successfully achieved the ultra-high quality SiC crystal utilizing the conversion phenomenon.

Several years ago, it was believed that the bulk growth of solution method was impossible because of low growth rate, the difficulty of polytype control, enlargement of crystal size and so on. Recently, many groups can overcome these problems. Each solution is still independent now, but we cannot realize them together. The last remaining problem that is to merge these solutions and develop an unified technique. We firmly believe that it will be completed within a few years.

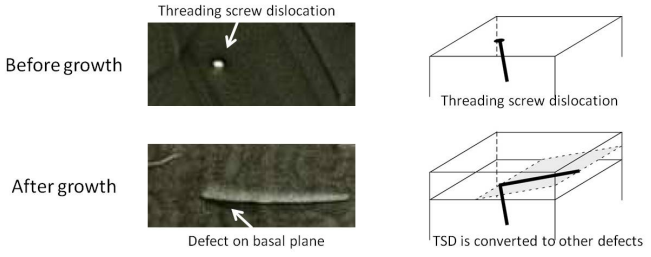

Fig. 1: X-ray topographic images of 4H-SiC grown on a vicinal (0001) seed crystal before and after growth. The rice-shape image (TSD) was changed to the line image (defect on basal plane).

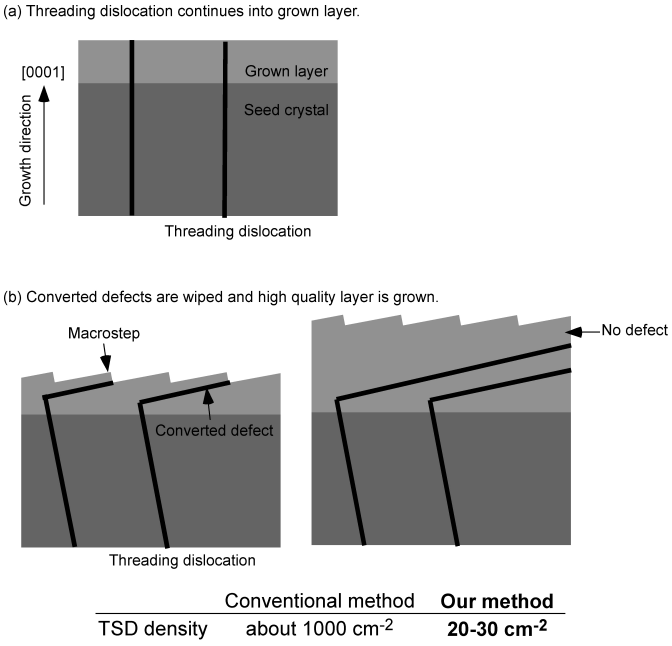

Fig. 2: (a) Without macrostep-flow, most of threading dislocations propagate to the grown layer. (b) With macrostep-flow, threading dislocations are converted to defects on basal planes and they are wiped. Consequently high-quality crystal is achieved.

15:45 Oral

Growth of Cr-containing topaz single crystals on a seed and their characterization

Vladimir S. Balitskiy[1], Liudmila V. Balitskaya[1], Denis V. Balitski[2], Viktor A. Rassulov[3], Tatiana V. Setkova[1]

1. *Institute of Experimental Mineralogy RAS (IEMRAS), Acad. Osipiana St, Chernogolovka 142432, Russian Federation* **2.** *Cristal Laser SA, 32 rue Robert Schuman, Messein 54850, France* **3.** *Federal state unitary enterprise "All-russian scientific-research institute of mineral resources named after N.M.Fedorovsky", Moscow 119017, Russian Federation*

e-mail: balvlad@iem.ac.ru

We report the first successful growth of Cr-containing topaz single crystals on seeds by hydrothermal method. Crystal growth was based on received earlier results of study of silica/alumina transport phenomena in supercritical water solutions. This study concerns investigation of growth conditions of Cr-topaz crystals: compositions of solution, TP parameters and nutrient materials. So, the principal condition of topaz crystal growth is neutral and acid fluoride solutions of density from 0.05 to 0.5 g/cm^3 at temperatures from 450 to 720°C. The nutrient consisted from mixture of both quartz and topaz places in the upper (colder) zone of autoclave. The topaz seeds best position is in lower (hotter) zone of autoclave. Some quantity of chrome ions were injected into solution by dissolution of chromium salts. Duration of the crystal growth runs was from 1 to 2 months.

As a result, topaz single crystals of bluish-green to yellowish green colour were grown (Fig. 1). The external morphology of the as grown crystals is determined by crystallographic orientation of seeds, their form and sizes. The crystals are characterized by a clear zoning and sectorial structure (see Fig. 1).

The described feature of colour change of natural Cr-topaz under different wavelength light was observed as well on synthesised Cr-topaz single crystals. At normal incandescent lamp illumination the Cr-topaz get a pink coloring, and at ultra-violet radiation (337 nm) as grown crystals demonstrate an intensive fluorescence of purple-red colour (see Fig. 1). The primary colouring of as grown crystals and also intensive fluorescence are connected with isomorphic occurrence of Cr^{+3}/Al^{+3} and confirmed by optical and fluorescent spectres. The content of Cr^{3+} in the crystals doesn't exceed 0.2-0.5 mass. %.

Thus, for the first time Cr-containing topaz single crystals with intensive fluorescence was grown in supercritical fluids and their structure characteristics and main properties were studied.

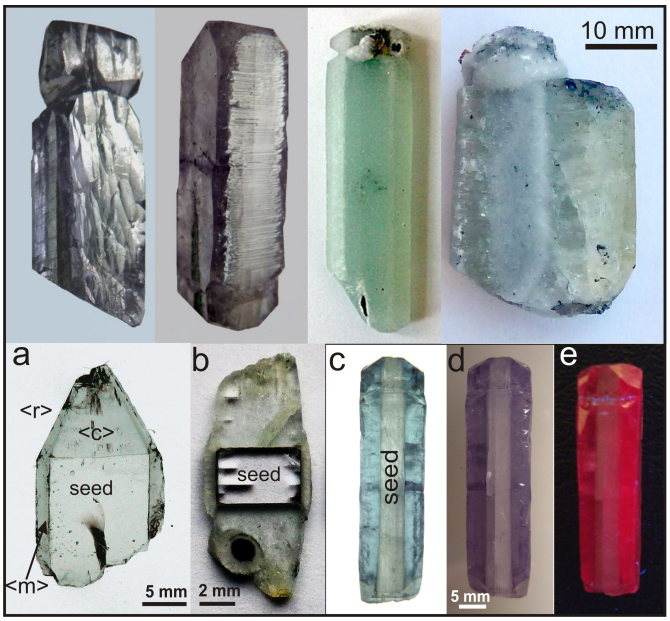

Fig. 1 The top line: Cr-containing topaz crystals for the first time grown in supercritical fluids; the bottom line: a,b - cross-section cuts of the grown crystals; Gr-containing topaz at daylight (c), electric (d) and ultra-violet (e) illumination.

16:00 Oral

Role and influence of impurities on GaN crystal grown from liquid solution under high nitrogen pressure in multi-feed-seed configuration

Michal Bockowski[1,2], Boleslaw L. Lucznik[1,2], Izabella Grzegory[1]

1. *Polish Academy of Sciences, Institute of High Pressure Physics (UNIPRESS), Sokolowska 29/37, Warszawa 01-142, Poland* **2.** *TopGaN Sp. z o. o., Sokolowska 29/37, Warsaw 01-142, Poland*

e-mail: bocian@unipress.waw.pl

There are some promising methods for obtaining good quality GaN crystals i.e. growth from the vapor phase, called HVPE[1] or crystallization from a solution: growth in gallium/sodium solution, the sodium flux method[2], or in supercritical ammonia, the ammonothermal method[3]. It is also well known that the High Nitrogen Pressure Solution (HNPS) growth allows obtaining high quality GaN crystals[4]. Recently, the multi-feed-seed (MFS) configuration in the HNPS growth method has been proposed and developed[5]. This configuration has been based on the conversion of free-standing HVPE-GaN crystals to the free-standing, pressure grown HNPS-GaN of much higher quality than the seeds. It has been already shown that the crystallization of GaN in the MFS configuration without an intentional doping results in growth of strongly n-type crystals with free electron concentration increasing with growth temperature. It has been suggested that so high free electron concentration in HNPS-MFS-GaN can be associated with high

oxygen concentration in the material. Obviously, the oxygen impurities in the GaN crystals can be compensated by magnesium. The HNPS-MFS-GaN:Mg crystallization has been already reported[6]. Highly resistive crystals have been obtained. However, one big difference in crystal growth procedure has been noted. The crystallization process has proceeded on the (000-1) GaN surface instead of the (0001) surface, typical for n-type GaN growth. It can be thus suggested that polarity of the GaN seed surface is determined and controlled by the Ga solution and its impurities.

In this paper the role and influence of impurities such as oxygen, indium and magnesium on GaN crystal growth from liquid solution in the MFS configuration will be presented and discussed in details. The differences in the properties of differently doped GaN crystals will be shown. It will be also demonstrated that HNPS-MFS-GaN crystals can be successfully used as substrates for epitaxy of optoelectronic and electronic devices.

[1] K. Motoki, SEI Technical Review, Number 70, April 2010; 28

[2] Y. Mori, M. Imade. K. Murakami, H. Takazawa, H. Imabayashi, Y. Todoroki, K. Kikamoto, M. Maruyama, M. Yoshimura, Y. Kitaoka, T. Sasaki, Journal of Crystal Growth, 350 (1), 72-74, (2012)

[3] R. Doradziński, R. Dwilinski, J. Garczynski, L.P. Sierzputowski, Y. Kanbara, in Technology of Gallium Nitride Crystal Growth, edited by D.Ehrentraut, E. Meissner, and M. Boćkowski, (Springer-Verlag, Heidelberg, ISBN 978-3-642-04828-9), 137-158, (2010)

[4] M. Bockowski, P. Strak, I. Grzegory, S. Porowski, in Technology of Gallium Nitride Crystal Growth, ed. by D. Ehrentraut, E. Meissner, M. Bockowski, (Springer-Verlag, Heidelberg, ISBN 978-3-642-04828-9), 207-220 (2010)

[5] M. Bockowski, I. Grzegory, B. Łucznik, T. Sochacki, G. Nowak, B. Sadovyi, P, Strak, G. Kamler, E. Litwin-Staszewska, S. Porowski, Journal of Crystal Growth 350 (1), 5-10 (2012)

[6] I. Grzegory, M. Bockowski, B. Lucznik, J. L. Weyher, E. Litwin-Staszewska, L. Konczewicz, B. Sadovyi, P. Nowakowski, S. Porowski. Journal of Crystal Growth 350 (1), 50–55 (2012)

16:15 Oral

4 inches langasite crystals growth along SAW-cut orientations

Xiaoniu Tu, Yanqing Zheng, Kainan Xiong, Yifan Tu, Erwei Shi

Shanghai Institute of Ceramics, Chinese Academy of Sciences, 1295 Dingxi Road, Shanghai 200050, China

e-mail: xiaoniu_tu@mail.sic.ac.cn

Langasite crystal possesses some excellent properties, such as higher piezoelectric constants and electromechanical coupling factor than quartz, no phase transition from room temperature to their melt point. Furthermore, langasite crystal can be grown by Czochralski method, and commercial three and four inch langasite wafers are available. Therefore, it becomes one of the most competitive candidate materials for high temperature (up to 1000 ^{o}C) sensors and acoustic electronic devices. However, there ere two issues prevented the large-scale application of langasite crystal, high cost and low homogeneity.

In this work, 4 inches langasite crystals along SAW-cut orientations had been grown successfully. The crystal shows in fig. 1 growth along Euler angles (0º, 22º, 90º) direction, and the crystal shows in fig. 2 growth along Euler angles (0º, 138.5º, 26.7º) direction. The growth morphology of those two types' as-grown crystals was discussed. The facet growth were compared with the as-grow crystal grown along Z direction. The high resolution X-ray diffraction surface mapping of 14 mm × 14 mm sample was measured. Frequency constant of 4 inches wafer has been tested by ALC-III frequency meter. Finally, resistivity was measured as a function of temperature. The results show that the 4 inches langasite crystals have high homogeneity, can satisfy the requirements of acoustic electronic devices and high temperature effective sensors applications.

Fig. 1 4 inches Langasite crystal growth along Euler angles (0º, 22º, 90º)

Fig. 2 4 inches Langasite crystal growth along Euler angles (0º, 138.5º,26.7º)

16:30 Oral

Top-seeded solution crystal growth of polar materials: design strategies and functional properties

Shiv Halasyamani, Weiguo Zhang

Department of Chemistry, Aalto University, Espoo FI-02150, Finland

e-mail: psh@uh.edu

Polar oxide materials – those with a macroscopic dipole moment – are ubiquitous in advanced technologies, i.e. computer memories, sensors, etc. The design and synthesis of new polar oxides, however, remains an ongoing challenge. Macroscopic polarity implies microscopic polarity, in other words some of the coordination polyhedra must be polar. As is often the case, the local dipole moment in the coordination polyhedra is directed in opposite directions resulting in a non-polar material. In this presentation we will discuss strategies toward designing new polar oxide materials, as well as the characterization of their functional properties. Specifically we will demonstrate that by exploiting second-order Jahn Teller distortions, we can design and synthesize new polar oxide materials. In addition we will describe the top-seeded solution crystal growth (tssg) of centimeter size crystals of $Na_2TeW_2O_9$, $LiFeP_2O_7$, and $K_3V_5O_{14}$. Functional properties will be

presented, and structure-property relationships will be discussed and explored.

16:45 Oral

Growth of Ce:$Li_6Lu(BO_3)_3$ Single Crystals for Neutron Detection

Shangke Pan, Dandan Sun, Guohao Ren

Shanghai Institute of Ceramics, Chinese Academy of Sciences, 1295 Dingxi Road, Shanghai 200050, China

e-mail: psk@mail.sic.ac.cn

Inorganic scintillation crystals are usually widely used in the detection of X- or gamma ray radiation. Recently, the interest in the detection of the thermal neutron has been increasing for the increasing need for neutron detectors in the fields of national security system and neutron scattering equipment, such as radiation portal monitors and spallation neutron sources. The neutron detection crystals of Eu:LiI and Ce:Cs_2LiYCl_6 can been obtained from the market. But they are very expensive for the sensitivity to water gas and the strictly control of the ^{6}Li isotopes. So crystals containing B elements may be promising cheap scintillators for neutron detection. Recently, we investigated the growth techniques of $Li_6Lu(BO_3)_3$ crystals and grew its single crystal by Czochralski technique.

The single crystal of Ce:$Li_6Lu(BO_3)_3$ with the diameter of about 30 mm (Fig 1) has been grown with the Czochraski technique under N_2 atmosphere. The effects of pulling rate on the crystal shape have been investigated.

The light yields of Ce:$Li_6Lu(BO_3)_3$ crystal excited by X-ray, gamma ray and α particles are comparable with Ce:$Li_6Gd(BO_3)_3$ crystal, which means that Ce:$Li_6Lu(BO_3)_3$ is a new promising neutron detection scintillation crystal for the ^{10}B(n,α) ^{7}Li reaction.

Fig 1. As-grown crystal of Ce:$Li_6Lu(BO_3)_3$ grown by the Czochralski technique

References:

[1] Chaminade J P, Viraphong O, Guillen F, et al. Crystal growth and optical properties of new neutron detectors Ce $^{3+}$:$Li_6R(BO_3)_3$ (R=Gd,Y)[J]. 2001, - 48(- 4): 1161.

[2] Pan S, Yang F, Ding D, et al. Czochralski Growth of Ce^{3+}-doped $Li_6Gd(BO_3)_3$ Single Crystals[J]. Nuclear Science, IEEE Transactions on. 2010, 57(3): 1300-1303.

[3] Yang F, Pan S K, Ding D Z, et al. Crystal growth and luminescent properties of the Ce-doped $Li_6Lu(BO_3)_3$[J]. Journal of Crystal Growth. 2010, 312(16-17): 2411-2414.

Corresponding author: E-mail address:psk@mail.sic.ac.cn. This work was supported by National Natural Science foundation of China (No. 51272263).

Break
Monday afternoon, 12 August, 17:00

MoP-G02
Monday afternoon, 12 August, 17:00
Rooms 105, 106, 107, Old Library

Tuesday, 13 August

TuO1

G02: Bulk crystal growth
Tuesday morning, 13 August, 10:20
Room A, Auditorium Maximum

10:20 Invited oral

Growth of AlN crystals and AlGaN epitaxy on AlN wafers

Zlatko Sitar

North Carolina State University, MSE (NCSU), 1001 Capability Dr., Raleigh, NC 27695, United States HexaTech, Morrisville 27560, United States

e-mail: sitar@ncsu.edu

For the first time in history of III-nitrides, the availability of low defect density (<10^3 cm^{-2}) native AlN substrates offers an opportunity for growth of AlGaN alloys and device layers that exhibit million-fold lower defect densities than the incumbent technologies and enable one to assess and control optical end electrical properties in absence of extended defects. Epi-ready AlN wafers are fabricated from AlN boules grown by physical vapor transport at temperatures between 2200 and 2300°C. Gradual crystal expansion is achieved through a scalable, iterative re-growth process in which the high crystal quality is maintained over many generations of boules.

Despite the excellent crystal quality, below bandgap optical absorption bands in the blue/UV range affect the UV transparency of wafers. We use density functional theory (DFT) to develop a model to understand the interplay of point defects responsible for this absorption. We show a direct dependence of the mid-gap absorption band with the carbon concentration within the AlN.

Low defect density AlN and AlGaN epitaxial films are grown upon these wafers that exhibit superior optical properties in terms of emission efficiency and line width and can be doped with an efficiency that is several orders of magnitude higher than possible in technologies using non-native substrates. UV LED structures and laser diodes were fabricated on these materials that exhibit low turn-on voltages and record low lasing threshold.

This presentation will review state-of-the-art of AlN-based technology and give examples of potential applications in future devices and contrast these with other wide bandgap technologies.

10:50 Oral

Vertical Bridgman Growth of Large $ZnGeP_2$ Single Crystals for High Power Applications

Chunhui Yang[1], Zuotao Lei[1], Chong-Qiang Zhu[1], Chao Xu[1], Galina A. Verozubova[2]

1. *Harbin Institute of Technology (HIT), No.92, West Da-Zhi Street,Harbin, Heilongjiang, Harbin 150001, China* **2.** *Insitute of Climatic and Ecological Systems of SB RAS (IMCES), 10/3 ave Akademicheskii, Tomsk 634055, Russian Federation*

e-mail: yangchh@hit.edu.cn

Zinc germanium diphosohide ($ZnGeP_2$) belongs to the chalcopyrite family with a direct band gap, and it is a ternary analog of the III-V group binary compound GaP with the zinc-blende structure. However, the chalcopyrite structure is tetragonally distorted from the simpler zinc-blende structure. Due to the distorted structure relative to its binary analogue, $ZnGeP_2$ exhibits a far wider range of physical properties. $ZnGeP_2$ has large nonlinear optical coefficient (d_{36}=75 pm·V^{-1}), a wide transparency range from 0.74 to 12μm, sufficient birefringence (Δn= 0.04) for type I and type II phase matching, and relatively high thermal conductivity (0.35W·cm^{-1}·K^{-1}) for high average power applications. All these physical properties make $ZnGeP_2$ suitable for frequency conversion applications such as tunable mid-infrared optical parametric oscillator (OPO) laser systems. The main goal of the present work is to systematically study and deeply discuss the growth, optical properties and applications of $ZnGeP_2$.

Firstly, $ZnGeP_2$ polycrystalline ingots were synthesized by two-temperature method, and the maximum mass is about 470g for one run. Fig.1 shows the synthesized $ZnGeP_2$ ingots with 470g. The XRD suggests that they show chalcopyrite structure, high pure and good crystallinity. The ingots are suitable for growth as raw materials. Moreover, the study indicates that the more the charge amount, the higher the yield of product.

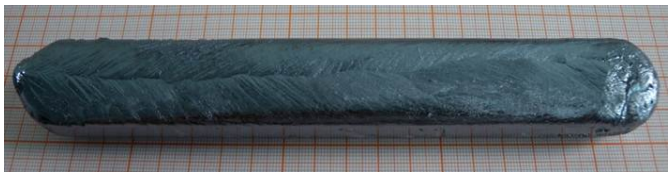

Fig.1 The synthesized $ZnGeP_2$ polycrystalline ingots with 470g

Secondly, $ZnGeP_2$ crystals were grown by Vertical Bridgman technique, and the largest size is about Φ50mm×140mm. Fig.2 shows the as-grown $ZnGeP_2$ crystals.The XRD and rocking curves suggest that they show good crystallinity and single phase, the XRF indicates that the as-grown $ZnGeP_2$ is stoichiometric, and the absorption coefficients of as-grown $ZnGeP_2$ are 0.05-0.08cm^{-1} at 2.05μm for *o*-light. However, the absorption coefficients of annealed and other post-treated $ZnGeP_2$ reduce to 0.01-0.03cm^{-1} at 2.05μm for *o*-light. The crystals are suitable for frequency conversion applications.

Fig.2 The as-grown $ZnGeP_2$ crystals

Finally, the $ZnGeP_2$ devices were tested for OPO. The $ZnGeP_2$ crystals were cut to 6mm×6mm×24mm in sizes after thermal annealing. Both surfaces of the crystal were carefully polished and antireflection coated for pump, signal, and idler lights. The $ZnGeP_2$-OPO devices are shown in Fig.3. Fig.4 shows the $ZnGeP_2$-OPO experiment setup. The OPO output wavelengths were in the spectral range of 3-5 mm. The results suggest that the output power of 30W is obtained pumping at 2.09μm and the conversion efficiency is 56%. Thus, $ZnGeP_2$ is an excellent OPO material and is acceptable for the fabrication of the infrared nonlinear optical device

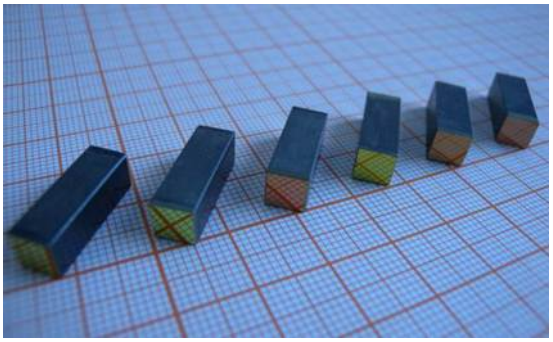

Fig.3 The $ZnGeP_2$-OPO devices

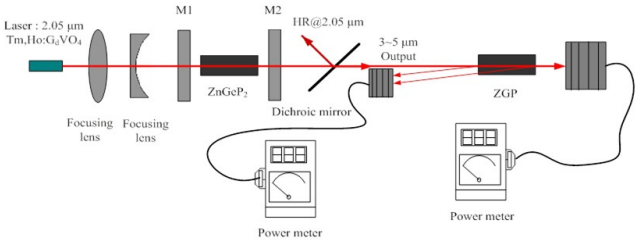

Fig.4 The $ZnGeP_2$-OPO experiment setup

11:05 Oral

Growth and Studies on Pure and Doped Magnetoelectric $GdMnO_3$ Single Crystals

Aditya A. Wagh, Anil Kumar P S, Suja E. Saji

Indian Institute of Science, Bangalore 560 012, India

e-mail: liz@physics.iisc.ernet.in

Various multiferroic materials classified as “improper ferroelectrics,” are known to posses polar state due to different types of ordering. They exhibit large magneto-electric coupling and are further sub-categorized as geometric, electronic and magnetic ferroelectrics. Divalent doping

is known to introduce significant changes in physical properties. Our studies on pure and strontium doped $GdMnO_3$ are discussed here. We have grown single crystals of $GdMnO_3$ and $Gd_{0.5}Sr_{0.5}MnO_3$ using float-zone method. Growth parameters are optimized to yield good quality single crystals. Preliminary characterization is carried out to ensure phase purity, crystallinity and composition. In order to investigate anisotropic properties of these crystals, they are oriented using back-reflection Laue technique and cut into appropriate dimensions for the experimental measurements. Magneto-dielectric and electric polarization measurements are performed in the temperature range, 5 to 100 K at applied magnetic fields ranging from 0 – 50 kOe. $GdMnO_3$ exhibits interesting antiferromagnetic transitions. At ~ 43 K, it transforms to long-wavelength modulated collinear structure, which is incommensurate [1]. At ~ 23 K, an A-type antiferromagnetic phase sets in [1]. Application of magnetic field (10 KOe) along b-axis induces ferroelectric phase along a-axis in $GdMnO_3$ crystal [1]. Tuning of electric polarization with magnetic field and magneto-dielectric effects are studied in this configuration. Specific heat measurements are carried out to probe low temperature magnetic transitions of both crystals. $Gd_{0.5}Sr_{0.5}MnO_3$

shows glass-like magnetic phase below ~ 32 K [2]. It also exhibits interesting features like, charge ordered insulating phase and colossal magnetoresistance [2,3]. Dielectric behaviour is investigated on oriented single crystals. Thermal, magnetic and dielectric properties as well as growth aspects of these gadolinium manganite crystals will be discussed in detail.

References:

(1) T. Kimura, G. Lawes, T. Goto, Y. Tokura, and A. P. Ramirez, Phys. Rev. B 71, 224425 (2005).

(2) A. A. Wagh, P. S. Anil Kumar, H. L. Bhat, and S. Elizabeth, J. Supercond. Nov. Mag., 24, 665 (2011), A. A. Wagh, P. S. Anil Kumar, H. L. Bhat, and S. Elizabeth, J. Phys. Condens.Matter 22, 026005 (2010).

(3) B. Garcia-Landa, J. M. De Terasa and M. R. Ibarra, J. Appl. Phys. 83, 12, 7664(1998).

11:20 Oral

Growth and Properties of Mid-infrared Chalcogenide Crystals

Shanpeng Wang, Xixia Zhang, Xiang Zhang, Huapeng Ruan, Chunlong Li, Zeliang Gao, Chunming Dong, Xutang Tao

State Key Laboratory of Crystal Materials, Shandong University, Jinan 250100, China Institue of Crystal Materials, Shandong University, Jinan 250100, China

e-mail: wshp@sdu.edu.cn

Over the past few decades, widely tunable coherent mid-infrared laser sources in the range of 3-20 μm, specially in band 3-5 μm and 8-14 μm of three atmospheric transparent windows, have become research focus of infrared (IR) laser technology[1]. Frequency conversion by an infrared nonlinear optical (NLO) crystal is an effective way of producing coherent mid-infrared light.

Lithium containing chalcogenide (such as $LiInS_2$, $LiInSe_2$ $LiGa_3Te_5$) are promising candidates for mid-IR optical frequency conversion. $LiInS_2$ has wide transparency range (0.35~12.5μm), high nonlinear coefficient and is phase matchable over a large wavelength range. Compared to other infrared nonlinear crystals, such as silver thiogallate ($AgGaS_2$) [2] and zinc germanium phosphide ($ZnGeP_2$) [3], $LiInS_2$ displays a nearly isotropic thermal expansion behavior and a 5-times-larger thermal conductivity. Owing to its wider band gap and lower absorptions in the range of near infrared, $LiInS_2$ crystals can be pumped by Nd: YAG laser. LISe is one of these few nonoxide nonlinear crystals whose band-gap (2.86 eV) and transparency allow operation in the nanosecond optical parametric above 4 μm without TPA for a pump wavelength of 1064 nm. $LiGa_3Te_5$ crystallizes in the noncentrosymmetrical system, space group *R32*. The transmission of LGT crystal is above a level 40% from 3.5 to 18 μm, and the cut-off edges at short and long wavelength are at 0.9 and 25 μm, respectively.

In this paper, we report the growth and properties of large-sized Lithium containing chalcogenide crystals. The crystals were grown by the modified Bridgman method. The characterizations such as XRD, high resolution X-ray diffractometor, the thermal properties, damage threshold and refractive index of the grown crystals are also discussed.

References:

[1] Fossier, S.; Salaun, S.; Mangin, J.; Bidault, O.; Thenot, I.; Zondy,J. J.; Chen, W. D.; Rotermund, F.; Petrov, V.; Petrov, P.; Henningsen,J.; Yelisseyev, A.; Isaenko, L.; Lobanov, S.; Balachninaite, O.; Slekys, G.; Sirutkaitis, V. *J. Opt. Soc. Am. B* 2004, *21*, 1981.

[2] G.A.Verozubova, A.I.Gribenyukov, V.V. Korotkova, O. Semchinova, D. Uffmann, *J. Crystal Growth*, 2000, 213, 334.

[3] D.Lee, T.Kaing, J.-J. Zondy, *Appl. Phys. B*, 1998, 67, 1259.

11:35 Oral

Crystal Growth and Neutron Diffraction Studies of $LiCoO_2$ Bulk Single Crystals

Uthayakumar Sivaperumal[1], Manoj S. Pandiyan[1], Daniel Porter[1], Matthias J. Gutmann[2], Jon Goff[1]

1. *Royal Holloway University of London (RHUL), Egham Hill, Egham TW200EX, United Kingdom* **2.** *Science and technology facilities council, Rutherford Appleton laboratory, Didcot OX110QX, United Kingdom*

e-mail: s.uthayakumar@rhul.ac.uk

There has been a renaissance of research on alternative energy sources to decrease global warming and environmental pollution. Hence energy generation and energy storage are two of the biggest challenges facing modern science. Lithium ion batteries are considered to be one of the most attractive technologies in recent years due to its high energy density and long service life. Such high performance batteries based on the movement of Li^+ ions in layered transition metal oxides such as $LiCoO_2$ have made a revolution possible in the technology industry in products from iPods to mobile phones. These materials are already used extensively in commercial applications, but until now it has not been possible to study their basic properties using single crystal neutron scattering. To develop this pollution free system further, it is imperative to understand the growth-structure interrelationship to shed light on material properties such as the electro chemical properties, capacity loss and cyclability.

Material synthesis is a key component in the discovery and design of energy related research. The most common method of preparing Li_xCoO_2 is by solid state reaction method. However the results obtained from polycrystalline samples lead to scattered results due to irregular morphology, grain boundaries or impurities. An alternative, the slow cooling technique, leads to particle coarsening and evaporation of lithium species. This in turn significantly hampers the electrochemical properties. To solve these issues we employed the optical floating-zone technique (FZ-T-10000-H-VI-VPO-PC, Crystal System) and found

that this favours improved morphological and chemical reactivity compared to slow cooling and the solid state reaction techniques.

The as-grown crystals were subjected to various characterizations. Fundamental understanding with regard to melt processing is essential for optimizing processing conditions. Hence, DTA–TGA analysis was made to optimize the thermal profile for the growth. The surface morphology was analysed by scanning electron microscope. Using a SQUID, magnetic measurements were performed in a field of 1Tesla in both the H || C and H ⊥ C configurations. A transition was observed at 10K. Analysis of small (<0.5mm) crystals using single crystal x-ray diffraction at RHUL indicate the high crystalline quality of the growth. A much larger boule was screened using neutron diffraction in SXD at ISIS. SXD combines the white beam Laue technique with area detectors covering a solid-angle of 2π steradians, allowing comprehensive surveys of 3D volumes of reciprocal space. We were able to cleave large samples (>1 cm) with sharp Bragg reflections from a single grain. The structure refined in the space group $R3^{-}$ m with an R_w-factor of 7.96 %. It was possible to accurately determine the Li concentration. This is the first time that it has been possible to grow a large high quality single crystal of Li_xCoO_2, allowing further measurements that require large single crystals, such as studies of diffusion using neutron scattering. The results and growth procedures will be presented in detail.

11:50 Oral

Investigation on the SR method Growth etching, birefringence, laser damage threshold and thermal characterization of Strontium bis (hydrogen L-malate) hexahydrate single crystal

Senthil Arumugam[1], Ramasamy Perumal[2]

1. *SRM University, Ramapuram, Bharathisalai, Chennai 600089, India* **2.** *Centre for Crystal Growth,SSN College of Engineering,Kalavakkam,Chennai, Chennai 603110, India*

e-mail: tasenthil@yahoo.co.in

In recent years the search for new nonlinear optical materials included semi-organic and coordination compounds due to their advantages over traditional inorganic and organic compounds. Semi-organic materials possess several attractive properties such as high damage threshold, wide transparency range, less deliquescence and high nonlinear coefficient, which make them suitable for frequency doubling. Dicarboxylic acids have attracted the specific attention of many researchers for long time due to their overwhelming practical applications in science and technology. The growth and characterization of metal complexes of dicarboxylate crystals like oxalates, malonates, maleates and substituted acids like tartrates and lactates caught major attention due to their optical and ferroelectric properties. L-malic acid ($C_4H_6O_5$) is one of the simplest chiral dicarboxylic acids, is a suitable building block in crystal engineering. Its chirality ensures the absence of a center of symmetry, essential for optical nonlinear second harmonic generation. Ammonium malate, racemic potassium malate, zinc malate 1,10-phenanthroline and cesium hydrogen malate are the famous reported semi-organic malic acid family crystals. The low-temperature solution growth is an important technique because large-size nonlinear optical and other crystals are being grown by this technique. In order to grow large crystals one has to ensure that, during the growth period, the available nutrient is deposited on the chosen seed only. Any spontaneous nucleation occurring during the growth will eat away a portion of the solute, thus making it difficult or impossible to grow a single large crystal. Crystals of different orientations with different morphology are grown by conventional solution growth technique but for application point of view, specific orientation with good quality is needed. The Sankaranarayanan–Ramasamy solution growth technique is suitable to grow high-quality large-size unidirectional L- Malic acid single crystals from solution. In the present investigation, semi-organic, good quality single crystals of strontium bis (hydrogen L-malate) hexahydrate (SrLM) were successfully grown by unidirectional SR method. Optically transparent SrLM crystal was grown by conventional slow cooling solution growth technique Based on the morphology of the conventional slow cooling grown SrLM crystal, the (010) plane was selected in the present study to impose the orientation in the growing crystal. The seed crystal started to grow after 12 days with growth rate of 1 mm/day. By this method, SrLM crystal with the diameter 10 mm and 50 mm length was grown in 34 days. The structural perfection and growth features of SrLM was analysed by chemical etching studies. The grown crystals were characterized by UV-Vis-NIR spectrum, birefringence, laser damage threshold and Thermal analysis (TG/DTA) studies. The UV-vis-NIR spectrum elucidates that the crystal is transparent between 230- 1100 nm and the lower cutoff is found to be around 226 nm. The value of birefringence and quality were ascertained by birefringence interferometer. The birefringence interferogram shows good refractive index homogeneity of the SrLM crystal grown by SR method. Optical damage tolerance of SR grown SrLM crystal was investigated by laser damage threshold studies. Laser damage value has been determined using Q-switched diode array side pumped Nd:YAG laser operating at 532 nm.

12:05 Oral

Bulk Single crystal growth and magnetic studies of $La_{2-x}Sr_xCoO_4$

Dharmalingam Prabhakaran, Andrew T. Boothroyd

University of Oxford, Department of Physics, The Clarendon Laboratory, Parks Road, Oxford OX13PU, United Kingdom

e-mail: d.prabhakaran@physics.ox.ac.uk

The discovery of charge and spin stripes in the high-T_c cuprate superconductors has motivated us to investigate other doped oxides possessing the K_2NiF_4 structure. The single-layered cobalt oxides $La_{2-x}Sr_xCoO_4$ are one such system with similar crystal structure. Although no superconductivity has been found at any doping level, compounds in this cobaltate family do exhibit charge stripe ordering and other phenomena similar to those found in the cuprates.

In order to understand the static and dynamic properties of the charge stripe phases in the cobaltates by neutron scattering, large single crystals are needed (1-3). We will report the optimisation and growth of large $La_{2-x}Sr_xCoO_4$ (x=0.0 to 0.9) crystals by the floating-zone technique in an image furnace. Crack-free single crystals of diameter ~10 mm and length up to 80 mm have been obtained. One of the major issues associated with this system was the oxygen non-stoichiometry. To over come this problem, we have post annealed the as-grown crystals in $CO:CO_2$ atmosphere. The phase-purity of the crystals has been checked by powder x-ray diffraction, and information on the crystal quality has been obtained by x-ray Laue and neutron diffraction. We will give an account of our investigations into the conditions needed to obtain the highest quality crystals. We will also provide some preliminary results on the spin and charge ordering in the crystals.

References

1. A. T. Boothroyd, P. Babkevich, D. Prabhakaran, and P. G. Freeman, *Nature***471** (2011) 341–344.

2. P. Babkevich, D. Prabhakaran, C. D. Frost, and A. T. Boothroyd, *Phys. Rev. B***82** (2010) 184425.

3. L.M. Helme, A.T. Boothroyd, R. Coldea, D. Prabhakaran, C.D. Frost, D.A. Keen, L.P. Regnault, P.G. Freeman, M. Enderle, and J. Kulda, *Phys. Rev. B***80** (2009) 134414.

Lunch (IOCG Exec. Com. meeting)

Tuesday afternoon, 13 August, 12:20

TuO2

G02: Bulk crystal growth
Tuesday afternoon, 13 August, 14:00
Room A, Auditorium Maximum

14:00 Invited oral

Growth of Bulk Crystals of Semiconductors by Electroepitaxy

Sadik Dost

University of Victoria, Victoria V8W3P6, Canada

e-mail: sdost@me.uvic.ca

The article presents an overview of the growth of single crystal bulk semiconductors by liquid phase electroepitaxy (LPEE). The talk covers the LPEE growth of III-V, II-VI, and IV-IV semiconductor materials.

Following a short introduction on early modeling and theoretical studies on LPEE, we will first introduce recent experimental results of the LPEE growth of GaAs/GaInAs single crystals under a static applied magnetic field. Crystal growth experiments carried out have shown that the application of a static magnetic field in the LPEE growth of GaAs increases growth rate very significantly. For instance the LPEE growth rate of GaAs under a 3-A/cm2 electric current density is about 0.5 mm/day. However, the growth under the same electric current is about ten times higher in the presence of a static magnetic field of 4.5 kGauss. In order to predict such a high growth rate, a continuum model was developed by giving a new definition to the process of electromigration in which a total electric mobility was introduced, i.e., "electromagnetic mobility". Introduction of the electromagnetic mobility allowed accurate predictions for both the growth rate and the growth interface shape. A thermodynamic and kinetic interpretation for this electromagnetic mobility was also given. Dimensionless electromagnetic mobility varies with the magnetic field intensity as 1+2B (up to B=4.5 kGauss).

LPEE growth CdTe single crystal experiments were also carried out. Although experiments led to the growth CdTe crystals of about 2mm thickness, we have failed to find an appropriate contact zone that would lead to a uniform passage of the applied electric current through the seed crystal, and would maintain to a prolong growth for ticker crystals. This issue of contact zone in LPEE growth of CdTe/CdZnTe crystals still remains unresolved.
In the talk we will also present the results of our recent LPEE growth experiments for SiGe bulk single crystals. Experiments were designed for the growth of crystals of 24mm in diameter, and were run under a 3 A/cm2 electric current density. Growth was achieved from the silicon side (on silicon seed).

14:30 Oral

Chemical segregation in micro-pulling-down process: analytical model and experiments

Abdeldjalil Nehari[1], Thierry Duffar[2], Kheirreddine Lebbou[1]

1. *Institut Matière et Lumière Université Lyon (CNRS), Villeurbanne cedex 69622, France* **2.** *SIMaP EPM, CNRS UJF, BP 75, Saint Martin d'Heres cedex 38402, France*

e-mail: thierry.duffar@grenoble-inp.fr

The micro-pulling down (μ-PD) process consists in pulling a crystal under a capillary channel placed at the bottom of a crucible. In spite of the fact that it is limited to rather small liquid volumes, it is used to grow single crystal fibers and shaped crystals of various cross sections, mainly applied industrially for optical applications such as lasers, optics or scintillators. Consequently those crystals should be doped with active elements in order to fit the target application. Unfortunately, whatever the growth parameters and the dopant type, quite often segregation problem is observed. It is generally believed that chemical segregations in μ-PD technique are restricted to the first grown millimeters, but some experiments show that it is not always the case.

An analytical one dimensional model is presented, aiming to predict the longitudinal segregation along the growth direction. It is shown that it depends in practice on growth parameters such as capillary length, meniscus height, crucible volume and growth rate. The characteristic numbers controlling the type of segregation that will be obtained are derived and a parametric study is performed in the case of Ti-doped sapphire single crystal fibers.

Such Ti:Al_2O_3 single crystal fibers oriented along c-axis have been grown under stationary stable regime using different pulling rates and the longitudinal chemical segregation has been characterized by photoluminescence. Results are in agreement with the model predictions.

14:45 Oral

Thermodynamic analysis of impurity partitioning in colloidal crystallization

Jun Nozawa, Yuhei Naradate, Haruhiko Koizumi, Kozo Fujiwara, Satoshi Uda

Institute for Materials Research, Tohoku University, 2-1-1, Katahira, Aoba-ku, Sendai 980-8577, Japan

e-mail: nozawa@imr.tohoku.ac.jp

Colloidal crystals are regarded as a promising tool to investigate diverse basic physical phenomena. We have applied this colloidal crystal to impurity partitioning in the melt growth. Since no research has been focused to detail partitioning behavior of colloidal crystals, the objective of the present work is to reveal a partitioning behavior during colloidal crystallization.

A few amount of impurities (2 percent) were doped to the colloidal dispersion, from which colloidal crystals were grown with convective assembly method. Polystyrene particles (PS) were used for fabricating colloidal crystals, and different sizes of PS and fluorescent bearing PS (w/fluor.) were doped as impurity particles.

In each particle size for two kinds of impurity, effective partition coefficient (k_{eff}) were measured at various growth rates. Obtained k_{eff} gives k_0 by using BPS plot. The k_0 is decreased as the difference between the size of the impurity and the 500 nm host particle increased. The k_0 of each w/fluor. was larger than that of the correspond-

ing pure PS. Moreover, the value of k_0 for the 520 nm w/fluor. surpassed unity, whereas the PS is always less than unity.

We have employed a Thurmond and Struthers (T&S) model (J. Phys. Chem. 57, 831 (1953)) to discuss the difference of k0 for PS and w/fluor. particles. T&S model shows k_0 as; $k_0 = \exp((\Delta G_{Tr}-\Delta H)/RT)$. Here, ΔG_{Tr} is free energy difference between the solid and liquid phases of an impurity at the transition temperature, T, ΔH is the excess enthalpy which is caused by incorporation of the impurity into the host material, and R is a gas constant. We have determined the phase transition volume fraction for PS and w/fluor. to evaluate the ΔG_{Tr}. It was shown that ΔG_{Tr} of w/fluor. is positive whereas PS is zero. This leads to larger $\Delta G_{Tr}-\Delta H$ of w/fluor. than that of PS, which corresponds to larger k_0 of w/fluor., and in a small $-\Delta H$ range, k_0 of w/fluor. surpasses unity. We have found the difference of k_0 for different kinds of impurity particles, and succeeded in applying concept of T&S model to partitioning of colloidal crystals.

15:00 Oral

Growth and characterization of 2-hydroxy biphenyl single crystals by top seeded melt growth method

Sadhasivam Subramani, Rajesh Narayana Perumal

Centre for crystal growth, SSN college of engineeting, kalavakkam, Chennai 603110, India

e-mail: sadha.phy1@gmail.com

In recent years, various seeding techniques were used for melt growth to obtain maximum perfect crystal. In order, delocalized electrons rich organic nonlinear optical single crystal 2-hydroxy biphenyl with dimension of 25x15x8mm^3 was grown by top seeded melt growth technique. The growth rate was observed 5mm/h. The seed orientation was optimized for fast growth. The morphological growth habits were analyzed. Scanning electron microscopy studies have been carried out on the surface of the grown crystal to investigate the nature of growth and defects on the crystal. The lattice parameters of the grown crystal were determined by single crystal X-ray diffraction technique. The grown crystals were characterized by powder XRD, FT-IR, FT-Raman and UV-Vis-NIR techniques. Thermal properties of grown crystal were studied by thermogravimetric analysis. The melting point of grown crystal was confirmed by differential scanning calorimetry analysis. The micro hardness values were measured for parallel and perpendicular face to growth direction. Second harmonic generation efficiency was measured using Q-switched Nd:YAG laser. Dielectric studies have been carried out for the grown crystal in the frequency range of 50Hz to 5MHz at various temperature and the results were discussed in detail.

15:15 Oral

Organic/inorganic doped aromatic derivatives crystals: growth and properties

Florin Stanculescu[1,2], Floricica Barvinschi[3], Iulian Ionita[1], Anca Stanculescu[4]

1. *University of Bucharest, Faculty of Physics, Str. Atomistilor nr.405, Bucharest- Magurele 077125, Romania* **2.** *ROMANIAN MATERIAL SCIENCE CRYSTAL GROWTH SOCIETY (ROMS-CGS), Str. Atomistilor nr.405, Bucharest- Magurele 077125, Romania* **3.** *Politehnica University of Timişoara, P-ţa Victoriei no. 2, Timisoara 300006, Romania* **4.** *National Institute of Materials Physics, 105 Atomistilor Street, Bucharest- Magurele 77125, Romania*

e-mail: fstanculescu@fpce1.fizica.unibuc.ro

In the last decades, the organic molecular crystals have been considered as potential substitutes for inorganic crystals in photonics for optical signal processing and integrated optics showing large second order non-resonant nonlinearities and fast response times. Their most significant advantages compared to inorganics are the high values for nonlinear coefficients, large birefringence values, high damage thresholds in laser beam and large transparency domain. These properties are associated with the presence of the delocalized π electrons cloud and, donor and acceptor substituent groups, which are generating important inductive and mezomeric effects at the molecular level and significant optical non-linear effect at the macroscopic scale.

Crystalline aromatic derivatives compounds such as meta-dinitrobenzene (m-DNB) and benzil are interesting for the above mention applications because they show large transparency domain, and theoretically study have anticipated high non-linear coefficients on one hand and the π-electrons systems that favour the emission property by fluorescence and/or intermolecular energy transfer on the other hand.

Additionally, substituted organics could show specific properties like important two photon absorption fluorescence emission (TPF) and are interesting for potential applications in frequency up conversion lasing, optical power limiting, three-dimensional (3D) fluorescence imaging, 3D optical data storage, 3D lithographic micro fabrication and photodynamic therapy.

In particular, the interest in studying crystalline benzil and m-DNB is explained mainly by their behaviour similar to that of the inorganic wide-gap semiconductors. This interest is also justify by the particularities of their molecular and crystalline structure that favors the appearance of the free space having diameter (~3 Å for both m-DNB and benzil evaluated from the molecular chemical structure taking into account the geometry of the molecule [1]) adequate for the inclusion of foreign atoms or molecules (doping), or for the development of specific internal microstructures of a different phase.

The type of dopant incorporation in the host matrix, substitutionally or interstitially, depends on the shape, volume and intermolecular bonding of the dopant molecule and, on the geometrical similarity between dopant and matrix. The investigation of the effect of the dopant incorporation and organization inside an organic matrix is important for obtaining a new class of materials combining the properties of the both components.

This paper presents some studies concerning the incorporation of inorganic (silver, iodine, sodium) and organic (naphthalene, m-DNB) single dopant in benzil or m-DNB matrix and of m-DNB+iodine; naphthalene+iodine) double dopant in benzil or m-DNB matrix.

Because both m-DNB and benzil are characterized by good thermal stability at the melting point (89^{o}C and 95^{o}C respectively), these organic molecular crystals have been grown from the melt in a Bridgman-Stockbarger vertical configuration (thermal gradient at the growth interface: 5-35^{o}C/cm; moving speed of the growth interface: 0.5-3 mm/h), which has been adapted to counteract the supercooling and low thermal conductivity characterizing the big molecule organic compounds. The starting material was purified by chemical methods/vacuum distillation/multiple passages (~20) zone refining process. The dopant concentration in wt% was well controlled.

Thick crystalline wafer (1.5-3 mm) with a diameter of ~8-12 mm, have been obtained by cutting these pure and doped ingots with a wire saw machine and mechanically polishing the slices with a mixture of alumina powder in ethyleneglycol.

We have analysed the dopant/matrix systems from the point of view of the growth interface stability emphasising the stability limits and the experimental conditions (temperature gradient, moving speed,

concentration gradient) for initiating the instabilities associated with defects in the final crystal.

To obtain high quality crystals, the temperature distribution both in melt and crystal must be accurately controlled. Controlling the local thermal distribution in the heater during the solidification process determined by the position of the growth ampoule in the heater we can control the position and shape of the solid-liquid interface. For this purpose we propose the numerical modelling of the heat transfer during the process of aromatic derivatives crystallization by firstly solving the steady-state heat transport model equation and subsequently considering the pseudo-transient heat transfer in the central zone of the furnace, simulated in a time-dependent model, assuming that the moving speed of the ampoule was equal to the solidification rate [2].

We have investigated the effect of the experimental conditions ($T_{hot\ zone}$ and ampoule position for charge melting; $T_{cold\ zone}$ and ampoule position for initiating the crystallization) on the growth interface shape and evaluated the interface deflection (curvature). This value was correlated with the growth interface shape, which is an important parameter associated with the structural quality of the crystal.

We have also realized a comparative study between the structural/morphological/optical (transmission, emission) properties of the pure and doped molecular crystals. We have evidenced an exponential sub band gap absorption process and estimated the corresponding Urbach energy. This parameter which is correlated with topological and/or structural defects is determined by two types of factors correlated: 1. to the growth regime (temperature gradient, moving speed); 2. to selected dopant.

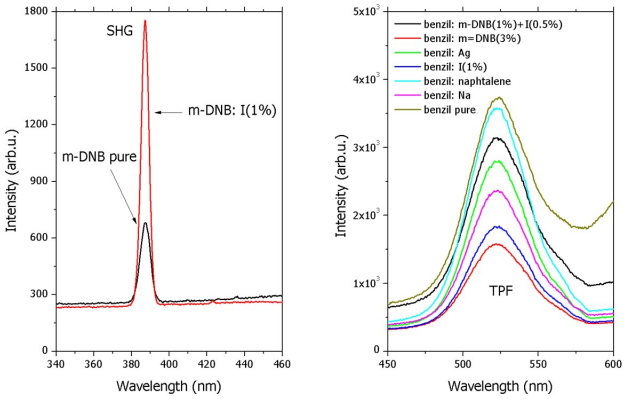

A special attention was paid to analyse the particularities of the interaction between the molecular crystal and a laser beam. We have used the ultrashort pulses of a pulsed laser Spectra Physics "Tsunami" with a maximum emission wavelength 800 nm, pulse duration of 60 fs and different medium power between 10 mW, and 500 mW.

We have analysed the effect of the doping on the second harmonic generation (SHG) and TPF signals (Fig. 1a and 1b), emphasising the dependence of the maximum intensity on the beam position, moving the beam focus across the wafer surface and depth inside the sample (Fig. 2). The effect of the dopant on the SHG will be estimated evaluating the non-linear coefficient of pure and doped organic crystal from the dependence of the SH intensity on the power of the incident laser beam.

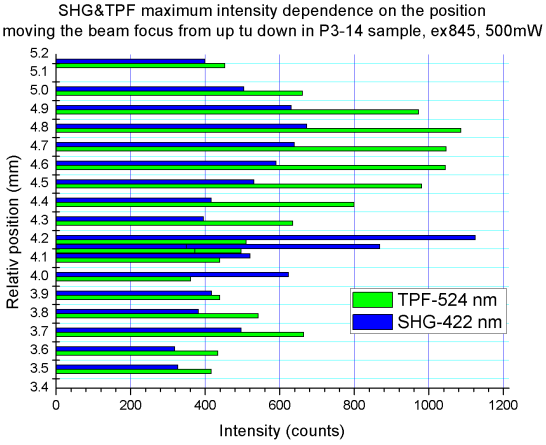

References

[1] A. Stanculescu, J. Optoelectron. Adv. Mater. 9 (2007) 1329.

[2] F. Barvinschi, A. Stanculescu, F. Stanculescu, J. Cryst. Growth 317 (2010) 23.

Break
Tuesday afternoon, 13 August, 15:30

Wednesday, 14 August

WeO1

G02: Bulk crystal growth
Wednesday morning, 14 August, 10:20
Room A, Auditorium Maximum

10:20 Invited oral

Growth and properties of bulk single crystals of selected transparent semiconducting oxides (TSOs): β-Ga_2O_3, In_2O_3 and SnO_2

Zbigniew Galazka, Reinhard Uecker, Klaus Irmscher, Detlef Klimm, Mike Pietsch, Martin Albrecht, Detlev Schulz, Steffen Ganschow, Albert Kwasniewski, Robert Schewski, Rainer Bertram, Matthias Bickermann, Roberto Fornari

Leibniz Institute for Crystal Growth (IKZ), Max-Born-Str 2, Berlin 12489, Germany

e-mail: zbigniew.galazka@ikz-berlin.de

β-Ga_2O_3, In_2O_3, and SnO_2 are attractive transparent semiconducting oxides (TSOs) with wide bandgaps of 4.8, 2.8, and 3.6 eV, respectively. They are however, chemically unstable at elevated temperatures and tend to decompose, therefore growing such single crystals from the melt is a very challenging task. Bulk β-Ga_2O_3 (MP=1820°C) single crystals were grown by the Czochralski method using a self-adjusting dynamic growth atmosphere. The crystal appearance and electrical / optical properties are strongly dependent on applied growth conditions. In_2O_3 (MP=1950°C) is much more unstable than Ga_2O_3 and ZnO, and for the purpose of growing bulk In_2O_3 single crystals from the melt we have developed a novel crystal growth method (PCT patent application, 2012), which will be disclosed for the first time at this conference. SnO_2 is the most chemically unstable compound at high temperatures (MP>2100°C) among other TSOs so that single crystals of SnO_2

cannot be grown from the melt. Therefore, bulk SnO_2 single crystals were obtained by the physical vapor transport (PVT). All these bulk TSO single crystals showed n-type conductivity with free electron concentrations in the range of $5x10^{16}$–$5x10^{18}$ cm^{-3} and electron mobilities between 120–220 $cm^2/(V\ s)$. A systematic annealing study of the bulk TSOs at different atmospheres, temperatures, and times revealed that all the crystals are thermo-chemically stable up to 1200°C in non-reducing and up to 600–700°C in highly reducing conditions. Moreover, in terms of electrical properties, bulk TSO single crystals are sensitive to annealing conditions: the free electron concentration of bulk In_2O_3 crystals could be modified by more than 2 orders of magnitude, while bulk β-Ga_2O_3 and SnO_2 crystals could be even switched interchangeably between semiconductor and electrical insulator just by suitable annealing. Availability of truly bulk TSO single crystals combined with their unique electrical and optical properties opens the door to new applications, such as high power electronics, transparent electronics, and light detectors.

10:50 Oral

Growth and EPR properties of $NdVO_4$, $HoVO_4$ and $NdVO_4$ single crystals

Slawomir M. Kaczmarek[1], Marek Berkowski[2], Grzegorz Leniec[1], Michał M. Głowacki[2], Tomasz Skibiński[1]

1. *West Pomeranian University of Technology, Szczecin (ZUT), Szczecin 70-310, Poland* **2.** *Polish Academy of Sciences, Institute of Physics, al. Lotników 32/46, Warszawa 02-668, Poland*

e-mail: skaczmarek@zut.edu.pl

Single crystals of $NdVO_4$, $HoVO_4$ and $ErVO_4$ were grown by the Czochralski method in an inductively heated iridium crucible of 40 x 40 mm and with an passive afterheater. Starting materials with 4N purity were heated at 1000 °C (Nd_2O_3, Ho_2O_3 and Er_2O_3) or at 300°C V_2O_5 for 6 hours before weighing, mixing and melting. Due to evaporation of vanadium from the melt during crystal growth process [1] composition of starting oxides was 1 mol.% shifted towards higher concentration of V_2O_5. Single crystals with 20 mm diameter were grown on an iridium 2 mm rod with pulling rate of 3-4 mm/h and a rotation of 4-6 rpm. Crystals were grown under ambient pressure in a nitrogen atmosphere. During crystallization strong tendency to spiral growth was observed, especially for $HoVO_4$. In spite of lack of crystal seed most crystals started to grow along direction close *c*-axis with *a*- and *b*-planes (cleavage planes) on the side. Obtained single crystals were transparent with strong coloring – violet for $NdVO_4$, yellow for $HoVO_4$ and pink for $ErVO_4$.

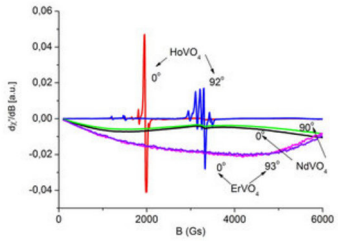

EPR spectra of the three well oriented crystals were recorded on a conventional X-band Bruker ELEXSYS E 500 CW-spectrometer (Bruker Analytik GmbH, Rheinstetten, Germany) operating at 9.5 GHz with a 100-kHz magnetic field modulation. The first derivative of the absorption spectra has been recorded as a function of the applied magnetic field. Temperature dependence of the EPR spectra of the samples in the 3–300 K temperature range was recorded using an Oxford Instruments ESP nitrogen-flow cryostat (Oxford Instruments Ltd., Witney, UK). EPR-NMR program was applied to recognize spin Hamiltonian parameters of the rare-earth ions [2].

[1] K. Oka, H. Unoki, H. Shibata, H. Eisaki, Journal of Crystal Growth 286 (2006) 288–293

[2] M.J. Mombourquette, J.A. Weil, and D.G. McGavi: EPR-NMR User's Manual (Department of Chemistry, University of Saskatchewan, Saskatoon, Canada, 1999).

11:05 Oral

Bulk crystals of ammonium acid phthalate single crystals for optical limiting applications grown by Sankaranarayanan- Ramasamy method

Arunkumar Alagesan, Ramasamy Perumalsamy

Centre for Crystal Growth,SSN College of Engineering,Kalavakkam,Chennai, Chennai 603110, India

e-mail: ramasamyp@ssn.edu.in

Transparent ammonium acid phthalate (AAP) crystal of length 140 mm long and 20 mm diameter has been grown from aqueous solution in <001> using Sankaranarayanan - Ramasamy method. The unit cell parameters were confirmed by single crystal X-ray diffraction analysis and it belongs to orthorhombic system. The crystalline perfection of grown crystals was analyzed by High-resolution X-ray diffraction. The UV-vis-NIR spectrum showed that the grown crystal is transparent in the entire visible region. Fluorescence studies were carried out in range of 200 – 700 nm. Thermogravimetric and differential thermal analysis was carried out to determine the thermal property of the grown crystal. The mechanical property of the grown crystal was studied by Vickers Microhardness measurement. Nonlinear optical absorption of the sample has been studied at 532 nm using single 7 ns laser pulses, employing the open-aperture Z-scan technique. It is found that the AAP molecule is a potential candidate for optical limiting applications. The laser damage threshold was measured using Q-switched Nd: YAG laser (1064 nm).

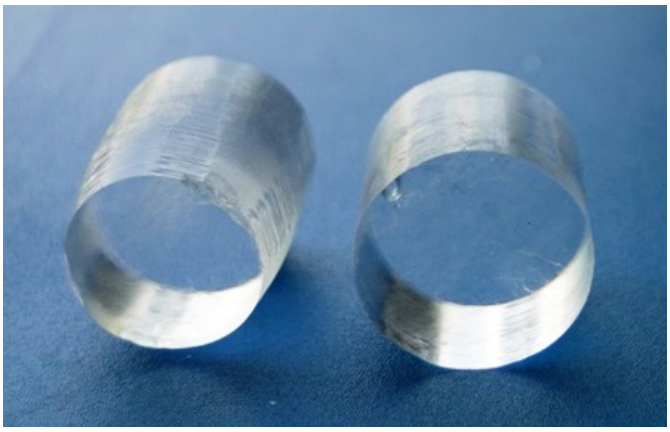

Photograph of SR grown ammonium acid phthalate crystal

11:20 Oral

Crystal Growth of pure and doped Potassium Titanyl Phosphate single crystal for E-O applications and its characterisation

Rajesh Narayana Perumal, Sadhasivam Subramani

SSN College Of Engineering (SSNCE), Kalavakkam, chennai 603110, India

e-mail: rajeshnp@ssn.edu.in

Nonlinear optics research and its needs require new materials for large variety of processes. The Potassium Titanyl Phosphate (KTP) is well known and prominent commercial material for harmonic generation. The KTP crystal used in integrated optics, optical parametric oscillator and high power laser generation for laser surgery. KTP have transparent through 350 nm to 4500 nm and good optical properties, which makes it is frontier single crystal for second harmonic generation at 532 nm of Nd-based fundamental lasers. Hydrothermal method also used but the risk is it needs several order pressure to reduce the growth temperature. Alternatively Flux growth (high temperature solution growth) using to grow Potassium titanyl phosphate material. Flux growth has many sub division and paths to grow crystal but in our investigation Top Seeded Solution Growth is chosen for obtaining good perfection of crystalline materials. The TSSG method is consist several parameters to get ideal technique.

The present investigation gives optimization during the growth of KTP crystal using TSSG technique such as vertical and horizontal temperature gradient optimizations, seed rotations and flow of melt causes the surface of crystal growth, interfacing effects of growing crystal with melt and growth rate, Solvent and solute concentration effects on viscosity and growth characteristics, ionic characteristics with defect relations. The inorganic material potassium titanyl phosphate single crystal has been grown using flux growth technique. The grown crystal analyzed by Atomic Force microscope for surface characteristics. The grown crystal confirmed using elementary dispersive analysis of X-ray (EDAX) and powder X-ray diffraction (XRD). The optical property of the grown crystal was analyzed by UV–vis–NIR, Raman scattering and photoluminescence (PL) spectral measurements. The dielectric measurements were carried out for three crystallographic planes at 10-10MHz frequency and the results discussed. The ferroelectric polarization with applied electric field measured. The indentation measurements were used to analyze the mechanical property of the grown crystal. Overcoming the growth obstacles were discussed as elaborately.

11:35 Oral

Development of Large Size Direction Controlled α-$NiSO_4$.$6H_2O$ Single Crystals and its Optical Studies for Bandpass Filters

Rajesh Paulraj, Ramasamy Perumalsamy

Centre for Crystal Growth,SSN College of Engineering,Kalavakkam,Chennai, Chennai 603110, India

e-mail: rajeshppraj@gmail.com

Optical band pass filters need normally a cylindrical plate crystal and perpendicular to the optical axis (0 0 1) and the crystal is directly applicable for the fabrication of the filters.Highly transparent single crystals of α- Nickel sulphate hexahydrate were grown by Sankaranarayanan-Ramasamy method. The size of the grown crystal is 150 mm in length and 25 mm in diameter. The grown crystals are shown in the Fig. 1. The element applied for filter, α -NSH crystal is normally a cylindrical sheet and perpendicular to the optical axis (0 0 1), while all the crystals grown by conventional method have a bitetragonal shape. The Sankaranarayanan-Ramasamy (SR) method has given the solution, and it is possible to grow bulk-size single crystals along a desired orientation needed for device fabrication. Its parameters of transmission spectrometry in the range from UV to near IR wavelengths, Microhardness, dislocation density, laser damage threshold and thermal properties are reported. It has the transmission of specific spectral wavelengths and rejection of others. The laser damage threshold studies show that SR method grown crystal has high laser stability compared to other crystals. Similar behaviour was reflected on the hardness measurements also.

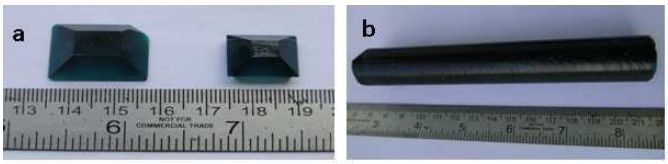

FIGURE 1. (a) Conventional method (b) SR method and grown NSH crystal

11:50 Oral

Bulk crystal growth and characterisation of nonlinear optical crystals by unidirectional growth method

Jerome S. Das

Department of Physics, Loyola College, Chennai, Chennai 600034, India

e-mail: sjeromedas2004@yahoo.com

In recent years there has been considerable interest to synthesize nonlinear optical materials with excellent second order optical non linearities owing to their potential application in electro-optic and opto-electronics devices. Nonlinear optics (NLO) is at the forefront of current research because of its importance in providing the key functions of frequency shifting, optical modulation, optical switching, optical logic and optical memory for the emerging technologies in the areas such as telecommunications, signal processing and optical interconnections. The rapid development of optical communication systems has led to a demand for nonlinear optical materials with high optical quality. Due to the technological importance of these nonlinear crystals, the need for good quality crystals has grown dramatically in the last few decades. The wide range of applicability of bulk single crystals is evident in the fields of semiconductors, infrared detectors, nonlinear optics, piezoelectric oscillators, photonics and optoelectronic industries. The key factors for materials selection depend not only on the laser condition but also on the physical properties of the crystal, such as transparency, damage threshold, conversion efficiency, phase matching, temperature stability and size of the crystal. Bridgeman-stockbarger method, Czochralski methods etc. are known for bulk crystal growth techniques from melt. However in these methods, the transparency and other mechanical properties of the grown crystals are affected due to thermal stress. The crystals, completely decompose at their melting point, cannot be grown by these methods. And also, growth technology plays a principal role for the non-linear optical susceptibilities. This is a main reason for the modification of the existed technological processes. It is reported that solution growth overcomes these difficulties due to its simplicity and convenience.

The unidirectional Sankaranarayanan - Ramasamy (SR) solution growth method attracted the researchers due to the growth of defect free transparent bulk single crystals along a particular axis. The unidirec-

tional growth of bulk single crystals and their characterization towards device fabrication have assumed great momentum due to their significance in both academic and applied research. Simple experimental techniques, unidirectional growth, 100% solute-solid conversion, minimum thermal stress and prevention of the microbial growth are the interesting features of this technique. Due to these reasons, our interest is focused towards the development of several NLO crystals by Sankaranarayanan – Ramasamy (SR) method. All the grown crystals were subjected to various characterizations such as single crystal X-ray diffraction analysis, FTIR analysis, optical and thermal studies and the results were discussed in detail.

12:05 Oral

Studies of solubility, metastable zone width, crystal growth morphology, mechanical and optical properties of UNBA NLO materials in different solvents

RamaNand Rai[1], Chung-Wen Lan[2]

1. *Banaras Hindu University, Varanasi 221005, India* **2.** *Department of Chemical Engineering, National Taiwan University, No. 1, Sec. 4, Roosevelt Road, Taipei city 10617, Taiwan*

e-mail: rn_rai@yahoo.co.in

The transparent single crystals of organic nonlinear optical (NLO) urea-m.nitrobenzoic acid, UNBA, material have been grown from methanol, acetone and ethanol solvents. The solubility and metastable zone width (solution stability) of UNBA have been studied in different solvents at different particular temperatures. Applying the van't Hoff equation the enthalpy, entropy and Jackson's roughness parameters were computed from the saturation temperature for each solvent. The deviation from ideal behavior of different solutions were assessed using the enthalpy of solution, determined applying van't Hoff equation, to that of heat of fusion value determined via differential scanning calorimeter (DSC). The temperature range of solution stability of different solution saturated at different particular temperature and optimum conditions to grow the good quality crystals from different solvents were studied. The crystals' habits of grown crystals from different solvents were found to be solvent dependence. The Optical transmittance, mechanical stability, band gap and refractive index of crystals grown from different solvents were also studied.

PACS: 47.70.M; 31.70.D; 42.25B; 64.75

Key word: Solubility; Metastable zone width; van Haff equation; pH measurements;

Solution crystal growth; Optical Transmittance; Band gap

*Corresponding author: E-mail:rn_rai@yahoo.co.in

Lunch (IOCG Council meeting)

Wednesday afternoon, 14 August, 12:20

WeO2

G02: Bulk crystal growth
Wednesday afternoon, 14 August, 14:00
Room A, Auditorium Maximum

14:00 Invited oral

CZ growth of large sapphire single crystals up to 8 inch diameter 300 mm length for multiple applications

Tsuguo Fukuda

Fukuda X'tal Laboratory, c/o ICR 6-6-3, Minami Yoshinari, Aoba-ku, Sendai 981-3204, Japan

e-mail: fukuda@fxtal.co.jp

The Sapphire substrate market is fast growing and driven by multiple applications such as LEDs, The SOS devices, RF devices, Cover lens and Power devices.

In Fukuda Crystal Labs, according to requirements from customers having many different purposes, CZ sapphire crystal growth technology of 1 inch to 8 inch diameter were developed. CZ crystal growth is historically proven and remains the major technique for producing Si wafer due to quality and cost of ownership requirements. Sapphire wafers would follow that same way at a stand point market expansions and cost reductions for the multiple applications. The development for resistance heating furnaces with Mo crucible has also progressed for lower cost solution as a key to the future markets. After sophisticated examinations with a number of suppliers including fabrication equipment such as multi wire saw, 8 inch sapphire wafers are in ready to markets.

Our efforts and the technology features including summary of melting points and choice of crucibles is also reviewed in this talk.

14:30 Oral

Growth of large-size sapphire and Ti:sapphire crystals with high optical and structural characteristics by HDC method

Viacheslav M. Puzikov, Georgyi Adonkin, Viacheslav Baranov, Aleksander Budnikov, Leonid Gryn, Sergii V. Nizhankovskyi, Natalia Sidelnikova, Alina Tanko

Institute for Single Crystals NAS of Ukraine (ISC), 60 Lenin Ave., Kharkov 61001, Ukraine

e-mail: grin@isc.kharkov.ua

Horizontally directed crystallization (HDC) is one of most effective methods for the obtaining of large-size sapphire windows for aerospace engineering and transparent armour, laser and scintillation crystals.

Studied in the present work were the conditions for the growth of sapphire crystals with rectangular parts measuring 350×500×40 mm^3 and large-size Ti:sapphire crystals by HDC method in reducing gaseous medium ($CO+H_2$). The structural, optical and laser characteristics of these crystals were investigated.

The distribution of the temperature fields in the crystals and the thermal convection in the melt were simulated in the frame of a two-dimensional model. The regions of non-uniform distribution of the thermal and stress fields in the crystals were established. The change of the density of dislocations and their distribution in the crystal bulk after making corrections of the technological growth conditions were considered. This made it possible to optimize the thermal conditions for the growth of large-size sapphire and Ti:sapphire crystals by the method of HDC.

The conditions for the growth of Ti:sapphire crystals with high optical homogeneity were established. Activator striation was shown to be essentially reduced by proper choice of the thermal and convective conditions in the melt. The investigation of the laser characteristics

testifies that the method of HDC is promising for the growth of wide-aperture Ti:sapphire crystals.

14:45 Oral

Effect of heat transfer on the crystal-melt interface shape of sapphire crystal grown using the vertical Bridgman method

Chihiro Miyagawa[1,2], Takumi Kobayashi[2], Toshinori Taishi[1], Keigo Hoshikawa[1]

1. *Shinshu University, 4-17-1 Wakasato, Nagano 380-8553, Japan* **2.** *Fujikoshi Machinery Corp. (FMC), 1650 Kiyono Matsushiro-machi, Nagano 381-1233, Japan*

e-mail: c_miyagawa@shinshu-u.ac.jp

In recent years, *c*-plane (0001) sapphire substrates have been used for the fabrication of GaN-based LED devices. We have applied the vertical Bridgman (VB) method to *c*-axis 3-inch diameter sapphire crystal growth, and crystals were successfully grown [1]. However, low-angle boundaries propagating from the seed-crystal interface were observed at the periphery of the crystal.

The quality of a crystal is affected by the shape of the crystal-melt interface. In order to control this interface shape, two crucibles were prepared for crystal growth by VB method, each with a different shape in order to control the change in heat flux. The crystal-melt interface shapes and resulting low-angle grain boundaries in grown crystals were investigated experimentally and numerically.

As-grown sapphire boules were cut into wafers. Polished sapphire wafers were evaluated using crossed polarizers and were also examined by X-ray topography. In addition, the influence of heat transfer using these crucibles on the crystal-melt interface shapes was numerically estimated using a 2D axisymmetric approach, performed using crystal growth simulator (CGSim) software.

Photographs using crossed polarizers and X-ray topographic images showed that the shape of the crystal-melt interface and the occurrence of low-angle grain boundaries in the crystals were influenced by the heat transfer characteristics of the different crucible structures. The numerical predictions shown in Fig.1 (a) and (b) are consistent with available experimental data.

[1] C. Miyagawa et.al, Demonstration of crack-free c-axis sapphire crystal growth using the vertical Bridgman method, J. Cryst. Growth (in press).

15:00 Oral

Growth and spectroscopic properties of ^{6}Li- and ^{10}B-enriched crystals for heat-scintillation cryogenic bolometers used in the rare events searches

Rekia Belhoucif[1,6], Matias Velazquez[1], Yannick Petit[1], Olivier Pérez[2], Benoît Glorieux[1], Oudomsack Viraphong[1], Pierre de Marcillac[3], Noël Coron[3], Lidia Torres[3,4], Emmanuel Véron[5], AbdelHamid Kellou[6], Philippe Veber[1], Rodolphe Decourt[1], Hassan El Hafid[1]

1. *Institut de Chimie de la Matiere Condensée de Bordeaux, ICMCB - CNRS, 87 avenue du Dr Albert Schweitzer, Pessac 33608, France* **2.** *Laboratoir CRISMAT, CNRS UMR 6508, Bd Marechal Juin, Caen F-14050, France* **3.** *Institut d'Astrophysique Spatiale (IAS), Bâtiment 121, UMR 8617 Université Paris-Sud 11/CNRS, Orsay 91405, France* **4.** *CEA-Saclay, Saclay 91191, France* **5.** *CEMHTI, 1D avenue de la Recherche Scientifique, Orléans 45071, France* **6.** *LEQ, BP 32 El alia, 16111 Bab Ezzouar, Alger 16111, Algeria*

e-mail: matias.velazquez@icmcb-bordeaux.cnrs.fr

he dark matter content of the Universe accounts for 23% of its total energy [1]. Dark matter particles from the halo of our galaxy can be, in principle, detected by the nuclear recoils that they produce in a detector when scattered off nuclei and great experimental efforts are nowadays dedicated to this subject [2]. In the past decade, improved sensitivity of this kind of experiments has come from the acquired capability of distinguishing nuclear recoils in the detector (like those presumably produced by WIMPs) from electronic recoils (produced by the most common radioactive background—gamma, electrons and alpha particles) [3-6]. Neutrons, which scatter off nuclei, are therefore the ultimate background of these searches. A bolometer consists of a crystal absorber strongly coupled to a thermometer, both weakly coupled to a heat sink maintained at 10-30 mK. When a particle of any kind interacts with the absorber, the energy released is seen as a temperature increase by the sensor. Scintillating bolometers are double readout (light and heat) detectors that measure simultaneously the heat and the light generated by a particle [7]. Particle discrimination is achieved by comparison of both signals, since the heat released by a particle is similar for all types of particles, and proportional to their energy, and the light yield strongly depends on the ionization power of the incident particle [3-7]. In this context, we are developing the growth of crystals with diameters of several centimeters and thicknesses several times the thermal neutron mean free path in ^{6}Li-based crystals and the range of neutron capture induced particles in crystals made of ^{6}Li or ^{10}B, typically 6 mm for alpha's and 34 mm for tritiums in lithium borates. As the ^{6}Li and ^{10}B isotopes, as well as several Gd isotopes, exhibit high neutron capture cross-sections (sigma$^{10}_{B\text{-}n}$~4sigma$^{6}_{Li\text{-}n}$(10 keV)~8.10^{-24} cm^{2}) [8,9], it soon turned out that crystals of the $Li_6Gd(BO_3)_3$-type would constitute ideal candidates for both tailoring HSBCs with high light yields over a wide neutron energy range and adapting them to powerful light detectors working at low temperature and available from UV to X-ray spectral ranges [3-7].

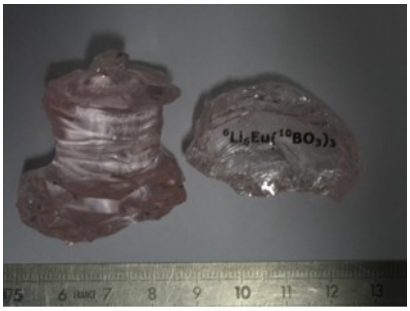

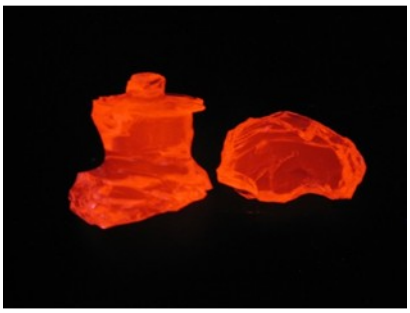

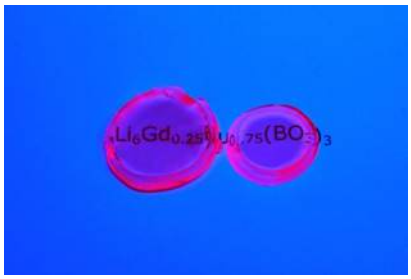

Figure 1.Top top : as-grown $^{6}Li_6Eu(^{10}BO_3)_3$ bulk crystals of 43.5 g and 17.7 g, respectively. Top bottom : the same crystals illuminated by 365 nm radiation. Bottom top : as-grown $Li_6Gd_{0.35}Eu_{0.65}(BO_3)_3$ bulk crystal of ~30 g. Bottom bottom : cut and polished $Li_6Gd_{0.25}Eu_{0.75}(BO_3)_3$ crystals 6 mm-thick and of diameters 30 mm and 23 mm, respectively. All crystals shown at the bottom are illuminated by 365 nm radiation.

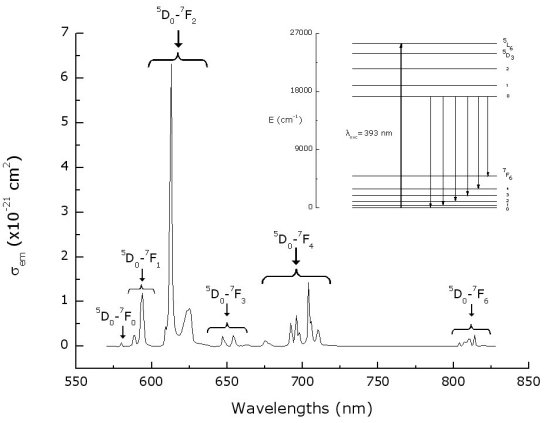

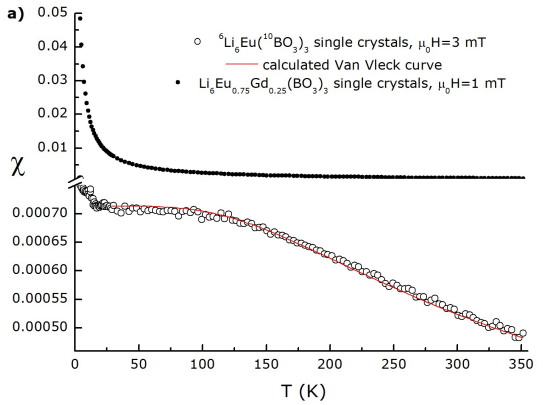

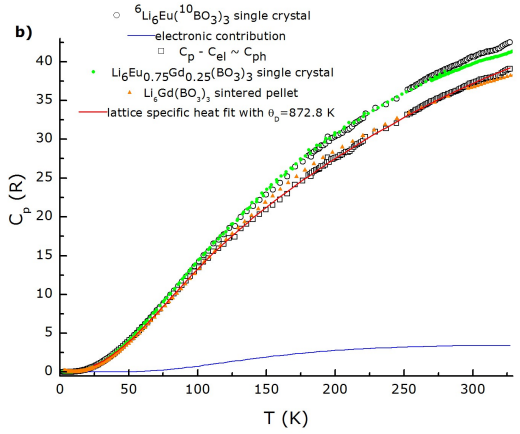

Figure 2. Top : FL-calibrated stimulated emission cross section of $^{6}Li_6Eu(^{10}BO_3)_3$ single crystals at room temperature. The inset shows an experimental energy level diagram of Eu^{3+} ions in $^{6}Li_6Eu(^{10}BO_3)_3$ that was cross-checked bya) MKSA magnetic susceptibility meausrements of unoriented $^{6}Li_6Eu(^{10}BO_3)_3$ and $Li_6Eu_{0.75}Gd_{0.25}(BO_3)_3$single crystals, and b) *specific heat measurements of $^{6}Li_6Eu(^{10}BO_3)_3$ and $Li_6Eu_{0.75}Gd_{0.25}(BO_3)_3$single crystalsand of $aLi_6Gd(BO_3)_3$sintered pellet.*

Moreover, in contrast with the ^{6}LiF bulk crystals which we recently developed, $^{6}Li_6(Eu,Gd)(^{10}BO_3)_3$ crystals are much less likely to exhibit thermoluminescence properties detrimental to HSCB applications [10]. In this work, we present the crystal growth by combined Czochralski and Kyropoulos methods, initiated on specifically oriented seeds, of centimeter-sized $^{6}Li_6Eu(^{10}BO_3)_3$ and $Li_6(Eu,Gd)(BO_3)_3$ single crystals with an heretofore unexplored concentration range for HSBCs application. The crystal structure and lattice thermal expansion of the former, obtained for the first time by single crystal X-ray diffraction (XRD), and the spectroscopic characterizations together with a consistent set of related thermodynamical properties measurements (magnetic susceptibility, specific heat), also unknown to date, are discussed. Finally, preliminary scintillation measurements at low temperature between 300 and 1100 nm under X-ray excitation are shown.

1 N. Jarosik *et al.*, *The Astrophysical Journal Suppl. Ser.*, 2011, **192:14**, 15 pp.

2 J. Beringer *et al.* (Particle Data Group), *Phys. Rev. D***86** 010001 (2012) 289-296.

3 P. de Marcillac, N. Coron, G. Dambier, J. Leblanc, J.-P. Moalic, *Nature*, 2003, **422**, 876-878.

4 N. Coron, P. de Marcillac, J. Leblanc, G. Dambier, J.-P. Moalic, *Opt. Eng.*, 2004, **43 (7)**, 1568-1576.

5 A. Calleja, N. Coron, E. Garcia, J. Gironnet, J. Leblanc, P. de Marcillac, M. Martinez, Y. Ortigoza, A. Ortiz de Solorzano, C. Pobes, J. Puimedon, T. Redon, M. L. Sarsa, L. Torres, J. A. Villar, *J. Low Temp. Phys.*, 2008, **151**, 848-853.

6 G. Angloher *et al.*, Eur. Phys. J. C, (2012), **72:1971**, 22 pp.

7 H. Kraus *et al.*, 2010, *PoS(IDM2010)* 109.

8 M. Knitel, In *New inorganic scintillators and storage phosphors for detection of thermal neutrons*, PhD thesis, Delft University of Technology, 1998.

9 G. F. Knoll, In *Radiation detection and measurement*, 4th edition, John Wiley & Sons (Ed.), 2010, chapters 14 & 15.

10. M. Martinez, N. Coron, C. Ginestra, J. Gironnet, V. Gressier, J. Leblanc, P. de Marcillac, T. Redon, P. Di Stefano, L. Torres, P.

Veber, M. Velazquez and O. Viraphong, *J. Phys. : Conf. Ser.*, 2012, **375**, 012025/1-4.

15:15 Oral

Crystallization rate control and growth parameters management for alkali halide crystal growth by VGF technique with the skull layer

Volodymyr Taranyuk, Alexander Gektin, Alexander Kolesnikov, Victor Liahov

Institute for scintillation materials of NAS of Ukraine (ISMA), 60 Lenin ave., Kharkov 61001, Ukraine

e-mail: v_taranyuk13@rambler.ru

Last years some experimental studies of VGF method use for alkali halide crystals were described [1]. These studies were directed to the development of an efficient industrial technique. The most important peculiarity is the use of skull layer for prevention of the melt-crucible contacts [2]. It allows to use Pt free crucible and minimize internal stresses due to the luck of adhesion between crucible and crystal.

This time the crystallization rate for such technique was studied by the melt level control from the melting stage to the full crystallization completed. The melt level control system as used for continuous halide crystal growth [3] was installed inside skull techniques furnace and successfully controlled the melt level. The melt level change (test accuracy was about 100 micro meters) allows to justify crystallization rate for flat shaped crystal-melt interface as this is typical for VGF technology [4]. Math simulation of the convection in the melt, the melt-interface shape and finally the crystallization rate was done on the base on CGSim softare [5]. Simulations corresponds to NaI crystal and melt parameter for the experimental set-up with crystallization volume 250x180x90mm^3.

The very good correlation between modeling and experimental data related to the melt level down and proper mass crystallization growth rate is found. This methodology was successfully used for the industrial sizes NaI(Tl) scintillation crystal growth. In particular, fully authomized VGF technology was developed for skull technique/technology.

[1] V. Taranyuk, A. Gektin, I. Kisil, A. Kolesnikov, NaI(Tl) and CsI(Tl) scintillation crystal growth by skull method, Journal of Crystal Growth 318 (2010) 820 – 822.

[2] I.I. Kisil, V.I. Taranyuk, S.V. Yaroslavkin, Growing of NaI:Tl crystal plates in garnissage, Functional Materials 15 4 (2008) 600-603.

[3] V.I. Goriletsky, V.A. Nemenov, V.G. Protsenko, A.V. Radkevich, L.G. Eidelman, J., Automated pulling of large alkali halide single crystals, Journal of Crystal Growth 52 (1981) 509-503.

[4] F.-M. Kiessling, F. Büllesfeld, N. Dropka, Ch. Frank-Rotsch, M. Müller, P. Rudolph, Characterization of mc-Si directionally solidified in travelling magnetic fields, Journal of Crystal Growth 360 (2012) 81-86.

[5] http://www.str-soft.com/products/CGSim

15:30 Oral

Growth of giant $CdWO_4$ crystals and properties of (010) cleaved surface

Vladimir N. Shlegel[1], Victor Atuchin[2], Evgeniy N. Galashov[1], Lev Pokrovsky[2], Aleksandr S. Kozhukhov[2]

1. *Institute of Inorganic Chemistry of RAS, Novosibirsk 630090, Russian Federation* **2.** *Institute of Semiconductor Physics SB RAS, pr. Lavrentieva 13, Novosibirsk 630090, Russian Federation*

e-mail: shlegel@niic.nsc.ru

Cadmium tungstate, $CdWO_4$, related to family of wolframite-type crystals $A^{2+}WO_4$ is one from the best scintillating mediums. Potentials of this material for laser techniques, acoustics and photocatalytic technologies are under considerations. The parameters of monoclinic cell of $CdWO_4$: a = 5.0400(8) Å, b = 5.8701(6) Å, c = 5.0841(7) Å, b = 91.476(19)° , V = 150.36(1) Å^3, Z = 2, space group P2/c. A chain-type structure is formed by parallel zigzag chains of distorted CdO_6 and WO_6 octahedrons, spreading along the c axis. The $CdWO_4$ crystals are characterized by good cleavage properties of (010) planes. Micromorphology, structural and electronic properties of $CdWO_4$ (010) cleaved surfaces are evaluated in present study.

High quality inclusion free $CdWO_4$ crystal of 80-90 mm in diameter and of 180-200 mm in length was grown by Low Thermal Gradient Czochralski Technique (LTG Cz). One of the essential features of the LTG Cz technique is the low thermoelastic stresses in the crystal. Respectively, the crystals are less susceptible to post-growth cracking and the dislocation density is much lower in the crystals grown by the LTG Cz technique. The results of $CdWO_4$ crystal growth along the [010] direction are considered in this report. The scintillation and optical properties of $^{116}CdWO_4$ crystals grown under the conditions were early reported in Ref. [1]. In practice, the $CdWO_4$ crystal growth along [010] direction is very hard to be realized by conventional high-temperature methods and, as a rule, is not used.

The substrates of $CdWO_4$ (010) with dimensions 12*0.7*12 mm^3 were fabricated by accurate cleaving of a single crystal parallelepiped. The top-surface crystallographic properties were evaluated with RHEED using EFZ4 device at electron energy of 50 keV. The surface micromorphology was studied by AFM with Solver P-47H device. The system of Kikuchi lines are found for cleaved $CdWO_4$ (010) by RHEED that confirms the high crystallographic state of cleaved surface. A substrate surface is formed by a system of wide plane terraces with as low rms as ~0.2 nm and typical area of 3-10 mm^2. At the terrace surface the point defects of 15-30 nm in diameter are present. Thermal stability of $CdWO_4$ (010) surface have been traced by annealing in the air over the temperature range of 400-700°C followed by RHEED analysis. High crystallographic quality of cleaved $CdWO_4$ (010) surface gives an opportunity to consider $CdWO_4$ as promising substrate material for epitaxial technologies. There is no foreign phase detected after annealing at 400-600°C. However, the low-intensity precipitation of WO_3 and W19O55 oxides was found after annealing at 650-700°C. The epitaxial relations have been obtained for the WO_3 and $W_{19}O_{55}$ precipitates on $CdWO_4$ (010) surface.

1. A.S. Barabash, P. Belli, R. Bernabei, R.S. Boiko, F. Cappella, V. Caracciolo, D.M. Chernyak, R. Cerulli, F.A. Danevich, M.L, Di Vacri, A.E. Dossovitskiy, E.N. Galashov, A. Incicchitti, V.V. Kobychev, S.I. Konovalov, G.P. Kovtun, V.M. Kudovbenko, M. Laubenstein, A.L. Mikhlin, S. Nisi, D.V. Poda, R.B. Podviyanuk, O.G. Polischuk, A.P. Shcherban, V.N. Shlegel, D.A. Solopikhin, Yu.G. Stenin, V.I. Tretyak, V.I. Umatov, Ya.V. Vasiliev and V.D. Virich, Low background detector with enriched $^{116}CdWO_4$ crystal scintillators to search for double β decay of ^{116}Cd, J. Instrumentation 6 (2011) P08011.

15:45 Oral

Growth and properties of BGO, BSO and BGSO scintillation crystals

Jiayue Xu[1], Yan Zhang[1], Xuefeng Xiao[1,2], Baoliang Lu[1,3], Yaoqing Chu[1], Hui Shen[1], Bobo Yang[1]

1. *School of Materials Science and Engineering, Shanghai Institute of Technology, Shanghai 201418, China* **2.** *Department of Fundamental Science, Shanghai Institute of Technology, Yinchuan 750021, China* **3.** *Shanghai Jingcui Material Technology Co., Ltd., Shanghai 200062, China*

e-mail: Xujiayue@sit.edu.cn

Inorganic scintillator plays an important role in radiation detection in many sectors of fundamental and applied research, such as nuclear and high energy physics experiments, and in almost all medical diagnostic imaging modalities that use X-rays or gamma rays, and many industrial measuring systems. The eulytite crystals $Bi_4M_3O_{12}$ (M=Si, Ge) have been investigated due to their excellent characteristics such as luminescent decay constant, absence of afterglow, light output, radiation hardness and nonhygroscopicity. $Bi_4Ge_3O_{12}$ (BGO) crystal has advantages of short radiation length X0=1.12 cm, light output as large as 10% of NaI:Tl but it has drawbacks of slow decay time (τ~300 ns) and expensive component GeO_2. On the other hand, $Bi_4Si_3O_{12}$ (BSO) crystal has faster decay time and cheaper raw materials but low light yield and difficult growth. Thus, $Bi_4(Ge_{1-x}Si_x)_3O_{12}$ (BGSO) solid solution was expected to modify their properties. In the present work, BGO, BSO and BGSO crystals have grown by the modified vertical Bridgman method. A comparative study on scintillation properties of as grown crystals has been reported. BGSO crystals with 0-15% BGO showed similar properties of pure BSO crystals, but the segregation of Bi2O3 in the mixed crystal was modified compared with pure BSO. The thermal and mechanical properties of BGO, BSO and BGSO were measured also.

Break
Wednesday afternoon, 14 August, 16:00

Posters

Monday, 12 August

Break
Monday afternoon, 12 August, 17:00

MoP-G02
Monday afternoon, 12 August, 17:00
Rooms 105, 106, 107, Old Library

17:00 Poster Mo39

Homoepitaxial HVPE-GaN growth on non-polar and semi-polar seeds

Mikołaj Amilusik[1,2], Tomasz Sochacki[1,2], Boleslaw L. Lucznik[1,2], Michal Bockowski[1,2], Michał Fijałkowski[1], Izabella Grzegory[1]

1. *Polish Academy of Sciences, Institute of High Pressure Physics (UNIPRESS), Sokolowska 29/37, Warszawa 01-142, Poland* **2.** *TopGaN Sp. z o. o., Sokolowska 29/37, Warsaw 01-142, Poland*

e-mail: amilusik@unipress.waw.pl

HVPE-GaN crystallization on non-polar and semi-polar HVPE-GaN seeds will be described. All seeds have been obtained by slicing them from the 5 mm thick HVPE-GaN boule (see Fig.1). This boule was grown in a few subsequent growth runs. The multistep growth process was performed in the following way. First, 500 nm thick MOCVD-GaN on 2 in. sapphire wafer was grown. Then, the template was patterned using a titanium mask. After that, the template was overgrown by the HVPE to a thickness of approximately 1 mm. Then, due to self-separation from the sapphire, a free standing HVPE-GaN crystal was obtained. In the next few steps, such crystal was overgrown by the HVPE to a thickness of about 5 mm. Finally, the HVPE-GaN boule was sliced along non-polar and semi-polar planes. Thus, many substrates in the form of stripes with a few centimeters length and five millimeters width were obtained (see Fig. 2). Their surfaces: (10-10), (11-20), (20-21) and (20-2-1) were prepared to the epi-ready state by mechanical and mechano-chemical polishing. These substrates were used as seeds for the HVPE growth in various directions. Four stripes with four different crystallographic surfaces and c-plane reference substrates were always used as seeds for one HVPE process.. This way, a growth rate and morphology at the same crystallization conditions, but in five crystallographic directions, could be determined and compared. Differences in morphology will be presented in this paper. It will be also shown that the growth rate can be changed more than 10 times (depending on the growth direction) and it can be also varied in the function of carrier gas used in the HVPE process.

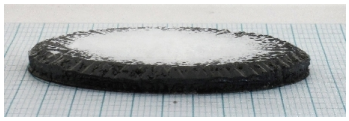

Fig. 1. 5 mm thick HVPE-GaN boule grown in a few subsequent growth runs.

Fig. 2. Stripes sliced from the HVPE-GaN boule with various exposed surfaces: a) (20-21); b) (10-10); c) (11-20); grid line 1 mm.

17:00 Poster Mo40

Study of Interphase Movement During Solidification of Zn-1wt.%Al and Zn-5wt.%Al Alloys

Alicia E. Ares

CONICET, Faculty of Sciences, Posadas 3300, Argentina

e-mail: aares@fceqyn.unam.edu.ar

The Zn based alloys, Zn-Al (alloys ZA or ALZEN) have called the attention like substitute materials of aluminum based alloys, fused irons and brasses. These alloys are of relatively low melting point, they are versatile and they can be manufactured for techniques of foundry, including solidification under pressure, compocasting and reocasting. ZA alloys have a high potential, they show a good performance in service and due to its low cost they have a great variety of industrial applications. The present study has as objective to analyze and to compare different solidification conditions of diluted Zn-Al alloys, Zn-1wt%Al, Zn-5wt%Al (% in weight): 1) alloys directionally solidified with predominant caloric extraction from the base and which have only two interphases [liquid/(solid+liquid)], IL and [(solid+liquid)/solid] IS and, 2) alloys directionally solidified in an horizontal form with caloric extraction from both ends, which gives place to four solidification interphases, two IL interphases and two IS interphases moving in contrary senses. The presence of four interphases determines that the end of the solidification occurs next to the geometric center of the samples and it seems to be related with the presence of pores or hollows derivated from subsuperficial internal contraction. For each alloy of the considered concentration the speeds of the interphases are determined as a function of time and position, and also their accelerations.

17:00 Poster Mo41

Parameters of Solidification of Metal Matrix Composites

Alicia E. Ares

CONICET, Faculty of Sciences, Posadas 3300, Argentina

e-mail: aares@fceqyn.unam.edu.ar

Composite materials obtained by adding particles to the metallic matrix (MMCs) have made remarkable progress in its development and applications in automotive and aerospace industries in recent decades. Among them the most current application is MMCs with zinc and aluminum matrix.

The present work is focused on the study of the effect of the directional heat extraction on the alumina distribution inside the zinc-aluminum matrix and on the columnar – to – equiaxed (CET) phenomenon in samples directionally solidified. The ZA-27 alloy was reinforced with ceramic-particulates of alumina (Al_2O_3) and then vertically directionally solidified and the following parameters were measured: cooling rates, temperature gradients, interphase velocities and the influence of heat transfer on the solidification microstructure of the MMCs is analyzed. Experimental results include transient metal/mould heat transfer coefficients, secondary dendrite arm spacings and particle distribution as a function of solidification conditions imposed by the metal/mould system. The results about the conditions for the CET in MMCs are compared with those obtaining in directional solidification of Zn-Al alloys.

17:00 Poster Mo42

Effective distribution coefficient of Nd^{+3} ion in YAG single crystal grown by Czochralski method

Morteza Asadian[1], Hossein Saeedi[1], Mehdi Yadegari[1], Naser Mirzaei[2]

1. *Iranian National Center of Laser Science and Technology, Tehran 14665-576, Iran* **2.** *Laser and Optics Research School, Tehran 14155-1339, Iran*

e-mail: morteza169@yahoo.com

The ratio of composition in the solid and the melt is a prominent quantity during crystallization of single crystals. This ratio which is known as the effective distribution coefficient is defined by $k_{eff}=C_S/C_L$. In fact, achieving a precise value of distribution coefficient could help to grow a crystal with high accurate dopant concentration and high optical quality.

In many crystal growth processes by Czochralski method, the distribution of solute can be approximately given by the Scheil equation,$C_s=k_{eff}(1-f_s)^{keff-1}$,[1]. So, the effective distribution coefficient (k_{eff}) can be derived as the form of $k_{eff}=W(z)/Ln(1-f_s)$ which z equals to $(Cs/C_0)(1-f_s)Ln(1-f_s)$. Where, the Lambert *W* function [2], represented by $W(z)$, is defined as the inverse of the function $f(z) = ze^z$, satisfying $W(z)e^{W(z)} = z$ for any complex number z.

In this study, four Nd:YAG crystals were grown by Czochralski method using induction heating equipment and auto diameter control software (ADC). The crystals were grown along the <111> crystallographic direction utilizing pure YAG seed crystal. They were pulled with a rate of 0.4 to 0.6 mm/h. The crystal rotation rate was varied from 16 to 20 rpm in order to improve structural and stoichiometric uniformity in the melt during all crystal growth processes. The initial concentrations of neodymium (C_0) into YAG melt were 2.73 at% and 3.33 at%. Each crystal was cut into 1.0 mm thick slices along growth direction of the boul. All samples have been polished on top and bottom planes to achieve good transparency. In the end, Neodymium concentration of samples was measured by Spectrometer instrument.

Because of interface flip, a sudden and uncontrollable interface inversion occurs during the growth of crystal with constant crystal rotation rate and increasing crystal radius (or with constant crystal diameter and decreasing melt level), Nd:YAG crystal is grown almost under convex interface. Utilizing the growth parameters (weight signal, level of melt and crystal diameter) recorded by ADC software is a new idea to calculate interface deflection and solid fraction (f_s). This technique eliminates the error created by Archimedes force during the measurement of crystal weight and causes more accurate k_{eff} using the Scheil equation. In conclusion, our results indicate that the average of effective segregation coefficients of neodymium in YAG crystals, respectively, are 0.28 and 0.24 for C_0=2.72 at% Nd^{+3} and C_0=3.33 at% Nd^{+3}.

References

[1] E. Scheil, Z. fur Metall., 34 (1942) 70

[2] R. M. Corless, G. H. Gonnet, D. E. G. Hare, D. J. Jeffrey, D. E. Knuth, Advances in Computational Mathematics 5 (1996) 329

17:00 Poster Mo43

Numerical study of silicon crystal ridge growth

Girts Barinovs, Andrejs Sabanskis, Andris Muiznieks

Faculty of Physics and Mathematics, University of Latvia, Zellu Street 8, Riga LV-1002, Latvia

e-mail: girts.barinovs@lu.lv

Growing cylindrical silicon (100) crystals from a melt, four crystal ridges appear on the external surface of the crystal, see Fig. 1 showing the cone of a Float zone single-crystal. The appearance of the ridges can be traced back to the presence of {111} crystal planes at the crystal-melt interface. The most detailed theoretical description of the crystal ridge growth has been presented by V. V. Voronkov [1]. The description analyses the effect of undercooling, needed to sustain 2D nucleation growth, on the crystal growth angle. To analyze the ridge growth we have solved Herring's equation describing the equilibrium orientation of crystal-melt, crystal-vapor and melt-vapor interfaces [2]. The equilibrium shape of silicon crystal was obtained from our molecular dynamics calculations. The equilibrium shape of crystal-vapor and melt-vapor interfaces was found in literature. The angular diagram showing equilibrium orientation of the crystal-melt and crystal-vapor interfaces as a function of the orientation of the free melt angle is used to calculate the shape of the crystal growth ridges and to predict the appearance of mirror like facets on the external surface of silicon crystals. The analytical solution of the Laplace equation for the perturbation of the melt surface in the presence of the crystal ridge together with the angular diagram was used to calculate the shape and the size of the crystal ridges for the Float zone crystal growth taking into account temperature gradients created in the melt by an inductor. Understanding of the crystal ridge growth, leads to better understanding of the physical conditions at the triple phase line during the silicon crystal growth from a melt.

Acknowledgements

The present work is carried out at the University of Latvia and has been supported by the European Regional Development Fund, project contract No. 2011-0002-2DP-2.1.1.1.0-10-APIA-VIAA-085.

References

1. V. V. Voronkov, Theory of crystal surface formation in the pulling process, Journal of Crystal Growth, 311 – 318 (1981) and references therein
2. G. Barinovs, A. Sabanskis, A. Muznieks, Study of silicon crystal surface formation based on molecular dynamics simulation results, submitted to Journal of Crystal Growth (2013)

17:00 Poster Mo44

Yb-doped $LiGd_{1-x}Lu_x(WO_4)_2$ single crystals fibers grown from the melt and optical characterization

Rekik Brahim[1], Mourad Derbal[1], Kheirreddine Lebbou[2]

1. *Saad Dahlab University (USDB), 270, route de Soumaa, Blida 09000, Algeria* **2.** *Institut Lumière Matière (ILM), Rue Ada Byron. 10., Lyon 69622, France*

e-mail: brahimre1@yahoo.fr

Because of their remarkable characteristics single crystalline fiber crystals receive an intense study. The growth of single crystals fibers is of low cost in comparison to Czochralski or Bridgman techniques. In addition, by micro-pulling down technique it is possible to grow fiber shape close to final geometry to be used in the final component. Yb-doped $LiGd(WO_4)_2$double tungstate crystal exhibit large absorption band and emission bandwidth. In spite of the optical performances of this material, only very few works were reported about single crystals fibers growth of Yb-doped $LiGd(WO_4)_2$.

Therefore, the main topic of this presentation is to investigate the fibers crystal growth from the melt of Yb3+:$LiGd(WO_4)_2$ using micro-pulling down (μ-PD) technique. The structure and spectroscopic characteristics of the single crystals fibers were evaluated to develop laser components based on active fiber shape. We have extended our research program to Yb3+-doped $LiGd_{1-x}Lu_x(WO_4)_2$ system to determine the solid solution range as a function of Lu3+ on Gd3+ sites.

Under stationary stable regime Yb3+-doped $LiGd_{1-x}Lu_x(WO_4)_2$ transparent and uniform single crystals fibers were grown by micro-pulling down technique. For $x \leq 0.025$, homogeneous fibers of diameter 700 μm were grown from the melt. The crystallization interface was flat, the meniscus length reach 150μm ± 20 and the liquid flow in the molten zone is laminar. For $x \geq 0.5$ the melt is not congruent and the grown materials were ceramic.

The Yb dopant distribution was examined parallel and perpendicular to the growth direction. For $x \leq 0.025$ the dopant distribution along the growth direction is homogeneous and no significant segregation has been observed. The pulling rate did not significantly affect Yb distribution. The absorption, Raman and excitation spectroscopy at room temperature were performed to investigate the lattice changes due to the Lu3+substitution in the $LiGd_{1-x}Lu_x(WO_4)_2$ host.

17:00 Poster Mo45

Flux growth and characterization of Mn- doped enstatite single crystals

Manuela Catalano, Valentino Pingitore, Enzo Cazzanelli, Domenico Miriello, Eugenio Barrese, Andrea Bloise

Universita' della Calabria, Rende, Cosenza 87036, Italy

e-mail: manuela.catalano@fis.unical.it

In recent years, particular interest has been addressed by researchers in the synthesis and study of enstatite ($MgSiO_3$). This is related with the good physical, chemical, electrical, mechanical properties of enstatite. In fact, it is useful for several technological applications such as substrates in electronics, as insulators at high frequencies, as materials for thermal insulation in applications at high temperatures, and mainly for laser technology luminescence. In view of its very good properties, mainly luminescence and to find others applications, in recent years syntheses and property studies have been conducted on enstatite doped with varying amounts of Cr^{3+}, $Li^{+}Sc^{3+}$, Ti^{4+} and Ni^{2+} [1]. In this contest, growth of Mn-doped enstatite was carried out in order to elucidate

the best conditions of its formation and to assess their potential in advanced technological applications. Mn- doped enstatite single crystals were grown in lithium-vanadomolybdate flux as melting agent, the following nutrients were used: SiO_2 (granular quartz), MgO (periclase), MnO (manganese oxide), before appropriately treated to make them more reactive. Several starting mixtures, with different MnO concentrations, were first held to 1350 °C, 1050 °C and 950 °C and then slowly cooled down to 700 °C or 600 °C with three different cooling rate (3.75 °C/h, 2.1 °C/h and 1.7 °C/h). The products were characterized and studied by stereo binocular microscopy, powder crystal X-ray diffraction (XRPD), and scanning electron microscopy with energy-dispersive spectrometry (SEM/EDS). Several crystals were further characterized by single-crystal X-ray diffraction (XRD), micro-Raman and cathodoluminescence (CL). Mn-doped enstatite crystals were magenta in colour and prismatic (Fig.1), and all appeared to be euhedral and elongate parallel to c-axis. Optical inspection and XRPD analyses of products revealed that hausmannite ($Mn^{2+}Mn^{3+}{}_2O_3$) and quartz were also found in some runs in addition to Mn-doped enstatite. According to the XRPD patterns, the major diffraction peaks of Mn-doped enstatite consisted of clinoenstatite associated with some orthoenstatite. The maximum size of Mn-doped enstatite was 8 mm in length when the cooling rate was 1.7 °C/h, becoming smaller when the cooling rate was faster. For all runs, the doped amount of MnO (wt %) in enstatite crystals ranged from 2.20 wt% to 12.60 wt% as calculated from EDS/SEM analyses. However, in some runs, enstatite crystals were zoned and had not the same MnO (wt%) dopant content, indicating crystallization in non equilibrium conditions. When the Mg/Mn molar ratio was > 0.43, no Mn-doped enstatite was produced. Raman spectrum of pure enstatite single crystal was compared with Mn-doped enstatite spectra in order to study the effect of the increasing doping on the position of Raman bands. For two different MnO values, about 6 wt% and 10 wt%, the following trends were observed in the Raman spectra: 1) a down shifting of the peak positions; 2) a widening of the peaks; 3) a general decrease of Raman intensity. The last effect is due to the increase in surface reflection as the MnO concentration increases. The other ones indicates changes in vibrational modes because of the increasing presence of MnO. In particular the Raman band at about 686 cm^{-1} in the pure enstatite spectrum, shifts down to 680 cm^{-1} for 10 wt% Mn doping, in good agreement with the data reported by Stalder *et al.* [2] for similar crystals doped with Fe. At room temperature, the CL spectrum of Mn-doped enstatite contains a broad emission located at 677 nm. As confirmed by Lin Lin *et al.* [3] this broad band is attributed to the transition $^4T_{1g}(G) \rightarrow {}^6A_{1g}(S)$ of Mn^{2+} substitutional to Mg^{2+} position in enstatite. The comparison of the CL spectrum of Mn-doped enstatite with the analogous spectrum of pure enstatite shows that the broad emission bands which appear in Mn-doped enstatite are completely absent in the CL spectrum of the no-doped enstatite.

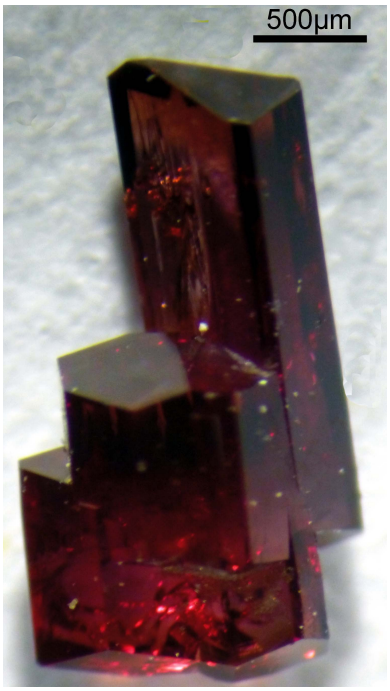

[1] A. Bloise, V. Pingitore, D. Miriello, C. Apollaro, D. Armentano, E. Barrese, A. Oliva, J. Cryst. Growth 329 (2011) 86.

[2] R. Stalder, A. Kronz, B. C. Schmidt, Eur. J. Mineral. 21 (2009) 27.

[3] L. Lin, Y. Min, S. Chaoshu, Z. Weiping, Y. Baogui, J. Rare Earths 24 (2006) 104.

17:00 Poster Mo46

Growth and Optical studies on Glycine Sodium Nitrate by Unidirectional Growth method

Mary J. Linet, Jerome S. Das

Department of Physics, Loyola College, Chennai, Chennai 600034, India

e-mail: sjeromedas2004@yahoo.com

Optically transparent bulk semi-organic single crystals of glycine sodium nitrate have been grown by unidirectional method. The grown crystal was identified using single crystal XRD analysis. The functional groups present in the crystal were confirmed using FTIR analysis. Optical absorption studies reveal very low absorption in the entire visible region, which reveals the good optical quality of the grown crystal. The mechanical properties of the grown crystal were studied using Vickers microhardness tester. Dielectric behaviour of the grown crystal was studied and the results are discussed in detail.

17:00 Poster Mo47

Unidirectional growth of potassium dihydrogen phosphate (KDP) single crystals by modified Sankaranarayanan–Ramasamy (mSR) method

Robert R R, Jerome S. Das

Department of Physics, Loyola College, Chennai, Chennai 600034, India

e-mail: sjeromedas2004@yahoo.com

Transparent single crystals of potassium dihydrogen phosphate (KDP) were grown by modified Sankaranarayanan–Ramasamy (SR) method. The band gap energy for the KDP crystals was calculated from optical transmission spectrum. The theoretical calculations to determine the optical constants of the material and a technique for photonic band gap tuning, which is essentially required to develop the optoelectronic devices, were determined using the optical studies. Further, theVicker's microhardness as well as parameters such as fracture toughness(Kc), brittleness index(B) and yield strength(sv) are presented.

17:00 Poster Mo48

Growth of 4H-SiC single crystals on the prismatic seeds

Alexey Fadeev[1], Andrey Lebedev[2], Dmitri Avrov[1], Sergey Dorozhkin[1], Yuri M. Tairov[1]

1. *State Electrotechnical University, Saint-Petersburg 197376, Russian Federation* **2.** *Ioffe Physico-Technical Institute, RAS, Saint-Petersburg, Russian Federation*

e-mail: alfadeus@gmail.com

Silicon carbide ingots grown by the modified Lely method on (0001)-plane are characterized by extremely developed defect structure. Thus, the study of non-basal plane growth of SiC became urgent for getting high quality non-basal substrates and further design of microelectronics devices as well as for so-called RAF-process and further getting defect-free (0001)-grown ingots. In this study the defect structure of the 4H-SiC crystals grown on (10-10), (11-20) and near to (8.3.-11.0) planes is considered. The last plane makes an angle of about 15° with (10-10) and (11-20).

Initial 4H-SiC (10-10), (11-20) and (8.3.-11.0) substrates were cut from the single [000-1] grown crystal. The SiC crystal growth was held on these three seeds in the same growth experiment simultaneously. The grown ingot was cut into the wafers in three perpendicular directions: (10-10), (11-20) and (0001) cuts for [10-10]- and [11-20]-grown crystals and (8.3.-11.0), (-3 4 -1 0) and (0001) cuts for [8.3.-11.0]-grown crystal. Defect analysis was held using optical microscopy after KOH etching (type of defects was identified by etch pits form) as well as X-ray topography.

Defect structure of grown crystals is shown in fig. 1. It is well known that the growth on prismatic seeds leads to stacking faults (SF) formation (linear defect in fig. 1a)-1c)). We have found that SF formation probability strongly depends on seed crystallographic orientation and gradually increases with seed inclination from (11-20)-plane to (10-10)-plane. For [11-20]-grown crystal it was also noticed that SFs prevail on the edges of crystal where convex growth front has maximal inclination from initial (11-20)-plane. In spite of relatively low quantity of SFs the growth on (11-20) seed was characterized by formation of a huge number of basal plane dislocations (BPD). The dissociation of these dislocations in (11-20)-plane with further SF formation is obviously impeded. So they keep being not dissociated during whole growth process.

Fig. 1d), f) and h) show (0001)-plane of grown crystals after KOH etching. This plane revealed BPDs as the only visible defect on the surface. The density of BPD is decreased from 4×10^3 cm^{-2} for [11-20] to 10^3 cm^{-2} for [10-10]. It is also clear that the inclination of the seed from (11-20)-plane to (10-10)-plane leads to merging of single BPDs and formation of low-angle grain boundaries (LAGB).

Fig. 1e), g) and i) show the edges of the planes parallel to the growth direction and normal to (0001)-plane. There are multiple terraces on the etched substrates extended along growth direction. The number of these terraces is obviously depends on number of SFs. More SFs are in the growth plane, more and narrower terraces are in the plane normal to the last and (0001) one.

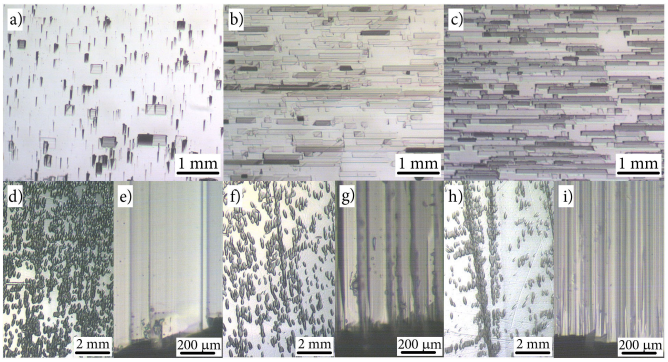

Fig.1. a), b), c): cuts normal to the growth direction; d), f), h): (0001)-plane; e), g), i): cuts parallel to the growth direction and normal to (0001)-plane for [11-20]-, [8.3.-11.0]- and [10-10]-grown crystals, respectively.

17:00 Poster Mo49

Precipitations of tungsten in quasicrystalline Al-Cu-Fe-W alloys

Jacek Krawczyk, Wojciech Gurdziel, Włodzimierz Bogdanowicz, Grzegorz Dercz, Robert Paszkowski

University of Silesia, Institute of Materials Science (INOM), 75 Pułku Piechoty 1A, Chorzów 41-500, Poland

e-mail: wojciech.gurdziel@us.edu.pl

The aim of presented paper is the analysis of precipitations morphology of tungsten in quasicrystal Al-Cu-Fe alloys. The composition of $Al_{65}Cu_{20}Fe_{14}W_1$ (at.%) was a base for preparation of bulk alloy in the form of ingot containing the icosahedral quasicrystalline phase.

The alloy was obtained in a two-stage process. At the first stage, the induction heating synthesis of alloy substrates and their preliminary homogenization were carried out using the mechanical mixing. The second stage was carried out by vertical directional solidification of the classic Bridgman method. The technological process was performed under protective atmosphere of helium (5N).

The samples were cut using electrical spark-erosion cutter. X-ray phase analysis, electron microscopy (SEM) and optical metallographic observations were performed.
The cubic β-phase, monoclinic λ-phase, quasicrystalline i-phase and tetragonal ω-phase were distinguished. It was stated that the needle-like precipitations of tungsten with the length-to-diameter ratio of 1:1000 were irregularly distributed in the volume of ingot. The presence of tungsten was confirmed by the powder phase analysis. The filaments of tungsten formed a clump-like aggregations. The tungsten filaments grow mainly on the crystalline β-phase.

17:00 Poster Mo50

Vertical Bridgman Growth of Sapphire Crystals with Thin Neck Formation Process

Etuko Ohba[1,2], Takumi Kobayashi[2], Jun Yanagisawa[2], Minami Shinozuka[2], Chihiro Miyagawa[1,2], Toshinori Taishi[1], Keigo Hoshikawa[1]

1. *Shinshu University, 4-17-1 Wakasato, Nagano 380-8553, Japan*
2. *Fujikoshi Machinery Corp. (FMC), 1650 Kiyono Matsushiro-machi, Nagano 381-1233, Japan*

e-mail: khoshi1@shinshu-u.ac.jp

A new technique is proposed, in which the thin neck formation process is adopted after the seeding process in the vertical Bridgman growth of sapphire crystals.

The process stages of the new technique are shown in figure 1. The raw materials are put into a Mo or W crucible from above and a c-axis seed crystal is inserted in the seed well at the bottom of the crucible as shown in Fig.1 (a). The growth processes consists of first seeding, after melting of all raw material and a part of seed crystal, as shown in Fig1(b) and then, as the crucible is pulled down, formation of thin neck, as shown in Fig1(c), and growth of the crystal body, as shown in Fig1(d). After cooling to room temperature, it was found that the seed and the body grown could be easily separated and released from the crucible[1)].

Samples cut from grown crystals were polished to mirror finish on both side and were characterized using a crossed polarizer and X-ray topography. It was confirmed that low angle grain boundaries generated at the periphery of seeding portion were eliminated at the thin neck and c-axis crystals free from low angle grain boundaries in the main body were successfully grown.

We concluded that the proposed new technique incorporating a thin neck formation process in the vertical Bridgman growth method promises high potential in growth of large-size and high quality c-axis sapphire crystals with high reproducibility.

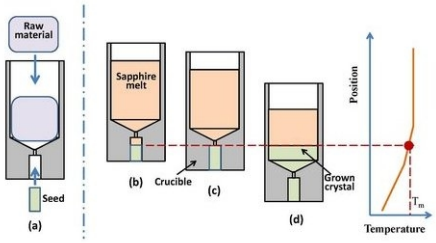

Fig.1 Vertical Bridgeman growth with thin neck formation process

(1) C. Miyagawa et.al: Demonstration of crack-free c-axis sapphire crystal growth using vertical Bridgman method, Journal of Crystal Growth. (in printing)

17:00 Poster Mo51

Vertical Bridgman Growth of Sapphire - Seed crystal shapes and seeding processes-

Keigo Hoshikawa[1], Etuko Ohba[1,2], Takumi Kobayashi[2], Jun Yanagisawa[2], Minami Shinozuka[2], Chihiro Miyagawa[1,2], Toshinori Taishi[1]

1. *Shinshu University, 4-17-1 Wakasato, Nagano 380-8553, Japan*
2. *Fujikoshi Machinery Corp. (FMC), 1650 Kiyono Matsushiro-machi, Nagano 381-1233, Japan*

e-mail: khoshi1@shinshu-u.ac.jp

Recently, significant attention has been paid to methods and techniques for growing sapphire crystals for use in the fabrication of GaN-based LED devices. We have investigated the growth of sapphire crystal using the traditional vertical Bridgman (VB) method, in which sapphire crystals were grown in a Mo or W crucible with rotation and translation in a hot zone to achieve an appropriate temperature distribution. Different types of seed crystals and the seeding processes using them were examined from the viewpoint of achieving single crystal growth.

The upper diagrams in Fig. 1 are schematic drawings showing the features of the crucibles and seed crystals used in the experiments. The full diameter, tapered and thin seed crystals and crucibles are shown in the upper parts of Fig. 1(a), Fig. 1(b), and Fig. 1(c) respectively. The full diameter portions of each crucible have a structure with a taper of a few degrees so that the grown crystals can be released easily from the crucible. Reproducible seeding processes have been established by using techniques which include precise temperature measurement and control by adapting a newly developed thermo-couple structure. Photographs of c-axis sapphire crystals grown using the three kinds of seed crystal, and using Mo or W crucibles of the suitable shape, are shown in the respective lower portions of Fig 1.

It is concluded that: (1) the newly developed thermo-couple enabled temperature measurement with accuracy of ±0.5 °C at about 2000 °C near the crucible bottom; (2) a seeding process which provides acceptable reproducibility in the very low temperature gradient of about 5 °C /cm at a high temperature near the melting temperature of sapphire has been established; (3) c-axis sapphire single crystals with a diameter of about 2 inches have been successfully grown from the three kinds of seeds, full diameter, tapered and thin seeds; and (4) it was found in the growth using thin seed crystals that a seed diameter of more than 20 millimeters was necessary in order for it to be possible to release the crystal easily from the crucible without breaking the grown crystal [1)].

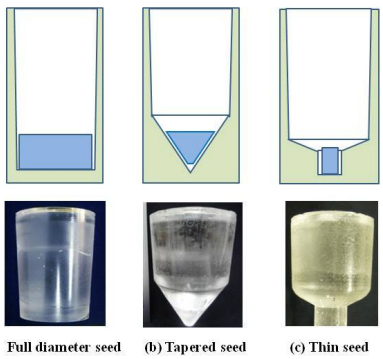

Fig. 1 Photographs (lower images) of crystals grown using (a) full diameter, (b) tapered and (c) thin seed crystals and schematics of the related crucibles (upper images).

(1) C. Miyagawa et. al: Demonstration of crack-free c-axis sapphire crystal growth using vertical Bridgman method, Journal of Crystal Growth. (in printing)

17:00 Poster Mo52

Sapphire for High Volume Cover and Touch Screen Applications

Weidong Huang

GT Advanced Technologies Inc., Merrimack 03054, United States

e-mail: ed.huang@gtat.com

The use of sapphire crystal in end user markets is poised for explosive growth. The increasing availability of high quality, low cost material is opening up new, high volume markets such as mobile and touch screen devices. This presentation will look at the factors that are contributing to this new opportunity. We will look specifically at advances in crystal growth methods that are leading to higher throughput, lower cost manufacturing of sapphire as well as the creation of a downstream, optimized fabrication channel capable of meeting these high volume market opportunities.

17:00 Poster Mo53

Dewetting as a powerful tool for thermoelectricity device applications

Khaled Ebnalwaled Hufny, Thierry Duffar, Lamin Sylla

South valley university, Qena 83523, Egypt

e-mail: kh_ebnalwaled@yahoo.com

InSb and GaSb polycrystals were grown using the dewetting technique. After optimization of the set up and growth parameters, four samples, 88 mm in length and 11 mm in diameter, have been obtained. The grown crystals were characterized by using X-ray analysis and thermoelectric power measurements. The effect of solidification type (attached, dewetted and so on) on the lattice parameters, microstrain and Crystallite size (D) of the obtained crystals was investigated. Their thermoelectrically properties were investigated also in relation to the type of solidification. Power factor values obtained for dewetted antimonide samples have shown the highest values obtained till now. These results indicate that dewetting can be used to produce InSb and GaSb with high power factor for thermoelectricity device applications.

17:00 Poster Mo54

The influence of the growth rate on the quality of BGO crystals and estimation of facet supercooling

Nina V. Ivannikova, Vladimir N. Shlegel, Yan V. Vasiliev

Nikolaev Institute of Inorganic Chemistry of SB RAS, Lavrentev 3, Novosibirsk 630090, Russian Federation

e-mail: nvi@niic.nsc.ru

Bismuth Orthogermanate ($Bi_4Ge_3O_{12}$) is widely used as a scintillation material. Although this crystal is grown for a long time, unsolved questions about the mechanisms of crystallization remain, in particularly, the influence of the growth rate on the quality of the crystals.
Commonly it is considered that the lower the crystallization rate, the higher crystal perfection. [1].
However, during growing the BGO crystals by the Low Thermal Gradient Czochralski Technique (LTG Cz) [2], just opposite behavior is observed. For the growth rate less than 1.5 mm/h, the amount of defects and impurities is higher than for the case of the growth rate 3.5 - 6 mm/h.
Small crystals (diameter 50 mm, length up to 170 mm) maintained steady growth to 10-11 mm/h. The upper limit of the growth rate of high quality crystals depends on the level of impurities in the charge and the homogeneity of the melt.
For estimation of supercooling the specified growth rate changed stepwise during the growth run while the crystal diameter maintained constant by the automatic weighing control system. Experiments were performed in the range from 0.3 to 15 mm/h for two polar growth directions <111>. Typical dependence of temperature drop at the middle section of three zone heated from the magnitude of step of the growth rated is shown in the Fig.

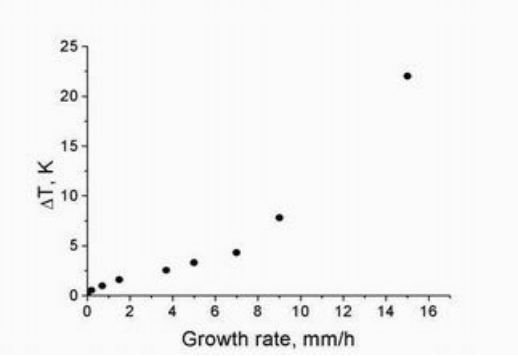

Change of temperature at the heater versus BGO crystal growth rate

The value of the temperature drop ΔT on the heater with increasing the crystallization rate $V_{cryst.}$ is determined by two main factors: the increase in supercooling and increase heat flow to remove the heat of crystallization. The contribution of the second factor is a linear function of growth rate and could be estimated from series experiments. The results are compared with data published in [3-5] where the values of supercooling were found by direct measurements of temperature on the crystal's face.

[1] H.J. Scheel // J.Cryst. Growth, 2000, v.211, p.1.
[2] Yu.A. Borovlev, N.V. Ivannikova, V.N. Shlegel et al. // J. Cryst. Growth. 2001, v. 229, p.305
[3] V.D. Golyshev, M.A. Gonik, V.B. Tsvetovsky // J. Cryst. Growth. 2002, v. 237, p.735
[4] S.V. Bykova, V.D. Golyshev, M.A. Gonik et al. // J. Cryst Growth. 2004, v. 266, p.246
[5] S.V. Bykova, V.D. Golyshev, M.A. Gonik et al. // Heat Transfer Engineering, 2006 v. 27, №2, p.43

17:00 Poster Mo55

Exploiting Inherent Thermodynamic Effects in Crystal Growth to Achieve Functionally Graded Thermoelectrics

Ellen M. Jensen Hedegaard, Simon Johnsen, Bo B. Iversen

Center for Materials Crystallography, Dept. of Chemistry, Aarhus University (AU), Langelandsgade 140, Aarhus DK-8000, Denmark

e-mail: ellenj@chem.au.dk

Exploiting waste heat by means of thermoelectric generators has long been proposed as one of the ways to meet the worlds rising energy demands. However, thermoelectric materials still need improvements to be cost-effective in most applications. Higher efficiency materials could be obtained by optimizing the materials through functionality grading to meet the changing temperature conditions within a thermoelectric leg in operation.

The physical parameters that influence the efficiency of a thermoelectric material are all strongly temperature dependent, and consequently the efficiency of a homogeneous material peaks in a narrow temperature interval. By grading these parameters though the material, the temperature at which the efficiency peaks can also be graded.

Opposed to most other techniques for functionality grading, graded materials can be achieved in one step though Czochralski or Bridgman/Stockbarger synthesis. It has previously been shown that thermoelectric materials graded in either composition, and thereby band gap [1], or doping [2???] can be prepared in this way, but by combining the two effects a potentially significant improvement in efficiency should be achievable.

This poster presents the idea behind and preliminary results of a study aiming at identifying and testing material systems capable of being graded in both doping and composition through either Czochralski or Bridgman/Stockbarger crystal growth in such a way that these effects enhance each other, and optimizing the synthesis of these materials.

1. Christensen, M., et al., *Fast Preparation and Characterization of Quarternary Thermoelectrics Clathrates.* Chem. Mater, 2009. 21(1): p. 122-127.
2. Kuznetsov, V.L., et al., *High performance functionally graded and segmented Bi2Te3-based materials for thermoelectric power generation.* Journal of Materials Science, 2002. 37(14): p. 2893-2897.

17:00 Poster Mo56

Structural, FTIR, thermal and dielectric studies of gel grown manganese-copper mixed levo tartrate crystals

Sudhir J. Joshi[1], Kashmira P. Tank[2], Poorvesh M. Vyas[2], Mihirkumar J. Joshi[2]

1. *Physics Department, Bahauddin Science College (BSC), Near-Bhutnath Temple, Junagadh 362001, India* **2.** *Saurashtra University, Department of Physics, Crystal Growth Laboratory, University Road, Rajkot 360005, India*

e-mail: energyjoshi@rediffmail.com

Manganese tartrate and copper tartrate find various applications, for example, copper tartrate stimulates Luteinizing hormone in vitro and manganese tartrate as chemical temperature sensor. In the present study manganese-copper mixed levo tartrate crystals have been grown by single diffusion gel growth technique in Silica hydro gel. Different compositions of manganese-copper mixed levo tartrate crystals were obtained by varying the amount of MnCl2 and CuSO4 in supernatant solution. Purple blue colored prismatic crystals were grown and the coloration changed from light purple blue to dark purple blue on increasing copper content. From the EDAX the exact content of manganese and copper in crystals was determined. The crystals exhibited orthorhombic crystal structure and the unit cell parameters changed with the composition of manganese and copper in the crystals. The FTIR spectra suggested the presence of functional groups O-H, C=O, C-O and C-H in the samples. The absorption bands shifted slightly to higher wave numbers on increasing copper in crystals. The thermogravimatry indicated that on heating the crystals first became anhydrous and then decomposed to respective oxides. All the crystals were having different amount of water of hydration. The dielectric study was carried out at room temperature by varying the frequency of applied field from 500 Hz to 1 MHz. The variation of dielectric constant with frequency indicated that as the frequency increased the dielectric constant decreased. The variations of dielectric loss and a.c. conductivity with frequency of applied field were studied. Results are discussed.

17:00 Poster Mo57

Analysis of dynamic parameters of sapphire crystallization by the Kyropulos method

Ievgenii V. Kryvonosov, Dmitrii I. Kryvonosov, Pavel V. Konevskyi, Leonid Lytvynov

Institute for Single Crystals NAS of Ukraine (ISC), 60 Lenin Ave., Kharkov 61001, Ukraine

e-mail: investig@inbox.ru

The Kyropoulos method is the technique most widely used for the growth of large-size sapphire crystals. The shape and quality of the crystals are defined by the thermal field configuration, the shape of the crystallization front (CF), the rates of crystallization and crystal pulling from the melt. The main problem to be solved in the process of crystal growth by the said method is the control of the growth dynamics from the changes of the weight sensor readings. The change of the CF shape in the process of crystal growth depends on the configuration of the thermal field of the used setup and the conditions of heat removal. The value of the increase of the crystal mass per unit of time and, consequently, the crystal's homogeneity, also change. Degradation of the thermal unit elements in the process of operation may modify the character of the change of the CF from process to process. Therefore, the crystallization conditions require correction each 5 or 6 crystallization processes.

There has been proposed a method for the determination, optimization and control of the main dynamic parameters of the crystallization process. This method implies the use of the computer program for the dynamic calculator developed in cooperation with Alyuda Research [1]. The program makes it possible to calculate the main crystal growth parameters and simulate the dynamic parameters of the crystallization process (the size and shape of the crucible, the quantity of the starting material, the CF shape, the rates of crystallization and crystal pulling from the melt), for different crystallization conditions. The program "SK Analysis" allows to analyze the dynamics of the change of the CF shape (Fig.), the shape and weight of the crystal, as well as the dynamics of the change of the weight sensor readings. By analyzing the dynamic characteristics one can virtually optimize the technological parameters using the program "SK Forecast", and establish the optimum dynamics of the increase of the crystal weight. Such a characteristic in the form of a time function is introduced into the program of a real crystallization process as a parameter of the heater power regulator.

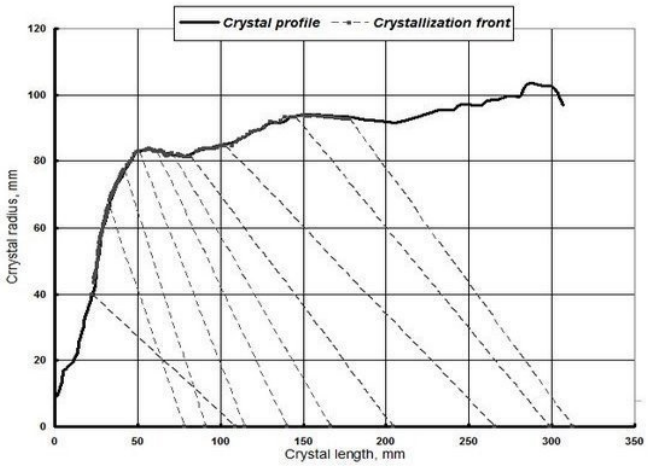

Fig. Simulation of the dynamics of CF shape for the grown crystal

Successive regular computer analysis, control and correction of the main dynamic crystallization parameters makes it possible to timely monitor and correct the changes in the thermal field during the growth equipment operation. Such a low-cost, on-line and addressed technological operation raises the efficiency of the growth process.

[1] Alyuda Research www.alyuda.com

17:00 Poster Mo58

Partially stabilized zirconia (PSZ): crystal growth and structure

Mikhail A. Borik[1], Vladimir T. Bublik[2], Alexey V. Kulebyakin[1], Elena E. Lomonova[1], Valentina A. Mizina[1], Filipp O. Milovich[2], Vjatcheslav V. Osiko[1], Natalia Y. Tabachkova[2]

1. *A.M. Prokhorov General Physics Institute of Russian Academy of Sciences (GPI), Vavilov Str. 38, Moscow 119991, Russian Federation* **2.** *National University of Science and Technology (MISIS), Leninsky prospect, 4, Moscow 119049, Russian Federation*

e-mail: kulebyakin@lst.gpi.ru

Currently, intensive research effort is focused all over the world on engineering novel nonmetallic structural materials that would combine high mechanical strength, fracture toughness, wear resistance, and chemical inertness with high stability in aggressive media in a wide temperature range. One such material is partially stabilized zirconia (PSZ) crystals — a zirconia-based solid solution containing small additions of stabilizing oxides.

The PSZ single crystals were grown by directional crystallization technique with direct RF-heating in the cold container (skull melting).The mechanical properties of PSZ crystals depend primarily on the synthesis procedure and conditions. PSZ single crystals possess very attractive mechanical properties owing to their unusual, twin domain structure.

PSZ crystals growing during melt synthesis initially have a cubic structure, and a phase transformations occur during cooling in the solid state. As the temperature decreases, the cubic phase becomes unstable and transforms to a tetragonal modification. The slight atomic shifts, mainly affecting the oxygen ions, distort the symmetry of the initial structure. The oxygen ions shift relative to the perfect fluorite lattice positions (1/4, 1/4, 1/4). Generally, the tetragonal phase lattice is slightly elongated along the c axis as compared to the cubic phase lattice.

X-ray diffraction from the PSZ phase showed that the material has two tetragonal phases (fig. 1). The simultaneous occurrence of the (006) and (600) reflections in the diffraction pattern is accounted for by twinning as will be shown below in the discussion of the transmission electron microscopy results. Phase constituent study of zirconia doped to different Y_2O_3 concentrations (2.8–5.0 mol.%) showed that all the specimens, regardless of the stabilizing impurity content, have two tetragonal zirconia modification phases with varying degrees of tetragonality. Both phases have a slightly distorted fluorite structure and differ in the ratio of their lattice parameters. For one tetragonal phase – t, the c/a ratio was 1.014–1.015, and for the other tetragonal phase – t', the c/a ratio was close to 1, i.e. 1.004–1.005. The yttrium rich t' phase is not transformable unlike the lower yttrium content t phase which undergoes a martensitic transformation to the monoclinic state under mechanical stress: this transformation may suppress the sources of stress concentration and increase the fracture toughness of the material.

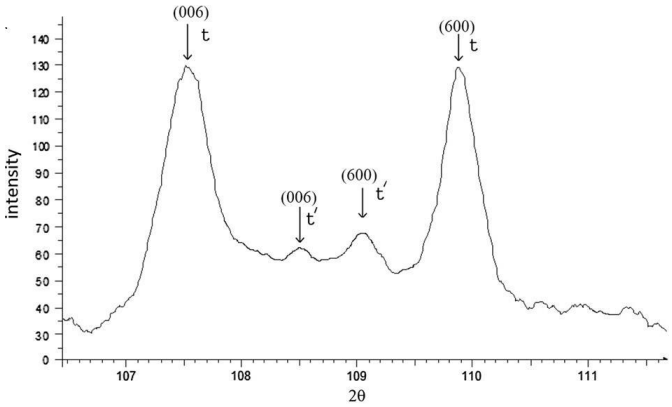

Fig. 1. X-ray diffraction patterns of the PSZ 2.8 mol.% Y_2O_3

TEM study of the PSZ crystals showed that all the specimens had a well developed twin domain structure. The twined structure forms due to the polymorphic transformation from the cubic to the tetragonal phase which occurs during single crystal cooling. Fig. 2 shows a typical example of the twined structure for the PSZ crystals. It can be seen that most domains have an elongated shape. The twinning plane is {110}. The primary twin plates also undergo secondary twinning to form a parquet-like structure consisting of twin domains. The twinning can occur on along the planes inclined to the fourth order axis c. Twinning may occur along the (101) and (011) planes cannot occur along the (110) plane which is parallel to the c axis.

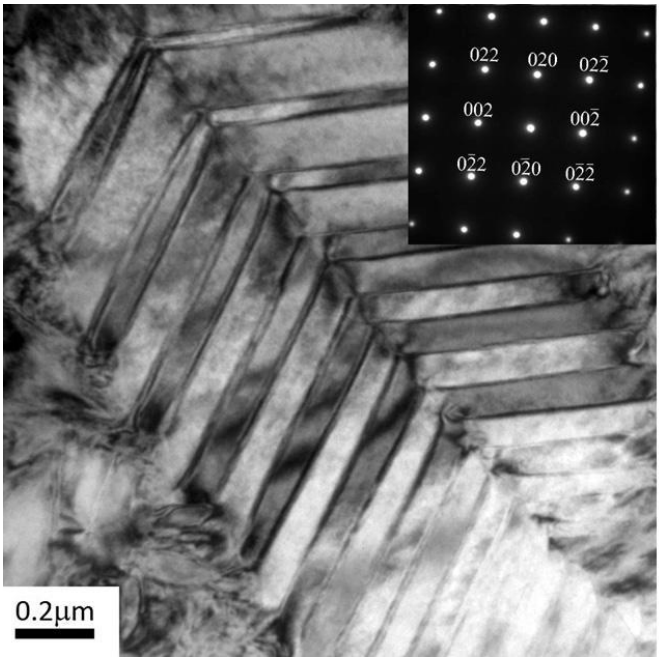

Fig. 2. Bright-field image of twin domains in the ZrO_2 2.8 mol.% Y_2O_3 sample, with selected area diffraction pattern in <100> orientation.

Study of the PSZ crystals with different stabilizing impurity concentrations showed that an increase in Y_2O_3 concentration controls the type and size of the twin domains. The twin structure also changes depending on the stabilizing impurity concentration. At Y_2O_3 concentrations from 2.8 to 3.2 mol.% twinning occurs first in larger domains which in turn also undergo twinning. High resolution study of the fine twin domain structure showed that nanosized twins only occur in specimens with the Y_2O_3 concentrations of up to 3.2 mol.%. At higher stabilizing impurity concentrations (3.7–5 mol.% Y_2O_3), no twinning hierarchy was observed, atomic plane traces inside twin domains were not broken, and minimum twin domain sizes could be identified in diffraction

contrast images. This suggests that twinning occurs simultaneously and is localized within small volumes. According to the phase diagram, the transition from the single phase cubic region to the two phase one during cooling occurs at lower temperatures if the yttrium oxide concentration is higher, and this controls the twin structure pattern.

The work was supported by the grant № 12-02-31751of the Russian foundation for basic research (RFBR) and the program of basic researches of Presidium of the Russian Academy of Sciences "Bases of basic researches nanotechnologies and nanomaterials"

17:00 Poster Mo59

Structural Role of Sodium Dithionate Impurity in Habit Modification of Sodium Chlorate Crystal

Xiaojun Lai

University of Leeds (SPEME), Leeds LS2-9JT, United Kingdom

e-mail: chexl@leeds.ac.uk

Research of crystal habit modification by impurity provides not only useful applications to achieve optimize crystal morphology for industrial crystallisation process, but also practical approaches to the fundamental aspects of surface chemistry and mechanisms involved in crystal growth. Sodium dithionate ($Na_2S_2O_6$) is used as the habit modifier for crystal growth of sodium chlorate ($NaClO_3$) as a representative system for such a study. Ordinary habit of pure sodium chlorate is cubic with dominant habit (100) type of faces. Presence of $Na_2S_2O_6$ (from 40ppm to 1000ppm) in the growing solution results in a significant decrease in the growth rates of (11), (11), (11) and ( ) faces, leading to tetrahedral morphology. Furthermore, crystal twinning is found to form under relatively high impurity concentration of 1000ppm and above.

X-ray topography has been applied to characterize growth history and defects of the crystals from various doping conditions (e.g. Fig.1). Having been identified to be the only system of impurity-induced crystal twinning, the two twin domains of the crystals are inter-grown each other (e.g. Fig.1 c) and only appear to be a mirror twining system. The twinning origin can be either on a modified-habit face or at the nucleation stage. By employing X-ray Multiple Diffraction (XRMD) based on synchrotron radiation, 004 reflection Renninger Scans (RS) for the doped crystals show a significant reduction in the secondary diffractions of (3-43)(3-41) and (343)(341), indicating these lattice planes are structurally disturbed by the impurity incorporation. Nevertheless, in 002 RS the overall lattice parameters on (1-11) and (-111) planes are found increasing as a function of impurity concentration, while that of (111) and (-1-1-1) planes decreasing. Local structural information of impurity obtained by applying X-ray Absorption Fine Structure (XAFS, synchrotron) provides direct proof on the impurity incorporation orientation and structural optimization (relaxation) on specific crystal planes. All experimental evidences are consistent with rational molecular model, in which the incorporation of dithionate impurity on {-1-1-1} faces is orientation-dependent.

17:00 Poster Mo60

Effect of high shear mixing and high frequency ultrasound on antisolvent crystallisation of sodium chloride

Judy Lee[1], Muthupandian Ashokkumar[2], Sandra E. Kentish[1]

1. *The University of Melbourne, Chemical and Biomolecular Engineering, Melbourne 3010, Australia* **2.** *The University of Melbourne, School of Chemistry, Parkville, VIC, Melbourne 3010, Australia*

e-mail: jytlee@unimelb.edu.au

Ultrasound has been shown to promote nucleation of crystals and produce narrow size distribution products without seeding. Crystallisation is initiated in a controlled and reproducible way that provides a well-defined starting point [1-5]. For these reasons, ultrasound has been beneficial in the pharmaceutical industry to enhance crystallisation of organic molecules [2] as well as in the mineral industry to crystallise alumina from Bayer's liquor [6]. Despite the large body of literature on sonocrystallisation, the exact mechanism behind its effects is still a subject of debate. Although there are various theories that suggest cavitation bubbles are responsible for sonocrystallisation, most studies use power ultrasonic horns that generate both intense shear and cavitation. The intense shear created can have a significant effect on crystallization, especially in antisolvent crystallization processes, making it difficult to see the role that cavitation bubbles play. The effect of cavitation bubbles without the intense shear can be examined using high frequency ultrasound, which generates stable cavitation bubbles without the intense shear seen with ultrasonic horns.

This study examined the effect of (i) mixing in the absence of ultrasound, (ii) sonication by an ultrasonic horn and (iii) high frequency ultrasound on the antisolvent crystallization of sodium chloride in ethanol. The degree of mixing was quantified by calculating the segregation index using a parallel competing reaction involving the reaction between iodide-iodate coupled with a neutralization reaction. The sodium chloride crystals were characterized for surface morphology using scanning electron microscope, size distribution using Malvern Mastersizer and crystal structure using X-ray diffraction.

The results show both mixing and ultrasound irradiation decreased the size of NaCl crystals. However, the crystals produced under mixing were irregular in geometry, whereas, crystals obtained under ultrasound sonication were more cubic and symmetric in geometry (Figure 1). Shown in Table 1 are the segregation index and the volume weighted mean diameter of the NaCl crystals. Increasing mixing decreased the segregaton index, which is as expected. The decrease in the NaCl crystal size with increasing mixing is due to the increase in the homogeneous nucleation and rate of nucleation. The results for a 20 kHz horn agree with what has been reported, which is a reduction in crystal sizes with segregation index. However, the use of 647 kHz ultrasound from a plate transducer provides a high segregation index but produces sodium chloride crystals of similar size distribution as the ultrasonic horn. At high frequency ultrasound, both large degas bubbles and cavitation bubbles may be responsible for the effect as gas bubble surfaces can act as nucleation sites for heterogeneous nucleation to occur. The advantage of high frequency ultrasound is that it allows a larger volume of liquid to be sonicated compared to ultrasonic horns where the active region is localized near the tip, making scaling up inefficient and difficult. Further, the reduction in shear is likely to lead to increased energy efficiency.

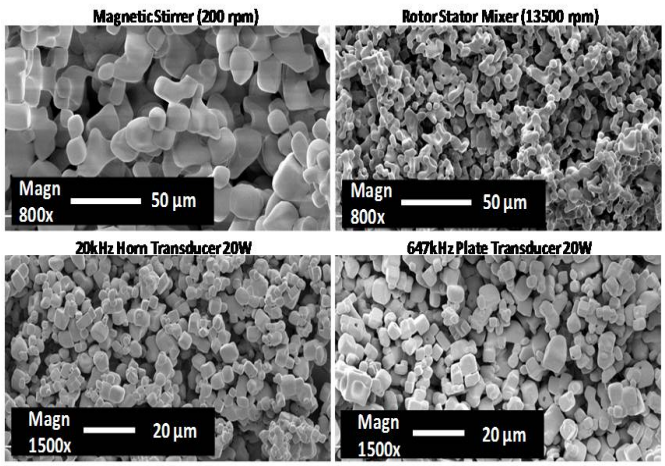

Figure 1: Scanning electron microscopic images of NaCl crystals obtained under different mixing and ultrasound irradiation.

Table 1: Segregation index and volume weighted mean diameter of particles obtained at various mixing and sonication conditions.

	Segregation Index (-)	D[4,3] (µm)
Mixing (200 rpm)	0.68	65.03
Mixing (13500 rpm)	0.42	27.81
20 kHz Horn transducer	0.30	16.67
647 kHz Plate transducer	0.89	16.68

References

[1] L.H. Thompson, L.K. Doraiswamy, The rate enhancing effect of ultasound by inducing supersaturation in a solid-liquid system, Chem. Eng. Sci., 55 (2000) 3085-3090.

[2] G. Ruecroft, D. Hipkiss, T. Ly, N. Maxted, P.W. Cains, Sonocrystallization: The use of ultrasound for improved industrial crystallization, Organic Process Research & Development, 9 (2005) 923-932.

[3] A. Abbas, M. Srour, P. Tang, H. Chiou, H.K. Chan, J.A. Romagnoli, Sonocrystallisation of sodium chloride particles for inhalation, Chem. Eng. Sci., 62 (2007) 2445-2453.

[4] R.K. Bund, A.B. Pandit, Sonocrystallization: Effect on lactose recovery and crystal habit, Ultrason. Sonochem., 14 (2007) 143-152.

[5] M. Ashokkumar, R. Bhaskaracharya, S. Kentish, J. Lee, M. Palmer, B. Zisu, The ultrasonic processing of dairy products - An overview, Dairy Sci. Technol., 90 (2010) 147-168.

[6] G. Ruecroft, D. Hipkiss, M. Fennell, Improving the bayer process by power ultrasound induced crystallization (sonocrystallization) of key impurities, in: H. Kvande (Ed.) 134th The Minerals, Metals & Materials Society Annual Meeting, TMS, San Francisco, California, 2005, pp. 163-166.

17:00 Poster Mo61

Study of the raw material, growth method on the optical properties of DKDP crystal

Baoan Liu[1], Mingxia Xu[1], Hailiang Zhou[1,2], Guohang Hu[3], Xun Sun[1], Xinguang Xu[1]

1. *State Key Laboratory of Crystal Materials, Shandong University, Jinan 250100, China* **2.** *School of Information Science and Engineering, Shandong Agricultural University, Taian 271018, China* **3.** *Shanghai Institute of Optics and Fine Mechanics China Academy of Sciences, Shanghai 201800, China*

e-mail: lba1101@hotmail.com

In this paper, three kind KH_2PO_4 raw materials were used to grow DKDP crystals by traditional and rapid method respectively. The growth habit dependence on the purity of the raw material is described and analyzed. The optical properties including transmission spectra and laser induced damage threshold of these crystals have been measured. We found that the growth method affects the crystal's optical properties more obviously than the raw material with the mass content of main metal ions below 1 ppm.

17:00 Poster Mo62

Bridgman growth and characterization of Ce:YAG single crystal for white LED applications

Baoliang Lu[1,2], Jian Tong[1,3], Xuejiao Niu[1], Jiayue Xu[1]

1. *School of Materials Science and Engineering, Shanghai Institute of Technology, Shanghai 201418, China* **2.** *Shanghai Jingcui Material Technology Co., Ltd., Shanghai 200062, China* **3.** *Shanghai Singlecrystal Instruments Co., Ltd, Shanghai 201109, China*

e-mail: cogaso@gmail.com

The combination of a GaN-based blue LED chip and an yellow phosphor (Ce^{3+}:$Y_3Al_5O_{12}$, Ce:YAG) packed with an epoxy resin is widely used to produce white LEDs. High irradiation and high temperature undercut the luminous efficacy and stability of high-power white LED due to the properties of resins and LED chip. To solve this problem, phosphor materials which are organic resin free, such as Ce:YAG transparent ceramics, low temperature Ce:YAG glass, and Ce:YAG single crystal, are developed. The optical, thermal, and electrical properties of Ce:YAG single crystal make it an important candidate for long lifetime and higher light output white LED applications. In the present work, 0.1~1 mol% Ce_2O_3 was added to the stoichiometric ratio mixture of Y_2O_3 and Al_2O_3 powders, and Ce:YAG single crystals were grown by the Bridgman method. The pulling down rate was 5-15mm/day, and as-grown crystals in diameter about 55mm were obtained. The defects such as inclusions and scatter particles were discussed and the optical and thermal properties are characterized.

17:00 Poster Mo63

Synthesis Of Multi Trace Element Doped $Fe_{0.6}Mn_{0.4}Ta_2O_6$ Tantalite Reference Crystals By Czochralski Method

Przemysław P. Michalak[1], Reinhard Uecker[2], Zbigniew Galazka[2], Frans F. Munnik[3], Axel A. Renno[3], Silke S. Merchel[3]

1. *Freiberg University of Mining and Technology, Mineralogical Institute, Brennhausgasse 14, Freiberg 09596, Germany* **2.** *Leibniz Institute for Crystal Growth (IKZ), Max-Born-Str 2, Berlin 12489, Germany* **3.** *Helmholtz-Zentrum Dresden-Rossendorf, Dresden 01314, Germany*

e-mail: Przemyslaw-Piotr.Michalak@student.tu-freiberg.de

Quality assurance of natural raw materials (e.g. ores) with beam-based microanalytical methods requires a proper set of homogeneous, matrix-matched reference materials (RMs) doped with trace elements relevant to resource technology applications. Natural minerals usually exhibit chemical heterogeneity at µg/g sampling masses and are unsuitable as RMs for in-situ chemical microanalysis. On the other hand, available synthetic RMs (e.g. glasses, pressed pellets) fail to satisfy matrix-match criterion.

A novel strategy has been established to obtaining such RMs through the synthesis of multi trace element doped phases that would be subsequently tested for chemical and structural homogeneity with both microscopic and spectroscopic spatially-resolved microanalytical methods.

A dark brown tantalite crystal from the melt of composition $Fe_{0.6}Mn_{0.4}Ta_2O_6$ has been grown by the conventional Czochralski method (melting point of about 1600°C) with the use of an Ir crucible and a protective atmosphere consisting of 85% Ar, 10% CO_2 and 5% CO. The growth rate of 1 mm/h and rotation rate of 10 rpm were applied. The boule was 17 mm in diameter and 30 mm in length (Fig. 1). Standard mineralogical thin sections were prepared for chemical analysis.

Back-scatter Electrons imaging (BSE) was implemented to check for the presence of impurities and other phases within the crystal. Electron Probe Microanalysis (EPMA) and Particle Induced X-ray Emission (PIXE) were used to determine the composition and homogeneity of the crystal. Compositional maps were prepared for each element for each method. As shown in Fig. 2 both BSE-EPMA and PIXE consistently proved stoichiometric composition of the crystal what is in agreement with stoichiometric composition of the melt. EPMA and PIXE compositional maps showed homogenous lateral distribution of all constituents of the crystal (Fig. 3).

The obtained tantalite phase turned out to be homogenous and stable. A matrix of the same stoichiometry will be used in further experiments – synthesis of tantalite crystals doped with different sets of technological trace elements - Sc, Ti; Y, Zr, W; La, Ce, Nd – each at concentration of 0,01 wt%.

Fig. 2

	Mg wt%	Ca wt%	Fe wt%	Mn wt%	Ta wt%	O wt%	Total
EPMA	0.000048	0.000131	5.9417	4.29268	70.3819	18.511	99.1275
PIXE	b.d.	b.d.	6.4367	4.0821	70.9777	18.503	100.00

b.d.= below limit of detection

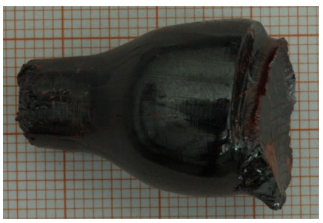

Fig. 1 Tantalite boule

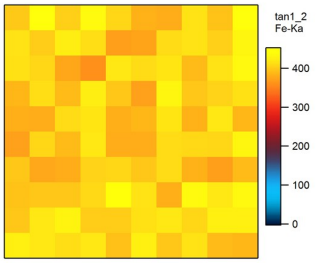

Fig. 3 PIXE Fe-Kα intensity distribution map

17:00 Poster Mo64

Preparation of Thiophen/Phenylene Co-Oligomer Crystals from Dropping of Their Solution into Poor Solvents

Hiroyuki Mochizuki[1], Fumio Sasaki, Shu Hotta[2]

1. *National Institute of Advanced Industrial Science and Technology (AIST), Central 5, 1-1-1 Higashi, Tsukuba, Ibaraki 305-8565, Japan*
2. *Kyoto Institute of Technology, Kyoto 606-8585, Japan*

e-mail: h-mochizuki@aist.go.jp

Organic crystalline solids have great potential for application to photonic and electronic devices. There have been many reports on preparation processes of organic crystalline solids, such as vapor and liquid processes. Minemawari *et al*. have recently reported organic crystals prepared using an ink-jet process.(1) Using this process, they demonstrated that mixing fine droplets of a poor solvent and a solution of an active semiconducting component can trigger the controlled formation of exceptionally uniform single crystal or polycrystalline thin films that grow at liquid-air interfaces.

Thiophene/phenylene co-oligomers (TPCOs) are expectable materials that have practical application to photonic and electronic devices. We have been studying the process of crystallizing TPCOs and have been developing more efficient processes of crystallizing them. Here, we report crystallization of TPCOs by mixing droplets of the poor solvent and the TPCO solution. The TPCO compound used in the present study was 2,5-bis(4-biphenylyl)thiophene (BP1T). BP1T was crystallized as follows: we first dropped *N*,*N*-dimethylformamide as a poor solvent onto a 1 × 1 cm^2 glass substrate to cover its surface. Three droplets of a chlorobenzene solution of BP1T were then consecutively dropped onto the poor solvent, mixing the poor solvent and BP1T solution. The chlorobenzene and poor solvent were then evaporated yielding the BP1T crystal on the glass substrate. The solubility of BP1T in chlorobenzene at 110°C was 4.1 mM. Dropping the 110°C chlorobenzene solution onto the poor solvent on an 80°C substrate formed a large planar BP1T crystal. Figure 1 shows the polarizing micrograph of the BP1T crystal on the glass substrate, and the crystal was 550 µm in size. The drying time of the sample was about 10 min. This method is efficient for preparing TPCO crystals on substrates.

Reference

(1) H. Minemawari *et al*., *Nature*, 475 (2011) 364.

Keywords: Thiophene/phenylene co-oligomer, Crystallization, Solution, Poor solvent

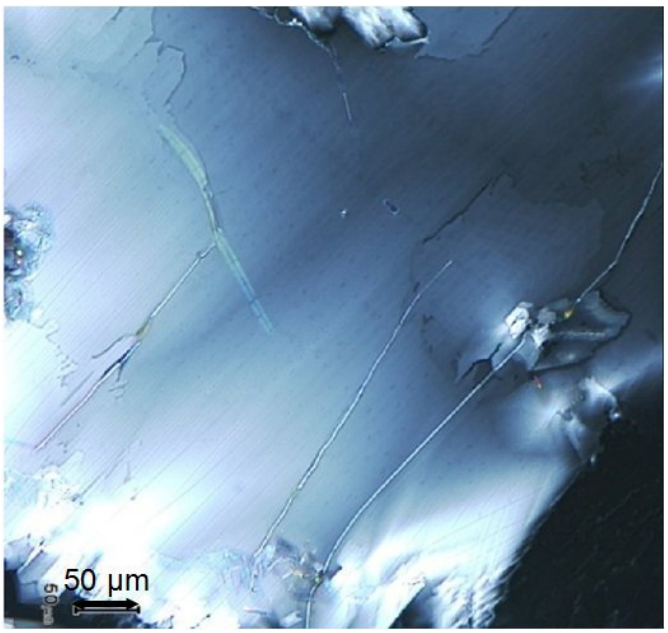

Figure 1. Polarizing micrograph of BP1T crystal crystallized from its chlorobenzene solution.

17:00 Poster Mo65

Method for producing High Purity raw materials for sapphire crystal growth

Radion Mogilevsky, Anna Oudodova

Emerging Material Technologies, Inc (EMT), 9931 Franklin Ave, Chicago, Il 60131, United States

e-mail: rnm@emtinc.us

Demand for high quality sapphire crystals grew ten folds within the last few years. Starting raw material significantly affects the quality of grown sapphire. Historically Vermeil crackles have been used to produce sapphire. Due to uncontrolled quality of Vermeil crackles it was challenging to grow sapphire with high and predictable yield.

EMT developed and patented plasma enhanced method to produce high purity high density ($HPDA^R$) raw material (purity more then 99.999%) to be used as starting material to grow sapphire crystals in which aluminum oxide is melted by a high temperature (> 10,000 ^oC) plasma torch. Optimum Al/O composition in melted HPDA is achieved by selecting proper gases combination that forms plasma. There is no hydrogen involved in the melting process. Water residual from starting material evaporates in high temperature plasma.

Details of the effect of the raw material produced via our patented technology on the properties of grown sapphire will be discussed.

17:00 Poster Mo66

NLO $LiInS_2$ single crystal grown by Bridgman technique for Mid IR application

Magesh Murugesan, Arunkumar Alagesan, Vijayakumar Palanimuthu, Anandha Babu Govindan, Ramasamy Perumalsamy

Centre for Crystal Growth,SSN College of Engineering,Kalavakkam,Chennai, Chennai 603110, India

e-mail: mage.radha@gmail.com

$LiInS_2$ material was synthesized in homemade graphite crucible by horizontal Bridgman furnace with high purity elements. $LiInS_2$ single crystal was grown by Bridgman gradient furnace with gradient of 10-15°C/cm. The grown crystal was subjected to various characterizations such as powder XRD, single crystal XRD, HRXRD, FTIR, UV-Vis-NIR studies, photoluminescence and Micro Raman spectroscopy. The grown $LiInS_2$ crystal was confirmed by single crystal and powder X-ray diffraction analyses. The grown crystal perfection was recorded by HRXRD which is 82 arc sec (FWHM). The FTIR transmission of grown $LiInS_2$ single crystal was measured to be around 80% which is very useful for mid IR laser, *Lidar* application. The band gap energy 1.99 eV was calculated from absorption spectrum. The photoluminescence spectrum was observed around 460 nm at room temperature, corresponding energy is 2.69eV. The structural and compositional uniformities of $LiInS_2$ were measured using micro-Raman scattering spectroscopy at room temperature. The insignificant change in the FWHM of the Γ_1 (W_1) measured at different regions of the crystal further reveals that the composition throughout its length is fairly uniform.

17:00 Poster Mo67

Formation processes of stable and metastable phases under Ostwald's step rule: a theoretical study

Natsuki Niekawa, Masao Kitamura

Kyoto University, Kyoto 606-8501, Japan

e-mail: niekawa@kueps.kyoto-u.ac.jp

Ostwald's step rule is widely known as an empirical rule that the thermodynamically less stable phase nucleates first, and then new phases are formed in order of increasing thermodynamic stability [1].

Solvent-mediated transformation is a good example of this step rule. In that, the stable phase nucleates and grows separately from preexistent crystals of the metastable phase. On the other hand, the metastable phase provides a substrate for nucleation of the stable phase. Indeed, a scenario where the stable phase nucleates on the surfaces of the preexistent metastable crystal and grows has been presented as for the origin of polycrystals such as tetrapod-like polycrystals of ZnO [2,3,4] and CdS [5], and a combination of bullets of snow [6,7]. Although, there have been few theoretical and universal studies on this phenomenon. In the present study, the conditions for as transformation induced by heterogeneous nucleation of a stable phase on the surface of the preformed metastable phase, referred as “epitaxy-mediated transformation” is studied theoretically.

We treated homogeneous 3D nucleation as the first process of Ostwald’s step rule and derived conditions for nucleation of the metastable phase from comparison of induction periods for nucleation and steady state nucleation rates of two crystal phases. It was revealed that if the surface free energy of critical 3D nucleus of the metastable phase is small enough and its shape is less anisotropic, nucleation of the metastable phase becomes dominant. The stable phase dominantly nucleates under the adverse conditions.

If any nuclei of the metastable phase are formed, three competitive following processes: growth of the metastable phase, solvent-mediated transformation, and epitaxy-mediated transformation, are envisioned. It was revealed that the later homogeneous nucleation of the stable phase, which accompanies solvent-mediated transformation, is possible only near the equilibrium concentration for the metastable phase. In contrast, epitaxy-mediated transformation arises under a high degree of concentration as well as near the equilibrium concentration of the metastable phase. The smaller edge energy and less anisotropy of a 2D nucleus of the stable phase work to the advantage of hetero-epitaxial

nucleation. And, the orientation giving the minimum value of the interfacial energy is selectively chosen for hetero-epitaxial nucleation. It should be noted that heterogeneous nucleation on the metastable phase can act as a trigger of direct transformation, as transformation proceeds from the surface to the center of the crystal.
[1] W. Ostwald, Z. Phs. Chem., 1987, 22, 289–330. [2] M. Shiojiri and C. Kaito, J. Cryst. Growth, 1981, 52, 173–177. [3] M. Kitano et al, J. Cryst. Growth, 1991, 108, 277–284. [4] T. Yoshioka et al, J. Electron Microsc., 1995, 44, 488–492. [5] C. Kaito, K. Fujita and M. Shiojiri, J. Cryst. Growth, 1982, 57, 199–202. [6] T. Takahashi, J. Cryst. Growth, 1982, 59, 441–449. [7] Y. Furukawa, J. Meteor. Soc. Japan, 1982, 60, 535–547

17:00 Poster Mo68

Effects of codoping on Scintillation Properties of Eu:SrI_2 Single Crystals

Kei Nishimoto[1], Yuui Yokota[2], Shunsuke Kurosawa[1,2], Akira Yoshikawa[1,2]

1. *Tohoku University, Institute for Materials Research (IMR), 2-1-1, Katahira, Aoba-ku, Sendai 980-8577, Japan* **2.** *New Industry Creation Hatchery Center, Tohoku University, Aoba-yama 6-6-10, Aoba-ku, Sendai, Miyagi, Sendai 980-8579, Japan*

e-mail: nishimotokei0909@imr.tohoku.ac.jp

Scintillator crystals have been widely applied in various fields such as medical imaging, homeland security and gamma-ray astronomy. The high scintillation light output and energy resolution are required for most of the applications. Among scintillator crystals, halide scintillator crystals with the small band-gap indicate relatively high light yield and energy resolution and especially Eu:SrI_2 single crystals have attracted attention recently [1]. However, the Eu:SrI_2 crystals is strongly hygroscopic and it is difficult to grow the single crystal of a high quality.

Therefore, we have developed the novel growth method for halide crystals which is called the atmosphere controled micro-pulling-down (m-PD) method [2]. One of its advantages is that the crystal can be grown at approximately ten times faster growth rate when compared to conventional methods. We have already reported the growth and scintillation properties of Eu:SrI_2 crystals by the m-PD method. However, the light yield and energy resolution were smaller than reported in the literature.

In this paper, we tried to improve the light yield and energy resolution by codoping the Eu:SrI_2 single crystals grown by the m-PD method. The emission at 430nm originates from 5d-4f transition of Eu^{2+} ion in the Eu:SrI_2 crystal. However, if the crystal included O^{2-} impurity at I^- site or cation vacancies, Eu^{2+} ion changes to the Eu^{3+} ion which does not have radiative 5d-4f transition. Therefore, the light yield could be increased by increasing the Eu^{2+} content in the crystal, which we tried to achieve by co-doping with the trivalent cation. The scintillation properties of the grown co-doped crystals were investigated and the results were compared to the Eu:SrI_2 crystals without co-doping.

Figure 1 is the schematic of the modified m-PD furnace with the removable chamber which can be moved in the glove box filled with Ar gas. Mixed powders with the nominal compositions of $(Sr_{1-x-y}Eu_xA_y)I_2$ $x = 0.05, 0.75$, $y = 0.01, 0.05, 0.1$, A = La, Gd, or Lu, were prepared with the starting materials of SrI_2 (4N), EuI_2(3N) and Co-dopants, LaI_3, GdI_3, LuI_3 (3N). The mixed powders were set into the carbon crucible with a f2 mm hole at the bottom in the glove box. The crucible together with the quartz insulator was placed in the center of chamber which was taken out from the glove box after the gate valve was closed. The chamber was connected with the turbo molecular pump and vacuumed up to 10^{-4} Pa. After the introduction of high purity Ar gas (99.9999%), the crucible was heated by the high-frequency induction coil up to the melting point of Eu:SrI_2. Crystal growth was performed by pulling-down from the melt using the Pt wire as a seed at 0.05~0.1mm/min growth rate. The grown crystals were cut and polished in the glove box for the measurements of optical and scintillation properties. The structural phases and the lattice parameters were measured by the powder X-ray diffraction using the tight chamber. Radioluminescence spectra were measured with the spectrometer and CCD camera using X-ray as the excitation source. To determine the light yield, the polished crystals were optically coupled with the PMT by optical grease in the glove box and pulse-height spectra under g-ray from ^{137}Cs radiation source were evaluated. At the same time, the decay time was also measured using the oscilloscope.

Figure 2 shows the La, Gd and Lu1% co-doped Eu5%:SrI_2 crystals grown by the m-PD method. All the crystals had f2 mm diameter and several centimeters length. All the polished crystals indicated high transparency and there were no visible cracks and inclusions in the crystals. The powder XRD patterns indicated these crystals were single phase of SrI_2 crystal structure. Figure 3 shows the pulse-hight spectrum of the La, Gd and Lu1% co-doped Eu5%:SrI_2. All the co-doped crytsals showed higher light yield than Eu5%:SrI_2 crystal without co-dopant. The other scintillation properties such as radioluminessence and decay time under g-ray irradiation will be reported.

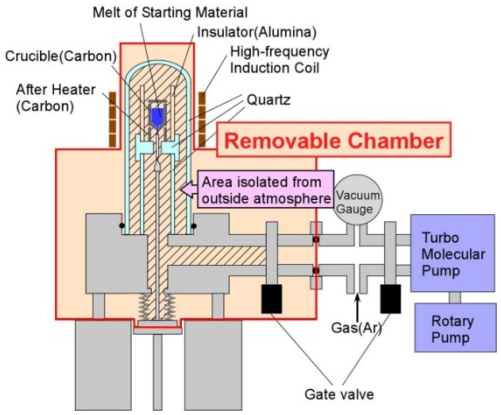

Fig 1. Schematic of the modified m-PD furnace

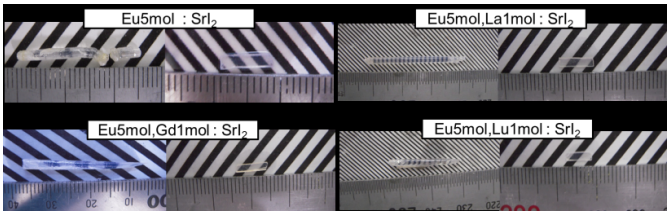

Figure 2 . La, Gd and Lu co-doped Eu5%:SrI_2 single crystals.

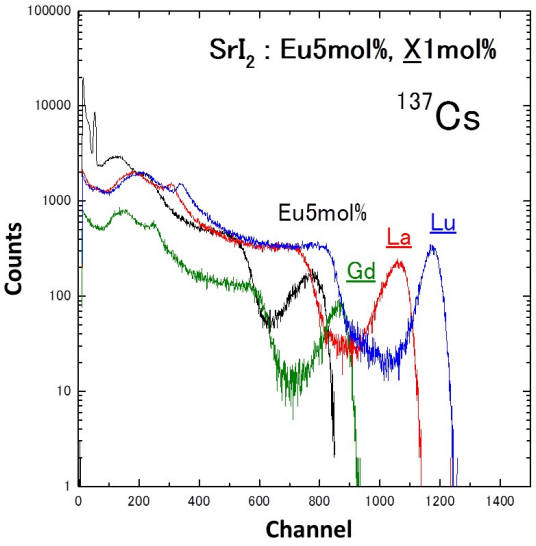

Figure 3. pulse-hight spectrum of La, Gd and Lu co-doped Eu5%:SrI_2 single crystals irradiated by g-ray.

[1] E.V.van Loef, C. M. Wilson, K. S. Shah, et.al., IEEE Trans.Nucl. Sci. 56, 869,(2009)

[2] Y. Yokota, A. Yoshikawa, et.al., J. Cryst. Growth 318 (2011) 908-911

17:00 Poster Mo69

Investigations on synthesis, growth and physical characterizations of Lithium selenoindate single crystal

Vijayakumar Palanimuthu, Magesh Murugesan, Arunkumar Alagesan, Anandha Babu Govindan, Ramasamy Perumalsamy

Centre for Crystal Growth,SSN College of Engineering,Kalavakkam,Chennai, Chennai 603110, India

e-mail: vijayakumarphy@gmail.com

Ternary chalcogenides with general formula $A^{I}B^{III}C^{VI}_2$ (A=Li,Cu,Ag; B=In, Ga; C=S,Se, Te) are of considerable interest because of their potential optoelectronic applications as nonlinear optical (NLO) devices, detectors, Light emitting diodes, and solar energy converters. The lithium containing $A^{I}B^{III}C^{VI}_2$ type semiconductors are little known because of difficulties in crystal growth caused by chemical activities of lithium and high vapour pressure of the chalcogens. The advantages of $LiInSe_2$ single crystal is the possibility of creating mid-IR parametric light oscillator pumped by radiation for near IR solid-state lasers (Nd:YAG) and thermal neutron detectors. $LiInSe_2$ polycrystalline material was synthesized from self-vapor transport with mechanical melt temperature oscillation method. Crack free $LiInSe_2$ single crystal of size 8mm diameter and 32mm length was grown using indigenous two zone tubular resistive heated furnace by modified vertical Bridgman- Stockbarger method with steady ampoule rotation. The single crystal wafer was made from grown crystal and characterizations were done using these wafers. Powder X-ray diffraction pattern was used to confirm the crystalline phase and the orientation of the grown crystal is <231>. Single crystal X-ray diffraction analysis confirms the orthorhombic crystal system and the lattice parameter values are a= 7.813 (Å), b= 8.398 (Å), c=6.781 (Å) and V=409.05 (Å)^3. Rutherford back scattering analysis analysis shows the grown crystal composition as $Li_{0.8}In_{1.16}Se_{2.04}$. The structural perfection of the grown crystals have been analyzed by High resolution X-ray diffraction rocking curve measurements. The single diffraction peak with reasonably low full width half-maximum (0.266 are. deg) indicated that the crystalline perfection is fairly good. From positron life time measurements, the average life time 278.03 ps has been observed, which corresponds to the vacancy clusters in $LiInSe_2$ single crystal. The crystal has transparency ranges from 0.62 µm to 20 µm and more than 80% has been observed in the mid-IR region.Hall effect measurements confirms the N-type semiconducting nature and has high resistivity (3.43×10^{10} Ω.cm). Thus $LiInSe_2$ single crystal can be used for frequency converters and detector applications.

17:00 Poster Mo70

Effect of the purity of starting materials on the growth and properties of KDP single crystals - A comparative study

Rajesh Paulraj[1], Urit Charoen In[2], Prapun Manyum[3], Ramasamy Perumalsamy[1]

1. *Centre for Crystal Growth,SSN College of Engineering,Kalavakkam,Chennai, Chennai 603110, India* **2.** *Mahasarakham University, Mahasarakham 44150, Thailand* **3.** *School of Physics, Suranaree University of Technology, Nakhon Ratchasima 30000, Thailand*

e-mail: rajeshppraj@gmail.com

A systematic study on the effect of purity of starting materials on the growth and properties of KDP single crystals is crucial for the future study of the material for NLO applications. KDP crystals were grown using high pure (99.999%) and ordinary (99.9%) starting raw materials using slow cooling method in identical conditions. Their optical transparency and crystalline perfection are studied by UV and HRXRD analyses respectively. The results are checked with the help of etching analyses. The full width at half maximum (FWHM) is 8 arc s which is close to that expected from the plane wave theory of dynamical X-ray diffraction for an ideally perfect crystal. Results of those studies are correlated with each other. The quantitative results show that how the raw material plays an important role in the growth of good quality crystals.

17:00 Poster Mo71

Investigation on solubility, growth, structural, optical, thermal, mechanical, dielectric, crystalline perfection and NLO properties of L-tyrosine added Potassium dihydrogen phosphate single crystal

Boopathi Kittusamy[1], Rajesh Paulraj[2], Ramasamy Perumalsamy[1]

1. *Centre for Crystal Growth,SSN College of Engineering,Kalavakkam,Chennai, Chennai 603110, India* **2.** *SSN College Of Engineering (SSNCE), Kalavakkam, chennai 603110, India*

e-mail: ramasamyp@ssn.edu.in

The KDP crystal is a type of nonlinear optical (NLO) crystal with outstanding physical properties and reproducible growth to large size. It is also a crucial ingredient in the inertial confinement fusion (ICF) system. Single crystals of L-tyrosine added potassium dihydrogen phosphate have been grown by slow cooling along with seed rotation method. The grown crystal has been characterized by powder X-ray diffraction, Fourier transform spectroscopy, UV-Vis-NIR spectroscopy, thermal analysis (TG/DTA), Vickers microhardness, dielectric measurements, laser damage threshold, HRXRD and second harmonic generation efficiency. The structural difference between pure and doped

crystal has been found by XRD analysis. Functional groups were identified by FT-IR spectroscopy. The transmittance of the grown pure and L-tyrosine added KDP crystals were 70%, 90%. Thermal analysis was performed to study thermal stability of the grown crystals. Vickers microhardness measurement reveals the higher hardness of the doped crystals. Low dielectric loss was observed from the dielectric measurements for the doped KDP crystals. The laser damage threshold study reveals the higher laser stability for doped crystals. The high resolution x-ray diffraction studies show that the crystalline perfection of the crystal is quite good. The SHG efficiency measurement reveals that dopant has enhanced the SHG efficiency. The obtained results are compared with pure KDP crystal.

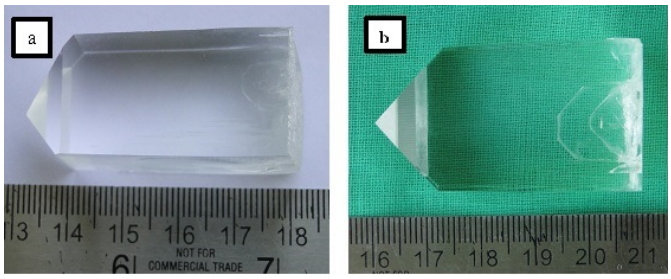

Photograph of (a) pure KDP (b) L-tyrosine added KDP crystal grown by slow cooling along with seed rotation method

17:00 Poster Mo72

Nucleation of Germanium Disulfide Determined by Image Analysis

Suresh kumar Pillai, Jiří Málek

University of Pardubice, Studentska, Pardubice 53210, Czech Republic

e-mail: sureshkumar.pillai@upce.cz

Chalcogenide glasses are used in a variety of applications, notably, in the fields of infrared optics, memory devices and photoresists. The kinetics of nucleation and growth of these materials is of critical technological importance owing to their increasing number of usage as phase-change memory materials. A simple chalcogenide system, GeS_2, is a key element in several complicated glasses.

In this work, the nucleation and early GeS_2 were studied by optical microscopy and differential thermal analysis (DTA). Bulk samples were subjected to a double stage heat treatment consisting of nucleation and growth stages for predetermined durations. Subsequently, isothermal nucleation rates were estimated by Image Analysis. The applicability of the classical nucleation theory (CNT) is examined utilizing the bulk viscosity data available in the literature.

The financial support from the Czech Science Foundation under grant, No. P106/11/1152 and from the Ministry of Education, Youth and Sports under project, CZ.1.07/2.3.00/30.0021 “Strengthening of Research and Development Teams at the University of Pardubice” is gratefully acknowledged.

17:00 Poster Mo73

Invstigation of the growth of LiH_2PO_4 crystals from phosphate solutions

Aleksey Voronov, Galina Babenko, Viacheslav M. Puzikov, Anton Yurchenko

Institute for Single Crystals NAS of Ukraine (ISC), 60 Lenin Ave., Kharkov 61001, Ukraine

e-mail: puzikov@isc.kharkov.ua

The obtaining of new single crystals for detection of thermal neutrons on the base of lithium dihydrophosphate LiH_2PO_4 (LDP) doped with Eu^{3+} is topical for neutron physical investigations and radiation monitoring.

However, the growth of LDP crystals from the solutions is bound up with certain difficulties. As established earlier while studying the solubility of the system $Li_2O–P_2O_5–H_2O$, at temperatures higher than 20°C LDP dissolves incongruently. However, some researches have managed to grow the crystals from the solutions with excessive content of phosphoric acid. In the present work we studied the influence of the concentration of phosphoric acid in the mother liquor on the solubility and crystallization of LDP.

The temperature dependences of LDP solubility in aqueous solutions of H_3PO_4 with the concentrations 20-; 40-; 50-; 60-; 75- and 85%, were investigated by the method of test seeds. In the interval $20 \div 80^0$C the solubility of LDP was found to change insignificantly (not more than by 5 mass %), irrespective of the percentage of the acid. There were obtained the isotherms of LDP solubility in aqueous H_3PO_4 solutions with different concentrations of the acid. It was established that with the rise of the percentage of the acid from 20 to 85 mass % the solubility diminishes (at 50^0C it changes from 53 to 16 mass %). This can be used for creating supersaturation in the solution and for the growth of the crystals.

When the supersaturation is achieved by evaporation of the solvent from the solution, the volume of the solvent and the concentration of the acid in the solution change simultaneously. As the numerical estimations show, in this case it is possible to raise the output of LDP crystal by five times in comparison with the growth by the method of temperature lowering.

There were studied conditions of LDP crystallization from aqueous solutions of phosphoric acid of different concentrations. It was found that with the rise of the concentration of H_3PO_4 acid in the solution the growth of the faces of the pyramid $\{11\bar{1}\}$ and the dome $\{01\bar{1}\}$ was suppressed, whereas the face of the pedestal $\{00\bar{1}\}$ continued to grow. The full-faced form of the crystal habitus was achieved for the samples obtained from the solutions containing 20 – 40 % H_3PO_4 ($0.6 > pH > 0.04$).

The model of the influence of hydrogen bonds on the habitus of the crystals was considered. The probability of the formation of hydrogen bonds between $H_2PO_4^-$ anions was shown to rise with the concentration of H_3PO_4. The increase of the acid concentration in the solution changed the habitus of the crystals due to the rise of the quality of $H_2PO_4^-$ dimers.

17:00 Poster Mo74

Unidirectional growth of cobalt nickel sulfate twelvehydrate (CNSH) single crystal

Samaneh Karvar, Hamid Rezagholipour Dizaji

Semnan University, Physics Department, Crystal Growth Lab., Tehran 35195-363, Iran

e-mail: hrgholipour@semnan.ac.ir

Nickel sulfate hexahydrate (NSH) crystals are commercially available as Ultraviolet light filters and UV sensors. They are particularly useful in solar-blind optical systems and sensing devices, which seek to identify the presence of UV light sources in the UV missile warning band [1, 2]. In order to improve the transmittance and the dehydration temperature, the two important parameters of a crystal when used as UV filter, other nickel sulfate based crystals such as ANSH, KNSH, CNSH etc. have been prepared [3-5].

In the present work, using a new unidirectional crystal growth from solution called Sankaranarayana-Ramasamy method (SR), a cylindrical shape $CoNi(SO_4)_2 \cdot 12H_2O$ (CNSH) crystal in the [001] direction has been grown.

The advantage of this method over the one applied by Su et al [5] lies in the nature of the SR method which offers a solution growth method at room temperature involving less-sophisticated equipment to grow unidirectional single crystal with cylindrical morphology, 100% solute–crystal conversion efficiency and ease in scaling up of crystal diameter [6]. The grown crystal was subjected to X-ray diffraction, UV-Vis spectroscopy and TGA/DTA analysis. It was observed that the grown crystal had three sharp discontinuous transmission bands in the range from ultraviolet to near IR wavelengths with transmission efficiency about 77.20% at 305 nm. This value is very near to the value obtained by Su et al] 5[.

[1] S. Livneh, S. Selin, I. Zwieback, and W. Ruderman, US Patent 6, 452, 189, (2002).

[2] M. Hemmati and H. Rezagholipour Dizaji, Cryst. Res. Technol. 47, (2012) 703.

[3] N. L. Sizova, V. L. Manomenova, E. B. Rudneva and A. E.Voloshin, J. Crystallography Reports 52 (2007) 884.

[4] Y. He, J. Chen, G.o Su, X.n Zhuang, G. Lee and R. Jiang J. Cryst. Growth 233 (2001) 809.

[5] G. Su, X. Zhuang, Y. He, Z. Li, G. Li, J. Ma, G. Wang, and Z. Huang, Cryst. Res. Technol. 38 (2003) 1087.

[6] N. Balamurugan, M. Lenin, G. Bhagavannarayana, and P. Ramasamy, Cryst. Res. Technol. 42, 151 (2007).

17:00 Poster Mo75

Crystal Growth, Crystalline Perfection And Optical Property Analyses Of Ru Doped Congruent $LiNbO_3$ Single Crystals At Different Axial Positions

Bright Riscob[1,2], Sarveswaran Ganeshamoorthy[3], Rajeev Bhatt[4], Narayanasamy Vijayan[1], Indranil Bhaumik[4], Mohd A. Wahab[2], Godavarthi Bhagavannarayana[1]

1. *National Physical Laboratory (NPL), Dr.K.S.Krishnan Road, Delhi 110012, India* **2.** *Jamia Millia Islamia (JMI), Jamia Nagar,new delhi, Delhi 110025, India* **3.** *X ray Crystallography and Crystal Growth Section, Condensed Matter Physics Division, Material Science Group, IGCAR (IGCAR), Kalpakkam, Tamil Nadu, Chennai 603 102, India* **4.** *Laser Materials Development and Devices Division, Raja Ramanna Centre for Advanced Technology (RRCAT), Indore 452013, India*

e-mail: riscob@gmail.com

The good quality single crystals of Ru doped congruent $LiNbO_3$ (LN) have been successfully grown by Czochralski (Cz) technique using Cyberstar make automatic diameter controlling system with RF furnace. The axial and radial gradient of the RF furnace was controlled properly in order to get crack free single crystal. The wafer was cut from the grown single crystals at different axial positions and then subjected to various characterization analyses in order to find its suitability for device fabrications. The concentration of the dopant was assessed by inductively coupled plasma mass spectroscopy (ICP-MS) and found that upper portion of the wafer contains more Ru in comparison with the other part of the wafers, which was expected because of Ru evaporation and it is in agreement with the reported literatures. To assess the crystalline perfection, the wafers which were cut from the different axial positions were subjected to high-resolution X-ray diffractometry (HRXRD) by employing an in-house developed multicrystal X-ray diffractometer. From this analysis one can understand that the as-grown cLN crystal is having excellent perfection with single and sharp diffraction curve (DC), whereas, Ru-doped specimens can be clearly visualized by the broadening of DC. The top and bottom portions of the same ingot show distinct nature of defect structure. The significant change observed in the absorption coefficient and band gap analysis proven that the concentration variation of Ru play a major role in LN application. The refractive index measurements were carried out to observe Ru effect on different pieces of crystal while concentration varies using a prism coupler technique. The optical homogeneity of the grown specimen was examined by using conoscopy method and observed that the grown crystals are having good optical homogeneity, free from residual strain and at the same time Ru doping does not influence its optic sign.

17:00 Poster Mo76

Rubidium-nickel and cesium-nickel sulphates hexahydrates: new crystals for UV band filters

Vera Manomenova, Elena Rudneva, Alexey E. Voloshin, Vadim Grebenev, Natalia L. Sizova, Lyudmila F. Malakhova

A.V.Shubnikov Institute of Crystallography The Russian Academy of Sciences, Moscow, Russian Federation

e-mail: rudneva.lena@inbox.ru

$Rb_2Ni(SO_4)_2 \cdot 6H_2O$ (RbNSH) and $Cs_2Ni(SO_4)_2 \cdot 6H_2O$ (CsNSH) crystals belong to the nickel Tutton salts.

The large single crystals of $Rb_2Ni(SO_4)_2{\cdot}6H_2O$ (RbNSH) and $Cs_2Ni(SO_4)_2{\cdot}6H_2O$ (CsNSH) were grown. Some properties of these crystals were studied such as their structure, transmission spectra, thermal stability.

We determined the solubility curves of these salts in preparation for the crystal growth process. Both crystals were grown from low temperature solutions: by temperature decrease and by the solvent-evaporation techniques. Due to different solubility the normal growth rates were 0.2-0.4 mm/day for RbNSH and 0.5-2.0 mm/day for CsNSH depending on the crystal faces.

The RbNSH structure was refined and CsNSH structure was determined. RbNSH and CsNSH crystals belong to monoclinic sp.gr. $P2_1/c$ and form isostructural series with ANSH and KNSH.

Transmission spectra demonstrate rather high transparence in UV band (220-320 nm) that makes them possible for application as UV-filters.

The thermogravimetric measurements were made for both crystals. It was shown that the process of the single crystal dehydratation starts at temperatures 107 ºC for CsNSH and 110 ºC for RbNSH (the sample heating rate was 5 K/min). So these crystals are more thermal stable than well known α-NSH, ANSH and KNSH.

For CsNSH crystal the microhardness of (010), (001) and (100) plates was studied. The distinction in the hardness of different faces indicates the presence of anisotropy of the second kind in these crystals with the anisotropy coefficient k_1=1.4.

The internal defect structure of RNSH and CsNSH crystals was studied by X-ray topography. It was shown that growing CsNSH crystals by the solvent-evaporation method preferable.

Due to their good optical and thermogravimetric properties both crystals could be used as material for UV filters

17:00 Poster Mo77

The study of heat transfer processes in the system shaper-melt-crystal in the process of growing massive sapphire profiles by Stepanov/EFG method

Roman I. Safronov, Yevgeniy Andreev, Leonid Lytvynov

Institute for Single Crystals NAS of Ukraine (ISC), 60 Lenin Ave., Kharkov 61001, Ukraine

e-mail: r.i.safronov@gmail.com

Stability of crystallization front is determined by heat dissipation through the crystal in the process of growing profiled sapphire crystals with large cross sections. Reduction of heat removal from the crystallization front and prevent rejection of the crystal shape from the set is achieved by selection of screens that are installed in the growth zone. The size and weight of the shaper contribute to heat transfer at the crystallization front.

The aim of this work is a study of the influence geometric parameters of the shaper on the heat transfer at the crystallization front during the growth of massive profiled sapphire crystals.
Heat transfer processconsidered for growing semi-infinite cylindrical sapphire rod in thermal zone with induction or ohmic heating. Capillary system firmly fixed in the crucible and the shaper is a removable cap, which are locatedat the endof the capillary system [1] In the calculations it was assumed that the heat transfer from the crystallization front through the crystal occurs by two mechanisms - the molecular through the shaper and radiation through the crystal. The heat balanceequation on the working surface of the shaper is:

$$Q_1(d_c,l_c,\nabla T)+Q_2(d_c,d_s,T_s)+Q_3(d_s,h,T_s,T_h)+Q_4(d_s,T_s,T_{cr})=c_{Mo}m_s(T_s-T_c)$$

where:

Q_1 – heat flux through the growing crystal [2],

Q_2 – heat flux through the top surface of the base shaper;

Q_3 – heat flux through the lateral surface of the base shaper;

Q_4 – heat flux through the film of the melt from the bottom surface of the shaper.

∇T- axial temperature gradient,

T_h – temperature of the heater,

T_s – temperature of the shaper,

T_{cr} – temperature of the crucible,

d_c – diameter of the crystal,

d_s – diameter at the base shaper,

T_s – temperature of the shaper,

C_{Mo} – specific heat of the shaper (molybdenum),

m_s – weight of the shaper.

The ranges of the axial temperature gradient, heater temperature, shaper and crucible were set on the basis of experimental data. Calculations have shown that the main parameters affecting the resulting heat flux are: axial temperature gradient, crystal diameter, diameter of the base shaper (its mass) and its temperature. The results of the calculations are shown in the diagram. The shaded area – the area of optimal weights of the shaper.

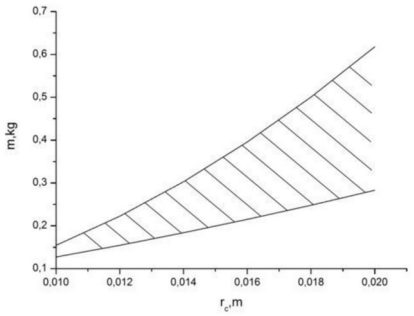

Fig. Dependent weight of a shaper on diametr of growing the crystall.

In the work shows a relationship between cross-sectional area of the crystal, axial temperature gradient and weight of the shaper. The results were used to develop the construction of shaper in the process of growing sapphire rods Ø35 mm and plates 15 x 55 mm optical quality.

1. Andreev Y.P., Lytvynov L.A. Device for growing shaped crystals // Patent of Ukraine № 89883, published in the Bulletin. №5,10,03,2010, in Russian.

2. P. I. Antonov et all. An Experimental and Theoretical Study of Temperature Distribution in Sapphire Crystals Grown From the Melt by Stepanov`s Method // Journal of Crystal Growth. 1980, V. 50, P. 62-68/.

17:00 Poster Mo78

Investigation of congruent composition of $(Gd_{2-x-y}La_xCe_y)Si_2O_7$ (Ce:La-GPS) scintillator and its single crystal growth

Yasuhiro Shoji[1,4], Shunsuke Kurosawa[1,2], Takayuki Nihei[3], Kei Kamada[2,4], Yuui Yokota[2], Kazushige Toota[3], Ko Onodera[3], Akira Yoshikawa[1,2,4]

1. *Institute for Materials Research, Tohoku University (IMR), Sendai 980-8577, Japan* **2.** *New Industry Creation Hatchery Center, Tohoku University, Aoba-yama 6-6-10, Aoba-ku, Sendai, Miyagi, Sendai 980-8579, Japan* **3.** *TDK Corporation, Akita 018-0147, Japan* **4.** *C and A corporation, Sendai 980-8579, Japan*

e-mail: y_shoji@imr.tohoku.ac.jp

A number of halide and oxide scintillator materials have been developed and they are applied to various fields such as astronomy, medical imaging, and homeland security. Although halide scintillators, such as Tl:NaI, Tl:CsI and Ce:$LaBr_3$, have high light outputs of more than 30,000 photons/MeV, they have hygroscopic nature. On the other hand, most oxide scintillators don't have hygroscopic nature. Ce:$Gd_2Si_2O_7$ (Ce:GPS) had a good light output of 30,000 photons/MeV and FWHM energy resolution of 6.0% at 662 keV at room temperature. However, according to the previous report [1], Ce:GPS crystals need to be grown with heavy Ce-doping (approximately, 10 mol%) in order to stabilize the crystal growth process. Such high Ce-concentration would lead to lower light output because of self-absorption or concentration quenching. The main reason is the fact that $Gd_2Si_2O_7$isn't congruently melt. When the chemicals with stoichiometric composition is melted, initial melt has apatite phase. Recently, we found substitution of La into Gd site gives positive effect of the phase stability of this pyrosilicate [2]. However, the ratio of La isn't optimized. In this study, variety of combination of x and y in $Gd_{2-x-y}La_xCe_ySi_2O_7$ are prepared and the optimum ratio of La into Gd site are investigated. Gd_2O_3, La_2O_3, CeO_2 and SiO_2 with 99.99% purity are used as starting chemicals. Ce:La-GPS single crystals were grown by the Micro-Pulling Down (m-PD) method with RF heating system using Ir crucible. The growth rate was 3-5mm/h and the atmosphere was under N_2. The Iridium rod was used as a seed in the first growth and the seed was gotten from this grown crystal.

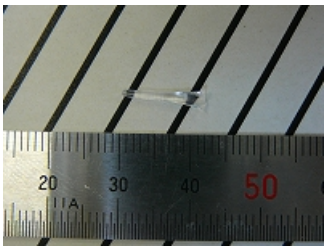

fig.1.Ce:La-GPS single crystal grown by m-PD method

The relationship between the amount of La and initial phase and structure will be discussed. Crystal growth attempts from the different x and y melt composition will be made and discussed with this relation. After thecrystal growth, photoluminescence, PL decay, radioluminescence, pulse height spectra and scintillation decay were measured and will also be reported taking the relation into account.

Reference

1. S. Kawamura, J. H. Kaneko, M. Higuchi,et.al., IEEE Trans. Nucl. Sci. **54**, (2007) 1383.

2. A. Suzuki, S. Kurosawa, A. Yoshikawa, et. al., Appl. Phys. Express **5** (2012) 102601.

17:00 Poster Mo79

Investigation on the Li, Ba // BO_2, F ternary reciprocal system and growth of bulk β–BaB_2O_4 crystals

Ekaterina A. Simonova[1], Nadegda G. Kononova[1], Pavel Fedorov[2], Alexander E. Kokh[1], Vladislav S. Shevchenko[1]

1. *Institute of Geology and Mineralogy SB RAS (IGM), Koptyuga ave., 3, Novosibirsk 630090, Russian Federation* **2.** *General Physics Institute, Vavilov Str. 38, Moscow 117942, Russian Federation*

e-mail: simonovakatherine1986@gmail.com

Single crystals of low temperature modification of barium borate β–BaB_2O_4 (BBO) are an important material for nonlinear optical application. Due to the phase transition at 925°C, β–BaB_2O_4 crystals are commonly grown from high temperature solution.

In present work phase equilibria in Li, Ba // BO_2, F ternary reciprocal system have been studied. LiF is considered as the promising solvent for β–BaB_2O_4 crystal growth due to the essential viscosity reduction. Also, lithium ions should not enter isomorphically into the structure of barium borate because of crystallochemical characteristics. In mentioned reciprocal system only boundary sections BaB_2O_4–$LiBO_2$ [1], BaB_2O_4–BaF_2 [2], BaF_2–LiF [3], $LiBO_2$–LiF [4] have been investigated yet.

We investigated phase equilibria in Li, Ba // BO_2, F ternary reciprocal system using the modified visual polythermal analysis (VPA), differential thermal analysis (DTA), methods of spontaneous crystallization on a platinum loop, solid–state synthesis and X–ray powder diffraction analysis.

It has been found that BaB_2O_4–LiF system is not quasi–binary. In the concentration interval of 32.5–40 mol % LiF and 40–60 mol % LiF the area of primary crystallization of β–BaB_2O_4 and $Li_2Ba_4B_{10}O_{20}$, respectively, were found.

The β–BaB_2O_4 crystal was grown by top–seeded solution growth (TSSG) technique in a precise furnace with a heat field of 3–fold axis symmetry *L3* [5]. A high–temperature solution of 1 kg 65 mol % BaB_2O_4 – 35 mol. % LiF composition was melted in a platinum crucible (90 mm in diameter and 95 mm in height). A crystal was grown on a 5 × 5 mm^2 seed oriented along the optical axis. The cooling rate was 0.2–0.3 °C/day. Total temperature decrease was only 21.5 °C due to the very narrow crystallization area, but the yield coefficient was as high as 7.44 g/(kg·°C). The crystal was 60 mm in diameter and 25 mm in height, its weight was 160 g.

There are the four invariant points in Li, Ba // BO_2, F ternary reciprocal system (except boundary sections). The BaB_2O_4–$LiBaF_3$, BaB_2O_4–(0.6 BaF_2–0.4 LiF), BaB_2O_4–(0.7 BaF_2–0.3 LiF) systems has been studied in detail and much broader crystallization area of BaB_2O_4 was found in Li, Ba // BO_2, F system. We suppose that the use of various compositions in this system is of great interest for the growth of large β–BaB_2O_4 crystals.

1. Shilie Pan, Jared P. Smit, Courtney H. Lanier, Michael R. Marvel, Laurence D. Marks, and Kenneth R. Poeppelmeier. Optical floating zone growth of β–BaB_2O_4 from a $LiBa_2B_5O_{10}$–based solvent// Crystal growth & design. 2007. V. 7. № 8. pp. 1561–1564.

2. Bekker T. B., Fedorov P. P., Kokh A. E. Phase formation in the BaB_2O_4–BaF_2 system // Crystallography Reports. 2012. V. 57. № 4. pp. 574–578.

3. Bychkova N.A., Bergman A.G. – ZHOKH, 1956, V.26, P.639 (in Russian).

4. Petit M.G., Jaeger M. – «C. r. Acad. Sci.», 1957, V. 244, № 13, P. 1734.

5. Kokh A.E., Kononova N.G., Mokruchnikov P.W., J. Crystal Growth 216 (2000) 369.

17:00 Poster Mo80

Preparation of free-standing GaN substrates from thick GaN layers crystallized by Hydride Vapor Phase Epitaxy on ammonothermally grown GaN seeds

Tomasz Sochacki[1,2], Michał Boćkowski[1,2], Izabella Grzegory[1]

1. *Polish Academy of Sciences, Institute of High Pressure Physics (UNIPRESS), Sokolowska 29/37, Warszawa 01-142, Poland* **2.** *TopGaN Sp. z o. o., Sokolowska 29/37, Warsaw 01-142, Poland*

e-mail: tsochacki@unipress.waw.pl

The best quality crystals of gallium nitride can be grown from the solution in supercritical ammonia [1]. This approach, which is known as ammonothermal method, is analogous to hydrothermal crystallization of quartz, however, ammonia is used in the place of water. The ammonothermal GaN crystals (Am-GaN) have many great attributes. They are extremely flat, with bowing radii of (0001) crystallographic planes reaching up to 100 m. Dislocations density is of the order of 10^4 cm^{-2} and free carrier concentration (for n-type crystals) can be varied from $5x10^{17}$ cm^{-3} to $5x10^{19}$ cm^{-3}. One of the biggest drawbacks of the ammonothermal growth of GaN is that it is very slow: growth at best 0.1 mm per day. A technique that has a relatively high growth rate, even up to 500 μm per hour, is a Hydride Vapor Phase Epitaxy (HVPE). This is the most common approach for manufacturing GaN substrates today. The HVPE involves crystallization from the vapor phase at ambient pressure, with GaN deposited on a foreign substrate through the reaction of ammonia with gallium chloride at temperatures of about 1300 K. Etching or self-lift-off techniques are used to separate the nitride film from the foreign substrate (typically sapphire or GaAs) and yield a large-diameter, free-standing (F-S) GaN substrates. Unfortunately, the F-S HVPE-GaN crystals often suffer from lattice bowing. This follows from significant differences between the lattice constants and thermal expansion coefficients of the foreign substrate and the nitride film. It seems, therefore, that a synergy of the HVPE method (the highest growth rate) and the ammonothermal crystallization (the highest structural quality) can create new opportunities for an efficient production of the GaN bulk crystals (then substrates). This can also be helpful to answer a few general questions. First of all, is it possible to combine the HVPE and ammonothermal methods and crystallize perfect HVPE-GaN on a perfect ammonothermal GaN seed? Second of all, is a nature andstructural quality of the seed a main barrier for crystallization of the bulk HVPE-GaN? Finally, if it is possible to multiply the Am-GaN crystal by the HVPE method, obtaining a new F-S HVPE-GaN by slicing it from the seed. Some answers for these questions are being given in this paper. Thus, the results of the HVPE-GaN crystallization on the ammonothermal GaN crystals are described. The starting conditions for the HVPE growth on the Am-GaN seeds are determined, presented and discussed. Smooth GaN layers of excellent crystalline quality, from 0.6 mm to 1.1 mm thick, without cracks, and with dislocation density of the order of $5x10^4$ cm^{-2} are shown. The result of slicing of a new HVPE grown material is demonstrated (see Fig. 1). Structural, optical and electrical properties of this new sliced F-S HVPE-GaN are examined and presented.

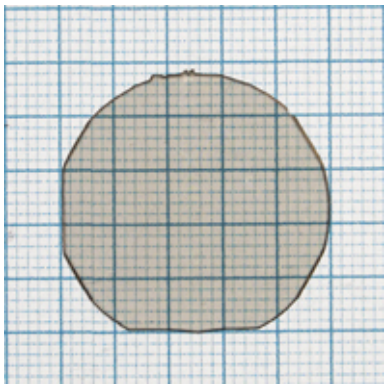

Fig1. Free standing HVPE-GaN sliced from the Am-GaN seed; both surfaces were mechanically polished after the slicing procedure.

1. R. Doradziński et al., in Technology of Gallium Nitride Crystal Growth, edited by D. Ehrentraut et al., (Springer-Verlag, Heidelberg, ISBN 978-3-642-04828-9), 137-158, (2010)

17:00 Poster Mo81

Growth and Optical characterization of Sodium Potassium Phthalate (NaKP) single crystals

Sivakumar Balaraman[1], Gokulraj Srinivasan[2], Rameshkumar Gubendiran[3], Mohan Rajagopal[1]

1. *Presidency College (PRESIDENCY), Kamarajar Salai, Chennai 600005, India* **2.** *VelTech Dr.RR and Dr.SR Technical University (VELTECH), No.42 VelTech Avadi Road, Chennai 600062, India* **3.** *University College of Engineering Arni, Chennai 632317, India*

e-mail: gokulrajs@yahoo.com

Single crystals of admixtured phthalates of sodium and potassium called as sodium potassium acid phthalate (NaKP) have been successfully grown from aqueous solution for the first time. The grown crystals were characterized by single crystal X-ray diffraction. The crystal belongs to Trigonalcrystallographic system with a non-centrosymmetric space group P-31c. Cell parameters are a = 16.731(3) Å; b = 16.731(3) Å; c = 18.276(5) Å α = 90°; β= 90°; γ= 120°; V=4430.5(17) $Å^3$. The vibrational structure of the compound has been elucidated through FTIR spectrum. Optical absorption properties of the crystal have been studied from UV-Vis-NIR measurements. Mass spectrometric analysis provides the molecular weight of the compound and possible ways of fragmentations that normally occur in the compound during thermal process have also been analyzed. Thermal stability of the crystal was studied by simultaneous TGA/DTA measurements. These preliminary results suggests that the crystal could be a potential candidate for higher order harmonic oscillators.

17:00 Poster Mo82

Bulk GaAs growth by Contactless Liquid Phase Electroepitaxy

Pawel Strak[1], Stanisław Krukowski[1,2], Zbigniew R. Zytkiewicz[3]

1. *Polish Academy of Sciences, Institute of High Pressure Physics (UNIPRESS), Sokolowska 29/37, Warszawa 01-142, Poland* **2.** *University of Warsaw, Interdisciplinary Centre for Mathematical and Computational Modelling (ICM), Pawinskiego 5a, Warsaw 02-106, Poland* **3.** *Institute of Physics, Polish Academy of Sciences, Warsaw 02-668, Poland*

e-mail: strak@unipress.waw.pl

LPEE has been found to be very effective for the growth of bulk crystals of multicomponent semiconductors. In particular, the LPEE grown crystals show compositional uniformity that is not attainable by other solution or melt growth methods (see [1] for a review). Unfortunately, as shown experimentally [2] and theoretically [3, 4] thickness of crystals feasible by LPEE is limited to ~3-4 mm. This is due to Joule heating in the body of growing crystal, which finally leads to complete termination of the growth. In this work we present a design for the growth of bulk III-V crystals by electroepitaxy which avoids severe drawbacks of standard LPEE. This liquid-phase technique allowing one to grow large-size single crystals in nearly isothermal conditions by application of electric current flow is presented. The technique, denoted as contactless liquid-phase electroepitaxy (CLPEE) method paves the way to obtain large-diameter high crystalline quality single crystals with potentially unlimited thickness. Systematic studies of influence of crucible design on uniformity of growth of bulk III-V crystals are reported. We found that CLPEE removes the most important drawback of standard liquid phase electroepitaxy, i.e. limited thickness of crystals being due to superheating of the growing crystals by Joule heat generation. However, the CLPEE method in its simplest version suffers from enhanced growth rate at the center of the crystal, which results from majority of electric current flowing to the center of the electrode and dragging solute species [5]. A number of various designs of growth crucible are examined showing that optimized triple-electrode system is capable to provide perfectly uniform growth rate distribution over a large portion of the surface of the growing crystal [6]. In this way the main obstacle in development of the CLPEE technique is removed allowing application of electroepitaxy to obtain large diameter high crystalline quality single crystals with potentially unlimited thickness.

[1] T. Bryskiewicz, Prog. Crystal Growth and Characterization 12 (1986) 29.

[2] Z.R. Zytkiewicz, J. Crystal Growth 146 (1995) 283.

[3] Z. R. Zytkiewicz, J. Cryst. Growth 172 (1997) 259.

[4] P. Strak, Z.R. Zytkiewicz, K. Sakowski, and S. Krukowski, Cryst. Res. Technol. 45 (2010)

1290.

[5] Z. R. Zytkiewicz, P. Strak, S. Krukowski, Crystal Growth and Design 11 (2011) 4684

[6] P. Strak, Z. R.Zytkiewicz, S. Krukowski, J. Crystal Growth, 355 (2012) 1

17:00 Poster Mo83

Control of the segregation coefficient for Eu doped LiSrAlF$_6$ by Co-doping

Shotaro Suzuki[1], Yuui Yokota[2], Akihiro Yamaji[1], Noriaki Kawaguchi[3], Kentaro Fukuda[3], Shunsuke Kurosawa[1,2], Akira Yoshikawa[1,2]

1. *Institute for Materials Research, Tohoku University (IMR), Sendai 980-8577, Japan* **2.** *New Industry Creation Hatchery Center, Tohoku University, Aoba-yama 6-6-10, Aoba-ku, Sendai, Miyagi, Sendai 980-8579, Japan* **3.** *TOKUYAMA Corp, Shunan 745-8684, Japan*

e-mail: suzuki_s@imr.tohoku.ac.jp

The interest in the neutron detection techniques have been increasing due to the increase of the need for neutron detectors in various applications. The proportional counters filled with ^{3}He gas have been mainly used in the applications because of the large cross-section to thermal neutron and low sensitivity to gamma-ray background. However, in recent years, great demand of the ^{3}He gas for homeland security applications resulted in the ^{3}He supply crisis, and then the development of alternative neutron detector has been strongly required. We have investigated the Ce^{3+} and Eu^{2+} dope $LiCaAlF_6$ (LiCAF) and $LiSrAlF_6$ (LiSAF) crystalline scintillators with relatively high light yield to thermal neutron as an alternative for the ^{3}He gas [1-3]. The Eu:LiCAF and Eu:LiSAF scintillator crystals have attractive performance such as high light yield and non-hygroscopic properties. However, the transparency drastically decreases due to the formation of milky parts which include the secondary phase by the increase of Eu concentration. The formation of secondary phase is attributable to the low effective segregation coefficient (k_{eff}) of Eu ion into the LiCAF and LiSAF crystals and this fact seriously decrease the yield of the bulk crystals. In this study, we grew Eu:LiSAF single crystals using Al metal as starting material to decrease the formation of milky parts and the optical and scintillation properties were investigated. Usually, the LiSAF single crystals were grown from LiF, SrF_2, AlF_3, EuF_3 starting material powders. However, the Eu^{3+} ion in EuF_3 substitutes to the Sr^{2+} site as a Eu^{2+} ion. Therefore, we tried to remove the extra fluorine ion (F^-) by doping of Al metal.

The Eu doped LiSAF crystals were grown as nominal compositions of $Li(Sr_{1-x}Eu_x)(Alm_{0.01}Al_{F0.99})F_6$ (x = 0.005, 0.01, 0.015, 0.02, 0.03) using starting materials of 4N LiF (7.5% ^{6}Li), SrF_2, AlF_3, EuF_3 (produced by Stera Chemifa) and Al metal powders. Al_m and Al_F are Al from Al metal and AlF_3, respectively. Crystal growth was performed by the micro-pulling-down (μ-PD) method with the tight-vacuum chamber. Mixed powders were set in the graphite crucible with a Φ3 mm die which has a Φ2 mm hole in the center and the crucible was heated by the high-frequency induction coil in Ar/CF4 mixed gas after baking process under high vacuum (~10^{-4} Pa). The melt in the crucible was pulled down using Platinum wire as the seed at approximately 0.1 mm/min. The detail of crystal growth by the μ-PD method was described in Ref. [4]. Rectangular samples with 1 mm thickness were obtained from the grown crystals and they were polished for the optical and scintillation measurements. Transmittance was measured by JASCO V550 spectrofluorometer in the range of 190-900 nm. Pulse height spectra and decay time under neutron excitation from ^{252}Cf radiation source were investigated. In the measurements, ^{6}Li-loaded glass scintillator (GS20; Saint Gobain) with the size of 1 × 2 × 6 mm^3 which had the light yield of 6000 ph/n [5] was used as a reference. The crystals were optically coupled to the window of photomultiplier tube (PMT, Hamamatsu R7600U) with an optical grease (OKEN 6262A). The polished $Li(Sr_{0.98}Eu_{0.02})(Al_{m0.01}Al_{F0.99})F_6$ single crystal is shown in Fig.1. The crystal indicated high transparency and there was no milky part in the all grown crystals. Transmittance of Al metal doped crystals showed approximately 80 % in the wavelength range of 380-900 nm, as it is illustrated in Fig. 2. In contrast, the crystals without Al metal indicated less than 50% transmittance due to the milk parts. In addition, the crystals had strong absorption peaks which were attributable to the 4f-5d transitions of Eu^{2+} ion at 200 and 300 nm. By the increase of Eu concentration, the intensities of absorption peaks systematically increased.

Figure 3 shows the pulse height spectra of Al metal doped Eu:LiSAF crystals. By way of comparison, the result of ^{6}Li-loaded glass scintillator was also indicated. Light yield of Al metal doped crystals systematically increased with the increase of Eu concentration up to 2 mol%. Meanwhile, the light yield of Eu 3 mol% doped crystal was almost same as that of Eu 2 mol% doped crystal. Decay times of Al metal doped crystals were 1400-1700 ns, as shown in Fig.4. Other optical and scintillation properties will be reported.

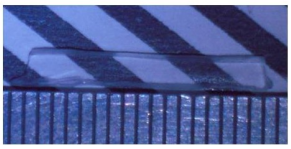

Fig.1. $Li(Sr_{0.98}Eu_{0.02})(Alm_{0.01}AlF_{0.99})F_6$ single crystal.

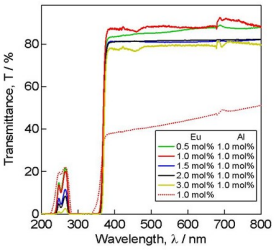

Fig. 2. Transmittance spectra of Al metal doped Eu:LiSAF crystals.

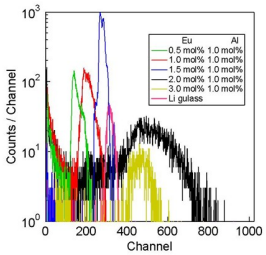

Fig. 3. Pulse height spectra of Al metal dope Eu:LiSAF crystals under neutron excitation.

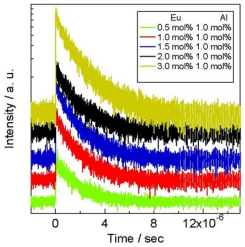

Fig. 4. Decay curves of Al metal dope Eu:LiSAF crystals under neutron excitation.

Reference

[1] A. Yoshikawa, T. Yanagida, Y. Yokota, N. Kawaguchi, S. Ishizu, K. Fukuda, T. Suyama, K. J. Kim, M. Nikl, M. Miyake, M. Baba, IEEE Trans. Nucl. Sci., 56 (2009) 3796-3799

[2] A. Yamaji, N. Kawaguchi, Y. Fujimoto, Y. Yokota, K. Watanabe, J. Pejchal, Nucl. Instr. Meth. Phys. Res A. 659 (2011) 368-372.

[3] T. Yanagida, N. Kawaguchi, Y. Fujimoto, Y. Yokota, A. Yamazaki, K. Watanabe, A. Yoshikawa, V. Chani, Measurements 46 (2011) 1708-1711.

[4] A. Yoshikawa, G. Boulon, T. Fukuda, Opt. Mater. 30 (2007) 6.

[5] E. Van, C.W.E., Radiat. Prot. Dosim. 110 (2004) 5-14.

17:00 Poster Mo84

Study of flow pattern by the measurement of temperature fluctuations in the solution during the growth of stoichiometric lithium niobate single crystals

Zsuzsanna Szaller, Ágnes Péter, Katalin Polgar, Éva Tichy-Rács

Wigner Research Centre for Physics, Hungarian Academy of Sciences (WIGNER), Konkoly-Thege Miklos út 29-33, Budapest 1121, Hungary

e-mail: szaller.zsuzsanna@wigner.mta.hu

Stoichiometric lithium niobate ($LiNbO_3$, sLN) shows improved performance for a number of applications compared to the congruent crystal, because of its nearly perfect crystal lattice containing low concentration of intrinsic structural defects ($[Nb_{Li}] < 0.01\%$). The photorefractive damage of sLN crystals is usually suppressed by less than 1mol% MgO doping. Optical device applications impose the growth of crystals in high quality and increased sizes.

Up to now methods have been applied for the preparation of sLN crystals, the one which resulted in the composition closest to 50% Li_2O is the high temperature top seeded solution growth (HTTSSG) method using potassium oxide containing flux [1]. Crystals grown by this technique show a pronounced tendency towards faceting. Pyramidal facets formed in sLN deteriorate the crystal quality, as the related strains may induce domain inversion, mechanical twinning and cracks. Faceted growth may enhance incorporation of flux inclusions and bubbles as well [2]. Near planar solid liquid interface can be ensured by applying gradually variable rotation rate all along the crystal growth process resulting in non-faceted crystal growth [3].

In this work we present investigations on the characteristics of the melt flow patterns during the growth process of Mg-doped sLN crystals from Li_2O–Nb_2O_5–K_2O flux (in diameter of 20-55 mm) using resistant heating furnace. Temperature gradient and fluctuations are measured in order to determine the Grashof and Reynolds numbers characterizing the flow patterns in the melt. A specific effort is made to determine the critical rotation rate and crystal diameter, optimal for establishing non-faceted growth.

References:

[1] K. Polgár, Á. Péter, L. Kovács, G. Corradi, Zs. Szaller: Growth of stoichiometric $LiNbO_3$ by Top seeded solution growth, J. Crystal Growth, vol. 177, pp. 211-216 (1997)

[2] K. Polgár, Á. Péter, I. Földvári, Zs. Szaller: Structural defects in flux grown stoichiometric $LiNbO_3$ single crystals, J. Crystal Growth, vol. 218, No.2-4, pp.327-333, (2000).

[3] Zs. Szaller, Á. Péter, K. Polgár, Gy. Szabó: High temperature top seeded solution growth of stoichiometric lithium niobate $LiNbO_3$ (sLN) with planar interface, J. Crystal Growth vol. 360 pp181-184 (2012)

17:00 Poster Mo85

Growth and spectrum of $Yb:Lu_xY_{1-x}PO_4$ crystal

Bing Teng

Qingdao University, College of Physics, Qingdao 0086-0532, China

e-mail: 5108tb@163.com

$Yb:Lu_xY_{1-x}PO_4$ mixed crystals were firstly grown by the high-temperature solution (or flux) growth process using lead pyrophosphate $Pb_2P_2O_7$ as the high-temperature solvent. The crystal structure of $Yb:Lu_xY_{1-x}PO_4$ mixed crystals was refined at room temperature by using single crystal X-ray diffraction data. Crystal structure analysis showed that $Yb:Lu_xY_{1-x}PO_4$ crystals possessed the tetragonal xenotime structure. The polarized absorption spectra were measured at room temperature.

17:00 Poster Mo86

A new kind of zone in sodium chlorate-bromate crystal grown in areas of temperature anomalies of growth rate («kinetic anomalies»)

Alexandr Vikharev, Sergey N. Bocharov

Saint-Petersburg State University (SPBSU), 7/9 University emb., S.Petersburg 199034, Russian Federation

e-mail: alexvikev@gmail.com

Detailed kinetic measurements show that growth rate in dependence on temperature is characterized by strongly nonmonotonous changes. Such phenomenon is known as “kinetic anomalies”. Kinetic anomalies investigation of mixed crystal growth showed that their chemical composition also changes nonmonotonically with temperature. It was assumed that such nonmonotonic changes of chemical composition will result in zone formation in bulk of crystal.

Sodium chlorate-bromate system was chosen for experiments since kinetic data and impurity (sodium bromate) concentration are known in dependence on temperature. Crystals for investigation have been received by three different methods. The first one (combined

method) is combination of temperature gradient and temperature decrease methods. Other two is spontaneous crystallization and constant supercooling method (microcrystallization). Last two of them were used for comparison of chemical composition distribution at crystals grown in different conditions from solution with the same composition.

Received crystals were investigated by two methods: optical microscopy and x-ray microtomography.

Crystals grown by combined method show zone distribution of interference colors. At the same time crystals grown by other methods have a domain or homogeneous distribution of interference colors. It means that tensions also as compounds distribution are different and show zone character only for crystals grown by combined method.

Microtomography investigation shows that crystals grown by combined method have zone distribution of grayscale index. Grown crystals have from one to three zones enriched by bromate compound in dependence on temperature range and amount of anomaly extremes located in this range. External zone has maximum intensity on grayscale index profile in every case where is more than one zone. It doesn't match to intensity of anomaly peaks and theoretical concentration of bromate. We link it to the features of X-Ray microtomography and reconstruction method where external zone "shields" internal zones.

Received data show that chemical composition can change nonmonotonic even in case of monotonic temperature decrease at growth process due to kinetic anomalies influence. This conclusion is supported by X-Ray microtomography data as well as data received by optical microscopy. There are some problems with investigations of our materials by x-ray microtomography method. Main of them is low contrast of received zonality. It results in additional treatment of microtomography slices and grayscale index profiles. Other one is higher intensity of external zone in comparison with theoretical prediction. Both of these problems might be solved with involvement equipment with higher energy tube.

The reported study was partially supported by Russian Foundation for Basic Research, research project No. 12-05-00876-a.

17:00 Poster Mo87

Temperature and frequency dependences of the electric properties of $CsLiB_6O_{10}$ (CLBO) crystals

Zhufeng Wang[1], Zengmei Wang[1], Zhenxiang Cheng[2], Hideo Kimura[3], Xinli Guo[1], Ji Chen[4], Yiping Wang[4]

1. *Southeast University (SEU), Nanjing 210000, China* **2.** *University of Wollongong, Wollongong NSW, Australia* **3.** *National Institute for Materials Science (NIMS), 1-2-1 Sengen, Tsukuba 305-0047, Japan* **4.** *College of Aerospace Engineering, Nanjing University of Aeronautics and Astronautics, Nanjing 210016, China*

e-mail: iamwangzhufeng@gmail.com

In this paper, CLBO crystals were grown by top-seeded solution growth (TSSG) method using self-flux. The temperature and frequency dependence of the dielectric constant, dielectric loss, a.c. conductivity and impedance spectroscopy for different cuts CLBO crystal were investigated, also temperature characteristics of the resonance frequency and electromechanical coupling were studied. The results show that (001)-plane of CLBO crystal has the highest dielectric constant in the order of 109, highest a.c. conductivity and highest electromechanical coupling factor of about 17% at elevated temperature, these make CLBO crystal excellent candidate for electrical application at elevated temperature. Also the anisotropy of electric properties has strong relationship with ion densities of different crystal plane.

17:00 Poster Mo88

Influence of different AlN surface preparation methods on the quality of AlN bulk crystals

Juergen Wollweber, Carsten Hartmann, Tom Neugut, Andrea Dittmar, Sandro Kollowa, Frank Langhans, Matthias Bickermann

Leibniz Institute for Crystal Growth (IKZ), Max-Born-Str 2, Berlin 12489, Germany

e-mail: juergen.wollweber@ikz-berlin.de

Nitride-based devices are reaching maturity. The next development stage could start by using AlN wafers as substrate. First companies are going to commercialize this material. Nevertheless, there are some open issues to be solved on the way to success. Basically, it is still a problem to prepare surfaces without damage layer. A solution of this problem is important not only for device application but also for seeding in bulk crystal growth.

This contribution will show in detail the structural consequences of different AlN surface preparation methods on the quality of AlN bulk crystals grown on it. Moreover, the practical effect on the overall growth concept will be discussed taking into account the cost-benefit ratio.

For this approach c-oriented seeds were prepared from spontaneously grown AlN crystals by sawing, lapping, and mechanical polishing of the N-polar (000-1) face using 2 µm diamond slurry. The seeds were further processed by chemical etching, thermal annealing, Ar-ion milling or chemical-mechanical planarization (CMP) to achieve structurally perfect surfaces. After that, the finished seeds were used in short time growth experiments at constant growth conditions (T=2150 °C, p=600 mbar N_2, t=1 h, grown layer thickness ~200 µm). All samples have been characterized before and after growth by X-ray rocking curve measurement, atomic force microscopy, and Nomarski microscopy.

In contrast to the well known thermal reconstruction of mechanically treated SiC surfaces, AlN does not show a comparable behavior. Maximum FWHM values of 60 arcsec have been found for Ar-ion milling and mechanical polishing. Thermal annealing and CMP led to the best FWHM values of about 15 arcsec. Large-area layer growth via well defined step flow was only observed after chemical etching or CMP finishing.

A detailed analysis of the defect situation of AlN bulk crystals grown on differently finished seeds shows that due to its enormous efforts in preparation time, CMP finishing is not the most cost-effective seed preparation method. The findings are compared to homoepitaxial MOCVD deposition results on AlN wafers with different surface finish.

17:00 Poster Mo89

Growth and characterization of birefringent crystal $NaNO_3$

Wei Xiong[1], Liang Chen[1], Lingxiong Huang[2], Yao Zhou[1], Baoliang Lu[3], Hui Yuan[1]

1. *Shanghai Institute of Ceramics, Chinese Academy of Sciences, 1295 Dingxi Road, Shanghai 200050, China* **2.** *Fujian Institue of Research on the Structure of Matter, Chinese Academy of Sciences, Fuzhou 350002, China* **3.** *Shanghai Jingcui Material Technology Co., Ltd., Shanghai 200062, China*

e-mail: xiongwei@mail.sic.ac.cn

With a bigger birefringence than calcite, sodium nitrate ($NaNO_3$) single crystals might have potential applications in opto-isolators, circulators

and polarizing prisms. However, it is difficult to grow large-size $NaNO_3$ crystals for their thermal conductivity anisotropy and phase transition at 275 ^oC. In this paper, crack-free $NaNO_3$ crystals with size of $\Phi 20\times 100mm^3$ were prepared by Bridgman method with lower growth rate and lower interface temperature gradient. The behaviors of time dependent on transmittance were measured and analyzed. The refractive indices of $NaNO_3$ crystal at wavelengths of 0.4730, 0.5320, 0.6328, 1.064 and 1.338 μm were measured by selfcollimating method. From which, we fitted and obtained the Sellmeier's equation of $NaNO_3$ crystal. Moreover, the photoluminescence spectra were detected under the excitation of 240 nm, and $NaNO_3$ crystal presented its fluorescence around 425 nm.

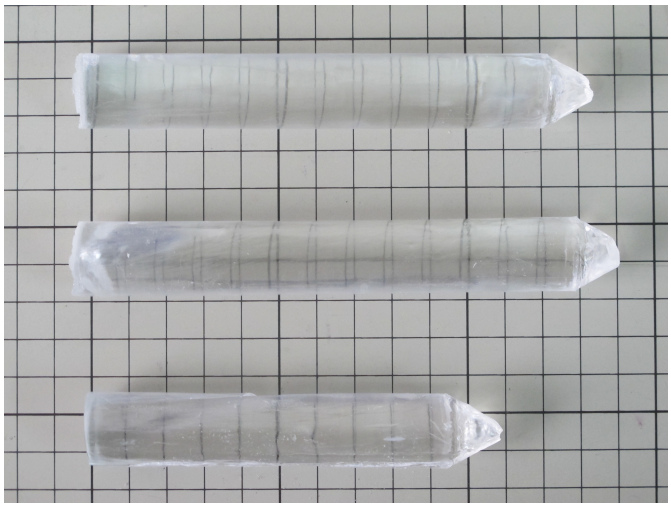

17:00 Poster Mo90

Characterization of dislocations in bulk GaN grown by HVPE

Ke Xu, Jianfeng Wang, Guoqiang Ren, Jun Huang, Zhenghui Liu, Demin Cai, Hui Yang

Suzhou Institute of Nano-tech and Nano-bionics (SINANO), Suzhou 215123, China

e-mail: kxu2006@sinano.ac.cn

Hydride Vapor Phase Epitaxy (HVPE) is an effective way to fabricate GaN substrate, however the big chanlenges are the residual stress and high dislocation density in GaN crystal compared with those grown by ammonothermal and Na-flux methods. In this work, we reported growth interface engineering in HVPE to control the stress and the threading dislocations in GaN crystals. Bulk GaN crystals with dislocation density in the order of 10^4cm^{-2} were demonstrated by HVPE. The mechanical properties dislocation in GaN were investigated by nanoidentation and cathodoluminescence. It was found that dislocation loops could multiply and move from plane to plane by cross slip, accomodating a wide plastic deformation in GaN during indentation. This mechanism is closely related to the threading dislocation generation during heteroepitaxial growth in large lattice mismatch system. The local carrier properties, including minority diffusion lengths and surface recombination velocities, were measured at single thread dislocations local in GaN by a combination of surface photovoltage spectroscopy and Kelvin probe force microscopy.

17:00 Poster Mo91

Crystal growth, spectroscopic characterization and laser performance of Yb-doped lead fluoride crystals

Jigang Yin, Yin Hang, LianHan Zhang, Peixiong Zhang, Kaijie Ning, Guangzhu Chen, Zhe Chen, Xiangyong Wang

Shanghai Institute of Optics and Fine Mechanics China Academy of Sciences, Shanghai 201800, China

e-mail: yjg@siom.ac.cn

Lead fluoride crystals doped with YbF_3, NaF or KF- codoped were grown using the vertical Bridgman method. Room-temperature absorption, photoluminescence spectra, fluorescence lifetimes and laser performance belonging to the transitions between ground state $^2F_{7/2}$ and the excited state $^2F_{5/2}$ of Yb^{3+} ions in these crystals have been investigated. Influence of the codoping with Na^+ and K^+ ions on the distribution coefficients, X-ray photoelectron spectrometry, absorption spectra and emission spectra of the Yb ions has been studied. With a 2 mol% Yb^{3+} and Na^+-codoped sample we obtained 2.65 W output power at 1045 nm for 7.5 W of incident power at 976 nm. The laser wavelength could be tuned from 1017 to 1078 nm, showing the great potential of Yb, Na: PbF_2 as an amplifier medium for femtosecond pulses.

17:00 Poster Mo92

Vertical Bridgman Growth and Optical Properties of Cd-SiP_2 Crystals

Guodong Zhang, Xutang Tao, Shanpeng Wang, Huapeng Ruan, Xiang Zhang

Shandong University, Jinan 250100, China

e-mail: zhguodong@126.com

Single crystals with the dimension of 8 mm in diameter and 40 mm in length were successfully grown using vertical Bridgman method. Optical observations showed the presence of macro-defects including flaws and inclusions in the as-grown crystals. The macro-defects can be restrained through controlling the process of polycrystalline synthesis and growth parameters. For the crystals with improved qualities, the high-resolution X-ray diffraction measurement on the (004)-faced plate indicates that the full-width at half-maximum (FWHM) of the rocking curve is 34". The phase-matching curves calculated from refractive indices indicate that, for 1.064 μm pumping, the CSP crystal will produce a noncritically phase-matched output at 6.2μm laser through a type-I parametric process, and a noncritically phase-matched output at 5.0 μm through a type-II parametric process. For 1.55 μm and 2.00 μm pumping, the crystal will yields continuous tunability from 2 to 6.5 μm through a type-I parametric process. The absorption coefficients for e-polarized light at 1.064 μm, 1.55μm and 2.0μm of the as-grown CSP crystal are 0.53 cm-1, 0.39 cm-1, and 0.25 cm-1, respectively.

17:00 Poster Mo93

Study on rapid growth of 98% deuterated potassium dihydrogen phosphate (98%DKDP) crystals

Lisong Zhang[1], Mingxia Xu[1], Baoan Liu, Shaohua Ji[1], Lili Zhu[1], Hailiang Zhou[1,2], Liang Li[3], Fafu Liu[1], Xun Sun[1], Xinguang Xu[1]

1. *State Key Laboratory of Crystal Materials, Shandong University, Jinan 250100, China* **2.** *School of Information Science and Engineering, Shandong Agricultural University, Taian 271018, China* **3.** *Advanced Research Center for Optics, Shandong University, Jinan 250100, China*

e-mail: zhls329747@gmail.com

Tetragonal98% deuterated potassium dihydrogen phosphate (98%DKDP) crystals were grown rapidly from synthetic higher deuterium content DKDP solution by using point seeds under high supersaturation at different temperatures ranging from 38.3°C to 51.0°C. It is found that the metastable region of DKDP solution is uncertain and DKDP crystal can start to grow from higher temperature. For comparison, monoclinic 98%DKDP crystals were also grown from the same solution. Surface morphologies of tetragonal 98%DKDP crystals grown under different temperatures and monoclinic 98%DKDP crystals were investigated by using AFM technique. The different growth habits of Tetragonal and monoclinic 98%DKDP crystals were studied according to their different crystal structures by using bond valence model.

17:00 Poster Mo94

Growth and optical properties of $LiLuF_4$ crystal co-doped with Ho^{3+} and Pr^{3+} at 2.9 μm

Peixiong Zhang[1,2], LianHan Zhang[1], Jigang Yin[1], Yin Hang[1]

1. *Shanghai Institute of Optics and Fine Mechanics China Academy of Sciences, Shanghai 201800, China* **2.** *Chinese Academy of Sciences, beijing 100190, China*

e-mail: pxzhang@yahoo.cn

In recent years, mid-IR (MIR) lasers operating around 3μm have attracted much attention for numerous applications in medical and sensing technologies because of the vibrational absorption band of water in this spectral region. Ho^{3+} is a well known ion with transitions in the IR region around 2.9 μm. However, the 2.9 μm emission cannot be obtained efficiently because the fluorescence lifetime of the upper $^5I_6$ level is considerably shorter than that of the lower level $^5I_7$. Co-doping of Pr^{3+} could be used as a feasible alternative to quench the lower level. $LiLuF_4$ (LLF) crystal has low multiphonon relaxation resulting in long radiative and fluorescence lifetimes of $^5I_6$ manifold, and the vibronic absorption bands appear in the MIR at a significantly higher wavelength. It has negative thermal dependence of refractive index, which leads to weak overall thermal lensing. In this poster session, Ho^{3+}- and Ho^{3+}, Pr^{3+}-doped LLF crystals were successfully prepared. The use of Pr^{3+} co-doping for enhancement of the Ho^{3+}:$^5I_6 \rightarrow {}^5I_7$ mid-IR emissions were investigated in the LLF crystal for the first time. It was found that Pr^{3+} greatly increased Ho^{3+} 2.9 μm emission by depopulating the Ho^{3+}:$^5I_7$ level while having little influence on the Ho^{3+}:$^5I_6$ level, leading to greater population inversion. The energy transfer efficiency from Ho^{3+}:$^5I_7$ to Pr^{3+}:$^3F_2$ is calculated to be 88%. Based on Judd–Ofelt theory, the 2.9 μm emission cross section is calculated to be 1.91×10^{-20} cm^2, and the gain property of the Ho^{3+}:$^5I_6 \rightarrow {}^5I_7$ transition is discussed. We propose that the Ho, Pr: LLF crystal may be a promising material for 2.9 μm laser applications.

17:00 Poster Mo95

Spectroscopic properties of Yb^{3+}-doped $Bi_4Si_3O_{12}$ single crystal

Yan Zhang, Jiayue Xu, Baoliang Lu, Bobo Yang

Shanghai Institute of technology (SIT), Haiquan Road, Fengxian, Shanghai 201418, China

e-mail: yanzhang@sit.edu.cn

Yb^{3+}-doped $Bi_4Si_3O_{12}$ single crystals with good optical quality have been grown by the modified vertical Bridgman method. The crystalline quality of the Yb^{3+}: $Bi_4Si_3O_{12}$ single crystal was verified by the width of the X-ray diffraction (XRD) peak in the X-ray rocking curves measurement. The absorption spectrum and emission spectra and fluorescence lifetime of the Yb^{3+}: $Bi_4Si_3O_{12}$ crystal were detected at room temperature. The spectral and laser parameters of Yb^{3+}: $Bi_4Si_3O_{12}$ crystal have been calculated.

17:00 Poster Mo96

Optical and Laser Properties of Gray Track Resistance KTP Crystals

Yang Zhang, Huaidong Jiang, Jiyang Wang, Jing Li

Shandong University, Jinan 250100, China

e-mail: zhangyang0115@yeah.net

KTiOPO4 (KTP) exhibits excellent nonlinear optical properties which have made it a widely used crystal in frequency conversion applications such as second-harmonic generation and optical parametric oscillation. When KTP is exposed to high power and high repetition frequency, the crystal will produce gray track effect. After gray track forms, the absorption will increase in visible and near-infrared light and thus, frequency doubling conversion efficiency will decline. So how to improve gray track resistance remains a challenge all the time.

There are always many potassium vacancies in flux-grown KTP crystals. Oxygen vacancies form to keep the lattice substitute for K^+ ions to provide charge compensation for potassium vacancies. Thus, oxygen vacancies, which are responsible for creating the detrimental gray-tracking centers by reducing the Ti^{4+} ions to Ti^{3+}, are needed no longer. In addition, PbO can reduce the viscosity of solution, increase growth velocity and decrease probability of sesondary nucleation events on the crucible wall.

This paper explores the reason of gray track formation. On the basis of the results, we succeed in improving the resistance of gray track using K_6-PbO as flux. The crystals grown in the solution containing PbO are difficult to produce gray track, while it tends to form gray track with K_6 as flux. We conducted X-ray absorption near edge structure(XANES) using total electron yield(TEY) method in the absorption of gray track formation in situ for the first time. The results of XANES and absorption spectrum of gray track region indicate that the formation of gray track is related to Ti^{3+} centers and the absorption of visible light will increase after gray track come into being. We also take a measurement of the optical and laser properties for comparing the difference between the crystal grown in the solution of K_6-PbO and the one grown in the solution of K_6. The results show that the crystal grown in the solution of K_6-PbO has lower absorption values at 532 nm and 1064 nm, lower absorption coefficients, higher resistance to gray track formation, and higher laser induced damage threshold(LIDT). PbO is a promising flux for crystal growth, and we expect that high quality and optically uniform gray-track-resistant KTP can be grown commercially.

17:00 Poster Mo97

Crystal Growth, Defects and Laser Action of Yb:$Y_xLu_{1-x}VO_4$ Mixed Crystals

Degao Zhong

Qingdao University, College of Physics, Qingdao 0086-0532, China

e-mail: zhdg2008@yahoo.com.cn

A new series of Yb:$Y_xLu_{1-x}VO_4$ mixed laser crystals were grown by the Czochralski method. The polarized absorption spectra were measured at room temperature. The continuous-wave (cw) laser action of diode-pumped Yb:$Y_xLu_{1-x}VO_4$ mixed crystal laser was reported. The laser emission spectrum and relationship curve between the output power and absorbed pump power (P_{abs}) were measured. The optical quality of Yb:$Y_xLu_{1-x}VO_4$ mixed crystal was determined using optical interferometer. The crystal defects were studied by chemical etching and X-ray topography.

17:00 Poster Mo98

Effect of solution flow velocity on the step bunching in solution growth of SiC

Can Zhu[1], Shunta Harada[1], Kazuaki Seki[2], Miho Tagawa[1], Yuji Matsumoto[3], Tomohisa Kato[4,5], Kazuhisa Kurashige[5,6], Hajime Okumura[4,5], Toru Ujihara[1]

1. *Department of Materials Science and Engineering, Nagoya University, Furo-cho, Chikusaku, Nagoya 464-8603, Japan* **2.** *Department of Crystalline Materials Science, Nagoya University, Furo-cho, Chikusa-ku, Nagoya 464-8603, Japan* **3.** *Materials and Structures Laboratory, Tokyo Institute of Technology, 2-12-1 Ookayama, Meguro-ku, Tokyo 152-8550, Japan* **4.** *National Institute of Advanced Industrial Science and Technology (AIST), Tsukuba Central 2-1-D811, 1-1-1 Umezono, Tsukuba 305-8568, Japan* **5.** *R D Partnership for Future Power Electronics Technology (FUPET), Onogawa 16-1, Tsukuba 305-8569, Japan* **6.** *Tsukuba Research Laboratory, Hitachi Chemical Co., Ltd., 48, Wadai, Tsukuba 300-4247, Japan*

e-mail: zchhuc@gmail.com

Silicon carbide (SiC) is a wide band gap semiconductor material for future electronics in high-power, high-temperature, and high-frequency applications. Solution growth is a promising method to achieve high quality crystals because the growth proceeds under the condition close to the thermal equilibrium. Recently we revealed that threading dislocations are converted to basal plane defects by the step-flow during the solution growth. By utilizing the threading dislocation conversion, we achieved drastic reduction of dislocation density. However, during the solution growth, step bunching always occurs. By the step bunching, the excess development of macrosteps can lead to the macroscopic defects such as rough growth surface and solvent inclusion. In this study, for the reduction of the step bunching during the solution growth of SiC, we investigated the effect of solution flow velocity on the step bunching behavior.

SiC crystal growth was conducted by the specially designed top seeded solution growth (TSSG) configuration. In our growth experiment, the seed crystals were placed at the position deviated from the center of the crucible. By only rotating the crucible, controlled solution flow was obtained on the growth surface. In this study, the off-angled 4H-SiC was used as seed crystals. We carried out the growth under two different solution flows, in which the solution flow direction and step-flow direction was the same (here we call parallel flow) and opposite (anti-parallel flow).

As shown in Figure 1, wide and flat macro-terraces were frequently observed under the parallel flow, while the step trains with narrow macro-terraces were observed under the anti-parallel flow. Figure 2 shows that the surface roughness of the grown crystal under the parallel flow was larger than that of anti-parallel flow. Under the parallel flow, the surface roughness increases with increasing solution flow velocity. On the other hand, the surface roughness was independent of the solution flow velocity under the anti-parallel flow. This can be explained by the change of solute concentration distribution above the crystal surface which controls the behavior of step bunching. Under the parallel flow, the high-concentration solution moves to the edge of macro-terrace, which results in the microsteps run into the macrosteps quickly and then the surface roughness increases. While under the anti-parallel flow, the high-concentration solution moves to the macrosteps from the front direction, thus the microsteps run out of the macrosteps, which keeps the surface roughness stable. We figured out that the solution flow control could be an effective way to control step bunching during the solution growth of SiC.

Acknowledgement: This study was partly supported by Novel Semiconductor Power Electronics Project Realizing Low Carbon-Emission Society of Ministry of Economy, Trade and Industry through R&D Partner-ship for Future Power Electronics Technology (FUPET).

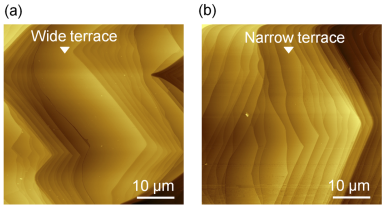

Figure 1. AFM images of surface morphology of grown crystals under (a) parallel flow and (b) anti-parallel flow.

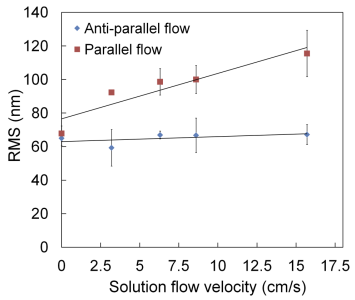

Figure 2. The RMS value V.S. solution flow velocity.

General Session 3

Biological and Biogenic Crystallization

Session Coordinators

Jolanta Prywer (Poland) *jolanta.prywer@p.lodz.pl*

Helmut Coelfen (Germany) *helmut.coelfen@uni-konstanz.de*

Abel Moreno (Mexico) IUCr representative *carcamo@servidor.unam.mx*

Programme

Monday, 12 August

MoO1

G03: Biological and Biogenic Crystallization
Monday morning, 12 August, 11:00
Room B, Auditorium Maximum

11:00 Invited oral

Bioinspired mineralization: branching growth and oriented attachment

Hiroaki Imai

Faculty of Science and Technology, Keio University (Keio Univ), 3-14-1, Hiyoshi, Kouhoku-ku, Yokohama 223-8522, Japan

e-mail: hiroaki@applc.keio.ac.jp

Biological inorganic crystals have a hierarchical structure that is different from geological minerals and artificial crystalline materials. Most biominerals are composed of nanometric oriented components, which are regarded as a mesocrystal. These specific architectures are generally produced through molecular controlled mineralization in aqueous solution systems. The biomineralization processes provide considerable inspirations in the fields of materials chemistry and crystal engineering. Recently, a wide variety of mesocrystals have been artificially produced by bioinspired techniques. In this presentation, the bioinspired processes for the mesocrystal formation are classified into two categories: branching in growth modulated with molecular species and self-assembly of nanoscale units via oriented attachment. The mineralization in a gel matrix is a typical example of the branching growth induced under a diffusion-limited condition. The particular interaction of molecular species and viscous media miniaturizes the unit size of growth. The mesostructures consisting of bridged nanocrystals are finally produced by the branching growth. The oriented attachment is obviously achieved by using rectangle nanoparticles as a structural unit. Another type of mesocrystals consisting of isolated units is obtained by self-assembly of the polyhedral particles covered with organic molecules. The homogeneity of the size and shape is important for construction of large-sized 3D architectures. The similarity and the difference between the branching growth and the oriented attachment are discussed for understanding and application of bioinspired mineralization.

11:30 Oral

Controlling of Morphology and Polymorph of Calcium Oxalate Crystals by Using Polyelectrolytes

Emel Akyol, Mualla Oner

Yildiz Technical University (YTU), Chemical Engineering Department Davutpasa Campus, Esenler, Istanbul 34210, Turkey

e-mail: eakyol@yildiz.edu.tr

In this study, we prepared polyelectrolytes to explore their effectiveness in controlling of crystallization of calcium oxalate. The effects were evaluated at different calcium to oxalate concentration ratios in the mother liquid. The polyelectrolytes affect morphology, phase, dimension and particle size distribution of the crystals. Our studies indicated that polyelectrolytes inhibit calcium oxalate monohydrate crystallization so that they are capable of increasing spontaneous nucleation of COD.

11:45 Oral

Hierarchically-structured inorganic-inorganic composite materials formed by crystal growth in hydrogels

Emily Asenath-Smith, Lara A. Estroff

Cornell University, Department of Materials Science and Engineering, Ithaca, NY 14853-1501, United States

e-mail: ea263@cornell.edu

Crystal growth in hydrogels is an extension of low temperature solution-based methods. Incorporation of the hydrogel matrix during growth was seen initially seen as a drawback to this method, but later proved to be a means to form composite crystals, similar to biogenic minerals that contain hierarchically ordered levels of structure. Translating these methods from organic-hydrogel, carbonate-mineral systems to inorganic-hydrogel, oxide-mineral systems is not a straightforward task, as most hydrogels lose their structure (melt) at the higher temperatures used for oxide synthesis. In this work, we report the growth of iron (III) oxide, hematite, in an inorganic silica hydrogel under hydrothermal conditions. The success of this approach stems from the parallel chemistries associated with the formation of each individual material (hematite in solution, silica as a hydrogel), and presents a means to form inorganic-inorganic composites with tunable hierarchical structures.

The well-known solution method for forming hematite pseudocubes (Fig. 1a) from iron (III) chloride under acidic conditions[1] was carried out within a silica hydrogel matrix. The resulting spherical particles (Fig. 1b) are not simply polycrystalline particles, but mosaic crystals that contain crystallographically-oriented subunits. Both the solution- and hydrogel-grown hematite particles (Fig. 1a&b, respectively) extinguish during rotation under cross-polarized light and diffract electrons as single crystals. The size of the crystalline subunits contained within these particles was calculated from x-ray powder diffraction data, and confirmed visually using transmission electron microscopy (TEM) with etching studies. The net relationship between the particle shape and the underlying hematite lattice was determined using high resolution TEM and selected area electron diffraction analysis on thin sections that were prepared using a focused ion beam. The macroscopic change in shape of the hematite crystals upon growing in a hydrogel is correlated to a change in the nano-scale, hierarchical structure of the subunits contained within hematite particles; formation of hematite in a silica hydrogel matrix is associated with an increase in the aspect ratio of the subunits, which become elongated along [110] of the hematite lattice.

The composite nature of the hydrogel grown particles is clearly demonstrated by their etching behavior. Upon etching in acidic solution, where hematite is soluble, a porous framework remains (Fig. 1c). Conversely, upon exposing the particles to basic media, where silica species have a higher solubility than hematite, layers of rods emerge from within a base-soluble matrix (Fig. 1d). These results indicate the two-phase nature of the hematite particles formed in silica hydrogel; crystalline hematite within a porous, silica-based matrix. The identity of the porous phase contained within the hydrogel grown hematite particles will be discussed in terms of chemical composition, crystallinity, and distribution within the interior of the particles with the goal of understanding of the molecular-level growth environment that leads to the levels of structure contained within hydrogel grown materials.

1. E. Matijevic and P. Scheiner, *J. Colloid Interface Sci.*, 1978, **63**, 509.

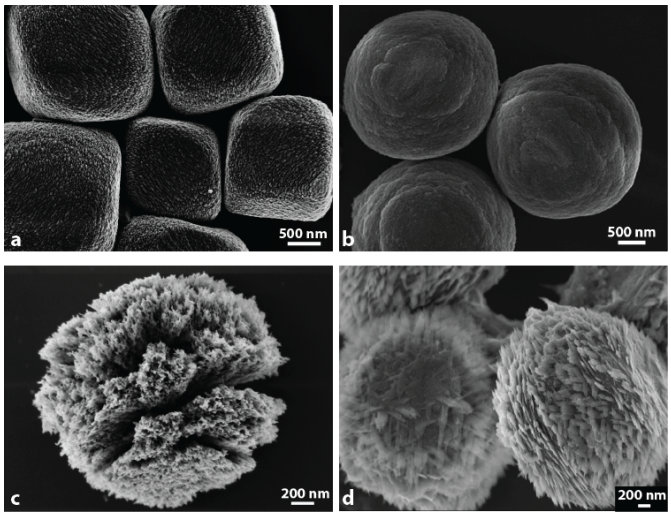

Figure 1. Scanning electron micrographs of hematite crystals formed under hydrothermal conditions in solution (a) and in a silica hydrogel matrix (b). (c) Acid- and (d) base-etched, hydrogel-grown particles showing the composite nature of the hydrogel-grown particles.

12:00 Oral

Growth and characterization of struvite-Na crystals

Chetan K. Chauhan[1,2,3], Mihirkumar J. Joshi[1]

1. *Saurashtra University, Department of Physics, Crystal Growth Laboratory, University Road, Rajkot 360005, India* **2.** *Government Science College, Sector 15, Gandhinagar 382015, India* **3.** *Knowledge Consortium of Gujarat, Dr Jivraj Mehta Bhavan, Gandhinagar 382010, India*

e-mail: ckc33@rediffmail.com

Sodium magnesium phosphate heptahydrate {$NaMgPO_4.7H_2O$}, also known as struvite-Na is the sodium analog to struvite. Among phosphate containing bio-minerals, struvite has attracted considerable attention, because of its common occurrence in a wide variety of environments. Struvite and family crystals were found as urinary calculi in humans and animals. Struvite-Na crystals were grown by single diffusion gel growth technique in silica hydro gel medium. Since the growth conditions play important role in the growth of crystals; in the present study, different growth parameters were used to grow struvite-Na crystals. Struvite-Na crystals with different morphologies having transparent to translucent diaphaneity were grown with different growth parameters. The phenomenon of Liesegang rings was also observed with some particular growth parameters. The crystals were characterized by powder XRD, FT-IR, thermal analysis and dielectric study. The powder XRD study confirmed the structural similarity of the grown struvite-Na crystals with struvite. It was found that struvite-Na crystallized in the orthorhombic $Pmn2_1$ space group with unit cell parameters as: a= 6.893 Å, b = 6.124 Å, c = 11.150 Å, $\alpha = \beta = \gamma = 90°$. FTIR spectra of struvite-Na crystals revealed the presence of functional groups and confirmed the presence of water of hydration, P – O and PO_4^{3-} ion and metal –oxygen vibrations. The TGA, DSC and DTA were carried out simultaneously. It was found that crystals started dehydrating and decomposing from 70°C and finally at 600°C temperature it became 63.9 % of the original weight and remained almost constant up to the end of analysis. The kinetic and thermodynamic parameters of dehydration / decomposition process were calculated. The variation of dielectric constant with frequency of applied field was studied in the range from 400 Hz to 100 kHz.

12:15 Oral

Calcium phosphate precipitation in hanging drop vapor diffusion monitored by in situ Raman microspectroscopy

Gloria Belén Ramírez-Rodríguez, José Manuel Delgado López, Jaime Gómez-Morales

Instituto Andaluz de Ciencias de la Tierra (LEC-IACT), Avda. Las Palmeras, nº 4. Armilla, Granada 18100, Spain

e-mail: jmdl@lec.csic.es

Calcium orthophosphates have a special interest in biomineralization and biomedical fields because of their presence in mineralized tissues of mammals and their wide variety of applications [1] ranging from biomimetic bone graft and tissue regeneration to carrier matrices of drugs and proteins. Among them, hydroxyapatite ($Ca_5(PO_4)_3(OH)$, HA), the thermodynamically most stable under physiological conditions, represents a model compound of the inorganic constituent of bones, teeth and many pathological calcifications [2]. Bone apatites are non-stoichiometric calcium and OH deficient nanosized crystals doped with carbonate (4–6 w/w%) and different foreign ions such as Na (0.9%) and Mg (0.5%).[2] Other phases such as dicalcium phosphate dihydrate ($CaHPO_4.2H_2O$, brushite, DCPD) and octacalcium phosphate ($Ca_8H_2(PO_4)_6.5H_2O$, OCP) are usually found in more acidic solutions [3]. In recent years, a huge number of studies on the crystallization process of these compounds have been carried out in order to analyse the mechanisms of precipitation and stability of each calcium phosphate (CaP) phase [4]. DCPD and OCP have been suggested as possible metastable precursors in the formation of apatite. This may occur by the precipitation of DCDP and/or OCP followed by its transformation to a more apatite phase.

We have studied the evolution of calcium phosphate precipitation by hanging drop vapor diffusion using the "*crystallization mushroom*" [5]. The hanged drops initially contained mixed solutions of $Ca(CH_3COO)_2$ and $(NH_4)_2HPO_4$. The diffusion of CO_2 and NH_3 gases released from NH_4HCO_3 solutions (located in the lower chamber of the device) at different concentrations (30 mM, 100 mM and 2 M) produced a gradual increase of the drop pH. The pH increase rate as well as the final pH strongly depends on the NH_4HCO_3 concentration. The evolution of the calcium phosphate precipitation was followed *in-situ* by confocal Raman microspectroscopy.Time-dependent in situ Raman spectra indicated that amorphous calcium phosphate (ACP) was the first precipitate appearing just after mixing the Ca- and PO_4-containing solutions. It transformed to dicalcium phosphate dihydrate (DCPD) a few minutes later. The lifetime of DCPD strongly depends on the concentration of the NH_4HCO_3 solutions and thus on the pH increase rate. The pathway for the phase transformation from ACP to DCPD and then to octacalcium phosphate (OCP) followed a

dissolution–reprecipitation mechanism. The precipitates obtained after 7 days of vapor diffusion also depends on the NH_4HCO_3 concentration. At lower concentrations (30 and 100 mM), OCP, micrometric HA and nanosized HA was obtained. OCP played the role as temporal template for the heterogeneous nucleation and crystallization of biomimetic carbonate–apatite nanocrystals. In contrast, working with the highest NH_4HCO_3 concentration the system evolved to the precipitation of elongated calcite crystals.

Acknowledgements. Financial support from Spanish MINECO (Projects MAT2011-28543 and Consolider-Ingenio 2010, Factoría de Cristalización) and CEI-BioTic (UGR) is greatly acknowledged.

References

[1] Dorozhkin S. Calcium Orthophosphates in Nature, Biology and Medicine. Materials 2009;2:399-498.

[2] Mann S. Biomineralization: principles and concepts in bioinorganic materials chemistry. Oxford: University Press; 2001.

[3] Johnsson MS-A, Nancollas GH. The Role of Brushite and Octacalcium Phosphate in Apatite Formation. Crit Rev Oral Biol Med 1992;3:61-82.

[4] Gómez-Morales J, Iafisco M, Delgado-López JM, Sarda S, Drouet C. Progress on the preparation of nanocrystalline apatites and surface characterization: Overview of fundamental and applied aspects. Prog Cryst Growth Ch 2013;59:1-46.

[5] Ramirez-Rodriguez GB, Delgado-Lopez JM, Gomez-Morales J. Evolution of calcium phosphate precipitation in hanging drop vapor diffusion by in situ Raman microspectroscopy. CrystEngComm 2013;15:2206-12.

12:30 Oral

Highlighting the role of citrate on the crystallization mechanism of nanocrystalline bio-apatites

Jaime Gómez-Morales[1], José Manuel Delgado López[1], Francisco Javier Martínez Casado[1], Gloria Belén Ramírez-Rodríguez[1], Michele Iafisco[2], Anna Tampieri[2], Maria Prat[3], Antonella Guagliardi[4]

1. *Instituto Andaluz de Ciencias de la Tierra (LEC-IACT), Avda. Las Palmeras, nº 4. Armilla, Granada 18100, Spain* **2.** *CNR-ISTEC, Institute of Science and Technology for Ceramics, Via Granarolo 64, Faenza 48018, Italy* **3.** *Università del Piemonte Orientale. Dip di Scienze della Salute, Via Solaroli 17, Novara 28100, Italy* **4.** *CNR, Istituto di Cristallografia, via Lucini 3, Como 22100, Italy*

e-mail: jaime@lec.csic.es

Nanocrystalline carbonate apatites constitute the main inorganic part of bone tissue, and a growing focus is devoted to prepare synthetic analogs, so-called "biomimetic", able to precisely mimic the morphological and physico-chemical features of bone apatite for new applications in nanomedicine [1,2]. The organic fraction is basically composed of type-I collagen, non-collagenous proteins (NCPs) and small molecules such as citrate, which represents around 5.5 wt% of the total organic matrix and has been found strongly bound to the nanocrystals [3]. Recent advances in the control of crystal growth of nanocrystalline apatites are related to the use of this additive [4]. The use of citrate in the production of synthetic nanoapatites will improve their biomimetism and, in addition, will increase the knowledge of its role in bone mineralization, which has been traditionally neglected. In this work we report recent advances of our laboratory in the preparation of nanocrystalline citrate functionalized apatite nanoparticles by decomplexing of metastable calcium/metal/citrate/carbonate/phosphate solutions including new insights on their formation mechanisms, and its relevance in apatite formation during bone mineralization. This method allowed us to tailor the carbonate and metal content, particle size and stability of the colloidal dispersions. In addition, the potential use of these citrate-functionalized nanoparticles as nanocarriers for pH-responsive drug delivery (doxorubicin) is under study.

Acknowledgements. Financial support from Spanish MINECO (projects MAT2011-28543 and Consolider-Ingenio 2010, Factoría de Cristalización) and CEI-BioTic (UGR) is greatly acknowledged.

References:

[1] J. Gómez-Morales, M. Iafisco, J. M. Delgado-López, S. Sarda, C. Drouet, Prog. Cryst Growth Char. Mater. 59 (2013) 1–46. [2] M. Iafisco, J.M. Delgado-López, E. Varoni, A. Tampieri, L. Rimondini, J. Gomez-Morales, M. Prat, Small (2013). In press. doi: 10.1002/smll.201202843.[3] Hu YY, Rawal A, Schmidt-Rohr K. Proc Natl Acad Sci USA 2010; 107:22425–9. [4] J.M. Delgado-López, M. Iafisco, I. Rodríguez Ruiz, A. Tampieri, M. Prat, J. Gómez-Morales. Acta Biomaterialia. 8 (2012) 3491–3499

12:45 Oral

The optimization of solution flow rate producing high-quality and large protein crystals

Yuki Hayashi[1], Mihoko Maruyama[1], Satoshi Nakayama[1], Yoshinori Takahashi[1], Hiroshi Yoshikawa[2], Masashi Yoshimura[1], Masaru Tachibana[3], Haruhiko Koizumi[4], Sigeru Sugiyama[5], Hiroaki Adachi[1,6], Kazufumi Takano[6,7], Satoshi Murakami[6,8], Hiroyoshi Matsumura[1,6], Tsuyoshi Inoue[1,6], Yusuke Mori[1,6]

1. *Graduated School of Engineering, Osaka University (OSAKAUNIV), Osaka, Japan* **2.** *Saitama University, 255 Shimo-ookubo, Sakuraku, Saitama 338-8570, Japan* **3.** *Graduate School of Nanobioscience, Yokohama City University, Yokohama 236-0027, Japan* **4.** *Institute for Materials Research, Tohoku University, Sendai 980-8577, Japan* **5.** *Graduate School of Science, Osaka University, Osaka 565-0871, Japan* **6.** *SOSHO Inc., Osaka 565-0871, Japan* **7.** *Kyoto Prefectural University, Kyoto 606-0823, Japan* **8.** *Tokyo Institute of Technology, Tokyo 152-8550, Japan*

e-mail: hayashi@cryst.eei.eng.osaka-u.ac.jp

Large protein crystals with high-quality are essential for determining the three-dimensional structure of proteins by X-ray diffraction measurement and neutron diffraction measurement. We have developed the top-seeded solution growth with the floating and solution-stirring technique (TSSG-FAST)[1] and succeeded to grow crystals of HIV-1 protease suitable for neutron diffraction measurement (Fig. 1). Using these crystals, structual information about the H atoms of HIV-1 protease was successfully determined. TSSG-FAST is an efficient technique for producing high-quality and large protein crystals. To make the technique highly-developed, we studied the correlation of the growth rate and the quality with the solution flow rate, and decided the best flow rate for growing high-quality and large crystals of proteins.

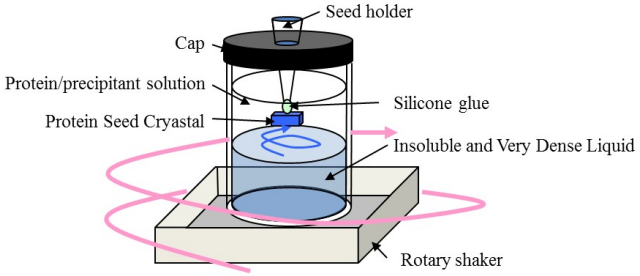

Fig. 1 Schematic illustration of the crystallization setup for TSSG-FAST

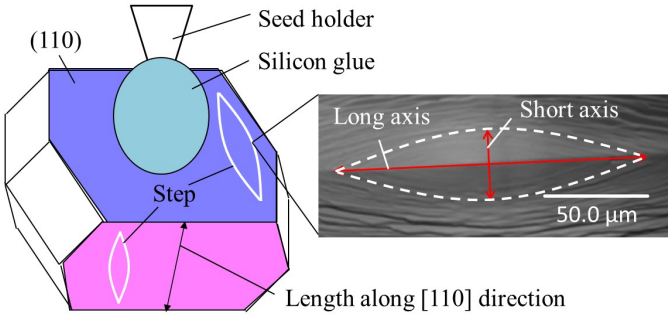

Fig. 2 Schematic illustration of the HEWL and the morphology of spiral growth hillock

Crystals of hen egg-white lysozyme (HEWL) were grown by the TSSG-FAST under various solution flow rates, which were determined by flow analysis. Growth rate of (110) face was obtained by observing the lengths along [110] direction at the starting and the ending day (Fig. 2). We also observed the morphology of spiral growth hillocks on {110} faces by laser confocal microscopy combined with differential interference contrast microscopy (LCM-DIM). The morphology is affected by impurities and the aspect ratio (long to short axes) of steps can be used as a measure of impurity effects (Fig. 2).[2] At the flow rate of 0 µm/sec, growth rate of (110) face was 0.2 µm/h and the aspect ratio of long to short axes was 4.1 ± 0.3 (Fig. 3). With increasing the flow rate, the both increased and had the maximum at the flow rate of 140 µm/sec, and then decreased. This result showed that there exists the best solution flow range, and solution flow faster than 140 µm/sec is not suitable for protein crystal growth. We consider that this result can be explained by the competition between the mass transfer of solutes and the inhibition effect of the impurities.[3]

Crystal defects (especially dislocations) in the HEWL crystal grown by the TSSG-FAST at the flow rate of 8 µm/sec were investigated by synchrotron monochromatic-beam X-ray topography (Fig. 4). The dislocation density of the crystal grown by TSSG-FAST was 10^1 ~ 10^2 cm^{-2}, which was lower than the dislocation density of a crystal grown by non-stirring technique.[4] This result shows that the TSSG-FAST have high possibility to reduce dislocations in crystals. As a result, we suggest that the TSSG-FAST can produce high-quality and large crystal of protein, especially at the flow rate lower than 140 µm/sec.

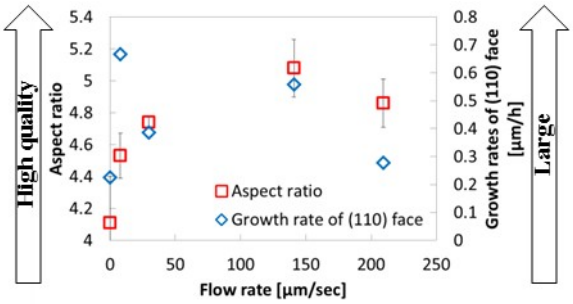

Fig. 3 Aspect ratio and Growth rates of (110) face as a function of the flow rate

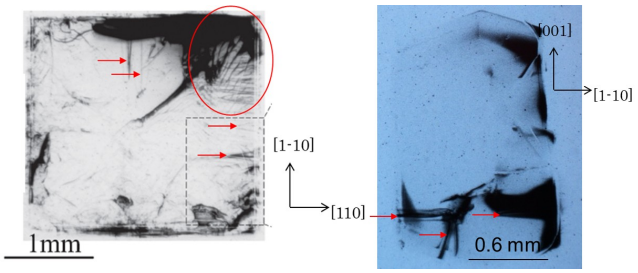

Fig. 4 Synchrotron monochromatic-beam X-ray topography (a)without stirring (b)TSSG-FAST

Reference

1) N.Shimizu, et al., Cryst. Growth Des. 10 (2010) 2990.
2) P. Dold, et al., J. Cryst. Growth 293 (2006) 102.
3) M. Maruyama, et al., Cryst. Growth Des. 12 (2012) 2856.
4) Y. Mukobayashi, et al., Phys. Status Solidi A206 (2009) 1825.

Lunch (JCG Editors meeting)

Monday afternoon, 12 August, 13:00

MoO2

G03: Biological and Biogenic Crystallization
Monday afternoon, 12 August, 15:00
Room B, Auditorium Maximum

15:00 Invited oral

Synthetic analogues of biomineralized materials

André R. Studart

ETH Zurich, Wolfgang-Pauli-Str. 10, Zurich 8093, Switzerland

e-mail: andre.studart@mat.ethz.ch

Biomineralized materials like seashells, teeth and bone often comprise of a soft organic matrix and hard reinforcing building blocks assembled into unique hierarchical architectures. The ubiquitous micro- and nanostructures of such natural materials lead to outstanding functional properties and find no counterparts within man-made composites. In this talk, I will present our recent attempts to replicate in artificial materials some of the unique architecture and design principles of biomineralized hybrid materials. First, I will show a new approach to obtain polymer-based composites exhibiting bioinspired deliberate orientation of reinforcing particles using ultra-low magnetic fields. The ability to control the position and orientation of reinforcing particles within a polymer matrix leads to heterogeneous structures with unusual out-of-plane stiffness, wear resistance and shape-memory effects. In the second part of the talk, I will show that an elastomeric polyurethane matrix can be hierarchically reinforced with nano- and microplatelets to form bioinspired hybrid materials with local elastic modulus varying up to five orders of magnitude. Control over the local reinforcement level enables the creation of polymeric substrates that can be stretched several times its initial length, while keeping the local strain on specific surface sites lower than 1%. Alike their biomineralized natural counterparts, the unusual mechanical properties achieved in these synthetic examples illustrate the great potential of nano- and microstructuring in creating bioinspired hybrid materials with rich functional behavior using a limited set of building blocks.

15:30 Invited oral

Nanocrystalline apatites analogous to bone mineral: review of surface state and derived interfacial behaviors

Christophe Drouet, David Grossin, Christele Combes, Christian Rey

CIRIMAT Carnot Institute, 4 allee Emile Monso, Toulouse 31030, France

e-mail: christophe.drouet@ensiacet.fr

Biomimetic nanocrystalline apatites are major candidates for biomedical applications including bone tissue engineering due to their high analogy to bone mineral. In particular, as for biological apatites, synthetic biomimetic analogs exhibit a structured but metastable non-apatitic surface layer which is at the origin of the exceptional reactivity of these compounds. This reactivity can be exploited for example by functionalizing the surface of apatite nanocrystals with drugs and biomolecules or interest in view of various biomedical applications, or by incorporating biologically-active ions within the apatite lattice, thus conveying new properties, or else for "low" temperature consolidation (typically in the range RT - 300°C).

In the last decade, significant advances have been made in the fine characterization of apatite nanocrystals (whether of biological or synthetic origins), enabling one to better understand the behavior of apatite nanocrystals when placed in varying conditions (upon drying, when re-immersed in aqueous media, ...) as well as biomineralization phenomena. Also interfacial events involving nanocrystalline apatites are bound to be directly related to their surface peculiarities (presence of a non-apatitic hydrated layer on the surface of the nanocrystals).

In this contribution, we will recall the specific surface state of biomimetic apatites which is at the origin of their very peculiar reactivity, and we will then overview the main interfacial aspects of interest in view of biomedical applications.

C. Drouet's brief biography:

http://science24.com/resources/paper/28802/0_Christophe_Drouet.doc

16:00 Oral

A controlled gradual desiccation strategy for improving the efficiency of protein crystallization screening

Qin-Qin Lu, Xu-Zhuo Xie, Rui-Qing Chen, Zi-Qing Wu, Da-Chuan Yin

Northwestern Polytechnical University, Xi'an 710072, China

e-mail: luqinqin@nwpu.edu.cn

It has been reported that a modification to the vapor diffusion technique, in which desiccant was used instead of reservoir solution to absorb the solvent evaporated from the protein crystallization droplets, increased the protein crystallization screening success rate. However, because the optimal amount of desiccant for a specific crystallization attempt is unknown, this desiccation method (one-time desiccation method) is not easy to apply broadly.

To solve this problem, we propose a further modification to the one-time desiccation method. We perform multiple desiccations (i.e., repeat the desiccation procedure more than once) until the droplets are dried out, so that the crystallization droplets can achieve a large concentration range. Compared with the one-time desiccation method, the gradual desiccation method (GDM) showed a higher crystallization screening success rate. In this report, the experimental results of crystallization using the GDM were discussed.

16:15 Oral

Polymorphism control of pharmaceutical compound acetaminophen by ultrasonic irradiation

Yoichiro Mori[1], Yoshinori Takahashi[1,2], Kenji Ikeda[1], Toshihiko Yamada[1], Ken Nishimura[1], Mihoko Maruyama[1], Hiroshi Yoshikawa[1,3], Shino Okada[2], Hiroaki Adachi[1,2], Shigeru Sugiyama[4], Hiroyoshi Matsumura[1,2], Kazuhumi Takano[2,5], Tsuyoshi Inoue[1,2], Satoshi Murakami[2,6], Masashi Yoshimura[1], Yusuke Mori[1,2]

1. *Graduated School of Engineering, Osaka University (OSAKAUNIV), Osaka, Japan* **2.** *SOSHO Inc., Osaka 565-0871, Japan* **3.** *Saitama University, 255 Shimo-ookubo, Sakuraku, Saitama 338-8570, Japan* **4.** *Graduate School of Science, Osaka University, Osaka 565-0871, Japan* **5.** *Kyoto Prefectural University, Kyoto 606-0823, Japan* **6.** *Tokyo Institute of Technology, Tokyo 152-8550, Japan*

e-mail: ymori@cryst.eei.eng.osaka-u.ac.jp

Polymorphs are solid phases in which the chemical composition is equal but the crystal structure differs. In the pharmaceutical industry, especially, most of compounds have polymorphs, and polymorphism control is very important because different polymorphs exhibit different stabilities, drug effects, formation properties, etc. Acetaminophen (Figure 1), which is one of the typical pharmaceutical compounds, has three known polymorphs, numbered I, II and III. The stable form I is the commercially used form because of its stability. In contrast, the metastable form II has been shown to be more soluble and more readily compressible into tablets than form I, and controlled crystallization of the form II is an important issue for practical use. Hence we attempted to control polymorphism of acetaminophen form II by ultrasonic irradiation in this study.

Acetaminophen aqueous solutions (32 mg/ml, total 50 bottles) were prepared, cooled to 0°C at a constant cooling rate (3°C/h), maintained at that temperature for about 2 days, and irradiated with ultrasound with different frequencies (no irradiation, 28, 45, 100 kHz) for investigating the effect of crystallization and polymorphism control. Figure 2 shows the probability of nucleation and form II crystallization on each condition. In the cases of no irradiation and 100 kHz irradiation, nucleation did not occur in solutions (no irradiation: 0/20 (0%), 100 kHz: 0/10 (0%)). In contrast, ultrasonic irradiation with the frequency of 28 or 45 kHz promoted the nucleation (28 kHz: 9/9 (100%), 45 kHz: 10/10 (100%)), and also increased probability of the form II crystallization as shown in Figure 2 (28 kHz: 6/9 (67%), 45 kHz: 6/10 (60%)).

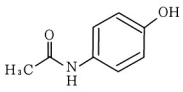

Fig. 1. Structural formula of acetaminophen

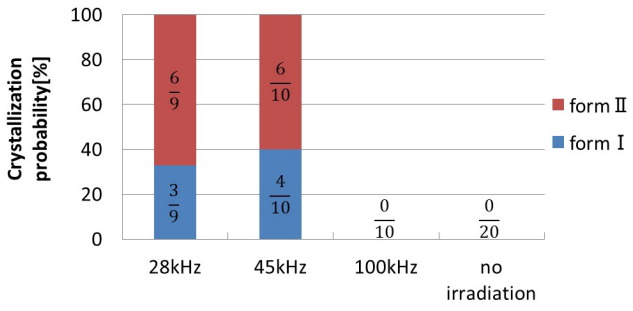

Fig. 2. Frequency dependence of crystallization probability

16:30 Oral

Improvement of femtosecond laser-induced nucleation technique for proteins: Studies of effect of gel-solution interface

Satoshi Nakayama[1], Hiroshi Yoshikawa[1,2], Yusuke Aoki[1], Masateru Kurata[1], Ryota Murai[1,3], Mihoko Maruyama[1], Yoshinori Takahashi[1], Masashi Yoshimura[1], Sigeru Sugiyama[4], Hiroaki Adachi[1,5], Kazufumi Takano[5,6], Satoshi Murakami[5,7], Hiroyoshi Matsumura[1,5], Tsuyoshi Inoue[1,5], Yusuke Mori[1,5]

1. *Graduated School of Engineering, Osaka University (OSAKAUNIV), Osaka, Japan* **2.** *Saitama University, 255 Shimo-ookubo, Sakuraku, Saitama 338-8570, Japan* **3.** *Kyoto University, Kyoto 606-8501, Japan* **4.** *Graduate School of Science, Osaka University, Osaka 565-0871, Japan* **5.** *SOSHO Inc., Osaka 565-0871, Japan* **6.** *Kyoto Prefectural University, Kyoto 606-0823, Japan* **7.** *Tokyo Institute of Technology, Tokyo 152-8550, Japan*

e-mail: snakayama@cryst.eei.eng.osaka-u.ac.jp

High-quality single crystals of protein are indispensable for determining the three-dimensional structure of protein by X-ray crystallography. However, the production of such high-quality protein crystals is still challenging because nucleation of proteins generally occurs at very high supersaturation. We previously reported a novel technique to induce nucleation at low supersaturation by focused femtosecond laser irradiation and obtained high-quality protein crystals of various proteins.[1)] We revealed that laser-induced cavitation bubbles transiently and locally concentrate a supersaturated solution.[2)] We are now investigating the detailed correlation between cavitation bubble behavior and protein nucleation.[3)] In this study, we studied the effect of gel-solution interfaces on the femtosecond laser-induced nucleation of proteins.

Supersaturated solutions of hen egg white lysozyme (HEWL) were pipetted onto agarose gel and irradiated with femtosecond laser pulses (800 nm, 200 fs). We found that the nucleation efficiency could be modulated by the distance between the laser focus and agarose gel surfaces (h). In particular, laser irradiation near the gel surface (h = 50 mm) could induce nucleation at very low supersaturation, where no nucleation could be induced in the bulk solutions even with femtosecond laser irradiation (h = 200 mm) (Fig. 1). Such enhancement of the nucleation was also confirmed for the membrane protein, acriflavine resistance protein B (AcrB). To gain further insights into the role of gel-solution interfaces, we conducted fast imaging of cavitation bubbles. We found that the cavitation bubbles shrank asymmetrically and then finally collapsed toward the solution side (Fig. 2b, h = 50 mm). This is in contrast to the symmetric collapse in bulk solutions (Fig. 2a, h = 200 mm), which generates a large amount heat and chemical decomposition at the focus[4)]. In addition, cavitation bubble behavior could be modulated by the gel concentration. These results indicate that the use of gel-solution interfaces is a successful method for the control of cavitation bubbles and can be cues to achieve effective nucleation. In this presentation, we will also discuss the correlation between the gel concentration and nucleation efficiency.

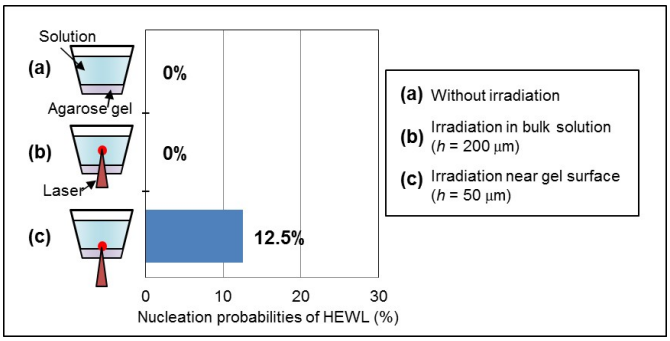

Fig. 1. Nucleation probabilities for HEWL on agarose gel.

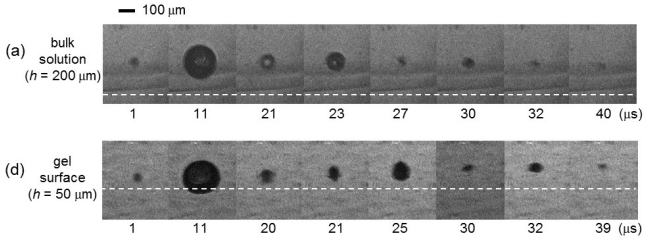

Fig. 2. Microscopic fast imaging of cavitation bubbles.

Reference
1) H. Adachi et al., Jpn. J. Appl. Phys. 42 (2003) L798.
2) H. Y. Yoshikawa et al., J. Cryst. Growth 311 (2009) 956.
3) S. Nakayama et al., Cryst. Growth Des 13 (2013) 1491.
4) K. S. Suslick et al., Annu. Rev. Mater. Sci. 29 (1999) 295.

16:45 Oral

Gelatin hydrogel porosity and crystallization of $CaCO_3$ phases and mesocrystals

Fitriana Nindiyasari[1], Lurdes Fernández-díaz[2], Erika Griesshaber[1], José Manuel Astilleros[2], Nuria Sánchez-Pastor[2], Wolfgang W. Schmahl[1]

1. *LM Universitaet, Institut, fuer Kristallographie, Munich, Germany* **2.** *Universidad Complutense de Madrid, Avda. de la Complutense s/n, Madrid 28040, Spain*

e-mail: f.nindiyasari@lmu.de

The influence of the porosity of the growth medium on the crystallization of calcite ($CaCO_3$) was explored using gelatin hydrogels with different solid contents in a counter diffusion arrangement. Increasing gelatin solid content resulted in decreasing pore sizes and more complex porosity structure in the hydrogel as seen by SEM after freeze drying. The changes in the porosity features affected the characteristics of calcite crystals, which showed smaller sizes, progressively rougher surfaces and a higher tendency to grow as aggregates rather than as single crystals as the gelatin content in the hydrogel increased. Moreover, the close observation of the calcite crystals grown in hydrogels with higher solid contents evidenced that they were mesocrystals built up by slightly misoriented rhombohedral subunits with sizes ranging between 1 and 10 μm (Fig. 1). The incorporation of small amounts of gelatin in the calcite mesocrystals was confirmed combining Raman spectroscopy and thermogravimetric analyses (TGA). The differences in the characteristics of the calcite formed in hydrogels with different gelatin contents are discussed considering the relationships between hydrogel porosity, diffusivity and supersaturation conditions during growth.

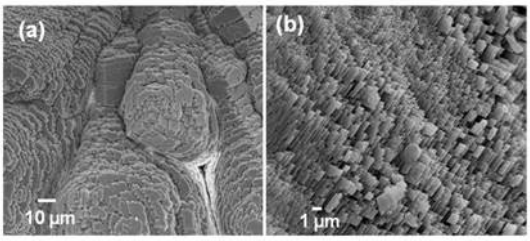

Figure 1. SEM images of **(a)** crystal growing in 10 wt% gelatin and **(b)** rhombohedral subunit building the calcite crystals.

MoP-G03
Monday afternoon, 12 August, 17:00
Room 205, Old Library

Break
Monday evening, 12 August, 18:30

Wednesday, 14 August

WeO1

G03: Biological and Biogenic Crystallization
Wednesday morning, 14 August, 10:20
Room B, Auditorium Maximum

10:20 Invited oral

The role of prenucleation clusters during (bio)mineral nucleation

Denis Gebauer

Universität Konstanz, Universitätsstr. 10, Konstanz 78457, Germany

e-mail: denis.gebauer@uni-konstanz.de

Recent work has highlighted the relevance of so-called prenucleation clusters during the nucleation of biominerals *in vitro* (1, 2). These stable ion clusters form in solution prior to nucleation, and the initial precipitation of amorphous nanoparticles appears to proceed *via* aggregation of the prenucleation clusters. In case of calcium carbonate, the processes lead to the development of distinct short-range structural features in amorphous intermediates (3). The distinct amorphous forms can be considered within the physical notion of amorphous polymorphism (polyamorphism), which is also observed in biomineralization, and may form the basis of polymorph selection (4).

The present contribution will summarize the notion of the prenucleation cluster pathway outlined above, paying special attention to most recent developments. *Inter alia*, this includes the physicochemical characterization of the multiple roles of different organic additives, which are relevant for biomineralization, during the early stages of precipitation.

1. D. Gebauer, A. Völkel, H. Cölfen, *Science***322**, 1819 (2008).

2. D. Gebauer, H. Cölfen, *Nano Today***6**, 564 (2011).

3. D. Gebauer, P. N. Gunawidjaja, J. Y. P. Ko, Z. Bacsik, B. Aziz, L. J. Liu, Y. F. Hu, L. Bergström, C.-W. Tai, T.-K. Sham, M. Edén, N. Hedin, *Angew. Chem. Int. Ed.* **49**, 8889 (2010).

4. J. H. E. Cartwright, A. G. Checa, J. D. Gale, D. Gebauer, C. I. Sainz-Díaz, *Angew. Chem. Int. Ed.* **51**, 11960 (2012).

10:50 Oral

Towards a better understanding of the nucleation behavior of α and γ polymorphs of glycine from aqueous solution in the presence of selective additives by charge compensation mechanism

Renuka Devi Krishnaraj, Srinivasan Karuppannan

Bharathiar University, Marudhamalai,Coimbatore, Coimbatore 641046, India

e-mail: nivas_5@yahoo.com

Polymorphism is the unique phenomenon by which a pure chemical compound can exist in more than one structural orientation, with different physical characteristics. This mere existence of disparity in physical properties among the polymorphs of the same material prompts the main essentiality to control and isolate the polymorphs at the level of nucleation for specified applications. In this regard, a thorough knowledge of the nucleation behavior of the polymorphs at different environmental circumstances is highly essential. Glycine, the organic molecule exists in three different polymorphic forms α, β and γ at ambient conditions. Existence of these three polymorphs is due to the difference in the stacking of the molecules which exist in the zwitterionic form in aqueous solution. This difference in stacking is mainly due of the lack or excess of certain electrostatic forces between the ionic charges in the solution. This deficiency of the necessary energy to withstand as a single molecule leads the molecular species in the solution to depend on their neighboring molecules for such charge compensation to ensure their stability and this is known as self-charge compensation. They pack as parallel dimers bilayer which is the preferable configuration of α polymorph and leads to their spontaneous nucleation in the solution. These bilayers are formed by strong NH….O hydrogen bonding interactions between cyclic hydrogen bonded zwitterionic dimers and these bilayers are packed by van der Waals interactions. When certain external force / parameters can overcome this situation then a good control over the nucleation behavior can be achieved. This deficient energy when supplied by some external force leads to a way to alter the configuration of molecules in the solution. This external force / parameter must be capable of overcoming the huge barrier / activation energy that prevents the singular existence of molecules with at most stability. This would finally lead to the monomeric existence of molecules in the solution which favors the β and γ forms of glycine. In the γ polymorph the dominating feature of the intermolecular packing is the hydrogen bonding between amino nitrogen and carboxyl oxygen atoms which links the molecule into helical chains about the threefold screw axis parallel to the c-axis. These chains are packed by lateral hydrogen bonding of monomers forming a three dimensional network of hydrogen bonds. In this paper the external forces are chosen to be sodium nitrate and sodium hydroxide. The nucleation behavior of the α and γ polymorphs of glycine in the presence of these two induced charge compensators has been investigated and explained based on the concept of charge compensation mechanism. This concept explains the mechanism behind the nucleation of polymorphs in the presence of sufficient externally added charged species which induce the required nucleation through charge compensation. In-situ micro droplet evaporation as well as slow evaporation has been applied as the appropriate methods to carry on this investigation. The induced charge compensators sodium nitrate (ICCsn) in the concentration range from 0.16 to 13.07 mole% and sodium hydroxide (ICCsh) in the concentration range from 0.13 to 3.19 mole% were used for these experiments. The added externally charged ions overcome the self-charge compensation and this is presented evidently through the variation in solubility, pH, polymorphic nucleation and morphology of the nucleated

polymorphs. The solubility of glycine aqueous solution increases from 34.68 to 101.03 g/100ml with ICCsn concentration and from 33.10 to 88.19 g/100ml with ICCsh concentration. This in turn alters the supersaturation of the solution which increases from 0.33 to 2.89 with ICCsn and from 0.02 to 1.73 with ICCsh concentrations. The pH increases from 6.05 to 6.99 and from 7.95 to 10.47 with ICCsn and ICCsh concentrations respectively. The ionic strength of the solution increases from 131.25 to 205.17 and from 127.19 to 169.91 mol L^{-1} with ICCsn and ICCsh concentrations. In the case of sodium nitrate, 100%α is observed up to 5.52 mole %. At the next concentration of 6.26 mole% γ nucleation appears with theα form. With further increase in the concentration of ICCsn the number of α decreases from 100 to 1% and γ increases from 17 to 99% at the final concentration of 13.07 mole %. In the case of sodium hydroxide, 100% α is observed up to 0.27 mole% and at the next concentration of 0.34 mole% γ appears along with the α form. With further increase in ICCsh concentration, the number of α decreases and γ increases. This proportionate appearance of the nucleated polymorphs shows that the self-charge compensation which was dominant up to 5.52 mole % in case of ICCsn and up to 0.27 mole % in case of ICCsh is overcome by induced charge compensation of additive ions at 6.26 mole% and 0.34 mole% respectively. The form of crystallization and the proportionate appearance of the nucleated polymorphs are confirmed by powder x-ray diffraction.

11:05 Oral

Synthesis of Fluorescent Gels of Gold made using Proteins

Radha Perumal Ramasamy[1], Shihabudeen M. Maliyekkal[2]

1. *Anna University, Department of Applied Science and Technology, ACT campus (ACT), Chennai 600 025, India* **2.** *VIT University,School of Mechanical and Building Sciences, Chennai Campus (VIT), Chennai 600 127, India*

e-mail: perumal.ramasamy@gmail.com

Gels are interesting class of materials that comprise of three dimensional networks swollen by large amount of solvent. In their rheological characteristics their storage modulus is lower than their loss modulus. They have solid like behavior in macroscopic scale and liquid like behavior in microscopic scales. They are classified as physical gels and chemical gels. Physical gels result due to formation of aggregates while chemical gels are formed due to covalent bonds. Gels have several applications that include biotechnology, micro fluidics and lab on a chip. In this research, gels were made using BSA. BSA is a globular protein. The presence of aminoacids like lysine can provide active sites on the surface of BSA for the formation of nanoparticles. Here solutions containing different concentrations of BSA were mixed with $HAuCl_4$ of concentration 5mM. To this NaOH was added to have a final concentration of 250mM NaOH. It was observed that for concentration of $HAuCl_4$ greater than 50 mg/ml, gels were formed. The gels were found to be fluorescent. Their photoluminescence properties were measured and emission peak was observed at 700 nm. Their rheological behavior was also examined. Interestingly, the gels were found to collapse after a while. SEM analysis showed that the solutions containing BSA of concentration 25 mg/ml had nanoparticles in it. In time all the samples became brown in color indicating the formation of nanoparticles.The formation and the collapse of the gel is attributed to the formation of nanoparticles and the subsequent weakening of the chitosan-chitosan bond due to the nanoparticles. The secondary structural modifications were characterized using FTIR spectroscopy and it was observed that as the concentration of the proteins decreased the second derivative peak shifted to position for random coil (1640 cm^{-1}). This indicates that the structure of the protein changes from helical to random coil as the nanoparticles form. XRD analysis was also done on the samples. A model is proposed for the formation of the fluorescent gels.

11:20 Oral

In situ observations of impurity effects during protein crystal growth

Mike Sleutel[1], Dominique Maes[1], Alexander E. Van Driessche[2]

1. *Vrije Universiteit Brussel (VUB), Brussels 1050, Belgium* **2.** *Instituto Andaluz de Ciencias de la Tierra, CSIC-UGR (LEC-IACT), Avda. Las Palmeras, nº 4, Granada 18100, Spain*

e-mail: mike.sleutel@gmail.com

Laser confocal microscopy combined with differential interference contrast microscopy (LCM-DIM) has emerged as one of the most powerful mesoscopic techniques for in situ observation of the protein crystal-liquid interface. We employ this technique to visualize non-invasively the surface topography of protein crystals that are in non-equilibrium with the surrounding mother liquor. From snapshots of growing crystals the dominating growth mechanisms are determined. Subsequent time-lapse imaging of a single observation area is then used for the study of growth and/or dissolution dynamics in response to the system's super/undersaturation. From the kinetics of elementary steps growing from high purity solutions, fundamental kinetics coefficients are determined. These measurements then serve as a benchmark for further studies of crystal growth kinetics in impure conditions. Two topics in particular will be highlighted. First, the concept of time-dependent impurity uptake will be discussed. Different growth mechanisms expose the crystal surface to the surrounding bulk liquid with varying characteristic times, coined the terrace exposure times. The ratio of the terrace exposure time with the characteristic time for impurity adsorption onto the crystal surface is put forward as an intrinsic constant that governs impurity incorporation. This model is then applied to the two main crystal growth mechanisms, i.e. spiral dislocations and two-dimensional nucleation, and differences will be commented upon.

11:35 Oral

Complete deracemisation of proteinogenic amino acids using Viedma ripening

Laura Spix, Hugo Meekes, Willem J. Van Enckevoort, Elias Vlieg

Radboud University Nijmegen, Heyendaalseweg 135, Nijmegen 6525AJ, Netherlands

e-mail: l.spix@science.ru.nl

Viedma ripening is a deracemisation method in which crystals in a saturated solution are vigorously ground and the chiral molecules are simultaneously racemised in the solution.[1] This leads to an enantiomerically pure solid state if the chiral molecules crystallize as a conglomerate. A conglomerate is equal to a mechanical mixture of pure (R) and (S) crystals. Unfortunately 90 % of the organic crystals form a racemic compound in which molecules of both handedness are present in the unit cell.[2] Hence they cannot be deracemised using Viedma ripening. We will present here two methods that allow a complete deracemisation on intrinsically racemic compound forming proteinogenic amino acids.

In the first case we make use of Ostwald's rule of stages (thermodynamically unstable phases appear first followed by recrystallisation to the thermodynamically stable phase). Glutamic acid forms a stable racemic compound.[3] Under well chosen experimental conditions a

metastable conglomerate is obtained and its stability is sufficient to enable a complete deracemisation.[4]

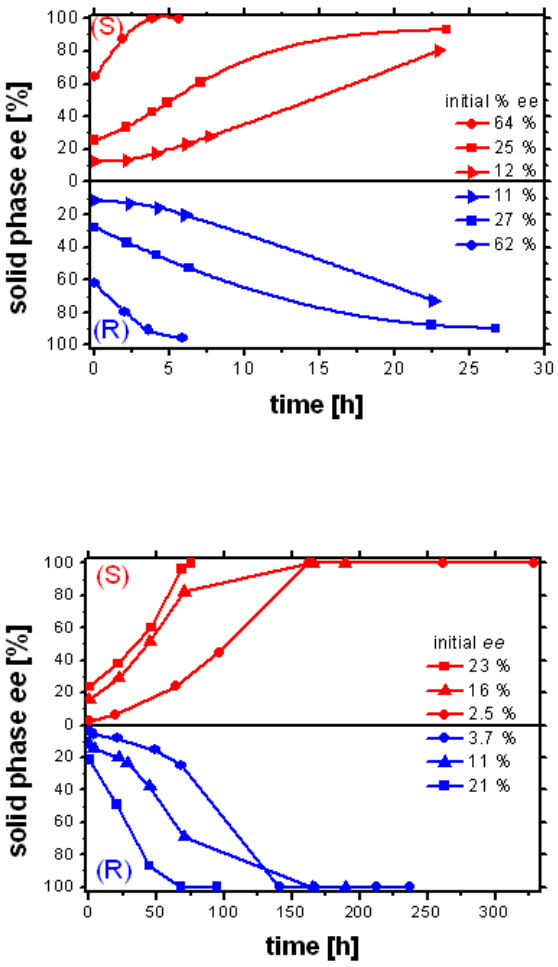

Figure 1: Attrition-enhanced evolution of solid-phase *ee* for Glutamic acid at 90 °C (upper) and Alanine 4-chlorobenzenesulfonate (Ala-CBS) at 70 °C. (lower) starting from initial values of the *ee* as shown.

In the second case a conversion into a salt is used. Alanine crystallizes in a 3D network structure as a stable racemic compound. Transformation into a 4-chlorobenzenesulfonate leads to a conglomerate with a layered structure.[5] The sulfonate conglomerate enables a complete deracemisation.

The enantiomerically pure final state has in both cases (Glu and Ala-CBS) a limited life time when left in the slurry. Glutamic acid transforms after a certain time into the most stable crystal structure which is a racemic compound and returns to a racemic state under deracemisation conditions. The alanine salt shows a different behavior. Sometimes the enantiomeric excess of the solid phase decreases after having reached 100 %. The epitaxial growth of the crystals could be the reason for this effect. (see picture 1)

picture 1: Etching experiment of an Ala-CBS crystal in a saturated solution of L-Ala-CBS (under the polarisation microscope)

[1] a)C. Viedma, *Phys. Rev. Lett.***2005**, *94*, 065504; b)W. L. Noorduin, T. Izumi, A. Millemaggi, M. Leeman, H. Meekes, W. J. P. Van Enckevort, R. M. Kellogg, B. Kaptein, E. Vlieg, D. G. Blackmond, *J. Am.Chem. Soc.***2008**, *130*, 1158; c)S. Yamada, C. Hongo, R. Yoshioka, I. Chibata, *J. Org. Chem.***1983**, *48*, 843.

[2] A. C. Jean Jacques, Samuel H. Wilen, *Enantiomers, Racemates, and Resolutions*, Krieger, Malabar, Florida, **1994**.

[3] J. D. Dunitz, W. B. Schweizer, *Acta Cryst.Sec. C***1995**, *51*, 1377.

[4] L. Spix, H. Meekes, R. H. Blaauw, W. J. P. van Enckevort, E. Vlieg, *Cryst.Growth Des.***2012**, *12*, 5796.

[5] H. Kimoto, K. Saigo, Y. Ohashi, M. Hasegawa, *Bull. Chem. Soc. Jpn.***1989**, *62*, 2189.

11:50 Oral

Vaterite intermediate phase: physicality and dynamics in presenting PO_4

Yuki Sugiura[1,2], Kazuo Onuma[2], Yuki Kimura[3], Koichi Momma[4], Atsushi Yamazaki[1]

1. *Waseda University, Tokyo 169-8555, Japan* **2.** *National Institute of Advanced Industrial Science and Technology (AIST), Tsukuba Central 2-1-D811, 1-1-1 Umezono, Tsukuba 305-856, Japan* **3.** *Earth and Planetary Science, Department of Science, Tohoku University, Sendai 984-0065, Japan* **4.** *National Museum of Nature and Science, Tsukuba 305-0055, Japan*

e-mail: arch.quartz@gmail.com

When Ca and CO_3 ions were mixed under highly supersaturated conditions in neutral to weak basic aqueous solution conditions which simulated biological environment, amorphous calcium carbonate (ACC) was appeared as an initial phase and rapidly transformed into vaterite. According to non-classical nucleation thesis, this phase transformation process is assumed as continuously structural reconstructions in cluster based phase transformation from amorphous phase to crystalline. Appearance of some intermediate phases during phase transformation in general. However, the phase transformation process has been little known, for examples, physicality, chemical composition and structure. Finely identify of the intermediate phase and measurement of their dynamics bring us new aspects for phase transformation of not only calcium carbonate but also other cluster based minerals like calcium phosphate.

Vaterite was often formed as round-shaped spherulites particles in supersaturated calcium carbonate solutions in around neutral to weak

based aqueous solutions. Sugiura et al. showed vaterite spherulites become hollow structure during dissolution process in a solution including PO_4 ions. This result suggests that vaterite spherulites were consisted of two or more vaterite like and lower stability phases and they were ranging inside part of vaterite spherulites and these phases were assumed as intermediate phases between ACC to vaterite.

We had done fine phase identification for inside phase of vaterite spherulites using powder X-ray structural analysis, selected area electron diffraction (SAED) analysis and measuring chemical composition, and estimated growth and dissolution rate of these intermediate phases in simulated biological temperature and pressure environment using optical in situ observation. In addition to these experiments, we investigated PO_4 effect into growth and dissolution dynamics of vaterite intermediate phases.

We discovered not only these intermediate phases were very similar to vaterite and ACC, but also there were obvious difference between their chemical compositions and structures. For example, C/Ca rate of the intermediate phases were higher than vaterite, SAED patterns corresponding to C-Ca bonds were very weak compare to that of vaterite. In dissolution experiment, this intermediate phase revealed small responsive toward to PO4 compare to outer vaterite. This difference was strongly affected dynamics, growth and dissolution process in PO_4 presence conditions.

Here, we will present about the details of vaterite intermediate phase structures and chemical compositions which were each ranging parts, growth and dissolution rate of each phase in various concentration of PO. In addition to reports about these intermediate phases, we will also introduce a formation of vaterites with unique morphologies during phase transformation based on in situ observation.

12:05 Oral

Jarosite crystallization in the presence of amino acids

Harrison Crabbe, Natalya Fernandez, Franca Jones

Curtin University, Perth 6845, Australia

e-mail: F.Jones@curtin.edu.au

The mineral jarosite ($KFe_3(SO_4)_2(OH)_6$) is commonly found in environments such as acid sulphate soils, acid mine wastes, saline lakes and hypogene systems. It is also produced in some hydrometallurgical operations (such as zinc processing) to remove unwanted iron and improve metal concentrates. In many, if not all, systems microbes also exist, often being a critical component of them. The relationship between jarosite and microbes is, however, not fully understood. In the case of acid mine drainage, jarosite formation could be extremely beneficial by locking away toxic metals often released by the high acidity but this depends on the stability of the jarosite in this environment. As a precursor to understanding the impact microbes have on jarosite formation, we have looked at small amino acids. Even if such small molecules are not incorporated into the jarosite mineral structure, it is probable that they will interact with growing crystallites to modify their growth rate, morphology and particle size.
Our studies focus on the formation of jarosite in the presence of amino acids and look at parameters such as i) yield ii) morphology and iii) phase. The talk will present the results of jarosite formation in the presence of four amino acids, and their impact on these crystallization properties.

Lunch (IOCG Council meeting)

Wednesday afternoon, 14 August, 12:20

WeO2

G03: Biological and Biogenic Crystallization
Wednesday afternoon, 14 August, 14:00
Room B, Auditorium Maximum

14:00 Invited oral

Growth mechanisms that trigger self-purification during protein growth

Alexander E. Van Driessche[1], Gen Sazaki[2], Dominique Maes[3], Mike Sleutel[3]

1. *Instituto Andaluz de Ciencias de la Tierra, CSIC-UGR (LEC-IACT), Avda. Las Palmeras, nº 4, Granada 18100, Spain* **2.** *Institute of Low Temperature Science, Hokkaido University (ILTS), N19-W8, Kita-ku, Sapporo 060-0819, Japan* **3.** *Vrije Universiteit Brussel (VUB), Brussels 1050, Belgium*

e-mail: sander@lec.csic.es

Crystals growing from contaminated solutions usually exhibit an altered surface topography and a reduction in step kinetics. In most cases, these effects are supersaturation dependent. The prevalent interpretation is that the crystal surface undergoes a self-purifying transition by moving from an impurity-saturated state at low supersaturation towards an effective state of impurity-repulsion at high driving forces [e.g. 1,2]. However, in recent years, motivated by *in situ* observations, we have perceived two models which can trigger the accelerated recovery of impurity poisoned surfaces. These events constitute an alternative route towards the self-purification scenario that would normally occur at higher supersaturation values.

One of the routes is linked to a non-classical growth mechanism. In this case the accelerated recovery of impurity poisoned surfaces is triggered when mesoscopic protein clusters, present in supersaturated solutions [e.g. 3,4], merge with the crystal surface and lead to a crystalline mound (i.e. multilayer island [e.g. 3,5]) relatively devoid of impurities. This was monitored *in situ* for lysozyme crystals growing from highly impure solutions (≈ 94.5% purity). When steps of areas free of multilayer islands and steps generated on areas enclosed by macrosteps are compared significant changes in step morphology and growth kinetics are observed. The freshly formed areas due to the solidification of a cluster on the crystal surface yield faster advancing steps with a morphology that more closely resembles the pure case [2]. This observation strongly suggests that these areas have a locally reduced surface impurity concentration surrounded by areas with high impurity coverage. The *de novo* formation of an impurity free terrace leads to an acceleration in the step velocity which reduces the terrace exposure time (compared to the surrounding regions) diminishing the probability that an impurity molecule will bind to the surface [6]. Eventually, a new steady-state will be established that is characterized by a higher lateral growth rate and quasi-pure morphology. These cluster-sedimentation events can therefore be considered as local hotspots of self-purification that grow in size with a velocity set by the rate of advancement of a macrostep across the impure surface. Once the edges of the surface are reached, the surface is effectively cleansed from impurity poisoning.

The second model was conceptualized when the growth dynamics of 2D islands and spiral hillocks of lysozyme crystals growing from purified and contaminated solutions were compared [7]. The morphology and step dynamics of spiral hillocks are less affected by the presence of impurities in the growth solution as compared to steps generated by 2D nucleation. Thus, when crystal growth is dominated

by spiral hillocks, fewer impurities are adsorbed onto the crystal surface and a more pure crystal lattice should be formed. This mechanism also operates under forced flow [8] indicating its general nature.

[1] Weaver M. L., et al. *Cryst. Growth Des.* 2010, 10, 2954–2959. [2] Van Driessche, A.E.S., et al. *Cryst. Growth Des*. 2009, 9, 3062–3071. [3] Gliko O., et al., *J. Am. Chem. Soc*. 2005, 127, 3433–3438. [4] Pan W., et al., *J. Phys. Chem. B* 2010, 114, 7620-7630. [5] Kuznetsov Y.G., et al., *Phys. Rev. B* 1998, 58, 6097–6103. [6] Sleutel M., et al., *Cryst. Growth Des.* 2013, 13, 688–695. [7] Sleutel M., et al., *Cryst. Growth Des*. 2012, 12, 2367–2374. [8] Maruyama M., et al., *Cryst. Growth Des*. 2012, 12, 2856–2863.

14:30 Invited oral

Protein conformational flexibility as a prerequisite for the formation of crystalline nuclei

Peter Vekilov, Maria Vorontsova, Vassiliy Lubchenko

University of Houston (UH), 4800 Calhoun Rd., Houston, TX 77204, United States

e-mail: vekilov@uh.edu

Nuclei of ordered solid phases of proteins in native conformations form within crucial precursors, which are metastable mesoscopic liquid clusters, existing both in the homogenous region of the solution phase diagram and in the region supersaturated with respect to an ordered solid phase. We show that the cluster exist due to the conformation flexibility of the protein molecules, leading to the exposure of hydrophobic surfaces and enhanced intermolecular binding. We show that additives known to destabilize the native protein structure lead to enhanced cluster formation. NMR characterization reveals that in solutions, in which clusters are present at concentrations allowing each protein molecule pass through a cluster within an hour, the protein conformational variability is significantly enhanced in comparison to solutions without clusters. These results indicate that protein conformational flexibility might be the mechanism behind the metastable mesoscopic complexes and, hence, behind the clusters and new-phase nucleation.

15:00 Oral

A Novel Delivery Mechanism of Topiramate_PFC drug for Lennox-Gas taut type of seizures through the growth of nano crystal

Ravi Sitaraman, Sundar T V, Natchimuthu V N

National College Autonomous, Tiruchirappalli 620001, India

e-mail: suga_ravi@yahoo.co.in

Lennox-Gas taut (L-G) type of seizures that affects the Central Nervous System (CNS), are facing drug administration problems. This is because of three basic reasons viz., a) the non soluble nature of almost all anti-epileptic drugs b) these drugs generally are not properly targeted towards the affected area of CNS c) generally it affects children. In this paper, a novel attempt has been made to solve the second one. Topiramate (TPM) is one of the most commonly prescribed medicine for L-G type of seizures. But still it is not that much adequate to serve the purpose of proper delivery to the affected seizures. To over come this, TPM is homogenized with certain PERFLUOROCARBONS (PFC) using ultrasound of 3-12 MHz on aqueous medium. Nano crystal is grown with the support of the ultrasound frequency. X-ray, solubility and SEM are made to analyze the structure of the crystal. The attachment of the PFC, which has got a very high oxygen carrying capacity to the CNS, to TPM reveals its capacity to detach and deliver TPM to the affected seizures in the CNS. That way TPM is made more effective on the affected seizures. Carbamazepine(CBZ), which is the best prescribed drug for such diseases do not get reacted with any kind of PFCs. Their attachment reveal that TPM is more effectively delivered than CBZ because of its mode of attachment along with PFC. Extensive study is also made on Lamotrigine which is also effective for Lennox-Gas taut type of seizures.

• PROJECT FINANCIALLY ASSISTED BY DEFENCE RESEARCH DEVELOPOMENT ORGANISATION – INDIA.

15:15 Oral

High resolution protein crystals using an efficient convention-free growth geometry

Elias Vlieg[1], Alaa Adawy[1], Etienne Rebuffet[2], Susanna Tornroth-Horsefield[2], Willem J. De Grip[1], Willem J. Van Enckevoort[1]

1. *Radboud University Nijmegen, Heyendaalseweg 135, Nijmegen 6525AJ, Netherlands* **2.** *Department of Chemistry, Biochemistry and Biophysics, University of Gothenburg, Göteborg 0000, Sweden*

e-mail: e.vlieg@science.ru.nl

The growth of high quality single protein crystals, yielding the highest X-ray resolution, remains a bottleneck in macromolecular crystallography. Convection-free conditions should lead to improved crystal quality, because in such a case growth is slow and the formation of defects and the incorporation of impurities minimized. Convection-free conditions have been achieved in the microgravity environment of space and in magnetic fields, but the impact on protein crystal growth has been limited due to the experimental difficulties with these methods.

Here we show that through a laboratory-based setup, an entirely convection-free crystallization environment is achieved, which enhances the purity and crystallinity of protein crystals [1]. This is accomplished by using an upside-down geometry, where crystals grow at the 'ceiling' of a growth cell completely filled with the crystallization solution. The 'ceiling crystals' experience the same diffusion-limited conditions as in space microgravity environments. The new method was tested on bovine insuline and two hen egg-white lysozyme polymorphs. In all cases, ceiling crystals diffracted X-rays to resolution limits beyond their current world records, even while solutions of moderate purity were used. The enhanced purification in the ceiling geometry is further demonstrated by comparing the crystal morphology and the fluorescence from impurities between normal batch-grown and ceiling crystals. Using phase-shifting interferometry, we show that indeed convection-free growth occurs.

[1] A. Adawy et al. (2013). *Cryst. Growth & Design,* **13**, 775.

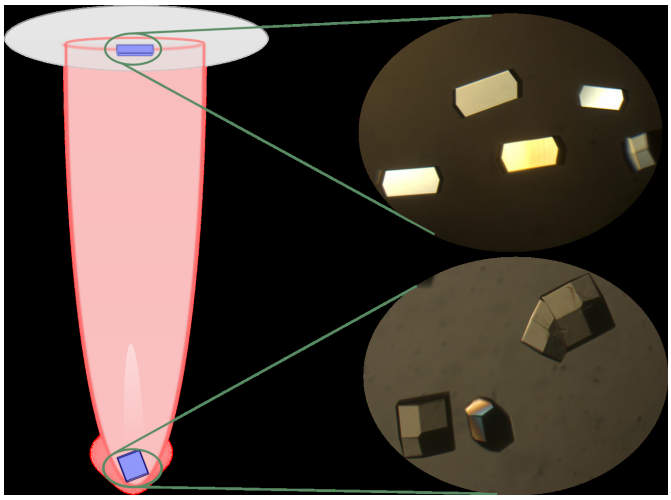

Break
Wednesday afternoon, 14 August, 16:00

Posters

Monday, 12 August

MoP-G03
Monday afternoon, 12 August, 17:00
Room 205, Old Library

17:00 | Poster | Mo100

The Effects of Turkish Cranberry Bush Fruit on the Growth Mechanism of the Calcium Oxalate Crystals

Emel Akyol, Kerim Ongun, Semra Kirboga, Mualla Oner

Yildiz Technical University (YTU), Chemical Engineering Department Davutpasa Campus, Esenler, Istanbul 34210, Turkey

e-mail: eakyol@yildiz.edu.tr

In this study, the effects of Turkish cranberry bush (Viburnum opulus L.) on crystal kinetics and morphology of calcium oxalate were investigated in vitro in an attempt to elucidate the mechanisms of formation of calcium oxalate calculi and further help in seeking inhibitors for preventing this disease. The results showed that Turkish cranberry bush fruit (TCBF) affected crystal growth mechanism of calcium oxalate. It was found that TCBF tested in this study is effective on crystallization rate and behaved as an inhibitor of calcium oxalate crystallization. Our data demonstrated that TCBF could play a potential role in the prevention of stone formation associated with hyperoxaluria. The presence of TCBF inhibited the crystal growth of calcium oxalate possibly through adsorption onto the active growth sites for crystal growth.

17:00 | Poster | Mo101

Crystallization in Chitosan Membrane due to Lithium – A Potential Topic in Solid State Polymer Electrolytes for Batteries

Suraiya Begum, Saravanan Annamalai, Radha Perumal Ramasamy

Anna University, Department of Applied Science and Technology, ACT campus (ACT), Chennai 600 025, India

e-mail: suraiya8786@gmail.com

Solid state polymer electrolytes for Lithium ion batteries using biodegradable polymers are gaining scientific attention recently. Chitosan is a biodegradable polymer which shows partly amorphous and partly crystalline nature. The most popularly used solvent for chitosan dissolution is acetic acid solution, which acts as a cross linker for the formation of membranes. Studies relating to the interactions between Lithium and Chitosan membrane are important for using chitosan as a membrane in batteries. In this work, we study the influence of lithium ions on the crystallinity of chitosan membrane. The polymer membranes containing chitosan, acetic acid and lithium ions were prepared using solution casting method. In our experiment to the chitosan solution (10g/L) acetic acid was added to have a final concentration of 0.25 M/L. The solution was stirred while heating at 60°C for 30 min. To this $LiClO_4$ was added to have a final concentration of 5g/L. The solution was mixed for 30 min and then casted as films using glass Petri dish. It was observed that the films made using $LiClO_4$ was more flexible than those made without it (Fig. 1).

XRD pattern for chitosan - acetic acid films (Fig. 2) shows peak with 2θ angle at 11.5° and broad peak at 18.2°, 30° and 42°. Previously it has been shown that chitosan films made with 0.5M/L of acetic acid and 10g/L of chitosan has two unit cells. The unit cell of crystals (1) is larger than that of crystal (2), also the intensities of 2θ angle at 18.2° was nearly the same as that of 11.5° [1]. For our samples the concentration of acetic acid is 0.25M/L and 10g/L of chitosan. The intensity for 2θ angle at 11.5° was found to be less than that of 2θ angle at 18.5°. Thus, the reduction in the intensity of peak with 2θ angle at 11.5° (crystal (1)) to the lesser acetic acid contribution (0.25m/L) as against 0.5M/L acetic acid used in Samuels et al [2]. Chitosan solution with 50%$LiClO_4$ did not show any peak at 11.5° or 18.2°. But it shows broad peaks with 2θ angles at 20°, 30° and 41°. The absence of peaks with 2θ angles at 11.5° and 18.2° indicate that the formation of crystals due to acetic acid has been suppressed due to incorporation of lithium, thereby reducing the interaction of acetic acid with chitosan. The suppression of interaction between acetic acid and chitosan by lithium should be the reason for the membranes containing lithium to be more flexible than those of without lithium. Also this could happen because of formation of complexes involving lithium and acetic acid (lithium acetate). AFM could not image the chitosan- lithium ion membrane as it was very smooth and soft and could not be scanned. Raman spectra showed that the films are amorphous. Light scattering showed that complexes were formed when $LiClO_4$ was incorporated. The sizes of the complexes are ~ 100 nm. Room temperature measurement of the conductivity of the films showed that the films containing Lithium had 2000 times the conductivity of chitosan films without $LiClO_4$. The mechanical properties and the electrical characteristics of the films will also be discussed.

A B

Figure 1: Optical images of (A) Chitosan (B) Chitosan with 50% $LiClO_4$

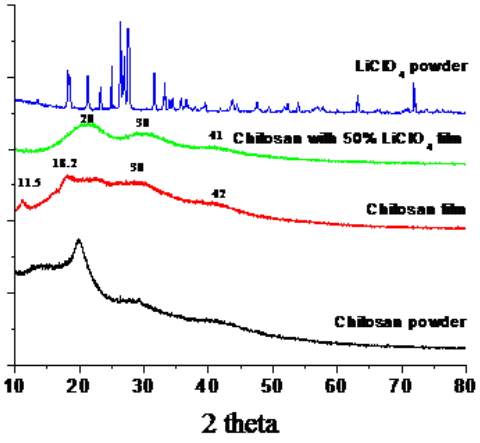

Figure 2: XRD pattern for the Chitosan films and powder.

References

1.C.G.A. Lima, DC conductivity and dielectric permittivity of collagen–chitosan films, Materials Chemistry and Physics 99 (2006) 284–288.

2 .R.J. Samuels, Solid state characterization of the structure of chitosan films, J. Polym. Sci., Polym. Phys. 19 (1981) 1081.

17:00 Poster Mo102

The attachment/detachment process of lysozyme molecules on a monoclinic lysozyme crystal surface studied by single-molecule visualization

Guoliang Dai[1], Gen Sazaki[2]

1. *Institute of Mechanics, Chinese Academy of Sciences, Beijing 100190, China* **2.** *Institute of Low Temperature Science, Hokkaido University (ILTS), N19-W8, Kita-ku, Sapporo 060-0819, Japan*

e-mail: dspr@imech.ac.cn

Attachment/detachment process of protein molecules on a crystal surface is one of the key elementary processes of protein crystal growth. In particular, how the attachment/detachment process happens and changes during crystallization process is still unclear. In this work, we conducted, by single-molecule visualization, the observation of fluorescent-labeled lysozyme molecules on {10-1} faces of a seed monoclinic lysozyme crystals under an almost equilibrium condition and a growth condition. We measured the changes in number density of florescent-labeled lysozyme molecules (whose positions were not changed, within an accuracy of one pixel size, for longer than a certain residence time) as a function of an adsorption time. We found that there was an induction period (~120 min) of the attachment/detachment process, during which period the number density remained constant, under both equilibrium and growth condition. After the "induction period", number density of florescent-labeled lysozyme molecules increased linearly with the adsorption time. Supersaturation significantly changes the attachment/detachment process: the increase in supersaturation obviously increases the adsorption (attachment) rate and decreased the induction period. We analyzed the changes in the ratio of adsorbed florescent-labeled lysozyme molecules (whose residence time was longer than 20 min) on steps of a seed crystal. The results showed that the induction period is an important factor affecting the adsorption position of molecules under equilibrium condition. Moreover, we tracked the changes of position of one labeled lysozyme molecule absorbed on steps under the growth condition. We found experimentally that the adsorbed molecule moved along a step under a low supersaturation condition.

17:00 Poster Mo103

Characterization of local rocking curves of protein crystals by X-ray digital topography with CCD camera

Takeharu Kishi[1], Daiki Fujii[1], Shiro Tsukashima[1], Kei Wako[2], Kenichi Kojima[2], Masaru Tachibana[1]

1. *Yokohama City University, Yokohama, Japan* **2.** *Yokohama Soei University, 1 Miho-tyou, Midori-ku, Yokohama, Yokohama 226-0015, Japan*

e-mail: tachiban@yokohama-cu.ac.jp

X-ray topography is one of the most powerful methods to characterize the imperfection or crystal defects in protein crystals. Recent development of high resolution CCD camera has led to X-ray digital topography which can acquire a lot of topographs as digital data in short time, depending on the rotation angle of the crystal sample around the Bragg angle for an interest reflection [1,2]. From the analysis of the digital data, we can plot X-ray intensities as a function of the sample rotation angle for any local areas in the topographs, called local rocking curves. Such analysis can lead to more detailed evaluation of the imperfection in protein crystals. In this paper, we report the characterization of local rocking curves of hen egg-white lysozyme (HEWL) crystals with monoclinic structure.

Monoclinic HEWL crystals were grown by a batch method and a liquid-liquid interfacial precipitation method. X-ray digital topography with CCD camera was carried out using synchrotron radiation in BL15B1 or 15C at PF in KEK. The wavelength of the incident beam was 1.2Å. The successive digital topographs were recorded in the interval of 0.00053 or 0.001 degree for the analysis of rocking curves.

Fig. 1 shows typical local rocking curves for monoclinic HEWL crystals. One is single peak and the other is double peak. In general, the full width of the half maximum of the single peak can be related to the mosaic structure. The double peak might be associated with larger sectors including mosaic structures. The difference between peak positions would correspond to misorientation between sectors with mosaic spreads. The characterizations of local rocking curves will be discussed and compared with other polymorphism such as tetragonal and orthorhombic structures.

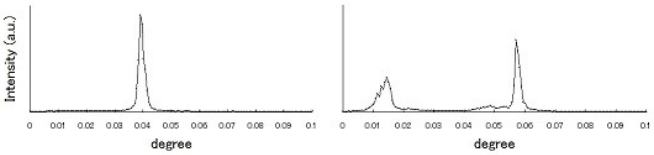

Fig. 1 A single peak (left figure) and a local rocking curve which peak was divided (right figure) in a monoclinic lysozyme crystal.

Reference

[1] H. D. Bellamy, et al. Acta Cryst. **D56**, 986-995 (2000)
[2] K. Wako, K. Kimura, Y. Yamamoto, T. Sawaura, M. Shen, M. Tachibana, and K. Kojima, J. Appl. Cryst. **45**, 1009-1014 (2012)

Corresponding author: Masaru Tachibana, Yokohama City University, 22-2 Seto, Kanazawa-ku, Yokohama 2360027, Japan, Tel &Fax: +81-45-787-2360, E-mail: tachiban@yokohama-cu.ac.jp

17:00 Poster Mo104

Effects of cyclic temperature change on camphor crystals in Storm glass solution, camphor-ethanol-water solution, and camphor-ethanol solution

Takuro Mitsuya, Kyohei Takahashi, Kazushige Nagashima

Meiji University, 1-1-1 Higashimita, Tama-ku, Kawasaki, Kanagawa 214-8571, Japan

e-mail: knaga@isc.meiji.ac.jp

Introduction: ‘‘Storm glass’’ (also referred to as storm bottle, camphor glass) consists of a sealed glass tube containing five components of camphor, ethanol, water, ammonium chloride (NH4Cl), and potassium nitrate (KNO3) [1]. The pattern and quantity of the crystals change according to daily variation of weather condition and were empirically interpreted as a weather forecasting tool mainly in 19th century England.

Nakamoto et al. [2] examined the effect of several parameters of weather condition on the storm glass. The change in the appearance of crystals in the solution in the “sealed” glass tube was not caused by a change in atmospheric pressure, humidity, electric field, or magnetic field, but solely by a change in temperature. It was difficult to find a correlation between the variations in the crystallization and the changes in the weather useful in forecasting the weather.

In our previous study [3], the pattern formation of the crystals in the storm glass solution was investigated by focusing on the applied temperature. The main results are summarized as follows. (i) XRD showed that the crystals in the storm glass were camphor. (ii) Typical crystal patterns that appear in the storm glass were obtained using a directional growth technique by controlling the growth rates (cooling rate). (iii) The effects of temperature changes on the appearance of camphor crystals were observed. Two runs of temperature changes, i.e. cooling from 30 to 20 deg C and heating from 10 to 20 deg C showed the completely different appearance of the crystals even after keeping the final temperature of 20 deg C for 24 hours. The result suggested that the storm glass does not act as a thermometer, but rather an apparatus affected by the history of the temperature change. (iv) A cyclic temperature change between 30 and 20 deg C with the period of 20 hours was applied to the storm glass. Two runs for different initial conditions of 20 deg C with crystals and 30 deg C without crystals were compared. The height of the precipitated crystals repeatedly changed with the temperature change. The ranges of crystal height for two cases of initial conditions finally coincided after about five periods of the temperature cycle. The crystals in the storm glass were found to be affected by the history of temperature change over several days.

Kaempfe et al. [4] also showed that the ambient temperature had a major influence on the state of the weather glass (storm glass). A cyclic temperature change between two temperatures showed that the storm glass reversibly formed the same amount of crystals at a given temperature. It was concluded that the storm glass is chemically a complex system that is near the temperature-dependent solubility of camphor. A prediction of the weather was not possible.

Despite of the negative results of storm glass as a weather forecasting tool, we still have a strong interest in it. Generally, the crystals behavior under temperature variation has not been well characterized. Fundamental studies of growth mechanism and pattern formation mechanism of crystals have been carried out experimentally and theoretically under ideal condition, i.e. growth of a single crystal under uniform applied temperature. In this sense, there remain questions how we can predict appearance of aggregate of crystals and patterns of crystals under repeated temperature change. The study of the storm glass can be a model study of crystals (or a single crystal) behavior under complex growth condition.

Difficulties in understanding the crystal behavior in the storm glass lie in changing temperature accompanying growth and dissolution, multi-crystals interaction throughout the diffusion field of solute, and multi-component solution system. Our approach in the present study is simplification of the solution system. The objective is to clarify the effect of the components of the storm glass solution on the appearance of camphor crystals under cyclic temperature change. In addition, equilibrium temperatures of camphor crystal as a function of the camphor concentration in the solutions are obtained to estimate the amount of camphor crystals to discuss the appearance of the crystals.

Experimental: Three types of sample solutions are used; (a) Storm glass solution (five-component system: camphor 1.210g, ethanol 3.560 g, water 3.920 g, NH4Cl 0.300 g, KNO3 0.300 g), (b) three-component system (camphor 1.169 g, ethanol 3.727 g, water 4.100 g), and (c) two-component system (camphor 5.911 g, ethanol 3.266 g). The camphor concentration in the solution (weight ratio of camphor to the total weight of the solution) is (a) C = 13.0 wt%, (b) C = 13.0 wt%, (c) C = 64.4 wt%, respectively. The weights of camphor in the solutions are decided in order not to completely dissolve the camphor crystals at a highest temperature of the temperature cycle.

The experiment runs of cyclic temperature change were carried out as follows. The glass tubes (16.5 mm in diameter and 105 mm in height) with the different sample solutions were sealed and immersed in a programmable temperature controlled water tank. At an initial condition of 45 deg C, there is no crystal in all samples. The cyclic temperature change of a triangle wave function between TH = 28 deg C and TL = 21 deg C with the period of 10 hours is applied. The experimental run was continued for 48 cycles of temperature changes. The appearance of crystals (the height of aggregated crystals in the glass tube and crystal patterns) were recorded by a high resolution digital camera using an interval timer.

The equilibrium temperatures of camphor as a function of camphor concentration were obtained by microscope observation of the zero growth condition of a quite small single crystal in each solution in a thin glass cell. The temperature was controlled to an accuracy of 0.1 deg C using a thermo-electric module with a temperature controller.

Results and discussion: First of all, the images of camphor crystals in the glass tubes are shown. Fig. 1 shows typical images of crystals at TL = 21 deg C and at elapsed time t = 490 hrs. The numbers of components in the samples are (a) 5 components (storm glass), (b) 3 components (camphor-ethanol-water), and (c) 2 components (camphor-ethanol). Note that the height of the solution surface from the bottom of the glass tube is almost the same. The crystal heights in the samples (a) and (b) are twice as large as that in the sample (c). The crystals in the solutions of (a) and (b) look feather-like. Each crystal has dendrite pattern. The crystals in the solution of (c) look densely packed.

Fig. 2 shows the crystal height ratio to the solution surface vs the elapsed time. During the initial cooling, the crystal heights rapidly increased in all samples. The maximum crystal heights for 5 and 3 components are higher than that for 2 components. In case of 5 and 3 components, nucleated tiny crystals sank to the bottom of glass tube. Then the crystals with dendrite pattern grew upward. The crystal height

ratios reached about 0.7 of solution surface. However, in case of 2 components, lots of tiny crystals repeatedly nucleated and sank to the bottom of the glass tube. The maximum height ratio resulted in 0.5 which is lower than the cases mentioned above.

In the process of the cyclic heating and cooling processes, the crystal height decreased and increased. Local maxima and minima of crystal heights for each sample gradually decreased repeating temperature cycles, and finally kept almost the constant values. It should be emphasized that not only the crystal height but also the amplitude of the height variation for 5 and 3 components are larger than those for 2 components.

The equilibrium temperatures , Teq, of camphor crystal as a function of camphor concentration were obtained (not shown). At the camphor concentrations of the three samples, the equilibrium temperatures are 31.1 deg C (5 components), 27.9 deg C (3 components), and 28.3 deg C (two components). Considering the temperature change applied, the weights, w, of the camphor crystals precipitated in the solutions were estimated simply assuming the equilibrium condition neglecting the concentration distribution in the solutions. For example, at TL = 21 deg C, the values of w are 0.30 g for 5 components, 0.20 g for 3 components, and 0.37 g for 2 components. The result showed that the values of w at TL in the solutions of 5 components and 3 components were smaller than that for 2 components, although the crystal heights as shown in Fig. 1(a) and 1(b) were much higher than that in Fig. 1(c).

In addition, at TH = 28 deg C the values of w are 0.11 g for 5 components, 0 g for 3 components, and 0.01 g for 2 components. The differences of crystal weight estimated, Δw, between TH and TL, is 0.19 g (5 components), and 0.20 g (3 components) which were much smaller than 0.36 g (2 components), although the amplitude of height variation in the solutions of 5 components and 3 components were much larger than that of 2 components. It should be noted that TH is close to the equilibrium temperatures, the local minima of the crystal height variation are much larger than 0. This might be the effect of increase in camphor concentration near the dissolving crystals in the solution.

Both results mentioned suggest that the porosities of the aggregate of crystals in the storm glass solution and the camphor-ethanol-water solution are quite high due to feather-like (dendrite) crystals. It is concluded that the large amplitude of height variation and dendrite pattern formation of crystals during the temperature change in the storm glass might be one of reasons that people in 19th century had an interest in the appearance of crystals in the storm glass in connection with the change in weather condition. The difference in crystal appearances between the storm glass solution and 3-component solution without NH4Cl and KNO3 was not clarified.

References:

[1] R. Fitzroy, The Weather Book, Longman, Green, Longman, Roberts, and Green, London, 1863, p. 439.

[2] Y. Nakamoto, M. Hiroi, Bull. Kobe Univ. Mercantile Mar. (Japanese) 38 (1990) 143.

[3] Y. Tanaka, K. Hagano, T. Kuno, K. Nagashima, J. Crystal Growth 310 (2008) 2668.

[4] P. Kaempfe, K. Molt, M. Epple, Chem. Unserer Zeit 46 (2012) 26.

Fig.1 Crystals images in three types of solutions at T_L and t =495 hrs. (a) 5 components, (b) 3 components (c) 2 components.

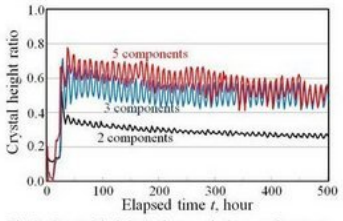

Fig.2 Crystal height ratio to solution surface vs t.

17:00 Poster Mo105

In vitro studies on disodium EDTA effect on mineralization of struvite and carbonate apatite

Marcin Olszynski, Jolanta Prywer

Institute of Physics, Technical University of Lodz, Wólczańska 219, Łódź 90-924, Poland

e-mail: 145010@edu.p.lodz.pl

Struvite ($MgNH_4PO_4 \cdot 6H_2O$) and carbonate apatite ($Ca_{10}(PO_4)_6CO_3$; CA) are the major components of infectious urinary stones. They are formed when the urinary tract is infected by urease positive microorganisms, mainly from *Proteus sp*. This kind of stones constitutes from 10% [1] to 30% [2] of all urinary stones. One of the most frequently used treatment procedures for urinary stones is extracorporeal shock wave lithotripsy and a long-term antibiotic treatment. Such a treatment should prevent also the recurrence and re-growth of stone after treatment. However, it is known that even bacterial substances and dead bacteria may serve as sites for heterogeneous nucleation and re-crystallization. Among other things, this is the reason that the recurrence after treatment is on the level of 50%. Therefore, in recent years, many studies on the crystallization processes have been made for providing effective treatment methods.

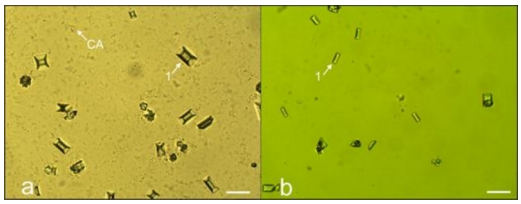

Fig. 1. Struvite crystals (1) and CA precipitation grown from artificial urine (a) in the absence of disodium EDTA and (b) in the presence of disodium EDTA (5 mM).
Scale bar: 50 μm.

In the present research we study the effect of disodium EDTA on the crystallization of struvite and CA. The growth of struvite crystals and CA occurred in the solution of artificial urine at 37°C. Mineral components in the artificial urine correspond to mean concentration found in 24-hour period in normal human urine. The crystallization process occurs after consecutive addition of aqueous ammonia solution to mimic urease activity under the control of pH value. Such an addition emulates real urinary tract infection [3]. The results demonstrate a clear relationship between disodium EDTA concentration and struvite crystallization and CA precipitation. Increasing the disodium EDTA concentration causes an increase in induction time and decrease in the growth efficiency (Fig. 1) compared to baseline (without disodium EDTA). Increasing the concentration of disodium EDTA reduces the mass of struvite and CA formed in the solution of artificial urine. Additionally, the struvite crystals are found to decrease, while the aspect ratio is found to increase in the presence of disodium EDTA. The results indicate that by dosing an appropriate concentration of disodium EDTA struvite and CA precipitation in artificial urine can be lowered or even prevented. The appropriate dose of disodium EDTA required preventing struvite nucleation and CA precipitation is predictable taking into account the pH of the solution of urine and the magnesium and calcium concentration.

References

[1] Bichler, K.H.; Eipper, E.; Naber, K.; Braun, V.; Zimmermann, R.; Lahme, S. *Int. J. Antimicrob. Agents* **2002**, *19*, 488–498.

[2] Chauhan, Ch.K.; Joshi, M.J. *J. Cryst. Growth***2013**, *362*, 330–337.

[3] Prywer, J.; Torzewska, A.; *Evidence-Based Complementary and Alternative Medicine*, vol. 2012, Article ID 862794, 7 pages, 2012.

17:00 Poster Mo106

Comparative in vitro studies on disodium EDTA effect with and without Proteus mirabilis on the mineralization of struvite and carbonate apatite

Jolanta Prywer[1], Agnieszka Torzewska[2], Marcin Olszynski[1]

1. *Institute of Physics, Technical University of Lodz, Wólczańska 219, Łódź 90-924, Poland* **2.** *Department of Immunobiology of Bacteria, Institute of Microbiology and Immunobiology, University of Lodz, Banacha 12/16, Łódź 90-237, Poland*

e-mail: jolanta.prywer@p.lodz.pl

Struvite ($MgNH_4PO_4 \cdot 6H_2O$) and carbonate apatite ($Ca_{10}(PO_4)_6CO_3$; CA) are the major components of infectious urinary stones. Urine of a healthy person is undersaturated with regard to struvite and CA formation. However, infectious stones are formed in the case of urinary tract infection by urease-producing bacteria. Urease – bacterially produced enzyme – splits urea, natural component of urine – into ammonia and carbon dioxide. This in turn raises the pH of the urine. Under alkaline conditions, an increase in the concentration of the ammonium, carbonate and phosphate ions occurs. These ions together with the ions of calcium and magnesium present in the urine lead to the crystallization of CA and then of struvite.

In the present study we describe the effect of disodium EDTA on the mineralization of CA and struvite in the solution of artificial urine in the absence and presence of *Proteus mirabilis* and the comparative study of the growth processes. The aim of this study is to determine and understand the role of *Proteus mirabilis* in the formation of CA and struvite with the presence of disodium EDTA. The present study is a continuation of the investigation of an influence of disodium EDTA on the growth of struvite and carbonate apatite in the absence of bacteria [1].

Microorganisms from *Proteus* species are isolated in the case of 70% of infectious stones [2,3]. *Proteus* includes, among others, *Proteus mirabilis* responsible for urinary tract infections and was chosen to our study. Crystallization occurs after addition of the suspension of bacteria to the solution of artificial urine and incubation at 37° C. The experiment designed in such a manner guarantees that the crystallization process occurs at conditions emulating the natural conditions existing in human body during the infection by *Proteus mirabilis*. Control experiments without bacteria were performed using artificial urine of the same composition. In this case the crystallization process occurs after consecutive addition of aqueous ammonia solution. Such an addition causes an increase in pH value and the concentration of the ammonium ions. In other words the addition of aqueous ammonia solution mimics urease activity and therefore emulates real urinary tract infection [4].

The results demonstrate that in both cases – in the presence and in the absence of bacteria – disodium EDTA reduces the mass of struvite and CA formed in the solution of artificial urine. The addition of disodium EDTA to the urine does not affect the morphology and habit of single crystals. However, in the presence of bacteria, when pH value increases, the presence of single crystals vanishes progressively and the majority of the crystals are hopper and dendrite-like. The evolution of dendrite-like crystals is mainly influenced by the rate of change in pH. Kinetics of pH changes is faster in the presence of bacteria compared to the absence of bacteria. Therefore, in the case of absence of bacteria, dendrite-like crystals are observed very rarely. In both cases (with and without bacteria), increasing disodium EDTA concentration causes the induction time increase compared to baseline (without disodium EDTA). Therefore, the pH level of urine increases much more slowly in the presence of disodium EDTA compared to baseline. For this reason urine is undersaturated with respect to struvite and CA formation for longer time compared with the control test (without disodium EDTA).

The results demonstrate also that in the presence of bacteria the number of formed nuclei decreases compared with the absence of bacteria. This means that the nucleation rate decreases in the presence of bacteria. The nucleation rate is defined as the number of nuclei generated per unit volume and per unit time and is correlated with surface energy crystal-solution denoted by γ. Our results suggest that the surface energy γ is enlarged in the presence of bacteria. Increasing the surface energy leads to decreasing in the nucleation rate. Consequently, the number of formed nuclei decreases. These nuclei grow to larger crystals compared with the crystals which grow in the case of absence of bacteria. Consequently, the struvite crystals which grow in the presence of bacteria are larger and the number of crystals is less compared with the absence of bacteria. To sum up, the results demonstrate that the growth process is modified in the presence of bacteria and provide evidence for the importance of biological regulation in crystallization process.

References

[1] Prywer, J., Olszynski, M. *J. Crystal Growth* **375** (2013) 108–114.

[2] Lerner, SP, Gleeson MJ, Griffith DP. *J. Urol.* **141** (1989) 753–758.

[3] Kramer G, Klinger HC, Steiner GE. *Curr. Opin Urol.* **10** (2000) 35–38.

[4] Prywer, J.; Torzewska, A. *Cryst. Res. Technol.* **45** (2010) 1283–1289.

17:00 Poster Mo107

Influence of Proteus mirabilis on the growth process and morphology of struvite crystals

Rafal R. Sadowski, Jolanta Prywer

Institute of Physics, Technical University of Lodz, Wólczańska 219, Łódź 90-924, Poland

e-mail: 145016@edu.p.lodz.pl

Struvite ($MgNH_4PO_4 \cdot 6H_2O$), is not only an important biomineral, but also a major component of the so called infectious urinary stones. It is formed when urinary tract becomes colonised by bacteria producing urease. Urease is a characteristic bacterial enzyme splitting urea [1] into carbon dioxide and ammonia. These products alkalinize urine. Under alkaline conditions, an increase in the concentration of the ammonium, carbonate and phosphate ions occurs. These ions together with the ions of calcium and magnesium present in the urine lead to the crystallization of struvite, according to the following reaction [2]:

$$Mg^{2+}+NH_4^{+}+PO_4^{3-}+6H_2O \rightarrow MgNH_4PO_4 \cdot 6H_2O. \quad (1)$$

The minor component which crystallizes as a result of the infection is carbonate apatite ($Ca_{10}(PO_4)_6CO_3$; CA) formed according to the general reaction [2]:

$$CO_3^{2-}+10Ca^{2+}+6PO_4^{3-} \rightarrow Ca_{10}(PO_4)_6CO_3. \quad (2)$$

This component is present as an amorphous precipitate and does not form crystals of defined morphology typical to struvite. Struvite together with small amount of CA forms the so-called infectious stones.

In the present study we describe mineralization of CA and struvite crystals in the environment of artificial urine in the absence and presence of *Proteus mirabilis* and the comparative study of the crystal

grown. The obtained crystals take habits typical for crystals growing in living animal and human organisms. Struvite grown in the presence of *Proteus mirabilis*, at first stage of growth (low pH), takes coffin-like habit and the crystals are mainly composed of the (001) and (00–1) pedions and the {101}, {10–1}, {011} and {01–1} forms [3]. At higher pH single crystals are observed rarely, and instead twins and dendritic structures appear. Twins may be divided into two groups. First group of twins is composed of two (or three) crystals one rotated 60 or 90 degrees relative to the other [4]. Second kind of twins is typical penetration twin with the (001) pedion as penetration plane. Dendrites are X-shaped or they are composed of one trunk and branches symmetrically distributed on two sides of the trunk. The evolution of dendrites is mainly influenced by the rate of change in pH with minor influence of the value of pH. The absence of dendrites is a key indication that sample did not experience a rapid change in pH value. The virtual boundary separating these two kinds of crystals (single and dendrites) can be considered as the limit between the slow and rapid growth.

From the comparison of this result with the results of the control experiments without bacteria, it can be concluded that in the case of absence of bacteria the crystals in most cases take also the coffin-like habits, but instead of the {011} and {01–1} forms, the {012} and {010} forms appear. Additionally, in the case of the absence of bacteria, it is observed very frequently, that the (001) pedion disappears totally and is not represented in the morphology. It is known that the changes in crystal habit and morphology are due to differences in relative growth rates of faces of which the crystal is composed. In this case, it is suggested that the changes in morphology are induced by the presence of bacteria. This may happen because the surface of bacterial cells usually demonstrates anionic character and therefore they have ability to trap positive ions from the surrounding environment. In the case of *Proteus mirabilis*, bacterial polysaccharides contain negatively charged residues, which are able to bind the Ca^{2+} and Mg^{2+} ions [5]. These ions accumulate around bacterial cells and the crystallization process appears to be mediated by specific molecular interactions between molecular structures of the crystal surface and molecular arrays around bacterial cells.

References

[1] Bichler, K.H.; Eipper, E.; Naber, K.; Braun, V.; Zimmermann, R.; Lahme, S. *Int. J. Antimicrob. Agents***2002**, *19*, 488–498.

[2] McLean, R.J.C.; Nickel, J. C.; Cheng, K. J.; Costerton, J.W. *Crit. Rev. Microbiol*. **1988**,*16* , 37–79.

[3] Prywer, J.; Torzewska, A. *Crystal Growth & Design***2009**, *9*, 3538–3543.

[4] Prywer, J.; Torzewska, A.; Płociński, T. *Urological Research***2012**, *40*, 699–707.

[5] Torzewska, A.; Stączek, P.; Różalski, A. *J. Medical Microbiol.***2003**, *52*, 471–477.

17:00 Poster Mo108

Rocky protein crystals grown in silica gel

Jose Antonio Gavira, Alexander E. Van Driessche, Juan Manuel Garcia-Ruiz

Instituto Andaluz de Ciencias de la Tierra, CSIC-UGR (LEC-IACT), Avda. Las Palmeras, nº 4, Granada 18100, Spain

e-mail: sander@lec.csic.es

Protein crystals are generally considered as soft material. The low reticular energy and the high solvent content make them very fragile and sensitive to any physical stress such as mechanical shocks, osmotic pressure, drying, etc. Fragility and stability are two of the main features of protein crystals that make difficult their manipulation and limit the feasibility of using them for technological purposes [1-3]. We have shown that macromolecular crystals grown in gelled media (such as agarose, sephadex, polyacrylamide or silica), incorporate large volumes of the solid gel network into the body of the crystals. In this communication we extend our results with lysozyme crystals grown in silica gels [4] to other proteins (thaumatin, insulin, ferritin, etc) proving that the phenomenon is universal.

Crystals were obtained by counter-diffusion or batch method in silica gels at silica concentrations ranging from 2 to 22% *(v/v)* . The protein crystals incorporate the solid silica fibers during their growth making the crystal appear optically translucent while maintaining crystal order at short and long-range scale. Silica incorporation was measured by termogravimetry, and the internal texture of the crystals showing the location of the silica fibers was studied by scanning electron microscopy. The mechanical properties and the stability of the crystals are improved by the incorporation of the highly hydrophilic silica phase. Increasing the silica gel concentration reduces the surface energy anisotropy to such an extend that spherical single crystals can be obtained as growth forms. The reinforced protein crystal enhances the mechanical stability and the drying behavior, as shown by scanning differential calorimetry. The crystals can be handled at room condition out of their mother solution using tweezers. X-ray diffraction data can be collected outside capillaries without mounting to preserve the moisture. The application of these rocky crystals in Materials Science and Chemical Engineering is also discussed.

[1] Y. Shen et al. (1993), Nature 366, 48.

[2] K. Douglas et al. (1992), Science 257, 642.

[3] T. Thomson. (1996), BYTE April 79.

[4] J.M. García-Ruiz et al. (1998), Materials Research Bulletin, Vol 33, 11, 1593

17:00 Poster Mo109

Unexpected growth behaviour: a first step to understand crystalline growth of non-model proteins?

Alexander E. Van Driessche

Instituto Andaluz de Ciencias de la Tierra, CSIC-UGR (LEC-IACT), Avda. Las Palmeras, nº 4, Granada 18100, Spain

e-mail: sander@lec.csic.es

In this work we report on the violation of the succession of crystal growth modes as a function of supersaturation [1]. Typically, a crystal transitions from spiral growth to two-dimensional (2D) nucleation mediated growth with increasing supersaturation. In the case of monoclinic xylanase crystals we observed, using LCM-DIM, strong lattice discontinuities protruding the surface from which 2D and/or spiral hillocks originate. The complex nature of such a step source yields nonequidistant step trains and on some occasions even macrosteps demonstrating that the xylanase crystals grown under these conditions are far from perfect and do not behave like the quasi flawless model systems such as high purity lysozyme and glucose isomerase crystals.

More importantly, these defect-prone monoclinic xylanase crystals also constitute an exception to this well-maintained rule. This is the result of a unique interplay between the dominating layer generation mechanism and the subsequent occurrence and propagation of large numbers of lattice discontinuities. The defect density becomes so high that, given enough time, a fully developed, crystal-wide network of interlinked stacking faults is generated. This network effectively abol-

ishes any advancement of steps emanating from the sole step source, being a spiral dislocation. The crystals manage to recover from this growth cessation by switching over to a secondary layer generating mechanism at lower supersaturation, that is, 2D nucleation. Several questions still remain open and need to be answered to fully elucidate the events observed on the monoclinic xylanase crystals. To what extent do these lattice discontinuities have an impact on the X-ray diffraction quality? The fact that high resolution structures of xylanase from Trichoderma are present in the protein databank (e.g., PDB-id: 2DFB [2]) suggests that these defects are not necessarily an intrinsic part of xylanase's growth modes. But remarkably, all high resolution structures were obtained from the orthorhombic polymorph; no structures obtained from the mononclinic polymorph are reported. Taking into account the observations done in this work, it seems reasonable to assume that the high density of defects is related to a specific space group, monoclinic in this case, and does significantly affect the diffraction properties.

This observation demonstrate that by simply departing from well-established purified protein model systems, one can obtain unconventional and highly complex protein crystals with nontrivial growth mechanisms which could help us to understand the growth or (non-growth) on non-model proteins, still a major setback in structural biology.

[1]. M. Sleutel, Van Driessche A.E.S., Maes D. Cryst. Growth Des. 2012, 12, 2986-2993.

[2]. Watanabe, N.; Akiba, T.; Kanai, R.; Harata, K. Acta Crystallogr., Sect. D 2006, 62, 784−792.

17:00 Poster Mo110

Crystallization of biomorphic aragonite in silica gel

Gan Zhang, José Manuel Delgado López, Duane Choquesillo-Lazarte, Juan Manuel Garcia-Ruiz

Instituto Andaluz de Ciencias de la Tierra, CSIC-UGR (LEC-IACT), Avda. Las Palmeras, nº 4, Granada 18100, Spain

e-mail: ganzhang@ymail.com

Calcium carbonate, as one of the most abundant biominerals, has attracted considerable interest and therefore it has been deeply studied throughout the past years. Calcium carbonate exists in a variety of polymorphic forms, including three anhydrous crystalline polymorphs, calcite, aragonite and vaterite. Under ambient conditions, calcite is the most stable phase and forms rhombohedral carbonate structures. Although the orthorhombic aragonite phase is less stable than calcite, its formation is also common in natural mineralization processes. Vaterite is described by a hexagonal unit cell. It is the less stable anhydrous $CaCO_3$ phase, and preferably transforms into more stable phases. However, it is also considered as a key phase in biomineralization and biomimetic crystallization.[1]

The common experimental pathway for biomimetic crystallization usually includes the presence of organic molecules, which has received an enormous amount of attention in the past.[2] However, biomimetic morphologies could also be achieved by pure inorganic crystallization. In fact, the crystallization of orthorhombic alkaline earth carbonates such as witherite ($BaCO_3$) and the strontianite ($SrCO_3$) in silica rich alkaline environment result a wide range of highly oriented self-assembled poly-nano-crystalline structures exhibiting non-crystallographic morphologies such as regular helicoids and filaments, which are reminiscent of the shape of living organisms. This kind of "life-like" orthorhombic (Ba or Sr) carbonates structures forming in pure inorganic silica-carbonate environments was called "silica biomorphs".[3-6] However, in the case of calcium carbonate, the phase forming under classical alkaline conditions is calcite, the rhombohedral polymorph. This difference makes a critical change on the morphology of the structures obtained that creates dendrites and fractal like formations, while witherite and strontianite exhibit complex biomorphic formation under the same conditions. Biomorphic structures with complex curvilinear forms of silica-calcium carbonate were only detected when the formation of orthorhombic aragonite was induced by temperature and using strontium as additive.[4,7]

In this study, the precipitation of calcium carbonate in silica gel under specific initial concentration and pH formed the biomorphic curvilinear structures at room temperature without the presence of any other additive. The crystallization procedure was performed by counter diffusion method in a lab made crystallization cell. The resulting biomorphic formation was characterized by X-ray diffraction (European Synchrotron Radiation Facility) and Raman microspectroscopy, and the results revealed that aragonite was the only crystalline phase. The growth behavior and morphological study was followed by optical microscopy and field emission scanning electron microscopy (FESEM). The crystal exhibited a petal-like structure with continuous smooth curvature and in some cases, regular helicoids were also observed. The detailed study by FESEM show that the biomorphic aragonite is a polycrystalline aggregates made of highly co-oriented nanorods with a size of hundreds of nanometer, thus similar to the case of barium and strontium biomorphs[5]. Notably, the biomorphic aragonite only occurred within a very specific narrow zone in the crystallization cell, inserted among the layers of elongated calcite and sheaf of wheat calcite.

1. F. C. Meldrum, *Int. Mater. Rev.*, 2003, **48**, 187-224.

2. F. C. Meldrum and H. Co□lfen, *Chem. Rev.*, 2008, **108**, 4332-4432.

3. J. M. García-Ruiz, S. T. Hyde, A. M. Carnerup, A. G. Christy, M. J. Van Kranendonk and N. J. Welham, *Science*, 2003, **302**, 1194-1197.

4. A. E. Voinescu, M. Kellermeier, B. Bartel, A. M. Carnerup, A.-K. Larsson, D. Touraud, W. Kunz, L. Kienle, A. Pfitzner and S. T. Hyde, *Cryst. Growth Des.*, 2008, **8**, 1515-1521.

5. M. Kellermeier, H. Cölfen and J. M. García-Ruiz, *European Journal of Inorganic Chemistry*, 2012, **2012**, 5123-5144.

6. A. E. Voinescu, M. Kellermeier, A. M. Carnerup, A.-K. Larsson, D. Touraud, S. T. Hyde and W. Kunz, *J. Cryst. Growth*, 2007, **306**, 152-158.

7. H. Imai, T. Terada, T. Miura and S. Yamabi, *J. Cryst. Growth*, 2002, **244**, 200-205.

General Session 4

Industrial crystallization

Session Coordinators

Kevin Roberts (UK) *K.J.Roberts@leeds.ac.uk*

Govindhan Dhanaraj (USA) *gdr_1998@yahoo.com*

Kullaiah Byrappa (India) IUCr representative *kbyrappa@rediffmail.com*

Programme

Tuesday, 13 August

TuO1

G04: Industrial crystallization
Tuesday morning, 13 August, 10:20
Room B, Auditorium Maximum

10:20 Invited oral

Size- and Shape-Controlled Continuous Flow Hydrothermal Synthesis of Inorganic Nanomaterials

Ed Lester, Christopher Starkey, Peter W. Dunne, Miquel Gimeno-Fabra

University of Nottingham, Nottingham, United Kingdom

e-mail: peter.dunne@nottingham.ac.uk

Continuous flow hydrothermal synthesis has proven itself to be a simple, scalable and relatively environmentally friendly method for the production inorganic nanomaterials. Much of the research effort in this area has focussed on the synthesis of metal oxide nanoparticles. We have recently been shown that continuous flow hydrothermal synthesis can be applied to the production of nanostructured phosphate materials, such as hydroxyapatite nanotubes. We are currently working to further extend the library of inorganic nanomaterials accessible by this technology.

Here we report for the first time a general continuous flow hydrothermal synthesis route to a variety of metal sulphide nanomaterials. Metal sulphides constitute a diverse and interesting class of materials with a wide range of structures and applications, with many sulphide systems exhibiting strongly size- and shape-dependent optical and electronic properties. Nanosized and nanostructured metal sulphides are thus of particular interest for their applications in biological labeling, photocatalysis, photovoltaics, LEDs and lithium-ion batteries.

The reaction of metal salts with thiourea under continuous flow hydrothermal conditions has been found to be a viable route to a wide range of metal sulphide nanoparticles; including zinc, cadmium, and lead sulphides. Furthermore, by varying reaction conditions it is possible to control the size and shape of the produced nanoparticles.

The continuous hydrothermal synthesis of lithium iron phosphate for lithium-ion battery applications is also reported. $LiFePO_4$ is a highly promising material for next generation battery materials, with high stability, as well as a high redox potential and theoretical capacity. The poor conductivity and lithium ion diffusivity of the material may potentially be overcome by limiting particle size to the nanoscale and controlling morphology in order to promote directional lithium ion diffusion. The direct continuous flow hydrothermal synthesis of lithium iron phosphate leads to spherical and diamond-shaped particles of 100 – 500 nm diameters, while shape control has been achieved by the addition of an organic chelating agent leading to the formation of elongated nanoplates.

This work is all part of a large EU FP7 funded project called SHYMAN – Sustainable Hydrothermal Manufacturing of Nanomaterials.

10:50 Invited oral

Development of continuous crystallisation processes of pharmaceutical compounds to achieve better control over final product attributes

Anna Jawor-Baczynska[1], Alastair J. Florence[2], Jan Sefcik[1]

1. *University of Strathclyde, Chemical and Process Engineering, 75 Montrose Street, Glasgow G11XJ, United Kingdom* **2.** *University of Strathclyde, Strathclyde Institute for Pharmacy and Biomedical Sciences, 27 Taylor Street, Glasgow G40NR, United Kingdom*

e-mail: anna.jawor-baczynska@strath.ac.uk

Crystallisation form solution is an important separation and purification process commonly used for a broad range of solid products. Many fine chemicals, such as dyes, explosive, and photographic materials, required crystallisation in their manufacture, as well as wide majority of active pharmaceutical ingredients and excipients[1]. Currently, pharmaceutical crystallisations are performed in batch mode which often leads to problems in achieving consistent product specifications, e.g. crystal form, particle shape and particle size distribution. Moving to continuous crystallisation technologies has the potential for huge increases the efficiency, flexibility and product quality[1,2]. However, the crystallisation process in continuous system is especially challenging due to lack of understanding particles nucleation and growth mechanism under flow conditions and challenges related to eliminate the crystal encrustation and fouling.

In this research we've designed and investigated an anti-solvent nucleation unit in order to continuously generate seeding suspensions for continuous crystal growth. We used two model compounds, paracetamol and DL-valine. The nucleator was constructed in such a way that warm solution is injected into cold antisolvent using a small diameter nozzle. The unit is composed of a jacketed vessel in which the temperature of the wall could be controlled to prevent the fouling problem; keeping the solution near the wall undersaturated. The encrustation problem was also eliminated by applying the ultrasound and effect of ultrasound on crystal size, crystal structures, morphology and yield was investigated. The control of crystal nucleation kinetics has been achieved by adjusting the mixing efficiency, solvent-antisolvent ratio, supersaturation level and residence time in the nucleator. Produced crystals may be used as a seeding suspension and be continuously introduced to a crystal growth unit (e.g. Oscillatory Baffled Crystalliser (OBC))[3]. Careful control of the crystal nucleation separated from subsequent crystal growth will allow a better control of the continuous crystallisation operation and production of the final product with desired properties.

1 Chen, J., Sarma, B., Evans, J. M. B. & Myerson, A. S. Pharmaceutical Crystallization. *Crystal Growth & Design***11**, 887-895, (2011).

2 Wong, S. Y., Tatusko, A. P., Trout, B. L. & Myerson, A. S. Development of Continuous Crystallization Processes Using a Single-Stage Mixed-Suspension, Mixed-Product Removal Crystallizer with Recycle. *Crystal Growth & Design***12**, (2012).

3 Mackley, M. R. & Ni, X. Experimental fluid dispersion measurements in periodic baffled tube arrays. *Chemical Engineering Science* **48**, 3293-3305,(1993).

11:20 Oral

Anionic, inorganic crystallization promoters - the curious case of sodium sulfite and sodium dithionate impacts on barium sulfate crystallization

Andrew Baynton, Mark I. Ogden, Tomoko Radomirovic, Franca Jones

Curtin University, Perth 6845, Australia

e-mail: F.Jones@curtin.edu.au

Phone: +618 9266 7677 Fax: +618 9266 4699

Crystallization promotion is a new and exciting field that offers the possibility of controlling crystallization to an even greater degree than previously imagined. Promotion has been observed for barium sulfate and calcium carbonate in the presence of organic molecules (for example, aspartic acid) and in the case of barium sulfate in the presence of inorganic cations of the alkaline earth metals. Inorganic anionic promoters of barium sulfate have yet to be reported, however, we will provide evidence here that such promoters exist.

We show that, indeed, the presence of sodium sulfite and sodium dithionate promotes barium sulfate crystallization. Morphology experiments show that the impact appears to be dominant in the *c* axis and AFM experiments show that this is due to the promotion of 2D nucleation. Comparison is made with sodium oxalate, which is found to inhibit rather than promote crystallization.

Finally, we discuss why this finding is curious and the possible mechanism by which this promotion may be occurring.

11:35 Oral

Nucleation control and separation of paracetamol polymorphs through swift cooling crystallization process

Sudha Chinnu, Srinivasan Karuppannan

Bharathiar University, Marudhamalai,Coimbatore, Coimbatore 641046, India

e-mail: nivas_5@yahoo.com

Polymorphism plays a significant role in pharmaceutics for drug designing because of their diversified properties. It has critical implications in pharmaceutical development as they impact the stability and bioavailability of the active drug ingredient. Paracetamol an excellent analgesic and antipyretic drug crystallizes in three different polymorphic forms mono, ortho and the unstable form. Crystallization of metastable orthorhombic and the unstable polymorph is highly elusive and moreover, the separation of these polymorphs remains as a challenging task today. In the present work, the polymorphic nucleation behaviour of pharmaceutical solid paracetamol has been investigated by performing cooling crystallization process at different cooling rates from 274-313 K with fixed agitation of the mother liquor at 100 rpm. Saturated pure aqueous solutions of paracetamol at fixed supersaturation conditions were stabilized for about 2 hours at 353 K and then swiftly cooled to a below ambient temperature of 274 K with continuous stirring by means of a DC micrometer with digital speed controlling facility. The resultant supersaturation generated in the mother solution favours the nucleation of desired polymorphs of paracetamol. The resulted nucleation in the solutions was investigated under in-situ optical microscopy and the type of polymorphs was identified according to their morphology. The phase diagram constructed to demonstrate the swift cooling experimental procedure clearly explains the reason for the occurrence of polymorphs and its stability by the movement of concentration position line into the metastable or labile zone region. The experiment was continued for different cooling rates in the range 274-313 K in steps of 1 K. The results elucidate a clear distinction of preferred nucleation regions of mono, ortho and unstable polymorph in the temperature range between 274 and 313 K. Very high supersaturation in the temperature range 274-281 K favours unstable polymorph with fibre-like morphology, the supersaturation generated in the temperature range 282-292 K yields orthorhombic polymorph with needle shaped morphology and the low supersaturation favours monoclinic polymorph with prismatic morphology in the temperature range 293-313 K. The nucleated metastable polymorph which possesses needle shaped morphology is quiet stable for about 10 minutes and after 15 minutes it undergoes dissolution. The nucleated unstable polymorph which possesses fibre-like morphology undergoes extensive dissolution within a short period and disappears within 7 seconds at that experimental condition. The form of crystallization of the obtained polymorphs was confirmed by PXRD. The type of nucleated paracetamol polymorphs in the solution is mainly influenced by the driving force created in the solution. Through swift cooling process the nucleation regions of the three different polymorphs were identified and separated for the first time. This novel specific cooling crystallization process seems as a promising one for the control of nucleation and separation of polymorphs.

11:50 Oral

Precipitation process and phase stability of calcium sulfate; The role of temperature, salinity and time of reaction

Mercedes Ossorio[1], Alexander E. Van Driessche[1], Pedro Perez[2], Juan Manuel Garcia-Ruiz[1]

1. *Instituto Andaluz de Ciencias de la Tierra, CSIC-UGR (LEC-IACT), Avda. Las Palmeras, nº 4, Granada 18100, Spain* **2.** *Universidad de la Habana, Departamento de Física General, La Habana 10400, Cuba*

e-mail: mercedes.ossorio@gmail.com

Three crystalline phases are known in the $CaSO_4$-H_2O system: gypsum ($CaSO_4 \cdot 2H_2O$), bassanite ($CaSO_4 \cdot 0.5H_2O$), and anhydrite ($CaSO_4$). Gypsum and anhydrite often form massive evaporite deposits [1] but gypsum can also appear as large crystals in caves [2,3]. But, gypsum and bassanite are also economically important materials (e.g. construction industry). On the other hand, the precipitation of calcium sulfate in mining or desalination plants is often an unwanted by-product [4,5], leading to costly production reduction. Despite the important role, marked inconsistencies still exist between solubility measurement data, thermodynamic predictions of stability and the experimental data obtained from precipitation experiments in the laboratory.

A series of experiments were conducted in which precipitation was carried out by chemical reaction in a wide temperature range, 40-120 ^{o}C, at three different salinities (0.8, 2.8 and 4.3 M NaCl). The phase stability was tested by varying the reaction time of the precipitate with the mother solution, from 2 min to 10 months.

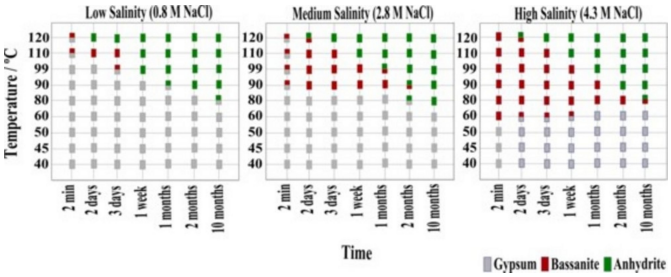

Fig. 1. Experimental results obtained by chemical reaction, as a function of salinity, temperature and time during which the precipitate was in contact with the solution.

The two main observations are: (I) Within its predicted stability field no primary anhydrite precipitation occurred from aqueous NaCl solutions (Fig. 1). (II) Bassanite occurs as an important metastable phase and the bassanite stability increases significantly with increasing salinity. At 4.3 M NaCl bassanite remains stable for more than two months at 80 ºC (Fig. 1). Previous studies [6,7] on growth dynamics of gypsum and anhydrite, show that anhydrite presents much slower kinetics than gypsum. Additionally, the significantly higher surface free energy of anhydrite leads to much longer induction times for nucleation. Both observations could be responsible for the observed metastable development of gypsum crystals for temperatures corresponding to the stability field of anhydrite. In a previous study [8] we have detected the presence of bassanite as a precursor phase during gypsum precipitation. The present observations show us that with increasing temperature and salinity the stability of this metastable phase is increased but at present the precise mechanism behind this stabilization is still unknown.
A better understanding of the precise precipitation dynamics and stability region of each phase will help understand natural occurring calcium sulfate deposits and is necessary to design more effective strategies to avoid the precipitation of these phases during industrial applications.

[1] Melvin (1991) Evaporites, Petroleum and Mineral Resources, 556;

[2] García-Ruiz et al., (2007) Geology, 35:327–330;

[3] García-Ruiz et al., (2008) McGraw-Hill Yearbook of Science and Technology, 154–156;

[4] Kagawa et al., (1981) Inorg. Nucl. Chem. 43:917–920;

[5] Stumm and Morgan (1995) Aquatic Chemistry, Wiley;

[6] Van Driessche et al., (2010) Cryst. Growth Des. 10:3909–3916;

[7] Morales et al., (2012) *Cryst. Growth Des.* 12; 414–421;

[8] Van Driessche et al., (2012) Science 336:69–72

12:05 Oral

Non-Classical Nucleation of Calcium Sulfate: A Novel View on the Origin of Scale Formation

Matthias Kellermeier[1], Andreas Kempter[2], Denis Gebauer[1], Helmut Coelfen[1]

1. *Universität Konstanz, Universitätsstr. 10, Konstanz 78457, Germany* **2.** *BASF SE, Carl Bosch Straße, Ludwigshafen 67056, Germany*

e-mail: matthias.kellermeier@uni-konstanz.de

Scale formation is a serious issue that affects both daily-life and industrial applications to a considerable extent. Due to changes in solubility and/or crystallization kinetics at elevated temperature, certain minerals precipitate from hard water and processing solutions under these conditions, leading to incrustation of pipes, kettles, and heating surfaces. While this may cause damage of household devices like laundry machines or dishwashers, scaling in industrial settings can be associated with a tremendous loss in performance, which eventually will necessitate shutdown of facilities and expensive cleaning. Thus, it is highly desirable to find ways to avoid the precipitation of solids in such environments, or at least prevent any nucleated particles from firmly depositing onto crucial components [1]. This, however, requires a fundamental understanding of the processes underlying mineral nucleation and subsequent crystallization from solution.
In this context, numerous studies have been devoted to calcium carbonate, one of the major scale-forming minerals in most waters. It was found that $CaCO_3$ precipitation frequently proceeds via a complex multi-stage scenario involving amorphous nanoparticles and metastable crystalline polymorphs as temporary intermediates [2]. Recently, it was furthermore demonstrated that calcium and carbonate ions assemble in solution to give stable associates, so-called pre-nucleation clusters [3], and that aggregation of these species is a possible pathway to nucleation [4]. This novel perspective opens up new promising strategies for scale inhibition that may rely on additives specialized to influence the crystallization at hitherto unknown stages [5].
Calcium sulfate is another mineral that often contributes substantially to water hardness and related problems. While it has long been believed that gypsum ($CaSO_4 \cdot 2H_2O$), the stable polymorph at ambient conditions, forms through a classical one-step mechanism directly from the dissolved ions, there is now increasing evidence that also this system may pass through non-classical reaction channels under practically relevant circumstances. Indeed, both amorphous calcium sulfate (ACS) and bassanite ($CaSO_4 \cdot 0.5H_2O$), a metastable crystalline modification, have been identified as possible precursor phases [6, 7], and the influence of selected additives on the stability of these intermediates has been explored on a qualitative level [8, 9].
In the present work, we have used a titration-based crystallization assay, originally developed for studying $CaCO_3$ nucleation [3], in order to monitor calcium sulfate precipitation under controlled conditions. By combining information gained from immersed ion-selective electrodes, conductivity sensors and turbidity probes, the different stages occurring on the way to final gypsum crystals are detected and characterized in situ. Corresponding results show that ion association in solution plays an important role during $CaSO_4$ mineralization, although the observed binding patterns are distinct from those in the $CaCO_3$ case. High-resolution techniques like cryo-transmission electron microscopy and analytical ultracentrifugation furthermore allow us to trace and directly observe the actual nucleation event, as well as to investigate early growth and phase transformation processes. Overall, the collected data paint a consistent molecular-scale picture that rationalizes the macroscopic precipitation behavior of calcium sulfate. In light of these new findings, we finally examine the effects of specific crystallization additives on the newly identified processes, and evaluate the potential of certain well-known antiscalants so as to ultimately delineate, as for calcium carbonate, alternative and perhaps more powerful concepts for scale inhibition.

References:

1. J. Rieger, E. Hädicke, I. U. Rau, D. Boeckh, Tenside Surfactants Deterg. 1997, 34, 430.
2. J. Rieger, T. Frechen, G. Cox, W. Heckmann, C. Schmidt, J. Thieme, Faraday Discuss. 2007, 136, 265.
3. D. Gebauer, A. Völkel, H. Cölfen, Science 2008, 322, 1819.
4. M. Kellermeier, D. Gebauer, E. Melero-García, M. Drechsler, Y. Talmon, L. Kienle, H. Cölfen, J. M. García-Ruiz, W. Kunz, Adv. Funct. Mater. 2012, 22, 4301.
5. A. Verch, D. Gebauer, M. Antonietti, H. Cölfen, Phys. Chem. Chem. Phys. 2011, 13, 16811.

6. Y. W. Wang, Y. Y. Kim, H. K. Christenson, F. C. Meldrum, Chem. Commun. 2012, 48, 504.
7. A. E. S. Van Driessche, L. G. Benning, J. D. Rodriguez-Blanco, M. Ossorio, P. Bots, J. M. García-Ruiz, Science 2012, 336, 69.
8. A. Saha, J. Lee, S. M. Pancera, M. F. Bräu, A. Kempter, A. Tripathi, A. Bose, Langmuir 2012, 28, 11182.
9. Y. Y. Wang, F. C. Meldrum, J. Mater. Chem. 2012, 22, 22055.

Lunch (IOCG Exec. Com. meeting)

Tuesday afternoon, 13 August, 12:20

TuO2

G04: Industrial crystallization
Tuesday afternoon, 13 August, 14:00
Room B, Auditorium Maximum

14:00 Invited oral

Analysis of the early stages of crystallization processes

Helmut Coelfen

Universität Konstanz, Universitätsstr. 10, Konstanz 78457, Germany

e-mail: helmut.coelfen@uni-konstanz.de

Analysis of the early stages of crystallization is of crucial importance to understand nucleation and growth processes. Several methods will be presented, which are able to deliver information in the size range between atoms and nanoparticles in solution. A particularly powerful method is Analytical Ultracentrifugation. It will be shown that species from prenucleation clusters to nanoparticles can be detected in solution with angström size resolution and high statistical significance since every particle is detected. An ultracentrifugation technique will be shown, which allows to perform nucleation experiments directly in the spinning rotor. Application of a newly developed UV/Vis detector allows to simultaneously obtain the UV/Vis spectra of all detected species which is very advantageous for metal and semiconductor nanoparticles. Other techniques like Taylor diffusion or mass spectrometry will also be discussed regarding their application to analyse early stages of crystallization processes.

14:30 Invited oral

90 years progress in shaped crystal growth

Vitali A. Tatartchenko

Shanghai CEC Zhenhua Crystal Technology Co., Ltd. (CECCG), Building 50, 1000 Zhangheng Road, Shanghai 201210, China

e-mail: vitali.tatartchenko@orange.fr

This year a shaped crystal growth technique has been amazing the crystal growth community: “Saint – Gobain Crystals, USA” announced construction of the new factory “Substrates of High Performance” for production of 6” sapphire substrates of high quality for LED application on the basis of EFG technique [1]. Without any doubt, it is an event of historical significance. Indeed, we know a lot of shaped growth advantages but up to now nobody had believed that their crystal quality can be the best one.

We would like to use this event to remind a shaped growth history. A priority in applying of a shaper (holes in plates placed onto the melt surface for shaping melt-pulled crystals) belongs to Gomperz [2]. In 1922, he used mica plates floating on melt surfaces to pull Pb, Zn, Sn, Al, Cd, Bi thin filaments through holes in the plates. In 1928, P. Kapitza, later the Nobel Prize rewarded, used this technique for Bi rods growth. In 1929, for Zn single crystalline filaments growth, for the first time, a single crystalline seed was used. Thus, during 1922 – 1931, six papers concerned with a shaper using were published, and the technique was titled as the Czochralski – Gomperz technique.

A development of shaped crystal growth for industrial application was begun from the set of papers published in 1958 – 1959. The first paper [3] informed that during 1938 – 1941, Russian scientist A. V. Stepanov had carried out experiments concerning pulling of shaped polycrystalline and single-crystalline specimens (sheets, tubes and so on) from melts of some metals, especially aluminum and its alloys. The Second World War interrupted these experiments and they have been continued since 50th in the Physical and Technical Institute of the USSR Academy of Sciences.

The very first theoretical analysis of the capillary shaping was reported by the author of this paper at the Internal Russian Conference in April 1967; later it was specified in the set of papers [4] published in the USA. Here is this approach. A crystal grows from a melt meniscus. As the Laplace capillary equation is a second order differential equation, the formulation of the boundary problem for melt meniscus shape calculation requires assignment of two boundary conditions. The first of them (the condition on the crystal-melt interface) is mutual for all techniques of crystal growth and follows from the existence of the growth angle. The second one is determined by a shaper. Shaping is accomplished either on the sharp edges or on the surfaces of the shaper. This corresponds to two different boundary conditions of the capillary boundary problem and as a result – two different techniques of shaped growth: Catching (attachment) and Angle fixation (Wetting) Boundary Conditions. It means that EFG was for the first time formulated in these papers as catching or attachment technique. It was shown that catching (attachment or EFG) boundary condition can be achieved for wetted as well as un-wetted shaper materials by using corresponding melt pressure. This strict formulation of boundary value problems allowed calculation of growth conditions and invention of many practical schemes of shaped crystal growth. But there is a violation in EFG (catching, attachment) boundary condition that never had been mentioned by other researches. The mathematical formulation of the problem requires a fixation of the meniscus edge. But from the physical point of view the melt has to form a wetting angle with the shaper surface. This discrepancy was explained in [5]. The paper contents well-grounded mathematical proof that edge has to be in reality sharp.

Thus, the real history of shaped crystal growth must be rewrite by the following way. A priority in shaped growth belongs to Gompertz (1922) but strict physical description belongs to the author of this paper who had published the full scheme of shaping (EFG and wetting including) much earlier than LaBelle and Mlavski [6].

In 1971, the very first paper concerning a crystal growth process stability investigation was submitted: Comparative analysis of stability of Czh and EFG techniques [7]. A fundamental result was obtained there – the Czh technique is not stable from capillary point of view, and a shaper can allow a capillary stability of process.

To resolve contradictions concerning different titles of shaped growth techniques: Czh – Gomperz, Stepanov's, EFG, etc., the author of this paper suggested [8] to use a title TPS (Technique of pulling from shaper). Here is the TPS definition [9]: TPS is the shape crystal growth technique which uses a solid body (shaper) to define a melt meniscus shape by means of either catching (on edges of shaper) or wetting (on surfaces of shaper) capillary boundary condition to obtain the crystal of predominant cross section and impurity distribution as a result of pulling it in a dynamically stable regime.

References:

1. V. A. Tatartchenko, C. D. Jones, S. A. Zanella, J. W. Locker, F. Pranadi, C – Plane Sapphire Method and Apparatus, USA Patent WO 2008036888 A1, 2006.

2. E. V. Gomperz: Untersuchungen an einkristalldrähten, Zeitschr. für Phys. **8,** 184 – 190 (1922).

3. A. V. Stepanov: A new technique of production of sheets, of tubes, of rods with different cross sections from a melt, J. Tech. Physics **29**, 382 – 393 (1959).

4. V. A. Tatarchenko, A. I. Saet, A. V. Stepanov: Boundary conditions of capillary shaping at crystallization from melts, Bull. Ac. Sc. of the USSR, Phys. Series, **33,** 1782 – 1787 (1969).

5. V. A.Tatarchenko, V. S. Uspenski, E. V. Tatarchenko, J. Ph. Nabot, T. Duffar, B. Roux: Theoretical Model of Crystal Growth Shaping Process, J. Cryst. Growth **180,** 615 - 626 (1997).

6. H. E. LaBelle: EFG, the invention and application to sapphire growth, J. Cryst. Growth **50,** 8 -17 (1980).

7. V. A. Tatartchenko: Influence of capillary phenomena on the stability of the crystallization process during pulling of shaped specimens from the melt, Phys. & Chem. Mater. Treat. **№6,** 47 – 53 (1973).

8. V. A. Tatarchenko: Shaped crystal growth (Kluwer Academic Publishers, London, 1993).

9. V. A. Tatartchenko: Shaped Crystal Growth, In: Springer Handbook of Crystal Growth, Ed. G. Dhanaraj, K. Byrappa, V. Prasad, M. Dudley, pp. 509 – 552 (Springer. Dordrecht, London, New York, 2010).

15:00 Oral

Toward Controlling Interface Shape during Bridgman Crystal Growth: Past, Present, and Future

Jeffrey J. Derby, Nan Zhang, Kristianto Tjiptowidjojo, Andrew Yeckel

University of Minnesota, Chemical Engineering and Materials Science, 421 Washington Ave. S.E., Minneapolis, MN 55455, United States

e-mail: derby@umn.edu

Percy Williams Bridgman received the 1946 Nobel Prize in Physics "for the invention of an apparatus to produce extremely high pressures, and for the discoveries he made therewith in the field of high pressure physics." He also invented an apparatus that has arguably proven to be even more important and pervasive, when in 1926 he developed a method to grow single crystals of non-cubic metals needed for his high-pressure studies. Of course, this technique is now commonly referred to as the Bridgman method.

The initial realization of the Bridgman method was quite crude, with a cylindrical tube being lowered into the air of the room or into a cooling bath of oil. Bridgman noted, "It is important that air drafts be kept from the emerging mold, as otherwise new centers of solidification may be started." In a "radical change of technique," Stockbarger (1935) pulled his samples of lithium fluoride from an upper furnace maintained at a temperature above the melting point into a lower furnace, whose temperature was set to achieve a suitable axial gradient.

Thus, Stockbarger was perhaps the first to advance the idea that careful control of temperatures and gradients would be needed to carry out the growth of high-quality single crystals. This idea will be examined and enlarged in this presentation, which endeavors to highlight many of the prior advances in understanding and technique that have led to the Bridgman-Stockbarger and gradient freeze processes of today. In particular, we will emphasize the role of heat transfer and furnace design in setting the macroscopic shape of the solidification interface.

It will be argued that modern ideas of model-based design and control can be used to influence this important characteristic of growth. Several examples from recent modeling of electrodynamic gradient freeze growth of cadmium zinc telluride will be presented. Notably, a strategy is presented to dynamically adapt the furnace profile so that uniform, convex interface shapes are maintained through an entire growth run. Realizing a convex solidification interface is postulated to result in better crystallinity and higher yields than obtained via conventional approaches.

Supported in part by DOE/NNSA, DE-FG52-08NA28768, the content of which does not necessarily reflect the position or policy of the United States Government, and no official endorsement should be inferred.

15:15 Oral

Numerical study of argon gas flow in a semi-industrial crystallization furnace for the production of multicrystalline silicon ingots

Martin P. Bellmann[1], Dag Lindholm[2], Dag Mortensen[2], Mohammed M'Hamdi[3]

1. *SINTEF Materials and Chemistry, Trondheim 7028, Norway* **2.** *Institute for Energy Technology (IFE), Institutveien 18, Oslo NO-2027, Norway* **3.** *SINTEF Materials and Chemistry, Oslo 0315, Norway*

e-mail: martin.bellmann@sintef.no

In directionally solidified multi-crystalline silicon, oxygen and carbon are the impurities that present by far the highest level. Oxygen from the silica crucible dissolves into the melt, incorporates into the crystal or forms silicon monoxide which evaporates from the free melt surface. Argon inert gas, injected into the furnace chamber, carries the silicon monoxide to the hot graphite fixtures where it reacts with carbon to form carbon monoxide and silicon carbide. Carbon monoxide is carried by the inert gas to the melt free surface, where it dissociates into carbon and oxygen. Finally, oxygen and carbon are incorporated into the crystal. Oxygen related defects, like thermal and new donors, can reduce the minority carrier lifetime in solar cells. Carbon precipitates can be responsible for the nucleation of new grains, the formation of locally induced stresses, wire-sawing defects and can cause ohmic shunts in solar cells.

The final impurity distribution in the solidified ingot strongly depends on the melt [1] and gas flow [2] velocity fields. Tailoring the melt flow, e.g. by external force fields [3], and the gas flow field, provides tools for controlling the impurity distribution in the ingot and gas phase. A global model of a semi-industrial crystallization furnace including heat transfer by conduction, convection and radiation is used to study the argon gas flow field. The induction heated furnace holds 120 kg of silicon, producing squared ingots of 55x55 cm and 16.5 cm in height. A special feature of the furnace is the argon gas injector, which consists of two nozzles allowing to control the flow in horizontal and vertical direction independently. In the paper the impact of different flow rate combinations (horizontal/vertical) on the gas flow pattern are studied and discussed with respect to impurity transport. The furnace model and the mesh are shown on the left hand side in Fig. 1 and the calculated argon gas flow field on the right hand side.

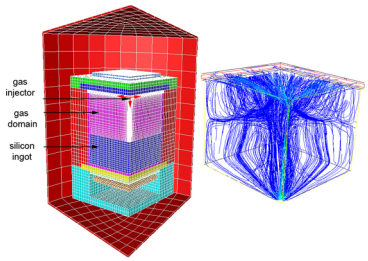

Fig. 1: Global furnace geometry with mesh and furnace parts and simulated argon gas flow field (pathlines).

[1] M.P. Bellmann et al., Journal of Crystal Growth 362 2013, 93.

[2] M.P. Bellmann et al., Journal of Crystal Growth 369 2013, 47.

[3] P. Rudolph, K. Kakimoto, MRS Bulletin 34, 251.

Break
Tuesday afternoon, 13 August, 15:30

Wednesday, 14 August

WeP-G04
Wednesday afternoon, 14 August, 16:00
Room 211, Old Library

Break
Wednesday afternoon, 14 August, 17:30

Thursday, 15 August

ThO1

G04: Industrial crystallization
Thursday morning, 15 August, 10:20
Room B, Auditorium Maximum

10:20 Invited oral

Formation and Industrial Application of Dispersive Nano-particles and Whiskers*

Lan Xiang

Tsinghua University, Tsinghua Garden, Beijing 100084, China

e-mail: xianglan@tsinghua.edu.cn

Our recent work was concerned mainly with the formation and industrial application of dispersive nano-particles and whiskers. A general dissolution-precipitation way was developed to synthesis dispersive nano-particles ($CaCO_3$, $Mg(OH)_2$, ZnO and $CaSO_4$, etc.) by controlling the crystallinity and the surface properties of the nano-particles. A general method induced by the inorganic ions as SO_4^{2-} and OH^-, etc. or by the surfactants was also developed to promote the one-dimensional growth of the whiskers (513MOS, $Mg(OH)_2$, $Mg_2B_2O_5$, AlOOH, ZnO and $CaSO_4.0.5H_2O$, etc.) at moderate hydrothermal conditions.

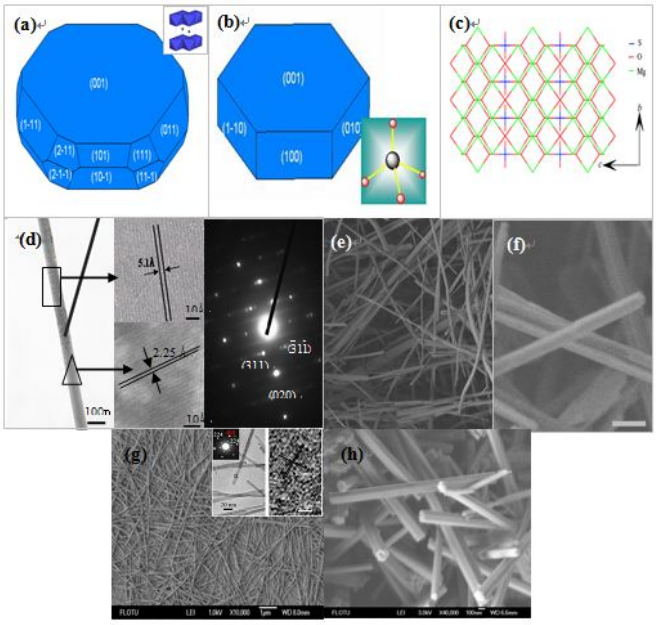

Fig. 1 Theoretical morphology of $Mg(OH)_2$ at 0K(a) and 473K(b); structure (c) and morphology (d) of 513MOS; morphology of $Mg(OH)_2$(e), MgO(f), AlOOH(g) and ZnO (h) whiskers.

* Project supported by the National Science Foundation of China (No. 51174125 and No. 51234003) and National Hi-Tech Research and Development Program of China (863 Program, 2012AA061602)

Corresponding author. E-mail: xianglan@mail.tsinghua.edu.cn

10:50 Invited oral

Challenges in the scale-up of crystallisation from process and product development through to manufacturing

Hongyuan Wei

School of Chemical Engineering, Tianjin University, 92 Weijin Road, Tianjin 300072, China

e-mail: david.wei@tju.edu.cn

Scale-up is always a hurdle for crystallisation processes. Conventionally, more attention has been given to achieving consistent size distribution and purity of crystal product in the scale-up from product development stage. However, in recent years, there are new challenges, especially in the pharmaceutical and fine chemical industries, which need to be faced such as polymorph control, cocrystal formation and micro particle or aggregate productions for manufacturing high value crystal products. Such crystal products normally have unique physical or chemical properties which must be maintained at high quality in large scale production. Major factors and criteria for the scale-up of crystallisation from the development stage to manufacturing scale are summarised and discussed in this paper and some novel approaches and attempts are also introduced through case studies.

11:20 Oral

Study of Crystallization and Kinetics Control in Metal Oxides using Novel Solution Routes

Kullaiah Byrappa[1], Namratha Keerthiraj[1], Lokanatha K. Rai[2]

1. *University of Mysore, Materials Science Center (UOM), P.B. No. 21 Manasagangothri P.O. Mysore, Mysore 570006, India* **2.** *University of Mysore, DOS in Chemistry (UOM), Manasagangothri, Mysore 570006, India*

e-mail: kbyrappa@gmail.com

Novel solution routes cover conventional hydrothermal, solvothermal and supercritical fluid processes with several other variants depending upon the solvent used. These solution routes have emerged as the most powerful tools in the preparative chemistry owing to their efficiency in crystallizing simple to most complex inorganic structures with controlled size, shape, dispersibility, and surface chemistry with or without *in situ* surface modification. Besides, these solution routes facilitate the growth of even high melting crystalline compounds at milder pressure temperature conditions.

In recent years, metal oxides such as TiO_2, ZnO, Fe_3O_4 play an important role in modern technology related to gas sensors, biomedical, photocatalysis, UV filters, etc. The synthesis of these metal oxides with tailor made physico-chemical characteristics is a challenging task to researchers, because, size, shape, dispersibility and surface chemistry control their applications. In this context, the experimental conditions, *in situ* surface modification, selective doping, and organic additives play an important role in the crystallization and kinetics control. The present authors have carried out a systematic study of these parameters in understanding the crystallization mechanism and the kinetics control in these compounds. The use of organic additives for example, has enhanced the kinetics of crystallization and the experimental duration has been reduced to a few hours from 48 hours. The experiments have been carried out under mild pressure and temperature conditions (P = autogeneous; T = 150 – 240^{o}C). The resultant products have been characterized using powder XRD, FTIR, UV-Vis Spectroscopy, SEM, TEM, DLS, BET surface area and the application potential has been explored vis-à-vis the experimental conditions.

11:35 Oral

Time Dependent Hydrothermal Crystallization Studies on $BiVO_4$ and its Photocatalytic Properties

Namratha Keerthiraj, Kullaiah Byrappa

University of Mysore, Materials Science Center (UOM), P.B. No. 21 Manasagangothri P.O. Mysore, Mysore 570006, India

e-mail: kbyrappa@gmail.com

Bismuth (III) vanadate ($BiVO_4$) shows multi-functional properties like ferroelastic, pyro-optical, electrolytic, and photocatalytic. It is classified as non-toxic and could replace toxic pigments such as cadmium and lead-based paints. However, it has been proven difficult to control the pigmentary colours of $BiVO_4$, which varies with the particle size. Three main crystal forms of $BiVO_4$ are known; tetragonal (zircon-type structure), monoclinic (distorted scheelite structure, fergusonite structure) and tetragonal (scheelite structure). The scheelite structure $BiVO_4$ shows good photocatalytic properties. The present authors have carried out homogenous hydrothermal chemical reactions using bismuth nitrate and ammonium vanadate solutions as precursors in the presence acid mineralizers like hydrochloric or nitric acids to synthesize scheelite type monoclinic $BiVO_4$. The pH of the solution was maintained at 6 using ammonia solution. *In situ* surface modification was carried out to control the size, shape and dispersibility of the title compounds. Sodium dodecyl sulphate was used as surfactant in different concentration. The experiments were carried out in mild hydrothermal conditions (T=180^{o}C; P= autogenous). Doping was carried out using Al or Mn with varying concentrations. The acid mineralizers are very effective in the crystallization of $BiVO_4$ and the experimental duration was varied accordingly from 12 to 4 h. The initial experiments with 12h duration yielded well crystallized $BiVO_4$ and authors slowly reduced the experimental duration to 4h in subsequent experiments by maintaining all others experimental parameters constant. Results of these experiments show that the product did not vary with experimental duration, but it is the role of mineralizers and surfactants which controls the crystal quality and size and morophology. Hence the time controlled study of crystallization vis-á-vis the experimental parameters is important in understanding the crystallization kinetics and mechanism. A systematic characterization of powder XRD, FTIR, UV- Vis Spectroscopy, SEM, TEM, DLS, BET surface area. Photocatalytic studies were carried out by using several organic dyes like Procion Red, Alizarin and Brilliant Yellow either individually or mixed with varying concentration.

11:50 Oral

Redox process catalysed by growing crystal – strengite, $FePO_4,2H_2O$, crystallizing from solution with iron(II) and hydroxylamine

Hans Erik Lundager Madsen

Faculty of Science (SCIENCE), Thorvaldsensvej 40, Frederiksberg C 1871, Denmark

e-mail: helm@life.ku.dk

In an attempt to grow pure crystals of the iron(II) phosphate vivianite, $Fe_3(PO_4)_2,8H_2O$, from a solution of Mohr's salt, $Fe(NH_4)_2(SO_4)_2,6H_2O$, added to a solution of ammonium phosphate, hydroxylammonium chloride, NH_3OHCl, was added to the stock solution of Mohr's salt to eliminate oxidation of iron(II) by oxygen from the air. However, the effect turned out to be the opposite of the expected: whereas hydroxylamine reduces iron(III) in bulk solution, it acted as a strong oxidant in the presence of growing iron phosphate crystals, causing the crystallization of the iron(III) phosphate strengite, $FePO_4,2H_2O$, as the only solid phase. Evidently the crystal surface catalyses oxidation of iron(II) by hydroxylamine, the actual precipitation process being

$$2\ Fe^{2+} + 2\ H_2PO_4^- + NH_3OH^+ + 3\ H_2O \rightarrow 2\ FePO_4,2H_2O + NH_4^+ + 2\ H^+$$

As H^+ is liberated, causing decrease in pH, the crystallization process may be monitored by recording pH versus time. The graphs of growth rate versus supersaturation as calculated from pH and initial solution composition were significantly more regular with this system than those for crystallization of vivianite or strengite from solutions without hydroxylamine. The usual composite kinetics of spiral growth and surface nucleation was found. At 25ºC the surface-nucleation part yielded the edge free energy $\lambda = 25 \pm 10$ pJ/m, which is about half the lowest value found for strengite crystallizing from an iron(III) solution without hydroxylamine and in the range of values previously found for vivianite. The scatter of values for λ presumably arises from contributions from different crystal forms to the overall growth rate. The low mean value points to strong adsorption of iron(II), which is subsequently oxidized at the crystal surface, forming strengite. The state of the system did not tend to thermodynamic equilibrium, but to a metastable state, presumably controlled by the iron(II) rich surface

layer of the crystal. In addition to crystal growth, it was possible to measure nucleation kinetics by light scattering (turbidimetry). A point of transition from heterogeneous to homogeneous nucleation was found, and from the results for the homogeneous domain a rather precise value of crystal surface free energy $\gamma = 55$ mJ/m^2 was found. This is a relatively low value as well, indicating that the redox process plays a role already at the nucleation stage.

12:05 Oral

Studies on the effect of different operational parameters on the crystallization kinetics of α-lactose monohydrate single crystals in aqueous solution

Parimaladevi Palanisamy, Srinivasan Karuppannan

Bharathiar University, Marudhamalai,Coimbatore, Coimbatore 641046, India

e-mail: nivas_5@yahoo.com

Carbohydrate is one among the four major classes of biomolecules. It serves as an important energy source in plants and animals. Lactose is the only carbohydrate naturally found in mammalian milk. It is widely used in dairy powders, food ingredients and pharmaceutical formulations. The presence of lactose in these products often related to stickiness and caking which cause blockages in pharmaceutical tableting machines and reducing the shelf-life of food ingredients by forming solid lumps. Appropriate size, shape, physical state, packing and flow characteristics of lactose crystals are essential for the food and pharmaceutical applications because a small change in these parameters can affect the overall performance of the product. Crystallization plays a vital role in controlling the size and morphology of lactose crystals. In our present work, the effect of supersaturation, time taken for the generation of supersaturation and volume of the solution on the size, morphology and crystallization kinetics of α-LM single crystals in aqueous solution was investigated. A range of supersaturation σ=0.05-1.30 was generated in 100 mL of α-LM aqueous solution at 307 K by employing slow evaporation process. While adopting this process, the induction time for the occurrence of nucleation was found to be varying from 131 h to 127 h. Size of the nucleated crystals varying from 80-60 μm in the supersaturation range σ=0.05-1.30. From the beginning to the end of the growth process, α-LM crystals were retaining the tomahawk morphology and there was no change observed in the entire ranges of supersaturation σ=0.50-130. A similar range of supersaturation σ=0.05-1.30 was generated in 500 μL of α-LM aqueous solution at 307 K by employing fast evaporation process. During this process, the induction time for the crystallization of α-LM was found to be greatly reduced and it was varied from 1.2 h to 0.03 h. By fast evaporation process the nucleations with tomahawk morphology was obtained initially at the lower supersaturation range σ=0.05-0.50, crystals with triangular morphology was obtained in the range σ=0.51-0.90 and crystals with triangular as well as diamond-like morphologies were observed in the supersaturation range σ=0.90-1.30. During growth, it was found that the morphology of the nucleated crystals changes from tomahawk to pyramidal shape with beveled faces at the bottom (within 65 min from the beginning of the nucleation) in the supersaturation range σ=0.05-0.50. Whereas the triangular morphology of the crystal changes to trapezoidal (within 35 min from the beginning of the nucleation) at the supersaturation range of σ=0.51 to 0.90. During growth there was a morphological change from diamond-like morphology to needle shape. Size of the nucleated crystals varies from 30 to 10 μm. Variation in the growth rate of different faces of the crystals at different supersaturation levels was found to be due to the difference in the strength of the intermolecular interactions between the respective faces and the solvent molecules. The nucleation kinetics of primary nucleated α-LM crystals were studied on the basis of classical nucleation theory. From the calculated values of nucleation parameters it was observed that only one type of nucleation is possible in all ranges of supersaturation from σ=0.05 to σ=1.30 while employing both the slow and fast evaporation process. In both the processes, similar range of supersaturation σ=0.50-1.30 was generated at different intervals of time and with difference in volume of the mother solution. Size and morphology of α-LM crystals were found to be varying with the different operational parameters employed. It is concluded that by optimizing the operational parameters, the size and morphology of α-LM crystals can be controlled to achieve the desired physico-chemical properties.

Lunch (EMCG meeting)

Thursday afternoon, 15 August, 12:20

ThO2

G04: Industrial crystallization
Thursday afternoon, 15 August, 14:00
Room B, Auditorium Maximum

14:00 Invited oral

Keeping a greener world on the move in winter: controlling crystallisation within fuels and biofuels in cold weather

Ken Lewtas, Peter Hutchins[1], Mark A. Price, Kevin J. Roberts[2], Chiu C. Tang[3], Elizabeth Shotton, Sarah A. Barnett, Joseph A. Hriljac[4]

1. *Infineum UK Ltd, Abingdom OX13 6BB, United Kingdom* **2.** *University of Leeds (SPEME), Leeds LS2-9JT, United Kingdom* **3.** *Diamond Light Source, Science Dept., Harwell Science and Innovation Campus, Chilton Didcot OX110DE, United Kingdom* **4.** *School of Chemistry, University of Birmingham, Edgbaston, Birmingham B152TT, United Kingdom*

e-mail: ken.lewtas@infineum.com

It seems appropriate, on the 50th anniversary of the first effective winter fuel additive (by modifying the wax crystals) that enabled the economic optimisation of distillate fuel production, to discuss the factors affecting the crystallization of conventional fuels and the differences which biofuel (e.g. fatty acid methyl esters (FAME)) have introduced into the complex crystallization behaviour.

The crystal structures of n-alkane waxes have been reported in-depth and the crystal structures of biofuel components are also referenced in the literature. New data will be discussed which shows significant differences with previously published data.

It will be shown how the molecular arrangements and energy minimisation controls the morphologies and habits of all these wax crystals precipitating from fuel and model solvents. Theoretical modelling of the most stable crystal structures gives crystal aspect ratios very different from those found in solution grown crystals. This is because the solvent has a profound effect on the growth rates of the different crystal surfaces and ultimately the fuel filterability performance.

The phase behaviour of mixtures will also be discussed. The compositions of the waxes and fuels can have dramatic consequences on the low temperature operation of diesel vehicles and heating oil systems.

The economic low temperature operation of these fuels can only be guaranteed by the use of specially designed additives. Such additives operate in different ways and these mechanisms will be illustrated with appropriate examples. The difficulties in controlling the crystal growth

when various FAME components are added will be shown together with the associated crystallization mechanisms.

14:30 Oral

Enantiospecific Cocrystallization, a New Method for Chiral Resolution.

Geraldine Springuel

Université Catholique de Louvain (UCL), Louvain-la-Neuve 1348, Belgium

e-mail: geraldine.springuel@uclouvain.be

Chiral resolution is common practice in the biomedical and pharmaceutical industry given the large number of chiral drug candidates. Beside diastereomeric salt crystallization and chiral chromatography, a new type of chiral resolution using the enantiospecific behavior of cocrystallization in solution was suggested over recent years.[1-8] This technique has the advantage of being economically and environmentally more interesting compared to chromatography and can furthermore be applied to compounds that do not or not easily form salts.

Prior to the development of this novel technique, it was shown that enantiospecificity can occur during the formation of cocrystal products between two chiral partners.[9] As a cocrystal can only be formed between a matching pair of enantiomers, this would imply that cocrystallization can be used as a resolution tool, provoking a specific interaction of a coformer of given chirality with the chiral API of interest, the unwanted enantiomer remaining in solution.

We will emphasize on the necessity of phase diagrams in the pursuit of optimal conditions for the development of a resolution. While ternary phase diagrams of cocrystals are nowadays commonly constructed, we are in here confronted with a quaternary phase diagram, as both quantities of R and S API, the quantity of chiral coformer, and the amount of solvent play a role. The overall description of the quaternary phase diagram will be illustrated by experimental results on a model compound. As a model pharmaceutical compound, we decided to use 2-(2-oxopyrrolidin-1-yl) butanamide which is a compound that does not easily form salts and which hitherto required chiral chromatography for effective resolution. This molecule, shown in Figure 1, is a racemic nootropic drug and its biologically activity is essentially associated with the S-enantiomer, marketed under the name Levetiracetam, an active anticonvulsant used to treat epilepsy.

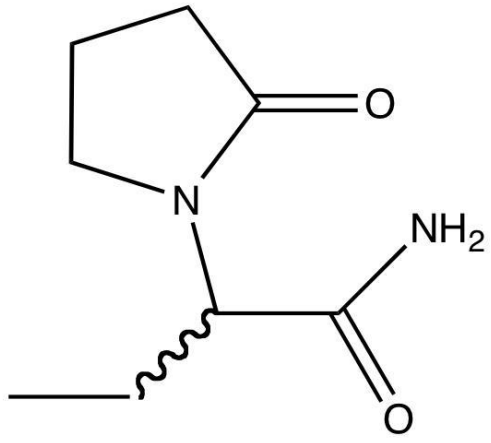

Figure 1. 2-(2-oxopyrrolidin-1-yl) butanamide

References:

1. G. Springuel, T. Leyssens, *Cryst. Growth Des.*, 2012, **12**, 3374.

2. C. Kassai, Z. Juvancz, J. Bálint, E. Forgassy, D. Kozma, Tetrahedron, 2000, **56**, 8355.

3. S. Hanessian, R. Saladino, R. Margarita, M. Simard, Chem. Eur. J., 1999, **5**, 2169.

4. P. Thorey, P. Bombicz, I. M. Szilágyi, P. Molnár, G. Bánsághi, E. Székely, B. Simándi, L. Párkányi, G. Pokol, J. Madarász, Thermochimica Acta, 2010,**497**, 129.

5. E. Székely, G. Bánsághi, P. Thorey, P. Molnár, J. Madarász, L. Vida, B. Simándi, Ind. Eng. Chem. Res., 2010, **49**, 9349.

6. M. Kawashima, A. Hirayama, Chem. Letters, 1991, 763.

7. M. R. Caira, L. R. Nassimbeni, J. L. Scott, A. F. Wildervanck, J. Chem. Crystallogr. 1996, **26**, 117.

8. K. Nemák, M. Ács, Z. M. Jászay, D. Kozma, E. Forgassy, Terahedron, 1996, **52**, 1637.

9. H. G. Brittain, Cryst. Growth Des., 2011, **11**, 2500.

14:45 Oral

Investigating Precipitation Kinetics of Sparingly Soluble Salts using Shock-Freeze TEM

Umraan Hendricks, Marcos Rodriguez-Pascual, Jillian F. Banfield, Alison E. Lewis

UNIVERSITY OF CAPE TOWN (UCT), RODENBOSCH, CAPE TOWN, CAPE TOWN 7701, South Africa

e-mail: hndumr001@myuct.ac.za

Reactive precipitation is defined as the process whereby a solid is formed after two reactant solutions are mixed together. The kinetic processes in precipitation include, nucleation, crystal growth, agglomeration and breakage of the particles. These processes are used extensively in the pharmaceutical industry, the fine chemical industry as well as the mining industry. When precipitation is used in industry, optimal process conditions are required in order to manufacture a product with specific physical properties. These physical properties include; particle structure, morphology and particle size distribution and are a function of several variables. Supersaturation, temperature and mixing rate are variables that can be controlled in order to achieve specific physical properties of the precipitate. Optimal conditions can be obtained by understanding the competing kinetic processes that occur during precipitation. Due to the short nucleation time in the precipitation of sparingly soluble salts, a fast mixing time is required in order to obtain experimentally measurable nucleation rates. Fast flow rates in the order of 100-250 $m.s^{-1}$ and accurate particle sizing techniques in the size range of 10-100 nm are required in order to achieve an experimental setup capable of measuring nucleation rates for these salts. Sparingly soluble salts produce nuclei that consist of 5-20 monomer units, which fall in the nanometer range and smaller. Therefore, in this study, cryofixation-TEM was used to measure the nucleation rate and kinetics during the precipitation of the reacting solutions. Liquid nitrogen (-196°) was used to quick freeze the nuclei in the solution and prevent further nucleation and growth. Copper nano tubes, with an outer diameter of 0.4 mm and an inner diameter of 0.3 mm were used to form the T-mixer reactor because of their high thermal conductivity. The use of TEM allowed for the determination of the number and size of the particles in micrometric slices taken along the reaction tube length. In this manner, the nucleation rate and kinetics, versus residence time of the precipitation reaction were determined. Residence times were calculated based on the flow rate and position of the micrometric slice along the copper tube. Three reactions were investigated.

$BaCl_2 + Na_2SO_4$ -> BaSO4 + NaCl (1)

$ZnSO_4 + Na_2S$ -> ZnS + $NaSO_4$ (2)

$CuSO_4 + Na_2S$ -> CuS + $NaSO_4$ (3)

The precipitation of barium sulfate has been widely studied, and therefore in this study it was used as a calibration/verification system. Barium sulfate (k_{sp}=1X10^{-10}) for a supersaturation range of 1.0E+2 - 1.0E+7 and zinc sulfide (k_{sp}=2X10^{-}25) and copper sulfide (k_{sp}=8X10^{-37}) for a supersaturation range of 1,0E+12 - 1,0E+16 were investigated. The number of particles for specific residence times along the reaction channel was measured, and the nucleation rates were calculated. The morphology and size of the nuclei were also determined using Cryo-TEM. Experimental data was compared to the corresponding theoretical values and correlations between the data were made. The mass and energy balance for each system was carried out in order to determine the role of each kinetic process.

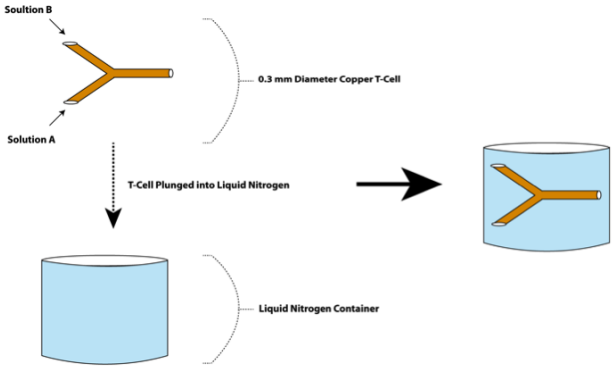

Figure 1. Cryofixation Experimental Procedure

15:00 Oral

A pneumatic micro-fluidic system for in-situ detection of mineralization with micro-Raman spectroscopy

Barbara M. Liszka[1], Aufried Lenferink[1], Yoonsun Yang[1], Hoon Rho[1], Geert-Jan Witkamp[2], Leon Terstappen[1], Cees Otto[1]

1. *University of Twente (UT), P.O. Box 217, Enschede 7500AE, Netherlands* **2.** *Delft University of Technology, Department of Materials Science and Engineering, Mekelweg 2, Delft 2628CD, Netherlands*

e-mail: b.liszka@utwente.nl

Mineralization in water processing is not desirable as it leads to a significant decrease of membrane efficiency by fouling processes and variation in surface properties. An increase of our understanding of early surface mineralization may lead to a better water quality control and improved surface protection.

Mineralization occurs under many conditions but of particular interest are condition in stages of the water treatment process where supersaturation occurs. Super-saturation may only arise locally at the surface of membrane systems. Therefore, a key question is whether nucleation and aggregation occurs in solution or at a surface. Recently, a novel theory (*Gebauer,Volkel,Colfen*) was proposed. In this theory nucleation followed the formation of nano-scale clusters stabe even in undersaturated solution. This opposes earlier notions that nucleation occurs only in supersaturated ions solution by stochastic solute clustering. One of the aims of this work is to investigate if prenucleation plays a role in mineralization at membrane surfaces and how early mineralization events may lead to scaling over time. Double pulse (DP) experiments were performed, which enable to assess the mineralization rate and seek evidence for the nature of prenuclation prior to a mineralization process. The DP experiment requires a model mineralization solution with a well-defined metastable region which depends on parameters, such as: super- saturation ratio, pH , ionic strength, temperature, etc. Moreover, an improved understanding of processes that occur in model mineralization solutions may lead to a better control of mineralization at surfaces.

In order to control experimental conditions as well as to monitor time evolution of crystal formation we have set out to develop a micro-fluidic system. The monitoring of prenucleation and mineralization events will be done by micro-Raman spectroscopy and imaging. The microfluidic system will for this reason be optically coupled in an efficient way to the Raman system. The ultimate aim will be to detect nano-sized crystals, which will give rise to only feeble Raman spectra.

A pneumatic micro-fluidic system has been developed to connect to the Raman micro-spectrometer. The micro-fluidic system will be prepared using standard PDMS technology in combination with masks made by photo-lithography. In order to create small chambers on a chip where prenucleation and mineralization will take place the PDMS walls will be pneumatically closed. The advantage of such a pneumatic micro fluidic device is that it enables a control over mass transport such that experiments can be carried out in a confined volume and under well-defined conditions in solution. Additionally, Raman-based micro-spectroscopic methods like spontaneous Raman scattering and coherent Raman imaging can be applied on samples under ambient conditions in the micro-fluidic device in real time. Another aim of this work is to show that micro-fluidic devices are promising tools for studies concerning mineralization processes and will provide rich information on underlying principles. The Raman spectra of minerals are directly informing on the chemical composition and can be directly interpreted in terms of the detailed symmetry of the crystals in case of different polymorphs. Furthermore, a great advantage is the sensitivity which is sufficient to detect nano-sized mineral particles.

Mineralization has been assumed to be highly dependent on the nature of the surface. A number of polymer materials was selected for mineralization experiments. The selected organic polymers are common in membrane technology and water filtration systems, namely polysulfone and poly(p-phenylene-oxide). Polystyrene has been added as a common material in technology. In order to observe the smallest possible nano-crystals at a polymer surface the Raman scattering of the crystals must be of the some order of magnitude as the Raman scattering from the organic layer. It was therefore decided to prepare very thin polymer films of the order of nanometers. These polymer films should preferably be homogeneous in thickness and contiguous. Quantitative Raman micro-spectroscopy and imaging was used to investigate thickness and contiguity in spin-coated systems. Extremely thin polymer films of less than 50 nm thickness can be easily observed with Raman micro-spectroscopy.

Results will be presented of hybrid micro-fluidic system-Raman microspectroscopy and imaging for the study of mineralization processes.

This research was supported by grant issued by FOM and Wetsus

15:15 Oral

The production of bulk thermoelectric materials based on bismuth and antimony chalcogenide solid solutions by hot extrusion

Mikhail V. Mezhennyi[1], Mikhail G. Lavrentev[2], Vladimir B. Osvenskyi[2], Vladimir T. Bublik[3], Natalia P. Tuchkova[3], Oleg M. Narva[4], Anatoly I. Prostomolotov[5]

1. *Technological Institute for Superhard and Novel Carbon Materials, Moscow 142190, Russian Federation* **2.** *State Institute of Rare Metals (GIREDMET), B. Tolmachevsky per., Moscow 119017, Russian Federation* **3.** *National University of Science and Technology (MISIS), Leninsky prospect, 4, Moscow 119049, Russian Federation* **4.** *LLC ADV-Engineering, Moscow 119049, Russian Federation* **5.** *Institute for Problems in Mechanics of RAS (IPMECH), Vernadskogo prospect 101, bl. 1, Moscow 119526, Russian Federation*

e-mail: mvmezh@gmail.com

Traditionally, since the 50-ies of the previous century, the production of thermoelectric materials (TEM) was carried out mainly by crystallization from a melt. However, the hot extrusion is hugely promising and technological method. It provides a production of the rods of thermoelectric materials with desired geometrical configuration and satisfied high mechanical and thermoelectric properties [1]. These mechanical properties play the particular importance at TEM applications in thermal generators and cooling micromodules.

The technological process of extrusion involves a lot of consecutive operations: synthesis of solid solution for required composition, grinding and dispersion of micron-sized powder, production of briquettes by powder cold pressing, hot extrusion and annealing of extruded rods. One of the factors, which may essentially impair the thermoelectric properties, is an interaction of the material with oxygen (oxidation process). Therefore all operations with its powder are carried out in an inert atmosphere.

The following questions are discussed in this presentation:
1. The production of extruded material from a micro- and nanopowder mixture.
2. The application of initial rod materials produced by different methods (preliminary extrusion and zone melting).
3. The influence of extrusion ratio on TEM properties of extruded rods.

The structure and texture distributions along a rod length were investigated by metallographic and X-ray methods for a compound $Bi_xSb_{2-x}Te_3$ extruded from solid solution. Some basic regularities of stucture formation for this material have been published in [2]. The mechanical properties have been investigated by means of the permanent record of the deformation diagram (load-deformation) in temperature range 293-623 K for the samples, which were cut in extrusion direction and perpendicular to it. The thermoelectric properties of extruded samples were measured by Harman's method.

The measurements at room temperature of mechanical and thermoelectric properties in p-type TEM samples showed the strength ~ 150 MPa and the thermoelectric efficiency ~ $3.5*10^{-3}$ K^{-1}, which satisfy the modern international standards.

ACKNOWLEDGMENTS

This investigation was supported by JSC "ROSATOM" (the state contract H.4б.44.90.13.1050) and Russian Foundation for Basic Research (the grants: 12-02-90027-Bel, 12-02-01126).

References

[1] Sabo Ye.P. // Journal of Thermoelectricity. 2005. V.3. P. 52-68.

[2] Lavrentev M.G., Osvenskii V.B., Mezhennii M.V. et al // Journal of Thermoelectricity.2012.V. 4.P. 36-42.

15:30 Oral

A novel stirred scraped wall crystallizer designed for melt and eutectic freeze crystallization

Marcos Rodriguez-Pascual, Alison E. Lewis

UNIVERSITY OF CAPE TOWN (UCT), RODENBOSCH, CAPE TOWN, CAPE TOWN 7701, South Africa

e-mail: marcos.rodriguezpascual@uct.ac.za

Many industrial processes involve one or more streams of electrolyte solutions. Melt crystallization is well known to be used for liquid purification been the limit of application eutectic conditions. In the other hand Eutectic freeze crystallization (EFC) has been reported to be economically more beneficial than the conventional techniques for the recovery of pure salt or acids and clean water (Van der Ham et al. 1999, Van der Ham et al. 2003, Vaessen et al. 2003). Van der Ham et al. showed that compared to triple-stage evaporative crystallization savings up to 70% of the energy consumption could be achieved depending on the type of salt. In an EFC process salt and ice are crystallized simultaneously at conditions just below the eutectic point of the aqueous solution. The selectivity of crystal growth leads to very pure products even when the solution contains many impurities as is often the case for industrial streams. Impurities can however, shift the eutectic point of the pure system. During eutectic freeze crystallization separation of the ice and the salt crystals can be perform gravitationally within the crystallizer or by centrifugal forces in or out of the crystallizer due to the difference in density between either the ice or the salt, and the mother liquor. In previous studies several prototypes of EFC crystallizers have been developed. The most important design characteristics of these crystallizers are the heat transfer rate that dictates the production rate, the residence time, the solid suspension and the separation efficiency, all them governed by the fluid dynamics in the crystallizer. Several Melt and EFC crystallizer designs and implementations have been reported in literature. As an example Vaessen et al. compared the performance of the Cooled Disk Column Crystallizer (CDCC-1) and the Scraped Cooled Wall Crystallizer (SCWC-1) (Vaessen et al. 2003). The heat transfer was higher in the CDCC-1 up to 7.2 kW m-2 compared with the 3.8 kW m-2 of the SCWC-1 due to the more effective removal of the developing ice scale layer from the heat exchanger surface. The gravitational separation on the other hand, was shown to proceed more effectively in the SCWC-1, because settling of the salt crystals and floatation of the ice crystals was not hampered by the horizontally positioned perforated cooling disks. However, separation difficulties still occurred at high solid percentages, and ice scale formation at low scraping rates (Genceli 2008). In this paper we present a novel Stirred Scraped Cooled Wall Crystallizer with an optimized fluid dynamics design for higher heat transfer, crystal suspension and for efficient gravitational separation to increase the throughput. Heat transfer and fluid dynamics were simultaneously investigated by using thermocromic liquid crystal slurry and crystallization kinetics were investigated in situ in a continuous crystallizer were crystal size distribution, morphology and purity of the crystals were determined.

References:

Genceli, F. E. Scaling-Up Eutectic Freeze Crystallization, PhD dissertation, Delft, 2008

Vaessen, R.J.C., Janse, B.J.H., Seckler, M.M., Witkamp, G.J. Evaluation of the Performance of a Newly Developed Eutectic Freeze Crystallizer Scraped Cooled Wall Crystallizer, Chemical Engineering Research and Design 81(2003), A10, 1363-1372

Van der Ham, F., Witkamp, G.J., De Graauw, J., Van Rosmalen, G.M. Eutectic Freeze Crystallization Simultaneous Formation and Separation of Two Solid Phases, J. Cryst. Growth 198-199(1999), 744-748

Van der Ham, F., Seckler, M.M., Witkamp, G.J. Eutectic Freeze Crystallization in a New Apparatus: The Cooled Disk Column Crystallizer, Chem. Eng. Proc. 43(2003), 161

Coffee
Thursday afternoon, 15 August, 16:00

Posters

Wednesday, 14 August

WeP-G04
Wednesday afternoon, 14 August, 16:00
Room 211, Old Library

16:00 Poster We168

The Effect of Ultrasonication on Calcium Carbonate Crystallization in the Presence of Biopolymer

Semra Kirboga, Mualla Oner, Emel Akyol

Yildiz Technical University (YTU), Chemical Engineering Department Davutpasa Campus, Esenler, Istanbul 34210, Turkey

e-mail: eakyol@yildiz.edu.tr

Synthesis of calcium carbonate (CaCO3) was carried out using sonication in aqueous solution medium. The effect of the probe immersion depth (PID) and the amplitude of sonicator on calcium carbonate crystallization were studied in the absence and presence of biopolymer, carboxymethyl inulin (CMI). Calcium carbonate crystals synthesized with and without ultrasound were compared. XRD analysis showed that calcium carbonate obtained in the presence of biopolymer was a mixture of calcite and vaterite whereas there was only calcite polymorph in the absence of biopolymer. In the presence of biopolymer, the relative fraction of vaterite increased with the application of sonication process. The higher amplitude resulted in the higher relative vaterite fraction. The results showed that the probe immersion depth and the amplitude affected the morphology of calcium carbonate.

16:00 Poster We169

Does Chirality Influence the Tendency of Co-crystal Formation ?

Fanny George[1], Bernadette Norberg[2], Johan Wouters[2], Tom Leyssens[1]

1. *Université Catholique de Louvain (UCL), Louvain-la-Neuve 1348, Belgium* **2.** *University of Namur (FUNDP), rue de Bruxelles 61, Namur 5000, Belgium*

e-mail: fannygeorge@gmail.com

One of the goals of crystallization processes is to obtain a pure form, especially when treating with active pharmaceutical ingredients (API). Different forms of these latter may be accessible (polymorphs of the pure compound, salts/hydrates/co-crystals ...). One form may differ significantly from another by its physicochemical properties, such as its solubility or bioavailability. A multitude of drug substances are marketed under salt form. As salt formation mainly depends on pKa differences between base and acid, an acid/base interacting with a given chiral API is also expected to interact with the racemic version of the API (containing both enantiomers). However, one can question whether this still holds for co-crystals, as these compounds, mostly depend on hydrogen-bonding interactions, which are directional.

We therefore decided to perform a systematic co-crystal search for the enantiopure and racemic version of a given compound, that does not form a salt. We recently identified a series of co-crystals for Levetiracetam, which is an anticonvulsant drug used in the treatment of epilepsy. Levetiracetam is the biologically active enantiomeric form of (RS)-2-(2-oxopyrrolidin-1-yl) butanamide.

Here we identified several co-crystals of Levetiracetam and the racemic equivalent using solvent drop grinding and a wide variety of coformers. XRPD was used to detect co-crystals. X-ray single crystal diffraction analysis was carried out to confirm positive hits. 20 co-crystals of the enantiopure compound were obtained, whereas 29 of the racemic compound were identified. Out of these, 17 share a common coformer.

16:00 Poster We170

Populations and size distributions of solute-rich mesoscale structures in aqueous amino acid solutions and their role in crystal nucleation

Anna Jawor-Baczynska[1], Barry D. Moore[2], Jan Sefcik[1]

1. *University of Strathclyde, Chemical and Process Engineering, 75 Montrose Street, Glasgow G11XJ, United Kingdom* **2.** *University of Strathclyde, Department of Pure and Applied Chemistry, 295 Cathedral Street, Glasgow G11XL, United Kingdom*

e-mail: anna.jawor-baczynska@strath.ac.uk

Aqueous solutions of well soluble molecules such as small amino acids are usually assumed to be essentially homogenous systems with some degree of local structuring due to specific interactions on the sub-nanometre scale (e.g. molecular clusters, hydration shells) usually not exceeding several solute molecules. However, recent theoretical and experimental studies have indicated presence of mesoscale structures in solutions of small organic and inorganic molecules as well as proteins[1].

We investigated both supersaturated and undersaturated aqueous solutions of two simple amino acids (glycine and DL-alanine) using Small Angle X-ray Scattering (SAXS), Dynamic Light Scattering (DLS) and Brownian Microscopy/Nanoparticles Tracking Analysis (NTA). Colloidal scale mesostructures were previously reported in supersaturated solutions of those amino acids and were implicated as intermediates species on non-classical crystallization pathways[2,3]. Surprisingly, we found that these mesostructures were also present in undersaturated solutions at solute concentrations well below the solid-liquid equilibrium (saturation) concentration at a given temperature, with mean sizes ranging from 100 to 300 nm and size distributions widening towards larger sizes with increasing solute concentrations. While DL-alanine mesostructures appeared to be solid-like and could be filtered out by 100 nm syringe PTFE filters, glycine mesostructures were comfortably passing through these filters and are thought to be liquid-like.
Using experimentally measured size distributions of these mesostructures from NTA, SAXS intensity data were fitted using various structural models and an excellent agreement was obtained using a mass fractal model with the fractal dimension d_f=2.7 suggesting fairly compact clusters with highly irregular interfaces. This is not surprising, since it is expected that the surface tension between the mesostructures and surrounding bulk solution would be very low as they only differ

in glycine concentration. The result may be an undulating interfacial topology similar to that found in complex surfactant or block-copolymer systems.

We note that these mesostructures are not a separate phase but a part of the liquid solution phase and are in equilibrium with the surrounding bulk solution. Therefore they are also in equilibrium with the solid phase when the overall solution concentration is equal to the saturation concentration at a given temperature. The local concentration of glycine in mesostructures is higher than that in the surrounding bulk solution so when the system is supersaturated nucleation is more likely to occur in them. However, if the nuclei produced are smaller than the critical nucleus size, they will redissolve when they are exposed to the surrounding bulk solution.

1 Vekilov, P. G. Dense Liquid Precursor for the Nucleation of Ordered Solid Phases from Solution. *Crystal Growth & Design***4**, 671-685, (2004).

2 Ma, Y., Cölfen, H. & Antonietti, M. Morphosynthesis of Alanine Mesocrystals by pH Control. *The Journal of Physical Chemistry B***110**, 10822-10828, (2006).

3 Jawor-Baczynska, A., Sefcik, J. & Moore, B. D. 250 nm Glycine-Rich Nanodroplets Are Formed on Dissolution of Glycine Crystals But Are Too Small To Provide Productive Nucleation Sites. *Crystal Growth & Design*, (2012).

16:00 Poster We171

Growth of scorodite crystals from an aqueous solution bearing arsenic by photo catalysis method

Hideyuki Okamura, Hironori Itoh, Ryuichi Komatsu

Yamaguchi University, 2-16-1 Tokiwadai, Ube 755-8611, Japan

e-mail: r-komats@yamaguchi-u.ac.jp

1. INTRODUCTION

Smelting copper and other metals actually produces arsenic as a by-product [1]. Currently, these arsenic has been simply stored because of no demand, and thus the technology required to make arsenic insoluble for safe storage has been developed vigorously. In these researches, scorodite crystals ($FeAsO_4 \cdot 2H_2O$) have been receiving attention because of their low solubility [3], and much efforts to synthesize easily scorodite are being widely performed [4-7]. Recently, novel scorodite synthesis technology by injecting O_2 gas under atmospheric pressure has been reported and is attracting much attention as simple and easy synthesis method [8-11]. In this method, Fe^{2+} ion in solution is oxidized to Fe^{3+} by O_2 gas injection, and scorodite crystals precipitate from the solution containing Fe^{3+} and As(V) ions. It has also been revealed that synthesized scorodite by this method has actually low solubility [11].

Products in this method, however, include small sized crystals with up to several μm in diameter to some extent [8]. Such small crystals dissolve more easily than large ones because of large surface area in unit volume, and the concentration of arsenic may suddenly increases in current water such as the subsurface water. In addition, such small crystals are actually grown under high super-saturation, and it is also reported that amorphous precipitations with scorodite composition having high solubility [3] are synthesized under high super-saturation [6]. Therefore, the development of new method to grow crystals with larger diameter has been required for more safety immobilization of arsenic.

Crystals with similar large particles can be synthesized under low super-saturation [12], whereas in O_2 gas injection method, it is difficult to form such crystals because the supersaturation of scorodite crystal growth with the flow quantity of O_2 gas is large [13].

Photocatalyst irradiated with UV light was frequently used in order to oxidize Fe^{2+} ions in solution [14, 15], and it also was considered that photocatalyst can easily control the oxidation rate of Fe ions, depending on the strength of UV light, and keep the super-saturation low.

Therefore, in this paper, growth of scorodite crystals has been investigated using a photocatalyst irradiated with UV light, and growth behavior of scorodite crystal in this method compared with scorodite synthesized by O_2 gas injection associated with particle size.

2. EXPERIMENTAL PROCEDURE

The experiment flowchart is shown in Fig.1. Figure 2 also depicts a schematic drawing of the experimental apparatus. As_2O_3 derived from the copper smelting process was used as starting material. Starting material (5.28g or 2.74g) was dissolved in 40ml of deionized water and then oxidized by adding molar equivalent hydrogen peroxide to produce As (V) solution. To this arsenic solution, $FeSO_4 \cdot 7H_2O$ (11.1g)(Analytical- reagent grade) and anatase TiO_2 (0.500g)(Titan Kogyo Ltd. , Japan) as a photocatalyst were added. Ultraviolet light from a UV lamp (λ=365nm, 810μW/cm3) irradiated this solution while it was stirred at 90°C to synthesize scorodite. The solution was filtered after experiment period and a powdered product was obtained through natural drying. For comparison, scorodite crystals were also synthesized by O_2 gas injection using a glass tube (inner diameter 5mm) that was just the same as the one used for synthesis by irradiation with UV light. All experiments were conducted in a glove box to ensure safety.

These products were identified by X-ray powder diffraction (XRD). Crystal morphology was observed on optical microscope and scanning electron microscope (SEM). To clarify the growth behavior, the particle density in the initial stage of reaction and the crystal size distribution (CSD) was measured. the crystal density was obtained by sampling 10μl of slurry using a microsyringe, spreading it on a glass plate to a diameter of 14mm, and then counting the number of crystals in that area. The CSD was obtained measured the ferret diameters [16] of 300 particles from the SEM photo of the filtered product.

3. RESULTS AND DISCUSSION

3.1 Product evaluation

XRD results of two products were shown in Fig.3. This figure indicates that only scorodite without another phase is synthesized by two methods. In particular, it was revealed for the first time that scorodite can grow using a photocatalyst.

Figure 4 shows SEM photo-images of synthesized scorodite. Synthesis by UV light irradiation yielded crystals with similar particle sizes. In contrast, crystals synthesized by O_2 gas injection were the mixture of large and small crystals with greatly different particle diameters. We were not able to observe the difference in morphology between crystals synthesized by each of the two methods. Also, in this study, it is clearly revealed that TiO_2 acted as catalyst to form the nucleation of scorodite crystal. However, we could not obtain new information on relationship between TiO_2 and scorodite as well as heterogeneous nucleation of scorodite on surface of TiO_2 catalysis has not been clear. Further information to clear such a relationship will be done.

3.2 Growth mechanism of scorodite crystal by photocatalyst

The color of the solution changed from pale-white to green within one hour in O_2 gas injection, whereas the change in color in UV irradiation took place at 12 hours. This change depends on the amount of scorodite crystals. Therefore, this result indicates that the growth rate of scorodite by UV light irradiation is clearly slower than that of synthesis by O_2 gas injection.

Measurement results of the number of crystals per unit area in the initial stage in two growth methods is shown in Table I. Although it was impossible to count the number of crystals in one hour of the reaction time by UV light irradiation because almost all of the unreacted mater-

ial and TiO_2 remained, in 3hours, the number of crystals by UV light irradiation was one-fifth that of O_2 gas injection. In addition, it was one-fourth the numbers of crystals after one hour of reaction by O_2 gas injection. This crystal density can be considered as the nucleation density in the solution.

From these experimental results, it was concluded that super-saturation is clearly lower in synthesis by UV light irradiation than in synthesis by O_2 gas injection.

Figure 5 illustrates CSD curves with time for each synthesis method. Curves in UV light irradiation show single peaks and the average was 5 to 10μm, whereas CSD curves with O_2 gas injection have two peaks, indicating a broader distribution of crystal sizes.

The CSD curve for UV light irradiation changed with reaction time from asymptotic to lognormal between three to five hours, but such changes occurred within three hours in O_2 gas injection. An asymptotic CSD curve is expected when both nucleation and crystal growth occur, while a lognormal curve is expected when crystal growth is predominant over nucleation [17]. It is considered that the CSD curve is asymptotic at high super-saturation and changes to lognormal curve as super-saturation decreases. The CSD curve produced by O_2 gas injection is asymptotic. But the CSD curve changes to lognormal curve in a short time. This reason is due to the rapid decrease of super-saturation, originated from large nucleation density and crystal growth of each nucleus crystal at high super-saturation. On the other hands, low nucleation density and slow crystal growth rate can be expected in UV light irradiation because of low super-saturation compared with O_2 gas injection, and the super-saturation will decrease more slowly compared with that in O_2 gas injection. As a result, the time for the CSD curve to change from asymptotic to lognormal with UV light irradiation is longer than with O_2 gas injection.

As depicted in Fig. 5 (b), bimodal peaks in O_2 gas injection was not observed in UV light irradiation. As for bimodal peaks, it has been reported that secondary nucleation, occurred by rapid nucleation at high super-saturation, causes such bimodal peaks in CSD [18]. Conversely, such peaks in CSD curve in UV light irradiation are not observed because of low super-saturation.

Compared with O_2 gas injection, it was revealed in UV light irradiation that number of crystals with less than 5 μm in diameter is smaller, but growth rate is slower. In order to synthesize rapidly scorodite crystals with similar diameter for a short time, it is also considered that synthesis of combining UV light irradiation and O_2 gas injection is required. Scorodite crystals are formed first by UV light irradiation to decrease concentration at which spontaneous nucleation can not take place, and then are grew further by O_2 gas injection.

4. CONCLUSIONS

Scorodite crystals have been successfully grown using a photocatalyst irradiated by UV light for the first time. It was also revealed that these crystals in UV light irradiation were grown in lower super-saturation compared with O_2 gas injection.

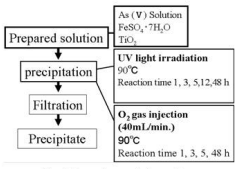

Fig.1 Experimental flow-chart

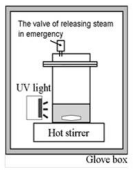

Fig.2 Schematic diagram of experimental apparatus in glove box.

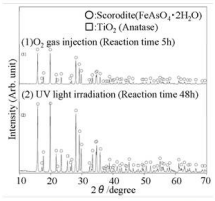

Fig.3 X-ray diffraction patterns of precipitated samples.

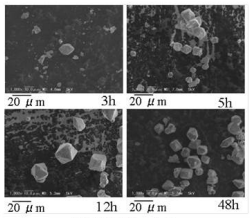

(a) UV light irradiation

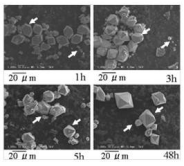

(b) O_2 gas injection

Fig. 4 SEM photo-images of grown crystals ((a) UV light irradiation and (b) O_2 gas injection).

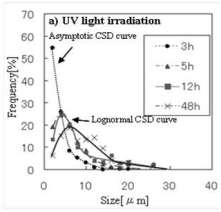

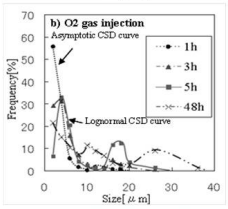

Fig. 5 Crystal size distributions with reaction time in each method ((a) UV light irradiation and (b) O_2 gas injection).

References

[1] J. E. Hoffmann, JOM, 45, 30-31 (1993).
[2] A. J. Monhemius and P. M. Swash, JOM, 51, 30-33 (1999).
[3] E. Krause and V.A. Ettel, Hydrometallurgy, 22, 311-337 (1989).
[4] M.A. Gomez, L. Becze, J. N. Cutler, and G.P. Demopoulos, Hydrometallurgy, 107, 74-90 (2011).
[5] M.A. Gomez, L. Becze, M. Celikin, and G.P. Demopoulos, J. Colloid Interface Sci., 360, 508-518 (2011).
[6] G.P. Demopoulos, D.J. Droppert, and G. Van Weert, Hydrometallurgy, 38, 245-261 (1995).
[7] D. Filippou and G. P. Demopoulos, JOM, 49, 52-55 (1997).
[8] T. Fujita, R. Taguchi, M. Abumiya, M. Matsumoto, E. Shibata, and T. Nakamura, Hydrometallurgy, 90, 92–102 (2008).
[9] T. Fujita, R. Taguchi, M. Abumiya, M. Matsumoto, E. Shibata, and T. Nakamura, Hydrometallurgy, 90, 85-91 (2008).
[10] T. Fujita, R. Taguchi, M. Abumiya, M. Matsumoto, E. Shibata, and T. Nakamura, Hydrometallurgy, 93, 30-38 (2008).
[11] T. Fujita, R. Taguchi, H. Kubo, E. Shibata, and T. Nakamura, Materials Transactions, 50, 321-331 (2009).
[12] H. A. Mohameed, B. Abu-Jdayil, M. Al Khateeb, Chemical Engineering and Processing, 41, 297–302 (2002).
[13] H. Okamura, bachelor thesis, Yamaguchi University (2009).
[14] W. Z. Tang and H. An, Chemosphere, 31, 4157-4170 (1995).
[15] H. Fei, W. Leng, X. Li, X. Cheng, Y. Xu, J. Zhang, and C. Cao, Environmental Science & Technology, 45, 4532–4539 (2011).
[16] T. Allen, "Particle size measurement", Chapman and Hall, London, (1968) pp.46-48.

[17] K. Sangwal, "Additives and Crystallization Processes: From Fundamentals to Applications", John Wiley & Sons, Inc., New York City, (2007) pp.291-295.
[18]R. Misumi, M. Tsukada, K. Nishi, and M. Kaminoyama, Journal of Chemical Engineering of Japan, 40, 939-946 (2008).

16:00 Poster We172

Influencing the crystallization behaviour of multi crystalline silicon in a R&D furnace

Iven Kupka[1], Christian Reimann[2], Jan Seebeck[2], Toni Lehmann[1], Ulrike Wunderwald[1], Jochen Friedrich[2], Kaspars Dadzis[3], Frieder Kropfgans[3], Lamin Sylla[3]

1. *Technologiezentrum Halbleitermaterialien, Freiberg 09599, Germany* **2.** *Fraunhofer Institut IISB, Schottkystr. 10, Erlangen 91058, Germany* **3.** *SolarWorld Innovations GmbH, Freiberg 09599, Germany*

e-mail: iven.kupka@iisb.fraunhofer.de

For a further improvement of the industrial crystallization process of multi crystalline silicon for PV application it is necessary to gain a fundamental understanding of the initial nucleation process of silicon on the crucible bottom, the subsequent grain selection process and the final grain growth behaviour over the crystal height. These phenomena have to be understood to decrease the amount of recombination active regions especially in form of harmful dislocation clusters and therefore to increase the resulting solar cell performance.
For this reason a R&D crystallization furnace was developed at Fraunhofer THM, which offers different ways to influence the grain structure and the defect formation during directional solidification of multi crystalline silicon ingots in G1 crucibles.
It is well known that on the one hand the nucleation process can be affected by the thermal conditions occurring during the start of crystallization. On the other hand the thermal field can be influence by the use of a time-dependent magnetic field in an elegant way. Therefore, we studied the nucleation and subsequent grain growth process under the action of a special configuration of a time-dependent magnetic field. Based on 3D numerical simulations [1] a heater configuration consisting of 3 side heaters with a standard AC power supply (fixed frequency of 50 Hz) was implemented in a new R&D furnace which allows the solidification of multicrystalline silicon ingots in G1 crucibles. Different Lorentz forces, which can vary in direction and magnitude, are generated in the silicon melt by changing the phase shift between the side heaters. This leads to various axial and radial temperature gradients caused by various convection conditions in the melt. Experimental and numerical investigations show clearly that the highest Lorentz force density, generated with a phase shift at the side heaters of 0°, leads to a strong melt mixing and small temperature gradients, whereas a small Lorentz force density, generated with a phase shift at the side heaters of 180° increases the temperature gradients in the melt because of lower melt mixing.
It will be shown that the initial nucleus formation is affected by the used convection conditions. In addition to the level of melt mixing the influence of the cooling conditions and the properties of the crucible bottom on the initial grain growth will be addressed.

16:00 Poster We173

Quantitative analysis of the cover effects on crystal growth in the industrial directional solidification process for silicon ingots

Zaoyang Li[1,2], Yunfeng Zhang[3], Zhiyan Hu[3], Genshu Zhou[2], Lijun Liu[1]

1. *School of Energy and Power Engineering, Xi'an Jiaotong University, Xi'an 710049, China* **2.** *School of Materials Science and Engineering, Xi'an Jiaotong University, Xi'an 710049, China* **3.** *Yingli Green Energy Holding Co. Ltd., Baoding 071051, China*

e-mail: ljliu@mail.xjtu.edu.cn

Directional solidification (DS) has been the main method to manufacture multi- and mono-crystalline silicon ingots for solar cells. The DS process is a highly coupled nonlinear thermal system with complex heat and mass transport. It includes solid thermal conduction, melt convection, argon flow, thermal radiation, phase change, as well as transport of oxygen, carbon and other impurities. These transport characteristics can influence the crystal growth of silicon ingots significantly [1]. Therefore, many measures are implemented to control the heat and mass transport in the DS process to optimize the crystal growth and improve the ingot quality.

For the industrial 500 kg DS process, a cover is usually fixed above the crucible, which is different from the previous furnace for silicon ingots of 240 kg [2]. The cover can uniform the thermal field and change the gas flow pattern as well as the pathway of argon gas flow, which is of benefit to the impurities control. Gao et al. [3] did almost the same thing for a laboratory-scale DS furnace to reduce oxygen and carbon concentrations in the silicon ingots. Teng et al. [4] investigated the cover effects on thermal field and oxygen distribution when crystal grows. As is known, the DS is a complex process including heating, melting, growing, annealing and cooling stages. However, few studies have been published regarding the cover's effects on heat and mass transport through the entire DS process.

In this paper, an industrial DS furnace that can produce 500 kg ingots is chosen to undertake the numerical study. Transient simulations of global heat transfer, including melt convection, argon flow, thermal conduction, radiation and phase change, are carried out and validated by comparing with the industrial experiment. Fig.1 compares the temperature variation at the crucible bottom between numerical simulations and experimental data for the entire DS process. Four solid vertical lines divide the curve sections into heating, melting, growing, annealing and cooling stages. The numerical predictions agree satisfactorily with the experimental measurements. Therefore, the transient global heat transfer model can reproduce the entire industrial DS process for production of large-size silicon ingots.

Fig.2 and Fig.3 show the stream lines of argon gas flow above the silicon melt for DS furnaces with and without a cover design. It is obvious that the cover can modify the argon flow pathway and thus affect the impurities transport. Furthermore, since the cover is fixed in the space between the graphite heaters and the silicon melt surface, radiant heat from the heaters to the silicon can be directly influenced. As the radiative heat transfer is dominant in high temperature environment, the crystal growth process for silicon ingots must be affected. Based on the above analysis, we quantitatively compare the power consumption, melting time and sequence, temperature distribution and solidification front surface shape, as well as thermal stress distribution after annealing for the entire DS processes with and without a cover design. The study can help us to deeply understand the important role of the cover effects

on crystal growth through the entire industrial DS process for silicon ingots.

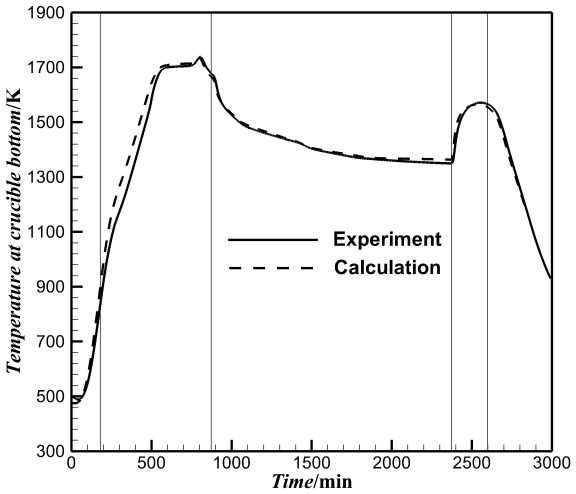

Fig. 1 Comparison of simulations with experiment: temperature evolutions at crucible bottom.

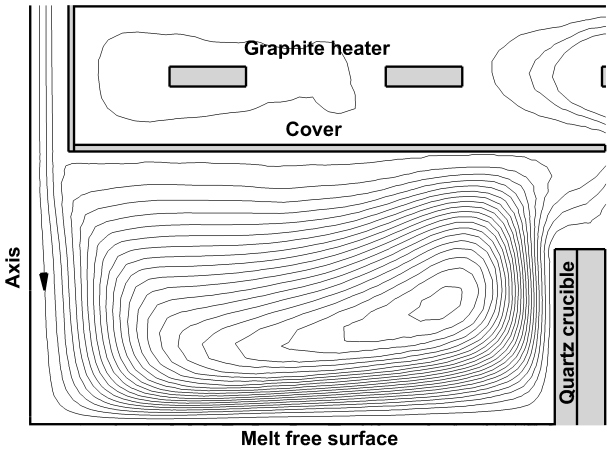

Fig. 2 Stream lines of argon gas flow above the silicon melt surface with a flat cover design.

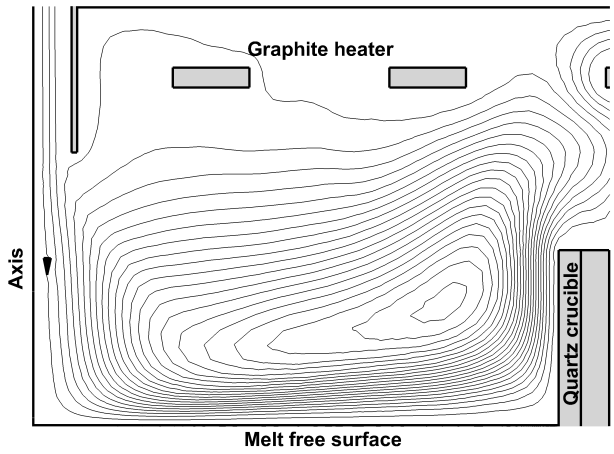

Fig. 3 Stream lines of argon gas flow above the silicon melt surface without a cover design.

References:

[1] P. Rudolph, Sel. Top. Cryst. Growth 1270 (2010) 107.
[2] H. Zhang, L. Zheng, X. Ma, B. Zhao, C. Wang, F. Xu, J. Cryst. Growth 318 (2011) 283.
[3] B. Gao, X.J. Chen, S. Nakano, K. Kakimoto, J. Cryst. Growth 312 (2010) 1572.
[4] Y.Y. Teng, J.C. Chen, C.W. Lu, C.Y. Chen, 360 (2012) 12.

16:00 Poster We174

Precipitation of Calcium Carbonate with Different Morphologies in the Resourcization of Distiller Waste

Yunzhao Li, Xingfu Song, Jianguo Yu

East China University of Science and Technology, Shanghai 200237, China

e-mail: liyunzhao@mail.ecust.edu.cn

Combined with circular economy and comprehensive utilization, a new method was put forward in this paper for the treatment of distiller waste produced in soda industry. Calcium chloride was changed into precipitated calcium carbonate through a reaction-extraction-crystallization process. The reaction equation was as follows:

$$CaCl_2 + CO_2 + H_2O + 2S \rightarrow CaCO_3\downarrow + 2S{\cdot}HCl$$

The effects of the concentration of extractant, phase ratio, the initial concentration of calcium chloride, partial pressure of carbon dioxide, stirring rate, reaction temperature and time on the conversion rate of calcium chloride and the size distribution and morphology of calcium carbonate were investigated with regard to the gas-liquid-liquid-solid system. The optimal operating variables were found and results showed that calcium carbonate particles with different morphologies could be prepared in the presence of different additives. The solid products were characterized with scanning electron microscopy, partial size analyzer and X-ray diffraction. The mass transfer mechanism was demonstrated simultaneously.

16:00 Poster We175

Study on the metastable zone width of potassium nitrate aqueous solutions by polythermal method

Ewa Mielniczek-Brzóska

Jan Długosz Academy, Al. Armii Krajowej 13/15, Częstochowa 42-200, Poland

e-mail: e.mielniczek@ajd.czest.pl

Results of an experimental study of the metastable zone width of pure potassium nitrate aqueous solutions contained in 4-cm^3 capacity cuvettes of a UV−Vis spectrophotometer investigated as functions of cooling rate R and saturation temperature T_0 of the solution by the polythermal method are described and discussed. The metastable zone width was measured as the maximum supercooling ΔT_{max} defined as the difference between the saturation temperature T_0 and the temperature T_{lim} at which first crystals are detected in the solution, i.e. $DT_{max} = T_0 - T_{lim}$. The changes occurring in the studied solutions during their cooling at constant predefined rates between 5 and 40 K/h were followed by registering changes in the intensity of transmitted light using the UV-Vis spectrophotometer. It was observed that the maximum supercooling ΔT_{max} for potassium nitrate aqueous solutions increases with increasing cooling rate R andsaturation temperature T_0. The experimental data on maximum supercooling ΔT_{max} corresponding to saturation temperature T_0 as a function of cooling rate R are analyzed by employing the following two approaches: self-consistent Nývlt-like approach and a novel approach based on the classical three-dimensional nucleation theory. The above results of the metastable zone width of potassium nitrate solutions contained in cuvettes are compared with the literature data on the metastable zone width of solutions of relatively large volume in the absence and presence of seeds.

16:00 Poster We176

Evolution of Sapphire Melt Convection at the Transition to Large Scale Ky Technology

Svetlana Demina[1], Vladimir Kalaev[1], Andrey Smirnov[1], Vadim Ivanov[2]

1. *STR Group, Inc., Engels av. 27, P.O. Box 89, St-Petersburg 194156, Russian Federation* **2.** *Crystal Development Ltd., Moscow 127083, Russian Federation*

e-mail: Andrey.Smirnov@str-soft.com

Sapphire wafers of large diameter make LED manufacturing process significantly more efficient. Leading LED chip manufacturers have already moved from 2-inch to 4-inch substrates, and coming transition to 8-inch wafers was announced. However, the wafer thickness may increase significantly with diameter due to requirements of MOCVD and processing. Hence, more sapphire material is needed to meet this increased demand.

Economical conditions force the industry to produce larger sapphire boules or plates with subsequent scaling up of manufacturing equipment. Kyropoulos growth technique is well developed for sapphire charges up to 90 kg in a single crucible. Further increase in sapphire charge weight and crucible size generates additional difficulties during seeding stage and reduces the range of parameters within which it is possible to grow high quality crystals with high yields.

Using 3D computer simulations [1] and experimental observations, we have studied sapphire melt convection in crucibles containing 1, 30, and 65 kg sapphire charge. Quite different flow patterns were observed on the melt free surface for different charges. It was found out that there is a star-like flow structure in small scale crucibles, being indicative of optimality condition for stable and rapid seeding. For 65 kg charge, the flow structure changes to chaotic if the hot zone design suitable for 30 kg charge is simply scaled up to a larger furnace. 3D computer simulation has been applied for optimization of the furnace design and stabilization of melt flow during seeding stage in 65 kg sapphire growth furnace. Modified conditions helped to reduce significantly the seeding time.

[1] S.E. Demina, V.V. Kalaev, J. Crystal Growth 320, 23 (2011)

16:00 Poster We177

Amino acids as zwitterionic co-formers for cocrystallization

Natalia Tumanova[1], Bernadette Norberg[2], Johan Wouters[2], Tom Leyssens[1]

1. *Université Catholique de Louvain (UCL), Louvain-la-Neuve 1348, Belgium* **2.** *University of Namur (FUNDP), rue de Bruxelles 61, Namur 5000, Belgium*

e-mail: shikina.n@gmail.com

Cocrystals belong to a relatively new class of compounds, which are of special interest in pharmaceutics, as they may serve as alternative drug formulations. Cocrystals may have improved properties, such as the solubility or dissolution rate, in comparison with other crystalline forms of active pharmaceutical ingredients (APIs). Moreover, the production of drugs in the form of cocrystals may be more feasible and provide improved stability.

We used amino acids as co-formers to obtain co-crystals of different APIs. Amino acids are natural to the body, which makes them perfect candidates for cocrystallization of APIs – the drug Spidifen® (Ibuprofen and L-arginine) being the perfect industrial example of the use of an amino acid as a cocrystal co-former. We screened amino acids and amino acid derivatives with S-Naproxen, Levetiracetam, and S-Oxiracetam by liquid-assisted grinding with methanol. The results were analyzed by X-ray powder diffraction. Only S-Naproxen showed positive hits. So far, we succeeded to obtain single crystals for a co-crystal hydrate containing S-Naproxen and D-tryptophan. The structural motifs in that cocrystal are similar to those observed in (1???): amino acid molecules form zwitterionic head-to-tail chains, thereby organizing columns, to which S-Naproxen connects via hydrogen bonds. It thus seems that zwitterionic amino acids can be successfully used as cocrystal coformers with carboxylic acids, but fail when dealing with amides, or alcohol compounds. These results should be definitely taken into account when developing new solid forms of APIs.

1. Tilborg A, Springuel G, Norberg B, Wouters J, Leyssens T. CrystEngComm. 2013.

General Session 5

Characterization

Session Coordinators

Maria Kaminska (Poland) *Maria.Kaminska@fuw.edu.pl*

Marek Skowronski (USA) *mareks@cmu.edu*

Programme

Monday, 12 August

MoP-G05
Monday afternoon, 12 August, 17:00
Room 215, Old Library

Break
Monday evening, 12 August, 18:30

Tuesday, 13 August

TuO2

G05: Characterization
Tuesday afternoon, 13 August, 14:00
Room D, Auditorium Maximum

14:00 Invited oral

Application of microwave spectroscopy to studies of electron transport properties

Agnieszka Wołoś[1,2], Aneta Drabińska[2]

1. *Polish Academy of Sciences, Institute of Physics, Lotnikow 32/46, Warsaw 02-668, Poland* **2.** *University of Warsaw, Faculty of Physics, Institute of Experimental Physics (IFDUW), Hoża 69, Warsaw 00-681, Poland*

e-mail: wolos@ifpan.edu.pl

Many research laboratories in the world are equipped with EPR (Electron Paramagnetic Resonance) spectrometers dedicated to investigations of paramagnetic defects in crystalline materials. Whereas conducting samples placed in a microwave cavity of the spectrometer can show also features related to their magnetoconductivity. A condition necessary to observe these types of signals is presence of electric component of microwave field in the spot where the investigated sample is placed. This may require the use of specially designed resonators, such as these exploiting TM_{010} mode. It turns out, however, that in a popular TE_{102} rectangular cavity dedicated to investigations of magnetic dipole transitions, and thus such requiring absorption of a quantum of microwave magnetic field, the electric field component of microwaves spontaneously occurs in the center of the cavity due to disruption of the perfect distribution of microwave field by the presence of the sample and quartz elements of the cryostat. In such a resonator, we observe signals related to magnetoconductivity which may constitute an undesired background or an interesting object for study. We will shortly introduce such features recorded for different novel materials, $GaN/Al_xGa_{1-x}N$ heterostructures, graphene, and topological insulators.

At the $GaN/Al_xGa_{1-x}N$ interface, the two-dimensional electron gas forms spontaneously with typical sheet electron concentration of the order of $10^{12} – 10^{13}$ cm^{-2}. The frequency of the popular microwave X-band is close but slightly higher than the typical plasma frequency in mm-sized $GaN/Al_xGa_{1-x}N$ samples, allowing thus to observe edge magnetoplasma resonance in the X-band EPR spectrometer [1,2], Fig. 1(a). It has been recently reported, that similar conditions are as well fulfilled for the two-dimensional electron system in $Mg_xZn_{1-x}O/ZnO$ [3]. The magnetoplasma resonance, the coupled plasmon-cyclotron resonance, allows to determine electron concentration and mobility without having to make electric contacts. It allows to probe electric parameters even when the substrate is conductive or the structure contains conducting interfaces. The effective masses can be also investigated in this way [3]. Additionally, Shubnikov – de Haas oscillations can be also observed in EPR spectrometers, if only the applied magnetic field is high enough [1, 4, 5], Fig. 1(b). In general, the observation of both cyclotron or plasmon-cyclotron resonance and Shubnikov – de Haas oscillations requires high-mobility samples, as both the line width of the resonance line and the magnetic field onset for Shubnikov – de Haas signal scale with the mobility.

Low-field magnetoconductivity related to quantum effects of weak localization and antilocalization can be as well successfully investigated with the use of the EPR spectrometer. Modern spectrometers allow to inverse the direction of the magnetic field with very smooth zero crossing. Fig. 1(c) shows examples of weak localization and antilocalization phenomena measured for graphene [6], Bi_2Te_2Se topological insulator, and $GaN/Al_xGa_{1-x}N$ heterostructure. These are non-resonant signals, arising due to changes of the cavity quality factor induced by the change in sample conductivity. Unlike the previous case, one can investigate low-mobility samples, so as many scattering events occur before electron wave function loses its ability to interfere. For such a condition, it is a DC measurement, although microwave frequency is used to probe the sample.

Cyclotron resonance due to relativistic Fermions in Bi_2Te_3 topological insulator is shown in Fig.1(d). In a case of topological insulators from bismuth compound family, high bulk conductivity due to high concentration of native crystal lattice defects is a major obstacle to observe cyclotron resonance of topological surface states using optical transmission method or electric transport. Placing the sample in a resonance cavity provided so far the only way for observation of this phenomenon [5].

We would like to acknowledge teams of A. Hruban and W. Strupinski from the Institute of Electronic Materials Technology, Warsaw, C. Skierbiszewski from the Institute of High Pressure Physics, Unipress, Warsaw, and Z. Zytkiewicz from the Institute of Physics Polish Academy of Sciences, Warsaw for supplying us with samples for the studies. We would like to thank Prof. M. Kaminska for many fruitful discussions. This work was partially supported by the NCN grant no 2011/03/B/ST3/03362, Poland and NCBiR grant GRAFTECH/NCBR/02/19/2012, Poland.

1. A. Wolos, W. Jantsch, K. Dybko, Z. Wilamowski, and C. Skierbiszewski, Phys. Rev. B **76**, 045301 (2007).
2. A. Wolos, Z. Wilamowski, C. Skierbiszewski, A. Drabinska, B. Lucznik, I. Grzegory, S. Porowski, Physica B **406**, 2548 (2011).
3. Y. Kasahara, Y. Oshima, J. Falson, Y. Kozuka, A. Tsukazaki, M. Kawasaki, and Y. Iwasa, Phys. Rev. Lett. **109**, 246401 (2012).
4. G. Hendorfer, M. Seto, H. Ruckser, W. Jantsch, M. Helm, G. Brunthaler, W. Jost, H. Obloh, K. Kohler, D. J. As, Phys. Rev B **48**, 2328 (1993).

5. A. Wolos, S. Szyszko, A. Drabinska, M. Kaminska, S. G. Strzelecka, A. Hruban, A. Materna, and M. Piersa, Phys. Rev. Lett. **109**, 247604 (2012).
6. A. Drabinska, A. Wolos, M. Kaminska, W. Strupinski, and J. M. Baranowski, Phys. Rev. B **86**, 045421 (2012).

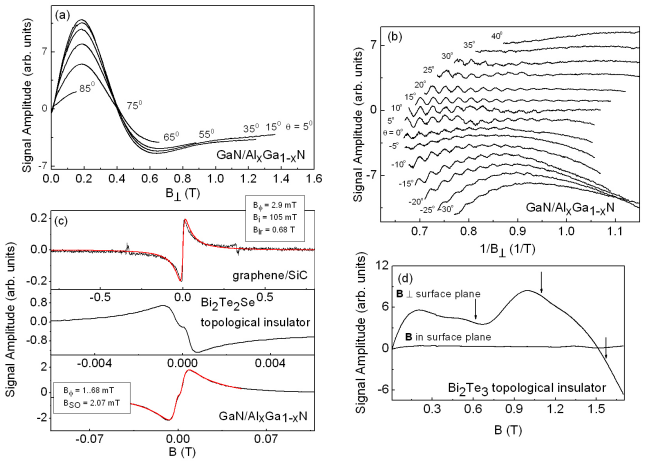

Figure 1. Signals recorded with the use of X-band EPR spectrometer. The temperature is about 5 K. (a) Edge magnetoplasma resonance in $GaN/Al_xGa_{1-x}N$ heterostructure. The angle between the direction of the magnetic field and the GaN c-axis (perpendicular to the plane of the two-dimensional electron gas) is given for each spectrum. (b) Shubnikov – de Haas oscillations in $GaN/Al_xGa_{1-x}N$ heterostructure dependent on the perpendicular to the sample plane component of the applied magnetic field. (c) weak localization (WL) and antilocalization (WAL) signals in: graphene grown on SiC (WL), Bi_2Te_2Se topological insulator (WL+WAL), $GaN/Al_xGa_{1-x}N$ heterostructure (WL+WAL). Fitted parameters are given. (d) Cyclotron resonance of relativistic Fermions in Bi_2Te_3 topological insulator. Arrows indicate position of the three distinguished resonance lines.

14:30 Oral

Optical Characterisation of Bulk ZnO Crystals Grown by CVT

Krzysztof P. Korona[1], Katarzyna Gas[2], Anna Reszka[2], Paweł Skupiński[2], Krzysztof Grasza[2], Bogdan J. Kowalski[2], Agnieszka Kamińska[3]

1. *Warsaw University, Institute of Experimental Physics (IEP UW), Hoża 69, Warszawa 00-681, Poland* **2.** *Polish Academy of Sciences, Institute of Physics, al. Lotników 32/46, Warszawa 02-668, Poland* **3.** *Institute of Physical Chemistry Polish Academy of Sciences (IPCPAS), Kasprzaka 44/52, Warsaw 01-224, Poland*

e-mail: kkorona@fuw.edu.pl

The ZnO crystals are interesting as substrate materials for ZnO homoepitaxy and for epitaxy of other II-VI materials. Such devices promise new applications in spintronics as well as for blue/UV optoelectronics, including light-emitting or even laser diodes.

ZnO crystals were grown by the chemical vapour transport method (CVT)

The time-resolved photoluminescence (TRPL) was measured using of a 30-cm spectrograph (0.05 nm resolution) and a synchroscan streak camera (2.5 ps resolution). For absorption measurements Cary 5000 spectrophotometer was used. Raman scattering was measured using Renishaw InVia Raman system

The as grown crystals had characteristic orange colour. Annealing in vacuum or oxygen led to transparent crystals. On the other hand, samples annealed in Zn stayed orange. In all cases the colour was caused by absorption band starting at 2.1 eV. Moreover, absorption band related to O vacancy at 3.1 eV was visible.

The photoluminescence spectra were composed of long-living ($\tau > 10$ ns), green (2.4 eV) band (GL), probably related to O vacancy and the near band-gap luminescence (NBL). It could be observed (see Fig. 1.) that samples with high red absorption showed lower luminescence, with shorter NBL lifetimes (of the order of 0.1 ns).

At low temperatures (below 100 K) NBL split into series of peaks with different lifetimes, what is due to exciton formation. At 4 K (see Fig. 2) a few distinct peaks were identified: $h\nu = 3.377$ eV, $\tau = 60$ ps - free exciton A (FX_A); 3.374 eV, 90 ps - donor bound exciton B(DX_B); 3.362 eV, 300 ps - donor bound exciton A (DX_A). The width (HWFM) of the DX_A peak was about 2 meV, what confirms good crystal quality of the samples.

Temperature-dependent measurements revealed interesting details about carriers dynamics. The increase of temperature from 4 to 100 K caused decrease of brightness and lifetime, but further heating, above 100 K, leads to increase of carriers lifetime (but decrease of brightness). It can be explained by assumption that carrier recombination is mainly radiative and defect-related decay is less important.

Raman spectroscopy shown that samples has sharp phonon spectra (width of E_2^H peak FWHM = 9 cm^{-1}). In the as grown material strong A_1(TO) phonon was observed. It vanished after annealing in O_2.

This work was partially supported by the National Centre for Research and Development (Poland) grant No. PBS1/A5/27/2012, by National Science Centre in Poland, grant UMO-2011/01/D/ST7/02657 and by European Union within European Regional Development Fund, through the Innovative Economy Grant: POIG.01.01.02-00-108/2009/3.

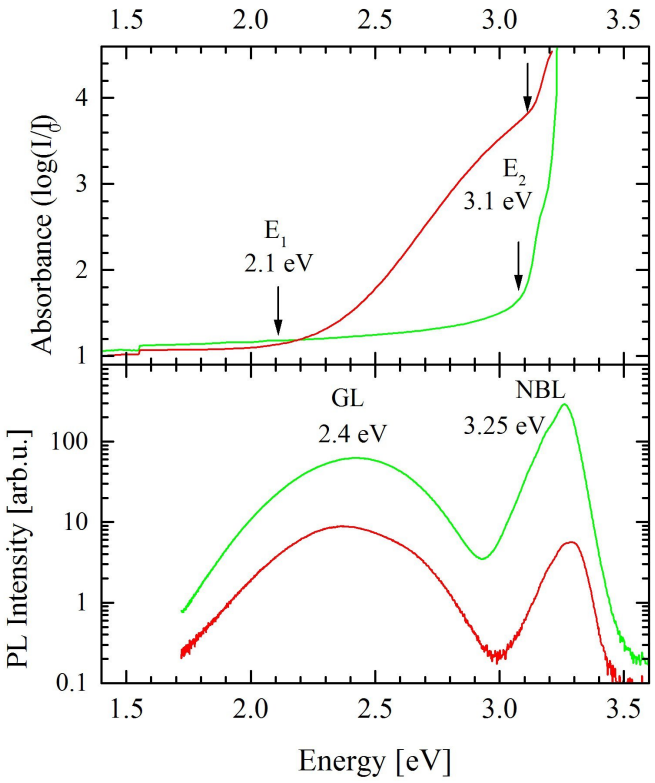

Fig. 1. Room temperature absorption and PL spectra of samples annealed in vacuum (green) and in Zn vapour (red).

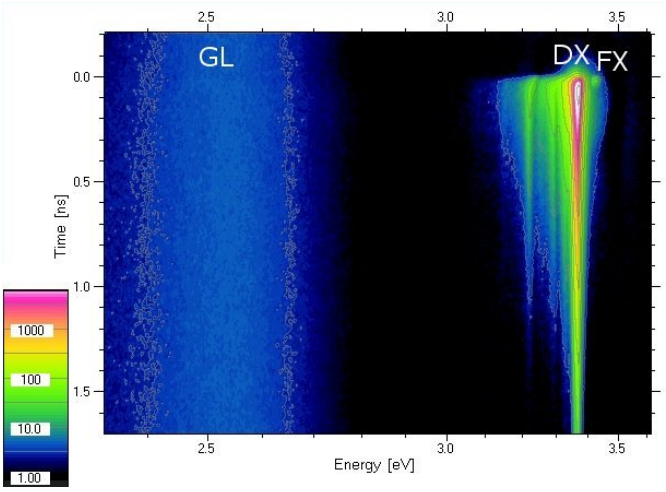

Fig. 2. Time resolved spectrum at 4 K.The GL band has so long lifetime that its decay is nearly unobservable. n the other hand the FX lifetime is so short that the peak look like a dot.

in Zn rich conditions at 950°C (temperature of ZnO source material was 1050°C). Hydrogen was used as a transport agent. Three samples from one crystal were annealed in three different atmospheres: oxygen, vacuum, or zinc vapour at ~1000°C for 39 hours.

14:45 Oral

Characterization of optical quality of GaSe:Al crystals by exciton absorption peak parameters

Konstantin A. Kokh[1,2], Yurii Andreev[3,4], Tatyana Izaak[4], Gregory Lanskii[3,4], Anna Shaiduko[3,4], Valery Svetlichnyi[4]

1. *Institute of Geology and Mineralogy SB RAS (IGM), Koptyuga ave., 3, Novosibirsk 630090, Russian Federation* **2.** *Novosibirsk State University (NSU), Pirogov 2, Novosibirsk 630090, Russian Federation* **3.** *Insitute of Climatic and Ecological Systems of SB RAS (IMCES), 10/3 ave Akademicheskii, Tomsk 634055, Russian Federation* **4.** *Tomsk State University (TSU), Lenina, 36, Tomsk 634050, Russian Federation*

e-mail: k.a.kokh@gmail.com

It is well known that doping of GaSe crystals with isovalent elements: Al [1], S [2, 3], In [4, 5], Te [6, 7] and Er [8] strengthens the structure and improves optical quality , which in turn increases efficiency of parametric frequency conversion into mid-IR and THz ranges. On the other hand, excess doping leads to destruction of the lattice structure [9]. So it is obvious that intermediate optimal doping should exist. Direct search of this concentration by conventional spectroscopic measurements is very complicated due to low optical losses of GaSe in the range of maximal trabsparency (absorption coefficient ≤0.1-0.2 cm^{-1}). Available data on the optimal doping in GaSe that resulted in the best optical quality and maximal conversion efficiency are limited by the only paper on tellurium doping [10]. The proposed method of characterization included two stages: (1) recording of absorption spectra of GaSe crystals with a set of doping concentration out of maximal transparency range, i.e. THz absorption spectra, (2) selection of a sample with maximal phonon peak intensities and narrowest spectral bandwidths. Optimal doping of selected samples was then confirmed by efficiency of SHG and optical rectification experiments. But to apply this method one needs quite rare and expansive facility. In this study we propose the recording of exciton absorption spectra by widespread and cheap UV-visible absorption spectrophotometer. Selection of optimally doped crystal can be carried out by: (1) choosing a crystal with maximal intensity and narrowest spectral bandwidth of exciton absorption peak, (2) choosing of a crystal with maximal gradient of the absorption end, and (3) with minimal absorption at the bottom of the absorption end (Fig. 1). Physical basis for this proposal will be discussed.

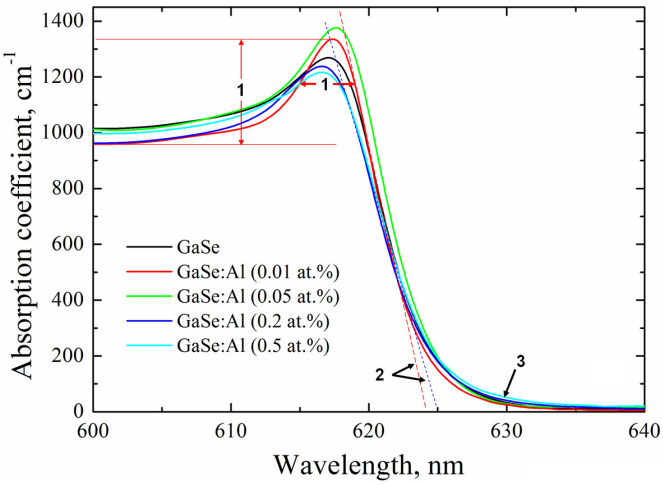

Fig.1. Characteristics of short-wave absorption diagram for Al-doped GaSe crystals.

In Fig. 1 it is seen that maximal intensity of the exciton absorption peak, minimal spectral bandwidth and absorption coefficient at the bottom of the short-wave absorption end are owned y 0.02 wt.% Al-doped GaSe crystals. Close characteristics are possessed by 0.05 wt.% of Al doped crystal. Thus, optimal Al doping has to be about from 0.02 to 0.05 wt.%. This proposal is confirmed by THz generation efficiency by optical rectification method.

References

1. Y.-F. Zhang, R. Wang, Z.-H. Kang, L.-L. Qu, Y. Jiang, J.-Y. Gao, Yu.M. Andreev, G.V. Lanskii, K.A. Kokh, A.N. Morozov, A.V. Shaiduko, V.V. Zuev AgGaS2- and Al-doped GaSe Crystals for IR Applications // Opt. Commun. 2011. V. 284. P. 1677-1681.

2. K.R. Allakhverdiev, R.I. Guliev, E.Yu. Salaev, V.V. Smirnov Investigation of linear and nonlinear optical properties of GaSxSe1-x crystals // Sov. J. Quantum Electron. 1982. V. 12, No. 7. P. 947-948.

3. H.-Z. Zhang, Z.-H. Kang, Yu. Jiang, J.-Yu. Gao, F.-G. Wu, Z.-S. Feng, Yu.M. Andreev, G.V. Lanskii, A.N. Morozov, E.I. Sachkova, S.Yu. Sarkisov. SHG phase matching in GaSe and mixed GaSe1-xSx, x<0.412, crystals at room temperature // Optics Express 2008. V. 16, № 13. P. 9951-9957.

4. D. R. Suhre, N. B. Singh, and V. Balakrishna, N. C. Fernelius and F. K. Hopkins Improved crystal quality and harmonic generation in GaSe doped with indium // Optics Letters. 1997. V.22, No.11. P.775-777

5. Z.-S. Feng, Z.-H. Kang, F.-G. Wu, J.-Yu. Gao, Yu. Jiang, H.-Z. Zhang, Yu.M. Andreev, G.V. Lanskii, V.V. Atuchin, T.A. Gavrilova. SHG in doped GaSe:In crystals // Optics Express 2008. V. 16, № 13. P. 9978-9985.

6. K.C. Mandal, S.H. Kang, M. Choi, J. Chen, Xi-Ch. Zhang, J.M. Schleicher, C.A. Schmuttenmaer, N.C. Fernelius. III–VI Chalcogenide Semiconductor Crystals for Broadband Tunable THz Sources and Sensors // IEEE Journal of Selected Topics in Quantum Electronics 2008. V. 14, № 2. P. 284-288.

7. Wei-Chen Chu, Shin An Ku, Harn Jiunn Wang, Chih Wei Luo, Yu. M. Andreev, Grigory Lanskii, T. Kobayashi. Widely linear and non-

phase-matched optics-to-THz conversion on GaSe:Te crystals. Optics Letters, 2012, V.37, No.5, P.945-947.

8. Yu-Kuei Hsu, Ching-Wei Chen, Jung Y. Huang, and Ci-Ling Pan, Jing-Yuan Zhang, Chen-Shiung Chang Erbium doped GaSe crystal for mid-IR applications // Optics Express. 2006. V.14, No.12. P.5484-5491

9. A. Gouskov, J. Camassel, L. Gouskov Growth and characterization of III-VI layered crystals like GaSe, GaTe, InSe, GaSe1-xTex and GaxIn1-xSe // Prog. Cryst. Growth Charact. Mat. 1982. V. 5. P. 323-413.

10. Shin-An Ku, Wei-Chen Chu, and Chih-Wei Luo, Yury Andreev, Grigory Lanskii, Anna Shaiduko, Tatyana Izaak, Valery Svetlichnyi, Kaung Hsiung Wu, T. Kobayashi. Optimal Te-doping in GaSe for nonlinear applications. Optics Express, 2012, V.20, No. 5, P. 5029-5037.

15:00 Oral

Polarized Raman Spectra in β-Ga_2O_3 Crystals

Takeyoshi Onuma[1,2,3], Shuhei Fujioka[2], Tomohiro Yamaguchi[2], Masataka Higashiwaki[3,4], Kohei Sasaki[3,5], Takekazu Masui[6], Tohru Honda[2]

1. *Tokyo National College of Technology (TNCT), 1220-2, Kunugida, Hachioji 193-0997, Japan* **2.** *Kogakuin University, Hachioji 192-0015, Japan* **3.** *National Institute of Information and Communications Technology (NICT), Koganei 184-8795, Japan* **4.** *PRESTO-JST, Chiyoda 102-0075, Japan* **5.** *Tamura Corporation, Sayama 350-1328, Japan* **6.** *Koha Co., Ltd., Nerima 176-0022, Japan*

e-mail: onuma@tokyo-ct.ac.jp

Monoclinic β-Ga_2O_3 has wide-bandgap energy of 4.8-4.9 eV, and has attracted much attention because of their potential use in UV transparent electrodes, photo detectors, substrates for GaN-based light emitters, and field-effect transistors (FETs). [1] Especially, an availability of low cost, large-area, and single-crystalline substrates is great advantage over GaN- and SiC-based FETs. On the contrary, complexity in emission processes in β-Ga_2O_3 constricts its application for deep UV light-emitters. In this paper, polarized Raman spectra are shown to discuss the relation between lattice vibration modes and emission processes in β-Ga_2O_3.

Samples investigated are single crystalline *a*, *b*, and *c*-plane β-Ga_2O_3 substrates grown by floating zone growth [2] or edge-defined film-fed growth methods. Unintentionally-doped (undoped), and intentionally Si-, Mg-, Zn-, or Fe-doped substrates were prepared. Polarized Raman spectra were recorded using JASCO NR-2000 system at room temperature. The samples were excited using a cw Ar ion laser emitting at 514.5 nm with a power of 20 mW. The back-scattered light was dispersed by a triple monochromator, and detected by a charge coupled device.

Relation between crystallographic *a*, *b*, *c* axes and observed X, Y, Z axes for β-Ga_2O_3 is shown in Fig. 1. The Y- and Z-axes are parallel to the *a*- and *b*-axes, respectively, and the X-axis is perpendicular to the *ab*-plane and is angled at 13.7º from the *c*-axis; it is abbreviated as c^*-axis. The a^*-axis is orthogonal to the *a*- and *c*-axes. The space group is C_{2h}^3. Two formula units are contained in the primitive unit cell. According to the factor group analysis at the Γ point, the irreducible representation for acoustical and optical zone center modes are $\Gamma_{aco}=A_u+2B_u$ and $\Gamma_{opt}=10A_g+5B_g+4A_u+8B_u$, respectively. For the optical modes, A_g and B_g modes are Raman active, while A_u and B_u modes are IR active. [3, 4] Representative polarized Raman spectra are summarized in Fig. 2. As expected from the polarization selection rules, the A_g modes were observed for the configurations Z(YX)Z, Z(XX)Z, Z(YY)Z, and X(ZZ)X [see Fig. 2(a)-2(d)], and the B_g modes were selectively observed for the configuration X(ZY)X [see Fig. 2(e)]. To the best of our knowledge, this is the first experimental observation of complete set of polarized Raman spectra of β-Ga_2O_3, in which the polarization selection rules are perfectly reproduced. The results are ensured by the high uniformity of crystalline orientation and surface flatness of the present substrates.

This work was supported in part by Grants-in-Aid for Scientific Research Nos. 23760021 and 21560361 under MEXT, Japan. T. O. is grateful to Prof. M. Sato, Prof. Y. Ito, Dr. H. Nagai, and Ms. C. Mochizuki for their help in the experiments.

[1] M. Higashiwaki *et al.*, Appl. Phys. Lett. **100**, 013504 (2012) and references cited therein.

[2] E. G. Víllora *et al.*, J. Crystal Growth **270**, 420 (2004).

[3] D. Dohy *et al.*, JSSC **79**, 419 (1982).

[4] B. Liu *et al.*, APL **91**, 172102 (2007).

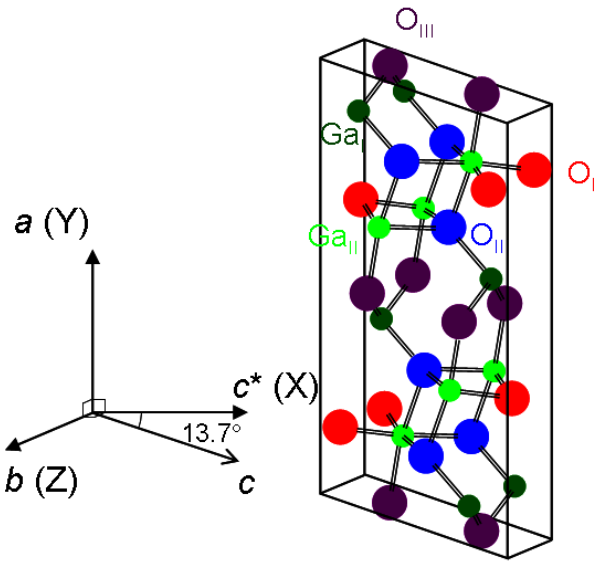

Fig. 1 Relation between crystallographic *a*, *b*, *c* axes and observed X, Y, Z axes for *b*-Ga_2O_3.

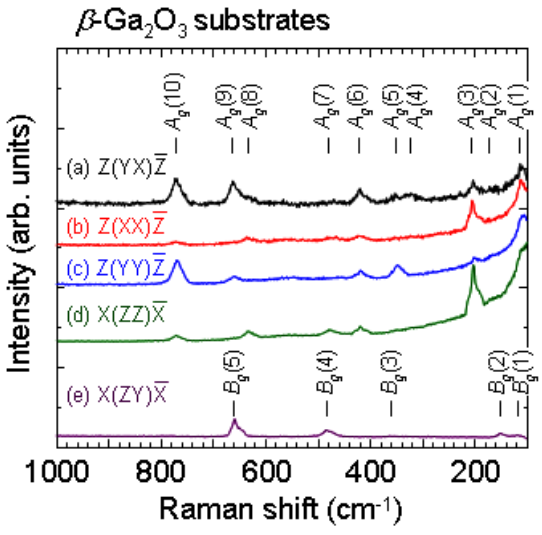

Fig. 2 Polarized Raman spectra of *b*-Ga_2O_3 substrates at room temperature.

Break
Tuesday afternoon, 13 August, 15:30

Wednesday, 14 August

WeO1

G05: Characterization
Wednesday morning, 14 August, 10:20
Room D, Auditorium Maximum

10:20 Invited oral

Visualization of Novel Electronic Structures in Topological Quantum Matter

Yulin Chen

Oxford University, South Parks Road, Oxford OX1 3QZ, United Kingdom

e-mail: yulin.chen@physics.ox.ac.uk

The discovery of materials with novel properties is one of the most fascinating aspects of physics, and such findings have always played important roles in the development of science and human life. A very recent example of conceptually new materials is the topological insulator. On the face of it, these are well-known, off-the-shelf materials, but they have previously overlooked properties which distinguish them from all other previously known quantum states. In its pure form, a topological insulator has a full energy gap in the bulk; while on the surface, it has massless and gapless metallic states formed by an odd number of relativistic Dirac fermions with helical spin texture. Within the last few years, topological insulators have grown as one of the most intensely studied fields in condensed matter physics due to their scientific significance and technological potentials.

The rapid development of topological insulators has also inspired the study of many other novel topological quantum states, such as quantum anomalous Hall states, topological semi-metals, and topological superconductors.

In this talk, I will show that by investigating these novel topological quantum materials with angle-resolved photoemission spectroscopy (ARPES), we were able to directly visualize their non-trivial electronic structures and unusual dynamics. In addition, I will briefly discuss the application potentials of these unusual materials, in electronics, spintronics and energy-related applications.

10:50 Oral

Magnetism and superconductivity in antimony doped binary and ternary iron chalcogenide single crystals

Dona Cherian, Nagendra G M, Suja E. Saji

Indian Institute of Science, Bangalore 560 012, India

e-mail: liz@physics.iisc.ernet.in

Since the discovery of superconductivity in Fe based compounds numerous studies have been carried out to synthesize new materials which can give a better insight into the mechanisms involved. Though Fe pnictides and chalcogenides share many common properties, the influence of composition on magnetic, structural and superconducting properties make Fe(Se,Te) more distinct. The key parameters controlling the physical properties of $Fe_{1+y}Te_{1-x}Se_x$ are excess Fe content(y) at the interstitial site and doping at the anion site. The parent compound $Fe_{1+y}Te$ shows a coupled magneto-structural transition (T_N) which decouples to two well separated transitions for certain concentration of excess Fe (y) [1]. On doping with Se, superconductivity emerges with a maximum T_C of 15 K for $Fe_{1+y}Te_{0.5}Se_{0.5}$ [2]. Also application of external pressure changes the superconducting and magnetic properties of $Fe_{1+y}Te$ and $Fe_{1+y}Se$ [3]. Assuming that doping impart chemical pressure we have doped Sb (2 % and 5%) on $Fe_{1+y}Te$ and $Fe_{1+y}Se_{0.5}Te_{0.5}$ while keeping y unchanged. Single crystals of $Fe_{1+y}Te_{1-x}Sb_x$(x= 0, 2%, 5%) and $Fe_{1+y}Te_{0.49}Se_{0.49}Sb_{0.02}$ were grown by modified horizontal Bridgman method. Growth parameters were optimized to obtain high quality single crystals. On doping $Fe_{1+y}Te$ with Sb, antiferromagnetic transition at T_N = 64 K shift to lower temperature. It is interesting to note that in antimony doped sample also the transition is first order in nature .This indicate the presence of structural transition even after doping. However on 5% doping the first order nature is not preserved. This indicates the tendency to suppress structural transition with higher doping. Subsequently we doped the chalcogen site of $Fe_{1+y}Se_{0.5}Te_{0.5}$ with Sb. The doped crystals preserve superconductivity even though superconducting transition (T_C) falls to slightly lower temperature with a concomitant reduction in superconducting volume fraction. Physical properties of different Fe chalcogenide crystals will be compared and discussed in detail.

References

1. S.Rößler et al. Phys. Rev. B, 84, 174506 (2011)

2. K -W Yeh et al., EPL , 84,37002 (2008)

3. S. Margadonna et al., Phys. Rev. B , 80, 064506 (2009)

11:05 Oral

Growth of Eu:SrI_2 Bulk Crystals by Modified μ-PD Method and the Scintillation Properties

Yuui Yokota[1], Shunsuke Kurosawa[1,2], Kei Nishimoto[2], Kei Kamada[1], Akira Yoshikawa[1,2,3]

1. *New Industry Creation Hatchery Center, Tohoku University, Aoba-yama 6-6-10, Aoba-ku, Sendai, Miyagi, Sendai 980-8579, Japan* **2.** *Institute for Materials Research, Tohoku University (IMR), Sendai 980-8577, Japan* **3.** *C and A corporation, Sendai 980-8579, Japan*

e-mail: yokota@imr.tohoku.ac.jp

The micro-pulling-down (μ-PD) method has been used for the material research of functional single crystals due to the higher growth rate compared to the conventional methods such as Czochralski (Cz) and Bridgeman (BS) methods and many novel functional crystals were developed. Recently, the halide scintillator crystals have been focused due to the high light yield and energy resolution originated from to the small band-gap. Especially, the Eu doped SrI_2 [Eu:SrI_2] and Ce and $LaBr_3$ [Ce:$LaBr_3$] crystals have gathering attentions due to the greatly high light yield and less than 3% energy resolution. However, most of halide materials have relatively high hygroscopicity and it is difficult to obtain their single crystals with high crystal quality. Therefore, the development of growth method for halide scintillator crystals have been required. Based on these background, we developed the modified μ-PD method for the growth of halide scintillator crystals with hygroscopicity. The Eu:SrI_2 and Ce:$LaBr_3$ crystals were grown by the modified μ-PD method and their scintillation properties were investigated in our previous reports. The modified μ-PD method can grow a fiber crystal at approximately ten times faster growth rate compared to the conventional methods. However, the modified μ-PD method

can grow only fiber crystal with diameter of 2~5 mm and bulk crystal with diameter of several inches can't be obtained. For the applications of radiation detectors, the size of halide scintillator crystals is required a minimum 1 inch in diameter and we developed the novel growth method of bulk crystal with diameter of 1 inch using the modified μ-PD method. Then, the scintillation properties of grown bulk crystal were investigated.

Eu:SrI_2 bulk single crystals were grown by the modified μ-PD method using the special shaped carbon crucible. Mixed powders were prepared from starting materials, SrI_2(4N, Alfa Aesar) and EuI_2(3N, Alfa Aesar) as nominal compositions of $(Sr_{0.925}Eu_{0.075})I_2$ in the glove box. Mixed powders were set in the carbon crucible and the crucible was set in the removable chamber. After the gate valve was closed, the chamber was taken our from the glove box and it was connected with the torbo morecular pomp and the inside was evacuated up to 10^{-4} Pa at 300°C to remove the moisture on the surface of starting materials, crucible, insulators and so on. After the baking process for sseveral hours, the high-purity Ar gas (99.9999%) was introduced in the chamber and the crucible was heated up to the melting point of Eu:SrI_2 by the high-frequency induction heating. Then the crucible was pulled down at 0.6 mm/h. After the crystal growth, the crucible was cooled to room temperature and the chamber was entered in the glove box again. Finally, the grown crystal was obtained. The grown bulk crystal was cut and polished in the glove box using 100% synthesis oil. The structural phase was identified by X-ray diffraction measurement using a tight chamber. Light yield and decay time under γ-ray irradiation were evaluated by the photomultiplier in the glove box using multichannel analyzer and ociloscope, respectively.

Eu:SrI_2 bulk crystal with diameter of 1 inch was grown by the modified μ-PD method as it is illustrated in Fig.1. Obtained Eu:SrI_2 bulk crystal had high transparency and almost all parts of the crystal were single crystal while it had several cracks in the crystal. The light yield of Eu:SrI_2 crystal irradiated under γ-ray from ^{137}Cs radiation source was evaluated by the pulse-height spectrum. Figure2 is the pulse-height spectra of Eu:SrI_2 crystal with a thickness of 5 mm cut from the bulk crystal and $Bi_4Ge_3O_{12}$ (BGO) as a reference. The light yield was calculated by comparing the position of photo-peak position to that of BGO. The light yield and energy resolution of Eu:SrI_2 crystal was 85,000 ph/MeV and 5%, respectively. The details of crystal growth and the scintillation properties of the Eu:SrI_2 bulk crystal will be reported.

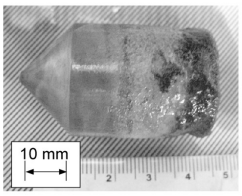

Fig.1 Eu:SrI2 bulk crystal with diameter of 1 inch grown by the modified μ-PD method.

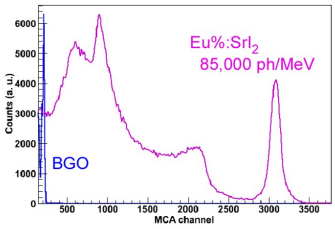

Fig. 2 Pulse-height spectra under γ-ray irradiation for Eu:SrI2 bulk crystal.

11:20 Oral

Crystal growth, structure, optical and scintillation properties of Ce^{3+}-doped $Tb_{2.2}Lu_{0.8}Al_5O_{12}$ single crystal

Yuntao Wu

Shanghai Institute of Ceramics, Chinese Academy of Sciences, 1295 Dingxi Road, Shanghai 200050, China

e-mail: caswyt@hotmail.com

Single crystals of undoped and 0.5at.%Ce^{3+}-doped $Tb_{2.2}Lu_{0.8}Al_5O_{12}$ (LuTbAG) with dimensions up to Æ25´30 mm^3 have been successfully grown by Czochralski pulling method. After the single-phase was confirmed using X-ray diffraction analysis, absorption coefficient of undoped LuTbAG was investigated. By using the results of Rietveld refinement and electron probe micro-analysis, the site occupation in undoped and Ce-doped LuTbAG crystals were indirectly revealed. The optical and scintillation characteristics of Ce^{3+}-doped LuTbAG crystal were investigated in detail. In the transmittance spectra, Ce^{3+}-doped crystals showed not only the absorption bands around 340 and 459 nm which are ascribed to the transition from 4f ground state to 5d excited state of Ce^{3+}, but the typical 4f-4f absorption of Tb^{3+}. Under the X-ray and UV excitation, strong emission peaks at 530 nm and 565 nm because of the Ce^{3+} 5d-4f transition and the line emission traces of Tb^{3+} featured 4f-4f transitions were both observed for Ce^{3+} doped crystal. The scintillation efficiency of LuTbAG:Ce crystal under X-ray excitation was about two times larger than that of BGO commercial crystal measured at the same conditions. Pulses X-ray luminescence measurements showed two exponential decay components of 1.8 ms and 161 ms. These initial results make LuTbAG:Ce crystal an attractive and promising scintillator for X-ray detection. In addition, the point defects in undoped and Ce-doped LuTbAG crystals were investigated by wavelength-resolved thermoluminescence technique.

11:35 Oral

The Analysis of Defects in $ZnGeP_2$ Single Crystals from Birefringence Images

Alexey Okunev[1], Galina A. Verozubova[2], Chunhui Yang[4], Chongqiang Zhu[4], Valery Tkal[3], Vladimir Staschenko[1], Inga A. Zhukovskaya[3]

1. *Yaroslav the Wise Novgorod State University, Bolshaya St-Petersburgskaya 41, Novgorod the Great 173003, Russian Federation* **2.** *Insitute of Climatic and Ecological Systems of SB RAS (IMCES), 10/3 ave Akademicheskii, Tomsk 634055, Russian Federation* **3.** *Saint Petersburg State University of Service and Economics (SUSE), Kavalergardskaja, 7, St-Petersburg 191015, Russian Federation* **4.** *Harbin Institute of Technology (HIT), No.92, West Da-Zhi Street,Harbin, Heilongjiang, Harbin 150001, China*

e-mail: alexei.okunev@mail.ru

Due to simplicity, exceptional clarity and reliability polarization-optical method (photoelasticity) occupies a special place among all experimental methods of determining of stresses. It is an optical method of stress investigation based on the phenomenon of induced birefringence (piezo-optical effect).

It is known that this method allows us to study not only the macroscopic internal stresses in the transversal and longitudinal cuts of single crystal ingots, but also to identify the microscopic stresses associated with individual dislocations [1]. In an optically isotropic crystals dislocations with non-zero edge component of Burgers vector, form a picture of the characteristic stresses, having a form of contrast rosette. Exploring the field of birefringence around the edge or mixed dislocation with line parallel to the axis of observation, we can determine position of the slip plane, the sign and magnitude of the Burgers vector. The method has demonstrated its great possibilities at the study of individual dislocations in silicon, garnet crystals, GaAs and GaP [2]. We studied types of dislocations in SiC single crystals and fine structure of photoelasticity rosettes from them by birefringence method [3, 4]. In some materials (alums, Rochelle salt and corundum) individual dislocations are not resolved and observed images in the photoelasticity method correspond to dislocation clusters or slip lines [2].

The image contrast, and thus the sensitivity of photoelasticity method are determined by many factors: the characteristics of the optical system, the size of the aperture diaphragm of the microscope, the polarizer's quality, the properties of the photographic material used to fix images, quality of the crystal surface. Despite an advanced theory of characterization of revealed dislocations, visibility and ease of implementation, the method of photoelasticity is relatively rarely applied to the study of structural defects of semiconductors. In this paper, we used the method of polarization-optical analysis to study of structural perfection of the $ZnGeP_2$ single crystals, grown by seeded vertical Bridgman method from melt [5]. Crystals were produced in Institute of Monitoring of Climatic and Ecological Systems SB RAS (Tomsk, Russia) and Single Crystal Laboratory in School of Chemical Engineering, Harbin Institute of Technology (Harbin, PRC). According to our earlier studies carried out by X-Ray topography, these crystals contain dislocations with straight lines [6], and one would expect to find a birefringence patterns from them. Indeed, at study of $ZnGeP_2$ plates, cut along the optical isotropy plane (001), birefringence images have been registered presumably from the slip bands as shown in Fig. 1. Fixed rosettes of photoelasticity from individual dislocations in low-angle boundaries also are inserted in Fig 1. Birefringence image of the entire volume of the sample composed from several single photographs is given in Fig. 2.

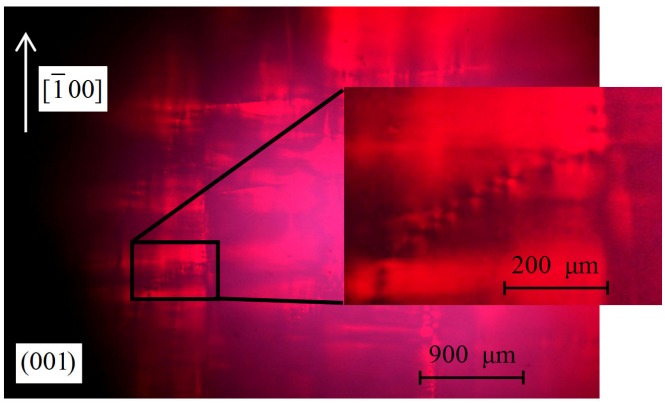

Fig. 1. Birefringence image of part of the $ZnGeP_2$ crystal with dislocation rows.

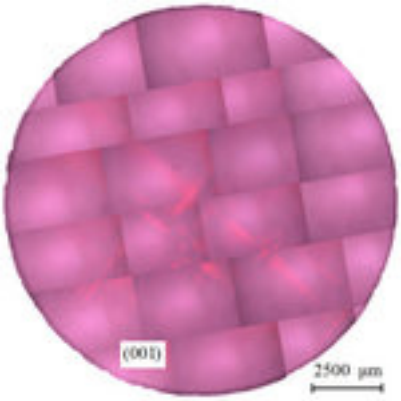

Fig. 2. The whole $ZnGeP_2$ plate, imaged with crossed nicols.

After the study by photoelasticity method crystals were thinning by chemical polishing for X-Ray topography. Fig. 3 shows topograph of the same crystal obtained by the method of the X-Ray topography on base of Borrmann effect. It is clear from X-Ray topographs that dislocations are distributed irregularly over the area of the plates, there are almost dislocation-free area of the small size and the areas in which a high density of defects leads to the disappearance of the anomalous transmission of X-Rays due to the strong distortion of the crystal lattice. The average dislocation density is about $N_d \sim 5 \cdot 10^3$ cm^{-2}.

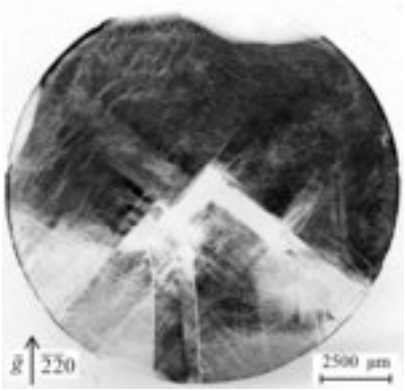

Fig. 3. X-Ray topograph of the same $ZnGeP_2$ plate.

Dislocations with curved lines, united in streams like structures and the slip bands are predominated. Comparison of X-Ray topographs and polarization-optical images shows their complete correlation. Birefringence images correspond mainly dislocation clusters in slip bands, the strongest contrast is observed at the boundaries of the slip bands and areas of relatively perfect crystal. As might be expected, the contrast is stronger for more defective crystals, in which large stresses arise. The contrast is also enhanced by increasing of the crystal thickness, since this increases the path length of the ordinary and extraordinary rays, and their path length difference at interference increases too.

Large and bright images in the form of rosettes creates by stresses around large inclusions in the sample volume as it is seen from Fig. 4. From a comparison of experimental images follows that similar SiC crystals [4], the method of polarization-optical analysis allows to obtain information, even in the case when the X-Ray topography methods do not work. In areas where the anomalous transmission of X-Rays is absent due to the high dislocation density, $N_d > 10^4$ cm^2, for example in area in Fig. 1, polarization-optical method allows to fix the defect images, investigate the stress field around them, and determine the characteristics of defects. In particular, the analysis of the form of photoelasticity rosette allows to determine the direction of dislocation line and the direction of the Burgers vector. The sign and magnitude of the Burgers vector are determined by means of optical compensators [1].

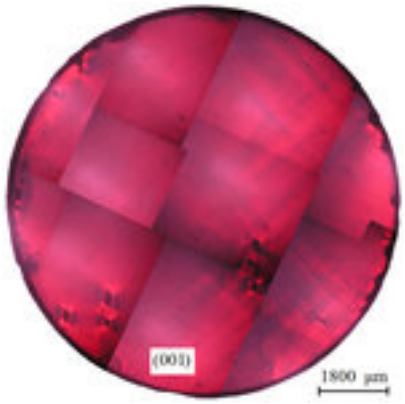

Fig. 4. Birefringence image of sample with large inclusions.

Studies facilitated by the fact that in the photoelasticity method we can get a continuous series of images of the dislocation at different angles between the dislocation slip plane and the polarization vector of the incident plane-polarized light. In contrast, in the X-Ray topography researcher can get a discrete set of images of the defect on the several "strong" reflections only.

Thus, the polarization-optical method was applied to study of defects in $ZnGeP_2$ crystals for first time. It is shown that this method is suitable to investigate the plates, cut perpendicular to the growth axis of the ingots [001]. Images of growth bands and individual dislocations were identified. Comparison of X-Ray and birefringence topographs shows great promise of this method for rapid analysis of the structural perfection of ingots and study of distribution and types of dislocations in them.

This work was partially supported by RFBR grant № 12-02-00201.

1. V.I. Nikitenko, Yu.A. Osip'yan, in book: Problems of Modern Crystallography: Collection of Articles in Memory of Academician A. V. Shubnikov (Nauka, Moscow, 1975), pp. 239-261.

2. K. Sangwal Etching of crystals: theory, experiment, and application (Amsterdam, North-Holland, 1987). P. 497.

3. Yu.A. Drozdov, A.O. Okunev, V.A. Tkal, I.L. Shulpina // Zavodskaja Laboratorija. Diagnostika materialov(rus). 2003. Vol. 69, No. 1, pp. 24–29.

4. A.O. Okunev, V.A. Tkal, L.N. Danil'chuk. The study of structure defects of single crystal silicon carbide by direct physical methods (Veliky Novgorod, Yaroslav-the-Wise NovSU, 2006). P. 252.

5. G.A. Verozubova, A.I. Gribenyukov // Crystallography Reports. 2008. Vol. 53, No. 1, pp. 158–163.

6. Okunev A.O., Verozubova G.A., Trukhanov E.M., Dzjuba I.V., Galtier P.R.J. and Said Hassani S.A. // J. Appl. Cryst. 2009. Vol. 42, No. 6, pp. 994–998.

11:50 Oral

Low-frequency noise in diagnostics of power blue InGaN/GaN LEDs

Evgeniia Shabunina, Anton Chernyakov, Michael Levinshtein, Natalia M. Shmidt, Nadezhda Talnishnikh

A.F.Ioffe Phisico-Technical Institute (FTI), Politekhnicheskaja 26, S.Petersburg 194021, Russian Federation

e-mail: jenni-85@mail.ru

Power blue InGaN/GaN light emitting diodes (LEDs) are the basis for the solid-state lighting. In spite of excellent success in the light-emitting devices technology, the physical mechanisms of non-radiative recombination and ones that responsible for the unpredictable failure after a comparatively shot operation time of some part of LEDs with the same values of external quantum efficiency as LEDs having long life time have not been clarified until now. The difficulties arisen under the study of the physical mechanisms are related to numerous forms of nano-structural arrangement (NA) in these LEDs and nano-scale phase separation (NPS) in InGaN both depending strongly on growth conditions. NA forms are determined by coalescence crystallites of near 3D growth mode to near 2D one and result in formation of the extended defect system (EDS) piercing the LED active region. EDS includes threading dislocations, their accumulations and numerous dilatation and dislocation boundaries. To study such complicated system not enough the traditional methods. It seems that the application of low frequency noise (LFN) techniques allows one to fully characterize these peculiarities. The methods are known to be an effective tool to obtain a comprehensive information not only on the generation-recombination (G-R) noise due to point defects, but also on charge fluctuations at surface states, presence of several barriers with close energy levels, nano-material disorder or local field fluctuation [1]. The behaviour of the defects can be investigated at the large current density range.

In this abstract we present the results demonstrating the efficiency of LFN methods for separation of the contribution of EDS and point defects to non-radiative recombination to clarify the causes of unpredictable failure of power blue InGaN/GaN LEDs. All results have been obtained on InGaN/GaN LEDs with the values of external quantum efficiency (η) 45-50% at wavelength 450-460 nm. Low frequency noise measurements in the frequency range 1 Hz – 10 kHz and spectral voltage $S_V(j)$ and current $S_I(j)$ noise density dependences at 10^{-4} – 50 A/cm^2 and η(j) dependencies were performed on all LEDs.

To separate the contribution of EDS and point defects in non radiative recombination the classification of LEDs on their leakage current (LC) values were used. The LC values at $U < 2$ V integrally characterize electrical properties of EDS. The lower LC values are, the smaller concentration of extended defects is [2]. It has been revealed that low-frequency noise peculiarities such as the shape of noise spectral density (S_I) on frequency (f) as 1/f and increase in S_I with an LC values growth are caused by EDS presence. The point defects (PD) contribution to non-radiative recombination processes is observed in current density region 10^{-2} – 10 A/cm^2 where radiative recombination prevails. The non-radiative recombination caused by EDS at $j < 10^{-2}$ A/cm^2 and at $j > 10$ A/cm^2 is predominated. The complicated behavior of EDS with an injection current change has been observed. The shape of the decreasing part at $S_I(j)$ dependences in the LEDs differs noticeably from the $S_I(j) \sim 1/j^2$ being typical for local trap filling mechanism.

In order to clarify the causes of unpredictable failure in LEDs with the same η and LC but different values of forward current at $U < 2.5$ V and remarkable discrepancy in the shape of I-V forward branches, which might be attributed to the presence of local regions with smaller E_g, were studied by LFN methods before and after 10-1000 hours aging at 35 A/cm^2 and 100^{o}C p-n junction temperature. No considerable change in η, I-V characteristics and $S_V(j)$, $S_I(j)$ dependences were observed for majority of LEDs under the study even after 1000 hours, except fort he LEDs with a remarkable discrepancy in the shape of I-V forward branches. $S_V(j)$ dependencies of these LEDs differ strongly from the law $S_V(j) \sim 1/j$ which is typical for p-n junction with uniform current distribution. Moreover $S_I(j)$ dependences at $j < 10^{-2}$ A/cm^2 increases as $S_I \sim j^4$. According to [1], this type of $S_I(j)$ is caused by appearance of local overheating regions. These peculiarities usually appear after 10-100 hours of aging process. Although any noticeable changes in but η values has not been observed, the life time of these LEDs are smaller than 1000 hours. The results of electroluminescence study enable us to suppose that redistribution of In between nano-scale regions of InGaN alloy with non-equilibrium composition takes place.

$S_I(j)$ dependences for InGaN/GaN LEDs at 77 K has been obtained. Their analysis allows us to separate the charge carriers transport along EDS from the one along nano-scale fluctuations of InGaN composition. Thus LFN methods let us obtain important and useful information about recombination and degradation mechanism in power blue InGaN/GaN LEDs.

References

[1] N.V. Dyakonova at al., Physics and techniques of semiconductors, **25(12)**, 2065 (1991)

[2] A.V. Kamanin al. Phys. stat.sol.(c), **3**, 2129 (2006).

[3] Schubert EF. Light-emitting diodes. 2nd ed. UK: Cambrige University Press (2006).

12:05 Oral

Growth mechanism of CeO_2 nanocrystals revealed by electron tomography

Ming Lin

Institute of Materials Research and Engineering, Singapore, Singapore

e-mail: m-lin@imre.a-star.edu.sg

Understanding the nucleation and growth of nanoparticles in solution plays the key role to control the shape and morphology of the products. The growth mechanism of nanocrystals can be revealed from their microstructural details, such as the presence of pores, twins, and dislocations etc. However, conventional TEM images only show two-dimensional projections of three-dimensional (3D) particles, in which much information is lost in such 2D images. Electron tomography is the only technique which can provide a detailed analysis of the 3D shape and morphology at nanoscale. Here, we have firstly conducted a detailed analysis on CeO_2 single crystals using electron tomography to demonstrate the shape and internal structures, thus revealing the growth mechanism of the CeO_2 in solution. The CeO_2 nanocrystals were synthesized by the hydrothermal method. With the assistance of electron tomography, it is found that the porous CeO_2 nanocrystals have an irregular truncated octahedral shape with internal pores elongated along the <110> directions. Thus, it is concluded that in the hydrothermal process, the oriented attachment of nuclei through a lattice matched surface and subsequent Ostwald ripening results in the growth of CeO_2 nanocrystals with the pores inside. The dominant mechanism for the ripening of nuclei in hydrothermal reactions is the oriented attachment. It is believed that the crystallographic orientation of the pores and corresponding aggregation mechanism for the single crystalline and porous CeO_2 discussed here can also be applied to other oxide materials synthesized by self-assembly in solution.

Lunch (IOCG Council meeting)
Wednesday afternoon, 14 August, 12:20

Posters

Monday, 12 August

MoP-G05
Monday afternoon, 12 August, 17:00
Room 215, Old Library

17:00 Poster Mo202

Effect of swift heavy ions induced modifications on some rare earth orthoferrite crystals

Krishan K. Bamzai, Monita Bhatt

CGMR Lab, Department of Physics, University of Jammu, Jammu 180006, India

e-mail: kkbamz@yahoo.com

Engineering the properties of materials using swift heavy ions (SHI) is an emerging field of research. It is known fact that when an energetic ion beam passes through the material, the modification in the material is caused due to Coulomb interaction between the target materials, the mean of the projectile ion, its energy and also type of irradiation like its flux, fluence and beam dimension. In the present presentation the results obtained on the 50 MeV Li^{3+} ion irradiation effect on various properties were studied on the perovskite type rare earth orthoferrite single crystals. The rare earth orthoferrite having general formula $REFeO_3$ where RE can be Yttrium or rare earth, possess distorted perovskite structure with four equal iron ions per unit cell. Three different compositions of $REFeO_3$ (where RE = Y, Er and Ho) grown by fluxed melt technique were used. Structural characterization by HRXRD indicated diffused peak in case of irradiated crystal which is attributed to creation of more defects upon irradiation. Mechanical characteristics were studied on pristine and irradiated crystals and it was found that microhardness decreases upon irradiation. The dielectric behavior shows complete dependence on frequency and temperature. Irradiation enhances the value of dielectric constant as well as conductivity and is attributed to disordering of the crystal lattice. The magnetic behavior were observed for these crystals across three different planes (110), (010) and (001). Irradiation affects the values of maximum magnetization, coercivity and remnant magnetization. From magnetization versus temperature curves, the magnetization decreases and Neel temperature was found to increase after irradiation. These studies summarizes that irradiation induces modification in material thus leading to change in the structural, mechanical, dielectric and magnetic properties of these crystal. The detail results will be presented and discussed.

17:00 Poster Mo203

Measurements of strain in AlGaN/GaN HEMT structures grown by plasma assisted molecular beam epitaxy

Jolanta Borysiuk[1], Kamil Sobczak[1], Aleksandra Wierzbicka[1], Kamil Klosek[1], Marta Sobanska[1], Zbigniew R. Zytkiewicz[1], Boleslaw L. Lucznik[2]

1. *Institute of Physics, Polish Academy of Sciences, Warsaw 02-668, Poland* **2.** *Polish Academy of Sciences, Institute of High Pressure Physics (UNIPRESS), Sokolowska 29/37, Warszawa 01-142, Poland*

e-mail: borysiuk@ifpan.edu.pl

The AlGaN/GaN high electron mobility transistor (HEMT) structures were grown on the (0001) HVPE bulk GaN substrates using plasma-assisted molecular-beam epitaxy (PAMBE). The AlGaN layers of content of 12% or 20% were grown to nominal 20nm thickness and the 3nm thick GaN cap was added. High-resolution X-ray diffraction (HRXRD) measurements were used to determine crystallographic quality of HEMT structures. Built-in strain was obtained from peak intensity analysis. An effective lattice constant was derived from the shifts of the peaks positions. These X-ray data were compared to local measurements performed by transmission electron microscopy (TEM) – Fig.1. Tetragonal distortion was used for lattice strain in the interface regions. Structure geometry was also obtained from TEM images. Overall quality of the structures and their performance was assessed.

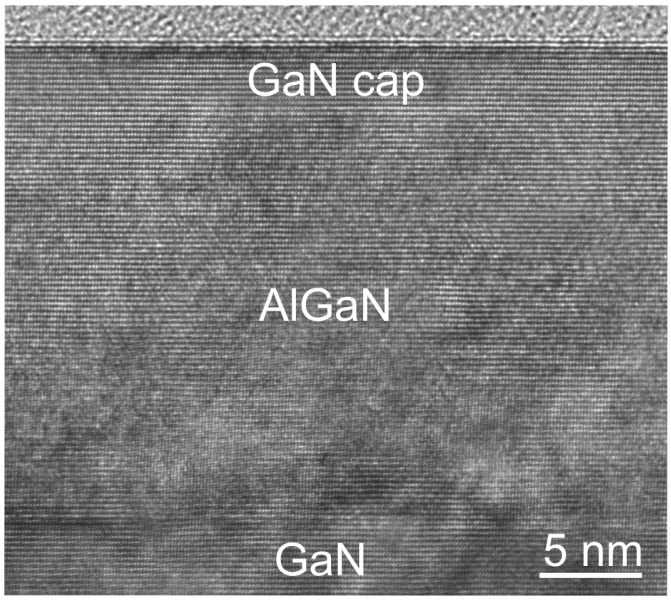

Figure 1. TEM image of HEMT structure.

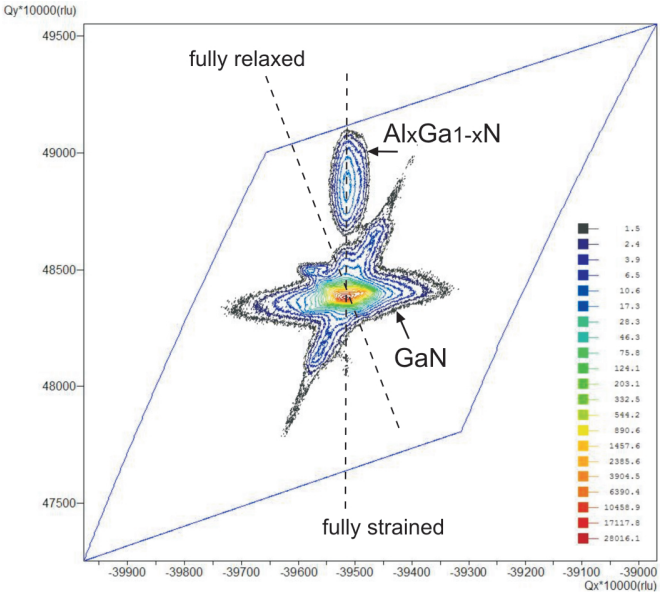

Figure 2. XRD map of the (11 4) reflection.

Acknowledgements

This work was partially supported by the European Union within European Regional Development Found, through grant Innovative Economy POIG.01.01.02-00-008/08 NanoBiom. One of the authors (JB) wishes to thank the National Science Centre (Poland) support by grant DEC-2011/03/B/ST5/02698.

17:00 Poster Mo204

Image contrast reversal of depletion regions in scanning capacitance microscopy

Mao-Nan Chang[1], Yi-Hao Chen[1], Yao-Jen Lee[2]

1. *National Chung Hsing University, Department of Physics (NCHU), No.250, Guoguang Rd., South Dist., Taichung City, Taiwan, Taichung 40227, Taiwan* **2.** *National Nano Device Laboratories (NDL), No. 26, Prosperity Road I, Science-based Industrial Park, Hsinchu 30078, Taiwan*

e-mail: changndl@yahoo.com.tw

For many years, scanning capacitance microscopy (SCM) has been an important method to observe and to analyse the carrier distributions and pn junctions in semiconductor materials and devices.SCM provides differential capacitance (dC/dV) images corresponding to carrier polarity and concentrations, which are important information forsemiconductordevices. For instance, SCM can identify p-type and n-type regions in semiconductors and map pn junctions. With SCM, one can profile the source and the drain regions as well as the channel length of a metal-oxide-semiconductor (MOS) device. It is well known that a typical SCM setup is based on an atomic force microscope (AFM) equipped with a conductive probe to synchronously provide AFM images and the corresponding carrier concentration profiles. Unfortunately, prior studies reported that the AFMlaser system may lead to photoperturbation problems in SCM measurements, including distorted junction profiles and false dC/dV signals. For a pn junction, the AFM laser could induce electron-hole pairs in the depletion region during SCM measurements. The photo-generated electron-hole pairs are separated by a built-in electric field, perturbing the dC/dV signals nearby the junction region. For this reason, a dark-mode SCM system has been developed to clearly observe *pn* junctions without photoperturbation problems. However, it is interesting to know if there is any physical information hid in the photoperturbed junction images observed by typical SCM. For a pn junction under continuous-wave (CW) laser illumination, the depletion region reaches a steady state but thermal equilibrium. Since *dC/dV* signals are very sensitive to the carrier polarity and concentration, it is expected that the dC/dV image may respond to the carrier distribution of a depletion region in steady state. In this work, we performed dark-mode SCM measurements combining with external laser illumination for investigating the subtle variation in pn junctions under various illumination intensities. Two series of samples were prepared by patterned n-type silicon wafers and boron ion implantation. The window width and the spacer of the pattern was 0.8 um and 2 um, respectively. The first series of the samples were treated by microwave annealing (MA) for 300 s after boron implantation. This series of samples was denoted as MA300. Another series of samples were treated by the same MA process followed by furnace annealing (FA) at 550 ^{o}C for 6 hours. This series of samples was denoted as MA+FA. The MA power is about 1800 W. In general, the effective temperature of MA for boron activation is less than 500 ^{o}C. A Bruker D3100 scanning probe microscope was used to obtain the cross-sectional dC/dV images of pn junctions. For all of the samples, the boron depth profiles were obtained by secondary ion mass spectrometer (SIMS). For all of the samples, there was no significant difference between the SIMS boron profiles since MA is a low-thermal-budget process. For the samples MA300, illumination-induced contrast reversal was clearly observed from the dC/dV images of the lateral pn junctions. It is found that the contrast reversal behavior depends on the intensity of the illumination. Due to the recombination of photo-generated electron-hole pairs and space charges, the p-side and the n-side of the junction region exhibits electron-rich and hole-rich, respectively. As

a result, the dC/dV images of the depletion regions with photo-illumination show a contrast reversal behavior. In addition, the influence of the electron drift from p-side to n-side on the *dC/dV* signals was also observed. For the vertical junctions, SCM cannot observe obvious contrast reversal since the effective space charge density in vertical direction is lower than that in lateral direction. In addition, for the samples MA+FA the dC/dV images exhibit a similar behavior before and after laser illumination. Section analysis of the dC/dV images revealed that FA induces boron deactivation, reducing the electric field in the lateral junction and leading to a shift of the electrical junction. Since the electric field in the lateral junction is reduced by FA, the *dC/dV* signal intensity induced by the electron drift from p-side to n-side also decreased. In summary, we have employed dark-mode SCM with external laser illumination to observe the image contrast reversal of pn junctions formed by boron implantation and MA treatment. For an abrupt pn junction, one can observe clear contrast reversal from the dC/dV image of the depletion region. Our experimental results indicate that the contrast reversal behavior in the dC/dV image of a depletion region can be an indicator of the space charge density.

17:00 Poster Mo205

Mechanism of band-edge luminescence in cuprous iodide single crystals

Pan Gao

Shanghai Institute of Ceramics, Chinese Academy of Sciences, 1295 Dingxi Road, Shanghai 200050, China

e-mail: gaopan601@gmail.com

The photoluminescence spectra of CuI crystals using synchrotron radiation as an excitation light source were obtained at 60K. The emission peaks at 405, 415, 420 and 443nm were observed respectively. The possible origins of these peaks were discussed by the temperature dependence of CuI luminescence. Meanwhile, the photoluminescence spectra of CuI powder with different excitation intensity were measured and the ultrafast component luminescence in CuI crystals was warranted to be attributed to the donor acceptor pair recombination. Furthermore, the excitation process was understood by the photoluminescence excitation spectra of CuI crystals and powder.

17:00 Poster Mo206

Surface charging of crystalline oxides in X-ray photoelectron spectroscopy - examples of $LiNbO_3$, Lu_2SiO_5 and $LuVO_4$

Ryszard J. Iwanowski[1], Markku Heinonen[2], Marek Berkowski[1], Michał M. Głowacki[1], Izabela Pracka[3], Hanna A. Dabkowska[4]

1. *Polish Academy of Sciences, Institute of Physics, al. Lotników 32/46, Warszawa 02-668, Poland* **2.** *Laboratory of Materials Science, Department of Physics, University of Turku,, Turku FIN-20014, Finland* **3.** *Institute of Electronic Materials Technology (ITME), Wólczyńska, Warsaw 01-919, Poland* **4.** *Brockhouse Institute for Materials Research, McMaster University, 1280 Main Street West, Hamilton L8S4MI, Canada*

e-mail: riwanowski@wp.pl

X-ray photoelectron spectroscopy (XPS) is one of the major research tools for studying solid surfaces, either of bulk materials or of thin films. For conducting solids it enables direct qualitative- and quantitative chemical analysis of the surface and subsurface region, also providing information about electronic structure of material (valence band, core-level structure). On the other hand, a positive surface charge induced by X-ray beam within the photoemission process is a main problem in the XPS study of insulating materials, including the large-gap oxide compounds.

The goal of this work was to exhibit certain aspects of surface charging by taking into account the results of XPS investigations of the following single crystalline oxides doped with rare earths: $LiNbO_3$:(Er,Yb), Lu_2SiO_5 :Dy and $LuVO_4$:Yb (the dopant symbols will be omitted further in the text).

XPS measurements were performed with a monochromatized Al Kalpha (E= 1487 eV) X-ray excitation source, where charging of the sample is very important. The spectra were acquired in two modes: (1) with use of surface charge neutralization by low-energy electron beam (electron flood gun), (2) without a charge neutralization. Their comparison enabled us to determine the binding energy (BE) shift (E_s) of the particular XPS spectrum and thus, the charge induced on the X-rayed surface of the crystal studied.

For $LiNbO_3$ we obtained the magnitude of BE shift equal E_s = 230 eV, i.e. the higher value than the relevant ones reported earlier (e.g. F.Bart et al., J. El. Spectr. Rel. Phenom. 69). It was accompanied by a modification of the spectral lineshapes. For example, in neutralization conditions (mode 1) the Nb 3d spectrum indicated a purely 5+ valence state of Nb ion, whereas in a lack of charge compensation additional contribution of the Nb^{4+} and Nb^{3+} centers appeared in the core-line. This could be ascribed to partial surface reduction of Nb^{5+} ions to Nb^{4+} and Nb^{3+} ions, although in this case the process is not irreversible.

The analogous XPS experiment for Lu_2SiO_5 gave unexpectedly high value of BE shift, i.e. E_s = 650 eV, which indicated very strong surface charging. A huge broadening of the most intensive XPS lines led to disappearance of the other spectral lines that excluded even a qualitative chemical analysis. On the contrary, the same experiment with charge neutralization mode (1) provided a high quality XPS spectrum. This has been compared with the relevant XPS data for $LuVO_4$, where much weaker surface charging occurred, namely: E_s = 130 eV. In the neutralization conditions both these Lu-based oxides exhibited good consistency between their valence-band spectra as well as between their Lu 4f and Lu 4d core-level spectra. In the latter case, we observed slightly higher (but not exceeding 7 %) widths of these core-lines in Lu_2SiO_5 , compared to the relevant ones of $LuVO_4$. It could suggest an indirect influence of stronger surface charging in Lu_2SiO_5.

The above results illustrate well particular problems related to surface charging (and its neutralization) as an inevitable effect in the X-ray photoelectron spectroscopy of insulating crystalline oxides.

17:00 Poster Mo207

Transmission Spectra and First-principles Study of Sulfate substituted Potassium Dihydrogen Phosphate

Liang Li[1,2], Xun Sun[1], Zhengping Wang[1], Shenglai Wang[1], Xinguang Xu[1], Xixiang Zhang[2]

1. *Shandong University, Jinan 250100, China* **2.** *King Abdullah University of Science and Technology, Jeddah 23955-6900, Saudi Arabia*

e-mail: mike1.732@gmail.com

Potassium dihydrogen phosphate KH2PO4 (KDP) is a remarkable electro-optic and nonlinear material which large single crystal can be grown [1, 2]. KDP crystal has been widely used in laser physics, such as frequency doublers and triplers in large laser systems. In practical applications, the major issue is that the laser induced damage threshold is an order of magnitude below the expected limits [3, 4]. Many former studies have been performed to understanding this phenomenon and

further more expecting contribution of improvement of the damage threshold.

KDP crystals were grown with the traditional temperature-lowering method from the aqueous solution with different sulfate. Transmission spectrum measurement was performed by HITACHI U-3500 spectrometer at room temperature. Sample with high sulfate concentration density exhibits heavy absorption property in the ultraviolet region, while only tiny difference was observed in the rest of the spectrum. This crystal is also studied by the first-principles simulation method and the density of its states was calculated. We found that sulfate can reduce the band gap of KDP crystal to 3.90eV (318nm), which is consistent with the experimental work and indicates that sulfate is an important source of the low damage threshold.

17:00 Poster Mo208

Thermal properties of a series of partially deuterated ADP crystals

Shaohua Ji, Lisong Zhang, Lili Zhu, Fafu Liu, Shenglai Wang, Zhengping Wang, Xun Sun

Institue of Crystal Materials Shandong University, Jinan 250100, China

e-mail: jesohua@163.com

A series of deuterated ADP crystals were grown from deuterated aqueous solution by point-seed rapid growth method in this paper. The specific heat, thermal diffusivity and thermal conductivity were examined with a simultaneous thermal analyzer and a laser thermal conductivity meter, respectively. The experiment results show that the specific heat improve with increasing deuterated level in ADP crystal (60% partially deuterated, 1.62 J/(g*C), 120 ^{o}C) which is superior to that of 74% partially deuterated KDP crystal (1.21J/(g*C), 120 ^{o}C). However, (100) and (001) directions of thermal diffusivity and thermal conductivity present different variation trends and have no significant variation with deuterium doped.

17:00 Poster Mo209

Comparison of LGSO:Ce scintillator crystals grown by micro-PD and Czochralski methods

Valerii Kononets[1,2], Kheirreddine Lebbou[2], Oleg Sidletskiy[1]

1. *Institute for scintillation materials of NAS of Ukraine (ISMA), 60 Lenin ave., Kharkov 61001, Ukraine* **2.** *Universite de Lyon, CNRS, Institut Lumiere Matiere, Villeurbanne 69622, France*

e-mail: kononets@isma.kharkov.ua

Ce-doped crystals based on complex oxides are known as fast, dense, and bright sicntillators. Recently, a set of new mixed crystals were developed with improved light yield and energy resolution [1, 2]. $Lu_xGd_{1-x}SiO_5$:Ce (LGSO:Ce) is one of them. It is formed as the result of Lu/Gd cation substitution and form lattices of two types of monoclinic space symmetry. Scintillation characteristics of $P2_1/c$ lattice LGSO:Ce are moderate, at the same time, crystals with C2/c structure possess a very attractive combination of characteristics for PET, introscopy, high energy physics.

The present report is devoted to growth of bulk crystals and fibers by Czochralski (Cz) and micro-pulling down (μ-PD) methods. LGSO:Ce fibers by μ-PD were obtained for the first time. μ-PD is an efficient method for prompt screening of crystal compositions. Besides this, fibers are promising for utilization in pixelated detectors without multistage procedure of crystal machining. Optimal ratio of substituted cations and activator concentration in LGSO:Ce was determined by Cz and μ-PD. Relative population of Lu^{3+} and Gd^{3+} in 7-fold and 6-fold cation positions not differs substantially in crystals grown by different methods. luminescence spectrum of LGSO:Ce consists of subbands associated with CeO_7 and CeO_6 polyhedra. Similar shapes of luminescence spectra of Cz and μ-PD grown crystals certifies no substantial difference in activator distribution between these sites.

The work is partially supported by the project No. 28317ZC in the framework of DNIPRO scientific collaboration between Ukraine and France.

corresponding author e-mail: kononets@isma.kharkov.ua

References
1. M. Fasoli, A.Vedda, M. Nikl et al. Phys. Rev., B 84, 081102(R) (2011).
2. O. Sidletskiy, A. Belsky, A. Gektin et al., Crystal Growth & Design 12, 4411 (2012).

17:00 Poster Mo210

Contactless methods of both conductivity and sheet resistance measurements of semiconductor crystals, wafers and epitaxial films deposited on semi-insulating substrates

Jerzy A. Krupka

Politechnika Warszawska (PW), pl.Politechniki, Warszawa 00-661, Poland

e-mail: krupka@imio.pw.edu.pl

These days contactless methods of conductivity measurements become more and more important due to the progress in materials technology and development of new materials intended for electronic industry such as GaN, SiC, graphene, etc. Some of these materials like GaN, SiC even if they are conducting they are not measurable with conventional four point probe technique. Furthermore contactless measurement techniques are fast and non destructive. Appropriate choice among these techniques makes it possible measurements of materials having resistivity in the range of more than 16 decades from 10^{-6} Wcm to 10^{12} Wcm, and sheet resistances in the range from 10^{-6} W to 10^{8} W. This presentation will overview the last achievements on this topic, especially microwave techniques that have been recently developed by the author.

17:00 Poster Mo211

Modelling of X-Ray diffraction curves for GaN nanowires on Si(111)

Vasyl Kladko[1], Andrian Kuchuk[1], Hryhorii Stanchu[1], Nadiia Safriuk[1], Alexander Belyaev[1], Aleksandra Wierzbicka[2], Marta Sobanska[2], Kamil Klosek, Zbigniew R. Zytkiewicz[2]

1. *V. Lashkaryov Institute of Semiconductor Physics NASU (ISP), 41, pr. Nauki, Kiev 03028, Ukraine* **2.** *Institute of Physics, Polish Academy of Sciences, Warsaw 02-668, Poland*

e-mail: an.kuchuk@gmail.com

Recently the GaN nanowires (NWs) grown on various substrates have been extensively studied. At the same time many diagnostic methods are developed that allow analysis of NWs properties. For structural characterization the nondestructive X-ray diffraction (XRD) is mainly used.

The structure of GaN NWs, as well as of planar layers, is described by mosaic model, which takes into account such parameters as tilt, twist and size of mosaic blocks. All these parameters cause broadening of the X-ray diffraction curves (XDC) for both types of epitaxial structures. However, there are a strong differences between the full width at half maximum (FWHM) of XDCs of nanowire and planar GaN layers. For GaN layers different types of dislocations contribute mainly to the XDC broadening, while for dislocation free GaN NWs broadening is cased by the their small size as well as by large values of tilt and twist (spatial orientation). Attempts to fit the XDC by Lorentzian and Gaussian functions, as well as their combinations, often do not describe experimental observations. Moreover, this approach doesn't give any information about physical parameters which affect the broadening of XDC. Only modeling of XDC and comparison of calculated and experimental curves allow obtaining real structure parameters of NWs.

In this paper, we study the profiles of X-ray diffraction peaks from self-assembled GaN NWs grown by PAMBE (760^{o}C) on Si(111) substrate. As the sizes of scattering objects (NWs) are small, the X-rays kinematic scattering theory is applied. The peak profile was calculated taking into account coherence of the x-ray beam, size and spatial orientation distributions of NWs. As it can be seen from Fig. 1a, the best fit of experimental and calculated ω-scan for 0002 reflection from NWs GaN/Si(111) was obtained considering both distributions of NW's tilt and diameter. Moreover, the diameter distributions obtained by calculation of XDC well correlate with distributions obtained by SEM (Fig. 1b). All results obtained by modeling of XDC from GaN NWs will be compared with results from other X-ray diffraction techniques (Williamson-Hall, reciprocal space mapping) as well as with complimentary methods (SEM, AFM etc.).

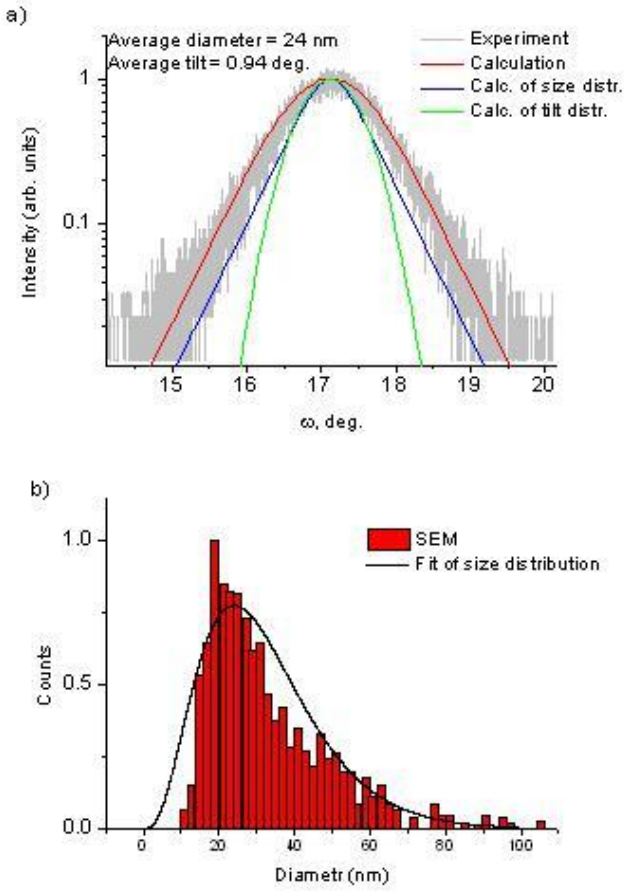

Fig.1. Calculated and experimental XRD ω-scan for 0002 reflection of GaN NWs (a); experimental and fitted diameter distributions (b).

This work was supported by the European Union within European Regional Development Fund, through grant Innovative Economy (POIG.01.01.02-00-008/08 NanoBiom).

17:00 Poster Mo212

Synthesis, growth, structure, optical and thermal properties of a new organic NLO crystal: 3-nitroanilinium trichloro-acetate

Selva Kumar[1], Chandra Mohan, Anandha Babu[2], Perumalsamy Ramasamy

1. *Sri ramakrishna mission vidyalaya (SRMV), periyanaciken palayam, Coimbatore 0422, India* **2.** *Centre for Crystal Growth,SSN College of Engineering,Kalavakkam,Chennai, Chennai 603110, India*

e-mail: eselvakumarsrmv@gmail.com

A new organic non-linear optical salt crystal 3-Nitro anilinium richloro-acetate (NAT) has been synthesized and single crystals were grown by slow solvent evaporation solution growth technique at room temperature using methanol as the solvent. The ^{1}H and ^{13}C NMR spectra were recorded to establish the molecular structure of the title salt. The crystal structure of NAT has been determined by single crystal XRD analysis and it belongs to monoclinic crystal system with noncentrosymmetric space group $P2_1$. Fourier transform infrared (FT-IR) spectral study has been carried out to confirm the various functional groups present. The UV-Vis-NIR transmittance spectrum was recorded in the range 200-2500nm, to find the optical transmittance window and lower cut off wavelength. The thermo gravimetric (TG) and differential thermal analyses (DTA) were carried out to establish the thermal stability of the title crystal. The second harmonic generation in the title complex was confirmed by the modified Kurtz-Perry powder test employing the Nd: YAG laser as the source for IR radiation.

17:00 Poster Mo213

X-ray diffraction studies of (Pb,Cd)Te solid solution – possible new material for thermoelectric applications

Roman Minikayev[1], Elzbieta Dynowska[1], Katarzyna Gas[1], Rafał Kuna[1], Andrzej Szczerbakow[1], Wojciech Szuszkiewicz[1], Anthony Bell[2], Patrick Baroni[3], Sylvain Petit[3]

1. *Polish Academy of Sciences, Institute of Physics, al. Lotników 32/46, Warszawa 02-668, Poland* **2.** *HASYLAB at DESY, Notkestr., Hamburg 22607, Germany* **3.** *Laboratoire Leon Brillouin, CEA-CNRS, CE Saclay (LLB), Gif-sur-Yvette 91191, France*

e-mail: minik@ifpan.edu.pl

Among a new materials for development of the mid-IR optoelectronic or the thermo-electric devices based on quantum dots the (Pb,Cd)Te solid solution attracted a lot of attention within the last few years. These crystals in the composition range corresponding to PbTe-based matrix containing a lot of CdTe precipitates may be considered as composites perfectly matching principal properties required for future thermoelectric applications. However, it is difficult to obtain a uniform material of such matrix. The reason is extremely low solubility limit of both materials [1] resulting from the difference in their crystal structure in spite of very similar values of lattice parameters. Both compounds crystallize in the *fcc* structure but of different type: PbTe in the rock salt (RS) type and CdTe in the zinc blende (ZB) one. So far, in the case of bulk crystals grown by the Bridgman technique or

by rapid quenching and annealing method only polycrystalline samples were obtained. For such samples the phase diagram and the solubility limit have been determined long time ago [1-3].

The recent successful growth of metastable, big, single, (Pb,Cd)Te crystals with the RS-type structure and the CdTe content up to about 12% at the Institute of Physics of the Polish Academy of Sciences in Warsaw opened new research opportunities. The crystals were grown by self-selecting vapour transport method (SSVT [4]), the details of the growth procedure can be found elsewhere [5, 6]. Characterization of numerous samples at ambient conditions allowed to determine their structure and the dependence of the lattice parameter value on the cadmium content in the solid solution. Due to their one-phase character and the perfect structure quality these samples were studied by several methods [5-8].

In this work we report the results of synchrotron X-ray diffraction studies in a wide temperature range from about 20 K to 1100 K, performed on a set of (Pb,Cd)Te solid solutions with different chemical compositions. These measurements were executed at the B2 beamline at Hasylab (DESY) using the polycrystalline diffractometerwith Debye–Scherrer geometry. The samples were prepared as a mixture of powdered (Pb,Cd)Te crystals and fine diamond powder (applied as an internal standard), and placed in a thin-wall quartz or glass capillary, rotating inside a graphite heater during measurements. Figure 1 show the typical pattern set for 5.6% CdTe reach (Pb,Cd)Te sample. The structural analysis of collected patterns sets was performed with the help of the Rietveld refinement and demonstrated non-monotonous evolution of the lattice parameter with temperature. The solubility limit calculated on the basis of present results does not agree with the previous data Ref. [1-3] and suggests the necessity of some correction of the relevant phase diagram in region of a low CdTe content. This correction will be shown, its possible influence on planned or expected applications of the solid solution under interest will also be discussed.

The big-size, single crystal containing about 9% of CdTe has also been characterized by neutron scattering technique at Laboratoire Léon Brillouin. Fig. 2 shows the map of 200 Bragg peak intensity distribution in the reciprocal space determined by the elastic neutron scattering. The measurements were performed at RT with the use of 2T1 spectrometer installed on the thermal neutron beam (k_f = 2.66 $Å^{-1}$). The result confirms the single crystal character of investigated sample, which has been then applied for further studies of the phonon dispersion. The preliminary results of the last experiment will also be shown and discussed in comparison to the last exciting findings for PbTe [9].

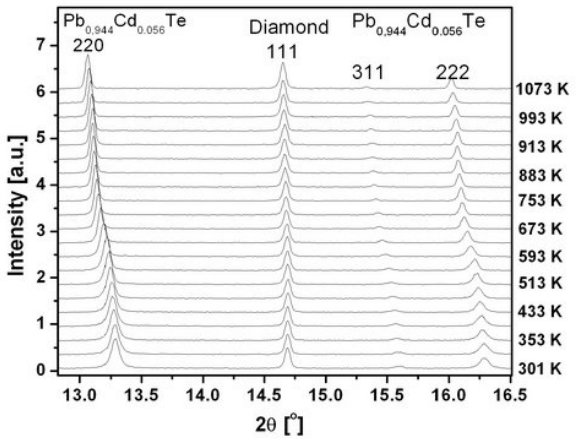

Fig. 1. X-ray powder patterns set accumulated for (Pb,Cd)Te solid solution containing about 5.6% of CdTe. The applied synchrotron radiation wavelength λ~0.52651 Å.

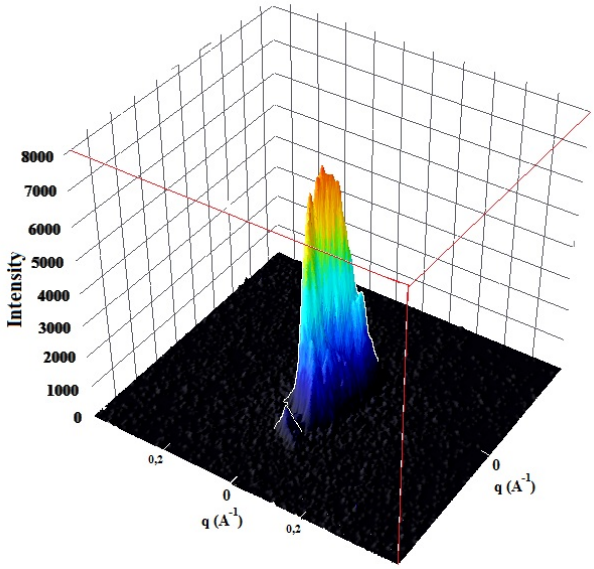

Fig. 2. The 200 Brag peak intensity distribution for a whole (Pb,Cd)Te crystal containing 9% of CdTe taken with the use of neutron scattering.

Acknowledgments:

This work has been partially supported by the European Community's Seventh Framework Programme (FP7/2007-2013) under grant agreement no. 226716 and by the European Union within the European Regional Development Fund, through grant Innovative Economy (POIG.01.01.02-00-108/09) and through the 'Research Infrastructures' action of the 'Capacities' Programme, NMI3-II Grant number 283883.

[1] A.J. Rosenberg, R. Gierson et al., *Trans. Metall. Soc. A.I.M.E.* **230**, 342 (1964).
[2] P.M. Nikolic, Brit. *J. Appl. Phys*. **17**, 341 (1966).
[3] V. Leute and R. Schmidt, *Z. Phys. Chem*. **172**, 81 (1991).
[4] A. Szczerbakow and K. Durose, *Prog. Cryst. Growth Character. Mater*. **51**, 81 (2005).
[5] M. Szot, A. Szczerbakow, K. Dybko et al., *Acta Phys. Pol. A***116**, 959 (2009).
[6] M. Szot, K. Dybko, P. Dziawa et al., *Cryst. Growth Des*. **11**, 4794 (2011).
[7] R. Minikayev, E. Dynowska, P. Dziawa, et al., *Synchr. Rad. Nat. Sci*. **8**, 83 (2009)
[8] R. Minikayev, E. Dynowska, E. Kaminska, et al., *Acta Phys. Pol. A***119**, 699 (2011).
[9] O. Delaire, J. Ma, K. Marty et al., *Nature Materials***10**, 614 (2011).

* Corresponding autor. E-mail address: minik@ifpan.edu.pl

17:00 Poster Mo214

Quantitative Criteria of Image Quality Evaluation, Theory and Experiment

Valery Tkal[1], Alexey Okunev[2], Anna V. Sharaeva[1], Inga A. Zhukovskaya[1]

1. *Saint Petersburg State University of Service and Economics (SUSE), Kavalergardskaja, 7, St-Petersburg 191015, Russian Federation* **2.** *Yaroslav the Wise Novgorod State University, Bolshaya St-Petersburgskaya 41, Novgorod the Great 173003, Russian Federation*

e-mail: alexei.okunev@mail.ru

By using different techniques of digital processing and different wavelet bases we can obtain processed images, similar in quality and visually indistinguishable, which actually contain differences due to "thin" features of experimental contrast. Several experts, analyzing the same contrast, may interpret it differently and, therefore, to identify structural defects in different ways. To reduce the influence of the subjective factor, that occurs at visual assessment of contrast, it is necessary to have a simple quantitative criteria for the objective assessment of the quality and efficiency of digital processing, the difference or identity of an analyzed image [1].

To date, existing methodology for quantifying image quality can be divided into two broad categories: subjective and objective techniques. Subjective techniques are used the human visual system to quantify the quality of the images and are based on the median estimate of observers. Objective techniques use mathematical models to simulate the results of a subjective quality assessment, and they based on objectively measurable criteria and metrics. Objective techniques are required repetition of tests to determine the parameters of the processing signal, which reduces the processing speed and complicates these methods. Therefore, it is necessary to find new and simple methods of objective quality assessment. In this contribution, the following objective methods of measuring the quality of images are considered - MSE (Mean Squared Error), PSNR (Peak Signal-to-Noise Ratio), SSIM (Structural Similarity Index). SSIM quality evaluation method is more promising than PSNR and MSE, as the calculation takes into account the brightness, contrast and structural features of the compared images.

All of these techniques have a major drawback – they need for time-consuming mathematical calculations, so in this study we used a more simple and easy to implement in practice method, which is based on the construction of brightness characteristics (BC), profiles of intensity (IP) and the difference of contrast (DC) in the program «Image-Pro Plus 6.0» [1, 3].

If one of the two comparable contrast perfectly identical to another, we get a zero DC, and corresponding to it BC and IP have the form of thin vertical and horizontal lines, respectively. If the images have visually indistinguishable minor differences, the DC is not zero, and the maxima of BC are different from ones for zero DC. This approach was tested on the test objects, which were used as a noisy and not noisy theoretical picture of structural defects further subjected to digital processing with different wavelets. Obtained results for the test objects are fully coincides with the results of digital processing of the experimental contrast. For simulation of noise factors – emulsion graininess and background inhomogeneity the expression *s2 = s1 + ((Random (10) / 10) - (5/10))* was use. Example of digital processing by different wavelets of noised after simulation test contrast of screw dislocation is shown on Fig. 1. The Fig. 1. shows the results of a similar processing of the experimental topograph of 6H-SiC crystal. The differences are revealed only when comparing of DC and maximum values of BC.

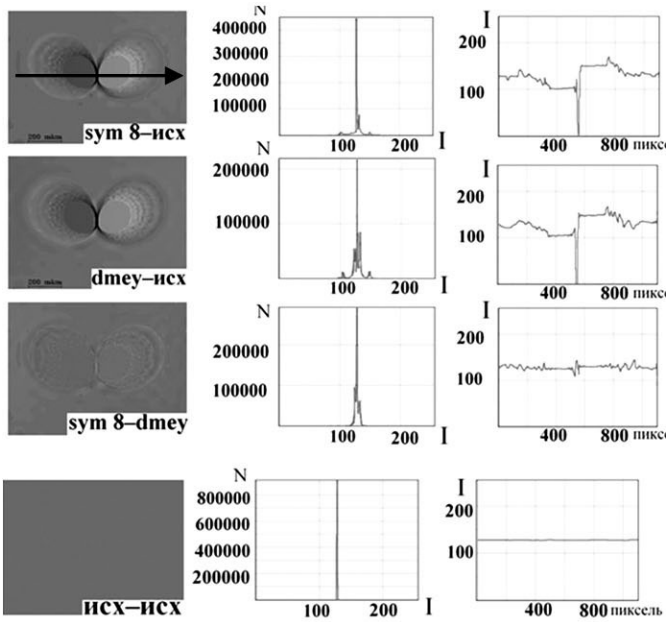

Fig. 1. Results of digital processing by *dmey* and *sym 8* wavelets of test image, based on the construction of the DC, BC and IP. The arrow shows the direction of the IP construction.

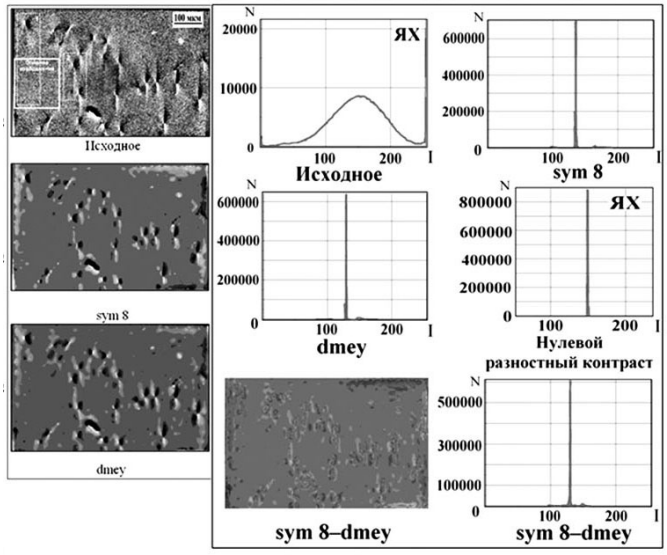

Fig. 2. Results of digital processing by *dmey* and *sym 8* wavelets of experimental topograph.

Maxima of BC in the case of processing of test (noised) and experimental contrasts were higher and closer to value for the initial contrast when choosing wavelet basis *sym 8* than for the wavelet basis *dmey*, and difference of contrast "*sym 8* - *dmey*" is not zero. Consequently, digital processing using wavelet *sym 8* gives better results than using wavelet *dmey*.

This method was successfully tested on the polarization-optical images with a strong background inhomogeneity, for comparing the effectiveness of different digital techniques and also for images presented in the 8-, 16- and 32-bit format, etc.

Thus, it is shown that the use of quantitative evaluation the quality of experimental contrast formed single crystal structure defects, can significantly reduce the subjective factor in its visual estimation and to

avoid errors in the identification and localization of defects in crystal volume.

Acknowledgments.

This work was performed in joint with Ioffe Physical Technical Institute RAS Laboratories "Computer technology in the diffraction diagnostics of materials" of SPbSUSE (Novgorod branch) and "X-ray topography methods at research of materials for electronic engineering" of NovSU with the support of RFBR grant № **12-02-00201**.

1. V. Tkal, A. Okunev, I. Zhukovskaya, The Brightness and Frequency Analysis of Images of Structure Defects (LAP LAMBERT Academic Publishing, Saarbrücken, 2012), p. 392.

2. V.A. Tkal', I.V. Dzyuba, L.N. Danil'chuk. Computer simulation of the theoretical contrast of various types of structure defects with noise factors. Journal of surface investigation: X-ray, synchrotron and neutron techniques. 2009. V3. No 5. P. 797-803.

3. V.A. Tkal, Quantitative criteria for efficiency evaluating of digital processing of single crystal structure defect images. Proceedings of "X-ray optics – 2010", Chernogolovka, IMT RAS. 2010. P. 37-39.

17:00 Poster Mo215

Computer Diagnostics of Crystal Quality

Valery Tkal[1], Alexey Okunev[2], Anna V. Sharaeva[1], Inga A. Zhukovskaya

1. *Saint Petersburg State University of Service and Economics (SUSE), Kavalergardskaja, 7, St-Petersburg 191015, Russian Federation* **2.** *Yaroslav the Wise Novgorod State University, Bolshaya St-Petersburgskaya 41, Novgorod the Great 173003, Russian Federation*

e-mail: alexei.okunev@mail.ru

Introduction and problem statement.

The estimation of quality and structural perfection of single crystals is not possible without of application of modern diagnostic techniques, including X-ray topography and a polarization-optical analysis, which are the direct and non-destructive methods. Among all the methods of X-ray topography it is possible to highlight a method based on the Borrmann effect (XRBT method), which has high sensitivity at the study of crystals with low dislocation density and dislocation-free crystals [1].

The contrast formed by various type structure defects in the XRBT method has the form of intensity rosettes, shape and number of lobes of which depends on the type of defect and its location in the volume of a single crystal, and the size of the rosettes depends on the type of the investigated crystal. The decoding of topography contrast images is carried out visually and complicated because of the noise factors - background inhomogeneity and granularity of experimental topographs, making it difficult to identify defects with dimensions comparable to the grain of nuclear emulsion plates, as well as defects in highly bright or dark areas. The use of different photographic techniques of eliminating of noise factors often does not lead to the desired result, but the process is generally laborious and inefficient. The result of crystal diagnostic depends on the skills, experience, and the visual acuity of the researcher.

Eliminating of noise factors and improving of reliability at the identification of structural defects is achieved by increasing the quality of the analyzed contrast through the use of digital methods of treatment [2]. Digital processing can be based on an analysis of brightness characteristics of experimental contrast or frequency characteristics at use Fourier and wavelet analysis.

Digital processing based on analysis of the brightness characteristics.

The method based on a filter with recursive accumulation has a high efficiency at granularity removal. The principle of the filter operation is based on the recognition of signal and noise regions in the image from difference between their average values. This allows us to do signal amplification and noise reduction through recursive accumulation with different weights for the signal and noise (Fig. 1).

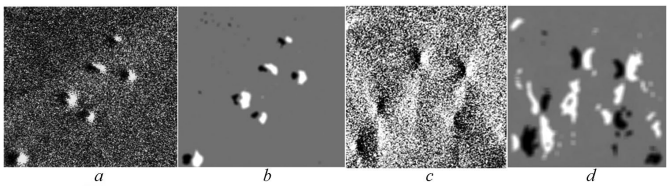

Fig. 1. Initial (a, c) and processed by filter (b, d) topographs containing images of structural defects: microdefects of interstitial type (a) and edge dislocations (c).

Effective elimination of background heterogeneity is achieved by using a high-frequency filter with pre-processing of the analyzed image by non-linear filter (with taking the logarithm or exponentiation of image). Filtering is done by mathematical processing of each pixel of the original image. The specific form of the selected processing function will depend from the average pixel values of the initial image (Fig. 2).

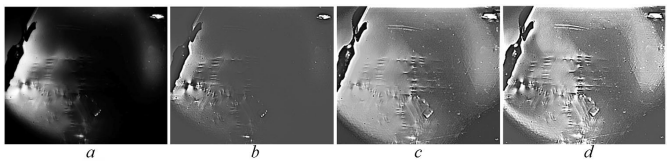

Fig. 2. The result of background inhomogeneity eliminating for single crystal 6H-SiC polarization-optical image: a – the original image; b – the image after high-frequency filtering with use image exponentiation only; c – the image after high-frequency filtering with taking the logarithm of image only; d – the high-frequency filtering with pre-processing by non-linear filter then taking the logarithm, and exponentiation do together.

Comparison of the structure defect images processed by these methods with the theoretically simulated from the modified Indenbom–Chamrov's equations ones shows that low-frequency peculiarities of experimental contrast (some lobes of intensity rosettes) may be lost, the processed contrast can be seen as a visual binary. However, digital processing stores all the basic features of the contrast formed by defects of various types, simplifies decoding and increases the reliability of the identification of structural defects.

Digital processing based on discrete wavelet analysis.

The most complete information about studied signal may exist in its frequency range. Discrete wavelet analysis is a kind of frequency analysis of complex signals, which include topography and birefringence experimental images. Experimental studies have shown a distinct advantage of the wavelet analysis in comparison with Fourier analysis [2].

At the core of the discrete wavelet analysis lays decomposition of the investigated contrast on a number of levels, depending on its size. As a result of the decomposition we obtain two types of factors that characterize the frequency spectrum of the image: scale factors containing low-frequency characteristics, and detailed (diagonal, vertical and horizontal) factors containing high-frequency image features. Selecting the optimal bandwidth at filtering and zeroing coefficients relating to the noise factors we obtain contrast at reconstruction (restoration),

containing purified from the noise images of structural defects. Background inhomogeneity refers to the low-frequency characteristics of the contrast and emulsion granularity – to high ones.

In comparison to methods based on the analysis of brightness characteristics, discrete wavelet analysis allows to keep the low-frequency characteristics of images of structure defects and improve the reliability of identification of the defect and its location in the crystal volume, reveals additional features of experimental contrast, not detected previously.

In this work we compare two methods of elimination of background inhomogeneity using the discrete wavelet analysis [2]. The first method is based on zeroing of scale factors at the signal decomposition. Further work is carried out with the detailing coefficients only at signal reconstruction with optimal selection of bandwidth. The second method involves four stages and can improve performance of wavelet processing by 10–12 times, as well as eliminate the aliasing phenomenon (intensity fluctuations at the boundaries of the single crystal and at the defects occurred during the surface processing): **stage 1** – zeroing of detailing coefficients and selection only background inhomogeneity after processing; **stage 2** – construction of a difference between the original contrast and contrast obtained at the first stage; **stage 3** – gauss blur of difference contrast (value is selected experimentally); **stage 4** – construct the final difference contrast between obtained at stage 3 (blurred contrast) and the difference contrast obtained at stage 2. For a better visual perception of the final contrast and for better details, optimal dynamic range is selected (Fig. 3).

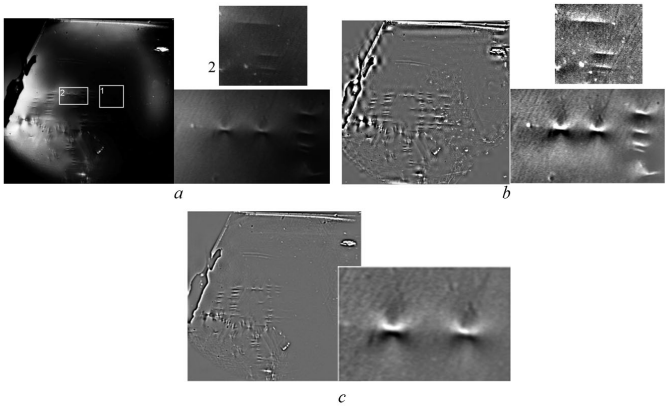

Fig. 3. The result of the wavelet processing of polarization-optical image of 6H-SiC single crystal and its fragments: a – the original image; b, c – images after digital processing with use of sym8 wavelet, through the first and second methods, respectively.

Best detailing of contrast is obtained by its rescaling and representation in 32-bit format (High-dynamic-range images or HDR-images). The processing time at this operation does not increase much.

The main result of the digital processing is the removal of noise factors, as well as more complete and reliable identification of crystal defects.

Acknowledgments.

This work was performed in joint with Ioffe Physical Technical Institute RAS Laboratories "Computer technology in the diffraction diagnostics of materials" of SPbSUSE (Novgorod branch) and "X-ray topography methods at research of materials for electronic engineering" of NovSU with the support of RFBR grant № **12-02-00201**.

1. L. Danilchuk, A. Okunev, V. Tkal, X-Ray topography on base of Borrmann effect (LAP LAMBERT Academic Publishing, Saarbrücken, 2012), p. 348.

2. V. Tkal, A. Okunev, I. Zhukovskaya, The Brightness and Frequency Analysis of Images of Structure Defects (LAP LAMBERT Academic Publishing, Saarbrücken, 2012), p. 392.

17:00 Poster Mo216

Defect distribution along needle-shaped $PrVO_4$ single crystals grown by the slow-cooling method

Jaroslaw Domagala[1], Wojciech Paszkowicz[1], Jadwiga Bak-Misiuk[1], Olga Ermakova[1], Hanna Dabkowska[2]

1. *Polish Academy of Sciences, Institute of Physics, al. Lotników 32/46, Warszawa 02-668, Poland* **2.** *Brockhouse Institute for Materials Research, McMaster University, 1280 Main Street West, Hamilton L8S4MI, Canada*

e-mail: paszk@ifpan.edu.pl

Rare earth orthovanadates (RVO_4) crystallizing in the tetragonal zircon-type structure have been reported to be applicable as scintillators, as laser and optical waveguide materials, as catalysts and to be useful for remote thermometry. Applications such as laser-directed ones require the use of defect-free crystals, as discussed in refs. [1, 2]. The defect structure strongly depends on the applied growth technology as well as on the doping details. Slow cooling method is known to provide crystals of small dimension but of relatively good quality [3, 4]. A limited information on growth of $PrVO_4$ single crystals can be found in literature, and very little is known about the nature and density of defect occurring in such crystals. Yadawa et al. [5] have concluded that the electrical conductivity of flux-grown PrVO4 single crystal is due to the point defects presence in the crystal. Nakahara et al. [6] have reported that the floating-zone-grown crystals do not contain macroscopic defects.

Spatially resolved X-ray diffraction techniques provide useful quantitative information on the defect structure distribution for single crystals, thin films or nanowires. In this work, general information on the defect structure is derived from reciprocal lattice-point maps at several selected points. Details of the defect nature and distribution along the crystals are obtained with the use of mapping of triple-axis rocking curves and of $2\theta/\omega$ diffraction curves.

Analysis of the obtained data permitted to extract the information on one-dimensional distribution of the lattice plane deformation, mosaic structure as well as on the lattice parameters variation in undoped and Yb-doped $PrVO_4$ crystals. The samples are typically single crystalline, some of them are built from several blocks with misorientation angles up to several arcmin. There is no particular difference between the defect nature of undoped and doped crystals. The full width at half maximum (FWHM) value at the central part of the crystals is as low as about 10-12 arcsec. There is a tendency of FWHM to increase at the crystal tips, demonstrating that the crystals are less perfect at these regions. The analysis for (100) and (010) crystal faces shows that there is a significant difference between their curvatures.

[1] J.B. LeBret, Defect Characterization of Yttrium Orthovanadate, Master Thesis, Washington State University, School of Mechanical and Materials Engineering (Pullman, WA, 2004).

[2] G.Yu. Orlova, V.I. Vlasov, Yu.D. Zavartsev, A.I. Zagumennyi, I.I. Kalashnikova, S.A. Kutovoi, V.S. Naumov, A.A. Sirotkin, Quant. Electron. 42, 208 (2012)

[3] B.K.Tanner, S.H. Smith, J. Cryst. Growth 30, 323–326 (1975)

[4] S.H. Smith, G. Garton, B.K. Tanner, D. Midgley, J. Mater. Sci. 13, 620 (1978)

[5] Y.P. Yadava, R.A. Singh, B.M. Wanklyn, J. Mater. Sci. Lett. 4, 224 (1985)

[6] T. Nakahara, M. Higuchi, J. Takahashi, T. Ogawa, S. Wada, J. Jpn. Assoc. Cryst. Growth 33, 195 (2006)

17:00 Poster Mo217

Precise lattice parameter measurements of the $Sr_{0.72}Ba_{0.25}Nb_2O_{5.97}$ single crystals

Robert Paszkowski[1], Krystyna B. Wokulska[1], Jan Dec[1], Tadeusz Łukasiewicz[2]

1. *University of Silesia, Institute of Materials Science (INOM), 75 Pułku Piechoty 1A, Chorzów 41-500, Poland* **2.** *Institute of Electronic Materials Technology (ITME), Wólczyńska 133, Warszawa 01-919, Poland*

e-mail: rpaszkowski@us.edu.pl

Strontium barium niobate ($Sr_xBa_{1-x}Nb_2O_6$ - SBN) is a ferroelectric material, which belongs to the tetragonal tungsten bronzes (TTB) family. At room temperature SBN crystallizes in a wide solid solution range - $0.25<x<0.75$. Below the Curie temperature - T_C, it has the P4bm space group [1]. In ferroelectric phase, SBN has the 4mm point group symmetry, which goes to centrosymmetric 4/mmm point group above T_C. SBN possesses many potential applications owing to its large pyroelectric and electrooptic coefficients and photorefractive properties.

Pure and undoped $Sr_{0.72}Ba_{0.25}Nb_2O_{5.97}$ single crystals with 72% at. content of strontium grown by Czochralski method were investigated. The real composition of the single crystals was determined using the Inductively Coupled Plasma-Optical Emission Spectroscopy (ICP-OES) method [2].

Basic measurements of the lattice parameter were have been carried out using the X-ray Bond's method which allows obtaining a accuracy of the order of $\Delta d/d = 10^{-5}$. For this purpose, the metric wavelength of $\lambda\ CuK_{\alpha 1} = 1{,}54059292 \pm 4{,}5\text{x}10^{-7}$ Å [3] is required. Measurements of the lattice parameters were performed using 15,4,0 ($\theta = 73.591°$) reflex for an orientation parallel to the crystallographic Z axis and 005 ($\theta = 77.029°$) reflex for an orientation perpendicular to the crystallographic Z axis. Details of measuring principles were presented earlier [4]. Measurements of *a* and *b* lattice parameters were repeated 10 times at 298 K. The obtained values of lattice parameters were $a = 12.43439 \pm 0.00027$ Å and $b = 12.43451 \pm 0.00014$ Å. Basing on the analysis of the obtained lattice parameter data it is ascertained that the investigated $Sr_{0.72}Ba_{0.25}Nb_2O_{5.97}$ single crystals crystallize in the tetragonal system.

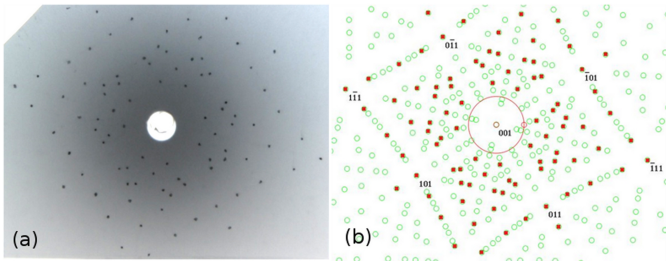

Fig. 1. Symmetry along [001]: (a) Laue backscattering pattern taken from (001) plane (b) simulated Laue pattern. Marked squares inside circles are the real equivalent Laue spots.

Large uncertainty of the measured lattice parameters could have been caused by vibrations of atoms when approaching the temperature T_C = 310K of the structural phase transition. Analysis of the diffraction patterns obtained by the Laue method confirmed the occurrence of a four-fold axis of symmetry (Fig. 1).

The additional observations of conoscopic figures using a polarizing microscope technique showed an optical pseudo-biaxiality of the investigated crystals [5]. Such results do not exclude the tetragonal symmetry in the investigated strontium barium niobate single crystals. The results obtained by different X-ray and optical methods are compatible and coincide with the literature data.

References

[1] M. Ulex, R. Pankrath, and K. Betzler, Growth of strontium barium niobate: the liquidus–solidus phase diagram, J. Crystal Growth 271 (2004) 128 - 133.

[2] T. Łukasiewicz, M.A. Świrkowicz, J. Dec, W. Hofman, W. Szyrski, Strontium-barium niobate single crystals, growth and ferroelectric properties, J. Crystal Growth 310 (2008) 1464 - 1469.

[3] G. Holzer, M. Fritsch, M. Deutsch, J. Hartwig, E. Forster, $K_{\alpha 1,2}$ and $K_{\beta 1,3}$ x-ray emission lines of the 3d transition metals, Phys. Rev. A 56 (1997) 4554-4568.

[4] K. Wokulska, P. Pacek, J. Dec, T. Łukasiewicz, M. Świrkowicz, Characterization of Phase Transition in Strontium Barium Niobate by Bond Method, Solid State Phenomena 163 (2010) 264-267.

[5] J. Dec, T. Łukasiewicz, Crystallooptics of tetragonal tungsten bronze materials, Book of Abstract of the XXII Conference on Applied Crystallography (2012) 73.

17:00 Poster Mo218

Birefringence and UV-Visible transmittance studies on unidirectional ADP single crystals

Rajesh Paulraj, Ramasamy Perumalsamy

Centre for Crystal Growth,SSN College of Engineering,Kalavakkam,Chennai, Chennai 603110, India

e-mail: rajeshppraj@gmail.com

Birefringence measurements on unidirectional ADP single crystals grown by SR method have been carried out. Pure ADP, slotted ampoule grown ADP, L-Asparagine monohydrate, ammonium chloride and nickel sulphate doped ADP crystals were selected for the measurements. It provides qualitative assessment of the uniformity of dislocation density inside the crystal. This technique is also used for precise determination of the birefringence along any preferred direction of the crystal. The uniformity of the fringes signifies that the grown crystals have good optical quality. The birefringence is practically zero, implying that the crystal plate is almost perpendicular to the optic axis direction. The birefringence value for < 0 0 1> direction of all crystals have been determined and these results are correlated with UV-Visible transmittance results.

Birefringence spectrum of (a) Slotted ampoule grown ADP (b) Pure ADP

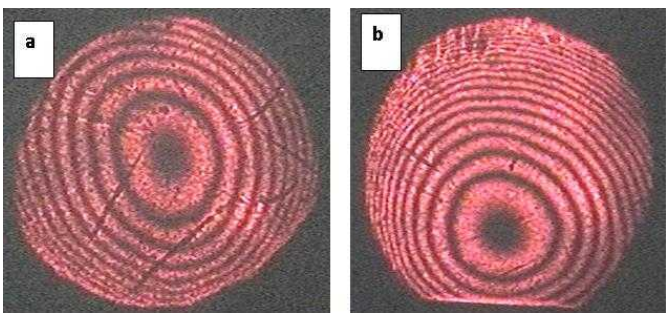

17:00 Poster Mo219

Micro-Raman scattering studies on silicon/quartz nanostructure

Sangeetha Periasamy[1], Jeyanthinath Mayandi[2], Ramakrishnan Veerabahu[3]

1. *Centre for Photonics and Nanotechnology, Sona College of Technology, Salem 636005, India* **2.** *Department of Material Science, School of Chemistry, Madurai Kamaraj University, Madurai 625021, India* **3.** *Department of Laser studies, School of Physics, Madurai Kamaraj University, Madurai 625021, India*

e-mail: geethu.laxi@gmail.com

The investigation on size effect of silicon/quartz nanostructure has been performed using micro-Raman spectroscopic technique. Micro Raman spectral measurements of silicon on quartz substrate prepared by the plasma enhanced chemical vapor deposition method (PECVD) with various deposition powers like 15, 30 and 50W have been made. Micro-Raman spectra of silicon show the T2g Raman active mode at 494, 499 and 504 cm-1 for these three different samples. The observed shift from 521 cm-1 (crystalline Si Raman line) indicates the samples are amorphous and crystalline in nature. We could notice large Raman mode shifts, up to 27 cm-1 and broadening up to 19 cm-1 of the T2g Raman-active mode, which is attributed to phonon confinement effect. The analysis of micro-Raman scattering data is useful to understand the role of deposition condition of the silicon sample.

17:00 Poster Mo220

Polytypic transitions during the growth on C and Si faces 15R-SiC single crystals

Narendraraj Chandran[1], Nikolaos Tsavdaris[2], Eirini Sarigiannidou[2], Didier Chaussende[2], Efstathios K. Polychroniadis[1]

1. *Department of Physics, Aristotle University of Thessaloniki, Thessaloniki 54124, Greece* **2.** *LMGP, CNRS UMR5615, GrenobleINP, Minatec 3 parvis Louis Néel, CS50257, Grenoble 38016, France*

e-mail: polychr@auth.gr

Silicon carbide (SiC) single crystals have been grown by Physical Vapor Transport (PVT) starting from 15R-SiC seeds. The aim of this work is to study the polytypic transition that usually occurs during the growth of 15R-SiC with a special focus on the interface structure and to analyze the associated mechanism by transmission electron microscopy (TEM). For both Si and C faces, on-axis 15R-SiC seeds have been used. Common growth conditions were employed, i.e. 2200°C for the growth temperature and a pressure comprised within the 15-20 mbar range. The thickness of the grown crystals was around 3 mm and the polytype was determined by Raman Spectroscopy. On the C-face, a mixture of 15R-SiC and 4H-SiC was obtained, while on the Si-face, 6H-SiC inclusions were observed.

Once the transition from 15R-SiC to 4H-SiC or 6H-SiC occurred, it rarely shifted back to 15R-SiC. Defects such as micro-pipes, Stacking Faults (SFs), Basal Plane Dislocations (BPDs), Screw and Edge Dislocation are abundant in 15R-SiC compared to 4H-SiC and 6H-SiC inclusions (Fig.1a). High Resolution Transmission Electron Microscope (HRTEM) was used to examine near atomic sequence at the interface. It revealed micro twin sequence with zigzag (32)/ (23) (Zhdanov notation) pattern in 15R-SiC which may have favored polytypic transformation to 4H-SiC without much disturbing atomic sequence at the interface (Fig.1b) The twin sequences were indistinguishable in Selected Electron Diffraction Pattern (SAED) due to hexagonal polytype inclusion later confirmed by FFT image. The 15R/6H interface was more complex with large transition region due the presence of numerous stacking faults.

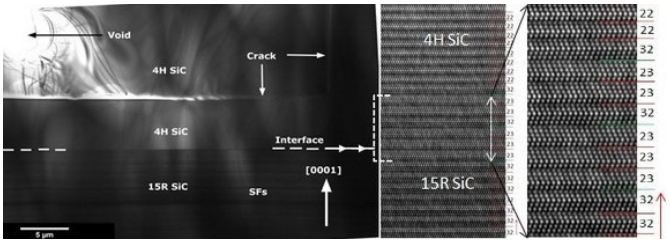

Fig1. (a) Convectional TEM image and (b) corresponding filtered HRTEM shows a coherent transition layer between 15R-SiC and 4H-SiC interface with alternating (32)/ (23) and finally transformed to (32)/(22) atomic sequence. The Zhhdanov notation of the stacking sequence is listed at right was measured as indicated by arrow.

17:00 Poster Mo221

Intrinsic crystal phase separation in the antiferromagnetic superconductor $Rb_yFe_{2-x}Se_2$: a diffraction study

Vladimir Pomjakushin[1], Anna Krzton-Maziopa[2], Ekaterina Pomjakushina[3], Kazimierz Conder[3], Dmitry Chernyshov[4], Volodymyr Svitlyk[4], Alexey Bosak[4]

1. *Laboratory for Neutron Scattering Paul Scherrer Institut, Villigen PSI 5232, Switzerland* **2.** *Warsaw University of Technology, Faculty of Chemistry, Noakowskiego, Warsaw 00-664, Poland* **3.** *Laboratory for Developments and Methods, Paul Scherrer Institut, Villigen PSI 5232, Switzerland* **4.** *Europen Synchrotron Radiation Facility (ESRF), 6, Jules Horowitz, Grenoble 38000, France*

e-mail: vladimir.pomjakushin@psi.ch

The crystal and magnetic structures of the superconducting iron-based chalcogenides
RbyFe2−xSe2 have been studied by means of single-crystal synchrotron x-ray and
high-resolution neutron powder diffraction in the temperature range 2–570 K. The ground state of the crystal is an intrinsically phase-separated state with two distinct-by-symmetry phases. The main phase has the iron vacancy ordered $\sqrt{5} \times \sqrt{5}$ superstructure (I4/m space group) with AFM ordered Fe spins. The minority phase does not have $\sqrt{5} \times \sqrt{5}$-type of ordering and has a smaller in-plane lattice constant a and larger tetragonal c-axis and can be well described by assuming the parent average vacancy disordered structure (I4/mmm space group) with the refined stoichiometry Rb0.60(5)(Fe1.10(5)Se)2. The minority phase amounts to 8–10% mass fraction. The unit cell volume of the minority phase is 3.2% smaller than the one of the main phase at T = 2 K and has quite different temperature dependence. The minority phase merges with the main vacancy ordered phase on heating above the phase separation temperature TP = 475 K. The spatial dimensions of the phase domains strongly increase above TP from 1000 to >2500 A° due to the integration of the regions of the main phase that were separated by the second phase at low temperatures. Additional annealing of the crystals at a temperature T = 488 K, close to TP, for a long time drastically reduces the amount of the minority phase.

17:00 Poster Mo222

Growth and characterization of L- glutamic acid and sodium sulphate doped triglycine sulphate single crystal

Siva Sankari Raghavan, Rajesh Narayana Perumal

Centre for Crystal Growth,SSN College of Engineering,Kalavakkam,Chennai, Chennai 603110, India

e-mail: r.shankarisai@gmail.com

Tri glycine sulphate is one of the most promising ferroelectric crystal exhibiting good pyroelectric properties,because of second order transition at room temperature (Curie temperature = 49^{o}C) and higher pyroelectric coefficient. TGS fits into polar point group2 with spontaneous polarization along b axis if the temperature is below curie temperature and centrosymmetric point group 2/m above the curie temperature. TGS can be depolarized by thermal,electric and mechanical power.In order to stabilize TGS ,an optically active molecule is done. The substitution of such a molecule creates an internal bias field into TGS by which crystal becomes permanently depolarized.In this paper, L -glutamic acid and sodium sulphate are selected as dopants.TGS crystal was doped with L- glutamic acid and sodium sulphate,harvested to study the change in phase transition temperature and electric studies.

TGS was synthesized by taking analar grade glycine and conc. sulphuric acid in 3:1 molar ratio. Then the dopnts L - glutamic acid and sodium sulphate were doped in 2 mol%, 4 mol% and 5 mol% molar ratio individually. Calculated amount of glycine was added with sulphuric acid which was diluted with millipore water, Once all dopants are clearly dissolved,they are filtered using whatman filter paper.Single crystalswere harvested by 30 days. Single crystal XRD anaysis was using Enraf - Nonius CAD4 diffarcto meter.The single crystal XRD shows a slight variation in the lattice parameters.This may be attributed to the effect of doping.The crystal retains its crystal system.FTIR analysis is done with perkins Elmer spectrophotometer.FTIR analysis was carried out to analyze the presence of L - glutamic acid sodium sulphate qualitatively.FTIR was done in the range 400cm-^{1} to 4000cm^{-1} The optical absorbance was recorded by Hitatchi spectrophotometer in the range 200 - 600 nm.The UV Cut off for the doped crystal is 235nm.The DSC analysis was done Metler Tledo DSC 821e caloriemeter,The phase transition temperature has increased to 50^{o}C.Dielectric measurements were made in the rangeHIOKI N3532-50 LCR Hitester with a temperature range 40^{o}C to 60^{o}C.The dielectric constant increases with temperature and reaches a maximum at 50^{o}C.AC conductivity also increases with temperature and reaches a maximum at the same temperature.The increase in phase transition temperature is due to thye effect of doping.The increase in phase transition temperature is shown in DSC studies

17:00 Poster Mo223

Structural and optical properties of $ZnGeP_2$ single crystals

Saïd Assoumani Saïd Hassani[1], A. Godard[2], Galina A. Verozubova[1,3], A. Lusson[1], J. Barjon[1], C. Vilar[1], M. Lefebvre[2], E. Rosencher[2], P. Galtier[1]

1. *GEMaC, CNRS-University of Versailles, 45 avenue des Etats-Unis, Versailles 78035, France* **2.** *Office National d'Études et de Recherches Aéospatiales Chemin de la Hunière, Palaiseau, Palaiseau F-91761, France* **3.** *Insitute of Climatic and Ecological Systems of SB RAS (IMCES), 10/3 ave Akademicheskii, Tomsk 634055, Russian Federation*

e-mail: said.hassani@uvsq.fr

Nonlinear optical infrared materials are needed for various applications. $ZnGeP_2$ is an interesting nonlinear optical material in the 0.7-13 mm spectral range due to its unique set of optical properties (wide potential transmission range and high value of nonlinear susceptibility). In this study, the vertical Bridgman technique was used for the growth of $ZnGeP_2$ monocrystals using a seed crystal with the <100> orientation. X-ray diffraction experiments show rocking curves with full width at half maximum of 35 arsec and demonstrate the high quality of the crystal. An excellent transmission is measured in the 2-12 μm range. We particularly focused our interest in the transmission in the 1.5-2 μm range because it corresponds to pump wavelengths for optical parametric oscillators (OPO) applications. In this range, the transmission was shown to be related to defects. In order to cure these defects, thermal annealing under various atmospheres has been investigated. Thermal annealing under Zn atmosphere (500°C, 24h) shows a catastrophic degradation of the transmission whereas annealing under P atmosphere shows a slight improvement for short time annealing (500°C, 3h) followed by a degradation for long time annealing (500°C, 72h). Thermal annealing under vacuum gives an improvement of ~30% in the transmission at 1.6 -1.8 μm. Cathodoluminescence investigation have been used to study the $ZnGeP_2$ based bulk. These results are discussed in relation with the creation and annihilation of stoichiometric and extrinsic defects.

17:00 Poster Mo224

The thermal properties and Stimulated Raman scattering of $Ba_2TiSi_2O_8$ single crystal

Chuanying Shen, Huaijin Zhang, Jiyang Wang

Institue of Crystal Materials, Shandong University, Jinan 250100, China

e-mail: shenshouchuan@163.com

Stimulated Raman scattering(SRS) used for shifting the frequency of laser radiation to new spectral regions where direct laser oscillation is not available or ineffective, has attracted much attention for their wide applications in medicine, ultra-fast laser spectroscopy, ecological monitoring techniques, laser guide stars and up-conversion fiber lasers. As one of the earliest third-order nonlinear optical process, SRS was discovered by Woodbury and Ng. Since then, intensive investigation were made on SRS and a large number of crystals were reported as promising candidates for efficient Raman shifting, including some tungstates ($BaWO_4$, $KGd(WO_4)_2$, $SrWO_4$, $PbWO_4$), nitrates($Ba(NO_3)_2$) and vanadates (YVO_4, $GdVO_4$). As one kind of perspective Raman materials, however, there have no reports about the SRS with $Ba_2TiSi_2O_8$ crystal.

The purpose of our experimental study was to examine the steady state Raman gain and the thresholds for the onset of SRS of BTS crystal with picosecond pumping. Stimulated Raman scattering of 30ps laser at 532 nm pulses were investigated in single-pass scattering arrangement. The first and second Stokes Raman gain coefficients were measured to be 5.08 cm/GW and 3.53 cm/GW at 532 nm, respectively. The highest first Stokes conversion efficient in a single-pass arrangement was 31.8%. Meanwhile, we measured the thermal properties of Ba2TiSi2O8, including the measured specific heat, thermal expansion, thermal diffusivity coefficient and thermal conductivity for the first time. The thermal expansions at room temperature are □a=3.72×10-6 K-1, □c=11.1×10-6 K-1. The thermal diffusivity coefficient at 296K are κ11=1.83 W•m-1•K-1, κ33=0.708 W•m-1•K-1. All the results show that $Ba_2TiSi_2O_8$ crystal is a new Raman material for the generation of frequency shifted Raman laser pulses.

17:00 Poster Mo225

Synthesis and structural and spectral analysis of new optical Di-Lithium Di-phthalate single crystals

Saravanan Devanathan[1], Sivakumar Balaraman[2], Gokulraj Srinivasan[3], Rameshkumar Gubendiran[4], Thangaraj Ka[5]

1. *Dr. Pauls Engineering College, VANUR T.K.,VILLUPURAM DT.,, Villupuram 605109, India* **2.** *Presidency College (PRESIDENCY), Kamarajar Salai, Chennai 600005, India* **3.** *VelTech Dr.RR and Dr.SR Technical University (VELTECH), No.42 VelTech Avadi Road, Chennai 600062, India* **4.** *University College of Engineering Arni, Chennai 632317, India* **5.** *Kongu Engineering college (KONGU), Erode 638052, India*

e-mail: gokulrajs@yahoo.com

A new mixed alkali phthale single crystal namely Di-lithium Diphthalate (DLDP) were crystallized for the first time and is being reported here. The crystal forms in a monoclinic system with a centrosymmetric space group having the unit cell parameters; a= 17.037(5) Å, b= 5.134(5) Å, and c=21.398(5) Å and α = 90.000(5) °, β = 113.195(5) °, and γ = 90.000(5) ° with Z= 2.

Spectroscopic measurements such as Fourier transform infrared (FTIR), UV-Vis-NIR analyses were carried out to confirm the functional groups and its optical transmittance. Thermal measurement reveals the stable nature of the compound. Thus wide transparency in the visible region and its centrosymmetric nature favours these crystals for its use as harmonic generators in third order regime. The obtained results have been discussed in detail.

17:00 Poster Mo226

Emission spectra and thermoluminescence of rare-earth-doped bismuth silicate crystal grown by modified Bridgman method

Zhengye Xiong[2], Jiayue Xu[1]

1. *Shanghai Institute of technology (SIT), Haiquan Road, Fengxian, Shanghai 201418, China* **2.** *Guangdong Ocean University (GDOU), East of Huguang Lake, Zhanjiang 524088, China*

e-mail: xiongzhengye@139.com

Undoped and rare-earth-doped bismuth silicate (BSO) crystals were grown in the same condition by modified Bridgman method. UV exited luminescence, thermoluminescence (TL) glow curves were investigated. The emission spectra of BSO crystals doped with Ce, Y, Gd, Yb ions respectively are similar to that of undoped crystal, but the emission spectra of BSO crystals doped with Dy and Eu respectively differ greatly from that of undoped crystal, and especially, the emission intensity of BSO:Dy is much more than that of undoped crystal. TL glow curves of BSO crystals coped with Y, Gd, Yb are similar to each other, but differ greatly from that of BSO crystals doped with Dy and Y respectively. Dy and Eu ions replace some Bi ions in BSO crystals and become new luminescence centers. Because Dy ions can boost up the luminescence intensity of BSO crystal, BSO:Dy can be a potential excellent scintillator.

17:00 Poster Mo227

Comparison of CdTe and ZnTe crystals grown under Te-rich condition

Yadong Xu, Hang Liu, Rui Yang, Yihui He, Tao Wang, Wanqi Jie

Northwestern Polytechnical University, Xi'an 710072, China

e-mail: xyd220@nwpu.edu.cn

II-VI compound semiconductor CdTe and ZnTe have attracted much attention in the fields of far-infrared and room temperature radiation detectors, solar cells, terahertz and photorefractive devices, etc. due to its excellent photoelectric properties. Recently, there has been a significant effort in developing CdTe and ZnTe single crystal growth. However, duo to the high melting point, abundance of structure imperfections usually positioned in the crystals when grown according to the stoichiometric composition. Therefore, the resistivity and charge transport behaviors of the crystals were degraded, which has consequently reduced the availability and prevented the wide-spread adoption of CdTe and ZnTe for various general applications.

In this work, CdTe and ZnTe crystals grown by the Te-solvent-vertical Bridgman method were evaluated. The size and density distributions of Te inclusions in CdTe and ZnTe crystals were examined using IR transmission microscopy. Current-voltage curves were measured at room temperature using a Kiethley 6517b picoammeter/ voltage supply. Charge transport mobility and conduction type was identified by Hall-effect measurements at room temperature. Upon comparing the corresponding electric properties and charge transport performance, the cut-off wavelength was analyzed according to the NIR transmittance spectra. In addition, the IR absorption within the wave-number range from 500 to 4000cm^{-1} was obtained, which potentially attributed to the shallow level defects.

17:00 Poster Mo228

Synthesis and physical properties of Li_8SiN_4 as a cathode material of lithium secondary batteries

Taiki Yamashita[1], Shinichi Kuwano[1], Kazuo Kuriyama[1], Kazumasa Kushida[2]

1. *Hosei University, Koganei, Tokyo 184-8584, Japan* **2.** *Osaka Kyoiku University, Kashiwara, Osaka 582-8582, Japan*

e-mail: taiki.yamashita.5a@stu.hosei.ac.jp

Li_8SiN_4 (Tetragonal structure; a = 10.21_7 Åand c = 9.53_6 Å[1], space group; P4/ncc or $P4_2nm$ [2]) has been expected as an electrode material of the Li secondary battery because it includes eight Li atoms in unit cell.

Li_8SiN_4 is synthesized by direct reaction between Li_3N (powder, 99.5% pure) and Si (powder, 99.999% pure). These elements with the molar ratio of 2.5:1 are charged in Ta crucible. The charged crucible is synthesized at 1073 K for 30 minutes under a nitrogen atmosphere of about 700 Torr. As-grown crystals, which are light orange in color, are confirmed to be single phase of Li_8SiN_4 with a = 10.30_0 Åand c = 9.50_9 Å by a powder x-ray diffraction method. Four Raman spectra are observed at 216, 431, 586 and 766 cm^{-1}. The 586 cm^{-1} Raman spectrum is the broad one with a full width at half maximum of 144 cm^{-1}, suggesting the disordered structure between Li and Si as observed in antifluorite type LiMgN, which is the disordered structure between Li and Mg [3]. The band gap of Li_8SiN_4 evaluated using optical absorption and photoacoustic spectroscopy is about 2.3 eV. This value is slightly larger than the d-d electron transition in spinel $LiMn_2O_4$ (1.63 and 2.00 eV [4]), which has been used for cathode materials.

The 5×5 mm^2 sized lithium secondary battery of Li_8SiN_4 cathode / propylene carbonate + $LiClO_4$ electrolyte / Li anode structure is charged at 10 μA for 20 minutes with the charge voltage of about 2.8 V. This battery shows a capacity of 66.7 μAh/cm^2 for a discharge current of 10 μA.

[1] H. Yamane, S. Kikkawa and M. Koizumi, Solid State Ionics, 25, 183 (1987).

[2] J. David, J.-P. Charlot and J. Lang, Rev. Chim. miner, 11, 415 (1974).

[3] K. Kuriyama, Y. Yamashita, T. Ishikawa and K. Kushida, Phys. Rev. B75, 233204

(2007).

[4] K. Kushida and K. Kuriyama, Appl. Phys. Lett. ,77, 4154 (2000).

*Corresponding author: e-mail: kuri@ionbeam.hosei.ac.jp

17:00 Poster Mo229

Structural peculiarities of undoped and Ce-doped solid solutions of rare-earth oxyorthosilicate crystals

Yuri D. Zavartsev[1,5], Alexander I. Zagumennyi[1,5], Sergey A. Kutovoi[1], Galina M. Kuz'micheva[2], Victor B. Rybakov[3], Irina B. Kaurova[4], Faouzi A. Zerrouk[5]

1. *A.M. Prokhorov General Physics Institute of Russian Academy of Sciences (GPI), Vavilov Str. 38, Moscow 119991, Russian Federation* **2.** *Lomonosov Moscow University of Fine Chemical Technology, Vernadskogo pr., 86, Moscow 119571, Russian Federation* **3.** *M.V. Lomonosov Moscow State University, Vorobyevy gory, Moscow 119992, Russian Federation* **4.** *Moscow State Open University, Institutskaya st. 1, Aleksandrov 60165, Russian Federation* **5.** *Zecotek Imaging Systems Pte Ltd, Division of Zecotek Photonics Inc., Richmond, BC V6W 1J, Canada*

e-mail: yu.zavart@gmail.com

The Ce-doped rare-earth oxyorthosilicate solid solutions are new, insufficiently explored field of scintillation materials researches. The first mixed oxyorthosilicate scintillate crystals, $Lu_{1-y}Me_yA_{1-x}Ce_xSiO_{5-z}\square_z$, were proposed in 1996, where A is Lu and at least one element selected from the group of the rare-earth elements, Me is element selected from the group consisting of K, Ca, Ti, Zr, Sn, Hf, As, V, Nb, Sb, Ta, Mo, and W [1]. The first solid-solutions of oxyorthosilicate scintillate crystals, $(Lu_{1-x}Gd_x)_2SiO_5$, were investigated in [2, 3]. Later, the lutetium-based oxyorthosilicate crystals of non-stoichiometry composition, LFS, containing at least one element selected from the group consisting of Ca, Gd, Sc, Y, La, Eu and Tb, were patented, [4]. Lutetium fine silicate, LFS, is a brand name of this family of Ce-doped solid-solution scintillation crystals comprising lutetium and crystallizing in the monoclinic system, space group C2/c, Z = 8. First mentioning of LFS crystal has occurred in 2004, [5].

In the Lu_2SiO_5 structure, there are two crystallographically non-equivalent sites with coordination numbers 6 and 7 for Lu^{3+} in oxyorthosilicate lattice host, whose unit cell contains 64 ions: eight lutetium ions (Lu1-type) are in the six-oxygen coordination, eight Lu3+ ions (Lu2-type) are in the seven-oxygen coordination, eight Si^{4+} ions and the forty O^{2-} ions of five types, O1, O2, O3, O4, O5 (eight O^{2-} ions in each type). Lutetium ions stand two right systems of points: $Lu(1)O_6$ is disordered octahedron; $Lu(2)O_7$ is disordered octahedron with one forked vertex, at that an average interatomic cation-anion distance is about 1.05 times larger in the $Lu(2)O_7$ polyhedron than that in the $Lu(1)O_6$ polyhedron. Si^{4+} ions are in disordered tetrahedron. The structural formula of a lutetium oxyorthosilicate crystal is $(Lu1)(Lu2)SiO_5$.

A content of the host elements in the crystals was measured by the ICP-MS method and the LECO combustion analysis method; concentration of the impurities was measured by the GDMS method. The crystals were grown by Czochralski technique from the melts containing a silicon oxide, a lutetium oxide, an yttrium oxide, a cerium oxide, and a scandium oxide of the different weights ratios. In particular, the crystals grown from the melts of $Lu_{2.06}Si_{0.97}O_{5.03}$, $Lu_{1.99}Si_{1.005}O_{4.995}$, $Lu_{1.98}Ce_{0.02}SiO_5$, and $Ce:Ca:Lu_{2+2y-z}Y_zSi_{1-y}O_{5+y}$ compositions were studied. The X-ray study of the samples cut from top and bottom of the crystals was performed. Precise measurement of the lattice parameters of the samples cut from the crystals grinded to powder allowed specifying structural chemical compositions of the crystals. The compositions of all crystallographic sites of oxyorthosilicate structure, namely Lu1, Lu2, Si, and oxygen, were taken into consideration.

Variation of cerium composition along a crystal length and related to it variation of structure parameters was found and explained. Distribution of Ce-ions in the Lu1 and Lu2 sites in the defect structure of lutetium oxyorthosilicate is established. Measured distribution coefficient of Ce^{3+} ions in LFS-3 crystal equals 0.365. The distribution coefficients in Ln_2SiO_5 calculated with Brandle's empirical formula [6] for the Ce^{3+}-ions in Ce2 and Ce1 sites are 0.39 and 0.17, respectively. Thus, the relative population of each site in crystal grown from a melt of the $Ce:Ca:Lu_{2+2y-z}Y_zSi_{1-y}O_{5+y}$ composition is found to be about 62% for Ce2 and 38% for Ce1 in contrast to the relative population in LSO crystal: 55% and 45% for Ce2 and Ce1 sites, respectively [7].

	$k_{Ce(\Sigma)}$	k_{Ca}	k_Y	k_{Ce2}	k_{Ce1}	Rel. population, Ce2 / Ce1	Ref.
Ce:YSO	0.25			-	-	-	[6]
Ce:LSO	0.206			-	-	55% / 45%	[7]
Ce:LYSO	0.22		-	-	-	-	[8]
$Ce:Ca:Lu_{2+2y-z}Y_zSi_{1-y}O_{5+y}$	0.365	0.4	0.75	*0.39	*0.17	62% / 38%	*this work*

The kind of point defects and non-stoichiometry in oxyorthosilicates are discussed. Existing experimental evidence suggests that in Lu-oxyorthosilicate with different Lu/Si ratios, vacancies of the Lu1 and Lu2 sites and possibility of interstitial ions presence are the point defects, while O vacancies and conduction-band electrons are the primary oxygen deficient defects.

References

[1] A.I. Zagumennyi, Yu.D. Zavartsev, and P.A. Studenekin, US Patent 6,278,832 (1996)

[2] I.A.Kamenskikh, V.V. Mikhailin, I.H. Munro, D.Y. Petrovukh, D.A. Shaw, P.A. Studenikin, A.N. Vasil'ev, A.I. Zagumennyi, Yu.D. Zavartsev, Radiation Effects and Defects in Solids 135 (1995) 391-396

[3] G.B. Loutts, A.I. Zagumennyi, S.B. Lavrishev, Yu.D. Zavartsev, P.A. Studenikin "Czochralski growth and characterization of $(Lu_{1-x}Gd_x)_2SiO_5$ single crystals for scintillators" J. Crystal Growth 174 (1997) 331-336

[4] A.I. Zagumennyi, Yu.D. Zavartsev, and S.A. Kutovoi, US Patent 7,132,060 (2004)

[5] Th.K. Lewellen, M.L. Janes, R.S.Miyaoka, A.F.Zerrouk, "Initial evaluation of the scintillator LFS for positron emission tomo-

graph applications" DOI:10.1109/NSSMIC.2004.1466296, Nuclear Science Symposium Conference Record, 2004 IEEE Vol.5 (2004) 2915-2918

[6] C.D. Brandle, A.J. Valentino and G.W. Berkstresser "Czochralski growth of rare-earth orthosilicates (Ln_2SiO_5)" J. Cryst. Growth **79** (1986) 308-315

[7] H. Suzuki, T.A. Tombrello, C.L. Melcher, and J.S. Schweitzer "Light emission mechanism of $Lu_2(SiO_4)O$:Ce" IEEE Transactions on nuclear science **40** #4 (1993) 380-383

[8] L.Pidol, O.Guillot-Noel, A.Kahn-Harari, B.Vianna, D.Pelenc, D.Gourier, Journal of Physics and Chemistry of Solids 67 (2006) 643-650

* Calculated with Brandle's empirical formula for rare-earth orthosilicates

17:00 Poster Mo230

Characterization of large scintillating Ce:LFS crystals

Alexander I. Zagumennyi[1,4], Yuri D. Zavartsev[1,4], Han Jianfeng[2], Xu Xuezhen[2], Mo Xiaogang[2], Valentin A. Kozlov[3], Mikhail V. Zavertyaev[3], Sergey A. Kutovoi[1], Faouzi A. Zerrouk[4], Ariffin Azman[4]

1. *A.M. Prokhorov General Physics Institute of Russian Academy of Sciences, Vavilova Str. 38, Moscow 119991, Russian Federation* **2.** *Beijing Opto-Electronics Technology Co., Ltd., No.4 Jiuxianqiao road, Chaoyang district, Beijing 100015, China* **3.** *P.N. Lebedev Physical Institute of Russian Academy of Sciences, Leninskii pr. 53, Moscow 117924, Russian Federation* **4.** *Zecotek Imaging Systems Pte Ltd, Division of Zecotek Photonics Inc., Richmond, BC V6W 1J, Canada*

e-mail: yu.zavart@gmail.com

Lutetium fine silicate, LFS, is a brand name of the set of Ce-doped solid solutions of rare-earth oxyorthosilicate scintillation crystals, comprising lutetium and crystallizing in the monoclinic system, spatial group C2/c, Z=4. The patented LFS compositions are $Ce_xLu_{2+2y-x-z}A_zSi_{1-y}O_{5+y}$ where A is at least one element selected from the group consisting of Ca, Sc, Y, and rare-earth elements, [1]. For the first time, the results of study of the LFS-5 and LFS-6 compositions crystals were presented in 2004, [2].

The LFS-3, LFS-7, and LFS-8 compositions crystal ingots of the up 10 kg weight, 10 cm diameter and 22 cm length have been grown by the Czochralski method. The LFS crystals are produced industrially by BOET, China. Compositions of the crystals have been studied. Concentrations of the host elements were measured by the ICP-MS method, oxygen concentration was measured by the Leco combustion analysis, concentration of the impurities was measured by the GDMS method. The existence of the two luminescence centres Ce2(7) and Ce1(6) in LSO crystal is a reason for the deterioration of luminescent properties of Ce-doped LSO. The emission from Ce1 centres should be controlled as much as possible in order to improve crystal performance. It may be achieved by means of: (a) an increasing the average distance of the two centres or (b) a decrease of the Ce1 centres concentration.

Results of the study of optical and luminescence characteristics of the LFS-3, LFS-7 and LFS-8 heavy scintillation crystals are presented. Emission spectra of LFS crystals were measured using a setup with luminescence excitation by X-ray photons with energy of 30 KeV. To determine the light yield scintillators, the total-absorption spectra of γ-rays from radioactive sources, i.e., so-called, photopeaks were used. The luminescence time of LFS scintillators was studied with a special installation using the delayed coincidence method consisting in measurements of the distribution of time intervals between scintillator excitation and photoelectron formation on the photomultiplier photocathode with the aid of a time-to-digital converter (TDC).

Using the average quantum efficiency of the R4125Q photomultiplier photocathode in the region of the LFS-3 emission spectrum to convert the number of photoelectrons per MeV to the photon yield, the LFS-3 light yield of 38000 photon/MeV was achieved. The reduction of the energy transfer between two Ce^{3+} centres improves the energy resolution to 7% and slows down the decay time to 35 ns due to the distortion of the crystal lattice in the Y-containing LFS-3 crystals of the 7.35 g/cm^3 density. The LFS-7 crystals of the 7.43 g/cm^3 density, exhibit high light yield, up to 36000 ph/MeV, good energy resolution, about 6 - 7.5%, a high uniformity and reproducibility of scintillation properties within the boule and from boule to boule. An insertion of Ca^{2+}-ions in LFS compositions and a proper non-stoichiometry compositional shift shortens decay time to 30 - 32 ns for the LFS-7 composition crystal, and results in superior short decay time of 14 ns - 19 ns for the LFS-8 composition crystal. Density of LFS-8 crystal is 7.4 g/cm^3, a light yield is up to 32000 ph/MeV.

Currently there is strong demand for new radiation hard scintillating materials for electromagnetic calorimeters of the HEP experiments. The stability of LFS-3 crystals to radiation damages caused by charged hadrons and γ-rays was studied. The samples were irradiated by the ^{60}Co radioactivity source (the maximum power is ~4krad/min). LFS-3 crystals were sequentially irradiated with three doses: 5, 23, and 68 Mrad. The optical transmission spectra were measured before and immediately after irradiation using a Kruess Optronic VIS 6500 spectrophotometer. An analysis of the transmission spectra shows that the optical transmittance in the LFS-3 emission region decreases by 2.5% for a dose of 68 Mrad. For the LFS-3 samples cut out from the upper, middle, and lower parts of the initial crystal, the dose of 23 Mrad had no appreciable effect on optical transmission.

Radiation damages of LFS-3 crystals during their irradiation with hadrons were studied in the proton beam of the synchrotron of the Institute of Theoretical and Experimental Physics (ITEP). LFS crystals were packed into a 3×2 matrix for simultaneous irradiation of six samples in the 50-mm-diameter proton beam. The LFS crystals were irradiated with 155-MeV protons. Due to the high level of induced radioactivity, the first measurements of the optical transmittance of crystal samples irradiated with protons were performed in 30 days after irradiation only. There are no damages in LFS-3 crystals for a fluence of 4.4×10^{12} particle/cm^2 [3].

References

[1] A.I. Zagumennyi, Yu.D. Zavartsev, S.A. Kutovoi, Patent US 7132060, 2004

[2] Th.K. Lewellen, M.L. Janes, R.S. Miyaoka, F.A. Zerrouk, DOI: 10.1109/NSSMIC.2004.1466296, Nuclear Science Symposium Conference Record, 2004 IEEE Vol.5 (2004) 2915-2918 "Initial evaluation of the scintillator LFS for positron emission tomograph applications"

[3] Yu.D. Zavartsev, M.V. Zavertyaev, A.I. Zagumennyi, A.F. Zerrouk, V.A. Kozlov, and S.A. Kutovoi, "New radiation resistant scintillator LFS-3 for electromagnetic calorimeters" Bulletin Lebedev Phys. Institute vol.40 (2013) 34-38 DOI:10.3103/S1068335613020024

General Session 6

In situ monitoring, new equipment and technologies

Session Coordinators

Thomas Zettler (Germany) *zettler@laytec.de*

Shiro Tsukamoto (Japan) *tsukamot@anan-nct.ac.jp*

Programme

Wednesday, 14 August

WeP-G06
Wednesday afternoon, 14 August, 16:00
Room 211, Old Library

Break
Wednesday afternoon, 14 August, 17:30

Thursday, 15 August

ThO2

G06: In situ monitoring
Thursday afternoon, 15 August, 14:00
Hall 16, Old Library

14:00 Invited oral

Next generation production MOVPE - on the role of in-situ metrology for process control and yield enhancement

Michael Heuken

AIXTRON SE, Kaiserstrasse 98, Herzogenrath 52134, Germany

e-mail: info@aixtron.com

The emerging GaN-on-Silicon technology for electronic and optoelectronic applications also has an impact on MOCVD reactor design as well as on the expected yield. To address these challenges we developed a Planetary Reactor for 5x200 mm GaN-on-Si applications. Advanced process control and yield improvement using metrology tools play a significant role to achieve the required production quality.

To assess the reactor performance we grew 5-fold InGaN LED structures with a total thickness of 5.9 µm on 200 mm (111) silicon wafer using a sequence of strain management AlGaN layers with Al-concentrations of ~67%, ~57% and ~32% followed by an in-situ deposited SiN mask. The GaN buffer had a total thickness of 6 µm with intermittent low temperature (LT) AlN strain management layers.

From in-situ curvature traces continuous buildup of compressive strain without signs of relaxation throughout the GaN buffer could be seen. Even during the 2 µm thick n-doped GaN layer no signs of tensile strain components are evident, as often seen in such layers. Apart from the outermost ~3 mm edge the layers were virtually crack free as determined by Candela measurements.

On wafer temperature measurements using pyrometer at different wavelength are developed to asses temperature distributions in the reactor. We found that the wafer surface shows a different temperature distribution than the wafer pocket due to wafer bowing issues.

White light interference maps yielded an average thickness across all wafers of 6.02 µm with a spread of +/- 25 nm. The on-wafer thickness standard deviation was 0.81% on average. Photoluminescence maps exhibited an average wavelength of 451 nm with on-wafer standard deviations of 2 nm without edge exclusion. The wafer-to-wafer wavelength spread was measured to 2.6 nm. These results show that the thermal management of the reactor allowed for uniform growth.

HR-XRD measurements at center, halfway and edge positions across the wafer were performed to assess the quality and composition of the structure. The GaN FWHM of the XRD traces were 412 arcsec and 682 arcsec for the (002) and (102) reflexes, respectively. Also clearly distinguishable are the three strain reduction AlGaN layers with their different compositions and the fringes of the MQW up to the 5th order which correspond to a uniform pair thickness of ~13 nm.

We will show additional results on uniformity, electrical properties and strain management. Special emphasis will be put on the interplay between in-situ metrology, shortening of development time and final yield improvement.

14:30 Invited oral

Growth monitoring of nitride semiconductors at its limit

Markus Pristovsek[1], Martin Leyer[2], Abdul Kadir[2], Michael A. Kneissl[2], Menno J. Kappers[1], Fabrice Oehler[1], Colin J. Humphreys[1]

1. *University of Cambridge, Department of Material Sciences and Metallurgy, Pembroke Street, Cambridge CB2 3QZ, United Kingdom*
2. *Technische Universität Berlin, Institute for Solid State Physics, Hardenbergstr. 36, Berlin 10623, Germany*

e-mail: markus@pristovsek.de

Reflectance together with pyrometry and deflection (bow) measurements are nowadays standard monitoring techniques during the epitaxy of nitride semiconductors. But even with those, the composition of a typical InGaN quantum well (QW) cannot be measured during growth. Also the defects are not seen since their densities usually are not high enough to influence the reflection. The only exceptions are defects that change the topography by causing roughness or facets.
Thickness and composition of QWs as well as defect densities can be found out afterwards. However, changes to the surface during growth (like single or double metal layers) cannot be found out later. For instance adding indium strong enhances the metal coverage on the surface. Using very sensitive optical monitoring with ellipsometry in the UV region (above 4.5 eV photon energy) allows following such surface changes. Altering the V/III ratio during growth of AlN showed similar indications for a surface transition. In both cases the topography of the layers was different depending on growth conditions.
Growing on patterned substrates/templates is another field where the analysis of reflectance signals is not straight forward. But in this case there is a signal that can be analyzed. From beating pattern coalescence as well as growth rate can be extracted. This will be demonstrated by the growth monitoring of semipolar GaN (11-22) grown on patterned silicon (113) or m-plane Sapphire templates. Still the growth monitoring is limited to the growth rate, and access to defect densities is not possible.
As an outlook, some further monitoring techniques will be discussed, which could improve resolution even in commercial epitaxy reactors.

15:00 Oral

In situ X-ray diffraction monitoring of GaInN growth by metalorganic vapor phase epitaxy

Motoaki Iwaya[1], Taiji Yamamoto[1], Daisuke Iida[1], Mihoko Sowa[1], Yasunari Kondo[1], Tetsuya Takeuchi[1], Satoshi Kamiyama[1], Isamu Akasaki[1,2]

1. *Faculty of Science and Technology, Meijo University (MU), 1-501 Shiogamaguchi, Tempaku-ku, Nagoya, Nagoya 468-8502, Japan* **2.** *Akasaki Research Center, Nagoya University, Nagoya 464-8601, Japan*

e-mail: iwaya@ccmfs.meijo-u.ac.jp

GaInN-based high-brightness LED have been achieved as a result of several breakthroughs. To improve the performance of these devices, it is necessary to understand their crystal growth mechanism. For this purpose, the use of an in situ observation system during crystal growth is effective. XRD can be used to determine the lattice constant, composition, crystalline quality, and thickness. As such, an *in situ* XRD (I-XRD) monitoring system is expected to serve as a very helpful tool for observing epitaxial growth in real time. In this study, we developed a novel I-XRD system to observe the crystal growth of a nitride using a MOVPE reactor. We also present the results of real-time I-XRD monitoring. In general, a conventional XRD system requires a long measurement time because it is necessary to scan the X-ray source, detector, and/or substrate. In this light, it is desirable for the I-XRD system to perform the analysis quickly without the need for scanning during epitaxial growth. Toward this end, it is necessary to establish a high-time-resolution system for accurately analyzing the growth process. The proposed I-XRD measurement system is attached to an MOVPE reactor. The MOVPE reactor, in turn, is attached to the flange of a window consisting of Be. This I-XRD system does not require scanning. X-rays from the tube spread out as shown in the figure. The spread X-rays are focused using a Johansson curved crystal. The irradiation of the focused X-ray on the substrate can be controlled without scanning the angle. In addition, diffracted X-rays were detected using a one-dimensional CCD. These configurations can be measured in a manner equivalent to a (0002) 2θ/ω scan without the need for an analyzer crystal. In addition, this system can perform measurements within at most 1 s. In this system, the tilt component and distribution of lattice constant c can be simultaneously characterized from the FWHMs. We characterized a GaInN/GaN heterostructure and GaInN MQWs by using the proposed I-XRD system. We also measured these samples by *ex situ* XRD through a 30-min-long process. An observation of the spectrum of the GaInN MQW measured at RT showed that although the proposed I-XRD system showed slightly lesser resolution compared to the conventional ex situ XRD system with an analyzer crystal, satellite peaks were confirmed between –2 and +2. As such, we consider that reasonably high resolution was achieved by the proposed system. Moreover, the I-XRD system revealed strain relaxation in GaInN films on GaN. The critical thickness of GaInN films could be estimated by the evolution of I-XRD with FWHMs as a function of GaInN thickness. The proposed I-XRD system enables measurements of the critical thicknesses that involve strain relaxation caused by the formation of surface pits with bent threading dislocations on GaInN during growth. This system is very useful for accurately evaluating the strain relaxation in the GaInN/GaN heterostructure during crystal growth.

15:15 Oral

Continuous in situ X-ray reflectivity measurement on InGaN epitaxial growth by MOVPE

Guangxu Ju[1], Yoshio Honda[1], Masao Tabuchi[2], Yoshikazu Takeda[3,4], Hiroshi Amano[1,5]

1. *Garaduate School of Enginnering, Nagoya University (NAGOYAU), Nagoya university, Furo-cyo, Chikusa-ku, Nagoya, Japan, Nagoya 464-8603, Japan* **2.** *Synchrotron Radiation Research Center, Nagoya Unviersity, Nagoya 464-8601, Japan* **3.** *Nagoya Industrial Science Research Institute, Aichi 464-0819, Japan* **4.** *Aichi Synchrotron Radiation Center, Aichi Science and Technology Foundation, Aichi 489-0965, Japan* **5.** *Akasaki Research Center, Nagoya University, Nagoya 464-8601, Japan*

e-mail: g_ju@nuee.nagoya-u.ac.jp

• 1. Introduction

High quality InGaN-based quantum wells (QWs) have undergone remarkable development because of their practicalapplications in high-frequency and high-power field-effect transistors, light-emitting diodes, and laser diodes. Metalorganic vapor phase epitaxy (MOVPE) has been the leading technique for the commercial growth of wide band-gap InGaN due to its big market. However, many problems are still unsolved and little is known what is going on during the growth process. Then, *in situ* measurements for InGaN growth are required to understand the growth of the layers under the growth conditions, and this may help to develop and fabricate better quality InGaN QWs. We have set up an MOVPE chamber installed in alaboratory level X-ray diffractometer (Rigaku RINT-TTRIII). In our previous work, the preliminary experiments of X-ray diffraction (XRD), X-ray crystal truncation rod (CTR) scattering and X-ray reflectivity (XRR) measurements at various growth temperatures of $In_xGa_{1-x}N$ growth were reported [1,2]. A combination of these techniques was used for investigation on the $In_{0.09}Ga_{0.91}N$ SQW structures with InGaN of several monolayers (MLs) thickness at 830 °C [3]. Annealed InGaN epilayers and GaN decomposition were also studied by using *in situ* XRR [4]. However, the measurement time of CTR and XRR measurements is too long to realize *real time* investigation during the formation of heterostructures, because of measuring with the angle scan.

In this work, a continuous*in situ*XRR observation on InGaN epitaxially grown on free-standing GaN substrate and GaN(2 mm)/sapphire template without the angle scan is reported. The analysis of the strain relaxation of $In_xGa_{1-x}N$ epilayers is conducted.

• 2. Experiments

Both the incident and reflected angle of X-rays were fixed at 0.6°. The growth of $In_xGa_{1-x}N$ and its continuous XRR measurements were simultaneously started and stopped without interruption. The indium composition was 0.09 and 0.13. In Fig.1, experimentally observed oscillations of XRR (red and black line) with growth time are shown. The red line is for thick $In_{0.09}Ga_{0.91}N$ epilayer and the black one is for thick $In_{0.13}Ga_{0.91}N$ epilayer. Both of them were grown on free-standing GaN substrates. An ideal reflectivity oscillation, assuming fully strained InGaN on GaN, with changing InGaN thickness is shown by the blue line. For the ideal reflectivity oscillation, one period of oscillation corresponds to the InGaN thickness of 8.9 nm. The changing InGaN thickness is equal to the growth time multiplied by the growth rate of InGaN epilayer, and then, the growth rate of InGaN epilayer can be estimated. Decrease of the experimental X-ray intensity with growth time is considered due to the increasing surface roughness of InGaN

epilayer caused by the relaxation. It is understood that InGaN is fully strained below the thickness of 14.0 and 8.5 nm with indium composition 0.09 and 0.13, respectively. It is in good agreement with the reported results by D. Holec *et al.* by calculation using the isotropic approximation and energy balance model [5].

Continuous *in situ* X-ray reflectivity was also conducted on InGaN epitaxially grown on GaN/sapphiretemplate with indium composition0.09 and 0.13. Figs. 2 and 3 show the comparison of InGaN epitaxially grown on free-standing GaN substrates with that on GaN/sapphiretemplates at each indium composition. These results show that the critical thickness of $In_{0.09}Ga_{0.91}N$ are 14.0 and 8.1 nm and that of $In_{0.13}Ga_{0.87}N$ are 8.5 and 5.3 nm, on free-standing GaN substrate and GaN/sapphire template, respectively. The dislocation density for free-standing GaN substrate and GaN/sapphire template is 2×10^7 cm^{-2} and 2.6×10^9 cm^{-2} respectively. High dislocation density of the templates accelerates the relaxation in InGaN epilayer, due to thread dislocation extended into the grown layer.

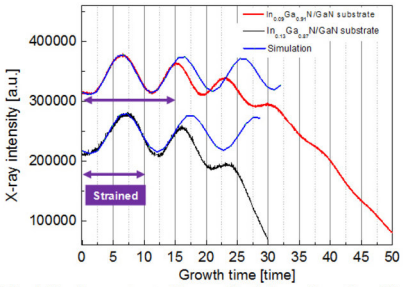

Fig. 1 Continuous *in situ* X-ray reflectivity on $In_{0.09}Ga_{0.91}N$ and $In_{0.13}Ga_{0.87}N$ epilayers grown on free-standing GaN substrate

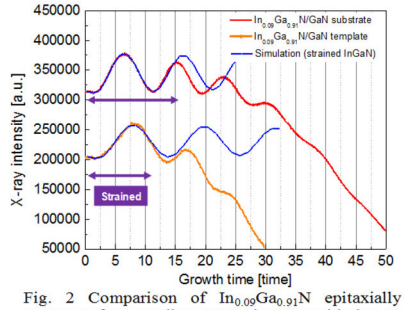

Fig. 2 Comparison of $In_{0.09}Ga_{0.91}N$ epitaxially grown on free-standing GaN substrates with that on GaN/sapphire template

• 3.Conclusions

Continuous *in situ* X-ray reflectivity observation on InGaN epitaxial growth without the angle scan was successfully achieved. The strain relaxation of $In_{0.09}Ga_{0.91}N$ and $In_{0.13}Ga_{0.87}N$ epilayers grown on free-standing GaN substrate was observed. The experimental results agreed with the calculated results using the isotropic approximation and energy balance model. Comparing $In_{0.09}Ga_{0.91}N$ and $In_{0.13}Ga_{0.87}N$ epitaxially grown on free-standing GaN substrates and GaN/sapphire templates, it was clearly and quantitatively observed by XRR that the critical layer thicknesses of InGaN grown on GaN/sapphire templates were thinner than those grown on free-standing GaN substrates.

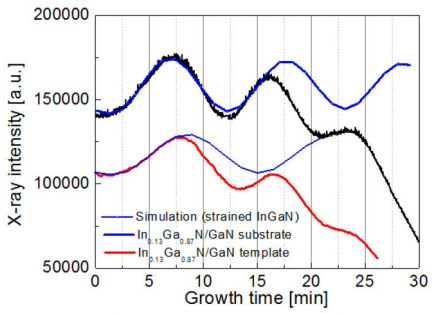

Fig. 3 Comparison of $In_{0.13}Ga_{0.87}N$ epitaxially grown on free-standing GaN substrates with that on GaN/sapphire template

• Acknowledgements

This work was partly supported by NEDO.

• References

[1] Y. Takeda *et al.*, IOP Conf. Ser.: Mater. Sci. Eng. **24** (2011) 012002.

[2] G.X. Ju *et. al.*, J. Cryst. Growth **318** (2011)1143.

[3] G. X. Ju *et al.*, J. Cryst. Growth**370** (2013) 36.

[4] G. X. Ju *et al.*, Jpn. J. Appl. Phys. (in press).

[5] D. Holec *et al.,* J. Cryst. Growth **30**3 (2007) 314.

Coffee

Thursday afternoon, 15 August, 16:00

ThO3

G06: In situ monitoring
Thursday afternoon, 15 August, 16:30
Hall 16, Old Library

16:30 Invited oral

Electronic processes in adatom dynamics at epitaxial semiconductor surfaces studied using MBE-STM combined system

Kiyoshi Kanisawa

NTT Basic Research Laboratories, NTT Corporation, 3-1 Morinosato Wakamiya, Atsugi 243-0198, Japan

e-mail: kanisawa.kiyoshi@lab.ntt.co.jp

It is essential to understand the epitaxial growth mechanism in order to precisely control thin film and nanostructure fabrication. *In situ* observation is a powerful tool for achieving atomic-level accuracy. For the molecular beam epitaxy (MBE) of III-V compound semiconductors, reflection high-energy electron diffraction (RHEED) [1] and the scanning electron microscopy (SEM) [2] are widely used *in situ* monitoring methods. At one extreme, real-time microscopy of transient process in 100 fs, i.e., atomic-scale imaging during single phonon absorption or emission, is long-awaited, though it has not been realized yet. Alternatively, *in situ* observation by scanning tunneling microscopy (STM) during MBE has been achieved [3]. During STM imaging at the MBE growth temperature T, however, the object of interest changes frequently and spectroscopic characterization is still difficult. The energy resolution is inherently limited by the thermal fluctuation (k_BT = 68.9 meV at 800 K; k_B: Boltzmann constant). At present, time-depend-

ent topographic imaging of the geometric transition at the scanning time in units of seconds is possible. More rapid scanning or a complementary nanoprobing technique is demanded to approach the growth dynamics more directly.

Epitaxial growth consists of microscopic processes at the surface. Among these processes, adatom dynamics is quite typical. According to *ab initio*-based theoretical calculations, substrate temperature shows limited contribution to adatom dynamics from the entropy and the statistics of kinetic energies [4, 5]. This means that higher temperature stimulates thermodynamic events more frequently, but the temperature does not change the elemental microscopic processes of events. This is consistent with previous STM experiments in an ultra-high vacuum (UHV) at the room temperature. It has been well confirmed that such non-real-time topographic STM characterizations still catch rich traces of thermodynamic events expected during MBE growth [6 - 8]. It is possible to further take advantage of this feature of UHV-STM by performing characterization at lower cryogenic temperature.

In this talk, adatom dynamics at the surface of InAs, one of the most important narrow-gap semiconductors, is discussed on the basis of low-temperature STM (LT-STM) observation of as-grown (111)A surface by MBE. LT-STM characterization is a promising complement to *in situ* STM observation during MBE. At the cryogenic temperature, the thermal fluctuation effect is markedly weakened and energy resolution becomes very high ($k_BT = 0.43$ meV at 5 K). Such high resolution allows us to interpret thermodynamic phenomena from the viewpoint of quantum mechanics. Since atomic structures have very long lifetimes at the cryogenic temperature, stable spectroscopy is possible repeatedly. For the interpretation of the desorption event, knowledge obtained by an atom manipulation at the compound semiconductor surfaces [9, 10] was applied. The desorption (detachment by phonon excitation) is regarded as an adatom 'pick-up' event (detachment by electron excitation). This scheme replaces the spontaneous and incontrollable phonon process with an intentional and controllable electron process. Using STM, we can easily control both the excitation energy and the frequency by the bias voltage and the magnitude of the tunneling current. Phonon frequency of 10 THz, for example, is regarded to be the inelastic excitation period of 100 fs. Electron injection by tunneling at the period of 100 fs corresponds to the tunneling current 10^{13} electrons/s = 1.6×10^{-6} A. If there is an inelastic event, it is immediately detected *in situ* by the tunneling current measurement at picometer spatial resolution. The desorption dynamics of cation adatoms was modeled in the context of the transition state theory. The model is based on the rate equation for the adatom charge state determined by the ratio of the electron lifetime in the adatom resonance state to the electron excitation period of the phonon-assisted inelastic tunneling. The predicted desorption temperature range excellently agreed with the reported one [11]. Thus, the equivalence of excitation sources is verified [12]. This equivalence allows us to make a giant leap in our understanding of epitaxial growth mechanism. It is suggested that adatom density at the MBE growth temperature is almost equal to that measured at 5 K and that the electron accumulation layer is maintained as it is induced by the MBE growth. Adatom desorption dynamics is found to be correlated to the surface electron accumulation. These results demonstrate that the LT-STM experiment is an excellent method for exploring individual quantum mechanical dynamic processes expected during the epitaxy.

References

1. J. H. Neave, P. J. Dobson, B. A. Joyce, and Jing Zhang, Appl. Phys. Lett. **47**, 100 (1985).
2. K. Yamada, N. Inoue, J. Osaka, and K. Wada, Appl. Phys. Lett. **55**, 622 (1989).
3. S. Tsukamoto and N. Koguchi, J. Crystal Growth **201-202**, 118 (1999).
4. N. Ishimure, T. Akiyama, K. Nakamura, and T. Ito, Physica E **42**, 2731 (2010).
5. K. Reuter and M. Scheffler, Phys. Rev. B **65**, 035406 (2001); **75**, 049901(E) (2007).
6. M. Tanimoto, J. Osaka, T. Takigami, S. Hirono, and K. Kanisawa, Ultramicroscopy **42-44**, 1275 (1992).
7. M. D. Johnson, K. T. Leung, A. Birch, B. G. Orr, and J. Tersoff, Surf. Sci. **350**, 254 (1996).
8. K. Kanisawa and H. Yamaguchi, Phys. Rev. B **56**, 12080 (1997).
9. S. Fölsch, J. Yang, Chr. Nacci, and K. Kanisawa, Phys. Rev. Lett. **103**, 096104 (2009).
10. K. Suzuki, S. Fölsch, and K. Kanisawa, Appl. Phys. Express **4**, 085002 (2011).
11. J. Zhang, E. M. Gibson, C. T. Foxon, and B. A. Joyce, J. Crystal Growth **111**, 93 (1991).
12. K. Kanisawa, J. Crystal Growth (2013). (in press)

17:00 Invited oral

In-situ monitoring of molecular-beam epitaxial growth of zero-, one-, and two-dimensional structures using synchrotron X-ray diffraction

Masamitu Takahasi

Japan Atomic Energy Agency (JAEA), 1-1-1 Kouto, Sayo-cho,Sayo-gun, Hyogo 679-5148, Japan University of Hyogo, Graduate School of Material Science, Kohto, Kamigori, Hyogo 678-1297, Japan

e-mail: mtaka@spring8.or.jp

The high controllability of molecular-beam epitaxy (MBE) for the growth of nanostructures relies on the use of a monitoring technique, which is reflection-high energy electron diffraction (RHEED) in a typical MBE system. Even sub-monolayer control of the thickness of quantum well structures is achievable using the RHEED oscillation. However, as the semiconductor nanostructures are diversified into lower-dimensional structures including quantum wires and dots, more sophisticated monitoring techniques has become required for full characterization of the nanostructures beyond the thickness of two-dimensional layered structures. In this work, we present in situ X-ray diffraction techniques enabling growth monitoring of a wide variety of low-dimensional structures. Our experiments were performed using a molecular-beam epitaxy (MBE) chamber integrated with an X-ray difftactometer at a synchrotron beamline, 11XU, at SPring-8 [1].

Among all the semiconductor nanostructures, quantum wells are playing the most important roles in technological applications today. Recently, considerable efforts have been devoted to the growth of relaxed layers with a small dislocation density in the aim of strained channel field effect transistors and multi-junction solar cells. In situ X-ray diffraction is suitable for monitoring the development of dislocations and residual strains because of its high angular resolution. Results of high-speed three-dimensional X-ray reciprocal space mapping during the growth of InGaAs on GaAs(001) will be presented [2,3]. Because of their extremely anisotropic shape, quantum wires are interesting from the viewpoints of crystal growth phenomena as well as the quantum effects in electronic structures. A remarkable phenomenon observed in III-V semiconductor nanowires is polytypism. The evolution of the crystal structure of semiconductor nanowires during growth has been investigated by in situ X-ray diffraction [4].

Finally, the growth of quantum dots, which are the ultimate quantum structure, has been investigated using in situ X-ray diffraction at different growth temperatures. The evolution of lateral and vertical size of self-assembled InAs/GaAs(001) quantum dots was determined

during growth. It was found that there was a good correlation between the structural and optical properties determined by in situ X-ray diffraction and post-growth photoluminescence spectroscopy, respectively [5].

[1] M. Takahasi, Y. Yoneda, H. Inoue, N. Yamamoto and J. Mizuki, Jpn. J. Appl. Phys. 41, 6247 (2002).

[2] H. Suzuki, T. Sasaki, A. Sai, Y. Ohshita, I. Kamiya, M. Yamaguchi, M. Takahasi and S. Fujikawa, Appl. Phys. Lett. 97, 041906 (2010).

[3] W. Hu, H. Suzuki, T. Sasaki, M. Kozu and M. Takahasi, J. Appl. Cryst. 45, 1046 (2012).

[4] W. Hu, M. Takahasi, M. Kozu and Y. Nakata, J. Phys.: Conf. Ser. 425, 202010 (2013).

[5] M. Takahasi and T. Kaizu, J. Crystal Growth 311, 1761 (2009).

17:30 Oral

3-dimensional InAs island growth on GaAs(001) at 500 °C observed by STMBE system

Takashi Toujyou, Teruki Teraoka, Shiro Tsukamoto

Anan National College of Technology, Anan 774-0017, Japan

e-mail: toujyou@anan-nct.ac.jp

Quantum dots (QDs) are unique nano structures that have received special attentions in recent years because these are strong candidates for advanced semiconductor quantum devices. From recently reports, 3-dimensional (3D) islands (between InAs QDs and 1ML high InAs 2-dimensional (2D) islands) were formed during the QD formation [1, 2]. But, the precise mechanism for forming the 3D islands was not well understood yet. In this report, we observed the InAs 3D islands grown by the STMBE system [3] which equipped with a scanning tunneling microscope (STM) inside a molecular beam epitaxy (MBE) growth chamber, performing true in situ imaging during the MBE growth [4].

An experimental procedure is as follows. We used undoped-GaAs(001) just substrates. After forming a GaAs buffer layer at 580 °C, a substrate temperature was decreased from 580 °C to 500 °C under an As_4 irradiation. When the substrate temperature was stabilized, we started in situ STM observation with the As_4 irradiation (a tip bias was -1.0 V, a tunneling current was 0.6 nA, and a scan speed was 6000 nm•s^{-1}). A tip scanned from left to right and moved from bottom to top of the image. Fig.1(a) show a STM image of GaAs buffer layer before supplying In and Fig.1(b) shows a line profile indicated as a white line. During the observation, we grow 2.6 ML InAs (growth rate was 2.8×10^{-3} MLs^{-1}). Fig.2(a) show a STM image of InAs WL during In supply and Fig.2(b) shows a line profile indicated as a white line. The amount of the InAs supply at the bottom of Fig.2(a) was 0.18 ML and that of its upper part was 1.27 ML. As the amount of the InAs increased, the number and volume of the InAs 2D island gradually increased. Moreover, a InAs 3D island (height: 0.4 nm, widhth: 20 nm) on the 2D island shown in Fig.2(b). InAs 3D islands appeared from the early stage of InAs supply (0.18 ML ~). The density of the 3D islands was same extent regardless of the amount of the InAs supply shown as Fig.3.

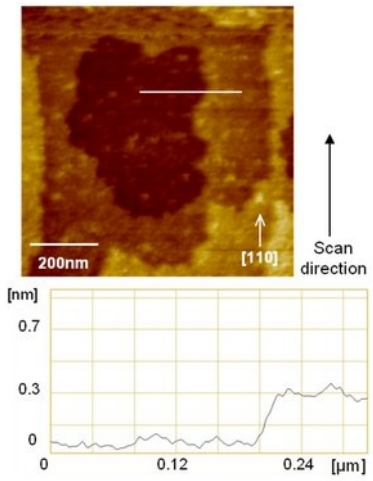

Fig.1 STM image and line profile. (a) STM image of before InAs supply, (b) line profile indicated as a white line.

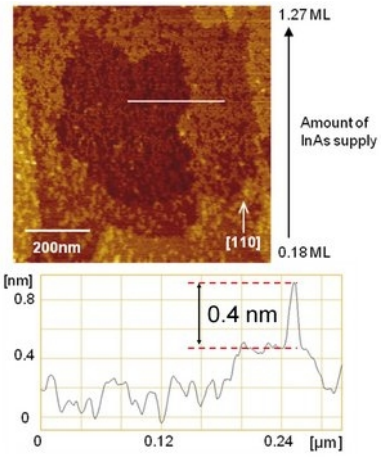

Fig.2 STM image and line profile. (a) STM image of during InAs supply, (b) line profile indicated as a white line.

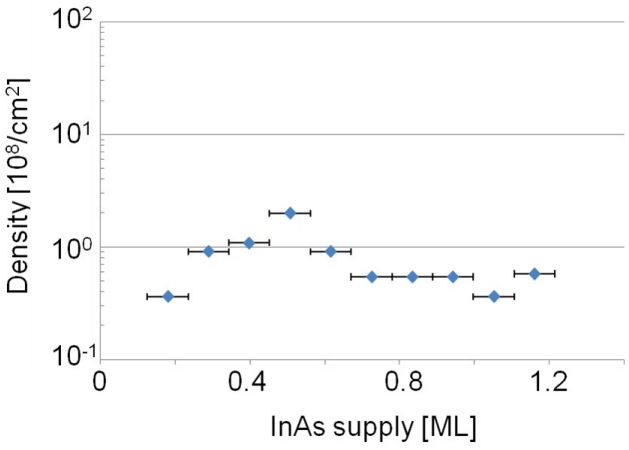

Fig.3 Densities of InAs 3D islands on GaAs(001) as a function of InAs supply.

[1] D.Tex and I.Kamiya, Phys. Rev. B. 83, 081309 (2011).
[2] T.R.Ramachandran, R.Heitz, P.Chen and A.Madhukar, Appl. Phys. Lett. 70, 640 (1997).
[3] S.Tsukamoto and N.Koguchi, J. Cryst. Growth 201/202, 118 (1999).
[4] S.Tsukamoto, T.Honma, G.R.Bell, A.Ishii, and Y.Arakawa, Small 2, 368(2006).

Break
Thursday evening, 15 August, 18:30

Posters

Wednesday, 14 August

WeP-G06
Wednesday afternoon, 14 August, 16:00
Room 211, Old Library

16:00 Poster We179

In-situ observation of faceted growth of benzophenone single crystals from melt

Veerabagu Natarajan[1], Mukannan Arivanandhan[2], Yuko Inatomi[3], Yasuhiro Hayakawa[2]

1. *Department of Physics, Aditanar College of Arts and Science,, Tiruchendur 628216, India* **2.** *Research Institute of Electronics, Shizuoka University, Johoku 3-5-1, Naka-Ku,, Hamamatsu 432-8011, Japan* **3.** *Institute of Space and Astronautical Science, Japan Aerospace Exploration Agency, 3-1-1 Yoshinodai, Sagamihara, Kanagawa, Fujisawa, Kanagawa 229-8510, Japan*

e-mail: arivucz@gmail.com

Understanding of crystal growth process is important not only for the fundamental science but also for the industrial crystallization. Many factors associated with structure of a crystal such as temperature gradient, cooling rates of a crystal influence in controlling the growth process. Therefore, it is indispensable to understand the primary growth process taking place during crystallization from solution and/or melt. The growth process at an initial stage of growth can be understood by in-situ observation of the growing crystal and the solid-liquid interfaces. In order to understand the growth process of benzophenone in detail, melt growth of benzophenone was in-situ observed under various cooling rate and temperature gradient. Growth rate and the profile of temperature in the vicinity of solid-liquid interface were investigated. The movement of growth interface with time was measured for various growth faces such as (001), (101) and (011) and the growth rates of the respective faces were calculated. It was found that the growth rate of all the faces increased with cooling rate. Steady state growth was observed in the experiments with low temperature gradient while the steep gradient leads to unstable growth of crystal. The observed growth rate variation was explained using the PBC and attachment energy models.

16:00 Poster We180

In situ diagnostics of SiC nanostructures growth process

Agnieszka M. Dąbrowska

Warsaw University, Department of Chemistry, Pasteura 1, Warsaw 02-093, Poland

e-mail: aggy-dab@wp.pl

Combustion synthesis (SHS, Self-sustainable High-temperature Synthesis), carried out in a modified calorimetric bomb, is a fast, efficient, self-sustainable, and one-step production method of new nanomaterials. Among them, SiC nanowires are one of the most interesting due to their properties and a variety of possible applications. However, as the growth process occurs probably partially under non-equilibrium conditions, its control and monitoring is rather difficult. Furthermore, the synthesis is very sensitive to any change of process variables, so that the growth mechanism knowledge is essential for the optimization of the synthesis. To overcome those drawbacks, the in-situ diagnostics of combustion is proposed. It is based on the photo registration of an optical signal (light emitted and observed via polycarbonate observation port). From full HD 25 frames per second with resolution 1920x1080, one may calculate the relative signal intensity, its time evolution and find the reaction fingerprint. The validation of experimental protocol consisted in confirmation of results reproducibility, crucial in case of nonlinear process, within different calculation alghoritms and registration conditions.

Acknowledgement. This work was supported by NCN through grant No. UMO-2011/03/B/ST5/03256.

16:00 Poster We181

Epitaxy during oriented nucleation of gold and other biomineral crystals at organic templates: in situ X-ray studies

Ahmet Uysal, Benjamin Stripe, Pulak Dutta

Northwestern University, Dept. of Physics and Astronomy, 2145 Sheridan Road, Evanston, Illinois 60208, United States

e-mail: pdutta@northwestern.edu

There has been considerable debate regarding whether epitaxy plays a major role in the oriented nucleation of biomineral crystals (with molecular surfaces as the proposed templates). The only direct way to settle this matter is to observe the organic and inorganic interfacial structures in situ during the process of nucleation, using a structural probe such as X-ray scattering. This has not yet been done in vivo, but we have studied biomimetic nucleation using molecular monolayers (Langmuir films) floating on aqueous solutions. Reversing the more familiar process of thiol monolayer self-assembly on gold (111) surfaces, we have used floating thiol monolayers to grow (111)–oriented gold nanocrystals. Calcium carbonate---a more common biomineral---will not grow oriented crystals under pure acid-terminated monolayers, but it will do so when the monolayers are mixtures of anionic and cationic molecules. Whether this is a result of charge balance, epitaxy or stereochemistry (e.g. molecular tilt) is revealed by the X-ray data. Our results illustrate the importance of in situ scattering studies that look at organic and inorganic structures simultaneously, and they show how soft (compliant) molecular templates are particularly effective at nucleating oriented crystals.

16:00 Poster We182

Method for determining chemical vapor deposition occurrence using langasite crystal microbalance

Hitoshi Habuka, Misako Matsui, Ayumi Saito

Yokohama National University (YNU), 79-5 Tokiwadai Hodogaya, Yokohama 240-8501, Japan

e-mail: habuka1@ynu.ac.jp

In order to develop the method determining the existence of surface chemical reactions, the frequency behaviour of the langasite crystal microbalance (LCM) set in a chemical vapour deposition (CVD) reactor was studied, in detail. The parameter, $C(T)$, of the equation for expressing the LCM frequency change, (: gas density, : gas viscosity), was evaluated. In a hydrogen-monomethylsilane system, the LCM frequency

very gradually increased after the monomethylsilane gas introduction above 500 ^{o}C, although that at lower temperatures was maintained flat. The difference of $C(T)$ values in monomethylsilane-hydrogen system from those in nitrogen-hydrogen system increased above 500 ^{o}C. Thus, the silicon carbide film deposition from monomethylsilane gas was determined to begin near 500 ^{o}C.

1. Introduction

Chemical vapour deposition (CVD) is the key technology [1] for producing various useful thin and thick films. When a new film deposition process is designed and developed, particularly employing new combinations between precursors, reactors and process conditions, the information on the occurrence of surface chemical reactions is often useful by some reasons.

For surveying the parameters producing significantly thin films, nanometre-thick or monolayer-thick, the critical temperature to initiate the surface chemical reaction can be key information. The success of the thin film formation can be validated typically by the transmission electron microscope (TEM), deposition by deposition [2]. However, because this technique is often expensive, an alternative low cost and easy method should be developed.

The temperature to initiate the surface chemical reaction is useful information, for designing and maintaining the practical thermal condition of the cold wall reactor. In a cold wall system, the substrate is very often heated using the infrared lamps from the outside of the transparent quartz vessel. When the film deposition occurs at the reactor wall, the formed film significantly absorbs the infrared light to increase the quartz wall temperature; the cold wall thermal environment cannot be maintained. Additionally, the film formed at the reactor inner wall often emits small particles to cause hillocks and various defects on the CVD film surface. Thus, in order to avoid these troubles, the reactor wall temperature must be maintained below the acceptable highest temperature, that is, the critical temperature, at which the surface chemical reactions by the precursors are completely suppressed.

The expected solution for detecting the surface chemical reaction occurrence is the *in-situ* monitoring technique using the langasite crystal microbalance (LCM) [2-4], because the LCM has a potential for sensitively working at low and high temperatures in various inactive and reactive gas ambient atmosphere. As shown in our previous studies [2, 4], the LCM has the potential to detect the various small changes in the heat and flow conditions in a reactor, caused by the nanometre-thick film deposition. In our extended study [5], parameters of the equation [6, 7] were optimized so that the LCM frequency behaviour could be simply expressed using the gas properties in an ambient of gas mixture of hydrogen and nitrogen. Next to be performed is the development of the systematic method which can detect significantly small change caused by the surface chemical reaction from the LCM behaviour in very wide ranges of the CVD conditions.

In this study for determining the surface chemical reaction occurrence, the LCM frequency behaviour was evaluated using gases, such as nitrogen and monomethylsilane in ambient hydrogen, over wide ranges of temperature and gas concentrations. The difference of the LCM frequency behaviours between the ambient containing nitrogen gas and monomethylsilane gas and that between the high and low temperatures was studied in detail.

2. Experimental procedure and equation

The horizontal cold wall reactor containing the LCM, shown in Fig. 1, was used. This reactor consists of a gas supply system, a quartz chamber and infrared lamps. The gas supply system can introduce hydrogen, nitrogen and monomethylsilane gases. Hydrogen is the carrier gas. The gas flow channel of this reactor has a low height and a small rectangular cross section in order to achieve a high consumption efficiency of the reactive gases. The height and the width of the quartz chamber were 10 mm and 40 mm, respectively, similar to those used in our previous studies [2, 4, 5, 8-12].

A 30-mm-wide x 40-mm-long (100) silicon wafer manufactured by the Czochralski method was horizontally placed on the bottom wall of the quartz chamber. The LCM (Halloran Electronics, Tokyo, Japan) was placed 5 mm above the silicon wafer and was connected to a personal computer in order to record its frequency.

The LCM has an intrinsic frequency of 10 MHz similar to our previous studies [2, 4, 5]. The silicon wafer and the LCM were simultaneously heated by infrared light from halogen lamps through the quartz chamber. The LCM was heated not only by the infrared light, but also by radiation heat and conduction heat from the hot silicon wafer. The temperature of the silicon wafer was measured prior to the CVD process using thermocouples. Because the position of the LCM was very near the silicon wafer, the temperature of the LCM was assumed to be the same as that of the silicon wafer.

A typical process used in this study is shown in Fig. 2. First, the LCM was heated to 300 - 600 ^{o}C in ambient hydrogen at atmospheric pressure. After waiting until the LCM frequency became stable, the nitrogen gas and monomethylsilane gas were introduced at atmospheric pressure into the reactor chamber. The flow rates of the nitrogen gas and monomethylsilane gas were 0 – 1.0 slm and 0.05 - 0.3 slm, respectively. The total gas flow rate was adjusted to 1 slm.

In the previous studies [5, 6], the parameters of equation for expressing the LCM frequency change using the fluid properties were optimized to linearly express the LCM frequency difference of the gas mixture from the ambient hydrogen, as

$$\Delta f_{gas} = -C(T) \rho_{Mix}^{\ y} \eta_{Mix}^{\ y}. \quad (1)$$

$$C(T) = A\, e^{(-B/T)}. \quad (2)$$

where the y and z values were 1.3 and 1.3, respectively.

The $C(T)$ value was expressed in a form of Arrhenius type equation, as Eq. (2), when any chemical reaction did not occur. Any chemical reactions for the film formation are expected to sensitively influence the $C(T)$ value.

3. Results and discussion

3.1 LCM frequency

First, the LCM frequency behaviours at various conditions were measured and evaluated in the monomethylsilane-hydrogen system. In order to recognize the entire behaviour of the LCM frequency, the LCM frequency differences from hydrogen ambient at 300 - 600 ^{o}C was shown in Fig. 3.

Immediately after opening the gas valve at 0 s for the monomethylsilane gas supply, the monomethylsilane gas at high concentration was introduced into the reactor, because the monomethylsilane gas at 100 % remained between the gas valve and the mass flow controller came to the reactor. During the high concentration gas passing through the reactor, the LCM frequency significantly decreased. After this, the monomethylsilane gas, which concentration was adjusted to the set value, reached the LCM in the reactor. Thus, the fluctuation of the LCM frequency became small.

As shown in Fig. 3, the LCM frequency difference measured at 300 ^{o}C was very stable after 20 s. This indicated that the gas temperature and the fluid properties, such as gas density and gas viscosity, were in a steady state. This simultaneously indicated that there was no chemical reaction at 300 ^{o}C, because of no thermal change caused by no reaction heat. The behaviour at 400 and 500 ^{o}C was similar to that at 300 ^{o}C. The trend of LCM frequency difference at 300, 400 and 500 ^{o}C was the same and parallel to each other. Thus, the monomethylsil-

ane-hydrogen system below 500 ^{o}C is concluded to have no chemical reaction.

Although the LCM frequency difference at 550 ^{o}C seemed to be relatively stable, it very gradually increased after 20 s. Similar to this, the LCM frequency difference at 600 ^{o}C also slightly increased with the larger gradient than that at 550 ^{o}C. This gradual increase in the LCM frequency difference indicated that any transient change relating to chemical reaction, such as temperature, gas density and gas viscosity, occurred and continued in the reactor during the introduction of monomethylsilane gas.

As reported in our previous study [8] and as shown in Fig. 3, the LCM frequency increased with the decreasing temperature. Additionally, the surface chemical reaction for silicon carbide film deposition from monomethylsilane gas is endothermic [8]. The frequency decrease due to the weight increase by the film deposition was overcompensated by the frequency increase due to the temperature decrease by the endothermic reaction. Thus, the LCM frequency could continue to increase till reaching the steady state. From Fig. 3, the chemical reaction occurring at the LCM surface is considered to continue after 200 s.

The temperature change should be enhanced by the increasing reaction rate, because of the greater reaction heat. In order to clearly show this trend, the LCM frequency gradient at various temperatures in the monomethylsilane-hydrogen system was evaluated, as shown in Fig. 4. As shown in this figure, the LCM frequency gradient in the low temperature range between 300 – 500 ^{o}C was less than zero Hz/s. This value should be recognized to show the state with no chemical reaction. In contrast, the LCM frequency gradient increased at 550 ^{o}C from the value less than zero to the positive value of 2 Hz/s. It further increased to the value higher than 4 Hz/s at 600 ^{o}C. Because the LCM frequency gradient increased with the increasing temperature, the surface chemical reaction at the LCM surface was initiated in the temperature range between 500 and 600 ^{o}C.

3.2 $C(T)$ Parameter

In the previous section, the chemical reaction occurrence could be determined using the LCM frequency difference from that measured in the ambient having no reactive gases. However, the LCM frequency is significantly sensitive to the fluctuation of various parameters. Thus, in this section, a systematic method to find the occurrence of the surface chemical reaction is studied.

Because the chemical reaction induces various changes, such as the temperature, gas composition and fluid properties influencing the LCM frequency, the relationship of Eq. (1) between the LCM frequency and the gas properties is evaluated.

Fig. 5 shows the LCM frequency change with the increase in of the gas mixture of monomethylsilane, nitrogen and hydrogen at 400, 500 and 600 ^{o}C. In this figure, the frequency differences of nitrogen-hydrogen system (white circles) follows the Eq. (1), shown as a linear relationship. The monomethylsilane-hydrogen system (triangles) at 400 and 500 ^{o}C coincided with the behavior of nitrogen-hydrogen system. In contrast to this, the monomethylsilane-hydrogen system showed a slightly large gradient in the region of small value. Thus, the $C(T)$ value of Eq. (1) is expected to indicate the surface chemical reaction occurrence.

The $C(T)$ values obtained using Eq. (1) are plotted against $1/T$. as shown in Fig. 6. This figure shows that the $C(T)$ values for nitrogen-hydrogen system entirely have a linear relationship following Eq. (2), at the temperatures from 300 to 600 ^{o}C. In contrast, the monomethylsilane-hydrogen system shows the increase of the $C(T)$ value at the higher temperatures.

In order to clearly understand the behavior difference of the C(T) values between monomethylsilane and nitrogen, the $C(T)$ value difference of monomethylsilane-hydrogen system from nitrogen-hydrogen system are shown in Fig. 7. As shown in this figure, the $C(T)$ value difference at the temperatures lower than 500 ^{o}C were around zero. This concludes the monomethylsilane gas at less than 500 ^{o}C was the same as that of nitrogen which had no chemical reaction. The monomethylsilane-hydrogen system showed the $C(T)$ value increase to higher than 1×10^{10} at the temperatures between 500 and 550 ^{o}C. Because these values were obtained being separated from the fluid properties, the $C(T)$ value change could be understood as the additional phenomena occurring at the higher temperatures, such as the surface chemical reaction for the film deposition.

As reported in our previous study [2] using the LCM and TEM, the nanometre-thick silicon carbide film could be formed at 600 ^{o}C from monomethylsilane gas. Taking into account that the film deposition rate significantly decreases with the 100 K decrease of the substrate temperature [14], the silicon carbide film produced around 500 ^{o}C is expected to be less than nanometre- or angstrom-thick. Thus, the temperatures near 500 ^{o}C can be the critical temperature for the silicon carbide film deposition from monomethylsilane gas.

4. Conclusions

In order to develop the method to determining the occurrence of the surface chemical reaction for the chemical vapour deposition, the LCM frequency behaviour was studied in detail. The LCM frequency immediately after the introduction of the monomethylsilane gas gradually increased at the temperature higher than 500 ^{o}C. The gradient of the LCM frequency increased with the temperature higher than this temperature. Simultaneously, the parameter, $C(T)$, to describe the LCM frequency difference in the monomethylsilane-hydrogen system consistently showed a discontinuity between the temperatures above and below 500 ^{o}C. Additionally, the prediction of nanometre- or angstrom-thick film deposition by the TEM, previously obtained, was consistent with this result. Thus, the method developed in this study is expected to determine the critical temperature of the surface chemical reaction for the chemical vapour deposition.

Acknowledgement

The authors would like to thank Mr. Nobuyoshi Enomoto of Halloran Electronics Co., Ltd., for his technical support.

References

[1] S. M. Sze, Semiconductor devices: physics and technology. (2008) John-Wiley, Hoboken, NJ, USA.

[2] H. Habuka and Y. Tanaka, J. Surf. Eng. Mater. Adv. Tech., 3 (2013) 61-66.

[3] M. Schulz, J. Sauerwald, H. Seh H. Fritze, H. L. Tuller, Solid State Ionics 184 (2011) 78-82.

[4] H. Habuka and Y. Tanaka, ECS J. Solid State Sci. Tech., 1 (2012), 62-65.

[5] H. Habuka and M. Matsui, EuroCVD19, (Varna, Bulgaria, 2013), accepted.

[6] K. K. Kanazawa and J. G. Gordon II, Anal. Chim. Acta, 175 (1985) 99-105

[7] G. Sauerbrey, Zeitschrift fur Physik, 155 (1959) 206-222.

[8] H. Habuka and K. Kote, Jpn. J. Appl. Phys. 50 (2011) 096505-1-4.

[9] H. Habuka H. Ohmori and Y. Ando, Surf. Coat. Tech., 204 (2010) 1432-1437.

[10] H. Habuka, and Y. Ando, J. Electrochem. Soc., 158 (2011) H352-H357.

[11] H. Habuka, M. Watanabe, Y. Miura, M. Nishida, T. Sekiguchi, J. Crystal Growth, 300 (2007) 374-381.

[12] H. Habuka, M. Watanabe, M. Nishida and T. Sekiguchi, Surf. Coat. Tech., 201 (2007) 8961-8965.

[13] H. Habuka, T. Nagoya, M. Mayusumi, M. Katayama, M. Shimada and K. Okuyama, *J. Crystal Growth*, 169 (1996) 61-72.

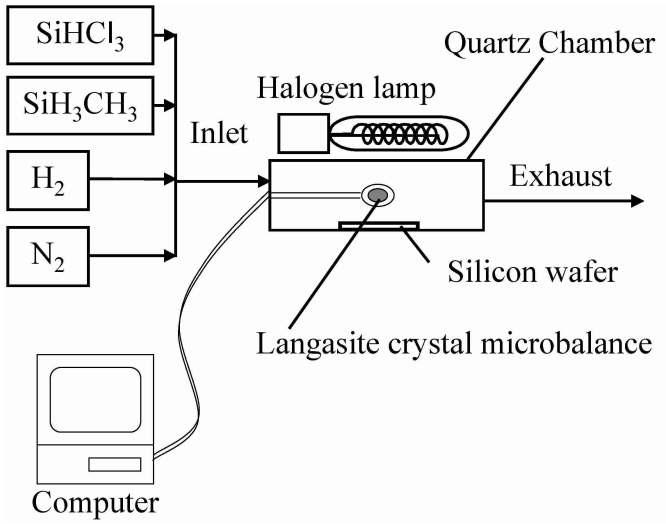

Figure 1 Cold wall chemical vapor deposition reactor containing the LCM system.

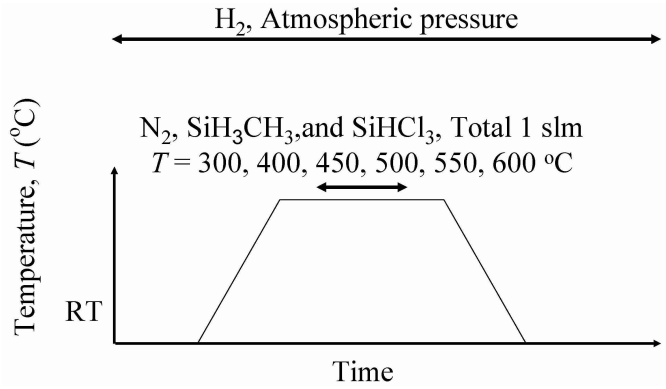

Figure 2 Process for measuring the LCM frequency using various gases.

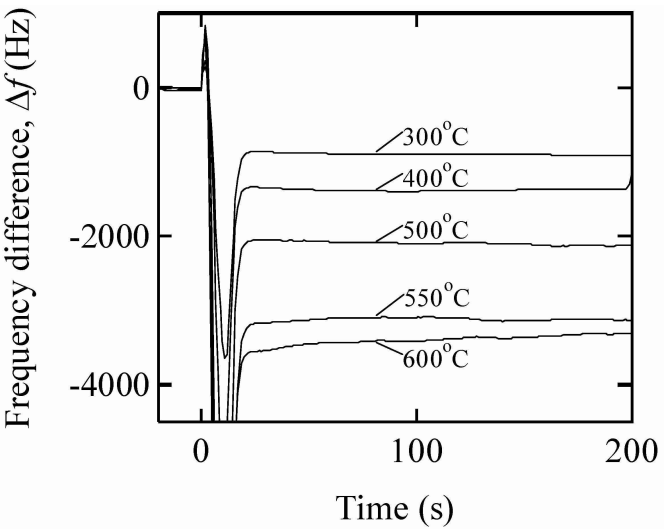

Figure 3 The LCM frequency change immediately after the introduction of monomethylsilane gas to hydrogen ambient atmosphere.

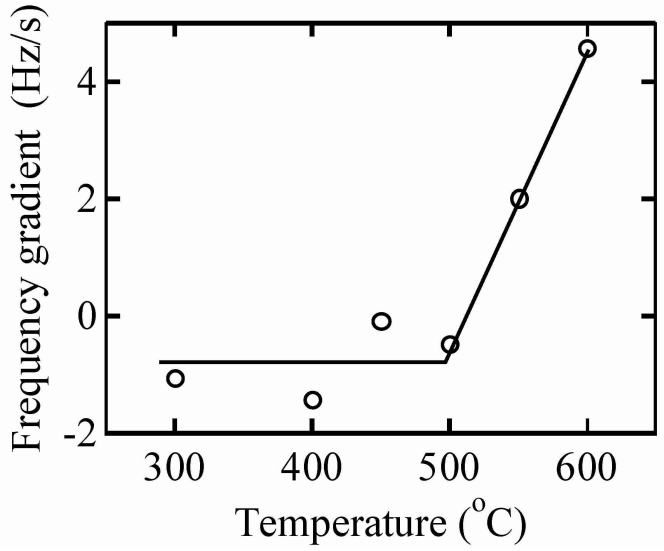

Figure 4 LCM frequency gradient immediately after introducing the monomethylsilane gas at various temperatures.

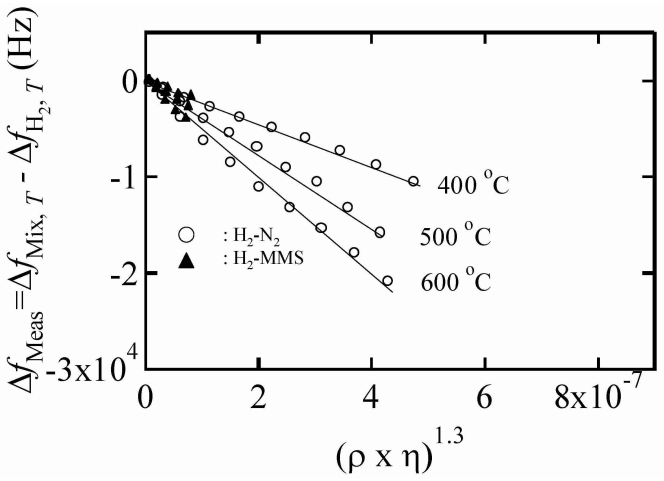

Figure 5 LCM frequency difference of monomethylsilane gas (dark triangle) and nitrogen gas (circle) from hydrogen ambient.

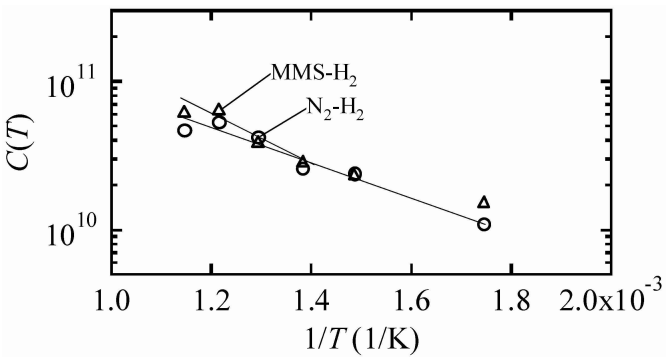

Figure 6 $C(T)$ values of monomethylsilane-hydrogen system (triangles) and nitrogen-hydrogen system (circles).

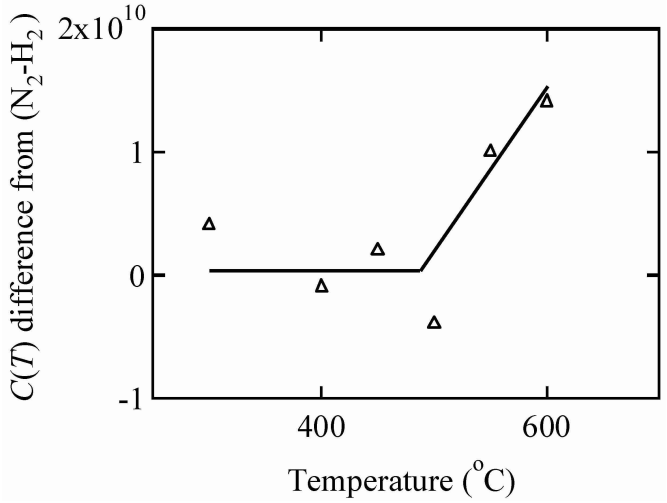

Figure 7 $C(T)$ value difference of monomethylsilane-hydrogen system from nitrogen-hydrogen system.

16:00 Poster We183

In-situ Observation of Melting and Crystallization of Si on Porous Si_3N_4 Substrate that Repels Si Melt

Hironori Itoh, Hideyuki Okamura, Kouhei Ikemura, Masaharu Nakayama, Ryuichi Komatsu

Yamaguchi University, 2-16-1 Tokiwadai, Ube 755-8611, Japan

e-mail: ito-hrnr@yamaguchi-u.ac.jp

Si is the most widely used material for solar cells but the cost of photovoltaic power generation is higher than other power generating systems. Many studies now under way seek to reduce the cost of Si solar cells. Some of these studies focus on spherical Si solar cells due to its conservation of Si material and reduction of Si consumption per unit electric power generation to less than 1/5 that of Si wafers because cutting of Si is not needed in the manufacturing process [1,2]. Spherical Si is currently produced by free-fall in a drop tower with very fast cooling of Si melt. Fabricated spherical Si crystals by this method are often composed of fine crystal grains due to high undercooling of Si melt that cause the reduction of the conversion efficiency of spherical Si solar cells [3]. To prevent this fine crystallization of spherical Si, the novel crystal growth technique that enables slow cooling of spherical Si melt is necessary. We have been successfully prepared the porous Si_3N_4 ceramic substrate that repels Si melt for the direct growth of spherical Si crystals on it [4]. This study describes in-situ observation of the melting and crystallization behavior of Si on the porous substrate. The clear observation of Si with high magnification under low oxygen partial pressure environment was achieved by using our originally developed in-situ observation furnace (Fig. 1).

The porous Si_3N_4 substrate was prepared by mixing and press-forming Si_3N_4, amorphous SiO_2, and PMMA spherical micro-particles (2-20 μm in diameter) at a weight ratio of 4:1:5. The molded object was degreased in air atmosphere at 873-1373 K, then fired in N_2 atmosphere at 1873 K. The porous structure in the substrate was formed during the degreasing process by thermal decomposition of mixed PMMA particles. Si material with 1 mg weight was placed on the substrate which is located between two tantalum heaters. High-purity Ar gas (G2 grade) was flowed in the furnace to prevent the oxidation of Si. Melting and crystallization behavior of Si on the substrate was observed horizontally using a long focal microscope (KEYENCE, VH-Z50L).

The Si melt became spherical shape with about 1 mm in diameter on the fabricated porous ceramic substrate and the measured contact angle between them was 160° at the maximum, which is the largest value ever reported for Si [5-7]. When spherical Si began to crystallize by slowly cooling the Si melt (Fig. 2), the line-shaped pattern was observed at the melt surface, which is considered to be the indication of low undercooling of Si melt (ΔT < 100 K) [8]. Then crystal growth advanced in one direction with about 14 seconds, so the growth rate is less than 0.1 mm/s. It was confirmed that the grown spherical Si crystals are composed of single grain or twin from the etching result of their cross section. Therefore, growth of high quality spherical Si crystals is stably possible with slow cooling condition on the porous substrate that repels Si melt.

This study is supported by Regional Innovation Cluster Program (Global Type) by Ministry of Education, Culture, Sports, Science and Technology; Yamaguchi Green Materials Cluster (2009-2013).

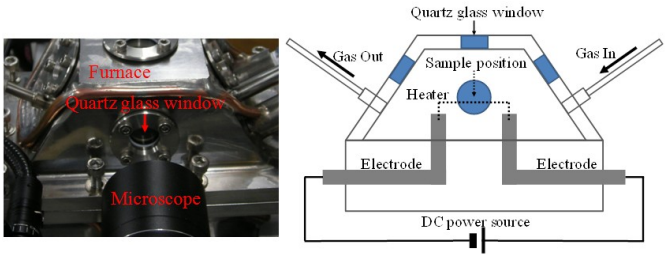

Figure 1. Developed high temperature in-situ observation furnace (left) and its schematic diagram (right).

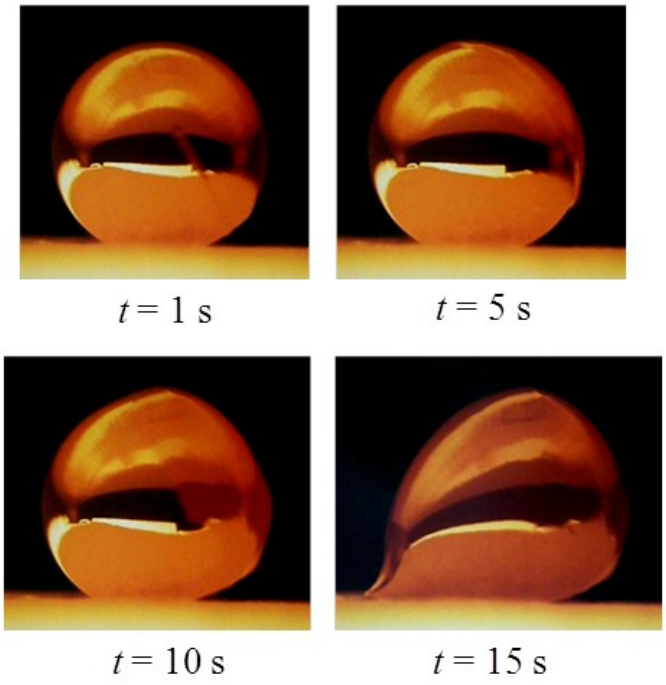

Figure 2. Crystal growth of spherical Si from low under cooling melt. Crystallization started at $t = 1$ s and finished at $t = 15$ s. A protuberance was formed at bottom left position due to volume expansion of Si accompanied by solidification.

References

[1] T. Minemoto *et al*., Jpn. J. Appl. Phys. 44 (2005) 4820-4824. [2] Z. Liu *et al*., Sol. Energy Mater. Sol. Cells 91 (2007) 1805-1810. [3] C. Okamoto *et al*., Jpn. J. Appl. Phys. 44 (2005) 7805-7808. [4] H. Itoh *et al*., J. Ceram. Soc. Jpn. (2013) in press. [5] K. Mukai and Z. Yuan, Mater. Trans. JIM 41(2) (2000) 338-345. [6] B. Drevet *et al*., J. Eur. Ceram. Soc. 29 (2009) 2363-2367. [7] I. Brynjulfsen *et al*., J.Cryst. Growth 312 (2010) 2404-2410. [8] K. Watanabe *et al*., J. Jpn. Soc. Microgravity Appl. 28(2) (2011) S64-S67.

16:00 Poster We184

The new approach to the weighing control of the CZ crystal growth

Pavel V. Kasimkin[1], Vitaly A. Moskovskih[1], Vladimir N. Shlegel[2], Yan V. Vasiliev[2], Vasiliy N. Zhdankov[3]

1. *Novosibirsk State Technical University (NSTU), K. Marx av., 20, Novosibirsk 630092, Russian Federation* **2.** *Institute of Inorganic Chemistry of RAS, Novosibirsk 630090, Russian Federation* **3.** *Crystal Manufacturing Lab (CML), Lavrentev 3, Novosibirsk 630090, Russian Federation*

e-mail: kaspavik@mail.ru

The crystal weighing technique of the automatic control of diameter in Czochralski growth process is widely used for years. Already in the one of the first publications on the method the certain troubles in application of it to control of diameter of semiconductor crystals were observed, and the cause of instability of control system for semiconductor materials was qualitatively explained [1]. If the melt is denser then material solid, then the apparent weight shows an anomalous time dependence and dependence of on crystal radius, which cause positive feedback in the servo-loop and lead to instability. The similar effect takes place if melts do not completely wet solid. The problem increases with decreasing pulling rate.

Later weighing signal behavior was investigated in many works. To overcome the problem it is necessary to provide a low noisy differentiation of weighing signal, to use effective algorithms of control object identification and to apply control units, which provide control actions both on the temperature and the pulling rate [2-6]. The recent example of sophisticated approach to the problem is the article series about nonlinear model-based control of the LEC Czochralski process [7].

Meanwhile a simple effective approach, free from problems with anomalous behavior, was realized for the melt-level technique of automatic Czochralski crystal growth [8]. For measuring a crystal diameter the stepped crystal pulling in combination with stepped feeding of raw material was performed. After rapid lifting the crystal holder at a small distance the melt level drop in the crucible was measured and fixed. From these two values and the crucible diameter a current diameter or more exactly cross-sectional area of crystal can be calculated. Then the feeding system restored the melt level to its initial value and the cycle was repeated. This approach can easily be extended to the case of weighing the crystal or the crucible of melt.

The essential development of the method presented in the report is the following. Under computer control small value periodical seesaw shifts are affecting the steady motion of the crystal holder. Buoyancy forces deviate as the crystal periodically moves across the melt level. Thus the weighting sensor generates buoyancy forces modulated signal. Neglecting the surface tension terms the growing crystal actual cross-sectional area is computed via the weighting modulated signal and the seesaw shifts of the crystal holder using the well-known formulas for buoyancy forces.

Automatic feeding of the raw material during crystal growth does not needed at this case. The magnitude of shift is established to be small enough and measuring cycle time to be short enough to prevent noticeable modulation of growth rate. It also should be noted measuring cycle time is much less than characteristic relaxation times of the processes that determine the dynamics of crystal growth. This is important factor in providing dynamical stability of the control system.

The method was checked on the growth of germanium crystal at low thermal gradients ~1 K/cm and at growth rate as low as 2 mm/h. It was found that the simple PI control law provides good system stability and dynamics.

The main advantage of weighing control with modulation of movement of the pulling rod is the possibility to provide good performance of diameter control of CZ growth process using simple control laws for materials with “anomalous” behavior of weight signal. That is correct for the wide range of crystallization rates and also for LEC CZ.

Another essential advantage is radical lowering of the requirements to zero drift of weighing cell. Besides effect of evaporation on the control system is eliminated with the method under consideration.

Corrections related to the effect of the meniscus on the results of measurement of the diameter of the crystal are discussed.

[1] W. Bardsley, G.W. Green, C.H. Holliday, D.T.J. Hurle. J. Cryst. Growth 16 (1972) 277.

[2] W. Bardsley, D.T.J. Hurle, G.C. Joyce. J. Cryst. Growth 40 (1977) 13.

[3] M. A. Gevelber, G. Stephanopoulos. J. Cr. Growth 84 (1987) 647

[4] G. Satunkin, A. Leonov. J. Cryst. Growth 102 (1990) 592.

[5] N.V. Abrosimov, V.N. Kurlov, S. N. Rossolenko. Prog. Cryst. Growth and Charact. of Materials 46 (2003) 1.

[6] G. Satunkin. Progress in Cryst. Growth and Charact. of Materials 56 (2010) 1.

[7] J. Winkler, M. Neubert, J. Rudolph. J. Cryst. Growth 312 (2010) 1005; ibid 312 (2010) 1019; M. Neubert, J. Rudolph. Ibid 360 (2012) 3.

[8] L.G. Eidelman, V.I. Goriletsky, V.G. Protsenko et al. J. Cryst. Growth, 128, (1993) 1059.

16:00 Poster We185

Electric Field and Temperature Introduced Dielectric Anomaly of [110]-oriented 65Pb($Mg_{1/3}Nb_{2/3}$)O_3-35$PbTiO_3$ (PMN-PT65/35)Single Crystal

Nengneng Luo[1], Qiang Li[1], Qingfeng Yan[1], Yiling Zhang[2], Zhiguo Xia[3], Xiangcheng Chu[2]

1. *Department of Chemistry, Tsinghua University, Beijing 100084, China* **2.** *State Key Laboratory of New Ceramics and Fine Processing, Tsinghua University, Beijing 100084, China* **3.** *School of Materials Science and Technology, China University of Geoscience, Beijing 100083, China*

e-mail: luonn1234@163.com

Electric field and temperature introduced dielectric permittivity of [110]-oriented 65Pb($Mg_{1/3}Nb_{2/3}$)O_3-35$PbTiO_3$ (PMN-PT65/35) single crystal near morphotropic phase boundary (MPB) was investigated by C-V curves and temperature dependent dielectric permittivity. Dielectric permittivity showed great dependence with DC bias field: when the applied DC bias field was below a threshold value, dielectric permittivity enhanced with elevated DC bias field and larger hysteresis was observed with higher DC field when it returned to the initial negative electric field, it attributed to the higher domain wall motion/switch ability at an intermediate electric field; when the applied DC bias field exceed the threshold value, dielectric permittivity first increased with an increasing DC bias field, then a decrease, forming a peak at the threshold field, due to the higher domain stability and field-introduced-phase transformation. Dielectric permittivity of poled single crystals was much lower than unpoled one at room temperature without DC bias field However, as temperature increased, dielectric permittivity of poled samples exhibited an abrupt enhancement at about 50^oC and reached much higher value than that of unpoled one, indicating a Rhombohedral-Orthohombic (R-O) phase transformation. The lower domain wall density and temperature introduced R-O phase transformation for poled samples might account for the temperature dependent dielectric anomaly.

16:00 Poster We186

Calculations of parameters of RHEED oscillations using different models of the scattering potential

Zbigniew Mitura

AGH University of Science and Technology, Faculty of Metals Eng. and Industrial Computer Sci., al. Mickiewicza 30, Kraków 30-059, Poland

e-mail: mitura@metal.agh.edu.pl

Nowadays, there is an interest in the growth of Ge nanolayers on different substrates (for example, on Ge, GaAs etc.) with the use of reflection high energy electron diffraction (RHEED) to monitor the preparation of samples. However, the interpretation of experimental runs of RHEED oscillations is still carried out mostly with the help of strongly simplified approaches which may cause some controversies.

In the current work RHEED oscillations and their parameters are computed for off-symmetry azimuths using dynamical diffraction theory. However, two substantially different models of the scattering potential are used. Calculations employing the realistic model are compared with calculations for the simple potential model. The realistic potential is defined with the help of sums of Gaussian functions determined for each atomic layer. On the other hand, in the simple model only two, volume-averaged, constants are taken into account to describe the potential (one value is set for the bulk, the other for the growing layer).

It is discussed that simplified approaches may be indeed helpful for describing basic features of RHEED oscillations. However, obtaining precise information on growing samples requires the use of realistic approaches.

16:00 Poster We187

Influence of mechanical deformations on morphology and kinetics of crystal growth in solution (AFM data)

Natalia N. Piskunova, Askhab M. Askhabov

Institute of Geology of RAS (IG), Pervomaiskaya st., Syktyvkar 167982, Russian Federation

e-mail: piskunova@geo.komisc.ru

Individuals growing or dissolving in real crystal-forming system are often exposed to the mechanical impact, the evidence of which is scratches and cracks, or rather defects initiated by them and the follow-up "healing" in the form of regeneration surfaces and anatomic peculiarities of the structure detected by a researcher. With the appearance of new methods it became possible to experimentally model similar processes and to observe in detail a growing crystal responding to the impact on its surface.

The purpose of the present work was to do an atomic-force microscopy (AFM) study of the evolution of a growing or dissolving crystal in the area of an intentional scratch on its surface. Dioxydine crystals (hydroxymethylquinoxalindioxyde, $C_{10}H_{10}N_2O_4$) served us as model objects.

In the contact mode, the AFM probe presses on a surface with the force of 10^{-9}N. In the operating mode, with the feedback regime on, this force of interaction is maintained stable and the needle-probe physically does not get in touch with the surface. When the scanning is off and the feedback is disconnected, the probe, nevertheless, can be moved intentionally over the surface for the purpose of mechanical impact, in particular, on high steps on its way. In this case, even short-term impact of this kind is capable to initiate, besides a visible scratch, an intense area round it. The influence of such contact has important crystal-genetic (morphological and kinetic) consequences and is perceptible even after a long time.

This way, in one of the experiments on a crystal surface in an undersaturated solution, we drew the letter "O" with the probe moving it counter-clockwise. Almost two hours of observations showed an intensive dissolution of the surface in the area of the scratch, which affects very little the surrounding surface.

Statistical calculations show that to the mid of the experiment there occurred enlargement of dissolving steps, and then they began to split into more thin ones. The average roughness of the surface changes non-monotonously, generally increasing by the end of the experiment end. We have discovered anisotropy of dissolution rates, connected with one of the axes of the second order, along which the pits are eventually extended.

The next experiment was carried out in conditions of crystals growth. We observed the process of regeneration of the surface damaged as a result of mechanical impact.

By means of AFM probe, two parallel furrows, each 5 mkm in length and 1 mkm in width, were drawn on two sides of the screw dislocation hillock from its top on face (100). The growth steps of the given hillock have height about 8Å that corresponds to the parameter *a* of an elementary cell. The AFM-images show how quickly the disturbed parts are healed on both sides (*the numbers indicate a picture serial number in the experiment, time interval between consecutive pictures of 4.5 min.*).

The healing rate of steps composing a scratch reaches 1.7 nm/sec, whereas the surrounding steps continue to grow with a very small rate from 0.1 to 0.6 nm/sec. Earlier [1] it was noted that for macroscale the mechanical impact on the surface, for example, pricking, increases the growth rate of faces more than twice. It was explained by the occurrence of more powerful centers of growth on the face. In this case, no new centers of growth are formed. Probably, it is energy factors that are responsible for the kinetic consequences at nano-level.

Observations show that the morphological structure of similar hillocks of growth on dioxydine is rather stable. Even after two or three hours of growth they retain their original outlines, having somewhat increased or reduced the number of steps. It was especially unexpected that after the impact, the growth rate of steps, even on those parts of surface which had no direct impact, experiences great fluctuation. This results in the loss of morphological stability: by the 45th minute, the steps to the right of the top lose the initial strict order in their position and alignment, and large curves were formed. The hillock top becomes more and more flat and asymmetrical. The steps going out from its center grow with the rate of 1.3 nm/sec in the beginning, and decrease their rate to 0.4 nm/sec by the end of the observation. This, probably, is connected with approaching an equilibrium state. At the same time, we observe the phenomenon of simultaneous growth and dissolution at the neighbouring steps, which is difficult to explain. Thus, after the 50th minute, some areas on the hillock top grow at a rate of 0.9 nm/sec, and the neighbouring ones are noticably dissolved at a rate reaching 2 nm/sec.

The investigation was carried out with the financial support of the Programs of the Russian Academy of Sciences, 12-U-5-1026, 12-P-5-1027, 12-P-5-1011, Scientific School 1310.2012.5, RFBR 11-05-00432a.

1. Askhabov A.M. Influence of mechanical deformations on crystals growth // Proceedings of the Institute of Geology, Komi Branch, USSR Acad. Sci. Issue 21. Syktyvkar. 1975. P. 3-11.

16:00 Poster We188

Morphology of the synthetic diamonds: dissolution on the defects

Natalia N. Piskunova, Vladimir I. Rakin

Institute of Geology of RAS (IG), Pervomaiskaya st., Syktyvkar 167982, Russian Federation

e-mail: piskunova@geo.komisc.ru

This work is aimed at a detailed investigation of surface of diamond crystals etched in HPHT cameras to macro-, micro, and nano-sizes by means of optical parabolic goniometry and AFM method.

As an object of investigation we used the diamond powder of two types. The examination of diamond crystal surface in the scope greater than 30 mkm revealed only growth surfaces. However, the crystal forming system going out of the growth mode, there can spontaneously occur conditions for transitory dissolution (etching) of diamond in the process of the residual melt degassing, which was proved by AFM examination of the negative pyramids of dissolution (etching pits) of micro- and nano-sizes on diamond faces.

The detected pits present sockets shaped as negative pyramids with the basis being a square whose sides are parallel to the directions [011]. This form of pits is conditioned by the symmetry of tetrad axis of diamond structure on the hexahedron face. AFM-images of some relatively large (about 5 mkm) pits have a clear stepped structure of inner sidewalls (the height of large steps being 40-60 nm) with visible terraces between the steps. According to the kinematic theory, pits terracing occurs due to disorientation of the etching surface in relation to the real crystallographic plane. It is also influenced by the slope of dislocation line in relation to the open surface.

Pits slope at a different angle that is not associated with any definite flat grids of diamond structure. This is caused by terracing. Our AFM-studies show that synthetic diamond crystals exhibit this effect on pits greater than 4–5 micrometers in size.

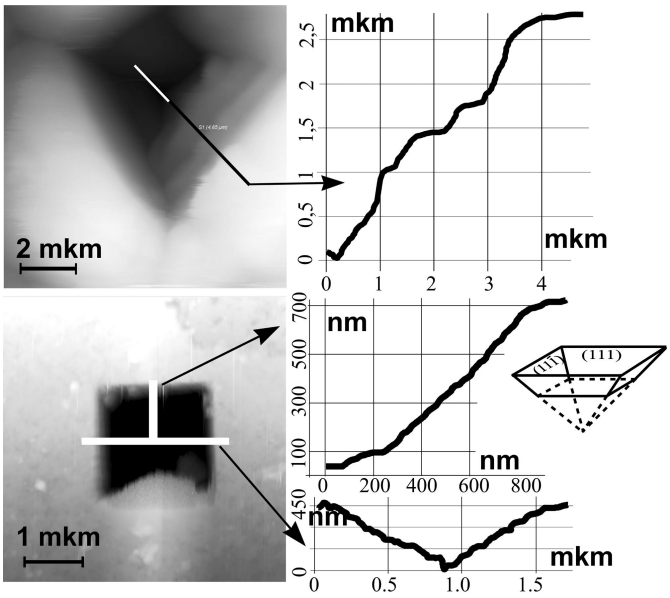

Etching pits smaller than 4 mkm on synthetic diamonds demonstrate a different structure. |Cross sections of five relatively large pits, 2-3 mkm in size (Figure), showed them to have even slopes and the average angle between the inner sub-face of the pit and crystal surface (100) of 54,3°, which allows to identify the etch pit sidewalls as flat lattices {111}. High resolution investigations have also revealed that faces of synthetic crystals may have square pits of a much smaller size, 30 – 70 nm. They show some competition character. Terraces between the nano-size etch pits can be uneven or, on the contrary, very even.

The standard AFM probes of pyramidal form with the needle curvature radius of 10 nm are known to misrepresent real morphology of nano-size pit slopes. If they don't reach the pit bottom, they may underrate their real depth. That is why the representations of the bottom and the walls of a 30 nm wide pit are not very reliable. The cuts of six pits of 70 and more nm wide showed that they present somewhat asymmetric near-pyramidal sockets with very mild slopes corresponding to flat lattices from {12.1.1} to {811} (deviation angles in relation to hexahedron face from 6 to 10°).

This used optical goniometry was established, that faceting of synthetic HPHT diamond crystals emphasizes the validity of Hartman and Perdok's periodic bond chain (PBC) theory. Consecutively considering

flat nets (hkl) with small Miller indices belonging to zone within 90° curve, we calculated with a list of all F- and S- diamond faces. Apart from cubic faces (100), octahedron faces (111) and rhombidodecahedron faces (011), this zone contains nets that form faces on diamond. The other diamond faces with large Miller indices, including all hexahedron faces, can be attributed to K-faces. Strictly following the criterion presented in Hartman and Perdok's theory, there are two forms that belong to diamond F-faces – octahedron and hexahedron, that contain three and two periodic bond chains correspondingly; as for S-faces, apart from rhombidodecahedron they include 13 kinds of trigontrisoctahedrons (hkk)h<k, and 5 kinds of tetragontrisoctahedrons (hkk)h>k.

Faces of hexahedron (two PBC-s) and octahedron (three PBC-s) belonging to F-faces are revealed in all diamond crystals. Rhombidodecahedron faces {110} (S-face – one chain of carbon bond) are present on one third of diamond crystals, and simple forms of tetragontrisoctahedron{311} and {433}, as well as trigontrisoctahedron {122}, also belonging to S-faces, appear only at the terminal growth stages connected with the off-effects. Theoretically, according to Hartman and Perdok's theory, apart from the above listed ones, diamond faces may have some other S-faces: three tetragontrisoctahedrons and twelve trigontrisoctahedrons. K-faces, which contain no bond chains, are not present in outer growth faceting of synthetic diamonds.

We think the peculiarities of the negative relief of synthetic diamonds have to do with the processes of thermal etching at the stage of synthesis termination. AFM-investigations showed that large etching pits (greater than 4 mkm) on cubic faces are made up of terraces that form protuberant surface. This surface can be composed of areas of flat nets of tetragontrisoctahedron, pertaining to either S- or K-faces. This is an evidence of non-equilibrium process of diamond etching over screw dislocations.

Numerous pits with a typical size of 2–3 mkm, on the contrary, possess even slopes, strictly corresponding to planes {111}. The appearance of equilibrium octahedron form {111} on the negative diamond relief in the etching process can indicate that there is another mechanism of such etch pits formation, which is not connected with linear defects of the structure. Micro- and nano-size etch pits can be associated with subsurface nano defects of the structure, formed during the terminal growth stage, i.e. be a result of the "off-effect". Plane {111} formation on microsize pits can be explained thermodynamically as reaching the minimum of surface energy at dying away of the tense defect area of the structure. Since nanosize pits demonstrate an unfinished non-equilibrium etching process, their faceting can be spontaneous.

The investigation was carried out with the financial support of Programs of Russian Academy of Sciences, 12-У-5-1026, 12-P-5-1027, Scientific School 1310.2012.5, RFBR 11-05-00432a

16:00 Poster We189

Effect of temperature and concentration on the particle size in lactose solution using dynamic light scattering analysis

Anna Pisponen, Avo Karus, Väino Poikalainen

Estonian University of Life Sciences, Kreutzwaldi 1a, Tartu 51014, Estonia

e-mail: anna.pisponen@emu.ee

Temperature and supersaturation are the major factors influencing nucleation in a solution. However, most data about the impact of various factors influencing the crystallization process, are obtained using microscopic studies. These provide the opportunity to explore quite large particles. Studies concerning particle size before nucleation have been carried out mostly at the theoretical level.

The objective of this work was to investigate the effects of temperature and concentration of a solution on the nucleation process, using the dynamic light scattering technique.

Solutions of different lactose concentrations were prepared. Each solution was cooled from a high temperature of 60 °C to 0 over a period of 2 hours and analysed using a Malvern Zetasizer Nano ZS.

Particle size distribution in lactose solution varied from 0.9 to 5 nm in diameter. Analysis of the results showed that, with increasing lactose concentration of a solution, the modes of the curves were displaced in the direction of increasing particle size (Fig. 1B). This finding accords with the theory that, in saturated solutions, molecules rapidly form aggregates. With decreasing of temperature the modes of the curves at all concentrations showed a displacement on the scale towards increasing particle size (Fig. 1A). This is due to the fact that a decreasing temperature promotes the growth of aggregates.

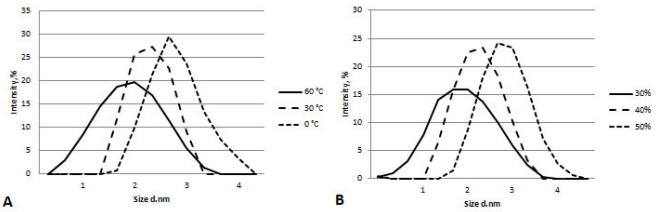

Fig.1 A - effect of temperature on particle size distribution in lactose solution of 40% w/v; B – effect of concentration of lactose solutions on particle size distribution at 30 °C

The results presented in this work indicate that the measurement of temperature and the concentration effect on particle size distribution in a lactose solution is now possible using the dynamic light scattering technique.

16:00 Poster We190

Synthesis of high-pressure $MgCO_3$ - $FeCO_3$ carbonate solid solutions: in situ Raman spectroscopy study

Anna V. Spivak[1], Natalia A. Solopova[1,2], Elena Bykova[2], Egor S. Zakharchenko[1], Yuriy A. Litvin[1], Leonid S. Dubrovinsky[2]

1. *Institute of Experimental Mineralogy RAS (IEMRAS), Acad. Osipiana St, Chernogolovka 142432, Russian Federation* **2.** *Bayerisches Geoinstitut Universität Bayreuth (BGI), Bayreuth D-95440, Germany*

e-mail: spivak@iem.ac.ru

There is growing mineralogical and experimental evidence that Ca-, (Ca, Mg, Fe)- and Na-Ca - carbonates are stable at the conditions of the Earth deep interior. Data on carbonate high-pressure high-temperature transformations would reveal their behavior at PT-conditions of the Earth's transition zone and lower mantle.

Fe^{2+} and Mg^{2+} substitution is common in mineral systems. Particularly, Fe^{2+} and Mg^{2+} form a complete solid solution in the $FeCO_3$-$MgCO_3$ system. Behavior of components of $Mg_{1-x}Fe_xCO_3$ solid solution (x=0.05, 0.09, 0.2, 0.4) is characterized *in situ* by Raman spectroscopy at high pressure and ambient temperature.

Samples of Mg-Fe carbonates of variable composition were synthesized using multianvil apparatus at 18 GPa and 2000°C. High-pressure experiments were carried out in a diamond anvil cell (DAC). The LabRam system (Horiba Sceintific Inc.) with a He-Nd-laser (excitation

wavelength 632 nm) was used for *in situ* registration of the Raman spectra.

Magnesite-stuctured carbonates with rhombohedral symmetry have six characteristic vibrational modes in Raman spectra. Four internal modes are connected with vibrations within the $(CO_3)^{2-}$ unit, and two modes - with external vibrations of the crystal lattice. For external modes T and L, (1) position of Raman band for end members siderite and magnesite are, correspondingly, 174/213 cm^{-1} and 273/330 cm^{-1}; (2) pressure – induced shiftfor solid-solution variable within $Mg_{0.6}Fe_{0.4}CO_3$-$Mg_{0.95}Fe_{0.05}CO_3$ composition are in the 197-210 cm^{-1} and 301-328 cm^{-1} range, correspondingly. The end member positions and solid solution pressure – induced shifts are characterized by the internal modes ν_4 (720/737 cm^{-1} and 730-737 cm^{-1} range), ν_1 (1074/1092 cm^{-1} and 1086-1092 cm^{-1} range), ν_3 (1425/1442 cm^{-1} and 1427-1442 cm^{-1} range), $2\nu_2$ (1711/1759 cm^{-1} and 1733-1758 cm^{-1} range). Raman shifts calibrated as a function of Mg or Fe carbonate content may be used in turn to evaluate the chemical composition of natural carbonate samples. Apart Raman bands characteristic for magnesite-type materials, it was observed the additional Raman peak in range 868-874 cm^{-1} for solid solutions of composition $Mg_{0.6}Fe_{0.4}CO_3$-$Mg_{0.95}Fe_{0.05}CO_3$. Similar peak was determined at 870 cm^{-1} for siderite and described as additional one not predicted by factor group analyses by Boulard et al. (2011). This peak may be explained to an infrared mode becoming Raman active due to a local loss of inversion symmetry as a result of Fe ordering [Langille and Oshea, 1977].

At high pressure *in situ* Raman study, it was analyzed the behavior of four modes of carbonates with following compositions $Mg_{0.6}Fe_{0.4}CO_3$, $Mg_{0.8}Fe_{0.2}CO_3$, $Mg_{0.91}Fe_{0.09}CO_3$ and $Mg_{0.95}Fe_{0.05}CO_3$. The high pressure Raman spectra show that the frequency of ν_1 of all studied carbonates increases monotonically up to 40-42 GPa, where addition peak appeared at 1220 cm^{-1}. Position of the peak of internal mode ν_4 is increases monotonically in all cases. Frequency of external modes T and L of $Mg_{0.91}Fe_{0.9}CO_3$ increase linearly up to 46 GPa, and above this pressure change it slope. For all carbonates with intermediate compositions additional peak in range 868-874 cm^{-1} at 0 GPa is observed. This peak not detectable in the DAC at low pressures, but become visible above 30 GPa with frequency increasing monotonically.

This work was funded by grant of the President RF MK-1386.2013.5, The Ministry of education and science of Russian Federation, project 8317, 16.740.11.0621 and grants RFBR 13-05-00835, 12-05-33044, 11-05-000401.

16:00 Poster We191

Development of refractive index matching cell for three-dimensional reconstruction of the concentration field around a growing crystal

Kenta Murayama[2], Atul Srivastava[1], Katsuo Tsukamoto[2]

1. *Indian Institute of Technology Bombay (IITBOMBAY), Powai, Mumbai 400076, India* **2.** *Graduate school of Scienece, Sendai 980-8578, Japan*

e-mail: atulsr@iitb.ac.in

Growth of a crystal from its aqueous solution is accompanied by the distribution of three-dimensional concentration gradients in the growth chamber. Under the influence of gravity, beyond a critical size of the growing crystal and the solution supersaturation level, gradients in the concentration field are responsible for the evolution of buoyancy-induced convection currents in the vicinity of the growing crystal [1]. The characteristic of the flow field thus generated is an important factor for crystal quality. Therefore, mapping of convection patterns is essential to understand the physical mechanism of crystal growth. In this regard, optical techniques are ideal since they are non-intrusive and inertia-free [2, 3]. However, the optical techniques provide only the two-dimensional information in the form of path-integrated concentration field along the direction of the propagation of the light beam. In order to retrieve the concentration field distribution in the third dimension, principles of tomography have been employed by various researchers in the recent past [4].

It has been experimentally as well as theoretically established that the resolution of tomography reconstruction strongly depends on the number of projection angles employed for recording the two-dimensional data of the field of interest. The literature on the three-dimensional reconstruction of concentration field around a growing crystal has revealed that researchers in the past have employed a maximum of only 4 projection data (recorded from 0, 45, 90 and 135 ^{o} viewing angles) for tomography reconstructions due to inherent curvature effects of cylindrical growth cells. Strong curvature effects of cylindrical growth cells lead to unwanted refraction and reflection errors as the light beam passes through the growth chamber and adversely affect the quality of the projection data. In order to circumvent this limitation, researchers have approximated the cylindrical growth cells by octagonal cells, thus restricting the number of views to a maximum of four. In view of this lacunae in the literature, we implemented the principle of refractive index matching to minimize the curvature effects of a cylindrical crystal growth cell so as to record the maximum number of projection data from any view angle in the span of 0 to 360 ^{o} . The present work is concerned with the details of the development and application of refractive index matching crystal growth cell for three-dimensional reconstruction of concentration field around a crystal growing from its aqueous solution. The crystal growth chamber, made of quartz, is cylindrical in shape with 4 mm inner diameter and a height of 20 mm. Thickness of the walls of the growth chamber is 0.5 mm. The cylindrical growth cell is placed inside an outer square chamber, also made of quartz, with dimensions 20 mm. The annulus region between the inner growth cell and outer square chamber is filled with refractive index matching liquid whose index of refraction is close to that of the cylindrical cell. The experiments have been performed in free convection regime of the growth process with Sodium Chlorate ($NaClO_3$) being the crystal material. A microscopic Mach-Zehnder interferometer has been employed for recording the projection data of concentration field. It is inferred that by using the cylindrical growth cell with the refractive index matching method, the projection data can be recorded from any arbitrary view angle within a span of 0 to 360 ^{o} . With larger number of projection data available, it is, therefore, expected to improve the spatial resolution of three-dimensional distribution of the concentration field. Detailed investigation of the three-dimensional reconstruction of the concentration field using the principles of tomography with varying number of projection data would be presented in the conference.

16:00 Poster We192

In-situ observation of mixing behavior in a tubular flow reactor for supercritical hydrothermal synthesis of nanocrystals using neutron radiography

Seiichi Takami[1], Ken-ichi Sugioka[2], Kyohei Ozawa[2], Takao Tsukada[2], Tadafumi Adschiri[3], Katsumi Sugimoto[4], Nobuyuki Takenaka[4], Yasushi Saito[5]

1. *IMRAM, Tohoku University, 2-1-1 Katahira, Aoba-ku, Sendai 980-8577, Japan* **2.** *Department of Chemical Engineering, Tohoku University, 6-6-07 Aramaki, Aoba-ku, Sendai 980-8579, Japan* **3.** *WPI-AIMR, Tohoku University, 2-1-1 Katahira, Aoba-ku, Sendai 980-8577, Japan* **4.** *Department of Mechanical Engineering, Kobe University, 1-1 Rokkodai, Nada-ku, Kobe 657-8501, Japan* **5.** *RRI, Kyoto University, 2 Asashiro-Nishi, Kumatori-cho, Sennan-gun, Osaka 590-0494, Japan*

e-mail: tsukada@pcel.che.tohoku.ac.jp

Hydrothermal synthesis at supercritical conditions is a useful method to produce metal oxide nanocrystals from metal salt aqueous solutions. The high reaction temperature and the properties of supercritical water as a reaction medium make the reaction rate quite fast and the solubility of dehydrated products extremely low. Consequently, a rapid increase in degree of supersaturation, very high nucleation rates and the mass production of nanocrystals can be achieved. In such a supercritical hydrothermal synthesis process, continuous flow reactors, in which two streams of metal salt aqueous solution and heated water are mixed at supercritical conditions, are commonly used. Rapid and uniform mixing of the streams is indispensable to produce metal oxide nanocrystals, and the size and its distributions of nanocrystals are strongly affected by how the reactants and supercritical water streams are mixed in the reactor. Therefore, it is important to understand the mixing behaviors of the streams, and the distributions of temperature and supersaturation in the reactor under supercritical conditions. However, the direct observation of the mixing behaviors in the reactor is difficult because the hydrothermal synthesis is performed at high pressure and high temperature in the reactor which is made of metal and consequently is opaque to visible light.

In this work, we have performed neutron radiography on a tubular flow reactor with a diameter of 1/8 inch which is commonly used for supercritical hydrothermal synthesis of metal oxide nanocrystals (J. Lu et al., ACS Appl. Mater. Interface, 4 (2012) 351), and visualized the mixing behaviors of supercritical water and room-temperature water (corresponding to metal salt aqueous solution) and moreover temperature distributions in the reactor. Here, hydrogen and water are opaque against neutrons, but heavier elements including iron, nickel, and chromium, i.e., the metal wall of the reactor, are more transparent. In addition, since neutron attenuation coefficient of water depends on its density, the difference between the densities of supercritical water and room-temperature water in the reactor can be visualized by neutron radiography. Figure 1 shows the schematic diagram of experimental setup, where a thermal neutron beam emitted from the B4 port of the KUR at the RRI, Kyoto University was used. The results demonstrated that the mixing behaviors, the distributions of water density and temperature in the reactor were clearly visualized by neutron radiography. The effects of the flow rates of supercritical water and room-temperature water on the temperature distributions in the reactor were also clarified. In addition, numerical simulations using a commercial software FLUENT were carried out to investigate the mixing behaviors in the reactor in detail. Figure 2 shows the comparison between experimental and numerical results of temperature distributions in a tubular flow reactor (imaging area in Figure 1), where the distributions in (a) were obtained using the relationship between the neutron attenuation coefficient of water and temperature measured experimentally.

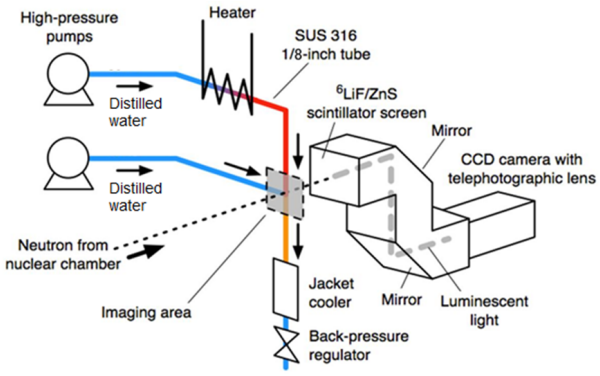

Figure 1 Schematic of experimental setup.

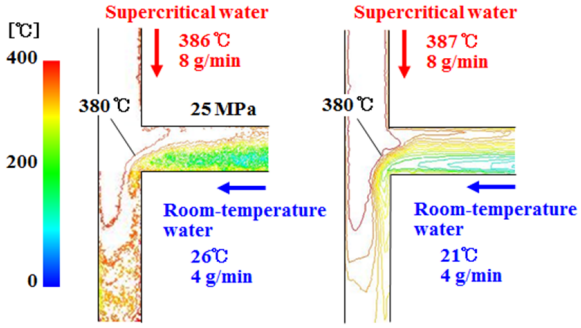

Figure 2 Comparison between experimental and numerical results of temperature distributions in a tubular flow reactor.

16:00 Poster We193

Real time observation of tellurium inclusion thermomigration and dissolution in CdZnTe crystals under infrared laser irradiation

Andrea Zappettini[1], Nicola Zambelli[1,2], Giacomo Benassi[1], Maura Pavesi[1,2], Davide Calestani[1]

1. *IMEM- CNR (IMEM), Parma, Italy* **2.** *Dipartimento di Fisica, Università, Viale G.P. Usberti 7/a, Parma 43100, Italy*

e-mail: zapp@imem.cnr.it

CdZnTe crystals are largely employed as substrates for IR devices, X-ray detectors, and electro-optic modulators. One of the main problems affecting device quality is the presence of tellurium inclusions. These form during crystal cooling due to the retrograde shape of the liquidus curve or are incorporated during growth. In fact, the maximum melting point is actually on the Te side of the phase diagram. Moreover, high resistivity is obtained by doping with In or Cl and by growing crystals from a Te-deviated charge.

Different approaches have been suggested for the elimination of tellurium inclusions by means of post growth treatments. One of them relies

on the observation that when CdZnTe crystals are annealed in a temperature gradient, Te inclusions drift towards the higher temperature region, due to the fact that CdZnTe solubility in tellurium increases with temperature. However, it was reported by many authors that after thermal treatment high resistivity can't be reproducibly recovered.

It was also shown that Te inclusions can experience thermomigration under the influence of a CO_2 laser irradiation at 10.6 micron [1]. The effect of the laser irradiation was evaluated comparing samples before and after irradiation.

In this work, we have studied the tellurium inclusion thermomigration induced by a pulsed Nd:YAG laser irradiation (1.064 micron). The inclusion movement was live-monitored *in situ* using our new IR microscopy system for 3D reconstruction of the position of tellurium inclusions in CdZnTe crystals [2].

First of all, with respect to the use of the CO_2 laser, it should be noted that a much larger thermomigration speed was in general observed, without the need to heat the sample. Secondly, thanks to the *in situ* observation, it was possible to conclude that inclusions migrate at different speed according to their dimension. Moreover, inclusions separates into smaller parts and finally dissolve in the CdZnTe matrix.

In conclusion, it was shown that laser irradiation at 1.064 micron is a powerful method to eliminate tellurium inclusions from CdZnTe crystals without heating the sample and that thanks to live monitoring it is possible to study the thermomigration dynamics and, thus, to tailor the process at best.

[1] M. Meier, M. J. Harrison, S. Spalsbury, D. S. McGregor, "Laser-induced thermomigration of Te precipitates in CdZnTe crystals", J. Crystal Growth 311 (2009) 4247-4250

[2] N. Zambelli, L. Marchini, M. Zha, A. Zappettini, "Three-dimensional mapping of tellurium inclusions in CdZnTe crystals by means of improved optical microscopy", J. Crystal Growth 318 (2011) 1167-1170

General Session 7

Defect formation/elimination

Session Coordinators

Andreas Danilewsky (Germany) *a.danilewsky@krist.uni-freiburg.de*

Michael Dudley (USA) *mdudley@notes.cc.sunysb.edu*

Thierry Duffar (France) IUCr representative

thierry.duffar@grenoble-inp.fr

Programme

Wednesday, 14 August

WeO2

G07: Defect formation/elimination
Wednesday afternoon, 14 August, 14:00
Room D, Auditorium Maximum

14:00 Invited oral

Synchrotron Topography Studies of the Operation of Double-Ended Frank-Read Partial Dislocation Sources in 4H-SiC

Balaji Raghothamachar[1], Huanhuan Wang[1], Fangzhen Wu[1], Shayan Byrappa[1], Michael Dudley[1], Ping Wu[2], Ilya Zwieback[2], Andy Souzis[2], Gary Ruland[2], Tom Anderson[2]

1. *Stony Brook University, Department of Materials Science and Engneering, Stony Brook 11794, United States* **2.** *II-VI Incorporated, New Jersey, NJ 07058, United States*

e-mail: balaji.raghothamachar@stonybrook.edu

Synchrotron White Beam X-ray Topography (SWBXT) is a powerful and versatile technique that enables rapid and non-destructive imaging of defects in thick and large-diameter wafers. Analysis of defect contrast facilitates determination of their configuration which, in turn, provides insight into their possible formation mechanisms. Here, we demonstrate the capabilities of SWBXT through the detailed characterization of a distinctive stacking fault pattern observed in 4H-SiC wafers. This fault has a shape of a six-pointed star comprised of rhombus-shaped stacking faults with three different fault vectors of the Shockley type. Transmission and grazing topography analysis reveals that the outline of the star is confined by 30° Shockley partial dislocations. Formation of the star fault is found to be associated with a micropipe at its center. It is well known that micropipes in SiC can act as nucleation sites for dislocation half-loops belonging to the primary basal (1/3<11-20> (0001)) slip system [1,2]. Occasionally, similar nucleation of slip on the secondary prismatic (1/3<11-20>{1-100}) slip system has also been reported [3,4]. In this case, the nucleation of the rhombus-shaped Shockley type stacking faults on the basal plane involves the reaction of 60° dislocations of a/3<-2110> Burgers vector on the basal plane and pure screw dislocations of a/3<11-20> Burgers vector on the prismatic plane and cross slip of the partial dislocation from prismatic plane to basal plane leading to the expansion of the faults [5]. The formation mechanism involves the operation of a double-ended Frank-Read partial dislocation source. Details of this mechanism will be discussed and we shall show that in the limit, this glide and cross-slip mechanism can lead to 4H to 3C polytype transformation in the vicinity of the micropipe by a mechanism similar to that proposed by Pirouz [6].

References:

[1] W. Vetter, Characterization of dislocation structures in silicon carbide single crystals, Ph.D. Thesis, Stony Brook University (1999).

[2] Jinwei Yang, SiC: Problems in Crystal Growth and Polytypic Transformation, Ph.D. Thesis, Case Western Reserve University (1993).

[3] S.Ha, N. T.Nuhfer, G. S.Rohrer, M. De Graef, M. Skowronski, J. Electron. Mater., vol. 29 L5-L8 (2000)

[4] H. Wang, S. Byrappa, F. Wu, B. Raghothamachar, M. Dudley, E. K. Sanchez, D. Hansen, R. Drachev, S. G. Mueller and M. J. Loboda, Mater. Sci. Forum, vols. 717-720, pp. 327-330, (2012).

[5] F. Wu, H. Wang, S. Byrappa, B. Raghothamachar, M. Dudley, P. Wu, X. Xu, I. Zwieback, J. Electron. Mater., doi: 10.1007/s11664-012-2379-9, (2012)

[6] P. Pirouz and J. W. Yang, Ultramicroscopy 51, 189-214 (1993)

14:30 Oral

Grain and Subgrain Boundaries in Multi-Crystalline Silicon

Eva-Regine Carl[1], Andreas Danilewsky[1], Arne Croell[1], Tobias Geiger[2], Elke Meissner[2]

1. *Kristallographie, Universität Freiburg (KI), Hermann-Herder-Str. 5, Freiburg 79104, Germany* **2.** *Fraunhofer Institute for Integrated Systems and Device Technology (IISB), Schottkystrasse 10, Erlangen 91058, Germany*

e-mail: eva-reginecarl@gmx.net

Multi-crystalline silicon is one of the most important photovoltaic materials. However, its microstructure lowers the efficiency of the cells with grain boundaries and highly dislocated areas acting as effective recombination centers. This is why the main challenge is to optimize the structural properties. For this, detailed knowledge about the formation of the microstructure is needed.

Grain and twin boundaries in multi-crystalline silicon grown by directional solidification were analyzed by means of Electron Backscatter Diffraction (EBSD) and Synchrotron X-Ray Topography (SXRT). Two nearest neighbor samples of one column were analyzed in order to get information about the development of grain boundaries during crystal growth. Thereby, the emphasis was placed on the evolution of one selected and its neighboring grains.

From the analysis of the EBSD data for the large angle grain boundaries and twins, it was found that the common interface of adjacent grains that forms the grain boundary is not correlated to the rotation axis that defines the type of boundary. The results show that the interfaces formed by lower symmetry operations are responsible for the trace of the grain boundary.

In the samples, significant changes with respect to non-“straight line” twin boundaries were found during the growth process. Grain boundaries of this type were formed or eliminated very quickly, while other types of grain boundaries experienced only small changes.

By means of SXRT, the microstructure of the analyzed grain shows numerous small-angle grain boundaries with angles in the range between 0.05 and 0.15 degrees, which is well below the EBSD angular resolution of about ± 0.5°. Fig. 1 compares a transmission X-ray topo-

graphy and an etch pit density map of the same small angle grain boundary. The small tilt of only w = 9 arcsecs (fig. 1 a) results after etching in a line of etch pits of such a high density, that the pits becomes uncountable (fig. 1b). It will be shown, that the "dislocation clusters" proposed from etch pit patterns are small angle grain boundaries with angles of 0.01 – 0.18 degrees, corresponding to a minimum theoretical dislocation density of about 10^8 cm^{-2} responsible for such a tilt value.

The experiments give evidence that the small-angle grain boundaries with larger angles extend, while the smaller ones vanished. This enlargement from 0.1° to 30° finally results in the formation of a twin boundary.

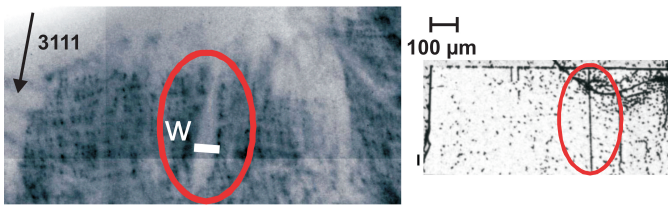

Fig. 1: Small angle grain boundary located in a single grain of mc-Si (a) Transmission X-ray topography: Opening w corresponds to a tilt of 9 arcsec.
(b) Etch pit density map of the same area: The aligned etch pits demark the small angle grain boundary.

14:45 Oral

Experimental study of the grain boundary orientations in multi-crystalline silicon

Thierry Duffar[1], C. T. Nwosu[1], I. M. Asuo[1], J. Muzy[1], Y. Duterrail-Couvat[1], F. Robaut[2]

1. *SIMaP EPM, CNRS UJF, BP 75, Saint Martin d'Heres cedex 38402, France* **2.** *INP-Grenoble, BP 75, Saint Martin d'Heres cedex 38402, France*

e-mail: thierry.duffar@grenoble-inp.fr

There are numerous Grain boundaries (GB) in photovoltaic multicrystalline silicon, with the drawback of decreasing the solar cell efficiency. We developed a theoretical model [1] in order to describe the origin and development of GB during the solidification of the silicon ingot. This model is used in a numerical code for the simulation of the GB distribution in industrial ingots [2]. One of the conclusions of the theoretical model is that facets may exist at the liquid-grain-grain triple line during growth. In this case, the orientation of the grain boundary is predicted to follow the bisector of the groove formed by the two facets.

The objective of this work is to validate experimentally this theoretical expectation. In this purpose, appropriate zones in Si ingots were selected, cut and polished at places showing interesting GB configurations with respect to the model hypothesis. These samples were analyzed by EBSD with a SEM in order to find the crystallographic orientation of the two grains forming the GB. Then the shape of the GB was analyzed by successive polishing and 3D reconstruction from successive pictures.

In the case where the crystallographic orientation of the two grains is compatible with the existence of (111) facets at the triple line, it was found that straight grain boundaries are always obtained. Comparison of the grain boundary orientation with the orientation of possible facets shows, within the error margin, that the GB follows the bisector of the two facets.

[1] « The solid-solid-liquid triple line and its effect on the grain structure of multi-crystalline photovoltaic silicon" T. Duffar and A. Nadri, C. R. Ac. Sci. Ser. Physique, 14 (2013) 185–191.

[2] " Numerical simulation of grain structure in PV Si" A. Nadri, Y. Du Terrail, T. Duffar, IWMCG7, 28-31 October 2012, Taipei, Taiwan, submitted for publication in the J. Crystal Growth.

15:00 Oral

Numerical study of dislocation formation during transient growth of multi-Si by the direct solidification technique

Vasif Mamedov, Vladimir Kalaev

STR Group, Inc., Engels av. 27, P.O. Box 89, St-Petersburg 194156, Russian Federation

e-mail: vasifm@mail.ru

The method of directional solidification (DS) is still the major technology to produce silicon wafers for photovoltaic. There are many factors responsible for the quality of the ingot such as impurity concentrations or grain structure. One of the most important parameters characterizing crystal quality is the dislocation density. The major factor responsible for generation and multiplication of dislocations inside the crystal bulk is the thermal stress. The thermal stress is produced by thermal deformation due to the temperature variation. A high stress level leads to the inelastic creep deformation providing the stress relaxation during the growth stage and resulting in high residual stress on the cooling stage. Thus there is a complex interaction of the stress field variation and generation of dislocations. Numerical simulation of transient growth of multi-Si by the DS technique has been performed to study the effect of growth conditions on formation of dislocations. Computer modeling has been provided by the specialized software CGSim [1]. This software allows one to simulate the DS growth as an unsteady continuous process from seeding stage to the end of cooling. The generation of dislocation has been calculated by Haasen- Alexander-Sumino model [2, 3] implemented into CGSim. This model provides the quantitative description of the relationship between plastic deformation and dislocation density. Different recipes of cooling and annealing have been simulated to find a promissing way to control of dislocation density. It is was shown that the most intensive multiplication of dislocations occurring after start of cooling while during the growth stage the dislocation density is quite stable. Despite of this the generation of dislocations on growth stage cannot be ignored because it strongly affects the stress-level inside Si ingot at the start of cooling.

1. www.str-soft.com
2. H. Alexander, P. Haasen, Solid State Phys. 22, 27 (1968)
3. M. Suezawa, K. Sumino, I. Yonegaga, J. Appl. Phys. 51, 217 (1979)

15:15 Oral

Quantitative analysis of correlations between the generation of dislocations and its influencing factors during cylindrical monocrystalline silicon growth

Bing Gao, Koichi Kakimoto

Kyushu University, Fukuoka, Japan

e-mail: gaobing@riam.kyushu-u.ac.jp

Solar cell efficiencies are generally governed by the concentration and type of impurities, and the density and electrical activity of exten-

ded defects such as grain boundaries and dislocations [1]. Dislocations have been identified to be one of the most efficiency-relevant defect centers in crystal silicon for photovoltaic [2]. The requirement of the increase of solar cell efficiencies necessitates a reduction of the crystal dislocations.

To reduce dislocation density, it is essential to know the relationships between the generation of dislocations and its influencing factors, such as geometry of crystal (diameter and height), temperature distribution in radial and axial directions. A quantitative study between the generation of dislocations and its influencing factors has been studied.

For radial temperature distribution, diameter of crystal and radial gradient of temperature have obvious effects on the generation of dislocations. If the radial gradient of temperature is fixed, the square root of maximum dislocation density in slices is proportional to the diameter of crystal; if the geometry of crystal is fixed, the square root of maximum dislocation density in slices is proportional to the radial gradient of temperature. We proposed a quantitative equation, which stated that the square root of maximum dislocation density in slices is proportional to the maximum value of rdT/dr in slices. Numerical simulations show that the proposed formulation can accurately predict the location and the value of maximum dislocation density in every slice. Further extension of the proposed equation indicates that the maximum dislocation density in slices is determined by the energy accumulation rate along radial direction.

For axial temperature distribution, height of crystal and axial second-gradient of temperature have obvious effects on the generation of dislocations. If the axial second-gradient of temperature is fixed, the square root of maximum dislocation density is proportional to the height of crystal; if the height of crystal is fixed, the square root of maximum dislocation density is proportional to the axial second-gradient of temperature. We proposed a quantitative equation, which stated that the square root of maximum dislocation density is proportional to the integration of d^2T/dz^2 along axial direction. Numerical simulations show that the proposed equation can accurately predict the value of maximum dislocation density in crystal. The proposed equation also indicates that the maximum dislocation density is determined by the energy accumulation rate along axial direction.

For mixed radial and axial temperature distribution, a proposed equation, which stated that the square root of maximum dislocation density in slices has a linear relationship with energy accumulation rate along radial direction and energy accumulation rate along axial direction. Therefore, in essence, maximum dislocation density in slices is determined by energy accumulation rate inside crystal.

The above analysis indicates a simple relationship between maximum dislocation density in slices, geometry of crystal, temperature distribution, which is very useful for crystal growers to control the generation of dislocations and optimize the distribution of dislocations.

Reference

[1] C. Häβler, G. Stollwerck,W. Koch,W. Krumbe, A. Müller, D. Franke, T. Rettelbach, Adv. Mater. 13 (23) 2001.

[2] H. El Ghitani, M. Pasquinelli and S. Martinuzzi, J. Phys. III 3 (1993) 1941.

15:30 Oral

Numerical Analysis of the Effect of Growth Rate Variations on Defect Formation in Czochralski Grown Silicon

Moez Jomâa[1], Mari Juel[2], Koichi Kakimoto[3], Rune Søndenå[4], Rajesh Selvaraj[5]

1. *SINTEF Materials and Chemistry, Oslo 0315, Norway* **2.** *SINTEF Materials and Chemistry, Trondheim 7028, Norway* **3.** *Kyushu University, Fukuoka, Japan* **4.** *Institute for Energy Technology (IFE), Institutveien 18, Oslo NO-2027, Norway* **5.** *FEMAGSoft S.A., Avenue Jean Monnet 1, Louvain-la-Neuve B-1348, Belgium*

e-mail: moez.jomaa@sintef.no

The type and distribution of grown-in defects formed in Cz grown silicon depends strongly on the growth parameters, like the furnace design, pull speed and crucible/seed rotation during crystal pulling. From the theory of Voronkov [1] a transition from self-interstitial rich material to a vacancy rich material happens when the v/G ratio (v is the growth rate and G is the thermal gradient) at the solidification front reach a critical value. The material quality from material that is solidified under conditions close to a critical v/G ratio can vary strongly from almost defect free (denuded zone) to regions where large oxygen precipitates are formed (OiSF-ring or p-band). A large problem for the solar cell producers is that the oxygen precipitates formed in the p-band often acts as recombination centres and decrease the efficiency of the solar cell significantly [2, 3]. Effort should therefore be use on investigations of the relation between growth conditions and the formation of the p-band and how it is possible to reduce its negative impact.

The aim of this work is to combine numerical and experimental techniques to study the effect of growth rate variations on the defect formation. Therefore, two n-type Cz-Si ingots have been grown with varying growth rates. Pull speed has been varied to cover different growth regimes. Experimental methods used for characterization of the p-band were Cu-decoration, wet oxidation flow by preferential etching [4]. Numerical simulations of the growth of the two crystals have been achieved. The predicted position of the p-band has been compared to the experimental observation and discussed.

References

[1] V.V. Voronkov, J. Crystal Growth 59 (1982) 625.

[2] J. Haunschild, J. Broisch, I. E. Reis, S. Rein, 26th European PV Solar Energy Conference and Exhibition, 5-9 September 2011, Hamburg, German

[3] J. Haunschild, I.E. Reis, J. Geilker, S. Rein, Phys. Status Solidi RRL. 5 (2011) 199-201.

[4] M. Juel, Y. Hu, V. S. Koien, M. Jomâa, S. Zhang, E. Øvrelid, The 6th International workshop on Crystalline Silicon for Solar Cells, October 8-11, 2012, Aix-les-bains, France.

15:45 Oral

Discrepancies between experimental results and simulations on point defects behavior during silicon crystal growth from the melt

Takao Abe[1], Toru Takahashi[1], Koun Shirai[2]

1. *Shin-Etsu Handotai Co., Ltd. (SEH), Isobe RD Center 2-13-1 Isobe, Annaka 379-0196, Japan* **2.** *Institute of Scientific and Industrial Research, Osaka University, Osaka, Japan*

e-mail: takao.abe@seh.jp

1. Introduction

In order to confirm justification for Voronkov's model, analyses were done by the detailed comparison between our experimental secondary defect distributions in CZ crystal and the simulation results on point defects distribution by Dornberger et al., who had explained our experimental distribution. The experimental secondary defect distributions were obtained from the defects formed in as grown crystal when the pulling rate is abruptly changed at a time. The simulation is based on Voronkov's model which gives the boundary between both interstitial and vacancy rich regions to be defined by the sign of CI-CV , where CI and CV are the concentrations of interstitial and vacancy, respectively. They have been performed the simulation for our transient growing process. It is shown from the analyses that there are the discrepancies between our experimental and their simulation results.

2. The experiments on decreasing abruptly pulling rate(DAPR)

2.1 Experiments

The measurable defects are not point defects but secondary defects which are formed by recombination and coalescence of point defects. Thus, the point defect distribution is always a speculated one from the secondary defect distribution. It is well known that these secondary defects are only voids and dislocation loops to correspond to vacancies and interstitials, respectively. However, the secondary defects are disclosed by many methods as lifetime, etching, and x-ray topograph, in particular, for the etchings it are well known FPD and OCP correspond to the void, and SEPD corresponds to the dislocation loop in CZ crystals. Also, the same says for the etching for FZ crystals When pulling rate was decreased abruptly, the distributions of secondary defects in the crystals were formed by the recombination and the coalescence of point defects. The distribution was obtained from the lifetime map of minority carriers injected by the infrared pulsed light [1,2]. The samples were prepared from the crystals in three different diameters (50 mm, 100 mm and 200 mm). The crystals were grown from the one crucible with the same melt volume to maintain the same growth condition. The growth condition is that pulling rate (v) is 1.0 mm/min after arriving at a stationary growth, and then abruptly decreased 0.2 mm/min at a time and kept for 30 min, and finally returned 1.0 mm/min again. These crystals were cut off wafers with 1.0 mm in thickness which were parallel to growth direction. And the wafers have the centers at abruptly decreased positions. The lifetime maps of minority carriers for their wafers were shown in Fig. 1(a), (b) and (c), respectively.

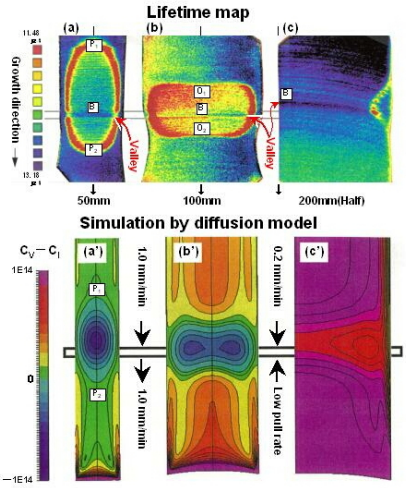

Fig. 1. (a), (b) and (c) show lifetime maps (WT-85 SEMILAB) of as-grown crystals of 50 mm, 100 mm, right half of 200 mm in diameter, respectively. (a'), (b'), (c') simulation results to correspond with (a), (b) and (c), respectively.

2.2 The interstitial type dislocation loops detected by the minority carrier lifetime

The lifetime values are not influenced by the existence of vacancies and their secondary defects so-called FPD (flow pattern defect) [3] or the void [4], but they are adversely proportional to the density of the dangling bonds of dislocations. The interpretation of the lifetime as described above has not yet reported but we show two examples for this interpretation to be true. Figure 2(a) shows an x-ray topograph of a vertical cut wafer along growth direction of an as-grown crystal of which slip dislocations were formed at the growth interface and were spread to the already grown dislocation-free region to relax the thermal stress contained in the CZ crystal grown with a dislocation-free state. Figure 2(b) also shows a lifetime map of the wafer in Fig. 2(a). Although all growth condition of the wafer from top to bottom is the same, the lifetimes largely decreased in the dislocated region, and also the lifetimes along the slip dislocations had lower values than those in the dislocation-free region. Figure 3(a) shows an x-ray topograph after copper decoration of the FZ wafer to have been cut parallel to growth direction. This crystal was grown with the abruptly changed pulling rate from 3.0 mm/min to 2.0 mm/min. The decreasing of pulling rate started from the left hand side. Before the change of pulling rate the all region of the crystal was filled with the FPD which is called the D defect in FZ crystals [5]. However, because of decreasing the pulling rate, the SEPD (Secco etch pit defect) [6] region which is called the A defect region in FZ crystals gradually spread into the insides but saturated soon. As shown in Fig. 3(b) which is the magnification of the part to be surrounded by the white lines in Fig. 3(a), the A defects were the arrays of small points which consist of interstitial type dislocation loops with several tens um in size [7] on the growth striations. On the other hand, the lifetime map of a neighboring as-grown wafer is shown in Fig. 3(c) and the A defect region corresponds clearly to the lower lifetime region. The cause of the lower lifetimes should be attributed to the density of the dangling bonds of the dislocation loops. Hence, it is concluded that the low lifetime distributions in Figs. 1(a), (b) and (c) correspond to the density distributions of the dangling bonds on the interstitial type dislocations which were formed by coalescence of interstitial point defects. This conclusion gives us one of the keys to translate the secondary defect distribution into the speculated distribution of point defects. The other key is the lifetime not to be influenced by the existence of vacancies and their secondary defects, that is, voids.

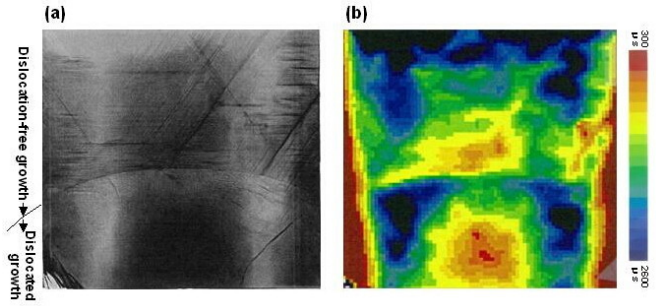

Fig. 2. (a) shows x-ray topograph of dislocated crystal part during (100) CZ growth. (b) Lifetime map (WT-2000 SEMILAB) of wafer (a).

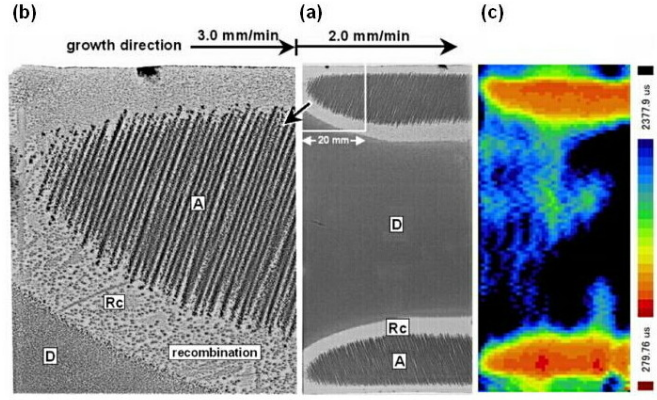

Fig. 3. (a) shows x-ray topograph after copper decoration of wafer cut parallel to growth direction from 100 mm FZ crystal which pulling rate was abruptly changed from 3 mm/min to 2 mm/min. (b) enlargement of upper left square of wafer (a). (c) Lifetime map (WT-2000 SEMILAB) of as-grown neighboring wafer of (a).

3. Discrepancies of the distributions of interstitials between the experimental and the simulation results

Using the each neighboring wafer of the lifetime measurements, the densities of the FPD and the SEPD were counted along the center lines indicated by the arrows in Figs. 1 (a), (b), (c) and their density distributions were shown in Figs. 4(a), (b), (c), respectively. The FPD distribution shows the flow pattern to spread from a void [4] to the upper side when the wafer was put vertically in etchant.

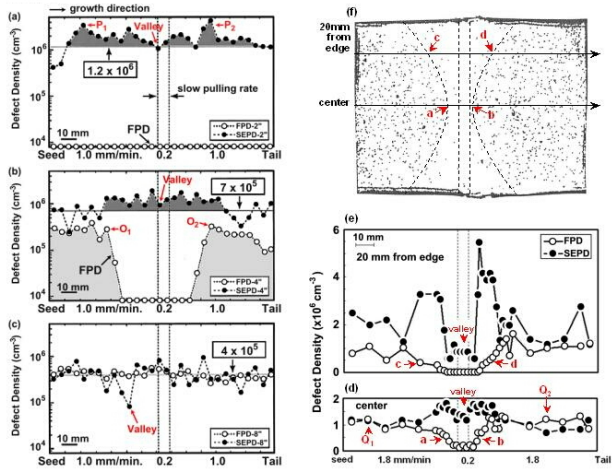

Fig. 4. Density distributions of FPD and SEPD measured along center lines of three wafers in Fig. 1(a), (b) and (c). Other examples of valley phenomenon are Fig. 4(d) and (e). Growth conditions of Fig. 4(e) and (d) are the same as that of Fig 1(b) except pulling rate (1.8 mm/min). Pulling rate of Fig. 1(b) is 1.0 mm/min. Fig. 4(d) and (e) are FPD and SEPD density distributions along center line and 20 mm from edge line, respectively. (f) is COP map measured by LS-6000 (Hitachi). COP is revealed by NH_4OH/H_2O_2 solution which is one of solution of RCA cleaning for 20 min and particle size counted is in the range of 0.1μm~0.13μm. **a**', **b**', **c**' and **d**' in Fig. 4(f) are corresponding to **a**, **b**, **c** and **d** in Fig. 4(d), (e), respectively.

The original pits of the voids with the exaggerated flow pattern are only counted, therefore there is no chance to count the SEPD as the FPD. On the other hand, the size of the SEPD is so small in μm order, so the SEPD was separately counted using 10 times higher magnification [1] than that of the FPD. The one of the example of the SEPD pit was observed by AFM as shown in Fig. 5(b).

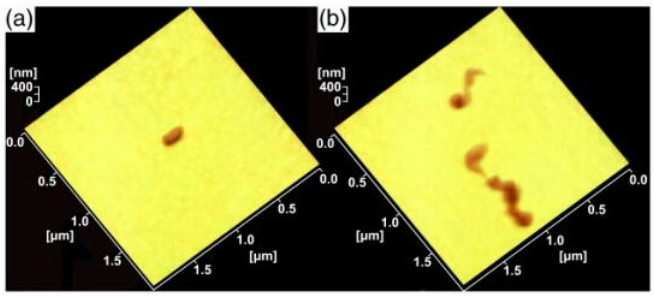

Fig. 5. (a) shows AFM images of a SF on ellipsoidal SF band, and (b) parts of interstitial type dislocation loops at inner part of ellipsoidal SF band in Fig. 1(a).

It was shown from the observation that SEPD corresponds to interstitial type dislocation loops with irregular shape [2]. The two points of the discrepancies between the experiments and the simulation are described as follows: First, in Fig. 4(a) of the 50 mm diameter crystal, it was found that the P1 and P2 peaks of the maximum densities of the SEPD consist of only stacking faults (SF) and correspond to P1 and P2 on the red ellipsoidal band in the lifetime map of Fig. 1(a), respectively. This shows that the points of the minimum lifetime correspond to those of the maximum density of the SEPD on the SFB (band). The SFB consists of only the SF which have a disk-like shape with a interstitial type dislocation loop to be surrounded by the dangling bonds. The existence of the SF's is confirmed not only by an optical microscope but also by AFM as shown in Fig. 5(a). On the crystal of 50mm in diameter, SEPD density was very high, but FPD density was nearly zero as shown in Fig. 4(a). This results show that the points P1 and P2 in Fig. 1(a) existed not in the V region but in the I region because the SF with dislocation loop is formed by the interstitials in the I rich region and the dangling bonds of the dislocations are the cause of the minimum lifetime. On the other hand, in the simulation by Dornberger et al. [8] shown in Fig. 1(a') the both positions corresponding to P1 and P2 exist in the V rich region in Fig. 1(a'). Also, this region is the outside of the diffused region of and far away from the growth interface that is only the source and the reservoir of interstitials. However, the experimental results showed that the SF density is of 3~4 x 106 cm-2 at these positions and the crystal has not vacancies to be confirmed by the zero density of the FPD as shown in Fig. 4(a). From the result described above, it is clear that there is the decisive discrepancy between the experimental and the simulation results. Second, as shown in Figs. 1(a') and (b') in the simulation, the low pulling rate region colored by blue indicates the maximum densities of interstitials by the boundary condition from Voronkov's model [9] that only the growth interface is the source and the reservoir of interstitials. However, the experimental results at the interface B including the SFB in Fig. 1(a) showed clearly not the maximum interstitial densities but rather depressed re-

gion denoted as "valley" in Fig. 1(a) and (b). Such interstitial depression distribution is also confirmed by the depressions of the SEPD densities as shown in the center region of Figs. 4(a) and (b). The depression region appeared not only in the 50 mm and 100 mm crystals but also in 200 mm crystal as shown by the growth interface B which is the concave shape with blue color in Fig. 1(c) and the corresponding minimum density of the SEPD in Fig. 4(c). This valley phenomenon by the low pulling rate was also reproduced by the other experiments as shown in Figs. 4 (d) and (e) and was shown in Fig. 2 in Roksnoer's paper [10] again. Figures 4(d) and (e) show clearly the valley phenomenon in the distributions of the SEPD of the 100 mm crystal along to the center line and 20 mm line from the edge, respectively. The growth parameters of this crystal were the same as those of the crystal of Fig. 1(b) except the higher stationary pulling rate of 1.8 mm/min instead of 1.0 mm/min. The average FPD densities in the outside region of Q1 and Q2 in Fig. 4(d) and (e) had the same value of 1 x 106 cm-3 , and this value was about three times higher than 3 x 105 cm-3 in Fig. 4(b). These results show that the FPD density depends on the pulling rate. The depleted FPD densities in Fig. 4(d), (e) are considered the effect of recombination with the increased SEPD due to the low pulling rate. A typical type of such recombination effect was also observed in the depression(from O1 to O2) of the FPD densities by the increasing of the SEPD densities due to the low pulling rate in Fig. 4(b). The depleted distribution of the FPD in Fig. 4(d) was also reconfirmed by the measurement of COP's (crystal originated particle) [11] using a particle counter. The COP is a void on a mirror- polished wafer which is the same as that of FPD [4]. The map of the COP in Fig. 4(f) was obtained from a neighboring mirror-polished wafer after so-called RCA cleaning. In the COP map each black point shows a scattered light point from a void. The positions of a, b in Fig. 4(d) and c, d in Fig. 4(e) correspond to the positions of a, b on center line and c, d on 20 mm from edge line in Fig. 4(f), respectively. In the simulation for the region of the low pulling rate, the interstitial density had the maximum as reservoir for interstitials [8] as seen from Figs. 1(a') and 1(b'). However, it was showed from the experimental results on the COP that the region of the maximum interstitial density in the simulation corresponded to that of the minimum interstitial density as described by the valley phenomenon. The FPD distributions in Fig. 4(d), (e) were reconfirmed by the COP distribution in Fig. 4(f). The speculated interstitial distribution to be deduced from the experimental results give the reverse distribution of that in the simulation. Hence, it is impossible for the simulation to give the experimental secondary defect distribution. Moreover, from AOP analyses [12, 13, 14] of the detaching experiments on crystals we clearly demonstrated that the growth interface is always filled with vacancies. The same result was also reported by Roksnoer in the detaching experiment of the pedestal crystals [10]. It will be reported in detail at the conference .

4. Conclusions

We showed that there are the many discrepancies between the point defects distribution by the simulation and the speculated point defect distribution by the analyses of experimental secondary defects as FPD, SEPD, COP, and AOP. Also, by the crystal detaching experiments from the melt, it is showed that the growth interface is always filled with vacancies. This shows that the growth interface is not the source and the reservoir of interstitials at the least. Moreover, Considering that the simulation is based on Voronkov's model, the discrepancies show that Voronkov's model itself is not suitable for the behavior of the intrinsic point defects in silicon crystals grown from the melt.

References

[1] T. Abe, K. Hagimoto, Proceedings of the Second International Symposium on Adv. Sci. and Tech. of Silicon Mat., 1996, p. 242.

[2] T. Abe, Materials Science and Engineerings, B73 (2000) 16.

[3] H. Yamagishi, I. Fusegawa, N. Fujimaki, M. Katayama, Semicond. Sci. Technol. 7 (1992) A135.

[4] M. Itsumi, H. Akiya, T. Ueki, M. Yamawaki, J. Appl. Phys. 78 (1995) 5984.

[5] M. Nishimura, Y. Yamaguchi, K. Nakamura, J. Jablonski, M. Watanabe, in: C.L. Cleays, P. Ray-Chauduhury, M. Watanabe, P. Stallhofer, H.J. Dawson (Eds.), High Purity Silicon V, The Electrochem. Soc. Ser. 98-13, Pennington, NJ, 1998, p.188.

[6] S. Sadamitsu, S. Umeno, Y. Koike, M. Hourai, S. Sumita, T. Shigematsu, Jpn. Appl. Phys. 32 (1993) 3675.

[7] H. Foell, B.O. Kolbesen, Appl.Phys. 8 (1975) 319.

[8] E. Dornberger, W. von Ammon, J. Virbulis, B. Hanna, T. Sinno, J. Cryst. Growth 230 (2001) 291.

[9] V.V. Voronkov, J. Cryst. Growth 59 (1982) 625.

[10] P.J. Roksnoer, J. Cryst. Growth 68 (1984) 596.

[11] J. Ryuta, E. Morita, T. Tanaka, Y. Shimanuki, Jpn. J. Appl. Phys. 29 (1991) L1947

[12] H. Harada, T. Abe, J. Chikawa, in: H.R. Huff, T. Abe, B.O. Kolbesen (Eds.) Semiconductor Silicon 1986, the Electrochem. Soc., Pennington, NJ, 1986, p. 76.

[13] T. Abe, T. Takahashi, J. Cryst. Growth 334 (2011) 16.

[14] K. Shirai, T. Abe, J. Cryst. Growth 351 (2012) 141.

WeP-G07
Wednesday afternoon, 14 August, 16:00
Room 211, Old Library

Break
Wednesday afternoon, 14 August, 17:30

Thursday, 15 August

ThO1

G07: Defect formation/elimination
Thursday morning, 15 August, 10:20
Room D, Auditorium Maximum

10:20 Invited oral

Imaging defects during growth of seeded directionally solidified mono-like silicon for photovoltaic applications

Maria Tsoutsouva[1], Denis Camel[2], Thu Nhi Tran Thi[1], José Baruchel[1], Benoit Marie[2], Vanessa Amaral de Oliveira[2], Tamzin Lafford[1]

1. *European Synchrotron Radiation Facility (ESRF), Grenoble 38043, France* **2.** *CEA-INES (INES), Savoie Technolac, Le Bourget du Lac 73370, France*

e-mail: maria.tsoutsouva@esrf.fr

The main challenge of industrial-scale production of photovoltaic devices is the growth of large, high quality Si monocrystals at a much lower cost than that of microelectronics quality crystals. Directional solidification has become a very promising method for achieving this. With the use of an extended monocrystalline seed, high quality "mono-

like" Si crystals [1, 2] can be grown. However, multiple seeds are needed in order to grow large crystals and that fact raises the question of growth at the boundary between seeds. In the present work, we investigate the early stages of Si solidification in the region where the liquid Si penetrates between two seeds, and the evolution of the crystal growth from this region. Synchrotron radiation Bragg imaging (white beam, monochromatic section topography, "weak beam" images) was applied to samples grown from melted silicon on oriented seeds with a small gap between them. The images showed the subgrain boundary and even very low subgrain misorientation could be measured, while the generation and evolution of dislocations during growth was followed. Besides X-ray diffraction imaging, Scanning Electron Microscopy (SEM) and micro-Fourier Transform Infrared Spectroscopy (μ-FTIR) mapping were applied, the latter showing the elemental distributions of oxygen, iron and carbon.

In the present study, two cases are examined of samples cut parallel to the growth directionas shown in the SEM images in Figure 1. In Figure 1A we observe the presence of two distinct, vertical, resolidified zones between the seeds; and in Figure 1B, the existence of a hole is observed in the same area. As the regrowth proceeded from the seeds, the presence of a sub-grain boundary was observed between the two seeds in both cases.

With the aid of white beam image topography (Figure 2) we observe that in both cases the solidified Si is built of two separate sub-grains which are slightly misoriented but both of them are well crystallized and follow the crystallographic orientation of the seed. However, in case A, networks of dislocations are generated at the top edges of the resolidified zones, while in case B, no such bunches of dislocations are observed.

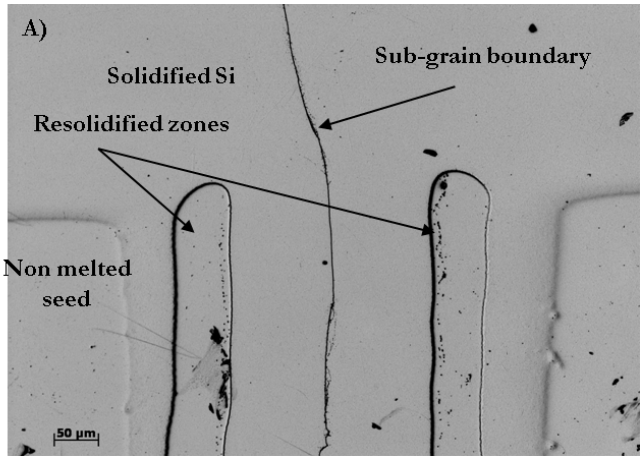

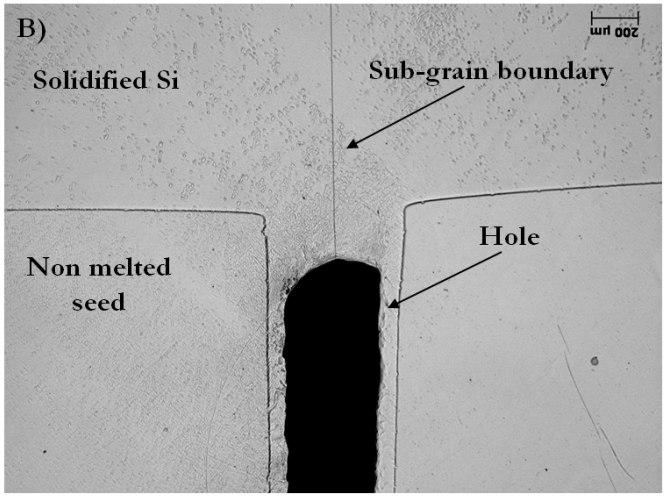

Figure 1: SEM images of the solidified zone between the seeds, parallel to the growth direction, for the two cases that are stud-

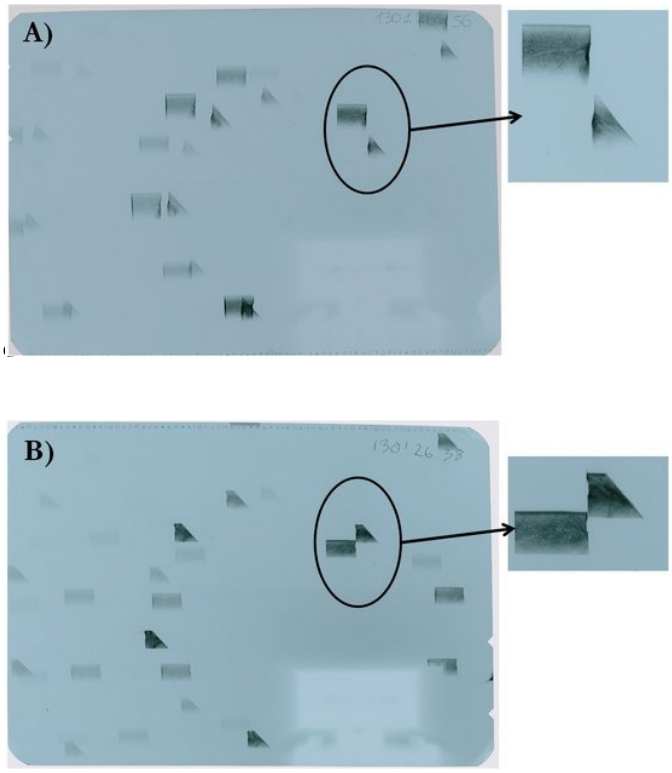

Figure 2: White beam diffraction images, of the solidified zone between the seeds, for the two cases, showing the misorientation between the two subgrains.

Dislocations are associated with deterioration in the minority carrier lifetime as measured using the Light-Beam Induced Current method. μ-FTIR mapping showed a particular distribution of contaminants in the resolidified zones in case A. A model is proposed in order to explain the probable formation mechanism of the resolidified zones between the seeds during the solidification process, and their possible influence on the observed development of a dislocation network is discussed.

[1] A. Jouini *et al*., Prog. Photovolt: Res. Appl.20 (2012) 735-746

[2] M. Trempa *et al*., J. Cryst. Growth 351 (2012) 131-140

10:50 Invited oral

Nucleation and dislocations cores in semi conductors: from macrostructures to nanostructures

Jacques Rabier, Jean-Luc Demenet, Julien Godet, Laurent Pizzagalli

Institut P', UPR 3346 CNRS université de Poitiers ENSMA (DPMM), Futuroscope 86962, France

e-mail: jacques.rabier@univ-poitiers.fr

Depending on their dimensions semiconductor materials can sustain very different stress levels before failure. Indeed nanostructures can support extremely high stresses as compared to those usually encountered at a macroscopic scale. As a consequence the nucleation of dislocations in devices or crystals with different sizes will occur at very different stress levels.

In order to reproduce the high stress conditions reached in nanostructures, two experimental techniques have been used: high-pressure deformation on bulk materials and plastic deformation of micro and nano pillars. Transmission Electron Microscopy (TEM) has been conducted

on deformation microstructures in order to analyze dislocation core structures. Concurrently the nucleation of dislocations has been studied in various conditions of stress and temperature by using atomistic simulations.

This paper aims at reviewing the effect of stress and size on the dislocation nucleation in semi conductor materials. Results on silicon will be presented. Both simulations and TEM observations converge in showing that in silicon dislocation core configurations have different nature depending on the temperature and nucleation stress [1]: perfect dislocations are found to be nucleated at high stress as compared to dissociated dislocations at moderate stress. The properties of such core structures will be discussed. Although most of the experiments and simulations are relevant to silicon, this behavior is common to a number of semiconductor materials. Indeed this impacts also silicon carbide [2] in which stresses usually favor polytypes formation whereas perfect dislocations nucleated at very high stresses do not contribute to any phase transformations.

[1] Rabier J, Pizzagalli L and Demenet J L 2010, Elsevier B.V. Dislocations in Solids, Edited by J.P. Hirth and L. Kubin (North-Holland, Amsterdam), 93, 47

[2] Demenet J L, Amer M, Tromas C, Eyidi D and J. Rabier J 2013, pssc 10, 64

11:20 Oral

Evolution of threading screw dislocation conversion during solution growth of 4H-SiC

Shunta Harada, Yuji Yamamoto, Kazuaki Seki, Atsushi Horio, Takato Mitsuhashi, Miho Tagawa, Toru Ujihara

Department of Materials Science and Engineering, Nagoya University, Furo-cho, Chikusaku, Nagoya 464-8603, Japan

e-mail: harada@numse.nagoya-u.ac.jp

Silicon carbide (SiC) is a promising material for next-generation power device because of its excellent physical properties. For high-performance SiC power devices with long-term reliability, the improvement of crystal quality is essential. Solution growth has an advantage to grow high quality crystals because the condition is close to thermal equilibrium. Recently, we have revealed that threading screw dislocations (TSDs) in seed crystal are efficiently converted into the defects on the basal plane during the solution growth of 4H-SiC. By using the TSD conversion during the solution growth, we have successfully grown high quality 4H-SiC with extremely low TSD density. However, the details of the highly efficient TSD conversion are still not clear. In the present study, we investigate the evolution of TSD conversion during the solution growth of 4H-SiC by synchrotron X-ray topography. Single crystals of SiC were grown on off-axis seed crystals by top-seeded solution growth method.

During the solution growth on a vicinal seed crystal, almost all TSDs were converted to the defects on the basal planes by the macrosteps advancing toward step-flow direction as shown in Fig. 1. In the X-ray topography image of the grown crystal, the length of the basal plane defects was different with each other. The length of the basal plane defect is proportional to the depth where the TSD conversion occurs. Therefore the distribution of the defect length indicates that the TSD conversion stochastically take place during the growth. Figure 2 shows the evolution of the residual TSDs with different growth thickness. The TSD density was exponentially decreased and after the 10 micrometer growth there are no TSDs in the measured area corresponding to the TSD density of below 25 cm^{-2}, which is smaller than that of the commercial SiC wafers by two orders of magnitude.

Similar TSD conversion has been reported in the epitaxial growth of SiC by chemical vapor deposition (CVD). However, the conversion ratio is as low as 1% in CVD within the growth of about 20 μm. The TSD conversions during CVD were reported to occur only at the interface between substrate and growth layer. On the other hand, the TSD conversions during solution growth intermittently take place during the growth, which leads to the highly efficient TSD conversion.

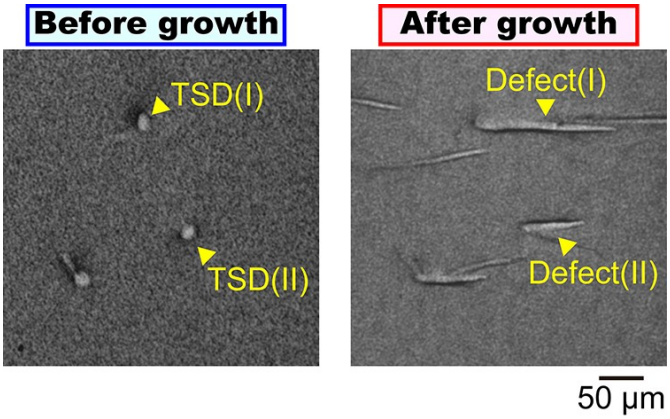

Figure 1. X-ray topography images before and after the solution growth. The length of the Defect (I) and Defect (II) is different, which indicates that the TSD conversions occurred at different depth.

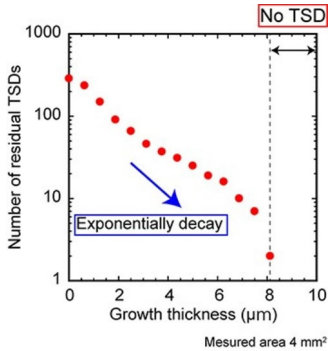

Figure 2. The number of residual TSD density with the different growth thickness in the area of 2 × 2 mm^2. The TSDs were exponentially decreased and after the 10 micrometer there are no TSDs in the measured area.

11:35 Oral

Coupling effects of Te inclusions and the surrounding extended defects in bulk-grown CdZnTe crystals

Yadong Xu[1,2], Wanqi Jie[1,2], Tao Wang[1,2], Yihui He[1], Yuecun Wang[1]

1. *Northwestern Polytechnical University, Xi'an 710072, China*
2. *State Key Laboratory of Solidification Processing, Xi'an 710072, China*

e-mail: xyd220@nwpu.edu.cn

Recently, CdZnTe (CZT) detectors have emerged as the dominant semiconductor room temperature radiation detectors. However, their wide deployment is hampered by the low availability of high-quality CZT crystals. Among which, material's inhomogeneity in bulk grown CZT crystals, especially due to the structure imperfections, still creates a 'bottle-neck' in state of the art wafer assessment and screening. It has been widely reported that the presence of Te-rich secondary phase

particles (inclusions) in CZT crystals tends to affect the structural uniformity, in turn dominates the properties of spectrometer-grade CZT crystals. Therefore, Te inclusions in CZT crystals and the effects of Te inclusions on the energy resolution of CZT detectors have been studied numerically and experimentally for the last years. However, more and more evidences suggest that not only Te inlusions, but also their induced extended defects would influence CZT detectors' performance.

In this work, the generation and coupling effects mechanisms of Te inclusions and their induced defects are discussed. Employing surface-etching techniques, Te inclusions on $(111)_{Cd}$, and $(111)_{Te}$ surfaces of CZT crystals were observed using a field emission scanning electron microscope (FE-SEM) and a cathodoluminescence (CL) microscopy. The coupling effects between Te inclusion and the induced dislocations were discussed by analyzing the dislocations rosette surrounding Te inclusions. Finally, a focused ion beam/scanning electron microscope (FIB/SEM) was used to prepare thin sections for transmission electron microscopy (TEM) studies. The phase structure and lattice deformation of local areas were identified by HRTEM. It was suggested that the dislocation enriched region was proportional to the volume of the originating Te inclusion.

11:50 Oral

The subgrain boundaries in CMSX-4 superalloy

Robert Albrecht[1], Włodzimierz Bogdanowicz[1], Jan Sieniawski[2], Krzysztof Kubiak[2]

1. *University of Silesia, Institute of Materials Science (INOM), 75 Pułku Piechoty 1A, Chorzów 41-500, Poland* **2.** *Rzeszow University of Technology, Rzeszów, Poland*

e-mail: ralbrecht@us.edu.pl

Single-crystal nickel-base superalloys are widely used as material for turbine blades in advanced aircraft engines and stationary gas turbines. As these elements are critical for flight safety much attention should be given for preventing the casting defects. However, dendritic structure and complex shape of turbine blades tend to create many growth defects. Therefore, the macroscopic investigation of the turbine blades is fundamental for preventing damage during service.

In the paper single-crystal turbine blade roots made of CMSX-4 have been investigated. Material for research was produced in Research and Development Laboratory for Aerospace Materials at Rzeszów University of Technology. Casts were obtained in ALD Vacuum Technologies by the Bridgman technique. One stage of solution heat treatment was then conducted on the samples. X-ray topography, Laue method, novel X-ray diffraction mapping and scanning electron microscopy were applied to study the crystal quality of the samples. It was found that in the root part of the blades the macroscopic low angle boundaries were present. The angles of subgrains misorientation were calculate from the X-ray topograms. Additionally, misorientation angles were defined from X-ray diffraction maps obtained by using the diffractometer of EFG company. By mapping the lattice parameter changes near the low angle boundary were presented. The presence of low angle boundaries were then confirmed by SEM . The mechanism of subgrains formation and influence of elements were described.

12:05 Oral

Self-organized substructuring during bulk crystal growth

Peter Rudolph

Crystal Technology Consulting (CTC), Helga-Hahnemann-Str. 57, Schönefeld 12529, Germany

e-mail: rudolph@ctc-berlin.de

Dislocation substructures belongs to small angle grain patterns which are already well studied in bended and rolled metals and alloys due to their essential effect on material strength. But there is also an increasing need for clarification of such features in semiconductors and dielectric crystals because they markedly influence the device quality. For instance, in as-grown semi-insulating GaAs, important for production of low-noise high-frequency devices, a mesoscopic resistivity variation does occur due to the accumulation of As_{Ga} antisite defects (EL2) along the low-angle grain walls that requires a well sophisticated after-annealing step. Further, the wide application of $Cd_{1-x}Zn_xTe$ crystals as most promising candidates for radiation-detection systems is still hindered by the charge-transport non-uniformities along such cellular substructures which, additionally, are decorated by impurities and secondary phase particles affecting the energy and spatial resolution too. Or, in multicrystalline silicon (mc-Si) for photovoltaic an enhanced recombination is occurred due to metal decoration in combination with oxygen at the subgrain boundaries leading to degradation of carrier life time and, thus, solar cell efficiency. Finally, as it is well known in crystals for optical applications, such as CaF_2 for UV photolithography, subgrain networks impair the transparency and resolution quality.

Undoubted, there is a correlation between substructures and stored dislocations. It is also well known that dislocation networks are observed in crystals independently by which method of phase transition they have been grown[1]. However, the origins and genesis of their appearance can be somewhat varied. Let's differ in three processes – i) dynamic polygonization (DP) in the course of plastic relaxation due to thermomechanical stress, ii) high-temperature dislocation dynamics (DD) combining glide with point-defect assisted claim, and iii) morphological instability of the propagating crystallization front in the form of cellular interface shape. Of course, i) and ii) are close correlating. However, whereas DP requires in any case stress-related driving force DD implies along with screening effects also evidences of self-organized (dissipative) structuring in the course of irreversible thermodynamics (de facto, each directional crystallization system is an "open" one steadily importing and exporting energy). DD takes place at high temperatures where the point defect diffusivity is still high enough. It is noteworthy that the formation of spatial cellular patterns is only possible when three-dimensional dislocation movements like climb and cross glide can take place. Glide alone could be not responsible for. Actually, as it was observed by real-time synchrotron x-ray topography on Al the cell formation takes place near (some millimetre) behind the propagating interface[2].

In general, dislocation cell structures consist of walls with high dislocation density separated by interiors of markedly dislocation-reduced or even dislocation-free material. The ripening level depends on various material and process parameters like dislocation density and mobility as well as stress-time devolution, respectively. The genesis is also markedly influenced by obstacles such as second phase particles, large angle grain boundaries or sessile dislocations.

The detailed analysis by x-ray synchrotron topography of dislocation cells in as-grown 6" vapor-pressure-controlled GaAs crystal showed that the dislocations are accumulated in fuzzy walls[3]. Typically, numerous junctions and pins form a sessile dislocation jungle which is rather

stable against post-growth annealing. Only very small mean tilt angles around 10 arcsec do exist between the cells. In comparison, in CdTe, PbTe, mc-Si and CaF_2 the matrix contains still numerous isolated dislocations and the cell walls are formed much sharper consisting of only one row of dislocation pits as it can be ascertained by transmission electron microscopy[4]. Such behaviour is well-known from the standard type of polygonized low-angle grain boundaries (primary subgrain formation) containing only the excess dislocations of similar Burgers vector after the annihilation is completed. Tilt angles of 60 - 120 arcsec were reported for such crystals[5]. Obviously, compared with GaAs in these materials the substructure reacts much more sensitively to variations of the stress field acting during crystal growth. Additionally, in II-VI and IV-VI substances the dislocation mobility is markedly enhanced compared with III-Vs. Finally, the point defect situation is of crucial influence on the DD. For instance, it was shown that the minimization of the native point defect content by nearly stoichiometric growth of compounds restrains cellular structures[6] as it was prognosticated numerically[7]. In mc-Si ingots grown under typical *v/G*-conditions (*v* - growth velocity, *G* - temperature gradient) > 1.34 x 10^{-3} cm^2/K min[8] the generation of vacancies dominates which are immediately absorbed by the presented dislocations. As a result, the dislocations are able to claim enhancing globular cell formation.

Ascertaining the mean cell diameter thanks to the rules of correspondence being valid for most materials[9] we are able to estimate the value of once acting thermo-mechanical stress. At first, after Holt's relation $dr^{1/2} \cong 10$ (*d* - cell diameter, *r* - dislocation density) there is a correlation between cell size and dislocation content. According to the rule of Kuhlmann-Wilsdorf $d = K\ G\ bt^{-1}$ (*G* - shear modulus, *b* - Burgers vector, *t* - shear stress, *K* - constant » 20) a mean cell diameter of 100 µm within in as-grown crystal correlates with a formerly *t* of about 3-5 MPa. Finally, Taylor's rule $t = KG\ br^{½}$ shows the relation between stress and expected dislocation density. Of course, from these relations follows that substructures should be damped by adherence of lowest as possible thermomechanical stress during growth, i.e. assurance either of even or as it was postulated by Indenbom[10] polynomial shaped isotherms. Additionally, solution hardening by doping in order to increase the critical resolved shear stress proves to be helpful[1].

As it was demonstrated by real-time synchrotron x-ray topography on Al-Cu alloys[11] also a cellular interface shape, generated by constitutional supercooling (origin iii), is able to redirect and collect growing-in dislocations along the elongated grain boundaries. It seems that charac-teristic substructures in low-temperature solution-grown THM $Cd_{1-x}Zn_xTe$ and $Hg_{1-x}Cd_xTe$ crystals are correlating with such mode, especially, due to the high Te enrichment as solvent ahead the crystallization front. An effective mixing measure is required to prevent morphological instability and tellurium inclusions.

Finally, as was mentioned above, locally and temporally varying growth parameters should be considered. This leads to gradients and flows - the basic preconditions of irreversible thermodynamics. According Kubin[12] in either case, the plastic flow is not uniform at a fine scale. The inhomogeneous release of elastic energy gives rise to the emission of acoustic waves (avalanches) interplaying with stored sessile dislocations and micro obstacles (precipitates, vacancy condensations). In the course of cooling down sporadic clouded dislocation patterns are frozen up remembering our well-known cluster structures in mc-silicon. Thus, it will be hard for crystal growers to maintain perfect homogeneously distributed stored dislocations.

1. P. Rudolph, Crystal Res. Technology 40 (2005) 7.

2. G. Grange, C. Jourdan, A.L. Coulet, J. Gastaldi, J. Crystal Growth 72 (1985) 748.

3. T. Tuomi et al., J. Crystal Growth 237 (2002) 350.

4. K. Durose, G.J. Russel, J. Crystal Growth 86 (1988) 471.

5. P. Rudolph, Progr. Crystal Growth and Characterization 29 (1994) 275.

6. P. Rudolph, C. Frank-Rotsch, U. Juda, F. Kiessling, Mat.Sci.Engin. A400 (2005) 170.

7. B. Bako et al, Computational Materials Science 38 (2006) 22.

8. V.V. Voronkov, J. Crystal Growth 59 (1982) 625.

9. M. Zaiser in: G. Müller et al. (eds.), Crystal Growth (Elsevier 2004) p. 215.

10. V.L. Indenbom, Kristall und Technik 14 (1979) 493.

11. G. Grange, B. Billia, J. Phys. France 4 (1994) 293.

12. L. Kubin, Dislocations, mesoscale simulations and plastic flow (Oxford Univ. 2013).

Lunch (EMCG meeting)

Thursday afternoon, 15 August, 12:20

ThO2

G07: Defect formation/elimination
Thursday afternoon, 15 August, 14:00
Room D, Auditorium Maximum

14:00 Invited oral

Thick metamorphic buffer layers grown by hydride vapor phase epitaxy as platforms for novel semiconductor devices

Kevin L. Schulte[1], Tae Wan Kim[2], Adam W. Wood[3], Brian T. Zutter[1], Nickolas T. Meyer[3], Susan E. Babcock[3], Luke J. Mawst[2], Thomas F. Kuech[1]

1. *University of Wisconsin-Madison, Department of Chemical and Biological Engineering, Madison, WI 53706, United States* **2.** *University of Wisconsin-Madison, Department of Electrical and Computer Engineering, Madison, WI 53706, United States* **3.** *University of Wisconsin at Madison, Department of Materials Science and Engineering, 1509 University Avenue, Madison, WI 53706, United States*

e-mail: kschulte2@wisc.edu

The design and manufacture of advanced, epitaxial semiconductor devices is critically dependent on the availability of single crystal substrates with negligibly low levels of extended defects. The substrates available commercially which posses sufficiently low defect densities and sufficiently large wafer areas only include 3 lattice constants: GaP/Si (5.45 Å/5.43 Å), GaAs/Ge (5.65 Å/5.66 Å), and InP (5.87 Å). Design of epitaxial devices is thus limited by this constraint, since the growth of a thin film with a lattice constant even a fraction of a percent different from that of the substrate soon accumulates significant numbers of defects once the 'critical' layer thickness is reached. The ability to develop devices without regard for lattice constant would fundamentally change the manner in which they are designed, and expand the palate of materials and alloy systems available to crystal growers. One of the most promising routes to new lattice constants is the metamorphic buffer layer (MBL), in which a ternary (or higher order) alloy is grown on a commercial substrate, starting at the lattice matching composition and grading until a composition corresponding to the desired lattice constant is reached. Instead of forcing a suboptimal device onto one of the commercially available substrates,

the device itself can be optimized and the substrate tailored to that device.
Since dislocations are required to accommodate the misfit between the substrate and epilayer, the goal of MBLs is to relax the misfit strain by introducing dislocations in a controlled manner which confines them to the graded region. An optimal MBL has zero residual strain and a threading dislocation (TD) density equal to, or even lower than, that of the original substrate. Limitation of processes which impede dislocation glide is crucial as blocked dislocations provide less strain relief compared to dislocations which can lengthen without limitation. Then fewer dislocation half loops are required to achieve the same strain relaxation and the total number of accompanying threading segments, which intersect the surface, is minimized. A common strategy in the literature involves the use of slow grading rates which space out dislocations, decreasing the likelihood that dislocations will interact and impede each other. Phase separation also creates glide impediments which lead to increased dislocation densities, and the choice of growth conditions that avoid phase separation is necessary as well.
Hydride vapor phase epitaxy (HVPE) is an attractive technique for the growth of MBLs. Its characteristically high growth rates makes the growth of thick grading layers at slow grading rates feasible, allowing ample spacing between dislocations. Growth is common at temperatures higher than those employed by molecular beam epitaxy (MBE) and metal-organic vapor phase epitaxy (MOVPE), which promotes rapid dislocation glide. Since HVPE growth temperatures are well above the spinodal temperatures of common ternary systems like $GaAs_xP_{1-x}$, $In_xGa_{1-x}As$, and $In_xGa_{1-x}P$ and growth proceeds much closer to equilibrium than in MBE and MOVPE, phase separation is potentially mitigated in HVPE layers. Lastly, the high growth rates make the growth of a sacrificial polishing layer possible. The use of chemical mechanical planarization techniques reduces the surface roughness inherent to mismatched growth by all types of vapor deposition allows the creation of an 'epi-ready' surface with a new lattice constant.
This work will demonstrate the growth and subsequent device integration of HVPE-grown $In_xGa_{1-x}As$ and $GaAs_xP_{1-x}$ MBLs. The relationships between grading style, grading rate, final x (in $In_xGa_{1-x}As$ or $GaAs_xP_{1-x}$), and deposition temperature on buffer layer properties were explored. The suitability of the MBLs as a platform for device growth was characterized through the measurement of surface residual strain, threading dislocation density, and root mean square (RMS) surface roughness. Defect structure was analyzed by transmission electron microscopy and related to measured macroscopic layer parameters. Guidelines for buffer layer design and optimization will be offered. The potential for device incorporation through the growth and polishing back of a sacrificial layer was demonstrated through the growth of quantum cascade laser type superlattices on planarized HVPE surfaces.

14:30 Oral

Behavior of defects in a-plane GaN films grown by Low-Angle-Incidence Microchannel Epitaxy (LAIMCE)

Noriyuki Kuwano[1], Yuki Ryu[2], Masatoshi Mitsuhara[2], Chia-Hung Lin[3], Shota Uchiyama[3], Takahiro Maruyama[3], Yohei Suzuki[3], Shigeya Naritsuka[3]

1. *University of Technology Malaysia (UTM), Jalan Semarak, Kuala Lumpur 50400, Malaysia* **2.** *Department of Applied Science for Electronics and Materials, Kyushu University (ASEM), Kasuga Kohen, Kasuga 816-8580, Japan* **3.** *Faculty of Science and Technology, Meijo University (MU), 1-501 Shiogamaguchi, Tempaku-ku, Nagoya, Nagoya 468-8502, Japan*

e-mail: noriyuki.kuwano.577@m.kyushu-u.ac.jp

Gallium nitride (GaN) grows usually in wurtzite structure ($P6_3mc$) that does not have the center of symmetry, and then it has the crystallographic polarity (thereafter called polarity). The polarity causes the piezoelectricity leading to the quantum-confined Stark effect. Since the wurtzite structure has the strong polarity along *c*<0001>, many efforts have been made so far to grow films along the direction other than *c*<0001>, such as non-polar direction m[01-10] or a[2-1-10] [1-4] and semi-polar direction normal to (11-22) or (1-101) [5-8]. Unfortunately, thin films grown in such directions usually contain a lot of lattice defects. In this work, a-plane GaN thin films were grown by a novel method of the "low-angle-incidence microchannel epitaxy (LAIMCE) " [9-10]. Cross sectional transmission electron microscope (TEM) observation was performed to analyze the behavior of lattice defects in order to clarify the effects of the present method on the growth of high-quality non-polar thin films. Special attention was paid to the difference in the behavior of defects between the wing-areas that grew along +*c* and -*c* directions.

An *a*(2-1-10) plane GaN template with a stripe type SiO_2 mask was prepared on a *r*(01-12) sapphire substrate. The mask had seed-windows of 3 μm wide and terraces of 7 μm wide. GaN was overgrown on the template by the metal-organic MBE using TMG and NH_3 at 860ºC. The source gases were injected from the direction of +*c*[0001] of GaN. The injection angles were 5º for TMG and 45º for NH_3. The polarity of GaN was distinguished from the difference in growth rate along *c*-direction under a certain growth condition (larger growth rate along +*c* direction). Thin foil specimens for TEM observation were made by using a focused-ion-beam (FIB) mill, followed by final finishing with an Ar^+ ion mill. TEM characterization was carried out with a microscope of JEM-2000EX at accelerating voltage of 200 kV. The polarity of GaN was also confirmed from the relationship between the +*c* direction of wurtzite structure and the direction of *c*-axis of the *r*-plane sapphire substrate [11]. Burgers vectors ***B*** of lattice defects were analyzed by the conventional ***gB*** method.

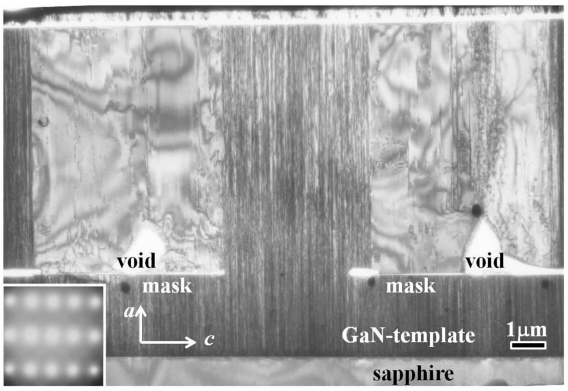

Fig.1 TEM bright-field image of *a*-plane GaN taken with [01-10] zone-axis incidence

Figure 1 shows a TEM micrograph of *a*-plane GaN grown by the present method. The micrograph was a bright field image taken with [01-10] zone-axis incidence. It is clearly seen that the overgrown thin film has a very smooth and flat surface of *a*-plane. The GaN template contains a large density of threading dislocations (TDs), and some of the TDs propagate through the seed-windows, running straight up to the top-surface of the overgrown thin film. The density of TDs in the GaN template was roughly estimated to be of the order of 10^{10} cm^{-2}, and the region in the overgrown layer has almost the same dislocation density over the seeding windows. From the ***gB*** characterization, most of the TDs were confirmed to be of (*a*+*c*) type. As these TDs do not bend in the overgrown layer, there are regions without TDs on the mask-terraces. The dislocation density is estimated to be less than 2 x 10^8 cm^{-2} at most.

Inside the overgrown GaN thin film, a large void and small ones remain on the center and the ends of mask-terrace, respectively. The large voids are thought to remain on the terrace of mask after the wing regions coalesce with each other. As the large void is located at the center of terrace, the growth rates at +*c* and -*c* direction were almost the same as each other under the present growth condition. In other words, the regions of right-hand side and left-hand side are formed by the growth along -*c* and +*c*, respectively. One can see faint image-contrasts in the both wing regions over the mask-terraces. They are due to lattice defects that have been formed during the lateral growth of GaN. When the incident beam of TEM was parallel to [1-100], stacking faults (SFs) on the basal plane usually cannot be observed. By observation after tilting the TEM specimen, it was found that the both wing regions contain SFs on the basal planes. In *c*-plane GaN layers grown by the conventional way, there are scarcely such SFs. This suggests that the growth process of the wing regions is different from the case of conventional *c*-plane growth in spite that the wing regions were thought to be formed also by the *c*- plane growth at the early stage.

We performed further TEM observation with different conditions in order to reveal the microstructure in the regions over the mask-terraces. Behavior of basal stacking faults and the effects of +*c*/-*c* growth direction on the lattice defects was discussed. A new method for a high quality GaN layer is proposed.

References

[1] F. Wu et al.: J. Appl. Phys., 94, 942 (2003).

[2] Z. Lilietan-Weber et al.: Opto-Electr. Rev., 12, 339 (2004)

[3] M. Araki et al.: Jpn. J. Appl. Phys., 47, 119 (2008)

[4] N. Kuwano et al.: Phys. Stat. Sol., C6(52), S494 (2009)

[5] A. E. Romanov et al.: J. Appl. Phys., 100, 023522 (2006).

[6] H. Masui et al.: IEEE Trans. Electr. Device, 57, 88 (2010).

[7] Z. H. Wu et al., Appl. Phys. Lett. 98, 051902 (2011).

[8] T. Kuwahara et al., Phys. Stat. Sol., C9(3/4) 488 (2012).

[9] G. Bacchin et al. J. Cryst. Growth 208, 1 (2000).

[10] C-H. Lin et al.: J. Cryst. Growth, 318, 446 (2011).
[11] J. K. Liu: J. Appl. Phys. 46, 3703(1975).

14:45 Oral

Morphology and formation mechanism of metallic inclusions in VB-grown sapphire crystals

Toshinori Taishi[1], Takumi Kobayashi[2], Minami Shinozuka[2], Etuko Ohba[2], Chihiro Miyagawa[1,2], Keigo Hoshikawa[1]

1. *Shinshu University, 4-17-1 Wakasato, Nagano 380-8553, Japan*
2. *Fujikoshi Machinery Corp. (FMC), 1650 Kiyono Matsushiro-machi, Nagano 381-1233, Japan*

e-mail: taishi@shinshu-u.ac.jp

With regard to microscale defects in sapphire crystals, many research studies reporting small bubbles of the size of 2 - 10 μm in EFG- [1] or CZ-grown crystals [2] have been published. However, there have been few reports about inclusions in sapphire crystals. Danko et al. reported hexagonal-shaped Al3O4 inclusions in sapphire crystals grown by the horizontally oriented crystallization method [3]. Recently, we reported the vertical Bridgman (VB) technique for growing c-axis sapphire crystal using a tungsten (W) or a molybdenum (Mo) crucible [4]. This paper reports the morphology and formation mechanism of inclusions observed in VB-grown sapphire crystals.

Sapphire boules grown by the VB process using a W or a Mo crucible in an Ar atmosphere at 1 atm were cut into wafers, which were lapped and polished. The wafers were evaluated using a laser scattering observation technique to confirm the distribution of microscale light-scattering defects. Inclusions in the sapphire wafers were characterized using an optical microscope and a field emission scanning electron microscope (FE-SEM). The compositions of the inclusions were evaluated by energy dispersive X-ray spectrometry (EDS) working in the FE-SEM.

Cubic, pentagonal or hexagonal-shaped inclusions with a size of 2 - 3 μm were observed in sapphire crystals grown using a W crucible. Figure 1 (a) shows a back-scattered electron image of an inclusion, and Figs. 1 (b) to (d) show the EDS mapping images of related elements Al, O and W, respectively. It was found that such inclusions consisted of W, which was the material used for the crucible. Similar-shaped Mo inclusions with the size of about 20 μm were observed in crystals grown using a Mo crucible.

We concluded that the morphology of inclusions reflects a rhombic dodecahedron, which is based on the cubic structure of W and Mo and is surrounded by {110} faces.

[1] K. Wada et al., J. Cryst. Growth **50** (1980) 151-159.
[2] H. Li et al., Optical Mater. in press.
[3] A. Ya. Danko et al., Functional Mater. **10** (2003) 217-223.
[4] C. Miyagawa et al., J. Cryst. Growth in press.

15:00 Oral

Defect elimination by optimizing starting materials in Lithium Niobate crystals

Ravi Ganesan[1], Kitamura Kenji[2]

1. *Department of Physics, Alagappa University,, Karaikudi 630 003, India* **2.** *National Institute of Material Science (NIMS), Tsukuba, Japan*

e-mail: gravicrc@gmail.com

Lithium niobate is one of the very promising materials found in the literature since its applicability in various field especially optical waveguides, SAW devices, optical modulators and optical data storage (1-5). In the present study, pure and doped near stoichiometric LN crystals have been grown by top seeded solution growth technique using platinum crucible at air atmosphere. The crucible placed inside a three-tier ceramic insulation tube coupled to the RF heating coil to reduce the axial temperature gradients. Various melt compositions were chosen to eliminate the inherent defects normally found in the LN crystals. The grown crystals were free from inclusions, twins, voids and cracks and were single domain in nature when observing through polarizing microscope. The effect of dopants on the homogeneity of the crystals has been studied. The determined Curie temperatures of all the samples taken from top to bottom are found to be same, which confirms that the crystals are highly homogeneous. The segregation coefficient of the dopants is found from the AES-ICP analysis. The improved light induced absorption has been obtained for the high Li content crystals. The properties related to optical data storage has been studied. The results will be presented in detail.

References:

1. Y.Yang, D. Psaltis, M. Luennemann, D. Berben, U. Hartwig and K. Buse, J. Opt. Soc. Am. B 20 (2003) 1491 - 1502.
2. Dongdong Teng, Biao Wanga, Tao Geng, Furi Ling Fu, Opt. Las. Tech. 39 (2007) 1125 – 1129.
3. S. Kar, Sunil Verma, M.S.Khan, K.S.Bartwal, Cryst. Res. Techn. (2009) 1-5.

4. T.Bodziony, S.M.Kaczmarek and R.Kruk, Rev.Adv.Mater.Sci. 23(2010) 1-7.
5. K. Buse, A. Adibi and D. Psaltis, Nature 393 (1998) 665 - 668.

15:15 Oral

Characteristic Void Alignment in Sapphire Crystals Grown by the Vertical Bridgman Method

Junya Osada, Takaomi Suzuki, Toshinori Taishi, Keigo Hoshikawa

Shinshu University, 4-17-1 Wakasato, Nagano 380-8553, Japan

e-mail: josada@shinshu-u.ac.jp

A relationship between growth rates and void alignments in sapphire crystals grown by the vertical Bridgman method is experimentally investigated and the alignments and shapes of voids are discussed in the context of the growth rate and temperature gradient in the growth process.

Sapphire crystals of about 50mm in diameter and about 100mm in length were grown in a sealed chamber including a hot-zone constructed with a graphite heater, carbon felt heat-shields and a crucible made of Mo or W. The shape, size and distribution of voids in three crystals grown with crucible translation speeds of 3, 5 and 10 mm/h respectively were characterized by optical microscope and laser scattering observation techniques.

Slight voids of the size of several or several tens of micro-meters were detected with irregular distributions in the crystals grown with translation speeds of 3 and 5 mm/h. On the other hand, a high density of voids with characteristic alignments was observed in the crystal grown of 10mm/h. The alignments consisted of three-fold symmetries of void distributions in the c-plane, perpendicular to the growth axis. The shapes of voids showed the characteristic facet corresponding to crystal symmetry and temperature gradient in the growth processes.

It was concluded that the generation of high density voids and their alignment was strongly related to the cellular growth and to the volumetric shrinkage when the sapphire melt solidified to crystal[1)].

<References>

(1) K. Wada et. al: Jpn. J. Appl. Phys. Vol.17 No.2 (1978) pp.449-450.

15:30 Oral

Investigation of Defects in $ZnGeP_2$ Single Crystals by X-ray Topography on Base of Borrmann Effect

Alexey Okunev[1], Galina A. Verozubova[2], Chunhui Yang[3], Chongqiang Zhu[3], Valery Tkal[4], Inga A. Zhukovskaya[4], Vladimir Staschenko[1]

1. *Yaroslav the Wise Novgorod State University, Bolshaya St-Petersburgskaya 41, Novgorod the Great 173003, Russian Federation* **2.** *Insitute of Climatic and Ecological Systems of SB RAS (IMCES), 10/3 ave Akademicheskii, Tomsk 634055, Russian Federation* **3.** *Harbin Institute of Technology (HIT), No.92, West Da-Zhi Street,Harbin, Heilongjiang, Harbin 150001, China* **4.** *Saint Petersburg State University of Service and Economics (SUSE), Kavalergardskaja, 7, St-Petersburg 191015, Russian Federation*

e-mail: alexei.okunev@mail.ru

Single crystals of ternary semiconductor compound $ZnGeP_2$ with chalcopyrite structure are used as a high-performance medium for conversion of laser frequency radiation in the middle IR, what allows to solve a lot of problems of high-resolution spectroscopy. The crystals are also very promising for creation of sources of tunable THz radiation. Literature data about real $ZnGeP_2$ structure are practically absent.

In present contribution an analysis of structural defects in $ZnGeP_2$ crystals by X-Ray transmission topography for the first time has been carried out. $ZnGeP_2$ single crystals are grown by seeded Vertical Bridgman method from melt in Institute of Monitoring of Climatic and Ecological Systems SB RAS (Tomsk, Russia) and Single Crystal Growth Laboratory in School of Chemical Engineering, Harbin Institute of Technology (Harbin, PRC).

The state-of-the-art results in $ZnGeP_2$ growth with sufficiently perfect structure allow to register a presence of Borrmann effect and to apply X-Ray topography method based on this effect (XRBT method) [1]. The method has a high sensitivity to defects of crystal lattice and it has already shown its high effectiveness for a wide group of semiconducting materials such as Ge, Si, GaAs, SiC, and monocrystalline alloys of Bi-Sb [2]. The identification of defects by X-Ray transmission topography, based on Borrmann effect also shows that our $ZnGeP_2$ has a rather perfect structure, since only perfect crystals can be studied by this method. Additional methods in this work were method of topography in back reflection geometry and the method of photoelasticity (birefringence contrast method). Comparison of the information received by various methods of topography is spent.

It was studied the distribution of defects in the crystal volume, the factors affecting for distribution and density of dislocations was identified. Examples of topographs of cross-section and longitudinal slices of $ZnGeP_2$ ingots are shown on Fig. 1 and Fig. 2 respectively.

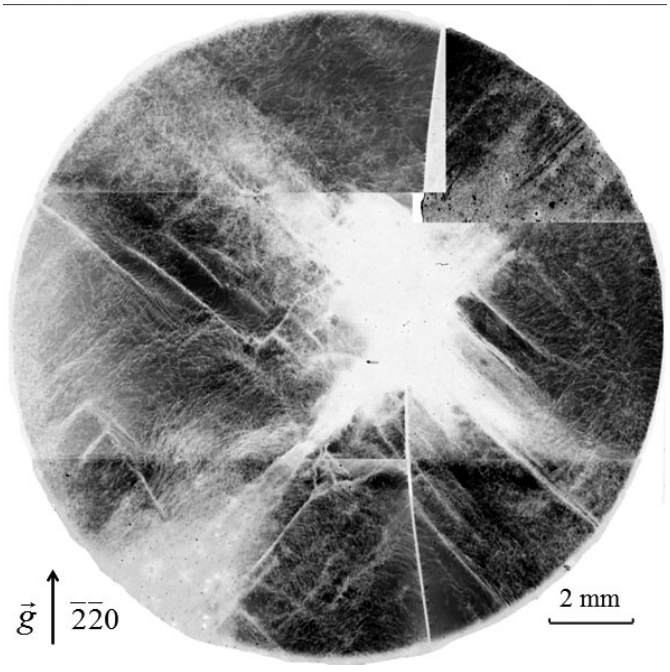

Fig. 1. Example of topograph of cross-section cut of $ZnGeP_2$ ingot.

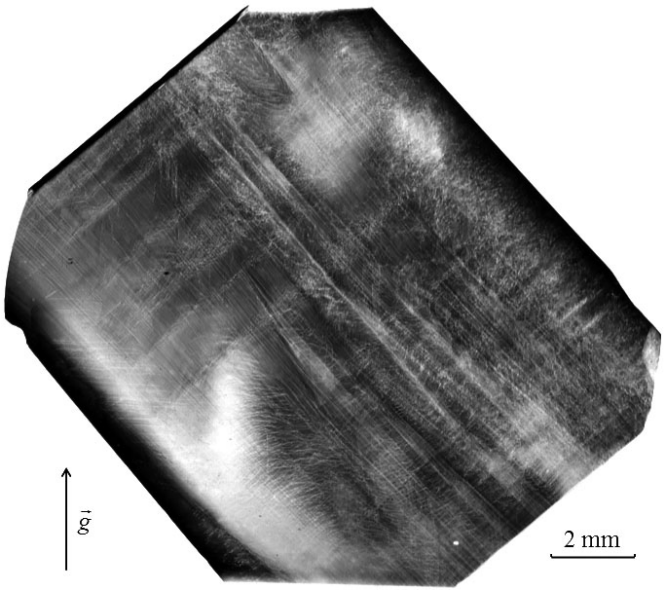

Fig. 2. Example of topograph of longitudinal cut of $ZnGeP_2$ ingot.

By XRBT method images of all the main types of defects of crystal lattice – three-dimensional, or volume (large inclusions, dislocation networks, the elastic stress fields), two-dimensional, or planar (twins and stacking faults, Fig. 3), one-dimensional (dislocations of different slip systems), quasi-point defects (micro-inclusions of various types and small dislocation loops) were found and identified in ZnGeP2 crystals.

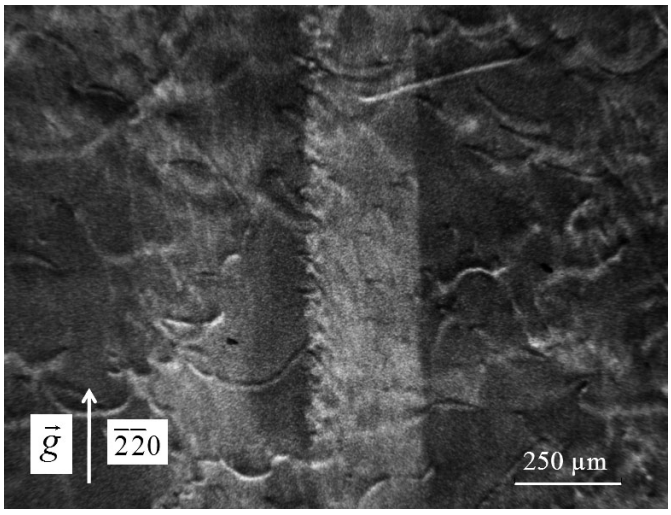

Fig. 3. Magnified image of giant growth stacking fault in sample cut perpendicular to the growth axis of the $ZnGeP_2$ crystal.

In addition, the contrast from specific defects of this material – dislocations with strong impurity atmosphere and chains of inclusions, known as «solute trails» was observed also. Images of these defects were studied and described.

Under certain conditions, at the XRBT method defect is formed an image in form of contrast rosette with multiple petals. For example, the rosette is formed, if the axis of the dislocation lies in the reflection plane of the crystal along the direction of propagation of the energy of the X-ray wave field. Microdefect forms a rosette of contrast, if it located at a smaller distance from the output to X-rays surface of the sample than the "depth of vision" of the defect. Examples of images in the form of contrast rosettes from edge dislocations are shown in Fig. 4. Fig. 5 and Fig. 6 demonstrate examples of images of microdefects (small dislocation loops and microinclusions of second phase, respectively).

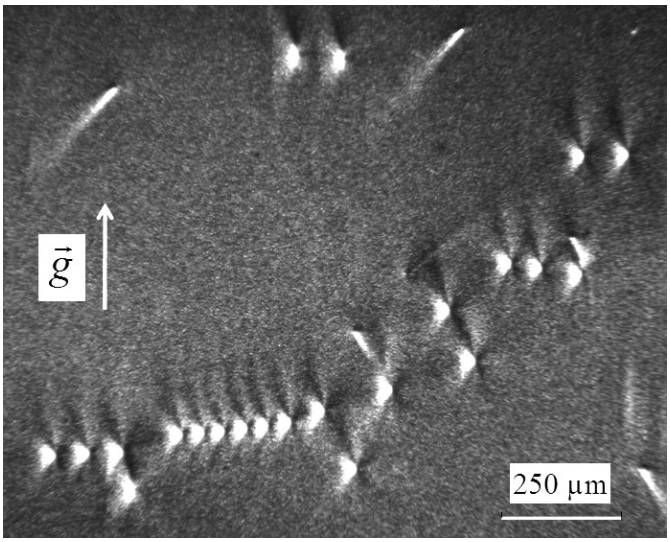

Fig. 4. Rosettes of contrast from edge dislocations in $ZnGeP_2$.

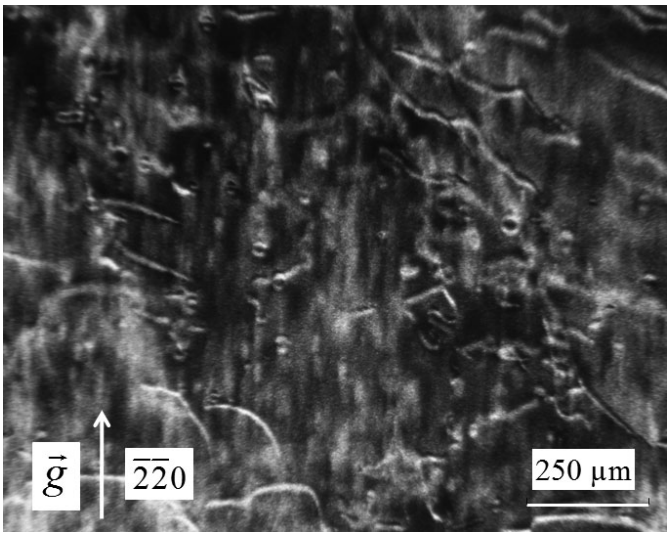

Fig. 5. Images of small dislocation loops.

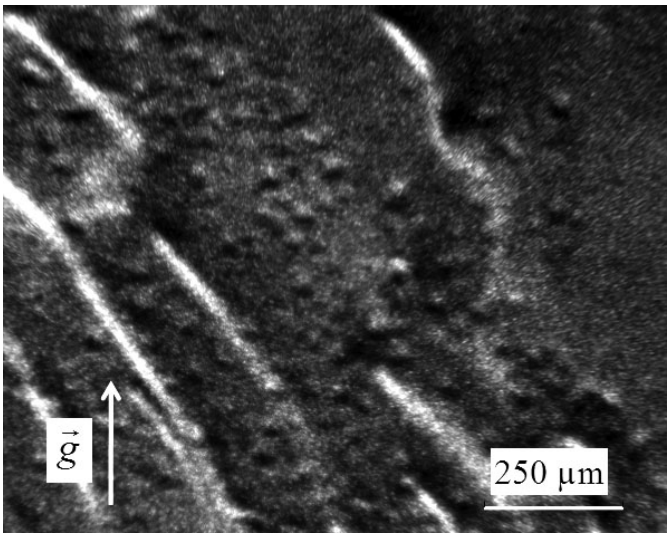

Fig. 6. Topograph of a sample area with high density of "vacancy" type microdefects.

Identification of defects is carried out by comparing of their images on the experimental topographs with simulation ones or with already decoded images of defects. For the computer simulation a semi-phenomenological theory of contrast on the basis of Indenbom–Chamrov's equations modified by L.N. Danil'chuk may be used. Recently the possibility of direct simulation of dislocation images in thick absorbing crystals by solving of Takagi equations was shown [3]. Images of "rosette" type for the same defect in different materials are similar, differing in size, proportions and the character of shape changes by varying one of the parameters (for example, at changing the depth of the microdefect location) [2]. XRBT method differs from other methods of X-ray topography due to higher informativeness and reliability. From the images in the form of contrast rosettes we can identify all main parameters of defects reliably and unequivocally: for dislocations these are direction of a dislocation axis, direction, sign and magnitude of the Burgers vector, and for microinclusions the type of lattice strain (microdefect of "vacancy" type or "interstitial" type), the power of the defect and the depth of its location in the crystal volume.

Obtained results show great possibilities of the "rosette" technique of topography in registration and study of structural defects in $ZnGeP_2$ crystals. A revelation of features of experimental topographs and their comparison with theoretically calculated will allow to create an atlas of experimental and calculated topographs of defects in $ZnGeP_2$, revealed by X-Ray transmission method based on Borrmann effect. This atlas in future should sufficiently simplify the study of real structure of $ZnGeP_2$ crystals.

This work was partially supported by RFBR grant № 12-02-00201.

1. A.O. Okunev, G.A. Verozubova, E.M. Trukhanov, I.V. Dzjuba, P.R.J. Galtier and S.A. Said Hassani // J. Appl. Cryst. (2009), Vol. 42, pp. 994–998.

2. L. Danilchuk, A. Okunev, V. Tkal, X-Ray Topography on Base of Borrmann Effect (LAP LAMBERT Academic Publishing, Saarbrücken, 2012), p. 348.

3. I.A. Smirnova, E.V. Suvorov, E.V. Shulakov // Fizika Tverdogo Tela (rus), 2007, Vol. 49, No. 6, pp. 1050–1056.

Coffee

Thursday afternoon, 15 August, 16:00

ThO3

G07: Defect formation/elimination
Thursday afternoon, 15 August, 16:30
Room D, Auditorium Maximum

16:30 Invited oral

Development of properties and functionalities by precise control of rare earth doping to semiconductors

Yasufumi Fujiwara, Atsushi Koizumi

Graduated School of Engineering, Osaka University (OSAKAUNIV), Osaka, Japan

e-mail: fujiwara@mat.eng.osaka-u.ac.jp

Luminescent and magnetic properties of rare-earth (RE) elements doped in insulators and metals have been well investigated and they have been successfully applied to practically-used fluorescent substances and magnets. In these applications, however, either luminescent or magnetic property has been independently used. Furthermore, research on the RE-doped materials has been based on experienced trial-and-error, not on *material design* by precise control of RE doping and understanding of energy-transfer mechanism.

RE-doped semiconductors are a new class of materials with various promising potentials. RE ions doped in semiconductors exhibit a characteristic emission due to the intra-*4f* shell transitions of RE ions. The intra-*4f* shell transitions give rise to sharp emission lines whose wavelengths are largely independent of both the host material and temperature. This stability occurs because the filled outer *5s* and *5p* electron shells screen transitions within the inner *4f* electron shell from the interaction with the host. We have intensively investigated RE-doped III-V semiconductors grown by atomically-controlled organometallic vapor phase epitaxy (OMVPE) and fabricated new types of light-emitting diodes (LEDs) with the materials.

In Er,O-codoped GaAs (GaAs:Er,O), one kind of Er center is formed selectively as an Er atom located at the Ga sublattice with two adjacent O atoms (hereafter referred as Er-2O) together with two As atoms, resulting in drastic enhancement in intensity of Er-related luminescence due to the intra-4*f* shell transitions of Er^{3+} ions [1]. GaAs:Er,O homostructure and double-heterostructure (DH) LEDs were fabricated by OMVPE, which exhibited successfully 1.5 mm electroluminescence (EL) due to the Er-2O center under forward bias at room temperature [2,3]. The dependence of the EL intensity on the injection current density indicated extremely large excitation cross section of Er ions by current injection ($1\sim2 \times 10^{-15}$ cm^2) in the LED, which is larger by five orders in magnitude than optical excitation cross section in conventional Er-doped fiber amplifiers ($10^{-20}\sim10^{-21}$ cm^2).

RE-doped GaN has been identified as a promising candidate for the realization of white LEDs, displays, and lasers. Eu^{3+} ions have been widely used as red-emitting phosphors for cathode ray-tube and plasma display panels. In these applications, the ions are doped into an insulator and red emission is obtained mainly by optical excitation. GaN is an attractive host material for Eu doping because its wide bandgap allows visible wavelength emission from Eu ions and reduces the thermal quenching effect for the emission intensity. We have grown Eu-doped GaN (GaN:Eu) by OMVPE and observed successfully bright red emission due to the intra-4*f*shelltransitions of Eu^{3+} ions from a LED with the GaN:Eu as an active layer[4]. The main emission line with a half-width of less than 1 nm was observed at 621 nm, which can be assigned to the $^5D_0$–$^7F_2$ transition of Eu^{3+} ions. Notably, no band-edge and defect luminescence was observed under bias conditions, indicating that the Eu luminescence is caused by the ultrafast energy transfer from the GaN host to the Eu^{3+} ions. These results suggest a novel method of realizing GaN-based red LEDs, which are an alternative to conventional toxic As-containing AlGaInP/GaAs red LEDs, and a monolithic device composed of red, green andblue GaN-based LEDs for full-color display or lighting technology.

Significant improvement in device performance has been achieved by optimizing growth parameters and device structures. The atmospheric-pressure growth of GaN:Eu drastically increased the light output power of the Eu emission, which is due to the increased number of optically active Eu centers and efficient energy transfer by the reduced non-radiative processes in the GaN host [5]. Furthermore, Eu,Mg-codoped GaN (GaN:Eu,Mg) showed an approximately five-fold improved Eu intensity at room temperature [6,7]. An additional emission center created by Mg codoping and its unique behavior under thermal annealing were also observed. With increasing active layer thickness in the LED, on the other hand, the output power increased monotonically. In the presentation, current status of the RE-doped semiconductors and their LEDs is reviewed.

References: [1] K. Takahei and A. Taguchi, J. Appl. Phys. **74**, 1979 (1993). [2] A. Koizumi, Y. Fujiwara, A. Urakami, K. Inoue, T. Yoshikane and Y. Takeda, Appl. Phys. Lett. **83**, 4521 (2003). [3] A. Koizumi, K. Inoue, Y. Fujiwara, T. Yoshikane, A. Urakami and Y. Takeda, Jpn. J. Appl. Phys. **42**, 2223 (2003). [4] A. Nishikawa, T. Kawasaki, N. Furukawa, Y. Terai, and Y. Fujiwara, Appl. Phys. Express **2**, 071004 (2009). [5] A. Nishikawa, N. Furukawa, T. Kawasaki, Y. Terai, and Y. Fujiwara, Appl. Phys. Lett. **97**, 051113 (2010). [6] D. Lee, A. Nishikawa, Y. Terai, and Y. Fujiwara, Appl. Phys. Lett. **100**, 171904(2012). [7] D. Lee, R. Wakamatsu, Y. Terai, and Y. Fujiwara, Appl. Phys. Lett. **102**, 141904(2013).

17:00 Oral

Influence of acceptor and donor dopants on PZN-PT single crystals

Srimathy Balasubramanian, Sharon Gloria, Jayavel Ramasamy, Kumar Janakiraman

Crystal Growth Centre, Anna University, Chennai, Chennai 600025, India

e-mail: marsjk@annauniv.edu

Single crystals of lead zinc niobium titanium oxide (1-x)$Pb(Zn_{1/3}Nb_{2/3})O_3$-x$PbTiO_3$ (PZN-PT) grown at their morphotrophic phase boundary (MPB) composition (x = 9 mol%) are widely used in multilayer capacitors, micro-electro mechanical systems (MEMS) and integrated devices owing to high values of piezoelectric coefficient (d_{33}) and electromechanical coupling factor (k_{33}). However, an urge to increase the d_{33} and quality factor (Q_m) of the material lead to adding dopants in PZN-PT to tune their properties. Hence PZN-9%PT single crystals were grown by doping 0.5 mol% Nd, 0.5 mol% W and 0.5 mol% Cr by high temperature solution growth (flux technique). For the growth of doped crystals, the soaking temperature and time was increased in order to achieve good solubility and homogeneity. Addition of donor dopants (Nd and W) lowered the growth rate which was inferred from the reduced size of the crystals whereas acceptor doping (Cr) doesn't have much influence on the crystal size. Also a notable colour change was seen after doping with Nd and W (brownish yellow) and with Cr (dark brown). Figure 1 shows the pictures of as grown crystals of (a) Nd-doped, (b) W-doped and (c) Cr-doped PZN-PT crystals respectively. Perovskite phases of the crystals were confirmed by X-ray diffraction. Influence of defects (oxygen vacancies) created during growth process because of Pb evaporation as well as due to doping on the dielectric, ferroelectric and piezoelectric properties of the crystals were investigated in detail and the results will be presented.

Fig. 1 As grown (a) Nd-doped PZN-PT (b) W-doped PZN-PT (c) Cr-doped PZN-PT

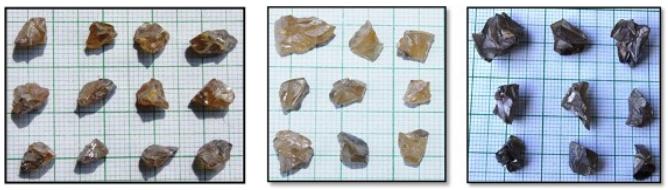

17:15 Oral

Structure, Domain Configuration and Frequency Dependent Dielectric Properties of PMN-PFN-PT Single Crystal

Nengneng Luo[1], Qiang Li[1], Qingfeng Yan[1], Yiling Zhang[2], Zhiguo Xia[3], Xiangcheng Chu[2]

1. *Department of Chemistry, Tsinghua University, Beijing 100084, China* **2.** *State Key Laboratory of New Ceramics and Fine Processing, Tsinghua University, Beijing 100084, China* **3.** *School of Materials Science and Technology, China University of Geoscience, Beijing 100083, China*

e-mail: luonn1234@163.com

$Pb(Mg_{1/3}Nb_{2/3})O_3$-$Pb(Fe_{1/2}Nb_{1/2})O_3$-$PbTiO_3$ (PMN-PFN-PT) single crystal was grown successfully by slow cooling method. Structure, domain configuration and frequency dependent dielectric properties of [001]-oriented as-grown single crystal had been analyzed. X-ray diffraction and polarized Raman spectra analyzed indicated a pure perovskite phase with tetragonal symmetry at room temperature. Domain configuration of the poled [001]-oriented PMN-PFN-PT was observed for the first time using a polarized light microscopy (PLM). Domain on (001) face exhibited a straight stripe-like morphology with domain size on the scale of 10um, and the extinction of 90^o domains at P/A:0^o revealed a tetragonal structure. Dielectric permittivity of [001]-oriented single crystal at room temperature exhibited a strong dependence with frequency and decreased sharply with increasing frequency.

17:30 Oral

Site structures and antisite defects of impurity-doped lithium niobate

Chihiro Koyama, Kensaku Maeda, Jun Nozawa, Kozo Fujiwara, Satoshi Uda

Institute for Materials Research, Tohoku University, 2-1-1, Katahira, Aoba-ku, Sendai 980-8577, Japan

e-mail: c.koyama@imr.tohoku.ac.jp

Lithium niobate ($LiNbO_3$: LN) is a piezoelectric material, and it has been used as nonlinear optical device. A crystal is grown from the congruent melt to obtain homogeneous composition. During the crystal growth, antisite defect (Nb_{Li}) is generated because of excess Nb in LN. The Nb_{Li} causes photorefractive damage, which hinders optical application of LN. Regarding this problem, Zhong et al. (1980) found that MgO doping increased the damage resistance. However, it has not been fully understood how doping of impurities such as MgO affects to the defect formation which lead to optical damage. In the present study, site structures and Nb_{Li} behavior have been investigated by measuring lattice constants and curie temperatures (T_c) of LNs with changing impurity concentration. Lattice constants of congruent LN(c-LN) doped with respective impurities (MgO, ZnO, Fe_2O_3, TiO_2, ZrO_2) were measured by XRD. Site structure changes caused by impurity doping were analyzed with variation of lattice constants with impurities. The analyses show that Mg, Zn and Fe were incorporated into Li-site, which decreased Nb_{Li}, in contrast Zr and Ti were incorporated into Nb-site, which increased Nb_{Li}. T_cs of impurity-doped LNs were measured by DSC with changing a composition of LN along with two different series of A and B. In A series, impurities were doped to stoichiometric LN keeping Nb_2O_5 concentration to be 50 mol%. In B series, they were doped to c-LN keeping Li/Nb to be constant. In A series, T_c didn't change, in which Li/Nb changed and Nb_{Li} was con-

stant. In B series, on the other hand, T_c changed, in which Li/Nb was constant and Nb_{Li} changed. T_c has been believed to depend on Li/Nb in the non-doped LN (O'Bryan et al. 1985). However, from these results, we can conclude that T_c of doped LN depends on Nb_{Li} concentration instead of Li/Nb. Measurement of lattice constants and T_c reveal that the Nb_{Li} to be decreased by doping of Mg, Zn and Fe whereas increased by Zr and Ti.

17:45 Oral

Study on Site Occupancy of Metal Vacancy in Langasite-type Crystal with Four Elements

Hengyu Zhao, Jun Nozawa, Kensaku Maeda, Haruhiko Koizumi, Kozo Fujiwara, Satoshi Uda

Tohoku University, Institute for Materials Research (IMR), 2-1-1, Katahira, Aoba-ku, Sendai 980-8577, Japan

e-mail: hengyu_zhao@imr.tohoku.ac.jp

Langasite-type (LGS-type) crystal with four elements in $A_3BC_3D_2O_{14}$ structure has been intensively studied as a group of piezoelectric crystal[1,2]. Recently, we have found the amount of thermally activated holes in LGS-type crystal depends on metal vacancy ($V_m^{\times}$), which crucially affects conductivity of bulk crystal[3]. However, no study on the site occupancy of $V_m^{\times}$ has been carried out in LGS-type crystal with four elements so far.

Site occupancy model (SOM) is able to raise all the possible site-structure of constituent elements and corresponding defects. In LGS-type crystal, $Ca_3TaGa_3Si_2O_{14}$ (CTGS), 6 site-structures out of 16 are possible but not essential to exist. So,solid solution range (ss range)was determined in CTGS to verify which site-structuresexist.

3 compositional series of CTGS were synthesized: 1. Ca,Ta-stoichiometric (-s), changing Ga and Si ratio; 2. Ca,Si-s, changing Ga and Ta ratio; 3. Ca,Ga-s, changing Ta and Si ratio, as shown in Fig. 1. Secondary phases were observed with backscattering electron image (BEI). In the sintered materials, four kinds of secondary phases in the composition of $CaTa_2O_6$ (CT2), $Ca_3Ta_2Ga_4O_{14}$ (CTG), $CaSi_2O_5$ (CS2) and $Ca_3Ga_4Si_2O_{13}$ (CGS) were recognized. The lever rule was applied to obtain ss range from composition and relative quantity of secondary phases. In CTGS, ss range locates at Ca-s, Ta, Ga-poor and Si-rich area, the calculated composition of the boundary of ss range was shown in Fig. 1. Only one of the 6 possible site-structures is applicable in CTGS, which shows B site accommodates $V_m^{\times}$. The quantitative relationship between $V_m^{\times}$and antisite defect is also deduced by this SOM site-structure: $5Si_{Ga}$- V_{Ta}=0, where Si_{Ga} is Si population in Ga site. This result indicates $V_m^{\times}$ in CTGS bulk crystal will generate significant amount of holes at elevated temperature, which is harmful to conductivity stability. This work suggests the method that SOM discussion accompanied with ss range measured by investigating secondary phase is valid to study site of $V_m^{\times}$in a certain LGS-type crystal.

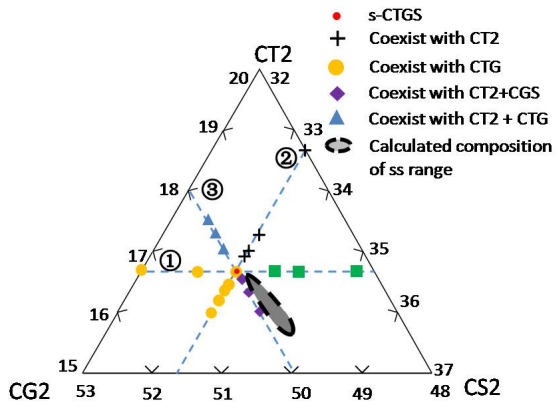

[1] S.Zhang, et al., J.Appl.Phys105, 114107 (2009).

[2] B.Mill,et al., Russ.J.Inorg.Chem.43, 1270 (1998).

[3] R. Yaokawa et al. J.Appl.Phys108, 064112 (2010)

18:00 Oral

Study on defects in hydrothermal-grown RbBe2BO3F2 crystals

Haitao Zhou[1], Lijuan Liu[2], Xiaoling He[1], Fuhua Lu[1], Changlong Zhang[1], Chuangtian Chen[2]

1. *China Nonferrous Metal Guilin Geology And Mining Co., Ltd. (CNMC), Guilin 541004, China* **2.** *Technical Institute of Physics and Chemistry, beijing 100190, China*

e-mail: haitao83@gmail.com

Several NLO crystals have been used in the past to produce DUV coherent light, but so far only $KBe_2BO_3F_2$ (KBBF) and $RbBe_2BO_3F_2$ (RBBF) can produce DUV harmonic generation by second harmonic generation (SHG). The major disadvantage of KBBF and RBBF is the crystal growth. Large sizes of high quality single crystals are very difficult to obtain, which seriously affects further applications. The hydrothermal growth of KBBF can yield much thicker crystals than flux method, but cannot be applied to generating DUV laser because of their much lower SHG conversion efficiency [1]. However, sizeable crystals of $RbBe_2BO_3F_2$ (RBBF) which grown by the hydrothermal method show similar capability for frequency conversion compared with flux grown crystals [2].

In order to find the reason, extensive studies on defects in hydrothermal-grown RBBF crystals were carried out for the first time. Dislocations, grain boundaries and twins were revealed and observed on the (001) plane of hydrothermal-grown RBBF crystals by chemical etching and microscopy. X-ray rocking curves indicate the hydrothermal-grown crystals are of high crystalline quality. Moreover, powder X-ray diffraction measurements show no unidentified peaks for hydrothermal-grown RBBF crystals. These indicate the hydrothermal-grown RBBF crystals may not contain structural defects, different from hydrothermal KBBF [3-4].

Acknowledgement: This work was supported by Guangxi Natural Science Foundation (2011GXNSFB018014).

**corresponding author e-mail: lufuhua81n@163.com*

References:

[1] Chen, C. T., et al. "Deep-UV nonlinear optical crystal KBe2BO3F2—discovery, growth, optical properties and applications." *Applied Physics B* 97.1 (2009): 9-25.

[2] Liu, Lijuan, et al. "Hydrothermal growth and optical properties of $RbBe_2BO_3F_2$ crystals." *Journal of crystal growth* 348.1 (2012): 60-64.

[3] Yu, Jinqiu, et al. "Superstructure and stacking faults in hydrothermal-grown KBe_2BO_3 F_2crystals." *Journal of Solid State Chemistry* 184.10 (2011): 2790-2793.

[4] Sang, Yuanhua, et al. "X-ray and neutron diffraction studies of flux and hydrothermally grown nonlinear optical material KBe2BO3F2." *CrystEngComm*14.18 (2012): 6079-6084.4

Break
Thursday evening, 15 August, 18:30

Posters

Wednesday, 14 August

WeP-G07
Wednesday afternoon, 14 August, 16:00
Room 211, Old Library

16:00 Poster We195

Effect of Gamma Irradiation on deep levels detected by DLTS in $GaAs_xN_{1-x}$ with different Nitrogen concentration

Mohsin Aziz[1], Jorlandio F. Felix[2], Riaz H. Mari[3], Noor alhuda Al saqri[1,4], Dler A. Jameel[1], David Taylor[1], Mohamed Henini[1], Almontaser Khatab[1]

1. *School of Physics and Astronomy, University of Nottingham, Nottingham NG72RD, United Kingdom* **2.** *Universidade Federal de Viçosa (UFV), Av. P. H. Rolfs, sn, Viçosa 36570-000, Brazil* **3.** *Institute of Physics, University of Sindh, Jamshoro 76080, Pakistan* **4.** *Sultan Qaboos University, P.O Box 36, Physics Dept.,, Muscat 0123, Oman*

e-mail: ppxma2@nottingham.ac.uk

Introduction: The addition of nitrogen atoms into gallium-arsenide (GaAs) leads to a remarkable band-gap reduction, which originates predominantly from a downward of the conduction band edge. Due to this circumstance, GaNAs as well as other III-V-N alloys are strong candidates for various applications in semiconductor electronics, such as solar cells and GaAs-based telecommunication laser diodes [1]. The scientific literature suggests that the Irradiation of GaAs samples with high-energy radiation can leads to production of lattice defects in the form of vacancies, defect clusters and dislocations. Thus in this work it was investigated the effect of gamma radiation (γ-ray) on GaAs samples prepared with different concentrations of Nitrogen. The results shown that the number of defects induced in the sample can be monitored, it indicates that this system can be possibly used as a material for the development of sensors devices to γ-ray.

Experimental: The GaAs samples used in this study were grown by different Nitrogen concentrations of 0.2%, 0.4%, 0.8% and 1.2% [2]. These samples were irradiated with a gammacell Cobalt Irradiator (dose rate of 5.143 KGy/hour) with various doses (up to 50 kGy). The effects of γ-ray were studied by deep level transient spectroscopy (DLTS) and Laplace DLTS [3].

Results and Discussion: GaAs with different Nitrogen concentrations were subjected to ^{60}Co γ-ray irradiation and the effects of γ-ray irradiation have been studied in this work by DLTS. DLTS is a powerful tool to study these effects, which induce to the formation of energy levels within the band gap which can act as trapping and recombination centers for carriers. The DLTS measurements on gamma irradiated sample found that with small Nitrogen contents (0.2% and 0.8%) most of defects are compensated. However irradiation did not compensate defects with higher Nitrogen concentration. If the defects induced by γ-ray can be monitored by electrical / electronic measurements techniques this system could be used as a semiconductor sensor device for gamma radiation.

References:

[1] M. Henini, Dilute Nitride Semiconductors (Elsevier Ltd., Oxford, 2005) and references therein.

[2] R.Kudrawiec, et al. (2012) Appl. Phys. Lett., *101*, 082109
[3] M. Shafi, et al. (2009) Phys. Status Solidi C *6*, No. 12, 2652–2654

16:00 Poster We196

The growth rate impact on the crystal perfection of single-crystalline CMSX-4 turbine blades

Jacek Krawczyk[1], Włodzimierz Bogdanowicz[1], Robert Albrecht[1], Jan Sieniawski[2], Krzysztof Kubiak[2]

1. *University of Silesia, Institute of Materials Science (INOM), 75 Pułku Piechoty 1A, Chorzów 41-500, Poland* **2.** *Rzeszów University of Technology, Department of Materials Science, W. Pola 2, Rzeszów 35-959, Poland*

e-mail: wlodzimierz.bogdanowicz@us.edu.pl

The single-crystalline turbine blades of CMSX-4 Nickel-based superalloy were studied. The turbine blades were produced by Research and Development Laboratory for Aerospace Materials in Rzeszów University of Technology by the Bridgman method. Five different withdrawn rates were used in the crystallization processes conducted in a ALD vacuum furnace.

The main phase in alloy of all obtained blades was the cubic γ′ phase. Samples for investigations were prepared by cutting the blades perpendicular to its axial direction. Changes in crystal orientation and lattice parameter of γ′ phase along the camber line of blades were analysed. The structural parameters maps (maps of γ′ lattice parameter and components of disorientation angles) were obtained by the original OD-EFG X-ray diffractometer. The changes of essential structure parameters between leading edge area and trailing edge area of the blades were determined. The SEM technique was used for complementing the X-ray mapping results, obtained by OD-EFG diffractometer. The results were compared with the results of X-ray topography reflection method.

16:00 Poster We197

Study of the zig-zag grain boundary in multicrystalline silicon

A. Nadri, Thierry Duffar, Y. Duterrail-Couvat, S. Epure

SIMaP EPM, CNRS UJF, BP 75, Saint Martin d'Heres cedex 38402, France

e-mail: thierry.duffar@grenoble-inp.fr

There are numerous Grain boundaries (GB) in photovoltaic multicrystalline silicon, with the drawback of decreasing the solar cell efficiency. While those GB are generally straight or bended, some of them have a zig-zag shape. We developed a theoretical model [1] in order to describe the origin and development of GB during the solidification of the silicon ingot. The theoretical model developed in [1] describes the origin and development of GB during the solidification of the silicon ingot. One of the conclusions of the model is that [111] facets may exist at the liquid-grain-grain triple line during growth. Zig-zag grains are predicted to occur when the facet of one grain becomes parallel or perpendicular to the solid-liquid interface. In such cases, another facet of the [111] family appears on this grain, replacing the wrongly oriented one. A numerical simulation (performed with ANSYS Fluent) of heat transfer in the vicinity of the faceted groove shows that the new facet is likely to subsist for some time. Consequently the GB orientation changes and the new facet becomes wrongly oriented, then shifting to the initial one.

The objective of this work is to validate experimentally this theoretical expectation. In this purpose, appropriate zones in Si ingots were selected, cut and polished at places showing zig-zag GB. These samples were analyzed by EBSD with a SEM in order to find the crystallographic orientation of the two grains forming the GB. The orientation of the [111] planes in both grains are compared and the possibility that one of them is perpendicular or parallel to the S/L interface is discussed. It appears that the experimental observations are in agreement with the model.

[1] "The solid-solid-liquid triple line and its effect on the grain structure of multi-crystalline photovoltaic silicon" T. Duffar and A. Nadri, C. R. Ac. Sci. Ser. Physique, 14 (2013) 185–191.

16:00 Poster We198

Comparison of various methods for large scale dislocation density characterization

B. Gallien[1], Thierry Duffar[1], J. P. Garandet[2], S. Bailly[2], G. Stokkan[3]

1. *SIMaP EPM, CNRS UJF, BP 75, Saint Martin d'Heres cedex 38402, France* **2.** *CEA-CNRS-Université de Savoie (INES), 24 Avenue Lac Léman, Le Bourget du Lac 73370, France* **3.** *SINTEF, R. Birkelands vei 2B, Trondheim 7034, Norway*

e-mail: thierry.duffar@grenoble-inp.fr

In the industry of silicon for photovoltaic application, the crystalline quality of the material is an important criterion as much as duration of the solidification process or the kerf loss due to the sawing of the ingot in wafers. Indeed, defects in the crystal lead directly to a decrease of photovoltaic efficiency of a solar cell.

Defects in the crystal matrix can be grain boundaries, precipitates, impurities or dislocations, which are the issue of this study. In the material, dislocations are generated by the application of a stress, generally created by the thermal field or the attachment between the crucible and the ingot. The dislocation have intrinsic activity due to the presence of dangling bonds at its core, but also act indirectly through the trapping of metallic impurities or their role as nucleation centers for oxygen precipitates, meaning that dislocations are often efficient minority carrier recombination centers. Due to the size of the ingots grown in industrial practice, where 450 kg is now a minimum, the characterization of dislocations in photovoltaic material requires a quick and efficient method which can be applied to large scale samples.

In this study, our purpose is to compare various characterization techniques on a sample of several square centimeters. To start with, the sample, a thin plate of silicon, is polished to obtain a mirror surface and etched to reveal dislocations. The reference method is to count them one by one with an optical microscope in order to obtain a precise and exhaustive map of dislocation density.

After this slow but necessary dislocation density characterization, the sample is submitted to different faster methods. First, a high resolution scanner is used to take a picture of the sample. The grey scale of this picture can be linked to dislocation density. In a second method, a Scanning Electron Microscope is used to take small pictures of several parts of the same sample. These pictures are treated with an image processing software, developed at INES laboratory, which recognizes and counts etch pits and gives the dislocation density. In a third method the sample is characterized by PVscan, an instrument used by photovoltaic industries to estimate the dislocation density of their wafers. The fourth method has been developed at NTNU and consists in illuminating the sample with an incident light and measuring the diffused light with a CCD camera. The results of these four methods are finally compared to the precise map obtained by the reference technique in order to draw conclusions concerning their accuracy and efficiency.

16:00 Poster We199

Real defect structure of GaSe grown by Bridgman method

Konstantin A. Kokh[1,2], Victor Atuchin[3], Tatyana Gavrilova[3], Aleksandr S. Kozhukhov[3], Evguenii Maximovskiy[4], Lev Pokrovsky[3]

1. *Institute of Geology and Mineralogy SB RAS (IGM), Koptyuga ave., 3, Novosibirsk 630090, Russian Federation* **2.** *Novosibirsk State University (NSU), Pirogov 2, Novosibirsk 630090, Russian Federation* **3.** *Institute of Semiconductor Physics SB RAS, pr. Lavrentieva 13, Novosibirsk 630090, Russian Federation* **4.** *Nikolaev Institute of Inorganic Chemistry SB RAS (NIIC), Acad. Lavrentiev Ave., 3, Novosibirsk 630090, Russian Federation*

e-mail: k.a.kokh@gmail.com

Gallium selenide, GaSe, is a well-known nonlinear optical crystal widely used for frequency conversion over visible, IR and THz spectral ranges. During last decade, the breakthrough application of GaSe for terahertz (THz) generation over extremely wide spectral range under the pump by near-IR coherent sources was reported. Most recently, efficient THz generation from two collinearly propagating CO_2 laser pulses was demonstrated that resulted by significant improvement of the frequency conversion efficiency of CO2 laser within mid-IR (second, third and forth harmonic generation) GaSe possesses layered crystal structure with high cleavage properties. Initially, 120-150 g of polycrystalline material was obtained in single-zone horizontal furnace using high purity (99.9999%) gallium (Ga) and selenium (Se). The synthesis was performed in sealed quartz ampoules by direct fusion of the elements and following homogenization for 1 day at 1000˚C. The crystals used in this study were grown by the conventional Bridgman technique in evacuated quartz ampoules 18 mm in diameter. The temperature gradient at the crystallization front was 10 deg/cm and the crystal pulling rate - 6 mm/day. The samples 20-22 μm, 70-80

μm, ~ 0.3̄-0.5 mm, and 3 mm in thickness were cleaved from the grown ingots parallel to (001) and were studied without any additional treatment and polishing. Micromorphology of cleaved GaSe(001) surface has been observed by AFM with Solver P-47H device in noncontact mode. SEM explorations were implemented using LEO 1430 and JEOL JSM 6700F devices. Structural properties were evaluated by TEM analysis. As it was shown by AFM observation, the cleaved GaSe(001) surface is almost entirely atomically flat with as low rms parameter as ~0.06 nm for an area of 5×5 μm^2. In several scans, a hillock-type formations were detected with bottom diameter of ~200 nm and height of ~20-35 nm. The hillocks were also detected in high-resolution SEM patterns. The Ga/Se ratio estimated by local chemical composition analysis was as low as 0.55-0.84 that indicates drastic depletion of the hillock material by gallium. Acknowledgements: This study is supported by SB RAS (Project 46.13) and Ministry of Education and Science of the Russian Federation (Contract 16.518.11.7091).

16:00 Poster We200

Scattering centers in as grown $AgGaS_2$ crystal

Konstantin A. Kokh[1,2], Dmitry Kokh[1]

1. *Institute of Geology and Mineralogy SB RAS (IGM), Koptyuga ave., 3, Novosibirsk 630090, Russian Federation* **2.** *Novosibirsk State University (NSU), Pirogov 2, Novosibirsk 630090, Russian Federation*

e-mail: k.a.kokh@gmail.com

Many crystals with chalcopyrite structure possess outstanding nonlinear optical properties. A common feature of these compounds is the presence of scattering centers in as-grown crystals due to decay of the solid solutions. While the basic principles of how to suppress the centers are known, this contribution is aimed to detailed microscopic study of these defects on the example of $AgGaS_2$ (AGS) crystals. Due to high sulfur pressure at the melting point of AGS (996˚C) a separate synthesis of raw material is necessary. In this work the synthesis of AGS was performed by direct fusion of the elementary compounds in the single-zone furnace. Then, the charge was placed in the double-wall ampoule for recrystallization by modified Bridgman method. Thin plates of AGS from as-grown crystal as well as from that annealed in Ag_2S and Ga_2S_3 atmosphere were taken for study. The annealing was done by heating the sample and the boat with agent in evacuated quartz ampoules. Various times and temperatures were tested. No difference was found between the samples by X-ray diffraction and Raman measurements. However, according to EDS X-ray microprobe analysis, the scattering centers consist from inclusions of $Ag_2Ga_{20}S_{31}$ phase. Elimination of these inclusions takes place after annealing of the samples in the atmosphere of Ag_2S. Diffusion of Ag-rich components into the bulk of AGS determines the time of annealing. Around 2 weeks are necessary for boundary between milky and optically clear AGS to propagate at 1 cm inside the sample at 850˚C. The composition of inclusions is also confirmed by the fact that annealing with Ga_2S_3 makes the inclusions larger which in turn results in cleavage micro cracks in the sample. A certain attention has been paid to acid etching of the samples. The treatment in HCl revealed morphological feature of the plate like inclusions which explains why they look like a dot-lines in transmitted light. Also this acid effectively dissolves defective outer layer on the polished surface of the AGS, while the undamaged cleavage plane {112} remains unchanged. On the other hand HNO_3 reacts with any surface of AGS, so this acid is suitable to reveal etch pits.

16:00 Poster We201

The role of voids in cracking of single crystal-matrix composites containing quasicrystal phase

Jacek Krawczyk

University of Silesia, Institute of Materials Science (INOM), 75 Pułku Piechoty 1A, Chorzów 41-500, Poland

e-mail: jacek.krawczyk@us.edu.pl

The fibrous composites of Al-Cu-Fe alloy containing quasicrystal phase fraction were studied. The composites were obtained *in situ* through the directional solidification by the Bridgman method in furnace with vertical gradient of temperature. The composites were subjected to X-ray powder phase analysis, the Laue diffraction and the X-ray topography study. Plate-like samples were cut from obtained ingots in parallel to vertical axis of ingots. Reinforcing fibers were arranged in parallel to the ingots axis and to the tensile direction in simple uniaxial tension tests of plate-like samples. Tension tests were performed up to the rupture.

The microstructure of the singlecrystal-matrix composites, especially tensile fracture surface were analyzed. The optical and electron microscopy were used. The voids distribution in the composite and their size were studied. The voids impact on the composites stability and the way of cracking were analyzed. The reason and region of voids formation and their role in cracking process were discussed. The influence of the pores on the brittleness of Al-Cu-Fe singlecrystal-matrix composites containing quasicrystal phase fraction were determined.

16:00 Poster We202

Polytypism in SiC: theory and experiments

Andrey Lebedev[1], Yuri M. Tairov[2]

1. *Ioffe Physico-Technical Institute, RAS, Saint-Petersburg, Russian Federation* **2.** *State Electrotechnical University, Saint-Petersburg 197376, Russian Federation*

e-mail: aswan@aport.ru

Silicon carbide (SiC) is one of the most promising materials for high temperature, radiation-hardened, power and high-speed electronics due to its unique physical and electronic properties. Silicon carbide exists in the form of different polytypes. Today the number of described structures of silicon carbide polytypes is about 200. Authentic causes of polytypism are unknown. In accordance with an accepted dislocation theory of polytypism [1], screw dislocations with Burgers vectors not multiple to the lattice parameters of basic polytypes (6H, 4H or 15R) may create new polytypes.

Model example: polytype 27R. In the dislocation theory the polytype 27R (2,2,2,3) is considered as a derivative structure based on 4H (2,2) polytype. Structure and polytype composition of 27R-samples grown by non-seeded Lely technique [2] have been investigated by X-ray Berg-Barrett topography, Laue pattern technique, X-ray diffractometry as well as by micro Raman spectroscopy. Extended 6H – polytype inclusions have been detected in about a half of samples. Polytypes form sintaxial joints (numerous sandwich structures) with the same arrangement of crystal axes. One sample had small misorientation (about 3 degrees) between C-axes of 6H- and 27R-polytypes. We have found no statistical disorder of 27R-polytype within the limits of resolution of used techniques. Also, we have not revealed any presence of presumed parent phase 4H within the representative set of 8 samples.

One-dimensional matrix assembly of basic polytypes. Ramsdell and Kohn proposed [3] so-called polymeric concept of polytypism assumed an existence of 7 various hypothetic polymeric group in gas phase having the following Zhdanov indexes (3,3), (3,2), (2,3), (2,2), (3,4), (4,3), (4,4). At the same time, taking into account the great difference in occurrence rate for various polytypes, it seems to be the most authentic to modify and to use this concept only for relatively small set of basic polytypes (6H, 4H, 3C, 15R).

The main molecular forms in a gas phase during the growth of silicon carbide crystals are Si(g), Si_2C(g) and SiC_2(g). Due to the first principles an interaction of these species could lead to occurrence of two intermediate stoichiometric forms, namely, so-called dimer Si_2C_2 and trimer Si_3C_3. Actual spatial configuration of activated clusters which forms a polytypic sequence is unknown. Therefore below we simply consider all possible results of one-dimensional cluster assembly from dimers and trimers (see table).

NN	Symmetry of element	Symmetry of chain, Ramsdell notation
1	(B) – A – B – (A)	2H
2	(B) – A – B – (C)	4H
3	(C) – A – B – (C)	3C
4	(B) – A – B – C – (A)	6H
5	(B) – A – B – C – (B)	9R
6	(C) – A – B – C – (A)	3C
7	(C) – A – B – C – (B)	6H
8	(B) – A – B – A – (B)	2H
9	(B) – A – B – A – (C)	9R
10	(C) – A – B – A – (C)	6H

As known, at rather low temperatures ($T<2200^oC$) gaseous silicon prevails and, according to this approach, leads to formation of 3C or 4H polytypes from dimers, in conformity with an experiment. Moreover, because of the concurrent creation of 4H and 3C polytypes being unlikely one polytype should replace another at elevating the temperature. Polytype chains of 2H, 3C, 6H or 9R should be formed from trimers. As known, polytype 2H-SiC is not grown in high-temperature Lely process while 3C and 6H polytypes meet most frequently. As for 9R version of silicon carbide this rare polytype is also known for a long time. Note that assembly of the chain of monomers (for example, during CVD growth of SiC) should lead to the occurrence of only two polytypes, i.e. 2H or 3C.

15R polytype. Co-polymer analogy. 15R polytype structure can not be described as the chain composed of the same elementary cluster but – similarly to a copolymer – of two alternating those. Considering the concurrent growth of 4H and 6H polytypes, in the framework of polymer analogy and kinetic approximation we obtain:

$$P_{4H} = K_{22}[M_2]/(K_{22}[M_2]+K_{23}[M_3]),\ P_{6H} = K_{33}[M_3]/(K_{32}[M_2]+K_{33}[M_3]),$$

where P_{4H}, P_{6H} are probabilities of growth of 4H and 6H polytypes, correspondingly, K_{AB} is a chain propagation reaction constant for an addition of A-mer to B chain, $[M_2]$, $[M_3]$ are the concentrations of dimers and trimers, accordingly.

Then, probabilities of failure of polytype sequence can be written down:

$$P_{4H\to6H} = 1 - P_{4H}\ ,\ P_{6H\to4H} = 1 - P_{6H}.$$

Assuming second-order reaction in the gas we have for concentrations:

$$[M_2] = K_2[Si][SiC_2],\ [M_3] = K_3[Si_2C][SiC_2],$$

where K2, K_3 corresponding reaction constants for dimer and trimer formation.

Using all expressions above we carried out qualitative simulation of concurrent growth in a wide range of parameters. All possible scripts of chain assembling are presented below:

(i) -222222333332222- growth of 4H-polytype containing bulk inclusions of 6H-polytype;

(ii) -23322232323223- growth of 15R polytype, with a great fraction of statistically disordered 15R-polytype (improbable variant);

(iii) -2323232323- ideal 15R-structure;

(iv) -222222232222223222222- prevailed growth of 4H, with small inclusions of trimers.

Note that ideal 15R structure could be composed when the growth of one polytype is suppressed by kinetic limitations, another – by an absence of "building material", i.e. by negligible concentration of dimers or trimers, accordingly. Also, presence of two polytypes (4H and 6H) in syntaxial joint could lead to an occurrence of elementary steps with motive of 15R-polytype. Results of HRTEM-analysis of 15R-inclusions in 4H-ingots grown by modified Lely technique [4] have been presented and interpreted. Possible restrictions of proposed approach are considered.

References

[1] Franc F.C. Phil.Mag.42, 1014(1951).

[2] Lely J.A. Ber.Deut.Keram.Ges. 32, 229(1955).

[3] Ramsdell L.S., Kohn J.A. Acta Cryst. 5, 215(1952).

[4] Tairov Yu., Tsvetkov V.F. J.Crystal Growth 43, 209(1978).

16:00 Poster We203

Investigations of chemical and phase composition of SBN solid solutions: charge and crystals grown by shaping techniques

Liudmila I. Ivleva[1], Pavel A. Lykov[1], Nina S. Kozlova[2], Elizaveta E. Dunaeva[1]

1. *A.M. Prokhorov General Physics Institute of Russian Academy of Sciences (GPI), Vavilov Str. 38, Moscow 119991, Russian Federation* **2.** *National University of Science and Technology (MISIS), Leninsky prospect, 4, Moscow 119049, Russian Federation*

e-mail: lykov@lst.gpi.ru

The search of new non-linear materials and development of technologies for producing optically perfect crystals remain actual up to now. Among solid-state materials an important role play ferroelectric crystals of strontium-barium niobate solid solutions $Sr_xBa_{1-x}Nb_2O_6$ (SBN:x), which belong to a class of active dielectric, exhibiting qualitatively new properties under influence of external factors. SBN single crystals are characterized by the extremely large electro-optical coefficients and high nonlinear optical properties. Doping of the SBN solid solutions by rare-earth and transition metals allows to control the properties of the crystals and to create new materials for different applications, particularly in the areas of pyroelectricity, piezoelectricity, electro-optics, photorefractive optics and non-linear optics.

The present investigation is directed on investigation of chemical and phase composition of the SBN solid solutions charge and crystals grown from the melt by shaping techniques. We studied influence of non-controlled charge impurities and special dopants introduced into the melt on chemical and phase homogeneities of SBN crystals obtained

in profiled configuration. The specific features of the shaping techniques, including form and capillary sizes of dies, were studied, their influence on chemical and optical homogeneities of the crystals were shown.
The SBN charge was prepared by solid phase synthesis at a temperature of 1200°C during 6h according to the reactions:
SBN:61:

$0.61SrCO_3+0.39BaCO_3+Nb_2O_5 \rightarrow Sr_{0.61}Ba_{0.39}Nb_2O_6+CO_2\uparrow$ (1)

SBN:75:

$0.75SrCO_3+0.25BaCO_3+Nb_2O_5 \rightarrow Sr_{0.75}Ba_{0.25}Nb_2O_6+CO_2\uparrow$ (2)

The method of scanning electron microscopy (SEM) combined with microanalysis was used for determination of morphology and the elemental composition of the SBN: 61 and SBN: 75 solid solutions (fig.1).

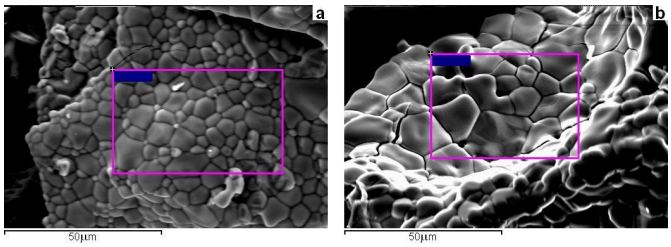

Fig.1 SEM images of surface micro-relief for SBN:61(a) and SBN:75 (b) solid solutions

It was estimated that the grain sizes in SBN:61 and SBN:75 samples vary from units to tens of microns. Content of Sr, Ba, Nb elements in separate grains does not correspond to the chemical formula. Deviation from the specified element composition was within 10%. The presence of calcium ions as uncontrollable impurities was registered in admixture. The phase composition of the charges was determined by XRD method. It was found that a monoclinic phase and tetragonal phase coexist in the temperature region of 950-1400°C. The monoclinic phase is stable at temperatures below 850°C. Temperature of the phase transition from monoclinic into tetragonal form depends on the aggregate state of sample and lies in the region of 1340°C. At higher temperatures the monoclinic phase quickly and completely converted in phase with tetragonal symmetry. The solid phase synthesis of SBN at temperature 1200°C leads to formation of both phases. At the same time the content of monoclinic phase in charge increases with increasing of strontium content in SBN solid solution.
The SBN crystals were grown from the melt by the modified Stepanov technique using special die of capillary type. Influence of constructive peculiarities of dies on chemical homogeneity of profiled SBN crystals was studied. In optimized conditions the crystals (14x24mm) in cross-section and up to 80 mm in length were grown. Effective segregation coefficients for crystals doped with Ce, Cr or Co ions were determined. It was shown that the content of uncontrollable impurities did not exceed 100 ppm, except Na, Al, Si (120-190 ppm). Nevertheless, the presence of non-controlled impurities leads to appearance of absorption band around 400 nm in transmission spectra of the material. The control of optical quality of the crystals was performed by optical and polarization-optical methods, laser radiation scattering control, the method of dynamic holography.

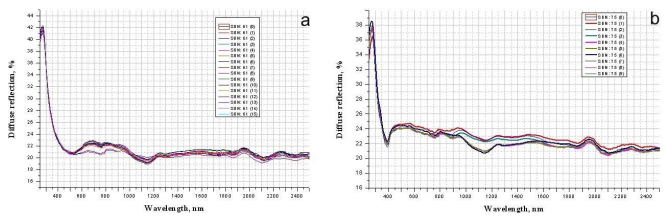

Fig.2 The dependence of full diffuse reflection on wavelength for SBN:61:Ce (a) and SBN:75 (b) crystals

Measurements of the optical homogeneity of crystals were also carried out by photometry method. Diffuse reflection coefficients and diffuse transmittance in the spectral range (250-2500 nm) were determined. The results are given in fig.2. The spectra, obtained in different points of the samples are identical within 1% (experimental error). It should be noted that the introduction of cerium dopant into the congruently melting SBN:61 gives total reflection coefficient less than one for the nominally pure SBN:75 crystal, which is characterized by the most disordered structure among SBN solid solutions.
The regimes of solid phase synthesis and growth parameters were optimized to provide the reproducible characteristics of SBN crystals of high homogeneity.

16:00 Poster We204

Computational analysis of precipitates, parasitic deposits and gas-to-particle conversion during Cz and DS Si-crystal growth

Andrei Vorob'ev, Vladimir Kalaev, Alexander Sid'ko

STR Group, Inc., Engels av. 27, P.O. Box 89, St-Petersburg 194156, Russian Federation

e-mail: andrei.vorobiev@str-soft.com

The present paper focuses on modeling Cz and DS *Si*-crystal growth. There are a few related problems in the performance of these technologies. We will emphasize three of them.
First, impurities contained in silicon feedstock and generated due to the melt-to-crucible contact strongly affect the efficiency of mono and multicrystalline silicon solar cells. Oxygen and nitrogen are mainly coming from quartz crucible wall and crucible coating, while the main sources for carbon are feedstock and graphite furnace elements. Carbon, nitrogen and oxygen dissolved in the melt interact with silicon and each other, generating such precipitates as *SiC*, Si_3N_4 and Si_2N_2O [1], [2].
Second, oxygen is mostly evacuated through the free melt surface and transported as silicon monoxide by argon flow downstream to the reactor outlet. Therewith, *SiO*-vapor chemically reacts with graphite elements, supplying such by-products as *CO* and *Si* in the gas-phase. In turn, *SiO*, *CO* and *Si* become sources of *SiC*- and *Si*-parasitic deposits on hot elements of reactor, shortening significantly, in particular, the heater lifetime. Moreover, SiO_2 or *SiO* can be deposited on the cold surfaces [3].
Third, *SiO*-vapor in some cooled regions, e.g., in outlet tubes and near upper part of the heat shield around the crystal turns out to be supersaturated and conversed into *SiO*-particles in the gas-phase. Their entry into the silicon melt may cause single crystal structure loss [3].
In this connection, the conventional heat and mass transport model [4] is extended to describe those phenomena. The model is verified by comparing our computations with available experimental data.
It is found for the DS method that maximum amount of Si_3N_4-precipitates is predicted near the crystal top where the nitrogen percentage is higher due to absence of its loss at melt free surface. As contrasted to Si_3N_4-precipitates, Si_2N_2O-concentration reaches its maximum near the crystal bottom. Obviously, its formation then is controlled primarily by the oxygen decreasing with the height. Therewith, in both cases the precipitates are accumulated along the crystal center. *SiC*-concentration exhibits a behavior similar to that of Si_3N_4 for the same reasons but is remarkably less localized near the crystal center. Accounting for the lack of detailed information on the process parameters and the reactor

design, our computations qualitatively agree well with experimental data presented in [5].

The developed chemistry is applied to modeling the Cz silicon growth for a 155-mm-diameter ingot in a Kayex CG6000 puller [3]. As it follows from our computations, a zone near the shield top is inconsiderably heated, and our model predicts SiO_2-deposit on upper part of the shield where it is just observed in experiment. In addition, *SiO*-vapor is supersaturated here and, hence, conversed into the particles. Further, *SiO* is transported downstream where it interacts with the hot graphite heater. As seen from simulation, *Si*-deposit of a short length is formed in region of relatively low temperature at the top and bottom of heater, while a central part is coated by silicon carbide. Their formation is accompanied by graphite etching. The same computation is performed for an optimized design of the furnace where the outlet is located opposite to the upper part of crucible, and insulation is added at the top of molybdenum shield. Our computations show that modification of the hot zone near the shield could help to suppress *SiO*- supersaturation and its condensation. Also, *Si*- and *SiC*-deposition rate on the shield and on the heater is predicted to be negligibly low due to the alternative location of reactor outlet. The results obtained are well consistent with experimental data [3].

To conclude, the advanced chemistry model for DS and Cz *Si*-crystal growth is developed to account for precipitation in the melt and parasitic deposits from the gas-phase as well as gas-to-particle conversion. The software tool, CGSim crystal growth simulator, based on the model allows optimization of reactor design and process conditions to avoid the gas-phase condensation and to minimize the parasitic deposits.

References

1. Liu L., Nakano S., Kakimoto K., Journal of Crystal Growth, 310 (2008) 2192-2197.

2. Hisamatsu S., Matsuo H., Nakano S., Kakimoto K., *Journal of Crystal Growth*, 311 (2009) 2615-2620.

3. C.W. Lan, *Chemical Engineering Science*, 59 (2004) 1437 - 1457.

4. A.D. Smirnov, V.V. Kalaev, *Journal of Crystal Growth*, 311 (2009) 829-832.

5. Matsuo H., Ganesh R.B., Nakano S., Liu L., Kangawa Y., Arafune K., Ohshita Y., Yamaguchi M., Kakimoto K., *Journal of Crystal Growth*, 310 (2008) 4666-4671.

16:00 Poster We205

Effects of 355nm subdamage laser fluence on characteristic of KDP

Fengrui Wang, Hongjie Liu, Decheng Guo, Jin Huang, Xiaodong Jiang, Weidong Wu, Wanguo Zheng

Central South University, Chemistry & Chemical Engineering College, Changsha, Hunan 410082, China Dipartimento di Chimica, Università di Firenze (UNIFI), Via della Lastruccia 3, Sesto Fiorentino (Firenze) 50019, Italy

e-mail: wfr2000@163.com

Damage properties of the frequency conversion crystal KDP limits the output fluence of high power laser facilities. Damage behavior of KDP was investigated for many years, and results show that intrinsic or extrinsic defects are responsible for highly localized absorption in the bulk of KDP materials may cause the damage. Irradiated by laser fluence under damage threslond would improve the damage performance of KDP crystal. The mechanisms of laser-induced damage and laser conditioning are still not well understood. Lots of research concerntrated on optimizing the laser parameters to improve the conditioning effect, since no visible damage pionts in the KDP ctrystal formed under subdamage fluence irradiation, few attention focused on changes of the intrinsic crytal.

We investigated the characterisitic of KDP crystal before and after laser irradiation. The crystal were irradiated by different fluences below damage threshold, and absorption coefficient, fluorescence spectrum, x-ray diffraction of the irradiated area were investigated, and obviously variation obtained.

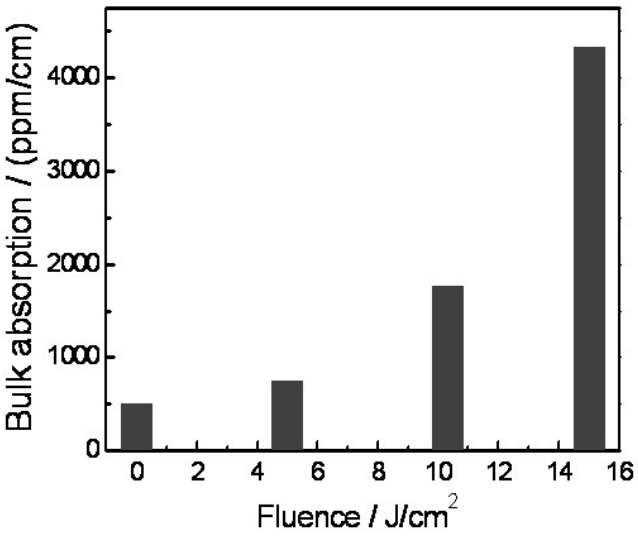

Bulk absorption vs laser fluence

Our results show that subdamage laser fluence irradiation modified performance of KDP crystal, such as absorption coefficient of the material, that is, as the damage threshold improve, the absorption of the material increase, too, considering the low threshold defect precursors have been eliminated, we wonder whether the damage occurred after laser conditioning has something to do with this.

16:00 Poster We206

Defect population in the High pressure rotator phase of n-tridecane, pentadecane and heptadecane observed by FT-IR

Motoi Yamashita

Chiba Institute of Technology, 2-1-1 Shibazono, Narashino, Chiba 275-0023, Japan

e-mail: motoi.yamashita@it-chiba.ac.jp

The effect of pressure on phase transition behavior and defect populations of *n*-tridecane, pentadecane and heptadecane has been investigated by using Fourier transform infrared spectroscopy at 25°C. The transition between the high pressure ordered (HPO) and high pressure rotator (HPR) phase has been observed in the pressure ranges of 270–220, 106–95 and 152–181 MPa for C_{13}, C_{15} and C_{17}, respectively, and the transition between the HPR and liquid phase was observed in the pressure ranges of 171–112, 73–47 and 43–70 MPa for C_{13}, C_{15} and C_{17}, respectively. The populations of the -gtg- + -gtg'-, -gg- and gt- defects determined from the methylene wagging mode are smaller in the HPR phase than in the liquid phase and are smaller under higher pressure in both of the HPR and liquid phases. A relationship has been found between the conformation and the intensity of the 890 cm^{-1} band, which has been assigned as the methyl rocking mode and has been considered as insensitive to conformation.

General Session 8

Nanomaterials and low dimensional structures

Session Coordinators

Torsten Boeck (Germany) *boeck@ikz-berlin.de*

Joan Redwing (USA) *jmr31@psu.edu*

Programme

Monday, 12 August

MoO1

G08: Nanomaterials and low dimensional structures
Monday morning, 12 August, 11:00
Room D, Auditorium Maximum

11:00 Invited oral

Growth of site-controlled single GaN/AlGaN nanowire quantum dots by MOCVD and their optical properties

Yasuhiko Arakawa, Kihyun Choi, Munetaka Arita, Mark Holmes, Satoshi Kako

University of Tokyo, Institute of Industrial Science, 4-6-1 Komaba, Tokyo 153-8505, Japan

e-mail: arakawa@iis.u-tokyo.ac.jp

Semiconductor quantum dots (QDs) formed by Stranski-Krastanow growth mode has enabled the realization of highly-efficient optoelectronic devices such as QD lasers. Also, unique features of the QDs are promising for the development of solid state quantum information processing technologies. Particularly, III-nitride QDs are important for high-temperature operation of quantum information devices. In this presentation, we discuss our recent advances in site-controlled single GaN/AlGaN nanowire quantum dots. We developed MOCVD selective area growth of nanowires embedding QDs in order to control the site of GaN QDs. High-quality single GaN QDs with intense photoluminescence were successfully obtained together with the observation of a large biexciton binding-energy, fine structure splitting (FSS), and strong interaction with phonons in the single GaN QDs. Moreover, the presence of the excited states in a single GaN QDs were evidenced by means of photoluminescence excitation (PLE) measurements, which was led to realization of coherent control of excitons in the single GaN QDs.

11:30 Invited oral

Growth and optical properties of nitride dot-in-a-wire structure on Si substrate

Yen-Ting Chen[1,2], Per Olof Holtz[2], Yasushi Nanishi[3], Li-Chyong Chen[1]

1. *Center for Condensed Matter Sciences, National Taiwan University, Taipei 10617, Taiwan* **2.** *Department of Physics, Chemistry and Biology, Linköping University, Linköping 58183, Sweden* **3.** *Ritsumeikan University (Rits), Kusatsu 525-8577, Japan*

e-mail: r93921104@ntu.edu.tw

Nitrides have been a mature class of material to the light emitting diode (LED) industry for years with high quantum efficiency at room temperature, and have many outstanding properties including doping characteristic, robustness, and wide optical emission range. GaN nanowire is an emerging structure for the next-generation LED due to its outstanding crystal and optical properties. Nitride quantum dots embedded in nanowires (dot-in-a-wire) have recently become a focus due to the advantage of dislocation-free crystal structure and the suppression of quantum confined Stark effect (QCSE) by taking advantage of the free-surface relaxation of lattices. However, challenges remain such as wire alignment, phase segregation, the formation of basal plane stacking faults due to the growth-temperature variation in the heterostructure, and the density and diameter control of the nanowires. In this talk, fabrication of single dot-in-a-nanorod with small rod diameter (9~35 nm) and low rod-density ($< 10^8$ cm^{-2}) fabricated without extensive processing steps will be reported. Excitation power-dependent PL spectrum of single QD reveals multi-excitonic peak with 0.75 meV (exciton) and 0.33 meV (trion) blue-shift across 3 orders of magnitude increasing power, indicating the present system is spectrally stable and nearly free of QCSE, due to the strain relaxation induced by free surface of small rod diameters. The emission of single quantum dot is fully polarized with degree of polarization around 90% and with a high working temperature. Optical property is further investigated by multiple methods including scanning near-field optical microscopy for the single dot-in-a-wire emissions. Diffusion length of photo-excited excitons in the nanowire is estimated and related to the surface effect of the nanowire which is crucial for the application of naon-devices. For the growth of nanowire, the nucleation mechanism crucial for the device fabrication remains unclear. We present direct evidences which show that the nucleation of GaN nanorods stems from the sidewall of the underlying islands and the Si(111) substrate surface. Accordingly, the growth and density control of low density, uniform, and narrow GaN nanorods is exploited by a 'narrow-pass' approach that only narrow nanorod can be grown, and wide rods merge to the surroundings automatically. A nucleation scenario based on statistical results will be reported as a tentative blueprint for the fabrication of uniform single nanorods.

12:00 Oral

Growth Dynamics of GaAs/AlGaAs Quantum dots by Droplet Epitaxy

Stefano Sanguinetti[1], Sergio Bietti[1], Claudio Somaschini[1], Alexey Fedorov[2]

1. *LNESS and Dipartimento di Scienza dei Materiali, Università di Milano-Bicocca, via Cozzi 53, Milano 20125, Italy* **2.** *CNR-IFN, Via Anzani 42, Como 22100, Italy*

e-mail: stefano.sanguinetti@unimib.it

Droplet epitaxy (DE) [1] is an emerging and powerful MBE growth technique alternative to the commonly used Stranski-Krastanov approach for the self-assembly of quantum dots (QDs). Strain-free GaAs quantum dots can be grown by DE crystallizing group III metallic atoms, stored in nanometer scale droplets, with a group V atomic flux. This allows for an independent control over size and density of the fabricated QDs. However, despite the high level of design control achieved by DE, the details of the growth kinetics of the DE-QDs is still unclear. This knowledge could be of the utmost importance for the optimization of the fabrication procedures of DE-QD materials. Two fundamental aspects of the QD growth kinetics by DE will be here presented: 1) The crystallization kinetics of a nanometer size Ga droplet in to a QD under As flux 2) The faceting of a DE-QD and its dependence on the growth parameters The crystallization kinetics of the metallic Ga contained in the droplet into GaAs nanocrystals under the As flux is followed step-by-step, investigating the amount and the morphology of the crystallized GaAs in the droplet at different As doses by means of a combination of selective wet chemical etching and Atomic Force Microscopy (AFM), in a nano-tomography approach (see Figure 1). The crystallization of the Ga in the droplet starts from a ring of GaAs which is formed just after the Ga deposition at the perimeter of the droplet. This ring acts as nucleation seed for the subsequent QD growth. During the As supply, the ring increases its size at the expenses of the metallic droplet. The QD growth the proceeds at the contact surface between the liquid Ga and the ring until the complete depletion of the Ga contained in the droplet. The control of the faceting of DE-QD is a fundamental aspect for the fabrication of QDs with on-demand density of states and a reduced electron-phonon interaction. We will show that it is possible to determine, by the control of the crystallization kinetic, the shape of DE-QDs. The QD shape depends on the Ga diffusion length in the crystallization condition, thus showing a marked dependence on As pressure and temperature (see Figure 2). The facet orientation evolves, by reducing As pressure or increasing substrate temperature, from {111} facets, exposed at low temperatures and high As presure, towards {311} facets. A model, based on the effect of the diffusion of the metallic Ga from the droplet during the crystallization step, is able to reproduce the observed faceting evolution on temperature and As pressure. [1] N. Koguchi, S. Takahashi, T. Chikyow, J. Crystal Growth 111 (1991) 688.

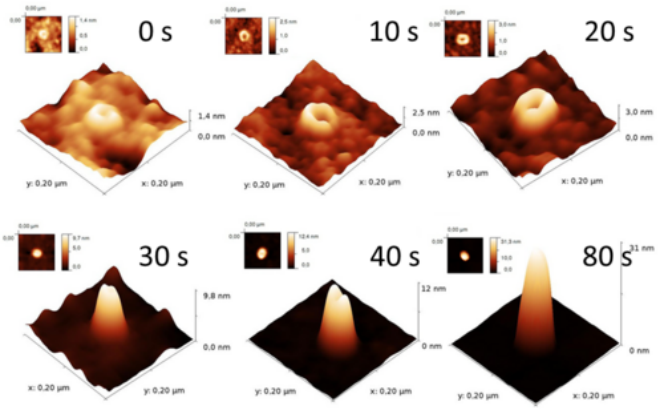

Figure 1: From left to right: crystallized GaAs morphology at different As irradiation times. The unreacted Ga in the droplet was removed by wet chemical etching.

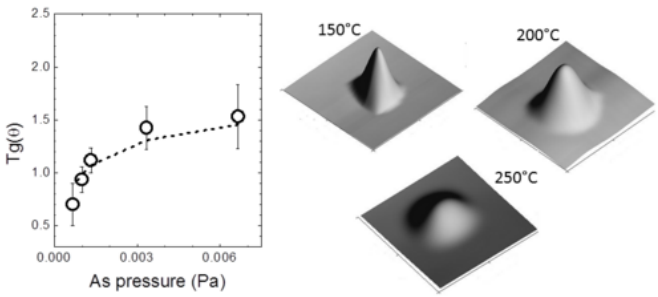

Figure 2. Left panel: Dependence of DE-QD facet orientation on As crystallization pressure at T_{SUBST}= 200 °C. θ is the angle between the substrate and the QD facet. The dashed line report simulation prediction based on Ga diffusion model. Right panel: AFM images of DE-QDs crystallized at different temperatures

12:15 Oral

GaAs/$Al_{0.3}Ga_{0.7}As$ Quantum Dot Intermediate-band Solar Cell by Droplet Epitaxy

Sergio Bietti, Andrea Scaccabarozzi, Maurizio Acciarri, Stefano Sanguinetti

LNESS and Dipartimento di Scienza dei Materiali, Università di Milano-Bicocca, via Cozzi 53, Milano 20125, Italy

e-mail: andrea.scaccabarozzi@mater.unimib.it

Quantum dot intermediate band (IB) solar cells have been proposed in order to increase the efficiency of traditional solar cells and immediately attracted a lot of attention and research since the time they were first proposed [1]. The IB introduces an extension of the absorption coefficient of the semiconductor to lower energies, allowing a more thorough collection of the solar spectrum, via a two-step absorption of low-energy photons. Quantum dot (QD) structures are good candidates for IB solar cells, because their confined energy levels can overlap and form a miniband in dense arrays and the position of these levels and bands can be tuned varying the size and spacing of the QDs. The IB working mechanisms have been demonstrated for InAs QDs in GaAs [2], and a lot of research is devoted to reduce the problems due to strain, and defect nucleation increasing carrier escape [3]. Droplet epitaxy (DE) [4] is a molecular beam epitaxy technique that allows for the growth of quantum dots of materials lattice matched to the barrier and the removal of the wetting layer. DE makes possible to indipendently control density, size and shape of the nanostructures. Densities as high as some 10^{11} cm^{-2} per layer have been reported [5] and potentially a large number of layers can be stacked because the system is strain-free, leading to a much higher density of states in the IB than the more conventional Stranski-Krastanov techniques. Since it is a strain-free technique, there are virtually no defects in DE-grown materials, and this is fundamental to have high performance devices. Moreover, DE nanostructures can be grown without the presence of a wetting layer [6], that would introduce unwanted quantum-well-like states in the system. By tuning the size of the QDs it is obviously possible to change the position of the IB, and by tuning their aspect ratio the high energy states of the QDs can also be tuned in order to have a small electron-phonon coupling with the barrier. The lack of defect and wetting layer states can greatly reduce thermal escape of carriers from the IB, leaving photon-induced transitions the dominant ones, as requested by IB theory [1]. For these reasons DE is a good candidate for the realization of QD-IB solar cells. We demonstrate the key working principle of IB materials, that is the production of sub-gap two-photon photocurrent, with $Al_{0.3}Ga_{0.7}$

As solar cells containing GaAs QDs grown by DE (figure 1a). The devices were illuminated at 15K by continuous monochromatic light and chopped broadband IR light (1.5 – 20 μm), and the signal was demodulated by a lock-in amplifier. The continuous light pumps electrons into the QDs and the chopped IR promotes them to the CB where they can be collected generating an electric signal. As a control, a reference sample without QDs was grown and measured in the same conditions, but no two-photon signal was detected (see figure 2b). Measurements show that the shape of the two-photon photocurrent signal is different from the VB-CB photoresponse, indicating clearly that a two-photon process involving the QD levels is taking place. The two-photon signal response is in good agreement with the PL spectrum of the QD samples (figure 1b), that lets us easily understand the position of the energy levels of the system. [1] A. Luque, A. Martì, Physical Review Letters, 78, 5014 (1997). [2] A. Martì, E. Antolìn, C. R. Stanley, C. D. Farmer, N. Lòpez, P. Dìaz, E. Cànovas, P. G. Linares and A. Luque, Physical Review Letters 97, 247701 (2006). [3] A. Luque and A. Martì, Prog. Photovolt: Res. Appl. 9, 73-86 (2001) [4] N. Koguchi and K. Ishige, Japanese Journal of Applied Physics 32, 2052–2058 (1993). [5] M. Jo, T. Mano, Y. Sakuma and K. Sakoda, Applied Physics Letters 100, 212113 (2012) [6] S. Sanguinetti, K. Watanabe, T. Tateno, M. Wakaki, N. Koguchi, T. Kuroda, F. Minami, and M. Gurioli, Applied Physics Letters 81, 613 (2002).

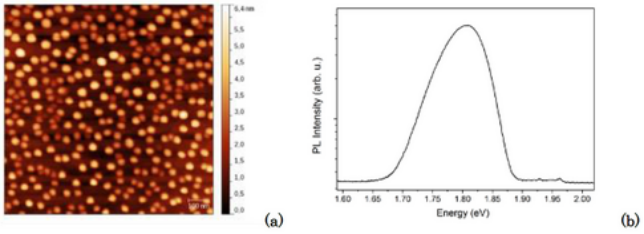

Figure 1: (a) AFM image of uncapped high density QDs grown by droplet epitaxy for the IB solar cell. (b) PL spectra of the QD sample at 15K with different excitation power. The QD emission energy indicates the IB energy level.

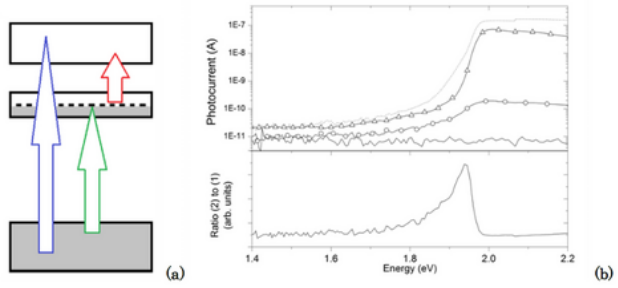

Figure 2: (a) Energy band diagram of the quantum dot solar cell with the main optical transitions outlined. (b) Upper panel: photocurrent signal of the QD and reference devices at 15K. Dashed curve is the AlGaAs reference cell single photon signal. Continuous, triangles and circles refer to the GaAs/AlGaAs QD photovoltaic cell: single photon signal (triangles), two-photon signal (circles) and noise level (continuous line). Lower panel: ratio of normalized two-photon to single-photon photocurrent signal, to better show the subgap photoresponse

12:30 Oral

Growth and multiple stacking of self-assembled InGaAsN/GaP quantum dot by molecular beam epitaxy

Noriyuki Urakami, Hironari Ito, Hiroto Sekiguchi, Hiroshi Okada, Akihiro Wakahara

Toyohashi University of Technology, Toyohashi Hibarigaoka, Tempaku-cho, Toyohashi, Aichi 441-8580, Japan

e-mail: urakami-n@int.ee.tut.ac.jp

Introduction: For the realization of future high integration optical interconnection devices such as optoelectronic integrated circuits, monolithic integration of III-V based optical devices to Si is key technology because Si has indirect band gap [1]. In particular, the conventional III-V based optical materials like GaAs or InP with low densities of crystalline defects such as threading dislocations and misfit dislocations are necessary to achieve long device lifetime. The dilute nitride GaAsPN (As > ~ 80 %) alloys shows direct band gap and is promising for the pseudomorphic quantum well grown on Si substrate [2]. However, high N incorporation (~ 7.5 %) into the GaAsPN/GaP QW structure has been designed to obtain conduction band offset (ΔE_c) and to close the lattice constant to that of Si, because conduction band energy and lattice constant of dilute nitride decrease with the increase of N composition. Point defects related N incorporation have increased with the increase of N composition in the dilute nitride [3]. Point defects generally act the nonradiative recombination centers. On the other hands, InGaAs/GaP quantum dot (QD) structure has been investigated for Si-based optical devices [4]. This structure has been expected higher carrier confinement and temperature stability compared to QW structure, because QD structure can been available to three-dimensional carrier confinement. However, low carrier confinement has been reported by band alignment calculation due to GaP barrier layer is indirect semiconductor and highly compressive strain applies to InGaAs [5]. Therefore, the increase of ΔE_c is necessary in order to realize high performance optical devices. The N incorporation into InGaAs QD is one of candidates to achieve higher ΔE_c. Here, it should be noted that N incorporation into QD structure may impact a growth behavior of three-dimensional islands such as size distribution reported InAsN/GaAs QD systems [6]. In this report, effects of N incorporation on form characterizations of self-assembled InGaAsN/GaP QD islands were investigated. The size fluctuation of islands height was optimized narrow by deposition thickness and N composition. Additionally, since critical thickness for GaP layer on Si substrate without misfit dislocation has been 50 – 70 nm [7], the GaP spacer layer in multiple stacked InGaAsN/GaP QD structure was studied as thin as possible by observation of luminescence spectra. Lastly, growth of the multiple stacking InGaAsN/GaP QD structure on Si substrate was demonstrated.

Experimental produce: Self-assembled InGaAsN/GaP QDs were grown by a conventional solid-source molecular beam epitaxy apparatus equipped with an As_2 valved cracker and radio frequency (rf)-plasma N cell. We used semi-insulating GaP (001) substrates. The growth temperature, growth rate and beam equivalent pressure (BEP) ratio of $BEP_{As2}/BEP_{(In+Ga)}$were set to 460 ºC, 0.3 monolayers per second (ML/s) and 20, respectively. The In composition was fixed 40% which was estimated by InGaAsN/GaAs QW. In the first step, uncapped InGaAsN/GaP QDs were fabricated to investigate islands density and height distributions. Prior to the growth of InGaAsN islands, a 100-nm thick GaP buffer layer was grown at 600 ºC. Subsequently, we switched the group-V beam from $P_2$to As_2. Then the substrate temperature was reduced to 460 ºC, self-assembled InGaAsN islands were formed by Stranski-Krastanov growth mode. After the

growth, the substrate was rapidly cooled under As_2irradiation in fabrication of uncapped samples. After the self-assembled InGaAsN islands formed as mentioned above, islands were embedded with a 20-nm thick GaP at 460 ºC in fabrication of GaP-capped to observe luminescence spectra. Where, to suppress the reduction of the density on the embedded islands by As/P exchange reactions, Ga adatoms corresponding to approximately 1 ML was deposited on the islands before P_2 beam supply [8]. The substrate temperature was then taken to 580 ºC and a 80-nm thick GaP layer was grown. The deposition thickness was 1.8 ~ 2.4 MLs. The N plasma power of N cell was 180 ~ 350W and N_2 flow rate was fixed 0.1 sccm. In the next step, GaP spacer layers thickness in the multiple staked InGaAsN/GaP QD structure were investigated. The GaP spacer layers thickness were investigated from 10 to 20 nm by the double stacked QD structure. Then, deposition thickness and N plasma power were 1.8 MLs and 180 W in a QD layer, respectively. Lastly, the five stacked InGaAsN/GaP QD structure on the dislocation free GaP/Si template was fabricated. The GaP/Si template was developed by migration enhanced epitaxy with optimized conditions with growth sequence and annealing [7]. Then, the GaP spacer layers thickness in the QDs structure were 10nm. The surface images of InGaAsN/GaP QD islands were characterized by atomic force microscopy. Photoluminescence (PL) spectra were measured by pumping with a 532-nm Nd: YVO_4 laser.

Results and discussion: Figure 1 shows amount of deposition dependence of height distribution on uncapped InGaAsN/GaP QD islands. The islands density was realized 10^{11} cm^{-2} in all samples as shown in the inset. Especially, high islands density of $4.1\times10^{11}cm^{-2}$ was available with 1.8 MLs deposition. This density is approximately 3 ~ 4 times higher than that of conventional self-assembled QD systems such as In(Ga)As on GaAs (001) substrates. Since the height fluctuation generally affects line width of luminescence spectrum, narrow height fluctuation is desired. The height fluctuation for 1.8 MLs deposition was the narrowest in this study and, then the average height was 2.6 nm. Figure 2 shows dependence of N plasma power on islands density of uncapped InGaAsN/GaP QD islands. The inset table shows islands density. In the GaAsN/GaP quantum well systems, the N composition of each samples were estimated to be 1.2, 2.5 and 3.0 % with N plasma power of 180, 300 and 350 W, respectively. The islands density grown with supplying N radicals was two orders higher than that without supplying N radicals. Migration length of In and Ga adatoms were decreased with supplying N radicals due to bonding energy of III-N are higher than that of III-As. Additionally, islands density and height distribution seems to be not depend on N plasma power. Here, N incorporation efficiency with compressive strain material systems has been shown the increase compared to unstrained material systems in dilute nitride. For GaPN alloys, the N composition grown on Si substrate has been increased 1.6 times more efficient compared to GaP substrate [9]. Therefore, plasma power of 180 W is sufficient. Figure 3 shows dependence of GaP spacer layer thickness on PL spectra from InGaAsN/GaP double stacked QD and single QD. The PL peak energy blueshifted with thinning the GaP spacer layer reducing from 20 nm to 10 nm. The mini-band formation caused by electron coupling in vertical direction was not dominantly indicated. If the mini-band formation occurred, the red-shift should be observed [10]. This finding was attributed to the increase of lateral compressive strain with thinning the GaP spacer layer [11]. On the other hand, PL intensity from double staked QD samples for any spacer thickness was monotonically increased approximately 1.5 times compared to single QD. Thus, the spacer layer thickness could be thinned to 10 nm without the degradation of PL intensity. From the above results, the deposition thickness, N plasma power and spacer thickness in the multiple stacked InGaAsN/GaP QD structure on GaP substrate were optimized to 1.8 ML, 180 W and 10 nm, respectively. Figure 4 shows luminescence spectra of InGaAsN/GaP 5QD structure on GaP/Si template and sample structure, respectively. This structure was consisted $In_{0.4}Ga_{0.6}AsN$/GaP 5QD active layer and $GaP_{0.97}N_{0.03}$ barrier layer. In order to improve luminescence intensity, the sample was performed thermal annealing in N_2 ambient for 1 minute at 700 ºC. Two different luminescence peaks from doped-Si substrate and InGaAsN/GaP 5QD were observed at 200 K. However, luminescence from InGaAsN/GaP 5QD was not observed at 293 K. The increase of active non-radiative recombination centers in the layer structure with rising measurement temperature was one of the reasons. In particular, many deep traps which are like isoelectronic traps existed in InGaAsN QD layers and the crystalline was not completely improved by annealing above. Additionally, InGaAsN QDs were selectively excited in active layer of InGaAsN/GaP 5QD structure because the absorption coefficient of GaP crystal is 1.25×10^{-2} cm^{-1} at 532-nm (2.33 eV) and absorption of GaP at the energy region is weak [12].

References

[1] H. Yonezu, Semicond. Sci. Technol. **17** (2002) 762. [2] B. Kunert, et al., Appl. Phys. Lett. **88** (2006) 182108. [3] I. A. Buyanova, et al., Solid-State Electron. **47** (2003) 467. [4] T. N. Thanh, et al., Appl. Phys. Lett. **99** (2011) 143123. [5] F. Fukami, et al., Phys. Stat. sol. C **8** (2011) 322. [6] J. F. Fälth, et al., Nanotechnology **19** (2008) 045608. [7] K. Yamane et al., J. Cryst. Growth **312** (2010) 2179. [8] K. Umeno et al., Physica E **42** (2010) 2772. [9] A. Utsumi et al., J. Cryst. Growth **295** (2006) 12. [10] G. S. Solomon et al., Phys.Rev.Lett.**76** (1996) 952. [11] Q. Xie, et al., Phys.Rev.Lett.**75** (1995) 2542. [12] S. Adachi, Optical Constants of Crystalline and Amorphous Semiconductor, Kluwer Academic Publishers, United States of America, 1999.

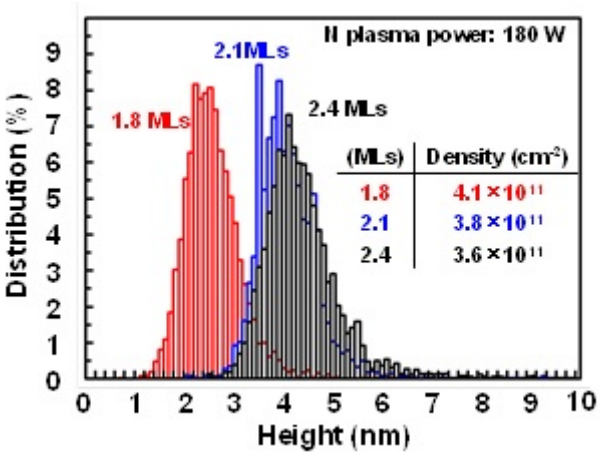

Figure 1. Amount of deposition dependence of height distribution for uncapped samples. The inset table shows islands densities.

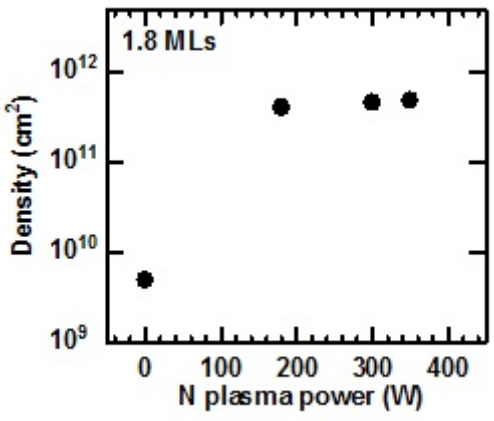

Figure 2. Dependence of N plasma power on islands density for uncapped samples.

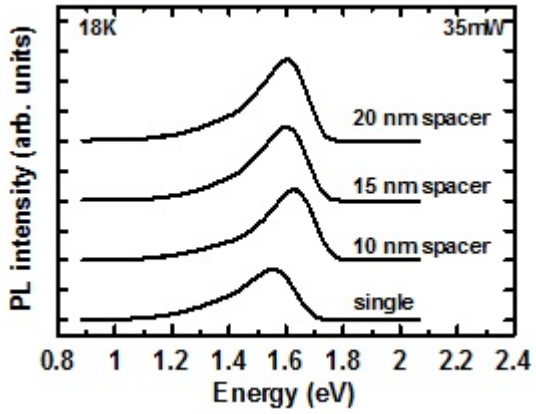

Figure 3. PL spectra at 18 K as a function of spacer layer thickness.

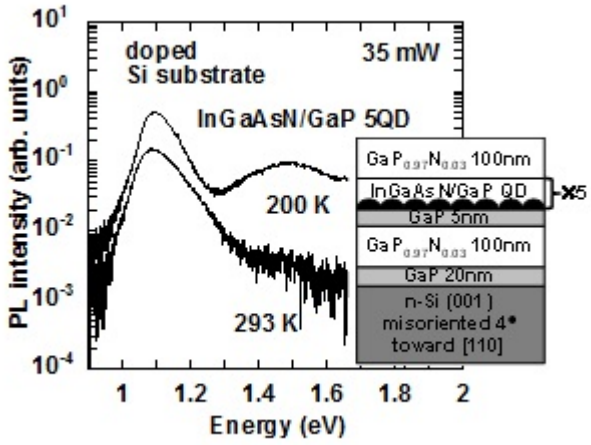

Figure 4. PL spectra at 200 and 293 K from InGaAsN/GaP 5QD on GaP/Si template. Inset shows layer structure.

12:45 Oral

High-uniformity GaAs/AlGaAs quantum dots coupled with GaAs wetting layer embedded in a GaAs/AlAs superlattice

Yu Chen Chang, Qiandong Zhuang, Alex Robson, Peter D. Hodgson, Manus Hayne, Ana M. Sánchez

Lancaster University, Lancaster LA1-4YB, United Kingdom

e-mail: y.chang4@lancaster.ac.uk

Self-assembled growth of high-quality quantum dots (QDs) is important for fabricating novel and effective electronic and photonic devices [???]. Typically, QDs are obtained via the Stranski-Krastanow (SK) growth mode, which reduces strain arising from lattice mismatch in underlying layers. A defining feature of SK growth is the formation of a wetting layer (WL) that precedes dot growth. The WL mediates the electronic interaction between the barrier states and the localized QD states influencing the optical properties of the QDs. Charge transfer between QDs via higher energy states can, for example, prove advantageous for laser operation [???]. SK growth is not possible in lattice-matched materials due to the absence of strain, droplet epitaxy (DE) is a promising technique, which enables self-assembly of strain-free QDs [???]. For the fabrication of GaAs/AlGaAs QDs, for instance, the size and density of the GaAs QDs is dependent on that of the Ga droplets, which is a function of growth temperature and Ga flux, and on the subsequent crystallisation process with As flux. However, QDs are formed without a WL, unless special growth conditions are used [???]. Besides potential advantages in terms of carrier transfer, inclusion of a GaAs WL is expected to improve the As adatom surface diffusion resulting in the growth of more uniform dots. Here, we report GaAs/AlGaAs QDs with highly uniform size and excellent optical properties.

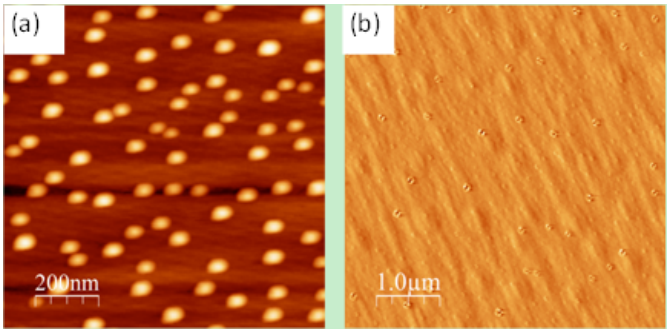

Figure 1: AFM image of (a) 3 MLs Ga droplets and (b) GaAs quantum dots

Figure 1(a) shows Ga droplets with an average diameter of 69±4 nm formed by the deposition of 3 monolayers (MLs) Ga on a GaAs substrate at 320ºC. GaAs/AlGaAs QDs with mean diameter of 99±10 nm were subsequently formed after supplying low As flux at 400ºC [Fig. 1(b)].

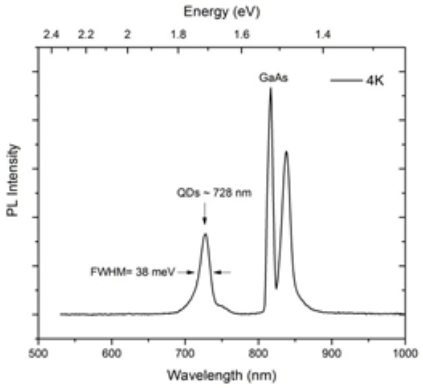

Figure2: 4K PL spectrum of GaAs QDs

The optical properties of GaAs QDs grown under similar conditions, but embedded in $Al_{0.3}Ga_{0.7}As$, were studied using photoluminescence (PL), shown in Fig.2. At 728 nm, the QD PL is at higher energy than the bulk GaAs emission due to confinement effects, but has lower intensity. The FWHM of the QD emission is 38 meV, which is typical for SK QDs, and indicates that although the initial size of Ga droplets is uniform, the final shape and size of the QDs on the crystallisation process during the supply of As flux. To improve the size uniformity of the QDs and the FWHM and intensity of their PL, new structure was grown where a GaAs WL was inserted immediately prior to the QD growth, and both Ga droplet deposition and crystallisation with As flux were at 320ºC. The GaAs/$Al_{0.3}Ga_{0.7}As$ structure was also embedded in a GaAs/AlAs superlattice (SL).

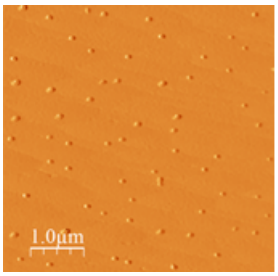

Figure3: AFM image of surface of GaAs QDs from the superlattice sample

Fig 3 shows that the surface of GaAs QDs for this sample have high uniformity (99±3 nm) and areal density of 10^8 cm^{-2} .

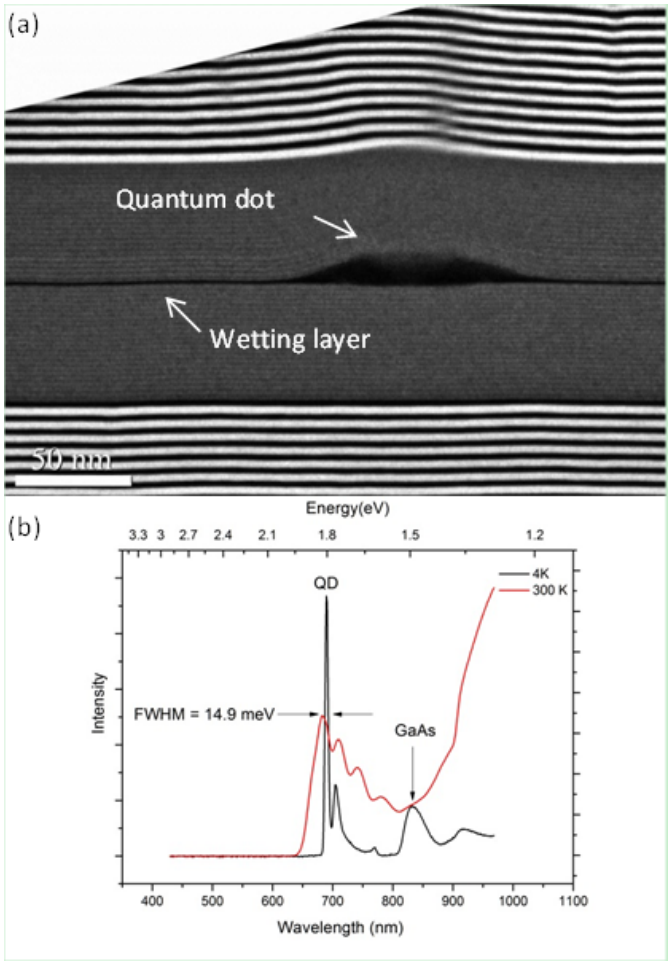

Figure 4: (a) TEM image of GaAs/AlGaAs QDs embedded in GaAs-AlAs SL and (b) 4K and 300K PL spectra

Fig 4(a) shows a transmission electron microscopy (TEM) image of a GaAs/AlGaAs QD embedded in GaAs/AlAs SL structure. A continuous WL under the QDs is clearly observed. Low-temperature and room temperature PL spectra from the same sample are shown in Fig. 4(b). The very narrow PL emission (FWHM of 14.9 meV) observed from the QDs at 4K (centred at 689 nm) indicates high optical quality and excellent dot uniformity. Despite the low areal number density of 10^8 cm^{-2} the QD peak in Fig. 3 is now more intense than the GaAs peak, which we attribute this to efficient transfer of carriers from the SL to the WL and from the WL to the dots. At room temperature, the PL shows a series of sub-peaks, which we attribute to different quantum confined dot states.

1. D Bimberg, M. Grundmann., and N.N Ledentsov, *Quantum Dots Heterostructures*1999, New York: Wiley.

2. C. Cornet, et al., *InAs/InP quantum dots (QD): from fundamental understanding to coupled QD 1.55 μm laser applications.* physica status solidi (c), 2007. **4**(2): p. 458-461.

3. M. Jo, T. Mano, and K. Sakoda, *Two-Step Formation of Gallium Droplets with High Controllability of Size and Density.* Crystal Growth & Design, 2011. **11**(10): p. 4647-4651.

4. S. Sanguinetti, et al., *Modified droplet epitaxy GaAs/AlGaAs quantum dots grown on a variable thickness wetting layer.* Journal of Crystal Growth, 2003. **253**(1–4): p. 71-76.

Lunch (JCG Editors meeting)

Monday afternoon, 12 August, 13:00

MoO2

G08: Nanomaterials and low dimensional structures
Monday afternoon, 12 August, 15:00
Room D, Auditorium Maximum

15:00 Invited oral

In situ TEM control growth of nanowire heterostructures and the nanoscale reactions

Yi-Chia Chou

National Chiao-Tung University, Institute and Department of Electrophysics, 1001 Ta Hsueh Road, Hsinchu 30050, Taiwan

e-mail: ycchou@nctu.edu.tw

Recent advances in nanotechnology have offered the hope of extending Moore's law of large scale integration of semiconductor device circuits to nanodevices. Nanostructures based on Si will play an important role in future semiconductor technology. In situ transmission electron microscopy is a powerful means to understand the kinetics of nanoscale reactions. In this talk, I will present in-situ transmission electron microscopy of solid-state chemical reactions in the nanowire-based nanostructures and the control of the formation of nano-heterostructures.

Transition metal silicide nanowires are strong candidates for circuit elements in one-dimensional nanodevices, with applications including ohmic contacts, Schottky barriers, gate electrodes and interconnects. Silicidation reactions take place at the point contact between adjacent nanowires or nanoparticles, and high resolution imaging allows the reaction to be followed in real time as each layer of Si is transformed. It is possible to control the formation of the metal silicide accurately enough to fabricate nano-gap heterostructures, where silicide regions are separated by just a few atomic planes of Si. The atomic-level details of the growth process can also be examined directly, and I will show axial epitaxial stepwise growth of CoSi2, NiSi, and NiSi2 in silicon nanowires. This growth process is unique, in that each atomic plane of silicide nucleates at the center of the nanowire cross-section in a homogeneous nucleation event that had been theoretically predicted but not observed previously. The oxidized surface structure of the nanowire is of key importance in this nucleation and growth process, and I will discuss the differences in growth mechanism and morphology when silicidation reactions are carried out in-situ on nanowires with atomically clean surfaces.

Recent experimental and theoretical studies show that, in metal-catalyzed nanowire growth, sharp interfaces within nanowires can be achieved by using solid catalysts (the VSS growth mode). Solid catalysts have low solubility for the growth species and hence do not act as a reservoir when switching between materials. We propose a method using solid silver-based catalysts to grow abrupt Ge layers embedded in Si nanowires, and demonstrate the results using in situ transmission electron microscopy. Ag is completely miscible with Au without intermetallic compounds, so homogeneous Ag-Au alloys can be formed and act as catalysts. Ag-Au alloys have two advantages compared to Au or solid alloy catalysts: The eutectic temperatures of Ag-Au alloys with Si are higher than pure Au with Si so that, compared to pure Au, solid alloy catalysts are stable at higher temperatures where growth rates are faster. Furthermore, the resistance of Ag to oxidation makes it easier to work with than say Al alloys and potentially allows scaling up to standard CVD growth systems. We will show that the temperatures at which liquid and solid Ag-Au catalysts are stable, and hence growth occurs by the VLS and VSS processes, are tuned by adjustment of the Ag/Au ratio. In situ movies show that VSS Si growth occurs by ledge propagation at the alloy/silicon interface, similarly to AlAu alloys. We will discuss the details of the growth process, in particular periodic changes in the catalyst shape and growth interface morphology as individual ledge flow events occur. We can switch growth mechanisms controllably between VLS and VSS, enabling optimization of growth rates and the formation of abrupt interfaces and thin layers, thus opening up a promising route towards control of nanowire and heterostructure growth and morphology.

15:30 Invited oral

Growth modeling of III-V semiconductor nanowires

Vladimir G. Dubrovskii

Ioffe Physico-Technical Institute, RAS, Saint-Petersburg, Russian Federation

e-mail: dubrovskii@mail.ioffe.ru

In this talk, I will review some recent achievements in modeling of growth and crystal structure of III-V semiconductor nanowires. These nanowires are usually grown by different epitaxy techniques via the vapor-liquid-solid mechanism. In this mechanism, a metal catalyst particle (Au or group III metal) is seated on the top of a nanowire and promotes its vertical growth by different kinetic pathways: directly from vapor or by surface diffusion of adatoms [1-3].

I will first discuss the growth modeling based on the material transport equations and nucleation theory. The latter is used to describe the nucleation-mediated growth at the liquid-solid interface under the droplet. Due to a small size of a catalyst particle, the vapor-liquid-solid nanowire growth usually proceeds in the so-called mononuclear regime, where only one island suceeds in nucleation in one layer and then rapidly spreads laterally to complete the naInowire monolayer slice. This entails major difference with nucleation in large volumes and gives rise to many interesting effects such as self-regulated pulsed supersaturation, temporal anti-correlation of nucleation events and periodically changing morphology of the growth interface [4-6].

I will then consider theoretical dependences of the nanowire growth rate on the nanowire radius and the growth conditions, and show how these results are used to describe and control the morphology of MBE and MOCVD-grown GaAs, InAs, InP and other III-V nanowires.

The second part of the talk will regard the surprising effect of wurtzite phase formation in the vapor-liquid-solid III-V nanowires of cubic zincblende materials. It will be shown that this effect originates from a lower surface energy of relevant sidewall facets of hexahedral wurtzite nanowires, but also depends on the level of liquid supersaturation in the catalyst droplet during growth. I will discuss the concept of the triple phase line nucleation [7] and show how the supersaturation dependence of the preferred crystal phase can be used to control the structure of catalyzed III-V nanowires [8,9]. In particular, the formation of abrupt zincblende-wurtzite crystal phase heterostructures in III-V nanowires [10] will be demonstrated.

Finally, I will consider the Ga-catalyzed MBE growth of GaAs nanowires on Si substrates and discuss the novel mode of the vapor-liquid-solid nanowire growth where the droplet wets the nanowire sidewalls [11]. This has an inetersting impact on the crystal phase purity and helps to avoid the polytypism on surface energetic grounds.

References

[1] V.G. Dubrovskii, N.V. Sibirev, G.E. Cirlin, I.P. Soshnikov, W.H. Chen, R. Larde, E. Cadel, P. Pareige, T. Xu, B. Grandidier , J.-P. Nys, D. Stievenard, M. Moewe, L.C. Chuang, and C. Chang-Hasnain, Phys. Rev. B **79**, 205316 (2009).

[2] V.G. Dubrovskii, N.V. Sibirev, G.E. Cirlin, A. D. Bouravleuv, Yu.B. Samsonenko, D.L. Dheeraj, H.L. Zhou, C. Sartel, J.C. Harmand, G. Patriarche, and F. Glas, Phys. Rev. B **80**, 205305 (2009).

[3] V.G. Dubrovskii, T. Xu, Y. Lambert, J.-P. Nys, B. Grandidier, D. Stievenard, W. Chen, and P. Pareige, Phys. Rev. Lett. **108**, 105501 (2012).

[4] C.-Y. Wen, J. Tersoff, K. Hillerich, M. C. Reuter, J. H. Park, S. Kodambaka, E.A. Stach, and F.M. Ross, Phys. Rev. Lett. **107**, 025503 (2011).

[5] F. Glas, J.C. Harmand, and G. Patriarche, Phys. Rev. Lett. **104**, 135501 (2010).

[6] V.G. Dubrovskii, Phys. Rev. B, accepted for publication (2013).

[7] F. Glas, J.C. Harmand, and J. Patriarche, Phys. Rev. Lett. **99**, 146101 (2007).

[8] V.G. Dubrovskii, N.V. Sibirev, J.C. Harmand, and F. Glas, Phys. Rev. B **78**, 235301 (2008).

[9] G.E. Cirlin, V.G. Dubrovskii, Yu.B. Samsonenko, A.D. Bouravleuv, K. Durose, Y.Y. Proskuryakov, B. Mendis, L. Bowen, M. A. Kaliteevski, R.A. Abram, and D. Zeze, Phys. Rev. B **82**, 035302 (2010).

[10] K.A. Dick, C. Thelander, L. Samuelson, and P. Caroff, Nano Lett. **10**, 3494 (2010).

[11] V.G. Dubrovskii, G.E. Cirlin, N.V. Sibirev, F. Jabeen, J.C. Harmand, and P. Werner, Nano Lett. **11**, 1247 (2011).

16:00 Oral

$In_xGa_{1-x}As$ alloy fluctuation and quantum dot nucleation mechanism

Tomoya Konishi[1], Gavin R. Bell[1,2], Shiro Tsukamoto[1]

1. *Anan National College of Technology, Anan 774-0017, Japan*
2. *University of Warwick, Department of Physics, Gibbet Hill Road, Coventry CV4 7AL, United Kingdom*

e-mail: konishi@anan-nct.ac.jp

For optimal use of semiconductor quantum dots (QDs), it is desirable to arrange them in a highly dense and site-controlled array. However, important gaps remain in the understanding of the Stranski-Krastanow-like growth mechanism of InAs-GaAs QDs, particularly the effects of surface reconstruction (SR) in the wetting layer (WL) prior to QD

nucleation. It is reported that the (n×3) SRs favour intermixing of Ga and In atoms. Furthermore, *ab initio* Monte Carlo simulations have shown that the migration barrier energy of mobile In adatoms becomes higher on Ga defects, implying that initial nucleation occurs preferentially on $In_xGa_{1-x}As$ alloy fluctuations within the WL, associated with (n×3) SR [1].

In order to test the ansatz experimentally, we carefully measured the spatial distribution of (n×3) SR in the WL using a unique scanning tunnelling microscopy / molecular beam epitaxy (STMBE) system. If QD nucleation is induced by (n×3) SR, it is likely that the spatial distribution of QD precursors resembles that of (n×3) SR [2]. In this study, we analyzed the spatial distribution of the SR on the 100×100 nm^2 STMBE images by using image processing techniques (Fig. 1). The SR is distinguished by As dimer row pitch ((n×2) (c(4×4)), (n×3), (n×4) regions). We finally obtained a precise map of SR patterns. We demonstrate that the frequency distribution of the measured pitches is comparable with the RHEED patterns and Fourier transformed STM images (Fig. 2).

From the SR map of WL, the spatial distribution function of (n×3) SR pattern was calculated and was compared to that of QD nucleation pattern. The similarity in the both functions suggested that QD nucleation is likely induced by $In_xGa_{1-x}As$ fluctuations forming (n×3) SR.

[1] S. Tsukamoto, T. Honma, G. R. Bell, A. Ishii, and Y. Arakawa, *Small* **2** 386 (2006).

[2] T. Konishi, S. Tsukamoto, *Surface Science***605** L1–L5 (2011).

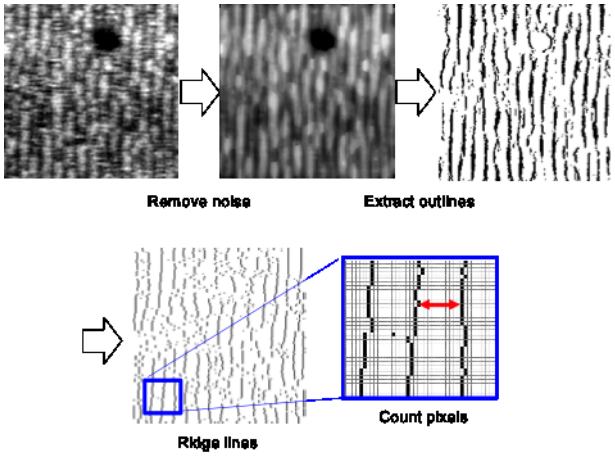

Fig. 1: Schematic diagram of surface reconstruction map generation on an example 20×20 nm^2 region.

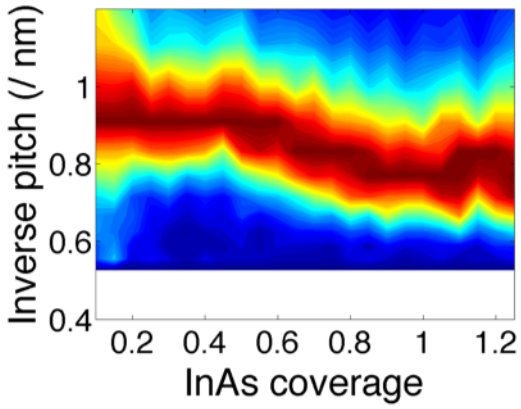

2: Evolution of As dimer row pitch as a function of InAs coverage. It is shown that the surface reconstruction changes from (n×2) to the mixture of (n×3) and (n×4).

16:15 Oral

Quantum-Dot Ring Formation by Strained Droplet Epitaxy

Suwit Kiravittaya[1], Poonyasiri Boonpeng[2], Wipakorn Jevasuwan[2], Somchai Ratanathammaphan[2], Somsak Panyakeow[2]

1. *Naresuan University, Phitsanulok 65000, Thailand* **2.** *Chulalongkorn University, Department of Electrical Engineering, Semiconductor Device Research La, Dep. Electrical Engineering, Faculty of Engineering, 254 Phyathai Road, Bangkok 10330, Thailand*

e-mail: suwitki@gmail.com

Recently, fabrication of advanced quantum-dot (QD) architectures gains a lot of interests due to its potential to realize novel nano-electronic and nano-photonic devices [1]. Self-assembled growth is a bottom-up process to create complex nanostructures without using cumbersome fabrication steps. Growths of self-assembled III-V QDs has continuously been investigated and applied with other techniques. In this work, we theoretically investigate the formation of QD ring in strained droplet epitaxy. A generic growth model is proposed to explain the experimentally observed results.

Conventional droplet epitaxy can divided into 2 steps, i.e., (i) deposition of group-III metallic nano-droplet and (ii) crystallization by group-V material. For *strained* droplet epitaxy, the strain will accumulated in the nanostructures and thus the self-assembly process will occurred as the latest step (Fig. 1). Models for growth of unstrained nanostructures have existed [2]. Here, we extend these models to account for the intrinsic strain accumulated in nanostructures. By using numerical finite element method, the strain distribution and total strain energy are analyzed. We perform energetic comparisons of total energy (strain energy and surface energy) between homogeneous ring and QD ring structure. According to our calculation (Fig. 2(a)), the critical size/volume for triggering the self-assembly process can be estimated. It agrees well with the experimental results (Fig. 2(b)) [3-4].

In conclusion, we have extend the growth scenario of conventional unstrained droplet epitaxy to the strained systems. This work will improve the understanding of nanostructure fabrication processes and thus open the door to realize more complex and controllable nanostructures.

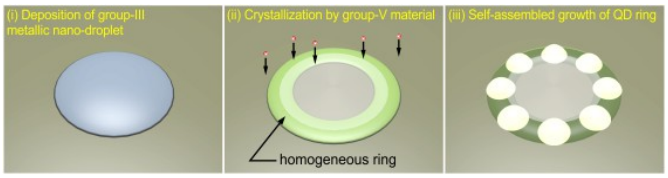

Fig. 1 Growth scenario for QD ring formation by strained droplet epitaxy

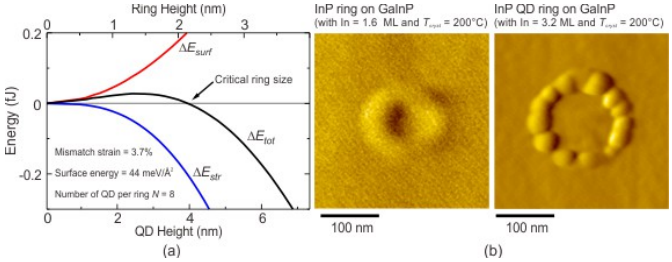

Fig. 2 (a) Variation of total energy showing critical size for nanostructure shape transition. Beyond the ring height of ~2.2 nm, QD is energetic preferential shape. (b) Atomic force microscopy images of single InP ring and QD ring obtained at different amount of indium deposition.

References

[1] S. Kiravittaya, A. Rastelli, and O. G. Schmidt, "Advanced quantum dot configurations," *Rep. Prog. Phys.***72**, 046502, (2009).

[2] X. L. Li and G. W. Yang, "On the physical understanding of quantum rings self-assembly upon droplet epitaxy," *J. Appl. Phys.***105**, 103507, (2009).

[3] P. Boonpeng, W. Jevasuwan, S. Suraprapapich, S. Ratanathammaphan, and S. Panyakeow, "Quadra-quantum dots grown on quantum rings having square-shaped holes: Basic nanostructure for quantum dot cellular automata application," *Microelectron. Eng.***86**, 853, (2009).

[4] W. Jevasuwan, P. Boonpeng, S. Thainoi, S. Panyakeow, and S. Ratanathammaphan, "InP ring-shaped quantum-dot molecules grown by droplet molecular beam epitaxy," *J. Cryst. Growth***323**, 275, (2011).

16:30 Oral

Molecular Beam Epitaxial Growth of GaSb Quantum Dots on Ge Substrates

Suwit Kiravittaya[1], Maetee Kunrugsa[2], Suwat Sopitpan[3], Somchai Ratanathammaphan[2], Somsak Panyakeow[2]

1. *Naresuan University, Phitsanulok 65000, Thailand* **2.** *Chulalongkorn University, Department of Electrical Engineering, Semiconductor Device Research La, Dep. Electrical Engineering, Faculty of Engineering, 254 Phyathai Road, Bangkok 10330, Thailand* **3.** *Thai Microelectronics Center, Chachoengsao 24000, Thailand*

e-mail: s_panyakeow@yahoo.com

Ge is a well-known bulk material for infrared detectors. Ge doped with transition metals such as gold and mercury have been used for far infrared applications and detectors for CO_2 lasers [1]. However, due to its low band gap, typical Ge detectors operate at low temperature of liquid nitrogen. GaSb/GaAs quantum dots (QDs) are type II nanostructures having also a potential for mid-infrared and far-infrared applications [1,2]. Based on quantum confinement behavior, GaSb can operate to operate at higher temperature.

We combine these two materials, i.e., Ge and GaSb in our samples grown by molecular beam epitaxy (MBE). At the beginning phase, we grew GaAs epitaxial layer on Ge substrates. Anti-phase domains (APD) of GaAs are distributed on the Ge surface due to the nature III-V compound growth on group IV semiconductors. We have experimentally investigated the growth of GaAs APD on Ge substrates as well as the growth of InAs QDs on APD epitaxial layers [3]. Figure 1 shows an AFM image of InAs/GaAs QDs on Ge substrate. The InAs QDs mainly locate near the domain walls due the high strain field and are elongated along [110] crystallographic directions in each GaAs domain. The elongation directions of APDs are typically perpendicular to each other.

For Sb-related growth, we have installed Sb cracker cell to our MBE system and have investigated the growth of GaSb QDs. Figure 2 shows an atomic force microscopy image of typical GaSb QDs having ~7 nm in height and ~80 nm in diameter. Optical properties of these nanostructures are characterized by photoluminescence measurement in order to investigate their quantum confinement behaviors.

In this contribution, we will report the MBE growth recipe and characterization of GaSb/GaAs QDs on Ge substrates. Details of our growth steps as well as the properties of obtained structures will be presented. Structural comparisons between conventional QD growth and the growth on Ge substrate will be discussed.

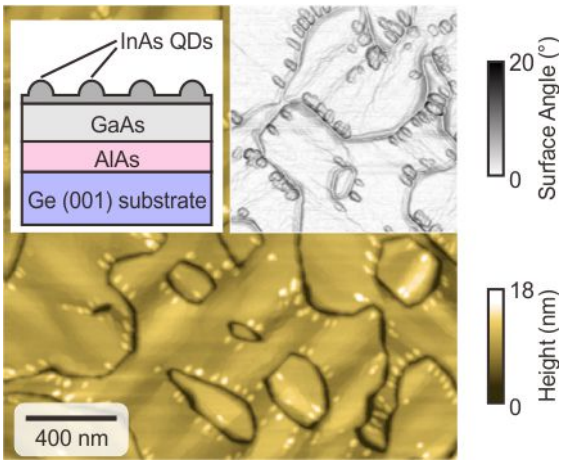

Fig. 1 An AFM image of InAs QDs on APD of GaAs on Ge substrate

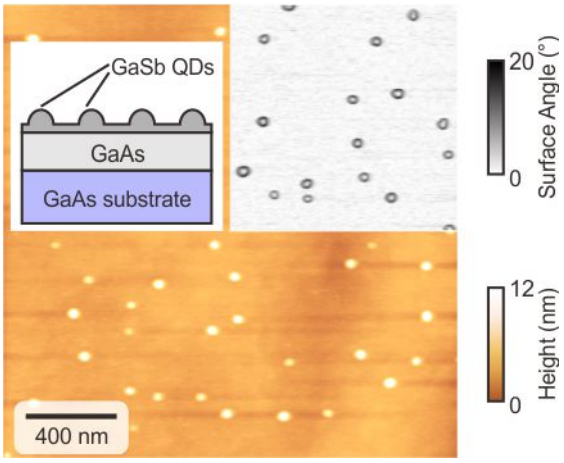

Fig. 2 A typical 2×2 μm^2 AFM image of GaSb QDs on GaAs substrate

References

[1] E H. Putley, "Far infra-red photoconductivity," *phys. stat. sol.***6**, 571 (1964). K. Kikuchi, M. Saguchi, and A. Oshimoto, "A new photoconductive sensor for 10.6-mm infrared radiation," *IEEE Trans. Instrum. Meas.***37**, 137 (1988).

[2] W.-H. Lin, C.-C. Tseng, K.-P. Chao, S.-C. Mai, S.-Y. Kung, S.-Y. Wu, S.-Y. Lin, and M.-C. Wu, "High-temperature operation GaSb/GaAs quantum-dot infrared photodetectors," *IEEE Photon. Technol. Lett.***23**, 106 (2011).

[3] W. Tantiweerasophon, S. Thainoi, P. Changmuang, S. Kanjanachuchai, S. Rattanathammaphan, and S. Panyakeow, "Self-assembled InAs quantum dots on anti-phase domains of GaAs on Ge substrates," *J. Cryst. Growth***323**, 254 (2011).

16:45 Oral

MBE grown microcavities based on selenide and telluride compounds

Jean-Guy Rousset[1], Tomasz Jakubczyk[1,2], Jakub Kobak[1], Piotr Piotrowski[1], Elżbieta Janik[1], Tomasz Slupinski[3], Andrzej Golnik[1], Piotr Kossacki[1], Michał Nawrocki[1], Wojciech Pacuski[1]

1. *University of Warsaw, Faculty of Physics, Institute of Experimental Physics (IFDUW), Hoża 69, Warsaw 00-681, Poland* **2.** *University of Bremen, Institute of Solid State Physics, P.O. Box 330440, Bremen 28334, Germany* **3.** *Faculty of Physics, University of Warsaw, Hoża 69, Warszawa 00-681, Poland*

e-mail: j-g.rousset@fuw.edu.pl

Light-matter coupling in semiconductor microcavities has been intensively investigated over the past twenty years. Microcavities containing quantum dots (QDs) or quantum wells (QWs), led to the achievement of various devices for optoelectronics such as vertical cavity surface emitting lasers (VCSELs) [1] or resonant cavity light emitting diodes (RCLEDs) [2]. Etched pillar microcavities containing QDs allow controlling spatial, energetic and temporal properties of light emission [3,4]. The coherent coupling between light and matter in such structures is of great interest for quantum information processing. Compared to III-V compounds, the stronger carrier confinement and more robust excitonic states exhibited by II-VI compounds is expected to extend the fundamental investigations on light matter coupling and the functionalization of the devices to higher temperatures [5]. In addition, II-VI compounds based emitters are good candidates to answer the problem of the low efficiency of III-V based emitters in the green yellow range [6].

The fabrication of high quality microcavities relies on opposite constrains: lattice matching of the layers with different refractive index (crystalline quality) and high refractive index contrast (optical quality, photon confinement efficiency within the cavity). The additional question of the implementation of efficient light emitters in the cavity dedicated to the desired application (spectrally narrow tunable light emitter, VCSEL, investigation of the photon-exciton strong coupling) makes the successful realization of II-VI based microcavities a real challenge.

In this work, we present three groups of microcavities: based on selenide compounds, based on telluride compounds, and structures based on mixed selenide and telluride compounds. We focus on their possible applications in the field of optoelectronic devices and fundamental physics (VCSELs, narrow range light sources, studies of photon-exciton coupling).

Selenide based microcavities built on (Zn,Mg)Se and (Zn,Cd)Se layers containing CdSe quantum dots present the advantage of exhibiting a relatively short wavelength absorption (near or under 520 nm). In addition, CdSe / ZnSe quantum dots are known to be good light emitters and good candidates for room temperature emission. However, we show that the relatively low refractive index contrast reachable limits the light confinement and the quality factor. As a resultmicrocavities based on these compounds could be used to build narrow range emitters in the green – yellow range since the quality factor of the cavity plays a secondary role for these devices. Telluride based microcavities allowed us to reach a higher refractive index contrast which resulted in the growth of a fully lattice matched structure containing (Cd,Zn)Te QWs [7]. Here we present the observation of the photon-exciton strong coupling for such structures with a single QW. However, the lower band gap of telluride based materials restrains the applications of such structures to the spectral range over 650 nm. Good candidates for a wide range of practical applications and fundamental studies are found to be selenide-telluride based structures [8,9] exhibiting a high refractive index contrast and lower absorption edge wavelength. We show that the cavity mode can be obtained for wavelength as short as 560 nm. We present results obtained with structures (planar and pillar microcavities) lattice matched to ZnTe for yellow optoelectronics applications and prospects for novel structures based on Zn(Se,Te) and (Cd,Zn,Mg)Se layers.

[1] M.E. Murtagh et al., Thin Solid Films, 450, 148 (2004).
[2] V. Vilokkinen et al., Mater. Sci. Eng. B, 74, 165 (2000).
[3] T. Jakubczyk et al., Appl. Phys. Lett., 101, 132105 (2012).
[4] J. M. Gerard et al., Phys. Rev. Lett., 81, 1110 (1998).
[5] C. Kruse et al., Appl. Phys. Lett., 92, 031101 (2008).
[6] M.R. Krames et al. , J. Display Techmology, 3(2), 2007
[7] J.-G. Rousset et al., ArXiv, 1210.1933 (2012).
[8] W. Pacuski et al., Appl. Phys. Lett., 94, 191108 (2009).

Break
Monday afternoon, 12 August, 17:00

Tuesday, 13 August

TuO1

G08: Nanomaterials and low dimensional structures
Tuesday morning, 13 August, 10:20
Room D, Auditorium Maximum

10:20 Invited oral

Structural aspects of nanoscale magnetic patterning of epitaxial metallic thin films

Andrzej Wawro[1], Ewelina Sieczkowska[1], Marcin Jakubowski[1], Lech T. Baczewski[1], Zbigniew Kurant[2], Piotr Mazalski[2], Andrzej Maziewski[2]

1. *Polish Academy of Sciences, Institute of Physics, al. Lotników 32/46, Warszawa 02-668, Poland* **2.** *University of Bialystok, Faculty of Physics, Lipowa 41, Białystok 15-424, Poland*

e-mail: wawro@ifpan.edu.pl

Magnetic layered structures spatially patterned in a nanoscale are of great scientific interest and high technological relevance. Such systems are excellent objects to perform fundamental studies on nanomagnetism as well as they are promising for practical applications: as magnonic crystals, sources of local magnetic fields in spintronics devices, or as magnetic recording media, in which undesired influence of superparamagnetic effects is substantially reduced. In this work we discuss different methods of magnetic patterning of Co-based sandwiches: by a spatially structured buffer and by irradiation with an ion beam. Magnetic properties studied by magnetometry utilizing magnetooptical Kerr effect (MOKE) and magnetic force microscopy (MFM) are correlated with structural features of the investigated patterned systems.

In the first method magnetic patterning is induced by deposition of a Co layer on a structured buffer in the form of Au islands, few hundred nanometers in lateral size, self-assembled on a Mo layer surface [1]. Observed Volmer-Weber growth mode is a consequence of surface energy interplay of low-index free atomic planes of Au and Mo and Mo/Au interface as well as elastic energy originating from a lattice mismatch. Due to strong dependence of magnetic anisotropy on a buffer/Co-film interface type, a system of elevated magnetic dots (Co layer grown on the top of the Au islands) embedded in the magnetic trench matrix (Co layer deposited between the Au islands on the Mo

layer surface) with various dot - matrix magnetization orientations (Fig. 1a) has been fabricated [2, 3]. A buffer material influences the surface anisotropy due to hybridization of electron orbitals at the interface and magnetoelastic contribution resulting from the lattice mismatch. Moreover, the structure of the buffer affects the growth of the Co layer and in consequence – the magnetocrystalline anisotropy. As the size of the magnetic dots is determined by dimensions of the Au islands, tuning of magnetic properties of the dots and their surface density becomes possible by control of the Au islands growth conditions on the Mo layer surface.

Combination of the results obtained from the PMOKE and MFM reveals magnetization switching mechanism of the dots by nucleation of a reversed domain followed by rapid and unpinned domain wall propagation (Fig. 1b). High crystalline quality of the studied epitaxial patterned structures, which are not exposed to any post-growth treatment, explains a monodomain character of the magnetic dots. Low amount of structural defects, confined dimensions and stiffer magnetization at the edges are responsible for higher nucleation field of the reversed domain in the dot in comparison with the uniform Au/Co/Au reference film. For the same reason the domain wall propagation is unperturbed. Thus, once nucleated, the reversed domain expands rapidly by the domain wall propagation over whole area of the dot.

In the second method the Pt/Co/Pt sandwiches are irradiated by an ion beam. As-deposited structure with in-plane magnetization exhibits consecutive reorientation spin transitions from in-plane to out-of-plane alignments and vice versa with an increasing fluence of the beam (Fig. 1c) [4, 5]. Observed behavior results from two competitive processes undergoing upon irradiation: (i) degradation of the interfaces (initially with a sharp chemical profile) which suppresses PMA and (ii) formation of ordered CoPt alloys exhibiting enhanced PMA. In-depth chemical profile and composition of the forming intermetallic alloys were estimated with use of TRIDYN simulations. Results obtained from these simulations and those revealed from XMCD measurements lead to a conclusion that $L1_0$ and $L1_2$ phases are responsible for PMA appearance with increasing irradiation fluence.

Controlled irradiation of the Pt/Co/Pt sandwiches with focused ion beam is expected to allow fabrication of structures periodically patterned in a nanoscale with desired properties of the irradiated spots.

Acknowledgement: This work has been partially supported by the National Science Center in Poland under the project no. DEC-2011/03/N/ST3/02662 and by the Foundation for Polish Science under the SYMPHONY project operated within the Team Programme, co-financed by the EU European Regional Development Fund, OPIE 2007-2013.

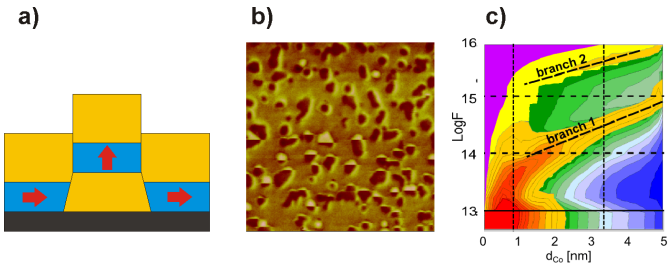

Fig.1. a) schematic representation of a magnetic dot with perpendicular magnetization embedded in a matrix magnetized in the plane (black: Mo buffer, blue: Co layer, yellow: Au island and cap layer, red arrows: magnetization directions); b) magnetization reversal (visible in the lower part of the MFM image) of the dots while scanning with a magnetic tip; c) a diagram (d_{Co} - Co layer thickness; F- Ga ion fluence) of magnetization orientation in Pt/Co/Pt sandwiches. Two branches of perpendicular magnetization are distinct (blue and green – magnetization in-plane; yellow and red – perpendicular magnetization, magenta – superparamagnetic state) [4].

[1] A. Wawro, M. Sobańska, A. Petroutchik, L. T. Baczewski and P. Pankowski, Nanotechnology 21, 335606 (2010).
[2] A. Wawro, A. Petroutchik, L. T. Baczewski, Z. Kurant and A. Maziewski, Europhys. Lett. 89, 37003 (2010).
[3] A. Wawro, E. Sieczkowska, A. Petroutchik, L.T. Baczewski, Z. Kurant, A. Maziewski, Phys Rev. B 83, 092405 (2011).
[4] A. Maziewski, P. Mazalski, Z. Kurant, M.O. Liedke, J. McCord, J. Fassbender, J. Ferré, A. Mougin, A. Wawro, L.T. Baczewski, A. Rogalev, F. Wilhelm, T. Gemming, Phys. Rev. B 85, 054427 (2012).
[5] P. Mazalski, Z. Kurant, A. Maziewski, M. O. Liedke, J. Fassbender, L. T. Baczewski, A. Wawro J. Appl. Phys. 113 17C109 (2013).

10:50 Oral

InZnO nanorods by liquid indium seeded vapour phase deposition

Andrea Zappettini, Sathish Chander Dhanabalan, Marco Villani, Laura Lazzarini, Davide Calestani

IMEM- CNR (IMEM), Parma, Italy

e-mail: zapp@imem.cnr.it

Metal oxide nanowires have received a continuously growing attention in the last years. Among them, in particular, zinc oxide nanowires (or nanorods) have been proposed for a large number of applications such as photovoltaics, UV emitters, piezo energy harvesting, gas sensing, and transparent electronics. Undoped zinc oxide shows typically n-type conductivity, generally ascribed to stoichiometric defects (e.g. oxygen vacancies or zinc interstitials) or due to unavoidable contamination of hydrogen that acts as interstitial donor. Most of the applications actually require a good control of electrical conductivity that can be achieved by doping or alloying ZnO. In particular, high n-type conductivity can be achieved by alloying zinc oxide with group III elements (such as Al, In or Ga) in ternary or even quaternary oxide compounds. Indeed, numerical calculations recently showed that 1-3% concentration of an element such as Al in a ZnO matrix, pushes Fermi level to penetrate into the conduction band, thus giving rise to a metallic behaviour [1]. Similar results were obtained in the case of doping with Ga or In. This is, for example, very important for the production of transparent conductors as in the case of TCOs in solar cells. Recently, a vapour phase technique to grow vertically self-aligned ZnO nanorods by a vapour-phase technique over a ZnO or Al:ZnO (AZO) film [2] has been reported. The main result of that growth technique is that, even if Zn vapours are used for the growth, the required temperature is low enough (450-480 °C) to allow the use of low-cost glass substrates, as the ones typically adopted for solar cell technology. By growing such nanostructures starting from a metallic Zn source, without the use of any catalyst or metal-organic precursor, contaminations from reaction environment (often intrinsic and noteworthy in wet chemical methods) has been drastically reduced allowing to grow ZnO nanorods with high crystalline quality and controlled physical properties. It is important to note that in the described technique a layer of liquid metal droplets is formed on the substrate during the first growth stage and that only afterwards, when oxygen is introduced, a corrugated oxide wetting layer is formed and nanostructures start to grow. This two-step process was successfully used in the past by our group also for growing SnO_2, In_2O_3, and ZnO nanowires and mainly differs from standard VLS (vapour-liquid-solid) growth techniques because in this case the liquid phase is not used as an inert solvent through which the solid phase of different materials precipitate but to induce a localized preferential fast nucleation point that also provides high metal vapour supersaturation for a self-catalyzed vapour-solid growth. In general, the growth of ternary oxides by a similar vapour deposition technique, starting directly from the co-evaporation of two different metals, is much more

difficult because vapour pressure of the two metals may differ by several orders of magnitude. This is the case, for example, of zinc and the mentioned group III elements, whose boiling point are generally over 2000°C and, hence, have insufficient vapour pressure around 500°C. For this reason, growth of InZnO nanowires was achieved up to now at temperatures well above 500°C (typically on the range 700-1400 °C), and thus not compatible with the use of low-cost glass substrates. In this work, we show that it is possible to grow indium zinc oxide nanorods by evaporating Zn and using liquid indium as a seed on the substrate at a temperature lower than 500°C. Microanalysis performed by TEM on single nanowires show an indium concentration larger than 1% (that is the concentration required to get metallic behaviour). The same technique has been also successfully used to grow at low temperature GaZnO and SnZnO nanowires. The possibility to use the same technique to grow nanowires of a wider family of ternary oxides is discussed.

[1] Mirco Bazzani, Andrea Neroni, Arrigo Calzolari, and Alessandra Catellani, , "Optoelectronic properties of Al:ZnO: Critical dosage for an optimal transparent conductive oxide", Applied Physics Letters, 98 121907 (2011)

[2] D. Calestani, M. Zha, L. Zanotti, M. Villani, A. Zappettini, "Low temperature thermal evaporation growth of aligned ZnO nanorods on ZnO film: a growth mechanism promoted by Zn nanoclusters on polar surfaces", CrystEngComm, Vol. 13 (2011) pp. 1707-1712

11:05 Oral

Combustion synthesis of crystalline nanomaterials

Andrzej Huczko[1], Magdalena Kurcz[1], Agnieszka M. Dąbrowska[1], Ajaya Bhattarai[2]

1. *Warsaw University, Department of Chemistry, Pasteura 1, Warsaw 02-093, Poland* **2.** *Departmenta of Chemistry M. M. A. M. C., Tribhuvan University, Biratnagar 00977, Nepal*

e-mail: ahuczko@chem.uw.edu.pl

Combustion synthesis is a novel type of highly exothermic, self-sustained reaction between a strong reducer and a strong oxidant. After combustion initiation, the chemical reaction propagates through the reactants as a rapidly moving combustion wave. High temperature and pressure gradients within the combustion wave result in a growth of different nanomaterials [1], i.e., we demonstrated earlier the efficient formation of silicon carbide nanowires [2]. The present study is a continuation of that research aimed at more-in-depth study of the combustion mechanism. In a typical combustion synthesis, Si powder or Si-containing powdered compound (silicides, alloys) were thoroughly mixed with poly(tetrafluoroethylene) - PTFE, in a stoichiometric ratio to obtain a homogeneous mixture. The following silicon compounds were tested: $CaSi_2$, Si_2Ta, Mg_2Si, $NbSi_2$, Cu_5Si, $MoSi_2$, Si_2Zr, $CrSi_2$, Si_2Sr, VSi_2, $FeSi_2$, Si_2Ti, WSi_2, $Mn_{15}Si_{26}$, $HfSi_2$, $Co_{0.5}Ni_{0.5}Si_2$, $Ni_{0.5}Fe_{0.5}Si_2$, $Co_{0.5}Fe_{0.5}Si_2$. Not all of them were reactive enough to instantly reduce PTFE so a small amount of a strong reductant (Mg powder) was added to commence such combustion. The reactants were transferred to a quartz crucible and then placed in a stainless steel high pressure reactor (Fig. 1) with a 350 cm^3 volume.

Fig. 1. High-pressure stainless steel reactor for combustion synthesis

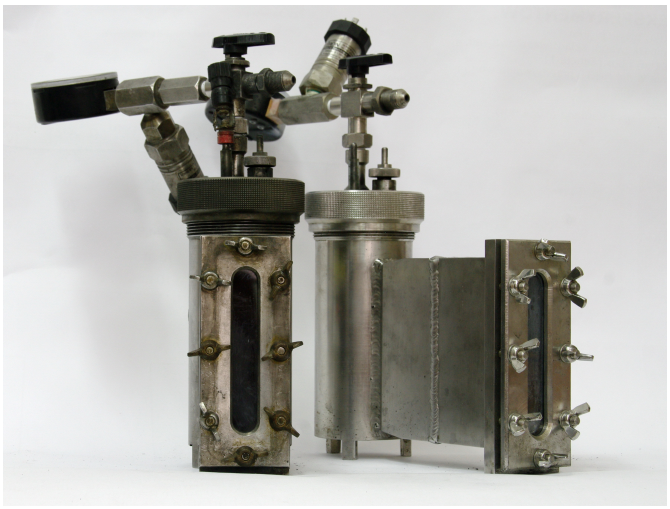

After filling the reactor with either argon or carbon dioxide to a pressure of 1 MPa, the combustion process was commenced using an ohmic heating. A mechanism of the reaction can be presented in a following simplified form

$MeSi + (CF_2)_n \rightarrow MeF + SiC + C + SiF_4$

Fig. 2 presents registered sequence of combustion stages in Si/PTFE system.

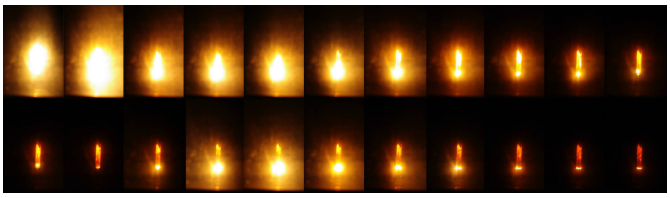

The time of reaction is about 1.2 s. The oscillation of signal intensity may be noted. Fig. 2. Registered sequence of combustion stages in Si/PTFE system The product was collected for SEM, TEM, XRD, and chemical analyses. Electron microscopy observation showed a presence of one-dimensional (1-D) silicon carbide nanocrystallites (Fig. 3) and fluoride nanoparticles along with soot agglomerates.

Fig. 3. SEM image of reaction products (starting mixture: Si/PTFE)

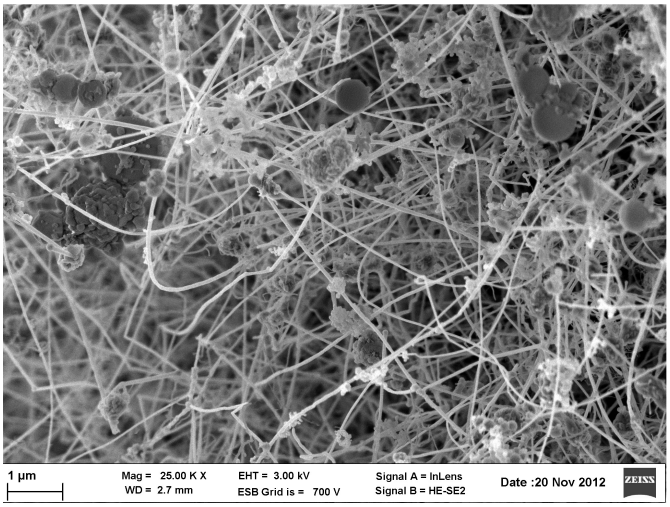

To accelerate the combustion, sodium azide (up to 85 wt%) was also added to the starting mixture. Branched and comb-like SiC nanocrystallites were found in products (SEM images in Fig. 4) .

Fig. 4. SEM image of reaction products (starting mixture: Si/PTFE/NaN_3)

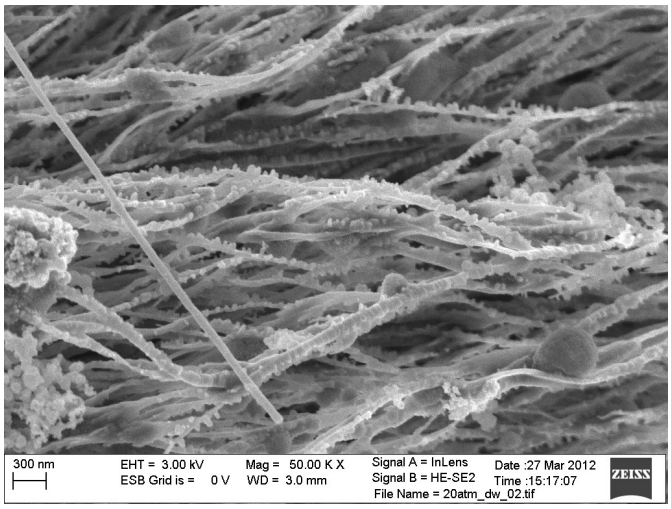

After combustion initiation, the high temperature causes the pyrolysis of PTFE into C_xF_y radicals and melting of silicon. The reaction of radicals with Si generates gaseous species forming 1-D SiC nanocrystallites presumably via a well-known VLS growth.

Acknowledgement. This work was supported by NCN through grant No. UMO-2011/03/B/ST5/03256 and 2012/05/B/ST5/00709.

References:

[1] A. Huczko, M. Szala, A. Dąbrowska, "Combustion Synthesis of Nanostructured Materials", Publ. Wydawnictwa UW, 2011, Warsaw.

[2] M. Soszyński, A. Dąbrowska, M. Bystrzejewski, A. Huczko, CrystalResearch and Technol., 45, 2010, 1241-1244.

11:20 Oral

Forming two-dimensional structure of DNA-functionalized Au nanoparticles via lipid diffusion in supported lipid bilayers

Takumi Isogai[1], Agnes Piednoir[2], Eri Akada[1], Yuki Akahoshi[1], Ryugo Tero[3], Shunta Harada[1], Toru Ujihara[1], Miho Tagawa[1]

1. *Department of Materials Science and Engineering, Nagoya University, Furo-cho, Chikusaku, Nagoya 464-8603, Japan* **2.** *Université de Lyon, 43 Bd du 11 Novembre 1918 Villeurbanne, Lyon 69622, France* **3.** *The Electronics-Inspired Interdisciplinary Research Institute, Toyohashi University of Technology, Aichi 441-8580, Japan*

e-mail: isogai@sic.numse.nagoya-u.ac.jp

Nanoparticle assemblies have recently attracted considerable interest because of their potential applications in the field of nanoelectronics, nanophotonics and other various nanodevices. To realize novel devices utilizing 'nano-specific' phenomena and effects, it is necessary to develop a method for programmable assembly of nanoparticles into one-, two- or three-dimensional arrays with nano-meter precision. In recent years, DNA has attracted much attention as an engineering tool for controlling the assembly of nanoparticles because it offers programmability in the arrangement of nanocomponents through base sequence design. As shown in Figure 1, nanoparticles bind each other via DNA strands, which are attached on nanoparticles, through DNA hybridization: the process of combining two complementary single-stranded DNA molecules and allowing them to form a double-stranded molecule through Watson-Crick base-pairing rules. By this technique, three-dimensional nanoparticle superlattices have already been made using DNA-functionalized nanoparticles (DNA-NPs). To assemble two-dimensional nanoparticle superlattices using DNA-NPs, we figured out to utilize surface adsorption and laterally-confined diffusion of DNA-NPs on a substrate surface. More specifically, to implement laterally-confined diffusion of DNA-NPs, we used supported lipid bilayer (SLB). Figure 2 shows schematic drawings of the process of forming two-dimensional nanoparticle array using lipid lateral diffusion: Firstly adsorption of DNA-NPs to SLB (left), secondly making DNA-NP diffuse via lipid (middle), and finally assembling two-dimensional superlattices of nanoparticles on SLB (right).

We prepared two types of DNA-functionalized Au nanoparticles (DNA-AuNPs) as shown in figure 1 and lipid bilayer on mica by vesicle fusion method using Dimethyldioctadecylammonium bromide (DDAB). The solution of DNA-AuNP mixture was deposited on DDAB SLB and temperature of the system was increased in order to promote lipid lateral diffusion. After that, the sample was annealed.

Figure 3(a) shows that an AFM image of DDAB SLB on mica. Small bilayer patches of DDAB were observed. Figure 3(b) shows an AFM image of DNA-AuNPs adsorbed on DDAB SLB. Close analysis of section profiles revealed that most of DNA-AuNPs adsorbed selectively on DDAB bilayers. As shown in Figure 3(c), after annealing, the morphology changed dramatically and densely-packed well-ordered two-dimensional arrays of DNA-AuNPs were observed. This result suggests that lipid diffusion was enhanced at high temperature and DNA-AuNPs were transported by high-mobility lipid molecules and then bind each other through DNA hybridization. In this system, the realization of two-dimensionally limited diffusion of DNA-NPs enables two-dimensional assembly of nanoparticles without creating any complex mechanism on nanoparticles to get their own anisotropies.

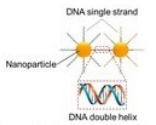

Figure 1. Schematic drawing of DNA-NPs.

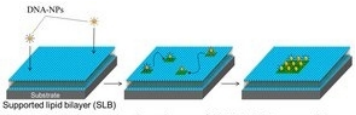

Figure 2. Schematic drawings of DNA-NP assembles on SLB. The lipid molecules, which attach to DNA-NPs, are indicated by green to distinguish from others.

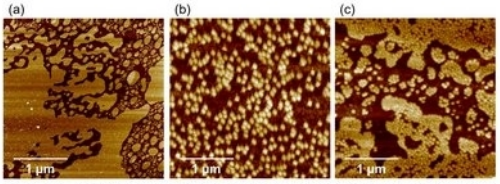

Figure 3. AFM images of (a) DDAB bilayer patches on mica substrate, (b) DNA-AuNPs on DDAB SLB and (c) DNA-AuNPs assembled on DDAB SLB after annealing.

11:35 Oral

Synthesis and luminescent characteristics of $NaYF_4$:Yb:Er powders for photodynamic cancer therapy

Sergey V. Kuznetsov[1], Darya S. Yasirkina[1], Anastasiya V. Ryabova[1], Darya V. Pominova[1], Pavel Fedorov[1], Valerii V. Voronov[1], Oleg V. Uvarov, Vjatcheslav V. Osiko[1], Alexander E. Baranchikov[2], Vladimir K. Ivanov[2]

1. *General Physics Institute, Vavilov Str. 38, Moscow 117942, Russian Federation* **2.** *Kurnakov Institute of General and Inorganic Chemistry RAS (IGIC), Leninsky prospect, 31, Moscow 119991, Russian Federation*

e-mail: kouznetzovsv@gmail.com

Photodynamic cancer therapy is one of the most promising ways treating cancer. It is based on the ability of photosensitizers (PS) to produce a reactive oxygen species in the cancer-affected tissues under photo-excitation by light of a certain wavelength. The major drawback of this method is the low penetration of visible light into tissues.

A novel approach to visible light delivery to the PS-saturated cancerous tissue includes the application of the up-conversion mechanism: instead of low-penetrating visible radiation, one can use much better penetrating IR radiation and up-convert it in situ, i.e., at the deep layers of damaged tissue, where visible radiation cannot penetrate. Yb/Er-, Yb/Tm-, Yb/Ho-activated $NaYF_4$ are some of the most efficient up-converting phosphors [1]. $NaYF_4$ forms two types of the solid solutions: a cubic fluorite structure $Na_{0.5-x}Y_{0.5+x}F_{2+2x}$ and a hexagonal gagarinite structure $Na_{3x}Y_{2-x}F_6$.

$NaYF_4$:Yb:Er powders can be easily synthesized by co-precipitation from aqueous solutions; and the following factors play crucial role in the preparation of products of acceptable quality: (1) initial concentrations and ratios of starting material solutions, (2) the order of their mixing, (3) concentration of polyethyleneimine (PEI) additive, and (4) pH of the initial solutions. Namely, 25% excess of NaF is required for the preparation of single cubic phase samples, and preparation should be carried out by addition of metal nitrate solutions to 9 g/L PEI-doped 0.35 M aqueous NaF at pH = 10. According to scanning electron microscopy (SEM) data, this leads to the formation of 50-90 nm particles of cubic phase. The use of PEI concentration of 9 g/L resulted in the precipitation of 100-150 nm particle agglomerates (0.3-1 mm elongated agglomerates, SEM data) (hexagonal phase). Transmission electron microscopy (TEM) study of cubic $NaYF_4$:Yb:Er samples indicated that they consisted of several nm primary particles with 50 nm embryo agglomerates and 160 nm particle agglomerates. TEM data confirm the realization of the non-classical mechanism of crystal growth via the nanoparticle agglomeration. Powder samples of cubic $NaYF_4$:Yb:Er provided up to 2% luminescence quantum yield and can be used as a working agent in photodynamic cancer therapy.

References

[1] P.P. Fedorov, A.A. Luginina, S.V. Kuznetsov, V.V. Osiko. // *J. Fluorine Chemistry.***Vol.**132. (2011) pp.1012-1039.

[2] S.V. Kuznetzov, A.V. Ryabova, D.S. Los`, P.P. Fedorov, V.V. Voronov, R.P. Ermakov, V.B. Loshchenov, V.V. Volkov, A.E. Baranchikov, V.V. Osiko. // *NanotechnologiesinRussia*. **Vol**.7. (2012) pp.615-628.

This work was supported by RFBR 12-02-00851-a (Russian Federation State Contract 14.740.12.1343). TEM measurements were carried at the Center of mutual use of equipment at Prokhorov General Physics Institute.

11:50 Oral

Growth of C_{70} nanosheet crystals by Liquid-Liquid Interfacial Precipitation Method

Kana Osonoe, Ryosuke Kano, Masaru Tachibana

Yokohama City University, Yokohama, Japan

e-mail: nano_solid@yahoo.co.jp

C_{70}, one of the higher fullerenes, has narrow band gap than C_{60}. So C_{70} is very interesting for the application to a nanoelectronic device. However, it is difficult to get a high quality C_{70} crystal because C_{70} has some phase transitions near room temperature and symmetry being lower than C_{60}. Therefore there are fewer studies on solid state properties of C_{70} than C_{60}. Recently, for the control of the crystal shape, much attention has been paid for the solution growth. A liquid–liquid interfacial precipitation method (LLIP method) leads to not only the control of crystal shapes but also the short time growth for the crystals [1]. The LLIP method is expected as an effective method for practical use. In this paper, we report the growth of C_{70} nanosheets by LLIP method.

C_{70} nanosheets were prepared by LLIP method with an interface between C_{70}-saturated toluene with ferrocene and IPA. Fig. 1 shows an optical microscopic image of C_{70} nanosheets grown for 24 hours by LLIP method. They exhibit hexagonal shapes with about 300 nm in thickness and 5 μm in diameter. Fig. 2 shows XRD pattern of C_{70} nanosheets. From the XRD pattern, the structure of C_{70} nanosheets exhibits a monoclinic structure including ferrocene (a = 27.15Å, b = 10.21Å, c = 19.25Å, β = 121.73°). In addition, it should be noted that the monoclinic structure of C_{70} nanosheets change to a face-centered cubic one with annealing at 200ºC. We present the growth of C_{70} nanosheets, and their physical properties such as structural, optical and electrical properties.

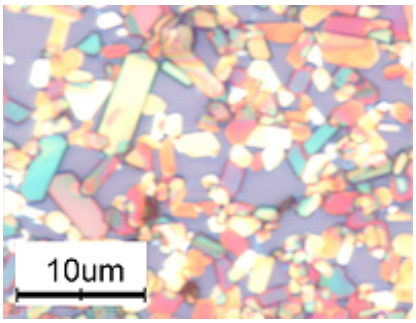

Fig.1 The optical microscopic image of C_{70} nanosheets.

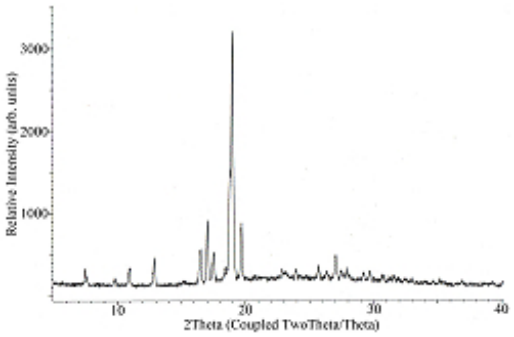

Fig. 2 The XRD pattern of C70 nanosheets.

[1] T. Wakahara et al. J. Am. Chem. Soc 131 (2009) 6372

Corresponding author: Masaru Tachibana, YokohamaCity University, 22-2 Seto, Kanazawa-ku,Yokohama 2360027, Japan, Tel &Fax: +81-45-787-2360,E-mail: tachiban@yokohama-cu.ac.jp

12:05 Oral

Field-Emission of Large Scale and Uniform Monolayer Graphene Sheet Supported on Patterned ZnO Nanowire Arrays

Lijing Zhang[1], Xiaomiao Liu[2], Qingfeng Yan[1], Xiaoqing Wang[1], Guangqiu Shen[1], Dezhong Shen[1]

1. *Tsinghua University, Tsinghua Garden, Beijing 100084, China*
2. *Hubei University, Wuhan 430062, China*

e-mail: zhanglijing_1124@126.com

Field emitters possessing needlelike shapes with sharp tips can dramatically reduce the strength of turn-on electric field by several orders of magnitude due to their enhanced local field at these tips. Graphene and its derivatives are expected to be potential field emitters due to their unique electronic properties. The sharp edges of graphene can produce significant enhancement of electron field emission due to the reduction of work function at the edges. Many efforts have been made in exposing the atomically thin edges and fabricating vertical sheets

in line with field direction such as screen printing graphene films, photolithographically patterned graphene arrays and graphene sheets supported on metal nanotips. Among them, supporting graphene sheet by well-aligned nanowire arrays can form nanometer-scale sharp protrusions. These high density protrusions localize and enhance the electric field, thereby allowing electrons to tunnel through the tips at very low electric fields and to produce stable emission in a large area.

Herein, we demonstrate a facile and effective route toward large scale and uniform graphene sheet supported on patterned ZnO nanowires with nanometer-scale sharp protrusions. The fabrication process is schematically illustrated in Figure 1. Monolayer colloidal crystal template was introduced to tailor the vertical ZnO nanowire (NW). Large-scale colloidal monolayer was prepared by the self-assembly of polystyrene (PS) nanospheres at the air/water interface. It was then transferred on a silicon substrate coated with ZnO seeds. The ZnO nanorods were grown via a hydrothermal growth approach with the colloidal sphere monolayer as a template. The size and period of the ZnO nanowires array synthesized could be controlled by the interstice size and sphere diameter of the colloidal monolayer template. Graphene was originally grown on copper foil by chemical vapor deposition method. The as-grown large area graphene was then transferred onto the patterned ZnO nanowires as a whole sheet by using the polymethyl methacrylate (PMMA) as an interfacial layer. The PMMA-supported graphene/ZnO wires nanocomposites were then washed with acetone followed by annealing in air at 350 °C for 30 minutes to remove the PMMA and PS spheres template as well as to optimize the ZnO nanowires performance. Highly efficient and stable field emission with a low turn-on field was observed from the resulted graphene sheet supported on patterned ZnO nanowire arrays. The enhanced field emission performances were attributed to the patterned and nanometer-scale sharp protrusions which locally enhanced the electric field and dramatically increased the field emission.

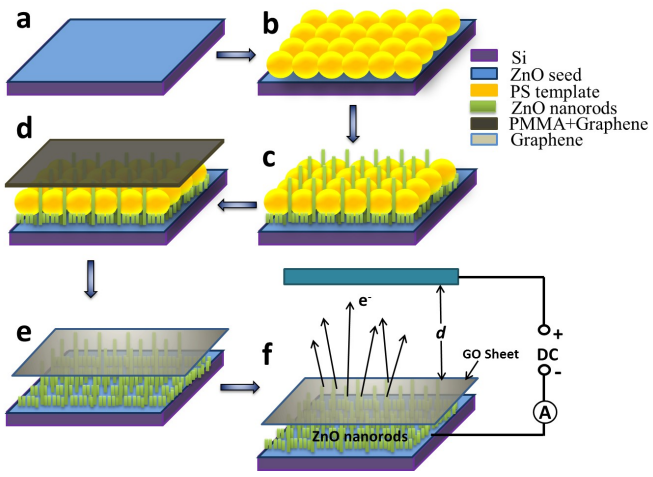

Fig. 1. A schematic illustration of the fabrication of the graphene/patterned ZnO nanowires composite. (a) A ZnO seed layer was coated on a silicon substrate, (b) A PS colloidal spheres monolayer was transferred onto the Si substrate, (c) Vertically aligned and patterned ZnO nanowire arrays were synthesized by the hydrothermal growth, (d) Graphene/PMMA film was transferred onto the ZnO nanowire arrays, (e) PMMA and PS template were removed to expose the graphene sheet that uniformly covered the patterned ZnO nanowire arrays, and (f) A schematic of the setup for field emission measurement.

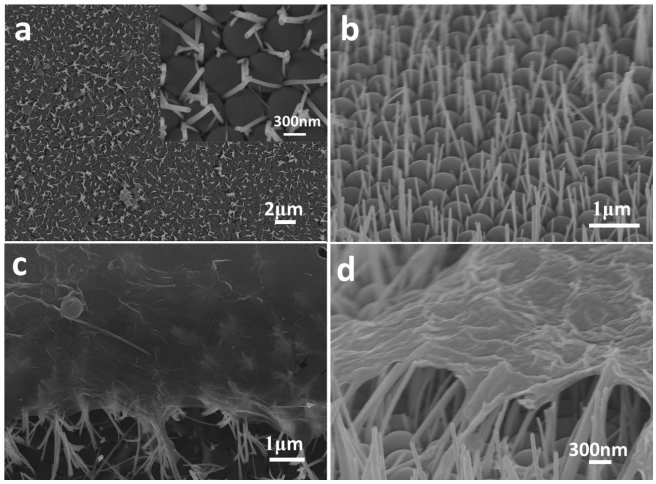

Fig. 2. (a) Top-view SEM image of the patterned ZnO nanowires array on a silicon substrate in a large scale. The insert is the corresponding high magnification image. (b) Cross-sectional SEM image of the patterned ZnO nanowires array on the silicon substrate. (c) Top-view and (d) cross-sectional SEM images of the graphene sheets supported by the patterned ZnO nanowires array.

Reference

[1] Z.C.Yang, Q. Zhao, Y. X. Ou, W. Wang, H. Li, D. P. Yu. Enhanced field emission from large scale uniform monolayer graphene supported by well-aligned ZnO nanowire arrays, Appl. Phys. Lett., 101(2012) 173107.

[2] D.X.Ye, S. Moussa, J.D. Ferguson, A. A. Baski, M. S. El-Shall, Highly Efficient Electron Field Emission from Graphene Oxide Sheets Supported by Nickel Nanotip Arrays, Nano Lett., 12 (2012) 1265-1268.

[3] C. K. Huang, Y. X. Ou, Y. Q. Bie, Q. Zhao, and D. P. Yu, Well-aligned graphene arrays for field emission displays, Appl. Phys. Lett., 98 (2011) 263104.

[4] H. B. Zeng, X. J. Xu, Y. Bando,U. K. Gautam, T. Y. Zhai,X. S. Fang, Fang, B. D. Liu, D. Golberg, Template Deformation-Tailored ZnO Nanorod/Nanowire Arrays: Full Growth Control andOptimization of Field-Emission, Adv.Funct.Mater,19(2009) 3165-3172.

Lunch (IOCG Exec. Com. meeting)
Tuesday afternoon, 13 August, 12:20

Wednesday, 14 August

WeP-G08
Wednesday afternoon, 14 August, 16:00
Rooms 205, 207, Old Library

Break
Wednesday afternoon, 14 August, 17:30

Posters

Wednesday, 14 August

WeP-G08
Wednesday afternoon, 14 August, 16:00
Rooms 205, 207, Old Library

16:00 Poster We96

Growth of pseudomorphic self-assembled quantum dots in the GaSb/GaP heterosystem

Demid S. Abramkin, Michael Putyato, Anton K. Gutakovskii, Boris R. Semyagin, Valerii V. Preobrazhenskii, Timur S. Shamirzaev

Institute of Semiconductor Physics SB RAS, Lavrentjeva 13, Novosibirsk 630090, Russian Federation

e-mail: demid@isp.nsc.ru

Epitaxial self-assembled quantum dots (SAQDs) semiconductor heterostructures are ones of the modern prospective objects for light-emitting devices application [1]. Three-dimensional exciton localization into SAQDs results in high efficiency of radiative recombination. Using wide-gap semiconductors as a matrix for SAQDs enables to fabricate devices emitting in the visible spectral range. The present report is devoted to investigation of GaSbP/GaP SAQDs heterostructures. Up to now, just fully relaxed surface nanoislands [2] and SAQDs [3] were investigated, because GaSb and GaP have huge lattice mismatch about 10.5% [4]. We report to the formation of pseudomorphic GaSbP/GaP heterostructures with SAQDs.

Series of the structures with SAQDs were grown on the semi-insulator GaP (100)-oriented substrates by molecular beam epitaxy. SAQDs was formed at $T_S = 420^0$C and $T_S = 470^0$C. Deposition of 1 monolayer GaSb was performed in atomic layer epitaxy mode.

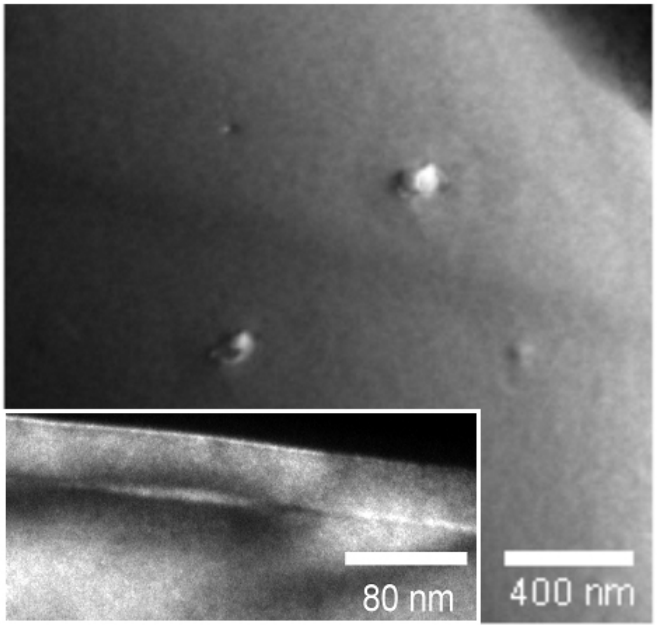

Fig. 1. TEM plan view and cross-section (inset) images of the GaSb/GaP heterostructure with SAQDs.

The TEM plan view and cross-section images of the GaSb/GaP structure with SAQDs are presented in fig. 1 (a). The SAQDs arrays in the all structures are characterized by low density ($< 10^8$ cm^{-2}) and the lateral diameter of 80÷120 nm. The height of SAQDs is about 10 nm. As it clear from TEM images, SAQDs are pseudomorphic strained. Taking into account the huge lattice mismatch of GaSb and GaP [4] and large SAQDs sizes, formation of dislocation-free pseudomorphic SAQDs allows us to conclude, that it consists of ternary alloy $GaSb_{1-x}P_x$.

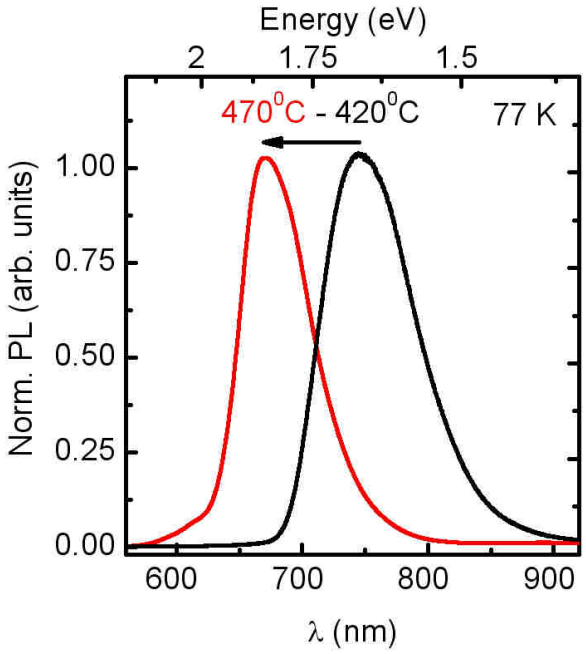

Fig. 2. Normalized steady-state PL spectra of GaSbP/GaP heterostuctures with SAQDs, grown at 420°C and 470°C, measured at 77 K and excitation density of 30 W/cm^2.

All investigated structures demonstrate high photoluminescence (PL) intensity at non-resonant excitation to the GaP matrix and temperature 77 K. Blue shift of steady-state PL spectra with increasing T_S from 420^0C to 470^0C (see fig. 2) evidences increasing of GaP fraction in $GaSb_{1-x}P_x$/GaP SAQDs. Average alloy composition x = 0.6 at $T_S = 420^0$C and x = 0.75 at $T_S = 470^0$C were estimated using comparison of PL data with SAQDs energy spectrum calculations.

This work was supported by the Russian Foundation for Basic Research (Projects No. 13-02-00073), the Dynasty Foundation, the Presidential Grants No. SP-985.2013.5 and the programs of the Ministry of Education and Science of Russian Federation (contract 16.552.11.7091).

Reference

1. D. Bimberg, M. Grundmann, and N. Ledentsov, Quantum Dot Heterostructures (Wiley, New York, 1999).
2. K. Posilovic, T. Kettler, V. A. Shchukin, N. N. Ledentsov, U. W. Pohl, D. Bimberg, J. Fricke, A. Ginolas, G. Erbert, G. Trankle, J. Jonsson, and M. Weyers, Appl. Phys. Lett. 93, 221102 (2008).
3. F. Bosc, J. Sicart, and J. L. Robert, J. Appl. Phys. 85, 6520 (1999).
4. Vurgaftman, J. R. Meyer, L. R. Ram-Mohan, J. Appl. Phys. 89, 5815 (2001).

16:00 Poster We97

Single Domain Maghemite Nanoparticles and Nanocomposites using Chitosan for Dye Removal from Industrial Waste Water

Saravanan Annamalai, Suraiya Begum, Radha Perumal Ramasamy

Anna University, Department of Applied Science and Technology, ACT campus (ACT), Chennai 600 025, India

e-mail: srisaran@gmail.com

Chitosan is a natural, biodegradable and biocompatible polymer which is having an excellent film forming ability [1]. Maghemite (γ-Fe2O3) is one of the oxides of the iron and it is used for the preparation of polymer magnetic nanocomposites because of its unique superparamagnetic behavior, biocompatibility, non-toxicity and low cost of production. Chitosan-maghemite nanocomposites have great potential applications in various biomedical fields and in environmental engineering like for heavy metal ion removal and dye detection. [2,3] In this work, chitosan-maghemite nanocomposites were prepared by the following steps. In the first step, single domain maghemite nanoparticles were prepared by a standard co-precipitation method [4]. The size of the nanoparticles was found to be ~ 3 nm using scherrer formula. In the second step, the as obtained mahemite nanoparticles were dispersed in to the 1(w/v) chitosan along with the 1.5% acetic acid solution by ultrasonic irradiation for 10 min at various concentrations of maghemite. After sonication, the composite solution was poured into a glass plate and dried at room temperature for 3 days. As obtained films were found to be flexible. The colour of the films turned from yellow to dark brown as the concentration of the maghemite nanoparticles increased from 0 to 50%. XRD, FE-SEM, VSM and dielectric measurements were taken for the obtained maghemite nanoparticles. The particles were found to be spherical, superparamagnetic and having high dielectric constant. The Chitosan – Maghemite nanocomposite showed that the particles are dispersed throughout the film [Fig. 1]. The structure of the chitosan-maghemite nanocomposites were characterized by XRD. Both high resolution scanning electron microscopy (HR-SEM) and Atomic Force microscope (AFM) were used to characterize the dispersion of γ-Fe2O3 NPs on the chitosan matrix and the surface morphology of the nanocomposites. The effect of the γ-Fe2O3 NPs on the chitosan also was studied by using the thermogravimetric analysis (TGA). The various dielectric charecteristics like dielectric constant, loss, electric modulus and conductivity were studied as a function of frequency (0.01Hz to 1MHz) and temperature (300C to 1500C). The morphology and the dielectric charecetristics were found to be dependent upon the concentration of the nanoparticles while the magnetic property was found to be nearly the same for low (5%) and high (50%) concentration of maghemite nanoparticles. The efficiency of the nanocomposites in removing methyl orange dye from water will also be discussed.

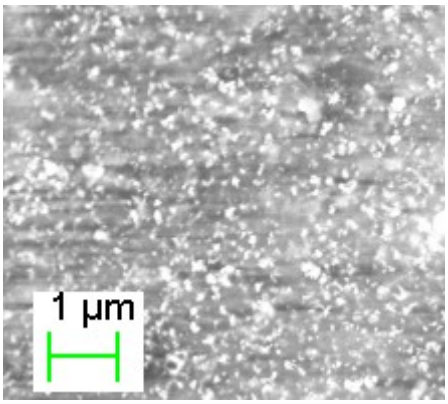

Figure 1 Optical and SEM images of the Chitosan - maghemite nanocomposites

References:
1. Denkbas E. B.et al, React. Funct.Polym., 50,225 (2002)
2. Chang YC et al., J. Colloid Interface Sci. 283, 446 (2005)
3. R. Jiang et al., J Appl Polym Sci 125, 540 (2012)
4. Laurent S et al.,Chem. Rev. 108, 206 (2008)

16:00 Poster We98

Organic luminophor metal complex in inorganic glass matrix – a new hybrid material

Olga B. Petrtova, Roman I. Avetisov, Oksana A. Mushkalo, Alexander G. Cherednichenko, Andrew Khomykov, Igor C. Avetissov

D.I.Mendeleyev University of Chemical Technology of Russia (MUCTR), Miusskaya sq. 9, Moscow 125047, Russian Federation

e-mail: igor_avetisov@mail.ru

Hybrid materials (HM) based on organic-inorganic substances are of a great interest due to specific properties of nanosize particles disordered or ordered into matrix. Organic luminescent materials demonstrate high efficiency both at optical and electric current excitation. But, in general, most of organic phosphors are unstable at room atmosphere and need to be protected. Incorporation of organic materials into transparent inorganic matrix could solve the problem of degradation and give an opportunity to get new materials with unique properties.

In the recent 15th years a lot of studies of HM's delt with an inorganic matrix, which based on glasses [1,2], silicon oxide nanospheres [3,4], thin amorphous films [5,6], xerogels [7,8], layered double hydroxides [9], single crystals [10,11].

HM's were synthesized by variations of sol-gel technique [1-9], single crystal based HM's [10,11] were grown from solutions. An application of these techniques results to incorporation of OH–group in HM's and correspondingly to luminescence quenching at the OH–group oscillations. Synthesis of new efficient phosphors based on organic metal-complex compounds with high decay temperature (higher 300 °C) makes possible a synthesis of hybrid optic materials using glass melt technology. In this case we could decrease the energy dispersion on residual anion groups.

In the present research we used low-melting borate glasses (B_2O_3, Na_2O-B_2O_3, PbF_2-B_2O_3) as a glass matrix and organic phosphor was a metal complex of Me^{3+} (Al, In) with 8-quinolinol (tris-(8-hydroxyquinoline) aluminum, Alq_3 and tris-(8-hydroxyquinoline) indium, Inq_3). They are stable up to 450°C melting temperature.

Meq_3 molecules exist as two geometrical isomers: *meridianal* and *facial* (*mer-* and *fac-*), and crystallized in some polymorphs *(mer-* in *α-,β-ε-*phase*, fac-* in *γ-, δ-*phase) [9, 12]. Meq_3 luminescent properties depend on the central metal ion, polymorph, and isomer.

Metal complexes were synthesized by the reaction:

$$3\ C_9H_7ON + Me^{+3} + 3OH^- = (C_9H_6ON)_3\ Me + 3\ H_2O$$

The synthesis was conducted during 1 hour at 25°C, continuous mixing, pH=10. The purification procedure included two stages. At the first stage impurities were extracted into hexane. At the second stage metal complexes was sublimated in vacuum under $p<10^{-5}$ Torr at stepped heating to 90→200→250→290°C and 1.5 hours exposure at the very temperature.

HM's were synthesized by melting of a mixture of 0.02-0.1 wt. % Meq_3 in dried B_2O_3 powder at temperatures below the decay temperature during 10-60 minutes. Glass samples were obtained by the melt freezing or thick thread pulling.

Hybrid samples were transparent in 250 – 2700 nm range and did not content visible inclusions and bulbs. The influence of glass melting parameters on HM's structure and spectral properties was studied.

We found out that in case of Alq_3 (Fig.) that an increase of synthesis duration resulted in linear shift of chromaticity coordinates according to the equation Y = 4.1093·X – 0.4859 from green (dot 1) to blue (dot 5) with corresponding changes luminescent maximum peak from 513 nm for pure Alq_3 to 443 nm for HM with maximum melting duration. Dots 1-5 forms the GB edge of the RGB triangle for full-color emitting devices using only Alq_3 as a luminophor component. This is perspective for development of new classes of emitting devices based on hybrid materials

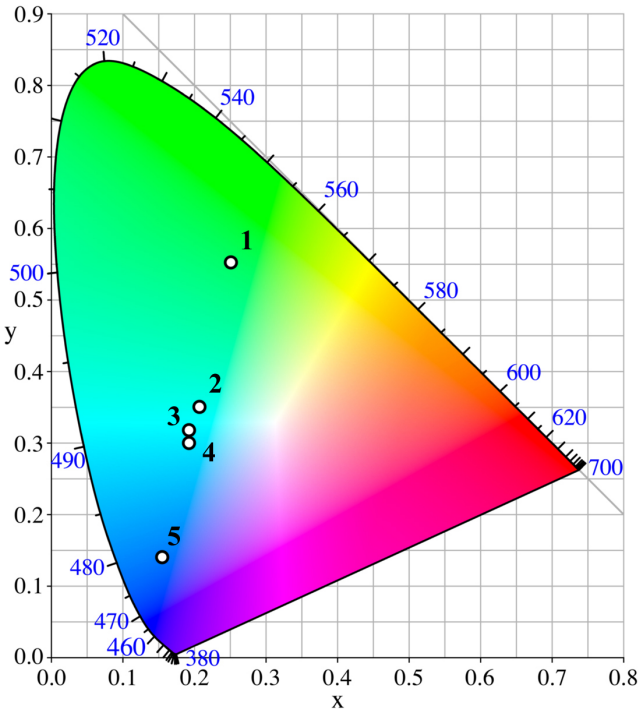

Fig. Chromaticity diagram (CIE) with marks corresponding to samples X-Y color coordinates: 1 – original Alq_3; 2 – 5 – Alq_3/B_2O_3 – hybrid materials, melted at: 2 – 400 °C, 8 min, 3 – 400 °C, 10 min; 4 – 390 °C, 30 min; 5 – 400 °C, 60 min

1. N.Sanza, P.L. Baldeckb, A. Ibane.// Synthetic Metals. V.115. 2000. p. 229-234
2. P. Innocenzi, A. Martucci, M. Guglielmi, L. Armela // Journal of Non-Crystalline Solids. 1999. Vol. 259. P. 182-190
3. D. Zhao, W. Qin, C. Wu, J. Zhang, G. Qin, H. Lin // Journal of Rare Earths. 2004. V. 22.№ 1. p. 49-52
4. C. Huang, T Sun, W. Tian, B. Zhao // Journal of Rare Earths. 2006. V. 24, № 2, p. 134-137
5. X. Hao, X. Fan, M. Wang. // Thin Solid Films.V. 353. 1999. № 1-2, p. 223-226
6. D. Bersani, P.P. Lottici, M. Casalboni, P. Prosposito// Materials Letters. V. 51. 2001. p. 208–212
7. L.D. Carlos, R.A. Sa Ferreira, V. de Zea Bermudez // Electrochimica Acta. V. 45. 2000. p. 1555–1560
8. X. Fan, Z. Wang, M. Wang // Journal of Luminescence.V. 99, 2002. № 3, p. 247-254
9. S. Li, J. Lu, M. Wei, D.G. Evans, X. Duan. // Adv. Funct. Mater. V. 20. 2010. p. 2848–2856
10.T. Watanabe, N. Doki, M. Yokota, K. Shimizu// Mat. APCChE 2010, October 5-8, 2010, Taipei
11. I. Pritula, V. Gayvoronsky, Yu. Gromov, at all // Optics Communications. V. 282. 2009. № 6, p. 1141-1147
12. I. Hernandez and W P. Gillin // J. Phys. Chem. B, V. 113, 2009. p. 14079–14086

16:00 Poster We99

The morphology, luminescence and photovoltaic characteristics of MEH-PPV/nanocrystal ZnO hybride films with perylene dyes as interface modifiers

Nataliya V. Babayevskaya, Yuri N. Savin, Valerii V. Vashchenko

Institute for Single Crystals NAS of Ukraine (ISC), 60 Lenin Ave., Kharkov 61001, Ukraine

e-mail: babayevskaya@isc.kharkov.ua

Solar cells based on hybrid photoactive films created from the organic and inorganic semiconductors are attracting attention as an alternative of Si based energy sources. The control of morphology of the photoactive layer and therefore improving the photoconversion efficiency of the cell are the challenging key issue for the fabrication of efficient photovoltaic devices. Now the hybrid composite films, which are blends of conjugated polymers (P3HT, MEH-PPV) and inorganic nanocrystals (TiO_2, ZnO) that offer high hole and electron mobility or improved spectral coverage are widely investigated for photovoltaic applications. However there are a little scientific work devoted to the investigation of the phase states in blend films and the influence of interface modifier (IM) deposited on the nanocrystal surface on phase separation and photovoltaic properties, particularly.

The present study is devoted to the obtaining and study of morphology, and photoelectrical properties of the MEH-PPV/ZnO/IM nanocomposite. The perylene derivates were chosen as IM. MEH-PPV/ZnO(IM) films were prepared by spin-coating onto substrates.

X-ray photoelectron spectroscopy analyses revealed that the IM are adsorbed and chemically bonded to ZnO. The morphology of the hybrid film was determined by TEM and is characterized by RDF (radial distribution function). It is found that RDF for ZnO nanocrystals with the dye (II) interface modifier corresponded to the case of spherical stabilization of NC in the polymer matrix. Unlike RDF of the blend with ZnO in the dye (II) shell corresponded to the case of vertical phase segregation (in accordance with Schweizer model). HOMO and LUMO levels of the dyes were calculated using E_{ox} measured by cyclic voltammetry method and E_g was determined by optical absorption in the dye films. The better photoluminescence quenching in the MEH-PPV/ZnO(IM) blends was observed for ZnO with dye (I). Photovoltaic

measurements on the cells with planar and BHJ geometry demonstrated that open-circuit voltage (V_{OC}) and (J_{SC}) correlated with a the radial distribution function (RDF) of ZnO in polymer matrix. This study provides a useful route for increasing the efficiency of hybrid solar cells *via* the control of distribution of ZnO in polymer matrix.

16:00 Poster We100

Structural and Morphologic Characterization of Zirconia-Silica Nanocomposites Prepared by Sol-Gel Methods

Marcela Stoia[1], Paul C. Barvinschi[2], Floricica Barvinschi[1]

1. *Politehnica University of Timişoara, P-ţa Victoriei no. 2, Timisoara 300006, Romania* **2.** *West University of Timisoara (UVT), Bd.V. Parvan nr.4, Timisoara 300223, Romania*

e-mail: fbarvinschi@gmail.com

The interest devoted to binary zirconia-silica oxides can be traced back to their enhanced catalytic, mechanical, electronic, thermal properties. These materials can be used as coatings, fibres, catalysts and high-refractive-index glasses [1]. The addition of zirconium in silica significantly improves their mechanic, electric and chemical properties, more particularly towards alkaline attacks [2]. The structure of mixed zirconia-silica oxides is very interesting because zirconium cannot substitute silicon, due to the different atomic radius and coordination number between these two elements. Thus zirconia will develop as distinct phase in the nanocomposites. It is interesting to study the evolution of zirconia crystalline phases inside the silica matrix. It has been reported in the literature the formation at temperatures lower than 1000°C only of the monoclinic zirconia [3]. It is interesting to find the conditions of synthesis and thermal treatment for the obtaining of tetragonal zirconia inside the silica matrix. The sol-gel process allows in principle to synthesize zirconia-silica nanocomposites for various zirconia contents at lower temperatures than the conventional methods. The reactivity of zirconium alkoxides towards hydrolysis being higher than that of silicon alkoxides, mixtures of zirconium oxides and alkoxides precipitate during hydrolysis instead of forming a homogeneous gel. The aim of this work is to study the local structure of ZrO_2-SiO_2 mixed oxides obtained from hybrid inorganic-organic materials with different Si/Zr atomic ratios as precursors. In this study, we have synthesized zirconia-silica nanocomposites using a modified sol-gel method, starting from TEOS – $Zr(NO_3)_4$ – poliol – H_2O sols that succesfully gelified to homogenous gels. We have studied the gels $Zr(NO_3)_4$-poliol (1,3-propanediol and poly(vinyl alcohol), and we have evidenced during gels heating that a redox reaction takes place between zirconium nitrate and poliol with formation of some carboxylate type compounds of Zr, that were used as precursor for zirconia powders. It has been concluded from the study that the use of PVA as poliol is favorable to the formation and stabilization of tetragonal zirconia [4]. Also the presence of SiO_2 in small amounts was reported as a stabiliser for tetragonal zirconia [5]. Thus we have decided to use as poliols in our gels 1,3-propanediol and poly(vinyl alcohol). The gels obtained at room temperature have been dried and then thermally treated at 160°C when the redox reaction took plase between the organic poliol and zirconia nitrate leading to the formation of zirconia nanoparticles precursors in the pores of silica matrix. These xerogels obtained at 160°C have been thermally treated at 400°C for 3 hours for the thermal decomposition of zirconia precursors, then annealed at higher temperatures in the range 400-1100°C. The obtained composites have been characterized by FTIR spectroscopy, X-ray diffraction, HR-TEM and SEM-EDX analysis. Depending on the thermal treatment zirconium silicate appeared as secondary phase. The working conditions for the obtaining of homogenously distributed $ZrO¬2/SiO_2$ nanocomposites have been established. The influence of zirconia/silica ratio on the evolution of zirconia phases was also studied.

16:00 Poster We101

Active media on based of solid SiO2 matrices with incorporated Polymethine dyes molecules

Olga N. Bezkrovnaya, Igor M. Prytula, Anna G. Plaksy

Institute for Single Crystals NAS of Ukraine (ISC), 60 Lenin Ave., Kharkov 61001, Ukraine

e-mail: bezkrovnaya@isc.kharkov.ua

Composite materials based on different nanoporous matrices with incorporated dye molecules are increasingly used to create tunable lasers, light guides and active elements for nonlinear optics and photonics. The unique properties of polymethine dyes converting of light energy in the visible and near infrared region of the spectrum allows their widely to use as sensitizers, active laser and nonlinear optical media, new tools for recording information. One of the most promising materials for the creation of composite optical materials based polymethine dyes are synthesized by the sol-gel SiO_2 matrices has a low light scattering, good thermal conductivity and low temperature coefficient of refractive index. The sol-gel technology allows incorporation of organic and inorganic additives during the process of the formation of SiO_2 network at room temperature. Introduction to the SiO_2 matrices polymethine dyes with different geometrical shape and concentration allows to obtain composites with desired properties. For regulation of these properties must be controlled pore size distribution of the dye molecules and their aggregation in the matrix.

The aim of the present work was the synthesis of transparent monolithic SiO_2 matrices with DCCA (formamide, FA) and polymethine dyes (SL2651, SL3021 and SL3104) to create of composite nonlinear optical media. SiO_2 based sols were prepared by hydrolysis and polycondensation of tetraethoxysilane in ethanol with citric acid used as a catalyst. The optimal physical and chemical conditions for obtaining nanoporous SiO_2 matrices with FA were installed. TEM method confirmed the formation of pores in the matrix size as 4-10 nm. By hydrostatic weighing method was determined that porosity of the matrices – 52%.

Organic dyes SL2651, SL3021 and SL3104 were injected into SiO_2 matrices directly in the sol at the synthesis stage. Based on a comparative analysis of the spectral-luminescent properties of dyes in various solvents and in the matrix, were found the effect of the microenvironment in the matrix pores on the dye molecules. Shown to increase the length of the polymethine chain in the dye SL2651 compared with dyes SL3021 and SL3104 leads to bathochromic shift of the absorption maximum for SL2651. The observed hypsochromic shift of the absorption maxima of dyes SL3021 and SL3104 in an aqueous solution with respect to ethanol and FA caused dimers of dye molecules. The polymethine dyes molecules with branched structure (SL2651, SL3021 and SL3104) form dimers in the pores of the matrices and in aqueous solutions due to their conformational features. Dimerization of the dyes in the gel due to the presence of water leads to a reduction of their luminescence in SiO_2 matrices. It was found that the dye does not form dimers SL2651 in the solvent (water) and in the pores of the matrices is in the monomeric state, resulting composite SiO_2: SL2651 has effective luminescence. Given the geometric and conformational parameters of molecules contained phosphors, and statistically derived pore sizes, was proposed the model of the location of the dye molecules in the pores of the matrix. Production of composite structures is of great interest for optoelectronics and photonics.

16:00 Poster We102

Nano- and microwhiskers of III-V solid solutions

Inessa Bolshakova, Yaroslav Kost, Olena Makido, Roman Stetsko, Fedir Shurygin

Lviv National Polytechnic University, Lviv, Ukraine

e-mail: inessa@mail.lviv.ua

Electronic devices produced from semiconductor compounds of III-V group and their solid solutions are coming into increasingly wider practical use. The interest taken in solid solutions is primarily associated with the ability to change band-gap width and other properties, depending on the ratio of binary compounds. Among the existing solid solutions of III-V compounds $InAs_{1-x}Sb_x$ and $Ga_xIn_{1-x}As$ solid solutions are considered promising for the needs of the electronics .

The basis for modern electronic devices is formed by the planar technology of semiconductor materials, which is characterized by continuous growth of requirements for the perfection of the crystal structure and uniformity of electrophysical characteristics in the material grown. Planar technologies for obtaining heterostructures imply coherence between substrate and epitaxial layer in terms of the lattice parameter. The limited choice of substrates with different lattice parameters places limits on the potential of planar technology and the possibility of obtaining solid solutions with different compositions. As an alternative to planar technology one may consider the technologies for obtaining semiconductor whiskers from vapour phase that do not require substrates. The technology is based on the transfer of components to the crystal growth area as a result of chemical transport reactions and initiation of crystal growth by the vapour-liquid-crystal mechanism.

The derived technology for obtaining nano- and microwhiskers consists of two stages. In the first stage semiconductor nanowhiskers are formed following the vapour-liquid-crystal mechanism. Here the triggering doping agent for nanowhiskers is gold, which together with the basic material forms a eutectic alloy on nanowhisker tips. Nanowhiskers are obtained in non-equilibrium mode with high oversaturation level, which is required to ensure efficient feed of the eutectic alloy drop with a small radius of curvature in accordance with the Gibbs–Thomson equation.

In the next stage, conditions are created for further growth from nanowhiskers to micron-diameter whiskers. This process is carried out in a different temperature range and is considerably longer than the previous one. The most important element in the suggested technology is to provide the correct conditions for transition from the first stage to the second stage as throughout this transition process nanowhiskers are selected for further growth to micron sizes. The selection is based on the Oswald ripening mechanism under the conditions of declining oversaturation of vapour phase in the reactor.

The developed technology makes it possible to grow microwhiskers of $InAs_{1-x}Sb_x$ and $Ga_xIn_{1-x}As$ solid solutions and provides control over the composition of the compound (parameter x) by changing the ratio of the partial vapour pressures of volatile group five components, which are controlled by the temperature of source area and temperature gradient in the reactor.

The paper presents technological modes for growing microwhiskers of $InAs_{1-x}Sb_x$ and $Ga_xIn_{1-x}As$ solid solutions by method of transport reactions with different component compositions. The conducted X-ray diffraction studies of the obtained solid solution microwhiskers showed that the change in lattice parameter of the solid solution depends on the ration of components.

Studies carried out into the electrophysical properties of obtained whiskers have shown that the developed technology for growing solid solution whiskers following the transport reaction method makes it possible to obtain crystals with predetermined parameters, which renders them promising for application as sensing elements in sensors of physical quantities.

16:00 Poster We103

Photoluminescence of CdS nanocrystals doped with Cu or Zn

Sergiy I. Budzulyak[1], Dmytro V. Korbutyak[1], Andrij O. Kuryk[1], Oleg M. Shevchuk[2], Stanislav V. Tokarev[2]

1. *V. Lashkaryov Institute of Semiconductor Physics NASU (ISP), 41, pr. Nauki, Kiev 03028, Ukraine* **2.** *Lviv Polytechnic National University, 12 Bandera, Lviv 79013, Ukraine*

e-mail: buser@isp.kiev.ua

Formation of the thin polymeric films with the embedded nanoclusters doped on the basis of CdS/ZnS and CdS/CuS was performed via several stages: At the first stage a solution of the polyfunctional copolymer (PFC) poly [(butyl acrylate)-co-(5-tert-butylperoxy-5-methylhex-1-en-3-yne)-co-(maleic anhydride)] modified dimethylaminoethanol, polyethylene glycol PEG-200 (taken in the amount of 10% respectively to PFK) and a mixture of two salts Cadmium Acetate Cd(Ac)2 with either Cu(Ac)2 or Zn(Ac)2 in dimethylformamide at their ratio as [Cd(Ac)2]:[Me(Ac)2]=99:1÷90:10. Theoretical content of MeS in the film was of 20%.

On glass plates from the obtained solutions were spin-coated the thin polymeric films containing metal ions bonded with polymeric matrix due to formation of both ionic and coordinate bonds. The film thickness was in average of ≈ 20 nm. Crosslinking of the films obtained occurred at their heating (T=100 ÷ 120˚C) as results of an esterification reaction between hydroxyl groups of bifunctional PEG-200 and the maleic anhydride moieties in PFC. At the final stage the CdS nanoclusters doped were formed by treatment of the films by Hydrogen Sulfide in gas phase.

Absorption maxima in the area of 2.6-2.85 eV depending on the nature and concentration of doping metal cations were observed in the UV-vis spectra of obtained thin films.

In the spectra of photoluminescence (PL) of the samples were observed two broad bands: one in the spectral region (1,6 - 2,3) eV, the second - in the (2,4 - 3,4) eV. The first is caused by structural defects in QDs CdS, the second (high-energy, with energy quanta greater than band gap of bulk CdS) related to the radiative annihilation of excitons. Characteristically, the introduction of Cu impurities in CdS QDs led to the quenching of "defect" PL band (1,6 - 2,3) eV while increasing the intensity of high-energy (2,4 - 3,4) eV PL band. This means that Cu enhances structural perfection CdS QDs. Introduction Zn impurities in QDs CdS, in contrast, did not lead to improved structural characteristics of QDs, as evidenced by the increase in the intensity of "defect" PL band with increasing zinc content of impurities.

16:00 Poster We104

Hydrothermal Synthesis and Characterisation of Zn_2SnO_4 Nanoparticles

Mary Jaculine, Jerome S. Das, Sheeba Anu Jacob, Prince Joshua

Department of Physics, Loyola College, Chennai, Chennai 600034, India

e-mail: sjeromedas2004@yahoo.com

Nanostructured Zn_2SnO_4 nanoparticles have attracted considerable interest owing to their applications in dye-sensitised solar cells (DSSCs), as an anode material of lithium-ion batteries, as photocatalytic materials and as a gas sensor. Ternary oxide Zn_2SnO_4 nanoparticle was successfully synthesized by a simple hydrothermal technique using NaOH as the mineralizer at 200°C for the reaction time of 24 h. Synthesized sample was characterized by powder X-ray diffraction, HRSEM and UV-visible spectroscopy measurements. The product phase and high crystallinity were confirmed using X-ray diffraction (XRD). Optical absorption study revealed the band gap energy to be lesser than that of the bulk Zn_2SnO_4.

16:00 Poster We105

Al-doped ZnO electrode formation for dye sensitized solar cell by gas evaporation method

Minoru Dohi, Ryo Koizumi, Tetsuo Ozawa

Shizuoka Institute of Science and Technology, Toyosawa 2200-2, Fukuroi 437-8555, Japan

e-mail: dohi@ee.sist.ac.jp

The dye sensitized solar cell, whose production is easy and cheap, is expected as a low cost solar cell. The aluminum-doped zinc oxide film and titanium oxide film are used as an electrode of a dye sensitized solar cell,. The dye adheres to this electrode and emits electrons. The formation of an electrode with large surface area, therefore, leads to production of a highly efficient solar cell. Researches of the electrode of porosity or whiskers are actually done widely. In this study, we produced the zinc oxide nanorod electrodes with large surface area for a dye sensitized solar cell by the gas evaporation method, which is one of the methods of producing metal ultrafine particles [1].

We used the powder Zn containing 2 wt% powder aluminum as the evaporation source materials. Ar atmosphere gas of pressure 0.01~0.8 atm was enclosed in the vacuum chamber evacuated to 4 Pa with the rotary pump. The nanorod film was deposited on the slide glass substrate, which was heated at 300~550 ^oC with a ceramic heater. The prepared film was observed with the scanning electron microscope. The nanorod wound intricately rather than was straight. The diameter of the nanorod was controlled by distance of an evaporation source and a substrate in 100 to 1000 nm. After the sample oxidized at 460-520 ^oC in the air, it was investigated by x-ray diffraction. The oxidized film was nonconductive. Therefore, 2 wt% aluminum-doped zinc oxide was sputtered on the film to have conductivity. The efficiency of the dye sensitized solar cell using this electrode will be discussed at the presentation.

[1] M.Dohi et al. Jpn. J. Appl. Phys. **29**, 2445(1990).

16:00 Poster We106

Optimization of the preparation, characterization, adsorption and photocatalytic properties of the samples containing nanoscale titanium dioxide with anatase and η-TiO_2 structures

Elena N. Domoroshchina[1], Lubov N. Obolenskaya[1], Alexandr M. Zybinsky[1], Asia A. Gaynanova[1], Evgeniy N. Kabachkov[2], Polina A. Demina[1], Galina M. Kuz'micheva[1], Elena V. Savinkina[1]

1. *Lomonosov Moscow University of Fine Chemical Technology, Vernadskogo pr., 86, Moscow 119571, Russian Federation* **2.** *Institute of Problems of Chemical Physics RAS (IPCPRAS), Akademika Semenova 1, Chernogolovka 142432, Russian Federation*

e-mail: elena7820@gmail.com

The development of materials with radically new properties is inextricably related with obtaining of nanoscale systems. One of the most promising materials in this area is TiO_2. Its nano-modifications are unique due to the formation of self-generating surface OH groups with a high reaction activity. From the 13 known stable and metastable modifications only one (η-TiO_2) was obtained just in the nanoscale form [1,2]. According to [1] this polymorph and anatase exhibit properties that distinguishes them from the another of nanoscale modifications. The purpose of the investigation is to optimize of sulfate method of samples preparation with nano-anatase and η-TiO_2 and establish the relationship between synthesis conditions, characteristics of the samples and their adsorption and photocatalytic properties. Samples with η-TiO_2 differ from samples with anatase by the presence of two distinct diffraction reflections at $2\theta \sim 4 \div 5°$ and $2\theta \sim 33°$ (CuKα). Based on the X-ray data of anatase and η-TiO_2, it is likely that the structure of η-TiO_2 should be derived from the structure of anatase, or rather, the superstructure to the structure of anatase. Nano-anatase is formed with the practical yield of > 90% in long-term (<4 h) hydrolysis of $TiOSO_4$ at 70°C to 98°C, therefore, in order to optimize its production process we searched the terms of its uniform formation and precipitation. In the results the synthesis parameters (the rate of dissolution of the starting reagent in the water, its amount, method of heating and the pH of the reaction mixture at different stages of the synthesis) were defined and their optimal values for laboratory obtaining of the product were found. Due to the metastability of the phase with η-TiO_2 we have to get it in a strong suppression of precursor hydrolysis, resulting in extremely low practical yield. Modification of the method of obtaining η-TiO_2, described in [1], is to replace the coagulant (solution of HCl [1]) to the more active solution of alkali metal - potassium and cesium halogenides which led to increasing of the practical yield from ~ 30% to ~ 90% [2]. Samples with different modifications differ in their characteristics: specific surface area (30 ÷ 170 m^2/g for anatase and 3 ÷ 18 m^2/g for η-TiO_2), a volume of nano-and ultrananopores (0.04÷0.48 and 0.0005÷0.06 cm^3/g for anatase, 0.0009÷0.004 and 0.008÷0.04 cm^3/g for η-TiO_2), the size of coherent scattering (5÷10 and 2÷4 nm for anatase and η-TiO_2, respectively), the size of crystallites (7÷10 nm), the size of the nanoparticles (~15÷~40 nm for anatase, 10÷~ 30 nm for η-TiO_2), aggregates (120÷150 nm for anatase and 400÷500 nm for η-TiO_2) and agglomerates (aglomerization of the particles with different sizes depending on the synthesis conditions was found in all samples, but mostly it is expressed in samples with η-TiO_2). It was established by IR spectroscopy that the intensity of the absorption bands of the deformation vibrations of the Ti-O-H bonds (about 1050-1150 cm^{-1}) and H-O-H bonds (about 1600-1650 cm^{-1}) in the spectrum of the sample with η-TiO_2 more than in the anatase one. This fact indicates greater content of OH groups on the surface of the particles with η-TiO_2 in comparison with anatase. Photocatalytic activity (PA) of the obtained samples (pure - in the UV, and sensitized by the cold impregnation of diazo- and thiazole dyes under visible light range) is lower than that of the not aggregated commercial Degussa (Evonik) P25 (a mixture of anatase and rutile) and Hombifine N (anatase). However, non-destructive conditions of synthesis for the dyes used (in contrast to pyrolysis that is used in obtaining of commercial analogs) allow sensitizing colloidal intermediate product and obtaining samples with greater PA in comparison with the commercial analogs after impregnation. In the UV range the samples with η-TiO_2 modified by $VO(NO_3)_2$ show larger PA in the reaction of photodegradation of dye Rhodamine B in comparison with Degussa P25, but lower in comparison with Hombifine N. However, when irradiated with visible light (λ= 450÷490 nm) PA of the sample with η-TiO_2 exceeds Hombifine N (Fig. 1).

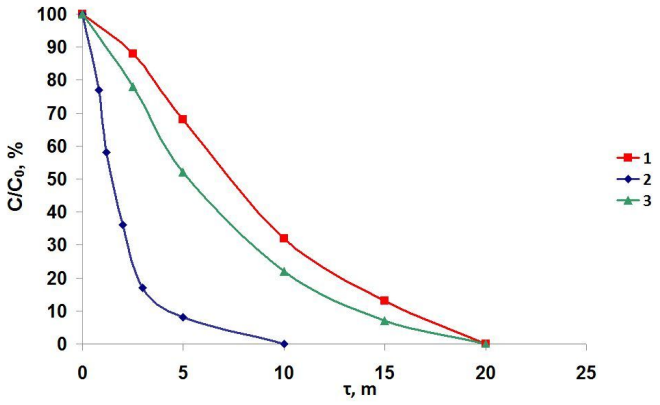

a.

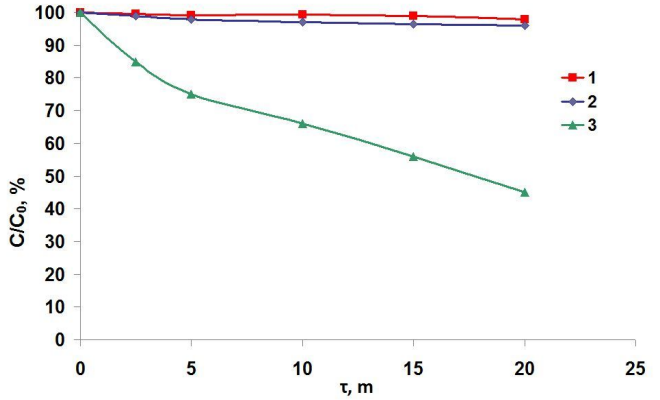

b.

Fig.1 Efficiency of photodegradation of Rhodamine B under UV (a) and visible irradiation (b) in the presence of various photocatalysts Degussa P25 (1), Hombifine N (2), η-TiO_2:V(3).

We have examined adsorption ability of the nano-TiO_2 samples with anatase structure and anatase modified with peroxide (H_2O_2) to extract from water environments Nb (V) and Ta (V) ions. It was found that the sorption degree (R=100-(Cf)/(Ci),%, where Cf and Ci are finish and initial concentrations of analytes, respectively) depends on the sorption conditions and the type of analyte. So, the R,% increases with the increasing of the sorption duration, decreases with the increasing of the sample weight for Ta(V) and does not change for Nb(V), decreases with the use of the membrane filter with 0.45 μm pores and dramatically increases with the use of centrifugation. The R,% weakly depends on the adsorbent characteristics (size of nanoparticles, specific surface area, volume of ultra- and nanopores), and is determined by the nature of the analyte (the degree of Nb (V) extraction is larger than found for Ta (V) one). The results led to the conclusion that the maximal recovery efficiency depends on the sample composition and concentration of adsorption centers – OH-groups – on the adsorbent surface. The amount of Nb (V) and Ta (V) ions adsorbed on the TiO_2 nanoparticles from aqueous solutions first decreases and then increases with increasing the temperature from 4°C to 10°C (Nb(V)) or 20°C (Ta(V)) and from 10°C or 20°C to 80°C, respectively (Fig.2a).

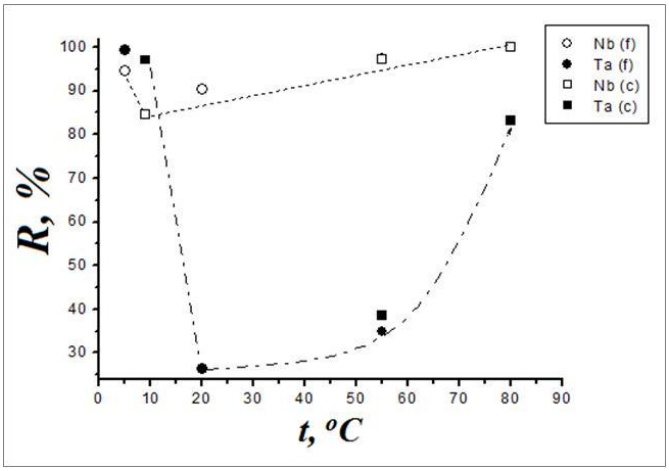

a.

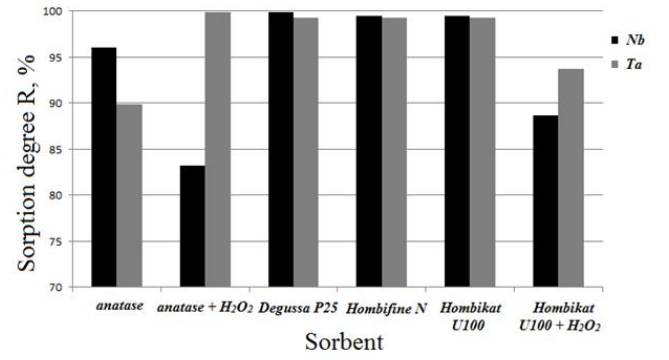

b.

Fig.2 The sorption degree (R,%) vs. the temperature (a) and the nature of the analyte (b).

This behavior suggests exothermic nature of the process (in range of 4°C-10°C for Nb(V) or 4°C -20°C for Ta(V)) which can be caused by physical modification of the adsorbents. Surfaces of metal oxides usually have positive charge at low pH (our case: pH=0.35, i=0.43(1), i-ionic strength). Mo(VI) and W(VI) ions in hydrated associates of different compositions probably have a negative charge (a similar to As(V) ions [3]-[5]). At low temperatures, they are adsorbed at the expense of forces of electrostatic character. With temperature increasing from 4°C to 10°C (Nb(V)) or from 4°C to 20°C (Ta(V)), the attractive forces between TiO_2 and analytes are weakened and the adsorption decreases. Besides, at increasing temperature the thickness of the boundary layer decreases, due to the increasing tendency of the adsorbate to escape from the surface of the adsorbent to the solution phase, which results in a decrease in adsorption. So, it was found that in the temperature range from 10°C to 80°C (Nb(V)) or 20°C to 80°C (Ta(V)) the process is endothermic, since the adsorption increases with increasing temperature. Therefore, the rate of physical adsorption and the amount of ions adsorbed by this way decrease, meanwhile the rate of chemical adsorption increases. As a result, we have found that the samples containing anatase modified with peroxide and Degussa P25 shown the maximum adsorption ability for Ta (V) ions (R = 99.9%) and for Nb (V) ions (R = 99.9%), respectively (Fig. 2b). Note that the sorption process was carried out at pH = 0.35 and a change of this magnitude can have a significant influence on sorption properties. Thus the obtained samples with nano-TiO_2 have a higher photocatalytic activity and comparable adsorption ability in comparison with analogs used at present with increasing of practical output and simplification of the preparation.

[1] Dadachov M. US Patent Application Publication. US 2006/0171877

[2] Kuzmicheva G. M. et al., Patent RU 2463252 C1.

[3] E. Valencia-Trejo et al., J.Applied Sciences in Environmental Sanitation. 5(2) (2010) 171-184

[4] Nabi Deedar et al., J.Environmental Sciences. 21 (2009) 402–408.

[5] By Xiao et al., Water Environ. Res. 79 (2007) 1015.

16:00 Poster We107

Cation distribution in Co-doped $MgGa_2O_4$ nanoparticles studied by X-ray photoelectron spectroscopy

Xiulan Duan, Duorong Yuan, Yuanchun Wu, Fapeng Yu

State Key Laboratory of Crystal Materials, Shandong University, Jinan 250100, China

e-mail: xlduan@sdu.edu.cn

$Co_xMg_{1-x}Ga_2O_4$ (x = 0~0.6) nanoparticles were synthesized by citrate sol-gel method and characterized by X-ray powder diffraction. X-ray photoelectron spectroscopy was used to study the distribution of the cations in the tetrahedral and octahedral sites in $Co_xMg_{1-x}Ga_2O_4$ nanoparticles as a function of composition. The results show that the as-synthesized samples exhibit spinel-type single phase when annealed at 800°C (Fig.1). The crystallite size is about 8-40 nm, and increases with increasing cobalt content. The Ga $2p_{3/2}$ XPS spectra are composed of two peaks for all the x values, indicating that Ga^{3+} ions occupy two different coordination sites (tetrahedral and octahedral) in the nanoparticles (Fig.2). The inversion parameter (two times the fraction of Ga^{3+} ions in tetrahedral sites) is estimated to be 0.48 for the pure $MgGa_2O_4$ (x=0) and the value increases to 0.72 when x is up to 0.6. The absorption spectra of Co-doped $MgGa_2O_4$ nanoparticles exhibit two absorption bands in the wavelength range 250-800 nm, which indicates that Co^{2+} ions are located in the tetrahedral sites as well as in the octahedral sites in the nanoparticles (Fig.3).

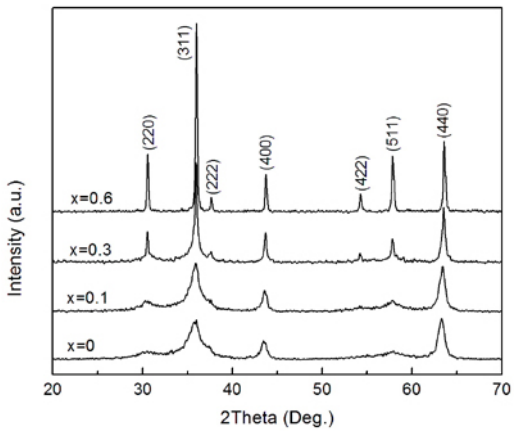

Fig.1 XRD patterns of $Co_xMg_{1-x}Ga_2O_4$ nanoparticles annealed at 800°C.

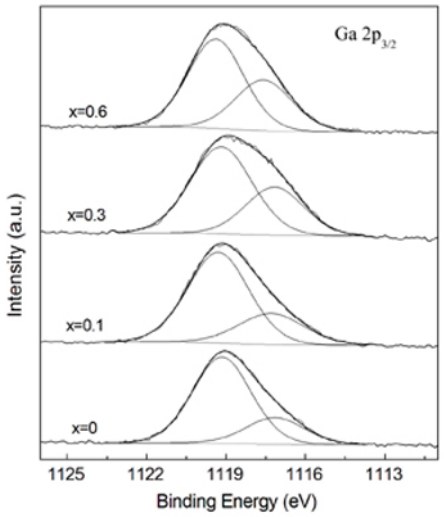

Fig.2 Ga $2p_{3/2}$ XPS spectra of $Co_xMg_{1-x}Ga_2O_4$ (x=0~0.6) nanoparticles annealed at 800°C.

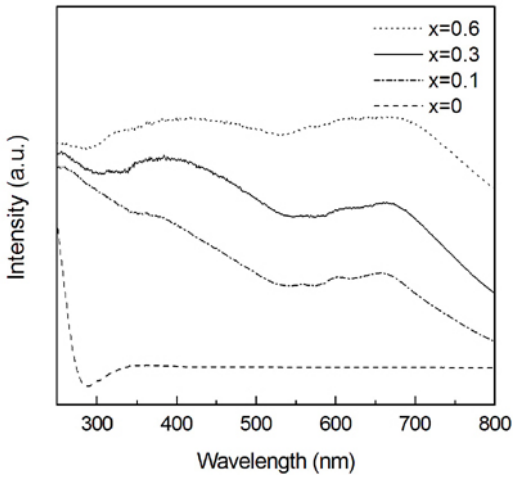

Fig.3 Absorption spectra of $Co_xMg_{1-x}Ga_2O_4$ (x=0~0.6) nanoparticles annealed at 800°C.

16:00 Poster We108

Structural and morphological properties of new composite nanocrystalline Y_2O_3/ZnO spheres

Nadya A. Dulina[1], Yuliya V. Yermolayeva[1], Alexander V. Tolmachev[1], Gennady A. Emelchenko[3], Alexander N. Gruzintsev[2]

1. *Institute for Single Crystals NAS of Ukraine (ISC), 60 Lenin Ave., Kharkov 61001, Ukraine* **2.** *Institute of Microelectronics Technology, Russian Academy of Science (IMTRAS), Institutskaja, 6, Chernogolovka 142432, Russian Federation* **3.** *Institute of Solid State Physics, RAS, Chernogolovka, Russian Federation*

e-mail: dulina@isc.kharkov.ua

Last years, an explosive growth of the number of researches devoted to the creation and design of the new crystalline nanocomposite materials has been observed. For example, composite nanoparticles (core–shell structured or hollow, raspberry-like and others), nanopowders and crystalline nanostructures attract considerable attention

due to the ability to adjust their properties in a wide range depending on the structure, composition and geometrical proportions. We propose mono-sized polycrystalline Y_2O_3 nano- and submicrospheres as matrix material for ZnO nanocrystals preparation. Y_2O_3 as well as other rare-earth oxides with the well-defined spherical morphology were successfully obtained by urea-based homogeneous precipitation (UBHP) by taking advantages of high control of the sizes (40-400 nm) and monodispersity of the particles as well as economic efficiency.

Highly UV luminescent ZnO nanocrystals were obtained in the voids of mesoporous Y_2O_3 spherical particles of different diameters by means of infiltration technique with subsequent thermolysis (T= 600 ºC). The main idea is the application of mesoporous UBHP–prepared Y_2O_3 spheres with the porosity till 50% as a matrix with high chemical and thermal stability for preparation of isolated ZnO nanocrystals. Nanostructure, morphology and composition of obtained composite particles were investigated by transmission electron microscopy (TEM), energy dispersive X-ray spectroscopy (EDS), thermal analysis (DTA-TG), BET, and X-ray diffraction (XRD) technique. The ZnO nanophase were found to begin crystallization in the Y_2O_3 matrixes at 300 °C and its crystalline structure was improved with the increase of annealing temperature till 900°C without anysolid-phase reactions between Y_2O_3 and ZnO. Room-temperature photoluminescence spectra of Y_2O_3-ZnO composite particles show intensive UV emission at 340 nm with almost absence impurity visible luminescence.It has been shown that the position of UV luminescence of the composites and its intensity strongly depends on the annealing temperature and the spheres diameter. The possible reasons of such phenomenon were also discussed.

16:00 Poster We109

Crystalline nanostructures of heavy metal halides

Laura Fornaro[1], Ivana Aguiar[2], María Eugenia Pérez Barthaburu[1], Alvaro Olivera[1], Isabel Galain[2], Maia Mombrú[2]

1. *Compound Semiconductors Group, CURE, Universidad de la República, Route 15, km 28.500 and route 9, Rocha 27000, Uruguay*
2. *Compound Semiconductors Group, Cátedra de Radioquímica, DEC, Facultad de Química, Universidad de la República, General Flores 2124, Montevideo 11800, Uruguay*

e-mail: lfornaro@gmail.com

Mercuric iodide, bismuth tri-iodide and mercuric bromide nanoparticles were synthesized by the suspension method, using 1-octadecene (ODE) as suspension agent, $Hg(NO_3)2.H_2O$ as Hg source, $Bi(NO_3)_3.5H_2O$ as Bi source and I_2 and NaBr as halides sources. The influence of Octadecanethiol (ODT) as capping agent was also studied. Syntheses were performed with one (at a temperature T1 and during a time t1) or two steps (with a second step at a temperature T2 and during a time t2). The best synthesis conditions for nanostructures of the three halides are summarized in Table 1.

Halide	Sample	T1(ºC)	t1(min)	T2(ºC)	t2(min)	Capping
HgI_2	H1	70	60	-	-	-
	H2	70	240	-	-	-
	H3	70	240	-	-	ODT
BiI_3	B1	100	240	200	10	-
	B2	80	240	180	10	-
	B3	200	10	-	-	ODT
$HgBr_2$	P1	100	240	200	10	-
	P2	80	240	200	10	-
	Pe	100	240	200	10	ODT

Table 1

The synthesized nanostructures were characterized by scanning electron microscopy (SEM), transmission electron microscopy (TEM) and high resolution TEM (HR-TEM), energy dispersive spectrometry (EDS), X-Ray diffraction (XRD) and selected area electron diffraction (SAED). Compounds identity was confirmed by XRD and EDS. Crystalline nanostructures were obtained for the three halides, with sizes from 5 to 500 nm. Mercuric iodide and mercuric bromide nanostructures have cubic and rod morphology, whereas bismuth tri-iodide ones have hexagonal and rod morphology. XRD, SAED and HR-TEM results show that the obtained nanostructures are crystalline, and that they have preferred orientations. In addition, nanostructures modification and coalescence was observed as consequence of the TEM beam irradiation.

Figures 1 to 3 show some examples of SEM, TEM, XRD and SAED results for representative samples of the three halides.

Taking into account the physical properties of these compounds, especially their high radiation absorption coefficients and wide band gaps, as far as the crystalline nature of the obtained nanostructures, the nanostructures are being used as nuclei for inducing oriented and epitaxial growth of films for ionizing radiation imaging, opening the possibility of a new generation of imagers with enhanced performances. In addition, these nanocrystals are being experimented as acceptors into hybrid solar cells.

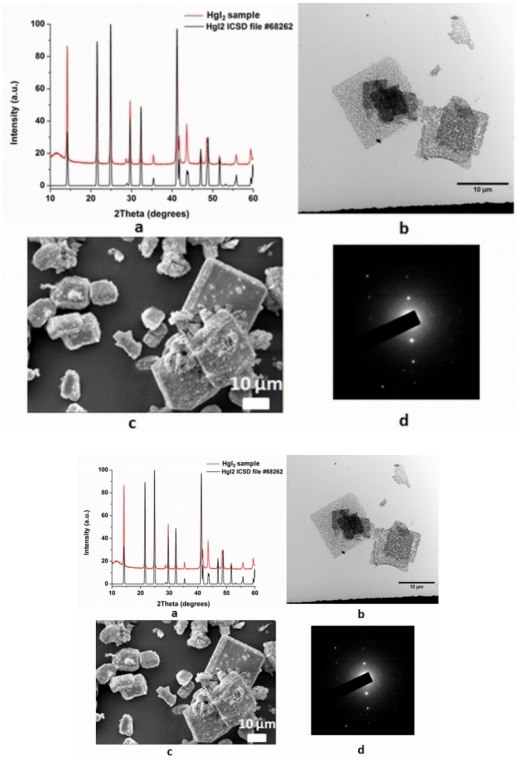

Figure 1: Characterizations of a representative HgI_2 sample, a: XRD diagram, b: TEM image, c: SEM image, d: SAED diagram

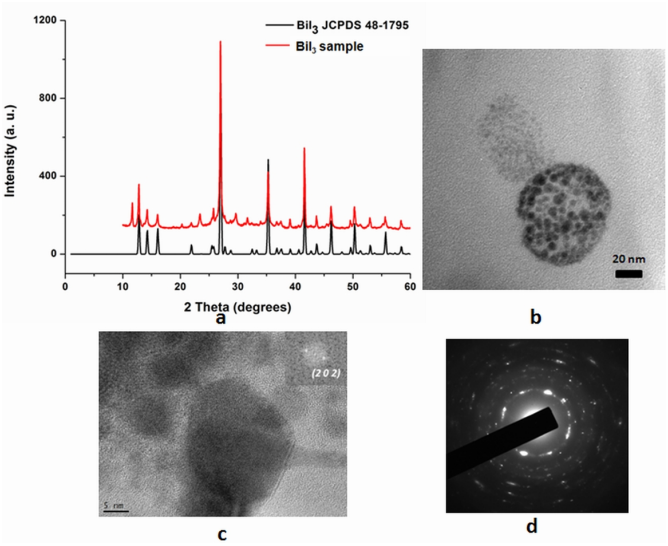

Figure 2: Characterizations of a representative BiI_3 sample, a: XRD diagram, b: TEM image, c: HR-TEM image, d: SAED diagram

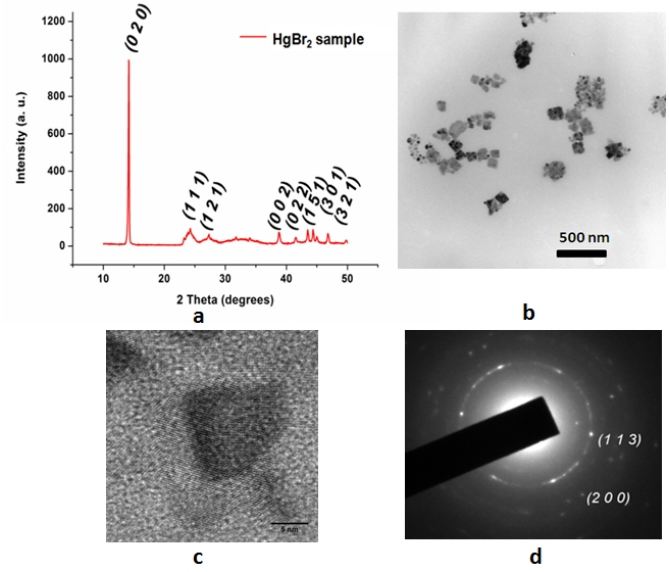

Figure 3: Characterizations of a representative $HgBr_2$ sample, a: XRD diagram, b: TEM image, c: HR-TEM, d: SAED diagram

16:00 Poster We110

Preparation and Characterization of Orthorhombic MoO_3 Nanostructures by VS growth method

Senthilkumar Rajamanickam[1], Ravi Ganesan[1], Hayakawa Yasuhiro[2]

1. *Department of Physics, Alagappa University,, Karaikudi 630 003, India* **2.** *Shizuoka University, Hamamatsu 432-8011, Japan*

e-mail: gravicrc@gmail.com

Molybdenum trioxide (MoO_3) is one of the transition metal oxides that have engrossed much interest for technological and industrial applications in recent years. Molybdenum oxide nanostructures film were grown on different substrates such as fluorine doped tin oxide (FTO), indium doped tin oxide (ITO) and ordinary glass substrates by simple thermal evaporation technique using tubular furnace. Using molybdenum trioxide (MoO_3) powder as a source material vaporized at high temperature without catalyst and then by transient sufficient oxygen, argon gas mixture (O_2/Ar) ratio for different flow rate. By changing the source and substrate temperature, different morphologies including dense nanobelts and nanohunk of MoO_3 nanostructures were obtained. Morphology, composition phase and micro structural parameters of the film have been characterized by scanning electron microscope (SEM), X-ray diffraction (XRD), Energy Dispersive analysis (EDAX) and Raman spectroscopy. The observed XRD patterns were compared with standard JCPDS cards (65-2421) and (05-0508). The samples were nanobelts with a width up to 800 nm, about 40 nm in thickness and from tens to several hundred micrometers in length. The analysis indicated that as-synthesized samples were orthorhombic structured MoO_3 grown with [0 1 0] preferred orientation and also confirmed by SEM images. Raman spectra of corresponding vibrational modes are due to a highly ordered structure. The EDAX spectra reveals that FTO substrates having good O/Mo ratio nearly equal to 3 that means the presence of stoichiometry of MoO_3 compared to ITO and glass substrates.

References

[1]. Dongmei Ban, Ningsheng Xu, Shaozhi Deng, Jun Chen and Juncong She, J. Mater. Sci. Technol., 26(7) (2010) 584-588.

[2]. Jian Zhen Ou, Jos L CampBell, David Yao, Wojtek Wlodarski and Kourosh Kalantar-Zadeh, J. Phys. Chem., C 115, (2011) 0757-10763.

[3]. Chirakkal V. Krishnan, Jinglu Chen, Christian Burger, and Benjamain Chu J.Phys. Chem. B 110 (2006) 20182-20188.

16:00 Poster We111

Surfactant Assisted Growth and Studies of $NiCo_2O_4$ Nanostructures through Microwave Heating Method

Anandha babu Ganesan[1], Ravi Ganesan[1], Hayakawa Yasuhiro[2]

1. *Department of Physics, Alagappa University,, Karaikudi 630 003, India* **2.** *Shizuoka University, Hamamatsu 432-8011, Japan*

e-mail: gravicrc@gmail.com

A fast and facile method has been imposed for the preparation of $NiCo_2O_4$ nanostructures using metal nitrate as a precursor materials and CTAB as a surfactant. The prepared samples were characterized by Thermo gravimetry differential thermal analysis (TG–DTA), Powder X-ray diffraction (XRD), Fourier transformation infrared spectroscopy (FT-IR), Scanning electron microscopy (SEM) and UV-Visible spectroscopy. It was found that the synthesis route proposed in this work favored the formation of $NiCo_2O_4$ spinel phase at low temperature. The surfactant CTAB was chosen to control over the nucleation, growth and agglomeration nature of observed $NiCo_2O_4$ nanocrystalline products. With the effect of surfactant, the obtained $NiCo_2O_4$ has been used for various promising potential applications. Based on the observed experimental observations and analysis, a possible microwave reaction mechanism is proposed to synthesis $NiCo_2O_4$ nanostructured materials to enrich the structural, morphological and optical properties of $NiCo_2O_4$ nanostructures.

References

[1] A.P.S. Peres, A.C. Lima, B.S. Barros, D.M.A. Melo, Materials Letters, 89 (2012) 36–39.

[2] Guo-Ying Zhang, Bing Guo, Jun Chen, Sensors and Actuators B, 114 (2006) 402–409.

16:00 Poster We112

The Solvent Effect on Size and Morphology of SnO Nanoparticles via Chemical Co-Precipitation Method

Vijayaprasath Gandhi[1], Ravi Ganesan[1], Hayakawa Yasuhiro[2]

1. *Department of Physics, Alagappa University,, Karaikudi 630 003, India* **2.** *Shizuoka University, Hamamatsu 432-8011, Japan*

e-mail: gravicrc@gmail.com

Stannous oxide (SnO) is an important functional material which contributes to a wide range of applications. The synthesis of energetically stable SnO, a p-type semiconductor with direct optical variable band gap of E_g= 2.7-3.4 eV has been attracted a considerable attention due to its specific functional characteristics and significance in various technological applications such as coating substance, catalyst, thin film transistors and a permissible anode material for lithium ion batteries. In the present study the SnO nanoparticles has been synthesized using different solvents by chemical co-precipitation method. Different morphologies of SnO nanoparticles have been achieved for different solvents. The size of SnO nanoparticles for various solvents was estimated by powder X-ray diffraction (PXRD) pattern and revealed that SnO crystallizes into tetragonal rutile phase. The chemical structure information of the synthesized nanoparticles was studied by Fourier transform infrared (FTIR) spectroscopy. The SnO absorption peaks are attributed to 650-550 cm^{-1} range and assigned to the stretching vibration of Sn-O bond. The strong prominent UV emission peak was observed at 413 nm in the luminance spectra, which was studied by photoluminescence (PL) spectroscopy. The composition of the product could be determined through X-ray photoelectron spectroscopy (XPS) spectra. The binding energies of O(1s) and Sn($3d_{3/2}$) were found to be centered at 530 and 492 eV respectively.

REFERENCES

1. M.Ahmad, Rafi-ud-Din, C.F.Pan, J.Zhu, J.Phys.Chem.C 114 (2010) 2560.
2. L.Y.Liang, Z.M.Liu, H.T.Cao, X.Q.Pan, ACS Appl.Mater.Interface, 2 (2010) 1060.
3. H.Kawazoe, M.Yasukawa, H.Hyodo, M.Kurita, H.Yanagi, H.Hosono, Nature, 389 (1997) 939–942.
4. X.Wu, B.Zou, J.Xu, B.Yu, G.Zhang, W.Chen, Nanostruct. Mater., 8(1997)179.

16:00 Poster We113

Synthesis and Study of Structural, Morphological and Magnetic properties of nanocrystalline Hausmannite (Mn_3O_4)

Shrividhya Thiagarajan[1], Ravi Ganesan[1], Hayakawa Yasuhiro[2], Mahalingam Taiyan[3]

1. *Department of Physics, Alagappa University,, Karaikudi 630 003, India* **2.** *Shizuoka University, Hamamatsu 432-8011, Japan* **3.** *Karunya university, karunya nagar, Coimbatore 641114, India*

e-mail: gravicrc@gmail.com

Mn_3O_4 is an important functional material with potential applications in batteries, high density storage devices, starting material for ferrites, catalytic and ion exchange reactions, electro-chromic displays and dilute magnetic semiconductors (DMS) [1-3]. This material has good magnetic and magneto optical properties due to the strong interaction of s, p-d interaction between the electron/hole band states of Mn [4-5]. Mn_3O_4 nanoparticle was prepared by co-precipitation method using $MnSO_4.H_2O$ and NaOH as starting materials. Ammonia was used to maintain the pH of the solution. The deposited nanoparticles were annealed at 300°C and 600°C. Nanoparticles synthesized by this method were characterized using X-Ray diffractometer, Raman spectroscopy, Scanning electron microscopy, Energy dispersive analysis of x-rays and vibrating sample magnetometer to analyze structural, functional, morphological, compositional and magnetic properties respectively. Microstructural parameters such as crystallite size, micro strain and dislocation density were calculated from the XRD data obtained. Structural changes between the as deposited and annealed Mn_3O_4 nanoparticles were observed. Raman spectra showed the presence of A_{1g} mode of vibration corresponding to Mn_3O_4 phase. Hysteresis loop of the as deposited Mn_3O_4 nanoparticles depicts paramagnetic behavior at room temperature. SEM micrographs showed spherical shaped particles with particle size 23.5 nm approximately. All results will be discussed in detail.

References

1. Ming Yin and Stephen O'Brien, J. Am. Chem. Soc., 125 (2003)10181.
2. Hassouna Dhaouadi, Ouassim Ghodbane, Faouzi Hosni and Fathi Touati, ISRN Spec., 2012 (2011) 706398.
3. Yu Li, Haiyan Tan , Xiao-Yu Yang , Bart Goris , Jo Verbeeck , Sara Bals , Pierre Colson, Rudi Cloots, Gustaaf Van Tendeloo and Bao-Lian Su, Small, 7 (2011) 475.
4. Tian Qin, Jun Lu, Shuo Wei, Pengfei Qi , Yiya Peng , Zhiping Yang and Yitai Qian, Inorganic Chem. Commun., 5 (2002) 369.
5. D.P. Dubal, D.S. Dhawale, R.R. Salunkhe, C.D. Lokhande, J. Electro.Chem., 647 (2010) 60.

16:00 Poster We114

1D ZnO-based structures obtained by thermal oxidation of ZnTe and ZnTe/Zn nanowires

Katarzyna Gas[1], Eliana Kamińska[2], Elzbieta Dynowska[1], Sławomir Kret[1], Maciej Wiater[1], Wojciech Zaleszczyk[1], Agnieszka Kamińska[3], Tomasz Wojtowicz[1], Wojciech Szuszkiewicz[1]

1. *Polish Academy of Sciences, Institute of Physics, Lotnikow 32/46, Warsaw 02-668, Poland* **2.** *Institute of Electron Technology (ITE), al. Lotników 32/46, Warszawa 02-668, Poland* **3.** *Institute of Physical Chemistry Polish Academy of Sciences (IPCPAS), Kasprzaka 44/52, Warsaw 01-224, Poland*

e-mail: kgas@ifpan.edu.pl

One-dimensional (1D) semiconductor nanostructures like, e.g., nanowires (NWs) or nanobelts recently attracted a great deal of attention due to their potential application in electronic and optoelectronic nanodevices. Among many materials zinc oxide is particularly intensively researched due to its wide direct-gap (3.37 eV at 295 K) and a large exciton binding energy of 60 meV. The non-intentionally doped ZnO usually exhibits n-type conductivity and it is difficult to convert it to p-type semiconductor. The inherent difficulties in obtaining p-type ZnO is the major obstacle in widespread device applications of this material. Contrary to ZnO, ZnTe can be relatively easy highly p-type doped. Moreover, as it was already shown thermal oxidation of nitrogen-doped ZnTe allows to obtain p-type ZnO [1, 2], therefore one possible way to produce p-type, ZnO-based NW structure would be through the oxidation of p-type ZnTe NWs.

In this paper we report on fabrication and characterization of 1D ZnO-based structures. The nanostructures have been obtained by thermal oxidation of ZnTe and ZnTe/Zn core/shell NWs. The ZnTe NWs were grown on GaAs substrates by molecular beam epitaxy employing a

gold-catalyzed vapor-liquid-solid mechanism [3, 4]. After the growth, the ZnTe-based NWs are annealed under different conditions: we vary the annealing time, temperature and atmospheres (O_2, Ar or mixture O_2 and Ar). The surface morphology of the nanostructures before and after thermal annealing process is examined by scanning electron microscopy. The structural characterization is performed by using transmission electron microscopy and X-ray diffraction. The energy dispersive X-ray spectroscopy is applied to examine the chemical composition of the resulting nanostrucrures. The optical characterization is carried out by room temperature micro-Raman spectroscopy, as well as, by cathodoluminescence.

The annealing of ZnTe NWs at 300°C for 4 h in O_2 led to formation of numerous 30-60 nm in diameter ZnO nanocrystals on the surfaces of the wires, whereas the same annealing procedure applied to ZnTe/Zn core/shell NWs does not change their morphology significantly (see Figure 1), indicating that the ZnTe/ZnO core/shell NWs are obtained in this case. The two-step oxidation process for core/shell ZnTe/Zn NWs in O_2 (in the first step the samples are annealed at 350°C by 1h and after that the temperature is increased to 400°C and oxidation process is continued by 1h) results in formation of nanotubes composed mostly of small ZnO and also of TeO_2 crystallites with random crystal orientations. These randomly oriented ZnO nanocrystals can get oriented along the crystal orientation of the Zn shell initially covering the ZnTe/Zn NWs when after normal oxidation they are subjected to 600°C argon annealing. Moreover, an additional annealing at 600°C in argon causes branching on the NWs into only a several nm in diameter but almost a micrometer long dendrites-like very straight and uniform nanowires. Presence of the gold droplets at the end of each wire indicates the same Au-driven catalytical grows mode. The annealing of the ZnTe NWs in O_2 at the temperature above 500°C destroys completely the NWs. However, we can increase the oxidation temperature up to 600°C by changing the annealing atmosphere to the mixture of 2% O_2 and 98% Ar. Thanks to such approach the obtained NWs contain only ZnO and shows characteristic for ZnO near-band edge and defect luminescence.

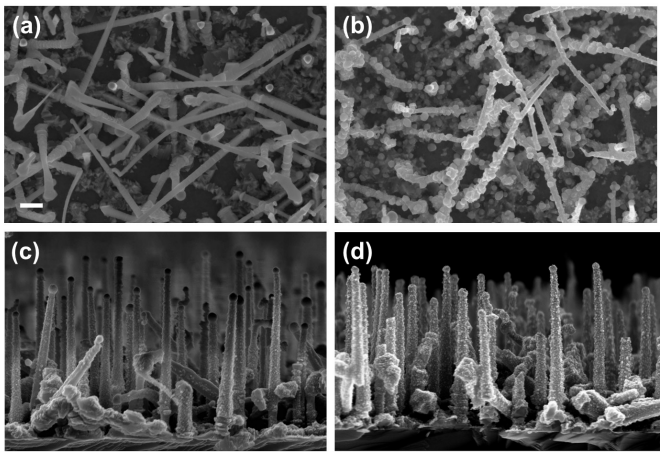

Figure 1: SEM images of (a) ZnTe NWs (b) oxidized ZnTe NWs (c) ZnTe/Zn core/shell NWs (d) oxidized ZnTe/Zn core/shell NWs. The NWs are oxidized in O_2 at 300°C for 4 h. The scale bar on the SEM picture corresponds to 200 nm.

The studies were partially supported by the European Union within European Regional Development Fund, through grant Innovative Economy (POIG.01.01.02-00-008/08).

[1] E. Przeździecka, A. Piotrowska, J. Kossut, R. Butkute, W. Dobrowolski, R. Łukasiewicz, A. Barcz, R. Jakieła, E. Dynowska, E. Przeździecka, M. Aleszkiewicz, P. Wojnar and E. Kowalczyk, *phys. stat. sol. (c)***3**, 988 (2006).

[2] E. Przeździecka, E. Kamińska, K. P. Korona, E. Dynowska, W. Dobrowolski, R. Jakiela, Ł. Kłopotowski, and J. Kossut, *Semicond. Sci. Technol*. **22**, 10 (2007).

[3] E. Janik, J. Sadowski, P. Dłużewski, S. Kret, L. T. Baczewski, A. Petroutchik, E. Łusakowska, J. Wróbel, W. Zaleszczyk, G. Karczewski, T. Wojtowicz, and A. Presz, *Appl. Phys. Lett.***89**, 133114 (2006).

[4] E. Janik, P. Dłużewski, S. Kret, A. Presz, H. Kirmse, W. Neumann, W. Zaleszczyk, L.T. Baczewski, A. Petroutchik, E. Dynowska, J. Sadowski, W. Caliebe, G. Karczewski, and T. Wojtowicz, *Nanotechnology***18**, 475606 (2007).

16:00 Poster We115

Nanoscale Schottky contacts to compound semiconductors based on metal nanoparticles

Jan Grym[1], Roman Yatskiv[1], Jan Lörinčík[1], Ondřej Černohorský[1,2]

1. *Czech Academy of Sciences, Institute of Photonics and Electronics, Chaberská 57, Prague 18251, Czech Republic* **2.** *Czech Technical University in Prague, Faculty of Nuclear Sciences and Physical Engineering, Department of Physical Electronics, Brehova str. 7, Prague 115 19, Czech Republic*

e-mail: grym@ufe.cz

Metal-semiconductor interfaces formed by thermal evaporation on n-type II-VI and III-V semiconductors frequently show low Schottky barrier heights (SBH). Attempts to increase the SBH by depositing metals with a large work function fail because of the strong Fermi level pinning (FLP). High-energy deposition processes cause large disorder at the interface and thus a high level of FLP. Substantial improvements can be reached by low energy deposition techniques.

We report on the electrophoretic deposition (EPD) of metal nanoparticles (MNPs) prepared by the reverse micelle technique onto bulk substrates and epitaxial layers of InP, GaAs, InGaAs, GaN and ZnO and on their application in hydrogen sensor elements. We describe the role of the EPD conditions (time, polarity, applied voltage regime) on the quality of graphite/MNPs/InP Schottky barriers and their hydrogen sensing properties. We show that the SBH can be greatly increased and that Schottky-based hydrogen sensor elements with excellent sensitivity response can be fabricated.

The work was supported by the project COST LD12014 of the Ministry of Education CR and by the international collaboration project M100671201 of the ASCR.

16:00 Poster We116

Growth and structure of nitrogen-doped carbon nanowalls by plasma-enhanced chemical vapor deposition

Miki Inoue[1], Akihiko Yoshimura[1,2], Masaru Tachibana[1]

1. *Yokohama City University, Yokohama, Japan* **2.** *IHI Corporation, Yokohama 235-8501, Japan*

e-mail: choco52244@gmail.com

Vertically oriented two-dimensional carbon sheets called carbon nanowalls (CNWs) have been fabricated on some substrates by dc plasma-enhanced chemical vapor deposition (dc-PECVD). Each CNW basically consists of several tens of graphene layers. The unique shape and structure can lead to various applications for electronic and energy devices [1]. Furthermore, the doping of nitrogen in CNWs can give rise to the improvement of electrical [2] and electrochemical properties [3]. The understanding of the growth process of CNWs is important for not only the growth control but also the technical applications.

Especially, the understanding of the interface between CNW and substrate is important for the construction of electronic circuit and electrodes for devices. Grazing incidence X-ray diffraction studies on CNW growth have showed that graphene layers parallel to the substrate surface are formed before the growth of graphene layers vertical to the substrate, i.e. CNW [4,5]. In this paper, we report the atomic force microscopy (AFM) and Raman spectroscopy study on the early stage of CNW growth by dc-PECVD.

CNWs were fabricated on Si (100) substrate by dc-PECVD with a gas mixture of CH_4, H_2 and Ar. The substrate was heated to a temperature of 973 K. The flow rates of CH_4, H_2 and Ar were 10, 10 and 80 sccm, respectively. In the case of the doping of nitrogen, N_2gas was introduced with gases as mentioned above. The dc plasma power was 3.0 kW. During the deposition reaction, the pressure of dc plasma reactor was kept at 1.0 Pa with a turbomolecular pump. Samples were prepared under various reaction times below several minutes. The surface morphologies of the samples were observed by AFM in dynamic mode. The Raman spectra were obtained using a micro-Raman system, equipped a single spectrometer (1800 g/mm grating) with an optical microscope (100 x objective), a holographic notch filter, and an air-cooled charge coupled device (CCD) detector.

From AFM and Raman analysis for samples with various reaction times, it is suggested that the growth as mentioned below occur in the early stage of the growth of CNW. First nanodiamond particles with highly defective graphene layers are formed over the substrate. Subsequently nanographite grains are grown on the nanodiamond film. The density of nanographite grains increases with increasing deposition time, and they coalesce to form a continuous graphite film. Finally, CNW is shown to grow vertically on the graphite film. In addition, the effect of nitrogen doping on CNW growth was also investigated by AFM and Raman spectroscopy. In this presentation, the growth process with nitrogen will be discussed compared with CNW growth without nitrogen.

[1] S. C. Shin et al., J. Appl. Phys. **110**, 104308-1-4 (2011)

[2] W. Takeuchi et al. Appl. Phys. Lett. 92, 213103 (2008)

[3] J. P. Mcclure et al. J. Electrochem. Soc. **159**, F733-F742 (2012)

[4] H. Yoshimura et al. Chem. Phys. Lett. **482,** 125-128 (2009)

[5] A. Yoshimura et al. Carbon **50**, 2698-2702 (2012)

Corresponding author: Masaru Tachibana, YokohamaCity University, 22-2 Seto, Kanazawa-ku,Yokohama 2360027, Japan, Tel &Fax: +81-45-787-2360, E-mail: tachiban@yokohama-cu.ac.jp

16:00 Poster We117

Comparative Study of Transport Properties in AlInSb/InSb and AlInSb/InAsSb Quantum Wells

Takusi Manago[1], Shuichi Ishida[2], Hirotaka Geka[3], Ichiro Shibasaki[4]

1. *Fukuoka University, 8-19-1 Nanakuma, Jonan, Fukuoka 814-0180, Japan* **2.** *Tokyo University of Science, Yamaguchi, Daigakudori 1-1-1, San'yo-Onoda 756-0884, Japan* **3.** *Asahi Kasei Corporation, Samejima 2-1, Fuji, Shizuoka 416-8501, Japan* **4.** *The Noguchi Institute, 1-8-1 Kaga, Itabashi, Tokyo 173-0003, Japan*

e-mail: shuisida@ymail.plala.or.jp

Two-dimensional electron systems (2DES) using narrow-gap semiconductors are important for high speed devices, infrared detectors, highly sensitive magnetic sensors and spintronic applications, because of high electron mobility and large effective g-factor. We have studied the well-width dependence of sheet resistivity, carrier density and mobility in $Al_{0.1}In_{0.9}Sb$/InSb and $Al_{0.1}In_{0.9}Sb$/$InAs_{0.1}Sb_{0.9}$ QWs, and found that the transport properties of InSb and $Al_{0.1}In_{0.9}Sb$ QWs are entirely different especially in low temperature. In this paper, we explain the result, based on the calculated band-alignment of these QWs.

The samples were grown by molecular beam epitaxy (MBE). The sample structures are GaAs cap (6.5 nm) /$Al_{0.1}In_{0.9}Sb$ cap (50 nm)/InSb or $InAs_{0.1}Sb_{0.9}$ active layer (L_w)/$Al_{0.1}In_{0.9}Sb$ buffer (700 nm)/GaAs (100) substrate. The layer structures are the same except the active layer for both QW structures. The substrate is a semi-insulating GaAs and all layers are undoped. The well width (L_w) of the active layer is 15 ~ 200 nm.

As shown in Fig.1, the resistivity in low temperature of $InAs_{0.1}Sb_{0.9}$ QWs is much smaller than that of InSb QWs. The difference has been found to result from the band alignment calculated for these QW structures. Fig.2 indicates that the bottom of the conduction band of InSb QWs is depleted above the Fermi level (E_F), while that of $InAs_{0.1}Sb_{0.9}$ QWs is just under E_F in low temperature. In addition, the mobility of InSb QWs falls markedly with decreasing L_w, while that of the $InAs_{0.1}Sb_{0.9}$ QWs hardly depends on the well width. The mobility decrease with narrowing L_w could originate from the possible strain-effect due to the lattice mismatch.

This work was partly supported by the Japan Society for the Promotion of Science (JSPS), Grant-in-Aid for Scientific Research (C: 24560034).

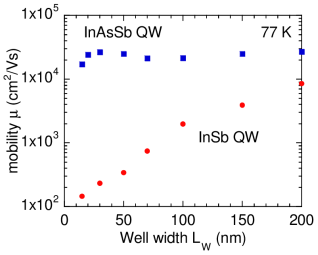

Fig.1 Well-width dependence of mobility

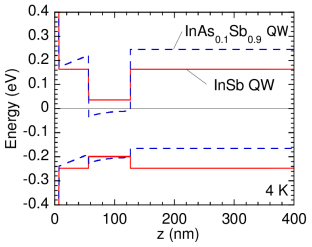

Fig.2 Energy-band diagram for Lw =70 nm

16:00 Poster We118

Nanocrystalline pure and doped Indium nitride

Bagavath Chandiran, Ashraf Ali A, Ramasubramanian Swaminathan, Kumar Janakiraman

Crystal Growth Centre, Anna University, Chennai, Chennai 600025, India

e-mail: marsjk@annauniv.edu

III-V nitride semiconductors are attracted much research attention for their applications in electrical and opto-electronic field. Gallium nitride (GaN) and Indium nitride (InN) are direct bandgap materials of optical bandgap 3.4 eV and 0.7 eV respectively. Many growth procedures have been adapted in growing the III- nitrides. Usually the preparation of GaN in these methods involves nitrification at higher temperatures. Synthesis of nanocrystalline GaN and InN has been done via modified sol-gel and ammonolysis methods. Both nitrides are prepared in successive steps: (i) preparing their elemental –citrate-amine crystals with optimization of pH (7 -8 for GaN, 2 -3 for InN) and (ii) followed with drying in air at 400 °C and (iii) subjected to ammonolysis at elevated temperatures. Experiments of nitridation process have been carried out with variation of temperature in a horizontal reactor with constant flow of ammonia (400 mlm). In the case of InN, the period of nitration process is found to have an important role in the formation of this nitride. Structural studies of X-ray diffraction and Raman showed the

successful synthesis of hexagonal GaN and InN. The optical properties of the synthesized nitrides have been investigated using diffusive reflectance spectra and room temperature photoluminescence studies. Different morphological shapes of these agglomerated nitrides are observed in the scanning electron microscopic images. The morphology and bandgap of the nitrides varied with the synthesis temperature. Barium doped InN nanocrystals have also been successfully grown. Ba doping is found to eliminate the presence of indium. The structural, morphological and optical properties of the Ba doped InN have been investigated and will be presented in detail.

16:00 Poster We119

Influence of capping agent ratio on the structural and morphology of $CuInSe_2$ nanoparticles

Ramkumar Jeyagopal, Ananthakumar Susaimanickam, Moorthy Babu Sridharan

Crystal Growth Centre, Anna University, Chennai, Chennai 600025, India

e-mail: rjramkumar@gmail.com

A facile route for synthesizing $CuInSe_2$ nanocrystals was developed using mercaptoacetic acid as capping agent and water as solvent. Two different mole ratios (5 & 10) of mercaptoacetic acid was used to synthesis $CuInSe_2$ nanoparticles by wet chemical method and similar ratio of capping agent was also used for the preparation by hydrothermal method. The synthesis method and the ratio of the capping agent have influence over the structure and morphology of the synthesised nanoparticles. There are some significant changes in the structure of the $CuInSe_2$ nanoparticles which was confirmed through the XRD. The samples prepared by wet chemical method shows wurtzite phase while the hydrothermally prepared samples shows chalcopyrite phase and at the same the crystallinity of samples increases with increasing the mole ratio of the capping agent as well as varying the synthesis method. Raman analysis shows a strong band at 233 cm^{-1} is due to the combination of B_2 + E mode. The surface capping was confirmed from the FTIR analysis. The thermal stability of the samples was also studied through the TGA-DSC analysis. The changes in morphology of the synthesized samples were analyzed from the SEM and it shows that the sample prepared by wet chemical method is spherical with 5 & 10 mole ratio of thiol while hydrothermally synthesized samples were nanotubes and nanoflakes. The TEM analysis shows larger grains for the hydrothermally prepared sample with 10 mole ratio of thiol. The results are discussed in detail.

SEM & TEM image of wetchemically synthesised $CuInSe_2$ nanoparticles with ten mole ratio of capping agents

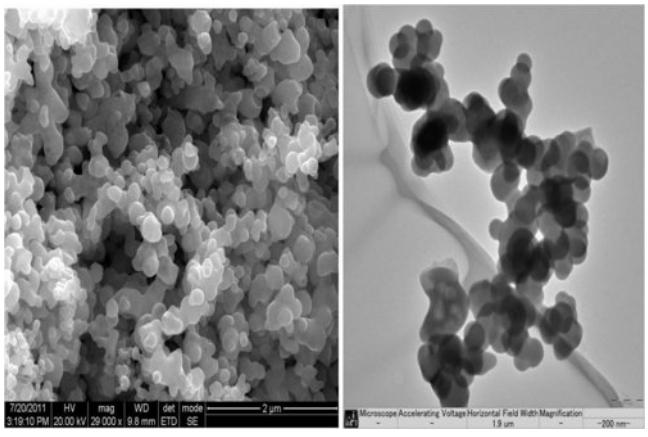

16:00 Poster We120

Synthesis and optical properties of the Eu^{2+} and Eu^{3+} doped GaN nanostructures

BongKyun Kang, Sung Ryul Mang, Dae Ho Yoon

Sungkyunkwan university (SKKU), 2066, seobu-ro, jangan-gu, Suwon 440-746, Korea, South

e-mail: kangbk84@skku.edu

In recent years, III-nitride nanostructures, such as nanoparticles, nanowires, and nanotubes, have attracted considerable attention, due to their unique electronic and optical properties. Gallium nitride (GaN) has a direct wide bandgap of 3.4 eV at room temperature and is a promising candidate material for short wavelength optoelectronic devices, such as light emitting diodes and laser diodes, as well as high power and high temperature operation devices. Forthermore, rare earth-doped GaN have a promising applications as multiple color electroluminescent (EL) devices due to the chemical stability and a large incorporation of rare earth dopants such as Eu, Er, Tb, Tm. In the case where Eu ions are doped into the host materials, distinctive optical properties are obtained, which commonly include a strong and sharp emission at around 612nm. It is caused by the f-f transitions of the Eu^{3+} ions. On the other hand, the Eu^{2+} ions show a broad blue emission at around 450nm. These two different emission effects depend on the environmental matrices surrounding the Eu ions, such as those in aluminates and silicate matrices. Compared with film and nanowires, GaN nanopowder could be alternative hybrid integration materials with a variety of optical properties because of the flexible powder form and controlled shape or size, as well as low fabrication cost.
In this work, Eu^{2+} and Eu^{3+} doped GaN nanostrucutures were synthesized successfully nitridation of Eu doped gallium oxide nanostrucutures by organic compound synthesis. In addition, the crystal structure, luminescence properties and particle size of the Eu^{2+} and Eu^{3+} doped GaN nanostrucutures were analyzed using powder X-ray diffraction (XRD), high resolution transition electron microscope (HT-TEM), photoluminescence spectrometry (PL) and energy dispersive X-ray analysis (EDX).

16:00 Poster We121

Red Fluorescence in LaF_3: Nd^{3+}, Sm^{3+} Nanocrystals Grown by Rapid Microwave Assisted Synthesis

Mahendra M. Khandpekar, Siddeshwar G. Gaurkhede

Birla College, Kalyan, Murbad Road, Kalyan, Mumbai 421304, India

e-mail: dr_mmk1968@yahoo.com

Lanthanum fluoride based nanoparticles have been of considerable interest owing to the luminescent properties exhibited by them. Elongated, hexagonal and assorted nanocrystals of LaF_3: Nd^{3+}, Sm^{3+} has been obtained by rapid microwave assisted synthesis in deionised water and methanol solvents. The crystals show luminescent and non linear optical behavior. The presence of elements has been verified by EDAX spectra. Comparative FTIR and FT Raman analysis has been carried out. Thermal (TGA /DTA) studies indicate continuous weight loss from 100°C to 900°C. The weight losses in range from 100°C – 300°C may be attributed to the loss of water molecules, NH_4Cl and NH_4F. The prominent peak in DTA spectrum at 300°C & 451°C in sample prepared in water & methanol respectively may be attributed to the temperature of formation and internal crystal structure adjustments. The thermal studies on LaF_3; Nd^3 , Sm^{3+} are found to be in close agreement with LaF3; Yb^{3+}, Er^{3+} reported by other authors. The

UV absorption edge was found to lie at 250 nm for samples synthesized in deionized water and methanol respectively corresponding to band gap energy of 4.9eV. A wide transparent window between 250 nm-800 nm has been observed. Emission of Red color (654 nm) has been recorded for LaF_3: Nd^{3+}, Sm^{3+} nanocrystals at an excitation wavelength of 357 nm. Relevant energy level scheme has been constructed. The I-V characteristics show current increases rapidly beyond 30 V/cm & 10 V/ cm with applied voltage for LaF_3; Nd^{3+}, Sm^{3+} nanocrystals in deionized water & methanol respectively indicating field dependent conductivity. The conductivity of the sample at room temperature is found to be of order 3×10^{-6} S cm^{-1}. The dielectric studies shows both dielectric constant and dielectric loss fall rapidly with applied frequency thereby exhibiting normal dielectric behavior. Graph of log dielectric loss vs. log frequency shows near linear nature and graph of tangent loss vs. log frequency shows presence of relaxation peak at about 2.9 KHz. The implications will be discussed.

16:00 Poster We122

Ni_2O_3-decorated In_2O_3 nanostructures for highly sensitive methane detection

Nguyen M. Vuong[1], Nguyen M. Hieu[1], Hwanpyo Lee[1], Dojin Kim[1], Hyojin Kim[1], Yong Shik Han[2], Myungbae Kim[2]

1. *Chungnam National University, Daejon 305764, Korea, South* **2.** *Korea Institute of Machinery and Materials (KIMM), Daejeon 305-600, Korea, South*

e-mail: dojin@cnu.ac.kr

Methane is a highly flammable gas that explodes in the air when reacting with other pollutants. The explosive limit of methane gas is 5%. However, detection of lower concentrations is necessary for prevention and warning purposes in a leaking system. We developed a simple method of fabricating thin films of granular indium oxide (In_2O_3) particles decorated with Ni_2O_3 nanoparticles for a high-response methane gas sensor. The In_2O_3 granular film was fabricated by sputter-deposition of indium followed by oxidation. Ni nanoparticles were deposited onto the In_2O_3 film by the arc-discharge deposition of single-wall carbon nanotubes followed by the burning out of these nanotubes. The catalyst Ni nanoparticles distributed in the single-wall carbon nanotubes were oxidized to Ni_2O_3. The sensors exhibited tens of % response per 100 ppm methane gas concentration.

16:00 Poster We123

Influence of microstructure of $Bi_{12}GeO_{20}$ doped with Ni and Co nanoparticles and $Tb_3Sc_2Al_3O_{12}$-$TbScO_3$ system grown by directional solidification on Faraday effect

Andrzej Kłos[1], Wojciech Gawlik[2], Mariusz Mrózek[2], Dorota A. Pawlak[1], Sebastian Turczynski[1]

1. *Institute of Electronic Materials Technology (ITME), Wólczyńska 133, Warszawa 01-919, Poland* **2.** *Jagiellonian University, Institute of Physics (IF UJ), Reymonta 4, Kraków 30-059, Poland*

e-mail: Andrzej.Klos@itme.edu.pl

It has been shown that additive effects such as the Faraday effect, the rotation of the polarization plane of linearly polarized light passing through a material placed in the longitudinal magnetic field, can be enhanced in periodic systems resembling photonic crystals [1, 2]. The Faraday effect was measured in $Bi_{12}GeO_{20}$ (BGO) single crystal doped with Ni and Co nanoparticles and in $Tb_3Sc_2Al_3O_{12}$-$TbScO_3$ (TSAG-TSP) eutectic. The measurements were performed in the visible region of the spectrum. The influence of microstructure of the above materials on rotation angle will be discussed.

Materials were obtained by micro-pulling down method utilizing the self-organization mechanism. In the TSAG-TSP eutectic the micro-rods of perovskite phase are packed pseudo-hexagonally in a garnet matrix [3] and the Faraday effect originate mainly from the terbium ions. The comparison of values of Verdet constant for different diameters of microrods and for light propagated perpendicularly and along the microrods will be presented. The value of the constant is much higher than those that have been reported for any garnet material. The influence of total concentration of Tb on the obtained results is discussed.

In BGO doped with Ni and Co the dependence of Verdet constant on concentration of nanoparticles up to 10 wt.% was investigated. The dependence of Faraday effect on sample orientation was also discussed. The angle of Faraday rotation is higher for BGO doped with Co than for material doped with Ni nanoparticles and increase with increasing of the nanoparticles concentration.

Acknowledgements

This work was partially supported by Polish National Science Centre under project MAESTRO.

[1] M. Inoue, A.V. Baryshev, *Magnetophotonic Crystals: The Way to Enhance the Faraday Rotation*, Encyclopedia of Materials: Science and Technology, **2008**, Pages 1–5.

[2] C. Koerdt, G. L. J. A. Rikken, E. P. Petrov, *Faraday effect of photonic crystals*, Appl. Phys. Lett., **2003**, 82, 1538.

[3] D. A. Pawlak, K. Kolodziejak, S. Turczynski, J. Kisielewski, K. Rożniatowski, R. Diduszko, M. Kaczkan, M. Malinowski, Chem. Mater.**2006**, 18(9), 2450-2457.

16:00 Poster We124

Formation of nanocrystals in $Bi_{0.9}Sb_{0.1}$ amorphous alloy

Gennadiy N. Kozhemyakin[1], Stanislav Y. Kovalev[1], Oleg N. Ivanov[2], Oksana N. Maradudina[2]

1. *Volodymyr Dahl East Ukrainian National University, Luhansk 91050, Ukraine* **2.** *Belgorod State University (BSU), Pobedy, Belgorod 308015, Russian Federation*

e-mail: genakozhemyakin@mail.ru

Bi_xSb_{1-x} alloys are the best *n*-type materials for thermoelectric and magneto-thermoelectric cooling at temperatures below 200 K [1]. It was shown that $Bi_{0.9}Sb_{0.1}$ reveals unique properties and is being investigated as a novel quantum material [2]. Nanostructured Bi_xSb_{1-x} materials draw attention because they have different properties due to quantum effects [3]. Many different methods can be employed to prepare nanomaterials. One promising method that provides control over nanocrystal formation is low-temperature annealing of amorphous metallic alloys [4,5]. Therefore, we used this method for preparation of nanostructured Bi_xSb_{1-x} alloys, which was not applied for these alloys earlier.

We used the spinning method for obtaining of amorphous Bi_xSb_{1-x} alloys. In this experiment, an alloy with composition $Bi_{0.9}Sb_{0.1}$ was prepared by melting and mixing components in a quartz crucible of a Czochralski apparatus at a temperature near 700 K for 2 h at 0.4 atm in high purity Ar. Bi of 99.9999% purity and Sb of 99.9999% purity were used as source materials. After crystallization, a $Bi_{0.9}Sb_{0.1}$ alloy polycrystal with weight 100 g was obtained in pieces smaller than 7 mm. These pieces were placed into a quartz ampoule with 8–20 mm inner diameter and 115 mm length, which had an external resistance

heater. High purity Ar at a gauge pressure of 0.1 atm was passed through the ampoule to prevent alloy oxidization. The melt temperature during spinning was controlled from 750 K to 920 K. After the alloy melted, and a steady state established, the melt was poured out onto a cold copper plate with 300 mm diameter, rotating at 1100 rpm. The amorphous alloy formed as a film with 20 μm thickness, 2–5 mm width, and 10–25 mm length. The alloy samples were annealed at temperatures above 80 °C for 1 h in a special cylindrical furnace with less than 1 K/cm temperature gradient in the axial and radial directions. A cross section of the films was prepared by breaking the samples in liquid nitrogen. The film microstructure was studied using a scanning electron microscope "Quanta 600 H".

The $Bi_{0.9}Sb_{0.1}$ films had many microcrystals with sizes 1–5 μm after spinning process with the melt temperature less than 800 K. Amorphous films were cooled from 920 K melt temperature by spinning. However, amorphous films had a few microcracks perpendicular to their surface under these conditions. The microcracks could appear at the moment of breaking in liquid nitrogen. Nanocrystals were detected in amorphous $Bi_{0.9}Sb_{0.1}$ films only after annealing at 150 °C. A small amount of individual nanocrystals with dimensions from 20 to 80 nm were sparsely located in a central part of the films. Vice versa, a large amount of nanocrystals with dimensions 40–100 nm formed densely at the film surface. From this study, we have shown the potential of using low temperature annealing of amorphous Bi_xSb_{1-x} alloys for formation of nanocrystals.

References

[1] G.N. Kozhemyakin, J. Crystal Growth, **257**, 237 (2003).

[2] D. Hsieh, D. Qian, L. Wray, Y. Xia, Y. S. Hor, R. J. Cava, M. Z. Hasan, Nature, **452**, 970 (2008).

[3] O. Rabin, Y.M. Lin, M.S. Dresselhaus, Appl. Phys. Lett. **79**, 81 (2001).

[4] K. Lu, J.T. Wang, W.D. Wei, Scrip. Metallurgica Mater., **25**, 619 (1991).

[5] T. Cheng, Nanostruct. Mater., **1**, 19 (1992).

16:00 Poster We125

Combustion synthesis of Si-related crystalline nanostructures

Michał Soszyński, Olga M. Łabędź, Andrzej Huczko

Warsaw University, Faculty of Chemistry, Pasteura 1, Warszawa 02-093, Poland

e-mail: olabedz@chem.uw.edu.pl

The unique technique of Self-Propagating High-Temperature Synthesis SHS [1] provides efficient, energy autogenic route to produce a variety of new materials, often nanostructured, nonstoichiometric or involving new phases, resulting from a fast reaction in a mixture of strong oxidant/strong reducer [2]. This is due to the specific process conditions - high temperature and pressure gradients, short reaction times and a very rapid "quenching" of gaseous reaction products. This presented efficient method includes here a production of at least gram quantities of silicon carbide nanowires (SiCNWs) (Fig. 1. A,B). Silicon carbide - due to its unique physical and chemical properties - is the primary representative of refractory ceramics with many practical applications [3,4]. The characteristics of this rapid process also make it possible to obtain other unusual materials such as silicon nanowires (Fig. 1. C,D).

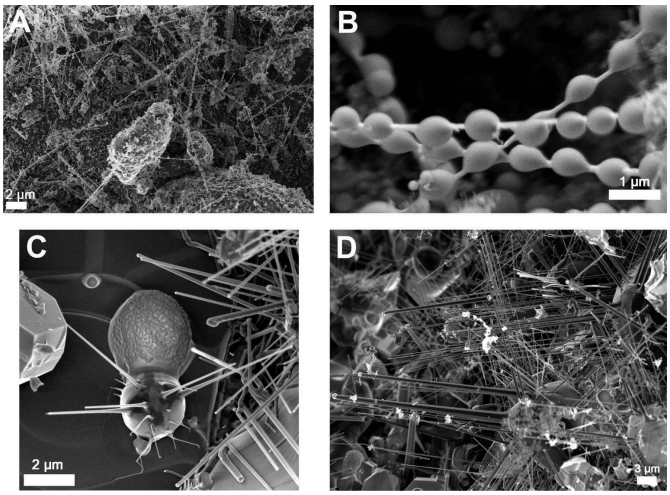

Fig. 1. SEM: SiCNWs morphology (A,B) and Si nanowires (C,D).

Efficiency of combustion synthesis depends on many parameters such as, for example: the atmosphere, the type, quantity and composition of the reactants and the initial pressure [2,5]. The authors present here the results of the parametric synthesis of SiCNWs and the preliminary studies on the preparation of silicon nanowires.

ACKNOWLEDGEMENTS: This research has been supported by the National Science Center founds awarded on the basic of decision No DEC-2011/03/N/ST5/04726 and 2011/03/B/ST5/03256 The SEM images were obtained using the equipment purchased within CePT Project No.: POIG.02.02.00-14-024/08-00.

REFERENCES:

[1] Huczko A., M. Szala, A. Dąbrowska, Synteza Spaleniowa Materiałów Nanostrukturalnych, Wydawnictwa Uniwersytetu Warszawskiego, Warszawa, 2011

[2] Soszyński M., Dąbrowska A., Bystrzejewski M., and Huczko A., Crystal Research and Technology 12, 1241 (2010).

[3] Seyller T., Appl. Phys. A 85, 2006, 371

[4] Lebedev A., Sbruyev C., Elektronika (ros.) 5, (2006), 28.

[5] Soszyński M., Dąbrowska A., and Huczko A., Phys. Status Solidi B 248, 11, 2708–2711 (2011).

16:00 Poster We126

Temperature driven 3D ordering of quantum dots in (InGa)As/GaAs superlattices grown under As_2 flux

Peter Lytvyn[1,2], Yuriy Mazur[1], Euclydes Marega Jr[1], Leonardo de Souza[1,3], Mourad Benamara[1], Morgan Ware[1], Igor Prokopenko[2], Gilmar Marques[3], Gregory J. Salamo[1]

1. *Institute for Nanoscience and Engineering, University of Arkansas,, 731 W. Dickson str., Fayetteville, AR 72701, United States* **2.** *V.Lashkaryov Institute of Semiconductor Physics NAS Ukraine (ISP), Nauky prosp., Kyiv 03028, Ukraine* **3.** *Departamento de Fisica, Universidade Federal de Sao Carlos, Sao Carlos, Sao Paulo 13-565-905, Brazil*

e-mail: plyt2007@gmail.com

Strain-driven self-assembly has matured into a promising method for the fabrication of semiconductor quantum dot (QD) nanostructures. The basic mechanism of QD nucleation and growth is well described by the classical Stranski-Krastanov growth model. However, more complex multi-component systems as well as strongly anisotropic structures are not completely described by the simplified basic model.

Elastic properties of the bulk crystal lattice and surface mass transport have a significant impact on the QD growth. So, in the case of multilayer structures of InGaAs QDs additional effects must be considered such as: the strain distribution through the spacer layers, In migration on the surface during the capping process, and possibly surface roughening throughout the deposition of the spacer layer. To control QD ordering the thickness and composition of corresponding layers are optimized as a rule. But, it is possible to achieve significant transformations in the three-dimensional ordering of the QDs by means of temperature control.

We systematically investigated the effect of deposition temperature of the QD layer on the three-dimensional ordering of InGaAs QDs within multilayer nanostructures grown using As_2 flux as the group V source. The threshold nature for 3D ordering was established using direct observation (TEM and AFM) for the 510-520 °C and 540-555°C growth temperature transitions. At these temperatures, there is a significant decrease in strain propagation through the system as the distances between QDs in one of the characteristics directions <011> exhibits a sharp increase. Changes of inter-dot distances are minimal at 530 and 540°C. There is an increase in the anisotropy of the strain in the system which leads to the appearance of some anticorrelation (slopes) in the alignment of the QDs through the superlattice growth and a more pronounced planar ordering along the preferred direction (fig.1). It is shown that this ordering is accompanied by transition of the almost continuous wetting layer (low temperature) into large QDs (high temperature) where no In detected between them (fig. 2). Critical changes in the overall period of the superlattice and the reduction of the spacer thickness over buried QDs are observed at the 555°C where an intense desorption of indium atoms becomes possible. The above changes in 3D QDs alignment correlated well with the assessment of quality of the structures through photoluminescence measurements.

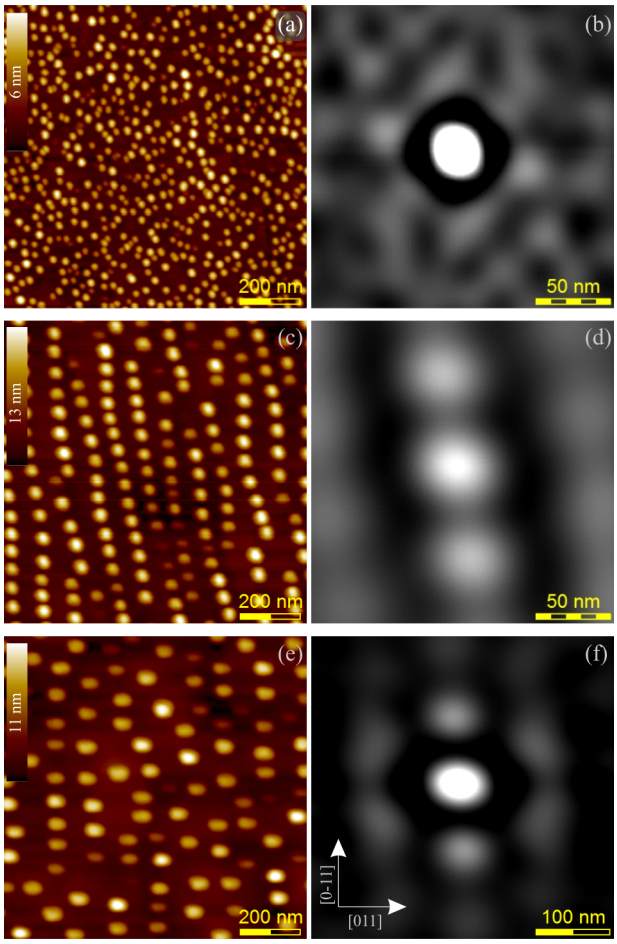

Fig.1. AFM height maps (left) and corresponding 2D autocorrelation functions (right) for the samples grown at 510, 530 and 555°C, (a,b), (c,d) and (e,f) correspondingly.

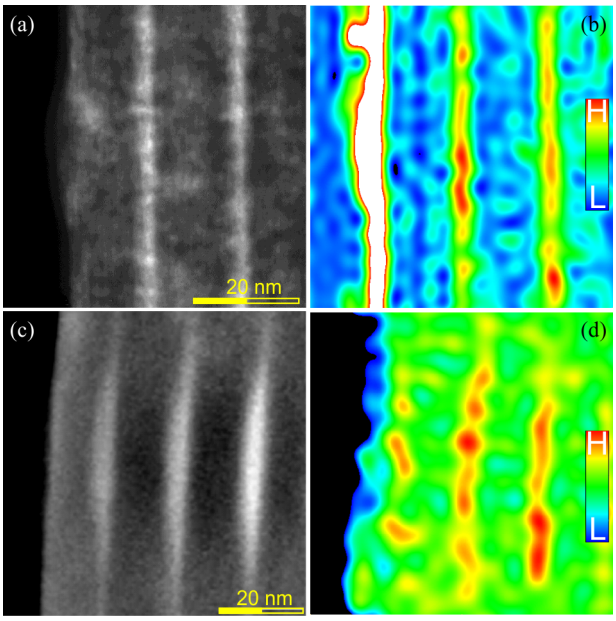

Fig.2. Bright field TEM images, taken under two-beam condition with (002) reflection and corresponding In distribution maps (electron energy loss spectroscopy) of the samples grown at 510°C (a,b) and 555°C (c,d).

These regularities can be explained by the competing processes of anisotropic mass transport on the growth surface and the influence of strain on the nucleation of 3D islands. Abrupt changes in the distances between QDs can be associated with changes in the surface atomic reconstruction which in turn affects the degree of anisotropy for the diffusion of adatoms. The indium surface segregation could play an important role in the behavior of the wetting layer. Less important are the effects of surface corrugation which caused fluctuations of superlattice period of ~0.5% in our case.

16:00 Poster We127

The phase state of polymer nanocomposite versus the surface modification of quantum dots

Oksana O. Matvienko, Yuriy N. Savin, Maxim F. Prodanov, Valerii V. Vashchenko, Oleg M. Vovk, Mariya V. Dobrotvorska

Institute for Single Crystals NAS of Ukraine (ISC), 60 Lenin Ave., Kharkov 61001, Ukraine

e-mail: tugai@isc.kharkov.ua

Polymer-quantum dots nanocomposites (PQDNCs) are a technologically important class of materials, with structural, biomedical, and optoelectronic applications. The properties of PQDNCs are sensitive to their microstructural features, which are difficult to control due to a complex interplay of entropic and enthalpic factors that determine dispersion of QD.

In this paper we examine the phase behavior of poly(9-vinylcarbazole) (PVK) – CdSe/ZnS QD thin films with 50 wt. % QD loading by ligand exchange.

PQDNCs (80-100 nm) are prepared by spin-coating method from the mixed toluene solution of QD and PVK. The morphology of PQDNCs has been investigated by using transmission electron microscopy and

X-ray photoelectron spectroscopy. The photoluminescence spectra were recorded on SDL–2 spectrophotometer. For investigation of the influence of the surface of QD on PQDNCs phase behavior the QD initial aliphatic ligand shell (trioctylphosphine oxide, (TOPO)) were exchanged by aromatic molecules: pyridine (PY), «cyanodendrone» (CD), «alkyldendrone» (AD).

Analysis of the 2-dimensional radial distribution function (RDF) and the potential of mean force (PMF) of the obtained composites PVK/QD/PY, PVK/QD/CD and PVK/QD/AD have revealed the three different phase states of QD spatial organization as a function of the polymer-QD interaction. The observation of the TEM images of PVK/QD/PY clearly demonstrates increasing agglomeration and lateral phase segregation of QDs in the film with increasing the fraction of surface sites capped by PY. Nanocomposite PVK /QD/AD as well as PVK/QD/TOPO tends to vertical phase segregation whereas PVK/QD/CD dispersion tends to uniformly QD distribution. The dispersion of QDs and their surface have a significant impact on the luminescence properties of PQDNCs.

16:00 Poster We128

Synthesis and characterization of new hollow calcium carbonate/polyanion microspheres

Marcela Mihai, Florica Doroftei, Bogdan C. Simionescu

Petru Poni Institute of Macromolecular Chemistry of the Romanian Academy, Aleea Grigore Ghica Voda 41A, Iasi, Romania

e-mail: marcelas@icmpp.ro

There is an intense interest in design simple strategy to synthesize hollow-structured spheres. Hollow calcium carbonate particles have attracted considerable attention owing to their excellent properties such as low density, high specific surface areas, and drugs, inks or pigments microencapsulation. Previous studies showed that the nucleation mechanism requires the presence of calcium-binding acidic groups on the polymer, thus providing the template upon which crystallization could occur. The formation of hollow shells of calcium carbonate, by the principle of controlled nucleation and growth on a polyanion substrate, is discussed in this paper. To initiate the nucleation mechanism, which required the presence of calcium-binding acidic groups, a strong/weak anionic copolymer, poly(2-acrylamido-2-methylpropanesulfonic acid–co-acrylic acid), was used. The influence of polyanion concentration (0.2 and 0.4 wt.%) on the $CaCO_3$ hollow microparticles growth from supersaturate aqueous solutions, at pH = 10.5 and after 8 h crystallization time, has been followed. The products were characterized by scanning electron microscopy, laser diffraction, X-ray powder diffraction, X-ray photoelectron spectroscopy, particle charge density, and zeta potential. In the presence of the copolymer, hollow-structured spherical particles, with medium sizes of 4 – 6 μm and containing just calcite polymorph, were obtained. The small increase of particles charge density, comparative with blank sample, showed that the polymer is located mainly inside the hollow particles and the calcite crystals on their surface.

Acknowledgment: *The research leading to these results has received funding from the European Union's Seventh Framework Programme (FP7/2007-2013) under grant agreement n°264115 - STREAM.*

16:00 Poster We129

Effect of reagents concentrations on the size of PbS nanocrystals prepared by chemical bath deposition

Takeshi Motomochi, Satoshi Oya, Takeshi Hirai, Toshitaka Nakada

Department of Physical Sciences, Ritsumeikan University, 1-1-1, Noji Higashi, Kusatsu, Shiga 525-8577, Japan

e-mail: rp0007rk@ed.ritsumei.ac.jp

In the last decade, there has been great interest in Lead Sulfide (PbS) quantum dots because of its potential application in multiple exciton generation solar cell. In order to fabricate the solar cell, it is necessary to synthesize PbS nanocrystals in the size less than 18 nm [1] on appropriate substrates. Chemical bath deposition (CBD) is one of the most popular solution-based processes for synthesis of PbS crystals on substrates. However, the typical size of CBD-synthesized PbS crystals is rather large, 0.1–1.0 μm in diameter [2]. Recently, Osherov et al. pointed out the possibility that the crystal size and shape could be controlled by varying the deposition conditions, such as reagents concentrations or temperature [3]. Nevertheless, to our knowledge, no successful synthesis of PbS quantum dots on substrates by CBD has been reported so far. In the present work, we have systematically studied the effect of reagents concentrations on the size of chemically deposited PbS crystals.

CBD experiments were performed on indium tin oxide coated glass substrates with basically the same method as described by Osherov et al. [3]. Atomic Force Microscopy showed that the dark brown films deposited on the substrates were composed of numerous polyhedral-shaped small particles. It was found that the particle size was strongly affected by $CS(NH_2)_2$ concentration: Increase of the concentration from 0.036 to 0.720 M lead to monotonous decrease of the particle size from 200 to 50 nm, while the density of the particles were increased. Moreover, X-ray diffraction spectra of the samples revealed that the deposited particles were face-centered-cubic rock-salt structured PbS, irrespective of concentration of $CS(NH_2)_2$. Taking into account the given equilibrium reagents concentrations, it is most likely that the change of the crystal size is due to the change of supersaturation in deposition solution. In this regard, we will also discuss the effect of NaOH and $Pb(CH_3COO)_2$ concentrations on the PbS crystal size in detail.

References

[1] A. K. Dutta, et al., Journal of Chemical Materials, 12 (2000) 1042.

[2] Z. Zhao, et al., Journal of Colloids and Surfaces A, 355 (2010) 114.

[3] A. Osherov, et al., Journal of Physical State Solid C 5, 11 (2008) 3431.

16:00 Poster We130

Growth and characterization of 3C-SiC nanowires on silicon substrates using different catalysts

Sathish Chander Dhanabalan[1], Marco Negri[1,2], Giovanni Attolini[1], Matteo Bosi[1], Francesca Rossi[1], Marco Campanini[1,2], Francesco Boschi[2], Paola Lagonegro[1], Pierpaolo Lupo[1], Giancarlo Salviati[1]

1. *IMEM- CNR (IMEM), Parma, Italy* **2.** *Dipartimento di Fisica, Università, Viale G.P. Usberti 7/a, Parma 43100, Italy*

e-mail: negri1@gmail.com

Nanowires (NWs) open promising near-future perspectives for the design and fabrication of nano-scale devices. The main interests are

in nanoelectronic devices (e.g. nano field-effect transistors), nano-electromechanical systems able to operate even in harsh environments, and nano-sensors exploiting the SiC NWs as biocompatible nanoprobes for biological systems.

Cubic silicon carbide (b-SiC or 3C-SiC) is a wide band-gap semiconductor with high hardness, high electron mobility, high thermal conductivity and high resistance to chemical attack. Those properties make them a promising material for devices operating in harsh environments.

Further, functionalized 3C-silicon carbide nanowires have the potential to act as highly sensitive detector elements in bio-chemical field.

Here we report on the properties of 3C-SiC nanowires prepared on (100) silicon substrate using three different metal catalysts: nickel, iron and gold and following different growth procedures.

A 2 nm thick Nickel film was deposited on Si(100) substrate using an e-beam system; iron and gold have been deposited as a thin layer (2 nm) using a sputtering system.

We used the more conventional nickel as reference catalyst, then Fe and Au to obtain better biocompatibility to use NWs in biological systems.

The nanowires have been grown in a home-made MOVPE reactor: the typical growth experiment involves two steps: thermal treatment for 2 min (dewetting) to obtain a pattern distribution of metals, and finally epi-growth in mixtures of SiH_4 , C_3H_8 for 5 minutes. The C/Si ratio used in each growth was 1.6.

The nickel-deposited substrate was preheated at 1100°C for 2 minutes; iron at 1250°C and gold at 600°C, before introducing reagents.

The growth temperatures were 1100°C, 1250°C when we used Ni and Fe respectively. When we used Au the temperature was increased from 600 °C to the growth temperature of 1100°C in presence of propane.

X-ray diffraction (XRD) has been used to identify the nanowires structure over large area. The morphology and crystal habit of the grown nanowires were further investigated by Scanning Electron Microscopy (SEM) while Transmission Electron Microscopy (TEM) imaging and SAD patterns were used to determine the nanowires structure at the nanoscale.

From morphological point of view the SiC nanowires appear similar with a dense network distributed on the substrate, but their diameter was smaller for those grown using Ni respect to those with iron. In samples where the gold has been used, only a few NWs were obtained with a presence of Si flakes.

For all samples the cubic structure has been confirmed with X-ray and TEM.

16:00 Poster We131

Numerical Computations of Metastable III-V Semiconductor Compounds' Surface Energy

Natalia I. Podolska[1,2,3], Maria A. Timofeeva[2], Nickolay V. Sibirev[2,4], Alexander I. Zhmakin[1,3], Maxim Nazarenko[2], Vladimir G. Dubrovskii[1,2]

1. *Ioffe Physico-Technical Institute, RAS, Saint-Petersburg, Russian Federation* **2.** *St Petersburg Academic University, Hlopina 8/3, Saint-Petersburg 194021, Russian Federation* **3.** *Saint-Petersburg Branch of the Joint Supercomputer Center, RAS (SPBSCC), 26 Politeknicheskaya str., Saint-Petersburg 194021, Russian Federation* **4.** *Saint-Petersburg State University, Saint-Petersburg, Russian Federation*

e-mail: natalya@scc.ioffe.ru

The zinc-blende lattice structure is the stable one of all bulk III-V semiconductor compounds except the group III-nitrides. However, nanowires (NW) of these materials grow having the metastable hexagonal lattice structure (wurzite, 4H polytype etc.) if their radius is smaller than the critical value [1]. The existence of the critical radius is commonly explained by the concurrence of the bulk and surface contributions to the NW formation energy [2]. To compute its value, the surface energy of the lateral NW facets in both stable and metastable phases should be known; note that this information is also relevant to the growth of quantum dots, nanoneedles, nanoislands. Experimental data on the surface energy in the metastable phases are absent.

The paper presents results of the computation of the surface energy of different facets of III-V compounds (GaAs, AlP, InSb and others) for both zinc blende and wurzite lattice. The results are compared to the known data for stable lattices on nitrides (wurzite), arsenides, antimonides and phosphides (sphalerite). The dependence of the surface energy on the NW size is obtained as functions of NW size and some other parameters of growth conditions. The effect of the catalyzer drop on the NW lattice structure is analyzed.

The paper presents results of the computation of the surface energy of different facets of III-V compounds (GaAs, AlP, InSb and others) for both zinc blende and wurzite lattice. The results are compared to the known data for stable lattices on nitrides (wurzite), arsenides, antimonides and phosphides (sphalerite). The dependence of the surface energy on the NW size is obtained as functions of NW size and some other parameters of growth conditions. The effect of the catalyzer drop on the NW lattice structure is analyzed.

Acknowledgements:

This study was supported by the Russian Foundation for Basic Research, the Presidium of the Russian Academy of Sciences, the Presidium of the St. Petersburg Scientific Center of the Russian Academy of Sciences, and the Federal Agency for Science and Innovation.

References:

[1] N.V.Sibirev, M.A.Timofeeva, A.D.Bol'shakov, M.V.Nazarenko, and V.G.Dubrovskii, Physics of the Solid State 52, 1531-1538 (2010).

[2] V.G. Dubrovskii, N.V. Sibirev, Phys.Rev.B 77, 035414 (2008).

16:00 Poster We132

Effect of transition metal(Fe, Mn) ion doping on TiO_2 nanoparticles

Dimple Shah, Kirit Siddhapara, Vipulkumar Kheraj

S.V. National Institute of Technology (SVNIT), Piplod,Ichchanath, Surat 395007, India

e-mail: dimpleshah73@yahoo.co.in

In this research, we have studied the doping behaviors of two transition metal ion dopants on the crystal phase, particle sizes, XRD patterns, EDAX spectra, and photoreactivity of TiO_2 nanoparticles. The crystallite size of TiO_2 particles is close to 4nm calculated from(10 1) peak by using FWHM method in Scherrer's equation. Test metal ion concentrations ranged from 1% to 4 at.%, we report the growth of Fe & Mn doped TiO_2 nanocrystals prepared by Sol-Gel technique, followed by freeze-drying treatment at -30°C temperature for 12hrs. The obtained Gel was thermally treated at different temperature like 200,400,600, 800°C. The Gouy balance study found samples to be paramagnetic at room temperature. The photoreactivities of transition metal ion-doped TiO_2 nanoparticles under UV irradiation were quantified by the degradation of formaldehyde.

16:00 Poster We133

Synthesis Bi_2S_3 Nanocrystals with Different Surfactant By Precipitation Method

Dimple Shah[1], Kirit Siddhapara[1], Mukesh Chavda[2], Hp Soni[2], Dhawani Chauhan[1]

1. *S.V. National Institute of Technology (SVNIT), Piplod,Ichchanath, Surat 395007, India* **2.** *The M.S.University of Baroda, Vadodara 390002, India*

e-mail: dimpleshah73@yahoo.co.in

Bismuth sulphide is a direct band gap material with Eg ~1.3eV Attracts high interest in thermo electronics investigation. Elegant Bi_2S_3 Nanostructure was grown by precipitation method using different surfactants. Nanocrystals were synthesized using Bismuth nitrate, Manganese acetate, Sodium Sulphide, with different Surfactant like Ammonium Bromide, Urea, and Sodium dodecyl sulfate. Nano flowers were obtained in the presence of Sodium dodecyl sulfate (SDS) while Nano rods have been observed in presence of Ammonium Bromide. we also report the growth of $[Fe]_xBi_2S_3$ (x=1,2 & 5%) nanocrystals prepared by same technique The structure was characterized by X-ray powder diffraction (XRD), Transmission electron microscopy (TEM), scanning electron microscopy (SEM), and Optical property studied by Ultra Violet Visible Spectroscopy (UV-Vis) absorption Spectra. It is expected that the present research may offer useful guidelines to the design and application of Bi_2S_3 Nanostructures. The determination of magnetic properties was also carried out by Gouy balance method.

16:00 Poster We134

Preparation of $La_2Ce_2O_7$ nanoparticles by co-precipitation method

Dimple Shah, Hozefa Tinwala, Jyoti Menghani, Ranjan Pati

S.V. National Institute of Technology (SVNIT), Piplod,Ichchanath, Surat 395007, India

e-mail: dimpleshah73@yahoo.co.in

Lanthanum cerium oxide ($La_2Ce_2O_7$) nanoparticles have been synthesized by co-precipitation method at low temperature (600ºC) using Lanthanum nitrate hexahydrate ($La(NO_3)_3.6H_2O$) and Cerium nitrate hexahydrate ($Ce(NO_3)_3$•6H2O) as source powder synthesis. Thermo gravimetric analysis (TGA), X-ray diffraction (XRD), Electron dispersive spectroscopy (EDS), Transmission electron microscopy (TEM) and Fourier transform infrared spectroscopy (FT-IR) were utilized to characterize the thermal, morphological, and chemical properties of the products. Thermo gravimetric analysis (TGA) of the material shows the removal of impurities at 600ºC, from X-ray diffraction (XRD) analysis the formation of cubic fluorite phase of lanthanum cerium oxide is observed, Electron dispersive spectroscopy (EDS) confirms the presence of both La and Ce. Particle size (55 to 80 nm) and cubic shape is observed from Transmission electron microscopy (TEM), and from Fourier transform infrared spectroscopy (FTIR) analysis the presence of residual water and nitrate is observed.

16:00 Poster We135

Synthesis of Silver Nanoparticles by using Peltophorum pterocarpum flower Extract

Balamurugan Matheswaran[1], Saravanan Shanmugam[1], Tetsuo Soga[2]

1. *Centre for Photonics and Nanotechnology, Sona College of Technology, Salem 636005, India* **2.** *Department of Frontier Materials, Nagoya Institute of Technology, Gokiso-cho, Showa-ku, Nagoya 466-8555, Japan*

e-mail: rasisaran@gmail.com

Ultrafine transition metal nanoscale materials have considerable attention due to their unique property. Silver nanoparticle (AgNP) is one of the more gorgeous because of its uses in various fields such as catalysis, sensors, photonics, solar cell and pharmaceuticals. Various physical, chemical and mechanical methods are available for synthesis of nanomaterials. However all the above methods are consuming more energy, toxic chemical and lengthy process. In the field of nanotechnology researcher are looking for natural systems to synthesize the nanomaterials in order to develop the environmental safe green process. The utilization of biological systems has the enormous benefits in the synthesis of nanomaterials. In this present study a facile methods is explored to prepare stable AgNPs by using *Peltophorum pterocarpum* (PP) flower extract as reducing and capping agent and aqueous silver nitrate as metal precursor. The use of plant extract for the synthesis of nanoparticles have advantages over microorganisms due to long process and cell cultural maintenance. AgNPs have been synthesized by adding different dosage of PP flower extract into the aqueous silver nitrate (0.001 M) solution. Instantaneously, the colour less solution was turned to brownindicating the formation of AgNPs. The synthesized nanoparticles are characterized by Ultra Violet – Visible spectrum (UV-Vis), High Resolution Transmission Electron Microscopy (HR-TEM), X-Ray diffraction and Fourier Transform Infra Red spectroscopy (FT-IR). HR-TEM image shows the nanostructures of prepared AgNPs. The UV-Vis spectrum shows an absorption peak around 420nm. The FWHM of the UV-Vis spectrum varies depend on the dosage of flower extracts. The XRD reveals that the prepared silver nanoparticles have crystalline nature.

16:00 Poster We136

Structural and Optical Properties of Fe-doped ZnO Nanoparticles Synthesized by Simple Solution Combusting Method

Silambarasan Murugesan[1], Saravanan Shanmugam[1], Tetsuo Soga[2]

1. *Centre for Photonics and Nanotechnology, Sona College of Technology, Salem 636005, India* **2.** *Department of Frontier Materials, Nagoya Institute of Technology, Gokiso-cho, Showa-ku, Nagoya 466-8555, Japan*

e-mail: rasisaran@gmail.com

Zinc Oxide (ZnO) is one of the most important II-VI group elements with wide band gap (3.37 eV) possessing size tunable optical transitions in solar cell, optoelectronics and wider range of application [1-2]. In this paper we report the structural and optical properties of Fe-doped ZnO Nanoparticles (NP) by solution combusting method. In a typical synthesis [2], 0.05M of zinc acetate dihydrate was dissolved in 100 mL of mixed solvent of ethanol and ethyleneglycol with a volume ratio of 60:40. Then, different mill mole of Ferrous Sulfate (0.5, 1, 2, 5 and 10 mmol) was introduced into the above solution under constant magnetic stirring. The solution was transferred into a spirit

lamp with an absorbent cotton lampwick and then the sprite lamp was fired. After the lampwick was extinguished, the samples were repeatedly dispersed into distilled water to wash and remove the impurity by ultrasonic process. Finally, the sample was dried at 150°C in hot air oven for 24 h. Powder X-Ray Diffraction (XRD), Field Emission-Scanning Electron Microscopy (FE-SEM), Raman and Photoluminescence (PL) spectrum were employed to characterize the structural, morphology and optical studies of pure and Fe-doped ZnO NP. The Rietveld refinement analysis of XRD data indicates that the particles are in the hexagonal wurtzite structure. The average particle size is around 80 nm which is confirmed by FE-SEM. Presence of some bigger particles might be attributed to aggregating or overlapping of smaller particles. Raman spectra of the Fe doped ZnO NP show remarkable effect on the polar as well as non-polar branches. The PL spectra indicates that blue shift of the UV-emission have occurred in Fe-doped sample due to Burstein-Moss effect.

References:

[1] J.J. Cole, X. Wang, R. J. Knuesel R J,H. O. Jacobs, Nano Lett. **8** (2008)1477.

[2] Y. Ni, X. Cao, G. Wu, G. Hu, Z. Yang, X. Wei, Nanotechnology **18** (2007)1556.

16:00 Poster We137

Synthesis and Characterization of Pure and Doped ZnO Nano-Crystals

Nidhi Sinha, Geeta Ray, Manoj K. Gupta, Binay Kumar

Department of Electronics, SGTB Khalsa College, University of Delhi, Delhi 110007, India

e-mail: nidhisinha5@yahoo.co.in

Zinc oxide (ZnO) is a highly sought after material in which electronic, semiconducting, optical, piezoelectric, etc properties can be integrated. It can be synthesized in different nano-configurations, apart from bulk crystals and thin films. It can be grown both in both n- and p-types nanostructures giving possibilities of electronic and optical applications. Additionally, ZnO is environmentally friendly and bio-compatible.

Pure and doped (rare earth, Cr, V, Li, etc) ZnO nanocrystals are grown by low cost chemical route and their structural, dielectric, optical, ferroelectric and piezoelectric properties are studied. They are mostly grown in the form of nanorods with diameter around 20 nm and length in the range of 50-300 nm. The effect of doping on size and structure are studies by microscopic and x-ray diffraction methods. In dielectric studies, room temperature dielectric constant has been found to change significantly as a result of doping. In all the cases, dielectric constant for nano crystals is higher than their bulk counterpart. While the pure ZnO showed no phase transition, ferroelectric to paraelectric phase transition is observed at different transition temperatures for different doping; the highest Tc was observed for V-doping at 345 ^{o}C. In optical studies, we report the results of UV-Vis, Raman, photoluminescence, band gap tuning studies as a result of above doping in which interesting improvement has been observed. The piezoelectric charge coefficient was found to be practically unaffected by doping and remained in the range of 1.5-2.0 pC/N. The change in ferroelectric properties viz shape of P-E loop, remnant and coercivity are significant. The results obtained in the case of rare earth doping have been compared with the results of other doping. In summary, it has been shown that various doping can be used to enhance the optical, ferroelectric or dielectric properties of ZnO.

16:00 Poster We138

Electronic structure of nanocrystals YF_3: RE

Aleksandra Skuta[1], Ewa Talik[2], Ludwika Lipińska[3], Monika Michalska[4]

1. *University of Silesia, Institute of Physics, Uniwersytecka 4, Katowice 40-007, Poland* **2.** *Institute of Physics, Silesian University, Uniwersytecka 4, Katowice 40007, Poland* **3.** *Institute of Electronic Materials Technology (ITME), Warszawa 01919, Poland* **4.** *Institute of Electronic Materials Technology (ITME), Wólczyńska, Warsaw 01-919, Poland*

e-mail: zaloga85@wp.pl

Up-conversion phosphors emit visible light after excitation by lower energy photons, usually in the near infrared spectral range. They have potential applications in different fields of science and technology, including luminescent displays, optoelectronic devices or lasers and amplifiers. Recently, a great interest has been devoted to their use in infrared (IR) and visible imaging for biological research and medical diagnosis, because of their important advantages when compared to the traditional biolabels such as organic dyes, semiconductors or metallic nanoparticles. For example, the up-conversion mechanisms are favourable compared to traditional down-conversion ones due to the higher penetration depth of light achieved in tissues under IR excitation wavelengths. Moreover, this excitation scheme also accounts for the lower photo-damage to living organisms, and the possibility of obtaining a higher spatial resolution and weak autofluorescence from cells or tissues. Additionally, it is possible to obtain nanophosphors with low toxicity, which is also one of the main points of interest in comparison with other bio-labels. Rare-earth (RE) based up-conversion nanophosphors are based on the combination of ion pairs acting as sensitizers–activators that allow a variety of excitation–emission choices.[1]

In the present work we have synthesized nanopowders using thermal decomposition method as follows. Firstly, the Y_2O_3 was dissolved in acetic acid, RE_2O_3in diluted nitric acid and NH_4F in deionized water. Next all solutions were mixed together and stirred for 6 h at 70 ºC. During slow evaporation of the mixture the volume was decreased 5 times. Then the concentrated solution was dried in 150C in order to total remove of water. Next the dry powder was calcined in air atmosphere in 400^{o}C during 2 h. Electronic structure and atomic concentration of samples were characterized by the following method X-ray photoelectron spectroscopy (XPS).

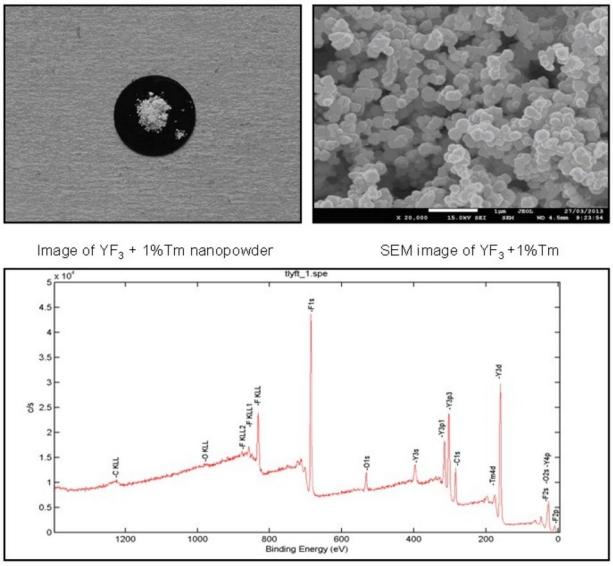

XPS spectrum of YF_3 + 1%Tm

References:

1. Marta Quintanilla, Nuria O. Nunez, Eugenio Cantelar, Manuel Ocana and Fernando Cusso, Tuning from blue to magenta the up-converted emissions of YF_3:Tm_3+/Yb_3+nanocrystals

16:00 Poster We139

Tuning of MBE growth of AlGaInAs-based microcavities with embedded QDots or QWells

Tomasz Slupinski, Piotr Stawicki, Barbara Pietka, Katarzyna Golasa, Jean-Guy Rousset, Wojciech Pacuski, Adam Babinski, Jacek Szczytko, Jerzy Łusakowski

Faculty of Physics, University of Warsaw, Hoża 69, Warszawa 00-681, Poland

e-mail: tomslu@fuw.edu.pl

Semiconductor microcavities with a high quality factor grown by MBE require high technological precision and knowledge of how optical constants of materials used change with temperature from a growth one to a measurement one (e.g. from ~900K to ~4K in case of AlGaAs). High quality microcavities enable studies of quantum cavity electrodynamics or are used in optoelectronics. By embedding quantum wells (QWells) or dots (QDots) in a microcavity the control of spontaneous emission is possible (Purcell effect) or a strong coupling of photons and excitons leading to a normal mode splitting (exciton polaritons) can be observed if the cavity quality factor is high enough. Optically active QDots emit light in a wider wavelength range than QWells, comparable to a shift of cavity mode's wevelength with temperature from growth one to low one, and so the optically active microcavity with QDots is easier to prepare epitaxially.

We present GaAs-AlAs-based microcavities growth by molecular beam epitaxy (MBE) with built-in InAs self-assembled QDots or InGaAs QWells. The Bragg mirrors are made of GaAs (high refractive index) and AlAs (low refractive index) λ/4 layers, the cavity is made of GaAs of λ width. We concentrated on a proper tuning of cavity mode's wavelength to the emission wavelength of QDots or QWells. We use modeling of optical properties of microcavities by the transfer matrix method taking into account a temperature dependence of refractive indexes of GaAs and AlAs materials reported in literature. We test growth procedures which take into account this temperature dependence of optical constants and try to minimize the limitations of MBE technology, like flow of molecular beams intensity over microcavity growth time. Properties of QWells embedded are modeled using NextNano software. Emission and reflectivity measurements from InAs QDots or InGaAs/GaAs QWells in GaAs-AlAs microcavities grown will be presented and discussed.

As an example we present in the Figure a high-resolution image of photoluminescence at low temperature T=4K, which illustrates dispersion of the cavity mode for light emitted by InAs QDots built-in in GaAs/AlAs microcavity. We observe that the emission from the cavity with QDots in wavevector space is composed of a number of discrete states laid along the dispersion curve. The number and shape of discrete states depend on a place in the sample probably indicating that the localized states are formed due to the imperfections of growth.

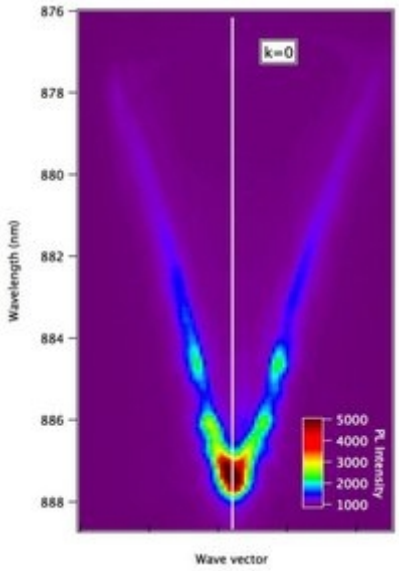

16:00 Poster We140

Synthesis and structural investigations of nanocrystalline multiferroic $YMnO_3$

Gokulraj Srinivasan[1], Rameshkumar Gubendiran[2]

1. *VelTech Dr.RR and Dr.SR Technical University (VELTECH), No.42 VelTech Avadi Road, Chennai 600062, India* **2.** *University College of Engineering Arni, Chennai 632317, India*

e-mail: gokulrajs@yahoo.com

The rare-earth manganites, $RMnO_3$, exhibit hexagonal and orthorhombic structure when 'R' the ionic radius is smaller (R = Ho, Er, Tm, Lu and Y) and for larger radius (R = La, Pr, Nd, Sm, Eu, Gd and Tb) respectively. $YMnO_3$ is one such compound that exhibits both ferroelectric and antiferromagnetic orders below 70 K. Ferroelectric ordering occurs only in the hexagonal phase, which belongs to the noncentrosymmetric *P*63*cm* space group, whereas an antiferromagnetic ordering occurs in both structural phases.

$YMnO_3$ powders were conventionally synthesized by solid-state reaction process by the use of Y_2O_3 and Mn_2O_3 as starting materials. The solid-state reaction process usually requires a calcination temperature above 1200 ^oC. The high calcination temperature inevitably leads to coarsening microstructures and, thus, the sinterability of the synthesized powders. As a result, extremely high sintering temperature is needed to obtain single phase $YMnO_3$.

In the present investigation, Yttrium nitrate, Yttrium acetate and yttrium chloride and their corresponding manganese counterpart were used to synthesis Yttrium Manganese oxide ($YMnO_3$) in a single step sol-gel synthesis by the use of citrate gel method. Phase analysis was investigated by powder X-ray diffraction analysis.For the powders calcined at 700 ^oC, $YMnO_3$ exhibits a well-defined hexagonal $YMnO_3$ phase. All the peaks can be identified with the single hexagonal$YMnO_3$ phase (JCPDS 25-1079). The lattice parameters of the nano powders was calculated from the XRD pattern and was found to be a = 6.135 Å, and c = 11.40Å which is in agreement with that of reported values. Spectral and thermal analyses were carried out to confirm its phase formation. Raman and PL was carried out investigate its spectral properties. Scanning electron microscope (SEM) and EXAX analysis was obtained to investigate it morphology and composition analysis.

16:00 Poster We141

Influence of 1D polymer network in TiO_2 nanoparticles/P3HT nanofibril blends

Ananthakumar Susaimanickam, Ramkumar Jeyagopal, Moorthy Babu Sridharan

Crystal Growth Centre, Anna University, Chennai, Chennai 600025, India

e-mail: ananthacgc@gmail.com

Titanium-di-oxide (TiO_2) nanoparticles were synthesized using non aqueous sol-gel route through oleic acid as the medium and capping agent. Pyridine was used to treat the prepared TiO_2 nanoparticles to remove the oleic acid from the surface. This surface treated nanoparticles were allowed to make the blend with Poly-3-hexyl thiophene (P3HT) nano fibrils in chloroform. P3HT nanofibrils were prepared by the solvent induced self assembly method with the addition of acetone. These blends were analysed using UV-Visible, PL , SEM and AFM analysis. The optical properties of the fibril P3HT with TiO_2 nanoparticles was compared with pristine P3HT/TiO_2 nanoparticles blend. Enhancement of absorption of P3HT was observed from UV-Visible analysis when acetone was added with chloroform. The emergence of new bands of P3HT after addition of acetone reveals the formation of fibril structure. Photoluminescence (PL) analysis of the pristine and fibril P3HT polymer with TiO_2 nanoparticles confirms the efficient charge separation through quenching of the luminescence. SEM and AFM analysis further confirms the formation of fibril structure of the polymer. The suitability of the blends for photovoltaic applications were analysed. The results are discussed in detail.

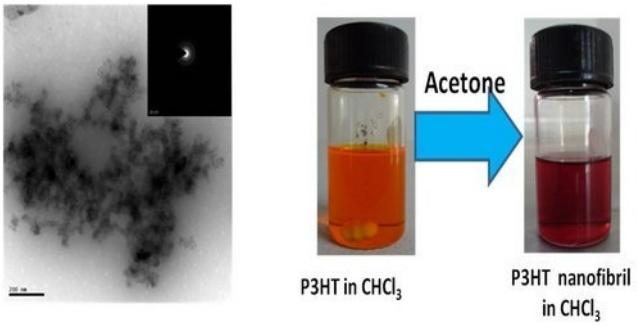

TEM and SAED pattern of TiO_2 nanoparticles

16:00 Poster We142

Effect of infiltrated CdSe nanoparticles / P3HT blends on TiO_2 nanotubes

Ananthakumar Susaimanickam, Ramkumar Jeyagopal, Moorthy Babu Sridharan

Crystal Growth Centre, Anna University, Chennai, Chennai 600025, India

e-mail: ananthacgc@gmail.com

Cadmium selenide nanoparticles were prepared in aqueous medium using sodium selenite as the selenium source. Thioglycolic acid was used as the ligand to stabilize the particles. The synthesized particles were surface modified by 1-dodecanethiol (1-DDT) to transfer the particles from aqueous to organic medium in the presence of acetone. The surface modified particles were finally blended with poly-3-hexyl-thiophene (P3HT) polymer in chloroform. The blends were infiltrated into the TiO_2 nanotubes through heating assisted method in dichlorobenzene. TiO_2 nanotubes were prepared by electrochemical anodization technique in the presence of a hydrogen fluoride (HF). The prepared particles and the CdSe/P3HT infiltrated nanotubes were analysed using UV-Visible, SEM,TEM, AFM and FT-IR. The increased absorption was observed through UV-Visible spectra for infiltrated TiO_2 nanotubes with CdSe/P3HT blends. TEM analysis shows that the prepared particles are spherical in nature. SEM images reveal the pore size of the TiO_2 nanotubes and the infiltration of P3HT polymer into the nanotubes. AFM images further confirm the morphological changes due to the P3HT after infiltration. FT-IR spectra show the corresponding bands of the polymer which ensures the incorporation into the tubes. The results are discussed in detail.

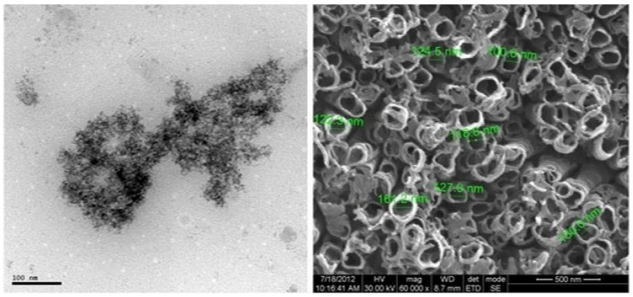

TEM image of CdSe-P3HT/TiO_2

SEM image of the infiltrated composites in TiO_2

16:00 Poster We143

Pure and zinc doped nano-hydroxyapatite : synthesis, characterization, antimicrobial and hemolytic studies

Kashmira P. Tank[1], Kiran S. Chudasama[2], Vrinda S. Thaker[2], Mihir J. Joshi[1]

1. *Saurashtra University, Department of Physics, Crystal Growth Laboratory, University Road, Rajkot 360005, India* **2.** *Saurashtra University, Department of Biosciences, University Road, Rajkot 360005, India*

e-mail: kashmira_physics@yahoo.co.in

Hydroxyapatite (HAP), $Ca_{10}(PO_4)_6(OH)_2$, has the ability to chemically interact with bone both *in vitro* and *in vivo*. For this reason it has been extensively studied as a possible bone substitute material. It also finds applications such as matrices for control drug release, bone cement,

toothpaste additives and dental implant. In the present study, pure zinc doped hydroxyapatite (Zn-HAP) nano- particles were synthesized and antibacterial activity was studied for their medical applications. Pure HAP and Zn-HAP nano-particles were synthesized by surfactant mediated approach. For the synthesis of pure HAP, aqueous solutions of calcium nitrate tetra-hydrate, nitric acid, potassium di-hydrogen phosphate and surfactant triton X – 100 were treated by ammonium hydroxide at appropriate temperature and pH. For the synthesis of Zn-HAP samples, different weight percentage of $Zn(NO_3)_2.6H_2O$ was added to the $Ca(NO_3)_2.4H_2O$ solution and the same procedure was followed as that for pure HAP nano-particles. The doping of zinc was estimated by EDAX. The average particle size was estimated by applying Scherrer's formula to the powder XRD patterns, which was found to be 16 nm to 33 nm. Doping of zinc with different percent changed the unit-cell parameters of HAP. The TEM images of pure and Zn-HAP nano-particles were also recorded. The pure HAP had needle type morphology and agglomeration increased with the increase of dopant concentration. The FT-IR spectra suggested the presence of O-H, O-P and C-O functional group. The antimicrobial activity was evaluated against four organisms *Pseudomonas aeruginosa* and *Shigella flexneri* as Gram negative as well as *Micrococcus luteus* and *Staphylococcous aureus* as Gram positive. The nano HAP and Zn-HAP possess the good antibacterial property. The ability of new apatite formation on the surface of pure and doped HAP samples was studied using Simulated Body Fluid (SBF) *in vitro*. Hemolytic study indicated that all samples were non-hemolytic defining potential application as bone implant material.

16:00 Poster We144

Examination of Modification of Mechanical and Electrical Characteristics of Chitosan – Lithium Films due to Chromium Nanoparticles for Solid State Batteries

Nivedhitha Venkatraman[1], Suraiya Begum[2], Saravanan Annamalai[2], Radha Perumal Ramasamy[2]

1. *Anna University, Department of Physics, Guindy campus, Chennai (AU), Chennai 600025, India* **2.** *Anna University, Department of Applied Science and Technology, ACT campus (ACT), Chennai 600 025, India*

e-mail: nivedhavenkat1990@gmail.com

Using Biopolymers for solid state batteries has gained great scientific interests in recent years. Biopolymers such as chitosan are abundantly available and are very environment friendly. Chitosan is a liner polysacchraide composed of deacetylated chitin units. Chitosan is well kown as an absorbing agent which forms chelate compounds with metal ions. Lithium ion batteries using biopolymers like chitosan can help the environment greatly. One important problem faced in making Chitosan-Lithium membranes is the change in the mechanical prperties of the films due to inclusion of Lithium. Incorporation of Lithium in Chitosan membranes during the formation of the membrane makes the films very flexible. It is therefore of importance to try to control the mechanical characteristics of the films. One method we are investigating in this research is by studying the mechanical characteristics of the films by incorporation of chromium into the membranes during its formation. Chromium compounds are of great practical importance. CrO_3 is a very good oxidizing agent. It is also useful in chrome plating. Cr(IV) can be chelated by chitosan via either the hydroxyl group or the protonated amine group by electrostatic attraction to chromium.

In our experiment 1 gm of chitosan was dispersed in 100 ml of water to which 1.5 ml of acetic acid was added. After mixing the sample, appropriate amounts of chromic acid was added to have a final chromium concentration of 20 mM. The solution was heated to 90ºC for 2 hr. It was observed that the solution changed its color from yellow to greyish green as the temperature increased. This is attributable to the formation of chromium nanoparticles. The solutions viscosity was also found to decrease. It was observed that the films were not formed and that lots of cracks developed in the film. It is therefore clear that the formation of chromium nanoparticles affects the mechanical properties of the films and it make it harder unlike Lithium which makes it softer. The effect of varying concentrations of chromic acid in chitosan films containing Lithium is presently being investigated. The characterization involving XRD, Raman, FTIR, AFM, SEM and impedance spectroscopy will be discussed.

16:00 Poster We145

Synthesis and characterization of 1-phenyl-3-(propan-2-yl)-1H-pyrazol-5-ol nano particles by using w/o microemulsion technique

Poorvesh M. Vyas[1], Jignesh D. Akbari[2], Satish D. Tala[2], Hitendra S. Joshi[2], Mihirkumar J. Joshi[3]

1. *Shri M and N Virani Science College, Physics Department, Kalawad Road, Rajkot 360005, India* **2.** *Saurashtra University, Department of Chemistry, University Road, Rajkot 360005, India* **3.** *Saurashtra University, Department of Physics, Crystal Growth Laboratory, University Road, Rajkot 360005, India*

e-mail: pm_crystal123@yahoo.co.in

The synthesis of pyrazoles is of great interest due to their wide applications in the pharmaceutical and agrochemical industry. Pyrazole derivatives are found to possess potent activities such as anti-inflammatory, anti-microbial, anti- HIV, anti-cancer, anti-allergic, anti-diabetic, cardiovascular and diuretic. The 1-phenyl-3-(propan-2-yl)-1H-pyrazol-5-ol was synthesized by using mixture of methyl-isobutylacetate and phenylhydrazine in methanol with the presence of a few drops of acetic acid as a catalyst. Light yellowish crystalline powder was obtained, which was further used to synthesize nano particles by water/oil micro-emulsion technique. In the present study, Triton X-100 was used as surfactant and n-heptane was used as oil phase. The single phase region was determined. The solution 1-phenyl-3-(propan-2-yl)-1H-pyrazol-5-ol in chloroform was added in a drop-wise manner under constant stirring to synthesize nano particles. The powder XRD study suggested triclinic structure with characteristic peak broadening indicating the nano structured nature having average particle size 33 nm obtained by using Scherrer's formula. The TEM study indicated nearly spherical nano-particles having diameter varied from 11 nm – 42 nm. The nanoparticles were also characterized by FT – IR spectroscopy and mass spectroscopy. From the FTIR study the functional groups C-H, C=C, =N-N- and –C=O were confirmed. The thermal stability of the nano particle was studied by using TG-DTA-DSC. The nano particles remained thermally stable up to 168^{o}C after that it started decomposing. Thermodynamic and kinetic parameters were calculated by using Coats-Redfern relation to the thermo-gram. Results are discussed.

16:00 Poster We146

Synthesis of ZnO Nano-whiskers with Varying Diameters from ε-$Zn(OH)_2$

Jing Wang, Chengxiang Liu, Lan Xiang

Tsinghua University, Tsinghua Garden, Beijing 100084, China

e-mail: wangjingflotu@gmail.com

As one of advanced functional materials, 1D ZnO with small diameter is a promising candidate for many applications as gas sensor, field emission, solar cell and photocatalyst, *etc.* since the electrical, optical and mechanical properties of 1D ZnO are closely related to its morphology and structure. The synthesis of 1D ZnO with small diameter via wet chemical routes was usually carried out in dilute solution, remaining the problem of poor efficiency. Recently, it was reported that **ε**-$Zn(OH)_2$ could be converted to 1D ZnO effectively under mild conditions, but it's still difficult to produce 1D ZnO with a diameter lower than 100 nm. In this work, a facile method was developed to synthesize ZnO nanowhiskers with a diameter of 20-80 nm and a length of 1-5 mm, using **ε**-$Zn(OH)_2$ as the precursor. It was found that the pre-ageing of **ε**-$Zn(OH)_2$ precursor in NaOH solution at 25 ^oC favored the formation of ZnO nano-whiskers with small diameter owing to the formation of minor amount of ZnO nucleus with a diameter of 10-30 nm on the **ε**-$Zn(OH)_2$ surface, which served as the seed for the subsequent growth of 1D ZnO at 80 ^oC. The enhanced photocatalytic activity was detected for the ZnO nano-whiskers with small diameters.

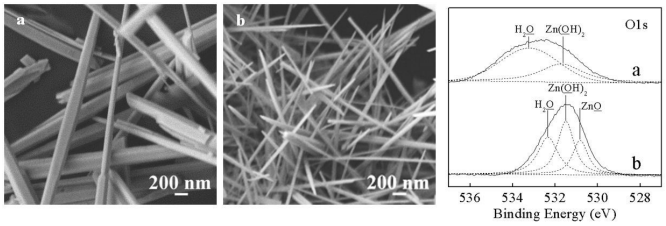

Figure 1 Morphology of ZnO whiskers and XPS spectra of **ε**-$Zn(OH)_2$

a: without pre-ageing, b: with pre-ageing

Project supported by the National Natural Science Foundation of China (No. 51174125 and 51234003).

Correspongding author: xianglan@mail.tsinghua.edu.cn

16:00 Poster We147

Nanosphere Lithography toward Corrugated Sapphire Nanocone Arrays for Antireflection Application

Chong Geng, Lu Zheng, Huajing Fang, Qingfeng Yan, Xiaoqing Wang, Dezhong Shen

Department of Chemistry, Tsinghua University, Beijing 100084, China

e-mail: yanqf@mail.tsinghua.edu.cn

Sapphire has found many device applications in optoelectronics and protective optics that require mechanical and temperature stability. However, the refraction index of sapphire (1.75-1.78 in the visible spectrum) is much larger than that of air, leading to strong reflection at the interface between sapphire and air. Such a drawback limits its application in devices that require high transmittance. Thin film coatings with intermediate or gradient refractive indexes are usually employed to suppress undesired reflection. However, the adhesiveness and thermal mismatch between the film and the sapphire may cause the stability problems. Surface-relief arrays with dimension smaller than the wavelength of incident light, also known as moth-eye structures, have been considered an alternative to the thin film coatings. Such kind of structures is more stable and durable than thin film coatings since only one material is involved. Furthermore, the moth-eye structure enables the reduction of optical reflection in the wider ranges of both spectrum and incident angles of light on condition that the periodic nanostructure is sufficiently smaller than the wavelength of antireflection spectrum. In the last years, various techniques for producing biomimetic moth-eye structures on sapphire have been reported, such as electron-beam lithography, laser interference lithography, and nanoimprint lithography. However, these techniques are restricted from practical application because of their expensive equipment and complicated procedures. Nanosphere lithography is a high-throughput and low-cost method to fabricate nanostructures with high uniformity over large areas, which can be used to pattern sapphire substrates. In this paper, corrugated sapphire nanocone arrays are fabricated on double-side polished sapphire substrates in order to increase the transmission over broadband spectra. The corrugated nanostructure is patterned by the combination of nanosphere lithography and inductively coupled plasma (ICP) dry etching. The etching process involves two steps, which utilizes two kinds of silica monolayer colloidal crystals in different sizes as masks, respectively. Firstly, the suspension consisting of silica colloidal spheres and 1-butanol was dropped on the water reservoir in a Petri dish. Then a monolayer of colloidal silica spheres was assembled on the air-water interface. Subsequently, the silica monolayer was transferred to a sapphire substrate and acted as a shadow mask for the first ICP etching. The residual silica spheres were removed after ICP etching by immersing in HF solution, resulting in a blunt cone array. A monolayer of smaller silica spheres were transferred to the surface of the resulting arrays of blunt cones. The corrugated sapphire nanocone arrays were obtained after the second ICP etching process using the smaller silica spheres as a mask. The optical reflection properties of the corrugated sapphire nanocone arrays are optimized by manipulating the size ratio of the two silica spheres and controlling the etching conditions. These surface-relief arrays are expected to improve the performance of optoelectronic devices such as light-emitting and photodetection devices due to their low reflection characteristics over a wide wavelength range.

16:00 Poster We148

Crystalline phosphors based on mono-sized $(R_{1-x}Eu_x)_2O_3$ (R=Lu, Y) nanopowders with the spherical morphology

Yuliya V. Yermolayeva, Oleksii S. Bezkrovnyi, Neonila A. Matveevskaya, Oleg M. Vovk, Alexander V. Tolmachev

Institute for Single Crystals NAS of Ukraine (ISC), 60 Lenin Ave., Kharkov 61001, Ukraine

e-mail: yu.yermolayeva@gmail.com

Within last several years, researchers have shifted the focus of their investigations toward the nanotechnology of new nano-objects based on rare-earth oxides ($(R1_{1-x}R2_x)_2O_3$, R1 = Y, Gd, Lu, R2 = Eu, Yb, Nd) from individual nanoparticles to bulk materials with ordered nanostructure. This new interest has emerged due to the prospective applications in photonics, lasers, energy and environmental technologies. To extend phosphor nanopowders to high resolution applications fine individual particles with ideal spherical morphology, controllable diameters, narrow size distribution as well as perfect crystalline structure and homogeneous composition can be highly desirable.

However, the principal drawback of the luminescent nano- and submicrospheres ($R1_{1-x}R2_x)_2O_3$ (D=70-400 nm) is lower luminescence efficiency comparatively with bulk materials due to the surface quenching processes through the decrease of the volume/surface ratio of the phosphor layer. That is why, it is necessary to establishment of the thermolysis parameters and crystallization processes of the spheres to minimize the activator activity diffusion, as well as select the optimal activator concentration to eliminate the of luminescence quenching. It was demonstrated in the present study for the model crystalline spheres phosphor $(R_{1-x}Eu_x)_2O_3$ (R=Lu, Y) ($^5D_0 \rightarrow {}^7F_2$ transition).

Polycrystalline, non-agglomerated nanopowders based on monosized $(R_{1-x}Eu_x)_2O_3$ nano- and submicrospheres were prepared by low-tem-

perature thermal decomposition of the amorphous precursor. The resulting structural, morphological and luminescence properties of obtained products were studied using the X-ray diffraction, X-ray photoelectron and FT-IR spectroscopy, SEM and HR-TEM microscopy methods. The mechanisms of the precursor decomposition, spheres crystallization and morphological evolution at the temperatures ranging from 60ºC to 1200ºC were studied. It was shown that the annealing temperature strongly influences on the structure, morphology and composition of the spherical $(R_{1-x}Eu_x)_2O_3$ phosphors obtained. The effects of annealing temperature as well as particles sizes and dopant Eu^{3+} concentration on the luminescence efficiency of $(R_{1-x}Eu_x)_2O_3$ phosphors were systematically investigated. It was shown that the concentration quenching effects of Eu^{3+} luminescence in the $(R_{1-x}Eu_x)_2O_3$ spheres with 100-250 nm diameter is shifted to lower Eu^{3+} concentrations (x = 0.05) compared with the microcrystalline powders with similar composition (x = 0.09). The reason of this phenomenon probably is formation of inhomogeneous phase of $(R_{1-x}Eu_x)_2O_3$ solid solution in the nanolayers with the primary location of bigger Eu^{3+} ions in the surface area due to active diffusion processes.

Detailed analytical data revealed that the luminescence intensity increased with the increase of crystallites size and particles size. The phosphor spheres developed in this work are attractive as building blocks for scintillation films for X-ray imaging and also for new types of photonic structures.

General Session 9

Surfaces and interfaces

Session Coordinators

Thomas Michely (Germany) *michely@ph2.uni-koeln.de*

Elias Vlieg (The Netherlands) *e.vlieg@science.ru.nl*

Programme

Wednesday, 14 August

WeP-G09
Wednesday afternoon, 14 August, 16:00
Room 207, Old Library

Break
Wednesday afternoon, 14 August, 17:30

Friday, 16 August

FrO1

G09: Surfaces and interfaces
Friday morning, 16 August, 8:30
Hall 16, Old Library

8:30 Invited oral

Growth and properties of epitaxial single and multi-layer silicene

Patrick Vogt[1], Andrea Resta[2], Thomas Bruhn[1,2], Paola De Padova[3], Guy Le Lay[2,3]

1. *Technische Universität Berlin, Institute for Solid State Physics, Hardenbergstr. 36, Berlin 10623, Germany* **2.** *Aix-Marseille University, CNRS-CINaM, Marseille 3288, France* **3.** *CNR-ISM, Roma 00016, Italy*

e-mail: patrick.vogt@tu-berlin.de

Since the discovery of graphene enormous efforts have been invested to search for other similar 2-dimensional materials, especially silicene, a 2D structure of Si atoms in a honeycomb-like arrangement. Silicene, a novel silicon allotrope, which does not exist in nature, was theoretically conjectured a few years ago [1] and was recently synthesized and experimentally investigated [2]. This new form of silicon has recently attracted considerable interest, because its topology confers to it the same remarkable electronic properties as those of graphene, with the potential advantage of being easily integrated in current Si-based nano/micro-electronics. Different technological applications have been suggested, such as gated silicene devices with a tunable electronic band gap [3] or spintronic applications [4].

We will discuss the epitaxial formation of single layer silicene on Ag substrates and its structural and electronic properties. Based on these results we will look at the growth of silicene multi-layers which can be explained by stacking of single silicene sheets. Different experimental techniques are used to investigate atomic structure and electronic properties of this layered system and to discuss its similarities to graphite. The formation of graphite-like silicon structures could open new possibilities for the technological application of this 2D material.

1. G. G. Guzmán-Verri, L. C. Lew Yan Voon, Phys. Rev. B 76, 075131 (2007); S. Lebègue and O. Eriksson, Phys. Rev. B, 79 115409 (2009); S. Cahangirov et al., Phys. Rev. Lett. 102, 236804 (2009).

2. P. Vogt et al., Phys. Rev. Lett. 108, 55501 (2012); C.-L. Lin et al., Appl. Phys. Exp. 5, 045802 (2012); A. Fleurence et al.,Phys. Rev. Lett. 108, 245501 (2012); L. Chen et al., Phys. Rev. Lett. 109, 56804 (2012); N. Zeyuan et al., Nano Lett. 12, 13 (2012); J. Gao, J. Zhao, Sci. Rep. 2, 1 (2012).

3. Z. Ni et al., Nano Lett. 12, 113 (2012).

4. Wei-Feng Tsai et al., Nat. Commun. 4, 1500 (2013)

9:00 Invited oral

Spontaneous formation of silicene on diboride thin films grown on Si wafers

Yukiko Yamada-Takamura

School of Material Science, Japan Advanced Institute of Science and Technology, Nomi, Japan

e-mail: yukikoyt@jaist.ac.jp

Silicene is an atom thick, honeycomb layer made from Si atoms, and thus the silicon counterpart of graphene. Epitaxial silicene forms spontaneously on single-crystalline zirconium diboride thin films grown on Si(111) wafers through surface segregation. The results of structural as well as electronic structure characterizations, which reveal the silicene nature of this surfactant layer, will be reported, and the possibility to synthesize two-dimensional materials in a similar way will be discussed.

9:30 Oral

Surface structure and diffusion of Si and C adatoms on bare SiC(0001) and SiC(0001) surfaces- density functional theory studies

Jakub Sołtys[1], Stanisław Krukowski[2], Jacek Piechota[3], Jolanta Borysiuk[4,5]

1. *University of Warsaw, Interdisciplinary Centre for Mathematical and Computational Modelling (ICM), Pawinskiego 5a, Warsaw 02-106, Poland* **2.** *Polish Academy of Sciences, Institute of High Pressure Physics (UNIPRESS), Sokolowska 29/37, Warszawa 01-142, Poland* **3.** *Interdisciplinary Centre for Mathematical and Compuerial Modelling, University of Warsaw (ICM), ul. Pawinskiego 5a, Warszawa 02-106, Poland* **4.** *Polish Academy of Sciences, Institute of Physics, al. Lotników 32/46, Warszawa 02-668, Poland* **5.** *Instytut Fizyki PAN, Al. Lotnikow 32/46, Warszawa 02668, Poland*

e-mail: qba@icm.edu.pl

Silicon carbide structures have extremely attractive properties for many applications in electronics. Thus detailed understanding of various stage growth process of SiC structures is of great importance. Density functional theory based ab initio calculations were used to obtain silicon and carbon adatoms energy landscape on both principal polar surfaces of silicon carbide: SiC(0001) and SiC(000$\bar{1}$). From these data the adsorption sites, the diffusion paths and energy barriers for the jumps between these minima were determined. The obtained data allowed to

describe energy characteristics for the motion of silicon and carbon adatoms on both Si- and C-terminated sides. The energy characteristics include the desorption energy of the adatoms from both surfaces. These data allows to obtain the diffusion length of these species in function of the temperature. In addition the DFT results shows the barrierless conversion of the topmost layer of C-terminated SiC(000) surface to sp^2-bonded configuration, that provides a nucleation center for creation of nanopipes, during growth of silicon carbide crystals by modified Lely method in carbon-rich environment. Thus molecular mechanism of nucleation of nanopipes is elucidated. The proposed mechanism also provides explanation of the early stages of growth of graphene layers on C-terminated surfaces of annealed SiC crystals. These hypothesis is supplemented by the transmission electron microscopy images of graphene layers on C-side SiC surfaces.

9:45 Oral

Monte Carlo simulations of 4H-SiC crystals sublimation from the stepped (0001) surface

Filip Krzyzewski[1], Magdalena A. Zaluska-Kotur[1,2]

1. *Polish Academy of Sciences, Institute of Physics, al. Lotników 32/46, Warszawa 02-668, Poland* **2.** *Cardinal Stefan Wyszynski University, Faculty of Mathematics and Natural Sciences, Dewajtis 5, Warszawa 01815, Poland*

e-mail: fkrzy@ifpan.edu.pl

We present the new kinetic Monte Carlo model of 4H-SiC crystals (0001) plane. The model consists of two species of atoms which form alternate layers of silicon and carbon building SiC double layers. Three different bonds are considered. The strongest one between silicon and carbon atoms binds nearest neighbors (NN) of a lattice, weaker one apears between two carbon atoms and the weakest one binds to Si atoms. C-C and Si-Si bonds connect next nearest neighbors (NNN) of a lattice. Every atom can form up to 4 NN bonds and 12 NNN bonds. Bonds of atoms forming consecutive double layers are rotated relative each other. Directions of those interactions are chosen in order to obtain ABAC stack of 4H politype. The model can be used to simulate growth and etchnig at both silicon and carbon faces of SiC. Moreover it can by easily transformed into simulations of other politypes formed by silicon carbide crystals.

Here we present results obtained during simulations of 4H silicon carbide sublimation at misoriented (0001) plane. Depending on the parameters of simulations we obtain step bunches, step trains, fourfold steps, waves and other surface structures observed during experiments. We show, that the type of structures at the surface affects the speed of etching. Despite higher desorption rates of silicon, evoporation at the surface with bunches is slower in comparison with waved surface and lower rate of individual Si adatoms desorption. We also show different surface structures obtained during simulations at diffrent etching conditions and present phase diagram of these structures.

10:00 Oral

Impact of surface phase transformation on the epitaxial growth of Si on Si(111)

Andreas Fissel[1], Jan Krügener[2], Jörg Osten[2]

1. *Leibniz University Hannover, Information Technology Laboratory (LFI), Schneiderberg 32, 30167 Hannover, Hannover D-30167, Germany* **2.** *Institute of Electronic Materials and Devices (MBE), Schneiderberg 32, 30167 Hannover, Hannover D-30167, Germany*

e-mail: fissel@mbe.uni-hannover.de

In Si technology, the continuous process of downscaling leads to problems related to atomic steps on the Si substrate surface. For example, thickness variation due to atomic steps is expected to have a significant impact on the properties of metal-oxide-semiconductor devices, where the oxide is only a few monolayers thick. Regrettably, step-free Si substrates are not available. Preparation of step-free surfaces demands a step-flow regime during growth, but unfortunately, Si adatoms migration length cannot reach typically substrate dimensions. This problem can only be overcome by preparation of step-free regions on substrates having smaller lateral dimensions. To realize step-free regions on a desired location on a substrate, patterned surfaces with trenches (mesas) are essential, which can be produced by standard Si processing steps. In this way, steps appearing on the surface are restricted to a small number within the patterned area and, moreover, step-free areas are well located at the surface allowing an exact positioning of the device on the step-free area. In this context, the pattering of the surface is also of advantage, since the edges of the mesa allow effective accumulation of steps during the growth leaving the rest of the region free of steps.

For epitaxial growth, two-dimensional terrace nucleation must be completely suppressed to achieve an atomically step-free surface. Among the epitaxial techniques, molecular beam epitaxy (MBE) is a sophisticated, finely controlled method for growing single-crystalline epitaxial layers in high vacuum. In Si-MBE, the growth temperatures are usually in the range of 700 K to 900 K, where the migration length of Si adatoms is only in the range of up to 100 nm. Therefore, temperature must be higher than those typically used in Si-MBE to realize step-free areas in the range of several micrometers suitable for device application. However, the Si surface exhibits surface phase transition at higher temperature, what could be of influence on the epitaxial growth. Therefore, it is desirable to have an understanding of morphology evolution of surfaces during Si-MBE also at higher temperatures.

In our work, we performed studies of Si-MBE on mesa-structured Si(111) at temperatures around the (7x7)-"1x1" surface phase transition (1030 K - 1120 K), which was controlled by reflection high-energy electron diffraction (RHEED). The surface morphology was investigated ex situ by atomic force microscopy. Significant changes in surface morphology were found for an only small increase in temperature near the surface phase transition., accompanied by a strong increase in step-free area dimension. This behaviour cannot be explained within a simple step-flow growth model. In particular, the simultaneous appearance of the two surface phases under certain conditions and their specific influence on the growth behaviour are discussed with regard to this matter. We presume that even at temperatures down to 1060 K the (7x7) and "1x1" surface phase coexist under dynamic condition of Si growth, whereas under near equilibrium condition the transition to the "1x1" surface phase is usually observed at temperatures around 1100 K. The appearance of both surface phases results in a strong variation of Si island size and shape. Furthermore, strong step-bunching was observed at temperatures around 1080 K. Stable step-flow without step-bunching was obtained for MBE at 1120 K, where only the "1x1" surface phase was visible in RHEED. Atomically flat step-free areas are formed over 10x10 μm^2 mesas under this conditions.

Coffee

Friday morning, 16 August, 10:30

FrO2

G09: Surfaces and interfaces
Friday morning, 16 August, 11:00
Hall 16, Old Library

11:00 Invited oral

Interface controlled crystalline organic layers

Christian Teichert

Montanuniversitaet Leoben, Franz Josef Str 18, Leoben 8700, Austria

e-mail: teichert@unileoben.ac.at

Crystalline films of conjugated organic semiconductors offer attractive potential for optoelectronic and electronic applications on flexible substrates. For device applications, the orientation of the molecules with respect to the substrate is crucial. In organic light-emitting diodes and solar cells, a lying orientation between the electrodes is desired whereas organic thin film transistors require in certain configurations that the molecules stand up between source and drain.

Using the small rod-like oligophenylene molecule parasexiphenyl (6P) as an example, it will be demonstrated how the substrate conditions help to tune the molecular orientation [1]. On clean mica(001), the self-organization of crystallites into one-dimensional chains is observed on a wetting layer in which the 6P molecules lie almost flat on the surface [2]. Also the crystallites are composed of lying molecules. On an ion bombarded, amorphous mica surface, the formation of terraced mounds composed of nearly upright standing molecules is observed by atomic-force microscopy(AFM). Quantitative analysis of the mound morphology together with transition state theory calculations reveals the existence of molecule bending during step edge crossing and level dependent Ehrlich Schwoebel barriers [3]. For the same system, the size of the critical nucleus has been determined from island size and capture zone distributions [4] and the subtle interplay of intra- and interlayer diffusion - resulting in elongated hexagonal second-layer islands - has been explored.

Finally, Low Energy Electron Microscopy (LEEM), micro Low Energy Electron Diffraction (μLEED), and AFM have been employed to study the initial growth of 6P on graphene which offers the potential to be used as a transparent flexible electrode. Due to the structural similarity between substrate and 6P one can expect that the molecules lie flat on the substrate. On Ir(111) supported graphene at 240 K, indeed layer-by-layer growth of lying molecules is observed as it is desired for OLEDs [5]. After formation of a low density layer, the full first monolayer already shows a bulk like structure. Up to at least four monolayers grow in this fashion. The nucleation of the 6P islands occurs at wrinkles in the metal supported graphene layer. Larger islands composed of flat-lying molecules detach from the original nucleation sites and move rapidly as entities across wrinkle free substrate areas [6]. In addition, μLEED reveals the surface unit cells in the different growth stages and at various substrate temperatures. At temperatures above room temperature, again crystalline needles appear on a molecular wetting layer [7] which is in agreement with AFM observations for 6P grown on exfoliated graphene transferred to silicon oxide [8].

This work has been supported by FWF project S9707-N20 and STW and FOM project 04PR2318. Contributions by G. Hlawacek, M. Kratzer, S. Klima, S. Lorbek, Q. Shen, P. Puschnig, D. Nabok, G. Biddau, C. Draxl (Leoben), P. Frank, T. Potocar, A. Winkler (Graz), F. S. Khokhar, R. van Gastel, B. Poelsema (Enschede), and B. Vasić, R. Gajić (Belgrade) are acknowledged.

[1]G. Hlawacek, C. Teichert, J. Phys.: Condens. Matter **25** (2013) 143202.

[2] C. Teichert, G. Hlawacek, A. Andreev, H. Sitter, P. Frank, A. Winkler, N.S. Sariciftci, Appl. Phys. **A 82** (2006) 665.

[3] G. Hlawacek, P. Puschnig, P. Frank, A. Winkler, C. Ambrosch-Draxl, C. Teichert, Science **321** (2008) 108.

[4] T. Potocar, S. Lorbek, D. Nabok, Q. Shen, L. Tumbek, G. Hlawacek, P. Puschnig, C. Ambrosch-Draxl, C. Teichert, A. Winkler, Phys. Rev. B 83 (2011) 075423.

[5] G. Hlawacek, F. S. Khokhar, R. van Gastel, B. Poelsema, C. Teichert, Nano Lett. **11** (2011) 333.

[6] G. Hlawacek, F. S. Khokar, R. van Gastel, C. Teichert, B. Poelsema, IBM J. Res. Devel. **55** (2011) 15:1.

[7] F. S. Khokhar, G. Hlawacek, R. van Gastel, H.J.W. Zandvliet, C. Teichert, B. Poelsema, Surf. Sci. **606** (2012) 47.

[8] M. Kratzer, S. Klima, B. Vasić, A. Matković, U. Ravelić, R. Gajić, C. Teichert, submitted to J. Vac. Sci. Technol.

11:30 Invited oral

In-situ observation of emergences of quasi-liquid layers from ice basal faces by advanced optical microscopy

Gen Sazaki, Harutoshi Asakawa, Ken Nagashima, Shunichi Nakatubo, Yoshinori Furukawa

Institute of Low Temperature Science, Hokkaido University (ILTS), N19-W8, Kita-ku, Sapporo 060-0819, Japan

e-mail: sazaki@lowtem.hokudai.ac.jp

Ice crystal surfaces melt at temperatures below 0°C, and then quasi-liquid layers (QLLs) are formed. However, revealing the dynamic behavior of QLLs, which dominates the surface properties of ice crystals at temperatures near the melting point, remains an experimental challenge. To observe ice crystal surfaces at the molecular level, we and Olympus Engeneering Co. Ltd. recently developed a laser confocal microscope combined with a differential interference contrast microscope (LCM-DM), which can directly visualize individual 0.37-nm-thick elementary steps on ice crystal surfaces [1, 2]. By utilizing LCM-DIM, we found the presence of two types of QLL phases that exhibit different morphologies and dynamics on ice basal faces [3]. In this study, we demonstrate the similarities and differences in the generation mechanisms of two types of QLL phases, as schematically shown in the figure [4].

We directly visualized the appearance of round liquid-like droplets (α-QLLs) and thin liquid-like layers (β-QLLs) on ice basal faces by LCM-DIM. We found that α-QLLs always appear at outcrops of dislocations, and that β-QLLs emerge from crystal surfaces where many microdefects are embedded. These results clearly demonstrate the similar function that strain induces the appearance of both types of QLLs. We also found that β-QLLs are spontaneously formed at interfaces between basal faces and α-QLLs when the diameter of the α-QLLs becomes larger than several tens of μm. This result arose from the different structures of α- and β-QLLs: the β-QLLs probably have a structure intermediate between those of basal faces and α-QLLs, resulting in a reduction of the total interfacial free energy. In the conference, we will also briefly demonstrate the thermodynamic stabilities of the α- and β-QLL phases.

References

1) G. Sazaki, et al., J. Crystal Growth, 262, 536-542 (2004).

2) G. Sazaki, et al. Proc. Nat. Acad. Sci. USA., 107, 19702-19707 (2010).

3) G. Sazaki, et al. Proc. Nat. Acad. Sci. USA., 109, 1052-1055 (2012).

4) G. Sazaki, et al. Crystal Growth & Design, 13, 1761-1766 (2013).

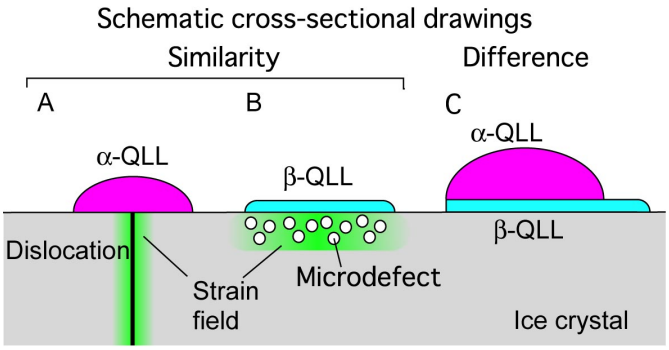

12:00 Oral

Gypsum crystal growth: from fast growth in the laboratory to ultraslow growth in Nature

Alexander E. Van Driessche[1], José Manuel Delgado López[1], Gen Sazaki[2], Hisao Satoh[4], Katsuo Tsukamoto[3], Juan Manuel Garcia-Ruiz[1]

1. *Instituto Andaluz de Ciencias de la Tierra, CSIC-UGR (LEC-IACT), Avda. Las Palmeras, nº 4, Granada 18100, Spain* **2.** *Institute of Low Temperature Science, Hokkaido University (ILTS), N19-W8, Kita-ku, Sapporo 060-0819, Japan* **3.** *Graduate school of Scienece, Sendai 980-8578, Japan* **4.** *Mitsubishir Materials Corporation Kitabukuro, Saitama 330-8508, Japan*

e-mail: sander@lec.csic.es

The importance of gypsum in both natural and industrial environments has motivated research on the fundamental aspects of gypsum crystallization over the last century. Even so, certain fundamental aspects, such as the growth mechanisms of the different crystal faces, the equilibrium and growth morphology, or the growth kinetics of gypsum at temperatures far above the gypsum-anhydrite transition curve of gypsum are poorly understood. Some of these unanswered questions are present in the giant selenite crystals in Mexico [1] Chile [2] and Spain [3,4] which put forth a challenging problem in the field of crystal growth in natural environments.

Laser confocal differential interference contrast microscopy, atomic force microscopy and white-beam phase-shift interferometry microscopy were used to observe in situ the step advancement and the evolution of the surface morphology of the (010) face of gypsum crystals growing from aqueous solutions prepared in the laboratory and natural solutions obtained from the Naica Mine.

When using supersaturated laboratory solutions we found that 2D nucleation is the main step generation mechanism, even at low supersaturations, and only indirect evidence of spiral hillocks was observed. Due to the elongated morphology of 2D islands along the *c*-axis and the frequent nucleation of multilayer 2D islands, the (010) develops a characteristic "hill and valley" topography. This type of surface topography is observed at all temperatures. The step kinetic coefficient, βst, was determined in the temperature range 20-80 ºC, and a steep increment in the kinetic coefficient is found with increasing temperature (step velocities as fast as 300 nm/s were measured at 80ºC, [5]). The second part of this work consisted in measuring the growth/dissolution rates of the (010) face of gypsum growing from current Naica waters at different temperatures (45-90ºC). The same "hill and valley" surface topography was observed and the slowest measurable growth rate was found at 55 °C, $1.4\pm0.2\times10^{-5}$ nm/s [6]. At higher temperatures, growth rates increase exponentially because of decreasing gypsum solubility and higher kinetic coefficient. At 50 °C neither growth nor dissolution was observed indicating that growth of giant crystals of gypsum occurred at Naica between 58 °C (gypsum/anhydrite transition temperature) and the current temperature of Naica waters, confirming formation temperatures determined from fluid inclusion studies [1,7].

Our results demonstrate the usefulness of applying advanced in situ optical techniques to gain a better understanding of crystal growth processes occurring at fast time scales (e.g. industry) but also at a geological time scale (e.g. giant gypsum deposits).

[1] Garcıa-Ruiz, J.; Villasuso, R.; Ayora, C.; Canals, A.; Otalora, F. *Geology* 2007, 35, 327–330.

[2] Cannell, J.; Cooke, R. D.; Walshe, J. L.; Stein, H. *Econ.Geol*. 2005, 979–1003.

[3] Garcıa-Guinea, J.; Morales, S.; Delgado, A.; Recio, C.; Calaforra, J. M. *Geol. Soc. J.* 2002, 159, 347–350.

[4] Bernardez Gomez, M. J.; Guisado di Monti, J. C. Pallas 2007, 75, 49–57.

[5] Van Driessche A.E.S., García-Ruiz J.M., Delgado-López J.M. Sazaki G.. *Crystal Growth Des.* 2010, 10, 3909-3916.

[6] A.E.S. Van Driessche, J.M. García-Ruiz, K. Tsukamoto, Patiño-López L.D., Satoh H. PNAS 2011, 108, 15721-15726.

[7] 5. Y. Krüger, J.M. García-Ruiz, A. Canals, D. Martí, M. Frenz Van Driessche A.E.S. Geology (2013)

12:15 Oral

Stabilities of Crystal Faces of Calcite Compared by AFM Observation of Facet Formation Processes during Dissolution in Dilute Aqueous Acetic Acid

Hitoshi Shindo[1], Yohei Ohtsu[1], Ryohei Yamamura[1], Tamon Kose[1], Kaori Niki[2]

1. *Chuo university, 1-13-27 Kasuga, Bunkyo-ku, Tokyo 112-8551, Japan* **2.** *Chiba University, 1-33 Yayoi-cho, Inage-ku, Chiba 263-8522, Japan*

e-mail: shindo@kc.chuo-u.ac.jp

Calcite($CaCO_3$) crystals are obtained in various forms in nature depending upon their origins[1]. The mineral, accordingly, is a good target in studying relationship between crystal morphology and the growth conditions. A series of crystal faces around the a_1-axis are shown in Figure 1. Depending on the inclination from the basal plane, electrically neutral *e*-, *m*- and *r*-faces, polar *c*- and *f*-faces, and other less polar faces are recognized. Many of them appear in natural crystal forms. Electrical polarity greatly affects stabilities of the crystal faces in polar solvents like water.

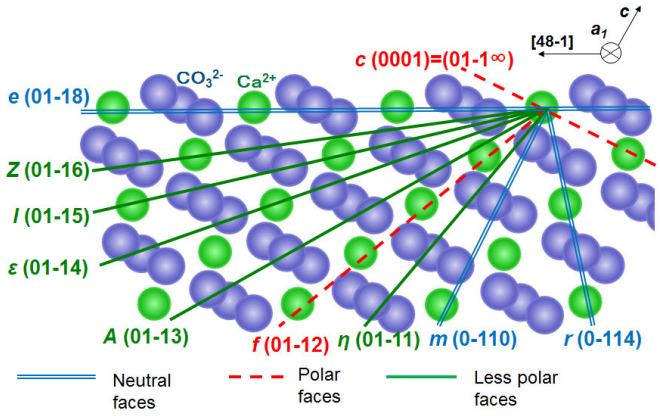

Figure 1. Structure of calcite crystal viewed along the a_1-axis. Hexagonal unit cell with the lattice constants of a =499.0 and c =1706.1 pm was chosen.

To study the relationship between crystal morphology and the growth conditions, we need to evaluate thermodynamic stabilities of various faces of crystals. We can experimentally compare relative stabilities of crystal faces, by observing, with atomic force microscopy(AFM), the formation processes of polyhedral micro-etch pits at various starting faces. Since diffusion is limited within tiny etch pits, especially for less soluble crystals, near equilibrium is obtained. By starting with a less stable crystal face, we can observe development of sidewalls formed by more stable facets. If we start with locally the most stable surface, atom-flat terraces are often obtained. The method was previously employed in studying crystal morphologies of aragonite-type carbonates[2-4], anhydrite($CaSO_4$)[5], and NaCl[6].

Calcite crystal faces in desired orientations were prepared by cutting natural calcite crystals buried in resin with Leica SP1600 microtome having a doughnut-shaped diamond saw. Fine-polished crystal plates in *m*(10-10) orientation were purchased from Furu-Uchi Chemicals. All the crystal faces shown in Figure 1 were prepared.

The crystal plates were soaked in dilute aqueous acetic acid or water in a flow-cell for AFM. When required, ethanol was added to the solvent to decrease polarity. The dissolution processes were observed with NanoScope III AFM of Digital Instruments in contact mode. Directions of ledges formed and dihedral angles between the sidewalls and the starting surface tell us the Miller indices of the facets stabilized in the solution.

Figure 2(a) shows an AFM image observed when η(01-11) face was dissolved in 1 mM aqueous acetic acid for 3 hours. Development of flat terraces shows us that the starting face is fairly stable. As shown in the sketch in (b), electrically neutral and stable *r*-faces form two sidewalls on the right-hand side. On the left-hand side, neutral *a*-facets give macro-steps and sidewalls. On the other hand, neutral but rugged *m*(01-10) face and polar *f*(01-12) facets do not appear in (a). We can tell that η-, *r*- and *a*-facets are more stable than *m*- and *f*-facets. By changing the starting faces, relative stabilities of calcite faces in aqueous acetic acid were determined as $r > e > \eta, \varepsilon, a > m > c, f$. Polar *c*- and *f*-faces are not stable in the solution.

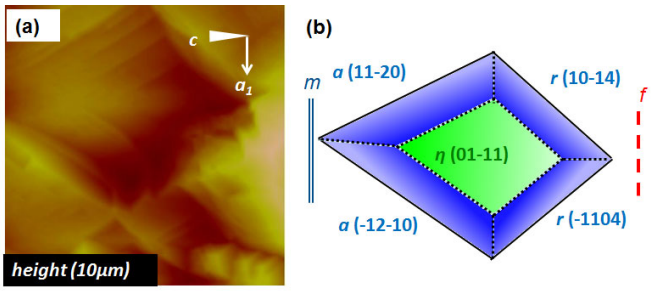

Figure 2. (a):AFM image observed during dissolution of η(01-11) face of calcite in 1mM aqueous acetic acid and (b): a sketch of an etch pit formed. More stable η-, *r*- and *a*-facets make the terraces and sidewalls, while less stable *m*- and *f*-facets do not appear in (a).

When ethanol was added to the aqueous acetic acid, however, polar *c*- and *f*-facets become much more stable. Adsorption of surface active ethanol molecules most probably stabilizes the polar faces. The polar faces often appear in natural crystal forms. The changes in the relative stabilities of crystal faces give us clues to the relationship between crystal forms and growth conditions.

Acknowlegement

This work was supported by JSPS KAKENHI 24510144, 20510097, 20225002, and The Institute of Science and Engineering, Chuo University.

References

[1] E. S. Dana, The System of Mineralogy –Descriptive Mineralogy, Wiley, New York, 6th ed. 1900, p.262.

[2] M. Kwak and H. Shindo, *J. Cryst. Growth,* **275** (2005) e1655-1659.

[3] H. Shindo and M. Kwak, *Phys. Chem. Chem. Phys.*, **7** (2005) 691-696.

[4] Y. Shirota, K. Niki and H. Shindo, *J. Cryst. Growth,* **324** (2011) 190-195.

[5] H. Shindo, T. Igarashi, W. Karino, A. Seo, M. Yamanobe-Hada and M. Haga, *J. Cryst. Growth*, **312** (2010) 573-579.

[6] W. Karino, H. Koda, K. Nakamura and H. Shindo, *J. Cryst. Growth,* **310** (2008) 676-681.

12:30 Oral

Submerged atomic resolution imaging of hydration structure on calcite

Yuki Araki[1], Katsuo Tsukamoto[1], Ryosuke Takagi[2], Tomoyuki Miyashita[2], Noriaki Oyabu[3], Kei Kobayashi[4], Hirofumi Yamada[3]

1. *Graduate school of Scienece, Tohoku University, Sendai 980-8578, Japan* **2.** *Department of Genetic Engineering, Kinki University, Wakayama 649-6493, Japan* **3.** *Department of Electric Science and Engineering, Kyoto University, Kyoto 615-8530, Japan* **4.** *Office of Society-Academia Collaboration for Innovation, Kyoto University, Kyoto 615-8530, Japan*

e-mail: y-araki@s.tohoku.ac.jp

Dehydration is an important growth rate-determing process in solution growth (Bennema, 1967). Recently, it has been suggested that hydration was eased by hydrophilic organic material from the result that the step velocity of calcite was increased by the addition of hydrophilic peptide (Elhadj et al., 2006). However, the influence of organic material on hydration has not been revealed. In order to verify the influence of the organic material on the hydration of the crystal surface visually, we

tried in situ observation of hydration structure on calcite surface in atomic level in supersaturated solution of calcium carbonate containing organic material.

The observation was conducted by a recently developed Frequency Modulation AFM (FM-AFM) working in liquids (Fukuma et al., 2005). Hydration imaging was realized by force mapping mathod (Kimura et al., 2010). The prove is scanned one-dimensionally in the vertical direction to the crystal surface. Hydration is detected by the slight frequency shift due to the interaction force between the tip and water molecule. By repeating 1D scanning with the change of the tip location to the next line, the 2D force map would be described.

The supersaturated solution of CaCO3 was prepared to be supersaturated for both calcite and aragonite at pH 8.1 and room temperature. A cleaved calcite crystal was glued to the bottom of an open fluid cell, and the solution was put on the surface. The synthetic polypeptide was adopted as organic material in our experiment. The synthetic polypeptide consists of fifteen amino acid residues including six aspartic acids periodically (Takagi and Miyashita, 2010). This polypeptide is considered as important material to control the polymorph of calcium carbonate in the field of biomineralization.

We obtained atomically image of lacy network of hydration on calcite (104) face. Water molecules formed four layers to be piled up alternately in the vertical direction of calcite surface. Water molecules were above gaps between calcium ions on calcite surface in the first and third layer. In the case of the second and fourth layer, water molecules were located above calcium ions. Furthermore, 3D hydration structure was constructed by multiple 2D hydration images which were taken at interval of 0.15 nm to the one direction. The hydration structure on each layer was described after construction of 3D image. As a result, it was confirmed that water molecules keep stable structure corresponding to the calcite surface structure until the height 0.5 nm above calcite surface.

Our result shows that the hydration can be visualized in the level that we can compare the structure in atomic resolution. It is strongly expected that the influence of organic material on hydration structure would be revealed.

12:45 Oral

Effects of TMSb overpressure on InSb surface morphologies during a thermal cleaning process by metal organic chemical vapor deposition

Sehun Park[1,2], Jinwook Jung[1,2], Sung Hyun Park[1], Chulkyun Seok[1], Keun Wook Shin[1], Yasushi Nanishi[2,3], Euijoon Yoon[1,2,4]

1. *Seoul National University (SNU), School of Mat. Sci. Eng., Seoul 151742, Korea, South* **2.** *WCU Hybrid Program, Department of Materials Science and Engineering, Seoul National University (SNU), Seoul 151744, Korea, South* **3.** *Department of Photonics, Ritsumeikan University, Kusatsu 525-8577, Japan* **4.** *Advanced Institutes of Covergence Technology (AICT), Suwon 443270, Korea, South*

e-mail: huf2002e@snu.ac.kr

In preparation for a high quality epitaxial layer of InSb by metal organic chemical vapor deposition (MOCVD), a substrate cleaning step such as *in-situ* thermal cleaning (TC), prior to the epitaxial growth, is an important process. This is a crucial step for preparing chemically clean, atomically flat and oxide-free surfaces. In contrary to the TC of III-V arsenic and phosphorus based compound semiconductors such as GaAs and InP etc, TC under Sb overpressure causes a controversial problem due to the low equilibrium vapor pressure of Sb during the growth of Sb-based compound semiconductors [1]. Precise control of Sb vapor pressure during TC process is very important in order not to form either Sb hillocks or rough surfaces [1].

In this study, InSb substrates were thermally cleaned in either H_2 or TMSb ambient to understand how the surface of InSb was affected by TC ambient. From the scanning electron microscope image as shown in Fig. 1-(a), we observed In droplets on the InSb surfaces when thermally treated at 515 ^{o}C in H_2 ambient. In droplets were generally formed by In oxides decomposition as well as InSb decomposition. The large In droplets with a diameter of about 2.5 μm were found within the rectangular etch pits on the surfaces. It was bounded with <111> sides. The facets in the etch pits were originated from the relative reactivity differences of various crystallographic planes of InSb [2]. Atomic force microscope was used to analyze surface morphology of InSb substrates thermally cleaned at 515 ^{o}C under TMSb overpressure. At a TMSb flow rate of 18.1 μmol/min, multi-layered mounds were formed on the InSb substrates as shown in Fig. 1-(b). This was caused by initial substrate morphologies, low Sb lateral diffusion length and Schwoebel potential barrier at the step edges [3, 4]. With increased TMSb flow rate of 126.7 μmol/min, the multi-layered mounds were evolved to a step-flow surface through the coalescence of mounds, as represented in Fig. 1-(c). The same surface evolution was also observed as TC time increases. The variation of TC temperature from 475 to 515 ^{o}C did not, however, affect the surface evolution of InSb substrate. The detailed experiment results and discussions about the effects of TMSb overpressure on InSb surfaces morphologies will be addressed.

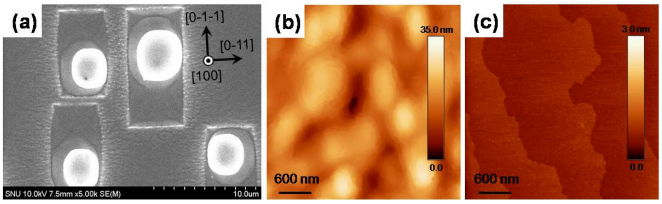

Fig. 1 InSb surface thermally treated under difference ambient conditions during thermal cleaning process: (a) H_2 ambient, (b) TMSb ambient at a flow rate of 18.1 μmol/min, and (c) TMSb ambient at a flow rate of 126. 7 μmol/min.

Reference

[1] R. M. Biefeld., Mat. Sci. Eng., **R 36**, 105 (2002)

[2] M. C. Lavine, A. J. Rosenberg and H. C. Gatos., J. Appl. Phys., **29**, 1131 (1958)

[3] R. L. Schwoebel., J. Appl. Phys., **40**, 614 (1969): R. L. Schwoebel and E. J. Shipsey., J. Appl. Phys., **37**, 3682 (1966)

Closing ceremony
Friday afternoon, 16 August, 13:00

Posters

Wednesday, 14 August

WeP-G09
Wednesday afternoon, 14 August, 16:00
Room 207, Old Library

16:00 Poster We150

Smoothing of a macro-step induced by discontinuous surface tension

Noriko Akutsu

Osaka Electro-Communication University, Hatsu-cho, Neyagawa, Osaka 572-8530, Japan

e-mail: nori3@phys.osakac.ac.jp

Discontinuous surface tension[1] (Fig. 1) of a restricted solid-on-solid (RSOS) model with point contact type step-step attraction (p-RSOS model)[1-3] is calculated numerically by using the product wave-function renormalization group (PWFRG) method[4]. The discontinuous surface tension induces a merging of steps at low temperatures near the equilibrium. The side surface of the merged step becomes smooth contrary to the capillary wave instability. As a result, the speed of motion of the merged step becomes slower than the dissolved steps.

The microscopic energy Hamiltonian of the p-RSOS model is as follows:

$$\begin{aligned}\mathcal{H}_{\mathrm{p-RSOS}} = \sum_{i,j} \epsilon[&|h(i+1,j)-h(i,j)| \\ &+|h(i,j+1)-h(i,j)|] \\ &+\sum_{i,j}\epsilon_{\mathrm{int}}[\delta(|h(i+1,j+1)-h(i,j)|,2) \\ &+\delta(|h(i+1,j-1)-h(i,j)|,2)], \qquad (1)\end{aligned}$$

where $h(i,j)$ represents the surface height at the site (i,j) on a square lattice, ε represents a microscopic step energy, $\varepsilon_{\mathrm{int}}$ ($\varepsilon_{\mathrm{int}}<0$) represents a microscopic step-step attractive energy, and $\delta(a,b)$ represents Kronecker delta.

Due to the sticky character of steps in the p-RSOS model, the surface free energy per projected area of the vicinal surface (Fig. 1) does not have the form of the 'one-dimensional free fermion universal type' or the 'Gruber- Mullins- Pokrovsky- Talapov (GMPT) universal type' but has a discontinuous one.

References

[1] N. Akutsu, Phys. Rev. E **86**, (2012) 061604. PRE Kaleidoscope Images: December 2012.

[2] N. Akutsu, J. Phys.: Condens. Matter **23** (2011) 485004.

[3] N. Akutsu, Appl. Surf. Sci. **256** (2009) 1205; J. Cryst. Growth, **318** (2011) 10.

[4] T. Nishino and K. Okunishi, J. Phys. Soc. Jpn. **64** (1995) 4084. Y. Hieida, K. Okunishi and Y. Akutsu, Phys. Lett. A **233** (1997) 464; New J. of Phys. **1** (1999) 7.

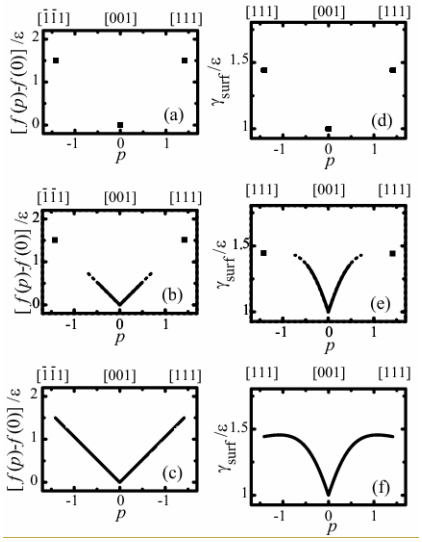

Fig. 1 Surface free energies per projected area $f(\boldsymbol{p})$ (left figures) and surface tensions $\gamma_{\mathrm{surf}}(\mathbf{p})$(right figures). $\boldsymbol{p}=(\partial z(x,y)/\partial p_x, \partial z(x,y)/\partial p_y)$ represents the surface gradient, $p=|\boldsymbol{p}|=\tan\theta$ represents the surface slope, and θ represents the tilted angle of the surface. $\varepsilon_{\mathrm{int}}/\varepsilon=-0.5$. (a) and (d) $k_BT/\varepsilon=0.35$, (b) and (e) $k_BT/\varepsilon=0.36$, and (c) and (f) $k_BT/\varepsilon=0.37$.

16:00 Poster We151

Structures of Chiral Crystal Faces Inducing Autocatalytic Chiral Amplifying Reaction of 2-Substituted Pyrimidine-5-Carbaldehyde

Takashi Fujioka[1], Tsuyoshi Takeshita[1], Yusuke Shirota[1], Hitoshi Shindo[1], Kaori Niki[2]

1. *Chuo university, 1-13-27 Kasuga, Bunkyo-ku, Tokyo 112-8551, Japan* **2.** *Chiba University, 1-33 Yayoi-cho, Inage-ku, Chiba 263-8522, Japan*

e-mail: tks.fuji0ka.328@gmail.com

Various hypotheses have been proposed to explain homo-chirality of biomolecules such as L-amino acids and D-sugars in nature. Frank proposed a purely chemical and homogeneous process of spontaneous symmetry breaking, assuming homochiral dimers of reaction products working as autocatalysts[1,2]. On the other hand, chiral crystal faces of minerals have always been considered to take a part in the selection processes of chirality. Soai and his group[3] have shown that various chiral crystals, inorganic or organic, induce autocatalytic chiral amplifying reactions of 2-substituted pyrimidine-5-carbaldehydes with diisopropyl zinc in non-polar solvents, leading to formation of corresponding pyrimidyl alkanols(structure in Figure 2) of chosen chirality in very high enantiomeric excess (Soai reaction). The combination of chiral-selective adsorption, a heterogeneous process, and autocatalysis, a homogeneous process, will make a good model to explain the mechanism of homochirality.

In order to study the selection mechanism of chirality at crystal surfaces, adsorption structures of the chiral product molecules of Soai reaction were observed with atomic force microscopy(AFM) at chiral (10-10) faces of *P*- and *M*-crystals of α-HgS(cinnabar), (100) faces of *d*- and *l*-crystals of $NaClO_3$, and (100) faces of (+)- and (-)-crystals of hippuric acid ($C_6H_5C(O)NHCH_2$-COOH). It should be reminded here that 2_1-screw axes penetrate these surfaces. Each chiral crystal leads to selective formation of (*R*)- or (*S*)-alkanol in the actual reaction processes[3].

Although atom-resolved AFM images were observed for the bare crystal surfaces before adsorption, chirality cannot be determined with the AFM images. Single crystal X-ray diffraction, optical rotation and circular dichroism were used to determine the chirality of HgS, $NaClO_3$ and hippuric acid crystals, respectively.

Each crystal face was soaked in 10mM toluene solution of the alkanol of chosen chirality for 3-12 hours. The AFM images of adsorption structures were observed in air after taking the samples out of the solutions. Although well-ordered 2D-adsorption structures were observed with AFM, no difference was clearly recognized with the chirality in the first layer.

After prolonged adsorption, however, marked differences occurred depending upon the combinations of the chiralities of the adsorbates and the substrates. The AFM images in Figure 1 show that (*R*)-alkanol molecules adsorbed at *P*-HgS, *l*-$NaClO_3$ and (-)-hippuric acid crystals form micro-crystals in regular shapes. On the other hand, (*S*)-alkanol molecules do not form such crystals on the same substrates. The combinations leading to the micro-crystal formation induce amplification of the same chirality in the Soai reactions. The micro-crystal formation is closely related to the autocatalysis. The chiral crystal faces may be supplying dimers or oligomers of the product molecules, in Zn-alkoxide forms, of chosen chirality, which work as the autocatalyst in the solution.

A mechanism explaining the chiral-selective formation of micro-crystals at (100) face of hippuric acid is proposed in Figure 2. With the alkanol molecule, one of the N-atom in the pyrimidine ring and the –OH group will participate in H-bonding with the –OH and carbonyl groups of the substrate as shown on the right-hand side of the figure in non-polar solvents. Depending upon the distribution of binding sites at the substrate, the chiral alkanol molecules adsorb at the surface in a slanted geometry as shown in the figure. If the substrate of different chirality was used, the molecules will adsorb in geometry slanted in the opposite way. The chiralities of the substrates determine the slant direction of the first adsorption layer.

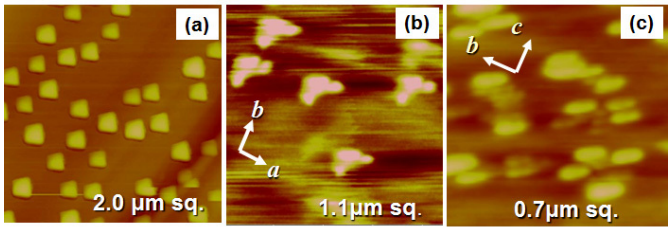

Figure 1. AFM height images of micro-crystals of (*R*)-pyrimidyl alkanol formed by adsorption at chiral (a):*P*-αHgS(10-10), (b):*l*-NaClO3(100) and (c):(100) face of (-)-crystal of hippuric acid.

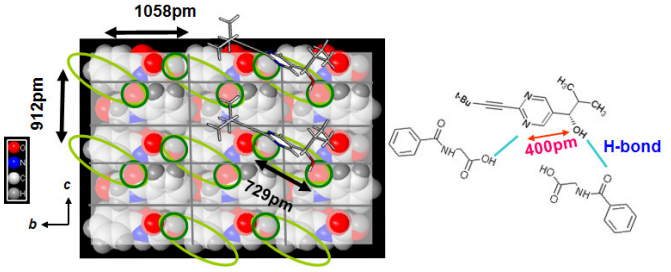

Figure 2. Adsorption structure proposed for (S)-2-substituted pyrimidyl 5-alkanol at (100) surface of (+)-crystal of hippuric acid. Binding sites are encircled.

On the other hand, the chiralities of the adsorbed molecules determine whether stable second-layer adsorption is possible or not. A pair of (*S*)-alkanol molecules adsorbed at (+)-crystal face of hippuric acid are shown in Figure 2. The separation of 912 pm between the two molecules is fairly close to the corresponding distance of *b'*=829 pm in the bulk crystal structure of the (*S*)-alkanol (orthorhombic $P2_12_12_1$). Adsorption geometry of the second layer should be considered in reference to the bulk structure. The same H-bonding sites of the alkanol molecule will be used in the adsorption of the second layer. Accordingly, on the pair of adsorbed (*S*)-alkanol molecules in Figure 2, another (*S*)-alkanol molecule, 180 degrees rotated, will adsorb, avoiding steric hindrance by the bulky isopropyl group, and make a structure resembling the bulk (*S*)- crystal. If (*R*)-alkanol molecules made the first layer on the same substrate, however, the second layer adsorption is impossible. Only (*S*)-homochiral oligomers and micro-crystals will be formed on the (+)-crystal face. On the other hand, (*R*)-homochiral oligomers and micro-crystals will be formed only on the (-)-crystal face. This explains why the micro-crystal structure as in Figure 1(c) was made only with the right combinations of chiralities of the substrate and the adsorbate.

In the cases of using α-HgS and $NaClO_3$ as substrates, binding sites will be Hg atoms, and Na and Cl atoms, respectively, all bearing positive charges. In these cases, too, the 2_1-symmetry allows two slanted geometries of adsorption of the chiral alkanol molecules, enabling selection of homochiral 3D adsorption structures. In the actual reaction conditions, clusters of the product molecules of selected chirality, in Zn alkoxide form, coming off the crystal face will be working as the autocatalyst.

Acknowlegement

This work was supported by JSPS KAKENHI 20225002, 20510097, 24510144, and The Institute of Science and Engineering, Chuo University.

References

[1] F. C. Frank, Biochim. Biophys. Acta, 11 (1953) 459.

[2] J. M. Brown, I. Gridnev, J. Klankermayer, *Asymmetric Autocatalysis with Organozinc Complexes; Elucidation of the Reaction Pathway*, in: K. Soai ed., *Amplification of Chirality,* Springer,, Berlin Heidelberg, 2008, pp.35-65.

[3] K. Soai, T. Kawasaki, *Asymmetric Autocatalysis with Amplification of Chirality*, in: K. Soai ed., *Amplification of Chirality*, Springer,, Berlin Heidelberg, 2008, pp.1-33.

16:00 Poster We152

Surface Characterization of $Bi_2Te_{2.9}Se_{0.1}$ single crystals

Maunik Jani, Manisha Patel, Sandip M. Vyas, Girish R. Pandya

e-mail: maunik_msu@yahoo.co.in

$Bi_2Te_{2.9}Se_{0.1}$ single crystal have been grown by bridgman technique with the freezing interface temperature gradient 65°C/cm and growth velocity 0.5 cm/hr. A parallel striations perpendicular to the ingot axis were observed on the top free surface of crystal, indicates layer growth mechanism is predominant among them.

16:00 Poster We153

Effect of immobile impurities on behaviors of a two-dimensional island

Hiroyasu Katsuno[1], Masahide Sato[2]

1. *Gakushuin University, 1-5-1 Mejiro,Toshima-ku, Tokyo 171-8588, Japan* **2.** *Kanazawa University, Kakuma-machi, Kanazawa 9201192, Japan*

e-mail: katsuno@sic.numse.nagoya-u.ac.jp

Foreign substitutional atoms attached on the surface act as trapping centers for adatoms and/or as obstacles preventing growth of an adsorbate, and affect behaviors of steps and surface morphology. It had been known that a step on crystal surface cannot advance when the period between impurities is shorter than the critical nucleus size[1]. Recently, spiral steps on monoclinic lysozyme crystal is observed and it is found that the interstep distance is about 50 times larger than the expected value[2]. This result suggests that the critical nucleus size in the experiment is much larger than that in pure system because of the impurity in the sample.

We have studied an impurity effect for the nucleus size from the thermodynamic point of view. When the free energy is taken account of the including impurities, the critical nucleus radius is large with increasing the concentration of impurities. The critical nucleus radius diverges when the concentration of the impurity is $(L_{\mathrm{imp}} r_{\mathrm{c}})-1$ where L_{imp} is the periphery length of the impurity and r_{c} is the critical nucleus radius in the pure system. In order to confirm above result, we have also performed the Monte Carlo simulation of a simple square lattice model. The simulation result is in good agreement with that of the thermodynamical analysis[3]. The nucleus, which forms eventually on surface, cannot grow. This interpretation is different from the ordinary impurity effect[1].

References:

[1] N. Cabrera and D. A. Vermilyea, Growth and Perfection of Crystals, edited by R. H. Doremus, B. W. Roberts, and D. Turnbull, (Wiley, New York, 1958), p.393.

[2] G. Dai et al., J. Cryst. Growth, 311, 548 (2009).

[3] H. Katsuno, K. Katsuno, and M. Sato, Phys. Rev. E, 84, 021605 (2011).

16:00 Poster We154

Adsorption of ammonia on hydrogen covered GaN(0001) surface – Density Functional Theory (DFT) study

Pawel Kempisty[1], Pawel Strak[1], Stanisław Krukowski[1,2]

1. *Polish Academy of Sciences, Institute of High Pressure Physics (UNIPRESS), Sokolowska 29/37, Warszawa 01-142, Poland* **2.** *University of Warsaw, Interdisciplinary Centre for Mathematical and Computational Modelling (ICM), Pawinskiego 5a, Warsaw 02-106, Poland*

e-mail: kempes@unipress.waw.pl

DFT calculations were used to investigate ammonia adsorption on GaN(0001) surface under mixed coverage composed of H adatoms, NH_2 radicals and NH_3 admolecules typical for the growth of GaN layers and crystals by MOVPE, HVPE and ammonothermal methods. The investigation elucidated role of electronic properties of the surface on the course of adsorption processes showing important role of electronic degrees of freedom in some cases. In the case of bare surface ammonia adsorption is dissociative: it leads to dissociation of ammonia and adsorption of NH_2 radicals and single H adatoms. The adsorption energy is close to 2.9 eV/molecule. For very low hydrogen coverage the ammonia adsorption follows the pattern of clean surface dissociation to NH_2 radicals and H adatoms which is caused by tendency to saturate broken Ga bonds. The increase of hydrogen coverage stabilizes ammonia molecule that is adsorbed in the molecular form at the surface with the reduction of adsorption energy to about 2 eV. This is related to tendency of GaN(0001) surface of to avoid pinning Fermi level at the surface states. In this case the adsorption of ammonia preserves its molecular structure, with only single molecular bond transformed into highly dispersive state located in the upper subband of GaN valence band. Finally for full coverage, the adsorption leads to creation of Ga-H-N bond weakly attaching the molecule with the energy. Further evolution of the system may either lead to return of the ammonia to the vapor or desorption of H_2 molecule with NH_2 radical attached to the surface. For higher content of ammonia admolecules or NH_2 radicals the pattern is changed, the adsorption affects the bonding of ammonia changing the bonding structure of the admolecule. This is related to change of the Fermi level at the surface which is shifted up into the conduction band. This change drastically reduces the bonding energy making the ammonia adsorbed admolecule unstable at the GaN(0001) surface for relatively high NH_3/NH_2 ratio.

16:00 Poster We155

Study of interaction and thermal properties between of copper-graphene sheets and LED interface

Sang Yeop Kim, Oybek Tursunkulov, Amir I. Abidov, Heung-Woo Jeon, Sungjin Kim

Kumoh National Institute of Technology (KIT), 61 Daehak-ro, Gumi 730-701, Korea, South

e-mail: saintkim1213@naver.com

A light-emitting diode (LED) light source have attracted considerable attention in modern lightening devices because of long lifetime, small size, producing different colored light and low energy consumption in comprising of traditional bulbs. However there is a problem of overheating and decreasing life time of LED chip performance at high temperature. Therefore it is necessary to research and develop new materials with optimal thermal conductivity and stable interface. Graphene sheets are alternative to conventional materials with excellent thermal properties. In this work we study of interaction and thermal properties of copper-graphene sheets attached onto arbitrary LED interface for controlling heat exchange process.

16:00 Poster We156

Temperature field measurement at simulated vertical Bridgman crystal growth

Robert Král[1], Karel Nitsch[1], Petra Zemenová[1,2], Jaroslav Hron[3]

1. *Czech Academy of Sciences, Institute of Physics, Cukrovarnicka 10, Prague 16253, Czech Republic* **2.** *Institute of Chemical Technology (VSCHT), Technicka 5, Prague 16628, Czech Republic* **3.** *Charles University, Faculty of Mathematics and Physics, Ke Karlovu 3, Prague 12116, Czech Republic*

e-mail: kralr@fzu.cz

This work reports on the study of the influence of temperature gradient in the furnace and the pulling rate on the position and the shape of the crystal/melt interface in a model system of lead chloride ($PbCl_2$) at simulated vertical Bridgman crystal growth. Its aim is to find suitable conditions for growth of high quality single crystals of lead halides and ternary alkali lead halides. Crystals of these compounds doped

with rare earth elements are promising materials as hosts for mid-IR lasers [1, 2].

The temperature field in our experimental setup was measured by four thermocouples placed in specially prepared quartz ampoule with four asymmetrically positioned capillaries along the ampoule axis. Two experimental configurations were used: stationary and dynamic. The measurement at the stationary arrangement, at which the ampoule was held at fixed position, the thermocouples were pulled up in the capillaries by step of 1 mm/h, was described in detail in [3].

At the dynamic one the ampoule was pulled down by pulling rates of 1 and 3 mm/hour through the same temperature gradients as those used in the stationary arrangement. When the ampoule reached the same position in the furnace as in the stationary arrangement, the temperature field was measured.

In the stationary arrangement, temperature gradient of 35 K/cm, and small volume of the crystalline phase in the ampoule, the shape of the crystal/melt interface obtained by temperature measurements was markedly convex. While at the dynamic arrangement the interface shape was planar and its position was lower by 2 – 3 mm than the position determined at the stationary arrangement. This can be explained by release of the latent heat.

Temperature data were used as boundary conditions for a modeling of the temperature field and the melt flow in the studied system using COMSOL Multiphysics 4.1 software.

This work was supported by the research project MSMT KONTAKT No. LH12150.

[1] T.T. Basiev, Yu.K. Danileiko, L.N. Dmitruk, B.I. Galagan, L.V. Moiseeva, V.V. Osiko, E.E. Sviridova, N.N. Vinogradova, Opt. Mat. 25 (2004) 295–299.

[2] L.I. Isaenko, I.N. Ogorodnikov, V.A. Pustovarov, A.Yu. Tarasova, V.M. Pashkov, Opt. Mat. 35 (2013) 620–625.

[3] R. Král, J. Crystal Growth 360 (2012) 162–166.

16:00 Poster We157

Morphology of the surface of modified AlN/sapphire substrates obtained by thermochemical nitridation method

Sergii I. Kryvonogov, Andrii A. Krukhmalev, Nataliya S. Sidelnikova, Elena A. Vovk, Aleksander Budnikov, Sergii V. Nizhankovskyi, Georgiy T. Adonkin

Institute for Single Crystals NAS of Ukraine (ISC), 60 Lenin Ave., Kharkov 61001, Ukraine

e-mail: ksicold@gmail.com

Sapphire is the material most widely used in the capacity of substrates for technical devices based on the nitrides GaN, InN, AlN and their solid solutions. However, the method of heteroepitaxy of the nitrides on sapphire substrates results in high dislocation density and other structure defects, due to discrepancy in the crystal lattice parameters and thermal expansion coefficients of these materials. This essentially complicates the obtaining of heterostructures with high functional characteristics. Since the commercial production of the substrates for homoepitaxial growth is expensive, much attention is being paid nowadays to the use of modified sapphire substrates with buffer nitride layers (GaN/sapphire or AlN/sapphire templates) which play the role of inherent nitride quasi-substrates. We have developed a new method for the obtaining of AlN/sapphire templates based on nitridation of sapphire in a gaseous mixture containing N_2, CO, CO_2, H_2, H_2O with low concentration of CO_2 and H_2O [1]. This method allows to obtain polar ((0001)AlN//(0001)Al_2O_3, (0001)AlN//(11-20) Al_2O_3), semipolar ((10-13) AlN//(10-10) Al_2O_3) and nonpolar ((11-20) AlN//(10-12) Al_2O_3) crystalline AlN layers on the surface of sapphire. Their thickness ranges between 20-30nm and several microns, the rocking curve half-width is less than 1º [2, 3]. In contrast to well-known deposition methods in which epitaxial films are obtained using external source, in the given method AlN layer is formed due to dissolution of nitrogen in anion-deficient corundum followed by crystal-chemical transformations in the surface-adjacent layer of sapphire substrate. Therefore, the nitride layer is to be formed after the stage of corundum reduction followed by etching of the substrate surface [4]. The goal of the present work was to establish regularities of the influence of reducing annealing of sapphire substrate on the morphology of the surface of AlN/sapphire templates.

The study was performed on sapphire substrates with a diameter of 50.8mm with the crystallographic orientation (0001) and a deviation angle of 3–9′. The substrate surface underwent chemico-mechanical polishing. The substrates were annealed at 1450°C. For reducing annealing there was used a mixture of Ar, CO, H_2 gases (0.1–0.12MPa, Ar and N_2 concentrations were ~ 99vol.%, ~ 0.1–0.4vol.%, respectively). Nitridization was realized in a mixture of N_2, CO, H_2 gases (0.1–0.12MPa, ~ 99vol.% concentration of N_2.

The surface morphology was investigated on an atomic-force microscope Solver 47 Pro (NT-MDT) in contact mode. After chemico-mechanical polishing the initial surface of the substrates had a surface with terraces and steps, the step width ranged between 30 and 140nm. Such a nanostructured lay may be formed on extremely smooth sapphire surface at low angles of inclination to the crystallographic plane. The roughness R_a was 0.2–0.4nm.

Shown in Fig.1 are the AFM images of the substrate inclination to the crystallographic plane. The roughness R_a was 0.2–0.4nm surface after reducing annealing in gaseous medium with low (Fig. 1 *a,c*) and high (Fig. 1 *b,d*) reduction potential which value is defined by the ratios CO_2/CO and H_2O/H_2 in the annealing medium.

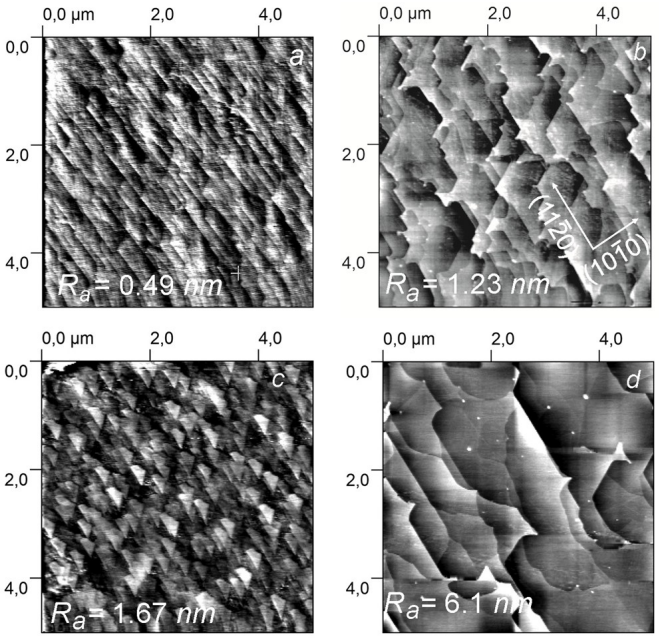

Fig. 1. AFM images of the surface of sapphire substrates after reducing annealing at different reduction potentials during 15min. (*a, b*) and 5 hours (*c, d*).

In the process of reducing annealing thermochemical etching leads to transformation of the initial surface structure accompanied with splitting and junction of the steps, increase of their width and height,

deformation of the edges. Within 15 min. of the annealing at low reduction potential (Fig. 1. *a*) the width of the steps is 0.3 μm, the roughness R_a is 0.49 nm. When the duration of isothermal holding increases to 5 hours, there is observed splitting of the surface structure followed by the formation of islets located in the direction which coincides with that of the terraces (Fig.1. *c*). In the process of annealing at high reduction potential the steps undergo essential deformation, their boundaries are sharper, the shape becomes toothed representing parts of etch patterns for the crystallographic orientation (0001) of sapphire (Fig. 1 *b*), the step width increases to 0.8–1.05μm, R_a = 1.23nm. At long-term holding (Fig. 1 *d*) the surface deformation is even more essential: the step width increases up to 1–2μm, the roughness R_a reaches 6.1nm. The crystallographic orientation of the steps is well defined from the etch patterns at their edges.

Fig. 2 presents the AFM images of the surface of AlN layer obtained on the substrate surface after preliminary reducing annealing (Fig. 2 *a*), and of the initial surface after chemico-mechanical polishing (Fig. 2 *b,c*). The nitride layer replicates the structure of the surface obtained after thermochemical etching of the substrate. On the surface of the sample which has not been subjected to preliminary reducing annealing the structure with steps is weakly pronounced, it is seen only at large magnification of the AFM images (Fig. 2 *c*).

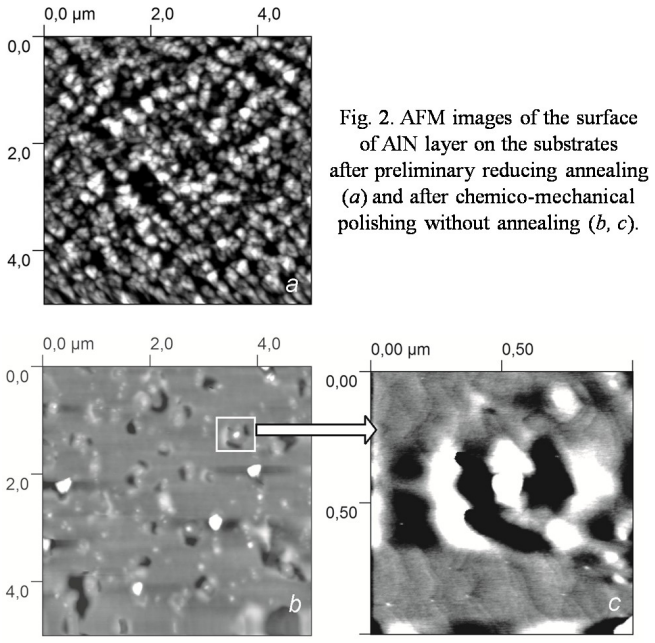

Fig. 2. AFM images of the surface of AlN layer on the substrates after preliminary reducing annealing (*a*) and after chemico-mechanical polishing without annealing (*b, c*).

Thus, the preformed investigation shows that the morphology of the surface of AlN obtained by the method of thermochemical nitridation of sapphire is essentially defined by thermochemical etching of the initial substrate realized prior to the formation of the nitride layer.

References

1. Pat. UA90239C2, C30B 25/00, C30B 29/38, C01B 21/072, C01F 7/00, Ukraine. Method obtainment of crystalline film of aluminum nitride / Kh. Sho. Kaltaev, N.S. Sidelnikova, S.V. Nizhankovskiy, A.Y. Dan'ko, M.A. Rom; Declar. 29.09.2009; Pablish. 12.04.2010, Byul. N7, 2010.

2. Kh. Sho. Kaltaev, N.S. Sidel'nikova, S.V. Nizhankovskiy, A.Y. Dan'ko, M.A. Rom, P.V. Mateychenko, M.V. Dobrotvorskaya, and A.T. Budnikov. Obtainment of Textured Films of Aluminum Nitride by Thermochemical Nitridation of Sapphire // Semiconductors, 2009, Vol. 43, N.12, P. 1606–1609.

3. S.V. Nizhankovskiy, A.A. Krukhmalev, H. Sh.-ogly Kaltaev, N.S. Sidelnikova, A.T. Budnikov, V.F. Tkachenko, M.V. Dobrotvorskaya, E.A. Vovk, S.I. Krivonogov, and G.T. Adonkin. Thermochemical Nitridation of Sapphire Substrates of Different Crystallographic Orientations // Physics of the Solid State, 2012, Vol. 54, N.9, P. 1896–1902.

4. Kh. Sh.-ogly Kaltaev, N.S. Sidelnikova, A.Ya. Dan'ko, A.T. Budnikov, S.V. Nizhankovskiy. Thermochemical etching of sapphire in $CO+H_2$ gas atmosphere // Functional Materials. 2010. Vol.17, N.3. – P.395–400.

16:00 Poster We158

Microscopic Studies on Crystals: Correlation Between Structural, Defects and Surface Features

Binay Kumar

Department of Physics and Astrophysics, University of Delhi, Delhi 110007, India

e-mail: b3kumar69@yahoo.co.in

Various surface features on crystals are beautiful manifestation of structural properties, growth pattern and defects in the crystal. Optical & Electron microscope are important tools to characterize crystals in respect of micro-morphology, growth features, etch pits, over growth, etc. In the micro- and macro-morphology, the information related to crystal habit, development of various planes along crystallographic directions, relative growth rate, etc can be drawn which is vital for the quality of grown crystals. In the growth features, the evidence of growth mechanism like spiral growth, two dimensional nucleation, dendritic growth, etc can be seen. Surface features are directly linked with the changes in the crystal structure through doping, annealing and other post growth treatment for improvement in material and crystallographic quality of crystals.

In the present talk, the above mentioned surface features are demonstrated in respect of crystals of wide range of materials like polytypic CdI_2/PbI_2 , high temperature superconducting Bi-2212, piezoelectric $LiNbO_3$ and PZNT, various semiorganic NLO (like L-HFB) and ZnO micro-crystals. These crystals are grown by various techniques like solution, vapour, melt (zone melting) and flux. The height of density and distribution of multiple spirals, etc provide micro-details of growth mechanism. The development of etch pits, their shape, size, density and distribution along selective crystallographic directions provide detailed information, both quantitative and qualitative, of dislocation present in the crystals. The slip lines and slip planes, overgrowth, hillocks, growth steps and their bunching, etc are other important features which have been studied. In the process, the fundamentals theories of spiral growth, 2D layer growth, dendritic growth, etc are discussed with clinching experimental evidences. The effect of growth technique, doping, etching, heat treatment, etc on various surface features will be discussed. A series of micrographs taken from optical, SEM, AFM and TEM will be presented.

16:00 Poster We159

Surface roughness analysis of Ni thin films electrodeposited onto rotating disk electrodes

Gholamreza Nabiyouni

Department of Physics, Arak University, Beheshti Avenue, Arak 38156, Iran

e-mail: g-nabiyouni@araku.ac.ir

Ni films were electrodeposited onto polycrystalline gold substrates mounted on a rotating disk electrode. The effect of rotating speed, film thickness and current density on the kinetic roughenin of the electrodeposited films were investigated. The film roughness surface was imaged using an atomic force microscope (AFM). The results indicate that the film roughness increases as the film thickness or the current density increase. We found that the electrodeposited Ni films exhibit anomalous scaling since both the local and long-scale roughness show a power law dependence of the film thickness. The effect of electrode rotating speed on the film thickness is also investigated.

16:00 Poster We160

Atomic or molecular resolution investigation of soluble crystals in liquid by frequency-modulation (non-contact) AFM

Ken Nagashima, Gen Sazaki, Harutoshi Asakawa, Yoshinori Furukawa

Institute of Low Temperature Science, Hokkaido University (ILTS), N19-W8, Kita-ku, Sapporo 060-0819, Japan

e-mail: nagasima@lowtem.hokudai.ac.jp

The most high resolution AFM images are obtained in vacuum by Frequency-Modulation AFM (FM-AFM). Recently, Fukuma et al. (2005) succeeded in obtaining true atomic resolution by FM-AFM in spite of liquid environment [1]. Subsequently, not soluble crystals but insoluble crystals have been observed in liquid by FM-AFM. Dissolution and growth processes are inconvenience for AFM observation. However, such processes at atomic levelare very important for crystal growth. Therefore, we tried to observe several soluble crystals in liquid by FM-AFM [2].

FM-AFM images were obtained using a modified commercial AFM (Shimadzu, SPM-9600) with open fluid cell. We intentionally observed soluble crystals in undersaturated solution at first. The concentration of solution gradually increased because of evaporation of water. Therefore, dissolution, near equilibrium, and growth conditions could be observed with increasing elapsed time. By using this method, crystal growth speed of vertical direction was suppressed and atomic resolution images could be obtained.

Figure 1 shows a KCl(100) cleaved surface in solution. We could observe a periodic structure, in which the wavelength is 6.29 Å. Therefore, only one kind of atom was probablyimaged in liquid environment as well as ultrahigh vacuum environment.

Figure 2 shows amolecular resolution image of lysozyme (110) in solution[2]. The surface unit cell (a black rectangle in fig. 2b, 11.2 × 3.8 nm) involves four molecules with the four unique orientations, which make two kinds of zigzag structures (circles and triangles) along the [001] direction. Figure 2 shows the individual four molecules in the unit cell and the image has higher resolution than images obtained by conventional contact mode or amplitude-modulation (tapping) mode AFM [3]. In addition, we could observe admolecule and point defect on the lysozyme(110) face (fig. 3).

Acknowledgments

We thank Prof. S. Morita of Osaka University, M. Abe of Nagoya University, and Shimadzu Corporation for observation of AFM.

[1] T. Fukuma rt al., *Appl. Phys. Lett.***87**, 034101 (2005).

[2] K. Nagashima et al., *J. Vac. Sci. Technol. B***28**, C4C11 (2010).

[3] J. H. Konnert et al., *Acta Crystallogr. D***50**, 603 (1994).

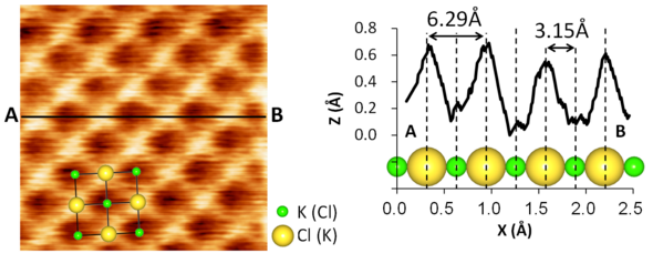

Fig.1 An atomic resolution image of KCl (100) surface in saturated solution. Crystal growth speed in the vertical direction $V < 0.005$ nm/s.

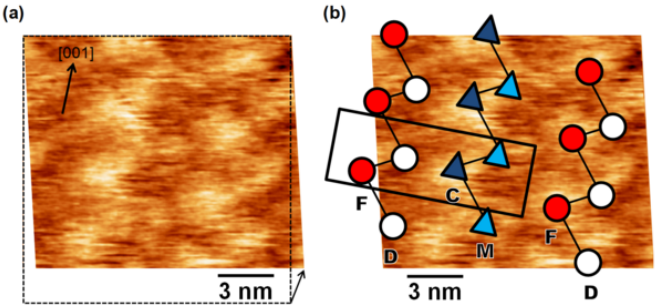

Fig.2 (a) Molecular resolution image of lysozyme(110) face in saturated solution. The image was already corrected for *XY* drift. (b) theoretical molecular packings on (a).

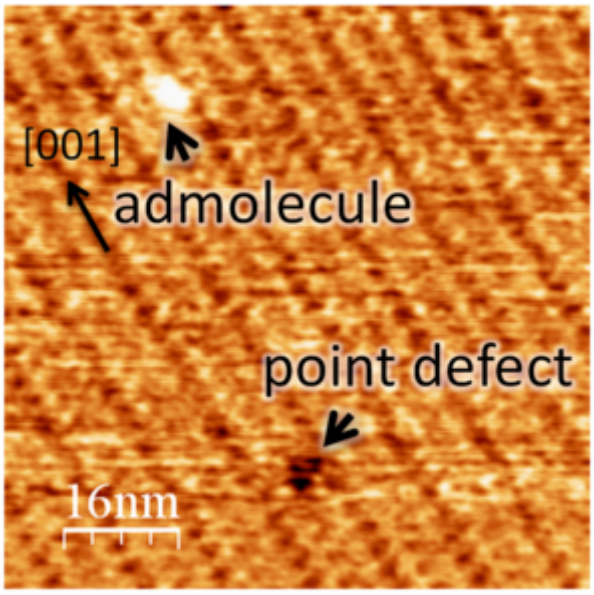

Fig.3 Admolecule and point defect on the lysozyme(110) face in saturated solution.

16:00 Poster We161

Relative Stabilities of Crystal Faces of Anatase Compared by AFM Observation of Micro-etch Pits Formed in Highly Oxidative Environment

Yohei Ohkawa, Shun-ichiro Saito, Hitoshi Shindo

Chuo university, 1-13-27 Kasuga, Bunkyo-ku, Tokyo 112-8551, Japan

e-mail: y_o0601@yahoo.co.jp

Titanium oxide(TiO_2) has three polymorphs, namely, rutile, anatase and brookite, each of them crystallizing in various forms in nature[1]. How are the morphology determined depending upon growth environ-

ments? Especially in the case of anatase, control of the crystal form has practical importance because its photocatalytic activity depends on the orientation of the surfaces. In order to control the crystal shapes, we need to know stabilities of crystal faces in various environments.

Stabilities of crystal faces can be compared by observing polyhedral micro-etch pits at crystal faces with atomic force microscope(AFM). One of the authors employed the method in studying relative stabilities of crystal surfaces of less water-soluble aragonite($CaCO_3$)[2-4] and anhydrite($CaSO_4$)[5] in aqueous solutions. Similar method can be applied to the studies of oxide crystals if appropriate etchants are obtained. In this study, three low-index faces of anatase were etched by heating with $KHSO_4$, which produces SO_3. The polyhedral etch pits formed were observed with AFM *ex situ*. The space group and lattice constants of anatase are tetragonal $I4_1/amd$, a=b=378.67, and c=951.49 pm[6]. The crystal faces studied are c(001), p(101) and m(100), where the alphabets were added to show the relationship with the classical nomenclature frequently used in mineralogy books[1]. The c- and p-faces used were naturally grown ones, while the m-face was sliced out of a natural crystal.

The AFM images shown in Figure 1 were observed after the c(001) surface was etched. With the smaller etch pit in (a), u{1,1,10} facets consisting of e{112} steps and c(001) terraces were stabilized. With the larger pit in (b), on the other hand, z{103} facets were observed in addition to x{116}=e{112}+4·c(001) facets. The e(112) and z(103) faces are nearly as stable as the c(001) face, since Ti atoms at the three faces are all 5-coordinated.

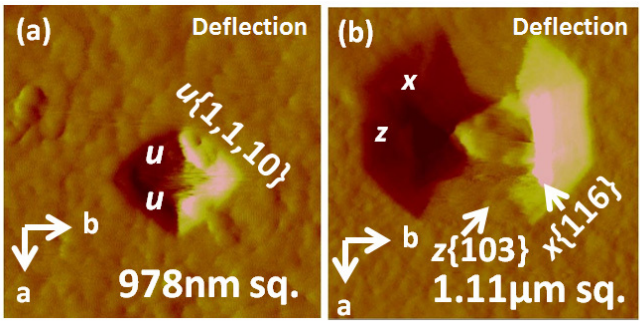

Figure 1. AFM images of TiO_2(001) surface after etching, where {11n} and {103} facets are stabilized.

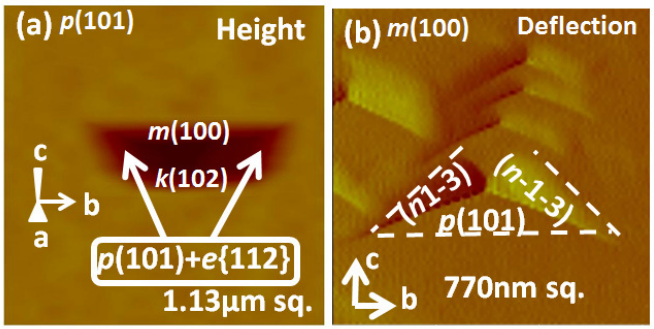

Figure 2. AFM images of (a)TiO_2(101) and (b)(100) surfaces after etching. Stable facets forming sidewalls of etch pits contain (100), (101) and (112) components.

The p(101) is considered to be the most stable surface since equal numbers of 6- and 5-coordinated Ti atoms are densely packed on it. In the etching of the p-face, trapezoidal etch pits were formed as the one shown in Figure 2(a). The bases are formed by m(100) and k(102)=(101)+(001) facets. The m(100) face is considered to be nearly as stable as the p-face, because equal numbers of 6- and 5-coordinated Ti atoms make the surface. Two other sidewalls of the pit are combination of e{112} ledges and p(101) terraces.

When the m(100) face was etched, triangular pits formed by p(101) and two {n13} facets were observed as shown in Figure 2(b). The (n13) facet is a combination of τ(213) ledges and m(100) terraces.

In the oxidative environment employed, relative stabilities of the crystal faces are determined by coordination numbers of Ti at the surfaces. The most stable p(101) and m(100) faces have 5- and 6-coordinated Ti atoms. Slightly less stable c(001), e(112), z(103) and k(102) faces have 5-coordinated Ti atoms on it. Other faces containing 4-cordinated Ti atoms, such as u(1,1,10) and x(116), appear only temporarily in the etching process. A natural crystal form of truncated tetragonal bipyramid having p-, m-, e-, c-,and u-faces is reported in literature[1]. The crystal was most probably formed in an oxidative condition like the one we used.

Acknowlegement

This work was supported by JSPS KAKENHI 24510144 and 20510097, and The Institute of Science and Engineering, Chuo University.

References

[1] E. S. Dana, *The System of Mineralogy –Descriptive Mineralogy,* Wiley, New York, 6th ed. 1900, pp.237-243.

[2] M. Kwak and H. Shindo, *J. Cryst. Growth,* **275** (2005) e1655-1659.

[3] H. Shindo and M. Kwak, *Phys. Chem. Chem. Phys.*, **7** (2005) 691-696.

[4] Y. Shirota, K. Niki and H. Shindo, *J. Cryst. Growth,* **324** (2011) 190-195.

16:00 Poster We162

PTCDA adsorption on KCl and NaCl(100) surface studied from first principles

Eva Rauls, Hazem Aldahhak, Wolf Gero Schmidt

Paderborn University, Department of Physics, Warburger Strasse 100, Paderborn 33098, Germany

e-mail: eva.rauls@upb.de

In recent years, various highly regular supramolecular architectures of self-organized molecules on crystals have been designed and used in the bottom-up device technology. In the past metal surfaces have frequently been used as substrate. However, metal substrates induce screening and quenching effects and thus hamper the detailed spectroscopy of the adsorbed overlayer. In contrast, molecular adsorption on ionic crystals like sodium or potassium chloride opens the possibility to study electronically decoupled molecules.

Here we present density-functional theory calculations on the adsorption of PTCDA on KCl and NaCl (100) surfaces. Thereby, the adsorption on flat surfaces as well as stepped substrates steps is investigated. The adsorption of PTCDA at special defective step sites is strongly favored over flat terraces and initiates film growth. Experimentally, both flat-lying (P-type) [1,5] as well as standing molecules (S-type) [1,2] are observed depending on the preparation conditions. In order to understand and rationalize the adsorption mechanisms leading to the formation of these structures, a large variety of interface geometries was studied and analyzed with respect to the contribution of ionic, covalent and van-der-Waals interactions between adsorbates and substrate. The influence of the substrate and bonding mechanism on the

molecular electronic structure is investigated in detail and compared with the experimental data available [3,4].

[1] M. Möbus et al. Thin Solid Films 175, 89 (1989).

[2] M. Möbus et al. Journal of Crystal Growth 116, 495 (1992).

[3] T. Dienel et al. Advanced Materials, 20, 959 (2008).

[4] H Karacuban et al. Nanotechnology, 22, 295305 (2011).

[5] Bruke et al PRL 100,186104 (2008)

16:00 Poster We163

Specific Surface Free Energy of Crucible Material for Sapphire Crystal Synthesis

Takaomi Suzuki, Kou Shirotsuki, Toshinori Taishi, Keigo Hoshikawa

Shinshu University, 4-17-1 Wakasato, Nagano 380-8553, Japan

e-mail: takaomi@shinshu-u.ac.jp

Vertical Bridgman method is one of the effective techniques to synthesize a single crystal of sapphire. In order to obtain high quality single crystal, removal of the voids or defects in the crystal is the important problem, and the material of crucible reflects the incidence of voids. When we use W-crucible, sapphire single crystal accompanies large voids at the boundary between the crucible and the crystal. On the other hand, Mo-crucible does not accompany voids at the boundary of crucible and the crystal. We are going to explain the mechanism of the incidence of voids by the specific surface free energy (SSFE) of the crucible materials.

W, Mo, and tungsten-molybdenum alloy (W-Mo) plates are used as the test pieces for crucible material. Water or formamide was dropped on the test pieces using micropipette. The contact angle of liquid droplet on the test piece was measured using a protractor and printed photos by a digital camera. SSFE was calculated using Forks approximation and Wu's harmonic mean equation. The SSFEs were 46, 48, and 52 mN/m for W, W-Mo, and Mo, respectively, indicating that the SSFE of Mo is larger than that of W. Even though the SSFEs were calculated from the contact angle of liquids at room temperature, they are considered to suggest the SSFE at high temperature. Contact angles of molten sapphire on test pieces were also measured by photograph, and they were 30.5, 27.5, 22.3 degree for W, W-Mo, and Mo, respectively. Molten sapphire is most wettable on the test piece of Mo. Voids at the boundary between sapphire and crucible can be removed, if the SSFE of crucible material is large enough to make the voids in spherical, and sphere voids easily detach from the crucible wall.

16:00 Poster We164

Changes in morphology and element composition of nitrided sapphire substrates at layer-by-layer polishing

Elena A. Vovk, Aleksander Budnikov, Sergii V. Nizhankovskyi, Sergii I. Kryvonogov, Mariya V. Dobrotvorska, Andrii A. Krukhmalev

Institute for Single Crystals NAS of Ukraine (ISC), 60 Lenin Ave., Kharkov 61001, Ukraine

e-mail: ovovk@isc.kharkov.ua

Semiconductor heterostructures based on III-Nitride materials are widely used in opto- and microwave electronics. Application of composit substrates or templates of GaN/sapphire, AlN/sapphire is perspective for the quality improvement of nitride heterostructures and cutting of production costs. Earlier we have shown the possibility to produce crystalline aluminum nitride layers on sapphire (AlN/sapphire templates) by thermochemical nitriding (TChN) of sapphire [1]. The essence of this method is the following. While annealing sapphire at temperatures of 1300-1450^{o}C in nitrogen-containing atmosphere under reductive conditions (CO, H_2 - reagents), there occurs nitriding of the surface layer followed by the formation of the crystalline phase of aluminum nitride of a varying composition AlN(O) with the wurtzite crystal structure.

The aim of the present work was to establish the conditions for chemical-mechanical polishing of the AlN/sapphire templates obtained by the TChN method , and to study the morphology and element composition of the surface at layer-by-layer removal of the nitridated layer.

The study was performed on (0001)AlN//(0001)Al_2O_3 templates. The thickness of AlN layers was determined by means of X-ray diffractometry from the interference lines intensity in the symmetrical Bragg geometry and run into 0.3-0.5μm. According to atomic forse microscopy the AlN surface with an initial roughness R_a=7.7nm represent the hills with a diameter up to 0.1 μm and a height up to 20nm, the depth of individual pores was 20nm.

Series of polishing suspensions based on colloidal silica, surfactants, alkaline agents were applied for polishing AlN/sapphire templates. The scratches appeared on the surface of nitrided layer or the etching of surface defects with formation of etch patterns occurred during the polishing in certain cases. The surface of the best quality has been produced at use of polishing suspension consisted aerosil and KOH at pH 10.3. Roughness R_a of 0.95 nm was achieved. Polishing with this suspension has allowed to produce a surface without scratches on whole thickness of nitrided layer.

The study of the element composition of template surface with X-ray photoelectron spectroscopy has shown gradual reduction of nitrogen atoms concentration at layer-by-layer removal of the nitrided layer. It is proving the diffusive mechanism of process of sapphire nitriding. However, even at achievement of a sapphire substrate (with the nitrogen concentration 1 at.%) the funnel-shaped pores of depth up to 10 nm was remained on the surface. The possible origin of these pores can be dissociative decomposing of sapphire with generation the gaseous products which form pores.

1. S.V. Nizhankovskiy, A.A. Kruhmaljov, N.S. Sidelnikova et al., Fiz.Tverd.Tela, 54, 1777 (2012) [in Russian].

16:00 Poster We165

Specific surface free energy of inorganic salt

Yuya Yamada, Takaomi Suzuki

Shinshu University, 4-17-1 Wakasato, Nagano 380-8553, Japan

e-mail: 10t6048k@shinshu-u.ac.jp

Introduction: Although specific surface free energy (SSFE) of inorganic crystal is discussed theoretically in many cases, experimental measurement of SSFE of inorganic is seldom performed. The measurement of SSFE of inorganic crystal is bereaved to be difficult. Recently, we determined the SSFE of some inorganic crystals, ruby, quartz, and apatite, using contact angle of liquid droplet. This time, we considered the basic meaning of SSFE, especially, polar and dispersion component of SSFE, and chose simple alkali halide crystals.

Experimental: Four kinds of alkali halide single crystals, NaCl, KCl, NaBr, and KBr, were used as sample crystals. Each alkali halide was saturated in water of 100mL, and kept it in incubator. Two or more well formed crystals were obtained, and the contact angle of liquid droplet on (100) face of the crystals were measured by the sessil drop method. Formamide and glycol was used as liquid droplet.

Result and discussion: Dispersion component and the polar component of SSFE were calculated using Young's equation, Fowks approximation and Wu's Harmonic mean equation. The calculated SSFE ware 88.63, 88.86, and 80.11mN/m for NaCl, NaBr and KBr, respectively. The polar components of SSFE ware 1.15, 1.08, and 0.81 mN/m for NaCl, NaBr, and KBr respectively. On the other hand, the distance between neighbor ions is 0.279, 0.294, and 0.329 nm for NaCl, NaBr, and KBr, resoectively. Therefore, the crystals with larger distance between neighbor ions have smaller SSFE. Such relationship between the polar component of SSFE and the neighboring ion distance can be explained by the rumpling of the crystal surface.

16:00 Poster We166

Thermodynamic interpretation of the morphology individuality of inorganic oxide single crystal

Mika Yoshida, Takaomi Suzuki

Shinshu University, 4-17-1 Wakasato, Nagano 380-8553, Japan

e-mail: 12tm630j@shinshu-u.ac.jp

Measurement of specific surface free energy (SSFE) of solid is very popular and well accepted in the field of polymer science. On the other hand, the measurement of SSFE of crystals face is believed to be difficult. Even though the significance of SSFE for crystal growth is well discussed, experimental determination of SSFE for crystal is very few. We performed the first trial to determine the SSFE of barium chlorapatite using the contact angle of liquids and reported[1]. This time we are going to study the SSFE of some inorganic single crystals and discuss the morphology individuality of each crystal.

Barium chlorapatite and ruby crystals were synthesized by flux method. The contact angles of water and formamide droplet on (10-10) face and (10-11) face of barium chlorapatite and (11-23) face of ruby were measured by sessile drop method. Contact angles were measured more than 300 times for each face.

Distribution of contact angle was approximately normal distribution. The average value of contact angle was nearly consistent with the angle of the highest frequency. The value of SSFE can be calculated using the Fowkes approximation and Wu's harmonic mean equations. Wide distribution of the SSFE is considered to cause the distribution of step density on crystal surface. The observed SSFE including step free energy was almost proportional to the grown length of the crystal, h. In the same system, for example the same crucible, the crystal has different shape each other, but the shape of each crystal is the resulted from minimum of the surface free energy including the step free energy.

[1] T.Suzuki, K.Nakayama, S.Oishi, Bull. Chem. Soc. Jpn. 77 (2004) 109.

General Session 10

Thin film and epitaxial growth

Session Coordinators

Michal Leszczynski (Poland) *mike@unipress.waw.pl*

Ferdinand Scholz (Germany) *ferdinand.scholz@uni-ulm.de*

Programme

Monday, 12 August

MoO1

G10: Thin film and epitaxial growth
Monday morning, 12 August, 11:00
Room C, Auditorium Maximum

11:00 Invited oral

Hollow nanostructure-assisted growth of GaN by MOCVD and its applications

Jonghak Kim[1], Heeju Woo[2], Kisu Joo[3], Sungwon Tae[1], Daeyoung Moon[1], Sunghyun Park[1], Junghwan Jang[1], Yigil Cho[4], Jucheol Park[1], Hwankuk Yuh[1], Gun-Do Lee[1], Jinsub Park[5], In-Suk Choi[4], Heung Nam Han[1], Yasushi Nanishi[6], Kookheon Char[2], Euijoon Yoon[1,7]

1. *Seoul National University (SNU), School of Mat. Sci. Eng., Seoul 151742, Korea, South* **2.** *Seoul National Unversity, School of Chemical and Biological Engineering (SNU), Seoul 151-744, Korea, South* **3.** *Seoul National University, Graduate School of Convergence Science and Technology, Suwon 443270, Korea, South* **4.** *Korea Institute of Science and Technology, High Temperature Energy Materials Research Center, Seoul 133791, Korea, South* **5.** *Hanyang University, Department of Electronic Engineering, Seoul 133791, Korea, South* **6.** *Department of Photonics, Ritsumeikan University, Kusatsu 525-8577, Japan* **7.** *Advanced Institutes of Covergence Technology (AICT), Suwon 443270, Korea, South*

e-mail: eyoon@snu.ac.kr

Light-emitting diodes (LEDs) become an attractive alternative to conventional light sources such as incandescent and fluorescent lamps due to their high energy efficiency, long device lifetime, and integration with other digital devices. However, different material properties between GaN and sapphire substrates cause several problems such as high dislocation density in GaN epitaxial layers, serious wafer bowing, particularly in large-area wafers due to thermal expansion mismatch, and poor light extraction efficiency of GaN-based LEDs due to total internal reflection. In this presentation, we propose a new growth strategy for the fabrication of high efficiency LEDs by incorporating artificial hollow nanospheres. In particular, polystyrene (PS)/silica core-shell nanospheres were synthesized and coated as a monolayer on a sapphire substrate by a modified dip coating technique. Sapphire substrates containing a monolayer of silica hollow nanosphere (S-HNS) could be prepared by the calcination of PS core and subsequent fixation to the substrate in a furnace. The subsequent growth of GaN by metal-organic chemical vapor deposition results in improved crystal quality due to nano-scale lateral epitaxial overgrowth. Moreover, well-defined voids embedded at the GaN/sapphire interface help scatter lights effectively with the maximum index contrast to increase the light extraction efficiency and reduced the wafer bowing due to partial alleviation of compressive stress in GaN. It was found that the GaN epilayer with embedded S-HNS had higher diffuse reflectance in all visible wavelength range, and reduced wafer bowing, and stronger integrated photoluminescence intensity. Detailed analyses of finite difference time domain (FDTD) simulation and finite element simulation were used to understand the effect of S-HNS on reflectance and structural properties, respectively. The blue LED with embedded S-HNS indeed had two-fold stronger light emission with respect to one without S-HNS, suggesting that the new GaN epitaxy scheme looks quite promising in achieving high external efficiency LEDs for solid-state lighting, particularly in the mass production of LEDs with large-area sapphire wafers.

11:30 Oral

Effect of nucleation islands coalescence on determining the quality of AlN layers grown by MOCVD

Balaji Manavaimaran, Baskar Krishnan

Crystal Growth Centre, Anna University, chennai 600025, India

e-mail: drbaskar2009@gmail.com

Aluminum Nitride (AlN) is an important material for ultraviolet emitters and detectors. AlN has wide band gap (6.2 eV), high thermal conductivity (3.2 W cm^{-1} K^{-1}), high breakdown voltage (12 MV cm^{-1}) and excellent lattice match with Gallium Nitride (GaN). However, growth of AlN always has many challenges due to the lack of native (AlN) substrates, high sticking coefficient of Aluminum (Al) that restricts the migration of Al atoms and unwanted parasitic reactions between Al and ammonia (NH3). Sapphire (Al_2O_3) and Silicon carbide (SiC) substrates have been used to grow AlN heteroepitaxially. Among these substrates c-plane sapphire is often used for AlN growth due to its affordability, despite the large lattice mismatch and large difference in thermal expansion.

In the present investigation, AlN epilayers were grown on 2” sapphire c-plane substrate by metal organic chemical vapor deposition system. High purity (7N) trimethyl aluminum and ammonia were used as the precursors for aluminum and nitrogen respectively. Hydrogen was used as a carrier gas. The effect of AlN nucleation layer (NL) deposition temperature on the surface morphology and structural quality of AlN epilayers has been studied using atomic force microscopy (AFM), high resolution X-ray diffraction and Raman spectroscopy. Figure 1(a) and 1(b) show the AFM images and X-ray rocking curve FWHM of AlN epilayers grown using the NLs deposited in the temperature range of 850 -1250 °C. It has been found that coalescence and size of nucleation island (NI) plays the vital role in determining the quality of AlN layer. The uniform size NIs of 80-100 nm range formed at a nucleation temperature of 950 °C tend to coalesce for a two dimensional specular AlN layer and resulted in the good crystalline quality.

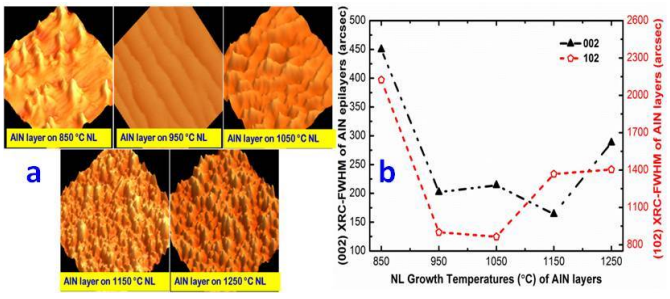

Figure 1 (a) AlN AFM images in the scan area of 10μm×10μm. (b) X-ray rocking curve FWHM of (002) and (102) reflections of AlN layers grown using the NLs in the temperature range of 850 - 1250 °C

11:45 Oral

Effect of process conditions on wafer curvature due to thermal stresses and wafer-to-carrier temperature gradient during MOCVD growth in vertical rotating disc reactors

Bojan Mitrovic, Aniruddha Bagchi, Alexander Manasson, Scott Maxwell, Russell Low

Veeco Instruments Inc. (VEECO), 394 Elizabeth Avenue, New Jersey, NJ 08873, United States

e-mail: bmitrovic@veeco.com

The LED industry is aggressively reducing manufacturing costs to compete economically with existing lighting technologies. Currently, the largest factor of the total cost associated with HB-LED manufacture is attributed to yield loss during the MOCVD epitaxial growth steps. One of the biggest contributors to the yield loss is wafer curvature, as it can induce large temperature gradients across the wafer surface. Critical LED parameters such as emission wavelength, electrical properties, and efficiency struggle to meet ever-tighter target specifications due to the high temperature sensitivity of the alloy compositions and doping levels. The curvature effect becomes even more important for growths on larger-diameter wafers, which is also one of the approaches for reducing the LED costs through back-end fabrication efficiency improvements. Thus, it is very critical to understand the physics affecting wafer curvature and how to minimize it in order to achieve optimal deposition uniformity and yield.

It is well-known that during thin film deposition, the wafer bows due to an intrinsic temperature gradient across the wafer thickness, lattice mismatch (tensile strain) that occurs between the substrate and the film, as well as from thermal expansion mismatch between the film and the substrate. This study focuses on the effect of process conditions, such as growth pressure, rotation rate, gas ambient, total flow rates, and gas inlet temperature, on wafer curvature induced by temperature gradient across the wafer. It will be shown that for transparent substrates such as sapphire, the wafer curvature is mostly dependent upon convective cooling above the wafer surface. A universal equation is derived from dimensionless Nusselt (Nu), Reynolds (Re) and Prandtl (Pr) numbers that can predict wafer curvature for a given process condition and wafer geometry. Predicted results from extensive thermal and flow modeling of various process conditions have shown good agreement with in-situ wafer curvature measurements taken during growth.

It will be demonstrated that convective cooling from the process conditions also defines the wafer-to-carrier temperature difference for a given carrier design. This is another important factor that can adversely affect the yield due to the thermal diffusion effects. The derived equation can be also used to predict relative wafer temperature changes for different process parameters, and has been confirmed by comparison with experimental data.

Differences between sapphire and silicon wafers curvature have additionally been explored. The study is aimed to help understanding how to optimize process conditions and wafer carrier design to maximize yield and optimize film thickness uniformity during MOCVD growth within vertical rotating disc reactors.

12:00 Oral

Growth and characterizations of nonpolar InN epitaxial film on LiGaO2 substrate by halide vapor phase epitaxy

Chu-An Li[1], ChenLong Chen[1], Da-Ren Hang[1], Li-Wei Tu[2], Chun-Yu Lee[1], Mitch Chou[1]

1. *Department of Materials and Optoelectronic Science, National Sun Yat-sen University, Kaohsiung 80424, Taiwan* **2.** *Department of Physics, National Sun Yat-sen University, Kaohsiung 80424, Taiwan*

e-mail: d983100006@student.nsysu.edu.tw

Growth and characterization of non-polar InN epitaxial films grown on β-LiGaO2 (100), (010) substrates by halide vapor phase epitaxy (HVPE) is presented here. InCl3 and NH3 are the source materials. InN is a promising material for optoelectronic devices because of its small effective mass, high electron drift velocity and small band gap (0.7eV). However, it is difficult to grow InN material with good quality because of its high dissociation pressure and poor thermal stability. Most of InN epitaxial films are grown on c-plane sapphire substrate, and it will be along the polar wurtzite c-plane orientation [1-3]. However, there are strong spontaneous and piezoelectric polarization-induced electric fields in III-Nitride heterostructures grown along c-axis [4]. It leads to a strong surface electron accumulation, which impedes the development in p-type InN [5]. One of the solutions to solve these problems is to grow InN films in nonpolar directions, such as m-plane (10-10), a-plane (11-20). We propose that LiGaO2 (LGO) single crystal substrate might be a potential substrate for the growth of nonpolar InN material. LiGaO2 has an orthorhombic structure with the lattice parameters of a = 5.402, b = 6.372, c = 5.007Å. X-ray diffraction pattern shows that as-grown InN films on LiGaO2 (100) and (010) are in non-polar m-plane (10-10) (Fig. 1) and a-plane (11-20) (Fig. 2) respectively. For (10-10) InN // (100) LGO, the lattice mismatch is 13.8%, while that for (11-20) InN // (010) LGO is 13.8%. Fig. 3 and Fig. 4 show the top view SEM images of InN films grown on (100) and (010) LGO substrates. To our understanding, (100) and (010) β-LiGaO2 substrates have not been used to the heteroepitaxy growth of non-polar InN growth yet. More details will be presented in the conference.

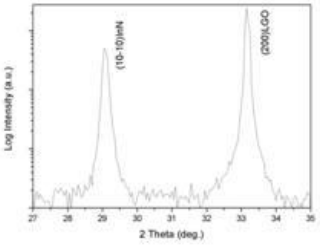

Fig.1 The θ–2θ XRD pattern of InN film on (100) LGO substrate.

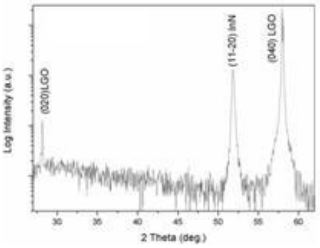

Fig.2 The θ–2θ XRD pattern of InN film on (010) LGO substrate.

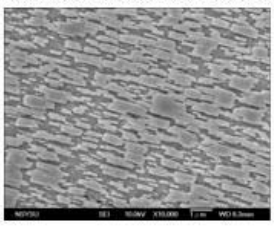

Fig. 3 The top view SEM image of InN film grown on (100) LGO substrate.

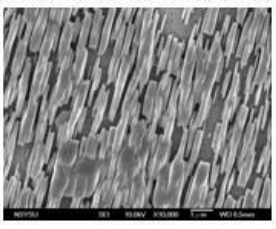

Fig. 4 The top view SEM image of InN film grown on (010) LGO substrate.

References

[1] Y. Kumagai et al., J. Cryst. Growth. 300(2007)57.

[2] Y. Sato et al., J. Cryst. Growth. 144(1994)15.

[3] G. Koblmüller et al., Appl. Phys. Lett. 93(2008)171902.

[4] X.L. Zhu et al. J. Cryst. Growth. 310(2008)3726.

[5] Ching-Lien Hsiao et al. J. Applied Physics. 107(2010)073502.

12:15 Oral

The epitaxial growth of Ge/Si structures on SiGe/Si(001) strain-relaxed buffers: transition from planar to island growth mode

Alexey V. Novikov[1], Mihail V. Shaleev[1], Dmitrij V. Yurasov[1], Dmitry N. Lobanov[1], Zaharij F. Krasilnik[1], Oleg A. Kuznetsov[2], Jean-Michel Hartmann[3]

1. *Institute for Physics of Microstructures Russian Academy of Sciences (IPM RAS), GSP-105, Nizhny Novgorod 603950, Russian Federation* **2.** *Nizhny Novgorod State University, Nizhny Novgorod 603950, Russian Federation* **3.** *CEA (LETI), 17 rue des Martyrs, Grenoble 38054, France*

e-mail: anov@ipm.sci-nnov.ru

The SiGe/Si(001) strain relaxed buffers can be used as templates for fabrication of various electronic and optoelectronic devices [1-4]. Control of strain in different layers of the structure grown on relaxed buffer provides significant bandgap engineering freedom and clears the way for fabrication of strain-compensated superlattices. Formation of structures on relaxed SiGe buffer requires an understanding of features of their growth mechanism. In particular, the transition from planar to island growth mode has to be known exactly for different growth conditions. In this paper features of the 2D-3D growth mode transition for Ge/Si structures fabricated on SiGe/Si(001) relaxed buffers are studied. The influence of Ge content in buffers and of strain in different layers on the critical thickness of 2D growth of Ge film is investigated.

$Si_{1-x}Ge_x$/Si(001) linearly graded relaxed buffers with Ge content up to 40% fabricated both by atmospheric and reduced pressure chemical vapor deposition were used as artificial substrates. Chemical-mechanical polishing (CMP) of grown buffer was used in order to reduce their surface roughness. The threading dislocation density in all SiGe relaxed buffer was less than 10^6 cm^{-2}. Investigated SiGe structures were grown by solid source MBE at 6500C on such relaxed buffers. Determination of the critical thickness of 2D growth of Ge film (h_c) was performed *in situ* using reflection high electron energy diffraction (RHEED) and *ex situ* by atomic-force microscopy (AFM). Deposition of the Ge film was interrupted immediately after the change of RHEED picture from "streaked" to "spotty," which indicates the 2D-3D transition.

At first sight, h_c should be higher for pure Ge growth on SiGe relaxed buffer as compared with growth on Si(001) due to the smaller lattice mismatch between the deposited film and the substrate. However, the experimental investigations have demonstrated unexpected results that values of h_c for Ge/SiGe growth are smaller than in the case of Ge/Si(001) growth under the same conditions (same temperature and growth rate) (fig. 1). Moreover h_c for Ge growth on SiGe buffer demonstrates a rather weak dependence on the composition of buffers and, consequently, on the lattice mismatch [5]. The decrease of critical thickness is related with Ge segregation and higher roughness of SiGe buffers in comparison with Si(001) substrates. According to the calculation Ge segregation during the MBE growth of unstrained SiGe layer leads to accumulation of approximately 0.8-0.9 ML (1 monolayer (ML)=0.136 nm) of Ge on the surface. As a result, the experimental value of h_c determined by RHEED during growth of pure Ge on relaxed buffer should be 0.8-0.9 ML smaller than the actual amount of Ge on the surface. AFM analysis of SiGe buffers revealed that, in spite of usage of CMP the surface roughness of the SiGe buffers was 2-3 times higher than that of Si(001) substrates. An increase in the surface roughness may also occur during the MBE growth of an unstrained SiGe layer on top of the relaxed buffer prior to Ge deposition [6]. In the Si/Ge system, a gradual roughening of the growing film surface may cause island formation [7]. The larger value of surface roughness in the case of direct deposition of Ge on SiGe relaxed buffer could be one of the reasons for the shift of the 2D-3D transition point to lower amounts of deposited Ge. The larger surface roughness of buffer with higher Ge content would then counter-balance the lower lattice mismatch between pure Ge and that buffer, resulting in a weak dependence of h_c on buffer composition (Fig. 1b).

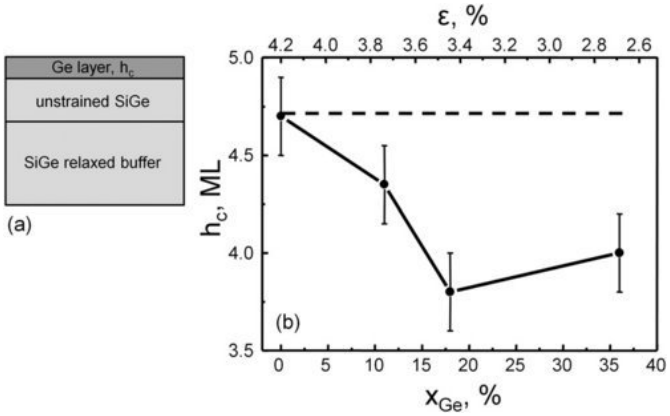

Fig. 1. a) - schematic view of the structures for investigation of the 2D-3D growth mode transition for direct Ge deposition on the SiGe/Si(001) relaxed buffer. b) - dependence of h_c on the Ge content in SiGe buffer (bottom scale) and lattice mismatch (top scale) for Ge deposition on SiGe buffer. Dashed line corresponds to the h_c value for Ge deposition on Si(001) substrates.

It was obtained that h_c of Ge film strongly depends on the thickness of tensile strained Si (sSi) layer deposited on the SiGe buffer before Ge growth (fig. 2). The value of h_c is increased with the increase of sSi layer thickness and in the case of growth of Ge on pre-deposited sSi layers with thickness > 2 nm the critical thickness of 2D Ge growth is larger than in the case of growth of Ge on Si(001) substrates (fig. 2). The distinct dependence of h_c on buffer composition is demonstrated in such structures.

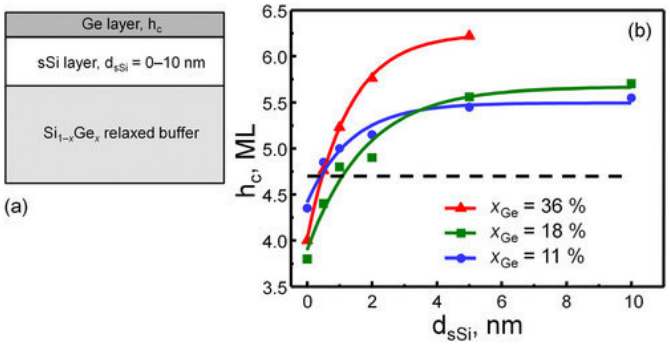

Fig. 2. a) - schematic view of the structures used for investigation of the 2D-3D growth mode transition for Ge growth on pre-deposited sSi layers. b) - dependences of h_c on sSi layer thickness for the structures with different SiGe buffer composition. Dashed line corresponds to h_c for Ge/Si(001) growth. Solid lines are guides for the eye.

The obtained experimental results for Ge growth on sSi layers can be also explained by the Ge segregation and dependence of surface roughness on the sign and value of strain of layers grown on SiGe relaxed buffer [5]. On the one hand, the deposition of sSi layer and the increase of its thickness results in decrease of amount of Ge accumulated on the surface due to segregation. On the other hand, the deposition of thin tensile-strained Si layers on SiGe relaxed buffer indeed leads to gradual surface smoothing [8]. Both these factors lead to increase of the critical thickness of 2D growth of Ge with the increase of sSi layer thickness (fig. 2). It should be noted that for the sake of generality, the relaxed buffers fabricated by different methods were used in all experiments described above. Therefore, the obtained results cannot be connected with some technological features of the employed buffers.

This work was supported by RFBR (grant # 13-02-01006-a), Scholarship for young scientists of the President of Russian Federation and programs of the Russian Academy of Sciences.

References:

1. M.L. Lee, E.A. Fitzgerald, M.T. Bulsara, M.T. Currie, and A. Lochtefeld. J. Appl. Phys., 97, 011101 (2005).

2. S. Tsujino, C.V. Falub, E. Müller, M. Scheinert, L. Diehl, U. Gennser, T. Fromherz, A. Borak, H. Sigg, D. Grützmacher, Y. Campidelli, O. Kermarrec, and D. Bensahel. Appl. Phys. Lett., 84, 2829 (2004).

3. Yu-Hsuan Kuo, Yong Kyu Lee, Yangsi Ge, Shen Ren, Jonathan E. Roth, Theodore I. Kamins, David A. B. Miller & James S. Harris, Nature 437, 1334-1336 (2005).

4. M. d'Avezac, Jun-Wei Luo, T. Chanier, A. Zunger, Phys. Rev. Lett. 108, 027401 (2012).

5. M.V. Shaleev, A.V. Novikov, D.V. Yurasov, J.M. Hartmann, O.A. Kuznetsov, D.N. Lobanov, Z.F. Krasilnik, Appl. Phys. Lett. **101**, 151601 (2012).

6. K. Sawano, S. Koh, Y. Shiraki, N. Usami, and K. Nakagawa, Appl. Phys. Lett. 83, 4339 (2003).

7. J. Tersoff, B. J. Spencer, A. Rastelli, and H. von K€anel, Phys. Rev. Lett. 89, 196104 (2002).

8. Y. Bogumilowicz, J. M. Hartmann, N. Cherkashin, A. Claverie, G. Rolland, and T. Billon, Mater. Sci. Eng.: B 124–125, 113 (2005).

12:30 Oral

Growth of ordered Ge nanoislands on Si surface patterned by ion irradiation

Zhanna V. Smagina[1], Anatolii V. Dvurechenskii[1,2], Alexey V. Nenashev[1,2], Pavel L. Novikov[1,2], Vladimir A. Zinoviev[1], Polina A. Kuchinskaya[1]

1. *Institute of Semiconductor Physics SB RAS, Lavrentjeva 13, Novosibirsk 630090, Russian Federation* **2.** *Novosibirsk State University (NSU), Pirogov 2, Novosibirsk 630090, Russian Federation*

e-mail: smagina@isp.nsc.ru

Self-organizing growth of Ge quantum dots (QDs) on Si carried out using molecular-beam epitaxy is characterized by the random process of Ge nanoisland nucleation that leads to disordered positions of QDs in plane of growth and QDs size dispersion. In this work the experimental and theoretical studies of the growth of dense space-ordered arrays of Ge QDs on prepatterned Si substrates, obtained by ion irradiation/plasma etching through specially prepared masks on Si surface are carried out. The formation of heterostructures with regular surface relief method is developed which is based on the ion irradiation of surface through masks formed by lithography to produce sites for favorable nucleation of nanocrystals during heteroepitaxy. The technology of pre-patterned substrate creation is based on the effect of Si etching sensitive to disordered structure in comparison with crystalline Si. It is developed with using nanoimprint/electron-beam lithography. The optimal conditions of ion irradiation are determined. Two regimes of Ge island growth on pre-patterned Si surface are observed: the growth nearby and inside the nucleation sites. Method of multilayer nanocluster structures growth on pre-patterned substrates is developed. It provides the formation of three-dimensional (3D) crystals of quantum dots in a crystalline matrix. By Raman scattering, high resolution electron microscopy and photoluminescense (PL) the chemical content, structure and electronic properties of the grown structures are studied. Intensity of PL of structures with space-arranged islands is found to be three times greater than that in case of randomly located islands.

The experimental results observed have been studied by molecular dynamics (MD) and Monte-Carlo simulation (MC). Microscopic mechanism of atom diffusion on pre-patterned surface is studied by MD (for the cases of pits and grooves). Energy surface of Ge/Si on pre-patterned Si substrate is mapped out. The activation energy and the main paths of surface diffusion of Ge on the pits walls are determined. It is shown that formation of 3D islands on defect-free prepatterned surface at the conditions close to experimental ones must occur mainly on the bottoms of the pits and inside the grooves.

The way of taking an account of strain effects in Monte Carlo simulation of epitaxial growth is suggested. Simulation of growth of multilayered Ge/Si structures is carried out. It is shown that areas of local surface extension above the ion-irradiation-induced clusters of interstitials become favourable sites for nucleation of Ge 3D islands. It is shown theoretically and experimentally, that in order to obtain high density of Ge islands in each next Ge layer of multilayered structures formed under ion-beam irradiation it is necessary to introduce interstitials, which play the main role in nucleation of 3D islands. The MC modeling reproduces the stacking effect in multilayered structures with Ge quantum dots.

12:45 Oral

Synthesis of defect-mitigating tunable dielectric materials by MBE

C. H. Lee[1,2], N. D. Orloff[3,4], T. Birol[5], Y. Zhu[5], V. Goian[6], R. Haislmaier[2], E. Vlahos[2], J. A. Mundy[5], Y. Nie[5], M. D. Biegalski[7], J. Zhang[1], M. Bernhagen[8], N. A. Benedek[9], Y. Kim[5], J. D. Brock[5], R. Uecker[8], X. X. Xi[10], L. F. Kourkoutis[5,11], V. Gopalan[2], D. Nuzhnyy[6], S. Kamba[6], D. A. Muller[5,11], I. Takeuchi[12], J. C. Booth[3], C. J. Fennie[5], Darrell G. Schlom[1,11]

1. *Cornell University, Department of Materials Science and Engineering, Ithaca, NY 14853-1501, United States* **2.** *Department of Materials Science and Engineering, Pennsylvania State University, Pittsburgh, PA 15131, United States* **3.** *National Institute of Standards and Technology (NIST), 100 Bureau Drive, MS-8362, Gaithersburg, Maryland 20899, United States* **4.** *Department of Physics, University of Maryland, Washington, DC 20742, United States* **5.** *School of Applied and Engineering Physics, Cornell University, Washington, DC 20037, United States* **6.** *Czech Academy of Sciences, Institute of Physics, Na Slovance 2, Prague 182-21, Czech Republic* **7.** *Center for Nanophase Materials Sciences, Oak Ridge National Laboratory, Washington, DC 20024, United States* **8.** *Leibniz Institute for Crystal Growth (IKZ), Max-Born-Str 2, Berlin 12489, Germany* **9.** *Materials Science and Engineering Program, The University of Texas at Austin, Austin, TX 78712, United States* **10.** *Temple University, Department of Physics, Philadelphia 19122, United States* **11.** *Kavli Institute at Cornell for Nanoscale Science, Ithaca, NY 14853, United States* **12.** *Department of Materials Science and Engineering, University of Maryland, Washington, DC 20742, United States*

e-mail: schlom@cornell.edu

The miniaturization and integration of frequency-agile microwave circuits—electronically-tunable filters, resonators, phase shifters and more—with microelectronics offers tantalizing device possibilities, yet requires thin films whose dielectric constant at GHz frequencies can be tuned by applying a quasi-static electric field. Appropriate systems, e.g., $Ba_xSr_{1-x}TiO_3$, have a paraelectric-to-ferroelectric transition just below ambient temperature, providing high tunability. Unfortunately such films suffer significant losses arising from defects. Recognizing that progress is stymied by dielectric loss, we start with a system with exceptionally low loss—$Sr_{n+1}Ti_nO_{3n+1}$ phases—where $(SrO)_2$ crystallographic shear planes provide an alternative to point defect formation for accommodating non-stoichiometry. We report the experimental realization of a highly tunable ground state arising from the emergence of a local ferroelectric instability in biaxially strained $Sr_{n+1}Ti_nO_{3n+1}$ phases with $n \geq 3$ at frequencies up to 120 GHz. In contrast to traditional methods of modifying ferroelectrics—doping or strain—in this rather unique system increasing the separation between the $(SrO)_2$ planes bolsters the local ferroelectric instability. This new control parameter, n, can be exploited to achieve a figure of merit at room temperature that surpasses all known tunable microwave dielectrics.

Lunch (JCG Editors meeting)

Monday afternoon, 12 August, 13:00

MoO2

G10: Thin film and epitaxial growth
Monday afternoon, 12 August, 15:00
Room C, Auditorium Maximum

15:00 Invited oral

In situ x-ray studies of epitaxial growth by MOVPE

Carol Thompson[1], Edith Perret[2], Matthew J. Highland[2], Peter Zapol[2], Stephen K. Streiffer[2], Brian Stephenson[2], Paul H. Fuoss[2]

1. *Northern Illinois University (NIU), De Kalb, Il 60115, United States* **2.** *Argonne National Laboratory (ANL), 9700 C. Cass Ave., Argonne, IL 60439, United States*

e-mail: cthompson@niu.edu

In situ, time-resolved techniques can provide valuable insights into the complex interplay of mechanisms during materials synthesis and processing. Our approach has been to measure the evolution of surface structure and morphology at the atomic scale in real-time during metal-organic vapor phase epitaxy (MOVPE) by using grazing incidence x-ray scattering and x-ray fluorescence. Our vertical-flow MOVPE chamber at the Advanced Photon Source at Argonne National Laboratory is mounted on a 'z-axis' surface diffractometer designed specifically for this purpose. We use ~30 keV x-rays from the Advanced Photon Source to penetrate the quartz chamber walls and the reactive vapor phase. By changing the chambers and associated gas handling systems, we have studied MOVPE of oxides (e.g., $PbTiO_3$) and III-V semiconductors.

These x-ray based techniques combine the ability of x-rays to penetrate chamber walls and realistic complex reactive environments, with the sensitivity of surface scattering techniques to quantify atomic and nanoscale structures during growth. In this presentation, I will discuss results from our III-nitride program; outlining both past and present examples from our in situ scattering studies of InN, GaN, and InGaN growth on GaN. I will describe the strengths and weaknesses of x-ray techniques for studying MOVPE processes and materials synthesis. X-ray experiments were carried out at beamline 12-ID-D of the Advanced Photon Source. Work supported by the U.S. Department of Energy under Contract DE-AC02-06CH11357.

15:30 Oral

Influence of CdS deposition technique on CdS/CdTe thin films

Sandra Rubio[1], Jose Luis Plaza[2], Ernesto Dieguez

1. *Laboratorio de crecimiento de cristales, Dpto Fisica de materiales, Facultad de ciencias, UAM (LCC, UAM), cantoblanco, Madrid, Madrid 28049, Spain* **2.** *Universidad Autonoma de Madrid (UAM), Cantoblanco, Madrid 28034, Spain*

e-mail: s.rubio@uam.es

The use of CdTe solar cells thin films is of great interest due to the fact that their band gap is optimum for efficient photo-conversion. Recent publications have shown that 12% efficiencies have been obtained using the Closed Space Sublimation (CSS) technique [1]. In this way the use of SiC electrical heating elements is a very promising approach [2] due to the fact that CdTe solar cells obtained by this way have high reproducibility and low manufacturing cost. The deposition parameters of CdTe layers and their influence on the structural and morphological properties have been studied by Luschitz et al. [3].

CdS/CdTe solar cells were developed in superstrate configuration on commercial TCO/glass substrates using Fluorine doped Tin Oxide (FTO) as the front contact.

The CdS window layer was deposited on FTO substrates by two different techniques: Chemical Bath Deposition (CBD), and CSS using SiC electrical heating elements. The morphology, crystalline structure and composition of the CdS thin films were analyzed by SEM, AFM, XRD and EDX. The results show that the CdS film obtained by CSS has better crystallography structure for 002 orientation, while the one prepared by CBD present a worse structure.

The CdTe absorber layer was deposited by CSS on top of the CdS window layer, using the same deposition parameters for all samples. The properties of CdS/CdTe thin films will be studied in order to analyze the influence of the deposition technique in the quality of the CdS window layer.

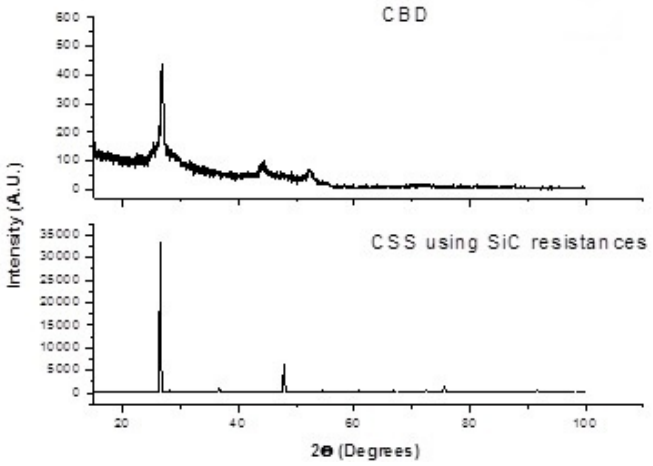

Fig 1: X-Ray Diffraction Patterns at Gracing Incidence (Angle = 0.5º) from CdS deposited by CBD and CSS

[1] J. Schaffner et al, Journal of applied phisics, 110, 064508, (2011).

[2] J. L. Plaza et al, CrystEngComm, 15, 2314-2318, (2013).

[3] J. Luschitz et al. Thin Solid Films 517, 2125-2131, (2009).

15:45 Oral

CdS and CdTe films grown by close space vapour sublimation using resistive heaters for solar cell applications: Experimental and numerical analysis

Jose Luis Plaza, Sandra Rubio, Ernesto Dieguez

Laboratorio de crecimiento de cristales, Dpto Fisica de materiales, Facultad de ciencias, UAM (LCC, UAM), cantoblanco, Madrid, Madrid 28049, Spain

e-mail: joseluis.plaza@uam.es

Thin Film Photovoltaic Cells (TFPV) with a reduced peak efficiency of 11%, represent nearly 8% world share of the actual solar cell market. This figure will be near too dramatic in the nearest future, because it seems it will reach the 20% of the market in the next few years, due to the scarcity of Si and the cost-cutting potential that many people perceive in TF technology [1]. For these reasons, a strong effort must be carried out in the research and development of TFPV experimental approaches which do not use Si as the matrix element.

Very recently Schaffner et al. have demonstrated 12% efficiency in CdTe/CdS solar cells developed by using low temperature close space sublimation (CSS) [2]. Our group has also recently demonstrated the feasibility to produce CSS-grown CdTe and CdS films for solar cell applications by using resistive heaters [3].

In this work we analyse both experimentally and numerically the growth of CdTe/CdS films by using Close Space Sublimation Transport (CSS) with resistive heaters. A photograph of two CdS and CdTe films are shown in Fig. 1.

The structure and composition of the films are studied as a function of different growth parameters. The properties of both CdTe and CdS films are studied by using High Resolution Secondary Electron Microscopy (HR-SEM), Energy Dispersive X-ray Analysis (EDX), optical absorption and X-Ray Diffraction. Numerical simulations have been performed in order to obtain information about the thermal field during the growth process for different boat materials and dimensions. These numerical results have been correlated to the structural properties of the films.

The analysis from SEM-EDX show good stoichiometry of the films, both in the case of CdS (S: 49.48 % at., 50.52 % at.), and CdTe films (51.29 % at., 48.71 % at.). SEM images on both CdTe and CdS films prepared in this work are shown in Figure 2.

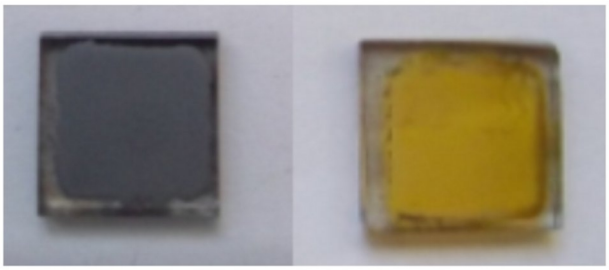

(a) (b)

Figure 1. (a) Photograph of a final glass/FTO/CdS/CdTe solar cell fabricated by using Close Space Sublimation. (b) Picture of the CdS window film deposited underneath CdTe.

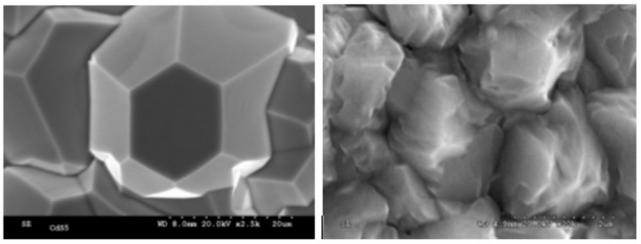

(a) (b)

Figure 2. SEM images taken from (a) CdS and (b) CdTe films prepared in this work by Close Space Sublimation.

References

[1] J .Heup, New Energy 1 (2009) 72.

[2] J. Schaffner, M. Motzko, A. Tueschen, A. Swirschuk, H.J. Schimper, A. Klein, T. Modes, O. Zywitzki, and Wolfram Jaegermann, J. Appl. Phys. 110 (2011) 064508.

[3] J. L. Plaza, O. Martínez, S. Rubio, V. Hortelano and E. Diéguez, CrystEngComm, 2013, 15, 2314–2318.

16:00 Oral

Low Temperature Amorphous Silicon Carbide Thin Film Formation Process on Aluminum Surface Using Monomethylsilane Gas and Trichlorosilane Gas

Hitoshi Habuka, Masaki Tsuji, Azumi Hirooka

Yokohama National University (YNU), 79-5 Tokiwadai Hodogaya, Yokohama 240-8501, Japan

e-mail: habuka1@ynu.ac.jp

The low-temperature chemical vapor deposition process of depositing silicon carbide on an aluminum surface was developed. In order to prepare the reactive substrate surface, a silicon interlayer containing silicon dimers at its surface was formed using trichlorosilane gas at 600 ^{o}C. After the reactive surface preparation, the silicon carbide thin film was formed at room temperature using monomethylsilane gas. The silicon carbide film was amorphous and about 5-nm thick. Silicon, carbon and silicon-carbon bond in the obtained film were detected by time of flight secondary ion mass spectrometry and energy dispersive X-ray spectrometry. Thus, the silicon carbide film formation is possible on an aluminum surface.

1. Introduction

Silicon carbide (SiC) is a suitable surface coating material, because the silicon carbide film is robust even in a harsh environment and at high temperatures. The typical application is the coating of the carbon susceptor used in a chemical vapor deposition (CVD) reactor [1]. However, one of the problems of the silicon carbide material is the very high temperature necessary for its film deposition [2-4]. Because the temperatures for depositing the silicon carbide film is often higher than the melting point of various useful metals, such as aluminum, the silicon carbide coating has been limited to only a few materials, such as carbon and silicon [4].

For achieving deposition on other metals, the low temperature amorphous silicon carbide film formation technology using monomethylsilane (MMS) gas [5-10] is expected to be applicable and hopeful. This technology consists of two steps, that is, (A) the reactive surface preparation, and (B) the silicon carbide film formation from monomethylsilane gas at room temperature. In order to apply this technology to various metal surfaces, the key issue is the development of a reactive surface preparation process at low temperatures.

In our previous studies [5-7, 10], the reactive surface has been prepared using the following three processes:

(I) The hydrogen annealing of a silicon surface at high temperatures, such as 1100 ^{o}C, and cooling to room temperature in ambient hydrogen [5, 6] in order to prepare the hydrogen-terminated silicon surface containing silicon dimers.

(II) The silicon thin film (silicon interlayer) formation at moderate temperatures, such as several hundred degrees, followed by cooling to room temperature in ambient hydrogen [7, SCT] in order to produce the surface condition the same as (I).

(III) The dangling bond formation on the substrate material surface by surface cleaning using an argon plasma at room temperature [8].

In our previous study [10], Process (II) was shown to be possible on an aluminum surface. However, the characteristics of the silicon carbide film and the silicon interlayer should be studied further.

In this study, the low-temperature process of amorphous silicon carbide film deposition on an aluminum substrate was performed. The quality of the silicon carbide film and the silicon interlayer was evaluated using Time-of-Flight Secondary Ion Mass Spectrometry (ToF-SIMS), Transmission Electron Microscope (TEM), and Energy Dispersive X-ray spectrometry (EDX).

2. Experimental

The film formation process used in this study is shown in Fig. 1. The silicon thin film is formed at 600 ^{o}C on the aluminum surface using trichlorosilane gas, as shown in Fig. 1 (b). The substrate is then cooled to room temperature in ambient hydrogen. Because the silicon interlayer surface has silicon dimers as shown in Figs. 1 (b) and (c), the amorphous silicon carbide film can be produced using the monomethylsilane gas, as shown in Figs. 1 (c) and (d).

The substrates used in this study were aluminum plates, which are low cost materials prepared for various handicrafts. The dimensions of the samples were 10-mm wide and 10-mm long, cut from a large 0.1 – 0.3-mm-thick plate. Due to their sufficiently long exposure to air, the surfaces of these plates were covered with a native oxide film. The sample surface was simply cleaned by ethanol without any additional wet cleaning. Thus, the native oxide film was not removed.

In order to obtain the silicon interlayer by the CVD method, the horizontal reactor shown in Fig. 2 was used, similar to those in our previous studies [5-7, 10]. This reactor consisted of a gas supply system, a quartz chamber and infrared lamps. The height and the width of the quartz chamber were 10 mm and 40 mm, respectively.

The gas supply system can introduce gases of hydrogen, nitrogen, trichlorosilane and monomethylsilane. Hydrogen gas is the carrier gas in the reactor used at 1 x 10^5 Pa and typically at the flow rate of 1 slm. The trichlorosilane and monomethylsilane gases diluted by hydrogen gas were used for the deposition of the silicon and silicon carbide, respectively.

Fig. 3 shows the steps for producing the silicon interlayer and the silicon carbide film. During Step (A), the silicon thin film was produced using trichlorosilane gas at 0.06 slm for 10 min at 600 ^{o}C. This film was cooled to room temperature in ambient hydrogen. In Step (B), the silicon carbide film was formed at room temperature using monomethylsilane gas at 0.1 slm for 7 min.

In order to obtain information about the chemical bonds in the very thin silicon carbide film formed on the silicon surface, a Time-of-Flight Secondary Ion Mass Spectrometer (ToF-SIMS) (TOF-SIMS300, ION-TOF GmbH, Münster, Germany) was used. The crystalline quality was evaluated using a Transmission Electron Microscope (TEM) (H-9000NAR, Hitachi High Technologies, Tokyo). Simultaneously, a energy dispersive X-ray spectrometer (EDX) (HD2700., Hitachi High Technologies, Tokyo) was used for evaluating the composition of the silicon, carbon and aluminum.

The ToF-SIMS, TEM and EDX were *ex situ* performed at the Foundation of Promotion of Material Science and Technology of Japan (Tokyo).

3. Results andDiscussion

The silicon carbide film deposition at room temperature was performed after the silicon interlayer formation at 600 ^{o}C followed by the cooling in ambient hydrogen in order to produce the silicon surface having silicon dimers as the reactive surface. This process was performed using the reactor shown in Fig. 2 and the process shown in Fig. 3. Fig. 4 shows the depth profiles of Al_2O_3, SiC_2, C_3, Si_4 and Si_2O_5 in the film obtained following the process shown in Fig. 3 on the aluminum substrate. These profiles were obtained by ToF-SIMS.

The species deeper than 1 nm was attributed to aluminum oxide. Si_4 has a peak at the depth of 0.8 nm from the surface, because the silicon thin film was in the range of 0.4 – 1 nm depth. Based on the ToF-SIMS profile, the silicon carbide film corresponds to the peak of SiC2 at the depth of 0.3 nm. Additionally, the C_3 peak at about 0.2 nm from the

surface was found; this position was the same as that of the silicon oxide, Si_2O_5. Although the C_3 peak might be mainly assigned to silicon carbide, the C_3 and Si_2O_5 peaks could be the by-product of the monomethylsilane oxidation. A part of the chemisorbed monomethylsilane still remaining in the intermediate form, as shown in Fig, 1 (d), was oxidized to form silicon oxide and a carbon layer at the surface.

In order to evaluate the film quality including the interface, a TEM image was taken and shown in Fig. 5. The silicon interlayer was intentionally formed thick by means of a longer deposition in order to clearly observe the stacked layers and their interface. Fig. 5 (a) shows the overall view of the obtained film. At the bottom of Fig. 5 (a), there was the aluminum substrate. The thin and low contrast layer on the aluminum substrate was aluminum oxide. The thick silicon interlayer existed on the aluminum oxide layer. The silicon carbide film existed on the silicon interlayer.

Because the original surface of the aluminum substrate was not flat, each interface consistently had hills and valleys. This TEM image additionally showed that that the interfaces between the aluminum oxide/silicon interlayer and silicon interlayer/silicon carbide were abrupt without any void.

Fig. 5 (b) shows the high resolution image of the silicon carbide and the silicon interlayer. In this figure, each spot indicates atoms. The upper half of this figure shows the non-periodic arrangement of the silicon and carbon atoms. This shows that the obtained silicon carbide film was amorphous, similar to our previous study [8].

Fig. 5 (b) includes the information in the wider region than that in our previous study [10] in order to evaluate the quality of the silicon interlayer, such as the existence of grains. There were periodic spots in the lower left half of Fig. 5 (b), but non-periodic spots in the lower right half of this figure. This shows the co-existence of silicon grains having various orientations formed on the aluminum oxide surface. Because this figure also shows that there was no void along the grain boundary, the silicon thin film formation on the aluminum oxide surface is possible without a fatal defect.

The existence of silicon and carbon was evaluated using the EDX at four points in Fig. 5 (b). Points #1 and #2 are in the upper half and lower half region, respectively, of the amorphous silicon carbide film. Point #3 is the silicon interlayer showing a non-periodic image; Point #4 is the silicon interlayer showing a non-periodic image.

Figs. 6 (a) and (b) show the existence of silicon and carbon at Points #1 and #2, respectively. This indicates that the film is silicon carbide. A considerable amount of oxygen indicates the oxidation of the intermediate species remaining after the deposition. This result is consistent with the existence of Si_2O_5 in Fig. 4.

In the silicon interlayer, the major element was silicon, as shown in Figs. 6 (c) and (d). A small amount of carbon in these figures is considered to be carbon contamination that occurred during the operation of the TEM and EDX sample preparation. Because the profiles of Figs. 6 (c) and (d) coincided with each other, the different appearance of the high resolution TEM image in the lower half of Fig 5 was due to the crystal grain orientation.

As shown in Figs. 6 (a) and (b), a small amount of aluminum was present in the amorphous silicon carbide film. Because aluminum was not present in the silicon interlayer as shown in Figs. 6 (c) and (d), aluminum was not incorporated during the silicon interlayer formation process at 600 ^{o}C. Taking into account that aluminum chloride is a volatile material [11], and also that the aluminum amount was higher in the lower region of the amorphous silicon carbide film, the aluminum chloride formed and vaporized at the aluminum substrate surface might be adsorbed at the silicon interlayer surface during the cooling process between Steps (A) and (B) in Fig. 3. Following such a process, aluminum might be incorporated in the amorphous silicon carbide film. The aluminum incorporation is considered to correspond to the dark contrast region at the lower position of the amorphous silicon carbide film in Fig. 5 (b).

The low temperature process employing the silicon interlayer as the reactive surface was successful in producing a silicon carbide film on the aluminum surfaces. Because the highest temperature in this process was 600 ^{o}C, the silicon carbide coating process shown in Figs. 1 and 3 is expected to be possible as a low temperature process for silicon carbide coating on aluminum.

4. Conclusions

The thin film formation process of amorphous silicon carbide on an aluminum surface was developed in order to extend the low temperature silicon carbide film formation on various low-melting point materials. In order to produce a surface which was reactive to monomethylsilane gas, the silicon interlayer on the aluminum surface was formed by means of a thin silicon film deposition using trichlorosilane gas at 600 ^{o}C. After cooling to room temperature in ambient hydrogen, the amorphous silicon carbide thin film was formed at room temperature and at atmospheric pressure using monomethylsilane gas. The various evaluation methods showed that the film obtained on the polysilicon interlayer was amorphous and consisted of silicon carbide. A low-temperature amorphous silicon carbide film formation process on an aluminum surface is possible.

References

[1] A. M. Rinaldi and D. Crippa, Silicon Epitaxy (Editor: D. Crippa, D. L. Rode and M. Masi), Chapter 1, P. 1 (2001) Academic Press (San Diego, USA).

[2] T. Kimoto and H. Matsunami, J. Appl. Phys., 75 (1994) 850-859.

[3] R. L. Myers, Y. Shishkin, O. Kordina and S. E. Saddow, J. Cryst. Growth, 285 (2005) 486-490.

[4] S. Kotamraju, B. Krishnan, G. Melnychuk, and Y. Koshka, J. Cryst. Growth, 312 (2010) 645–650.

[5] H. Habuka H. Ohmori and Y. Anndo, Surf. Coat. Tech., 204 (2010) 1432-1437.

[6] H. Habuka, and Y. Ando, J. Electrochem. Soc., 158 (2011) H352-H357.

[7] H. Habuka and Y. Ando, J. Nanosci. Nanotech., 11 (2011) 8374-8377.

[8] H. Habuka, Y. Ando and M. Tsuji, Surf. Coat. Technol., 206 (2011) 1503–1506.

[9] S. Klein, R. Carius, F. Finger, L. Houben, Thin Solid Films 501 (2006) 169-172.

[10] H. Habuka and M. Tsuji, Surf. Coat. Technol., 217 (2013) 88-93.

[11] D. R. Lide, CRC Handbook of Chemistry and Physics, 78th edition, CRC Press Boca Raton, New York(1997-1998).

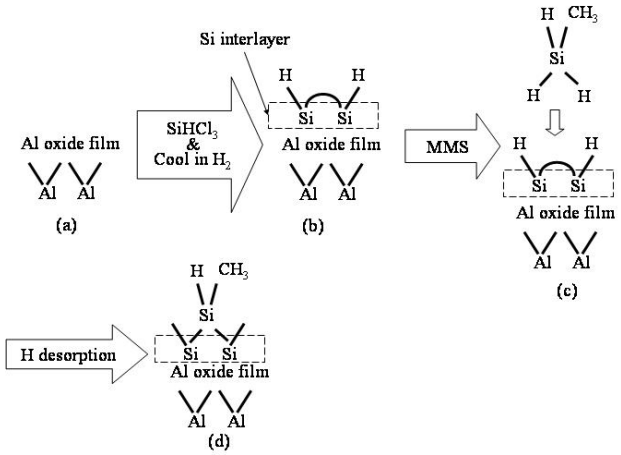

Figure 1 Silicon carbide film deposition process using silicon interlayer (Process (II)).

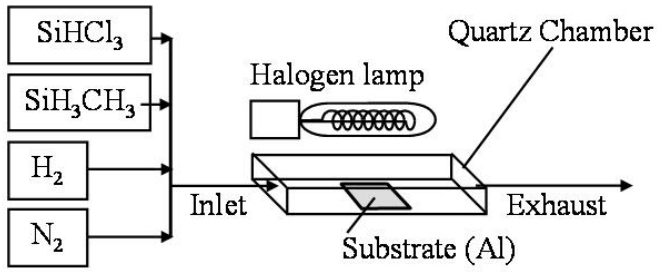

Figure 2 Horizontal cold-wall chemical vapor deposition reactor used for film deposition of silicon and silicon carbide.

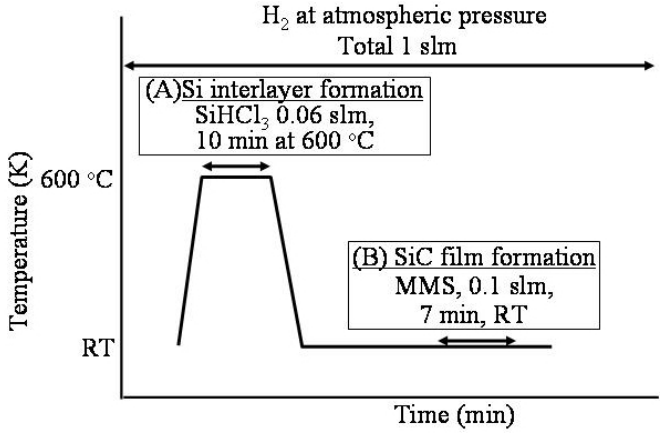

Figure 3 Steps for formation of silicon (silicon interlayer) and amorphous silicon carbide film. Step (A): silicon film formation for 10 min at 600 ^{o}C using trichlorosilane gas at 0.06 slm. Step (B): Amorphous silicon carbide film formation at room temperature using monomethylsilane gas at 0.1 slm for 7 min.

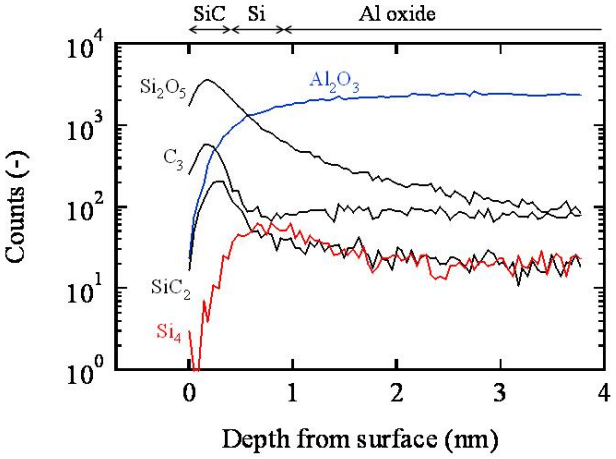

Figure 4 Depth profiles of Al_2O_3, SiC_2, C_3, Si_4 and Si_2O_5 in the film obtained on aluminum substrates measured by ToF-SIMS. Amorphous silicon carbide film deposition was performed after the silicon interlayer formation at 600 ^{o}C and cooling in ambient hydrogen.

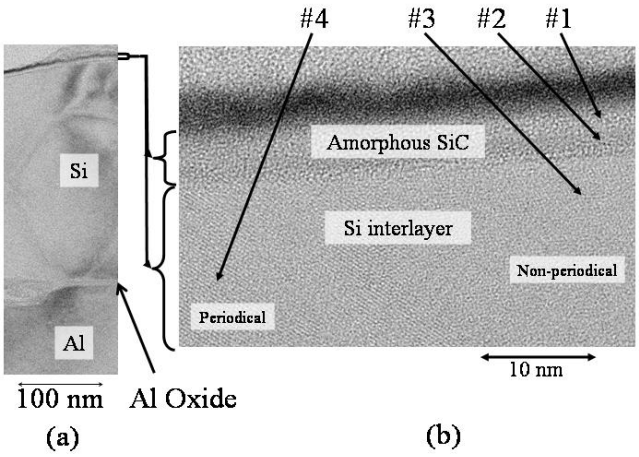

Figure 5 TEM image of the film obtained on aluminum substrates using 6% trichlorosilane gas at 600 ^{o}C and 10 % monomethylsilane gas at room temperature. (a): Overall view of the obtained film consisting of an aluminum substrate, aluminum native oxide, silicon interlayer and silicon carbide film. (b): High resolution image of silicon carbide film and silicon interlayer. EDX was performed at the four points of #1-4.

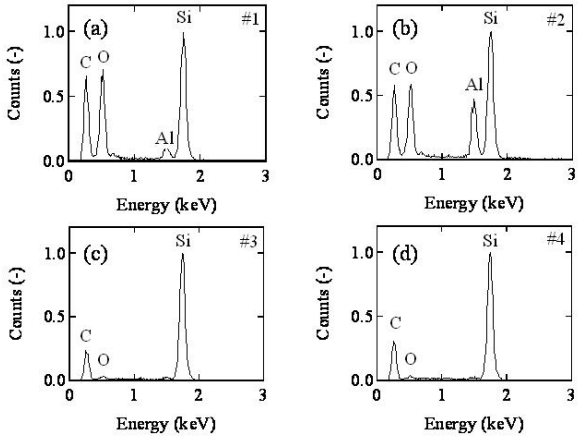

Figure 6 Silicon, carbon, oxygen and aluminum in the silicon carbide film and the silicon interlayer measured by EDX. (a), (b), (c) and (d) are the normalized counts at #1, #2, #3 and #4, respectively, in Fig. 5.

16:15 Oral

Liquid phase epitaxy of rare earth doped $LiYF_4$ layers for the elaboration of compact laser planar waveguides

Florent Starecki, Western Bolanos, Gurvan Brasse, Abdelmjid Benayad, Vivien Menard, Jean-Louis Doualan, Richard Moncorge, Patrice Camy

CIMAP, CNRS-ENSICAEN-CEA-UCBN, 6 Boulevard Maréchal Juin, Caen 14050, France

e-mail: gurvan.brasse@ensicaen.fr

Introduction:

The miniaturization of optical devices generates a growing interest, especially in the laser domain, in order to develop more and more compact photonic devices for their integration in various systems. The targeted applications increase considerably in various domains like the detection of atmospheric pollutants, biomedical applications, Lidar technologies, RGB display or quantum information. Laser planar waveguides have thus been elaborated, especially Tm^{3+} doped or Pr^{3+} doped $LiYF_4$ (YLF) thick layers epitaxially grown on undoped YLF substrates, to get original emissions in the visible domain or in the mid-infrared spectral range.

Description of the experimental process:

Two crystal growth techniques have been used successively to obtain crystalline optical waveguides : the Czochralski technique, first, to synthesize pure $LiYF_4$ substrates, then the liquid phase epitaxy (LPE) technique for the homoepitaxial growth of Tm^{3+} and Pr^{3+} doped $LiYF_4$ monocristalline layers on the substrates.

A fluorination step of the oxides raw materials required for the preparation of the melts at the origin of the substrates and the epilayers, is needed to get pure fluoride precursors. For that purpose, the NH_4HF_2 chemical precursor is used as fluorinating agent and the resulting chemical equation of the reaction is:

$$RE_2O_3 + 6NH_4HF_2 \xrightarrow{\text{Stirring + heating at } 240^\circ C} 2REF_3 + 6NH_4F + 3H_2O\uparrow$$

The so prepared material is then annealed at 650°C during few hours to eliminate the excess of NH_4HF and the residual water.

The bulk crystals obtained by using the Czochralski technique (boules of about 3 cm in diameter and 6 cm long) are cut perpendicularly to the (001) growth axis and prepared in the form of plates with a thickness of about 2 mm and rectangular faces of about 1x3 cm^2 to be used as substrates. Then, the rectangular faces on which the crystal growth occurs during the LPE process are very carefully and finely polished, in order to present a roughness of the order of a few nm and a flatness of few fringes. Such a step is crucial to obtain layers with a good crystalline quality and to limit the internal optical losses as much as possible.

The molar composition of the LPE bath is determined from the phase diagram of the system LiF-YF_3 [1] and is composed as follows: 73% of LiF and 27% of a mixture composed of YF_3 and of a few percents of GdF_3.GdF_3 is used to ensure the necessary refractive index contrast between epitaxial layer and substrate and also because Gd^{3+} ions only absorb light in the near UV, thus in a spectral region which does not interfere with the mid-infrared and visible optical transitions of the Tm^{3+} and Pr^{3+} dopants considered in the present work.

The substrates were thus immerged in the LPE bath at a temperature slightly lower than the saturation temperature, to initiate the epitaxial process, and the growth occurs on both sides of the substrates. The thickness of the layers is a function of the immersion duration and can be varied from a few microns to a hundred of microns. Moreover, the purity of the growth atmosphere, which has to be absolutely oxygen free, is also a key parameter for the crystal growth of fluoride layers. Once the epitaxial layers have been grown with the required thickness, the samples are cooled down to room temperature very slowly to avoid cracks and structural defects. They are then polished on the both faces to remove the residual deposit of LiF and also to adjust the thickness of the guiding layers.

To finalize the preparation of the waveguide samples before testing them in a laser cavity, it was also necessary to polish their input and output faces to have good pump and laser input and output coupling efficiencies and to ensure a good parallelism of the faces, thus optimal lasing conditions.

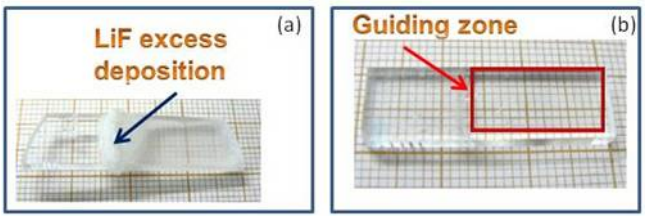

Figure 1: (a) Sample just after the LPE growing process, (b) sample prepared as planar waveguide.

Characterizations of the epitaxial layers and laser performances of the planar waveguides:

The obtained layers were all initially characterized by controlling the nature of the crystallized phase by using X-Ray Diffraction, then by determining the real dopant concentrations in the deposited layers by using absorption spectroscopy and EDX analysis. The refractive index contrast between the layers and the substrates, which is an important parameter for the final laser device, was also measured by using the M-Lines technique.

The planar waveguides were then tested optically to estimate the internal optical losses. Assuming nearly 100% coupling efficiency and subtracting for the Fresnel reflection losses (4%) occurring at the end faces of the waveguides, upper limits for the internal optical losses of 0.64 and 0.80 ± 0.03 dB/cm were obtained for the $LiY_{0.935}Gd_{0.05}Pr_{0.015}F_4$ and $LiY_{0.885}Gd_{0.05}Lu_{0.05}Pr_{0.015}F_4$ layers, and optical losses of 0.11 dB/cm and 0.26 dB/cm were obtained for the $LiY_{0.907}Gd_{0.024}Tm_{0.069}F_4$ and $LiY_{0.887}Gd_{0.024}Tm_{0.089}F_4$ layers, respectively. These losses are thus extremely low, attesting of the excellent crystalline quality of the epitaxial layers.

The good quality of the layers has been confirmed with the laser measurements. We have indeed demonstrated the first epitaxially grown Tm^{3+}-doped crystalline fluoride waveguide laser operating at 1.87 µm with an efficiency of 76% and a record output power of 560 mW [2]. we have also demonstrated, what we believe to be the first epitaxially grown Pr3+-doped fluoride planar waveguide laser operating in the red (639.4 nm) and orange (604.2 nm) spectral range with output powers up to about 25 and 12 mW, respectively [3].

By adjusting the Tm^{3+} and Pr^{3+} ion concentrations in the layers, by adjusting the width and the length of the waveguides to the pump and laser conditions, and by structuring these planar waveguides to form linear waveguides, it is now expected to reach even better laser performance (lower laser threshold and higher overall laser efficiencies), which definitely open the way to the fabrication of compact, integrated, high-power, and highly efficient devices for various applications. More details and results will be given at the conference.

References:

[1] R.E.Thoma, C.F. Weaver, H.A. Friedman, H. Insley, L.A.Harris, H.A. Yakel, Jr, J. Phys. Chem. 65, 1096-1098 (1961)
[2] W. Bolanos, F. Starecki, A. Benayad, G. Brasse, V. Ménard, J.L. Doualan, A. Braud, R. Moncorgé, and P. Camy, Opt. Lett. 37 (19) 4032-4034 (2012)
[3] F. Starecki, W. Bolaños, A. Braud, J.L. Doualan, G. Brasse, A. Benayad, V. Nazabal, B. Xu, R. Moncorgé, and P. Camy, Opt. Lett. 38 (4) 455-457 (2013)

16:30 Oral

Epitaxial growth of molecules and salts on muscovite mica

Wester De Poel[1], G. S. Pintea[2], S. Bozelie[1], J. Münninghoff[1], D. Lensen[1], J. Drnec[2], F. Carla[2], R. Felici[2], P. Mulder[1], J.A.A.W. Elemans[1], W.J.P. van Enckevort[1], A.E. Rowan[1], E. Vlieg[1]

1. *Radboud University Nijmegen, Toernooiveld 1, Nijmegen 6525ED, Netherlands* **2.** *European Synchrotron Radiation Facility (ESRF), Grenoble 38043, France*

e-mail: w.depoel@science.ru.nl

Muscovite mica is a very commonly used material for scientific study because of its atomically flat surface, which is easily prepared by cleavage. To see how flat muscovite mica really is we examined the surface of this crystal using atomic force microscopy (AFM), phase contrast microscopy and surface X-ray diffraction (SXRD). AFM revealed only one step in over 2500 unique measurements of 2.5 by 2.5 micrometer surface areas. This indicates that the occurrence of steps is very rare. Phase contrast optical microscopy was used to investigate larger surface areas (figure 1)and showed that areas the size of $1mm^2$ exist that are atomically flat. To investigate even larger surface areas SXRD was used, employing an X-ray beam footprint of 3 by 3 millimetres. Steps can be detected because of the difference in orientation between two neighbouring potassium layers separated by a 1 nm step, as a result from the glide plane in the crystal structure. Using the symmetric (11) and (1-1) crystal truncation rods, SXRD revealed that areas of 5 by 5 millimetres in size exist that are atomically flat. When this flatness is compared to the surface area of the USA, there would only one step dividing the country of two meters in height.

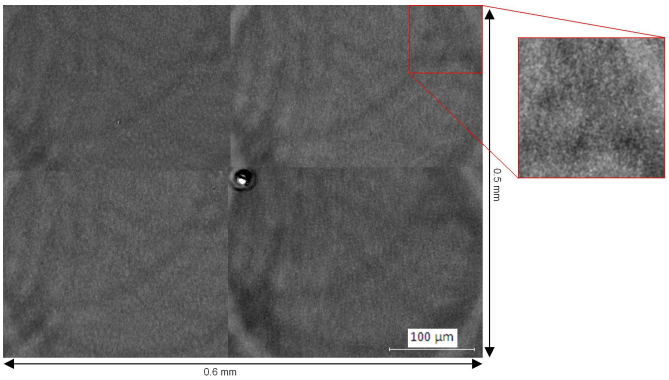

Figure 1 Phase contrast microscopy image of muscovite mica, showing a step-free area of 0.6 by 0.5 millimetres. The rings are an artefact from the microscope, the lines in the middle, both horizontal and vertical, are a result from merging four images and the spot at the centre is a dust particle.

The rare occurrence of steps on the muscovite surface means that step-induced nucleation is negligible to epitaxial nucleation on the flat areas of the substrate. Hence, growth in all directions is equally likely and epitaxy is easier to detect. For this reason muscovite mica is suited to grow epitaxial salt crystals. A large range of salts was investigated and analyzed with AFM and optical microscopy. The crystallographic plane with which the salt coordinates to the muscovite was established using X-ray diffraction and from these measurements a relationship between lattice mismatch and the occurrence of epitaxy could be determined.

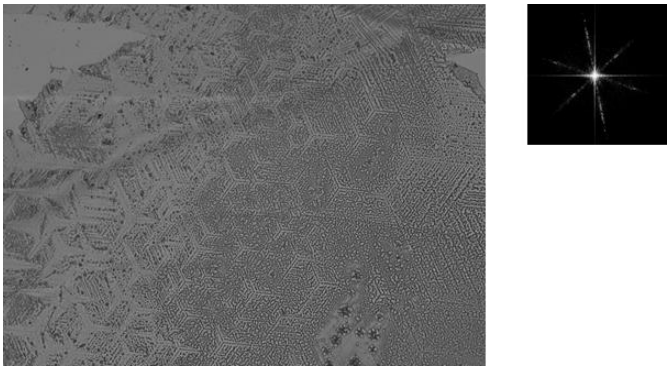

Figure 2 Optical microscopy image of epitaxially grown silver nitrate on muscovite mica (left) and Fourier transform showing the six fold symmetry of the deposit.

Finally, molecular monolayers and epitaxial layers were produced on muscovite mica. Crown-ethers are known for their ability to specifically bind to certain metal ions. Muscovite mica has potassium ions at its surface, while dibenzo-18-crown-6 specifically binds to potassium. This molecule should therefore form monolayers, which was indeed observed with AFM. The charge on the surface of muscovite can also be used to produce molecular layers, by binding molecules which have a dipole moment or contain acidic groups. Molecular (epitaxial) monolayers have been produced in this way with porphyrins and benzene-derived molecules.

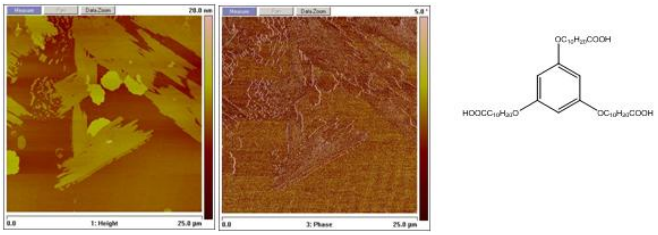

Figure 3 AFM height (left) and phase (middle) images of epitaxial layers of a benzene-derivative (right).

The final aim of this project is to use the epitaxial molecular monolayers as a template for protein crystallization.

16:45 Oral

Development of novel scintillating screens based on thesingle crystalline films of Ce doped multi-component $(Gd,Y,Lu,La)_3(Al,Ga,Sc)_5O_{12}$ garnets by LPE method

Yuriy V. Zorenko[1], Vitaliy Gorbenko[2], Volodymyr Savchyn[2], Tetyana Zorenko[2], Alexander Fedorov[3]

1. *Instytut Fizyki, Uniwersytet Kazimierza Wielkiego w Bydgoszczy (UKW), Powstancow Wielkopolskich, Bydgoszcz 85-822, Poland* **2.** *Electronics Department, Lviv National University, 50 Dragomanov str., Lviv 79005, Ukraine* **3.** *Institute for Scintillation Materials NAS of Ukraine (ISMA), Lenina ave., 60, Kharkov 61001, Ukraine*

e-mail: zorenko@ukw.edu.pl

The fast development of 2D/3D micro-imaging techniques using X-ray radiation strongly demands single crystalline film (SCF) scintillating screens with high ability of X-ray absorption and submicron spatial resolution [1]. Our report presents the results of pioneer research directed on the creation of new types of screens based on the SCF of Ce doped multi-component $(Gd,Y,La,Lu)_3(Al,Ga,Sc)_5O_{12}$ garnets by liquid phase epitaxy (LPE) method. In our work we try to applied the *combination of the "band-gap engineering" [2] and "5d-level positioning" strategies* [3] to the basic materials - the Ce doped $Y_3Al_5O_{12}$ (YAG) and $Lu_3Al_5O_{12}$ (LuAG) garnets, using the alloying with Sc and Ga ions in the octahedral positions and Gd and La ions into the dodecahedral position of the LuAG and YAG hosts.

The main task in the growth SCF based on the multi-component garnets by LPE method is the decreasing of the misfit Δa between the lattices of SCF and substrate to condition of the SCF growth (Δa <0.1 % [4]). That can be achieved by the respective choice of substrate and SCF cation content. Apart the YAG substrate with lattice constant a=12.01 Å, typically using for growth of YAG and LuAG based SCF, we consider also in our work the possibility of SCF crystallization by LPE method onto $Gd_3Ga_5O_{12}$ (GGG) substrates with a=12.38 Å. Namely, we successfully crystallized of the Ce-doped of the SCF of $Lu_{3-x}Gd_xAl_5O_{12}$ and $Lu_3Sc_2Al_3O_{12}$ garnets onto YAG substrates as well as the SCF of $Gd_{3-x}(Y,Lu)_xGa_{5-y}Al_yO_{12}$, $Gd_{3-x}(Y,Lu)_xSc_2Al_3O_{12}$ and $Lu_{3-x}La_x(Ga,Sc)_2Al_3O_{12}$ garnets onto GGG substrates using the typical $PbO\text{-}B_2O_3$ flux. The values of x and y in compositions of these garnets were changed from x=0 to 1.5 formula units.

The SCF were characterized by XRD and content analyses as well as by the absorption and cathodoluminescence (CL) spectra, light yield (LY) of CL under e-beam excitation and scintillation LY under excitation by α–particles of Pu^{239} (5.15 MeV) source. We found that from all SCF, grown onto YAG substrates, the best LY possess the SCF of Ce doped $Lu_{3-x}Gd_xAl_5O_{12}$ garnets at x=0.8-1.0. From all studied SCF, grown onto GGG substrates, the best LY possess the SCF of $Gd_{3-x}Y_xSc_2Al_3O_{12}$ and $Gd_{3-x}Lu_xSc_2Al_3O_{12}$ garnets at x=0.5-0.75. We also noted the significantly large content of Pb^{2+} flux related impurity and their higher influence on the LY of the Ce doped SCF of multi-component garnets, grown on the GGG substrates, in comparison with SCF of garnets, grown on the YAG substrates.

For determination of the fundamental optical characteristic of studied garnets (the band gap values, the positions of Ce^{3+} f-d levels relatively band gap extremes; the energy formation of excitons bound with the Ce ions), the luminescent spectroscopy of $(Gd,La,Y,Lu)_3(AlGaSc)_5O_{12}$ SCF were performed at the Superlumi station, HASYLAB, DESY under excitation by synchrotron radiation in 3.7-25 eV range.

[1] T. Martin, A. Koch, Journal of Synchrotron Radiation, 13**,** 180 (2006).

[2] M. Fasoli, A. Vedda, M. Nikl, C. Jiang, et all., Phys. Rev.,B 84, 081102 (2011).

[3] K. Kamada, T. Endo, K. Tsutumi, T. Yanagida, et all., Cryst. Growth Des., 11, 4484 (2011).

[4] Y. Zorenko, V. Gorbenko, Radiation Measurements 42, 907 (2007).

MoP-G10
Monday afternoon, 12 August, 17:00
Room 205, Old Library

Break
Monday evening, 12 August, 18:30

Tuesday, 13 August

TuO1
G10: Thin film and epitaxial growth
Tuesday morning, 13 August, 10:20
Room C, Auditorium Maximum

10:20 Invited oral

Plasma-Assisted MBE of III-nitride semiconductors: From two-dimensional layers to nanostructures

Eva Monroy

CEA-CNRS,Institut Nanosciences et Cryogénie, 17 rue des Martyrs, Grenoble 38054, France

e-mail: eva.monroy@cea.fr

Due to the low growth temperature and in-situ monitorization capabilities, Molecular-Beam Epitaxy (MBE) is the most suitable growth technique for devices or structures with low dimensionality, critical interface sharpness or immiscibility challenges. This talk will start with an introduction to plasma-assisted MBE of III-nitride materials, discussing the surface energy role on the control of the growth morphology. For growth temperatures high enough to grant a certain mobility of the group-III species at the growing front (>700°C in the case of GaN), variations of the III/V flux ratio result in changes of the surface potential that allow switching from Frank-Van der Merwe to Stranski-Krastanow growth mode. The transition from two-dimensional to three-dimensional growth can also be induced by a growth interruption due to the variation of the surface stoichiometry associated to the metal desorption in vacuum. The application of these principles to the synthesis of (0001)-, (000-1)- and (11-22)-oriented nanostructures (quantum wells, quantum dots) will be addressed, paying attention to

the particularities of those surfaces in terms of adatom mobility and metal wetting properties. Starting from the growth diagrams of the various GaN faces, we will study the incorporation of In or/and Al to form ternary or quaternary compounds. The modification of the growth kinetics in presence of dopants (Si, Mg, Mn) will be analyzed. The growth of a complete device structure requires specific growth processes, conditioned by the less thermally stable layer and by the specifications in terms of interface quality. Interfacial reactions, defects and interdiffusion will be discussed for the case of GaN/AlGaN and GaN/InGaN.

The advantages of plasma-assisted MBE find direct application in GaN/AlGaN intersubband (ISB) optoelectronics, technology that requires the control of the nanostructure dimensions and interface sharpness at the atomic scale. III-nitride heterostructures are excellent candidates for high-speed ISB devices thanks to their large conduction band offset (~1.8 eV for the GaN/AlN system) and subpicosecond ISB scattering rates. However, due to the rather large GaN electron effective mass (m* = 0.2m0), quantum wells as thin as 1-1.5 nm are required to achieve ISB absorption at 1.3-1.55 μm. In this talk, we will summarize the latest achievements in terms of MBE growth and characterization of ultra-thin GaN/Al(Ga)N QW and QD superlattices in polar and semipolar crystallographic orientations for the fabrication of ISB optoelectronic devices.

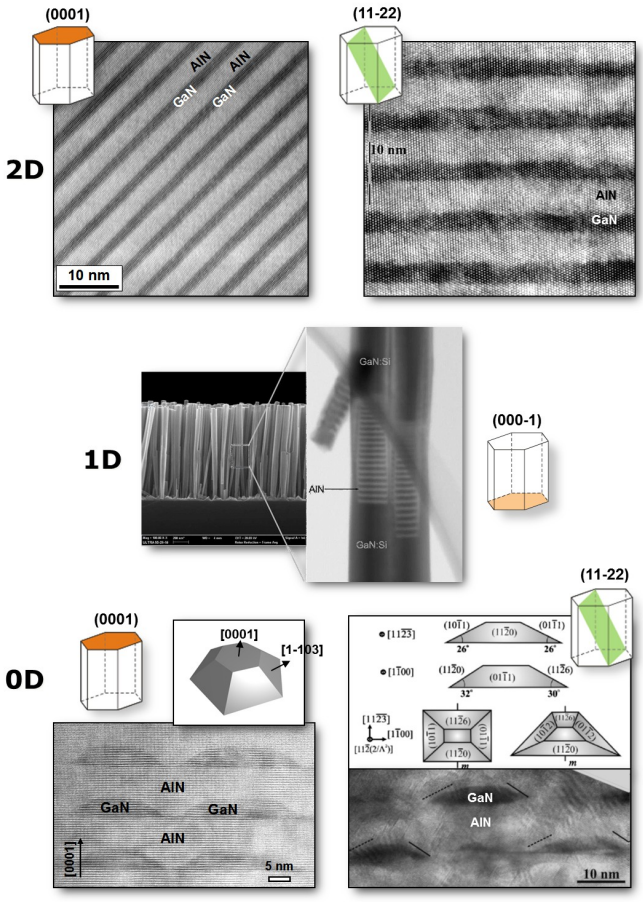

Fig. 1. GaN/AlN nanostructures (quantum wells, nanorods, quantum dots) synthesized by plasma-assisted MBE in various crystallographic orientations.

10:50 Invited oral

Growth Methodologies for Overcoming the Perceived Limitations of Phase Separation and p-type Doping in InGaN

William A. Doolittle, Brendan P. Gunning, Chloe Fabien, Michael W. Moseley

School of Electrical and Computer Engineering, Georgia Institute of Technology, Atlanta, GA 30332, United States

e-mail: alan.doolittle@ece.gatech.edu

While the InGaN material system is attractive for a wide variety of electronic and optoelectronic device applications, its potential is hindered by significant growth challenges such as p-type doping and the inability to grow thick, non-phase-separated films. Large background donor concentrations, particularly in high-indium composition InGaN, and the deep Mg acceptor level combine to make p-type doping above 10^{18}cm^{-3}very difficult. Simultaneously, InGaN films with indium fractions between 20% and 80% are notorious for phase separation where the film preferentially forms into discrete regions of varying indium composition rather than a single homogeneous alloy. More recently, a modified form of MBE called Metal-Modulated Epitaxy (MME) has shown the ability to overcome both of these challenges.

MME uses metal-rich fluxes, shuttering the metal sources while impingent nitrogen remains constant in order to consume any accumulated metal on the surface. This technique allows for lower substrate temperatures in order to facilitate the growth of high-indium content, non-phase-separated InGaN films. The samples here were grown well within the miscibility gap, from 22% to 67% indium fraction. Key growth considerations will be discussed in details, with a focus on transient RHEED analysis which plays a critical role in optimizing the InGaN growth chemistry. By monitoring the growth surface with RHEED, phase separation can be avoided without sacrificing crystal quality as is traditionally seen for nitrogen-rich growth. The InGaN films grown demonstrate GaN template-limited crystal quality with (0002) rocking curve FWHM less than 420 arcseconds in all cases, as well as smooth surfaces with less than 1nm RMS roughness. Figure 2 shows the XRD spectrum and AFM morphology for one such InGaN film with 67% indium fraction.

MME has also been a highly successful growth method for p-type GaN and InGaN films. Compared to the traditional hole concentrations in GaN of $10^{17}$to 10^{18}cm^{-3}, MME has demonstrated hole concentrations of up to 7.9x10^{19}cm^{-3}in GaN and 3x10^{19}cm^{-3}in InGaN films with up to 15% indium content. Moreover, MME-grown p-type GaN films have shown Mg acceptor activation efficiencies greater than 50%, compared to less than 10% as is traditionally reported. As with the high-indium InGaN films above, transient RHEED analysis is used to facilitate the extremely high Mg acceptor incorporation and activation, for which specific conditions and signatures will be discussed. Temperature-dependent Hall Effect is used to explore the electrical properties of these highly p-type GaN and InGaN films. A moderately-doped p-type GaN sample with a room temperature hole concentration of 3x10^{18}cm^{-3}showed significant carrier freeze-out and donor-compensated conductivity at low temperatures. In contrast, a heavily-doped sample with room-temperature hole concentration of 2x10^{19}cm^{-3}exhibited minimal carrier freeze-out and remained p-type throughout the measured temperature range, with a hole concentration of 5x10^{18}at just 82K. Similarly, a heavily-doped InGaN sample with 7% indium fraction and room temperature hole concentration of 3x10^{19}cm^{-3}also exhibited little carrier freeze-out with nearly 1x10^{19}cm^{-3}hole concentration at 90K. Figure 2 is the temperature-dependent resistivity of these three samples, where the resistivity of the sample with moderate

doping (black) exhibited a 150x increase in resistivity at low temperature, compared to just a minor increase for the highly doped GaN (blue) and InGaN (green).

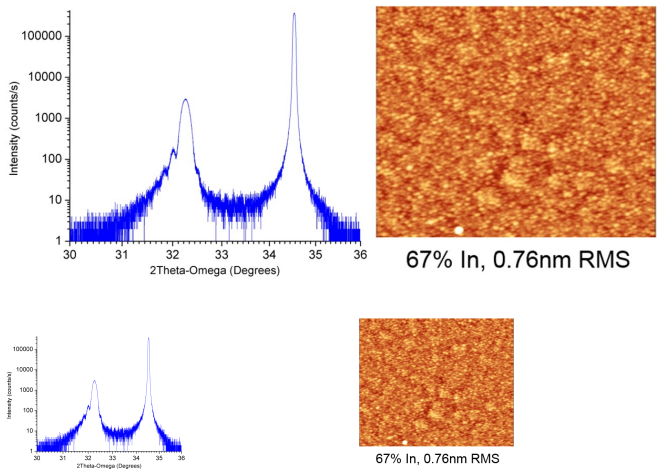

Figure 1. XRD spectrum and AFM surface morphology of 50nm-thick, single-phase InGaN with indium fraction of 67%.

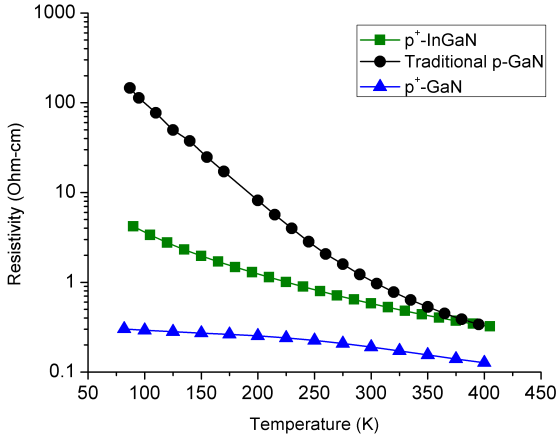

Figure 2. Temperature-dependent of resistivity of a traditional p-type GaN (black) which exhibits carrier freeze-out, compared to the highly-doped p^+-GaN and p^+-InGaN grown by MME.

11:20 Oral

Indium incorporation mechanism during InGaN growth by plasma-assisted molecular beam epitaxy

Henryk Turski[1], Marcin Siekacz[1,2], Grzegorz Muzioł[1], Marta Sawicka[1,2], Sylwester Porowski[1], Czeslaw Skierbiszewski

1. *Polish Academy of Sciences, Institute of High Pressure Physics (UNIPRESS), Sokolowska 29/37, Warszawa 01-142, Poland* **2.** *TopGaN LTd, Sokolowska 29/37, Warszawa 01-142, Poland*

e-mail: henryk@unipress.waw.pl

The prospects for InGaN in optoelectronic applications are excellent due to the wide range of accessible band gap covering the whole visible light spectrum. However the growth of high quality InGaN with indium (In) concentrations of more than 20% (imperative for long wavelength emitters) is still challenging. Growth of high optical quality InGaN structures has been recently demonstrated on c-plane GaN in excess of In flux by plasma-assisted molecular beam epitaxy (PAMBE) [1] at considerably lower temperatures then those used in MOVPE. It has been also established that In content can be increased by decreasing the growth temperature [2] or decreasing miscut angle of a substrate [3].

In this work we study the mechanism of In incorporation into InGaN layers in PAMBE environment. Based on experimental data obtained for structures grown using different Ga and N fluxes, a phenomenological model of InGaN growth was proposed. We found that both Ga and N fluxes influence composition and morphology of InGaN layers. This effect is explained by the growth kinetic dependence of the decomposition rate of In-N fraction [3]. The functional dependence of In content on atomic fluxes is deduced taking into account the existence of nonequivalent growth nucleation centers on neighboring atomic steps for InGaN surface. This observation, previously reported for GaN [4], has significant consequences for the InGaN growth.

We will discuss the model predictions for the maximum indium content of InGaN layers grown at a given growth temperature and show the proper conditions for the growth of efficient high indium content quantum wells.

[1] M. Siekacz et al. *J. Applied Physics***110**, 063110 (2011)

[2] R. Averbeck and H. Riechert, *Physical Status Solidi A***176**, 301 (1999)

[3] H. Turski et al., *J. Vac. Sci. Technol.B***29**, 03C136(2011)

[4] M. H. Xie et al. *Physical Review Letters***82**, 2749 (1999)

Acknowledgements: *This work was supported partially by the National Science Centre Grant No. 02938, the National Centre for Research and Development Grant No. IT13426, INNOTECH 157829, and the European Union within European Regional Development Fund, through the Innovative Economy Grant No. POIG.01.01.02-00-008/08, and the European Union funds within the European Social Fund.*

11:35 Oral

Semipolar (2021) UV LEDs and LDs grown by PAMBE

Marta Sawicka[1,2], Grzegorz Muzioł[1], Henryk Turski[1], Grzegorz Cywiński[1], Szymon Grzanka[1,2], Ewa Grzanka[1,2], Marcin Krysko[1], Marcin Siekacz[1,2,3], Martin Albrecht[4], Oliver Brandt[3], Christian Hauswald[3], Caroline Cheze[2,3], Robert Kucharski[5], Czeslaw Skierbiszewski[1,2], Piotr Perlin[1,2]

1. *Institute of High Pressure Physics, Polish Academy of Sciences (UNIPRESS), Sokołowska 29/37, Warsaw 01-142, Poland* **2.** *TopGaN Sp. z o. o., Sokolowska 29/37, Warsaw 01-142, Poland* **3.** *Paul-Drude-Institut (PDI), Hausvogteiplatz 5-7, Berlin 10117, Germany* **4.** *Leibniz Institute for Crystal Growth (IKZ), Max-Born-Str 2, Berlin 12489, Germany* **5.** *AMMONO S.A., Czerwonego Krzyża 2/31, Warsaw 00-377, Poland*

e-mail: sawicka@unipress.waw.pl

The advent of non-c-plane GaN substrates opened up new possibilities for the fabrication of nonpolar and semipolar nitride devices [1]. The majority of the light emitting diodes (LEDs) and laser diodes (LDs) is grown by metal-organic vapour phase epitaxy (MOVPE), but there are few exceptions that include optically pumped nonpolar laser [2] or recently reported semipolar LEDs [3] fabricated by plasma assisted molecular beam epitaxy (PAMBE).

In this work we report on the efficient LEDs and electrically driven LDs emitting in near-UV range grown by PAMBE on semipolar (20$\underline{2}$1)

ammono-GaN substrates. We present smooth semipolar surface morphologies after growth under metal-rich conditions obtained by atomic force microscopy (AFM) and we confirm the high structural quality of the structures presenting detailed transmission electron microscopy (TEM) studies.

In Fig. 1 we show the high resolution TEM image of the multi-quantum well $In_{0.06}Ga_{0.94}N/In_{0.01}Ga_{0.99}N$ (MQW) structure that has been implemented in the active region of the LED and LD. The QWs are very uniform with sharp interfaces that, along with the efficient n- and p-type doping, was essential to achieve both, electroluminescence and lasing from the semipolar devices. Using secondary ion mass spectroscopy (SIMS) we found similar Mg and Si concentrations for the (Al,In,Ga)N layers grown on semipolar (20$\underline{2}$1) GaN substrate in comparison to c-polar (0001) layers grown under the same growth conditions. The electroluminescence of the semipolar LED peaked at 387 nm while the optical output power obtained from nonprocessed wafer structure was 0.3 mW @ 100 mA. We will discuss the detailed electrical LED characteristics and its structural quality.

The semipolar LDs were processed with a ridge waveguide oriented along [11$\underline{2}$0] direction. The light-current-voltage (L-I-V) characteristics for room-temperature pulse mode operation are shown in Fig. 2(a). The threshold current density is 13.2 kA/cm^{-2} and the threshold voltage is about 10.8 V. The high resolution laser emission spectra is shown in Fig. 2(b), while the inset shows the magnified part of the spectrum. Laser emission wavelength is 388.2 nm. We observe a very small wavelength difference between the stimulated and spontaneous emission that is attributed to (i) the small electric fields in the semipolar structure and (ii) homogenous QWs and high interface quality in the active region. Further improvements in the LD electrical characteristics is expected for the devices processed with a ridge waveguide along the [$\underline{1}$014] direction [4].

Acknowledgements: Authors would like to thank A. Feduniewicz-Żmuda, B. Grzywacz, A. Nowakowska-Siwińska, A. Sarzyńska for help with sample preparation and device processing. This work has been partially supported by the National Science Centre Grant No. 02950, the National Centre for Research and Development Grant No. IT13426, INNOTECH 157829, the European Union within IAPP project SINOPLE grant No. 230765 and European Union funds by the European Social Fund.

References:

[1] R.M. Farrell, E.C. Young, F. Wu, S.P. DenBaars and J.S Speck, *Semicond. Sci. Technol.***27**, 024001 (2012).

[2] H. Teisseyre, C. Skierbiszewski, A. Khachapuridze, A. Feduniewicz-Zmuda, M. Siekacz, B. Łucznik, G. Kamler, M. Krysko, T. Suski, P. Perlin, I. Grzegory, and S. Porowski, *Appl. Phys. Lett.***90**, 081104 (2007).

[3] M. Sawicka, C. Cheze, H. Turski, G. Muziol, S. Grzanka, C. Hauswald, O. Brandt, M. Siekacz, R. Kucharski, T. Remmele, M. Albrecht, M. Krysko, E. Grzanka, T. Sochacki, C. Skierbiszewski, *Appl. Phys. Lett.***102**, 111104 (2013).

[4] W. G. Scheibenzuber, *GaN-Based Laser Diodes Towards Longer Wavelengths and Short Pulses*, PhD Thesis, Berlin Heidelberg (2012).

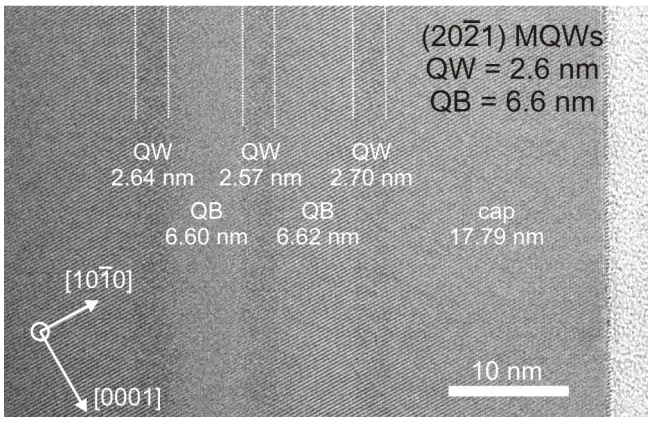

Fig 1: High resolution transmission electron micrograph (HRTEM) of the semipolar multi-quantum well structure grown by PAMBE that builds the LED and LD active region. Both the surface and interfaces are very smooth. The thickness of the respective layers is indicated in the image, dash lines mark the position of the interfaces.

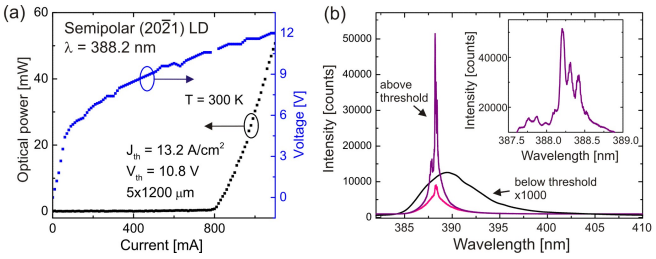

Fig 2: (a) Light-Current-Voltage characteristics of the semipolar LD with laser stripe along the [11$\underline{2}$0] direction. (b) Room temperature high resolution spectra of the semipolar laser diode below (pink and violet curves) and above the lasing threshold. Inset shows the magnified spectrum around the lasing wavelength 388.2 nm..

11:50 Oral

Effects of ceiling temperature on In incorporation and optical properties of InGaN epilayers grown by two-heater MOCVD reactor

Shao-fu Fu[1], Wei-Kuo Chen[1], Fang-Wei Li[1], Bo-Wei Liao[1], Wen-Cheng Ke[2], Szu-Yu Chen[1]

1. *National Chiao-Tung University, Institute and Department of Electrophysics, 1001 Ta Hsueh Road, Hsinchu 30050, Taiwan*
2. *Yuan Ze university,Department of mechanical engineering, Taoyuan 32003, Taiwan*

e-mail: flora.ep96g@nctu.edu.tw

We have conducted a series of InGaN growths using a modified MOCVD horizontal reactor, namely two-heater MOCVD reactor, by varying substrate temperature, ceiling temperature and growth pressure. When the ceiling temperature is fixed at 800^{o}C, the measured InN growth efficiency in InGaN exhibits an activation energy of 0.97 eV for substrate temperature >650^{o}C, a value close to InN decomposition energy (1.2 eV), indicating the InGaN growth at high temperatures here is governed mainly by the dissociation of InN, similar to the case by conventional MOCVD. More interesting results are observed on the series of ceiling temperture samples. At a substrate temperature of 625^{o}C, where the decomposition of InN, if exists, is insignificant, the InN growth efficiency is observed to remain almost constant with increasing ceiling temperature and begin to drop considerably for ceiling temperature >800^{o}C. Such a declining in InN growth efficiency is

ascribed to the parasitic reactions involved with TMIn reactants in the gas phase, as confirmed by the results of growth pressure experiment.

Additionally, we have found that the PL properties of InGaN films strongly depend on the ceiling temperature. As the ceiling temperature is increasing from 700 to 800°C, the peak energy of films grown at 625°C is found to be nearly unchanged at ~1.73 eV (730 nm), however, its intensity improves remarkably, nearly by two orders of magnitude. Our results demonstrate that the use of ceiling temperature can effectively improve the luminescence efficiency of MOCVD-grown InGaN film, which may shed a light on the exploration of high quality InGaN materials emitting at long wavelengths.

12:05 Oral

Structural and optical characterization of AlGaN/GaN layers

Jayasakthi Mathaiyan, Ramesh Raju, Arivazhagan Ponnusamy, Loganathan Ravi, Prabakaran Kandhasamy, Balaji Manavaimaran, Baskar Krishnan

Crystal Growth Centre, Anna University, chennai 600025, India

e-mail: drbaskar2009@gmail.com

Group III-nitride semiconductors of wurtzite structure are of great scientific and technological interest due to their potential application in short-wavelength light-emitting devices such as light-emitting diodes (LEDs) and laser diodes (LDs), in high temperature and high power electronic devices [1]. Aluminum rich $Al_xGa_{1-x}N$ alloys are promising materials for deep ultraviolet light emitting diodes (DUV-LEDs). DUV LEDs hold enormous potential for many applications such as sterilization, water purification and chemical agent detection [2].

$Al_xGa_{1-x}N$/GaN epilayers were grown on c-plane sapphire substrate by Metal-Organic Chemical Vapor Deposition (MOCVD). The reagents were 7N pure ammonia (NH_3), trimethylgallium (TMGa) and trimethylaluminum (TMAl). Hydrogen and nitrogen purified by purifier were used as carrier gas. During the growth TMAl flow was varied whereas the reactor pressure, NH_3 flow, reactor temperature, TMGa flow were kept constant.

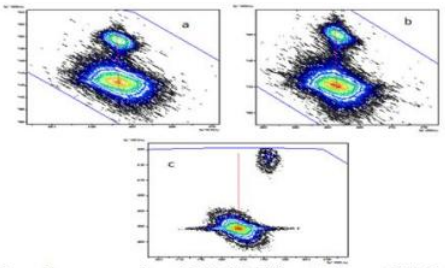

Fig. (1) Reciprocal space mapping of (20-25) different planes of (a) $Al_{0.15}Ga_{0.85}N$, (b) $Al_{0.25}Ga_{0.75}N$, (c) $Al_{0.52}Ga_{0.48}N$

The crystalline quality of the samples was determined by high resolution X-ray diffraction (HRXRD) rocking curve of symmetric (0004) and asymmetric reflection (10-12) for GaN and AlGaN. The thickness of the AlGaN was determined from (0004) ω/2θ-scan. HRXRD reciprocal space mapping (RSM) of (20-25) axis is used to estimate the strain in the AlGaN/GaN layers as shown in fig (1). The estimated degree of lattice relaxation of 2.29 x 10^{-4} for $Al_{0.15}Ga_{0.85}N$, indicates that the AlGaN epilayers is fully strained and pseudomorphic to the underlying GaN layer. RSM results indicate that in low Al composition AlGaN and GaN layers are fully strained and no cracks were observed in SEM. In high Al composition (> 0.33) strain relaxation between AlGaN and GaN epilayers resulted in cracks on the surface of the samples. Also the growth rate of AlGaN decreases on increasing the aluminum composition in fig (2).

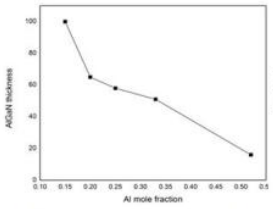

Fig. (2) Al mole Percent vs Thickness

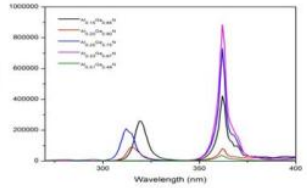

Fig. (3) PL emission wavelength of AlGaN with different Al composition

The optical properties were studied by room temperature PL. The GaN emission wavelength of 362 nm and the AlGaN emission wavelengths in the region 324-287 nm were estimated for different Al composition fig (3). The surface morphology and cracks in AlGaN epilayers were studied by Scanning Electron Microscopy (SEM). The surface roughness of AlGaN epilayers was studied by Atomic Force Microscopy (AFM). The surface roughness was found to be increased in AlGaN layers and strain relaxation between AlGaN and GaN were observed in higher aluminum composition. Higher in-plane tensile strain due to lattice and thermal mismatch between high Al content AlGaN layers and GaN buffer might be attributed to the formation of cracks. An increase in flow rate of TMAl, decreased the growth rate and thickness. Efforts are being made to introduce strained layer super lattices and thick AlN buffer layers to grow high quality crack free high aluminum containing layers of AlGaN for UV applications and results will be discussed.

References

1. W. Saito, T. Nitta, Y. Kakiuchi, Y. Saito, K. Tsuda, I. Omura, and M. Yamaguchi, "ON-resistance modulation of high voltage GaN HEMT on sapphire substrate under high applied voltage", IEEE Electron Device Lett, 28, 676 (2007).
2. J. P. Zhang, S. Wu, S. Rai, V. Mandavilli, V. Adivarahan, A. Chitnis, M. Shatalov, and M. Asif Khan, "AlGaN multiple-quantum-well-based, deep ultraviolet light-emitting diodes with significantly reduced long-wave emission", Appl. Phys. Lett. 83, 3456 (2003).

Lunch (IOCG Exec. Com. meeting)

Tuesday afternoon, 13 August, 12:20

TuO2

G10: Thin film and epitaxial growth
Tuesday afternoon, 13 August, 14:00
Room C, Auditorium Maximum

14:00 Invited oral

Epitaxial growth of wide band gap oxide semiconductor thin films

Shizuo Fujita

Photonics and Electronics Science and Engineering Center, Kyoto University, Katsura, Nishikyo-ku, Kyoto 615-8520, Japan

e-mail: fujitasz@kuee.kyoto-u.ac.jp

Wide band gap semiconductors are gaining increasing interest in order to meet the recent trends of such as high-power devices and UV light emitters. Exploration of new and novel materials has been the motive

force for the development of the merging field. Oxide semiconductors have been recognized as low-cost and multifunctional materials since the evolution of ZnO-based semiconductors, and more recently, the target has been extended from II-O materials to III-O materials such as Ga_2O_3 and In_2O_3 owing to their unique properties. In this presentation, the up-to-date achievements on III-O materials, focusing on Ga_2O_3 and related alloys, will be summarized in order to call interest of participants on these materials as a possible candidate for next-generation new and novel devices.

The researches Ga_2O_3 are now accelerating due to that highly-crystalline orthorhombic b-Ga_2O_3 substrates are available by solution methods and that its band gap is wider compared to GaN and SiC. Homoepitaxial growth by MBE has brought demonstration of Schottky diodes and MESFETs with high endurance against applied voltages[1,2], and is continuing to formation of MOSFETs.

On the other hand, corundum-structured a-Ga_2O_3 is another target of the research, because orthorhombic crystals are rare in semiconductor family and there hardly are other semiconductors of the same crystal structure for alloys or multilayer structures with b-Ga_2O_3. We found that highly-crystalline corundum-structured a-Ga_2O_3, as evidenced by the very narrow w-scan x-ray diffraction FWHMs of 40-60 arcsec, can be formed on sapphire substrates by using the mist CVD growth method[3]. Doping of Sn realized n-type conductivity[4]. It should be noted that there are many corundum-structured crystals beside Ga_2O_3, as shown in Fig. 1. Band gap engineering is expected for the Al_2O_3-Ga_2O_3-In_2O_3 system, with which we may obtain semiconductor alloys with band gaps of 3.8-7.8 eV, similarly to the nitride semiconductor alloy system of AlN-GaN-InN. Composition (x) control of a-$(Al_xGa_{1-x})_2O_3$ alloys from x=0 to 0.78 was successful, followed by the band gap tuning from 5.3 to 7.8 eV. For a-$(In_xGa_{1-x})_2O_3$, single-phase alloys are at present made for the composition close to Ga_2O_3 or In_2O_3 and marked phase separation is seen for x between 0.2 and 0.6. It is interesting that the phenomenon is similar to InGaN at the early stage. Significant enhancement of conductivity for slight addition of In to a-Ga_2O_3 (x~0.05) is seen, suggesting enhanced semiconductor property without marked reduction in band gap.

In addition to the above compounds, there are several transition-metal corundum-structured oxides, as shown simultaneously in Fig. 1. These compounds possess a variety of magnetic and electrical properties. Alloying or layering with Al_2O_3-Ga_2O_3-In_2O_3 alloys may create unique functions, that is, allow function engineering. For example, highly-crystalline alloys of a-$(Ga_{1-x}Fe_x)_2O_3$ were grown for the entire range of x from 0 to 1 keeping good crystallinity as highlighted by the w-scan x-ray diffraction FWHMs of smaller than 100 arcsec and no noticeable phase separation observed by TEM-EDX. As shown in Fig. 2, the a-$(Ga_{1-x}Fe_x)_2O_3$ films showed magnetization characteristics, more enhanced than Fe_2O_3. The hysteresis was as seen at room temperature for a-$(Ga_{0.41}Fe_{0.59})_2O_3$ (Fe=59%). Doping of Sn increased the coercive force, suggesting enhanced spin-carrier interaction. Similar phenomena were also seen for a-$(In_{1-x}Fe_x)_2O_3$. New and multifunctional devices are expected by band gap engineering and function engineering of a variety of corundum-structured oxides.

[1] K. Sasaki *et al*., Appl. Phys. Express **5**, 035502 (2012), [2] M. Higashiwaki *et al*., Appl. Phys. Lett. **100**, 013504 (2012), [3] D. Shinohara and S. Fujita, Jpn. J. Appl. Phys. **47**, 7311 (2008), [4] K. Akaiwa and S. Fujita, Jpn. J. Appl. Phys. **51**, 070203 (2012).

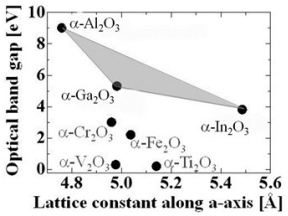

Fig. 1. Band gaps and lattice constants of corundum-structured oxides.

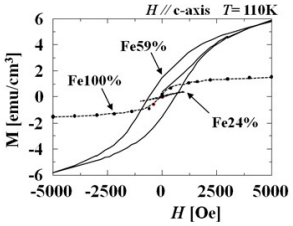

Fig. 2. Magnetization characterstics of α-$(Ga_{1-x}Fe_x)_2O_3$ thin films.

14:30 Oral

Crystal growth of $RbTiOPO_4$ epitaxial layers and optical waveguide applications

Ali Butt, Jaume Cugat, Rosa Solé, Maria Cinta Pujol, Joan J. Carvajal, Xavier Mateos, Jaume Massons, Francesc Díaz, Magdalena Aguiló

FiCMA-FiCNA, Universitat Rovira i Virgili (URV), Marceli Domingo s/n, Tarragona 43007, Spain

e-mail: f.diaz@urv.cat

$RbTiOPO_4$ (RTP) is an orthorhombic material, isostructural to $KTiOPO_4$ (KTP), which crystallizes in the *Pna2₁* space group [1]. It has high nonlinear optical and electrooptical coefficients, high damage threshold and chemical stability, which make it very interesting for optical and photonic applications [2]. RTP is a positive biaxial crystal with $n_x<n_y<n_z$. It is known that the substitution of Rb by K in the RTP structure produces a decreasing of the refractive indices [2], which is interesting in order to obtain epitaxial layers of $RbTiOPO_4$ on $Rb_{1-x}K_xTiOPO_4$ useful for making waveguides (refractive indices of the epilayer higher that those of the substrate). On the other hand, the RTP doping with Yb and Nb produces an increasing of the refractive indices with respect to those of RTP, which makes possible to guide the light through an epitaxial layer of (Yb,Nb):RTP grown on a RTP substrate. The presence of Yb, as an active ion, allows the possibility to obtain self-frequency doubling at the same crystal.

Thus, in this work, we have grown epitaxial layers of RTP on KRTP substrates and (Yb,Nb):RTP on RTP substrates in order to obtain planar waveguides. The crystals to be cut for substrates were grown from high temperature solutions using the top seeded solution growth technique. These crystals were cut in (001) oriented plates, which will be used as substrates. Figure 1 shows a RTP single crystal grown for substrates.

The epitaxial layers were obtained by the liquid phase epitaxy technique. The first step was to determine accurately the saturation temperature of the solution for growing the epitaxial layers. After that, the substrates, previously cleaned, were slowly introduced into the furnace to avoid thermal shocks and maintained for about 30 min slightly above the surface of the solution. After that, the substrate was dipped in the solution at 1K above the saturation temperature for 5 minutes, followed by decreasing the solution temperature to 2 K down the saturation temperature, in order to grow the epitaxial layer for about 2 hours. During all the growth process, the crystal rotated at 65 rpm. After that, the crystal was removed from the solution, maintained at a few mm above the solution surface and the furnace was cooled slowly to room temperature.

The doping concentration in the KRTP substrates and in the (Yb,Nb):RTP epitaxial layers and the concentration change through the substrate/epitaxial layer interface was measured by electron probe

microanalysis. The unit cell parameters of the substrates and epitaxial layers were obtained from X-ray measurements. The refractive indices at room temperature and a wavelength of 632 nm were measured using the dark modes technique.

In the $RbTiOPO_4/Rb_{1-x}K_xTiOPO_4$ (001) epitaxial layers, the lattice mismatch $f_{(001)}$ calculated using the formula $f_{(hkl)} = 100 \times (S_{(hkl)}(\text{layer}) - S_{(hkl)}(\text{substrate})) / S_{(hkl)}(\text{substrate})$ [3],

was 0.303, while the n_z refractive index contrast measured was 0.0047. The surface of the epitaxial layer showed in some parts, a capping effect due to the fast growth in the non natural face.

The chemical composition of these single crystals grown for substrates was $Rb_{0.9}K_{0.1}TiOPO_4$.

EPMA analysis also showed K^+ diffusion from the substrate into the epilayer with a non-sharp interface (Figure 2). This diffusion implies that these epitaxial layers can't work as step-index waveguide, but graded index waveguide.

In the $RbTi_{1-x-y}Yb_xNb_yOPO_4$/ $RbTiOPO_4$ (001) epitaxial layers, the lattice mismatch $f_{(001)}$ was 0.473 and the n_z refractive index contrast was 0.0077. The chemical composition of the epitaxial layer measured by EPMA was $RbTi_{0.958}Yb_{0.016}Nb_{0.026}OPO_4$, with a distribution coefficient of Yb and Nb of K_{Yb}=0.14 and K_{Nb}=0.66, respectively. Figure 3 shows the composition change at the interface of a (Yb,Nb):RTP/RTP epitaxial layer. As can be seen in the figure, the Yb and Nb diffusion from the epitaxial layer to the substrate is only around 3 mm. This means that this kind of epitaxial layers can be used for fabricating step-index waveguides. Figure 4 shows the TM_0 mode obtained by guiding the light through a (Yb,Nb):RTP/RTP planar waveguide.

Acknowledgements

This work was supported by the Spanish Government under Projects MAT2011-29255-C02-02, TEC2010-21574-C02-02, by the Catalan Authority under Project 2009SGR235 and by the European Union under Project No. FP7-SPA-2010-263044. M. Ali Butt and J. Cugat thanks the Catalan Government and the Spanish Government for the funds provided through the FI-DGR fellowships.

References

[1] P.A. Thomas, S.C. Mayo and B.E. Watts, Acta Crystallogr. B **48**, 401 (1992).

[2] M. N. Satyanarayan, A. Deeptly, H.L. Bhat, Critical Reviews in Solid State and Materials Sciences, **24**, 103 (1999).

[3] J. Cugat, R. Solé, J.J. Carvajal, M.C. Pujol, X. Mateos, F. Díaz and M. Aguiló, CrystEngComm, **13**, 2015 (2011).

Figure captions

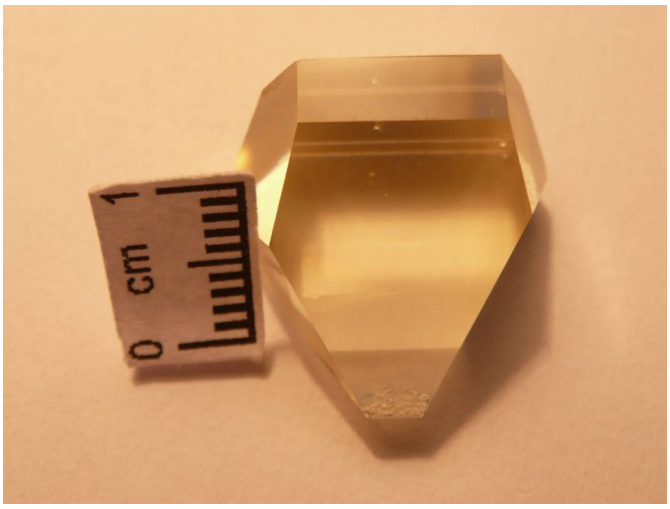

Figure 1.- As-grown RTP single crystal

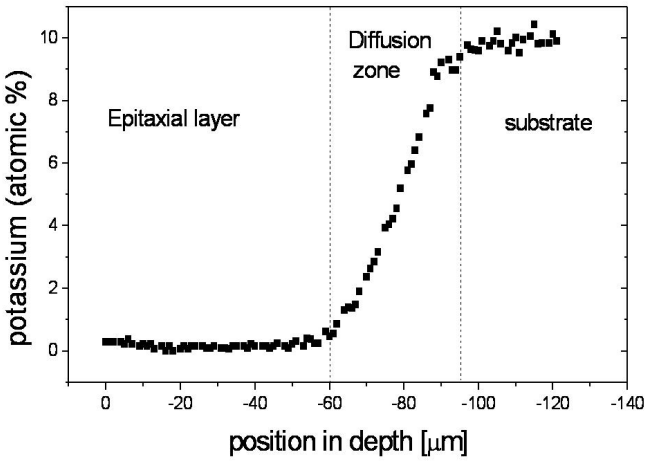

Figure 2.- K^+ atomic concentration through the interface in a RTP/KRTP epitaxial layer

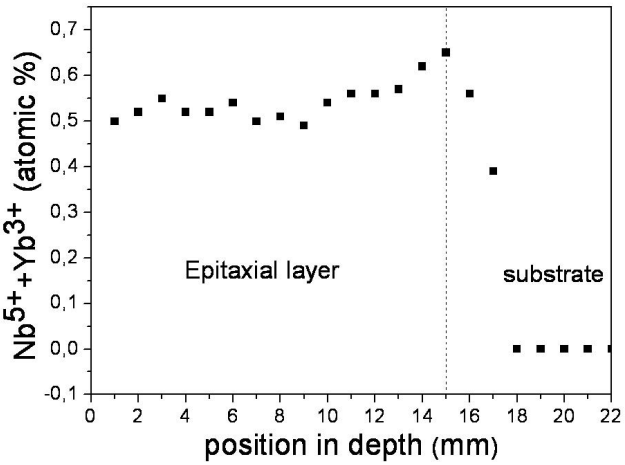

Figure 3.- [Nb^{5+},Yb^{5+}] atomic concentration through the interface in a (Yb,Nb):RTP/RTP epitaxial layer

Figure 4.- TM_0 mode in (Yb,Nb):RTP/RTP planar waveguide

14:45 Oral

High-temperature growth and comparative characterization of (Er,Yb):$YAl_3(BO_3)_4$ and $NdAl_3(BO_3)_4$ epitaxial layers

Elena A. Volkova, Victor Maltsev, Olga Kolganova, Nikolay I. Leonyuk

M.V. Lomonosov Moscow State University, Vorobyevy gory, Moscow 119992, Russian Federation

e-mail: volkova@geol.msu.ru

Development in compact solid-state lasers requires extensive study of highly efficient single crystals and crystalline layers to be used, for example, as miniature disk lasers and active waveguides with different pumping configurations including laser and amplifier applications. In this connection, borate crystals with general formula $RAl_3(BO_3)_4$ (*R*=Y, Pr - Lu) can be considered as polyfunctional solids having device potential due to their possibility of wide isomorphous substitutions, good mechanical hardness, and thermal conductivity. Of them, $NdAl_3(BO_3)_4$ (NAB) possess above mentioned requirements for weaker luminescence quenching micro-lasers [1]. Recently, excellent laser performance of (Er,Yb):$YAl_3(BO_3)_4$ (Er,Yb :YAB) crystal has been demonstrated. Diode-pumped (Er,Yb):YAB laser exhibit a slope efficiency as high as 35 % and output power of 0.8-1 W at several wavelengths between 1531 and 1602 nm [2]. Mode-locked regime has been realized with pulse duration of about 4 ps and average output power of 270 mW [3]. Among the waveguide fabrication methods, liquid-phase epitaxy (LPE) was found to be reliable, simple and low-cost technique allowing to produce the waveguides of low propagation losses and high crystalline quality [4,5]. In this report, experimental results on the LPE of (Er,Yb):YAB and NAB low-dimensional layers and their growth kinetics peculiarities are summarized.

Single crystal layers of (Er,Yb):$YAl_3(BO_3)_4$, Er:$YAl_3(BO_3)_4$ and $NdAl_3(BO_3)_4$ were grown from $K_2Mo_3O_{10}$-B_2O_3 based fluxed melts by the LPE method. For LPE growth of the *R*:YAB (*R*=Er,Yb) layers, (10`11) – oriented YAB plates were used. NAB films were obtained on (11`1) and (001) substrates with and without Pt buffer layer. YAB and NAB single crystals were grown using dipping seeded solution growth (DSSG) technique.

The observed growth rates were similar for all the investigated *R*:YAB layers, because a small amount of dopant does not change the nucleation and formation of the layers. The linear growth rates were estimated to be within the ranges of 1.5-12 μm/h. Growth steps with almost flat terraces cover the epitaxial film surface. Also, the growth hillocks were particularly typical for the corners and edges of the substrate. Most of the grown *R*:YAB layers were crack-free without visible inclusions of the mother solution.

The NAB layers thickness was typically 120-260 μm after 24 h- growth period depending on the fluxed melt supersaturations. These values give a mean linear growth rates of 5-11 μm/h. Growth steps and hillocks were also observed on the surfaces of almost all NAB grown layers.

These results were compared with previous investigations of growth kinetics of YAB, NAB and YFe-borate single crystals in $K_2Mo_3O_{10}$ based high-temperature solutions. A major problem which awaits clarification concerns controlled growth of these layers with optimal composition and thickness.

This research was supported in part by the RFBR grants ## 12-05-90010-Bel_a and 12-05-00912_a.

[1] Sh. Amano, S. Yokoyama, H. Koyama, et al, Rev. Laser. Eng. **17,** 48 (1989)

[2] N.A. Tolstik, S.V. Kurilchik, V.E. Kisel, et al, Opt. Lett. **32**, 3222 (2007)

[3] A.A. Lagatsky, V.E. Kisel, A.E. Troshin, et al, Optics Letters **33**, 83 (2008)

[4] Y. Romanyuk, C. Borca, M. Pollnau, et al, Opt. Lett. **31**, 53 (2006)

[5] M. Pollnau, Y. Romanyuk, C. R. Physique **8**, 123 (2007)

[6] S.-T. Jung, J.-K. Kang, S.-J. Chung. J. Crys/ Growth, **149**, 207 (1995)

15:00 Oral

The controllable growth and properties of self-assembly Ni-$BaTiO_3$/ $SrTiO_3$ nano-composite epitaxial film by laser molecular beam epitaxy

Weidong Wu, Zhengwei Xiong, Xueming Wang

Research Center of Laser Fusion, CAEP, MianYang 621900, China

e-mail: wuweidongding@163.com

Complex oxide epitaxial films with embedded magnetic metal nanocrystals (MNCs) have attracted more and more attention. On one hand, this interest has been driven by the exciting possibility of using those films for electronic and optic applications. On the other hand, problems associated with applications of those films, such as controllable growth, structure, dielectric and electronic transport properties, third order nonlinear optical properties etc., generated intensive research of the fundamental properties of the complex oxide films with embedded MNCs. In this report, growth behaviors, structure, electronic and optical properties of the epitaxial $BaTiO_3$/ $SrTiO_3$ super-lattice films with embedded Ni-MNCshave been reviewed in detail.

The main contents of this report contain the following aspects:

1. Ni nanocrystals (NCs) were embedded in $BaTiO_3$ epitaxial films using LMBE method. The processes involving the self-organization of Ni NCs and the epitaxial growth of $BaTiO_3$ were discussed. With the *in situ* monitoring of RHEED, the nanocomposite films were controllably engineered by the fine alternation of the self-organization of Ni NCs and the epitaxial growth of $BaTiO_3$. The transmission electron microscopy and the X-ray diffraction characterization confirmed that the composite film consist of the Ni NCs layers alternating with the (001)/(100)-oriented epitaxial $BaTiO_3$ separation layers. In addition, Ni-$BaTiO_3$/ $SrTiO_3$ nanocomposite films (Ni NCs are embedded in $BaTiO_3$/ $SrTiO_3$ superlattice films) were also fabricated with the same method.

2. The third order nonlinear optical properties of Ni-$BaTiO_3$ nanocomposite films were investigated by the z-scan technique. It was observed that the embedding of Ni NCs would significant improve the nonlinear optical property compare to $BaTiO_3$ single crystal films.

3. The stress of the composite films was increased with the increasing concentration of embedded Ni NCs, as investigation in stress calculation. The influence with the various concentrations of Ni NCs embedded in $BaTiO_3/SrTiO_3$ superlattices was also discussed. The internal stress of the films was too strong to epitaxial growth of $BaTiO_3/SrTiO_3$ superlattices. Compared with the pure $BaTiO_3/SrTiO_3$ superlattices, the $BaTiO_3/SrTiO_3$ superlattices with lower concentration of embedded Ni NCs had higher permittivity and dielectric loss. Furthermore, the dielectric enhancement of $BaTiO_3/SrTiO_3$ superlattices with embedded Ni NCs was proposed to explain by Drude quasi-free-electron theory.

4. The increasing sizes and irregular shapes of nickel nanoparticles were observed as the increase of laser energy density. By the absorption spectra investigation, the absorption peak presented red-shift and broadening phenomenon with the increase of the sizes. The results were explained by the calculation of real and imaginary permittivity of bulk nickel.

5. The electronic transport properties of Ni-$BaTiO_3$/ $SrTiO_3$ nanocomposite films were also studied with different concentration of embedded Ni NCs.

15:15 Oral

Origin of the room-temperature magnetoelectric coupling in multiferroic $Bi_5Ti_3FeO_{15}$

Hongyang Zhao

Shanghai Institute of Ceramics, Chinese Academy of Sciences, 1295 Dingxi Road, Shanghai 200050, China

e-mail: zhy@mail.sic.ac.cn

The quest for materials showing simultaneous ferromagnetism and ferroelectricity at room temperature remains a major challenge. Ferroelectricity and ferromagnetism are usually mutually exclusive, because of their requirement for empty and partially filled transition metal 3d orbitals, respectively. Materials design in a single-phase multiferroic material is keeping as a challenge, although robust magnetoelectric coupling could be achieved by an inverse Dyaloshinski–Moriya (DM) effect in improper ferroelectric systems. However, this usually happens at very low temperature.

In the search for new room-temperature multiferroicity, we have focused on $Bi_5Ti_3FeO_{15}$ (n = 1, m = 4) (BTFO) which belongs to the class of Aurivillius compounds $Bi_4Ti_3O_{12}\times nBiMO_3$ (M = Fe, Mn; n = 1, 2). Aurivillius compounds with the formula $(Bi_2O_2)^{2+}(A_{m-1}B_mO_{3m+1})^{2-}$ display an amazing variety of both structural and physical properties by changing the A and B cations as well as the number of perovskite-like units (m). BTFO crystallizes in the polar space group $A2_1am$ at room temperature, in which smaller Fe ions are also incorporated into B (Ti) sites, which may cause new magnetically ordered structures. Even so, BTFO has been neither fully characterized nor documented in the multiferroic database for its magnetoelectric coupling performance. Here, we present the first characterization of the magneto-dielectric, magneto-ferroelectric, and ME properties of BTFO thin film. All the evidences point to that $Bi_5Ti_3FeO_{15}$ is a single-phasemultiferroic material with a robust ME effect at room temperature.

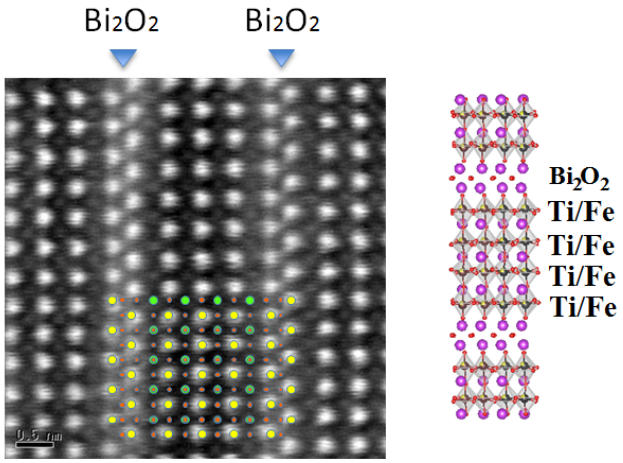

Figure 1. High-angle annular dark-field scanning TEM (HAADF STEM) picture and structure diagram of BTFO film.

***Presenting author's email:** zhy@mail.sic.ac.cn

Break
Tuesday afternoon, 13 August, 15:30

Wednesday, 14 August

WeO1

G10: Thin film and epitaxial growth
Wednesday morning, 14 August, 10:20
Room C, Auditorium Maximum

10:20 Invited oral

Novel dilute nitride III/V-semiconductor laser system for the monolithic integration to Si-microelectronics

B. Kunert[1], K. Volz[2], Wolfgang Stolz[2]

1. *NAsP-III-V GmbH, Marburg 35041, Germany* **2.** *Philipps-University, Material Sciences Center, Marburg 35032, Germany*

e-mail: wolfgang.stolz@physik.uni-marburg.de

The novel dilute-nitride material system Ga(NAsP) can be grown lattice-matched to (001) Si-substrate. The incorporation of N in the Ga(NAsP)-material allows for a significant reduction in the lattice constant, which leads on one side to a dislocation free deposition on Si. On the other side the specific conduction band formation process in these materials is used to realize a direct band gap semiconductor. By applying a variety of physical investigation techniques the high crystalline quality as well as the direct band gap character of the novel Ga(NAsP)-material system have been verified. Ga(NAsP)/(BGa)(AsP)-MQWH were grown on exact oriented (001) Si substrates embedded in thick (BGa)P separate confinement hetero-layers by metalorganic vapour phase epitaxy (MOVPE). The incorporation of B into GaP and Ga(AsP) allows for a precise strain management of the whole III/V laser stack towards the lattice constant of Si. The optoelectronic properties and first lasing characteristics of Ga(NAsP)-MQWH on (001) Si-substrate will be presented and discussed.
These results form the basis for a unique realization of monolithic integration of III/V-based optoelectronic and Si-microelectronic

functionalities in the near future. The challenges of this integration concept will be discussed and possible solutions will be presented.

10:50 Oral

Ab initio Study of GaAs(100) Surfaces Under As_2, H_2, and N_2 Influence, as a Model for Vapor-Phase Epitaxy of $GaAs_{1-x}N_x$

Hubert Valencia, Yoshihiro Kangawa, Koichi Kakimoto

Kyushu University, Fukuoka, Japan

e-mail: hubert.valencia@riam.kyushu-u.ac.jp

$(In_{1-y})Ga_yAs_{1-x}N_x$ materials are the focus of a growing interest to provide an efficient layer for four-junction solar cell[1]. However, the high quality growth of a simpler $GaAs_{1-x}N_x$ material remain an experimental challenge, due to low nitrogen content (x) and formation of defects and/or incorporation of impurities that are linked to the growth conditions[2]. In order to better understand the influence of these conditions, we examine the atomic and electronic structures of GaAs(100) surfaces by ab initio calculations, within the adsorption of As_2 and H_2 molecules, and As ↔ N substitution, as a model for GaAs(100) surfaces during vapor-phase epitaxy. Using a simple model, derived from previous studies[3], it was shown to be possible to examine the composition change of surfaces by first studying elementary adsorption and substitution reactions, then considering the relative stability of the resulting surfaces against the chemical potential of As_2, H_2 and N_2 gas (see figure). Finally, for this simple model a picture of the temperature and pressure stability domains for each surfaces can be drawn, which should allow us to better understand and control the surface states under specific growth conditions. We found that several different configurations are possible for N incorporation (N-H_2, N-H and N site), depending on the conditions. Since this incorporation often leads to the apparition of defects and impurities, linked to the presence or absence of H atoms on the N site, this result could enable a better understanding and control of the experimental condition needed to realized a high quality crystal growth.

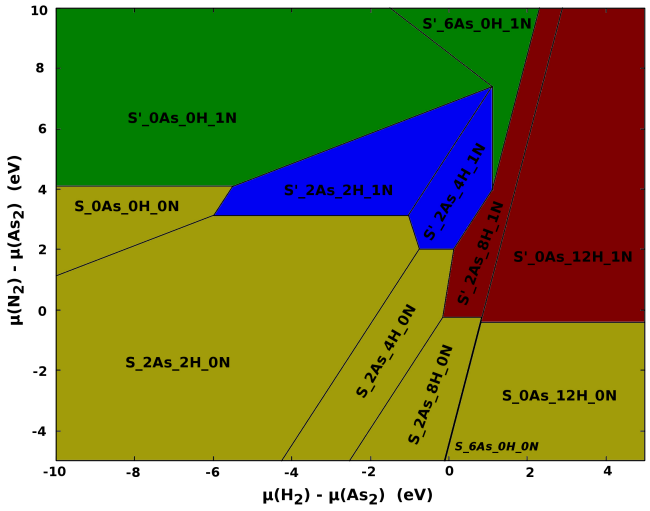

Figure. GaAs(100) surfaces under As_2, H_2 and N_2 conditions. The surface is called S when not N substituted, and S' otherwise; followed by the number of As, H and N atoms added as compared to the free (S_0As0H0N) surface. Yellow region stands for N-free surfaces, while red, blue and green one represent N-H_2, N-H, and N sites respectively. The S_6As_0H_0N surface is placed in a narrow domain between S_2As_8H_0N and S_0As_12H_0N.

[1] H.S. Lee et al., *J. Cryst. Growth***275**, pp. e1127-e1130 (2005).

[2] J. Kawano, Y. Kangawa, T. Ito, K. Kakimoto, and A. Koukitu, *J. Cryst. Growth***343**, pp. 105-109 (2012).

[3] J. Kawano, Y. Kangawa, and K. Kakimoto, *Jpn. J. Appl. Phys.***51**, pp. 81-84 (2012).

11:05 Oral

Dislocation and antiphase domain-free microscale GaAs crystals grown on SiO_2 from (001) and (111) Si nano-areas

Charles Renard[1], Nikolay Cherkashin[2], Alexandre Jaffre[3], Laetitia Vincent[1], Amélie Michel[2], Timothée Molière[1,2], Redouane Hamouche[1], José Alvarez[3], Denis Mencaraglia[3], D. Bouchier[1]

1. *Institut d'Electronique Fondamentale, UMR-CNRS 8622, 91405 Orsay Cedex, France, France* **2.** *CEMES-CNRS (CEMES-CNRS), 29, rue Jeanne Marvig, Toulouse F31055, France* **3.** *Laboratoire de Génie Electrique de Paris (LGEP), Plateau de moulon 11, rue Joliot Curie, Gif-sur-Yvette 91192, France*

e-mail: charles.renard@ief.u-psud.fr

The interest paid to the heteroepitaxy of GaAs on Si has never failed in the last years due to the potential for monolithic integration of GaAs-based optoelectronic devices with Si integrated circuits (OEICs)[1]. However, three major problems remain unresolved in GaAs layers grown directly on plain silicon substrates, i) the high density of threading dislocations due to the large lattice mismatch with Si (around 4%), ii) the formation of anti-phase domains due to the presence of polar/non-polar interfaces and iii) the formation of cracks due to the difference in thermal expansion coefficients between the two materials[2]. Significant improvements have been reported for many years, thanks to selective area epitaxy (SAE) of GaAs on Si substrates patterned with dielectric film[3-6]. These problems have been overcome, for the case of Ge on Si hetero-epitaxy, and we have previously demonstrated defect free Ge regions grown on thin SiO_2 layer where the crystalline order between epi-Ge and Si substrate was transferred through nano-holes in the SiO_2 layer[7].

Besides, to demonstrate compatibility with the Si CMOS technology platform, growth temperature should be preferably limited to a maximum of 600°C. That was achieved, in our growth process, by the use of tertiarybutylarsine (TBAs) instead of AsH_3 which has a higher cracking temperature. Thus, such epitaxy step could be added at any time in a CMOS process without degrading preexisting MOS device elements.

In this work, GaAs crystals were obtained by epitaxial lateral overgrowth (ELO process) directly grown on Si substrates at low temperature (ranging from 550 to 600°C) by chemical beam epitaxy (CBE). The investigated approach consisted in growing the GaAs layer from Si nanoscale seeds opened through a 0.6 nm thick SiO_2 layer chemically formed on (001) and (111) Si substrate. The use of a sufficiently small nucleation area is expected (i) to enable the relaxation of the mismatched material without emission of misfit dislocations[8] and (ii) to avoid the formation of steps and therefore to result in a perfect alignment of group III or group V elements at the interface between Si and GaAs within the seed area.

Coherent growth without misfit dislocation and antiphase domain formation was confirmed at the hetero interface of GaAs islands and Si substrate for small width openings. The density of initial seeds islands was choosen low enough to avoid any coalescence, which is assumed to result in additional defects, but the resulting islands are large enough to serve as a possible III-V plateform in CMOS or optoelectronic integrated circuit processings.

This technique allows us to obtain perfect integration of heterogeneous GaAs islands of microscopic size through a Si substrate (Figure 1). The analysis performed on these 3D objects by X-ray diffraction (XRD) and transmission electron microscopy (TEM) indicate that GaAs islands are perfectly relaxed and in epitaxial relation with the Si substrate. Additional measures performed by confocal Raman microscopy on these islands help us to determine different structural parameters, such as stress induced during growth, chemical compounds, doping, crystalline quality and the presence of defects. Finally, the micro-photoluminescence (μ-PL) measurements allow us to probe precisely the discrete electronic states and to give information on the quality of surface interfaces.

These different results will be presented and discussed during the communication.

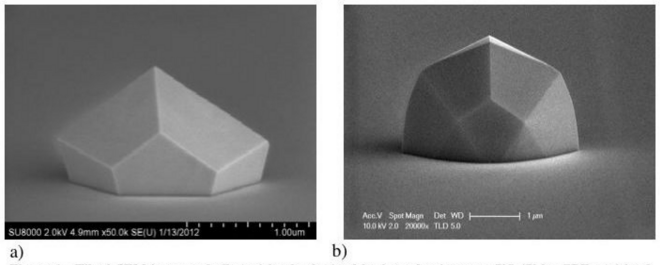

a) b)

Figure 1 : Tilted SEM images of GaAs islands obtained by lateral epitaxy on SiO_2/Si by CBE, a) island obtained with a growth temperature of 575°C, b) island obtained with a growth temperature of 550°C.

Reference :

[1] R. Chau, S. Datta, M. Doczy, B. Doyle, B.Jin, J. Kavalieros, A. Majumdar, M. Metz, and M. Radosavljevic, IEEE Trans. Nanotechnol. 4, 153 (2005)

[2] S. F. Fang, K. Adomi, S. Iyer, H. Morkoc, H. Zabel, C. Choi, N. Otsuka, J. Appl. Phys. 68, R31 (1990)

[3] J. Z. Li, J. Bai, J.-S. Park, B. Adekore,K. Fox, M. Carroll, A. Lochtefeld, Z. Shellenbarger, Appl. Phys. Lett. 91, 021114 (2007)

[4] J. Z. Li, J. Bai, C. Major, M. Carroll, A. Lochtefeld, Z. Shellenbarger, J. Appl. Phys. 103, 106102 (2008)

[5] M. Deura, T. Hoshii, M. Takenada, S. Takagi, Y. Nakano, M. Sugiyama, Journal of Crystal Growth 310, 4768 (2008)

[6] C.-W. Hsu, Y. -F. Chen, Y. -K. Su, Appl. Phys. Lett. 99, 133115 (2011)

[7]M. Halbwax, C. Renard, D. Cammilleri, V. Yam, F. Fossard, D. Bouchier, Y. Zheng and E. Rzepka, J. Crystal Growth 308 26 (2007)

[8]S. Luryi, E. Suhir, Appl. Phys. Lett. 49, 140 (1986)

???

???

11:20 Oral

Heteorepitaxy of high quality GaAs crystals on Silicon

Sergio Bietti[1], Andrea Scaccabarozzi[1], Roberto Bergamaschini[1], Monica Bollani[2], Emiliano Bonera[1], Claudiu Valentin Falub[3], Emanuele Grilli[1], Cesare Frigeri[4], Hans Von Känel[3], Leo Miglio[1], Stefano Sanguinetti[1]

1. *LNESS and Dipartimento di Scienza dei Materiali, Università di Milano-Bicocca, via Cozzi 53, Milano 20125, Italy* **2.** *CNR-IFN, Via Anzani 42, Como 22100, Italy* **3.** *ETH Zürich (ETHZ), Wolfgang-Pauli-Strasse 10, Zürich 8093, Switzerland* **4.** *CNR-IMEM, Pavia 43010, Italy*

e-mail: stefano.sanguinetti@unimib.it

In the quest for a viable path towards the monolithic integration of an quantum and optoelectronic devices onto a CMOS chip, we show that the recently developed approach for the hetero-epitaxial growth of Ge structures onto Si substrates [1], is also applicable to the GaAs on Si direct hetero-epitaxial growth. Fig. 1 shows an example of the three-dimensional hetero-epitaxy, namely GaAs micro-crystals (MCs), grown in a self-aligned manner on a periodic array of Si seeds. The seeds were formed by deep micro-machining of (001)-oriented, 6° off toward [110] Si substrates into pillars from 8 μm in height, with base width of 2 (not shown), 5 and 9 μm and spacing of 2 to 4 μm. Up to 8 μm of GaAs were deposited by MBE at a rate of 0.48 ML/s, a V/III ratio of 50 and a growth temperature of 580°C. This set of parameters was chosen to limit the diffusion length of Ga adatoms on GaAs, thus driving the growth toward kinetic limited morphologies. Depending on the choice of substrate pattern and the amount of material deposited, the arrays visible in Fig. 1 can cover almost the entire substrate surface, resulting in a measured space fillings of 90%. By preventing the formation of a continuous layer, crack propagation and wafer bowing are inhibited, even at large thickness GaAs deposit. An enlarged SEM image of the a GaAs crystal grown on Si pillars in shown in Fig. 1, in the case of pillar base width of 5 μm. The deposition is highly non-conformal, characterized by limited lateral expansion. The GaAs MC top is limited by clearly defined facets, with an anisotropy between the (110) and (1-10) directions due to the substrate miscut. The TEM analysis of the 5X5 2μm sample (Fig. 2) shows the presence of defected zones at the GaAs/Si interface and at the periphery of the crystal (Fig. 2), the latter characterized by the presence of stacking faults and threading dislocation arms. Due to 3D geometry of the deposit, such defects are readily expelled at the crystal sides. Antiphase domains are annihilated within few hundreds of nanometers from the interface. The topmost part of the GaAs MC, according to Raman measurements, appears completely relaxed. In order assess the GaAs crystal quality removing any interference from the low-quality material grown at the GaAs/Si interface, we realized GaAs crystals on Si pillars with an GaAs/AlGaAs heterostructure at the top, constituted by 200 nm of $Al_{0.3}Ga_{0.7}$

As topped with 300 nm of GaAs. For comparison, the same heterostructure was realized on GaAs-SI substrates (reference). The optical quality of the GaAs in the MC is confirmed by the intense room temperature emission, comparable to that of the GaAs bulk sample (Fig. 2c). The effect of growth conditions, pillar edge length and GaAs deposit thickness on the III-V material quality will be discussed. [1] C.V. Falub et al., Science 335, 1330 (2012).

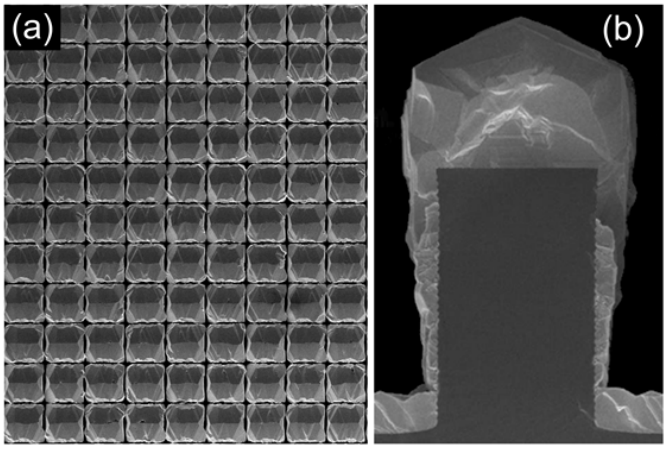

Figure 1: Panel (a): SEM top view of MC array obtained by heteroepitaxy of 8 µm of GaAs on Si patterned substrates (9×9 µm^2 pillars with 4 µm trenches). Panel (b): SEM cross section of a single GaAs/Si pillar structure (5×5 µm^2 pillars with 4 µm trenches). Dark areas correspond to Si.

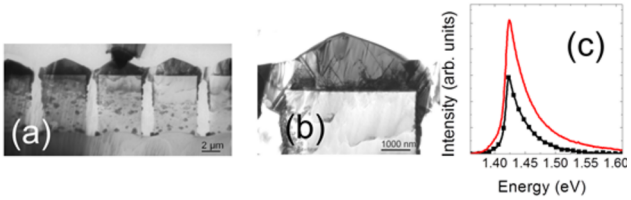

Figure 2 Panel (a): TEM images of MCs (2 µm thick GaAs on 5×5 µm2 pillars, 2 µm trenches). Panel (b): Image of a single MC. Panel (c) Room Temperature photoluminescence of Bulk GaAs (Black dots) and GaAs MC (4µm)

11:35 Oral

Strontium Doped ZnO Grown by Pulsed Laser Deposition: Structural and Optical Properties

Anwar Q. Alanazi[1], Essa Alfaifi[1], Hassen Alshahrani[1], Mudhi Almutairi[1], Joselito P. Labis[1], Ahmed Alyamani[2], Zeyad A. Alahmed[1], Ahmed Elnaggar[1], Asghar Kayani[3], Hamad A. Albrithen[1]

1. *King Saud University (KSU), P.O. Box 2455, Riyadh 11451, Saudi Arabia* **2.** *King Abdulaziz City for Science and Technology (KACST), Riyadh P.O. Box 6086, Riyadh 11442, Saudi Arabia* **3.** *Western Michigan University (WMU), Kalamazoo 49008, United States*

e-mail: brithen@ksu.edu.sa

Strontium-doped ZnO films have been grown by pulsed laser deposition on different substrate, mainly sapphire (0001). The doping was achieved by utilizing targets of $(SrO)_x$ $(ZnO)_{1-x}$ mixtures in the ZnO rich regime, having SrO up to 25%. The films were examined by different techniques to investigate the structural and optical properties. The main orientation of the film, indicated by XRD, is (001); however, other peaks of (100) and (101) were observed for higher Sr contents. Under certain growth conditions, the main peak was noticed to be apparent for even high Sr content, yet the peak intensity was decreasing as Sr increases. This in fact suggests the reduction of the grain size, induced by Sr. Moreover, the existence of other orientation, even though they are small, might be attributed to the change of the surface energies due to Sr incorporation. Optical measurements of different samples by spectrophotometer and ellipsometer exhibit variation of the index of refraction in the transparent regime as strontium concentration changes in the targets. Other analysis such as RBS measurements and HRTEM are being carried out to inspect the effect of SrO ratio (x), in targets, on the film structural properties and correlate that to the resultant optical properties. Funding is provided by Saudi National Plan for Science and Technology; the project # is NAN1197.

11:50 Oral

Pinning of steps near equilibrium without impurities, adsorbates, or dislocations

Noriko Akutsu

Osaka Electro-Communication University, Hatsu-cho, Neyagawa, Osaka 572-8530, Japan

e-mail: nori3@phys.osakac.ac.jp

Using the Monte Carlo method with the Metropolis Algorithm, we show that steps on a vicinal surface can be pinned without impurities, adsorbates, or dislocations (Fig. 1)[1].

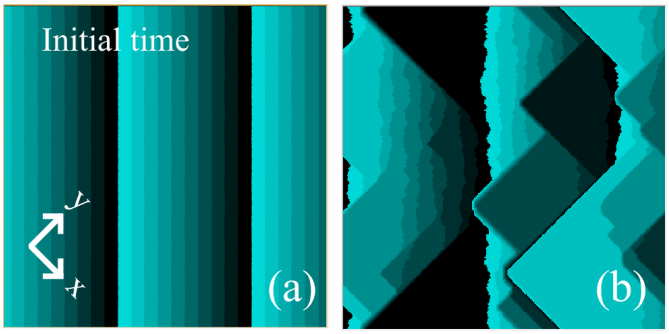

Fig. 1 Top view of a vicinal surface. The brighter, the higher, with 10 gradations. N_{step}=24. $\varepsilon_{int}/\varepsilon$ = - 0.5. Driving force for growth: $\Delta\mu/\varepsilon$ = 0.1. k_BT/ε= 0.1. (a) Initial configuration, and (b) 3000 Monte Carlo Steps per site (MCS).

The microscopic model of the vicinal surface is a restricted solid-on-solid (RSOS) model with point-contact-type step-step attraction (p-RSOS model)[1-3]. The Hamiltonian of the p-RSOS model is written as follows:

$$\begin{aligned}\mathcal{H}_{\text{p-RSOS}} = &\sum_{i,j} \epsilon[|h(i+1,j)-h(i,j)| \\ &+ |h(i,j+1)-h(i,j)|] \\ &+ \sum_{i,j} \epsilon_{\text{int}}[\delta(|h(i+1,j+1)-h(i,j)|,2) \\ &+ \delta(|h(i+1,j-1)-h(i,j)|,2)], \qquad (1)\end{aligned}$$

where $h(i,j)$ represents the surface height at the site (i,j) on a square lattice, e represents a microscopic step energy, ε_{int} (ε_{int}<0) represents a microscopic step-step attractive energy, and δ(a,b) represents Kronecker delta.

The step-step attraction causes a *discontinuity in the surface tension* at low temperatures[1-3]. This discontinuity leads to inhomogeneity on the vicinal surface[2]. Since the side surfaces of merged steps have few numbers of kinks, the dissolved steps grow faster than the merged steps. The difference of growth speed between the dissolved steps and the merged steps cause the pinning of steps[1].

References

[1] N. Akutsu, Phys. Rev. E **86**, (2012) 061604. PRE Kaleidoscope Images: December 2012.

[2] N. Akutsu, J. Phys.: Condens. Matter **23** (2011) 485004.

[3] N. Akutsu, Appl. Surf. Sci. **256** (2009) 1205; J. Cryst. Growth, **318** (2011) 10.

Lunch (IOCG Council meeting)
Wednesday afternoon, 14 August, 12:20

Posters

Monday, 12 August

MoP-G10
Monday afternoon, 12 August, 17:00
Room 205, Old Library

17:00 Poster Mo112

Microstructural analysis and optical characteristics of Cu-doped ZnO thin films prepared by DC magnetron sputtering

Bunyod Allabergenov, Oybek Tursunkulov, Amir I. Abidov, Sang Yeop Kim, Jeong Soon Wook, Sungjin Kim

Kumoh National Institute of Technology (KIT), 61 Daehak-ro, Gumi 730-701, Korea, South

e-mail: bunyod_kit@yahoo.com

The study of the processes interactions near the surfaces and bulk area of functional metal oxide semiconductor materials play important role for nanodevice application. Especially it is necessary to investigate the morphological, optical and physical properties of the synthesized semiconductor oxides modified by different state of dopant elements. Because this is allows making compound system with unique characteristics and novel properties. In this work the pure and Cu-doped zinc oxide (CZO) thin films were deposited on silicon oxide (SiO_2/Si) substrate by using direct current reactive magnetron sputtering technique. Synthesized samples were annealed at 500 ^oC, 700 ^oC, and 850 ^oC temperatures under oxygen atmosphere to order good quality crystal structure. Then microstructural and optical properties of the pure and CZO films are systematically investigated by X-ray diffraction, scanning electronic microscopy, and spectrophotometer. The results indicate that Cu-doped ZnO films show stronger preferred orientation toward the c-axis and lattice mismatch, uniform grain size after doping of Cu. The effect of thermal annealing to morphologic and physical parameters of metal oxide thin films was analyzed as functions of the Cu dopant.

17:00 Poster Mo113

Structural properties of epitaxial $La_{0.66}Sr_{0.33}MnO_3$ films with increased temperature of metal-insulator transition

Marianna Španková, Štefan Chromik, Alica Rosová, Ivo Vávra, Edmund Dobročka, Vladimír Štrbík

Slovak Academy of Sciences, Institute of Electrical Engineering (IEE SAS), Dubravska cesta 9, Bratislava 841 04, Slovakia (Slovak Rep.)

e-mail: stefan.chromik@savba.sk

Since the discovery of colossal magnetoresistivity (CMR) effect in perovskite manganites with general formula $A_{1-x}B_xMnO_3$ (where A is a lanthanum (La) and B an alkaline-earth (Ba, Ca, Sr) element), the magnetic and transport properties of these materials and their relations to microstructures have attracted much interest. The CMR effect occurs in the $0.2< x <0.5$ doping range. Among these materials $La_{1-x}Sr_xMnO_3$ ($La_{0.7}Sr_{0.3}MnO_3$, $La_{0.66}Sr_{0.33}MnO_3$) group has been intensively studied because of their high Curie temperature (T_C) (higher than room temperature), making these materials suitable for uncooled bolometric detectors, sensors, etc. At this temperature the materials undergo a ferromagnetic-paramagnetic transition and simultaneously, in most cases, a metal-insulator transition- when they reach the resistivity maximum at a temperature T_{MI}. For possible industrial applications, these materials have to be prepared in thin film form. Various single crystalline substrates, such as dielectric ($SrTiO_3$, $LaAlO_3$, $NdGaO_3$, YSZ, MgO) or semiconducting (Si, GaAs) are used for the $La_{0.66}Sr_{0.33}MnO_3$ (LSMO) films. Beside preferred substrates with a perfect matching to the LSMO significant results on MgO substrates or MgO buffer layers have also been obtained with a T_C=365 K [1], T_{MI} = 416 K [2] and a T_{MI} = 382 K [3], respectively.

LSMO has a perovskite structures with a rhombohedral distortion. In the pseudocubic description the lattice parameter and the unit cell angle are 0.3873 nm and 90.26°, respectively. The MgO substrate has the rock-salt cubic structure with a lattice parameter of 0.421 nm. The lattice mismatch between the LSMO film and the MgO substrate is 8 %.

The LSMO films were deposited using two different deposition techniques, on axis dc magnetron sputtering or pulsed laser deposition (PLD) onto a one-side polished MgO (001) substrate. The thickness of the films was about 50 nm, the growth rate of the sputtered and the laser ablated LSMO were 1.2 nm/min and 6.5 nm/min, respectively.

Both types of LSMO films exhibited a significant increased temperature of metal-insulator transition, measured using a standard four-point method, T_{MI} of about 400-458 K.

X-ray diffraction (XRD) analyses were carried out using Bruker D8 DISCOVER diffractometer equipped with X-ray tube with rotating Cu anode operating at 12 kW. We revealed different shape of the rocking curves measured on the (004) diffractions of the LSMO - in case of the sputtered LSMO film two distinct maxima of the rocking curve, while in case of the laser ablated LSMO film simple shape of the rocking curve with one maximum were observed. To explain the origin of the rocking curve splitting reciprocal space maps were recorded around the (004) and (204) Bragg reflections. The LSMO films prepared by sputtering exhibited splitted Bragg reflections in the direction parallel to the sample surface, indicating a distorted orthorombic LSMO unit cell. On the other hand, no splitting of the Bragg reflections was observed in case of laser ablated films. These films possess a pseudocubic structure.

The microstructure of the films was investigated by the use of transmission electron microscopy (TEM) Jeol 1200EX. Cross-section and planar view TEM samples were prepared in the conventional way with a final ion milling process. TEM analyses revealed an epitaxial growth of both types of the LSMO films. From the selected area diffraction pattern we determined a cube on cube relationship of the LSMO film to the MgO substrate. Cross-sectional TEM micrograph demonstrates a columnar epitaxial structure of the films with Moiré fringes clearly visible in the blocks.

XRD and TEM analyses have revealed that the LSMO films grown on the MgO are completely relaxed with respect to the substrate. The LSMO lattice parameters calculated from the reciprocal space maps are different from the LSMO bulk value, indicating a presence of some strains in the LSMO films. However, these strains are created during

the film growth and are brought into by the adjusting of the deposition conditions of the films. In this paper we discuss the influence of the deposition parameters on the increased temperature of metal-insulator transition.

[1] S.Y.Yang et al., J. of Magnetism and Magnetic Materials 226-230 (2001) 690.

[2] Š. Chromik et al., Applied Surface Science 269 (2013) 98.

[3] I. Khartsev et al., J. of Crystal Growth 284 (2005) 1.

17:00 Poster Mo114

Epitaxial growth on porous substrates of III-V semiconductors

Jan Grym[1], Peter Gladkov[1], Jan Vaniš[1], George P. Dimitrakopulos[2], Calliope Bazioti[2], Philomela Komninou[2], Eduard Hulicius[3], Jiří Pangrác[3], Oliva Pacherová[3]

1. *Czech Academy of Sciences, Institute of Photonics and Electronics, Chaberská 57, Prague 18251, Czech Republic* **2.** *Dept. of Physics, Aristotle University of Thessaloniki, Thessaloniki 54 124, Greece* **3.** *Czech Academy of Sciences, Institute of Physics, Cukrovarnicka 10, Prague 16253, Czech Republic*

e-mail: grym@ufe.cz

In mismatched heteroepitaxial growth on a conventional substrate, a thin epitaxial layer accommodates all of the mismatch strain so that this layer must be kept below the critical layer thickness to avoid generation of misfit dislocations, which are detrimental for the performance, reliability and lifetime of semiconductor devices. Enhancement of the critical layer thickness would be beneficial in many applications. One of the unexplored approaches to achieve the enhancement consists in the growth on a porous substrate, which, thanks to its compliance, is supposed to be capable of accommodating elastic strains at the heteroepitaxial interface.

We report on the electrochemical preparation of porous substrates of InP and GaAs and discuss specific problems related to their application in epitaxial growth from the liquid and vapor phase.

The pore etching was carried out in an electrochemical cell using a three-electrode configuration. A home-made potentiostat/galvanostat was computer-controlled and allowed to register all process variables. The porous substrates and epitaxial layers were prepared by liquid phase epitaxy (LPE) and metal-organic vapor phase epitaxy (MOVPE) were characterized by scanning electron microscopy (SEM), focused ion beam microscopy (FIBM), cross sectional transmission electron microscopy (XTEM), atomic force microscopy (AFM), x-ray diffraction (XRD), and low temperature photoluminescence spectroscopy (PL).

Porous substrates with low surface roughness and low density of pores in the nucleation layer (on the substrate surface) are appreciated to be easily laterally overgrown at an early stage of epitaxy; the pores should branch below this nucleation layer and thus allow for a high porosity and uniformity of a porous layer. This was achieved in highly concentrated HCl for InP substrates and HF-KI based electrolyte for GaAs substrates.

A set of samples of InGaAs/GaAs MOVPE experiments with a different composition of the ternary alloy (5, 10 and 20 % of In) and different thickness of the layer below and above the expected critical value on both porous and monolithic substrates was intentionally prepared for XRD and TEM measurements. Significantly higher amount of elastic strain was retained in the layers deposited on porous substrates and the density of misfit dislocations was reduced as compared to the layers grown on conventional substrates in the same growth run.

Several systems on porous substrates were also grown by LPE. Direct LPE deposition of InAs on conventional InP substrates (lattice mismatch approximately 3.4%) resulted in extremely poor structural quality polycrystalline deposit. On a porous InP substrate, epitaxially textured monocrystalline grains of InAs were obtained. Stress at the interface was proved to have a large impact on the mass transport velocity within the porous layer at elevated temperatures. A large set of InGaAs layers grown on porous GaAs was prepared at 590 C. Layers on porous substrates were systematically thicker, had higher integral luminescence intensity and allowed to introduce larger amount of indium. Growth conditions for the preparation of smooth layers with a good surface morphology were established.

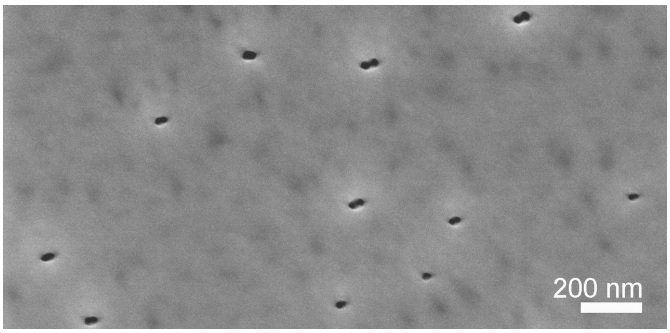

SEM picture of the surface of the low-roughness porous GaAs substrate

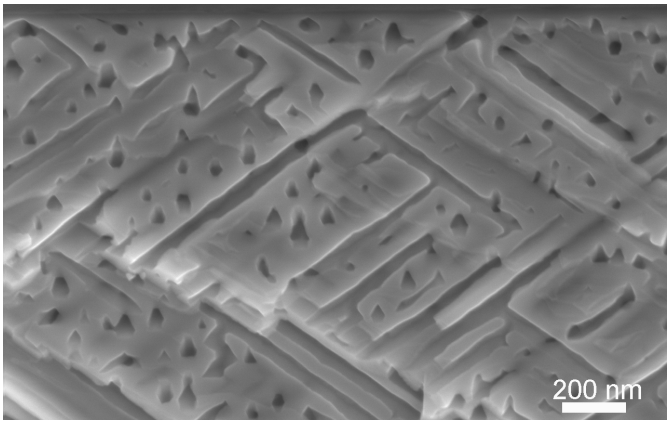

SEM picture of the cross-section of the low-roughness porous GaAs substrate

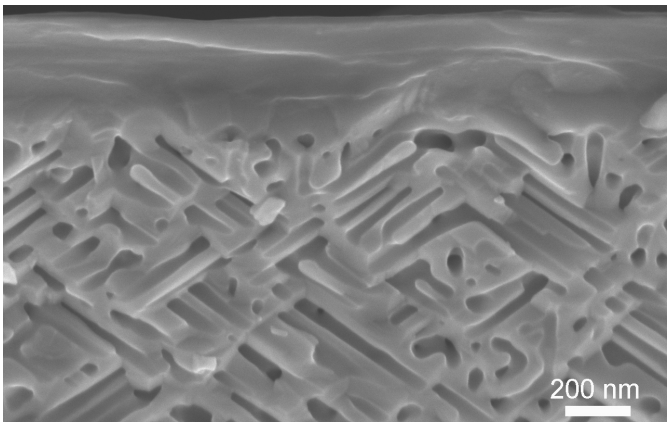

SEM picture of the cross-section of the InGaAs layer with 20 % of In grown by MOVPE on porous GaAs substrate

Work supported under the 2011-2013 Greece-Czech bilateral R&D collaboration project "III-V semiconductor heterostructures/nanostructures towards innovative electronic and photonic applications".

17:00 Poster Mo115

Selective growth of (001) GaAs using patterned graphene mask

Yujirou Hirota, Yuya Shirai, Hiromu Iha, Yusuke Kito, Manabu Suzuki, Hironao Kato, Nao Yamamoto, Takahiro Maruyama, Shigeya Naritsuka

Department of Materials Science and Engineering, Meijo University, 1-501 Shiogamaguchi, Tempaku-ku, Nagoya 468-8502, Japan

e-mail: 123434037@ccalumni.meijo-u.ac.jp

Selective growth is important not only for the fabrication of nanostructures but also the dislocation reduction in highly lattice-mismatched heteroepitaxy [1]. We have been studying selective growth of GaAs using molecular beam epitaxy (MBE) [2]. However, the window for the selective growth is very narrow because the selective growth is achieved by the re-evaporation of the adatoms on the mask. At the same time, the surface of the epitaxial layer becomes rough because of the high temperature of the growth. Therefore, a new material for the mask is requested to realize selective growth at low temperature. In this study, we focus on graphene as a mask material because graphene has two-dimensional structure and no bond towards the vertical direction. The critical temperature for the selective growth is firstly investigated with changing the growth temperature. Then, a pattered graphene mask is used to selectively grow GaAs.

The critical temperature for the selective growth of GaAs on graphene was studied with changing the substrate temperature from 580 to 600^{o}C. After finding the growth condition, the selective growth was performed on a patterned graphene mask, which was prepared by alcohol chemical vapor deposition (CVD). To form a patterned graphene mask, a 400nm-thick cobalt catalysis deposited by e-beam vapor deposition was firstly pattered into 7μm-wide stripes with period of 20μm using lift-off technique, as shown in Fig.1. Then, the graphene was grown by alcohol CVD on the Co catalysis. The CVD growth temperature and time was chosen to 450^{o}C for 10 min. After forming the graphene mask, the selective growth of GaAs was performed using MBE. The growth temperature and the thickness of the layer were set at 600^{o}C and 240nm, respectively. The grown layers were investigated using a scanning electron microscope (SEM).

Figure 2 shows SEM plane-view images of the selectively grown GaAs layers on graphene masks. Though several small polycrystalline of GaAs are observed on the sample grown at 580^{o}C, no polycrystalline are found on the graphene masks of the samples grown above 590^{o}C. On the other hand, a lot of polycrystalline were occurred on the SiO_2 mask even at 600^{o}C (not shown in the figure). The result indicates that the critical temperature of the selective growth on graphene is lower than that on SiO_2. The latter critical temperature is about 630^{o}C [2]. The weak bonding characteristics of the graphene is thought to increase the re-evaporation and/or the surface migration of the Ga adatoms. Consequently, the selective growth is able to realize about 30^{o}C lower on the graphene.

The selective growth of GaAs on a patterned graphene mask is shown in Fig.3. This figure clearly shows that a superior selectivity of growth and an extremely flat GaAs layer were obtained by the selective growth with the pattered graphene mask at 600^{o}C. The detailed mechanism of the growth using graphene will be discussed at the conference site.

Acknowledgments

This work was partly supported by Grant-in-Aid for Priority Area (B) No.22360131 from the Ministry of Education, Culture, Sports, Science, and Technology of Japan.

Reference

[1] For example, G.Bacchin and T.Nishinaga : J. Crystal Growth 208 (2000) 1-10.

[2] S. Naritsuka, S. Matsuoka, Y. Yamashita, T. Maruyama, J. Crystal Growth, 310 (2008) 1571-1575.

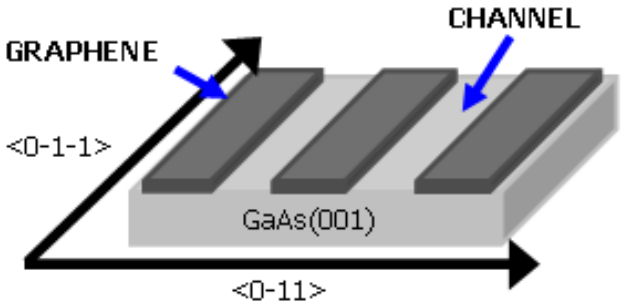

Fig.1 Patterned graphene mask for selective growth

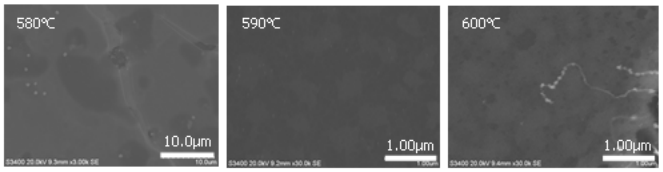

(a) (b) (c)

Fig.2 GaAs selective growth on graphene

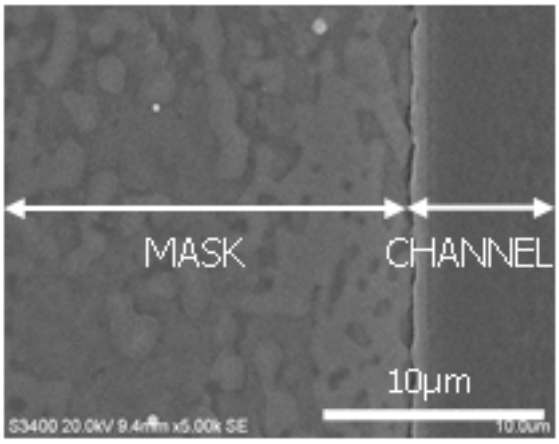

Fig.3 GaAs selective growth on patterned graphene

17:00 Poster Mo116

Nano-scale characterization of GaAsP/GaAs strained superlattice structures by nano-beam electron diffraction

Xiuguang Jin[1], Hiroko Nakamura[1], Koki Saito[1], Nobue Tanaka[1], Yoshikazu Takeda[2,3]

1. *Nagoya University, Aichi 4648603, Japan* **2.** *Nagoya Industrial Science Research Institute, Aichi 464-0819, Japan* **3.** *Aichi Synchrotron Radiation Center, Aichi Science and Technology Foundation, Aichi 489-0965, Japan*

e-mail: jinxg@nagoya-u.jp

Nanomaterials and low dimensional structures have been used for a wide variety of device applications. To achieve higher performance of such devices, a characterization technique in nano-scale is required. In this paper, we present strain and crystal structure evaluation with high spatial resolution using a nano-beam electron diffraction (NBD) [1] for GaAsP/GaAs strained superlattice layers.

Following the growth of a 2 mm thick $GaAs_{0.65}P_{0.35}$ layer and a 100 nm thick GaAs layer on the (001) GaP substrate, 6 pairs of the $GaAs_{0.65}P_{0.35}$(4 nm)/GaAs(4 nm) superlattice layers were grown. The NBD measurement was carried out using a TEM at an acceleration voltage of 120 kV. The electron beam size was about 15 nm in diameter.

TEM observation showed that the 100 nm GaAs layer consisted of (001) planes and slopes with an inclination angle of about 15° from the (001) plane. The superlattice layers on the (001) plane showed uniform thickness while those on the slope showed variable thickness. The NBD measurement indicated that the constant strain was introduced in the superlattice on the (001) plane while the non-uniform strain was introduced in the superlattice on the slope. From the NBD measurement, it was also found that the crystal orientation of the GaAsP superlattice layers on the slope was inclined by 1° from the [001] direction.

Using the strain values and thicknesses of the layers, the average mismatches of each pair of the superlattice were calculated. In the superlattice on the slope, the average mismatches decreased obviously with growth. It is believed that the change of the strain and the thickness contributed to decrease the strain effect. On the other hand, the average mismatches in the superlattice on the (001) plane showed much smaller values than that on the slope. The smaller values were the reason for the growth of uniform superlattice layers.

The formation mechanism of the different superlattice structures on the (001) plane and on the slope will be discussed.

Reference

[1] K. Saitoh, H. Nakahara, N. Tanaka, Microscopy, accepted (2013).

17:00 Poster Mo117

Solution growth of single crystalline organic semiconductor thin-films controlled by high magnetic field

Ryosuke Kamiya, Junichi Teramoto, Hiroyuki Fujishiro, Noriyuki Yoshimoto

Iwate University, Morioka 020-8551, Japan

e-mail: t5512001@iwate-u.ac.jp

In recent years, organic thin-film transistors (OTFTs) have attracted great attention, and their performance has continually improved. OTFTs fabricated by solution process have advantages in terms of a low-cost, printing process and compatibility with flexible substrates. Mobility and stability in solution processed OTFTs are still scarce, because crystallinity of organic semiconductor thin-films fabricated by solution process is generally low. Therefore, investigation and control of crystal growth are demanded to improve device performance of OTFTs. To control the crystal growth of organic semiconductors from solution phase, application of high magnetic field is effective. In this study, shape of solution is controlled by using high magnetic field which is provided by a bulk superconducting magnet. Solution including organic semiconductor and diamagnetic solvent is dropped onto substrate just above the magnet. The thickness of the diamagnetic solvent became very thin by means of the Moses effect. Evaporating the solvent slowly, a high concentration region occurs at thin place of the solution. As a result, a nucleation occurs selectively of the magnetic center. In this study, TIPS-pentacene and monochlorobenzene were employed as the organic semiconductor and solvent, respectively (Fig. 2). When crystals grow without the magnetic field, the nucleation occurs randomly and each crystal grows in disordered orientations (Fig. 3 (a)). In contrast, under the magnetic filed of 4 T, nucleation occurs preferentially of the center of the magnetic field, and the crystals grow radially as shown in fig. 3 (b). Figure 3 (c) and (d) show the in-plane X-ray rocking curves of fabricated TIPS-pentacene thin-films. The crystals obtained in the magnetic field were well orientated in in-plane direction. From these results, it is shown that application of the magnetic field is effective to improve the crystallinity of organic semiconductors using solution growth.

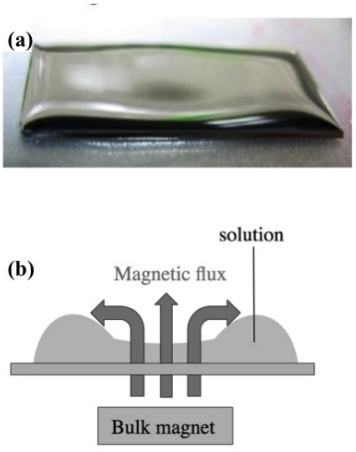

Figure 1. Effect of magnetic field on morophology of solution on substrate.

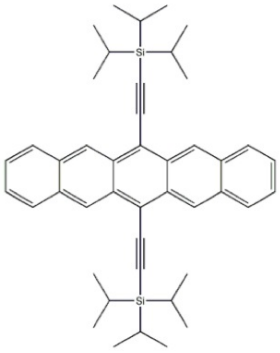

Figure 2. Molecular structure of TIPS-pentacene.

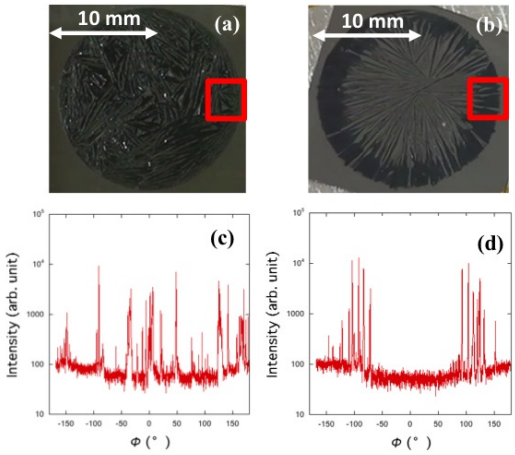

Figure 3. Picture and in-plane XRD rocking curves of fabricated TIPS-pentacene thin-films. Without the magnetic field ; (a) and (c), Under the magnetic field ; (b) and (d).

17:00 Poster Mo118

Optical properties and crystallinity of the GaN film grown on the SiO_2 based nanocomposites by MOCVD

BongKyun Kang, Sung Ryul Mang, Dae Ho Yoon

Sungkyunkwan university (SKKU), 2066, seobu-ro, jangan-gu, Suwon 440-746, Korea, South

e-mail: kangbk84@skku.edu

Recently, Gallium nitride (GaN) has been applied successfully as the high performance light emitting devices (LEDs), solar-blind ultraviolet photo detectors, and high power, high temperature devices. In spite of these developments, the performance of GaN-based LEDs is commonly reduced by fundamental problems that are associated with the large lattice mismatch and thermal expansion coefficients between hetero substrates and GaN films. These problems could lead to a significant number of defects such as threading dislocations (TDs) and associated point defects. Also, the degradation of efficiency results mainly from the TDs in the GaN films. To mitigate the TDs problem, the epitaxial lateral overgrowth (ELOG), selective area growth (SAG) and patterned sapphire substrate (PSS) techniques, in situ deposited SiN_x and ex situ TiN_x have been developed and widely used to reduce TDs densities. However, these techniques require complex and expensive processes such as depositing SiO_2 thin film and removing the SiO_2 film by selective etching.

In this work, we grew GaN films on the SiO_2 based nanocomposites by MOCVD to improve crystallinity and photoluminescence property**.** The size of SiO_2 bsased nanocomposites is approximately 200 nm. The TDs on the SiO_2 based nanocomposites were investigated by transmission electron microscope (TEM). The surface morphology and structural properties were investigated by Atomic Force Microscope (AFM), scanning electron microscope (SEM) and X-ray diffraction (XRD). the In addition, the optical properties of GaN films were examined by cathodo luminescence (CL) as well.

17:00 Poster Mo119

Selective epitaxial growth of compressively strained Ge layers on Si in 40-nm trench arrays

Byongju Kim, Sun-Wook Kim, Hyunchul Jang, Jeong-Hoon Kim, Sangmo Koo, Dae-Hong Ko

Yonsei University, School of Advanced Materials Science and Engineering, Seoul 120-749, Korea, South

e-mail: kimbj80@yonsei.ac.kr

Because of the technical difficulties in manufacturing nano-scaled semiconductor devices and also the inherent property of a low mobility, Si is not adequate for next generation high speed complementary metal oxide semiconductor (CMOS) logic devices beyond 10 nm nodes. In order to overcome these limitations, many researchers have explored Ge in order to replace Si for *p*-channel materials owing to its high hole mobility of 4 times higher than that of Si [1-4]. Despite such a merit of achieving high speed, the issues of a high cost of Ge wafers and the compatibilities with conventional Si CMOS processes have limited Ge's applications for replacing conventional Si channels. Although the epitaxial growth of the strain-relaxed Ge layers on Si wafers somewhat provides resolution from an economic perspective, high defect density in the Ge layers as well as their rough surfaces due to its large lattice mismatch of 4.2% with Si do not allow the integration of the Ge channel on Si substrates.

The aspect ratio trapping (ART) process, which involves selective growth of Ge on the Si regions between SiO_2 trench walls, has recently been reported to significantly reduce the magnitude of the defect density in the epitaxial Ge layers [5-11]. Despite the successful demonstration of the epitaxial Ge layers by ART process in the wide trenches and discrete holes, the fundamental understanding of the defect generations in the Ge layers in the narrow trenches have not been investigated, yet [6-11]. Indeed for the application to the nano scale Si devices, this issue of the buildup of the residual strain and consequent defect formations should be resolved. Therefore an in-depth research on the Ge growth in narrow (< 50 nm) trench arrays is needed.

In this paper we report the fabrication of high quality and compressively strained Ge epilayers on Si substrate using ART technology with a template of 40 nm SiO_2 trench array patterns. The cross-sectional shape of Ge layers was monitored by scanning electron microscopy (SEM) (JEOL, JSM-7001F). High resolution transmission electron microscopy (HR-TEM) measurements were carried out using a JEOL JEM-2100F. In order to analyze the strain in the Ge layers nanobeam electron diffraction (NBD) measurement was performed using TEM with a 2.5 nm diameter probe size.

Figures 1(a) and 1(b) depict the SEM images of the 40-nm-width trench arrays before and after the deposition, respectively. As can be seen in Fig. 1(b), Ge layers in each trench were deposited on a Si substrate with a uniform surface. Figures 1(c) and 1(d) show the cross-

sectional TEM images of Ge epilayers. In Figure 1(c) the cutting direction of the sample was [110], which is perpendicular to the direction of trenches and the Ge sample was prepared by the conventional ion milling method. Figure 1(d) shows the TEM image of the Ge specimen prepared by focused ion beam method along the trenches to reveal a single Ge epilayer. Despite a large lattice mismatch Ge was grown epitaxially with a low defect density. In a Ge/Si system, the critical thickness to nucleate a dislocation at the interface is estimated to be ~ 10 Å [11]. Therefore there are misfit dislocations at the Ge/Si interfaces that propagate to Ge epilayers forming threading dislocations. Since Ge has a diamond cubic crystal structure, its Burgers vector is **b** = $a/2$<110> and dislocations formed glide on (111) planes [12]. In addition, stacking faults are observed on the (111) planes with an angle of 54.7° to Si surface indicated by arrows as shown in Figs. 1(c) and 1(d). Nevertheless an upper region of Ge layers, of which heights are larger than critical thickness, reveals defect-free regions and top surface is formed with side facets.

In order to investigate the crystal quality, HR-TEM analyses were performed. Figures 2(a) and 2(b) show the HR-TEM images of the Ge epilayer inside the SiO_2 walls at upper region and in the vicinity of the Ge/Si interface, respectively. It is noted that the Ge layer was epitaxially grown with bottom Si substrate. Based on the diffraction pattern obtained from the dashed rectangular area in Fig. 2(a), we conclude that the Ge epilayer is surrounded by simultaneously flattened (001), (113), and (111) facets, as shown in Fig. 2(c). The epitaxial growth is also confirmed in the direction parallel to the trench [-110] (See Fig. 2(d)). In this case, as mentioned before, there are the stacking faults propagating from the Ge/Si interface to Ge top surface while maintaining a regular interval. Figure 2(d) displays clearly that the stacking fault is on the (111) plane making an angle of 54.7°.

Despite the large lattice mismatch and the condition where the height of Ge films is well above the critical thickness, a defect density is lower than expected and no surface roughening is observed as compared to the growth of Ge on bare Si wafers. It is likely that in the case of growing Ge layer in a narrow trench, SiO_2 mask prevents misfit dislocations from gliding to the side due to the constraint of lateral space along [110]. We attribute the low defect density of Ge to the growth of compressively strained layer. In order to measure the residual strain we performed the NBD analyses and these results will be presented in the conference.

Due to an increasing demand on high mobility devices and a low cost strategy, Ge has been grown on Si substrates in SiO_2 trenches using ART technology. Starting with a SiO_2 trench array pattern with a width of ~ 40 nm, we obtained high quality Ge epilayers with a low defect density despite the lattice mismatch of 4.2% between Ge and Si. HR-TEM analyses demonstrate that threading dislocations are located in a lower region of Ge epilayers and at regions above that the defect-free Ge layers are achieved.

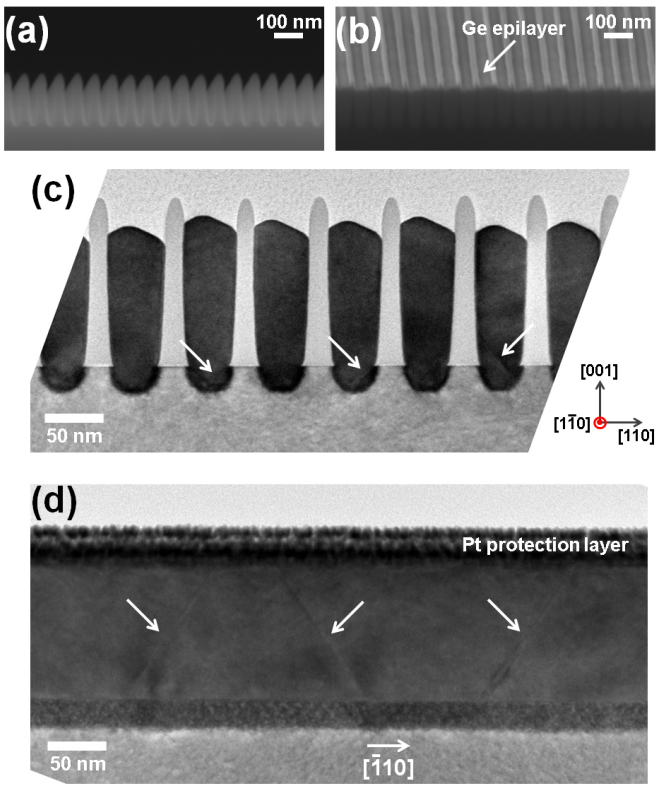

Figure 1. SEM images of the Ge trench patterns (a) before the deposition and (b) after the deposition, TEM images of Ge epilayers along two mutually perpendicular directions (c) [110] and (d) [-110], showing the defects indicated by the arrows

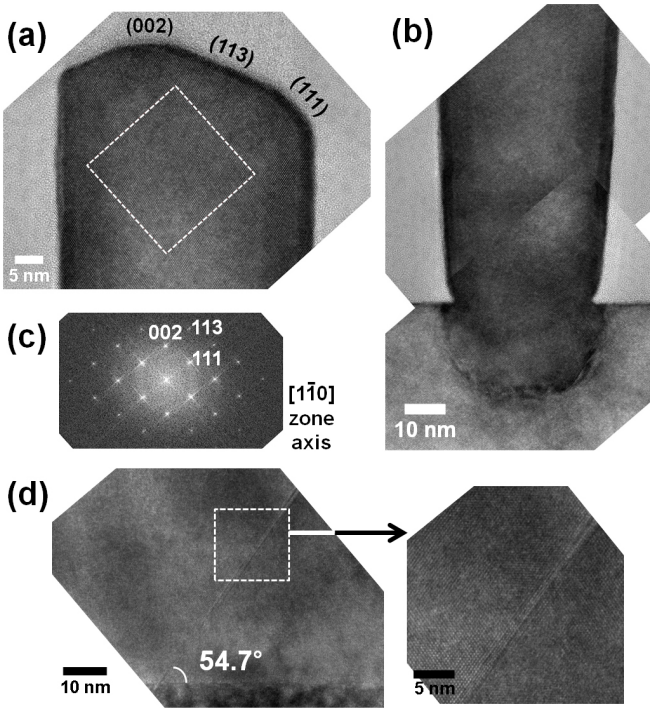

Figure 2. HR-TEM images of the Ge epilayer (a) at top region, (b) in the vicinity of the Ge/Si interface, (c) diffraction pattern for the selected area indicated by the dashed rectangle in (a), and (d) HR-TEM image of the Ge epilayer along the direction of the trench, showing the stacking fault and an enlarged atomic-scale view

References

[1] Minjoo L. Lee *et al*., Appl. Phys. Lett. **79**, 3344 (2001).

[2] C. O. Chui *et al*., Tech. Dig. - Int. Electron Devices Meet. **2001**, 437.

[3] Donald A. Neamen, *Semiconductor Physics and Devices: Basic Principles 4th ed*., (McGraw-Hill, New York, 2012).

[4] Darin Leonhardt *et al*., J. Appl. Phys. **110**, 073516 (2011).

[5] E. A. Fitzgerald *et al*., J. Electron. Mater. **20**, 839 (1991).

[6] T. A. Langdo *et al*., Appl. Phys. Lett. **76**, 3700 (2000).

[7] J.-S. Park *et al*., Appl. Phys. Lett. **90**, 052113 (2007).

[8] J. Bai *et al*., Appl. Phys. Lett. **90**, 101902 (2007).

[9] D. Pawlik *et al*., Electron. Lett. **44**, 930 (2008).

[10] G. Wang *et al*., J. Appl. Phys. **108**, 123517 (2010).

[11] J. W. Matthews *et al*., Thin Solid Film **33**, 253 (1976).

[12] D. Hull *et al*., *Introduction to Dislocations 5th ed*., (Elsevier, New York, 2011).

17:00 Poster Mo120

Mechanism of in-plane orientation of GaN self-induced nanowires grown on Si(111) substrates

Andrian Kuchuk[1], Vasyl Kladko[1], Peter Lytvyn[1], Andriy Efremov[1], Hryhorii Stanchu[1], Aleksandra Wierzbicka[2], Marta Sobanska[2], Kamil Klosek[2], Zbigniew R. Zytkiewicz[2]

1. *V. Lashkaryov Institute of Semiconductor Physics NASU (ISP), 41, pr. Nauki, Kiev 03028, Ukraine* **2.** *Institute of Physics, Polish Academy of Sciences, Warsaw 02-668, Poland*

e-mail: an.kuchuk@gmail.com

GaN nanowires (NWs) are extensively studied due to their perfect structural characteristics in comparison with planar epitaxial layers. This allows creation of new electronic devices with improved parameters. In this work, the mechanism responsible for in-plane arrangement of self-induced GaN NWs grown by plasma-assisted molecular beam epitaxy (PAMBE) on Si(111) substrate was investigated.

We show that the process of substrate nitridation performed at various temperatures prior to the MBE growth leads to creation of thin Si-N film on Si(111) substrate. Our XRD data indicates that a coherency of in-plane orientation of NWs strongly depends on temperature T_{ni} at which this Si-nitride film is grown.

First, the nitridation process of Si substrate was carried out at low temperature (LT). AFM measurements performed after nitridation process show that Si-N film is atomically smooth. However, GaN NWs grown on Si substrate with LT Si-N layer are twisted randomly. When the nitridation process of Si(111) substrate was carried out at high temperature (HT) post-growth AFM studies revealed formation of Si-N terraces with edges orientated along the <112> Si directions. In that case GaN NWs grown on HT Si-N film were ordered in-plane relative to Si substrate, i.e. the GaN basal <-1-120> directions were aligned with the Si <1-10> directions. This is the same epitaxial relationship between GaN and Si lattices as commonly observed in planar GaN layers grown on Si(111).

On the contrary, both SEM and XRD confirm that independently on substrate nitridation conditions NWs were grown with the c-axis being perpendicular to the substrate surface. As will be discussed, this indicates on quite different mechanisms responsible for in-plane and out-of-plane arrangements of the nanowires on the substrate.

This work was supported by the European Union within European Regional Development Fund, through grant Innovative Economy (POIG.01.01.02-00-008/08 NanoBiom).

17:00 Poster Mo121

Epitaxial growth of $SmFe_7$ films on Ta-buffered sapphire substrate using the RF magnetron sputtering method

Takeshi Kusumori, Kenta Takagi, Hiroyuki Nakayama, Mizue Mizoshiri, Kimihiro Ozaki

National Institute of Advanced Industrial Science and Technology (AIST), 2266-98 Anagahora, Shimoshidami, Moriyama-ku, Nagoya 463-8560, Japan

e-mail: t.kusumori@aist.go.jp

Rare-earth-based iron-rich compounds are important industrially in high-performance magnets used in the motors of hybrid and electric vehicles. Following the discovery of Nd-Fe-B magnets there has been intensive pursuit of new permanent magnets based on rare-earth-iron systems. Sm-Fe-N compounds, which are produced mainly as powder, are promising materials because of their higher Curie temperature than Nd-Fe-B magnets. To investigate their magnetic properties and how they have superior characteristics as permanent magnets, single crystals or epitaxial films are necessary.

We report here the fabrication of epitaxial films of $SmFe_7$, which is a starting alloy for Sm-Fe-N permanent magnets with $TbCu_7$-type crystal structure, upon Ta-buffered sapphire substrates. These films were prepared by the RF magnetron sputtering method, using Sm and Fe targets for $SmFe_7$ films and Ta target for Ta buffer layers. The substrate temperature during film deposition was maintained at 400°C. The thickness of the $SmFe_7$ and Ta layers were respectively about 40 nm and 360 nm.

The orientation of the films relative to the substrate was examined by XRD measurements. XRD spectra from 2 theta-omega scanning indicate that $SmFe_7$ (0001) films and the Ta (111) buffer layer grow normal to the sapphire (0001) substrate surface. Phi scanning measurements show 6-fold symmetry of (11-21) diffraction lines for hexagonal $SmFe_7$, 3-fold symmetry of (22-2) diffraction lines for cubic Ta, and 3-fold symmetry of (10-14) diffraction lines for rhombohedral sapphire, indicating epitaxial growth of the Ta buffer layer and $SmFe_7$ film.

We undertook TEM observations of cross-sections of the films. $SmFe_7$ grains grew in a columnar manner. Precipitation of α-Fe was found in the film, due presumably to Fe-enhanced deviation from the stoichiometric ratio. An amorphous area in the $SmFe_7$ film was identified adjacent to the Ta layer. The bottoms of the $SmFe_7$grains were V-shaped, suggesting that formation of the amorphous area began near the interface and proceeded to form a facet.

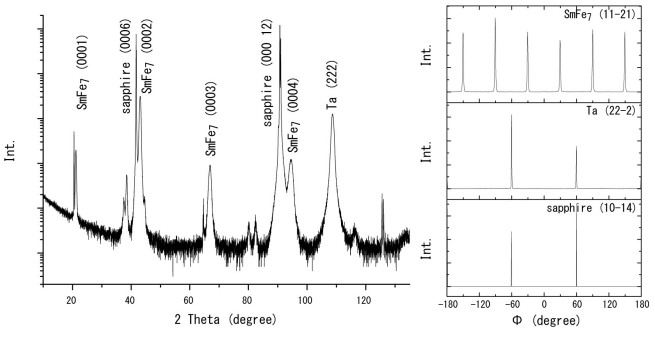

XRD profiles of 2 theta-omega scanning (left) and phi scanning (right) for the $SmFe_7$ film.

17:00 Poster Mo122

Structural and optical properties of GaPN(As) and InGaPN layers grown by MBE

Aleksandra Lazarenko, Ekaterina Nikitina, Evgeny Pirogov, Maksim Sobolev, Anton Egorov

St Petersburg Academic University, Khlopina Str 8/3, S.Petersburg 194021, Russian Federation

e-mail: lazarenko@spbau.ru

Growing high-quality III–V compound semiconductors with a direct band-gap on Si substrates is the key to implementation of optoelectronic integrated circuits (OEIC) on Si substrates. Physicists have long wished to create a single chip, combining III–V compounds with Si. The main problem in the growth of III–V compounds on Si is the unwanted generation of structural defects such as dislocations, stacking faults and anti-phase domains. A large number of dislocations is formed during the growth of light emitting III-V compounds on Si substrates due to the large lattice mismatch [1].

GaP has almost the same lattice constant as Si, but has indirect band gap. This problem can be overcomed by growing III–V–N alloys which are lattice-matched to Si and has the direct band-gap [2].

Growing dislocation-free GaP(As)N and InGaPN layers with direct band-gap on GaP substrate is the first step of creating OEIC on Si [3,4].

We investigated optical and structural properties of $GaP_{1-x}N_x$ bulk layers and $In_{1-x-y}GaP_yN_x$ and $GaP_yN_xAs_{1-x-y}$ quantum wells grown by molecular-beam epitaxy on GaP (001) substrates. The influence of various growth parameters (substrate temperature, growth rate and power of radio frequency (rf) plasma source of nitrogen) on the quality of layers and nitrogen content in heterostructures was studied. The epitaxial growth was realized with rf plasma nitrogen source. The structural investigations was performed by high-resolution X-ray diffraction (XRD). Room temperature (RT) photoluminescence (PL) of these samples was studied.

The samples demonstrate intensity room temperature photoluminescence (PL) in the red-orange spectral range. It means that the addition of nitrogen in GaPN(As) and InGaPN films leads to the direct band gap structure formation.

With the decrease of growth temperature of GaPN films the nitrogen mole fraction increase and luminescence intensity decrease (fig. 1). The decrease in the PL intensity implies that the GaPN layer contains a large number of non-radiative recombination centers and/or deep-levels. These defects could be generated due to large miscibility gap and fluctuations of nitrogen compositions in the GaPN layer. The rapid thermal annealing can improve the crystalline quality of GaPN layer [5].

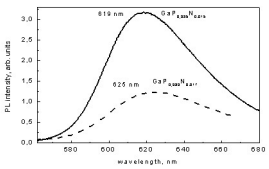

Figure 1.RT PL spectra of $GaP_{1-x}N_x$/GaP, grown at 470 ^{0}C (dashed) and 510 ^{0}C (solid).

The dependence of varying the rf power plasma source and growth rate on N incorporating was investigated. (fig. 2) The increase in the growth rate and/or rf power increases the N content and decreases the PL intensity.

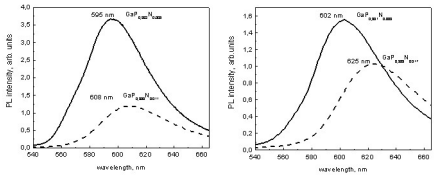

Figure 2. RT PL spectra of $GaP_{1-x}N_x$/GaP, grown at a) 300 W (solid) and 470 W (dashed) rf power plasma source; and b) at growth rate 1.7 Å/c and 400 W rf power (solid), 0.8 Å/c and 500 W (dashed).

The N content in $GaP_{1-x}N_x$ films with $0.004 \le x \le 0.018$ was investigated using XRD (fig. 3). The peak separation increases with increasing the nitrogen content, because the lattice constant decrease. The composition of $GaP_{1-x}N_x$ was determined by peak position.

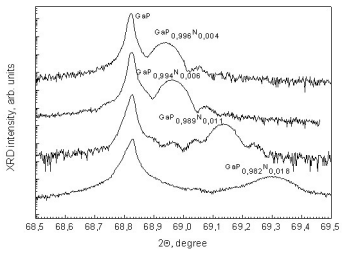

Figure 3. XRD curves of $GaP_{1-x}N_x$ films

Nitrogen addition in GaP and decreases the lattice constant and so leads to emergence of elastic stress. Addition of As or In increase the lattice constant of the solid solution.

A comparative analysis of samples with InGaPN and GaPNAs quantum wells was performed (fig. 4). It was shown that the PL intensity of heterostructures with InGaPN is much lower due to the large number of defects [6]. Indium is embedded in sublattice of III group, but elastic stress appears in sublattice of V group. Arsenic embedded in sublattice of V group compensates elastic stress and prevents the formation of defects. Thereby GaPNAs quantum wells have better crystalline quality.

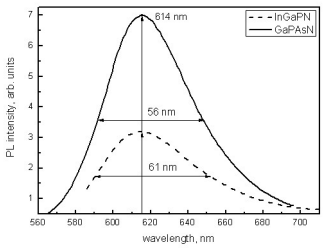

Figure 4. RT PL spectra of GaPAsN/GaP (solid) and InGaPN/GaP (dashed) quantum wells.

In summary, we investigated optical and structure properties of GaPN(As) and InGaPN layers. We also studied the influence of growth parameters on the nitrogen incorporation in GaPN/GaP layers.

A comparative analysis of samples with InGaPN and GaPNAs quantum wells was performed. It was shown that heterostructures with GaPNAs quantum wells have better crystalline quality.

[1] Y. Furukawa, H. Yonezu and A. Wakahara, «Monolithic integration of light-emitting devices and silicon transistors», SPIE Newsroom, (2007)

[2] B. Kunert, S. Reinhard, J. Koch, M. Lampalzer, K. Volz, and W. Stolz, Phys. stat. sol. (c) 3, No. 3, 614–618 (2006)

[3] S. Y. Moon, H. Yonezu, Y. Furukawa, Y. Morisaki, S. Yamada A. Wakahara, phys. stat. sol. (a) 204, No. 6, 2082–2086 (2007)

[4] H. Yonezu,Y. Furukawa, A. Wakahara, Journal of Crystal Growth, 310, 4757–4762, (2008)

[5] A. Utsumi et al, phys. stat. sol. (c) 0, No. 7 (2003)

[6] O.I. Rumyantsev, P.N. Brunkov, E.V. Pirogov, A.Yu. Egorov, Seniconductors, 44 (7), 923-927 (2010)

17:00 Poster Mo123

$ZnWO_4$ films obtained by ion–beam sputtering and hydrothermal method

Oleksiy Lebedynskiy[1], Ianina Boiaryntseva[1], Alexander Dubovik[1], Alexander Fedorov[1], Konstantin Katrunov[1], Dmitriy Sofronov[1], Irina Tupitsyna[1], Anna Yakubovskaya[1], Stanislav Yakovin[2], Alexander Zykov[2], Volodymyr Savchyn[3], Yuriy V. Zorenko[3]

1. *Institute for Scintillation Materials NAS of Ukraine (ISMA), Lenina ave., 60, Kharkov 61001, Ukraine* **2.** *Kharkov National University, 4 Svoboda Sq., Kharkov 61077, Ukraine* **3.** *Laboratory of Optoelectronic Materials Electronic Department Ivan Franko National University of, Lviv 79017, Ukraine*

e-mail: lebed@xray.isc.kharkov.com

$ZnWO_4$ has the monoclinic structure with the space group P2/c and two formula units per unit cell. It is a wide band gap (about 4 eV) compound. $ZnWO_4$ is considered as an attractive material for different applications due to its optical and chemical properties. Its potential application fields are wide from laser host material to scintillation detector.

$ZnWO_4$ are usually used in a form of single crystals produced by Czochralski method from a melt. In order to extend application area many efforts are made to obtain and study $ZnWO_4$ in film form. $ZnWO_4$ films can be prepared by different methods: sol–gel, spray pyrolysis, RF sputtering of WO_3 and ZnO mixture. In this work $ZnWO_4$ films were obtained by ion-beam sputtering and hydrothermal method.

Films produced by ion beam sputtering were deposited on the glass and KBr substrates in a vacuum chamber equipped with gridless closed drift ion source of the "Radikal" type. Pure Ar and O_2 at pressures $5 \cdot 10^{-4}$ Torr and $4 \cdot 10^{-4}$ Torr, respectively, were used for sputtering. The cleaved facet (010) of Chochralski grown $ZnWO_4$ crystal or ZnO-WO_3 hot-pressed mixture with matched to $ZnWO_4$ weight ratio were used as a targets for ion beam sputtering. Films of 1-10 mkm thickness were obtained in a time 30-180 min at the substrate temperatures 473-573 K.

The hydrothermal synthesis of $ZnWO_4$ films was realized with stainless-steel autoclave. For this purpose the amorphous $ZnWO_4$ precursor was obtained according to the reaction $Zn(NO_3)_2 + Na_2WO_4 \rightarrow ZnWO_4 \downarrow + 2NaNO_3$ and then filled in a stainless steel autoclave. Clean glass substrate was placed into the autoclave above the suspension surface. The tightly closed autoclave was heated to 473 K and kept at this temperature during 24 h without shaking or stirring. Thereafter autoclave was allowed to naturally cool down to room temperature. This process resulted in formation of a dense thick 10-20 mkm film on the sides of substrate.

The structure and optical properties of films obtained by both methods as well as comparison of methods applied for film production are discussed.

17:00 Poster Mo124

Fabrication of $BiFeO_3/LaNiO_3$ epitaxial superlattice structures by RF sputtering

Hsin-Yi Lee[1], Yen-Ting Liu[2], Shang-Jui Chiu[1], San-Yuan Chen[2]

1. *National Synchrotron Radiation Research Center (NSRRC), 101 Hsin-Ann Rd, Hsinchu Science Park, Hsinchu 30076, Taiwan* **2.** *Department of Materials Science and Engineering, National Chiao Tung University, Hsinchu 30050, Taiwan*

e-mail: hylee@nsrrc.org.tw

Artificial superlattice structures consisting of alternating epitaxial layers of materials with dissimilar physical properties offer exciting new possibilities both in the investigation of fundamental physical phenomena and in the exploitation of novel properties for diverse applications. In this work, symmetric epitaxial superlattice structures of multiferroic $BiFeO_3$ (BFO) and conductive $LaNiO_3$ (LNO) sublayers were grown on a Nb-doped $SrTiO_3$ substrate with rf magnetron sputtering at temperature 660 ^oC. The superlattices contained 6 – 30 periods of BFO/LNO bilayers with a sublayer thickness in a range 1.7 – 8.5 nm; the total thickness of the films was fixed at ~ 100 nm. We characterized the structure of the interface and the surface morphology of these films by measuring X-ray reflectivity (XRR) and diffraction. The formation of a superlattice structure was confirmed from the appearance of satellite features on both sides of the main feature in the X-ray diffraction (XRD) pattern. The periods and thickness of the superlattice confirmed by XRD and XRR are consistent with the results of secondary-ion mass spectrometer (SIMS). X-ray measurements show that these superlattice films become subject to greater tensile stress along the c-axis and increased compressive stress parallel to the surface plane with decreasing thickness of the sublayer. The BFO sulayer in the artificial superlattice is under biaxial compressive stress whereas the LNO sublayer is under biaxial tensile stress. The smaller is the thickness of the sublayer, the greater is the crystalline quality and the strain state. The hysteresis loops show a large leakage current at frequencies 0.5 and 1 kHz; the polarization decreases with increasing frequency. An intrinsic remanent polarization of the superlattices was observed at the thickness of a sublayer in the range 1.7 – 8.5 nm at 5 kHz. The rounded shape of the hysteresis loop at frequency ≤ 2 kHz resulted from large dc leakage and extrinsic interface effects.

17:00 Poster Mo125

Supphire Substrates With The Regular Relief Surface

Arsen Muslimov, Vladimir M. Kanevsky, Andrey Butashin, Alex Deryabin, Elena Rakova

A.V.Shubnikov Institute of Crystallography The Russian Academy of Sciences, Moscow, Russian Federation

e-mail: amuslimov@mail.ru

Application of the crystal substrates with the regular microrelief surface results in considerable reduction of the dislocation density in heteroepitaxial films like *GaN* on sapphire for example [1]. Such microrelief is usually created by the photolithography method and consequent etching of the substrate surface. Regular relief in a form of parallel steps and terraces of nanometer sizes can be created on the vicinal surface of sapphire substrates by their annealing in air at temperatures ≥1000ºC (Fig. 1.b). Application of such sapphire substrates with the

regular nanorelief surface results in improvement of the crystal quality of the heteroepitaxial $A^{II}B^{VI}$ semiconductor films [2], and permits to form ordered ensembles of nanoparticles, like *Au* particles for example [3] on such surface.

In present work regular microrelief on the sapphire substrate surface was created by following:

- standard vacuum evaporation method to deposit the metal mask layer of about 0,35 μm in thickness;

- standard photolithography method to obtained the windows of desired forms and sizes in the layer;

- the *Cl*-ion reactive plasma etching of the surface in opened windows to the depth of about 1,5 μm.

Obtained microrelief was formed by the circular or pseudo-triangle pits (Fig. 1.a) with the typical cut sizes 1÷7 μm and depths 1÷2 μm.

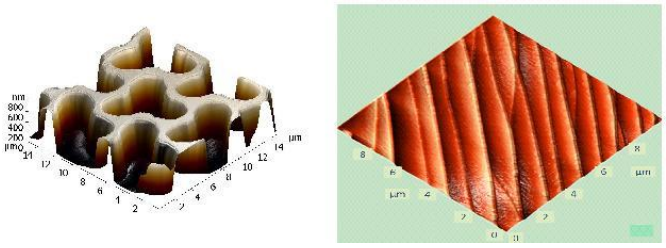

a b

Fig. 1. AFM image of sapphire substrate surface with regular relief, created by the lithography and etching methods (a), and by annealing the vicinal (0001) sapphire substrate in air at 1400°C

In addition experimental processes including vacuum deposition of *Al* metal on sapphire substrate surface through the regular pattern with the holes sizes 0.2÷40 μm and consequent oxidization and annealing were carried out to form regular microrelief on the surface (Fig. 2). Preliminary RHEED data, obtained from continuous film created by this method, indicate the film to be the sapphire single crystal. The jut lateral sizes are only defined by the pattern holes sizes, but the jut height does not exceed 20 nm for the moment, since it strongly depends upon the oxygen atoms diffusion length through the alumina layer from atmosphere to *Al* metal at its oxidization and the sapphire single crystal growth speed in the solid state as well.

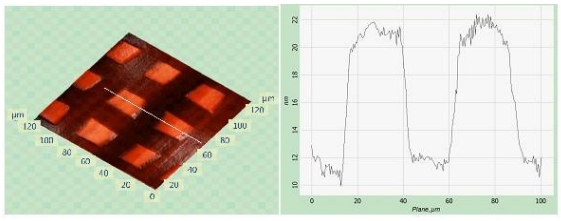

a b

Fig. 2. AFM image (a) and cross-section (b) of microrelief on the sapphire substrate surface, which is created by the vacuum deposition of *Al* metal through the regular pattern and consequent annealing at 1400°C in air

This study was performed using the equipment of the Mixed-Use Center of the Institute of Crystallography, Russian Academy of Sciences (RAS), and supported by the Ministry of Education and Science of the Russian Federation and the RAS Presidium (Basic Research Program no. 24, “Fundamentals of the Technology of Nanostructures and Nanomaterials”).

REFERENCES

1. Y. H. Kim, H. Ruh, Y. K. Noh, et. al. // J. Appl. Phys. 2010, V. 107, 063501.

2. V. I. Mikhailov, A. V. Butashin, V. M. Kanevsky, et.al. // J. Surf. Invest. 2011, Vol. 5, p. 595.

3. A. E. Muslimov, A. V. Butashin, A. A. Konovko, et. al. // Cryst Reports, 2012, Vol. 57, p. 415.

17:00 Poster Mo126

3C-SiC growth and characterization using methyltrichlorosilane

Marco Negri[1,2], Matteo Bosi[1], Giovanni Attolini[1], Béla Pécz[3], Ferenc Riesz[3], Lazlo Dobos[3], Mario P. Rotonda[4], Chris Cornelissen[4]

1. *IMEM- CNR (IMEM), Parma, Italy* **2.** *Dipartimento di Fisica, Università, Viale G.P. Usberti 7/a, Parma 43100, Italy* **3.** *Hungarian Academy of Sciences, Research Institute for Technical Physics and Materials Science, P.O.Box 49, Budapest H-1525, Hungary* **4.** *Lintes Research Laboratory, via Isola 2, Teramo 64010, Italy*

e-mail: negri1@gmail.com

Silicon carbide (SiC) is mechanically robust, chemically inert, non toxic and biocompatible, so is a good material for application in harsh environment and for biomedical purpose.

3C-SiC layers are commonly prepared by Vapour Phase Epitaxy (VPE) on silicon substrates. Due to the large mismatch between the two materials it is necessary to grow a buffer layer with a carburization of the silicon surface. However, this does not prevent the appearance of a large amount of structural and morphological defects in the film.

In this work we study the growth of 3C-SiC/Si by adding methyltrichlorosilane (MTS) to a standard process for 3C-SiC deposition using SiH_4 and C_3H_8.

A baseline SiC/Si growth process was developed with a carbonization at 1125 °C, addition of SiH_4 and C_3H_8 during the heating from 1125 °C to the thick film growth temperature and finally the deposition of a SiC layer at different temperatures, from 1300 °C to 1400 °C with Si/C ~ 1.4 at 200 mbar.

We investigate how the addition of MTS at different growth temperatures (1300 °C to 1400 °C) affects the SiC layer growth. We varied MTS/SiH_4 ratio from 1/20 to about 1 and we analyzed the samples by means of Transmission Electron Microscope (TEM), Fourier Transform Infrared Spectroscopy (FT-IR) and ellipsometry to study the structural quality of the films and to compare the results between the standard growth procedure and the one with MTS addition. The film thickness was measured by means of optical reflectivity and the study of the growth rate with and without MTS gives informations about the kinetics of the reactions.

We found that even with a small MTS/SiH_4 ratio of 1/20 in the gas phase is sufficient to increase significantly the growth rate, due to the fact that Cl species binds to Si atoms in the gas phase and prevents the formation of Si condensates. Quality of the film grown with and without MTS, as observed by XRD and TEM, is comparable for small MTS partial pressures but decrease if MTS/SiH_4 is increased to about 1. Surface, as observed by AFM, maintains a smooth morphology with very low mean square roughness, below 1nm for area of 1x1 mm^2.

Strain due to lattice and thermal mismatch is common problem in SiC/Si heteroepitaxy and, in order to study how MTS addition affects it we imaged the samples by means of Makyoh, in order to study the substrate bending. Low amount of stress was found.

17:00 Poster Mo127

Influence of the growth conditions on the properties of Germanium epilayers grown by MOVPE on Si

Giovanni Attolini[1], Matteo Bosi[1], Sophia J. Ponraj[2], Dakshinamurthy Arivuoli[2], Cesare Frigeri[1], Elisa Buffagni[1], Claudio Ferrari[1], Marco Negri[1], Tarik Asar[3], Nahida Musayeva[4,5], Rasim Jabbarov[4,5]

1. *IMEM- CNR (IMEM), Parma, Italy* **2.** *Crystal Growth Centre, Anna University, Chennai, Chennai 600025, India* **3.** *Physics Department of Arts and Science Faculty, Gazi University, Ankara 06500, Turkey* **4.** *Research and Development Center for Hi-Technologies (MCIT), Inshaatchilar ave., Baku AZ1073, Azerbaijan* **5.** *Azerbaijan National Academy of Science, Institute of Physics, H.Javid str.33, Baku AZ1143, Azerbaijan*

e-mail: negri1@gmail.com

Germanium (Ge) is an interesting material for high efficiency solar cell applications. Ge cells are also employed in thermophotovoltaic devices and photovoltaic multiple junction solar cells which is the current technology used to obtain Ge p/n junction by dopant diffusion. Ge is a low bandgap semiconductor (E_g= 0.67 eV) that also finds application in infrared detection. The study of mechanical properties of the germanium thin films has gained much attention in recent days and is required to use them as structural and functional elements in device fabrication. Heteroepitaxial Ge layers were deposited by means of metal organic vapor phase epitaxy (MOVPE) on Si (001) substrates using iso-butyl germane (iBuGe) as organic precursor and hydrogen as carrier gas. Germanium layers were grown at low pressure (60 mbar) and in the temperature range of 550-675°C at a growth time of 15 minutes. The removal of native oxide from the Ge substrate prior to the growth was done with HCl wet chemical etching and by performing a thermal annealing of the substrate at 650 ºC for 5 minutes.

The deposited epilayers were characterized by atomic force microscopy (AFM), scanning electron microscopy (SEM), high resolution X-ray diffraction (HRXRD) and transmission electron microscopy (TEM) and SPM coupled Hysitron TI950 Triboindenter. The AFM analysis shows that the surface was rough in general and with 3D islands, regardless of growth conditions such as temperature, pressure and iBuGe partial pressure. The HRXRD profile of the epilayers confirmed good crystallographic quality of the Ge epilayers. The growth rate was influenced by the growth temperature and partial pressure. The TEM results have been confirmed good interfaces and many defects were found. The mechanical deformation behaviour has been investigated by nanoindentation technique using Berkovich and Vickers indenters to study the properties such as hardness and elastic modulus. The occurrence of elbow phenomenon and their elasto-plastic properties appears to be related to sudden propagation of threading dislocation by pre-existing defects in the materials with the indentation load.

References

1. D.J. Oliver, J.E. Bradby, J.S. Williams, Journal of Applied Physics, 101, p. 043524, (2007)

2. G. Timò, C. Flores, R. Campesato, Cryst. Res. Technol. 40, (2005),pp. 1043-1047.

3. V.M. Andreev, V.P. Khovostikov, N.A. Kalyuzhnyi, S.S. Titkov, O.A. Khvostikova, M.Z. Shvarts, Semiconductors 38, (2004), pp. 355-359.

17:00 Poster Mo128

Growth condition dependence of electric properties of ScN films on (100) MgO substrates prepared by molecular beam epitaxy

Takeshi Ohgaki, Ken Watanabe, Yutaka Adachi, Isao Sakaguchi, Shunichi Hishita, Naoki Ohashi, Hajime Haneda

National Institute for Materials Science (NIMS), 1-1 Namiki, Tsukuba, Ibaraki 305-0044, Japan

e-mail: OGAKI.Takeshi@nims.go.jp

With the progress of GaN devices, ScN has attracted much attention in the recent decade. As 111-orieted ScN is lattice-matched to 0001 oriented wurtzite GaN, ScN is a potential material for development of GaN devices. In this study, the ScN films were grown on (100) MgO single crystals by a MBE method, and the electric properties of MBE grown ScN films were measured by temperature dependence Hall effect. The effect of the growth condition, the Sc/N ratio, growth temperature and nitrogen-radical state, on the electric properties of ScN films was studied.

ScN films were prepared by MBE using an RF plasma discharge cell as the nitrogen source. A conventional K-cell was used for evaporation of Sc metal. The K-cell temperature was varied from 1270–1310°C to examined the effect of Sc-flux on the surface morphology and the electric properties. A nitrogen radical beam, generated by the RF discharge cell, was irradiated on the film surface. MgO single crystals with a well polished (100) face were used for the substrates of ScN films. Before the growth, the substrates were thermally cleaned in a vacuum at 850°C for 30 min. The growth temperature was varied between 300 and 850°C to evaluate the effect of the substrate temperature. The crystalline phase and lattice orientation of the films were determined from XRD measurements. The surface of the films were observed by an AFM. The electric resistivity, the carrier concentration and the Hall mobility of the films were measured by Hall effect at 80–400K.

The ScN films were grown epitaxially on the MgO (100) substrates. Hall coefficient measurement confirmed that the ScN films grown under N-rich condition were highly degenerate n-type semiconductor, and the carrier concentration of the ScN films were 10^{19}–10^{21} cm^{-3}, and the Hall mobility were 50–150 $cm^2 \cdot V^{-1} \cdot s^{-1}$ even as the undoped films. The carrier concentration and the Hall mobility of the ScN film were sensitive to the growth temperature and the nitrogen-radical state compared to the Sc/N supplying ratio during the deposition, and the Hall mobility of the ScN films increased with increasing carrier concentration. The temperature-dependence Hall coefficient measurement revealed that the carrier concentration is nearly independent of temperature, indicating that the change of the resistivity with temperature is explained by the change of the Hall mobility. The Hall mobility of the ScN films increased with decreasing the measurement temperature, and the decrease of the Hall mobility at the lower temperature region due to ionized impurity scattering was not observed in temperature range from 80-400K.

17:00 Poster Mo129

Self-compensation effect of the silicon impurity in heavily doped AlGaN layers

Igor V. Osinnykh[1,2], Konstantin S. Zhuravlev[2], Dmitry Y. Protasov[2], Timur V. Malin[2], Valentin V. Ratnikov[3], V. Y. Davydov[3], Alexander N. Smirnov[3], Reginold N. Kyutt[3]

1. *Novosibirsk State University (NSU), Pirogov 2, Novosibirsk 630090, Russian Federation* **2.** *Institute of semiconductor physics (ISP), Lavrentiev, Novosibirsk, Russian Federation* **3.** *Ioffe Physico-Technical Institute (Ioffe), Polytechnicheskaya, 26, Saint-Petersburg 194021, Russian Federation*

e-mail: igor-osinnykh@nlstar.com

Due to wide and direct band gap AlGaN alloys have a wide application in light emitting diodes, high electron mobility transistors, high-density optical storage devices, ultraviolet emitters, and photodetectors. Doping of AlGaN layers is needed to fabricate multilayer device structures. Silicon is usually used in molecular beam epitaxy (MBE) for n-type doping of AlGaN layers. However, influence of silicon on AlGaN properties is very complicated and complex. Impurity causes formation of defects in epitaxial layers. Aim of this work was to investigate effect of silicon on electron concentration in AlGaN layers.

Sets of GaN and $Al_{0.3}Ga_{0.7}N$ layers were grown by MBE using ammonia as source of active nitrogen and silane (SiH4) as source of Si on (0001)-oriented sapphire substrates. Thickness of the layers was about 1.1-1.3 mm. In order to characterize the structural properties of the AlGaN layers, atomic force microscopy (AFM) and X-ray diffraction (XRD) were used. Concentration of silicon atoms in layers was found from secondary ions mass spectrometry (SIMS) data. Electron concentration (n) was evaluated by Hall measurements and Raman spectroscopy. Optical properties were studied by photoluminescence (PL) techniques. All measurements were carried out at 300K. PL of GaN layers was excited by laser with photon energy of 3.81 eV, and for excitation of PL of $Al_{0.3}Ga_{0.7}N$ layers two types of lasers with photon energy of 466 and 5.08 eV respectively.

In both materials, the concentration of silicon atoms in the layers increases linearly with the silane flux. The dependence of the electron concentration on the concentration of impurity atoms is different in the case of GaN and $Al_{0.3}Ga_{0.7}N$: if the layers of GaN observed a linear increase with increasing concentrations of silicon, in $Al_{0.3}Ga_{0.7}N$ electron concentration saturates. The difference is explained by a high degree of self-compensation $Al_{0.3}Ga_{0.7}N$ which is caused by either an increase in the number of defects, point or extended, or embedding the silicon atoms in place of nitrogen in the crystal lattice, which is why he is an acceptor. Gallium and aluminum vacancies form deep acceptor levels in AlGaN, the energy of formation of cation vacancies decreases with increasing Fermi energy. As $Al_{0.3}Ga_{0.7}N$ having a wide band gap, it has more cation vacancies. Transitions with vacancy's deep levels lead to appearance of wide yellow band in PL spectra. Experimental results show that in the case of GaN increase of doping leads to suppression of the defect band in the PL spectra induced cation vacancies, while the growth of silicon concentration in AlGaN its intensity increases. However, with increasing concentration of the donor concentration of cation vacancies in AlGaN is growing more slowly than in GaN, so the saturation of the electron concentration on the contrary should occur faster in GaN. Concentration of edge dislocations in AlGaN increase faster with increasing silicon content than in GaN, therefore we assume that rise of concentration of this type defects leads to decline of efficiency of dopind in $Al_{0.3}Ga_{0.7}N$. In addition, the visible surface of the AlGaN extended defects in heavily doped, they are replaced by defects of hexagonal shape, with the doping concentration of defects increases strongly. Presumably, these defects occur at the grain boundaries during the growth layers and may make compensation centers.

17:00 Poster Mo130

Spectroscopic characterization of high-quality polycrystalline Bi-Te films grown by thermal evaporation

Rafał M. Rapacz, Katarzyna Balin, Krzysztof Smuda, Anna Nowak, Jacek Szade

University of Silesia, August Chełkowski Institute of Physics, Department of Solid State Physics, Uniwersytecka 4, Katowice 40-007, Poland

e-mail: rapaczrafal85@gmail.com

Topological insulators form a group of materials exhibiting unusual metallic properties of the surface with an insulating gap in the bulk. One of the 3D topological insulator is Bi_2Te_3. Which is concerned as promising material for multiple applicationsin future electronics, particularly in spintronics.

The synthesis high-quality thin films of topological insulators on various substrates including silicon is an important technological challenge. Although the synthesis of monocrystalline films of Bi_2Te_3 was achieved we focused in our work on growth of polycrystalline Bi-Te films. The important question from the point of view of applications and future industrial technology is to find out if the polycrystalline films show the satisfactory properties and what are the conditions for the growth of high-quality polycrystalline samples.

In our studies we concentrated on the growth of high-purity Bi-Te films with varying stoichiometry and on their complex characterization. A particular attention has been devoted to the films with the Bi/Te ratio close to 2/3 as in the standard 3D topological insulator Bi_2Te_3. Additionally, we tested electronic structure and structural properties of Bi-Te films with different Bi/Te ratio as well as characterized those properties for pure Bi and Te films of the same thickness.

The Bi-Te films were obtained by thermal evaporation method in ultrahigh vacuum cluster system consisting of a Molecular Beam Epitaxy (MBE) growth chamber, Reflection High Energy Electron Diffractometer (RHEED), X-Ray Photoelectron Spectroscopy (XPS) Ultraviolet Photoelectron Spectroscopy (UPS) and Scanning Probe Microscopy (AFM and STM). Further characterization was realized ex-situ with the use of X-Rey Reflectometry technique (XRR) and X-Ray Diffractometry (XRD).

The Bi-Te films were deposited on the silicon (100) substrate with which was prepared *in-situ* using Ar-ion beam sputtering and annealing at temperature of 970K for 1h. The Bi-Te films were grown in the co-deposition mode from the effusion cells on monocrystalline Si (100) substrate kept at about 400K. The deposition rate of tellurium and bismuth were matched to obtain the appropriate stoichiometry (established rate for Te was 1.4 times higher than Bi) and were controlled by the quartz weight. The deposition was held under ultra-high vacuum conditions, the pressure during the growth did not exceed the level of $5 \cdot 10^{-9}$ mbar. The thicknesses of deposited films was of about 20-30nm.

In-situ RHEED measurements were preformed immediately after the deposition process. The diffraction pattern obtained after the growth process showed a set of rings indicating the formation of polycrystalline films. The RHEED patterns showed in some cases the diffused spots indicating texturization of the films. The *ex-situ* XRD studies indicated polycrystalline structure of grown films with relatively small size of the crystallites. XRR confirmed the assumed value of the thickness of the Bi-Te films.

Analysis of the XPS spectra of Bi-Te films indicated that only the deposited elements are the components of the film - no oxygen, carbon or other contamination were visible in the XPS survey spectra even after several days in the vacuum chamber.The chemical state of bismuth and tellurium was obtained from the detailed analysis of the Bi 4f and Te 3d multiplets. The valence band was studied for the excitation by x-rays, He I and He II radiation. Moreover, by changing the geometry of photoelectron analysis we were able to tune the surface sensitivity of the spectra. The photoemission data enabled us to draw conclusions about the influence of growth conditions on the electronic structure and film structure in the vicinity of the surface – the crucial element of a topological insulator.

17:00 Poster Mo131

An Investigation on Optical and Structural Properties of Nanocrystalline CdTe Thin Films Growth by Employing a New Vapor Flow Controlling System

Fatemeh Hosseini Siyanaki, Shiva Khorramabadi, Hamid Rezagholipour Dizaji, Mohammad H. Ehsani

Semnan University, Physics Department, Crystal Growth Lab., Tehran 35195-363, Iran

e-mail: hrgholipour@semnan.ac.ir

Cadmium Telluride (CdTe) polycrystalline layers can be prepared by several techniques among which, vacuum thermal evaporation is known as a suitable one to produce nanocrystalline thin films [1]. CdTe is regarded as one of the most promising absorber material for fabrication of high efficiency thin film solar cells [2]. In the present investigation, Cadmium CdTe thin films with thickness of 350nm, and grain sizes between 15nm to 40nm have been prepared by vacuum thermal evaporation technique, conventional and the one in which a novel vapor flow controlling system was employed. This system, as shown in Fig.1, consists of a rotating cylinder with one semi-closed end named shutter. The shutter includes two slits and is in the vicinity of the substrate. The other end of cylinder is completely open and close to the source. Placing this equipment in the way of vapor flux from the source to the substrate cut the depositing flux of vapor periodically and can change the way of vapor flux. It led to considerable change of optical properties, nanocrystalline structure, and also stochiometery of the thin films.

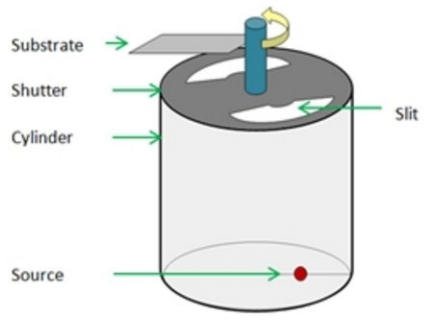

Figure 1: Schematic view of the vapor flow controlling system

The thin film deposited by conventional thermal evaporation method named S1, and the ones prepared by using the shutter and cylinder at 25, 50 and 75 rpm rate of rotation named S2, S3 and S4 respectively. Three other samples were prepared by applying the shutter alone, i.e. without the cylinder. They deposited at 25, 50 and 75 rpm rate of rotation and named S5, S6 and S7 respectively. The optical parameters such as absorption coefficient, bandgap, refractive index, and structural parameters such as texture coefficient, preferential orientation factor, crystallite size, were obtained. Also EDAX and FESEM result of samples were compared with each other in this study.

The most considerable increase in absorption coefficient was observed in S7 (9.8×10^4 cm^{-1}) in comparison with S1 (5.5×10^4 cm^{-1}) at 520nm wavelength of light (Fig. 2). By increasing the absorption coefficient, the light can be absorbed in a thinner layer of substance, considering following formula:

$$\mathbf{I/I_0 = \exp(\alpha d)} \qquad (1)$$

In this formula **α** is absorption coefficient and **d** is a thickness of film in which a light with intensity of $\mathbf{I_0}$ reduce to **I** because of absorption [3]. Therefore it seems that S7 is highly preferable in providing thinner layer of CdTe with similar result in absorbing the light.

The most considerable change in the bandgap also was observed in S6 (1.66 eV) in comparison with S1 (1.54 eV).

The changes of XRD patterns of S6 and S7 in comparison with S1 are illustrated in Fig. 3.

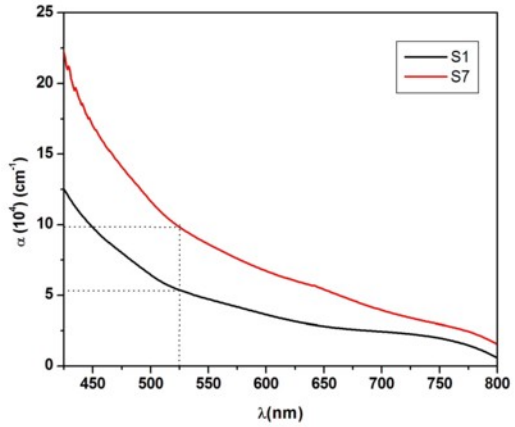

Figure. 2 absorption coefficient of S1 and S7

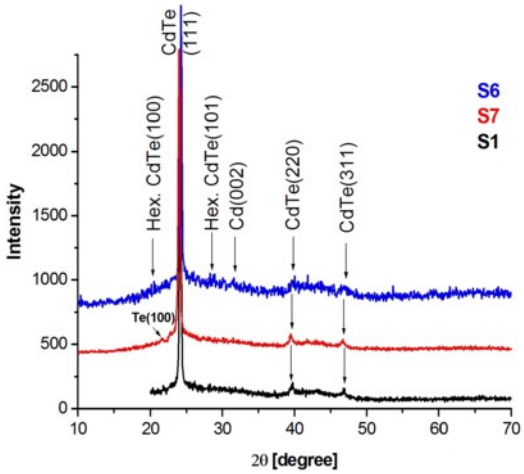

Figure. 3 XRD pattern of S1, S6, and S7.

The reasons and consequences of mentioned changes investigated by analyzing the structural and optical parameters of films, and will be presented in details.

References

[1] S. J. Ikhmayies and R. N. Ahmad-Bitar, “Optical Properties of Nanocrystalline CdTe Thin Films”, Phys. B., 405 (2010) 3141.

[2] V. D. Novruzov, et. al., "CdTe thin film solar cells prepared by a low-temperature deposition method", Phys. Status Solidi A 207 (2010) 730.

[3] M. Ohring, "The Materials Science of Thin Films', Academic Press, 1992.

17:00 Poster Mo132

The Improved Procedure of Ga-doped PbTe Films One Stage Synthesis by Modified HWE Technique

Alexander M. Samoylov, Sergey V. Belenko, Alexey I. Dontsov, Sergey V. Kannykin, Valentin M. Ievlev

Voronezh State University (VGU), Universitetskaya Sq., 1, Voronezh 394006, Russian Federation

e-mail: samoylov@chem.vsu.ru

Temperature T, K	Composition of initial melts	Ga pressure p_{Ga}, Pa	Integral pressure P_{int}, Pa	Predicted value of z^*_{Ga} in synthesizing films	Experimental value z_{Ga} in $Pb_{1-z}Ga_zTe$ films
1023 ± 3	$Ga_{0.15}Pb_{0.85}$	0.000733	2.25556	0.0011	0.0010±0.0005
1023 ± 3	$Ga_{0.95}Pb_{0.05}$	0.001	0.20261	0.0127	0.0132±0.0005
1103 ±3	$Ga_{0.15}Pb_{0.85}$	0.00634	10.5588	0.0020	0.0016±0.0005
1103 ± 3	$Ga_{0.95}Pb_{0.05}$	0.00956	0.83397	0.0195	0.0207±0.0005
1153 ± 3	$Ga_{0.15}Pb_{0.85}$	0.02178	24.8461	0.0025	0.0021±0.0005
1153 ±3	$Ga_{0.95}Pb_{0.05}$	0.03327	1.7808	0.0284	0.0298±0.0005

Table 1. The comparison of the estimated data z^*_{Ga} and the real experimental results z_{Ga} concerning the concentration of Ga atoms in $Pb_{1-z}Ga_zTe$ films fabricated by the improved one stage synthesis.

The thin films and single crystals of PbTe doped with Ga are the perspective materials for fabrication of the optoelectronic devices employed in infrared (IR) radiation middle wave range [1]. The IR sensitivity of these materials is similar to that of $Cd_{1-x}Hg_xTe$ but processing procedures are much less demanding. Under influence of the presence of III A group metals the energy spectrum of PbTe and its solid solutions can change significantly and depends not only the concentrations of the impurity atoms but from the method of investigated samples synthesis also [2].

The main purpose of this work is to emphasize the improvements of Ga-doped PbTe films one stage synthesis with predicted concentration of the impurity atoms by modified HWE technique. Earlier, Ga-doped PbTe thin films on Si-substrates had been prepared by the two stage procedure [3]. This doping procedure was based on the two-zone annealing in atmosphere of the saturated vapor, which corresponds th the three-phase equilibrium L1 + GaTe(S) + V in Ga - Te binary system, of the undoped PbTe/Si heterostructures previously formed by modified HWE technique. The EPMA and XPS experimental results clear demonstrated that after this treatment Ga impurity atoms have distributed on the surface layers quiet irregular. Later, another method of PbTe<Ga> heterostructures preparation was created. This procedure offers direct one stage synthesis, in which the doping and the layer condensation processes proceed simultaneously [4]. Despite the greater difference in fugitives between pure Pb and Ga the results of high-temperature mass-spectroscopy study have shown that saturated vapor phase over $Ga_{1-x}Pb_x$ is enriched with IIIA group metal at temperature interval T = 980 - 1300 K [5].

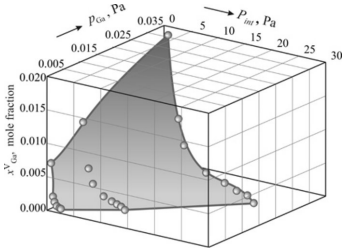

Fig. 1. The dependence of Ga atoms concentration in saturated vapor over $Ga_{1-x}Pb_x$ melts x^V_{Ga} upon the values of Ga partial pressure p_{Ga} and the integral pressure P_{int} of all components in Ga - Pb binary system.

At the first step of this work the mass-spectroscopic experimental data [5] allow us to determine the concentration of Ga atoms in the saturated vapor over $Ga_{1-x}Pb_x$ melts x^V_{Ga} dependence upon the values of Ga partial pressure p_{Ga} and the integral pressure P_{int} of all components in Ga - Pb binary system (Fig. 1). For x^V_{Ga} - p_{Ga} - and x^V_{Ga} - P_{int} - projections of the convolute shown in Fig. 1 it has been established that concentration of Ga atoms in equilibrium vapor phase may be expressed by the equations:

$$x^V_{Ga}(p_{Ga}) = A_1 + B_1 \times \exp(C_1 \times p_{Ga}) \quad (1a)$$

$$x^V_{Ga}(P_{int}) = A_2 + B_2 \times \exp(-C_2 \times P_{int}) \quad (1b)$$

At the second step by the general solution of the equations (1a) and (1b) the regimes (the values of p_{Ga}, p_{Pb}, P_{int}, temperature T, and compositions of initial $Ga_{1-x}Pb_x$ melts) of $Ga_{1-y}Pb_y$ binary layers have been defined. The synthesis of $Ga_{1-y}Pb_y$ samples is necessary to evaluate the degree of the discrepancy from the thermodynamic equilibrium in the HWE reaction chamber. The results of EPMA have shown that in prepared $Ga_{1-y}Pb_y$ binary layers Ga atoms concentration is higher than x^V_{Ga}. In order to take into account the major part of physicochemical processes resulting in the discrepancy from the thermodynamic equilibrium the analitical equation of factor $K_1 = y_{Ga}/x^V_{Ga}$ as the function of p_{Ga}, P_{int}, and the concentration of Ga atoms in initial $Ga_{1-x}Pb_x$ melts has been defined.

At the third step we have realized the results of the detail analysis of the quantitative composition of $Ga_{1-y}Pb_y$ binary layers in the improving of the one stage synthesis of ternary $Pb_{1-z}Ga_zTe$ films. It has been found that the presence of tellurium vapor has increased in the degree of the deviation from thermodynamic equilibrium in HWE reaction chamber. The values of factor $K_2 = z_{Ga}/x^V_{Ga}$ are higher than the values of K_1 in the most cases. On the basis of the general solution of the equations (2*a*) and (2*b*):

$$z^*_{Ga}(p_{Ga}) = A_1 + B_1 \times p_{Ga} + C_1 \times p^2_{Ga} \quad (2a)$$

$$z^*_{Ga}(P_{int}) = A_2 + B_2 \times P_{int} + C_2 \times P^2_{int} \quad (2b)$$

the improved conditions of ternary $Pb_{1-z}Ga_zTe$ films one stage synthesis have been designed. The comparison of the estimated z^*_{Ga} and the real experimental results z_{Ga} concerning the concentration of Ga atoms in fabricated $Pb_{1-z}Ga_zTe$ films is presented in Table 1. It has been established that compositions of $Pb_{1-z}Ga_zTe$ samples synthesized by improved one stage method are characterized by the complete concurrence to expected z^*_{Ga} values practically.

References:

1. M. Rahim, A Khiar, M. Fill, F. Felder, H. Zogg. *Electron Lett*. 18, 1037 (2011).

2. *Lead Chalcogenides: Physics and Application*. Ed. D. Khohlov. (Gordon & Breach, NY) 687 (2002)
3. A.M. Samoylov [et al]. *Journ. Cryst. Growth*. **38**, 340 (2002).
4. S.V. Belenko [et al] *Journ. Surface Investig. X-Ray, Synchrotron and Neutron Techn*., **4**, 170 (2010)
5. A.M. Samoylov [et al]. *Russian Journ. General Chem*. **81**, 27 (2011)

17:00 Poster Mo133

Surface morphology and structure of CaF_2/BaF_2–on-Si epitaxial layers and the electronic properties of the interface with the substrate

Alexander M. Samoylov[1], Alexandr E. Klimov[2], Aleksey N. Akimov[2], Nikolay S. Paschin[2], Vladimir N. Shumsky[2], Sergey P. Suprun[2], Evgeniy V. Fedosenko[2], Vladimir G. Erkov[2], Dmitriy V. Scheglov[2]

1. *Voronezh State University (VGU), Universitetskaya Sq., 1, Voronezh 394006, Russian Federation* **2.** *Rzhanov Institute of Semiconductor Physics SB RAS, Lavrentjeva 13, Novosibirsk 630090, Russian Federation*

e-mail: samoylov@chem.vsu.ru

Molecular-beam epitaxy was used to grow layers of alkaline-metal fluorides CaF_2 and BaF_2 (lattice mismatch values 0.6 and 14%) on (001)- and (111)-oriented Si substrates. In AFM images of the surface of BaF_2/CaF_2 films on (111)-oriented Si, smooth ordered steps of height (0.4±0.05) nm and length 2 μm were observed (Fig. 1); such steps correspond to half the principal diagonal of the unit cell of BaF_2 (0.876 nm).

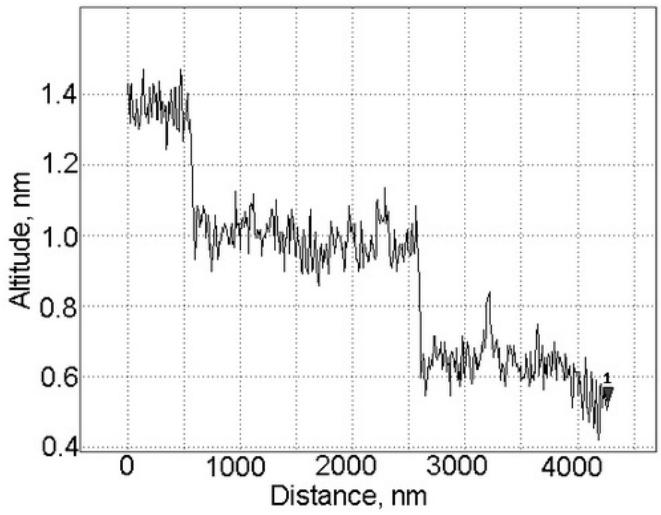

Fig. 1. Surface relief of a $BaF_2/CaF_2/Si$ (111) structure as measured by a Solver P-47H> (NT-MDT) atomic force microscope.

As it was shown in [1], the capacitance-voltage curves of CaF_2-on-Si (111) structures proved to be temperature-dependent. The capacitance modulation becomes less pronounced with increasing the growth temperature of the CaF_2 layers, and it finally vanishes in samples grown at temperatures above 500°C. Our data and data previously reported by other authors show that, with increase in temperature, for the interfacial region the x-ray photoelectron spectra exhibit a growth of the component due to Si 2*p*, corresponding to the Si-Ca bond, and a decrease of the component due to the Si-F bond. A similar tendency in the evolution of the physico-chemical interfacial structure was also observed for BaF_2 layers grown on Si (001); here, capacitance modulation was observed even in samples obtained at 780°C. In the latter case, the energy density of states at the interface with the substrate was $\sim 10^{11} eV^{-1} cm^{-2}$, and the built-in charge density was (4 to 5)×10^{11} cm^{-2} (Fig. 2). Our estimates show that the density of dangling bonds at the interface from the side of Si, which features a shorter lattice constant in comparison with BaF_2, reaches ~ $3 \times 10^{14} cm^{-2}$, the misfit dislocations forming a dislocation network with a step of 3 nm.

Thus, the explanation to the observed correlation between the built-in charge and the physico-mechanical structure of the heterointerface proposed in [1] for CaF_2/Si structures turns out to be inappropriate for BaF_2/Si structures. Moreover, the difference by three orders between the density of Si dangling bonds at the BaF_2/Si interface and the density of electron states determined from measured C-V and G-V characteristics of the samples makes the correlation between the indicated quantities doubt-

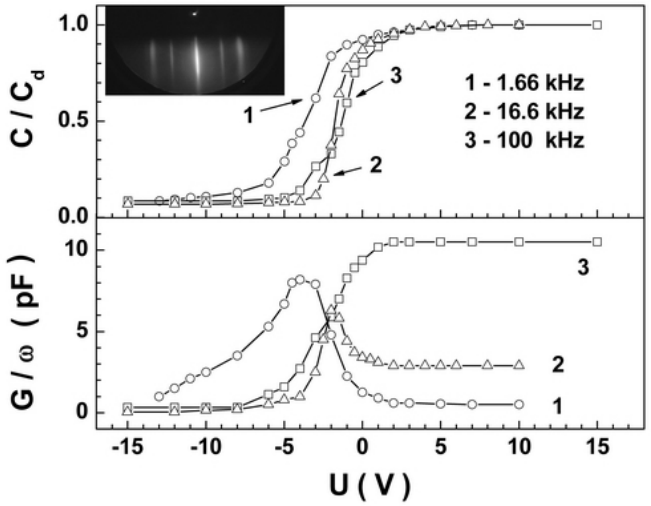

Fig. 2. C-V characteristics (upper panel) and G-V characteristics (lower panel) of BaF_2-Si(001) MIS structures measured at three frequencies. The inset shows a reflection electron diffraction pattern obtained on exposing the surface of the BaF_2-on-Si(001) film to fast electrons.

The spatial period of the misfit dislocation network is close to the size of the cells formed as a result of 7×7 reconstruction of the Si (111) surface, such reconstruction being accompanied by transformation of the Si (111) surface electronic structure. It can be hypothesized that spatially ordered defects present in the samples in a high density could also form a quantum subsystem "deactivating" the interfacial states. In principle, the electron states in the system may appear superimposed upon one of the allowed bands of Si, and they therefore can escape detection with standard observation means [2].

Also, we examined the influence which the diffractometer electron beam had on the growth and morphology of CaF_2 and BaF_2 layers. It was shown that electron-beam irradiation leads to formation of voids in the material. The size and density of the voids depended on the irradiation dose, thus being defined by the integral beam charge falling onto the sample. The mechanism underlying the formation of voids in the material involves, first, the beam-induced decomposition of the material and fluorine desorption in it and, second, the loss of positively charged metal ions in the material caused by their drift escape from the region to which the negative charge due to fast electrons sank [3].

References

1. C.-C. Cho, T.S. Kim, B.E. Gnade, H.Y. Liu, Y. Nishiokaa, Appl. Phys. Lett. **60**, 383 (1992).

2. S.P. Suprun, D.V. Shcheglov, JETP Letters **88**, 365 (2008).

3. S.P. Suprun, V.G. Kesler, E.V. Fedosenko, Observation of chemical reactions in solid phase using X-ray photoelectron spectroscopy, in:

"Stoichiometry and Materials Science - When Numbers Matter", 285-326, InTech, Rijeka, Croatia, 2012.

17:00 Poster Mo134

Heterostructures PbTe:Ga/BaF_2/CaF_2/Si for IR photodetectors

Alexander M. Samoylov[1], Alexandr E. Klimov[2], Aleksey N. Akimov[2], Nikolay S. Paschin[2], Sergey P. Suprun[2], Vladimir N. Shumsky[2]

1. *Voronezh State University (VGU), Universitetskaya Sq., 1, Voronezh 394006, Russian Federation* **2.** *Rzhanov Institute of Semiconductor Physics SB RAS, Lavrentjeva 13, Novosibirsk 630090, Russian Federation*

e-mail: samoylov@chem.vsu.ru

In the present publication, we report data gained in experiments on growing PbTe:Ga films on Si substrates and on examining the properties of In/(p-PbTe:Ga) test photosensitive structures based on such films. The various processes for production of PbTe layers on Si have long been under study (see, e.g. [1]). Advantageous features of such heterostructures include the possibility of fabricating large-format IR photodetectors on individual silicon chips and the possibility of fabricating flip-chip photodetectors, for which matching of multiplexer crystal and FPA substrate in terms of thermal expansion coefficients is not required. Also, experiments on doping PbTe films on BaF_2 substrates with gallium were previously reported in the literature [2]. From the standpoint of photodetector applications, the main result obtained in [2] was the revealed possibility of obtaining PbTe films with an extremely low concentration of charge carriers, which, in principle, enables the fabrication of photosensitive structures based on such films.

The process used in the present study for growing CaF_2/BaF_2 buffer layers on (111)-oriented Si substrates was described elsewhere [3]. The Si substrates with CaF_2/BaF_2 layers used for growing PbTe films on such layers were loaded into the MBE facility in the atmosphere of dry pure nitrogen. The thickness of the PbTe films was about one micrometer. The films were doped with gallium in a gas atmosphere as described in [4]. The source of Ga was $Ga_{0.6}Te_{0.4}$ alloy. A typical dependence of current on reciprocal temperature in our PbTe:Ga films is shown in Fig.1.

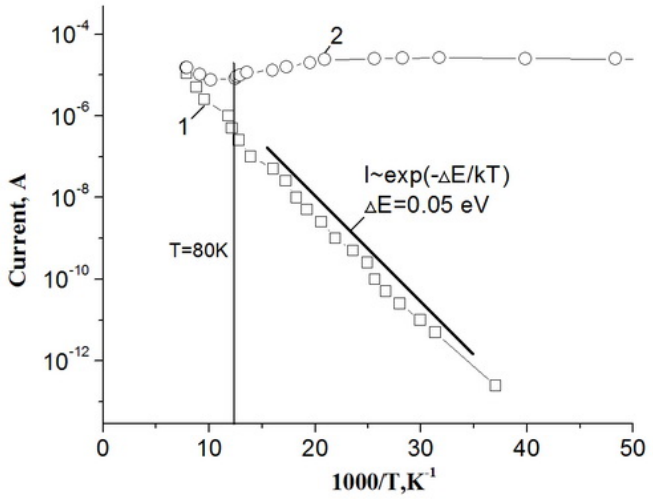

Fig.1. The electric current through a PbTe:Ga/BaF_2/CaF_2/Si film versus the reciprocal temperature. The sample was shaped as a square, and the bias voltage was U=1.5 V. Curve 1 was measured in the dark, and curve 2, under illumination. The straight line shows an Arrhenius dependence with activation energy ΔE=0.05 eV.

As it is evident from the data in Fig. 1, the sheet resistance of our films was rather high, $\rho > 10^6$ Ω at T=80 K, and the films were quite sensitive to illumination; these findings prove that the film systems obtained offer promise in fabrication of photoconductor-type photodetectors. However, the main focus in the present study was on the possibility of fabricating diode-type photodetectors based on PbTe films.

PbTe:Ga films of p-type conductivity with hole concentration p=(1-50)×10^{12} cm^{-3} and hole mobility $\mu_p > 10^4$ cm^2 V^{-1} s^{-1} at T=80 K were used. Indium contacts to the samples ranging in area from 75x75 to 1200x1200 μm^2 were obtained using thermal evaporation of In in vacuum. Anneals were given to the samples in argon ambient. Measurements were made on non-annealed (Schottky barriers) and annealed (shallow n-p junctions) structures. During measurements, the samples were held at temperature T=80 K in a nitrogen cryostat. The spectral sensitivity of measured structures, generally consistent with the behavior of PbTe photosensitivity in the fundamental absorption region of the material, exhibited interference-induced features, which, in principle, enables optimization of photosensitivity at a desired wavelength through film thickness adjustment. Current-voltage characteristics of a structure 200 μm in diameter measured prior to and after the annealing of the sample in argon atmosphere are shown in Fig.2; during measurements, the structure was shielded from background radiation.

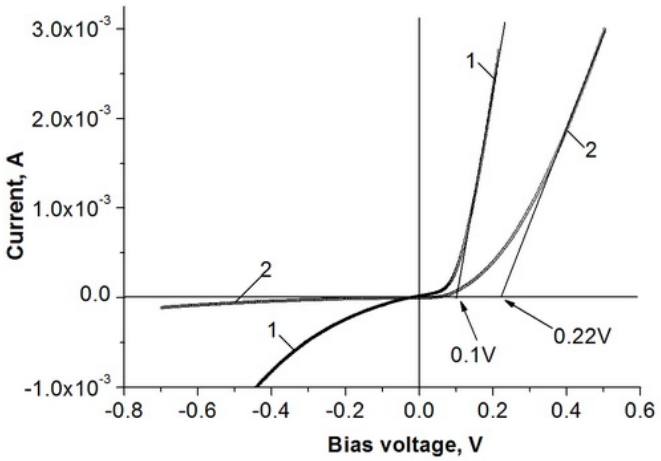

Fig. 2. Current-voltage characteristics of a structure 200 μm in diameter measured prior to (1) and after (2) the annealing of the sample in argon on screening the sample from background radiation. The straight lines show approximations of the linear portions of the characteristics.

Approximation of the linear portions of the forward branches of the current-voltage curves has yielded offset voltage values 0.1 V and 0.22 V, which can be identified as the diffusion potential values for Schottky barriers and n-p junctions (before and after annealing of the samples). Photosensitivity and noise measurements performed under low background illumination conditions have yielded for the maximum detectivity a value $D^* > 10^{11}$ W×cm×$Hz^{-0.5}$. Charge transport mechanisms in the films and available potential for improving characteristics of the photodetectors and for use of obtained film structures in the development of FPA photodetectors on silicon chips are discussed.

This work was supported by the Ministry of Science and Education of the Russian Federation under Grant No. 2012-1.1-12-000-2003-120.

References

1. C. Maissen, J. Masek, H. Zogg, S. Blunier. Appl. Phys. Lett. **53**, 1608 (1988).

2. B.A. Akimov, V.A. Bogoyavlenskii, L.I.Ryabova, *et al.* Phys. Rev. B **61**, 16045 (2000).

3. S.P. Suprun, and D.V. Shcheglov. JETP Letters **88**, 365 (2008).

4. L.F. Vasil'eva, A.E. Klimov, N.I. Petikov, and V.N. Shumsky. Inorganic Materials **37**, 144 (2001).

17:00 Poster Mo135

Anisotropic characteristics of a-plane GaN grown on r-plane sapphire by metalorganic chemical vapor deposition

Yong Gon Seo, Sun Hye Shin, Doo Soo Kim, Sung-Min Hwang

Korea Electronics Technology Institute, Seongnam 463-816, Korea, South

e-mail: ygseo@keti.re.kr

Nonpolar nitrides have attracted considerable attention due to the potential for eliminating undesirable electric field effects and the possibility of producing devices with higher efficiencies than conventional *c*-plane nitrides [1]. The nonpolar nitride films with *a*-plane and *m*-plane have been grown on *r*- and *m*- plane sapphire, (302) and (100) LiAlO2, *a*- and *m*-plane SiC, and *a*- and *m*-plane GaN substrates [2]. The structural anisotropies of the nonpolar nitride films were expected due to the unequal growth rate [3] so there is a dependence of the full widths at half maximum (FWHMs) of X-ray rocking curves (XRCs) on the azimuth angle. In this work, we report on the anisotropic characteristics of *a*-plane GaN films that have an M-shape or W-shape dependence on the azimuth angle with minimum FWHM along the *c*-axis or *m*-axis directions of *a*-plane GaN.

Nonpolar *a*-plane GaN films were grown on 2 inch *r*-plane sapphire substrates by metalorganic chemical vapor deposition. With the control of nucleation and three-dimensional growth conditions, we obtained M-shape (sample A) and W-shape (sample B) *a*-plane GaN films depending on the azimuth angle. The surface morphology and the crystalline quality of samples A and B were characterized by high resolution X-ray diffraction and atomic force microscopy (AFM). For optical properties, photoluminescence (PL) measurements at room temperature were carried out using a 266 nm laser.

1 x 1 μm^2 AFM images of the surface morphologies of samples A and B are shown in Fig. 1(a) and (b). Both samples had a smooth surface and the root mean square (RMS) of samples A and B was found to be 0.5 and 0.8 nm, respectively. The structure qualities of samples A and B were evaluated from the FWHM of XRC. Figure 2 shows the FWHMs of XRC of *a*-plane GaN films along with the azimuth angle. Azimuth angles of 0^o and 90^o were defined as the projection of the incident beam being parallel to the [0001] and [1-100] directions, respectively. The FWHMs of the (11-20) XRC for samples A and B were found to be dependent on the azimuth angle. Sample A had M-shape behavior and the FWHM values of the [0001] and [1-100] directions were 474 and 638 arcsec, respectively. The FWHMs of the [0001] and [1-100] directions for sample B with W-shape anisotropy were found to be 856 and 542 arcsec, respectively. The crystal quality of sample A along the [0001] direction was better than sample B and the reverse was found for crystal quality along the [1-100] direction. Room temperature PL spectra of samples A and B are shown in Fig. 3. Both spectra displayed the near band-edge emission at 363.4 nm and the FWHMs of the PL for samples A and B were 12.9 and 12.7 nm, respectively. The PL intensity of sample B was 1.7 times stronger than that of sample A although the average crystal quality of sample A was better than that of sample B. This indicates that the PL intensity of *a*-plane GaN layer is more affected by the crystal quality of the [1-100] direction rather than the [0001] direction.

References:

[1] P. Waltereit, O. Brandt, A. Trampert, H. T. Grahn, J. Meinnger, M. Ramsteiner, M. Reiche, and K. H. Ploog, Nature (London) 406, 865 (2000).

[2] V. Darakchieva, M.-Y. Xie, N. Franco, F. Giuliani, B. Nunes, E. Alves, C. L. Hsiao, L. C. Chen, T. Yamaguchi, Y. Takagi, K. Kawashima, and Y. Nanishi, J. Appl. Phys. 108, 073529 (2010).

[3] H. Wang, C. Chen, Z. Gong, J. Zhang, M. Gaevski, M. Su, J. Yang, and M. A. Khan, Appl. Phys. Lett. 84, 499 (2004).

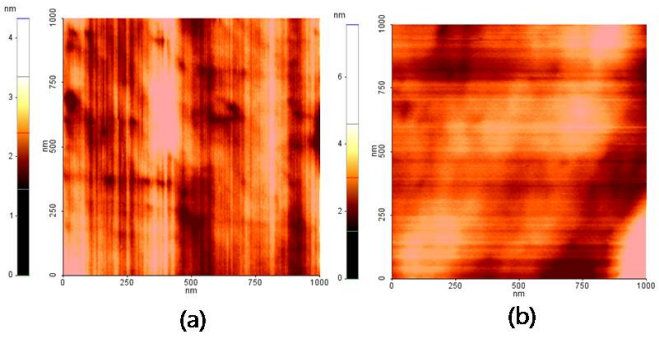

Figure 1. AFM images of a-plane GaN films: (a) sample A and (b) sample B.

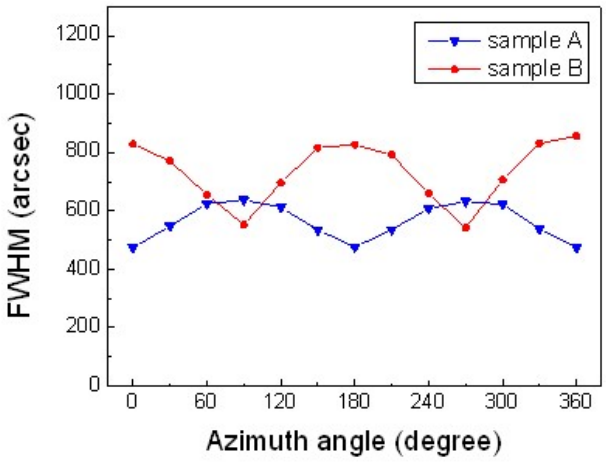

Figure 2. Azimuth angle dependence of the FWHM of the (11-20) rocking curves for *a*-plane GaN films.

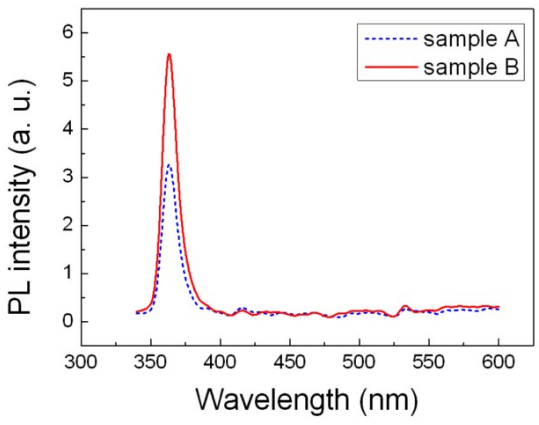

Figure 3. PL intensities for samples A and B at room temperature.

17:00 Poster Mo136

Epitaxial growth of Ga-rich tourmaline on natural elbaite seed in boric hydrothermal solutions

Tatiana V. Setkova, Vladimir S. Balitskiy

Institute of Experimental Mineralogy RAS (IEMRAS), Acad. Osipiana St, Chernogolovka 142432, Russian Federation

e-mail: setkova@iem.ac.ru

Crystal growth of tourmaline connected to a number of difficulties such as high temperature and pressure of crystallization, low growth rate, etc. [1,2]. At the same time, the synthesis of structural analogues of natural minerals in which aluminum and silicon are completely or partially substituted by gallium and germanium (gadolinium gallium, yttrium aluminum, and yttrium iron garnets, germanium oxide, etc.) can reduce significantly the temperature and pressure of the process and to improve functional properties.

Studies were performed under thermogradient conditions using chromium–nickel alloy autoclaves at temperature of 450-650°C and pressure of 100 MPa. Plates made from natural tourmaline crystals of elbaite (chemical formula is $Na(Li,Al)_3Al_6Si_6O_{18}(BO_3)_3(OH,F)_4$) were used as seed crystals in the experiments. Single crystals of quartz and corundum with addition of gallium oxide was used as charge material. The autoclave was filled with solution of boric acid and mineralizer in accordance to autoclave-filling factor,then sealed, and placed into electric furnace with two-section heaters. The duration of the runs was 14 days.

As a results, the epilayer of Ga-rich tourmaline wherein part of aluminum are substituted by gallium was grown on natural elbaite seed for the first time. The thickness of this layer was up to 100 μm, and the gallium content was up to 12 wt. %. Along with epilayer of Ga-rich tourmaline, a small amount of fine (10-30 micron in size) long prismatic Ga-rich tourmaline crystals of spontaneous nucleation was observed on surface of the seed and in the charge.

This work was supported by the RFBR (Grant no. 12-05-31030) and Ministry of education and science of Russian Federation (Agreement no. 8612 and 8378).

[1] London, D. (2011) Canadian Mineralogist, **49**, 117–136. [2] T. Setkova, Yu. Shapovalov, V. Balitsky (2011) Journal of Crystal Growth, **318**, 904–907.

17:00 Poster Mo137

Modeling of heat and mass transfer in GaN MOVPE reactor

Jakub Skibinski[1], Tomasz Wejrzanowski[1], Piotr Caban[2], Włodzimierz Strupiński[2]

1. *Warsaw University of Technology, Faculty of Materials Science and Engineering (InMat), Wołoska 141, Warszawa 02-507, Poland*
2. *Institute of Electronic Materials Technology (ITME), Wólczyńska 133, Warszawa 01-919, Poland*

e-mail: j.skibinski@inmat.pw.edu.pl

In the present study, the quantitative relationship between gas flow and epitaxial growth of GaN is addressed. Since there are many agents influencing reaction on crystal area such as temperature, pressure, gas flow, reactor geometry, it is difficult to design optimal process. Experimental analysis is difficult mainly due to high temperature and flow disturbance caused by introducing measuring probes. Numerical simulations allow to understand the process by calculation of heat and mass transfer distribution during growth process of GaN.

This study concerns influence of the inlet gases on the process of crystal growth. In order to investigate this subject a series of computer simulations and experimental processes have been performed. The software used for these calculations was ANSYS Fluent.

To study the influence of reagents mass flow rate on the crystal growth, model of MOVPE reactor has been created. The finite element mesh of 300.000 triangular elements has been created for the geometry of the reactor. The mesh is refined over the chemical reaction area, since it's the area of biggest importance, and mesh should be the most accurate above it.

Preliminary results show, that flow parameters change according to mass flow rates of gases. The study exhibited that velocity profile in reactor depends on temperature of the reactor walls, mass flow rate on the inlet and rotation of the plate. Reactor geometry gets a symmetric plane but because of the rotation of the plate, velocity profile inside the reactor doesn't get such plane. This asymmetric flow changes the proportion of hydrogen and gases that participate in chemical reactions over plate. It was found that the rotation of the plate does not influence temperature distribution over the growth area.

17:00 Poster Mo138

InGaN light-emitting diodes with an asymmetric multiple quantum well

Chia-Lung Tsai, Wei-Jhih Huang, Wei-Che Wu, Chih-Ta Yen, Chia-Lin Chang

Electronic Engineering, Chang Gung University, Taoyuan, Taiwan, Taoyuan 00333, Taiwan

e-mail: cltsai@mail.cgu.edu.tw

In this study, an asymmetric multiple quantum well (AMQW) with quantum wells of different thicknesses was used as the active regions of InGaN light-emitting diodes (LEDs) to achieve improved performance. The active region of normal LEDs is composed of a six-pair InGaN (2.5 nm)/GaN (10 nm) MQW for 455 nm emission; nevertheless, in the proposed LEDs, three quantum wells adjacent to the n-GaN have gradually increased well thickness from the p-side to n-side layers while the remaining structure is identical to those of normal LEDs. High-resolution transmission electron microscopy (HRTEM) image and high-resolution X-ray diffraction (HRXRD) analysis show that the modified MQWs have a reasonable crystalline quality even though two kinds of quantum wells with different thicknesses are combined together to form the active region of the InGaN LEDs. In wafer-level testing, both LEDs have similar effective series resistance (~4 Ω) and forward voltage (~3.1 V @ 20 mA). This indicates that the incorporation of an AMQW into the LED structures has little impact on the electrical properties of the fabricated LEDs. In addition to the peak intensity shifted towards higher current levels, the maximum light output power of the LEDs with an AMQW is superior to that of their counterparts, i.e., 14.97 and 13.88 mW at 580 and 500 mA for the LEDs with and without an AMQW. For the temperature dependent photoluminescence (PL) measurements, the thermal activation energy (E_a) of the LEDs with and without an AMQW extracted from the high-temperature section (> 100 K) of the Arrhenius plots is evaluated as 36.8 and 26.7 meV, respectively. Such result suggests that the localization effect is relatively strong in LEDs with an AMQW, which will help injection carriers radiatively recombine at the indium-rich localized states [1]. Experimentally, variations in indium content and well width during epitaxial growth may be responsible for the different levels of indium segregation in the InGaN MQWs [2]. For the LEDs with an

AMQW, the phenomenon of light intensity degraded at elevated current levels could be attributed to improved uniformity of carrier distribution among the quantum wells provided a graded-thickness MQW was used [3].

Reference

[1] T. Wang, J. Bai, S. Sakai, and J. K. Ho, "Investigation of the emission mechanism in InGaN/GaN-based light-emitting diodes," Appl. Phys. Lett., vol. 78, pp. 2617–2619 (2001).

[2] J. H. Na, R. A. Taylor, K. H. Lee, T. Wang, A. Tahraoui, P. Parbrook, A. M. Fox, S. N. Yi, Y. S. Park, J. W. Choi, and J. S. Lee, "Dependence of carrier localization in InGaN/GaN multiple-quantum wells on well thickness," Appl. Phys. Lett., vol. 89, pp. 253120-1~3 (2006).

[3] J. Y. Zhang, L. E. Cai, B. P. Zhang, X. L. Hu, F. Jiang, J. Z. Yu, and Q. M. Wang, "Efficient hole transport in asymmetric coupled InGaN multiple quantum wells," Appl. Phys. Lett., vol. 95, pp. 161110-1~3 (2009).

17:00 Poster Mo139

u-GaN buffer resistivity control for AlGaN/GaN HEMT's

Mateusz Wośko, Bogdan Paszkiewicz, R. Paszkiewicz, Marek Tłaczała

Wrocław University of Technology, Faculty of Microsystem Electronics and Photonics (WEMIF), Janiszewskiego 11/17, Wrocław 50-372, Poland

e-mail: mateusz.wosko@pwr.wroc.pl

Material quality (crystal perfection, electrical resistivity) of GaN buffer layers has great impact on the nitride based HEMT's (high electron mobility transistor) performance. On the one hand, buffer should have at least sheet resistivity in the range of 1E4 - 1E5 ohm/sq, to reduce leakage current, on the other hand, the surface roughness and dislocation density at the AlGaN/GaN heterostructure interface should be low enough to suppress electron scattering mechanism of 2DEG (two dimensional electron gas). So far, the lowest achievable background contretrations of u-GaN on the order of 1E16 cm^{-3}, are not sufficient to give sheet resistance higher than 1E4 ohm/sq. Due to the difficulties in fabrication of pure low dislocated GaN crystal, the only way to obtain high resistivity GaN layers is intentional compensation with acceptor. In general there are two different methods of deposition resistive GaN layers by MOVPE. First, not desirable for HEMT purposes due to strong impact on material mobility, is the doping with acceptors (Fe, Cr, Mg) [1,2,3], second is the self compensation of the material [4,5] by tuning the growth conditions of GaN buffer [6,7,8].

The self compensation of the GaN material is explained by the introduction of acceptor levels in the crystal structure. The main source of acceptors are probably C atoms comes from TMGa precursor. Experimental results indicate, that compensation effect, is strongly affected by the edge-type TD (threading dislocations) related to the MOVPE growth parameters. It was shown, that laser interferometry is useful method of growth process monitoring, and crystal quality prediction. It is possible to link growth conditions and material properties with reflectance trace.

In this contribution we demonstrate the statistical study of over 50 reflectance traces recorded during MOVPE growth of GaN buffer layers. The correlation between reflectance signal (i.e. signal recovery time) and electrical properties of the buffer (thickness of buried conductive layer, buffer resistivity) obtained by impedance spectroscopy are presented. This results shows, that in-situ laser interferometry can be used as a fast method of prediction of GaN buffer resistivity during AlGaN/GaN HEMT's growth. Based on this observation, the impact of the nucleation layer growth and annealing conditions (thickness/time, pressure, temperature) on the electrical properties of GaN buffer is demonstrated.

Acknowledgements:

This work was co-financed by the European Union within European Regional Development Fund, through grant Innovative Economy (POIG.01.01.02-00-008/08-05), National Centre for Science under the grant no. N N515 495740, by National Centre for Research and Development through Applied Research Program grant no. 178 782, by Wroclaw University of Technology statutory grant S20010, B20011 and Slovak-Polish International Cooperation Program nos. SK-PL-0017-09 & 0005-12,Mateusz Wosko benefited from fellowship co-financed by European Union within European Social Fund.

Bibliography:

[1] S. Heikman, S. Keller, S.P DeenBaars, U.K. Mishra, Appl. Phys. Lett. 81 (2002) 439.[2] A.Y. Polyakov, N.B. Smirnov, A.V. Govorkov, S.J. Pearton, J. Vac. Sci. Technol. B 22 (2004) 120.[3] N.I. Kuznetsov, A.E. Nikolayev, A.S. Zubrilov, Y.V. Melnik, V.A. Dmitriev, Appl. Phys. Lett. 75 (1999) 3138.[4] D.D. Koleske, A.E. Wickenden, R.L. Henry, M.E. Twigg, J. Cryst. Growth 242 (2002) 55.[5] A.E. Wickenden, D.D. Koleske, R.L. Henry, M.E. Twigg, M. Fatemi, J. Cryst. Growth 260 (2004) 54.[6] S.M. Hubbard, G. Zhao, D. Pavlidis, W. Sutton, E. Cho, J. Cryst. Growth 284 (2005) 297.[7] A.P. Grzegorczyk, L. Macht, P.R. Hageman, M. Rudzinski, P.K. Larsen, Phys. Stat. Sol. (c) 2 (2005) 2113.[8] S. Mita, R. Collazo, R. Dalmau, Z. Sitar, Phys. Stat. Sol. (c) 4 (2007) 2260

17:00 Poster Mo140

Growth and luminescent properties of Ce and Ce-Tb doped $(Y,Lu,Gd)_2SiO_5$:Ce single crystalline films

Yuriy V. Zorenko[1], Vitaliy Gorbenko[2], Volodymyr Savchyn[2], Tetyana Zorenko[2], Boris Grinyov[3], Oleg Sidletskiy[3], Alexander Fedorov[3]

1. *Instytut Fizyki, Uniwersytet Kazimierza Wielkiego w Bydgoszczy (UKW), Powstancow Wielkopolskich, Bydgoszcz 85-822, Poland* **2.** *Electronics Department, Lviv National University, 50 Dragomanov str., Lviv 79005, Ukraine* **3.** *Institute for scintillation materials of NAS of Ukraine (ISMA), Lenin avenue, 60, Kharkov 61158, Ukraine*

e-mail: zorenko@ukw.edu.pl

The single crystalline films (SCF) of undoped, Ce and Ce-Tb doped Y_2SiO_5 (YSO), Lu_2SiO_5 (LSO) and $(Lu_xGd_{1-x})_2SiO_5$ (LGSO) orthosilicates with a thickness from 2.5 to 100 μm were prepared by the liquid phase epitaxy (LPE) method onto undoped YSO and LSO substrates with different orientation from melt-solution (MS) based on PbO-B_2O_3 flux. These SCF can be used as scintillating screens for 2D X-ray microimaging [1]. In case LSO and LGSO SCF growth onto YSO and LSO substrates we did not use any additional doping to reduce the misfit between the SCF and substrate lattice parameters.

Luminescence of undoped YSO and LSO SCF is caused by the UV emission of Pb^{2+} flux impurity in the bands at 365 and 348 nm, respectively, related to the $^3P_{1,0}$-$^1S_0$ transitions, and by a visible band at 445 and 438 nm, ascribed to luminescence of excitons localised around the Pb^{2+} centers.

The luminescent properties of YSO:Ce, LSO:Ce and LGSO:Ce SCFs were compared with YSO, LYSO and LSO:Ce single crystal (SC). We found that the luminescence of YSO:Ce and LSO:Ce SCF caused by the $5d_1$-4f radiative transition of Ce^{3+} ions is red-shifted in comparison

with SC counterparts. This shift can be caused by (1) different relative occupancy of Y1/Lu1 and Y2/Lu2 sites of YSO and LSO hosts by Ce^{3+} ions in the case of SCF and SC growth due to very different temperatures for SC (2100^{o}C) and SCF (~1000^{o}C) crystallization; (2) luminescence of Pb^{2+} centers, overlapping with the emission of Ce^{3+} ions. We also found that the emission spectrum of LGSO:Ce SCF is systematically red-shifted with respect to spectrum of LSO:Ce SCF with increasing the Gd content in range of 0-0.7 formula units due to the increasing of the relative content of Ce2 centers in LGSO host. Such a red shit of the luminescence spectra of LGSO:Ce SCF is accompanied by decreasing their light yield (LY) down to 65 % for $Lu_{0.3}Gd_{0.7}SO$:Ce SCF in comparison with LY of LSO:Ce SCF. We would like also to note that LGSO:Ce SCF, despite of lower LY in comparison with LSO:Ce, possess much higher signal/noise ratio due to drop of afterglow level by ~100 times, by analogy with SC [2]. Therefore, image contrast at X-ray visualization should be better with LGSO screens.

The LY of YSO:Ce and LSO:Ce SCF reaches the value equal to 95-145 % of that for a LSO:Ce SC under excitation by α–particles of Am^{241} sources (5.5 MeV) but only ~40-60 % of the LY of high-quality LYSO:Ce SC. The lower LY of (Y,Lu,Gd)SO:Ce SCF with respect to the best SC analogues is caused by quenching induced by Pb^{2+} flux impurity. Therefore, the usage of the lead-free fluxes is strongly needed for crystallization by the LPE method of (Y.Lu,Gd)SO:Ce SCF scintillators to increase their LY.

[1] T. Martin, at al. IEEE TNS **56** (2009) 1412.

[2] O. Sidletskiy et al. Journal of Crystal Growth 312 (2010) 601-606

Topical Session 1

Intermetalic and highly correlated electron materials

Session Coordinators

Dariusz Kaczorowski (Poland) *d.kaczorowski@int.pan.wroc.pl*

Yoshichika Ōnuki (Japan) *onuki@phys.sci.osaka-u.ac.jp*

Programme

Wednesday, 14 August

WeP-T01
Wednesday afternoon, 14 August, 16:00
Room 107, Old Library

Break
Wednesday afternoon, 14 August, 17:30

Thursday, 15 August

ThO2

T01: Intermetalic and highly correlated electron materials
Thursday afternoon, 15 August, 14:00
Mickiewicz Hall, Auditorium Maximum

14:00 Invited oral

Crystal growth and magnetoelectric properties of multiferroics

Tsuyoshi Kimura

Osaka University, Machikaneyama, Toyonaka 560-8531, Japan

e-mail: kimura@mp.es.osaka-u.ac.jp

A new class of multiferroics such as $TbMnO_3$ exhibit gigantic magnetoelectric (ME) effects accompanied by a magnetic phase transition into a spiral magnetic ordered phase. Thus, the spiral magnetism is the key to understanding the ferroelectric and ME properties in these systems. In spiral magnets, inversion symmetry is broken owing to magnetic order, and some spiral-ordered structures such as a cycloidal one make the system polar. This means that a magnetic order can induce ferroelectricity. The ferroelectricity in the new class of multiferroics can be explained in terms of this scheme. Because spiral order often arises from the competition between nearest-neighbor and further-neighbor magnetic interactions, systems containing competing magnetic interactions are promising candidates for multiferroics. On the basis of this strategy several new multiferroics related to spiral magnetic orders have been discovered in the past few years. In this presentation, I show recent progress on the study of crystal growth and magnetoelectric properties in several multiferroics especially in which non-collinear spiral spin arrangements play crucial roles. (For example, low-field ME effect at room temperature in hexaferrite compounds, ferromagnetic and ferroelectric nature in an olivine compound, and antisymmetric off-diagonal ME effects in a spin-glass system.)

This work has been done in collaboration with Y. Hiraoka, Y. Yamaguchi, T. Honda, T. Ishikura, K. Okumura, Y. Kitagawa, H. Nakamura, Y. Wakabayashi, M. Soda, T. Asaka, T. Nakano, Y. Nozue, Y. Tanaka, S. Shin, J. S. White, and M. Kenzelmann.

14:30 Invited oral

LnFeAsO single crystals grown at high pressure: influence of doping and substitutions on superconducting properties and structure

Janusz Karpinski[1], Nikolai D. Zhigadlo[2], Sergiy Katrych[1], Philip J. Moll[2], K. Rogacki[3], Roman Puzniak[4], Andrea Pisoni[1], Bertram Batlogg[2], Stephen Weyeneth[5], Hugo Keller[5], Laszlo Forro[1]

1. *Institute of Condensed Matter Physics EPFL, Ecublens, Lausanne 1015, Switzerland* **2.** *Laboratory for Solid State Physics ETH (ETH), Schafmatstr. 16, Zürich 8093, Switzerland* **3.** *Polish Academy of Sciences, Institute of Low Temperature and Structure Research (INTiBS), Okólna 2, Wrocław 50-422, Poland* **4.** *Polish Academy of Sciences, Institute of Physics, al. Lotników 32/46, Warszawa 02-668, Poland* **5.** *Physik-Institut der Universität Zürich, Winterthurerstrasse 190, Zürich CH-8057, Switzerland*

e-mail: karpinski@phys.ethz.ch

For the investigations of intrinsic properties relevant for applications of FeAs based superconductors studies on single crystals are necessary. LnFeAsO (Ln=La, Pr, Nd, Sm, Gd) single crystals were grown from flux at high-pressure of 30 kbar. Two kind of fluxes have been used: NaCl/KCl and NaAs/KAs. An overview of the basic superconducting properties measured on single crystals of LnFeAsO will be presented. LnFeAsO compounds show the highest T_c up to 55K and the highest upper critical fields. Superconductivity in LnFeAsO single crystals has been induced by partial substitution of O by F or by H, Sm by Th, Fe by Co, As by P or by oxygen deficiency. Single crystal structure investigations show structure modifications due to substitutions which are linked to superconducting properties. Especially substitution of H for O is important, because it allows much higher doping rate than substitution of F for O. Detailed study of the transport properties of SmFeAs(O,F) single crystals reveals a promising combination of high ($> 2\ 10^6$ A/cm^2) and nearly isotropic critical current densities up to 30 T at low temperatures. In the frame of these studies new superconductor related to LnFeAsO, but with much larger c lattice parameter with T_c up to 40K has been discovered. Properties of new superconductor will be presented.

1. J. Karpinski, Phil. Mag. 92 (2012) 2662.
2. Philip J.W. Moll et al., Nature Mat. 12 (2012) 134.

15:00 Oral

Crystal growth and physical property of Bi-Sb-Te-Se topological insulator materials, and Cu-Bi-Se and Sn-In-Te topological superconductors

Genda Gu, Alina Yang, John Schneeloch, Ruidan Zhong, John Tranquada

Brookhaven National laboratory (BNL), Bldg 510, New York, NY 11973, United States

e-mail: ggu@bnl.gov

The discovery of 3D topological insulator materials and topological superconductor opens up a new research field in the condensed matter physics. We have grown a number of Bi-Sb-Te-Se topological insulator, and Cu-Bi-Se and Sn-In-Te topological superconductor single crystals. We have measured the physical properties on these single crystals. We have studied the effect of growth condition and impurity on the bulk electrical conductivity of these single crystals. We try to answer two questions for the topological insulator materials if it is possible to grow the bulk-insulating topological insulator single crystals and Which maximum resistivity of these topological insulator single crystals we can grow. For the topological superconductor, we have got the bulk superconducting single crystals with a maximum Tc=4.5K.

15:15 Oral

Czochralski single crystal growth in the Ga-Pd system

Judith Schwerin, Sandra Kiese, Peter Gille

LMU München, Department of Earth and Environmental Sciences, Crystallography section (LMU), Theresienstr. 41, Munich 80333, Germany

e-mail: peter.gille@lrz.uni-muenchen.de

Some intermetallic compounds in the Ga-Pd system have recently been explored as highly selective heterogeneous catalysts in the semi-hydrogenation of acetylene [1] which is a huge business in chemical industry. Compared to pure Pd or alloyed catalysts, intermetallic compounds with well-defined crystalline structures and therefore fixed sites of the catalytically active element have a considerably higher long-term stability. This has been explained according to the *active-site isolation concept* [2].

Although the technical application of catalysts made from intermetallic phases will be based on ultra-fine powders or even nanoparticles, single crystals of these compounds are needed to study their intrinsic properties, e.g. their anisotropic surface structures, and basic processes of catalysis. It is only recently that advances in the growth of large single-grain crystals allow the UHV preparation of low-index atomic surfaces to perform fundamental investigations by means of surface analytical tools.

Especially the phases PdGa (FeSi structure type, space group $P2_13$), Pd_3Ga_7 (Ir_3Ge_7 structure type, space group *Im3m*) and Pd_2Ga (Co_2Si structure type, space group *Pnma*) have shown their high potential as heterogeneous catalysts [3]. That is, why we try to grow cm^3-size single crystals of these Ga-Pd phases. Each phase needs specific conditions for crystallization that can be deduced from the phase diagram, see Fig. 1 [4].

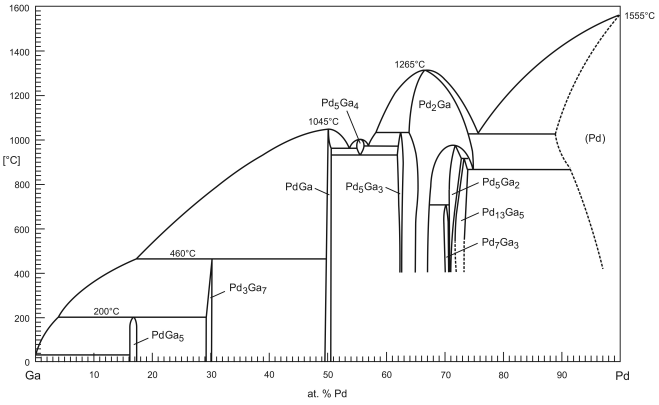

Fig. 1: Ga-Pd phase diagram, after [4].

PdGa can be grown either from a congruent melt or from Ga- or Pd-rich high-temperature solutions. The same options principally exist for growing Pd_2Ga, but quite high liquidus temperatures and accordingly a high Ga vapour pressure suggest crystallization from a Ga-rich melt. Contrary, Pd_3Ga_7 is only stable at temperatures lower than 460°C and crystal growth is limited to a crystallization from a Ga-rich solution at relatively low temperatures making materials transport and the preparation of inclusion-free single crystals the main problem.

We have grown single crystalline samples of Pd_3Ga_7, PdGa and Pd_2Ga by the Czochralski method from off-stoichiometric melts. The obtained PdGa single crystals (Fig. 2) show a fairly high structural perfection [5] and offer a wide scientific playground based on the complexity of enantiomorphism and the polarity of specific faces. Pd_2Ga is characterized by a broad stability region with retrograde solubility of the excess component. Thus, precipitation of the orthorhombic Pd_5Ga_3 phase may occur during post-growth cooling depending on the growth temperature. With Pd_3Ga_7 the inclusion of liquid solution droplets during growth is the most severe problem. These inclusions can even destroy the already grown crystal because of density changes occurring during the low-temperature peritectic reaction. What is common in Czochralski growth of these intermetallic phases is the need for a fully metal-sealed growth chamber to prevent traces of oxygen from entering the system and covering the melt surface. A very low pulling rate (typically 100 µm/h) combined with additional tools to assist materials transport adjacent to the growth interface is a prerequisite to avoid mother liquid inclusions in the growing crystals.

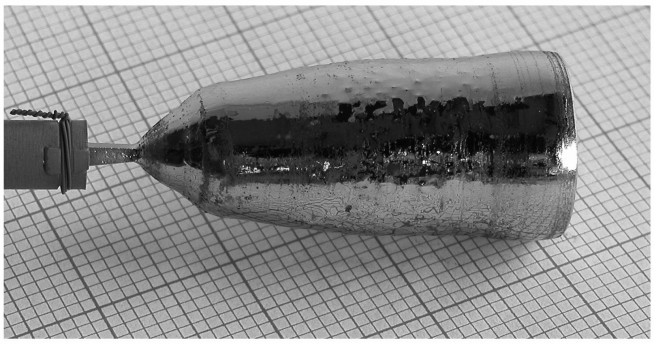

Fig. 2: PdGa single crystal grown from a $Pd_{45}Ga_{55}$ melt (grid size: 1 mm).

[1] J. Osswald et al., J. Catal. **258** (2008), 210.
[2] W.M.H. Sachtler, Catal. Rev. Sci. Eng. **14** (1976), 193.
[3] M. Armbrüster et al., J. Am. Chem. Soc. **132** (2010), 14745.
[4] H. Okamoto, J. Phase Equilibria Diffusion **29** (2008), 466.
[5] P. Gille et al., Intermetallics **18** (2010), 1663.

15:30 Oral

Czochralski crystal growth of the intermetallic compound InPd

Michael Hahne, Peter Gille

LMU München, Department of Earth and Environmental Sciences, Crystallography section (LMU), Theresienstr. 41, Munich 80333, Germany

e-mail: michael.hahne@lrz.uni-muenchen.de

Conventional catalysts for heterogeneous catalysis usually consist of finely dispersed particles of noble metals or their alloys on an oxide support material. Recent research has shown that also intermetallic compounds have a high potential as good catalysts being highly active with respect to a specific reaction and showing advantages in long-term stability and selectivity. For instance this was found for Pd-Ga intermetallic compounds used as semi-hydrogenation catalysts [1].

Due to the well-ordered crystal structure of the intermetallic compounds segregation effects are avoided and isolation of the active sites is assured (*active-site isolation concept* [2]).

The intermetallic compound InPd (CsCl prototype, *Pm*3*m*) is a promising catalyst material for methanol steam reforming. This reaction is a possibility to produce hydrogen for fuel cells in-situ from methanol. So the problems of storage and transportation of hydrogen could be avoided.

In order to understand the basic mechanisms of the catalysis and to enable a knowledge-based development of new catalysts, a number of characterization methods require cm-large and well-defined single crystalline samples. For example as catalysis takes place at the surface, it is important to investigate the surface structure and surface terminations for different crystallographic orientations. For this purpose it is necessary to grow cm^3-size single crystals of InPd, although of course in possible future applications fine powder or even nanoparticles will be used as for effective catalysts high specific surfaces are needed.

The Czochralski technique was applied to grow InPd crystals from In-rich solutions instead of growth from a congruent melt (melting point: 1285°C [3]) to reduce the relatively high vapour pressure of indium. The main problem of incorporation of In-rich solution droplets during growth could be solved by applying very low pulling rates in the range of 100 µm/h or even less and adjusting other experimental parameters.

We will present our Czochralski growth setup as well as the experimental conditions to get single-phase crystals and will discuss the results of the characterization of the grown crystals.

[1] M. Armbrüster et al., J. Am. Chem. Soc. **132** (2010), 14745.
[2] W.M.H. Sachtler, Catal. Rev. Sci. Eng. **14** (1976), 193.
[3] H. Okamoto, J. Phase Equilib. **24** (2003), 481.

15:45 Oral

Czochralski growth of R_2TSi_3 single crystals

Maria Szlawska, Dariusz Kaczorowski

Institue of Low Temperature and Structure Research, Polish Academy of Sciences (INTIBS-PAN), P.Nr 1410, Wrocław 50-950, Poland

e-mail: m.szlawska@int.pan.wroc.pl

The Czochralski process of crystal growth, named after Polish scientist Jan Czochralski, who invented the method in 1916 while investigating the crystallization rates of metals, is used in the semiconductor industry for the purpose of obtaining large single crystals of silicon with low density of defects. Application of the technique has induced technological revolution that led to advanced electronic devices being nowadays in common usage. The Czochralski technique is also widely employed in the area of fundamental research, as advanced studies on well-defined high-quality single crystals are indispensable for gaining important information on the physical properties of novel materials, which cannot be inferred from analogous characterization carried out on polycrystalline specimens.

Most of the Czochralski furnaces used in industry and in research laboratories utilize high-frequency electric induction heaters or resistance heaters to melt substrate. Their fundamental disadvantage is the presence of a hot crucible that may contaminate the grown material, especially if the latter has a high melting point. This problem is absent in cold-heart-type furnaces, which employ electric arcs ignited between tungsten-made cathodes and a water-cooled copper anode that serves as a crucible. Usually, three or four electric arcs are being lit and slow rotation of the heart is applied in order to provide uniform heating of molten material.

The Czochralski furnace installed at the Institute of Low Temperature and Structure Research, Polish Academy of Sciences in Wrocław (see the photograph on Fig. 1) is one of very few tetra-arc pulling furnaces available worldwide, and to the best of our knowledge the only one in Poland. Since its delivery from Japan in 2006,

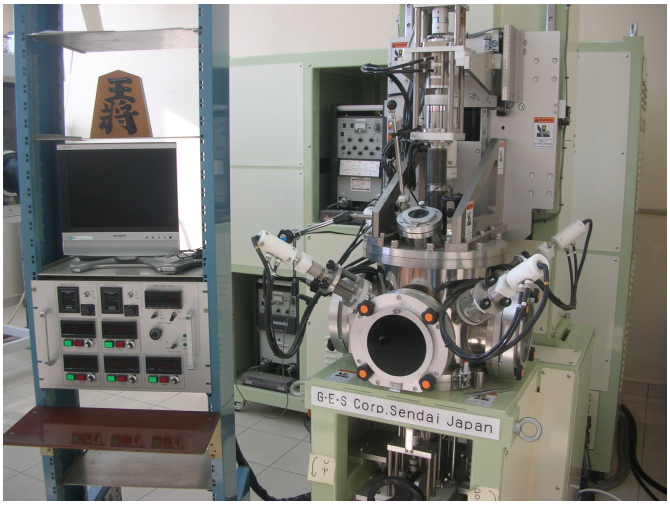

Fig. 1. The tetra-arc Czochralski furnace installed at the Institute of Low Temperature and Structure Research, Polish Academy of Sciences in Wrocław.

it has been successfully used to grow numerous excellent quality single crystals of various intermetallic compounds, with a special focus on cerium- and uranium-based ternaries. As 4*f*- and 5*f*-electron based phases usually melt at rather high temperatures, yet possess relatively low vapor pressures and many of them melt congruently, using this type of Czochralski technique seems to be the best way of obtaining well developed crystals. They have a shape of cylindrical rods with a diameter up to 3-4 mm and typical length of a few dozen mm.

Among the many compounds obtained to date in our Crystal Growth Laboratory in the form of excellent-quality single crystals, there is a series of ternary silicides with the overall composition R_2TSi_3, where R = Ce, U and T = Ni, Co, Rh, Ir. These phases crystallize with hexagonal disordered AlB_2-type structure (space group *P*6/*mmm*) or its more or less ordered derivatives. In the parent-type unit cell, R atoms occupy Al position and form triangular planar networks, while T and Si atoms share B site. Such arrangement of atoms inherently introduces frustration and randomness of exchange interactions between magnetic atoms, which may result in highly unusual magnetic properties. As an example, Fig. 2 displays a Czochralski-grown single crystal of Ce_2IrSi_3, which was recently comprehensively investigated by means of X-ray diffraction, magnetic, electrical transport and heat capacity measurements, performed in wide ranges of temperature and magnetic field strength [1,2]. The compound was found to form with a fully-ordered unit cell, which is doubled within the basal hexagonal plane with respect to the parent AlB_2-type substructure. As can be inferred from Fig. 3, it orders antiferromagnetically at T_N = 1.3 K with the magnetic susceptibility taken within the *ab* plane, χ_{ab}, being distinctly larger than that measured along the *c* axis, χ_c. Remarkably, the latter component hardly shows any anomaly at T_N. A distinct magnetic anisotropy is observed also in the field dependencies of the magnetization measured deeply in the ordered state (see the inset to Fig. 3). The component σ_c is roughly proportional to B, while that taken within the *ab* plane has much larger values and σ_{ab} (B) is strongly curvilinear. These results concomitantly indicate that the magnetic moments in the compound studied are probably confined to the basal hexagonal plane.

The long-range antiferromagnetic ordering in Ce_2IrSi_3 is accompanied by strong

Fig. 2. A single crystal of Ce_2IrSi_3 grown by Czochralski technique in the tetra-arc furnace.

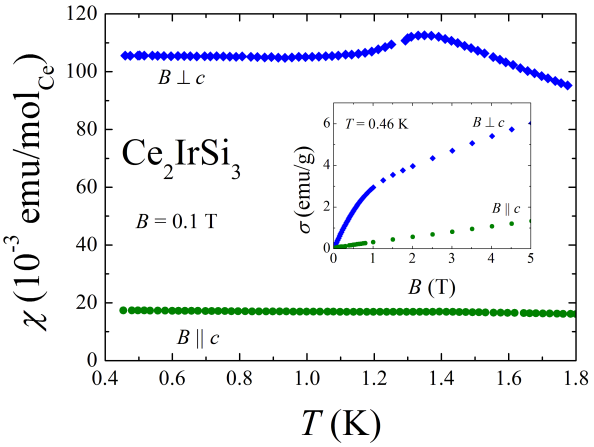

Fig. 3. Temperature variations of the magnetic susceptibility of single-crystalline Ce_2IrSi_3, measured in the magnetic field of 0.1 T oriented parallel and perpendicular to the *c* axis of the hexagonal unit cell. The inset presents magnetic field variations of the magnetization measured at 0.46 K.

electronic correlations effects, which manifest themselves in an enhanced low-temperature linear contribution to the specific heat, large negative values of the paramagnetic Curie temperatures, as well as in clear negative logarithmic slopes in the electrical resistivity. Based on all the experimental findings, Ce_2IrSi_3 can be categorized as an antiferromagnetic Kondo lattice with a moderate-heavy fermion ground state.

[1] M. Szlawska, D. Kaczorowski, Phys. Rev. B **84**, 094430 (2011)
[2] M. Szlawska, D. Kaczorowski, to be published in J. Korean Phys. Soc.

Coffee

Thursday afternoon, 15 August, 16:00

ThO3

T01: Intermetalic and highly correlated electron materials
Thursday afternoon, 15 August, 16:30
Mickiewicz Hall, Auditorium Maximum

16:30 Invited oral

Growing uranium and cerium pnictide crystals by chemical vapor transport and flux methods

Zygmunt Henkie

Institute of Low Temperature and Structure Research, Polish Academy of Sciences, P.Nr 1410, Wrocław 50-950, Poland

e-mail: Z.Henkie@int.pan.wroc.pl

Our knowledge of various compounds increases more effectively when they are studied within series of their homologs. Sometimes however, chemical properties of compounds in series strongly vary and growing their crystals requires serious modification of used methods. We illustrate this problem with an example of crystal growth of binary uranium pnictides of UX, U_3X_4 and UX_2 stoichiometries (X = P, As, Sb, and Bi). Uranium phosphides and arsenides of U_3X_4 and UX_2 composition could be grown by chemical vapor transport (CVT) in quartz ampoules at temperatures in range 750 - 950 ^oC, with iodine as a transporting agent and temperature gradient ~ 100 ^oC. Grown crystals were of excellent quality allowing quantum oscillations studies. UP, UAs, USb, and U_3Sb_4 could be grown by the CVT on tungsten rings heated up to temperature 1200 ÷ 1400 ^oC by induction furnace. The rings were suspended in a quartz bulb with substrates at its bottom - the coldest place in the bulb (600 ÷ 700 ^oC). Keeping a respectively low temperature of the quartz its reaction with uranium was greatly reduced. USb_2 and UBi_2 were grown by the self-flux method, where the driving force of the crystal growth was gradual decrease of temperature at rate ranging from 0.5 ^oC/hr at 1000 ^oC to 4 ^oC/hr at room temperature. Crystals of U_3Bi_4 were grown at constant temperature of 1080 ^oC in a U-Bi solution attaining over-saturation by slow evaporation of Bi due to the special construction of a graphite crucible heated with induction furnace. Various RET_4As_{12} (T = Fe, Ru and Os; RE = La, Ce, Pr, and Nd) skutterudite crystals first-ever obtained, were grown in Cd:As or As fluxes in a self made pressure cell. Owing to high sensitivity of $CeFe_4As_{12}$ hybridisation gap semiconducting state on stoichiometry defects we observed a clear dependence of the grown $CeFe_4As_{12}$ crystals morphology on very low amount of stoichiometry defects.

17:00 Invited oral

Pyrochlores Grown by Optical Floating Zone Method

Hanna A. Dabkowska[1], Kate A. Ross[2], Katharina Fritsch[2], Hilary M. Noad[2], Casey Marjerrison[2], Jacob P. Ruff[2], Bruce D. Gaulin[1,2], Teresa Medina[2], Robert M. D'Ortensio[2], Tim Munsie[2], Jose A. Rodriguez[2], Graeme M. Luke[2], Antoni Dabkowski[1]

1. *Brockhouse Institute for Materials Research, McMaster University, 1280 Main Street West, Hamilton L8S4MI, Canada* **2.** *McMaster University, Department of Physics, 1280 Main Street West, Hamilton L8S 4M1, Canada*

e-mail: dabkoh@mcmaster.ca

In this presentation I would like to stress the importance of high quality, well characterized crystals of complex oxides and their solid solutions for understanding geometrically frustrated magnetism.

My example are cubic rare earth pyrochlores $RE_2M_2O_7$ (where RE is an rare earth element and M = Ti, Sn, V or Zr), hosting many of the unusual, magnetic, frustrated states which are in the centre of attention of solid state physics.

As the rare earth pyrochlores melt congruently at temperatures above the melting point of Pt, the Optical Floating Zone [OFZ] technique

proved to be an efficient, crucible-free method for growth of relatively big single crystals. Using oxidizing or neutral growth atmosphere it was possible to crystallize $Y_2Ti_2O_7$ – diamagnet, a potential inert matrix for actinides transmutation [1], $Tb_2Ti_2O_7$ - a spin liquid, with thermal longitudinal spin fluctuations which break spin ice rules [2,3], $Ho_2Ti_2O_7$ and $Dy_2Ti_2O_7$ – classical, but still not well enough understood, spin ice systems [4-7], mysterious, frustrated XY antiferromagnet $Er_2Ti_2O_7$ [8] and $Yb_2Ti_2O_7$ which displays unexpected, quasi-two-dimensional (2D) magnetic correlations within a cubic lattice environment at low temperatures before entering an exotic disordered ground state below T = 265mK [10-12].

Moreover, $Lu_2V_2O_7$ melts congruently only in reducing conditions and shows ferromagnetic properties.

To investigate even further physical, crystallographic and optical properties of RE pyrochlores by directionally sensitive methods such as neutron scattering or muons experiments, high quality single crystals are essential.

In the presentation effects of growth conditions and composition on crystal properties of these pyrochlores are discussed.

1. Johnson MB, James DD, Bourque A, Hanna A Dąbkowska; Bruce D Gaulin; J. Solid State Chemistry, **182** (2009) 725-729

2. S. Legl, C. Krey, S. R. Dunsiger, H. A. Dabkowska, J. A. Rodriguez, G. M. Luke, and C. Pfleiderer PRL **109** (2012) 047201

3. K. Fritsch, K. A. Ross, Y. Qiu, J. R. D. Copley, T. Guidi, R. I. Bewley, H. A. Dabkowska, and B. D. Gaulin, Phys. Rev. B **87** (2013) 094410

4. J.A. Quilliam, L.R. Yaraskavitch, H.A. Dąbkowska, B.D. Gaulin, J. Kycia Phys. Rev. B, **83** (2011) 094424

5. H. M. Revell, L. R. Yaraskavitch, J. D. Mason, K. A. Ross, H. M. L. Noad, H. A. Dabkowska, B. D. Gaulin, P. Henelius and J. B. Kycia, Nature Physics **9** (2013) 34–37

6. D. Pomaranski, L. R. Yaraskavitch, S. Meng1, K. A. Ross, H. M. L. Noad, H. A. Dabkowska, B. D. Gaulin and J. B. Kycia, Nature Physics Letters (2013) *DOI:10.1038/NPHYS2591* .

7. L. R. Yaraskavitch, H. M. Revell, K. A. Ross, H. Noad, S. Meng, H. A. Dabkowska, B. D. Gaulin, and J. B. Kycia Phys. Rev. B, **85** (2012) 020410

8. J. P. C. Ruff, J. P. Clancy, A. Bourque, M. A. White, M. Ramazanoglu, J. S. Gardner, Y. Qiu, J.

R. D. Copley, M. B. Johnson, H. A. Dąbkowska, and B. D. Gaulin, Phys. Rev. Letters **101** (2008), 147205

9. Craig Bryan, Catherine A. Whitman, Michel B. Johnson, Patrick Murray, Alex Bourque, Hanna A. Dabkowska, Bruce D. Gaulin and Mary Anne White Phys. Rev. B 86 (2012) 054303

10. Ross KA, Ruff JPC, Adams CP, J. S. Gardner, H. A. Dąbkowska, Y. Qiu, J. R. D. Copley, and B. D. Gaulin Phys. Rev. Letters **103** (2009) 227202

11. K.A. Ross, L.R. Yaraskavitch, M. Laver, J.S. Gardner, J. A. Quilliam, S. Meng, J.B. Kycia, D. K. Singh, Th. Proen, H.A. Dabkowska, and B.D. Gaulin Phys. Rev. B **84** (2011) 174442

12. K.A. Ross, Th. Proen, H.A. Dabkowska, J. A. Quilliam, L.R. Yaraskavitch, J.B. Kycia, and B.D. Gaulin Phys. Rev. B **86** (2012) 174424

17:30 Oral

The effect of process parameters on floating zone crystal growth of selected cuprates

Nadja Wizent[1], Patrick Ribero[1], Günter Behr[1], Wolfgang Löser[1], Rüdiger Klingeler[2], Bernd Büchner[1]

1. *Leibniz-Institute for Solid State and Materials Research, P.O.Box 270116, Dresden D-01171, Germany* **2.** *Universität Heidelberg, Im Neuenheimer Feld 253, Heidelberg 69120, Germany*

e-mail: w.loeser@ifw-dresden.de

Single crystals of cuprates are unique subjects of fundamental research because of their high-T_c superconducting properties but also as excellent model systems for low-dimensional quantum antiferromagnetism. Here the crystal growth of selected cuprates by the floating zone (FZ) method with optical heating is analysed. Two different FZ facilities with vertical double ellipsoid optical configuration were primarily applied because of the radial symmetry of light flux and sharper focussing of the light leading to a steep temperature gradient at the crystal/melt interface. The compact growth chamber enables high gas pressure up to 15 MPa.

Process parameters for FZ crystal growth principally depend on the constitution of the systems. In case of congruent melting compounds, such as Li_2CuO_2, a growth velocity of 10 mm/h has been reached. In this case, the elevated total pressure of 50 bar of a gas mixture of Ar:O_2 4:1 has minimized the vaporization of the volatile element Li and prevented the crystallization of a secondary phase.

Cuprates with incongruent melting behaviour were grown with the travelling solvent floating zone (TSFZ) method at low velocities of the order of 1 mm/h or less. Because of the considerable composition difference at the crystal/melt interface steep temperature gradients and counter-rotation of crystal and feed rod are favourable for suppressing constitutional supercooling. Often phase diagrams of the cuprate systems are not precisely known. Phase equilibria were analysed by quenching the ultimate zone after the growth process (Fig.1).

The floating zones in TSFZ growth of multicomponent cuprates are not only enriched in CuO, but display diverse other element segregation. In TSFZ growth of the $Nd_2Ca_2Cu_5O_{10}$ crystal (Fig. 2), depletion of Ca and Nd in the solvent was revealed. For $Ca_{2+x}Y_{2-x}Cu_5O_{10}$ even liquid phase separation was detected in the floating zone where the crystal grew from a Y-depleted melt contrasted by the Y-rich melt adjacent to the feed rod.

Oxygen is a main constituent of the cuprates, and therefore the ambient atmosphere in the growth chamber affects the thermodynamic equilibria. Because copper can change its valence state, oxygen is often released on melting of cuprates whereas crystallization requires oxygen uptake. The TSFZ process proceeds with oxygen depleted melt zone. Elevated oxygen pressure up to 15 MPa can alter the solidification mode towards congruent melting [2], which is beneficial for achieving higher growth rates. It even enables the crystallization of novel compounds not stable at normal pressure, e.g., $Sr_{14-x}Ca_xCu_{24}O_{41}$ compounds with high Ca fractions x > 12. By using O_2/Ar gas mixtures, the oxygen partial pressure in the growth chamber can be controlled independently. Harmful formation of gas bubbles in the floating zone is diminished, which often arises in growth at high oxygen pressure (*cf.* Fig. 1).

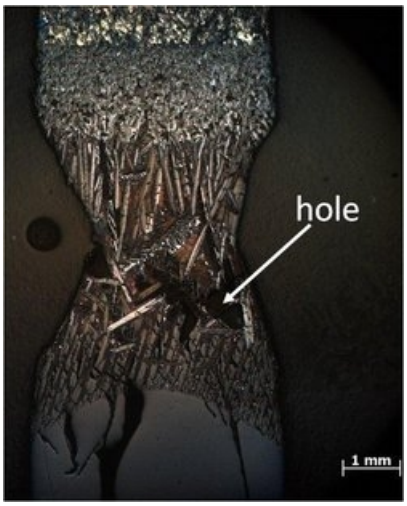

Fig. 1. Quenched last zone between feed rod (top) and $Nd_2Ca_2Cu_5O_{10}$ crystal (bottom).

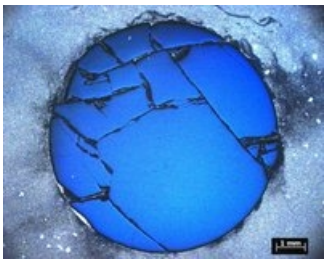

Fig. 2. Cross section of $Nd_2Ca_2Cu_5O_{10}$ crystal grown at oxygen pressure 4 MPa and v = 2 mm/h [1].

The control of the temperature profile, stable FZ geometry and a proper crystal/melt interface shape are other necessities for the TSFZ process. In the vertical crystal growth apparatus the irradiation profile is modified by the lamp position, but by higher rotation rates of the seed via melt convection the interface shape can also be flattened. In TSFZ growth of some cuprates spikes of refractory phases often crystallize at the surface of the partially melted feed rods. This is caused by grazing rays close to the optical axis, which must be eliminated from the incident light flux by a light blocker.

[1] N. Wizent, Thesis, TU Dresden 2009.

[2] N. Wizent , L. Schramm, G. Behr, W. Löser, W. Gruner, A. Voß, B. Büchner, L. Schultz, J. Solid State Chem. 182 (2009) 2036–2040.

17:45 Oral

Floating zone growth of $Co_2Cr_{1-x}Fe_xAl$ Heusler compounds

Ahmad Omar, Maria Dimitrakopoulou, Christian G F. Blum, Horst Wendrock, Steven Rodan, Silke Hampel, Wolfgang Löser, Bernd Büchner, Sabine Wurmehl

Leibniz-Institute for Solid State and Materials Research, P.O.Box 270116, Dresden D-01171, Germany

e-mail: a.omar@ifw-dresden.de

Many Heusler compounds are predicted to be half-metallic ferromagnets and find extensive interest as materials for spintronic applications, an example of which is the $Co_2Cr_{1-x}Fe_xAl$ series. So far, bulk samples of that series, in particular Cr-rich samples, do not verify those predictions and various studies yield results which are fraught with anomalies. Thin films as well do not meet the expectations in magnetoresistance ratio nor in degree of spin polarization and magnetic moments. In the present work, crystal growth of $Co_2Cr_{1-x}Fe_xAl$ Heusler compounds has been done, as a step towards understanding the intrinsic material properties of this series. To begin with, polycrystalline samples of Co_2CrAl, Co_2FeAl and $Co_2Cr_{0.6}Fe_{0.4}Al$ were prepared and found to be phase segregated, a hurdle already reported and easily tackled by using the Optical Floating Zone technique (FZ). Our results demonstrate that, although this phase segregation is eliminated in the FZ grown samples, an unexpected phase transformation via spinodal decomposition is taking place in samples containing Cr. This phase decomposition is found to strongly affect the magnetic properties and hence also other properties as e.g. the spin polarization. Our finding presents new insight into the phase dynamics in this system and provides answers to many of the issues in this series of half-metallic ferromagnets.

18:00 Oral

Crystal growth of intermetallic clathrates: floating zone process and ultra rapid crystallization

Andrey Prokofiev, Xinlin Yan, Matthias Ikeda, Silke Paschen

Institute of Solid State Physics, Vienna University of Technology, Wien, Austria

e-mail: andrey.prokofiev@ifp.tuwien.ac.at

Intermetallic clathrates are at the forefront of research in novel thermoelectrics. They are inclusion compounds in which atoms of one type (guest) are enclosed in oversized cavities formed by the framework atoms of another type (host). This structural feature leads to extremely low and even "glass-like" thermal conductivity whereas the electrical conductivity remains high and "crystal-like". This concept which is usually referred to as "phonon glass - electron crystal" (PGEC) makes clathrates a promising class of thermoelectric materials.

Synthesis of single phase clathrates is often problematic even when X-ray powder diffraction of polycrystalline samples shows no foreign phases. The foreign phases appear as thin intergrain layers, which can have a great impact on transport properties. Because these phases are very air sensitive the polycrystalline samples are chemically and mechanically unstable. Therefore investigations of intrinsic properties of some clathrate phases should be performed on single crystals.

Here we present our study of crystal growth of type-I transition metal clathrates $Ba_8TM_xSi_{46-x}$ and $Ba_8TM_xGe_{46-x}$ (TM = Cu, Au) in two different regimes. Bulk single crystals were grown in a floating zone furnace. We studied segregation effects of main constituting elements and of low doping impurities by investigation the composition profiles along the growth direction. Because of absence of air sensitive intergrain inclusions the grown single crystals, contrary to polycrystalline samples, are chemically and mechanically very stable.

The structural feature of clathrates and their extremely low thermal conductivity imply their specific growth behaviour. It manifests itself most pronounced in a rapid crystallization process. Ultra rapid crystallization in our study was realized using the melt spinning technique. This technique which provides the cooling rate of about 10^5-10^6 K/s was originally developed for the production of amorphous metallic materials and is used also for preparation of nanograined materials. Our numerous experiments on melt spinning of various clathrates have revealed surprisingly large grains of at least 1 μm [1-4]. Because of the anomalously high growth rate of the clathrate phase the formation of impurity phases is kinetically suppressed, and the melt spun samples appear to be air stable, too. We present our transmission electron microscopy (TEM) investigation of melt spun samples and discuss thermodynamic and kinetic aspects of the unusual clathrate crystallization: the interplay of nucleation and bulk growth as well as the effect of composition on the grain size.

[1] A. Prokofiev, S. Paschen, H. Sassik, S. Laumann, P. Pongratz, Utility patent AT: 10749 U1 2009-09-05, DE: 20 2008 006 946.7, patent applications US: 12/231,183, JP: 135994/2008.
[2] S. Paschen C. Gspan, W. Grogger, M. Diensleder, S. Laumann, P. Pongratz, H. Sassik, J. Wernisch, and A. Prokofiev. J. Cryst. Growth, 310, 1853 (2008)
[3] S. Laumann, M. Ikeda, H. Sassik, A. Prokofiev, and S. Paschen. J. Mater. Res. 26, 1861 (2011)
[4] S. Laumann, M. Ikeda, H. Sassik, A. Prokofiev, and S. Paschen. ZAAC 201100353 (2011)
We acknowledge financial support from the Austrian Science Fund (FWF project TRP 176-N22)

18:15 Oral

Growth of $(Na_xK_y)Fe_zSe_2$ crystals aided by reduction reaction from chlorides flux at low temperatures

Gang Wang, Tianping Ying, Yaobo Huang, Shifeng Jin, Lei Yan, Hong Ding, Xiaolong Chen

Institute of Physics, Chinese Academy of Sciences (IOPCAS), No.8 Nansanjie, Zhongguancun, Beijing 100190, China

e-mail: gangwang@iphy.ac.cn

The discoveries of superconductivity at about 30 K in $A_xFe_{2-y}Se_2$ (A = K, Cs, Rb, Tl/Rb, Tl/K)[1-5] have stimulated significant interest for the remarkably distinct structural and physical characteristics displayed in these metal-intercalated iron selenide superconductors. However, the presence of phase separations in the materials severely thwarts the attempts to unambiguously identify the superconducting phases and to understand the underlying mechanisms. Many efforts have been devoted to obtain phase-pure or superconducting-dominated single crystals by high-temperature routes and not succeeded. New strategies are needed to overcome this key problem. Here we report that $(Na_xK_y)Fe_zSe_2$ crystals are successfully prepared in NaCl/KCl flux at low temperatures~720 °C. A reduction reaction that converts K in KCl into metal K by metal Na plays a crucial role in the growth of crystals. It is found that K is more preferred than Na to enter in between FeSe layers and forms the superconducting phase. Thus-obtained superconducting crystals contain more superconducting phase in volume fraction than those by high-temperature routes and exhibit new features in transport property. Our results provide a new effective synthetic route for preparing quality crystals of iron selenide superconductors.

[1] J. G. Guo, S. F. Jin, G. Wang, S. C. Wang, K. X. Zhu, T. T. Zhou, M. He, X. L. Chen, *Phys. Rev. B*, **2010**, 82, 180520(R).

[2] A. Krzton-Maziopa, Z. Shermadini, E. Pomjakushina, V. Pomjakushin, M. Bendele, A. Amato, R. Khasanov, H. Luetkens, K. Conder, *J. Phys.: Condens. Matter*, **2011**, 23, 052203.

[3] A. F. Wang, J. J. Ying, Y. J. Yan, R. H. Liu, X. G. Luo, Z. Y. Li, X. F. Wang, M. Zhang, G. J. Ye, P. Cheng, Z. J. Xiang, X. H. Chen, *Phys. Rev. B*, **2011**, 83, 060512.

[4] H.-D. Wang, C.-H. Dong, Z.-J. Li, Q.-H. Mao, S.-S. Zhu, C.-M. Feng, H. Q. Yuan, M.-H. Fang, *Europhys. Lett.*, **2011**, 93, 47004.

[5] M.-H. Fang, H.-D. Wang, C.-H. Dong, Z.-J. Li, C.-M. Feng, J. Chen, H. Q. Yuan, *Europhys. Lett.*, **2011**, 94, 27009.

Break
Thursday evening, 15 August, 18:30

Posters

Wednesday, 14 August

WeP-T01
Wednesday afternoon, 14 August, 16:00
Room 107, Old Library

16:00 Poster We60

Single crystal growth and structural characterization of iron telluride doped with transition metals

Izabela I. Kruk, Paweł Ł. Zajdel

University of Silesia, August Chełkowski Institute of Physics, Department of Physics of Crystals, Uniwersytecka 4, Katowice 40-007, Poland

e-mail: iza.oshaughnessy@gmail.com

Tetragonal FeTe is an non-superconducting parent compound of the Fe(Te,Se,S) families of superconductors (SC), which under doping with selenium or with small amounts of sulphur becomes superconducting. So far, it was impossible to grow ideally stoichiometric 1:1 composition due to extra iron ions present in the lattice and the chemical composition of known bulk crystals can be described with general formula $Fe_{1+x}Te$, where x ranges from about 4% to 17%. The additional iron has been found to negatively correlate with the level of anion site doping and subsequently with hindering the superconductivity.

In our work, we attempt to create and investigate the situation equivalent to 1:1 stoichiometry by varying the amount of excess electrons present in the system. This is achieved by chemical means by doping $Fe_{1+x}Te$ with zinc ($3d^0$), chromium (3d electron deficient) or nickel (3d electron reach). This report presents our recent results obtained for zinc doped FeTe.

The single crystals of FeTe doped with zinc were grown using modified Bridgeman method. The characterization was performed using SEM, single crystal diffraction, magnetization measurements and for a powdered specimen - neutron diffraction.

The samples, several millimeter in size, were easily cleaved along 001 direction revealing terraced surface covered with cavities. The magnetic transition temperature was found to decrease with doping up to 5% Zn. Neutron powder diffraction for the sample with the highest zinc doping revealed well established long range magnetic order and the monoclinic distortion.

Such behavior, on the contrary to anion site doping, indicates that the removal of additional iron is not sufficient to significantly change the magnetic properties of the system.

This work is supported by the Polish National Science Centre grant No 2011/01/B/ST3/00425

Corresponding author pawel.zajdel@us.edu.pl

16:00 Poster We61

Bulk single crystal growth of $ErPd_2Si_2$ intermetallic compound by a floating zone method

Chongde Cao[1], Wolfgang Löser[2], Günter Behr[2]

1. *Northwestern Polytechnical University, Xi'an 710072, China* **2.** *Leibniz-Institute for Solid State and Materials Research, P.O.Box 270116, Dresden D-01171, Germany*

e-mail: w.loeser@ifw-dresden.de

Bulk single crystals (d = 6 mm, l = 50 mm) of the $ErPd_2Si_2$ compound have been successfully grown at a velocity of 10 mm/h by using the floating zone method with optical heating. Fig. 1 shows a cross section of an $ErPd_2Si_2$ single crystal. The morphology of a longitudinal section of the initial part grown from the seed shows a rapid grain selection in the early stage of the $ErPd_2Si_2$ crystal growth (Fig. 2). X-ray Laue back-scattering analysis indicates that the crystal growth direction is close to [110] orientation with an inclination angle of about 15° against the rod axis. Energy Dispersive X-ray (EDX) analysis revealed that the composition of the $ErPd_2Si_2$ single crystal is about 21.8 at% Er, 36.8 at% Pd, and 41.4 at% Si. The melting point of the $ErPd_2Si_2$ compound, 1461°C, is determined by differential scanning calorimetry (DSC). The lattice constants of the single crystal, a = 4.104 Å and c = 9.878 Å were measured by X-ray diffraction analysis. Significant anisotropy has been observed in the magnetic susceptibility. The temperature coefficient of electrical resistivity is isotropic, and no feature resulting from magnetic ordering was detected on the electrical resistivity at low temperatures.

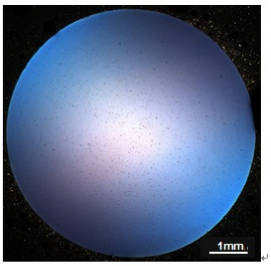

Fig. 1. Micrograph of a cross section of the $ErPd_2Si_2$ single crystal from the polarized-light optical microscope.

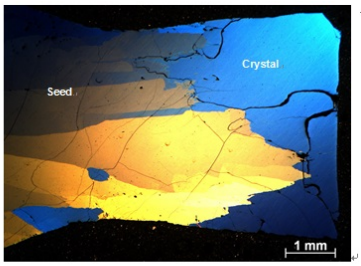

Fig. 2. Morphology of a longitudinal section of the initial part grown from the seed.

16:00 Poster We62

Floating Zone Crystal Growth of Lu_2PdSi_3 Silicide

Chongde Cao[1], Christian G F. Blum[2], Wolfgang Löser[2], Steven Rodan[2], Dirk Bombor[2]

1. *Northwestern Polytechnical University, Xi'an 710072, China* **2.** *Leibniz-Institute for Solid State and Materials Research, P.O.Box 270116, Dresden D-01171, Germany*

e-mail: w.loeser@ifw-dresden.de

The single crystals of various rare earth (R) – transition metal intermetallic compounds within the class of R_2PdSi_3 with hexagonal AlB_2-type crystallographic structure exhibit a systematic dependence of anisotropic magnetic properties governed by the interplay of crystal-electric field effects and magnetic two-ion interactions. Lu_2PdSi_3 represents a non-magnetic member of the class of R_2PdSi_3 intermetallic compounds. No information has been available on the crystal growth, structure and physical properties of Lu_2PdSi_3 intermetallic compound. In this work, single crystals of the Lu_2PdSi_3 compound have been successfully grown at velocities of 5 and 3 mm/h by using the floating zone method with optical heating. The axial temperature profile across the floating zone indicates a steep temperature gradient at the interface of the growing crystal, which is a prerequisite for suppression of the morphological instability of the crystal/melt interface at moderate growth rates despite the sizeable composition difference between the crystal and the travelling solvent. Microstructure analysis of the quenched liquid zone shows that a structure of Lu_2PdSi_3 dendrites with interdendritic binary eutectic is formed. Energy Dispersive X-ray (EDX) analysis reveals that the Lu_2PdSi_3 crystal has a Pd-depleted composition. The electrical resistivity and specific heat of the Lu_2PdSi_3 single crystals show this compound resembles a normal metal with relatively low Debye temperature. But the electrical resistivity displays a high anisotropy between orientations along the c-axis and within the plane perpendicular to the axis, respectively.

16:00 Poster We63

Preparation of $NdMn_{1-x}Fe_xO_{3+\delta}$ single crystals – effect of preparation atmosphere and iron doping

Matúš Mihalik[1,2], Slavomír Mat'aš[2], Martin Vavra[1,3], Jaroslav Briančin[4], Marian Mihalik[1], Magdalena Fitta[5], Viktor Kavečanský

1. *Institute of experimental Physics, Kosice (IEP SAS), Watsonova 47, Kosice 04353, Slovakia (Slovak Rep.)* **2.** *Hahn-Meitner-Institute (HMI), Glienicker Str. 100, Berlin D-14109, Germany* **3.** *P. J. Safarik University, Moyzesova 11, Kosice 04001, Slovakia (Slovak Rep.)* **4.** *Institute of Geotechnics SAS, Watsonova 45, Kosice 04353, Slovakia (Slovak Rep.)* **5.** *Institute of Nuclear Physics Polish Academy of Sciences, Kraków 31-342, Poland*

e-mail: matmihalik@saske.sk

We study the effect of crystal growth atmosphere (argon or air) and chemical doping (iron) on the quality of the single crystals with the general formula $NdMn_{1-x}Fe_xO_{3+\delta}$, which were grown by the optical floating zone method. The grown ingots were characterized in the manner of X-ray powder diffraction (XRPD), X-ray Laue diffraction, scanning electron microscopy (SEM), energy-dispersive X-ray spectroscopy (EDX), iodometric titration and single crystal neutron diffraction.

Single crystals of $NdMnO_{3+\delta}$ are usually grown following two main sets of preparation conditions: 1) ambient air atmosphere, rotation of 60 rpm and growing speed 10 – 20 mm/h [1] or 2) argon atmosphere of pressure 6 to 8 bars with 1 to 5 % of oxygen impurity, rotation of 40 rpm and growing speed of 6 – 8 mm/h [2]. Since both sets of preparation conditions might have the consequences on the oxygen non-stoichiometry δ [3] and thence on the physical properties of the prepared samples, or can lead to the decomposition of the material [4], a comparative study of crystal growth conditions with respect to crystal grown atmosphere is important. That is why we have prepared several rods of $NdMnO_{3+\delta}$ with different preparation conditions (see Table 1) and have studied the prepared crystals by different characterization techniques.

Table 1: The studied sets of the preparation conditions.

Trial number	atmosphere	power (kW)	pulling speeds* (mm/h) upper/lower shaft	rotation (rpm) upper/lower shaft

1	Ar, ambient, bubbling	2×1.5	8/8	10/10
2	Ar, ambient, bubbling	2×1.5	10/10	25/25
3	air, ambient, flowing 2 l/min	4×1	6/8	30/30
4	air, ambient, flowing 2 l/min	4×1	5/6	15/15
5**	air, ambient, flowing 2 l/min	4×1	5/5	10/10

* Speed relative to furnace lamps
** As a seed the grown ingot from previous trial was used

The XRPD experiments revealed that the rods prepared in the air atmosphere are clean from the impurities, but the rods prepared in the argon atmosphere were free from impurities only at the beginning of the rods, but at the end the small fraction (about 2 %) of MnO impurity was detected. This impurity is probably caused by the evaporation of oxygen from the melt which resulted to the reduction of some manganese atoms to oxidation state +2. The subsequent EDX analysis of samples from trials 3 to 5 revealed that the samples are clean from impurities within the precision of the EDX technique (0.5 %).

The iodometric titration experiments resulted to the oxygen nonstoichiometry δ = 0.04; 0.14; 0.13; 0.19 and 0.02 for trials 1; 2; 3; 4; and 5 respectively.

The check of the grown ingot by Laue diffraction (trials 1 and 2) revealed the twinning of the crystals. The single crystal neutron diffraction experiments (trials 3 – 5) revealed that in the bulk material there are two types of grains: one type of grains grows in the manner that (101) axis is parallel to the growing direction, but in the same grown ingot there exist also the grain with the (020) axis parallel to the growing direction (see figure 1). Fit of the neutron single crystal data revealed that the best crystal from the crystallographic point of view was crystal from trial 5, where the full width at half maxima (FWHM) for grain (101) was 0.76° and FWHM for (020) grain was 0.7°.

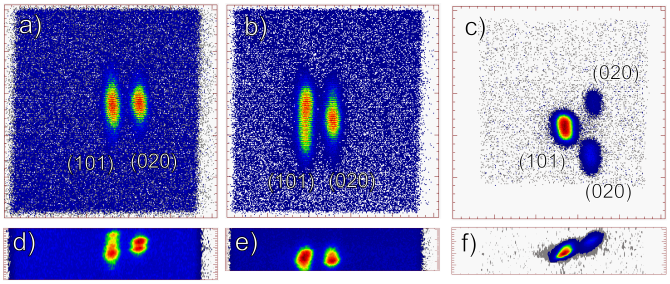

Figure 1: The omega scans as appear on the 2D neutron detector a) trial 3; b) trial 4; c) trial 5, data summed through the omega; d) trial 3; e) trial 4; f) trial 5, data summed through out of the scattering plane component. The position of the middle of the detector was trial 3: 36°; trial 4: 38°; trial 5: 36°; the detector covers angle range of 15.3 degree in 2θ and ± 7.65 degrees above and below scattering plane (at distance 748 mm from sample).

Concerning the iron doping for $NdMn_{1-x}Fe_xO_{3+\delta}$ compounds, we have prepared several samples up to x = 0.3. For these experiments we have used the following crystal growth parameters: air atmosphere, flowing 2 l/min, growing speed between 6 and 8 mm/h; rotation of 30 rpm. All samples from this series were proven by XRPD and EDX analysis to be single phased and with the expected chemical concentration within the experimental error. The subsequent iodometric titration experiments revealed the small excess of the oxygen δ = 0.04; 0.10; 0.07; 0.11 and 0.14 for x = 0; 0.1; 0.2; 0.25 and 0.3, respectively.

In conclusion the air atmosphere is better choice than the argon atmosphere for crystal growth of NdMn1-xFexO3+δ single crystals. The iron solubility in NdMnO3 is very good and it is possible to obtain the series of NdMn1-xFexO3+δ compounds at least up to x = 0.3.

[1] A. M. Balbashov, S. G. Karabashev, Ya. M. Mukovskiy and S. A. Zverkov, J. Cryst. Growth **167** (1996), 365-368
[2] D. Prabhakaran, A. I. Coldea, A. T. Boothroyd and S. J. Blundell, J. Cryst. Growth **237 – 239** (2002), 806 – 809
[3] V. A. Cherepanov, L. Yu Barkhatova, A. N. Petrov and V. I. Voronin, J. Sol. Stat. Chem. **118** (1995), 53 – 61
[4] N. Kamegashira, Y. Miyazaki and Y. Hiyoshi, Mater. Chem. & Phys. **10** (1984) 299-304

16:00 Poster We64

Optical Absorption in $Mo_xW_{1-X}Se_2$ (x=0, 0.25, 1) Single Crystals

Deepa S. Narang[1], Rajendra Prasad Pathak[2], Kirit D. Patel[3], Vivek M. Pathak[3], Ram Srivastava[3]

1. *Alliance College of Engineering and Design (ACED), Alliance University, Chandapura, Anekal, Bangalore, Karnataka, Bangalore 562106, India* **2.** *RR Mehta College of Science CL Parikh College of Commerce Palanpur (RRMS/CLPC), GD Modi Vidysnakul, Opp-ST Workshop, Highway, Palanpur, Ahmedabad 385001, India* **3.** *Department of Physics, Sardar Patel University, Vallabh Vidyanagar-388120, Gujarat, India, Vallabh Vidyanagar 388120, India*

e-mail: deepamakhija23@gmail.com

The transition-metal dichalcogenides (TMDC) such as MX_2 (M=W or Mo and X= S, Se) show a wide variety of interesting anisotropic optical and electrical properties. They display a whole spectrum of electronic properties covering semiconductors, metals, insulators and superconductors. Most TMDCs form hexagonal layered structures. Structurally, these compounds can be regarded as strongly bonded two dimensional X – M – X layers or sandwiches which are loosely coupled to one another by relatively weak Van der Waals type forces. This structure makes these compounds extremely anisotropic in character and leads to unusual structural properties. The band gaps of many of these materials are around 1 eV and it has been suggested that the band gaps are indirect. These TMDCs have been used for many years as solid state lubricants, photovoltaic/photocatalytic solar energy converters, Schottky and liquid junction solar cells as catalysts in many industrial applications and in secondary batteries etc. Looking to such diverse applications of TMDCs, the molybdenum diselenide, tungsten diselenide and mixed compounds of molybdenum and tungsten diselenides belonging to this family have been grown by direct vapour transport (DVT) technique using a two zone horizontal furnace. Optical absorption spectra of these compounds have been measured in the range 200–2000 nm at room temperature near the fundamental absorption edge using light parallel to c – axis incident normally on the basal plane. Results have been analyzed on the basis of two dimensional (2D) and three dimensional (3D) models. Both direct and indirect transitions are involved in the absorption process. Absorption near the fundamental edge was found to be due to indirect and direct allowed transitions on the basis of 3D model and indirect allowed transition on the basis of 2D model. The optical energy gaps corresponding to both transitions have also been determined. Some feeble disorder in the crystals is conceived to be present.

16:00 Poster We65

Comparison of magnetic properties of the monocrystalline and microcrystalline Gd_7Pd_3 compound

Monika Oboz, Ewa Talik, Grzegorz Ziółkowski, Antoni Winiarski

University of Silesia, Institute of Physics, Uniwersytecka 4, Katowice 40-007, Poland

e-mail: monika.oboz@us.edu.pl

Materials based on gadolinium are prospective for applications in magnetic refrigeration cycles. Recently, magnetic materials with relatively high Curie temperatures (T_C) are researched as potential candidates for magnetic refrigeration if they show large enough magnetocaloric effect (MCE). Several intermetallics based on rare earth and transition metals show interesting magnetocaloric properties [1-4]. However, their ordering temperatures are very often below room temperature. As a part of current research concerning the development of new magnets for magnetic refrigeration devices we characterized the monocrystalline and microcrystalline Gd_7Pd_3 compound. A single crystal of Gd_7Pd_3 of Th_7Fe_3-typewas grown by the Czochralski method from a levitating melt while microcrystalline Gd_7Pd_3 sample was obtained by rapid cooling of the melt (Figure). The samples were characterized by the following methods: X-ray diffraction, SQUID magnetometry, X-ray photoelectron spectroscopy and scanning electron microscopy (SEM/EDX). The SEM images showed grains size of the microcrystalline Gd_7Pd_3 sample. Magnetic and magnetocaloric properties were compared. The exchange interactions between Gd ions have a dominating mechanism being responsible for the formation of a magnetic ordering. It is realized by the RKKY interactions via the conduction electrons. From *ac* and *dc* magnetic susceptibility a transition to the ferromagnetic state has been found below T_C = 334 K for mono- and microcrystalline Gd_7Pd_3. It seems that microcrystalline Gd_7Pd_3 exhibits similar behaviour to *a* axis of monocrystalline Gd_7Pd_3 while Gd_7Pd_3 in powder form shows similar behaviour as *c* axis of monocrystalline Gd_7Pd_3. For both compounds the saturation magnetic moment per Gd ion is enhanced in relation to the theoretical value. Such behavior can be well ascribed to the contribution of itinerant ferromagnetism induced in the *d*-bands by the *f–d* exchange interactions.The value of the magnetocaloric effect is the highest for monocrystalline Gd_7Pd_3 and then decreases for microcrystalline and powder form of Gd_7Pd_3. The calculated entropy changes ΔS_m for the examined compounds amount to -6.7 J/Kkg, -5.3 J/Kkg and -2.8 J/Kkg for Gd_7Pd_3 single crystal and -5.4 J/Kkg, -4.2 J/Kkg and -2.07 J/Kkg for microcrystalline Gd_7Pd_3 at 7, 5 and 2 T respectively.

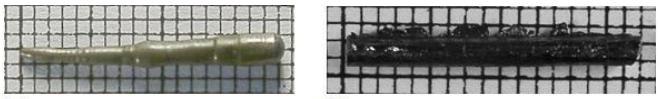

Fig. (a) Monocrystalline and (b) microcrystalline Gd_7Pd_3 compound.

Acknowledgements

This work was financed by the Polish National Science Centre (Narodowe Centrum Nauki) under grant no. 2011/03/B/ST5/01035.

References:

[1] V. K. Pecharsky, K. A. Gschneidner, Jr., Int. J. Refrig. **29**, (2006) 1239.

[2] K. A. Gschneidner, Jr., V. K. Pecharsk, A. O. Tsokol, Rep. Prog. Phys. **68**, (2005) 1479.

[3] D. T. Cam Thanh, E. Brück, O. Tegus, J. C. P. Klaasse, K. H. J. Buschow, J. Magn. Magn. Mater. **310**, (2007) e1012.

[4] E. Brück E, J. Phys. D Appl. Phys. **38**, (2005) R381.

Topical Session 2

Materials for spintronics

Session Coordinators

Maciej Sawicki (Poland) *mikes@ifpan.edu.pl*

Fumihiro Matsukura (Japan) *f-matsu@riec.tohoku.ac.jp*

Acknowledgements

This Topical Session is financially supported by the European Union 7th Framework Programme under the grant REGPOT-CT-2013-316014 (EAgLE).

Programme

Monday, 12 August

MoP-T02
Monday afternoon, 12 August, 17:00
Room 211, Old Library

Break
Monday evening, 12 August, 18:30

Friday, 16 August

FrO1

T02: Materials for spintronics
Friday morning, 16 August, 8:30
Mickiewicz Hall, Auditorium Maximum

8:30 Invited oral

From GaMnAs to CuMnAs: growth by Molecular Beam Epitaxy (MBE)

Richard P. Campion[1], P. Wadley[1,2], Vit Novak[2], C. Rinaldi[2,3], X. Marti[2,4,5], H. Reichlova[2,4], J. Zelezny[2], J. Gazquez[6], M. A. Roldan[7,8], M. Varela[7,8], D. Khalyavin[9], S. Langridge[9], D. Kriegner[10], F. Maca[11], J. Masek[11], R. Bertacco[3], V. Holy[4], A. W. Rushforth[1], K.W. Edmonds[1], B. L. Gallagher[1], C. T. Foxon[1], J. Wunderlich[2,12], T. Jungwirth[1,2]

1. *School of Physics and Astronomy, University of Nottingham, Nottingham NG72RD, United Kingdom* **2.** *Czech Academy of Sciences, Institute of Physics, Cukrovarnicka 10, Prague 16253, Czech Republic* **3.** *LNESS and Dipartimento di Fisica del Politecnico di Milano, via Anzani 42, Como 22100, Italy* **4.** *Charles University, Faculty of Mathematics and Physics, Ke Karlovu 3, Prague 12116, Czech Republic* **5.** *Department of Materials Science and Engineering, University of California, Berkeley, CA 94720, United States* **6.** *Institut de Cincia de Materials de Barcelona (ICMAB-CSIC), Bellaterra ES-08028, Spain* **7.** *Departamento de Fisica Aplicada III, Universidad Complutense de Madrid , Madrid 28040, Spain* **8.** *Oak Ridge National Laboratory, Solid State Division, Oak Ridge, TN, United States* **9.** *Rutherford Appleton Laboratory (RAL), Chilton, Didcot, Oxon OX11 0QX, United Kingdom* **10.** *Institut für Halbleiterphysik Universität Linz, Altenberger Str. 69, Linz A-4040, Austria* **11.** *Institute of Physics ASCR, v.v.i., Na Slovance 2, Prague CZ-18221, Czech Republic* **12.** *Hitachi Cambridge Laboratory, Cambridge CB3 0HE, United Kingdom*

e-mail: richard.campion@nottingham.ac.uk

The ferromagnetic semiconductor GaMnAs has proven to be a very successful prototype material that has enabled us to study the fundamentals of spintronics. In particular, a number of generally applicable concepts have been discovered in this material system, which can be readily applied to other ferromagnetic materials [1-3]. However, for successful device applications the Curie temperature must be well above room temperature and this does not seem likely to be the case in GaMnAs. Many groups are therefore looking for altenative options. Amongst the various options, antiferromagnetic materials in general seem to offer Neel temperatures in the appropriate temperature range. Antiferromagnets have long been key components in hard disk read heads, due to the exchange bias effect, while recent studies have demonstrated the potential of antiferromagnets as the active component in spintronics devices [4-8]. Our first studies involved the growth and characterisation of LiMnAs [7], which has an appropriate Neel temperature, but the inclusion of the alkali metal element represents a challenge both in terms of the growth and the stability of devices. However, LiMnAs is one of a family of antiferromagnetic I-II-V materials, which may be semiconductors or semi-metals, that could potentially be used for device applications.

Here we report the epitaxial growth of a new high temperature antiferromagnetic material, tetragonal CuMnAs, which exhibits excellent crystal quality, chemical order and compatibility with existing semiconductor technologies. We demonstrate growth on the III-V semiconductors GaAs and GaP, and show that the structure is also lattice matched to Si in-plane. The CuMnAs was grown by MBE in a Veeco Gen III system using elemental sources for the Cu,Mn and the As. Extensive structrual characterisation has been performed including Z-contrast TEM, X-ray and neutron scattering: this data will be presented. CuMnAs is shown to be a collinear antiferromagnet with a high transition temperature. Layers capped with Fe are used to demonstrate a large and stable room temperature exchange bias. This material may

offer new possibilities for spintronic applications combining antiferromagnetic and semiconducting materials.

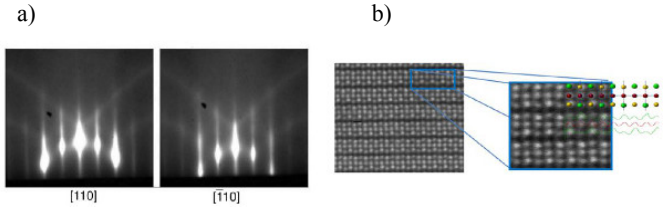

a) RHEED images of the surface of a CuMnAs layer during growth on a GaP substrate. b) Z-contrast TEM image of CuMnAs along the [1 0 0] direction. The As positions are clearly visible as the brightest atoms, and intensity analysis along the rows reveal a highly ordered compound in complete agreement with the overlaid model structure

[1] Chiba, D.; Y. Sato, T. Kita, F. Matsukura, H. Ohno. "Current-Driven Magnetization Reversal in a Ferromagnetic Semiconductor (Ga,Mn)As/GaAs/(Ga,Mn)As Tunnel Junction". Phys. Rev. Lett. 93 (21): 216602.

[2] Gould, C.; C. Ruster, T. Jungwirth, E. Girgis, G. M. Schott, R. Giraud, K. Brunner, G. Schmidt, L. W. Molenkamp. "Tunneling Anisotropic Magnetoresistance: A Spin-Valve-Like Tunnel Magnetoresistance Using a Single Magnetic Layer". Phys. Rev. Lett. 93 (11): 117203.

[3] Giddings, A. D.; M. N. Khalid, T. Jungwirth, J. Wunderlich, S. Yasin, R. P. Campion, K. W. Edmonds, J. Sinova, K. Ito, K.-Y. Wang, D. Williams, B. L. Gallagher, C. T. Foxon. "Large Tunneling Anisotropic Magnetoresistance in (Ga,Mn)As Nanoconstrictions". Phys. Rev. Lett. 94 (12): 127202.

[4] Park, B. G.; Wunderlich, J.; Marti, X.; Holy, V.; Kurosaki, Y.; Yamada, M.; Yamamoto, H.; Nishide, A.; Hayakawa, J.;Takahashi, H.; Shick, A. B.; Jungwirth, T. Nature Mat. 2011, 10, 347.

[5] Martı, X.; Park, B. G.; Wunderlich, J.; Reichlova, H.; Kurosaki, Y.; Yamada, M.; Yamamoto, H.; Nishide, A.; Hayakawa, J.;Takahashi, H.; Jungwirth, T. Phys. Rev. Lett. 2012, 108, 017201.

[6] Shick, A. B.; Khmelevskyi, S.; Mryasov, O. N.; Wunderlich, J.; Jungwirth, T. Phys. Rev. B 2010, 81, 212409.

[7] Jungwirth, T. et al. Phys. Rev. 2011, B 83, 035321.

[8] Cava, R. J. Physics 2011, 4, 7.

9:00 Oral

Growth and doping of (Ga,Mn)N epitaxial films

Gerd Kunert[1], Sylwia Dobkowska[2], Tian Li[3], Carsten Kruse[1], Alberta Bonanni[3], Jörg Grenzer[4], Johannes V. Borany[4], Wiktor Stefanowicz[2], Maciej Sawicki[2], Tomasz Dietl[2,5], Detlef Hommel[1]

1. *University of Bremen, Institute of Solid State Physics, P.O. Box 330440, Bremen 28334, Germany* **2.** *Polish Academy of Sciences, Institute of Physics, al. Lotników 32/46, Warszawa 02-668, Poland* **3.** *Institut für Halbleiter und Feskörperphysik, Johannes Kepler Universität (FKP-JKU), Altenbergerstr. 69, Linz 4040, Austria* **4.** *Institute of Ion Beam Physics and Materials Research, Helmholtz Zentrum Dresden Rossendorf (HZDR), Bautzner Landstrasse 400, Dresden 01328, Germany* **5.** *Japan Science and Technology Agency, Semiconductor Spintronics Project (ERATO), al. Lotników 32/46, Warszawa 02-668, Poland*

e-mail: kunert@ifp.uni-bremen.de

Owing to the lack of band carriers, and to the highly localized nature of electrons residing on Mn, (Ga,Mn)N has been classified as dilute magnetic insulator, where spin-spin interactions proceed via short ranged superexchange coupling [1,2]. In the case of compensated samples, in which Mn^{2+} prevails, this interaction is antiferromagnetic [1], like in Mn-based II-VI dilute magnetic semiconductors (DMSs). However, in high quality weakly compensated epilayers that contain merely Mn^{3+} ions, the superexchange acquires a ferromagnetic character [1,2,4], leading to Curie temperatures below 10 K [2,4], as predicted a time ago for Cr doped II-VI DMSs [5] and widely studied by first principle methods [6].

In this work we report on the growth of (Ga,Mn)N films by molecular beam epitaxy (MBE) which show the highest ever reported for any DMS (to our knowledge) field-induced magnetization M(H) [7]. It reaches 150 emu/cm^3 at 70 kOe, to be compared the value of 90 emu/cm^3 attained in (Ga,Mn)As [8]. Sapphire substrates and MOVPE GaN buffers have been employed. According to high resolution x-ray diffraction (HRXRD) investigations, the films show a linear dependence of the c-lattice parameter on the amount of Mn incorporated (figure 1). Reciprocal space maps reveal that the layers are fully strained. Furthermore, according to high resolution transmission electron microscopy (HRTEM) measurements there are no secondary crystalline phases in these samples. The magnitudes of the Mn concentrations x_{eff} provided by SQUID measurements have been cross-checked by secondary ions mass spectroscopy (SIMS). For a more detailed analysis of the crystalline structure of the layers, Rutherford backscattering (RBS) studies have been performed along the (0001)-direction. It has been found that the signal in the channelling mode drops to 3 % of its magnitude in the random mode, which is among the lowest values reported for GaN and, thus, confirms the high structural quality of the (Ga,Mn)N layers.

For achieving high Curie temperature the inclusion of carriers in GaMnN is essential. Therefore codoping experiments have been performed on GaMnN layers with Mg as well as Si as dopands. Additional Mg shifts the fermi-level to lower energies and surpresses the inclusion of Mn as seen in figure 2. Additional Si-doping, can in contrast increase the fermi-level, and therefore the amount of Mn incorporated.

References

1 A. Bonanni *et al.*, Phys. Rev. B, **84**, 3 (2011).

2 M. Sawicki *et al.*, Phys. Rev. B, **85**, 20 (2012).

3 E. Sarigiannidou *et al.*, Phys. Rev. B, **74**, 041306 (2006).

4 J. Blinowski *et al.*, Phys. Rev. B **53**, 9524 (1996).

5 K. Sato *et al.*, Rev. Mod. Phys. **82**, 1633 (2010), and references therein.

6 G. Kunert *et al.*, Appl. Phys. Lett. **101**, 022413 (2012).

7 D. Chiba *et al.*, Appl. Phys. Lett. **90**, 122503 (2007).

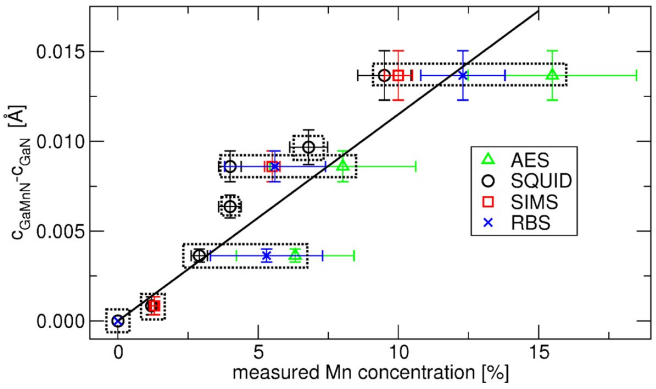

Figure 1: Change of c-lattice parameter with Mn content, determined by different methods. Measurements belonging to the same sample are marked by a dashed rectangle.

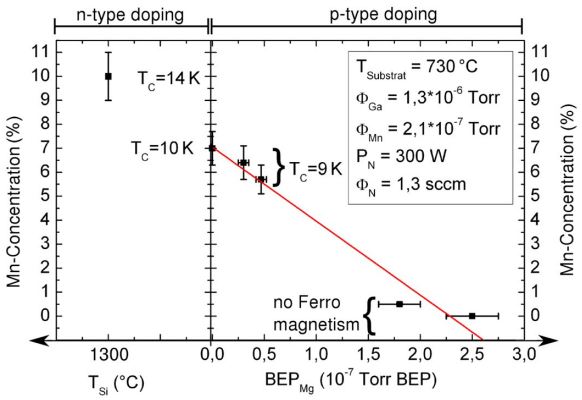

Figure 2: A shift in the fermi-level by Si- or Mg-doping leads to a significant change in the Mn concentrations incorporated under the same growth conditions.

9:15 Oral

Critical exponents of dilute ferromagnetic semiconductors (Ga,Mn)N and (Ga,Mn)As

Sylwia I. Stefanowicz[1], Gerd Kunert[2], Wiktor Stefanowicz[3], Janusz Sadowski[3,4,5,6], Detlef Hommel[7], Tomasz Dietl[3,8], Maciej Sawicki[3]

1. *Institute of Physics, Polish Academy of Sciences, Warsaw 02-668, Poland* **2.** *University of Bremen, Institute of Solid State Physics, Semiconductor Epitaxy, P.O. Box 330440, Bremen 28334, Germany* **3.** *Polish Academy of Sciences, Institute of Physics, al. Lotników 32/46, Warszawa 02-668, Poland* **4.** *University of Copenhagen, Universitetsparken 5, Copenhagen DK-2100, Denmark* **5.** *Chalmers University of Technology, Göteborg S-412 96, Sweden* **6.** *Lund University, MAX-lab, Lund SE-221 00, Sweden* **7.** *University of Bremen, Institute of Solid State Physics, P.O. Box 330440, Bremen 28334, Germany* **8.** *Japan Science and Technology Agency, Semiconductor Spintronics Project (ERATO), al. Lotników 32/46, Warszawa 02-668, Poland*

e-mail: sstefanowicz@ifpan.edu.pl

There are two compounds which arguably demonstrate the highest potential for studying novel spintronics-related phenomena: (Ga,Mn)As, the 'canonical' dilute ferromagnetic semiconductor (DFS) and (Ga,Mn)N, the emerging member of this family [1,2]. Whereas (Ga,Mn)As has become the model material to test semiconductor spintronics concepts, the importance of (Ga,Mn)N stems from a different origin of magnetism and the already dominating role of GaN in photonics and high power electronics. Due to the strong p-d hybridization the $Mn^{2+/3+}$ acceptor level occupies the mid band gap position in GaN, and, interchangeable, either a high p-type doping or high Mn content x is possible. Nevertheless, in uncompensated films, where Mn^{3+} ions prevail, the superexchange interaction becomes ferromagnetic for all Mn-Mn distances resulting in a ferromagnetic order [1] characterized by the Curie temperature T_C = 13 K for x = 0.10 [3].

In this context it becomes of a paramount importance to provide the most comprehensive characterization of the magnetic ground state of this insulating DFS. To this end we investigate the static critical behavior of MBE grown (Ga,Mn)N layers [3] with $0.04 < x < 0.10$ and compensation free, high-T_C (Ga,Mn)As layer, utilizing direct DC field dependent magnetization and temperature dependence of AC susceptibility. From the analysis we establish for each sample its T_C and critical exponents a, b, and g. In both systems we find g @ 2.6 to exceed about twice its typical value for most common (Stoner) ferromagnets, a value indicative of the profound role of disorder [positional of Mn in (Ga,Mn)N and electrical in (Ga,Mn)As] in the setting of the ferromagnetic state in these two system. We further find that, the Widom relation, d = 1 + g/d, holds precisely only in (Ga,Mn)As. Such calculated d in (Ga,Mn)N considerably overshoots its experimental value. This interesting discrepancy needs further clarification.

The work has been in part supported by FunDMS Advanced Grant of ERC within the Ideas 7th FP of EC and by (Polish) National Science Centre through project MAESTRO "Quantum phase transitions in magnetic layers driven by an electric field" (Decision 2011/02/A/ST3/00125).

[1] M. Sawicki, T. Devillers, S. Gałęski, C. Simserides, S. Dobkowska, B. Faina, A. Grois, A. Navarro-Quezada, K. N. Trohidou, J. A. Majewski, T. Dietl, and A. Bonanni, Phys. Rev. B 85, 205204 (2012).

[2] G. Kunert, S. Dobkowska, Tian Li, H. Reuther, C. Kruse, S. Figge, R. Jakieła, A. Bonanni, J. Grenzer, W. Stefanowicz, J. von Borany, M. Sawicki, T. Dietl, and D. Hommel, Appl. Phys. Lett. 101, 022413 (2012).

[3] S. Stefanowicz, G. Kunert, Tian Li, H. Reuther, C. Kruse, S. Figge, W. Stefanowicz, A. Bonanni, M. Sawicki, T. Dietl, and D. Hommel, in preparation, arXiv 2013.

9:30 Oral

Electric field-effect on magnetic properties of thin (Ga,Mn)Sb layers

Hsiao-Wen Chang[1], Shingo Akita[1], Fumihiro Matsukura[2,3], Hideo Ohno[1,2,3]

1. *Laboratory for Nanoelectronics and Spintronics, Research Institute of Electrical Communication, 2-1-1- Katahira, Aoba-ku, Sendai 980-8577, Japan* **2.** *WPI-AIMR Tohoku University, 2-1-1 Katahira, Aoba-Ku, Sendai 980-8577, Japan* **3.** *Center for Spintronics Integrated Systems, 2-1-1 Katahira, Aoba-ku, Sendai 980-8577, Japan*

e-mail: f-matsu@wpi-aimr.tohoku.ac.jp

III-V based magnetic semiconductors show hole-induced ferromagnetism [1], and their magnetic properties can be modulated by the application of electric fields E through the change of hole concentration p [2]. It was reported that the relationship between the Curie temperature T_C and p for thin (Ga,Mn)As layers is expressed as $T_C \propto p^{0.2}$, where p was controlled by using a field-effect structure by the application of E [3]. The result can be reproduced by an adapted p-d Zener model with non-uniform hole distribution due to the depletion region at the interface between gate insulator and (Ga,Mn)As [3,4]. Since the exponent is expected to depend on the material dependent pinning position of the Fermi level at the interface [5], in this work, we adopt (Ga,Mn)Sb as a channel layer in a field-effect structure.

5 nm-thick (Ga,Mn)Sb layers are grown by low temperature molecular beam epitaxy on 5 nm GaSb / 300 nm $A_{0.8}Ga_{0.2}Sb$ / 10 nm AlSb onto semi-insulating GaAs (001) substrate [6,7]. The field-effect structure has a Hall-bar shape for transport measurements. The measurements are performed under perpendicular magnetic field $\mu_0 H$ ($|\mu_0 H| < 0.5$ T, μ_0: permeability in vacuum) at various temperature T and E. We determine p from the E dependence of the channel conductivity and T_C from the H dependence of Hall resistance by making the Arrott plots. We determine to be the exponent $\gamma \sim 1$ in $T_C \propto p^{\gamma}$, and show that it can be reproduced by the adapted p-d Zener model with hole accumulation at the interface of (Ga,Mn)Sb and gate insulator, which is consistent with the Fermi energy pinning position of p-GaSb at the interface [8]. We show also that a perpendicular magnetic anisotropy of (Ga,Mn)Sb is E dependent.

We would like thank M. Sawicki and T. Dietl for discussion. This work was supported in part by the FIRST program of JSPS.

[1] T. Dietl, H. Ohno, F. Matsukura, J. Cibert, and D. Ferrand, Science **287,** 1019 (2000).
[2] H. Ohno, D. Chiba, F. Matsukura, T. Omiya, E. Abe, T. Dietl, Y. Ohno, and K. Ohtani, Nature **408,** 944 (2000).
[3] Y. Nishitani, D. Chiba, M. Endo, M. Sawichi, F. Matsukura, T. Dietl, and H. Ohno, Phys. Rev. B **81,** 045208 (2010).
[4] M. Sawicki, D. Chiba, A. Korbecka, Y. Nishitani, J. A. Majewski, F. Matsukura, T. Dietl, and H. Ohno, Nature Phys. **6,** 22 (2010).
[5] H. Ohno, J. Appl. Phys. **113,** 136509 (2013).
[6] E. Abe, F. Matsukura, H. Yasuda, Y. Ohno, and H. Ohno, Physica E **7,** 981 (2000).
[7] Y. Nishitani, M. Endo, F. Matsukura, and H. Ohno, Physica E **42,** 2681 (2010).
[8] H. Hasegawa, H. Ohno, and T. Sawada, Jpn. J. Appl. Phys. **25,** L265 (1986).

9:45 Oral

Quaternary (Ga,Mn)BiAs ferromagnetic semiconductor - MBE growth, structural and magnetic properties

Janusz Sadowski[1,2], Jaroslaw Domagala[2], Aloyzas Šiušys[2], Oksana Yastrubchak[3], Luikasz Gluba[3], Miroslaw Kulik[3], Michal Rawski[3], Maciej Sawicki[2]

1. *Lund University, MAX-lab, Lund SE-221 00, Sweden* **2.** *Polish Academy of Sciences, Institute of Physics, al. Lotników 32/46, Warszawa 02-668, Poland* **3.** *Uniwersytet Marii Curie-Skłodowskiej, Lubin 20-033, Poland*

e-mail: janusz.sadowski@maxlab.lu.se

(Ga,Mn)As ternary alloy is a canonical ferromagnetic semiconductor (FMS) studied for almost two decades by a number of research groups. After over15 years of extensive research activity (Ga,Mn)As became a prototype FMS used in the context of basic research of fundamental properties of FMS materials as well for the construction of novel spintronic devices using the new functionalities associated with the spin orientation of the charge carriers [1]. In spite of that, some basic issues concerning the mechanisms responsible for the FM phase transition in (Ga,Mn)As are still being debated [2,3]. Hence studying quaternary alloy whose band structure is modified by the introduction of an additional V-group element is highly interesting. So far, to our knowledge, only quaternary alloys of this kind reported in the literatures are (Ga,Mn)AsP [4] and (Ga,Mn)AsSb [5]. Thus we have investigated (Ga,Mn)As alloyed with another V element, namely Bi. It is well known that Bi partially replacing As in GaAs considerably shifts the position of the valence band maximum in the resulting ternary alloy[6]. On the other hand for the FM properties of (Ga,Mn)As (and other Mn-doped FMS materials) the position of Mn acceptor level is detrimental. This feature can be effectively tuned in (Ga,Mn)AsBi by choosing the appropriate Bi content in the quaternary alloy. (Ga,Mn)AsBi layers with the Bi content of up to 1% have been grown on GaAs(001) substrates by molecular beam epitaxy (MBE) at low substrate temperature (200 - 230 ^{o}C). In each case the MBE growth of a quaternary alloy was followed by the growth of the ternary (Ga,Mn)As layer with the same Mn content, at nominally identical growth conditions. Thus the influence of Bi on basic characteristics of FMS layers such as Curie temperature, lattice parameter can be investigated. The essential parameters of quaternary (Ga,Mn)BiAs layers, as mentioned above, are investigated by the standard techniques such as SQUID magnetometry and X-ray diffraction. The other features like electronic properties and defect structure are studied by photoreflectivity, transmission electron microscopy and Rutheford backscattering techniques. Our first investigations of magnetic properties of (Ga,Mn)BiAs have shown that Bi considerably changes the magnetic anisotropy of a quternary alloy, with respect to that of ternary (Ga,Mn)As. The origin of this effect will be discussed.

[1] T. Dietl, Nature Materials **9**, 965 (2010).
[2] M. Dobrowolska et. al. Nature Materials **11**, 444 (2012).
[3] P. Nemec et. al. Nature Communications **4**, 1422 (2013).
[4] M. Cubukcu et. al., Phys. Rev. B **81**, 041202R (2010).
[5] B. Howells et al. Appl. Phys. Lett. **102**, 052407 (2013).
[6] S. Francoeur et. al. Phys. Rev. B **77**, 085209 (2008)

10:00 Oral

Neutron scattering studies of short-period MnTe/ZnTe superlattices: magnetic order, magnon propagation and confinement

Wojciech Szuszkiewicz[1], Bernard Hennion[2], Sylvain Petit[2], Elzbieta Dynowska[1], Elżbieta Janik[1], Grzegorz Karczewski[1], Tomasz Wojtowicz[1]

1. *Polish Academy of Sciences, Institute of Physics, al. Lotników 32/46, Warszawa 02-668, Poland* **2.** *Laboratoire Leon Brillouin, CEA-CNRS, CE Saclay (LLB), Gif-sur-Yvette 91191, France*

e-mail: szusz@ifpan.edu.pl

MnTe is well-known magnetic semiconductor which can crystallize it two phases. The stable MnTe crystal phase is the hexagonal one of the NiAs type. The metastable MnTe phase with the zinc blende (ZB) structure can be obtained with the use of non-equilibrium growth techniques only, such as MBE. This phase exhibits an antiferromagnetic (AF) order of type-III at low temperatures (Néel temperature of about 65 K). This kind of magnetic order persists also in MnTe layers in MnTe/ZnTe superlattices (SLs). Because of the distortion of the *fcc* lattice an energy-minimizing magnetic configuration with the unit cell doubling direction along the SL growth axis is realized in such structures. Due to this property the SLs above mentioned are characterized by the single orientation of magnetic domains. The presence of an interlayer exchange coupling has been reported for selected MnTe/ZnTe short-period SLs previously [1,2] but details of this coupling and an anomalous temperature behavior of features observed by the neutron diffraction were not fully understood. The goal of the current research was to get more information on the magnetic properties of various SLs mentioned above.

Several MBE-grown, MnTe/ZnTe short period SLs with various numbers of monolayers (MLs) in magnetic and non-magnetic slabs were grown by MBE at the Institute of Physics PAS in Warsaw. Prior to the growth of the SL the ZnTe buffer layer was deposited onto (001)-oriented 2°off GaAs substrate. The typical SL single bilayer was composed of 15 or 20 MnTe MLs and of 4 to 10 ZnTe MLs. In every case the SL contained 200 periods, so its thickness was close to 1 micrometer. The separate set of SLs corresponded to structures with similar period values as those mentioned above but with much smaller number of MnTe MLs (7, 8 or 9) and 18 ZnTe MLs. The crystal quality of grown samples and their structure parameters were checked by the high-resolution XRD measurements with the use of Cu K_{a1} radiation. The typical diffraction pattern obtained at RT for one from our samples is shown in Fig. 1. The real and the nominal values of parameters describing typical SL bilayer were the same (possible difference in the case of the highest number of MnTe MLs does not exceed 0.5 ML).

Next, the samples were analyzed by elastic and inelastic neutron scattering performed at Laboratoire Léon Brillouin in Saclay. The first type of measurements tooks advantage of 4T2 spectrometer installed on the cold neutron source. The results of these measurements demonstrated a magnetic coherence in selected SLs for a distance as high as 900 Å at low temperatures. The temperature behavior of spectra observed in our experiments was found to be quite different from that previously reported in the literature. Due to careful analysis of the form of neutron diffraction structures at a few Brillouin zones we were able to propose the model of local magnetic order in SL. Possible physical mechanisms responsible for observed magnetic correlation in AF-ordered MnTe layers of these SLs given in the literature are mentioned and discussed.

In our earlier studies we have determined the collective magnetic excitations (magnons) dispersion in quasi-bulk ZB-MnTe slab at low temperature (in AF-III phase) by inelastic neutron scattering [3]. In current research we have observed not only a long-range coherency between AF layers for ZnTe spacer thickness up to ~25 Å, but also the propagation of collective magnetic excitations (magnons) along the SL-stacking direction in short-period SLs. For large enough ZnTe spacers, on the other hand, the AF MnTe layers are no longer correlated and size quantization effects (confinement) for magnons take place. The effective magnetic volume for investigated SLs varied between 0.15 mm^3 and 0.30 mm^3 so the counting time was equal to about 20 minutes per step. The experimental evidence of both effects mentioned above was found in our inelastic neutron scattering measurements, performed with the use of thermal neutron beams. A similarity of theoretically predicted and experimentally observed magnon spectra was also shown. To the best of our knowledge presented results constitute the first clear evidence of magnon propagation and magnon confinement in SLs containing magnetic semiconductor that was demonstrated with the use of inelastic neutron scattering technique.

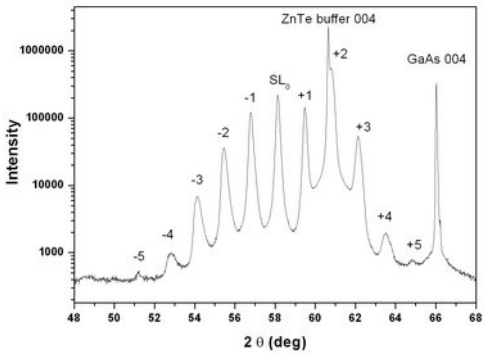

Fig. 1. The X-ray diffraction pattern collected for the $(MnTe)_{18}/(ZnTe)_7$ SL.

This work was partially supported by the research grant N N202 128639 from Ministry of Science and Higher Education (Poland) and by the European Commission under the 7th Framework Programme through the 'Research Infrastructures' action of the 'Capacities' Programme, NMI3-II Grant number 283883.

[1] J. Lin, J.J. Rhyne, J.K. Furdyna, T.M. Giebultowicz, *J. Appl. Phys.***83**, 6554 (1998).
[2] L.E. Stumpe, J.J. Rhyne, H. Kaiser, S. Lee, et. al., *J. Appl. Phys.***87**, 6460 (2000).
[3] B. Hennion, W. Szuszkiewicz, E. Dynowska, E. Janik, T. Wojtowicz, *Phys. Rev. B*, **66**, 224426 (2003).

* Corresponding author. E-mail address: szusz@ifpan.edu.pl

Coffee

Friday morning, 16 August, 10:30

FrO2

T02: Materials for spintronics
Friday morning, 16 August, 11:00
Mickiewicz Hall, Auditorium Maximum

11:00 Invited oral

Growing semiconductor nitrides into spintronic and magnetooptic materials

Alberta Bonanni

Institut für Halbleiter und Feskörperphysik, Johannes Kepler Universität (FKP-JKU), Altenbergerstr. 69, Linz 4040, Austria

e-mail: alberta.bonanni@jku.at

Due to their unique photonic properties, gallium nitride (GaN) and related compounds have already raised to the position of technologically most significant semiconductors next to Silicon. The addition of magnetic functionalities to these materials systems is expected to open striking views in both fundamental and application-oriented research.

I will review our recent work on the metalorganic vapor phase epitaxy (MOVPE) of magnetic nitrides and summarize how - by exploiting in particular synchrotron-radiation and microscopy techniques - we have correlated the growth parameters and procedures to the structural, magnetic, optical properties of the epitaxial layers. I will give an overview on how we have unraveled and we can now control a number of non-anticipated features of these systems, like the nature of super-exchange ferromagnetic interactions and the self-aggregation of functional magnetic cations and magnetoopticl impurity complexes driven by fabrication parameters and co-doping [1-13].

[1] A. Bonanni, et al., Phys. Rev. B 75, 125210 (2007).
[2] W. Pacuski, et al., Phys. Rev. Lett. 100, 037204 (2008).
[3] A. Bonanni, et al., Phys. Rev. Lett. 101, 135502 (2008).
[4] M. Rovezzi, et al., Phys. Rev. B 79, 195209 (2009).
[5] A. Navarro-Quezada, et al., Phys. Rev. B 81, 205206 (2010).
[6] I. A. Kowalik, et al., Phys. Rev. B 85, 184411 (2012).
[7] A. Navarro-Quezada, et al., Phys. Rev. B 84, 155321 (2011).
[8] W. Stefanowicz, et al., Phys. Rev. B 84, 035206 (2011).
[10] J. Suffczyński, et al., Phys Rev. B. 83, 094421 (2011).
[11] A. Bonanni, Semicond. Sci. and Technol. 22, 41 (2007).
[12] A. Bonanni and T. Dietl, Chem. Soc. Rev. 39, 528 (2010).
[13] T. Devillers et al., Scientific Reports 2, 722 (2012).

11:30 Oral

Growth and electronic properties of antiferromagnetic semiconductor LiMnAs

Stepan Svoboda[1,2], Vit Novak[1], Miroslav Cukr[1], Tomas Jungwirth[1], Lukas Horak[3], Xavier Marti[1], Vaclav Holy[3], Nada Tesarova[3], Petr Nemec[3], Ineke Wijnheijmer[4], Paul M. Koenraad[4]

1. *Czech Academy of Sciences, Institute of Physics, Cukrovarnicka 10, Prague 16253, Czech Republic* **2.** *Czech Technical University in Prague, The Faculty of Nuclear Sciences and Physical Engineering, Trojanova 13, Prague 2, Prague 12000, Czech Republic* **3.** *Charles University, Faculty of Mathematics and Physics, Ke Karlovu 3, Prague 12116, Czech Republic* **4.** *Eindhoven University of Technology, P.O. Box 513, Eindhoven 5600MB, Netherlands*

e-mail: vit.novak@fzu.cz

The first successful MBE growth of the antiferromagnetic material LiMnAs has been reported recently [1], opening one possible route to spintronics based on antiferromagnets. Although the ab-initio calculations predict the material to be a semiconductor, its detailed electronic structure still has not been fully experimentally explored. We present experimental study of the electronic and optical properties of LiMnAs by means of in situ optical reflectometry, cross sectional STM spectrocsopy, Auger spectroscopy and capacitance spectroscopy. Furthermore, we observed and analyzed the growth oscillations in the RHEED image at the early stages of the film growth. Combined with the SEM and XRD structural analysis this allowed us to identify coexistence of two closed phases of the material.

[1] T. Jungwirth, Phys. Rev. B 83, 035321 (2011)

11:45 Oral

Epitaxial magnetostrictive Galfenol thin films for spintronics

Duncan Parkes[1], L. R. Shelford[2], P. Wadley[1,3], V. Holy[3], M. Wang[1], A.T. Hindmarch[1], G. Van der Laan[2], Richard P. Campion[1], K.W. Edmonds[1], S.A. Cavill[2], Andrew W. Rushforth[1]

1. *School of Physics and Astronomy, University of Nottingham, Nottingham NG72RD, United Kingdom* **2.** *Diamond Light Source, Science Dept., Harwell Science and Innovation Campus, Chilton Didcot OX110DE, United Kingdom* **3.** *Charles University, Faculty of Mathematics and Physics, Ke Karlovu 3, Prague 12116, Czech Republic*

e-mail: ppxdep@nottingham.ac.uk

Multiferroic composite materials, consisting of coupled ferromagnetic and piezoelectric phases, are of great importance in the drive towards creating faster, smaller and more energy efficient devices for information and communications technologies. Such devices require thin ferromagnetic films with large magnetostriction and narrow microwave resonance linewidths. Both properties are often degraded, compared to bulk materials, due to structural imperfections and interface effects in the thin films. Here we present the development of cubic single crystal thin films of Galfenol ($Fe_{81}Ga_{19}$) grown by molecular beam epitaxy onto GaAs(001) substrates. We show that the thin films possess a magnetostriction as large as the best reported values for bulk single crystals. When incorporated into hybrid piezoelectric/ferromagnetic devices, this allows the magnetic anisotropy and microwave resonant frequency to be tuned by voltage-induced strain. Combined with the cubic magnetocrystalline anisotropy, this has enabled the demonstration of useful functionalities such as voltage induced non-volatile switching of the magnetisation direction [1] and the modification of ordered magnetic domain patterns [2].

The excellent magnetic properties of the single crystal thin films make them promising candidates for developing tunable devices for magnetic information storage, processing and microwave communications.

[1] D.E. Parkes, et al., Non-volatile voltage control of magnetization and magnetic domain walls in magnetostrictive epitaxial thin films, Appl. Phys. Lett. 101, 072402 (2012).

[2] S.A. Cavill, et al., Electrical control of magnetic reversal processes in magnetostrictive structures, Appl. Phys. Lett. 102, 032405 (2013).

12:00 Oral

Structure-Dependent Ferromagnetism in Mn-Doped III-V Nanowires

Marta Galicka, Ryszard Buczko, Perla Kacman

Institute of Physics, Polish Academy of Sciences, Warsaw 02-668, Poland

e-mail: galicka@ifpan.edu.pl

Several attempts to grow Mn-doped GaAs nanowires (NWs), motivated by the hope to obtain one-dimensional spintronic structures, have been reported in the literature [1]-[3]. The diverse conditions, in particular different optimal temperatures, needed for the growth of GaAs NWs and for doping them with Mn ions, make this task very challenging. We report our theoretical studies of the impact of crystallographic structure of the GaAs and InAs NWs on doping them with Mn ions and their magnetic properties.

First, to find the distribution of Mn impurities in a GaAs (InAs) NW, we compare the total energies of NWs with one Mn ion substituting different nonequivalent cation sites in the wire, [4]. We incorporate the Mn ion into two types of GaAs (InAs) wires: wurtzite (WZ) NWs grown along the <0001> direction and zinc blende (ZB) NWs along the <111> axis. Segregation energy for an impurity in a given site of the wire is the energy difference between the NW with the impurity in this site and NW, in which the dopant occupies the site exactly in the center. The most important result of the study of segregation energy is that while in WZ NWs a nearly homogeneous distribution of Mn ions can be expected, in ZB NWs the Mn ions are trapped at the lateral surfaces of the wires.

The comparison of the energies of the NWs with two Mn ions with parallel (ferromagnetic) and antiparallel (antiferromagnetic) spin alignment has shown that the ferromagnetism can be expected in III-V NWs only of WZ structure. In III-V NWs with ZB structure the ferromagnetic coupling is considerably suppressed. Moreover, in contrast to the (Ga,Mn)As layers but similarly to the situation observed in (Ga,Mn)As nanocrystals [5,6], this Mn-Mn interaction is a short-range one.When two Mn atoms in the wire are separated by more than one bridging As atom, the energy difference between FM and AFM phases decreases rapidly.

The research leading to these results has received funding from the European Community's Seventh Framework Programme [FP7/2007-2013] under grant agreement n° 215368 and from the project of Polish Ministry of Science and Higher Education. Calculations were carried out at the Academic Computer Center in Gdańsk.

[1] J. Sadowski et al., *Nano Lett***7**, 2724 (2007).

[2] A. Rudolph et al., *Nano Lett.***9**, 3860 (2009).

[3] M. Hilse et al., *Appl. Phys.Lett*. **95**, 133126 (2009).

[4] M. Galicka et al., *Nano Lett*. **11**, 3319 (2011).

[5] S. Sapra et al., *Nano Lett.* **2**, 605 (2002).

[6] H. Xiangyang et al., *Phys.Rev. Lett*. **94**, 236801 (2005).

12:15 Oral

Optical properties of GaAs:Mn nanowires

Katarzyna Gas[1], Janusz Sadowski[1,2], Jean-Francois Morhange[3], Aloyzas Siusys[1], Wojciech Zaleszczyk[1], Tomasz Wojciechowski[1], Takeshi Kasama[4], Abdulmenaf Altintaş[5], Hongqi Xu[5,6], Wojciech Szuszkiewicz[1]

1. *Polish Academy of Sciences, Institute of Physics, Lotnikow 32/46, Warsaw 02-668, Poland* **2.** *Lund University, MAX-lab, Lund SE-221 00, Sweden* **3.** *Institut des nanosciences de Paris (INSP), 140 rue de Lourmel, Paris 75015, France* **4.** *Center for Electron Nanoscopy, TUD, Kongens Lyngby DK-2800, Denmark* **5.** *Division of Solid State Physics and the Nanometer Structure Consortium, Lund University, Box 118, Lund SE-221 00, Sweden* **6.** *Key Laboratory for the Physics and Chemistry of Nanodevices and Department of Electronics, Peking University, Beijing 100871, China*

e-mail: kgas@ifpan.edu.pl

GaAs nanowires (NWs) are attractive for potential applications in nanodevices, since they are built from a material which is widely used in optoelectronics. For functional devices the control over the polarity and concentration of charge carriers, i.e., doping of the given semiconducting materials is essential. Particularly interesting is doping of GaAs NWs with Mn. In GaAs the Mn^{2+} ions occupy Ga sites. They provide magnetic moments, due to the spin polarisation of the half filled 3d shell, and act as effective acceptors. Such behaviour opens the possibility of using Mn-doped GaAs NWs for studying interesting phenomena associated with interactions between charge carriers or photons with localized, single Mn spins.

In this work we focus on optical properties of GaAs:Mn NWs measured by photoluminescence (PL), cathodoluminescence (CL) and micro Raman scattering (μ-RS). The NWs were grown in self-catalytic growth mode on oxidized Si(100) surface by MBE and characterized by SEM, TEM, and electron transport measurements. In order to analyze the influence of Mn on the physical properties of NWs the undoped GaAs NWs obtained in otherwise exactly the same manner as those containing Mn were also investigated. The NWs are quite uniform in terms of sizes (diameters and lengths being close to 150 nm and 5 μm, respectively) – see Figure 1. A slight decrease of the NW diameter with an increasing distance from the NW top can be noticed.

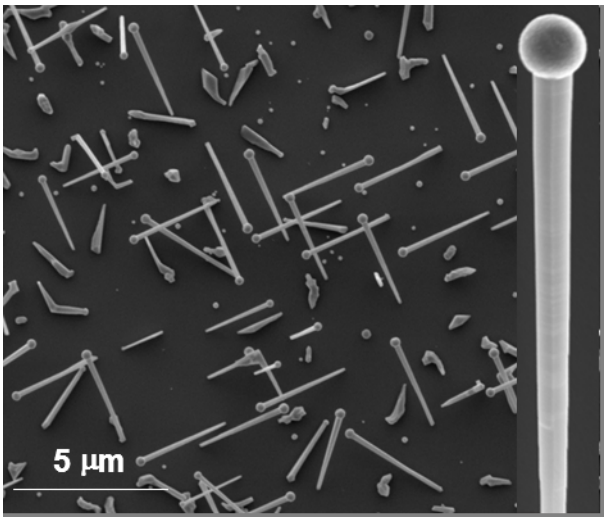

Figure 1. Scanning electron microscopy images of GaAs:Mn nanowires grown on Si(100).

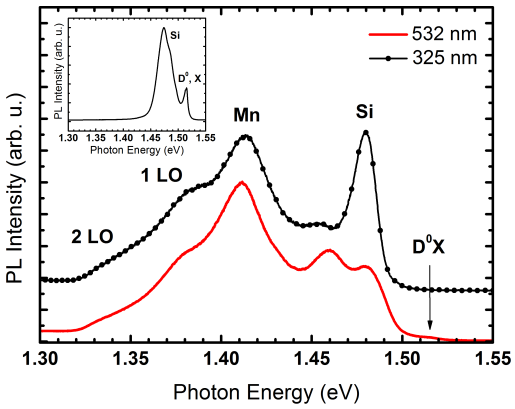

Figure 2. Low temperature PL spectra (normalized to the highest intensity) for GaAs:Mn NWs at different excitations (532 nm and 325 nm laser lines). The inset shows the low temperature PL spectrum of GaAs NWs at excitation of 532 nm laser line.

The comparision of PL spectra measured for GaAs and GaAs:Mn NWs is presented in Figure 2. The transitions related to the Si impurities, introduced into NWs from the substrate during the growth, are present both in undoped and Mn-doped NWs. In the latter case a transition at 1.41 eV associated with Mn acceptor states was also detected. This is a direct proof that the Mn^{2+} acceptors are located at Ga sites of the GaAs host lattice of the NWs. CL measurements performed on the single NW proved definitely that the PL signal came from the NWs only, not from the sample surface between them. An anomalous temperature dependence of the exciton emission was also found for GaAs:Mn NWs and explained by the thermal activation of Mn acceptor states. The μ-RS spectra, taken for the single NW revealed that the Mn concentration in GaAs:Mn NWs should not exceed 0.05% ($1 \cdot 10^{19}$ cm^{-3}). This value is much lower than the Mn/Ga flux ratio (about 3%) applied during the MBE growth. For both GaAs and GaAs:Mn the structures resulting from surface optical phonon modes were also found. The results of resistivity measurements as a function of temperature showed that contrary to undoped GaAs NWs the Mn doped ones are conductive. The p-type of this conductivity confirms the acceptor character of Mn impurities embedded into NW. The direct evidence that a substantial accumulation of Mn takes place inside the catalyzing Ga droplets at the top of the nanowires only was also found by TEM investigation.

This work was partially supported by the EU within European Regional Development Fund through grant Innovative Economy (POIG.01.01.02-00-008/08) and by the grant N N202 128639 from the Ministry of Science and Higher Education (Poland).

[1] K. Gas, J. Sadowski, J.F. Morhange, A. Siusys, W. Zaleszczyk, T. Wojciechowski, T. Kasama, A. Altintaş, H. Q. Xu, and W. Szuszkiewicz, sent to Nanoscale

12:30 Oral

MBE growth, structural, magnetic, and electric properties of (In,Ga)As-(Ga,Mn)As core-shell nanowires

Aloyzas Šiušys[1], Maciej Sawicki[1], Tomasz Wojciechowski[1], Serhii Trushkin[1], Maciej Zgirski[1], Anna Reszka[1], Sylwia I. Stefanowicz[1], Bogdan J. Kowalski[1], Andras Kovacs[3], Piotr Dłużewski[1], Slawomir Kret[1], Jaroslaw Domagala[1], Krzysztof Dybko[1,2], Janusz Sadowski

1. *Polish Academy of Sciences, Institute of Physics, al. Lotników 32/46, Warszawa 02-668, Poland* **2.** *Lund University, MAX-Lab, Lund 221 00, Sweden* **3.** *Forschungszentrum Jülich, IFF, Streumethoden, Jülich 52425, Germany*

e-mail: siusys@ifpan.edu.pl

Ferromagnetic nanowires (NWs) have been proposed as a new type of nanomagnetic memory structures [1]. In this context, the investigations of NWs combining ferromagnetic materials with commercially used semiconductors like Si or GaAs are desirable. GaAs NWs combined with (Ga,Mn)As ferromagnetic semiconductor or MnAs ferromagnetic metal were recently grown by molecular beam epitaxy [2-5]. In our studies the core NWs have been grown by two methods: (i) by autocatalytic growth mode on Si(111), (ii) by Au-catalyzed growth on GaAs(111)B. The (In,Ga)As nanowire cores were grown at high temperatures (550-630 °C) whereas the (Ga,Mn)As shells were grown at low temperatures (below 250 °C). Depending on composition of the (In,Ga)As core the (Ga,Mn)As shell can be either in the compressive strain (for low In content) or in the tensile strain (for high In content) state. This influences the magnetic anisotropy of (Ga,Mn)As shell. For NWs also shape magnetic anisotropy is important, hence these two factors are determining the magnetic properties of the shells. Structural properties of the core-shell (In,Ga)As-(Ga,Mn)As NWs were investigated by scanning and transmission electron microscopy as well as x-ray diffraction techniques revealing zinc blende monocrystalline (In,Ga)As cores with nanowire axis along [111] crystal direction and side facets of (110) orientation. The NWs grown on Si possess typical diameters of about 100 nm, lengths up to 15 µm. The Au-catalyzed NWS grown on GaAs(111)B are much shorter and thinner (70 nm and 3 µm, respectively). Magnetic properties of NWs ensemble were studied by SQUID magnetometry method revealing the ferromagnetic transition around $T_C \approx$ 20 - 30 K and only moderate magnetic anisotropy for magnetic field applied along the nanowire axis or normal to it. In some (Ga,Mn)As/(In,Ga)As NWs the ferromagnetic features were observed up to room temperature due to the formation of MnAs nanoclusters. Comparison of electrical measurements of individual nanowire terminated either by platinium contacts prepared by FIB-GIS method or by titanium-gold contacts prepared by lithographic methods will be presented.

References

[1] M. Hayashi et al., Science 320, 209 (2008).

[2] J. Sadowski et al., Nano Lett. 7, 2724 (2007).

[3] A. Rudolph et al., Nano Lett. 9, 3860 (2009).

[4] J. Sadowski et al., Phys. Stat. Sol. B 248, 1576 (2011).

[5] X. Yu et al., Nano Lett. doi**:** 10.1021/nl304740k (2013).

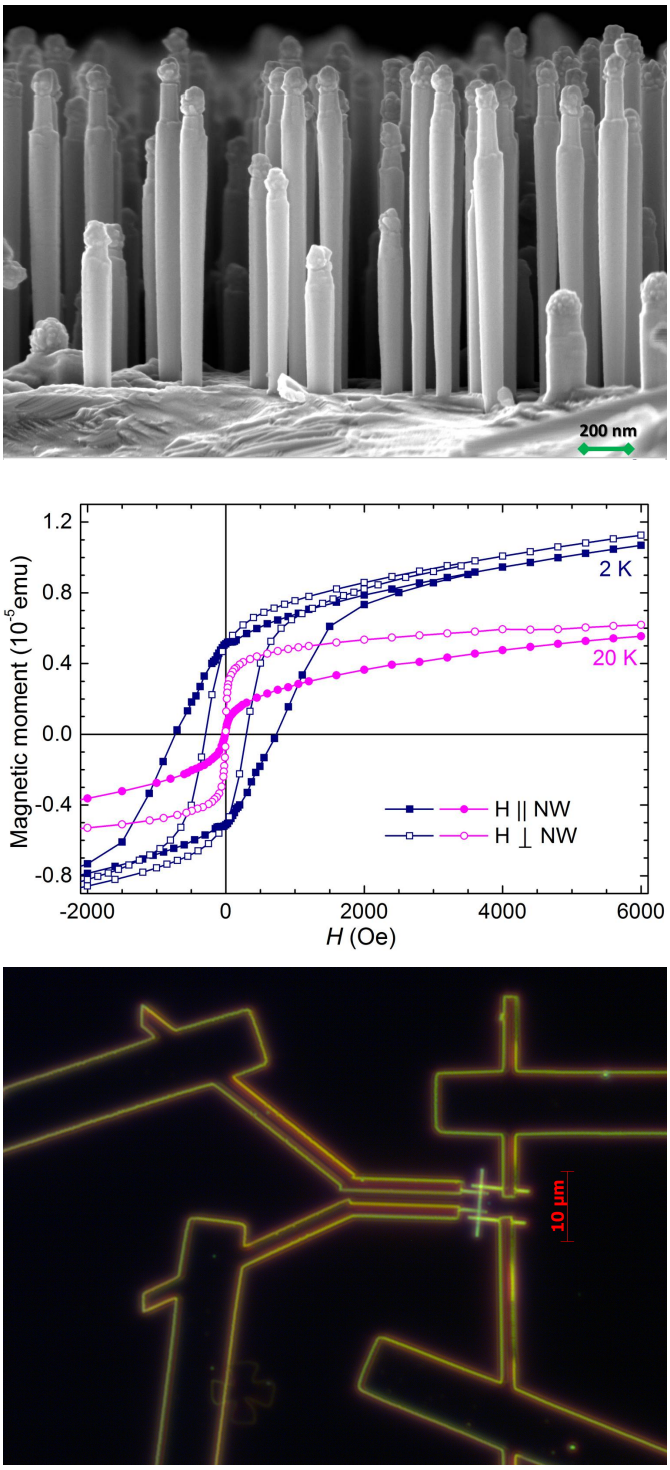

Figure 1: SEM picture of Au-catalysed (In,Ga)As-(Ga,Mn)As core-shell nanowires grown on GaAs(111)B substrate (upper panel); magnetic properties of nanowires ensemble (midlle panel); optical image in dark field of isolated nanowire on Si/SiO2 substrate contacted to four terminals by e-lithographic methods (lower panel).

Closing ceremony
Friday afternoon, 16 August, 13:00

Posters

Monday, 12 August

MoP-T02
Monday afternoon, 12 August, 17:00
Room 211, Old Library

17:00 Poster Mo185

Study on Ag modified TiO_2 thin films grown by sputtering deposition using sintered target

Amir I. Abidov, Bunyod Allabergenov, Oybek Tursunkulov, Sang Yeop Kim, Jeonghwan Lee, Xiao Feiyi, Sungjin Kim

Kumoh National Institute of Technology (KIT), 61 Daehak-ro, Gumi 730-701, Korea, South

e-mail: abidov_kit@yahoo.com

Ag modified thin films were grown by sputtering method using sintered Ag/TiO_2 target. Sputtered films were deposited on glass at room temperature. After sputtering samples were heated at different temperatures and time in order to stabilize structure. Microstructural properties were examined using X-ray diffraction (XRD) and Field emission Scanning Electronic Microscope (FESEM). X-Ray photoelectron spectrophotometer (XPS) was used to analyze chemical composition and stoichiometry of doped thin films. Photocatalytic properties were examined by liquid phase photodegradation of organic dyes under visible and UV light. Bandgap energy of doped films was determined using UV-visible absorbance spectrophotometer. It was found that photocatalytic activity depends on morphology and thickness of deposited film. In this study optimum sputtering parameters for achieving the highest phocatalytic properties of doped films were determined.

17:00 Poster Mo186

On the formation of magnetic nanocomposites and impurity complexes in GaN doped with Fe and Mn

Andrea Navarro-Quezada[1], Giulia Capuzzo[1], Sylwia I. Stefanowicz[2], Thibaut Devillers[1], Wiktor Stefanowicz[2], Tian Li[1], Bogdan Faina[1], Maciej Sawicki[2], Tomasz Dietl[2,3,4,5], Alberta Bonanni[1]

1. *Institut für Halbleiter und Feskörperphysik, Johannes Kepler Universität (FKP-JKU), Altenbergerstr. 69, Linz 4040, Austria* **2.** *Polish Academy of Sciences, Institute of Physics, Lotnikow 32/46, Warsaw 02-668, Poland* **3.** *Japan Science and Technology Agency, Semiconductor Spintronics Project (ERATO), al. Lotników 32/46, Warszawa 02-668, Poland* **4.** *Institute of Theoretical Physics, University of Warsaw, Warsaw 00-681, Poland* **5.** *WPI-AIMR, Tohoku University, 2-1-1 Katahira, Aoba-ku, Sendai 980-8577, Japan*

e-mail: alberta.bonanni@jku.at

The control over the aggregation of magnetic ions in a non-magnetic semiconductor matrix constitutes a new way to realize semiconductor/ferromagnetic nanocomposites with hitherto unexplored but striking functionalities.

With this work we show – in the case of the model systems (Ga,Fe)N and Ga,Mn)N fabricated by metalorganic vapor phase epitaxy – that there is a critical and systematic dependence of the crystalline structure, magnetic ions incorporation and macroscopic properties of these composite material systems on the fabrication conditions and on the co-doping with shallow impurities.

For phase-separated (Ga,Fe)N, we show that the controlled formation of various Fe-rich embedded nanocrystals with peculiar stoichiometry and magnetic properties is responsible for the observed contributions to the overall magnetization of the layers, namely: i) paramagnetic – due to dilute Fe3+; ii) ferromagnetic; and iii) a component linear in the magnetic field, associated with antiferromagnetic interactions – originating from FexN ($x \leq 2$) [1]. Furthermore, the effect of Mg co-doping and deposition mode on the Fe distribution is discussed, together with the ways to obtain a controlled and well-defined arrangement of monophase Fe-rich nanocrystals embedded in the GaN host [2].

In the case of (Ga,Mn)N, we demonstrate that co-doping with Mg over a certain threshold of doping allows to modify the charge- and spin-state of Mn via the formation of impurity complexes Mn-*k*Mg, where *k* depends on the fabrication conditions. The significance of these results is discussed in view of the prospects of embedded magnetic nanocrystals and impurity complexes for photonics and solotronics applications [3].

[1] A. Navarro-Quezada et al., Phys. Rev. B. 84, 155321 (2010)

[2] A. Navarro-Quezada et al. Appl. Phys. Lett. 101, 081911 (2012)

[3] P. Koenraad and M. Flatté, Nat. Mat. 10, 91-100 (2011)

17:00 Poster Mo187

Spin texture of topological crystalline insulator surface states in $Pb_{1-x}Sn_xSe$

Piotr Dziawa[1], Bastian M. Wojek[3], Ryszard Buczko[1], Shiva Safaei[1], B. J. Kowalski[1], Magnus H. Berntsen[3], Thiagarajan Balasubramanian[2], Mats Leandersson[2], Andrzej Szczerbakow[1], Perla Kacman[1], Tomasz Story[1], Oscar Tjernberg[3]

1. *Polish Academy of Sciences, Institute of Physics, al. Lotników 32/46, Warszawa 02-668, Poland* **2.** *Lund University, MAX-lab, Lund SE-221 00, Sweden* **3.** *Royal Institute of Technology (KTH), Brinellvagen 23, 2tr., Stockholm SE10044, Sweden*

e-mail: dziawa@ifpan.edu.pl

In recent years theoretical predictions [1-3] as well as experimental confirmations bring on new class of materials called topological insulators (TI). These materials are characterized by inverted electronic bands with an odd number of Dirac cones of metallic surface states with specific spin texture. Both spin-orbit coupling and time reversal symmetry protect spins against local non-magnetic perturbations and guarantee preservation of spin features of surface states. Lately the novel class – topological crystalline insulators (TCI) – was anticipated theoretically [4-5]. The exploration of TCIs has been directed onto SnTe, lead salts and related alloys from IV-VI group of narrow gap semiconductors, which was shortly confirmed experimentally [6-8]. Differently to TIs, in these materials the crucial role plays crystalline mirror symmetry originating from the rock-salt crystal structure.

In contrast to SnTe the ternary compounds provide the ability to manipulate both spin-orbit interaction and band gap. The increasing tin content in $Pb_{1-x}Sn_xSe$ and $Pb_{1-x}Sn_xTe$ leads to closing the bulk band gap at some specific composition x_c. For higher values of x the band structure undergoes inversion, band gap opens and distinct Dirac-like surface states appear [6]. The same effect can be achieved by changing the temperature, i.e. high temperatures correspond to topologically trivial state while at low temperatures TCI state with inverted bands is established [6].

To check spin phenomena in $Pb_{1-x}Sn_xSe$ we used angle-resolved as well as spin-resolved photoelectron spectroscopy at the MAX III synchrotron at MAX-lab, Lund University (Sweden). We studied (001) surface of n-type monocrystalline $Pb_{0.73}Sn_{0.27}Se$ grown by self-selected vapour method. From the evolution of the band gap the temperature of transition into closed gap state for this crystal composition was estimated to be approximately 250 K. The formation of metallic surface states revealed by the birth of Dirac-cones was clearly observed at low temperatures TCI state. The spin polarization was investigated in both trivial (at T=300 K) and TCI (at T=80 K) states at 2D Brillouin zone in vicinity of X (the projection of the L(111) points in the bulk crystal onto the (001) surface). The experimental results revealed that both trivial and TCI states posses spin polarization with the chiral spin textures. These findings are consistent with our using tight-binding calculations for high-symmetry directions of (001) surface Brillouin zone.

[1] C.L. Kane and E.J. Mele, Phys. Rev. Lett. **95** (2005) 146802.

[2] L. Fu and C.L. Kane, Phys. Rev. B **76** (2007) 045302.

[3] M. Hasan and C.L. Kane, Rev. Mod. Phys. **82** (2010) 3045.

[4] L. Fu, Phys. Rev. Lett. **106** (2011) 106802.

[5] T.H. Hsieh et al., Nature Communications **3** (2012) 982.

[6] P. Dziawa et al., Nat. Mater. **11** (2012) 1023.

[7] S.-Y. Xu et al., Nat. Commun. **3** (2012) 1192.

[8] Y. Tanaka et al., Nat. Phys. **8** (2012) 800.

17:00 Poster Mo188

Growth, characterization and study of ferromagnetism of bismuth telluride doped with manganese

Irina V. Fedorchenko[1], Sergey F. Marenkin[1], Andrei Avdonin[2], Viktor Domukhovski[2], Witold Dobrowolski[2], Janne Heikinheimo[3], Esa Korhonen[3], Filip Tuomisto[3]

1. *Kurnakov Institute of General and Inorganic Chemistry RAS (IGIC), Leninsky prospect, 31, Moscow 119991, Russian Federation* **2.** *Polish Academy of Sciences, Institute of Physics, al. Lotników 32/46, Warszawa 02-668, Poland* **3.** *Aalto University, Department of Applied Physics, P.O.Box 11100, Aalto FI-00076, Finland*

e-mail: fedorkin-san@rambler.ru

A number of publications, reporting ferromagnetism at low temperatures (about 10 K) in Bi_2Te_3 doped with manganese appeared recently. The work presented in this report was targeted at preparing a good quality $Bi_{2-X}Mn_XTe_3$ crystals and studying the mechanisms of formation of ferromagnetism in this material. The samples were studied by means of x-ray diffraction, energy dispersive x-ray analysis (EDX), AC susceptibility measurements, magnetization measurements, electronic transport measurements, magnetoresistance measurements and positron annihilation lifetime spectroscopy.

Crystals containing up to x=0.02 of manganese were grown by Bridgman technique using material synthesized in advance as the ampule charge. The concentration of manganese was estimated from EDX, magnetic susceptibility and magnetization measurements. The obtained values of concentration are consistent. This and the analysis of x-ray diffraction data suggest that manganese is scattered in the Bi_2Te_3 matrix and $Bi_{2-X}Mn_XTe_3$ is a true diluted magnetic semiconductor.

In heavily doped samples the ferromagnetic phase transition was observed. From the temperature dependence of AC magnetic susceptibility the temperature of the phase transition was estimated to be about 5.3 K. Comparison with other reports shows that the temperature of phase transition depends on manganese concentration. The hysteresis curves measured at 4.5 K have zero coercive field which is explained by closeness of the measurement temperature to Curie temperature.

The phase transition was also observed in electron transport measurements. An increase of resistivity, with the maximum at about 6 K, is observed in the ferromagnetic sample in the vicinity of the phase transition temperature. Such increase of resistivity, related with the increase of scattering, is typical for ferromagnetic materials. It is a further clue that manganese is randomly distributed in the crystal lattice. Anomalous Hall effect however was not observed in the ferromagnetic samples. Since a strong spin-orbit interaction is expected in bismuth telluride, this means that there is no spin polarization of the free carriers in the ferromagnetic state of the material.

The magnetoresistance was measured in the magnetic fields up to 13 T. The magnetoresistance of the ferromagnetic sample is linear above 2 T, reaches 30 % at 13 T and does not show signs of saturation both above and below phase transition temperature. The linear dependence of the magnetoresistance is typical for nonuniform materials in which the adjacent microscopic regions have slightly different properties. An additional component of magnetoresistance which appears at low temperatures and saturates at about 0.3 T is attributed to weak antilocalization phenomenon.

In positron annihilation lifetime spectroscopy two lifetime components of 250 ps and 480 ps were observed. The short lifetime component is attributed to annihilation events of the delocalized positrons in the bulk of the crystal. The 480 ps component should be related with clusters of vacancies or larger void structures. It may also be related with the layered structure of the Bi_2Te_3 crystal lattice.

This work was supported by RFBR project No 11-02-00363.

17:00 Poster Mo189

Influence of Mn δ-doping on formation of CdTe/ZnTe quantum dots with single magnetic ions

Karol Gietka[1], Jakub Kobak[1], Maciej Koperski[1], Tomasz Smoleński[1], Mateusz Goryca[1], Jean-Guy Rousset[1], Elzbieta Janik[1], Tomasz Slupinski[2], Andrzej Golnik[1], Piotr Kossacki[1], Wojciech Pacuski[1]

1. *Institute of Experimental Physics, University of Warsaw, Hoża 69, Warszawa 00-681, Poland* **2.** *Faculty of Physics, University of Warsaw, Hoża 69, Warszawa 00-681, Poland*

e-mail: karol.gietka@gmail.com

We report on technological and magneto-optical investigations of formation of quantum dots (QDs) with single magnetic ions. Motivation of our study is to control ion-exciton interaction by controlling position of magnetic ion in QD. In particular, we studied impact of position of Mn δ-doping on optical properties of QDs.

The first reported QDs with single magnetic ions were obtained by Mn δ-doping of ZnTe barrier, a few nm below CdTe QDs layer [1]. The method was further improved by simultaneous deposition of Mn and CdTe layer [2,3] what increased probability of good overlap of Mn and QD exciton. Within this work Mn was introduced at the bottom, in the middle and on the top of CdTe layer.

Quantum dots were grown using molecular beam epitaxy and a method of amorphous tellurium deposited after CdTe layer [4]. We used very thin CdTe layer (1-3 monolayers (MLs), instead of the typical 5-8 MLs [4]) in order to lower QDs density [5,6] and to study individual QDs with various sizes and emission energy, not limited to low energy tail. In order to get very low concentration of Mn ions, crucial for incorporating one Mn ion per QD on average, we have

calibrated the Mn molecular beam of our effusion cell using the giant Zeeman effect in (Cd,Mn)Te and (Zn,Mn)Te [6] layers.

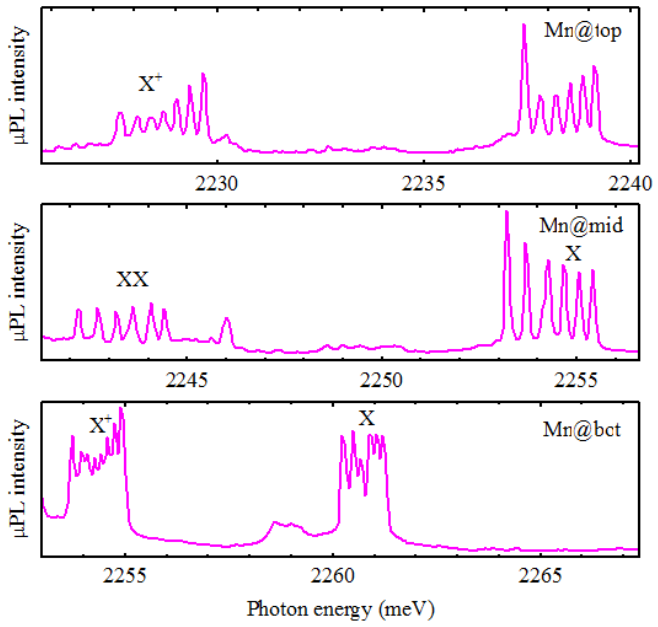

Fig.1. μPL lines of quantum dots with single manganese ions: excitons (X), trions (X^+) and biexcitons (XX).

In layers of dilute magnetic semiconductors, exciton lines split at low temperature (1.7K) and magnetic field (up to 5T) due to the giant Zeeman effect which is proportional to manganese concentration. Experimentally observed exciton splitting was fitted using modified Brillouin function [7,8] and Mn concentration was determined. Mn concentration appears to be in the range from 0.02% to 8%. The source calibration for the lowest Mn concentration was used for further growth of magnetic quantum dots.

Low temperature μ-photoluminescence (μPL) study shows that for all samples in the series we can identify QDs with exactly one Mn ion (Fig. 1). Independently on position of Mn δ-doping we observe QDs with large exciton splitting of about 2 meV, what indicates good overlap of Mn and exciton. This surprising result doesn't indicate how to improve control of Mn position in QD. On the other hand we observe strong impact of position of Mn δ-doping on QDs density and on amount of Mn incorporated into QDs. We discuss it as a consequence of modification of surface atom mobility [9].

The advantage of having QDs with low density is that we can study not only large QDs with emission lines in the low energy tail of QDs ensemble as it was typically studied before [3,10] but also access typical QDs having PL in the middle of spectrum. This opens a possibility to study statistics of incorporation of manganese into QDs. The analysis of μPL spectra shows that there is a clear dependence between the energy of a quantum dot and the probability of presence of manganese ions as shown on Fig. 2. The ratio of the number of quantum dots with Mn ions and all QDs within the constant area (1 μm2 given by our laser spot) decreases with the spectral energy. We interpret this effect in the following way: due to the quantum confinement large dots have lower energy than small dots hence manganese ions are more likely to arrange in dots with more space within.

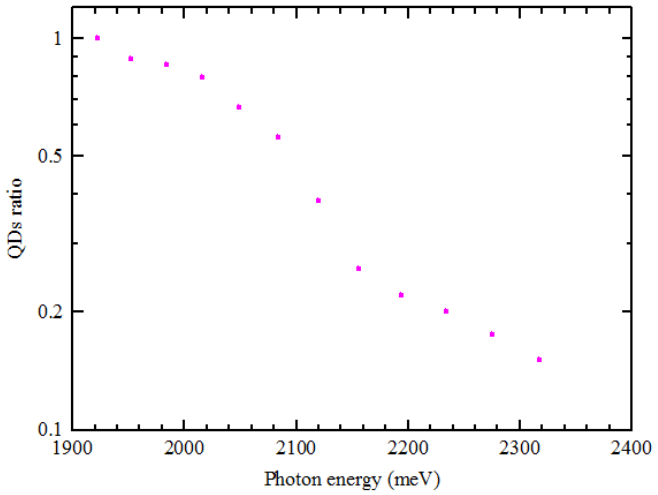

Fig. 2. The probability of finding Mn in a QD. We divided spectra into 45 meV wide parts and count the ratio between QDs with Mn ions and all QDs in each part. There are no dots with energy lower than 1900 meV and higher than 2400 meV. The probability decreases with emission energy. Statistics made for 15 points on the samples.

Large s,p-d splitting of QDs excitons with single Mn ions allow us to resolve well all six lines related to Mn spins and perform exciton decay measurements for various lines. Our results allow us to conclude on temporal evolution of exciton-magnetic ion complex.

[1] L. Maingault, L. Besombes, Y. Leger et al., *Appl. Phys. Lett.* **89**, 193109 (2006).
[2] P. Wojnar, J. Suffczynski, K. Kowalik et al., *Phys. Rev. B* **75**, 155301 (2007).
[3] M. Goryca, T. Kazimierczuk, M. Nawrocki et. al., *Phys. Rev. Lett.* **103**, 087401 (2009).
[4] F. Tinjod, B. Gilles, S. Moehl et al., *Appl. Phys. Lett.* **82**, 4340 (2003).
[5] J. Kobak, J.-G. Rousset, R. Rudniewski et al., arXiv:1210.2946 (2012).
[6] K. Gietka, J. Kobak, J.-G. Rousset et al., *Acta Physica Polonica A* **122**, 1056 (2012).
[7] J.A. Gaj, W. Grieshaber, C. Bodin-Deshages et al., *Phys. Rev. B* **50**, 5512 (1994).
[8] A. Twardowski, P. Świderski, M. von Ortenberg et al., *Solid State Commun.* **50**, 509 (1984).
[9] S. Kuroda, Y. Terai, K. Takita et al., *J. Cryst. Growth* **214-215**, 140 (2000).
[10] L. Besombes, Y. Léger, L. Maingault et al., *Phys. Rev. Lett.* **93**, 207403 (2004).

17:00 Poster Mo190

Photoreflectance study of Ga(Bi,As) and (Ga,Mn)As epitaxial layers grown under tensile and compressive strain

Łukasz Gluba[1], Oksana Yastrubchak[1], Janusz Sadowski[2,3], Jaroslaw Domagala[2], Jerzy Żuk[1], Tadeusz Wosiński[2]

1. *Uniwersytet Marii Curie-Skłodowskiej, Wydział Matematyki, Fizyki i Informatyki (UMCS), pl. MC-Skłodowskiej 5, Lublin 20-031, Poland* **2.** *Polish Academy of Sciences, Institute of Physics, al. Lotników 32/46, Warszawa 02-668, Poland* **3.** *Lund University, MAX-lab, Lund SE-221 00, Sweden*

e-mail: gluba@hektor.umcs.lublin.pl

(Ga,Mn)As has become a model diluted ferromagnetic semiconductor, in which ferromagnetic ordering between substitutional Mn^{2+} ions occurs owing to interaction with spin-polarized holes, as it was successfully explained within the frames of the *p-d* Zener model just over a decade ago [1]. However, the theoretical understanding of the band structure and the underlying ferromagnetic interactions are still under debate. An alternative model assuming an anticrossing-induced formation of a Mn-related impurity band in the band gap and the Fermi-level location in that band was proposed [2]. The band anticrossing model was developed previously to account for the observed strong red shift of the interband optical transition and a giant spin-orbit splitting in Ga(Bi,As) alloy [3].

In the present study, we have investigated thin 50-100nm (Ga,Mn)As and Ga(Bi,As) layers (Mn: 4% - 7%, Bi: 1 - 2%). These films were grown on semi-insulating (001) GaAs substrates with LT-GaAs and InGaAs (with the In content from 3.4% to 30%) buffers in order to introduce compressive or tensile strain in the (Ga,Mn)As or Ga(Bi,As) epitaxial layers. Some of the Ga(Bi,As) epi-layers were grown pseudomorphically on the LT-GaAs and InGaAs (with 10% of In content) buffers or partially and fully relaxed on InGaAs buffers with 20% and 30% of In content. The most of (Ga,Mn)As epitaxial films were fully strained, only few of them, grown on the InGaAs with high In composition were partially relaxed. The alloys compositions and the nature and magnitudes of the strain in the investigated epitaxial films were analysed by the high resolution X-ray diffractometry results. These investigations were supported by Raman spectroscopy measurements. The analysis of the fundamental properties of the epi-layers were performed using the modulation PR spectroscopy measurements, which enabled the determination of the band gap (E_0) and spin-orbit split-off (E_{SO}) band-to-conduction-band optical transitions. The full-line-shape analysis of experimental PR spectra allowed us to determine the energies of interband transitions and the electro-optic energies for light and heavy holes in all the investigated layers. Photoreflectance results for Ga(Bi,As) have shown significant red shift of E_0 transition energy with increasing Bi content. This shift is strongly depended on the strain parameters. On the other hand, small changes of fundamental gap (blue or red shift) have been observed in (Ga,Mn)As epitaxial layers subjected to different value of Mn content and type and magnitude of the strain.

Our experimental results are consistent with the valence-band origin of mobile holes mediating ferromagnetic ordering in the (Ga,Mn)As and in agreement with the anti-crossing model in case of the Ga(Bi,As).

[1] T. Dietl, H. Ohno and F. Matsukura, *Phys. Rev. B***63**, 195205 (2001)

[2] K. Alberi, K.M. Yu, P.R. Stone, O.D. Dubon, W. Walukiewicz, T. Wojtowicz, X. Liu and J.K. Furdyna, *Phys. Rev. B***78**, 075201 (2008)

[3] K. Alberi, J. Wu, W. Walukievicz, K. M. Yu, O.D. Dubon, S.P. Watkins, C.X. Wang, X. Liu, Y.-J. Cho and J. Furdyna, *Phys. Rev. B***75**, 045203 (2007)

17:00 Poster Mo191

Effect of codopants (Li, Na and K) on the magnetic properties of Co doped ZnO thin films

Ramasubramanian Swaminathan, Kumar Janakiraman

Crystal Growth Centre, Anna University, Chennai, Chennai 600025, India

e-mail: marsjk@annauniv.edu

Zinc oxide (ZnO) is studied for a variety of electrical and optical applications because of its wide band gap, transparency and its high exciton binding energy (60 meV) [1]. Since the last decade, considerable work has been devoted in realizing ZnO as a Dilute Magnetic Semiconductor (DMS) by doping transition (TM) metals in it. Among the TM ions, Cobalt doping is one of the most investigated and is considered to yield high magnetic moment in ZnO [2].The nature of the observed magnetism in Co doped ZnO is not being clear as it is intrinsic or because of the presence of metallic cluster. The presence of defects or impurities are also affects the magnetic property in the Co doped ZnO. In this work, we report the study on the impact of I group codopants (Li, Na and K) on the magnetic properties of the Co doped ZnO thin films. $Co_yZn_{1-y}O$, $Li_xCo_yZn_{1-x-y}O$, $Na_xCo_yZn_{1-x-y}O$ and $K_xCo_yZn_{1-x-y}O$ (x, y =0.03) thin films were grown on sapphire (0001) substrates using Sol-gel spin coating technique. Sol-gel technique has been adapted inorder to realize the homogeneous and atomic scale doping in the films. Structural properties of the films were analyzed using X-ray diffraction. Raman scattering techniques indicated the substitution of the dopants in the ZnO matrix.The amount of incorporated K^+ ions in the $K_xCo_yZn_{1-x-y}O$ films was found to be minimal. Surface morphology of the films was found to be of densely packed grains of varied sizes between 120 – 150 nm. The introduction of codopants was resultant in reducing the average grain sizes in the grown films. The transmittance spectra of all the films showed the characteristic Co^{2+} absorptions in the visible region at the wavelengths of 567, 619 and 673 nm. The optical bandgap energies of Co doped ZnO, (Li, Co) codoped ZnO, (Na, Co) codoped ZnO and (K, Co) codoped ZnO films were estimated to be 3.24 eV, 3.2 eV, 3.27 eV and 3.26 eV respectively. Photoluminescence measurement demonstrated the distinct variations in the nature of the intrinsic defects (V_o, Zn_i, V_{zn}

) in the different codoped ZnO films. Magnetic measurements showed the observation of the room temperature ferromagnetism in all the films. The magnetic moments found to be varied with the amount of incorporated Co in the grown films. Magnetic force microscopy was used to analyze the magneitc regions on the surfaces of the films. Presence of small metallic clusters of Co were observed along the grain boundaries. Figure 1 shows MFM images of Co doped ZnO. The introduction of Li and Na as codopants found to significantly reduced the amount of metallic cobalt in the grains. Our studies showed the nature of magnetism observed in the Co doped ZnO films could get changed by the use of codpants.

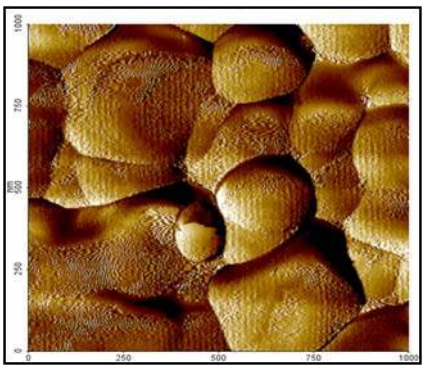

Figure 1: MFM image of the Li,Co codoped film over scan area of 1000 nm × 1000 nm. References: 1. U. Ozgur, Ya. I. Alivov, C. Liu, A. Teke, M. A. Reshchikov, S. Dogan, V. Avrutin, S.J. Cho, and H. Morkoc, J. Appl. Phys. 98, (2005) 041301 2. M. Venkatesan, C. B. Fitzgerald, J. G. Lunney and J. M. D. Coey, Phys. Rev. Lett. 93 (2004) 177206.

17:00 Poster Mo192

Multiferroic $Bi_4Ti_3O_{12}$-n$BiFeO_3$ (n= 1-5) crystals by pulling down technique

Hideo Kimura[1], Hongyang Zhao[1,2], Rumi Tanahashi[1], Lei Guo[1], Qiwen Yao[3], Zhenxiang Cheng[3], Xiaolin Wang[3], Zengmei Wang[4]

1. *National Institute for Materials Science (NIMS), 1-2-1 Sengen, Tsukuba 305-0047, Japan* **2.** *Shanghai Institute of Ceramics, Chinese Academy of Sciences, 1295 Dingxi Road, Shanghai 200050, China* **3.** *University of Wollongong, Wollongong NSW, Australia* **4.** *South-east University (SEU), Nanjing 210000, China*

e-mail: kimura.hideo@nims.go.jp

Aurivillius phase bismuth layer-structured materials with the formula of $(Bi_2O_2)^{2+}$ $(A_{m-1}B_mO_{3m+1})^{2-}$ are expected an amazing variety of both structural and physical properties by changing the A and B cations as well as the number of perovskite-like units (m). In recent years, number of paper is increased on those Aurivillius compounds with m=4, 5 or more complicated one.

In this paper, we report the crystal growth of these oxides compound; $Bi_5Ti_3FeO_{15}$ (BTFO) (m=4); i.e., $Bi_4Ti_3O_{12}$-n$BiFeO_3$ (n= 1-5). BTFO crystallizes in the polar space group A21am at room temperature. However, the structure of $Bi_4Ti_3O_{12}$- n$BiFeO_3$ (n= 2-5) compound are not so clear. In these cases, smaller Fe ions are also incorporated into B (Ti) sites, which may cause new magnetically ordered structures. BTFO starting ceramics were synthesized by conventional solid state method. The crystals were grown by our original floating-zone pulling down (Fz-PD) method.

In the past papers, we succeeded to grow long single crystals using modified pulling down method on Rb (Cs), Na: $KNbO_3$ series single crystals [1, 2]. This system is installed conventional double ellipsoidal mirror halogen lamps and Pt tube in 4 mm diameter. At least single-phase crystals could be grown in the present. At past time, no rotation of Pt wire is necessary to grow on single crystals on Rb (Cs), Na: $KNbO_3$ series. On the other hand in the present, the rotation of Pt wire is necessary to grow single crystals in long size due to keeping good temperature conditions. We believe the difference on the rotation is up to molten zone properties. But in this paper, we don't treat the molten zone properties. We focus on crystal properties only. Thus Characterizations were carried out for electric properties, such as dielectric constant and impedance etc.

Part of this work was supported by GRENE (Green Network of Excellence) project from Ministry of Education, Culture, Sports, Science and Technology- Japan.

[1] H.Kimura, R.Tanahashi, H.Y.Zhao, K.Maiwa, Cryst.Res.Technol. 46(1) (2011) 37.

[2] H.Kimura, R.Tanahashi, H.Y.Zhao, Q.W.Yao, Z.X.Cheng, X.L.Wang, Ceram. Int. 38S, (2012) S109.

17:00 Poster Mo193

Magnetic anisotropy in ferromagnetic (Ge,Mn)Te epitaxial layers with varying Mn content

Wojciech Knoff[1], Andrzej Szczerbakow[1], Badri Taliashvili[1], Viktor Domukhovski[1], Andrzej Lusakowski[1], Agnieszka Wołoś[1,2], Tomasz Story[1]

1. *Polish Academy of Sciences, Institute of Physics, al. Lotników 32/46, Warszawa 02-668, Poland* **2.** *University of Warsaw, Faculty of Physics, Institute of Experimental Physics (IFDUW), Hoża 69, Warsaw 00-681, Poland*

e-mail: knoff@ifpan.edu.pl

(Ge,Mn)Te is a IV-VI diluted magnetic semiconductor exhibiting ferromagnetic transition induced by a very high conducting hole concentration. The Curie temperature in crystalline (Ge,Mn)Te layers can be increased up to T_C = 190 K by independent optimization of Mn^{2+} ions content and carrier concentration [1,2]. GeTe and (Ge,Mn)Te crystals are known to undergo structural (ferroelectric) transition in which high-temperature cubic (rock-salt) structure becomes distorted along cube's diagonal to form low-temperature rhombohedral structure. Recent magnetization and ferromagnetic resonance (FMR) studies of (Ge,Mn)Te epitaxial layers on BaF_2 (111) substrates revealed that in monocrystalline layers with 10 at. % of Mn content the easy axis of magnetization is perpendicular to the layer (perpendicular magnetic anisotropy - PMA) while the usual easy-plane anisotropy is observed in layers with 20 at. % of Mn content. Additional annealing of layers results in the change of the easy axis of magnetization to the in-plane direction in samples with Mn content 10 – 20 at. %. These experimental findings indicate the key role of lattice distortions (the change of rhombohedral angle) in magnetic anisotropy of (Ge,Mn)Te layers. In this work, we quantitatively examine this effect by FMR and SQUID superconducting magnetometry techniques in monocrystalline (Ge,Mn)Te layers (thickness of 0.7 μm) grown on BaF_2 (111) substrates by molecular beam epitaxy with Mn concentration varying from 10 to 20 at. %. Post-grown annealing was performed to compare magnetic properties of as-grown and annealed samples. Our experimental results on the angular dependence of the FMR resonant field are analyzed in model calculations taking into account the contribution of demagnetization fields and the magnetocrystalline anisotropy terms in magnetic free energy. We propose a microscopic model of the PMA effect in (Ge,Mn)Te/BaF_2(111) layers with the key role of the hybridization of $3d^5$ electronic orbitals of Mn^{2+} ions and the valence band states of rhombohedrally [111] - distorted crystal lattice of *p*-(Ge,Mn)Te. [1] Y. Fukuma et al., Appl. Phys. Lett. 93, 252502 (2008) [2] R.T. Lechner et al., Appl. Phys. Lett. 97, 023101 (2010) [3] W. Knoff et al., Phys. Stat. Sol. (b) 248, 1605 (2011)

This work was supported by the research project UMO 2011/01/B/ST3/02486 of Polish National Science Center (NCN).

17:00 Poster Mo194

Confinement-dependent ferromagnetism in Mn-doped InAs quantum dots embedded in InP nanowires: an ab initio study

Erika N. Lima, Tome M. Schmidt

Universidade Federal de Uberlandia (UFU), Av Joao Naves de Avila, 2121, Uberlandia 38400902, Brazil

e-mail: erikanascimentolima@yahoo.com.br

Mn-doped InAs quantum dots (QDs) embedded in InP nanowires have been studied by first-principles calculations. The Mn-Mn ferromagnetic (FM) coupling is stronger in quantum dots than in nanowires and even greater than that of GaMnAs. We show that the ferromagnetic stability of Mn-doped InAs nanostructures is dependent on the confinement effects. InAs QDs embedded in InP NWs present stronger FM coupling than InAs bulk and NWs, and it is even greater than that of GaMnAs [1]. The magnentic-phase stabilization is due to a strong AFM *p-d exchange* between the Mn $3d^5$ states and the hole bound to the magnetic impurity [2]. This AFM coupling is dependent on the quantum-confinement effect, resulting in a total FM coupling in QDs. The magnetic coupling in these embedded QDs is a short-range one, presenting strong intradot Mn-Mn interaction and weaker interdot coupling.

References

[1] Marta Galicka et al. *Nano letters***11**, 3319 (2011)

[2] Gustavo Martini Dalpian et al. Solid State Communications **138,** 353(2006)

17:00 Poster Mo195

Photoluminescence studies of giant Zeeman effect in MBE-grown cobalt-based dilute magnetic semiconductors

Michał Papaj, Jakub Kobak, Jean-Guy Rousset, Elżbieta Janik, Michał Nawrocki, Piotr Kossacki, Andrzej Golnik, Wojciech Pacuski

University of Warsaw, Faculty of Physics, Institute of Experimental Physics (IFDUW), Hoża 69, Warsaw 00-681, Poland

e-mail: michal.papaj@student.uw.edu.pl

Cobalt introduced into wide gap semiconductor is known to quench its excitonic photoluminescence (PL). Therefore magneto-photoluminescence study of cobalt based dilute magnetic semiconductors is an experimental challenge. Using (Zn,Co)Te and (Cd,Co)Te layers grown for this work it was, however, possible to study the giant Zeeman effect both in reflectivity and photoluminescence spectroscopy.

About 1 μm thick layers were grown using molecular beam epitaxy (MBE) on GaAs substrates, at conditions optimized for growth of nonmagnetic ZnTe and CdTe. Using reflection high-energy electron diffraction (RHEED) we observe, that cobalt only weakly affects growth of (Zn,Co)Te layers with x_{Co} = 0.56%, but the same cobalt flux leads to degradation of (Cd,Co)Te. As revealed by RHEED, good quality (Cd,Co)Te layer was obtained for lower concentration of x_{Co} = 0.2%. Concentration of cobalt was determined from analysis of the giant Zeeman effect observed using magneto-reflectivity of excitonic transitions (Fig.1) [1-4].

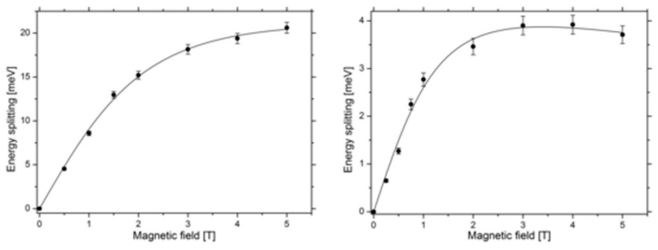

Figure 1. Exciton energy splitting vs magnetic field for: (a) – (Zn,Co)Te, (b) – (Cd,Co)Te. The solid line is a fit of a modified Brillouin function from Ref. [2]

Low temperature (1.5-10 K) PL was excited using 405 nm laser. Free exciton photoluminescence was observed at high excitation power only for (Zn,Co)Te (x_{Co} = 0.56%). Bound exciton transitions were observed for both (Zn,Co)Te (x_{Co} = 0.56%) and (Cd,Co)Te (x_{Co} = 0.2%). PL of (Cd,Co)Te was significantly weaker so that for higher Co concentration in (Cd,Co)Te (bad RHEED quality) the near band gap PL was not observed at all.

Under magnetic field in Faraday configuration PL lines are split and circularly polarized due to the giant Zeeman effect. Additionally, total PL intensity strongly increases with magnetic field, which shows that recombination channel through magnetic ions is less effective at high magnetic fields. For (Zn,Co)Te (x_{Co} = 0.56%) we observe twofold increase, whereas for (Cd,Co)Te (x_{Co} = 0.2%) integrated PL intensity increases by a factor of 30 (at B = 5 T compared to B = 0 T, shown in Fig.2).

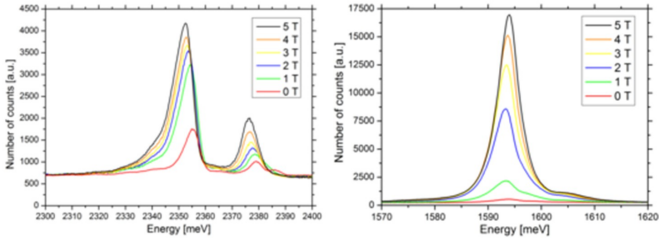

Figure 2. Photoluminescence spectra in σ+ polarization for: (a) – (Zn,Co)Te, (b) – (Cd,Co)Te. Increase of PL intensity with magnetic field is particularly visible for (Cd,Co)Te.

Such difference observed for this two samples has to be a consequence of more efficient PL quenching in (Cd,Co)Te as compared to (Zn,Co)Te. The intraionic Co^{2+} transitions $^4A_2$ - $^4T_1$ (^4P) are in resonance [5] with energy gap of CdTe, so energy transfer from excitons to cobalt ions is significantly faster for (Cd,Co)Te than for (Zn,Co)Te.

[1] M. Papaj, J. Kobak, J.-G. Rousset, E. Janik, A. Golnik, P. Kossacki and W. Pacuski,
*Acta Phys. Pol. A***122**, 1010 (2012).

[2] M. Zielinski, C. Rigaux, A. Lemaitre, A. Mycielski, and J. Deportes, *Phys. Rev. B***53**, 674 (1996);

[3] M. Zielinski, C. Rigaux, A. Mycielski, and M. Menant, *Phys. Rev. B***63**, 035202 (2000);

[4] H. Alawadhi, I. Miotkowski, V. Souw, M. McElfresh, A. K. Ramdas, S. Miotkowska, *Phys. Rev. B***63**, 155201 (2001)

[5] J. M. Baranowski, J. W. Allen, and G. L. Pearson, *Phys. Rev*. **160**, 627 (1967).

17:00 Poster Mo196

Enhanced superconducting transition temperature T_c by the carrier modulation in a high quality single crystal Cu_xPdTe_2

Gihun Ryu[1], Mingtao Li[1,2], Chengtian Lin[1]

1. *Max-Planck-Institut FKF, Heisenbergstr. 1, Stuttgart D70569, Germany* **2.** *Universityof Shanghai, Shanghai, Shanghai 200444, China*

e-mail: G.Ryu@fkf.mpg.de

Two dimensional (2D) layered transition metal dichalcogenide (MX_2) is one of interesting materials because of their unusual physical properties such as charge density wave (CDW) [1] and superconductivity [2,3]. In particular, MX_2 compound also has a Van Der Waals gap between layers so that the intercalation or doping of cation dopant can be efficiently considered and studied. Among 4*d* transition MX_2

compounds, CdI_2-type $PdTe_2$ compound is very attractive due to the peculiar electronic structure, in which the Fermi level (E_F) locates at the valley of density of states [4]. Superconducting transition temperature T_c in BCS-type superconductors dominantly depends on the carrier density at around E_F as one of main factors. Herein, we report superconductivity in Cu_xPdTe_2 single crystal with the large size of ~1´1.8cm^2, which is successfully synthesized by the conventional self-flux method as well as the vertical Bridgman method. Enhanced superconducting T_c from 1.7 to 2.6K is obtained by the carrier introduced in Cu_xPdTe_2 as defined in the electro-magnetic and Hall measurements. These results obviously indicate that Cu_xPdTe_2 compound could be considered as a new example of carrier modulated MX_2 superconductor like the intercalated or electric field induced MoS_2 superconductors with superconducting T_c depending on the carrier density at E_F [2].

References

[1] E. Morosan, H. W. Zandbergen, B. S. Dennis, J. W. G. Bos, Y. Onose, T. Klimczuk, A. P. Ramirez, N. P. Ong and R. J. Cava, Nature, **2**(2006)544

[2] J. Y. Ye, Y. J. Zang, R. Akashi, M. S. Bahramy and Y. Iwasa, Science, **338**(2012)1193

[3] Y. Qi, S. Matsuishi, J. Guo, h. Mizoguchi and H. Hosono, Phys. Rev. Lett. **109**(2012) 217002

[4] H. W. Myron, Solid State Commun. **15**(1974) 395

17:00 Poster Mo197

Electronic and diffusion properties of Li in III-V semiconductors

Stepan Svoboda[1,2], Vit Novak[1], Miroslav Cukr, Tomas Jungwirth[1,3], Nada Tesarova, Petr Nemec[4], Kamil Olejnik[1,4]

1. *Czech Academy of Sciences, Institute of Physics, Cukrovarnicka 10, Prague 16253, Czech Republic* **2.** *Czech Technical University in Prague, Faculty of Nuclear Sciences and Physical Engineering, Department of Physical Electronics, Brehova str. 7, Prague 115 19, Czech Republic* **3.** *School of Physics and Astronomy, University of Nottingham, Nottingham NG72RD, United Kingdom* **4.** *Charles University, Faculty of Mathematics and Physics, Ke Karlovu 3, Prague 12116, Czech Republic*

e-mail: svobost@gmail.com

Elemental Lithium from thermal source has recently been used as the first alcali metal ever in Molecular Beam Epitaxy technique when preparing the room-temperature antiferromagnetic semiconductor LiMnAs [1]. At the same time, Li was shown to penetrate deep into the substrate material during the epitaxial growth, significantly changing its electrical and optical properties. We demonstrate that Li behaves as a shallow donor in InAs, whereas it acts as a deep compensating impurity in GaAs. We present a systematic study of diffusion of Li atoms in both of these materials. Li diffusion coefficients are obtained by comparing the experiment with numerical simulation, their temperature dependence is used to determine the activation energy of the diffusion process. Photoluminescence spectrum is investigated and its correspondence to Li content is discussed.

[1] T. Jungwirth, Phys. Rev. B 83, 035321 (2011)

17:00 Poster Mo198

Hexagonal MnTe with NiAs structure: thermal expansion coefficients and exchange striction

Wojciech Szuszkiewicz[1], Roman Minikayev[1], Elzbieta Dynowska[1], Barbara Witkowska[1], Anthony Bell[2]

1. *Polish Academy of Sciences, Institute of Physics, al. Lotników 32/46, Warszawa 02-668, Poland* **2.** *HASYLAB at DESY, Notkestr., Hamburg 22607, Germany*

e-mail: szusz@ifpan.edu.pl

Magnetic or diluted magnetic semiconductors have been intensively studied in the past, but recently, the possibility of applications in spin electronic devices has renewed the interest for this kind of materials, especially when they exhibit magnetic properties at room temperature. Among binary manganese compounds MnTe with a hexagonal crystal structure of NiAs type is particularly interesting because of its relatively high Neel temperature (T_N = 310 K). The successful growth of such MnTe thin layers by molecular beam epitaxy [1] opened a possibility of potential applications of this material in multilayer structures. The expansion coefficients of materials constituting given structure belong to important parameters required for correct interpretation of the physical properties of considered multilayer. For magnetic materials details of the exchange striction are also of great interest. The relevant MnTe literature data published long time ago were limited to narrow temperature range from 170 K to 350 K only [2, 3]. Moreover, the authors of both mentioned papers demonstrated a sharp decrease of the *c* parameter value with decreasing temperature below T_N unaccompanied by any significant change in the *a* parameter temperature dependence. This information was a little bit surprising taking into account a typical behaviour of other magnetic compounds also crystallizing in the hexagonal structure of NiAs type.

The goal of present paper was to investigate the evolution of the MnTe lattice parameter values in a wide temperature range and to check the relevant information given in the literature. The determination of the linear expansion coefficient value at several hundreds Centigrades should be very helpful when considering possible growth of structures containing MnTe layers. In particular, the thermal strain resulting from different expansion coefficient values for the substrate and for the layer under interest when cooling the structure from the growth temperature to the room temperature can be estimated. On the other hand the numerical values of linear expansion coefficients at the low temperature range can be useful for possible analysis of the exchange striction, present below the magnetic phase transition temperature.

The bulk, single MnTe crystals were grown at the Institute of Physics PAS in Warsaw. Their structure quality at room temperature was confirmed by the results of high-resolution X-ray diffraction measurements, performed with help of Panalytic X'Pert MRD diffractometer iat the same institute. For that purpose the CuK_{a1} radiation was applied, within the experimental accuracy possible presence of precipitates or secondary phases was excluded. The HT and LT measurements were carried out using a synchrotron radiation and taking advantage of a powder diffractometer installed at the B2 beamline at Hasylab/DESY in Hamburg. The samples were prepared as a mixture of powdered MnTe crystals and fine diamond powder. For sample mounting a thin-wall quartz or glass capillary was applied. During all measurements the capillary rotates inside a temperature chamber. The radiation wavelength (about 0.538 Å) was calibrated *in situ*, using the diamond. The 10 K – 1163 K temperature range was investigated. Structure analysis has been provided by using the Rietveld-refinement procedure (an example is shown on figure 1).

The linear expansion coefficients were determined for the *a(T)* and *c(T)* dependences. At limited area of high temperature range a partial transformation of MnTe into $MnTe_2$ (phase absent at RT) was observed, the supplementary phase vanished above 1043 K. Below T_N value not only the *c* parameter, but also the *a* parameter exhibit a kink in its temperature dependence. The relative modification of the *a* parameter value is less pronounced than that corresponding to the *c* value but nevertheless well visible. Present low-temperature data are in general agreement with our previous neutron scattering data taken with slightly smaller accuracy a few years ago [4]. The observed modifications of lattice parameter values at low temperature resulting from the exchange interactions are compared with a few known, similar data obtained for other magnetic materials with the same type of crystal structure. A little bit surprising decrease of a distance between Mn ions observed in plane perpendicular to the hexagonal MnTe crystal axis in spite of the ferromagnetic exchange integral between the nearest neighbours in plane [5] is discussed.

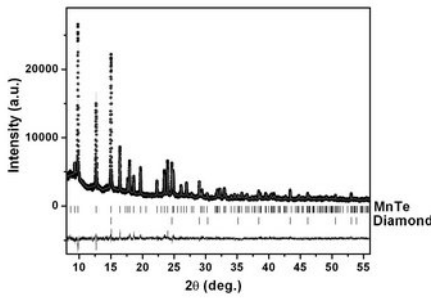

Fig. 1. The X-ray diffraction pattern collected at T = 40 K for investigated sample.

Portions of this research were carried out at the light source DORIS III at DESY, a member of the Helmholtz Association (HGF). This work was partially supported by the research grant N N202 128639 from Ministry of Science and Higher Education (Poland) and by the EU under contract II-20100155.

[1] E. Przeździecka, E.Kamińska, E. Dynowska et al., *Phys. Stat. Sol. C***2**, 1218 (2005).
[2] S. Greenwald, *Acta Cryst*. **6**, 396 (1953).
[3] N.P. Grazhdankina and D.I. Gurfel', *Soviet Phys. JETP***35**, ***631*** (1959).
[4] W. Szuszkiewicz, B. Hennion, B. Witkowska, E. Łusakowska and A. Mycielski, *Phys. Stat. Sol. C***2**, 1141 (2005).
[5] W. Szuszkiewicz, B. Hennion, E. Dynowska and B. Witkowska, *Phys. Rev. B***73**, 104403 (2006).

* Corresponding author. E-mail address: szusz@ifpan.edu.pl.

17:00 Poster Mo199

Room-temperature ferromagnetism in V doped 6H-SiC single crystal

Shi-Yi Zhuo, Xue-Chao Liu, Hong-Ming Chen, Xin Jun, Jian-Hua Yang, Er-Wei Shi

Shanghai institute of ceramics, Chinese academy of sciences, Shanghai 201800, China

e-mail: syzhuo@mail.sic.ac.cn

Room-temperature ferromagnetism has been reported in silicon carbide (SiC) powder, epilayer and single crystal [1,2,3]. However, the ferromagnetic mechanism of this kind of diluted magnetic materials is still controversial. In this paper, we focus on the relationship of ferromagnetism and crystalline quality of vanadium (V) doped 6H-SiC single crystals. It is found that the defect-rich sample shows stronger ferromagnetism. The V-doped 6H-SiC single crystals, with dopant ranging from 0 to 6.14×10^{17} at./cm^3 (labeled as sample I, II and III), were prepared by physical vapor transport technique. The 6H-SiC without V doping shows a diamagnetic behavior, while clear ferromagnetism is observed in V- doped 6H-SiC single crystals, as shown in Figure 1.It can be seen that the 6H-SiC single crystal with a lower V dopant exhibits a larger magnetization saturation. However, in-depth structural characterizations by optical microscope, high-resolution X-ray diffraction and Raman spectroscope indicate a poor crystalline quality of sample II (Figure 2). These results imply that both V dopant and defects are essential in inducing ferromagnetism of 6H-SiC, and the ferromagnetism can be enhanced by defects in poor crystalline quality single crystal.

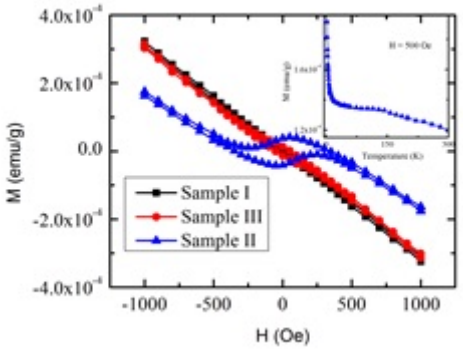

Figure 1. Room-temperature M-H curves of sample I, II and III. The inset shows M-T curve of sample II.

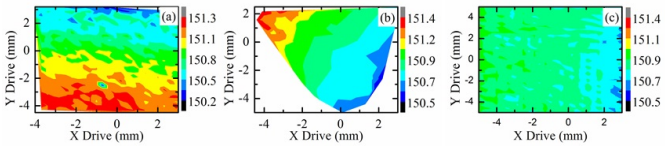

Figure 2. The mapping review of Raman peak intensity for sample I, II, and III.

[1] Hui Wang, Chen-Feng Yan, Hai-Kuan Kong, Jian-jun Chen, Jun Xin, and Er-Wei Shi, Investigation of room temperature ferromagnetism of 3C-SiC by vanadium carbide doping, Appl. Phys. Lett., 101 (2012) 142404.
[2] K. Bouziane, M. Mamor, Ph. Djemia and S.M. Cherif, Defects and magnetic properties in Mn-implanted 3C-SiC epilayer on Si(100): Experiments and first-principles calculations, Phys. Rev. B, 78 (2008) 195305.
[3] Zhuo Shi-Yi, Liu Xue-Chao, Xiong Ze, Yan Wen-Sheng, Xin Jun, Yang Jian-Hua, and Shi Er-Wei, Defects mediated ferromagnetism in V-doped 6H-SiC single crystal, Chin. Phys. B, 21 (2012) 067503.

Topical Session 3

Wide bandgap semiconductors

Session Coordinators

Marek Godlewski (Poland) *godlew@ifpan.edu.pl*

Bruno Daudin (France) *bruno.daudin@cea.fr*

Programme

Wednesday, 14 August

WeO2

T03: Wide bandgap semiconductors
Wednesday afternoon, 14 August, 14:00
Room C, Auditorium Maximum

14:00 Invited oral

Ammonothermal growth of GaN substrates

Robert Dwilinski, Roman Doradziński, Leszek P. Sierzputowski, Marcin Zajac, Malgorzata Iwinska, Robert Kucharski

AMMONO S.A., Czerwonego Krzyża 2/31, Warsaw 00-377, Poland

e-mail: dwilinski@ammono.com

Gallium Nitride (GaN) is a new generation semiconductor of wide, direct energy gap of 3.44 eV at room temperature. Among many advantages of GaN, a special attention is attracted to its high thermal, mechanical and chemical resistance, as well as high breakdown voltage and operating current. Wide spectrum of GaN applications includes both production of optoelectronic devices (blue and green light emitting diodes and laser diodes, UV detectors) and high power-high frequency devices used in modern satellite and surface communication systems (including mobile) and navigation.

At present commercially available GaN-based electronic devices are manufactured mainly by heteroepitaxy of quantum structures on non-native substrate (sapphire, SiC), leading to generation of large threading dislocation density, limiting power, efficiency and lifetime of the devices. High dislocation density (at the level of 10^6-10^9 cm^{-2}) is the reason of narrowing the range of operation parameters. The ideal solution of this problem would be use of bulk GaN substrates for homoepitaxy. Recently, large interest has been devoted to ammonothermal method, which is at present regarded as one of the key technologies of bulk GaN substrates manufacturing. It uses supercritical ammonia to dissolution of feedstock material and crystallization of GaN on native seeds due to convection-driven transport and supersaturation of the solution.

The ammonothermal method enables growth of large diameter crystals (now surpassing two inches) of high crystalline quality. It is well controlled, reproducible process performed at relatively low temperature and is perfectly scalable method (with autoclave size), enabling simultaneous growth of many crystals in one run under minimal material costs. The produced GaN crystals demonstrate exceptionally high crystalline properties curve, large lattice curvature radius and the lowest dislocation density (of the order of 10^4 cm^{-2}). Different orientations GaN substrates (polar, nonpolar, semipolar) and wide spectrum of electronic properties can be achieved. Substantial progress has been done to obtain high purity and transparency both n-type and semi-insulating substrates. Special technological procedures were applied to reduce concentration of oxygen and other contaminants, leading to a reduction of free carrier and impurity absorption bands, decreasing by several times the absorption coefficient to very few cm^{-1} at 450 nm.

The usefulness of ammonothermal GaN substrates in production of high quality devices was confirmed by latest achievement of Watt-class violet laser diode made on such substrates. New examples of devices, such as Schottky diodes, HEMT transistors (of low leakage current), blue and green lasers, grown on ammonothermal GaN wafers of various orientations, will be shown. Low dislocation density ammonothermal GaN substrates may then cause next breakthrough in production of high power optoelectronic and electronic devices.

This work was partially supported by the National Centre for Research and Development, under Applied Research Programme Contract Number PBS1/A3/9/2012 and PBS1/B5/8/2012 and under Innotech Programme, Contract Number INNOTECH - K1/IN1/44/158851/NCBR/12

14:30 Invited oral

Fabrication of bulk GaN crystals by Na flux method with a necking technique and a coalescence growth

Yusuke Mori, Masayuki Imanishi, Kosuke Murakami, Daisuke Matsuo, Hiroki Imabayashi, Hideo Takazawa, Yuma Todoroki, Akira Kitamoto, Mihoko Maruyama, Mamoru Imade, Masashi Yoshimura

Graduated School of Engineering, Osaka University (OSAKAUNIV), Osaka, Japan

e-mail: mori.yusuke@eei.eng.osaka-u.ac.jp

Na flux method developed by Yamane can grow GaN crystals in a Ga-Na mixed solution at relatively low pressure of nitrogen atmosphere (<5MPa) and at temperature range of 750~900 deg.C. At the beginning, we have utilized the seed crystal fabricated by the vapor phase growth method in order to make a large diameter GaN crystal. In spite of the poor quality seed substrate with high dislocation density, high quality GaN crystal with the dislocation density around $10^3/cm^2$ could be obtained. It is possible to grow a 4-inch GaN crystal on a HVPE-GaN substrate. However, there should be the limitation of the quality and size of GaN crystal grown on the HVPE substrate containing the residual stress.

Recently, we have developed two new techniques to grow large dislocation-free GaN by Na flux method. First one is necking technique, similar to the key technology in Cz growth of Si. This necking can be realized by putting a sapphire plate with a small hole (0.5 – 1.5 mm in diameter) on a GaN plate seed. The GaN point seed was placed in a ceramic crucible and the starting materials of metallic Ga, Na and graphite grains were added to the crucible in an Ar-filled glovebox. The crucible was transferred to a pressure-resistant stainless tube. The growth of GaN single crystals proceeded with nitrogen dissolution into a Ga–Na–C melt at 870- 890□ at a N2 pressure of 3.6- 4.0 MPa. Centimeter-sized bulk GaN single crystals with large dislocation-free areas could be fabricated by this technique. Cathodoluminescence measurement at the interface between the seed and the grown crystal has revealed that almost all dislocations propagated from the GaN seed were bent and terminated at the initial growth stage.

Second one is coalescence growth of multi-GaN crystals in order to fabricate a large diameter single GaN crystal within a short period. As a first step, we grew two GaN point seeds and coalesced them. Two

GaN point seeds were established by mounting a sapphire plate with two small holes. The coalescence direction was a-direction. Other experimental conditions were same as above. We have found the two GaN crystals grown from two separate holes of sapphire plate coalesced without generating dislocations at a coalescence boundary. X-ray rocking curve measurements revealed that miss-orientation of c-axis of two crystals around a coalescence boundary gradually diminished during the growth. The grown GaN crystal can remove from substrate easily during the growth. This phenomenon is effective to reduce the stress in the grown GaN crystal. The size of the GaN crystal can be increased as increasing the number of seed crystals. Up to now, we succeeded to fabricate 2-inch GaN crystals by the coalescence technique. Some of the crystals have very large curvature radius (~100 m), which exceed the detection limit of a Rigaku SmartLab X-ray diffractometer. Additionally, the point contact Schottky diode at the coalescence boundary of the crystal could work normally. These results indicate the high potential of the new two techniques to realize dislocation-free GaN crystals with large diameter and low strain.

14:45 Oral

First-principles calculation of the carbon-added Na-flux GaN growth on GaN(0001)

Takahiro Kawamura[1,2], Hiroki Imabayashi[2], Mihoko Maruyama[2], Mamoru Imade[2], Masashi Yoshimura[2], Yusuke Mori[2], Yoshitada Morikawa[2]

1. *Mie University, 1577 Kurima-Machiya, Tsu 5148507, Japan*
2. *Osaka UNIV., Yamadaoka 2-1, Suita 565-0871, Japan*

e-mail: tkawamura@mach.mie-u.ac.jp

The Na-flux method [1] is employed to grow large bulk GaN crystals for freestanding substrate. In the past, the polycrystal generation due to heterogeneous nucleation near gas-liquid interface was a crucial problem that inhibits a large crystal growth. This problem was solved by C addition to Na-Ga melts [2]; however, the fundamentals of the effect of C atoms and growth process under C-added condition are not understood. We previously reported that C and N atoms are strongly bonded in Ga-Na melts and it prevents Ga-N bond formation and GaN heterogeneous nucleation [3]. In this study, we simulated C-added Na-flux GaN growth on GaN(0001) surface using first-principles calculations and investigated the process of N incorporation into the crystal surface.

We used a first-principles molecular dynamics simulation program "STATE (Simulation Tool for Atom TEchnology)-Senri". Figure 1 shows a simulation model of the C-added Na-flux growth, which was composed of 133 atoms. The bottom part was a GaN crystal. The GaN(000-1) surface was terminated by 3/4-charged H atoms. Na atoms were placed above the GaN(0001) surface as Na melt. We removed a N atom in the top layer of the GaN(0001) surface to open a N site. We initially put a CN cluster over the open N site at several heights. The N atom of the CN cluster was arranged on the side of the GaN crystal. The interatomic distance between the C and the N atoms was initially set to be 1.2 Å, which is stable distance in Na-Ga melts. We carried out structural optimization calculations for three CN cluster positions and compared total energy and C-N interatomic distance of them.

Figure 2 shows the atomic coordinates after the structural optimization. It seems that Figs. 2(a), 2(b) and 2(c) sequentially show the process of the N atom of the CN cluster will be incorporated in the GaN(0001) surface. The total energy and the C-N interatomic distance of them were listed in Table 1. These results show that the following two situations were energetically stable: (i) the CN cluster was on a Ga atom of the GaN(0001) surface (Fig. 2(a)) and (ii) the N atom of the CN cluster was at the N site in the GaN(0001) surface and the C atom moved away from the N atom (Fig. 2(c)). In addition, the total energy of the situation (ii) was smaller than that of the situation (i). Considering these results and our previous paper [3], we speculate the process of the C-added Na-flux GaN growth on GaN(0001) as follows: CN clusters generated in the melt are transported to the crystal surface, the CN clusters obtain sufficient energy to overcome the energy barrier corresponding to the result of Fig. 2(b), the N atoms of the CN clusters are incorporated in the crystal surface and on the other hand the C atoms depart from the crystal surface. The GaN growth will develop by repeating these processes.

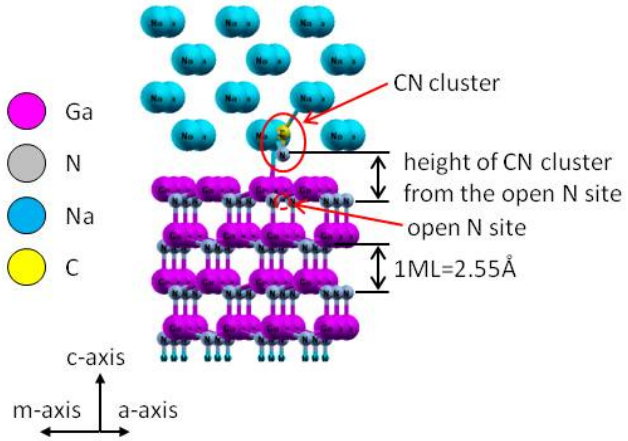

Figure 1 Simulation model of C-added Na-flux GaN growth.

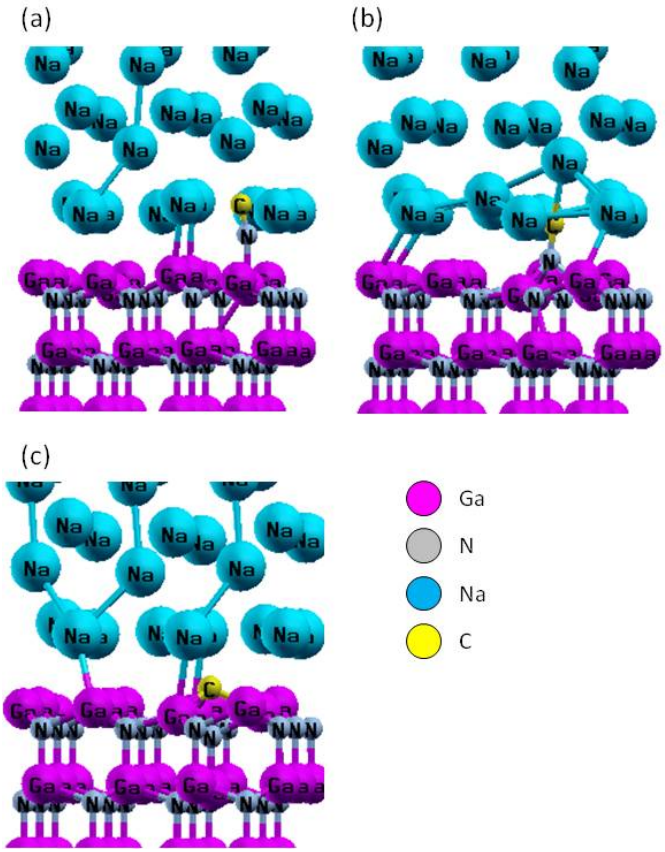

Figure 2 Atomic coordinates after structural optimization calculation. (a) The CN cluster was on a Ga atom. (b) The N atom of the CN cluster bonded to Ga atoms. (c) The N atom of the CN cluster was at the N site in the (0001) surface.

Table 1 Relative total energy and C-N interatomic distance for the carbon-added Na-flux GaN growth shown in Fig 2. The energy for Fig. 2(c) was set to be zero.

	Total energy [eV]	C-N distance [Å]
Fig. 2(a)	0.107	1.20
Fig. 2(b)	1.351	1.36
Fig. 2(c)	0.000	1.70

[1] H. Yamane, M. Shimada, S. J. Clarke and F. J. DiSalvo, Chem. Mater. 9 (1997) 413.

[2] M. Imade, Y. Hirabayasi, Y. Konishi, H. Ukegawa, N. Moyoshi, M. Yoshimura, T. Sasaki, Y. Kitaoka and Y. Mori, Appl. Phys. Express 3 (2010) 075501.

[3] T. Kawamura, H. Imabayashi, Y. Yamada, M. Maruyama, M. Imade, M. Yoshimura, Y. Mori and Y. Morikawa, Jpn. J. Appl. Phys. in press.

15:00 Oral

Processes of dissociative evaporation involved into sublimation growth of bulk AlN crystals

Boris Epelbaum, Octavian Filip, Paul Heimann, Ulrich Seitz, Albrecht Winnacker

CrystAl-N, GmbH, Dr.-Mack-Strasse 77, Fuerth 90762, Germany

e-mail: boris.epelbaum@ww.uni-erlangen.de

Single-crystalline AlN is the best substrate material for high Al content AlGaN-based optoelectronic devices performing in deep UV spectral range. High-purity AlN is optically transparent in UV and closely lattice and thermally expansion matched to the layers needed for the device structure, allowing for low dislocation density in the active region of the device. During last years the feasibility of bulk AlN growth using sublimation growth method at temperatures above 2200 C has been demonstrated by few research teams including our CrystAl-N GmbH (former research group at University of Erlangen; Germany). However, an understanding of sublimation and growth mechanisms of AlN during high-temperature PVT is still quite limited (an example here could be the well-known fact that nobody until now was able to explain very different growth habit of the crystals obtained in different crucibles/hot zone materials).

In his pioneering work [1] G. A. Slack assumed the growing (as well as evaporating) surface of AlN to be covered with a layer of liquid Al metal. This layer captures monatomic nitrogen atoms with unit probability, but it is unable to utilize N_2 molecules, as their dissociation energy is too large. Slack proposed crystal growth rate to be limited by supply of thermally dissociated (active) nitrogen. An interesting model for thermal decomposition of nitrides has been proposed by B. V. Lvov [2]. He succeeded to fit main kinetic characteristics of AlN evaporation considering partial evolution of nitrogen in the form of free atoms according to the equation AlN(s)->Al(g)+0.6N+0.2N2.

In this presentation we will discuss different aspects of dissociative evaporation involved into sublimation growth of bulk AlN crystals and show the influence of liquid Al condensation on the interface of the growing crystal on its morphological stability and crystalline perfection:

(i) Evaporation process inside the charge powder. Evaporation rate in the beginning of the process is strongly different from that of the later stages. Complex character of the initial evaporation stage is the result of superposition of two contrary effects: (1) enhanced evaporation of small particles/sharp corners consumed within the initial process stage and (2) slowed evaporation during the incubation period of accumulation of Al-melt having strong catalytic influence on evaporation process. Charge powder will be shown to be an important source of active (atomic) nitrogen additionally to thermal activation.

(ii) Growth process. Correct prediction of crystal growth rate requires consideration of transport mechanisms relevant for *both* components: aluminium gas and atomic nitrogen (including its recombination into N2). Al-melt accumulation on the growth surface depends on component supply rate and also on growth temperature. Surface diffusion driven by radial temperature gradient appears as an important redistribution mechanism of Al-melt adsorbed on the growing surface.

(iii) Specific crystal defects related to dissociation are bubble-like Al inclusions ranging from sub-micron up to 10 µm in diameter and locally disturbed crystal areas grown under strong excess of bulk Al-melt.

Finally the latest results of successful growth of large (> 2 inch) AlN crystals nearly free of Al inclusions achieved by CrystAl-N GmbH will be presented. The crystals grown in tungsten crucibles are of excellent chemical high purity ensuring their transparency to UV.

[1] G. A. Slack: Aluminum nitride crystal growth, Final Report, Contract No. *F49620*-78-C-0021 (1979)

[2] B. V. Lvov. Thermochimica Acta 373 (2001) 97-124

15:15 Oral

Influence of growth orientation on microstructure of AlN grown by solid-source solution growth (3SG) method

Yoshihiro Kangawa[1], Shunro Nagata[2], Boris Epelbaum[3], Koichi Kakimoto[1]

1. *Kyushu University, Fukuoka, Japan* **2.** *JFE Mineral Co., Ltd., Chiba 260-0826, Japan* **3.** *University Erlangen-Nürnberg, Inst. for Material Science, Martensstr. 7, Erlangen 91058, Germany*

e-mail: kangawa@riam.kyushu-u.ac.jp

Al(Ga)N is a candidate material for an optoelectronic device such as a deep UV-LED (Light Emitting Diode). In order to fabricate the Al(Ga)N device with low dislocation density, it is indispensable to develop a high quality AlN substrate. Recently, bulk AlN with low dislocation density was produced by PVT (Physical Vapor Transport). However, the growth process requires high temperatures exceed 2000ºC. We consider an another possibility, i.e., solution growth, to produce AlN template. Solution growth was generally performed under low temperatures, thus it may reduce the production cost of the crystal. In the present study, we discuss the crystalline quality of AlN grown by our original solution growth method.

In 2011, we have developed a solid-source solution growth (3SG) method which used Li_3N as a nitrogen source instead of N_2 gas [1]. In this method, we can control a nitrogen composition of the source materials, i.e., Al-Li_3N mixture. We confirmed that a 5mm-thick AlN epitaxial layer grew on AlN seed crystal along [1-100] under the condition of Al:Li_3N = 4:1. The TD density in the seed crystal was below the detection limit of TEM analysis. Though dense threading dislocations (TDs) were generated in the initial stage of 3SG (TD density = 10^9 cm^{-2}), it was decreased to 10^8 cm^{-2} at 5mm-thick region. Next, we grew AlN by 3SG on the AlN(0001) substrate which was grown by PVT. In this experiment, the TD density was decreased from 10^9 to 10^8 cm^{-2} at 2mm-thick region. That is, an annihilation ratio of TDs during the growth along [0001] was larger than that in the case of [1-100]. This is due to the difference in annihilation mechanisms of TDs. The TDs were annihilated by forming half-loops when the growth

direction was [1-100]. On the other hand, the TDs were annihilated by forming bundle structures in the latter case. These results imply that the growth along [0001] is better than that along [1-100] to obtain a low dislocation density crystal by 3SG.

Acknowledgement

This work was supported by a JST PRESTO program.

References

[1] Y. Kangawa et al., Appl. Phys. Express **4** (2011) 095501.

15:30 Oral

Achievement and advancement in the hetero-epitaxial growth of AlN single crystals on SiC substrates by PVT approach

Rajappan Radhakrishnan Sumathi, Peter Gille

LMU München, Department of Earth and Environmental Sciences, Crystallography section (LMU), Theresienstr. 41, Munich 80333, Germany

e-mail: sumathi@lrz.uni-muenchen.de

Large-diameter aluminium nitride (AlN) single crystals are essential for producing deep ultra violet light-emitting diodes and laser diodes, which are expected to have a major environmental impact by replacing the presently used toxic mercury lamps, both in water and air purifications. Besides that, currently AlN is also being exploited for its efficient use in the development of new power-semiconductor technology for the electric power grid modernisation or "smart grid". Various growth techniques have been attempted for producing large-diameter, high-quality AlN single crystals namely hydride vapour phase epitaxy, physical vapour transport (PVT) and solution growth methods. Until now, only PVT growth of AlN has been successfully demonstrated for producing bulk crystals with realistic growth rates of hundreds of microns per hour. However, most of the currently available commercial wafers are smaller than 25 mm in size and are in very limited quantities, besides the high cost. We have successfully grown AlN single crystals exceeding 1-inch diameter, on silicon-terminated, both 6H-silicon carbide (SiC) [1], 4H-SiC [2] substrates with very good structural quality by hetero-epitaxial seeding method. Most of the encountered problems in this hetero-epitaxial method namely, cracks (due to thermal mismatch), micro-pipes (propagation from the substrate), 3D-nucleation (preferable spiral growth due to screw dislocation), very high dislocation density (due to lattice mismatch) were effectively mitigated. While the other remaining issues such as presence of low-angle grain boundaries, high incorporation of unintentional impurities, very low electrical conductivity will be addressed in this work. Synchrotron white beam Laue topography was made in the transmission geometry to investigate lattice imperfection. Unintentional silicon and carbon concentration, incorporated from the SiC substrate, was about 1.5 – 2 *wt%* observed on the top part of the grown crystals. Incorporation of these impurities seemed to vary for different facets (*c*-, *r*- and *m*-facets) as revealed by EDX and EPMA measurements and also by different CL intensities.

In this paper, we also present the growth of AlN on the carbon-terminated SiC substrates for obtaining N-polar AlN substrates and to explore the influence of polarity on the properties. But, the growth on C-face was not straightforward because of obvious reasons. Usually our (0001) AlN single crystals were more than 5 mm in thickness, 28 mm in diameter and flat *c*-facets were obtained for all substrate off-orientations. Depending on the off-orientation of the substrate and supersaturation in the gas phase, 3D island nucleation as well as 2D step-flow growth modes were observed. AlN growth on carbon-face SiC was dominated by multi nucleation [Fig.1] and further, an abrupt interface was observed between the AlN layer and the substrate, in contrast to the growth on Si-face, where there was a formation of hexagonal hillocks at the interface. Very high supersaturation resulted in a spiral growth mode even on highly off-oriented substrates and the whole crystal grew as a single spiral [Fig.2], exhibiting a single nucleation centre with well pronounced hexagonal morphology. Broad XRD rocking curves of the sample (FWHM ~ 300 arcsec), indicated a high density of misfit dislocations near the interface and further a 2 cm^{-1} shift of E_2(high) phonon mode in the Raman measurements showed a significant misfit stress. By defect-selective etching with molten KOH:$NaOH_2$ the dislocation density was found to be in the range of (1 – 4) x 10^5 cm^{-2} in the middle of the grown crystal. We will report the detailed results on the morphology and structural imperfection of the crystals grown on C-face SiC substrates. These results will further be presented in comparison with the growth on Si-face SiC.

Fig. 1 Multi nucleation during the hetero-epitaxial growth of an AlN single crystal on C-face SiC substrate

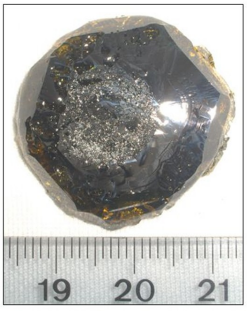

Fig. 2 Single nucleation spiral growth mode of an AlN single crystal on C-face SiC substrate

Reference

[1] R. R. Sumathi, P. Gille, R. U. Barz and T. Straubinger, Phys. Status Solidi C 8 (2011) 2107-2109.

[2] R. R. Sumathi, R. U. Barz, A. M. Gigler, T. Straubinger and P. Gille, Phys. Status Solidi A 209 (2012) 415-418.

WeP-T03
Wednesday afternoon, 14 August, 16:00
Room 105, Old Library

Break
Wednesday afternoon, 14 August, 17:30

Thursday, 15 August

TuO1

T03: Wide bandgap semiconductors
Thursday morning, 15 August, 10:20
Room C, Auditorium Maximum

10:20 Invited oral

Zinc oxide films grown by atomic layer deposition: from material properties to device applications

Grzegorz Łuka

Polish Academy of Sciences, Institute of Physics, al. Lotników 32/46, Warszawa 02-668, Poland

e-mail: gluka@ifpan.edu.pl

Atomic layer deposition (ALD) method, also known as atomic layer epitaxy (ALE), offers very conformal thin film growth over large area substrates at low growth temperatures. These features are caused by two principles, under which ALD operates: a sequentiality of precursor doses and the saturation effect. They also ensure an uniform coverage of porous or nanostructured surfaces by films with precisely controlled thicknesses. ALD is especially useful for deposition of various metal oxides including high-k materials or wide band gap semiconductors such as zinc oxide (ZnO). ZnO films attract a lot of attention in recent years due to their prospective applications in optoelectronics, photovoltaics, transparent electronics or hybrid heterostructures with organic materials. A possibility of applying low deposition temperatures is of great advantage, since the usage of organic or flexible substrates limits a device processing to temperatures well below 200 °C.

In my talk, I will focus on low temperature growth of ZnO films by the ALD method and show how choosing various ALD growth conditions results in ZnO films having different structural, optical and electrical properties. In particular, I will show that electrical properties of ALD-grown ZnO films can be controlled over a wide range of free electron concentrations as well as electron mobilities, measured at room temperature. Depending on this, different applications of ZnO or doped ZnO films in electronic devices, namely as an n-type partner to p-type semiconductors or as a transparent electrode, will be presented.

This work was partially supported by the European Union within the European Regional Development Fund, through the Innovative Economy grant (POIG.01.01.02-00-108/09).

10:50 Oral

Hydrothermal growth of bulk ZnO:Ga crystals and their physical properties

Mengde Ren, Xiaoling He, Yanbin Zuo, Haitao Zhou, Changlong Zhang, Jinliang Wang

China Nonferrous Metal Guilin Geology And Mining Co., Ltd. (CNMC), Guilin 541004, China

e-mail: just.mymail@163.com

To grow high-quality p-type ZnO layers is prerequisite to develop a low-temperature growth technique for high-quality ZnO layers.[1]ZnO:Ga has been known as an ultra-fast scintillator for a long time, but up to now, it has not been used in practice due to the growth difficulties of ZnO:Ga single crysltals.[2]In this paper, a large size ZnO:Ga (*30.44 mm×24.84 mm×5.40 mm*) with high crystalline quality was grown by Guilin hydrothermal method. The growth performed with KOH+LiOH+H_2O_2 as mineralizer and Ga_2O_3 powder for dopant . The growth characterization of ZnO:Ga influenced by concentration of Ga^{3+} and mineralizer was emphatically studied.We also discussed the influence of other factors including PH, temperature of dissolving growth zone and concentration of H_2O_2.A systematic characterization of Ga-doped ZnO was investigated by X-ray diffraction, chemical etching, X-ray rocking curve, inductively coupled plasma mass spectrometry (ICP-MS), and transimission spectrum. The results show that: 1) High-crystallinity product of ZnO:Ga single crysltal(fig. 1(a)) have been synthesized and its FWHM is 11 arcsec of the (002) reflection ofX-ray rocking curvewhich was lower than pure ZnO (fig. 1(b)). 2) ZnO:Ga crystal displays a high transmittance performence among 450-860 nm wavelength, and a total absorption performance in the wavelength range of >1750 nm. 3) ZnO:Ga crystal have a conductivity of 0.36 S/cm. A deeper pragmatic synergism between theory and experiment will greatly aid in developing more application of ZnO crystals.

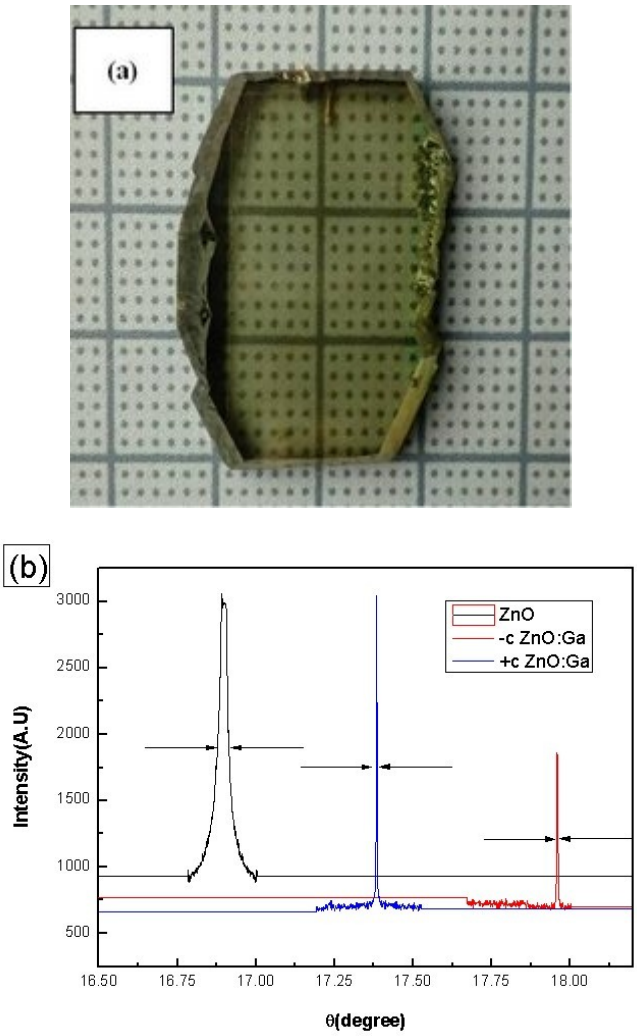

Figure 1: (a). Ga:ZnO single crystal grown by hydrothermal method.(b). X-ray rocking curve of ZnO and Ga:ZnO single crystal.

Acknowledgments:This work was supported by National Natural Science Foundation of China(51102057),GuangxiNaturalScienceFoundation(2013GXNSFBA019262) and Program on technology development of research institute of China (2012EG115007).

* corresponding author e-mail: zyb1976@126.com

References

[1]. S.H.Park, H.Suzukial. Low-temperature groth of high-quality ZnO layers by surfactant-mediated molecular-beam epitaxy [J]. Journal of Crystal Growth ,2007,309:158-163

[2]. E.D.Bourrent-Courchesne, S.E.Derenzo, M.J.Weber. Development of ZnO:Ga as an ultra-fast scintillator[J]. Nuclear Instruments and Methods in Physics Research A 601(2009)358-363.

11:05 Oral

Epitaxial growth and characterization of zinc oxide nanorods obtained by the hydro-thermal method

Łukasz Wachnicki[1], Bartłomiej S. Witkowski[1], Sylwia Gierałtowska[1], Aleksandra Wierzbicka[1], Marek Godlewski[1,2]

1. *Instytut Fizyki PAN, Al. Lotnikow 32/46, Warszawa 02668, Poland* **2.** *Cardinal Stefan Wyszynski University, College of Science, Deptartment of Mathematics and Natural Sciences, Warszawa, Poland*

e-mail: lwachn@ifpan.edu.pl

Zinc oxide which is a II-VI semiconductor with a 3.37 eV direct band gap at room temperature. This material has been extensively investigated in the past years for a large variety of potential applications. For example, it can be used in light-emitting diodes and transistors, or as a transparent conductive oxide in solar cells. ZnO is also a prospective material for sensor technology, where developed surface morphology is very important.

ZnO nanostructures were grown by a hydro-thermal method at extremely low temperature of 50°C. We used deionized water and zinc acetate as an oxygen and zinc precursors, respectively. The gold on the surface nucleates growth of the ZnO nanorods. In reaction we used a mixture consisting of water, zinc acetate and sodium hydroxide. The latter is used as a pH regulator.

We present the influence of the process parameters on the growth of zinc oxide nanorods. The difference in crystalline quality and orientation of zinc oxide nanorods grown on various substrates like a gallium nitride, zinc oxide, silicon and silicon dioxide will be presented. Structural properties of the ZnO nanorods were characterized using X-ray Diffractiometer and Scanning Electron Microscope.

The research was supported by the European Union within European Regional Development Fund through grant Innovative Economy (POIG. 01.01.02-00-108/09)

11:20 Oral

Hydrothermal growth of ZnO nanorods for solar cells applications

Bartłomiej S. Witkowski[1], Łukasz Wachnicki[1], Rafał Pietruszka[1], Sylwia Gierałtowska[1], Grzegorz Łuka[1], Marek Godlewski[1,2]

1. *Institute of Physics, Polish Academy of Sciences, Warsaw 02-668, Poland* **2.** *Cardinal Stefan Wyszynski University, College of Science, Deptartment of Mathematics and Natural Sciences, Warszawa, Poland*

e-mail: bwitkow@ifpan.edu.pl

Zinc oxide is a II-VI semiconductor material that focused a growing interest in various fields such as biology, medicine or electronics. It has a direct energy gap of about 3,37eV at room temperature and high transparency in a visible light spectral region. This semiconductor reveals very special physical and chemical properties, which imply many applications including a active layer or transparent electrode in solar cells or LED diodes. ZnO is also tested for applications in new generations of electronic devices as an active part of transparent transistors and cross-bar memories.

Among many applications, ZnO is also a prospective material for PV and sensor technologies, where developed surface morphology is very important. In this work we present growth of ZnO nano-columns using a new approach to the hydro-thermal method.

We used p-type silicon as a substrate with a thin gold layer (1nm) on the surface. ZnO nanostructures were grown from the water solution at extremely low temperature of 50°C. We used deionized water and zinc acetate as an oxygen and zinc precursors, respectively. The gold on the surface nucleates growth of the ZnO nanorods. In reaction we used a mixture consisting of water, zinc acetate and sodium hydroxide, which act as a pH regulator.

The method is characterized by extremely high growth rate (it takes only few minutes) and simple solution. It allows to regulate orientation and sizes of the ZnO nanorods in a large extent. Due to simplicity and safety of this method, it is suitable for industrial applications. Low costs relate also to the fact that our approach does not require a vacuum, high temperature, pressure, or hazardous chemicals.

In this work we present the properties of nanorods grown using hydro-thermal method for photovoltaic applications. On the nanorods grown on p-type Si we deposited a layer of ZnO:Al as a transparent electrodes using Atomic Layer Deposition method. Thrimetylaluminium was used as aluminum precursor to dope zinc oxide layer. Ohmic contacts to p-Si were deposited by e-beam evaporation. The obtained PV heterostructure, Au/Si/ZnO_{NR}/ZnO:Al showed a clear photovoltaic response. Current-voltage characteristic at 100mW/cm^2 illumination conditions will be presented. The details of the ZnO nanorods growth using hydro-thermal method and photovoltaic response will be discussed.

The research was partially supported by the European Union within European Regional Development Fund through grant Innovative Economy (POIG. 01.01.02-00-108/09).

11:35 Oral

Growth of corundum-structured α-$(In_xGa_{1-x})_2O_3$ alloy thin films on sapphire substrates with buffer layers

Norihiro Suzuki[1], Kentaro Kaneko[1], Shizuo Fujita[2]

1. *Department of Electronic Science and Engineering, Kyoto University, Katsura, Kyoto 615-8510, Japan* **2.** *Photonics and Electronics Science and Engineering Center, Kyoto University, Katsura, Nishikyo-ku, Kyoto 615-8520, Japan*

e-mail: suzuki.norihiro.56z@st.kyoto-u.ac.jp

Corundum-structured gallium oxide (a-Ga_2O_3), due to its expectably high breakdown electric field judging from wide band gap of 5.3 eV, is a novel candidate for high-voltage power devices as well as deep ultraviolet photonic devices. Band gap engineering is the basic requirements for heterostructure device applications, and has basically been achieved by alloying two or more binary semiconductors of the same crystal structure. We have showed the band gap engineering with a-$(AlGa)_2O_3$ from 5.3 to 7.8 eV for Al concentration from 0 to 0.81, keeping well-defined corundum structure [1]. The next target study is the band gap engineering with a-$(InGa)_2O_3$, which has been ready owing to our recent demonstration of a-In_2O_3 grown by the mist chemical vapor deposition (CVD) method [2]. The band gap engineering with these ternary alloys will be followed by the composition control of a-$(AlGaIn)_2O_3$ quaternary alloys, which will achieve a variety of heterostructures with unique properties, like (AlGaIn)N. In this presentation we will show the growth characteristics of a-$(InGa)_2O_3$ alloys.

The growth of α-$(In_xGa_{1-x})_2O_3$ was achieved by using α-Ga_2O_3 buffer layers on c-plane sapphire substrates by the mist CVD method, which is a safe technology with low energy consumption allowing the

growth of high-quality α-Ga_2O_3 [3]. The growth temperature was 500 ^oC. The growth time of an α-Ga_2O_3 buffer layer and α-$(In_xGa_{1-x})_2O_3$ were kept at 1 and 30 minute, respectively. Here gallium(III) acetylacetonate and indium(III) acetylacetonate were used as the sources of Ga and In, respectively.

Fig.1 is the results of XRD measurement of α-$(In_xGa_{1-x})_2O_3$ which has been grown by intentionally changing the In concentration x. The systematic shift of the XRD peaks suggests the successful growth of α-$(In_xGa_{1-x})_2O_3$ alloy thin films with x = 0, 0.05, 0.08, 0.67. Fig 2 shows the band gap and resistivity in terms of the In concentration. The band gap was calculated from the transmittance of the films, and was moderately changed with x. The resistivities were calculated from the value of the sheet resistance meter. The drastic decrease of resistivity was confirmed by slight addition of In (x = 0.05, 0.08) to α-Ga_2O_3, suggesting significant enhancement of semiconductor properties without marked reduction of the band gap. At the conference the detailed electrical and optical properties of α-$(In_xGa_{1-x})_2O_3$ alloy thin films will be shown to discuss their potential for wide band gap device applications.

References

[1] H.Ito, K.Kaneko, and S.Fujita, Jpn. J. Appl. Phys. **51** (2012) 100207.

[2] N.Suzuki, K.Kaneko, and S.Fujita, J. Cryst. Growth **364** (2013) 30.

[3] D. Shinohara and S. Fujita, Jpn. J. Appl. Phys. **47** (2008) 7311.

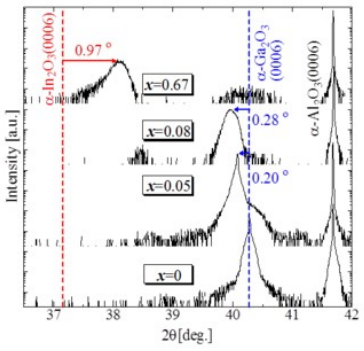

Fig1. XRD 2θ/θ scan profile of α-$(In_xGa_{1-x})_2O_3$

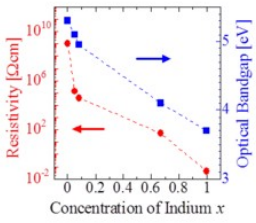

Fig2. Bandgap and resistivities as a function of the indium concentration

11:50 Oral

Nanoporous GaN epitaxial layers grown by Chemical Vapor Deposition

Oleksandr V. Bilousov, Joan J. Carvajal, Xavier Mateos, Rosa Solé, Jaume Massons, Francesc Díaz, Magdalena Aguiló

FiCMA-FiCNA, Universitat Rovira i Virgili (URV), Marceli Domingo s/n, Tarragona 43007, Spain

e-mail: joanjosep.carvajal@urv.cat

Hexagonal gallium nitride (GaN) is considered one of the most important wide band-gap semiconductors for a number of applications in electronics and optoelectronics. Porous GaN, due to its optical and electronic properties, is particularly interesting for developing optoelectronic devices with improved efficiency, such as LEDs with enhanced efficiency and sensors with enhanced sensitivity. Porous GaN has been typically fabricated by (photo)electrochemical and chemical etching methods. These methods generally suffer from a lack of control on the size, morphology and distribution of the generated pores. Thus, the poor reliability and reproducibility of these methods in the production of porous GaN had difficulted up to now the fabrication optoelectronic devices based on porous GaN.

In 2009 we have shown that it was possible to produce nanoporous GaN microparticles in a simple chemical vapor deposition (CVD) system [1] without any secondary etching or chemical treatment after growth in order to generate the porosity. The porosity in these particles is only present on the (0001) face. Recently, we demonstrated that these nanoporous GaN particles can be deposited also on silicon substrates using a metallic catalyst, obtaining porous particles with a low density of defects, as revealed by the emission arising only from the band-edge of the particles obtained in the cathodoluminescence studies [2]. Also, by using this methodology of growth, we demonstrated the formation of low resistivity near ohmic Pt and Au metallic contacts on porous n-type GaN by the formation of intermetallic seed layers through the vapour-solid-solid (VSS) mechanism [3].

Using our method we started studying possibilities of orientation of nanoporous GaN along [0001] crystallographic direction, since it has potential interest for fabrication of LED with higher efficiency. As substrates for oriented growth of nanoporous GaN can be used hexagonal SiC and sapphire, since they crystallize in the same crystallographic systems with relatively small lattice mismatches, and also epitaxial GaN (0001).

Here, we present an important step further in the crystal growth of nanoporous GaN, such it is the epitaxial growth of nanoporous GaN layers oriented along the [0001] crystallographic direction on epitaxial GaN (0001) substrates grown on sapphire substrates. In this way, all the pores of GaN are oriented along the same direction. We found that the lattice mismatch between the substrate and the porous GaN layer, plays an important role in order to obtain a continuous layer or a layer formed by discrete porous microparticles, as can be seen in Figure 1.

The obtained porous GaN layers can be doped with magnesium (Mg) to get *p*-type conductivity, that combined with the inherent n-type of undoped porous GaN allows the fabrication of totally porous *p-n* junctions, with potential application in high brightness unencapsulated GaN-based light emitting diodes and sensors with high sensitivity.

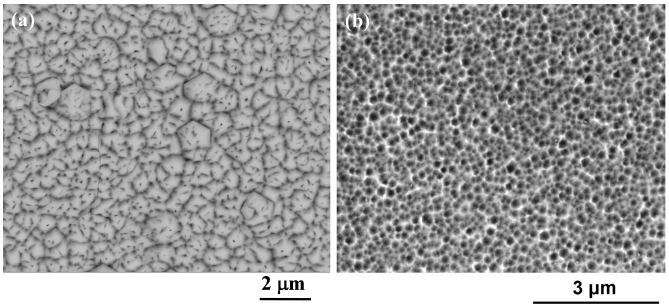

Figure 1. SEM images of epitaxial porous GaN grown on (a) SiC and (b) GaN on sapphire substrates.

Acknowledgements

This work was supported by the Spanish Government under Projects MAT2011-29255-C02-02, TEC2010-21574-C02-02, by the Catalan Authority under Project 2009SGR235 and by the European Union under Project No. FP7-SPA-2010-263044. O.V. Bilousov thanks the Catalan Authority for the funds provided through the FI 2011FI-B-00975 fellowship.

[1] J.J. Carvajal and J.C. Rojo, Crystal Growth Des., 9 (2009) 320.

[2] J.J. Carvajal, O.V. Bilousov, D. Drouin, M. Aguiló, F. Díaz and J.C. Rojo, Microsc. Miocroanal., 18 (2012) 1.

[3] O.V. Bilousov, J. J. Carvajal, D Drouin, X. Mateos, F. Díaz, M. Aguiló and C. O'Dwyer, ACS Appl. Mater. Interfaces 4 (2012) 6927.

12:05 Oral

c-plane GaN selective growth by liquid phase electroepitaxy under atmospheric pressure

Shigeya Naritsuka, Daisuke Kambayashi, Hiroyuki Takakura, Masafumi Tomita, Takahiro Maruyama

Department of Materials Science and Engineering, Meijo University, 1-501 Shiogamaguchi, Tempaku-ku, Nagoya 468-8502, Japan

e-mail: narit@meijo-u.ac.jp

Sodium addition and high ambient pressure are mandatory to grow GaN in the conventional liquid phase epitaxy (LPE). To solve these difficulties, Hussy et al. proposed low-pressure solution growth (LPSG), where GaN is able to grow without the use of Na at atmospheric pressure [1]. The growth rate of LPSG is not high because the solubility of nitrogen is low. Therefore, liquid phase electroepitaxy (LPEE) was applied to improve the growth rate. On the other hand, the selective growth is useful not only for the fabrication of nanostructures but also the dislocation reduction in highly lattice-mismatched heteroepitaxy [2]. In this paper, LPEE is applied to selective growth of c-plane GaN layer using LPSG without the use of Na at atmospheric pressure. The lateral growth over the mask is also attempted by the technique.

GaN template was used as a substrate. Straight line-openings with a width of 20μm and period of 40μm were cut into a W mask on the template substrate in the [11-20] direction. Using a mixture of Ga:Ge = 75:25 as a solution, LPEE was conducted under H_2 ambient at atmospheric pressure. Other growth parameters were set as followings ; the growth temperature of 960°C, the growth time of 20h, the current flow of 4.0A, and the flow rate of NH_3 mixed gas (NH_3:H_2 = 1:99) of 30.0sccm, respectively. The electrodes were immersed into the solution to flow electric current through the solution, as shown in Fig.1. In addition, the bottom electrode was contacted with the W mask on the substrate to uniformly flow the current. The shape and the arrangement of the bottom electrode are shown in Fig.2.

A scanning electron microscope image of the selectively grown GaN layer is shown in Fig.3. The figure shows both a selective growth and a lateral growth was achieved. The white areas in the figure show the side slopes of the selective growth. Then, the area surrounded by the slope is the region where the W mask is appeared. It indicates an excellent selectivity of the growth was performed. On the other hand, a flat place with no white line over the W mask suggests the adjacent grown stripes met together to form a flat area. The lateral growth is thought to enhance by the increased density of the solute over the mask, which was caused by the current flow toward the W mask and the suppression of the growth on the mask. The detailed mechanism of the growth will be discussed at the conference site.

Acknowledgements

This work was supported by Grant-in-Aid for Priority Area (B) (No.22360131) from the Ministry of Education, Culture, Sports, Science and Technology of Japan.

Reference

[1] S. Hussy, E. Meissner, P. Berwian, J. Friedrich, G. Müller, J. Cryst. Growth 310 (2008) 738-747.

[2] For example, G.Bacchin and T.Nishinaga : J. Crystal Growth 208 (2000) 1-10.

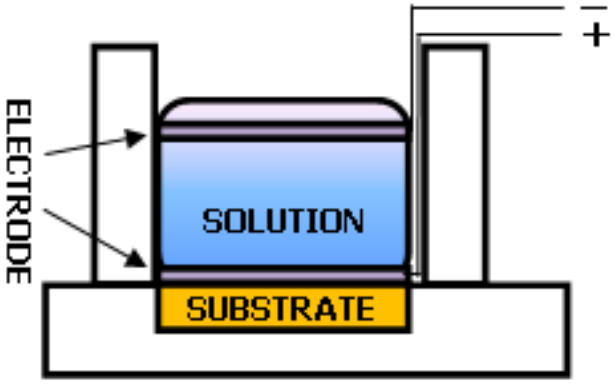

Fig.1 Schematic of LPEE equipment

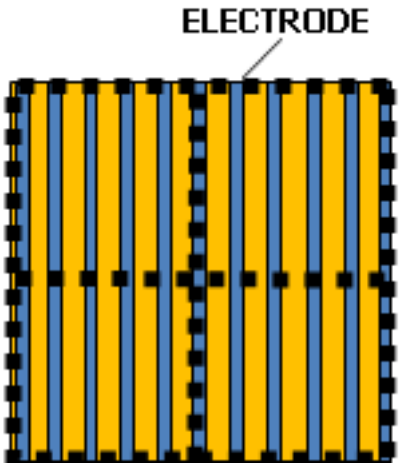

Fig.2 Arrangement of electrode on substrate

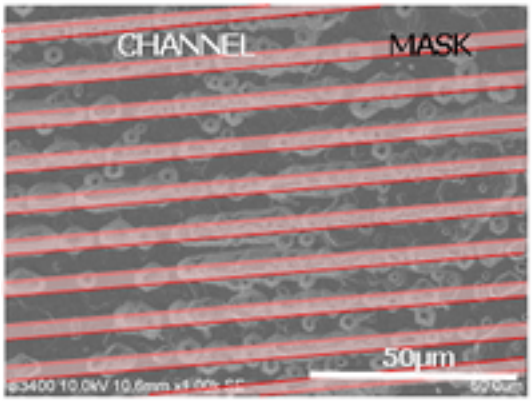

Fig.3 Selectively grown c-plane GaN layer using patterned W mask. The position of the mask are shown by the shaded areas.

Lunch (EMCG meeting)

Thursday afternoon, 15 August, 12:20

TuO2

T03: Wide bandgap semiconductors
Thursday afternoon, 15 August, 14:00
Room C, Auditorium Maximum

14:00 Invited oral

Nucleation and growth of GaN nanowires by molecular beam epitaxy

Lutz Geelhaar

Paul-Drude-Institut (PDI), Hausvogteiplatz 5-7, Berlin 10117, Germany

e-mail: geelhaar@pdi-berlin.de

Growth in the form of nanowires instead of planar films offers the advantage that the interface between adsorbate and substrate is very small and the aspect ratio of the structure is high. Hence, strain induced by mismatch in lattice constant or thermal expansion coefficient can elastically relax at the free sidewalls, and dissimilar materials can be combined in high crystal quality. This advantage is particularly relevant for group-III-nitrides because bulk substrates are still not readily available for this material class.

Already in the late nineties it was discovered that GaN forms nanowires when grown by molecular beam epitaxy (MBE) under suitable conditions [1], i.e. at fairly high substrate temperature (>750°C, higher than for the growth of planar films) and under excess of nitrogen. These nanowires are of excellent structural as well as optical quality [2], and thus very attractive both for fundamental studies and applications such as solid state lighting, sensing, and energy harvesting. Very interestingly, the formation of these nanowires does not require any guidance by a mask or catalyst and is not mediated by droplets or particles at the tips of the nanowires. Also, they can be grown on a number of different substrates including silicon. The aim of this talk is to provide an overview of what we know about the self-induced nucleation and subsequent growth of GaN nanowires by MBE with a focus on recent insights.

In particular, recently we showed that the nucleation of such nanowires can occur spontaneously, i.e. does not require any structural defects or irregularities in substrate morphology [3]. Also, even on an AlN buffer layer of Al-polarity that should lead to the growth of Ga-polar GaN nanowires, we found only N-polar nanowires. Thus, this type of polarity must play an important role for the microscopic growth mechanisms. In addition, a kinetic growth model will be presented that explains why nanowire growth requires effectively N-rich conditions and how the nanowire radius depends on the V/III ratio.

[1] M. Yoshizawa, A. Kikuchi, M. Mori, N. Fujita, and K. Kishino, Japanese Journal of Applied Physics **36**, L459 (1997); M.A. Sanchez-García, E. Calleja, E. Monroy, F.J. Sanchez, F. Calle, E. Muñoz, and R. Beresford, Journal of Crystal Growth **183**, 23 (1998).

[2] L. Geelhaar, C. Chèze, B. Jenichen, O. Brandt, C. Pfüller, S. Münch, R. Rothemund, S. Reitzenstein, A. Forchel, T. Kehagias, P. Komninou, G.P. Dimitrakopulos, T. Karakostas, L. Lari, P.R. Chalker, M.H. Gass, and H. Riechert, IEEE Journal of Selected Topics in Quantum Electronics **17**, 878 (2011).

[3] S. Fernández-Garrido, X. Kong, T. Gotschke, R. Calarco, L. Geelhaar, A. Trampert, and O. Brandt, Nano Letters **12**, 6119 (2012).

14:30 Oral

Impact of substrate microstructure on self-induced nucleation and properties of GaN nanowires grown by plasma-assisted MBE

Marta Sobanska, Kamil Klosek, Aleksandra Wierzbicka, Jolanta Borysiuk, Slawomir Kret, Giorgi Tchutchulashvili, Sylwia Gierałtowska, Elżbieta Lusakowska, Piotr Nowakowski, Zbigniew R. Zytkiewicz

Institute of Physics, Polish Academy of Sciences, Warsaw 02-668, Poland

e-mail: sobanska@ifpan.edu.pl

Recent in-situ studies of growth of GaN nanowires (NWs) by plasma-assisted molecular beam epitaxy on silicon by Hestroffer et al. [1] show that a massive self-induced nucleation of GaN NWs starts only after partial amorphization of the silicon nitride film that inevitably forms on silicon substrate under nitrogen flux. This result indicates existence of a barrier for GaN nucleation on monocrystalline substrate, so creation of nucleation sites (e.g. by partial amorphization of the substrate) seems to be needed to enhance nucleation rate of GaN NWs. To explore this effect in a more details we have compared efficiency of self-induced nucleation of GaN NWs on three different substrates, namely on bare c-oriented sapphire, on Si(111) with a native silicon nitride layer and on Si(111) coated with a thin amorphous Al_2O_3 buffer deposited at low temperature by atomic layer deposition. On all substrates catalyst-free growth of NWs proceeded under the same, highly nitrogen-rich conditions at ~750 ^{o}C [2].

Comparison of nucleation kinetics by RHEED showed that no NWs nucleation occurred on sapphire. This agrees with observation by Geelhaar et al. [3] who have reported that on the crystalline sapphire NWs do not form under any PAMBE growth conditions. Slow GaN nucleation was observed on partially amorphous silicon nitride film naturally created on the surface of Si(111) due to a high affinity of nitrogen to silicon. Finally, significantly enhanced nucleation of GaN NWs was observed on amorphous Al_2O_3 buffer. Post growth analysis by scanning and transmission electron microscopy show separated NWs on a bare silicon whereas high density of GaN nuclei are found between NWs grown on Al_2O_3 buffer (Fig. 1).

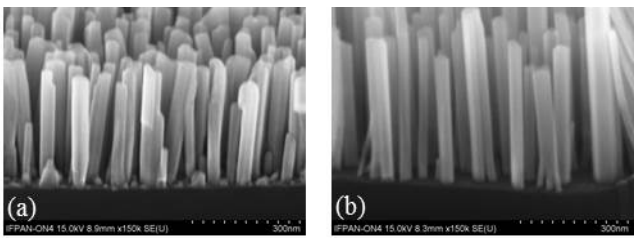

Fig. 1 Cross-section SEM views of GaN NWs (a) on Si(111) substrates with 2 nm thick amorphous Al_2O_3 buffer and (b) on bare Si(111).

Energy electron loss spectroscopy was used to check if creation of any AlN islands that might make GaN nucleation on amorphous Al_2O_3 easier as compared to crystalline sapphire took place in our case. However, precise analysis of oxygen and nitrogen distributions across the GaN/Al_2O_3 interface eliminated such explanation. Instead, we consider defects in Al_2O_3 buffer as possible GaN nucleation sites. Localization of Ga adatoms at these defects should speed up creation of supercritical nuclei and lead to shorter NWs incubation times.

Finally, arrangement on the substrate as well as structural and optical properties of GaN NWs are studied and correlated with microstructure of substrates on which they are grown.

This work was partly supported by the European Union within European Regional Development Fund, through grant Innovative Economy (POIG.01.01.02-00-008/08). MS thanks for support from European Social Fund through Human Capital Program and local authorities (Samorząd Województwa Mazowieckiego - „Potencjał naukowy wsparciem dla gospodarki Mazowsza – stypendia dla doktorantów").

[1] K. Hestroffer et al., Appl. Phys. Lett. 100, 212107 (2012).
[2] A. Wierzbicka et al., Nanotechnology 24, 035703 (2013).
[3] L. Geelhaar et al., Appl. Phys. Lett. 91, 093113 (2007).

14:45 Oral

GaN substrates with variable surface miscut for laser diode applications

Marcin Sarzynski[1], Robert Czernecki[1], Ewa Grzanka[1], Jaroslaw Domagala[2], Mike Leszczynski[1]

1. *Polish Academy of Sciences, Institute of High Pressure Physics (UNIPRESS), Sokolowska 29/37, Warszawa 01-142, Poland* **2.** *Polish Academy of Sciences, Institute of Physics, al. Lotników 32/46, Warszawa 02-668, Poland*

e-mail: sarzyn@unipress.waw.pl

All modern GaN-based optoelectronic devices consist of a stack of epitaxial layers, with different chemical composition and thickness, grown on different kind of native or foreign substrates. In case of laser diodes (LDs), the substrate is always freestanding GaN, preferably with threading dislocation density not exceeding $10^6/cm^2$. For LD structure growth by MOVPE, the substrate crystal must not be exact oriented. Instead, a small off-cut (0.3-0.6 degree) of the surface is needed to maintain the step-flow growth mode.

In case of III-nitride optoelectronic devices, the active region (most often quantum well structure) is made of the ternary compound, InGaN, and adding more indium to the compound lowers its bandgap from 3.5 eV for pure GaN down to about 0.9 eV for InN. Interestingly, for a fixed set of growth parameters (MOVPE), when the off-cut angle of the substrate is increrased, indium content in the layer decreases, respectively. This effect is also present when the off-cut angle is changed only locally (by special patterning technique), in several micrometer sized regions of the substrate.

GaN substrates with differently angled regions can be fabricated using the well known technique for diffraction optics elements fabrication. In our case, it was special laser protholithography, capable of producing multilevel photoresist patterns, and ion etching, see Fig. 1. With this technique we were able to fabricate ridge-waveguide, edge emitting laser diodes with different amount of indium in the QWs (and emitting at different wavelengths) on a single substrate.

In the present paper we will show how the local off-cut angle of the substrate influences LDs parameters such as the wavelength, threshold current and differential eficiency. We will also support the results by AFM and CL measurements. Next, we will show how the discussed substrate patterning technique could be used to obtain multiwavelength laser diode mini-arrays (see Fig. 2a.) and LDs with lower amount of indium near the mirror facet regions (Fig. 2b). In the latter case, we expect less light absorption, less heating and longer lifetime of high-power LDs.

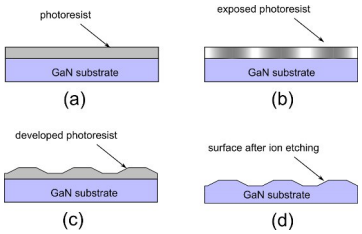

Fig. 1. Process flow for fabrication of GaN substrate with variable off-cut angle. (a) Exact oriented GaN substrate with uniform photoresist layer, (b) photoresist exposed by a laser writer with variable light dose, (c) photoresist profile after development, (d) GaN profile after ion ething.

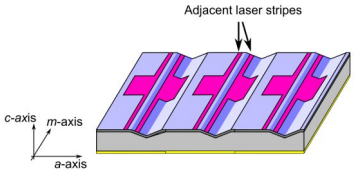

(a)

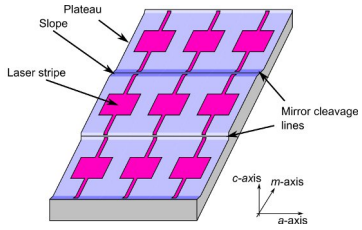

(b)

Fig. 2. (a) Schematic of a laser diode mini-array. Due to different substrate off-cut (and different indium content of the active region), each stripe emits at a different wavelength. (b) Schematic of a single stripe laser diode with non-absorbing mirrors. Due to increased substrate off-cut near the mirror facets, the amount of indium is lower in those regions than in the laser stripe region. Thus, light emitted in the stripe region is not absorbed in the facet region.

15:00 Oral

Plasma-assisted molecular beam epitaxy of AlGaN-based quantum well structures demonstrating spontaneous and stimulated emission in mid-ultraviolet spectral range

Valentin N. Jmerik[1], Dmitrii V. Nechaev[1], Alla A. Sitnikova[1], Valentin V. Ratnikov[1], Yana V. Kuznetsova[1], Evgenii A. Shevchenko[1], Alexey A. Toropov[1], Peter S. Kop'ev[1], Evgenii V. Lutsenko[2], Mikalai V. Rzheutskii[2], Gennadii P. Yablonskii[2], Ahmed Alyamani[3], Sergey V. Ivanov[1]

1. *Ioffe Physico-Technical Institute, RAS, Saint-Petersburg, Russian Federation* **2.** *B.I. Stepanov Institute of Physiscs National Academy of Sci. of Belarus (IF), Independence Av., 68, Minsk 220072, Belarus* **3.** *King Abdulaziz City for Science and Technology (KACST), Riyadh P.O. Box 6086, Riyadh 11442, Saudi Arabia*

e-mail: jmerik@pls.ioffe.ru

We report on development of plasma-assisted molecular beam epitaxy (PA MBE) of AlGaN-based quantum well (QW) heterostructures with high Al-content (>30%), exhibiting spontaneous and stimulated emission within mid-ultraviolet (UV) spectral range. The threading dislocations density in the active regions of the QW structures grown on standard c-Al_2O_3 substrates have been reduced to 10^8-10^9 cm^{-2} through

the optimization of initial growth stage and growth conditions of several-µm-thick AlN buffer layers, incorporation into them ultrathin comressively strained GaN layers, and employing both intentionally and spontaneously formed AlGaN-based superlattices. Special attention is paid to threading dislocation filtering mechanism originated from the latter. Metal-rich PA MBE conditions provided atomically smooth (rms~1 nm) morphology of $Al_yGa_{1-y}N$ (y=0.4-1) barier layers, while the $Al_xGa_{1-x}N$ (y-x=0.1-0.15) QWs were formed by sub-monolayer digital alloying technique. The structures emitted within the spectral range of 230-320 nm under both electron-beam and optical pumping. In addition, it was observed that 2D PA MBE growh led to pseudomorphic comressively-strained AlGaN QW active regions over the relaxed AlN buffer layers, which demonstrated TE-polarized spontaneus and stimulated emissions at minimum wavelengths of 254 and 259 nm, respectively. The compressive stress value achieved in the QWs was found to exceed the calculated elastic stress necessary for preventing the polarization switching from TE to TM mode in the $Al_xGa_{1-x}N$ QW structures with x>0.7. The paper also discusses peculiarities of stimulated emission in the mid-UV spectral range from 259 to ~303 nm, namely its peak position relative to spontaneous emission spectra, the polarization type and degree, the threshold power densities ranging from several MW/cm^2 to few hundreds kW/cm^2, as well as spectral-angular characteristics.

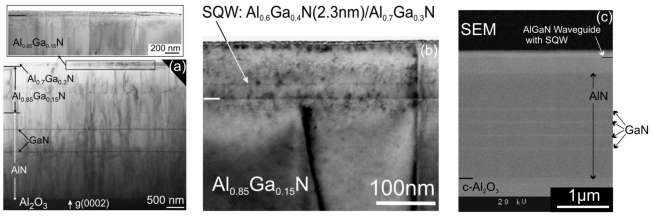

Fig. 1. TEM images of the AlGaN heterostructure on a substrate c-Al_2O_3 (a) and its active region - the waveguide layer QW $Al_{0.60}Ga_{0.40}N$ (2.3nm) / $Al_{0.70}Ga_{0.30}N$ (b). (c)- SEM image of cleaved edge of the AlGaN laser structure on c-Al_2O_3.

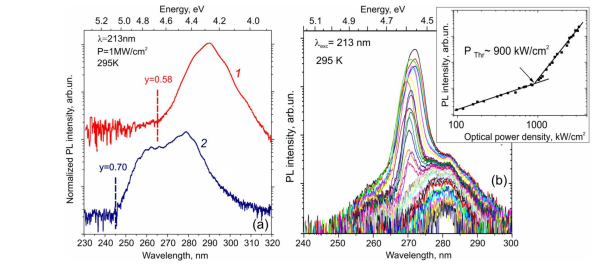

Fig. 2. (a) - PL spectra of the SQW $Al_{0.60}Ga_{0.40}N/Al_{0.70}Ga_{0.30}N$ (*1*) and $Al_{0.7}Ga_{0.3}N/Al_{0.6}Ga_{0.4}N$ (*2*) structures, measured at 295K and power density of 1 MW/cm^2. Dotted lines indicate the energy positions corresponding to the expected values of band gap (*Eg*) of the barrier layers in these structures. (b) - The PL spectra of the AlGaN-based SQW heterostructure measured from edge of a sample at the different excitation levels. The inset shows the dependence of the integrated PL intensity on the excitation level, which was used to measure the threshold power density of stimulated emission.

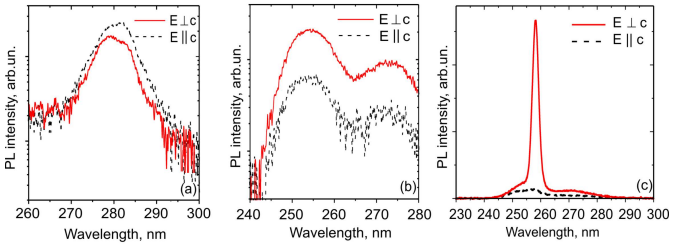

Fig. 3. Polarised PL spectra of spontaneous emission (295K) in the relaxed (a) and pseudomorphical (b) SQW-$Al_xGa_{1-x}N$/AlN(x>0.6) heterostructures grown on standard c-Al_2O_3 substrates.
(c)- stimulated emission spectra of the structure with a spontaneous spectrum presented in (b).
The spectra were measured under marked conditions of excitation.

15:15 Oral

Semipolar GaInN-GaN hetero structures on large area substrates

Ferdinand Scholz[1], Tobias Meisch[1], Marian Caliebe[1], Sabine Schörner[1], Klaus Thonke[2], Willem Van Mierlo[3], Johannes Biskupek[3], Ute Kaiser[3], Sondes Bauer[4], Sergey Lazarev[4], Tilo Baumbach[4]

1. *University of Ulm, Institute of Optoelectronics, Ulm 89069, Germany* **2.** *University of Ulm, Institute of Quantum Matter, Ulm 89069, Germany* **3.** *University of Ulm, Central Facility of Electron Microscopy, Ulm 89069, Germany* **4.** *Synchrotron Facility at ANKA, KIT Karlsruhe, Eggenstein-Leopoldshafen 76344, Germany*

e-mail: ferdinand.scholz@uni-ulm.de

Green light emitting diodes based on group-III nitrides still suffer from fairly low performance as compared to shorter wavelength blue emitters. One possible reason is the lattice mismatch induced strain of the GaInN quantum wells in the active region in such devices having a comparably large In content. This causes the formation of huge piezoelectric fields within the GaInN quantum wells separating electrons and holes locally and hence reducing their recombination probability. By changing the main epitaxial growth direction from the conventional polar c-direction into less polar crystal directions, the internal fields can be strongly reduced. This approach is currently investigated by growing on semipolar GaN wafers cut from thick c-plane material grown by other methods like hydride vapour phase epitaxy or ammonothermal crystal growth. However, owing to the limited size of those c-plane wafers, the semipolar substrates are limited in size to a few square millimetres. On the other hand, approaches to grow semipolar GaN on flat foreign substrates of accurate orientation other than c-plane typically result in highly defective layers. Obviously, growth in c-direction leads to lowest defect densities. Therefore, we currently study some hetero-epitaxial approach where the epitaxial process starts from c-plane-like sidewalls of trenches etched into sapphire wafers. To this end, either n-plane or r-plane sapphire wafers can be used. In both cases, the c-direction is inclined by about 60° from the surface normal. In a later stage, these inclined stripes coalesce forming (10-11) or (11-22) semipolar surfaces for the n-plane and r-plane wafers, respectively. This procedure can be easily applied to large size sapphire wafers. In this contribution, we will describe how to optimize such large area semipolar GaN layers grown by metalorganic vapour phase epitaxy. Similar as for regular c-plane growth, we start with an optimized low-temperature oxygen-doped AlN nucleation layer. After growing few 100 nm GaN, a very thin SiN nanomask layer is deposited in-situ acting as a defect-blocking layer. Hence, excellent semipolar layers have been achieved. Although the (10-11) semipolar planes show a much lower roughness than the (11-22) planes, we found lowest stacking fault densities below 10^4 cm^{-1} on the latter samples. On those surfaces, GaInN multi quantum well structures have been deposited which emit bright luminescence in the green spectral range. We observed a higher In incorporation efficiency on the (10-11) plane as compared to c-plane and (11-22). Moreover, first p-doping experiments revealed a fairly low Mg incorporation efficiency on our (11-22) planes.

15:30 Oral

Pulsed metal organic chemical vapor deposition growth, fabrication, and characterization of nearly lattice-matched InAlN/GaN high electron mobility transistors on sapphire substrate

JunShuai Xue, JinCheng Zhang, Yue Hao

Xidian University, School of Microelectronics (XIDIAN), South TaiBai Road, No.2, Xi'an 710071, China

e-mail: junshuaixue@hotmail.com

As a promising candidate for AlGaN barrier, InAlN-based nitride heterostructures offer a unique opportunity to develop high frequency and high power electronic device, and have been extensively studied in the past five years. In this work, high quality nearly lattice-matched InAlN/GaN heterostructures were successfully grown on sapphire by pulsed metal organic chemical vapor deposition (PMOCVD) based on series optimization of growth parameters, such as growth temperature and pressure, pulse duration and waveform. Simultaneously, the epitaxial growth and material characterization of InAlN/GaN heterostructures give a further understanding of growth mechanism and provide a useful guide to achieve high quality to satisfy diversity of requirements. In addition, high electron mobility transistors (HEMTs) are fabricated on this PMOCVD-grown nearly lattice-matched InAlN/GaN heterostructures, which exhibit a high 2DEG density of 2.15×10^{13} cm^{-2} and electron mobility of 972 cm^2/Vs for the barrier thickness of 13 nm measured by Hall effect in Van der Pauw configuration at room temperature. The processed HEMTs with gate dimensions of $(0.5\times50)\times2$ μm^2 and source-drain spacing of 3.5 μm provide a maximum drain current of 1279 mA/mm, a maximum extrinsic transconductance of 308 mS/mm, and current gain and maximum oscillation cutoff frequencies of 18 GHz and 27 GHz, respectively. For comparison, we also fabricated a conventional AlGaN/GaN HEMT with the same gate geometry and device process, which shows lower maximum drain current of 875 mA/mm and extrinsic transconductance of 198 mS/mm. The remarkably improved device performance is ascribed to the higher sheet carrier density and relatively thinner barrier thickness compared to AlGaN/GaN heterostructures. The obtained results demonstrate the promising potential of PMOCVD approach for applications in InAlN-related electronics' epitaxy. Aggressive shrinking of gate length by adopting advanced electron beam lithograph and reduction of Ohmic contact resistance by optimization of Ohmic contact metals and annealing conditions can be pursued and applied to the future device process to further improve the device characteristics including output drain current density and operation frequency.

15:45 Oral

Absorption and emission spectra of InN/GaN superlattice structures by DFT methods

Pawel Strak[1], Pawel Kempisty[1], Stanisław Krukowski[1,2]

1. *Polish Academy of Sciences, Institute of High Pressure Physics (UNIPRESS), Sokolowska 29/37, Warszawa 01-142, Poland*
2. *University of Warsaw, Interdisciplinary Centre for Mathematical and Computational Modelling (ICM), Pawinskiego 5a, Warsaw 02-106, Poland*

e-mail: strak@unipress.waw.pl

New types of InN/GaN heterostructures obtained by Yoshikawa et al.[1, 2] and Yuki et al.[3] opened new hopes for applications of theses structures for optoelectronic devices operating in the visible optical region. Unfortunately, ambiguity is introduced by the strong local electric field induced by the polarization charge density and the background doping. The detailed model of the absorption and emission spectra in the vicinity of the fundamental gap is therefore of fundamental importance in studying such systems. Systematic studies were conducted to determine an influence of change of the well/barrier width ratio on the physical properties of InN/GaN superlattice system, such as the electric field, polarization charges and polarization dipoles. To overcome the Kohn-Sham band gap (BG) underestimation of experimentally measured values, we have applied two different approaches i.e. empirical LDA+U correction method [4] and a method proposed recently by Ferreira et al., called LDA-1/2 which approximately includes the self-energy of excitations in semi-conductors, providing BG energies, effective masses, and band structures in very good agreement with experimental bulk properties [5]. The results obtained within this two approaches were compared. It was shown that the electric fields depend critically on the well-barrier thickness ratio. The overlap of wavefunctions of electrons and holes is calculated, showing considerable separation in space which significantly reduces the oscillator strength of the optical transitions, and consequently, the optical efficiency of nitride based light emitting diodes (LED) and laser diodes (LD). We have determined the dependence of the absorption spectra edge on the type of structure and also on the carrier concentration. Blue shift of the emission peak has been observed when comparing structures with higher dopants concentration.

[1] A. Yoshikawa, S. B. Che, W. Yamaguchi, H. Saito, X. Q. Wang, Y. Ishitani, E. S. Hwang, Appl. Phys. Lett. **90**, 073101 (2007)

[2] A. Yoshikawa, S. B. Che, N. Hashimoto, H. Saito, Y. Ishitani, X. Q. Wang, J. Vac. Sci. Technol. B, **26**, 1551 (2008)

[3] A. Yuki, H. Watanabe, S. B. Che, Y. Ishitani, A. Yoshikawa, Phys. Status Solidi C **6**, S417-S420 (2009)

[4] A. I. Liechtenstein, V. I. Anisimov and J. Zaane, Phys. Rev. B **52**, R5467 (1995)

[5] L.G. Ferreira, M. Marques, and L.K. Teles **78**(12), 125116 (2008)

Coffee

Thursday afternoon, 15 August, 16:00

TuO3

T03: Wide bandgap semiconductors
Thursday afternoon, 15 August, 16:30
Room C, Auditorium Maximum

16:30 Invited oral

Advance in Epitaxial Growth of SiC for High Power Devices

Jawad Ul Hassan, Louise Lilja, Ian Booker, Ildiko Farkas, Jianwu Sun, Olle Kordina, Peder Bergman, Erik Janzén

Department of Physics, Chemistry and Biology, Linköping University, Linköping 58183, Sweden

e-mail: jawul@ifm.liu.se

Low doped thick epilayers free of basal plane dislocations and with very low density of epitaxial defects are the basic requirements for high power bipolar devices. We have developed fast speed homoepitaxial growth process of 4H-SiC, using chlorinated chemistry (hydrogen+trichlorosilane+propane+HCl) and high growth rate of 100 μm/h.

The growth process is highly suitable for the production of device quality thick layers on 4-inch wafers in considerably short growth time and high reproducibility. The layers grown on 4° off-cut substrates has shown very smooth surfaces, completely free of surface step-bunching and ultra low epi defect density. Also, basal plane dislocation density is reduced to less than 1 cm^{-2} without using any special surface treatment of the substrate prior to the epitaxial growth.

We have also developed on-axis homoepitaxial growth process on 3-inch 4H-SiC wafers using standard chemistry (hydrogen+silane+propane). The major advantage of on-axis epitaxial growth is that epilayers completely free of basal plane dislocations and other epitaxial defects can be obtained. The major issue of the formation of 3C-SiC inclusions was solved through in-situ etching in Si-rich environment and 100% 4H-SiC polytype was obtained in over 100 µm thick epilayers grown at a growth rate of 7 µm/h. However, the surface morphology of the epilayers is not uniform due to surface step-bunching and spiral growth around threading screw dislocations and is not suitable for device fabrication. Epitaxial growth of complete PiN structure along with possible solutions to optimize the surface morphology will also be presented.

17:00 Oral

HCl assisted growth of thick 4H-SiC epilayers by chemical vapour deposition

Christian Ehlers, Birgit Kallinger, Patrick Berwian, Jochen Friedrich

Fraunhofer Institute of Integrated Systems and Device Technology (IISB), Schottkystraße 10, Erlangen 91058, Germany

e-mail: christian.ehlers@iisb.fraunhofer.de

Due to its outstanding material properties, 4H-SiC is well-suited for the production of energy efficient power electronics. Power electronic devices such as bipolar diodes with a high blocking voltage require thick n-type 4H-SiC epilayers with a high minority carrier lifetime [1] and low defect density especially basal plane dislocation (BPD) density. For high quality epilayers, the growth rate is limited to 30 µm/h for the conventional epitaxial process on 4° off-cut substrates. In the transport limited regime, an increase of the growth rate is only possible by increasing the silane partial pressure. However, if Si species supersaturate normal step-flow growth is inhibited and polycrystalline growth is observed. However, by adding hydrogen chloride (HCl) to the process, step-flow growth can be conserved even at growth rates up to 100 µm/h, therefore, making thick epilayers economically feasible [2]. It has been reported [3] that the addition of HCl reduces the concentration of certain point defects which act as recombination centers and hence, increases the minority carrier lifetime. Furthermore, the surface morphology and defects could be optimized by HCl assisted growth [4]. Most of these studies have been performed on 8° and 0° off-cut substrates.

In recent years we optimized extensively our growth process on 4° off-cut substrates with respect to BPD density and suitability of the thick epilayers for production of bipolar devices [5]. This paper investigates the benefits of HCl assisted growth with respect growth rate, surface morphology and minority carrier lifetime.

Therefore, homoepitaxial 4H-SiC epilayer were grown by chemical vapour deposition (CVD) in a horizontal hot wall reactor (Epigress VP508GFR). The epilayers were grown on the (0001) Si-face on substrates with a 4° off-cut towards the <11-20> direction. HCl is added to the conventional CVD growth process of 4H-SiC where silane and propane act as precursors and hydrogen as carrier gas.

The process conditions are described by the Cl/Si, Si/H and C/Si ratios while keeping the growth temperature, reactor pressure and total flow constant. Nominally undoped epilayers as well as nitrogen doped n-type epilayers with a donor concentration of 1×10^{15} cm^{-3} were grown.

The Cl/Si, Si/H and C/Si ratio of the HCl assisted growth was varied systematically on 4° off-cut substrates in order to investigate the surface morphology, BPD density, reduce deep level defects and increase the minority carrier lifetime. Epilayers grown by the conventional process and HCl assisted growth will be compared and tested for their suitability for bipolar devices.

This work was part of the SiC-WinS project funded by the Bavarian Research Foundation (BFS) under contract number AZ-1028-12.

References:

[1] J. Cooper et al.: Proceeding of the IEEE 90 (2002) 0018-9219

[2] H. Pedersen et al.: Chemical Reviews 112 (2012) 2434-2453

[3] L. Calcagno et al.: Journal of Applied Physics 102 (2007) 043523

[4] J. Zhang et al.: Material Science Forum 600-603 (2009) 103-106

[5] B. Kallinger et al.: Journal of Crystal Growth 314 (2011) 21-29

17:15 Oral

Suppression of step bunching generated on 4H-SiC Si-face substrates with vicinal off-angle

Keiko Masumoto[1,2], Kentaro Tamura[1,3], Sachiko Ito[1,2], Kazutoshi Kojima[1,2], Hajime Okumura[1,2]

1. *R D Partnership for Future Power Electronics Technology (FUPET), Onogawa 16-1, Tsukuba 305-8569, Japan* **2.** *National Institute of Advanced Industrial Science and Technology (AIST), Tsukuba central 2, Ibaraki 305-8568, Japan* **3.** *Rohm Co.,Ltd, Kyoto 615-8585, Japan*

e-mail: keiko-masumoto@aist.go.jp

SiC homoepitaxial layers grown on substrates with vicinal off-angle (epi-layers with vicinal off-angle) are effective for suppressing anisotropy of SiC trench devices. Step bunching, however, is easily generated on the substrates with vicinal off-angle during increase in temperature at H_2 atmosphere prior to the growth of the epi-layers. It is indispensable to suppress the generation of step bunching during increase in temperature in order to improve the surface morphology of the epi-layers with vicinal off-angle. It is thought that the etching reactions between the surface of the substrates and H_2 gas should be suppressed in order to suppress the generation of step bunching. In this study, we have investigated the process for suppressing the etching reactions during increase in temperature prior to the growth of the epi-layers.

We used the 4H-SiC Si-face substrates with vicinal off-angle (0.9 deg.). The etching process was conducted in a horizontal hot-wall CVD reactor at a temperature of 1660 °C and a pressure of 10.3 kPa for 1 min. It has been reported that the etching rate is lowered by adding a source gas such as SiH_4 and C_3H_8 and by reducing the flow rate of H_2 [1,2]. Therefore, we investigated the effects of adding SiH_4 and C_3H_8 and of reducing the flow rate of H_2 on the etching depth and the generation of step bunching.

Firstly, we observed a substrate etched by using H_2 of 100 slm. The etching depth was estimated at 7 nm. It has been reported that basal plane dislocations generate giant step bunching with finite length which is called short step bunching (SSB) [3]. We found that SSB, whose height and length was over 5 nm and about 1 mm, respectively, was generated on the substrate. The density of SSB generated on the substrate was about 200 cm^{-2}. Secondly, we investigated substrates etched

by adding each of SiH_4 and C_3H_8. The etching depth of the substrate was decreased to 3-4 nm by adding each of SiH_4 and C_3H_8. The density of SSB was not reduced by adding C_3H_8 but reduced by adding SiH_4. It is thought that both the reduction of the etching depth and the etching in an Si-rich environment are important for suppressing the generation of SSB. Finally, we tried to suppress the etching reactions by reducing the flow rate of H_2 added by SiH_4. The etching depth was decreased to 1 nm by reducing the flow rate of H_2 to 30 slm. As a result, the density of SSB was decreased to 16 cm^{-2} as shown in the Figure.

We have found that the etching reactions between the SiC substrates with vicinal off-angle and H_2 gas were suppressed by adding SiH_4 and reducing the flow rate of H_2 at once. As a result, we have succeeded in drastically decreasing the density of SSB. We will present the detail of the differences between the addition of SiH_4 and that of C_3H_8, and the growth of epitaxial layers using this process at the conference.

Acknowledgement

This work is supported by Novel Semiconductor Power Electronics Project Realizing Low Carbon Emission Society under New Energy and Industrial Technology Development Organization (NEDO).

References

[1] K. Kojima *et.al.*, Mater. Sci. Forum **556-557** (2007) 85.

[2] J. Zhang et.al., Mater. Sci. Forum **389-393** (2002) 239.

[3] K. Tamura *et.al.*, Ext. Abstr. 21st Meeting on SiC and Related Wide Bandgap Semiconductors (2012) 6 [in Japanese].

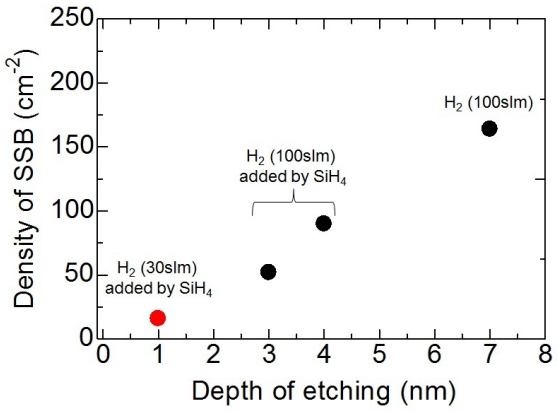

17:30 Oral

C-face epitaxial growth of 4H-SiC on quasi-150mm-diameter wafers

Johji Nishio[1,2], Chiaki Kudou[1,3], Kentaro Tamura[1,4], Keiko Masumoto[1,5], Kazutoshi Kojima[1,5], Toshiyuki Ohno[1,6]

1. *R D Partnership for Future Power Electronics Technology (FUPET), Onogawa 16-1, Tsukuba 305-8569, Japan* **2.** *Toshiba Reserch and Development Center (TOSHIBA), 1, Komukai Toshiba-cho, Saiwaiku, Kawasaki 212-8582, Japan* **3.** *Panasonic Corporation, 700 Tomonobu, Bizen, Okayama 705-8585, Japan* **4.** *Rohm Co.,Ltd, Kyoto 615-8585, Japan* **5.** *National Institute of Advanced Industrial Science and Technology (AIST), Tsukuba central 2, Ibaraki 305-8568, Japan* **6.** *Hitachi, Ltd., 1-280, Higashi-koigakubo, Kokubunji 185-8601, Japan*

e-mail: johji.nishio@toshiba.co.jp

Thick silicon carbide (SiC) epitaxial layers with low background doping are required for high-voltage devices to reduce the maximum electric fields at large reverse biases. SiC {0001} is a polar face, being either silicon-face (Si-face) or carbon-face (C-face). Currently, the Si-face is widely used in research and production of power devices, since the reproducible production of epitaxial layers having background doping levels less than 10^{15} cm^{-3} can be easily realized by using a site-competition technique [1-3].

On the other hand, the C-face of 4H-SiC is considered potentially useful for SiC-MOSFET fabrication, because of the higher inversion channel mobility [4]. Due to the background doping level in the C-face epitaxial layer is higher than Si-face epitaxial layer [2], C-face epitaxial layers are getting less popular when used in higher-voltage application. Accordingly, there has been almost no report on the higher growth rate study by using C-face substrate.

In our current investigation, reduction in background doping level on C-face epitaxial layers was targeted by increasing the growth rate of 4H-SiC film using a multiple-wafer (3x 150 mm-diameter) epitaxy system with a horizontal low-pressure hot-wall reactor [5]. Precursor gases used were monosilane and propane in hydrogen atmosphere. Growth pressure and temperature were kept 6.3 kPa and 1725 ^oC, respectively. The substrate used was n-type (000-1) 4H-SiC 4^o off-cut toward <11-20>. Two 76.5 mm-diameter wafers were aligned in a 150 mm-diameter pocket to cover radial direction of a rotating susceptor wafer plate holder. Figure 1 shows the experimental set-up.

Specular surface was maintained up until the growth rate was 50.9 μm/h when the input C/Si ratio was 0.9. Even when the growth rate was lower than this, outermost position of the wafer became partly frosty in case of making the input C/Si ratio too high or too low. Higher C/Si ratio was found likely to form triangular morphology to retard mirror like surface. Lower than 0.8 in C/Si ratio was found likely to generate silicon droplet also retarding smooth surface growth. The highest growth rate in our system was found limited by morphology deterioration with large density of downfalls. These results were summarized in fig. 2. The uniformity of the film thickness was measured by FTIR and found 2.42% of sigma/mean value on the wafers with the growth rate was 50.9 μm/h. The doping control was found possible with the background level of as low as $4x10^{14}$ cm^{-3} by assuming that residual nitrogen in the atmosphere plays an important role and by reducing it with employing high vacuum process prior to the start of epitaxial growth recipe. Since the formation of in-grown 8H Schokley stacking faults was reported when the SiC epitaxial growth rate was higher [6], photoluminescence imaging was examined with and without the band-pass filter and found that the density of such stacking faults was as low as 0.24cm^{-2}. In addition, surface morphological defects were evaluated using confocal differential interference microscope and the triangular defects were counted. It was found that the defect density becomes larger by increasing the growth rate. However up until the growth rate was within 43.1 μm/h, the triangular defect density was less than 0.32 cm^{-2}.

In summary, epitaxial growth on 4H-SiC C-face substrates with the size corresponding to 150 mm was carried out. As high as 50.9 μm/h was achieved as the growth rate without appearing frosty part on the wafers. High uniformity in the film thickness and low doping level control were satisfied at the same time. Also, there has not been found significant density of defects such as in-grown 8H Schockley stacking faults and surface morphological triangular defects within the range of 43.1 μm/h growth rate.

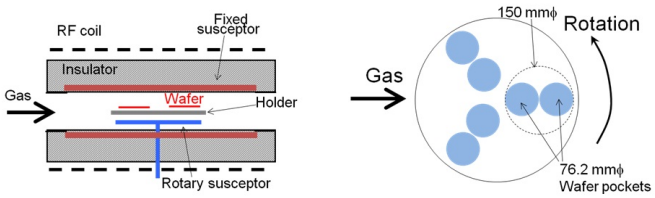

Fig. 1 Experimental set-up used in the present study.

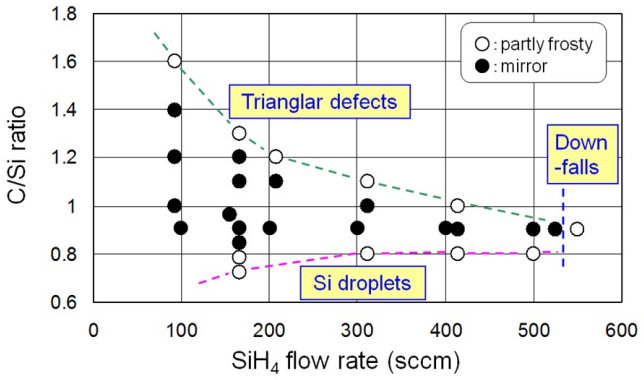

Fig. 2 Surface morphology variation by changing monosilane flow rate and C/Si ratio

Acknowledgements:

This work is supported by Novel Semiconductor Power Electronics Project Realizing Low Carbon Emission Society under Ministry of Economy, Trading Industry (METI) and New Energy and Industrial Technology Development Organization (NEDO).

References:

[1] H. S. Kong, J. T. Glass and R. F. Davis, J. Appl. Phys. 64 (1988) 2672.

[2] T. Kimoto, A. Itoh and H. Matsunami, Phys. Stat. Solidi (b) 202 (1977) 247.

[3] D. J. Larkin, P. G. Neudeck, J. A. Powell and L. G.. Matus, Appl. Phys. Lett. 65 (1994) 1659.

[4] K. Fukuda, M. Kato, J. Senzaki, K. Kojima and T. Suzuki, Mat. Sci. Forum 457-460 (2004) 1417.

[5] C. Kudou, K. Tamura, T.Aigo, W. Ito, J. Nishio, K. Kojima and T. Ohno, Mat. Res. Soc. Symp. Proc. Vol.1433 (2012) H1.2.

[6] S. Izumi, H. Tsuchida, I. Kamata and T. Tawara, Appl. Phys. Lett. 86 (2005) 202108.

17:45 Oral

Study of the effect of doped nitrogen and aluminum on polytype stability during PVT growth of SiC using 2D nucleation theory

Koichi Kakimoto, Takuya Shiramomo, Bing Gao, Frederic Mercier, Shin-ichi Nishizawa, Satoshi Nakano

Kyushu University, Fukuoka, Japan

e-mail: kakimoto@riam.kyushu-u.ac.jp

There are many papers on crystal growth of SiC, which is a promising material for use in devices operating at high temperature, power and frequency. Modified Lely technique is currently the most common method for growth of bulk SiC crystals. More than 200 polytypes of SiC with different properties such as band gap and lattice constant have been reported. Polytype should be controlled to produce SiC with consistent electrical characteristics, especially band gap and doping behavior to control of electronic conduction type. There are many papers discussion on polytype control, particularly the effect of impurity doping on polytype.

The influence of many parameters of crystal growth such as temperature, pressure, supersaturation, vapor-phase stoichiometry, impurities, and polarity of seed surface on polytype stability has been investigated. In this study, we investigated the effects of doping with nitrogen and aluminum impurities on the formation of specific polytypes of SiC during PVT. The classical thermodynamic nucleation theory reported by Fissel was used in conjunction with a global model to analyze the effects of these impurities on SiC polytype. The effect of nitrogen and aluminum as doped impurities on the stability of SiC polytypes (C- or Si-face 4H and 6H substrates) formed by physical vapor transport (PVT) was investigated. The stability of the polytypes was analyzed using classical thermodynamic nucleation theory with numerical results obtained from a global model including heat, mass and species transfer in a PVT furnace. The results reveal that the formation of 4H-SiC was more stable than that of 6H-SiC when a grown crystal was doped with nitrogen using C-face 4H- and 6H-SiC as seed crystals. In contrast, formation of 6H-SiC was favored over 4H-SiC when Si-face 4H- and 6H-SiC seed crystals were used. Meanwhile, the formation of 4H-SiC was more stable than that of 6H-SiC when aluminum was the dopant and C- and Si-faces of 6H-SiC were used as seed crystals. Formation of 6H-SiC occurred over that of 4H-SiC in the cases of C- and Si-faces of 4H-SiC as seed crystals.

18:00 Oral

Growth rate and surface morphology of 4H-SiC crystals grown from Si-Cr-C based solutions under various temperature gradient conditions

Takeshi Mitani[1,2], Naoyoshi Komatsu[1], Tetsuo Takahashi[1,2], Tomohisa Kato[1,2], Toru Ujihara[3], Yuji Matsumoto[4], Kazuhisa Kurashige[1,5], Hajime Okumura[1,2]

1. *R D Partnership for Future Power Electronics Technology (FUPET), Onogawa 16-1, Tsukuba 305-8569, Japan* **2.** *National Institute of Advanced Industrial Science and Technology (AIST), Tsukuba West, 16-1, Onogawa, Tsukuba, Tukuba 305-8569, Japan* **3.** *Department of Materials Science and Engineering, Nagoya University, Furo-cho, Chikusaku, Nagoya 464-8603, Japan* **4.** *Materials and Structures Laboratory, Tokyo Institute of Technology, 4259 Nagatsuta, Midori-ku, Yokohama 226-8503, Japan* **5.** *Tsukuba Research Laboratory, Hitachi Chemical Co., Ltd., 48, Wadai, Tsukuba 300-4247, Japan*

e-mail: t-mitani@aist.go.jp

In recent years remarkable progress has been made in solution growth of 4H-SiC crystals [1-4]. However, slow growth rate and surface roughening during growth are serious problems to be solved for applications of this method for industrial production of very-low-dislocation-density 4H-SiC wafers. Especially, step bunchings of several-hundred-nanometers height are always formed, and which often lead to macroscopic surface defects with incorporation of solvent and parasitic polytypes. Generally, growth rate and surface morphology are strongly influenced by supersaturation of solute elements and also by elemental compositions of alloy solvents. In order to find adequate conditions for high speed bulk growth with keeping a smooth surface, we have

investigated the feature of the solution growth with SiCr and SiCrAl solvents. Since solubility of carbon in $Si_{0.6}Cr_{0.4}$ melt becomes larger than that in pure-Si melt by approximately 20 times, $Si_{0.6}Cr_{0.4}$ melt can satisfys the conditions of high C solubility and low supersaturation. In this paper, we present the growth rate and surface morphology of 4H-SiC grown from Si-Cr-C based solutions under various temperature gradient conditions. In addition, according to our preliminary growth experiments with Si_xAl_{1-x} (x=0.01~0.2) solvents, the decrease in average step-width was observed with the addition of Al to Si solvent. Since the surface modification by Al is expected to promote step-flow growth and possibly reduce macroscopic surface defects, the changes in surface morphology for $SiCr_{0.4}Al_x$ (x=0.01~0.05) solvents were also investigated.

A schimatic illustration of the growth cell is shown in Fig. 1. Temperatures at seed crystals (T_S) and crucibles (T_C) were measured by pyrometers. Solution growth was carried out with $Si_{0.6}Cr_{0.4}$ and $Si-Cr_{0.4}Al_x$ (x=0.01~0.05) at 2050 ºC for T_C. The crucibles were used both as a container for the solvent and as a carbon source. Figure 2 (a) shows the dependence of growth rate on temperature difference (ΔT) between T_S and T_C ($\Delta T=T_S-T_C$). The dependence of growth rate on ΔT in $Si_{0.6}Cr_{0.4}$ melt is approximately 15 times larger than that in pure-Si melt. In Fig. 2 (b), growth rate is shown as a function of supersaturation of C. The supersaturation was calculated from the temperature difference between T_S and T_C refering liquidus curve for Si-C and Si-Cr-C phase diagrams. Figure 2 (b) shows that the growth rate in $Si_{0.6}Cr_{0.4}$ melt is much higher than that in pure-Si melt even for small increase in supersaturation. This indicates that the increase of C concentration in Si-Cr-C solution gives significant contribution on the growth rate. Though the solution growth was carried out under the conditions of higher C solubility and lower supersaturation, as seen in Fig. 3 (a) the surface roughening is still observed in $Si_{0.6}Cr_{0.4}$ melt. By the addition of Al the surface was improved. In $Si_{0.56}Cr_{0.4}Al_{0.04}$ solvent, high growth rate with smooth surface is achieved as shown in Fig. 3 (b). Step-flow growth was promoted very much by the addition of Al. Mechanism of surface modification by Al is now under investigation. Based on the results shown in Figs. 2 and 3, growth of 4H-SiC crystal in 2" diameter has been performed. 4H-SiC crystals in 3 mm-thick were succesfully grown with smooth step-flow surface from Si-Cr-Al-C solution.

Acknowledgement: This work is supported by the Novel Semiconductor Power Electronics Project Realizing Low Carbon Emission Society under the New Energy and Industrial Technology Development Organization (NEDO).

[1] Ujihara et al., Mater. Sci. Forum 717-720 (2012) 351. [2] Yamamoto et al., Appl. Phys. Express 5 (2012) 115501. [3] Daikoku et al., Mater. Sci. Forum 717-720 (2012) 61. [4] Kado et al., Mater. Sci. Forum 740-742 (2013) 73. [5] Komatsu et al. Mater. Sci. Forum 740-742 (2013) 23.

Fig. 1: A schimatic illustration of the growth cell.
Fig. 2: Dependence of growth rate on (a) temperature difference between T_S and T_C ($\Delta T=T_S-T_C$) and (b) supersaturation of C for the growth in Si, SiCr, and SiCrAl solvents.
Fig. 3: Micrographs of 4H-SiC crystals grown in (a) $Si_{0.6}Cr_{0.4}$ and (b) $Si_{0.56}Cr_{0.4}Al_{0.04}$ solvents. Diameters of crystals were 18 mm.

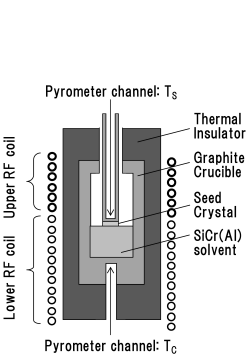

Fig. 1

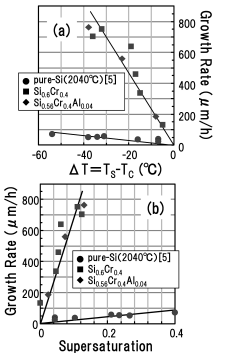

Fig. 2

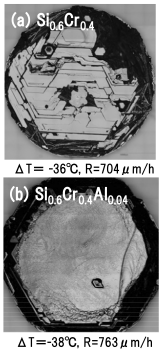

Fig. 3

18:15 Oral

Growth of high quality 3C-SiC on hexagonal SiC seed using TSSG method

Kazuaki Seki[1], Shota Yamamoto[2], Shunta Harada[2], Toru Ujihara[2]

1. *Department of Crystalline Materials Science, Nagoya University, Furo-cho, Chikusa-ku, Nagoya 464-8603, Japan* **2.** *Department of Materials Science and Engineering, Nagoya University, Furo-cho, Chikusaku, Nagoya 464-8603, Japan*

e-mail: seki@sic.numse.nagoya-u.ac.jp

Silicon carbide (SiC) is a promising semiconductor material for fabricating a high voltage power device. SiC has several polytypes such as 3C-SiC, 4H-SiC and 6H-SiC. In particular, 3C-SiC-based MOSFET shows higher channel mobility compared to other polytype because of low density of interface traps between SiO2/SiC [1]. We have developed the bulk growth technique of high quality 3C-SiC using top-seeded solution growth (TSSG) method. For the development, the most important issues were the polytype control of 3C-SiC and the elimination of double positioning boundaries (DPBs). In this paper, we review our trials for them: the kinetic approach of the polytype-selective growth and the elimination of DPBs by utilizing the step advance velocity depending on crystal orientation.

(1) Selective growth of polytype 3C-SiC is often grown on Si, 4H-SiC or 6H-SiC heteroepitaxially because of the lack of a high quality 3C-SiC bulk crystal. However, various polytypes can grow simultaneously during 3C-SiC growth on hexagonal SiC. In this study, we have achieved the selective growth of 3C-SiC single polytype by using the difference of growth rate among the polytepes. On the growth of 3C-SiC on the (0001) plane of hexagonal SiC seed, the 3C-SiC could grow via 2D nucleation mode, whereas the hexagonal polytype could grow via spiral growth mode from screw dislocations in the seed. Each polytype has the supersaturation dependence of growth rate as shown in Figure 1 [2]. This graph means that 6H-SiC preferentially grows in the range of A, and 3C-SiC grows in the range of B. In actual, we demonstrated the 3C-SiC growth regulating the supersaturation in TSSG method. At a higher supersaturation, only 3C-SiC grew on 6H-SiC seed. In contrast, at a lower supersaturation, 6H-SiC overgrew 3C-SiC [3]. Moreover, we performed the bulk crystal growth of 3C-SiC, of which the size 10×10 mm^2 and the thickness is approximately 1 mm in the maximum [4]. The conventional method of growth polytype control, e.g. step-controlled epitaxy [5], is based on the concept of the inheritance of stacking sequence. In contrast, our method based on growth kinetics is quite different from conventional techniques.

(2) Suppression of double positioning boundary Two twinned variants of 3C-SiC can grow on hexagonal SiC (0001) plane and DPBs are formed between them. The DPBs is the critical issue because they

cause a leakage current. When 3C-SiC domain grows by the step-flow growth toward [1-100] of hexagonal SiC, the step of each variant advances toward [11-2] and [-1-12]. The step velocity of each variant is different from each other due to the discrepancy between their atomic structures. Therefore, the grown surface could be covered with the variant of higher step advance velocity as shown in Figure 2. In actual, we performed the 3C-SiC growth on 6H-SiC off-oriented toward [1-100] by TSSG method. Consequently, we obtained the DPB-free 3C-SiC with a range of about 10 mm^2.

This study was supported by a Grant-in-Aid for JSPS Fellows (22·8543), Industrial Technology Research Grant Program in 2007 from NEDO, and Adaptable and Seamless Technology Transfer Program through targetdrive R&D from JST.

Reference

1) H. Uchida et al., Mater. Sci. Forum, **717-720** (2012) 1109,

2) K. Seki et al., J. Cryst. Growth, **335** (2011) 94,

3) K. Seki et al., J. Cryst. Growth, **360** (2012) 176,

4) K. Seki et al., Mater. Sci. Forum, **740-742** (2013) 311,

5) H. Matsunami et al., Mater. Sci. Eng: R, **20** (1997) 125.

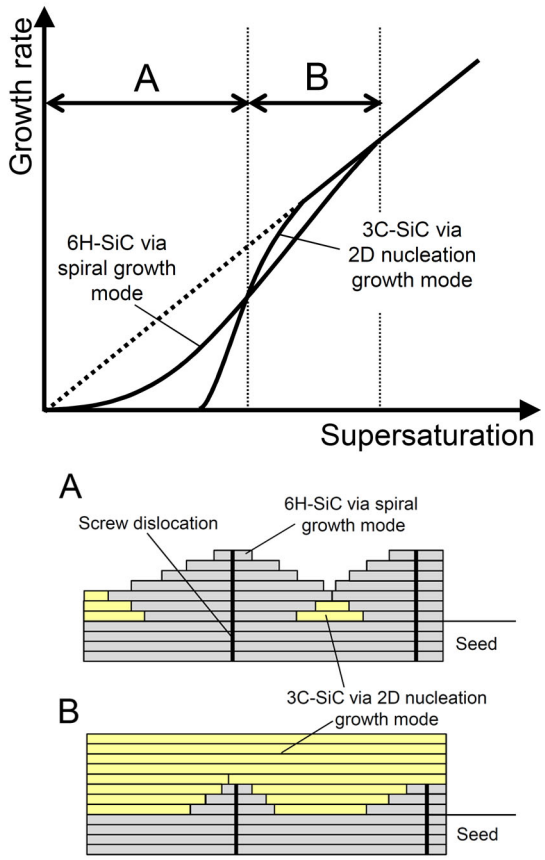

Figure 1. 3C-SiC and 6H-SiC have the different supersaturation dependence of growth rate. The 6H-SiC preferentially grows in the supersaturation range of A, whereas 3C-SiC grows over the 6H-SiC in the range of B.

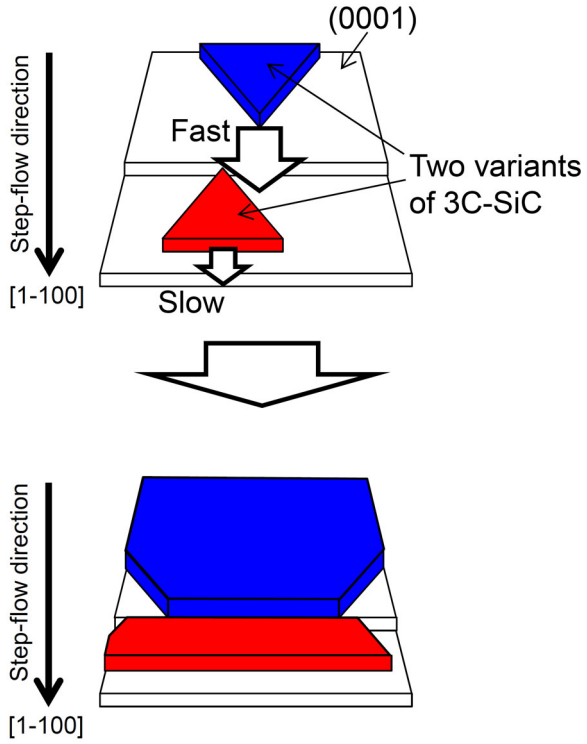

Figure 2. Two variants of 3C-SiC have the different step velocity toward [1-100] of hexagonal SiC seed crystal. The variant growing faster (blue) grows on the other (red).

Break
Thursday evening, 15 August, 18:30

Posters

Wednesday, 14 August

WeP-T03
Wednesday afternoon, 14 August, 16:00
Room 105, Old Library

16:00 Poster We1

Impurity Influence On Polytype Generation At SiC Vapor Growth

Igor C. Avetissov[1], Elena Mozhevitina[1], Andrew Khomykov[1], Valerii Khnykov[2], Yurii Petrov[2]

1. *D.I.Mendeleyev University of Chemical Technology of Russia (MUCTR), Miusskaya sq. 9, Moscow 125047, Russian Federation*
2. *Grannik Ltd., Trubnaya ul.17, build.2, Moscow 127051, Russian Federation*

e-mail: igor_avetisov@mail.ru

SiC crystals are widely used in electronic devices due to their unique properties [1]. Nowadays there is a lot of types of SiC wafers with different polytypes on the market.

In the present research we study the influence of impurity concentration on SiC polytype formation at different growth parameters and source materials. A special procedure of full dissolving of SiC crystals was developed. The solution was analyzed by ICP-MS technique (NexION 300D, Perkin Elmer) with the limits 10^{-10}-10^{-11} g/g, which provided the detection of impurities in crystals 10^{12}-10^{11} cm^{-3}. To detect O, N, F, Cl, Br in bulk crystal with the limits 10^{14}-10^{15} cm^{-3} we used SIMS technique (MiniSIMS, MillBrook).

SiC polytypes were detected by Raman spectroscopy technique.

The research was supported by Ministry of Education and Science of Russia, Contract no. 16.552.11.7046

1. https://www.ecscrm-2012.org

16:00 Poster We2

Substrate orientation, temperature and energetic atomic collisions effects on the structure of GaN films grown by reactive sputtering

Ziani S. Schiaber[1], Douglas M G. Leite[1], Jose R R. Bortoleto[2], Paulo N. Lisboa-Filho[1], Jose H. Dias da Silva[1]

1. *UNESP Univ Estadual Paulista (MAV), Av. Eng. Luís Edmundo C. Coube, 14-01, Bauru SP 17033-360, Brazil* **2.** *UNESP Univ Estadual Paulista (LAPTEC), Av. 3 de Março, 511, Sorocaba SP 18085-180, Brazil*

e-mail: jhdsilva@fc.unesp.br

The recent development of magnetron sputter epitaxy to the growth of high quality GaN films[1] and the incorporation of high concentrations of transition metals to GaN without segregation[2] has brought bold interest to deposition routes using reactive magnetron sputtering. In special this investigation reports on the combined effects of substrate orientation, temperature, and energetic particle collisions on the structure of GaN films deposited using radio frequency (RF) reactive magnetron sputtering. In the process a liquid Ga target was exposed to a plasma, generated from a gas mixture of N_2 and Ar. C-plane and a-plane sapphire and silica glass were used as substrates, with temperatures varying in the 100-1000°C range. X-ray diffraction, optical absorption, atomic force and scanning electron microscopies have been employed to characterize the films. The energy distribution of the species generated in the plasma and colliding with the growth surface were estimated using Monte Carlo based computer simulations.

All films are polycrystalline, presenting wurtzite structure ($P6_3mc$ spatial group), and different degrees of orientation texture with a tendency of the c-axis of the film being perpendicular to the substrate surface. The rocking curves are much sharper (of the order of 1°) on films deposited in the 600-800°C for depositions onto c- and a- plane sapphire substrates, while on amorphous silica the rocking curves remain broad, so the tendency to epitaxy is clearly noticed. An increase on interplanar spacings of different planes (compatible with the increase of both a and c lattice parameters) for depositions at higher substrate temperatures (T_s = 700°C) is observed. It is suggested that the effect is associated with the presence of a high density of self interstitial atoms produced by the incidence of energetic N^+ ions from the plasma and correlates well with the observed redshift of the optical bandgap. The effects of the swelling produced by self interstitials are observed to dominate the structural characteristics of the analyzed films grown at in the 700-1000°C range. The optimization of growth parameters and alternatives to minimize the defects produced by ion collisions in reactive magnetron sputtering are discussed.

[1] M. Junaid, et al. Applied Physics Letters, Vol. 98, 141915 (2011).

[2] D.M.G. Leite, et al. Journal of Crystal Growth. , Vol. 327, p.209 – 214 (2011).

16:00 Poster We3

Evaluation of different baffle geometries in an ammonothermal system by a local numerical 3D model

Jürgen Erlekampf[1], Elke Meissner[1,2], Jan Seebeck[2], Ashwin K. Ghanta[1], Jochen Friedrich[2], Lothar Frey[1,2]

1. *Chair of Electron Devices, Friedrich-Alexander-University of Erlangen-Nuremberg, Cauerstrasse 6, Erlangen 91058, Germany* **2.** *Fraunhofer Institute for Integrated Systems and Device Technology (IISB), Schottkystrasse 10, Erlangen 91058, Germany*

e-mail: juergen.erlekampf@leb.eei.uni-erlangen.de

The ammonothermal synthesis is a promising technology for bulk growth of GaN crystals. According to literature, ammonothermal grown crystals are strain free and often exhibit two orders of magnitude lower dislocation densities compared to other bulk growth methods. To optimize the ammonothermal crystal growth process, detailed knowledge of convection and temperature fields inside the growth autoclave is utmost important, but not well understood so far. Since in-situ analyzing means are difficult to apply under ammonothermal conditions (100-300 MPa, 400-600°C, sc NH_3), CFD calculations for the heat and mass transport become important. However, the few existing numerical simulations are based on axial symmetric calculations even though the flow is expected to be non-symmetrical. Moreover, not even the thermal model as a basis for further calculations was experimentally validated.

As a first toehold an axial symmetric thermal model of a lab-scale ammonothermal autoclave was developed in order to investigate different heater configurations and their influence on the temperature distribution inside the autoclave. This thermal model used in the calculations was validated by special in-situ temperature measurements directly under ammonothermal conditions. The results of the numerical 2D studies were presented elsewhere.

Based on the results of the global thermal 2D simulations of the autoclave, a transient local 3D model was developed for calculation of convective phenomena. The GaN feedstock is considered as a porous medium and was calculated by the Darcy-Brinkman-Forchheimer model. The residual volume is considered as a fluid layer and was solved by a large eddy simulation with a one equation turbulence model. The temperature and flow distribution for different baffle geometries, as well as for different temperature gradients, were investigated, since baffles are used to control the flow pattern in ammonothermal systems. CFD calculations of an inclined baffle construction revealed the formation of a jet stream through the baffle opening depending on the angle.

Generally, large fluctuations of the temperature as well as of the velocities occur, indicating that 3D considerations are absolutely necessary for an accurately evaluation of the heat and mass transport in ammonothermal systems. Further studies will include mineralizers and the mass transport during the crystal growth process.

16:00 Poster We4

Physical properties of unique ZnO single crystals from Oława Foundry

Katarzyna Gas[1], Elzbieta Dynowska[1], Roman Minikayev[1], Andrzej Witowski[2], Krzysztof P. Korona[2], Jean-Francois Morhange[3], Wojciech Zaleszczyk[1], Łusakowska Elżbieta[1], Jarosław Domagała, Anna Reszka[1], Paweł Skupiński[1], Patrick Baroni[4], Łukasz Kilański[1], Anna Dużyńska[1], Rafał Kuna[1], Anthony Bell[5], Wojciech Szuszkiewicz[1]

1. *Polish Academy of Sciences, Institute of Physics, Lotnikow 32/46, Warsaw 02-668, Poland* **2.** *Warsaw University, Institute of Experimental Physics (IEP UW), Hoża 69, Warszawa 00-681, Poland* **3.** *Institut des nanosciences de Paris (INSP), 140 rue de Lourmel, Paris 75015, France* **4.** *Laboratoire Leon Brillouin, CEA-CNRS, CE Saclay (LLB), Gif-sur-Yvette 91191, France* **5.** *HASYLAB at DESY, Notkestr., Hamburg 22607, Germany*

e-mail: kgas@ifpan.edu.pl

ZnO is a wide band-gap semiconductor with unique physicochemical properties. This material is high-energy radiation and ambient atmosphere resistant and is relatively non-toxic to living organisms. ZnO alloyed with transition metals promises an above-room-temperature ferromagnetism and hence wide applicability in semiconductor spintronics. Its high exciton binding energy of 60 meV allows to reduce the lasing threshold and increases the efficiency of ultraviolet luminescence at room temperature. Despite these great advantages, development of ZnO-based electronics is strongly limited by the lack of large crystals of high quality suitable for industry as substrates for the homoepitaxy.

The main goal of this work is a comprehensive investigation of physical properties of ZnO bulk crystals obtained as by-product of zinc white production in Oława Foundry [1]. A very intriguing aspect of these crystals is their sheer size, as far as we know, exceeding the typical size of commercially available ZnO. The crystals which are the subject of this paper are about 1 cm wide and about 12 cm long rods of a hexagonal basis. They are transparent and reddish.

In order to verify the purity of ZnO crystals a number of experimental methods were applied. The energy-dispersive X-ray (EDX) spectroscopy analysis have shown that the crystal consist of Zn and O only (the concentration of possible impurities is below the detection limit of EDX method). The powder X-ray diffraction measurements have demonstrated a hexagonal wurtzite structure of the samples and yielded no additional peaks resulting from possible precipitates or other crystal phases. The crystal orientation was determined by the Laue method. The crystal face parallel to its axis was analyzed at several points along the length of the sample. The investigated face corresponds to a (110) orientation, thus the crystals' axis coincides with the wurtzite c-axis, and the investigated crystal has the same orientation throughout its length. In order to check are the structure properties of investigated single crystals uniform or not the intensity of the Bragg peak 200 was measured in several places along the sample surface on the distance exceeding 10 mm. The analysis of the intensity distribution maps in the reciprocal space demonstrated a very homogeneous distribution of defects and small scattering of the mosaic block orientation in a big sample area. The analysis of the 110 Bragg peak intensity distribution, obtained by the neutron diffraction with the use of modern 2D neutron detector have demonstrated that the sample has indeed a form of a single crystal – see Figure 1(a). In order to determine the linear expansion coefficients for the a and c parameters the X-ray powder diffraction was performed with the use of synchrotron radiation in the temperature range from 15 K to 1100 K at Hasylab (the diffraction pattern obtained at 20 K is exemplified in Figure 1 (b)).

Samples were characterized by various optical methods: photoluminescence (PL), cathodoluminescence (CL), Raman scattering (RS), and optical absorption (OA). The as grown crystals have strong red absorption that can be related to Fe or Mn impurities. The PL spectra have exhibited broad defect-related green luminescence (GL) band – see Figure 2. The GL band is very wide, indicating a presence of a variety of defects in these crystals. The room temperature time-resolved PL have revealed that the life-time of near band-gap luminescence (NBL) and GL is 60 – 110 ps and 6 – 12 ns, respectively. Short lifetime of NBE indicates fast recombination on defects. The single-phonon excitations were studied by the infrared reflectivity and by the first-order RS. Infrared plasma reflection measurements yielded the magnitude of the electron concentration of 2.7 x 10^{16} cm^{-3} what was roughly confirmed by the Hall effect measurements.

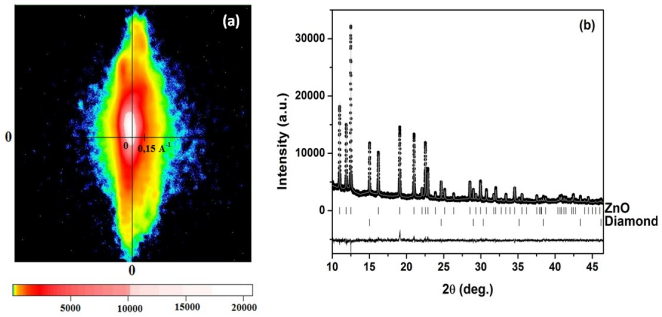

Figure 1. (a) The intensity distribution for 110 Bragg peak for the whole crystal obtained by the neutron diffraction with the use of a 2D detector. (b) Rietveld refinement plots for ZnO sample at 20 K. The observed data are indicated by dots and the calculated ones by the solid gray line. The vertical bars mark the positions of Bragg reflections, whereas the lower curve represents the difference between the observed and calculated powder diffraction patterns. The used X-ray wavelength was about 0.53836 Å.

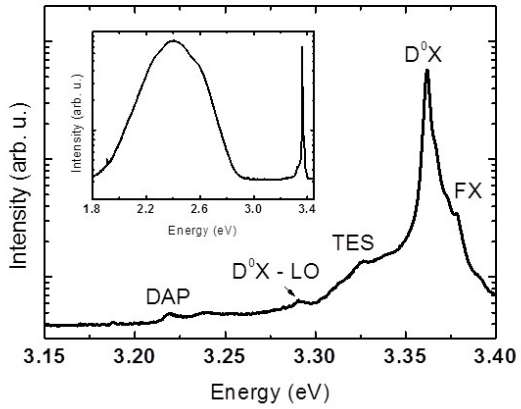

Figure 2. The photoluminescence spectrum of ZnO crystal at T = 5 K.

The studies were partially supported, by the European Union within the European the European Regional Development Fund, through grant Innovative Economy (POIG.01.01.02-00-008/08), and by the Polish National Science Centre grant No: DEC-2011/03/B/ST3/02664. Portions of this research were carried out at the light source DORIS III at DESY, a member of the Helmholtz Association (HGF). This work was partially supported by EC under contract II-20100155.

[1] J.W. Nowak R.S.W. Braithwaite, J. Nowak, K. Ostojski, M. Krystek, W. Buchowiecki, *Journal of Gemmology***30**, 257 (2007).

16:00 Poster We5

Growth of zinc oxide and dielectric films using Atomic Layer Deposition method from organic precursors

Sylwia Gierałtowska[1], Łukasz Wachnicki[1], Bartłomiej S. Witkowski[1], Elżbieta Guziewicz[1], Marek Godlewski[1,2]

1. *Polish Academy of Sciences, Institute of Physics, al. Lotników 32/46, Warszawa 02-668, Poland* **2.** *Cardinal Stefan Wyszynski University, College of Science, Deptartment of Mathematics and Natural Sciences, Warszawa, Poland*

e-mail: sgieral@ifpan.edu.pl

Thin films of ZnO and high-k oxides are materials with a wide range of technological applications that are extensively studied to optimize their physical characteristics and growth processes. Properties of these oxides have dramatically increased the interest to apply their as insulators in electronic devices, resistance switching materials in semiconductor memories, optical coatings in lasers or microscopes and barrier, compact or active layers in photovoltaic structures. We report on growth of zinc oxide (ZnO), hafnium dioxide (HfO_2), aluminum oxide (Al_2O_3) and zirconium dioxide (ZrO_2) thin films on n-Si and amorphous glass substrates using the Atomic Layer Deposition (ALD) technique with all the method-related controls of the growth parameters (growth temperature, pulse length, number of cycles, etc.). The properly selected growth parameters allowed deposition of homogeneous thin films with precisely controlled thickness and low concentration of defects from organic precursors (diethylzinc, tetrakis(dimethylamido)hafnium, trimethylaluminum and tetrakis(dimethylamido)zirconium) as metal precursors and de-ionized water as an oxygen precursor at low temperature in the range of 60–350° C. We studied the effect of growth temperature, number of cycles and post-deposition annealing on growth rate, structural and electronic properties and increase of defect concentration. Crystallization and increasing surface roughening were demonstrated, but were not observed a noticeable growth rate change with increasing film thickness. Our research lead to preparation of good quality thin films with properties as required for transparent electronic and photovoltaic applications.

The research was financially supported by the European Union within European Regional Development Fund through grant Innovative Economy (POIG.01.01.02-00-108/09) and by the National Science Centre (decision No. DEC-2012/06/A/ST7/00398).

16:00 Poster We6

A study on n-type doping of β-Ga_2O_3 layers grown by MOCVD

Daniela Gogova, Guenter Wagner, Michele Baldini, Klaus Irmscher, Martin Schmidbauer, Roberto Fornari

Leibniz Institute for Crystal Growth (IKZ), Max-Born-Str 2, Berlin 12489, Germany

e-mail: daniela.gogova@ikz-berlin.de

Although known since decades, only recently III-sesquioxides have received attention as a new class of wide-band-gap semiconductors. In the past polycrystalline highly doped In_2O_3:Sn was actually used as high-conductivity material for transparent electrodes in "smart windows" [1], photovoltaics [2] and chemical sensors [3]. Nowadays, the research is focusing on single-crystalline oxide layers with low defect densities and semiconducting behavior. β-Ga_2O_3 is the most attractive representative of this class of materials due to the large band-gap (4.9 eV) and high break-down field (8 MV/cm) promising applications in transparent electronics [4], short wavelength photonics, optoelectronics, etc.

We recently started a research program aiming at depositing epitaxial thin films of β-Ga_2O_3 on sapphire (0001) and also on native Ga_2O_3 substrates. Low-pressure MOCVD, with trimethylgallium as a source of gallium and water vapors as a source of oxygen, was employed for this study. The thickness of the samples was varied in the 80-250 nm range. For optimal growth a temperature 800°C was selected. Different structural, compositional and optical methods were employed to characterize the properties of the material grown. The MOCVD-grown epitaxial films are very pure and insulating owing to the large band gap of β-Ga_2O_3. To make them semiconducting, impurities such as Sn or Si have to be incorporated on Ga sites. We have chosen to study the behavior of Si since the Si atomic radius is smaller than that of Sn, which should favor its incorporation. In the literature however the Si-doping is discussed controversially [5,6], although there is some consensus that Si substitutes Ga in the crystal lattice. A parallel activity at IKZ on bulk β-Ga_2O_3 grown by the Czochralski method evidenced that single crystals were contaminated by Si from the growth environment or residual in the Ga_2O_3 source powder [7]. The crystals were *n*-type with an electron concentration in the range from $5x10^{16}$ cm^{-3} to $5x10^{17}$ cm^{-3}.

The present study aims at checking the Si doping potential in the MOCVD process. As silicon source we have taken tetra-ethyl-orthosilicate since it is well-developed for SiO_2 dielectric thin films growth. By adjustment of Ga to Si molar fraction ratios, a series of β-Ga_2O_3 epilayers with Si in the range from 10^{16} to 10^{19} cm^{-3} (determined by SIMS) were prepared. Hall effect measurements performed at room temperature demonstrated that the resulting material was not conductive. SIMS shows that Si is physically incorporated in the films homogeneously but it is obviously not electrically active. To activate the Si species the epitaxial layers were additionally annealed at temperatures from 800 to 1000°C with steps of 50°C. The structural, optical and electrical properties for as-grown and annealed samples have been studied in detail by different characterization methods. The interplay between temperature regimes, structural, optical and electrical properties will be discussed.

References:

[1] D. Gogova, L. -K. Thomas and B. Camin, Thin Solid Films 517 (11) 3326 (2009).

[2] J. Herrero, C. Guillén, Thin Solid Films 451–452 (2004) 630.

[3] P. Sowti Khiabani, E. Marzbanrad, C. Zamani, R. Riahifar, B. Raissi, Sensors and Actuators B: Chemical, 166–167 (2012) 128.

[4] J. Wager, Science 300 (5623) (2003) 1245.

[5] Encarnación G. Víllora, Kiyoshi Shimamura, Yukio Yoshikawa, Takekazu Ujiie, and Kazuo Aoki, Appl. Phys. Lett. 92, 202120 (2008).

[6] Kenichiro Takakura, Suguru Funasaki, Isao Tsunoda, Hidenori Ohyama, Daisuke Takeuchi, Toshiyuki Nakashima, Mutsuo Shibuya, Katsuya Murakami, Eddy Simoen, Cor Claeys, Physica B: Cond. Matter 407 (2012) 2900.

[7] K. Irmscher, Z. Galazka, M. Pietsch, R. Uecker, and R. Fornari, J. Appl. Phys. **110**, 063720 (2011).

16:00 Poster We7

Growth of thick InGaN by Hydride Vapor Phase Epitaxy

Takahide Hirasaki, Masato Ishikawa, Hisashi Murakami, Yoshinao Kumagai, Akinori Koukitu

Tokyo University of Agriculture and Technology, Department of Applied Chemistry (TUAT), 2-24-16 Naka-cho, Koganei, Tokyo, Japan, Tokyo 184-8588, Japan

e-mail: 50012832701@st.tuat.ac.jp

InGaN ternary alloys are exhaustively investigated as potential materials for high efficiency optical devices such as light-emitting diodes (LEDs) and laser-diodes (LDs) operated from infrared (IR) to ultraviolet (UV) spectrum range. Generally, MOVPE growth is employed to grow InGaN layer on GaN layer. It is well known that high efficiency of LEDs using InGaN is realized at blue spectrum region and the luminous efficiency decreases with increasing emitting wavelengths. This is because the degradation of crystalline quality is caused by increasing the In composition. In addition, it is difficult to obtain compositional uniform InGaN layer with high In content due to its compositional unstable nature in MOVPE [1]. Therefore, it is essential to fabricate a high crystalline quality thick InGaN layer and to use it as initial substrate for InGaN-related devices.

On the other hand, it is expected that hydride vapor phase epitaxy (HVPE) can control In composition over entire compositional range without inhomogeneity and grow InGaN thick layer due to its high free energy change of the formation [2]. In this work, the growth of InGaN by HVPE was investigated.

InGaN epitaxial layers were grown by a horizontal atmospheric-pressure HVPE system. C-plane freestanding GaN substrate was used as an initial substrate. N_2 was used as a carrier gas. $InCl_3$ and $GaCl_3$ were used as the group III source precursors, which were generated by the reactions between metallic Ga and In, and Cl_2 in the upstream region of the reactor [3]. NH_3 was mixed with the group-III precursors at deposition zone. InGaN grown layers were characterized by X-ray diffraction (XRD), scanning electron microscopy (SEM) and photoluminescence (PL) measurements.

Figure 1 shows 2θ-ω mode XRD profiles of InGaN grown on GaN substrate at various group-III input partial pressures. It is clear that InGaN layers can be epitaxially grown on GaN substrate without metal droplet under all growth conditions. Though the input concentration of the group-III was changed, In solid composition was kept constant approximately at 0.15, where In solid composition of grown InGaN layer was estimated by (0002) peak in XRD 2θ-ω measurement using vegard's low. Figure 2 shows the dependence of growth rate as a function of group-III input partial pressure. The growth rate of InGaN linearly increases with increasing the group-III input partial pressure. These results imply that InGaN growth is limited by the mass-transport of precursors under these conditions. The growth rate of 15.6 μm/h was obtained in this growth system, which was over hundred times faster than that by MOVPE.

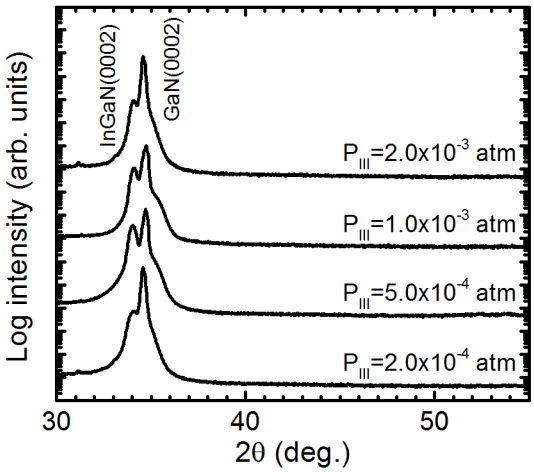

Figure 1 2θ-ω mode XRD of InGaN layers grown on GaN substrate at various group-III input partial pressures

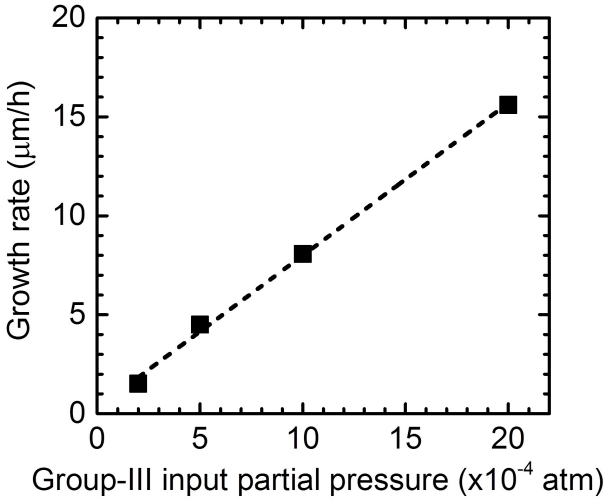

Figure 2 Dependence of growth rate on group-III input partial pressureReference

[1] A. Koukitu and H. Seki, J. Cryst. Growth, **189/190** (1998) 13-18.

[2] Y. Kumagai *et al*., J. Cryst. Growth, **231** (2001) 57-67.

[3] K. Hanaoka *et al*., J. Cryst. Growth, **318** (2012) 441-445.

16:00 Poster We8

Crystal orientation variation of nonpolar AlN films grown with III/V ratio on r-plane sapphire substrate by plasma-assisted molecular beam epitaxy

Le Duy Duc, Nguyen Hoang Thanh, Soon-Ku Hong

Chungnam National University (CNU), Yuseong, Daejeon 305-764, Korea, South

e-mail: soonku@cnu.ac.kr

Aluminum nitride (AlN) has a direct band gap exceeding 6 eV, so it is a promising material for light-emitting devices (LEDs) with ultra-short wavelengths[1]. Conventional AlN are grown on polar c -plane, especially commercial products. In this case, due to spontaneous/piezo-electric polarization of wurtzite structure, large internal electric field

is induced along the [0001] direction, which spatially separates electrons and holes to degrade the performances of devices. Furthermore, due to the strong polarization, the a-plane AlN LED showed strong emission along the surface normal, while the conventional c-plane AlN LED showed weak emission along the surface normal[2]. To obtain higher efficiencies, research on nonpolar AlN is necessary due to the suppression of built-in electrostatic fields in the polar direction.

This study reports the growth of nonpolar AlN films on r-plane sapphire substrate by plasma-assisted molecular beam epitaxy (PAMBE) with different III-V ratio. Sapphire substrates of r-plane orientation were cleaned by organic solvents and thermally cleaned in UHV. The growths of main AlN films were started after a substrate-nitridation step at 860 °C. The effects of III-V ratio on the films were characterized by reflection high energy diffraction (RHEED), atomic force microscopy (AFM) and high-resolution x-ray diffraction rocking curves (XRCs). RHEED in-situ observation showed that these films had two crystal orientations or only one crystal orientation depended on the III-V ratio. The higher III-V ratio growth condition prefers a-plane AlN films growth direction. More interesting, in only one growth process, there could be a change from two crystal orientations to one crystal orientation of AlN film and vice versa. From the AFM results, the AlN film which was grown with higher III-V ratio provides smoother surface and smaller grains. The crystal qualities of these films were compared based on the full width at half maximum values measured by XRCs. The a-plane AlN film grown in higher III-V ratio has better crystal quality. It is opposite to the case of c-plane AlN grown on c-plane sapphire in the same condition of our survey.

References

[1] J. Li et al., Appl. Phys. Lett. 83, 5163-5165 (2003).
[2] Y. Taniyasu et al., Appl. Phys. Lett. 96, 221110 (2010).

16:00 Poster We9

Zinc oxide wire-like thin films as nitrogen monoxide gas sensor

Nguyen L. Hung, Hyojin Kim, Soon-Ku Hong, Dojin Kim

Chungnam National University (CNU), Yuseong, Daejeon 305-764, Korea, South

e-mail: hyojkim@cnu.ac.kr

Recent anthropogenic environmental destruction and ecological crisis are urgently demanding relevant gas sensors for detecting various harmful air pollutants including carbon oxides and nitrogen oxides. In the field of solid-state gas sensors, chemiresistive gas sensors based on semiconducting metal oxides have been extensively investigated since the observation of the gas sensing effect in zinc oxide (ZnO) films via a change in electrical resistivity for a variation of the gas composition by Seiyama et al. as early as 1962. Among useful semiconducting metal oxides as sensing materials, tin oxide and zinc oxide are known to be two of the most reliable materials in the fabrication of semiconducting metal oxide gas sensors for the detection of various gases. Here, our attention is focused on the detection of nitric oxide (NO) because the NO gas is an air pollutant produced by cigarette smoke, automobile engines and power plants. In this study, we report the NO gas sensing properties of the polycrystalline ZnO wire-like films synthesized by thermal oxidation of sputtered Zn nanowire films in dry air. Structural and morphological characterization reveal that we synthesize polycrystalline hexagonal wurtzite ZnO films of a wire-like nanostructure with a width of 100-150 nm and a length of several microns. It is found from the gas sensing measurements that the ZnO wire-like thin film gas sensor shows a significant high response with a maximum value of 29.2 for 2 ppm NO at 200 ºC as well as a reversible fast response to NO with a very low detection limit of 50 ppb. In addition, the ZnO wire-like thin film gas sensor also displays the NO-selective sensing response for NO, O_2, H_2, NH_3 and CO gases. Our results illustrate that the polycrystalline ZnO wire-like thin films are potential sensing materials for the fabrication of NO-sensitive high-performance gas sensors.

16:00 Poster We10

MBE growth of GaN nanowires on Si(111) substrates for gas sensor applications

Kamil Klosek[1], Marta Sobanska[1], Zbigniew R. Zytkiewicz[1], Anna Reszka[1], Renata Kruszka[2], Krystyna Golaszewska[2], Maciej Setkiewicz[3], Tadeusz Pustelny[3]

1. *Polish Academy of Sciences, Institute of Physics, Lotnikow 32/46, Warsaw 02-668, Poland* **2.** *Institute of Electron Technology (ITE), al. Lotników 32/46, Warszawa 02-668, Poland* **3.** *Silesian University of Technology, Gliwice 44-100, Poland*

e-mail: klosekk@ifpan.edu.pl

Nanowires (NWs) made of GaN and related group III-N alloys, having a huge potential for new devices, attract much attention recently. The GaN-based materials are very thermally and chemically stable. This makes them very suitable for operation in chemically harsh environments. Therefore, wide band-gap group III nitride compound semiconductors are alternative options to supplement silicon, in particular in chemical sensor applications [1].

The aim of this paper is to report on our developments in plasma-assisted MBE growth of GaN NWs on Si(111) substrates and on their application in gas sensors. Two types of growth procedures were used to prepare GaN NWs structures. The first one, standard catalyst-free MBE growth at N-rich conditions, resulted in a dense ensemble of GaN NWs being ~400 – 500 nm long with diameter of 20 – 30 nm (see Fig. 1). They were homogenously distributed and well oriented with the c-axis being perpendicular to the substrate. Density of nanowires was quite large. Therefore, even a small tilt of some of them, estimated from XRD to be below ±2°, led to a partial coalescence in upper parts of NWs. In the second procedure, after growth of ~1 μm long NWs the conditions were changed to Ga-rich by increasing the Ga flux and reducing growth temperature. As the result the NWs were overgrown with a planar GaN layer (see Fig. 2).

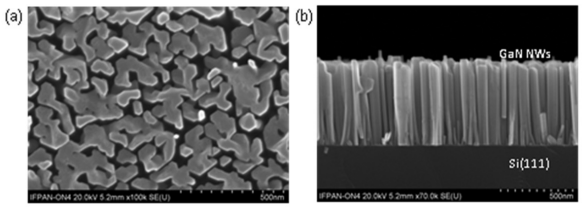

Fig.1: SEM images, plan view (a) and cross-section (b) of GaN NWs on Si(111) sample.

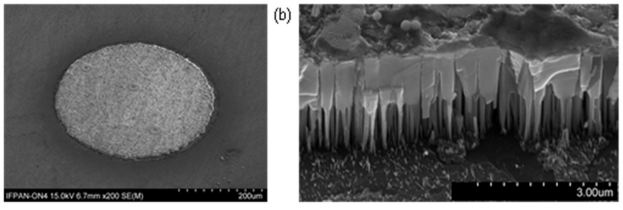

Fig.2: SEM images, plan view (a) and cross-section (b) of mesa-type sensor device based on fully overgrown GaN NWs.

Two types of GaN NWs based gas sensors were fabricated. For the planar device samples with ensemble of GaN NWs grown on semiinsulating Si(111) substrates were used. Then, Ti/Al/Au electrical con-

tacts having diameters of 400 μm were defined on the surface by standard photolithography and lift-off processes and annealed to form low resistance source and drain electrodes. Since NWs were closely packed thin bridges connecting them were created in the active area of the device between the electrodes. In vertical sensor devices electrical resistivity *along* the NWs, *not across* the NWs as in a planar geometry, is measured. In such a case, we used conductive Si substrate and overgrowth of NWs with a compact GaN layer. Then, a mesa-type sensors were made by dry etching and metal deposition techniques. Finally, both types of structures were electrically tested in NO_2, NH_3 and hydrogen atmospheres at temperatures up to 80 ^oC to check and compare their gas sensing properties.

This work was partly supported by the European Regional Development Fund through grant Innovative Economy (POIG.01.01.02-00-008/08 NanoBiom). Some of us (MS and TP) are grateful for support from the POIG.01.03.01-00-159/08 Project.

[1] S.J. Pearton, et al., Prog. Mat. Sci. 55, 1-59 (2010);

16:00 Poster We11

Optical and mechanical properties of a hexagonal single crystals of $Zn_{1-x}Mn_xS:Fe^{2+}$ solid solution

Alexey K. Kapustnik[1], Nazar O. Kovalenko[1], Vladimir A. Khristyan[1], Dmitriy Sofronov[2]

1. *Institute for Single Crystals NAS of Ukraine (ISC), 60 Lenin Ave., Kharkov 61001, Ukraine* **2.** *Division of Chemistry of Functional Materials of SSI 'Institute for Single Crystals' of National Academy of Sciences of Ukraine, Lenina Ave, 60, Kharkov 61001, Ukraine*

e-mail: nazar@isc.kharkov.ua

The search for new materials for laser systems, which would extend the spectral range of the lasers is one of the priorities of modern material science. And one of the promising areas of this investigations is the development of new active materials for vibronic lasers [1,2,3]. A broad band of tuning range so-called "vibronic" lasers is determined by features of the energy spectrum of activator in chalcogenide matrix. This feature determines the broad band luminescence in ZnSe matrix in a range 2-3 mmdoped Cr^{2+} and 4-5.5 mm for the Fe^{2+} [2]. The further development directions of the laser physics is to improve both the performance of well-known materials and searching for new matrices, which have a decisive influence on the energy spectrum of the active ions. This article presents the research results of semiconductor single crystals of substitution solid solution $Zn_{1-x}Mn_xS$ doped with Fe^{2+} ions.

Using the method of Vickers microhardness testing are measured the microhardness of a hexagonal $Zn_{1-x}Mn_xS:Fe^{2+}$ single crystals grown at an overpressure excessive pressure of inert gas in graphite crucibles (vertical Bridgman). The measurements were performed on samples with different concentrations of manganese in the load range from 0.25N to 2N. Indentation was performed on close-packed planes and the cleavage planes of these crystals. The obtained dependences are characterized by the type I and II microhardness anisotropy and defined the corresponding coefficients of anisotropy. Obtained microhardness values were compared with the corresponding values for the ZnS single crystals.

The spectra of the optical transmission of single crystals$Zn_{1-x}Mn_xS:Fe^{2+}$ in the visible, near-and mid-IR ranges are obtained. Investigated and explained the differences in the optical spectra of $ZnS:Fe^{2+}$ crystals. The dependence of the position of the absorbance maximum of Fe^{2+} ions on the concentration of manganese in the studied samples are established.

1. I. T. Sorokina. Cr^{2+}-doped II–VI materials for lasers and nonlinear optics. Optical Materials 26(4), 395–412 (2004).

2. Sergey Mirov, Vladimir Fedorov, Igor Moskalev, Dmitri Martyshkin, Changsu Kim. Laser & Photon. Rev. 4, No. 1, 21–41 (2010)

3. Zagoruiko Yu.A., Kovalenko N.O., PuzikovV.M., Fedorenko O.A., BasievT.T., Doroshenko M.E., OsikoV.V., Jelinkova H., KorandaP. Functional Materials **16**, No.3 (2009).

16:00 Poster We12

Studies on dislocation and surface morphology of $Al_xGa_{1-x}N$/GaN heterostructures grown by MOCVD

Loganathan Ravi, Jayasakthi Mathaiyan, Ramesh Raju, Arivazhagan Ponnusamy, Prabakaran Kandhasamy, Balaji Manavaimaran, Baskar Krishnan

Crystal Growth Centre, Anna University, Chennai, Chennai 600025, India

e-mail: drbaskar2009@gmail.com

Group III-nitride semiconductors have attracted huge research interest due to its unique properties and potential application for short-wavelength light emitters, high temperature and high frequency devices [1]. Successful fabrication of III-nitride based devices depends on the ability to grow epitaxial films on sapphire with low defect density. The large lattice mismatch and thermal expansion coefficient mismatch between AlGaN/GaN and sapphire substrate generally cause high-density of threading dislocations (TDs). TDs are very harmful to electronic and photonic devices [2]. GaN epilayer on sapphire typically contains the high-density of dislocations in the order of 10^8 to 10^{10} cm^{-2}

. Therefore, it is of great interest to explore a reliable and quick method for investigating dislocations in AlGaN/GaN heterostructures. To characterize the dislocation density of AlGaN/GaN heterostructures, various evaluation techniques such as high resolution X-ray diffraction (HRXRD), cathodoluminescence (CL), photoluminescence (PL), atomic force microscopy (AFM), and transmission electron microscopy (TEM) have been adopted [3].

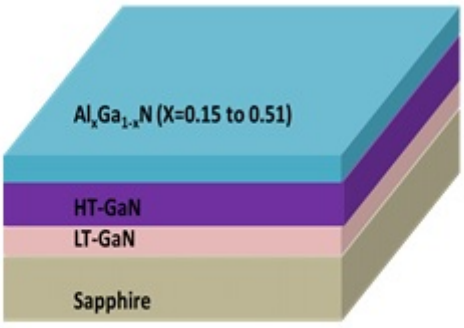

Fig 1 Schematic cross-sectional view of $Al_xGa_{1-x}N$

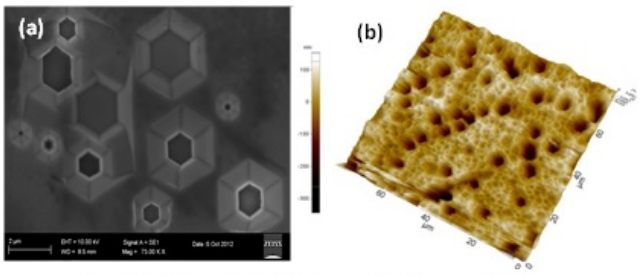

Fig 2(a) SEM and (b) AFM image of $Al_xGa_{1-x}N$ Etch pits

In the present study, the $Al_xGa_{1-x}N$ epilayers with $0 \le x \le 0.51$ on GaN layers were grown by Metal Organic Chemical Vapour Deposition (MOCVD) method. Fig (1) shows typical cross-sectional view of $Al_xGa_{1-x}N$ /GaN heterostructures on sapphire substrate. The dislocation density of the samples has been estimated through wet-chemical etching and HRXRD. The FWHM of (002) plane of GaN layers, estimated from ω-scan was in the range of 342-404 arc-sec, whereas FWHM of (102) plane was in the range 632-999 arc-sec. Ortho phosphoric acid (H_3PO_4) has been used as chemical etchant for AlGaN/GaN samples. The wet etching process has been optimized by varying the etching time and temperature. H_3PO_4 at 180 ºC for 90 seconds has been found as the optimal etching condition for AlGaN/GaN samples. After etching, the AlGaN/GaN samples have been analysed by SEM and AFM. Figure 2(a) shows the SEM image of etch pits and figure 2(b) shows the AFM image of etch pits formed on the surface of AlGaN layers. The dislocation density of the samples was found to be between $2.1x10^8 cm^{-2}$ and $1.9x10^9 cm^{-2}$. Photoluminescence studies reveal that the near band edge (NBE) emission intensity of AlGaN and GaN layers increases after etching due to increases the surface roughness. The dislocation density estimated from etch pits has been correlated with HRXRD results.

References

[1] Yitao Liao, Christos Thomidis, Chen-kai Kao, and Theodore D. Moustakas, "AlGaN based deep ultraviolet light emitting diodes with high internal quantum efficiency grown by molecular beam epitaxy" Appl. Phys. Lett., Vol. 98, pp. 081110, 2011.

[2] D. Kapolnek, X. H. Wu, B. Heying, S. Keller, B. P. Keller, U. K. Mishra, S. P. DenBaars, and J. S. Specka, "Structural evolution in epitaxial metalorganic chemical vapor deposition grown GaN films on sapphire" Appl. Phys. Lett., Vol. 67, pp. 1541-1543, 1995.

[3] J.L. Weyher, S. Lazar, L. Macht, Z. Liliental-Weber, R.J. Molnar, S. Mu¨ ller,V.G.M. Sivel, G. Nowak and I. Grzegory "Orthodox etching of HVPE-grown GaN" Journal of Crystal Growth, Vol. 305,pp. 384–392, 2007.

16:00 Poster We13

Growth and characterization of $Al_xGa_{1-x}N$/GaN/ Al_2O_3 heterostuctures

Arivazhagan Ponnusamy, Ramesh Raju, Jayasakthi Mathaiyan, Loganathan Ravi, Prabakaran Kandhasamy, Balaji Manavaimaran, Baskar Krishnan

Crystal Growth Centre, Anna University, Chennai, Chennai 600025, India

e-mail: drbaskar2009@gmail.com

The strain free $Al_xGa_{1-x}N$(x= 0.23) and partially strained $Al_xGa_{1-x}N$(x= 0.27) have been grown on GaN/sapphire template using MOCVD. The composition of Al in AlGaN layer has been determined from the ω-2Θ scan. Figure.1 shows the ω-2Θ scan for $Al_{0.27}Ga_{0.73}N$ /GaN layer. The Reciprocal space mapping (RSM) of (105) reflection has been carried out for $Al_xGa_{1-x}N$(x= 0.23 and 0.27)/GaN layers and the in-plane strain of the $Al_xGa_{1-x}N$ epilayers with respect to GaN has been estimated. Figure.2 illustrates the RSM of (105) reflection for $Al_{0.27}Ga_{0.73}N$ /GaN layer. Figure .3 shows the band edge emissions at 320 nm and 312 nm corresponding for $Al_{0.23}Ga_{0.77}N$ and $Al_{0.27}Ga_{0.73}N$ respectively, whereas the 362 nm emission is for GaN. The root mean square (RMS) surface roughness of $Al_{0.23}Ga_{0.77}N$ and $Al_{0.27}Ga_{0.73}N$ has been estimated as 0.37 nm and 0.30 nm respectively using atomic force microscopy.

Ti/Al/Ni/Au: 200/1000/400/500 Å metal layers were deposited on-$Al_xGa_{1-x}N$(x= 0.23) and $Al_xGa_{1-x}N$(x= 0.27) layers by E-beam evaporation technique. The samples were annealed with two step annealing in rapid thermal annealing system at optimum conditions of 550 ˚C under N2 ambient for 60 s and at 780 ˚C for 30 s.

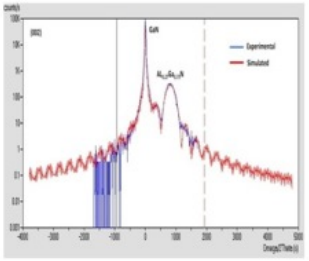

Figure. 1. HRXRD ω-2Θ scan of $Al_{0.27}Ga_{0.73}N$ (50nm)/GaN.

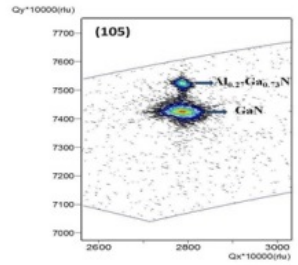

Figure. 2. Reciprocal space mapping of $Al_{0.27}Ga_{0.73}N$ /GaN (105) reflection.

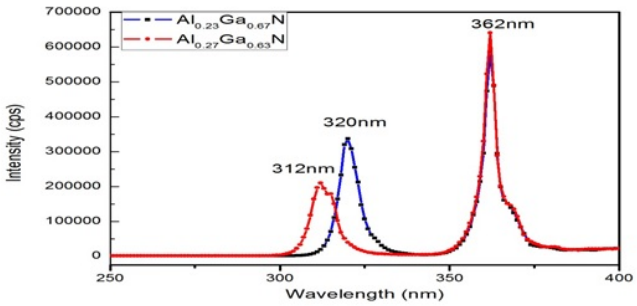

Figure. 3. PL spectrum of $Al_{0.23}Ga_{0.77}N$/GaN and $Al_{0.27}Ga_{0.73}N$/GaN

Circular Transmission Line Measurement (CTLM) has been adopted to find the variation in contact resistance (Rc), transfer length (L_T)and specific contact resistance(ρ_c) between metal contacts (Ti/Al/Ni/Au: 200/1000/400/500 Å) and $Al_xGa_{1-x}N$ layers were determined using I-V characteristics of diodes.

In addition the schottky behavior of Ni/Au: 400/1500 Å contacts on the strain free $Al_xGa_{1-x}N$(x= 0.23) and partially strained $Al_xGa_{1-x}N$(x= 0.27) layers have been studied using current -voltage (I-V) and capacitance-voltage(C-V) measurements. The device characteristics have been correlated with the structural quality of $Al_xGa_{1-x}N$ layers.

REFERNCES:

[1] P. Gay, P. B. Hirsch and A. Kelly, Acta Metall. 1, 315 (1953).

[2] C. G. Dunn and E. F. Koch, Acta Metall. 5, 548 (1957).

[3] G. S. Huang, T. C. Lu, H. H. Yao, H. C. Kuo, and S. C. Wang, Appl. Phys. Lett. 88, 061904, (2006).

[4] B. Jacobs, M.C.J.C.M. Kramer , E.J. Geluk, F. Karouta, Journal ofCrystal Growth, Vol. 241, pp. **15,** 2002.

[5] L.F. Lester, J.M. Brown, J.C. Ramer, L. Zhang, **S.** D. Hersee, J.C. Zolper, Applied Physics Letters, Vol. 69,No. l8,p. 2737, 1996.

16:00 Poster We14

Strain relaxation behavior of ultra-thin ZnO films on m-plane sapphire growth by atomic layer deposition

Ching-Shun Ku, Hsin-Yi Lee

National Synchrotron Radiation Research Center (NSRRC), 101 Hsin-Ann Rd, Hsinchu Science Park, Hsinchu 30076, Taiwan

e-mail: csku@nsrrc.org.tw

Non-ploar ZnO ultra-thin films were grown epitaxially on (10-10) sapphire substrate at 220 ^{0}C by flow-modulation atomic layer deposition method. Synchrotron X-ray scattering was employed to analyze the surface roughness, lattice constant, strain states and orientation of ultra-thin films. The results indicated the full-strained ZnO orientation rotate from (100) atomic plane to miscut plane at 7 monolayers and suddenly release at 8 monolayers. Besides, we also simultaneously observed quantum dots formation on 8 monolayers ZnO film surface by atomic force microscopy.

16:00 Poster We15

Structural and luminescent properties of ZnO thin films doped with Cu, Ga, Ag

Vladimir I. Kushnirenko[1], Viktoria S. Khomchenko[2], Tetiana G. Kryshtab[3], Tamara V. Zashivailo[4]

1. *V. Lashkarev Institute of Semiconductor Physics, NASU, Pr. Nauki 45, Kyiv 03028, Ukraine* **2.** *V. Lashkarev Institute of Semiconductor Physics, NASU, Pr. Nauki 41, Kiev 03028, Ukraine* **3.** *Instituto Politécnico Nacional, ESFM, Av. IPN, Ed. 9 U.P.A.L.M., México 07738, Mexico* **4.** *National Technical University of Ukraine "KPI", Pr. Pobedi 37, Kiev 03056, Ukraine*

e-mail: vl_kush@ukr.net

We report the studies of ZnO:[Cu, Ga] thin films deposited by electron-beam evaporation method (EBE) and of ZnO:[Cu, Ga] thin films doped additionally with silver by means of close space sublimation technique (CSS).

On first stage, ZnS and ZnS:[Cu, Ga] films were deposited onto glass substrates by EBE. Then, ZnO and ZnO:[Cu, Ga] films were prepared by an oxidization of ZnS and ZnS:[Cu, Ga] films at 600–650^{o}C in air or in wet air. Some ZnO:[Cu, Ga] films were doped with silver. Ag doping was accomplished by CSS in air at atmospheric pressure.

The structural characteristics and surface morphology of the films were studied by X-ray diffraction (XRD) and atomic force microscopy (AFM), respectively. Photoluminescence (PL) and PL excitation (PLE) spectra of the films were investigated in the temperature range of 30-300 K. The excitation of emission was carried out by light from intrinsic absorption and extrinsic absorption regions. For PL and PLE measurements, we used an N2-laser
and an Xe-lamp, respectively.

As-deposited ZnS films were of sphalerite structure grown along a <111> direction. PL was not observed. At optimal conditions, the oxidation of ZnS and ZnS:[Cu, Ga] led to a complete transformation to ZnO and ZnO:[Cu, Ga] with a slightly marked grains orientation in a <0002> direction. Silver doping of ZnO:[Cu, Ga] films led to the mean grain orientation in a <0002> direction. XRD and AFM studies showed that the average grain size of the films oxidized in wet air (WA) were larger than of the films oxidized in dry air (DA).

PL intensity for the films after WA was higher than after DA. A strong influence of the water vapor on shape and intensity of the emission was observed. PL of ZnO:[Cu, Ga] films exhibits UV (380 nm) and green emission (500 nm). The intensity of UV band increases at additional Ag doping. The shape and intensity of PL depended on the doping and oxidation conditions. PLE spectra exhibited the maximum at 370–380 nm. Origin of observed emission bands is discussed.

16:00 Poster We16

Synthesis and physical properties for Al-doped ZnO nanostructure powders with the chemical precipitation method

Hisn-Tzu Liu[1,2], Shi-Yao Zhong[3], Ming-Fong Tai[4], Chih-Ming Lin[3]

1. *Department of Chemical Engineering, National Tsing Hua University, Hsinchu, Taiwan, Hsinchu 30013, Taiwan* **2.** *Chemical Systems Research Division, Chung-Shan Institute of Science and Technology, Taoyuan, Taiwan, Taoyuan 3251, Taiwan* **3.** *Department of Applied Science, National Hsinchu University of Education, Hsinchu 30013, Taiwan* **4.** *Department of Physics, National Tsing-Hua University, Hsinchu 30013, Taiwan*

e-mail: cmlin@mail.nhcue.edu.tw

Plate-like or granular aluminum-doped zincite (AZO) nanostructure powders (NPs), $Zn_{1-x}Al_xO$, x=0.01, 0.03, 0.06, 0.09 and 0.11, were synthesized using a chemical precipitation method. Using of both reactants of zinc nitrate and aluminum nitrate as well as urea as the precipitating agent to get precursors. Then the precursors were calcined at 500^{o}C for three hours. The structure and morphology of the products were characterized by X-ray diffraction (XRD), scanning electron microscopy (SEM) and Raman spectroscopy. By the thermogravimetric analysis (TGA), precursors converted to oxides from hydroxides near about 250^{o}C and then take 500^{o}C for the temperature of the thermal processes of the precursor species. The results of inductively coupled plasma atomic emission spectrometer (ICP-AES) measurement ensured the stoichiometric ratio of Al/Zn in our ZAO NPs. XRD results showed that ZAO NPs with Al content less than 11% exhibited würtzite ZnO structure and there was no other impurity phase in the AZO NPs and Al atoms were doped into the ZnO lattice by substituting for zinc atoms. The grain size of AZO NPs were estimated as 31.9, 32.5, 16.9, 16.9 and 18.5 nm for x=0.01, 0.03, 0.06, 0.09 and 0.11 by using the Williamson-Hall equation, respectively. SEM images showed plate-like or granular. Raman data indicated that the more the concentration of the aluminum atoms is, the more the reduction of intensity of the polar mode A1(TO). This study provides a simple and efficient approach for synthesizing plate-like or granular AZO nanostructure.

16:00 Poster We17

Evaluations of GaN film grown on patterned Si (111) templates substrates

Kung Liang Lin[1,2], Chen-Chen Chung[1,2], Chih-Yung Huang[1], Chien-Chih Chen[1], Shih-Hsiang Lai[1], Ching-Chiun Wang[1], Edward-Yi Chang[1,2]

1. *Industrial Technology Research Institute, 195 Chung Hsing Rd., Sec.4, Hsinchu 3100, Taiwan* **2.** *Department of Materials Science and Engineering, National Chiao Tung University, Hsinchu 30050, Taiwan*

e-mail: kllin@itri.org.tw

Low stress, low defect density GaN was successful grown on circle array patterned Si (111) substrate using AlN as the nucleation buffer

followed by two steps growth of the GaN film. Raman measurement shows a reduction of in plane biaxial stress for the GaN film grown on patterned substrate. The slight blue-shift of the band edge PL peaks further provides the evidence that the tensile stress in the GaN film was relaxed in the patterned Si substrate. It's believed that the grain boundaries of the polycrystalline AlN buffer layer and the dislocations in the GaN film grown helped to relieve the stress induced by the lattice and the thermal coefficient mismatches during growth.

16:00 Poster We18

Influence of surface orientation on the In-incorporation of HVPE-grown InGaN studied by theoretical calculations

Hisashi Murakami, Rie Togashi, Yoshinao Kumagai, Akinori Koukitu

Tokyo University of Agriculture and Technology, Department of Applied Chemistry (TUAT), 2-24-16 Naka-cho, Koganei, Tokyo 184-8588, Japan

e-mail: faifai@cc.tuat.ac.jp

InGaN ternary alloys have been extensively investigated as possible materials for the optoelectronic devices such as light emitting diodes (LEDs) and laser diodes (LDs), and multi-junction solar cells with extremely high efficiency. Recently, non-polar and semi-polar surfaces are intensively attracted much attention for the growth of InGaN quantum wells suitable for true green lasers [1]. These surfaces are expected not only to reduce the spontaneous polarization in InGaN quantum wells but also to enhance the In-incorporation due to the surface structural properties [2]. Our group has reported on the growth of InGaN by hydride vapor phase epitaxy (HVPE) using $InCl_3$ and $GaCl_3$ as precursors by thermodynamic analyses [3]. Actually, we succeeded in the growth of thick InGaN ternary alloy by HVPE system constructed based on the thermodynamic analyses. However, thermochemical data such as Gibbs' free energy change, which are available from the database, do not take the surface orientation of crystal into consideration. Therefore, it is difficult to consider the behavior of vapor-solid relationship including the information of surface orientation by conventional thermodynamic analysis. Yayama et al. investigated the dependence of In solid composition on surface orientation for metalorganic vapor phase epitaxy (MOVPE) by the combination of first principles calculation and statistical thermodynamics [4]. In this study, we will report the influence of surface orientation on the In solid composition of HVPE-grown InGaN by taking the surface orientation into consideration.

In the calculation, the values of Gibbs' free energy change for InN deposition and GaN deposition were estimated by first principles calculation combined with statistical thermodynamics. We constructed the slab models of 8ML (before deposition) and 10ML (after deposition), and performed the vibration analysis to obtain the values such as entropy and heat capacity. And finally, Gibbs' free energy change DG (equilibrium constant K_i) was estimated. In order to predict the In-incorporation on each crystal surface, solid composition index normalized by c-plane was calculated through $[K_{InN}/(K_{InN}+K_{GaN})]_{each\text{-}orientation}/[K_{InN}/(K_{InN}+K_{GaN})]_{c\text{-}plane}$.

Figure 1 shows the values of Gibbs' free energy change for InN deposition at various temperatures and various surface orientations. From this figure, the order of deposition superiority for InN was revealed as (10-1-1)>(000-1)>(10-10)>(10-1-3)>(10-12)>(0001). Thus, solid composition index of HVPE-grown InGaN was estimated from the equilibrium constants of InN deposition and GaN deposition calculated by above mentioned method (Fig. 2). Growth temperature was selected at 1000K. Although it is not accurate to consider the In solid composition in InGaN by equilibrium constant, it is possible to grasp the tendency of In-incorporation when we change the only surface orientation as the growth condition is fixed. Figure 2 shows the solid composition index of InGaN normalized by the value of (0001) plane. The order of superiority for In-incorporation was revealed. Wernicke et al. [2] reported the high In-incorporation for (10-11) surface orientation and that was consistent with our calculated value. We believe that it is possible to expect the suitable surface orientation by theoretical calculations and feed it back to growth experiments.

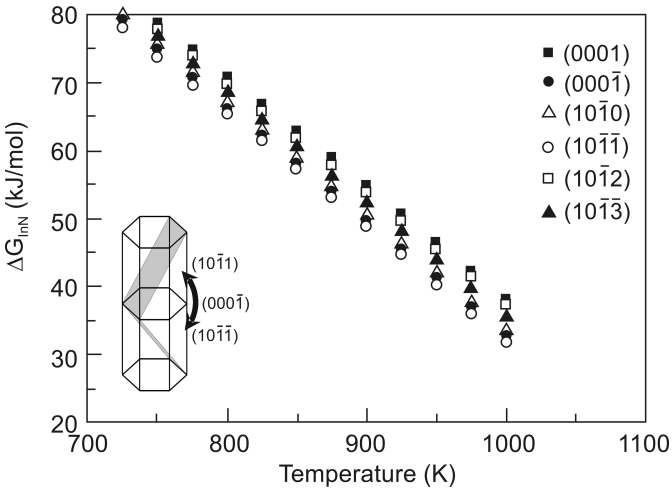

Figure 1 Dependence of Gibbs' free energy change for InN deposition on various temperatures for each surface orientation.

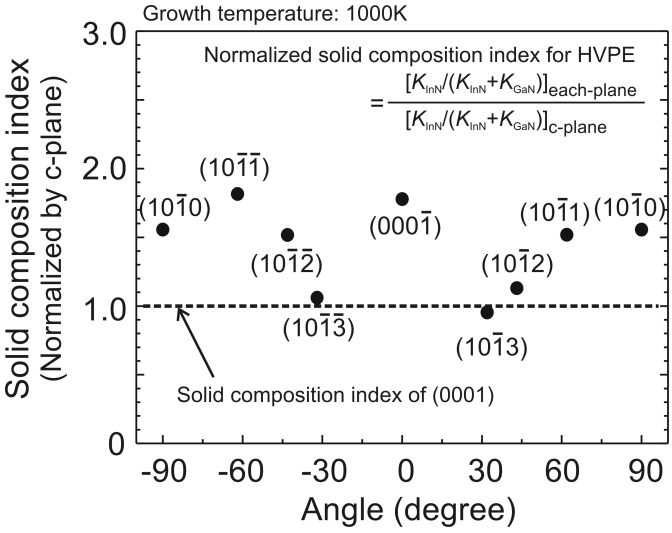

Figure 2 Normalized solid composition index of InGaN for each surface orientation. Growth temperature was set to 1000K.

References

[1] S. Takagi *et al.*, Appl. Phys. Express **5** (2012) 082102.

[2] T. Wernicke *et al.*, Semicond. Sci. Tech. **27** (2012) 024014.

[3] K. Hanaoka *et al.*, J. Cryst. Growth, **318** (2012) 441.

[4] T. Yayama *et al.*, Jpn. J. Appl. Phys. in press.

16:00 Poster We19

Far field pattern of AlGaN cladding free blue laser diodes grown by PAMBE

Grzegorz Muziol[1], Henryk Turski[1], M. Siekacz[1,2], Marta Sawicka[1,2], Paweł Wolny[1], Emilia Pruszyńska-Karbownik[3], Kazimierz Regiński[3], Bohdan Mroziewicz[3], Piotr Perlin[1,2], Czeslaw Skierbiszewski[1,2]

1. *Polish Academy of Sciences, Institute of High Pressure Physics (UNIPRESS), Sokolowska 29/37, Warszawa 01-142, Poland* **2.** *TopGaN LTd, Sokolowska 29/37, Warszawa 01-142, Poland* **3.** *Institute of Electron Technology (ITE), al. Lotników 32/46, Warszawa 02-668, Poland*

e-mail: gmuziol@unipress.waw.pl

Electrically driven laser operation from InGaN based devices had been shown in wide optical range from UV to green. Applications of laser diodes (LDs) to data storage technology and laser projectors demand very high beam quality. Nitride based LDs suffer from leakage of optical modes to GaN substrate which is pronounced as ripples in the far field pattern [1] which significantly worsens the beam quality. The amount of light leaking to the substrate increases for LDs emitting at longer wavelengths.

Leakage of optical modes to GaN substrate is often reduced by increasing the n-type AlGaN cladding thickness. Strauss et al. had shown that for LDs emitting at λ=440 nm a cladding as thick as 3 μm is needed to fully suppress ripples in far field pattern and obtain a Gaussian shaped beam. Growth of such thick AlGaN claddings without cracks in the structure is demanding for epitaxy.

In this work we present another way to obtain Gaussian shaped far field pattern for blue LDs. We have grown AlGaN cladding free LDs by Plasma Assisted Molecular Beam Epitaxy (PAMBE) [3,4], where the optical mode is confined by thick, high In content InGaN waveguide. Growth of thick high quality InGaN layers needed for waveguides is crucial to obtain good LD characteristics. Recent advantages in understanding of growth mode of high In content InGaN layers by PAMBE [5] allowed us to obtain high quality InGaN waveguide.

Due to the fact that effective refractive index of the light propagating in InGaN waveguide is higher than refractive index of GaN there is no leakage of optical modes to the GaN substrate. We show Gaussian shaped far field patterns with no ripples. AlGaN cladding free blue and green LDs can prove to be the choice for new generation laser projectors.

[1] V. Laino et al., Substrate Modes of (Al,In)GaN Semiconductor Laser Diodes on SiC and GaN Substrates, IEEE Journal of Quantum Electronics, vol.43, no.1, pp.16,24, Jan. 2007

[2] U. Strauss et al., Beam quality of blue InGaN laser for projection, Phys. Status Solidi C 5 (2008) 2077

[3] C. Skierbiszewski et al., AlGaN-Free Laser Diodes by Plasma-Assisted Molecular Beam Epitaxy, Appl. Phys. Express 5 (2012) 022104

[4] C. Skierbiszewski et al., True-Blue Nitride Laser Diodes Grown by Plasma-Assisted Molecular Beam Epitaxy, Appl. Phys. Express 5 (2012) 112103

[5] H. Turski et al., Nonequivalent atomic step edges—Role of gallium and nitrogen atoms in the growth of InGaN layers, Journal of Crystal Growth, Volume 367, 15 March 2013, Pages 115-121

Acknowledgements: This work was supported partially by the Polish Ministry of Science and Higher Education Grants No IT 13426 and INNOTECH 157829.

16:00 Poster We20

Growth of atomically-smooth droplet-free $Al_xGa_{1-x}N$ (x>0.5) layers by plasma assisted molecular beam epitaxy under strong metal-rich conditions

Dmitrii Nechaev[1], Valentin N. Jmerik[1], Pavel N. Brunkov[1], Sergey I. Troshkov[1], Ahmed Y. Alyamani[2], Sergey V. Ivanov[1]

1. *Ioffe Physico-Technical Institute, RAS, Saint-Petersburg, Russian Federation* **2.** *King Abdulaziz City for Science and Technology (KACST), Riyadh P.O. Box 6086, Riyadh 11442, Saudi Arabia*

e-mail: nechayev@mail.ioffe.ru

Plasma assisted molecular beam epitaxy (PA MBE) is one of the main technologies for manufacturing AlGaN heterostructures with a high Al content, emitting within wide UV spectral range down to a wavelength of 210 nm. The structural quality of UV-emitting devices can be improved by a precise control of the stoichiometric conditions during PA MBE that allows one to grow AlGaN layers with either rough or atomically smooth droplet-free surface morphology at the nitrogen- or metall-rich conditions, respectively. The paper reports on growth kinetics of $Al_xGa_{1-x}N$ films with high Al content (x>0.5) at the metal-rich conditions. Also we propose a new pulsed growth technique to achieve the atomically-smooth droplet-free film surface. The $Al_xGa_{1-x}N/AlN/c\text{-}Al_2O_3$ (x=0.5-0.8) samples were grown at substrate temperature (T_S) gradually varied from 650 to 800ºC using the group-III-to-activated nitrogen flux ratio (III/N) in the 1.1-2.2 range. *In situ* laser reflectometry and pyrometry measurements were used to determine growth rate (or alloy composition) as well as to estimate the metal(Ga) desorption rate and group III excess on the growth surface. The AlGaN growth kinetics data were used to obtain droplet-free AlGaN layers under the strong Ga-rich conditions at T_S=700-730ºC by using the controlled short-term interruptions of either only metal or all growth fluxes. Although optical and scanning electron microscopes revealed the droplets-free surface for the films grown by both techniques, the cracking effect was observed for the growth with only metal flux interruptions. This is explained by the formation of strained GaN insertions due to Ga surface segregation, leading to the tensile stress in AlGaN layers. Uncracked atomically-smooth surface with RMS~0.4 nm over area of 2x2 μm^2 was achieved for the 600-nm-thick $Al_{0.8}Ga_{0.2}N$ films grown at III/N=2.2 with the short-term interruptons of all fluxes.

16:00 Poster We21

Activity modulation and role of nitrogen radicals in PA-MBE for growth of group III nitrides and their alloys

Tadashi Ohachi[1], Yuuki Sato[2], Shinzo Yoshikado[2], Motoi Wada[2], Osamu Ariyada[3]

1. *Doshisha University (IREL), Jizoutani, Koudo, Kyoutanabe, Kyoto 610-0322, Japan* **2.** *Doshisha University, 1-3 Miyakotani, Kyotanabe, Kyoto 610-0321, Japan* **3.** *ARIOS INC., 3-2-20 Musashino, Akishima, Tokyo 196-0021, Japan*

e-mail: tohachi@me.com

Production of high quality epitaxial films of group III nitrides and their alloys on a large size Si wafer is requested for high frequency and high power electronics devices. Plasma assisted molecular beam epitaxy (PA-MBE) method, which uses radio frequency inductively coupled plasma (rf-ICP), is the most suitable one for growth of the group III nitrides on a Si wafer. From an original Si wafer a double buffer layer (DBL) AlN/β-Si_3N_4/Si(111) is grown by interface reaction epitaxy

(IRE) of Si and successive IRE of β-Si_3N_4 to form AlN. The rf-ICP plasma produces nitrogen radicals such as chemically active nitrogen atoms (N+N*) and physically active excited nitrogen molecules(N_2*).

A DBL of AlN(0001)/β-Si_3N_4/Si(111) has been studied by Wu et. al [1] and present authors [2-4]. Controlling exposure of both (N+N*) and N_2* fluxes is able to use an activity modulation migration enhanced epitaxy (AM-MEE)[4, 5]. On the DBL an AlN(0001) template is grown by an AM-MEE method of PA-MBE. This method is able to make a electronic or optical device from Si wafer with in a one MBE chamber.

In this presentation a new one-chamber growth system for group III nitrids on a large size Si wafer using PA-MBE system is demonstrated. In order to improve quality of the epitaxial films the interface properties of the AlN template and Si substrate is studied by grazing incidence-angle X-ray reflectivity (GIXR) measurement [6].

References

[1] C.L.Wu, J.C.Wang, M.H. Chan, T.T. Chen, S.Gwo, Appl. Phys. Lett. 83 (2003) 4530.

[2] N. Yamabe, H. Shimomura, T. Shimamura, and T. Ohachi, J. Cryst. Growth 311, 3049 (2009).

[3] N. Yamabe, Y. Yamamoto, and T. Ohachi, Phys. Status Solidi C 8, 1552 (2011).

[4] T. Ohachi, N. Yamabe, Y. Yamamoto, M. Wada, and O. Ariyada J. Jpn. Appl. Phys. 50, 01AE01(1)-(8) (2011).

[5] T. Ohachi, Y. Yamamoto, O. Ariyada, Y. Sato, S. Yoshikado, and M. Wada, P hys. Status Solidi C 10, No. 3, 429–432 (2013).

[6] Y. Yamamoto, N. Yamabe, and T. Ohachi, J. Cryst. Growth 318, 474 (2011).

16:00 Poster We22

AlN single crystal growth on sapphire substrate under atomic nitrogen plasma

Tetsuo Ozawa

Shizuoka Institute of Science and Technology, Toyosawa 2200-2, Fukuroi 437-8555, Japan

e-mail: ozawa@ee.sist.ac.jp

GaN and InN are promising materials for optoelectronic device applications such as light-emitting diodes (LEDs) and laser diodes (LDs). The method to prevent a large mismatch with sapphire substrate and to avoid the high equilibrium pressure and temperature environment is required to grow high crystalline GaN and InN. The paper demonstrates the effects of sapphire (Al_2O_3) substrate nitridation with plasma mixture of nitrogen. A (0001) sapphire substrate with atomically smooth surface was placed into a pyrolytic boron nitride crucible. Nitridation was performed for 2 to 4 h at 680 ˚C. AlN was formed by Al_2O_3 substrate nitridation. XRD patterns was shown It shows that the layer was nearly oriented to (0001)AlN//(0001) sapphire substrate. We have carried out experiments to grow thick single InN crystal films for use as substrate. It was successfully that AlN was formed to Al_2O_3 substrate nitridation by microwave plasma. By using same growth apparatus, the transparent GaN layer was grown on AlN/Al_2O_3 substrate by using plasma mixture of nitrogen and hydrogen.

16:00 Poster We23

A density functional theory study of the Zn, O, O_2, and H_2O adsorption on the polar ZnO(0001) and ZnO(000-1) surfaces

Jakub Sołtys[1], Jacek Piechota[1], Stanisław Krukowski[1,2]

1. *University of Warsaw, Interdisciplinary Centre for Mathematical and Computational Modelling (ICM), Pawinskiego 5a, Warsaw 02-106, Poland* **2.** *Polish Academy of Sciences, Institute of High Pressure Physics (UNIPRESS), Sokolowska 29/37, Warszawa 01-142, Poland*

e-mail: jp@icm.edu.pl

An extensive theoretical investigation of adsorption Zn and O atoms, as well as O_2 and H_2O molecules on polar ZnO(0001) and ZnO(0001) surfaces was performed. It was found that Zn atom is weakly bonded in a bridging configuration with the Zn surface atoms to the ZnO(0001) surface at the distance of 2.2 Å. On the opposite side, Zn atom is strongly bonded to the ZnO(0001) surface. On the other hand, it is demonstrated that the O_2 molecule is strongly bonded to the ZnO(0001) surface and is not bound to the ZnO(0001) surface at all. Energetically favorable configurations of single O atoms and H_2O molecule on the ZnO surfaces have also been discussed.

16:00 Poster We24

Electronic and optical properties – As and As+Sb doped ZnO grown by PA-MBE

Ewa Przezdziecka[1], Marcin Stachowicz[1], Rafał Jakieła[1], Elżbieta Guziewicz[1], Jacek M. Sajkowski[1], Anna Reszka[1], Aleksandra Wierzbicka[1], Anna Droba[1], Krzysztof Kopalko[1], Adam Barcz[1], A Kozanecki[1], Wojciech Lisowski[2], Janusz W. Sobczak[2], Mirosław Krawczyk[2], Aleksander Jabłoński[2]

1. *Polish Academy of Sciences, Institute of Physics, al. Lotników 32/46, Warszawa 02-668, Poland* **2.** *Polish Academy of Sciences, Institute of Physical Chemistry, Kasprzaka 52/56, Warszawa 01-224, Poland*

e-mail: eilczuk@ifpan.edu.pl

Zinc oxide with its Eg=3.37 eV room temperature energy gap and large exciton binding energy is a prospective material for a number of applications such as ultraviolet light emitters and detectors. For applications in optoelectronic devices p-type doping of ZnO is necessary. However, this it is a difficult task due to the background n-type doping associated with high hydrogen (H) level, O vacancies (Vo) or Zn interstitials (Zni), compensating p-dopants. For obtaining p-type ZnO V group elements such as As and Sb are often used. Understanding of how As and Sb build in to ZnO matrix is valid for p-type doping.

The ZnO:As and ZnO:(As+Sb) were grown by PA-MBE method on GaN templates. The concentration of As and Sb atoms ware relatively high ~$1*10^{20}$ at/cm^3. The quality of the samples was examined by PL, AFM, CL, SEM and X-ray photoelectron spectroscopy (XPS). The XPS measurements showed that the As3d core level in the obtained ZnO:As films consists of two components located at 40 eV and at 43.7 eV below the Fermi level. It was found that intensity of the As3d component at binding energy of 43.7 eV is correlated with appearance of the acceptor line free electrons to acceptor FA observed in low temperature photoluminescence. This observation strongly supports the previously postulated assumption that the origin of the 43.7 eV component of the Ad3d spectra derive from arsenic atoms in As_{Zn}-$2V_{Zn}$ complexes. In the case of dual doped ZnO:As+Sb both As3d and Sb3d

bands with binding energy 44.2 eV and 539.5 eV was observed. The binding energy of Sb3d suggests location of Sb atoms at Zn site (Sb_{Zn}). Additionally, the valence band shift towards the Fermi level and As3d shift in the ZnO:As+Sb film was also observed.

Acknowledgements. The work was supported by the European Union within the European Regional Development Fund, through the Innovative Economy grant (POIG.01.01.02-00-008/08)

16:00 Poster We25

Grown ZnMgO/ZnO/ZnMgO heterostructures on p-type Si(111) by MBE method

Mieczyslaw A. Pietrzyk, Anna Reszka, Marcin Stachowicz, Anna Droba, Aleksandra Wierzbicka, Jacek M. Sajkowski, Ewa Przezdziecka, A Kozanecki

Polish Academy of Sciences, Institute of Physics, al. Lotników 32/46, Warszawa 02-668, Poland

e-mail: eilczuk@ifpan.edu.pl

Zinc oxide layers, ZnO/ZnMgO and ZnMgO/ZnO/ZnMgO heterostructures deposited on p-type Si (111) substrates are very important for applications in optoelectronics and integrated optoelectronic circuits. Silicon, the material which keeps the dominant place on the commercial market, is used to fabricate the discrete devices and integrated circuits for computing, data storage and communication. ZnMgO alloy has been considered as a suitable material for the barrier layers in ZnO/ZnMgO structures because alloying of ZnO with MgO (Eg~7.7 eV) enables widening of band gap of ZnO.

We present ZnO/ZnMgO heterostructures grown on Si (111) by molecular beam epitaxy method.with single and double quantum wells. The samples were grown at temperature about 550°C and 940°C. For structures with one well no specific buffer layers were deposited on silicon except a 2 nm layer of Zn. ZnMgO capping layers of the same composition as the ZnMgO barrier were deposited. The samples with single quantum well were grown as follows: first the ~100 nm ZnMgO layer, then ZnO quantum well (QW) (about 3 nm) and finally ~25 nm ZnMgO cap layer. For structures with the double quantum wells, first a very thick (400 nm) low temperature buffer (450^{o}C) was grown and then about 250 nm ZnMgO barrier (in high temperature), then two ZnO QWs (3 nm and 6 nm thick) and 15 nm ZnMgO cap layer. During the growth the RF power of oxygen plasma was fixed at 350 W. For the characterization of these samples, X-ray diffraction, AFM, SEM microscopy, photoluminescence and cathodoluminescence were used.

The photoluminescence for a series of ZnO/ZnMgO single quantum wells of different widths were carried out within a temperature range of 4-300K. In the ZnO wells with thicknesses smaller than 3 nm a blue shift of excitonic emission in comparison to bulk ZnO was observed, which demonstrates a quantum confinement. We also show that excitonic emission from QWs is dominated by localized excitons. The characteristic energy of PL decay of the dominant excitonic lines agrees well with the values of localization energies of excitons to donor centers.

In the CL spectrum two major peaks are observed: the higher energy peak from the ZnMgO barrier/capping layers and the other at the lower energy side, originating from the confined excitons in the ZnO wells. At room temperature, the emission coming from the QW dominates.

On the SEM images we can see a uniform sample surface however the uniformly distributed arrays of hillocks are observed. A typical cross-section SEM image of ZnMgO films with the thick buffer reveals that nanocolumns were grown. The XRD spectra suggest that ZnMgO films grow with the c-axis preferred orientation. No other phases of ZnO and ZnMgO were found.

Acknowledgement: Work supported in part within European Regional Development Fund, through grant Innovative Economy (POIG.01.01.02-00-008/08).

16:00 Poster We26

Dual-acceptor doped p-ZnO:(As+Sb)/n-GaN heterojunctions grown by PA-MBE as a highly selective UV detector

Ewa Przezdziecka, Krzysztof Gościński, Aleksandra Wierzbicka, Marcin Stachowicz, Anna Reszka, Anna Droba, Rafał Jakieła, Jacek M. Sajkowski, Mieczyslaw A. Pietrzyk, A Kozanecki

Polish Academy of Sciences, Institute of Physics, al. Lotników 32/46, Warszawa 02-668, Poland

e-mail: eilczuk@ifpan.edu.pl

Zinc oxide (ZnO) is a promising candidate for application in ultraviolet (UV) photodetectors due to the large direct band gap and the high absorption coefficient in the UV spectrum range. UV detectors based on wide bandgap semiconductors like SiC, GaN and ZnO have received more and more attention due to their chemical and thermal stability in harsh environments. For applications in *p-n* diode detectors *p*-type doping of ZnO is necessary. It is known, however, that it is a difficult task due to the background n-type doping .

High quality dual acceptor doped ZnO:(As,Sb) films were grown on *n*-type GaN templates by plasma-assisted Molecular Beam Epitaxy (PA-MBE)and *p*-ZnO/*n*-GaN heterojunction structures have been fabricated [1]. The structure consists of a 3.5 um thick GaN layer on sapphire substrate covered by a 60 nm thick As and Sb-doped ZnO film. The quality of the heterojunction was examined by X-ray diffraction, atomic force microscopy (AFM) and *scanning electron* microscopy (SEM). The As and Sb concentration in ZnO, measured by secondary ion mass spectroscopy (SIMS), is $1x10^{20}$ cm^{-3}. The maximum forward-to-reverse current ratio I_F/I_R in the obtained diode is of about 10^5 at the applied voltage of ±4 V, which is a very good result for this type of heterojunction. Electronic properties were examined by XPS study and the presence of As acceptors was also confirmed by low temperature PL study. Photodetector's response to the pulse of light in the UV region is relatively fast <<1 ms. Photodetectors based on a presented diodes are highly selective (FWHM photocurrent peak ~12 nm), work both in atmospheric pressure and in vacuum.

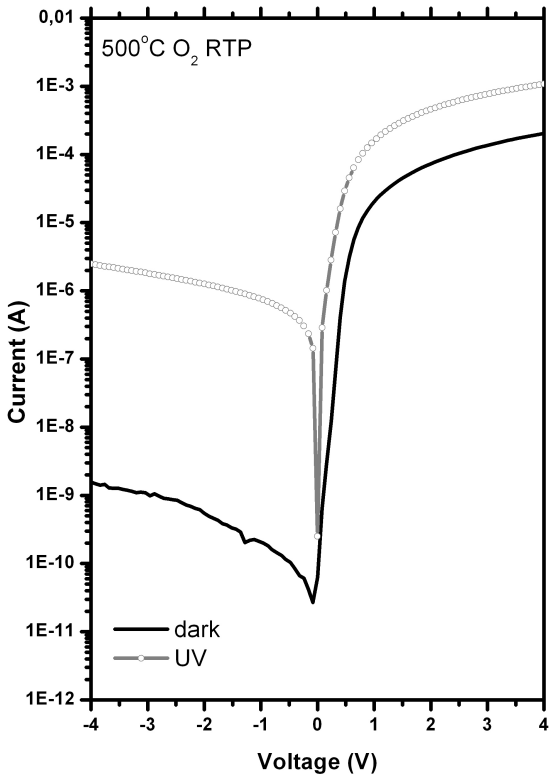

Fig 1 Cuurent-voltage characteristics ZnO/GaN diodes dark and with UV illumination.

The research was partially supported by the European Union within European Regional Development Fund, through grant Innovative Economy (POIG.01.01.02-00-008/08).

[1]E. Przeździecka, K. Gościński, M. Stachowicz, D. Dobosz, E. Zielony, J. M. Sajkowski, M. A. Pietrzyk, E. Płaczek-Popko, A. Kozanecki *Sensors & Actuators: A. Physical* (2013), pp. 27-31

16:00 Poster We27

Growth of SiC by PVT method with different sources of the cerium impurity, CeO_2 or $CeSi_2$

Katarzyna Racka[1], Emil Tymicki[1], Krzysztof Grasza[1,2], Rafał Jakieła[1,2], Marcin Pisarek[3], Barbara Surma[1], Andrei Avdonin[2], Paweł Skupiński[2], Jerzy Krupka[4]

1. *Institute of Electronic Materials Technology (ITME), Wólczyńska 133, Warszawa 01-919, Poland* **2.** *Polish Academy of Sciences, Institute of Physics, al. Lotników 32/46, Warszawa 02-668, Poland* **3.** *Polish Academy of Sciences, Institute of Physical Chemistry, Kasprzaka 44/52, Warszawa 01-224, Poland* **4.** *Warsaw University of Technology, Institute of Microelectronics and Optoelectronics (PW), Koszykowa 75, Warsaw 00-662, Poland*

e-mail: Katarzyna.Racka@itme.edu.pl

Rare-earth ion doped semiconductors are usually investigated as potential candidate materials for promising applications in optoelectronic devices. Many reports concern the structural and optical investigations of materials doped with optically active Ce^{3+} ions (e.g. YAG:Ce, Lu_2SiO_5:Ce, Ce-doped fluoride crystals) for applications as phosphors, scintillators and tunable lasers operating in the UV-blue region [1-4].

The Ce-doping of SiC is an interesting issue, because there is a lack of data in the literature, concerning this topic. There exists only one communication by Itoh et al. [5] concerning the PVT growth of bulk SiC crystals. For 4H-SiC crystals, which were grown using CeO_2 or $CeSi_2$ as the sources of the Ce impurity, the authors report the non-uniform concentrations of Ce atoms at levels less than 10^{17} cm^{-3} (which was a detection limit in their secondary ion mass spectroscopy (SIMS) measurements) up to 10^{20} cm^{-3}. This constituted a motivation for us to search for a confirmation of these results, in particular, if such a high cerium doping levels are possible in SiC crystal grown by PVT method. Our goal was: (1) to confirm that the cerium vapor was present in the growth atmosphere, (2) to study the effects of possible cerium incorporation into the crystalline lattice of SiC, and (3) to investigate possible effects induced by the presence of the oxide impurity in the growth atmosphere.

In this study we present a detailed investigations on structural, optical and electrical properties of SiC bulk crystals, which were grown on the Si- or C-faces of the crystal seeds and in the presence of a different Ce impurity content (from 0.1wt% up to 5.0wt%) in the SiC source materials. As the source of the cerium we used a commercial cerium dioxide (CeO_2) powder or granules of cerium silicide ($CeSi_2$).

The SiC crystals were studied by using a variety of experimental techniques, such as: X-ray diffraction (XRD), energy dispersive X-ray spectroscopy (EDX), X-ray photoemission spectroscopy (XPS), scanning electron microscopy (SEM), optical absorption (OA), photoluminescence measurements (PL), secondary ion mass spectroscopy (SIMS) and the contactless method at microwave frequencies at 300 K (to characterize the electrical properties). The results obtained by EDX and XPS point out the condensation of cerium vapor species at the crystallization fronts of the SiC crystals upon cooling-crystallization process, after the effective crystal growth stage. When CeO_2 was used as the source of Ce impurity, the cerium oxides Ce_2O_3 and CeO_2 were found to coexist on the SiC crystallization fronts, whereas in the case of the $CeSi_2$ source, there was found a mixture of CeO_2 and some unidentified (at this stage) Ce-species on the crystallization fronts. The presence of the cerium oxides and Ce-species on the SiC crystallization fronts proves of the gradual dosage of cerium from the SiC source materials and also, confirms the continuous presence of the cerium vapor over crystallization fronts during the crystal growth processes. A possible concentration of Ce atoms in bulk SiC crystals is at the level less than 10^{17} cm^{-3} (which is a detection limit in our SIMS measurements), while at the SiC crystallization fronts it reaches a value of 0.1 at.% (estimated from the XPS results).

For SiC crystals grown in the presence of the cerium impurity, a very interesting results of the investigation of electrical properties have been obtained. The electrical properties of bulk SiC crystals turned out to be a completely different in two cases, when CeO_2 or $CeSi_2$ were used as the source of Ce impurity. For both 4H- and 6H-SiC crystals, which were grown in the presence of $CeSi_2$, there were found the low values of resistivities at 300 K, within the range of ~0.02-0.57 Ωcm. From SIMS measurements it was found that the nitrogen donor impurity was a dominating impurity in all these crystals. For 4H-SiC crystals, which were grown in the presence of $CeSi_2$ on the C-face of the crystal seed, there was observed a very low concentration of boron atoms ([B] ~10^{12} cm^{-3}), in comparison with the SIMS results obtained for the reference SiC crystal ([B] ~10^{16} cm^{-3}), which was grown without the cerium additive, on the C-face of the crystal seed, and with the same growth parameters. For 6H-SiC crystals, which were grown in the presence of $CeSi_2$ on the Si-face of the crystal seed, the concentra-

tions of boron atoms were at the same level as in the case of the undoped reference 6H-SiC.

For 6H-SiC crystals, which were grown in the presence of CeO_2 on the Si-face of the crystal seed, there were found the high values of resistivities at 300 K. For some areas of different SiC wafers cut from these crystals, the high resistivity values up to ~1.70×10^4 Ωcm were observed. From SIMS measurements, the oxygen impurity was found to be a dominating impurity in the SiC wafers, besides the wafers, which were cut near the crystal seeds and thus represented the early stage of the crystal growth (they were the low-resistivity wafers with a dominating nitrogen impurity). But, regarding to a weak incorporation of Ce into the SiC lattice, it can be concluded that these high resistivities may be the result of a dominant oxygen impurity and the charge-carrier compensation effects between common residual donors (such as N or O) and acceptors (such as Al or B) in SiC, rather than from the impact of the Ce impurity. Moreover, some intrinsic defects and/or complex defects, e.g. B-O complexes, can provide deep levels in the band gap of SiC and, as compensating defects, they can take part in electrical compensation. The formation of electronically active B_s-O_{2i} defect (consisted of a substitutional boron atom and an interstitial oxygen dimer), acting as a electron-hole recombination center, was reported in the literature e.g. for compensated p- and n-type samples of Czochralski-grown silicon wafers [6].

Acknowledgements: This work was supported by the Polish Research Center under Grant No. 5043/B/T02/2011/40.

References:

[1] Y.C. Kang et al., Mater. Res. Bull. 35 (2000) 789.
[2] G. Ren et al., Nucl. Instr. Meth. Phys. Res. A 531 (2004) 560.
[3] F. Okada et al., J. Appl. Phys. 75 (1994) 49.
[4] C.D. Marshall et al., J. Opt. Soc. Am. B 11 (1994) 2054.
[5] A. Itoh et al., Appl. Phys. Lett. 65 (1994) 1400.
[6] J. Geilker et al., J. Appl. Phys. 109 (2011) 053718_1.

16:00 Poster We28

Drift-diffusion simulations of gallium nitride based heterostructures

Konrad Sakowski[1,2], Pawel Strak[1], Stanisław Krukowski[1,3], Leszek Marcinkowski[2]

1. *Polish Academy of Sciences, Institute of High Pressure Physics (UNIPRESS), Sokolowska 29/37, Warszawa 01-142, Poland*
2. *Warsaw University, Faculty of Mathematics, Computer Science and Mechanics (MIMUW), Banacha 2, Warszawa 02-097, Poland*
3. *Interdisciplinary Centre for Mathematical and Compuerial Modelling, University of Warsaw (ICM), ul. Pawinskiego 5a, Warszawa 02-106, Poland*

e-mail: iccge17sec@mail.unipress.waw.pl

We present a computer code for simulations of gallium nitride semiconductor devices. Our program is based on the drift-diffusion approximation. It is capable of simulating of the IV characteristics of the laser diodes and light-emitting diodes under the forward and reverse bias. It also provides approximations of the electrostatic potential, quasi-Fermi levels, carrier concentrations and many other derived values.

The implemented model accounts for radiative and Shockley-Read-Hall recombination, with or without trap-assisted tunneling, piezoelectric effect and interfacial charges. The program is written in a way that allows modifications of the underlying model, so this list is not final and we will include additional phenomena in the future. Our program is written in mixed Octave/C++, which makes it computationally effective and rather flexible in modification.

On our poster we present the model, algorithm, and examples of simulations performed with this program. In particular, simulation results of AlInGaN multiple quantum well heterostructures are discussed.

The research was supported by the European Union within European Regional Development Fund, through grant Innovative Economy (POIG.01.01.02-00-008/08).

16:00 Poster We29

Vapour phase growth of single crystalline GaN layers in hot microwave plasma

Radoslaw Zwierz, Sebastian Golka, Krzysztof Kachel, Dietmar Siche, Roberto Fornari

Leibniz Institute for Crystal Growth (IKZ), Max-Born-Str 2, Berlin 12489, Germany

e-mail: dietmar.siche@ikz-berlin.de

Gallium nitride (GaN) is already used as basic semiconductor for opto- and high frequency power electronics. The lack of cost effective bulk crystals drives the search for alternative growth methods to prepare homo-epitaxial substrates. We are using for Ga the Physical Vapor Transport (PVT) and microwave plasma for the N_2 activation, to grow first layers on double side polished sapphire substrates. The main challenge is to improve the plasma process stability when interaction between microwaves and plasma does not allow accurate prediction of the desired microwave resonator adjustment at growth temperature.

The spectra of Optical Emission Spectroscopy (OES) were utilized as markers for excitation efficiency, representing the operation parameters for controlled GaN growth in the metastable region of the phase diagram. Additionally, unfavorable vaporized impurities like Mo as cavity material can be detected, but there was no indication that it is sputtered. In contrast to spectra taken at RT, the lines of neutral and ionized molecules, N_2^* and N_2^+, and atomic nitrogen N could not be detected at growth temperature. Surprisingly, CN species were unambiguously detected, which means that reactive nitrogen was indeed present and reacted with carbon from insulation felt and susceptor graphite. The Ga related lines suggest that screening effects by Ga vapour and/or droplets do not severely affect the plasma formation.

Figs. 1a and 1b show typical GaN layers after 4 h growth on sapphire and etching of excess Ga in HCl:H_2

O mixture (1:2). In case of sample (a), plasma was not burning steadily during the whole growth time and a large amount of Ga excess was found on the seed after the process. Ga catalyses GaN decomposition may hinder the coalescence of crystallites by in-situ etching action and leads to the formation of small pits on their top surface. The crystallites shown in Fig. 5b are smaller, without top surface pits and were grown without visible Ga excess. EDX maps confirmed that thecrystallites consist of GaN, but the carbon map showed some particle-like spots, which might be tiny dust from the surrounding graphite susceptor and isolation felt transported into the cavity by carrier gas. The full width at half maximum (FWHM) of high resolution X-ray diffraction (HRXRD) measurements was 0.60 deg (2160 arcsec). This high value is reasonable since crystal quality improves with layer thickness and stress relaxation after delamination from the sapphire substrate.

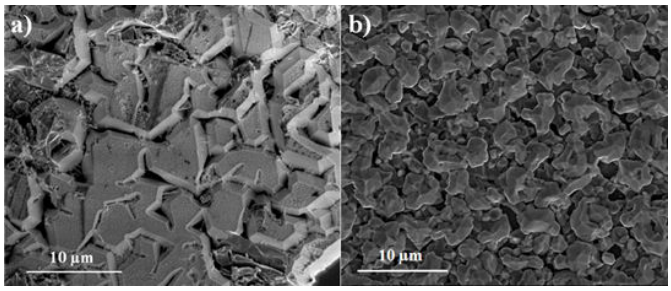

Fig. 1: Sample surfaces of GaN crystallites on sapphire grown with (a) and with no visible (b) Ga excess (SEM image) (T_{source} = 1300°C, T_{growth} » 1000°C, p = 400 mbar, growth duration 4 h)

16:00 Poster We30

The influence of growth atmosphere on the self-selection of the grains during ZnO crystal growth

Paweł Skupiński[1], Krzysztof Grasza[1,2], Elżbieta Łusakowska[1], Wojciech Paszkowicz[1], Anna Reszka[1], Rafał Jakieła[1], Andrei Avdonin[1], Emil Tymicki[2], Katarzyna Racka-Dzietko[2], B. J. Kowalski[1], Andrzej Mycielski[1]

1. *Polish Academy of Sciences, Institute of Physics, al. Lotników 32/46, Warszawa 02-668, Poland* **2.** *Institute of Electronic Materials Technology (ITME), Wólczyńska 133, Warszawa 01-919, Poland*

e-mail: skupin@ifpan.edu.pl

The self-selection of grains during crystal growth is a very useful phenomenon which enables one to obtain large size single crystals without using a seed during the first stage of the growth process. In this work the ZnO crystals were grown by chemical vapour transport (CVT). The hydrogen gas was used as the transport agent. Initially the growth processes were carried out in the zinc-rich growth atmosphere (a mixture of zinc vapour and molecules composed of oxygen and hydrogen). The overabundance of one of the crystal forming components, the zinc, results in a diffusion barrier for the second crystal forming component, that is oxygen bound with hydrogen. Such condition ensures stable growth of the crystals. However, the self-selection of crystal grains in such case is poor. The number of grains in the grown crystals is strongly dependent on the first stage of growth process, the spontaneous seeding. To avoid the problems with the randomly appearing seeds in this first stage of the growth process, a specially prepared piece of crystal (seed) mounted inside the growth ampoule was used. This approach allowed us to demonstrate that the Zn-terminated (0001) surface of the crystallization front gives the highest growth rate and the largest single grain volume [1].

In order to achieve an improvement of the self-selection, the influence of a variety of chemical reagents added to the growth atmosphere, on the growth conditions was investigated. Crystals obtained as the result of the most successful experiments were polycrystalline but with largest single grains exceeding a half of the area of the crystallization front. Even in the case of spontaneous seeding, where more than ten seeds appeared at the beginning of the growth process, in 80% of the experiments one large grain was found at the crystallization front of the resulting crystal at the end of the growth. The halogens and their components with manganese, when added to the growth atmosphere were found to give much better and reproducible results. In this case the largest grains of the crystal were oriented along directions other than [0001].

These observations were confirmed in experiments carried out with two differently oriented seeds, placed together into the same growth ampoule. These experiments allowed to compare the growth rate for various crystallographic directions in different growth ambiences. We believe that in the CVT growth of ZnO the improvement of the self-selection by addition of halogens and their components is a result of combining of two phenomena: (i) the increase of the diffusion barrier and (ii) the passivation of some of the ZnO crystallographic surfaces by the added components. The increase of the diffusion barrier caused by the presence of added components made it possible to improve the growth stability. The grains growing in the crystallographic directions which are blocked by the added components are being quickly overgrown by the other more favourably oriented grains. This passivation effect is responsible for the decreasing of the number of grains in the crystal.

In our report, an analysis of the influence of growth atmosphere composition on the self-selection of the crystal grains will be presented. The findings will be supported by microscopic investigations, X-ray diffraction and secondary ion mass-spectrometry studies of the crystals.

[1] P. Skupinski, K. Grasza, A. Mycielski, W. Paszkowicz, E. usakowska, E. Tymicki, R. Jakiea, B. Witkowski, phys. stat. sol. (b), 247 (2010) 1457

This work was partially supported by the National Science Centre in Poland, grant UMO-2011/01/D/ST7/02657

16:00 Poster We31

Absorption and emission spectra of AlN/GaN superlattice structures by DFT methods

Pawel Strak[1], Pawel Kempisty[1], Stanisław Krukowski[1,2]

1. *Polish Academy of Sciences, Institute of High Pressure Physics (UNIPRESS), Sokolowska 29/37, Warszawa 01-142, Poland* **2.** *University of Warsaw, Interdisciplinary Centre for Mathematical and Computational Modelling (ICM), Pawinskiego 5a, Warsaw 02-106, Poland*

e-mail: strak@unipress.waw.pl

Ambiguity introduced by the strong local electric field induced by the polarization charge density and the background doping strongly disturbs the optical properties of nitrides. The detailed model of the absorption and emission spectra in the vicinity of the fundamental gap is therefore of fundamental importance in studying such systems. Systematic studies were conducted to determine an influence of change of the well/barrier width ratio on the physical properties of AlN/GaN superlattice system, such as the electric field, polarization charges and polarization dipoles. To overcome the Kohn-Sham band gap (BG) underestimation of experimentally measured values, we have applied two different approaches i.e. empirical LDA+U correction method [1] and a method proposed recently by Ferreira et al., called LDA-1/2 which approximately includes the self-energy of excitations in semi-conductors, providing BG energies, effective masses, and band structures in very good agreement with experimental bulk properties [2]. The results obtained within this two approaches were compared. It was shown that the electric fields depend critically on the well-barrier thickness ratio. The overlap of wavefunctions of electrons and holes is calculated, showing considerable separation in space which significantly reduces the oscillator strength of the optical transitions, and consequently, the optical efficiency of nitride based light emitting diodes (LED) and laser diodes (LD). We have determined the dependence of the absorption spectra edge on the type of structure and also on the carrier concentration. Blue shift of the emission peak has been observed when comparing structures with higher dopants concentration.

[1] A. I. Liechtenstein, V. I. Anisimov and J. Zaane, Phys. Rev. B **52**, R5467 (1995).

[2] L.G. Ferreira, M. Marques, and L.K. Teles **78**(12), 125116 (2008).

16:00 Poster We32

The influence of the PVT growth conditions on the SiC crystal shape

Emil Tymicki[1], Katarzyna Racka[1], Krzysztof Grasza[1,2], Paweł Skupiński[2], Tomasz Wejrzanowski[3], Janusz Dagiel[3]

1. *Instytut Technologii Materiałów Elektronicznych (ITME), Wólczyńska, Warszawa 01-919, Poland* **2.** *Polish Academy of Sciences, Institute of Physics, al. Lotników 32/46, Warszawa 02-668, Poland* **3.** *Warsaw University of Technology, Faculty of Materials Science and Engineering (InMat), Wołoska 141, Warszawa 02-507, Poland*

e-mail: Emil.Tymicki@itme.edu.pl

The slightly convex crystallization front is necessary to ensure a bulk single crystal growth and formation of an appropriate surface morphology of SiC crystals [1]. These shape, morphology and the optimal growth conditions of crystallization process allow to obtain crystals with a good quality of the crystalline structure [2].

The crystallization front is an interface between a solid state and the gas phase, therefore its shape is affected by the temperature distribution in the crystal, and the way of providing of the SiC vapor components. In the SiC crystal growth by physical vapor transport (PVT) method it is a necessary the temperature gradient along the crystal growth direction. In order to obtain crystals with a slightly convex crystallization front there should be also applied the temperature gradient in the perpendicular direction. This shape provides a polytype and doping uniformity and also allows to control the propagation of defects, such as micropipes and dislocations.

In this work we investigate the factors, which can affect the shape of the SiC crystallization front. These factors cause mainly the change of the temperature field in the crystal and its surrounding. The first factor is the way of heating of the growth chamber by the heating system. A commonly used is an inductive or resistive heating, in which there are one or two heating sections. Our experiments have been done in the furnace, which was equipped with two independent resistance heaters. Thus, it was possible to control the axial and radial temperature gradients in the growth chamber during the crystallization processes [3]. The second important factor is an insulation, which is located above the growing crystal. In the experiments there was investigated the influence of the size of the channel through which the heat from the backside of the crystal is radiated. The radial temperature gradient in the crystal can be also affected by placing of the growth chamber in a different place of the heater. There were performed experiments in which the crucible was placed near the bottom of the heater or it was raised by a distance of 7 cm. The temperature and its distribution on the crystallization front may be also affected by the active interaction between the crystal growth surface and SiC source material [4]. There have been done the experiments with a different shape of the source materials and small distances between the crystallization front and the SiC source. Additionally, the effect of the open seed backside method [5] on the shape of the crystallization front in the first growth stage was investigated.

The aim of our research was to improve the crystallization growth conditions in order to obtain the SiC crystals with a slightly convex crystallization front. This crystal shape ensures a stable growth, in which there is minimalized a risk of polycrystal formation between the SiC crystal and the graphite ring. The lack of polycrystal allows to increase the diameter and the thickness of the obtained SiC crystals. Our works are fundamental studies to develop of the SiC crystallization growth conditions for growth processes, which result in lack of contact between the crystal and the wall of the graphite ring. The obtained SiC crystals will be free from defects and stresses originating from the contact between the crystal and a graphite ring.

Acknowledgements: This work was supported by the SICMAT Project co-financed by the European Regional Development Fund under the Operational Programme Innovative Economy (Contract No. UDA-POIG.01.03.01-14-155/09).

[1] Z. Herro, B. Epelbaum, M. Bickermann, P. Masri, A. Winnacker, J. Cryst. Growth, Vol. 262 (2004) 105.
[2] R. Yakimova, M. Syväjärvi, T. Iakimov, H. Jacobsson, R. Råback, A Vehanen, E. Janzén, J. Cryst. Growth, Vol 217 (2000) 255
[3] K. Grasza, E. Tymicki, K. Racka-Dzietko, M. Orzyłowski, Mater. Sci. Forum 679-680 (2011) 16
[4] K. Grasza, E. Tymicki, J. Kisielewski, Mater. Sci. Forum, 527-529, (2006) 87
[5] E. Y. Tupitsyn, A. Arulchakkaravarthi, R. V. Drachev, T. S. Sudarshan, „J. Cryst. Growth 299 (2007) 70.

16:00 Poster We33

The influence of atmosphere on β-Ga_2O_3 single crystal growth by floating zone

Marya E. Voronchikhina[1], Anatoly M. Balbashov[1], Boris I. Galagan[2], Ilia L. Shulman[2]

1. *Moscow power engineering institute (MPEI), Moscow 111250, Russian Federation* **2.** *A.M. Prokhorov General Physics Institute of Russian Academy of Sciences (GPI), Vavilov Str. 38, Moscow 119991, Russian Federation*

e-mail: asdf2984@mail.ru

β-Ga_2O_3 single crystal is the semiconductor material. It has IR and UV transparent. The material can have different applications in optic and optoelectronic fields, such as photodetectors, light-emitting diodes, conductive windows, transparent field effect transistors, phosphors, high temperature oxygen sensors and substrates for field-effect transistors [1].

β-Ga_2O_3 single crystals were grown by floating zone method at URN-2-ZM machine produced in MPEI [2].

Single crystals were grown from ceramic bar obtained by ceramic technology. The seed orientation was along (010) plane. At 10 mm/h growth rate the processes were stable. The growth processes were carried out in a variety of atmospheres, such as in air, Ar and O_2 atmosphere, under pressure of Ar and O_2 (up to 60 bar). The lengths of grown crystals were about 80 mm and diameter up to 15 mm. We used Laue method for single crystal orientation and twin definition. It was defined lattice parameters, they confirm with well-known data. We obtained transparent anisotropic single crystals with two clear marked parallel facets.

We couldn't grow single crystal in 80% Ar + 20 % H_2 mix atmosphere (1.5 bar), because of restoration Ga_2O_3 and strong evaporation.

The color of single crystals depends of growth atmosphere (type of gas and pressure). Influences of these two factors are different. It is seems that oxidizing atmosphere promote discoloration. We obtained colorless crystals when growth was under pressure of O_2 at 60 bar, and bluish crystals when growth was in air and Ar atmosphere.

The quality of growth single crystals depends on atmosphere and pressure too. The high quality crystal was grown under high pressure of oxygen.

Color and low quality can be associated with oxygen vacancies formation during crystal growth at weak oxidizing atmosphere. So at high

temperature, under low pressure and small oxygen concentration it is intensification of Ga_2O_3 decomposition [3].

Investigating transmission spectra It was occurred that colorless sample has enhanced transmission from 300 nm and over 1000 nm. Bluish samples have several bands at about 410, 480, 600 nm and sharp lose transparent in IR region. So it can be proposed that these bands correspond to oxygen vacancy appearance.

It was measured conductivities and permittivity. The results received was confirmed with assumption that oxygen vacancy appearance in violet single crystals grown at weak oxidizing condition.

β-Ga_2O_3 single crystal doped Ni was grown too. It shows a good width luminescence with maximum at 1430 nm and decay time 600 μs.

1. E. G. Villora, K. Shimamura, Y. Yoshikawa, K. Aoki, and N. Ichinose, J. Cryst. Growth 270, 420 (2004) 462-468
2. A.M. Balbashov, S.K. Egorov J. Cryst. Growth, 52 (1981) 498-504
3. Z. Galazka, R. Ueker, K. Irmscher, M. Albrecht, D. Klimm, M.Pietsch, M. Brützam, R. Bertram, S. Ganschow, and R. Fornari, Cryst, Res. Technol. 45, No. 12, (2010) 1229-1236

16:00 Poster We34

Modeling of growth kinetics of SiC single crystal in PVT process

Tomasz Wejrzanowski[1], Janusz Dagiel[1], Mateusz Grybczuk[1], Jakub Niescior[1], Emil Tymicki[2], Krzysztof J. Kurzydlowski[1]

1. *Warsaw University of Technology, Faculty of Materials Science and Engineering (InMat), Wołoska 141, Warszawa 02-507, Poland* **2.** *Institute of Electronic Materials Technology (ITME), Warszawa 01919, Poland*

e-mail: twejrzanowski@inmat.pw.edu.pl

The present paper deals with the design of optimal process conditions for manufacturing of single crystalline SiC with high quality. Different aspects of the technology have been taken into account. The geometry of the reactor was modified to obtain optimal mass transport and temperature profile. The influence of process conditions on the SiC crystal growth kinetics has been also studied. The results of modeling have been implemented in the SiC growth process developed for commercial use.

In these studies the Finite Volume method was applied to understand the phenomena taking place in the PVT (Physical Vapor Transport) reactor during growth of bulk SiC single crystal.

Numerical simulations predict the temperature distribution and growth kinetics at satisfactory level. It was found that especially the early stage of crystal growth might be controlled by changing the insulation types. Apart from the thermal conditions, which can be controlled directly by setting up the temperature on the heaters or indirectly by modification of insulation geometry, the gas pressure in the chamber is of key importance for the growth rate of SiC bulk single crystal.

16:00 Poster We35

Investigations on recombination mechanisms in InGaN/AlGaN multiple quantum wells

Ya-Fen Wu[1], Jiunn-Chyi Lee[2], Jeng-Kuang Huang[1], You-Wei Liu[1]

1. *Ming Chi University of Technology, Department of Electronic Engineering, New Taipei City 24301, Taiwan* **2.** *Taipei Chengshih University of Science and Technology, Department of Electrical Engineering, Taipei 11202, Taiwan*

e-mail: yfwu@mail.mcut.edu.tw

InGaN alloy system is attracting much attention because of its importance in both scientific and technological aspects. The wavelength emitted from InGaN can be tuned from visible red to ultraviolet by changing the alloy composition. The emission mechanism that occurs in the InGaN-based structures arises primarily from localized exciton emission. The localization of radiative electron-hole recombination is namely in a band-tail. These band-tail states are believed to be formed in local potential minima resembling quantum dots due to composition fluctuations, high density of impurity states and/or inhomogeneous lattice deformations. In addition, the quantum-confined Stark effect due to the presence of a large piezoelectric field in the quantum well is also considered to act as an important role in the emission mechanisms. The quantum-confined Stark effect (QCSE) arises from the presence of a large piezoelectric field in the quantum well. It has been discussed that the strain-induced piezoelectric polarization field plays an important role in carrier recombination in III-nitride quantum structures.

In this paper, we investigate the temperature and excitation intensity dependences of the photoluminescence (PL) spectra of InGaN/AlGaN multiple-quantum-well (MQW) heterostructures with different indium and aluminum content in the well and barrier layers. Three InGaN/AlGaN MQW samples used in this study were grown by metal-organic chemical vapor deposition system. Four pairs of InGaN/AlGaN MQWs were used as the active region and then 200-nm-thick p-GaN capping layer was grown above MQW region. During the growth of InGaN well layers and AlGaN barrier layers, the samples were grown under different trimethylindium (TMIn) and trimethylaluminum (TMAl) flow rates. The TMIn flow rates for sample A, sample B, and sample C were 128, 112, and 112 sccm, respectively; and the corresponding TMAl flow rates were 3, 3, and 6 sccm, respectively. The temperature dependent PL spectra were measured using a continuous wave He-Cd laser with a wavelength of 325 nm as the exciting source. The temperature and incident-power dependent PL spectra were measured using a He-Cd laser with a wavelength of 325 nm and the average excitation intensity was in the range from 1 to 30 mW. The samples were mounted in a closed-cycle He cryostat where the temperature was varied from 10 to 300 K. The luminescence was dispersed by a monochrometer and detected by photomultiplier using a standard lock-in technique.

Figure 1 shows the PL spectra of the InGaN/AlGaN MQW samples recorded at temperature 10 K with an incident power 30 mW. We observed InGaN-related main emissions with peak energies of 2.46, 2.47, and 2.42 eV for samples A, sample B, and sample C, respectively. Compare sample A and sample B with the same TMAl flow rate during the growth of MQW barriers, because the radiative recombination of InGaN-based MQWs is mainly due to excitons localized at deep traps originating from indium-rich regions in the wells, the slightly smaller PL peak energy of sample A is due to the more and deeper localized states in the well layers, resulting from its higher indium content. The indium content of sample C is lower than sample A; however, it exhibits the smallest PL peak energy among the samples. We attribute the result

to the large piezoelectric field and the induced QCSE in it, resulting from its highest aluminum content in the MQW barrier layers. The strain-induced polarization field tilts the potential profile, spatially separates between the electron and hole wave functions and significantly reduces the overlap integral between the electron and hole wave functions, which results in a redshift of the emission energy.

The emission energy as a function of temperature for the samples is shown in Fig. 2. With increasing temperatures, the PL peak energy of all the samples does not follow the Varshni law. The "S-shaped" temperature dependence of the PL peak energy is a fingerprint of the existence of the localization effect. It is strongly affected by the change in carrier dynamics with increasing temperature, and attributed to band-tail states in the density of states. The evident 'S-shaped' behavior observed for the temperature dependent PL peak energy of sample A implies that the carrier-localization effect is the dominant mechanism in this sample, mainly due to the higher indium content and the broadening band-tail states.

Figure 3 depicts the emission energy as a function of the incident power for the samples measured at 300 K, which is used to investigate the QCSE. When the samples are driven with an incident power, the piezoelectric fields in the strained well layer are screened by the injected carriers, thus weakening the QCSE. With the increasing incident power, because of the further weakened QCSE, the blueshift of peak energy occurs. We can judge the strain effect of these samples from the magnitude of the blueshift. Observing the measured results shown in Fig. 3, the blueshifts of the peak energy for samples A, sample B, and sample C are 10.2, 13, and 27.2 meV, respectively. It implies a stronger QCSE in sample C. Consequently, the inference obtained from the analysis of Fig. 1 for sample C is confirmed by the measurements of incident-power dependent PL spectra.

In this study, we investigate the emission mechanisms in the InGaN/AlGaN MQWs heterostructures with different indium and aluminum contents. Based on the measurements of temperature and incident-power dependent PL spectra from the samples, the exciton-localization effect and the QCSE are discussed. The 'S-shaped' variation of PL peak energy with temperature is enhanced for sample with higher indium content in the well layers, consistent with the band-tail states model. For sample with higher aluminum content in the barrier layer, the QCSE acts as an important role in the emission mechanisms.

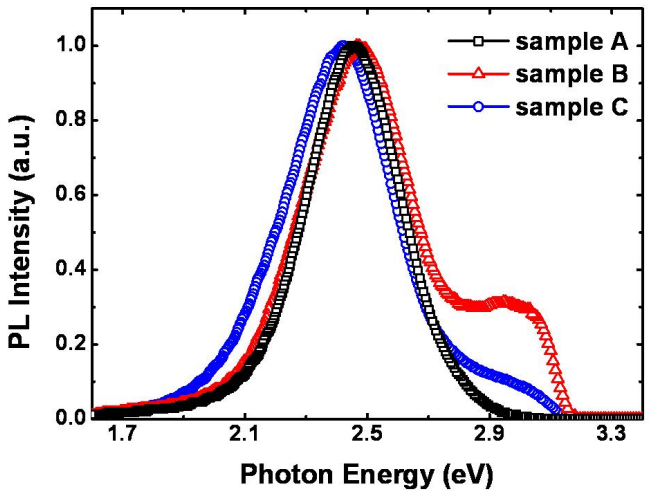

Fig. 1 Normalized PL spectra for sample A, sample B, and sample C at 10 K. The incident power is 30 mW.

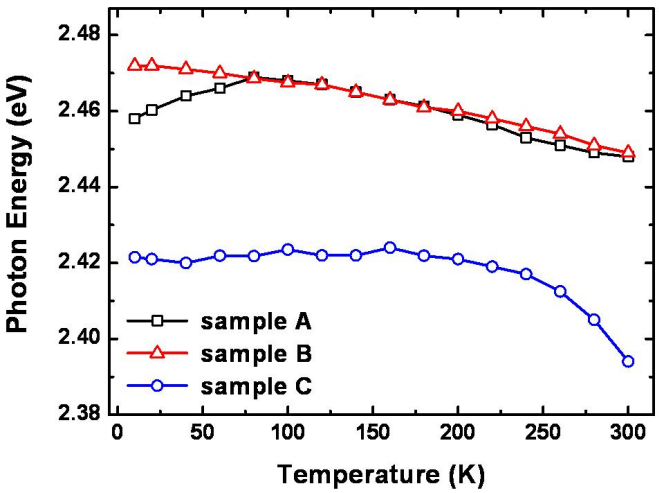

Fig. 2 Temperature dependence of peak position of luminescence spectra from sample A, sample B, and sample C at an incident power of 30 mW.

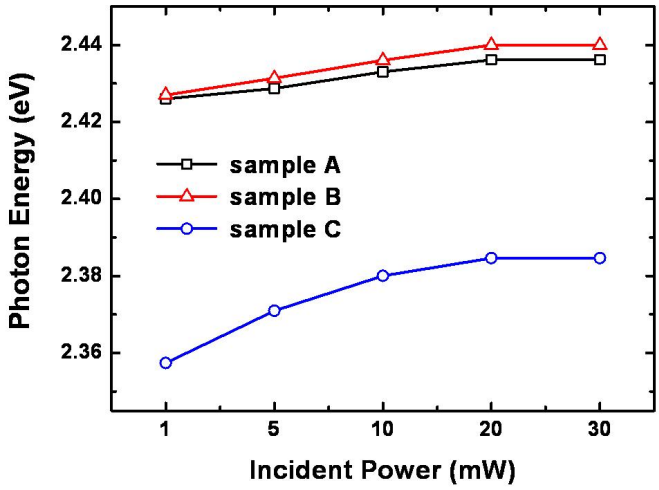

Fig. 3 Dependence of the spectral peak position on the incident power of the sample A, sample B, and sample C at 300 K.

16:00 Poster We36

Investigation of TMIn pulse duration effect on the properties of InAlN/GaN heterostructures grown on sapphire by pulsed metal organic chemical vapor deposition

JunShuai Xue, JinCheng Zhang, Yue Hao

Xidian University, School of Microelectronics (XIDIAN), South TaiBai Road, No.2, Xi'an 710071, China

e-mail: junshuaixue@hotmail.com

In this abstract, we report an experimental investigation of the effect of TMIn pulse duration on the properties of InAlN/GaN heterostructures grown on *c*-plane sapphire by pulsed metal organic chemical vapor deposition (PMOCVD). It is found that the TMIn pulse duration significantly influences the structural and electron transport properties of InAlN/GaN heterostructures.

High resolution X-ray diffraction and atomic force microscopy (AFM) measurements indicate that the crystalline quality of InAlN barrier is

strong dependent on the TMIn pulse time. With increasing TMIn pulse during from 0.1 to 0.4 min at intervals of 0.1 min, the indium content increases from 7.7 to 18.8 %, and a nearly lattice-matched indium content of 17 % is obtained at a TMIn pulse duration of 0.3 min. Simultaneously, an increase of electron mobility from 989 to 1538 cm^2/V s and a reduction of 2DEG density from 2.69×10^{13} to 1.17×10^{13} cm^{-2} accompany with the change of TMIn pulse duration. Upon an optimized TMIn pulse time of 0.3 min, a high electron mobility of 1428 cm^2/V s and a 2DEG density of 1.73×10^{13} cm^{-2} are achieved for nearly lattice-matched InAlN/GaN heterostructures, along with a smooth surface morphology with a root mean square roughness value of 0.21 nm observed by AFM in a 2×2 μm^2 scan area. While for the TMIn pulse duration of 0.1 and 0.4 min, small spiral hillocks and trench-like morphology appear on the surface of InAlN barrier, respectively.

In our work, the different dependence of structural and electrical properties on TMIn pulse time gives a further understanding of growth mechanism, and provides a useful guide to achieve high quality InAlN/GaN heterostructures with excellent transport properties by controlling the growth parameters of PMOCVD, such as pulse number and duration, pulse overlap and waveform. The presented results demonstrate the great potential application of PMOCVD in high quality InAlN/GaN heterostructures growth. As a promising approach besides of MOCVD and MBE, PMOCVD offers some advantages and provides more degree of freedom and flexibility to epitaxy of InAlN-related electronic and optoelectronic structures.

16:00 Poster We37

RF-MBE growth of GaN films on nitridated α-Ga_2O_3 buffer layer

Tomohiro Yamaguchi[1], Takumi Hatakeyama[1], Daiki Tajimi[1], Yohei Sugiura[1], Takeyoshi Onuma[2], Tohru Honda[1]

1. *Kogakuin University, 2665-1 Nakanomachi, Hachioji-city, Tokyo 1920015, Japan* **2.** *Tokyo National College of Technology (TNCT), 1220-2, Kunugida, Hachioji 193-0997, Japan*

e-mail: t-yamaguchi@cc.kogakuin.ac.jp

GaN and related alloys are one of the promising materials for applications in optoelectronic devices. These materials are typically grown on sapphire (α-Al_2O_3) substrates. Surface nitridation of α-Al_2O_3 is one of effective methods to obtain high-quality GaN films. However, there still has a lattice mismatch of more than 3 % between GaN and $AlON_x$ formed by the surface nitridation of α-Al_2O_3. Recently, the growth of high-quality α-Ga_2O_3 by mist chemical vapor deposition (CVD) was reported on a sapphire substrate [1]. When the α-Ga_2O_3 film is utilized as a novel buffer layer for the growth of GaN films, the lattice constant of α-Ga_2O_3 surface is expected to match with that of GaN after the surface nitridation of α-Ga_2O_3. This may lead the realization of higher-quality GaN films. In this study, GaN films were grown by radio-frequency plasma-assisted molecular beam epitaxy (RF-MBE) on the α-Ga_2O_3 buffer layers deposited on α-Al_2O_3 substrates by mist CVD. Effect of α-Ga_2O_3 surface nitridation was also investigated.

α-Ga_2O_3 buffer layers were grown on (0001) α-Al_2O_3 substrates by mist CVD. Typical full-width at half maximum (FWHM) value of (0006) α-Ga_2O_3 rocking curve measured by X-ray diffraction (XRD) was approximately 100 arcsec. After the growth of α-Ga_2O_3, the samples were introduced to the MBE chamber. Since α-Ga_2O_3 is a metastable phase in Ga_2O_3 structures, the surface of the α-Ga_2O_3 buffer layer was nitridated by irradiating a nitrogen radical beam under the temperature where no transformation of α-Ga_2O_3 to stable β-Ga_2O_3 phase occurred. Then, GaN films were grown on the nitridated α-Ga_2O_3 buffer layers by RF-MBE. As *in-situ* observation, reflection high-energy electron diffraction (RHEED) was utilized. The samples were also measured *ex-situ* by XRD analysis.

When the α-Ga_2O_3 buffer layer was annealed in a vacuum, the RHEED diffraction pattern intensity of α-Ga_2O_3 started to weaken at 620°C. From the result of XRD θ-2θ scan measurement, the new diffraction peaks different from the peaks of α-Ga_2O_3 were observed in the sample annealed at over 660°C. This suggests that the transformation of α-Ga_2O_3 to other structures occurred at over 620°C in a vacuum. When the surface nitridation of α-Ga_2O_3 buffer layer was carried out, the distance between streaks of the α-Ga_2O_3 RHEED pattern became close with that between streaks of the GaN RHEED pattern after the surface nitridation of 2 hours. The GaN films grown on the nitridated α-Ga_2O_3 buffer layers were found to have the epitaxial relationship of $[0001]_{GaN}//[0001]_{\alpha\text{-}Ga2O3}//[0001]_{\alpha\text{-}Al2O3}$ from the profile of XRD θ-2θ scan. The in-plane epitaxial relationship between GaN, α-Ga_2O_3 and α-Al_2O_3 was also found to be $<10\text{-}10>_{GaN}//<11\text{-}20>_{\alpha\text{-}Ga2O3}//<11\text{-}20>_{\alpha\text{-}Al2O3}$ from the results of XRD φ-scan measurements. These epitaxial relationships were the same as the cases without the use of α-Ga_2O_3 buffer layer. Details on the crystal quality of the GaN film will also be reported.

The authors would like thank Prof. Fujita and Dr. Kaneko of Kyoto Univeristy for technical supports of mist CVD growth. This work was partly supported by JSPS KAKENHI Grant Numbers #25706020, #25420341 and #25390071, TEPCO Memorial Foundation and ALCA project of JST.

[1] D. Shinohara and S. Fujita, Jpn. J. Appl. Phys. **47**, 7311 (2008).

16:00 Poster We38

Direct Comparison of ZnO single crystal grown by the hydrothermal and Pressurized melt growth method

Jigang Yin, Guangzhu Chen, Zhe Chen, Yin Hang, Kaijie Ning, Xiangyong Wang, LianHan Zhang, Peixiong Zhang

Shanghai Institute of Optics and Fine Mechanics China Academy of Sciences, Shanghai 201800, China

e-mail: yjg@siom.ac.cn

Among wide-band-gap semiconductors ZnO is one of the promising materials for the fabrication of UV and visible light emitting devices, which recently attracted particular attention due to its remarkable optical properties. Recently the melt and hydrothermal methods have been successfully used to grow two-inch, and even larger crystals. However, there still remain serious problems with bulk-ZnO crystals. The origin of the green emission in the ZnO is the most important among them. In this paper, a contrastive research was used to investigate the growth of ZnO single crystals grown by the hydrothermal and pressurized melt growth method. The crystals were processed under several annealing conditions and were characterized by photoluminescence spectroscopy (PL), Raman scattering and Electronic paramagnetic resonance (EPR) at room temperature. The origin of a green emission in undoped ZnO is discussed.

Topical Session 4

Compound semiconductors

Session Coordinators

Michael Fiederle (Germany) *michael.fiederle@fmf.uni-freiburg.de*

Gunther Springholz (Austria) *gunther.springholz@jku.at*

Programme

Wednesday, 14 August

WeP-T04
Wednesday afternoon, 14 August, 16:00
Room 107, Old Library

Break
Wednesday afternoon, 14 August, 17:30

Friday, 16 August

FrO1

T04: Compound semiconductors
Friday morning, 16 August, 8:30
Room C, Auditorium Maximum

8:30 Invited oral

Czochralski Growth of Indium Iodide

Aleksandar G. Ostrogorsky[1], Irina Nicoara[1], Dimitru Nicoara[1], Zhaopeng Xu[1], Charles Bertorrello[1], Michael Groza[2], Arnold Burger[2]

1. *Illinois Institute of Technology, 10 West 33rd Street, Chicago, Il 60616, United States* **2.** *Fisk University, Department of Physics, Materials Science and Applications Group, 1000 17th Ave. N., Nashville, TN 37208-305, United States*

e-mail: AOstrogo@IIT.edu

There has been only a small number of reported attempts to use the Czochralski process for growing the wide bandgap compound semiconductors, needed for the room temperature operated nuclear detectors.

The main difficulty is in the low chemical stability and high vapor pressure of the group II, V, VI and VII elements, leading to the off-stoichiometric composition, and various related defects. Among the heavy metal halides, indium mono-iodide presents an interesting exception. InI has a high disassociation energy and low relatively low vapor pressure, allowing for Czochralski pulling. We will describe the procedures used for synthesis, zone refining, Czochralski growth and characterization of indium iodide.

9:00 Oral

Nonstoichiometry of ZnTe and CdTe vapor grown crystals

Igor C. Avetissov[1], Elena Mozhevitina[1], Andrew Khomykov[1], Roman I. Avetisov[1], Albert A. Davydov[2], Vladimir P. Chegnov[2], Olga I. Chegnova[2], Nikolai V. Zhavoronkov[2]

1. *D.I.Mendeleyev University of Chemical Technology of Russia (MUCTR), Miusskaya sq. 9, Moscow 125047, Russian Federation* **2.** *Research Institute of Material Science and Technology (NIIMV), Проезд 4806, д.4, стр.2, Zelenograd Moscow 124460, Russian Federation*

e-mail: igor_avetisov@mail.ru

Extra pure ZnTe and CdTe single crystals were grown by Markov-Davydov vapor growth method [1] on a sapphire substrate. Crystals were formed at 1150-1350 K temperature range at pressures close to congruent sublimation conditions (Fig.1).

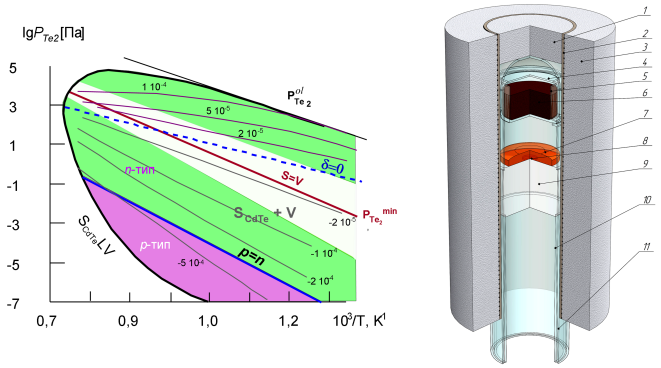

Fig.1. The scheme of CdTe and ZnTe vapor crystal growth by Markov-Davydov technique. Setup scheme (right) 1- thermo insulating cover, 2- ceramic tube, 3- thermoinsulation, 4- quartz glass reactor, 5- polycrystalline ingot, 6- quartz glass crucible, 7- growing crystal, 8- seed, 9- sapphire piedestal, 10- quartz glass tube, 11- plung for vacuume system connection. P_{Te2}-T projection of Cd-Te (left). Figures on isoconcentration lines shows the excess Te ("-" Cd) concentration at bivariant $S_{s\text{-}CdTe}V$ equilibrium. The white area covers the range of stable single crystal growth conditions.

The study of ZnTe and CdTe homogeneity ranges by direct physico-chemical method [2] in the temperature range 750-1365 K added by XRD analysis let us proposed the scheme of 3C-2H polymorphous transition in ZnTe and CdTe compounds. We proposed that polymorphous transition is followed by peritectic reactions at both Te-riched and Zn(Cd)-riched sides (Fig.2,3).

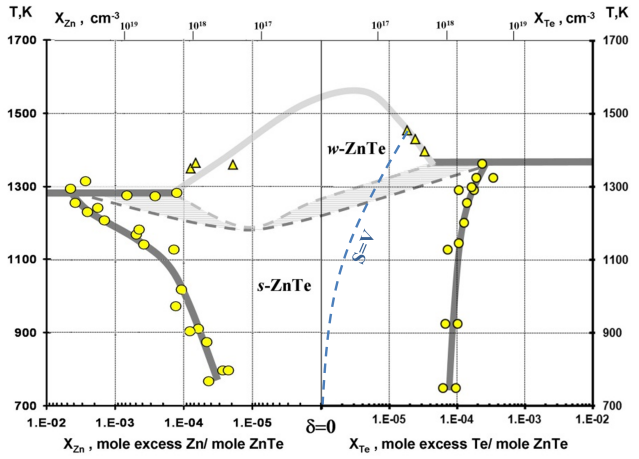

Fig.2. Homogenity region of ZnTe with the proposed scheme of 3C-2H polymorphous transformation

For the first time it was demonstrated that homogeneity region of undoped ZnTe included stiochiometric composition.

Analysis of luminescent and electrical properties of the as-grown and heat treated at different partial pressures single crystals was conducted.

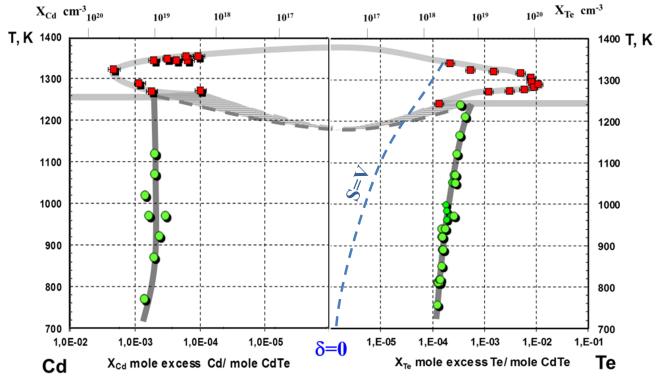

Fig.3. Homogenitty region of CdTe with the proposed scheme of 3C-2H polymorphous transformation

The research was supported by Ministry of Education and Science of Russia by grant N 16.513.11.3144

1. A.A.Davydov, et.al. (1992) *Neorg. Mater.* (*in Russian*), **28**, 42
2. I.Ch.Avetisov (2008) *Izvestia VUZov ser. Materialy Electronnoi Techniki* (*in Russian*), **3**, 68-75

9:15 Oral

Comparative studies on structural, compositional, morphological and optical properties of ZnSe and ZnSSe single crystals grown by CVT method

Perumal Kannappan, Ramasamy Dhanasekaran

Crystal Growth Centre, Anna University, Chennai 600 025, India

e-mail: kanna.phy6@gmail.com

Corresponding Author Email: *rdcgc@yahoo.com* ; Tel: +91-44 2235 8317

The ZnSe and ZnSSe single crystals are wide and direct band gap II-VI compound semiconductors. These single crystals are of immense importance in visible optoelectronic applications such as light emitting diodes (LEDs), laser diodes (LDs) and many electronic devices. The ZnSxSe1-x is a solid solution of two binary compound semiconductors ZnS (3.67 eV) and ZnSe (2.67 eV) where the band gap energy changes continuously with the composition of x. The ZnSe and ZnSSe single crystals were grown by chemical vapour transport (CVT) with iodine as a transporting agent. The source and growth temperatures of the reactor are 850˚C and 900˚C respectively using the two zone horizontal resistive heating furnace. The growth period was 15 days for ZnSe and 10 days for ZnSSe single crystals. The maximum dimension of the grown crystal is 9 x 7 x 5 mm^3. The grown crystals were characterized. The XRD pattern shows the peaks corresponding to (111), (200) and (311) planes which confirm the formation of crystalline phase. ZnSe and ZnSSe crystals belong to cubic zinc-blende structure. The composition of the grown ZnSe crystal were studied by EDAX analysis as Zn (52.5%) and Se (47.5%) and ZnSSe crystal has Zn (43.56%), S (29.86%) and Se (26.58%). The surface morphology of ZnSe and ZnSSe single crystals shows the parallel step growth pattern in the order of micrometer regions. The optical absorption study reveals the cut off wavelength as 483 nm (2.57 eV) for ZnSe and the 441 nm (2.81 eV) for ZnSSe single crystals. The photoluminescence show the band edge emission 440 nm and defect level emission at 590 nm. FT-Raman study shows the lattice vibrations of LO and TO modes which confirm the tetrahedral site symmetry of ZnSe and ZnSSe single crystals.

Key words: Crystal growth, Structural, Compositional, Surface morphological, Optical proeprties

9:30 Oral

CVT of Chalcopyrite Semiconductors

Rudolf Lauck[1], Manuel Cardona[1], Reinhard K. Kremer[1], Gisela Siegle[1], Jayprakash S. Bhosale[2], Anant K. Ramdas[2], Alfonso Muñoz[3], Aldo H. Romero[4]

1. *Max Planck Institute for Solid State Research, Stuttgart D-70569, Germany* **2.** *Purdue University, West Lafayette 47907, United States* **3.** *Universidad La Laguna, La Laguna 38206, Spain* **4.** *Unidad Querétaro, Querétaro 76230, Mexico*

e-mail: R.Lauck@fkf.mpg.de

Apart from the possible applications of I-III-VI_2 chalcopyrite-type semiconductors in opto-electronics and nonlinear optics, there has been a significant interest in the investigation of their physical properties. Unlike their II-VI analogs, the anomalous behavior displayed by these semiconductors is of particular interest.

In the present work, $CuGaS_2$ (CGS) and $AgGaS_2$ (AGS) crystals with different isotopic compositions were synthesized from their constituent elements in order to study their electronic, vibrational and thermodynamic properties. Before employing the chemical vapor transport (CVT) as growth method [1, 2], sulfur and copper were purified by sublimation and etching, respectively. The ^{109}Ag and the etched ^{71}Ga isotopes were purified from oxides by vacuum annealing. Elemental iodine or AgI was then added as transport agent with a concentration of 2-4 mg/cm³ (CGS) and 0.5-1.2 mg/cm³ (AGS). The source temperature was set to 880-940°C, yielding yellow, orange and green colored crystals (in the temperature range of 800-880°C) in the shapes of platelets, chunks, rods and needles of up to 7 mm (CGS) and 30 mm (AGS) in sizes. The surfaces of these crystals were observed to be plane (faceted), rounded or rough. At the source, crystals grew in dark and even in black color. The deposition of binary sulfides and iodides on the crystal surfaces during the ampoule cooling was prevented by a cold trap in order to preserve the surface quality. The ternary com-

pound compositions of the grown crystals were confirmed with Raman-spectroscopy.

The higher excitonic states (n = 2, 3) observed in these crystals at low temperatures with wavelength-modulated reflectivity indicate an excellent surface and crystalline quality. In addition, the experimentally determined non-monotonic temperature dependence of excitonic energies produces a good agreement with the Bose-Einstein oscillator model [3, 4]. Isotopic shift of excitonic energies has also been successfully observed in these crystals [5] and experimental results of heat capacities show a good agreement with the *ab initio* calculations [6, 7].

References:

[1] Y. Noda et al., J. Cryst. Growth 99 (1990) 757

[2] R. Lauck, J. Cryst. Growth 312 (2010) 3642

[3] J. Bhosale et al., Phys. Rev. B 86 (2012) 195208

[4] J. Bhosale et al., APS March Meeting 2013

[5] J. Bhosale et al., APS March Meeting 2012

[6] A.H. Romero et al., Phys. Rev. B 83 (2011) 195208

[7] M. Cardona et al., AIP Conf. Proc. 1506 (2012) 40

9:45 Oral

Growth of ZnTe - based microcavities on GaSb substrates

Tomasz Jakubczyk[1,2], Carsten Kruse[2], Wojciech Pacuski[1,2], Piotr Kossacki[1], Detlef Hommel[2]

1. *University of Warsaw, Faculty of Physics, Institute of Experimental Physics (IFDUW), Hoża 69, Warsaw 00-681, Poland* **2.** *University of Bremen, Institute of Solid State Physics, P.O. Box 330440, Bremen 28334, Germany*

e-mail: Tomasz.jakubczyk@fuw.edu.pl

We report on the molecular-beam epitaxy growth of ZnTe-based distributed Bragg reflectors (DBRs) and CdTe-based quantum wells on GaSb substrates. The aim is to use these structures as building blocks for future optoelectronic devices working in the yellow-orange spectral region.

We present details on the growth and discuss the photoluminescence measurements of a series of $Zn_xCd_{1-x}Te$ quantum wells with varying Zn/Cd ratio and thickness. The well with the highest Cd content exhibits emission at 600 nm at room temperature.

For the DBRs a MgSe/ZnTe/MgTe superlattice (SL) [1] is used as the low refractive index material. The structures were characterized by high resolution X-ray diffraction in order to find a thickness ratio for the SL that allows for lattice matching to the GaSb substrate.

The obtained results pave the way for the realization of a monolithic VCSEL that shows emission in the yellow-orange spectral region.

[1] W. Pacuski et al., Appl. Phys. Lett., 94, 191108 (2009).

10:00 Oral

Growth and Surface Studies of $Mo_XW_{1-x}Se_2$ Crystals

Rajendra Prasad Pathak[1], Dipakkumar Sahay[2], Ripal Parmar[1], Bhavesh Thakar[3], Kirit Patel[4], Vivek Pathak[4]

1. *R.R. Mehta College of Science C.L. Parikh College of Commerrce, Palanpur (RRMSCLPC), GD MODIVIDYSANKUL, OPP-ST WORKSHOP, HIGHWAY, PALANPUR, Palanpur 385001, India* **2.** *Govt. Engineering College, Gandhinagar (GECG), Gandhinagar, Gandhinagar 382017, India* **3.** *BS Patel Polytechnic, Ganpath Univeristy, Kherva, Gujarat (BSPP), Ganpath University, Kherva, Gujarat, Kherva 382041, India* **4.** *Department of Physics, Sardar Patel University, Vallabh Vidyanagar-388120, Gujarat, India, Vallabh Vidyanagar 388120, India*

e-mail: pathakrj@rediffmail.com

Recently, there has been a rise of interest in layered crystals, particularly transition metal dichalcogenides show signs of layered structures. The group VI Transition Metal Dichalcogenide compounds have been found to be highly stable against the environment. Several TMDCs are semiconducting compounds and widely used as a PEC solar cells, catalysts and also as a good lubricants. The compounds of TMDCs consists sandwiched layers i.e. X – M – X in which M atom layer is enclosed within two X chalcogenes layers. The interlayer binding forces are of van der Waals nature resulting in large interlayer distances and easy cleavability of these crystals. The crystals are anisotropic and leads to unusual structural properties. The Molybdenum diselenide, tungsten diselenide and mixed compounds of molybdenum and tungsten diselenides are diamagnetic indirect semiconductors belonging to this family.

Besides some technical complications the vapour transport technique has been proved to be very good technique to grow good quality single crystals. Single crystals of $MoSe_2$, WSe_2 and mixed system of these two compounds have been grown by direct vapour transport (DVT) technique using a two zone furnace from stoichiometric mixture of molybdenum (99.95% pure), tungsten (99.99% pure) and selenium (99.9 % pure). The source zone and growth zone temperatures were 1075^0C and 1055^0C respectively. The grown crystals were found to be gray and shiny irregular platelets. The average crystal dimensions were 3-10mm^2 in cross sectional area and few micrometers in thickness. The surface features of as grown crystals have been studied with the help of Optical Microscopy. The crystals grown by DVT technique possess 2H-hexagonal structure having /mmc space group and also contain only a little proportion of 3R polytype form. The optical micrograph shows the presence of screw dislocation on the surface of the grown crystals, which is clearly an indication that the growth of present materials in the form single crystals takes place via screw dislocation mechanism. Also the simultaneous presence of 2H and 3R polytypes is clearly seen in the optical micrograph, which confirms the results of XRD. On the other hand, the size and properties of grown crystals has been found to depend on the growth conditions also.

10:15 Oral

Te solution growth of twin-free CdMnTe crystal for detector applications

Tao Wang, Yuanyuan Du, Xin Zheng, Yadong Xu, Gangqiang Zha, Wanqi Jie

Northwestern Polytechnical University, Xi'an 710072, China

e-mail: czt.nwpu@gmail.com

CdMnTe is considered as the candidate material for x-ray and gamma ray detector applications. Production of CdMnTe crystal suffers from the low yield because of the severe twinning problem, which is caused by the transformation of the crystal structure of CdMnTe ingot during growth, when cooling to room temperature.

In this work, twin-free CdMnTe crystal was grown from Te solution with vertical Bridgman method. By adding excess Te, the growth temperature was lowered to 1293 K, 70 K below the melting point of $Cd_{0.9}Mn_{0.1}Te$. The phase transformation was thus avoided. Fewer twins were found in the as-grown CdMnTe crystal, compared with which grown from the traditional Bridgman method. The growth interface was studied. By using the optical microscope, SEM, IR transmission microscope and the confocal laser scanning microscope, the morphology of the growth interface was described macroscopically and microscopically. The possible growth mechanism was discussed. The optical and electrical properties of CdMnTe crystal were also investigated. PL spectrum showed good crystalline quality. High resistivity up to 2×10^{10} Ω·cm and good mutau products of electrons up to 1.6×10^{-3} $cm^2 \cdot V^{-1}$ was obtained. CMT detector was fabricated with planar electrode. Preliminary result with resolution of 10% for ^{241}Am@59.5keV was given. Further improve was expected with the optimization of the growth process and the detector evaluation system.

Coffee

Friday morning, 16 August, 10:30

FrO2

T04: Compound semiconductors
Friday morning, 16 August, 11:00
Room C, Auditorium Maximum

11:00 Invited oral

Vertical gradient freeze growth of GaAs using a heater magnet module (HMM)

Christiane Frank-Rotsch, Natasha Dropka, Alexander Glacki, Uta Juda

Leibniz Institute for Crystal Growth (IKZ), Max-Born-Str 2, Berlin 12489, Germany

e-mail: christiane.frank-rotsch@ikz-berlin.de

The development of GaAs vertical gradient freeze (VGF) growth process is focused on the increase of process efficiency by a reduction of the production costs with simultaneous improvement of the crystal quality. To meet this technological and scientific challenge, different strategies were proposed, e.g. an increase of crystal size, simultaneous crystallization in multi crucible furnace or an increase of growth rate. For process enhancement, an exact and permanent control of the melt flow is of crucial importance that is easily provided by traveling magnetic fields (TMF). The beneficial influence of Lorentz forces of crystal quality, which were generated by a KRIST*MAG*® internal heater-magnet module (HMM), was already reported for VGF Ge growth [1,2]. In analogous way to germanium growth, in the present investigation the HMM was positioned sidewise around the crucible and was supplied by a combination of direct current (DC) and alternating current (AC) for a coupled generation of thermal and magnetic fields. Thereby a wide range of electromagnetic parameters (frequency, current amplitude, phase shift) were available for process optimization. The influence of these magnetic parameters on the crystals growth in a HMM will be presented. Figure 1 shows an image of a 4 inch VGF GaAs single crystal grown in the HMM.

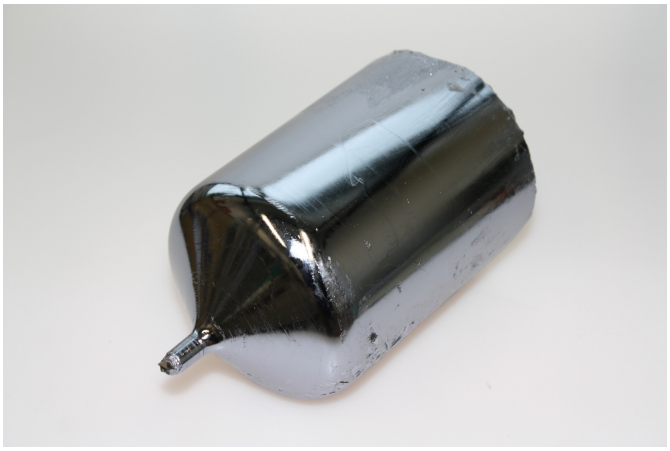

Fig. 1: Si doped 4 inch VGF-GaAs crystal grown in HMM

The key aspect of the presented investigation was the well-defined control of the solid/liquid interface bending in the grown VGF crystals. Therefore, a numerous preliminary 3D CFD global simulations of the whole furnace are inevitable. The both results, numerical and experimental, showed that the downward directed Lorentz forces generated near the crucible wall, if properly adjusted, may lead to a significant reduction of the concavity of the solid-liquid interface in comparison to the deflection characterizing crystals grown without TMF and to the data reported in the literature [3].

Study of charge carrier concentrations by Hall measurements also pointed out the differences in the crystals that were grown with and without TMF. The crystals exposed to TMF showed higher axial charge carrier densities. The radial charge carrier distribution was flattened due to the reduction of the interface deflection.

Moreover, simulation results revealed a potential for a further process improvement by an increase in a crystallization rate using TMF [4].

[1] Ch. Frank-Rotsch, P. Rudolph, Journal of Crystal Growth, 311 (2009) 2294-2299.

[2] Ch. Frank-Rotsch, U. Juda, B. Ubbenjans, P. Rudolph, Journal of Crystal Growth352 (2012) 16-20.

[3] R. Lantzsch,PhD Thesis, TU Freiberg (2009)

[4] N. Dropka, Ch. Frank-Rotsch, Journal of Crystal Growth, 367 (2013) 1-7.

11:30 Oral

Modeling of Dislocation Dynamics and Facet Formation in VGF of GaAs

Vasif Mamedov, Vladimir Artemyev, Andrey Smirnov, Vladimir Kalaev

STR Group, Inc., Engels av. 27, P.O. Box 89, St-Petersburg 194156, Russian Federation

e-mail: Andrey.Smirnov@str-soft.com

GaAs wafers are used for production of high-frequency microelectronics, multijunction solar cells, LED devices and in other applications. Requirements for wafer quality and price motivate crystal manufacturers for optimization of crystal growth technology to increase furnace productivity, wafer yield, and improve crystal quality. Since it is difficult to get accurate information about the crystal growth conditions

experimentally, computer modeling is being applied in industry for analysis and optimization of crystal growth processes. Specialized modeling capabilities of the software are important for quick and efficient technology optimization.

In the present work, we perform comprehensive analysis of 6-inch VGF GaAs crystal growth process using a specialized software for modeling of crystal growth, CGSim. Within this work, we performed unsteady modeling of GaAs growth process [1] coupled with melt and encapsulant flow, and melt/crystal interface shape evolution. Computation of the melt/crystal interface including facet formation [2] has been performed taking into account crystal orientation and local melt supercooling along the melt/crystal interface, which allowed us to estimate the probability of single crystal structure loss. Thermal stress evolution in the crystal during the growth process and cooling, and thermal stress release into dislocations within Haasen-Alexander-Sumino model [3, 4] have been calculated simultaneously with crystallization dynamics. As a potential direction of process optimization, different hot zone designs and configurations of traveling magnetic fields have been applied. The effect of TMF and furnace design on the melt flow pattern, interface shape and crystal quality is presented and discussed.

[1] K. Koai, K. Sonnenberg, H. Wenzl, J. of Crystal Growth 137 (1994) 59 – 63
[2] O. Weinstein, W. Miller, J. of Crystal Growth 312 (2010) 989–996
[3] H. Alexander, P. Haasen, Solid State Phys. 22, 27 (1968)
[4] M. Suezawa, K. Sumino, I. Yonegaga, J. Appl. Phys. 51, 217 (1979)

11:45 Oral

Some Optical Thermal and Electrical Properties of Bulk InP Crystal

Zhiguo Liu, Ruixia Yang, Fan Yang, Mustafa S. Omar, Goran M. Khalil, Tongnian Sun, Niefeng Sun

Hebei Semiconductor Research Institute, Scicence and Techonology on ASIC Laboratory, Shijiazhuang 050051, China

e-mail: niefengsun@gmail.com

Undoped InP single crystals were prepared with a rapid P-injection in situ synthesis liquid encapsulated Czochralski(LEC) method in an independently manufactured InP high pressure crystal puller, the physical properties were measured for the as grown single crystals by using the temperature control multipurpose cryostat, and all measurements were carried out under a vacuum of 10^{-3}mbar. The temperature dependent photoconductivity measurement was investigated. The photosensitivity spectrum at room temperature showed a peak at about 1.2869eV and shoulders around 1.2955, 1.3256, and 1.3392eV. The room temperature energy gap as 1.3392eV and its temperature coefficient in the range of 295-318K was found to be as $-3x10^{-4}$eV/K. The magneto-optical properties measurement up to 1.8 Tesla gave the magnetic coefficient of Eg as $8.6x10^{-4}$eV/Tesla. From this value, the reduced effective mass of electrons m_r* found to be as $0.0671m_0$. Measurements of Hall coefficient R_H, between 288K and 319K, were performed. Hall measurement for this sample at room temperature gave the Hall mobility and carrier concentration as $2950cm^2/V•S$ and $5.53x10^{15}cm^{-3}$ respectively. From thermoelectric power measurements, the room temperature Seebeck coefficient found to be as 565μV/K. This value, with that of the Hall measurements, the density of state effective mass m_d* was calculated and found to be as $0.0757m_0$. This value with that of the reduced effective mass of electrons mentioned above gave the effective mass of electrons in the valance band m_v* in this InP sample as $0.591m_0$.

12:00 Oral

Defect and Strain Analysis of Selective GaAs Epitaxy in STI Patterned Si (001) Substrate

Sun-Wook Kim[1], Young-Dae Cho[1], Won-Kyu Park[2], Chan-Soo Shin[2], Dae-Hyun Kim[3], Dae-Hong Ko[1]

1. *Yonsei University (Yonsei UNIV.), Sinchon-dong, Sudaemoon-ku, Seoul 120-749, Korea, South* **2.** *Korea Advanced Nano Fab Center, Suwon 443-270, Korea, South* **3.** *SEMATECH, Albany 12203, United States*

e-mail: shun701@yonsei.ac.kr

It is believed that the introduction of III-V materials in CMOS technologies needs to take advantage of the mature Si based technologies [1]. Among the significant progress in reducing the defect density in epitaxial GaAs grown on Si substrates, the selective epitaxial growth of the lattice mismatched materials in high aspect ratio trenches is well investigated route involving the elimination of dislocations by trapping of threading dislocations within trenches [2,3].

In this study, we carried out the epitaxial growth of GaAs layers in shallow trench isolation (STI) structures patterned on (001) Si substrates. The trench widths were 30 nm and 65 nm, and STI depths were 145 nm. The GaAs layer was deposited by metalorganic chemical vapor deposition (MOCVD) at 450~670°C. Patterned Si substrates with a Ge seed layer were also used to reduce the lattice mismatch between GaAs and Si. The microstructure and the channel strain were characterized using several techniques of TEM (JEOL, JEM-2100F) including nanobeam diffraction (NBD). The spatial resolution of NBD method was estimated to be around 2 nm with 0.1% strain resolution [4]. The TEM samples were fabricated using a focused ion beam (FIB) with 100 nm thickness.

Figures 1 show the low magnification TEM cross-sectional images of GaAs layers in trenches of 30 nm (Fig. 1(a)), 65 nm (Fig. 1(b)) widths, and 65 nm widths with Ge seed layers (Fig. 1(C)). In all the samples, the TEM image shows that all of the trenches are well filled with a GaAs layer and the defect free region is observed near the top region of the trench, except the stacking faults originating from the top oxide layer, and boundaries in the overgrown regions. This result indicates that the dislocations originating at the GaAs/Si or GaAs/Ge interface were trapped within trench region. Figures 2 are the high resolution TEM images of GaAs layers for each sample. For the case of the samples without Ge seed layer, the threading dislocations, micro-twins and stacking faults are clearly observed forming an about 55°angle with the [11] direction. <110>-oriented threading segments would all be inclined to the (11) oxide sidewalls in <110> {111} slip system [2]. The dislocations from the GaAs/Si interface terminate at the oxide sidewall within 50 nm heights. On the contrary, defect formation becomes more pronounced in GaAs layers with Ge seed layer due to the presence of interfacial oxide layer between Ge and GaAs, and the defect free region is shown above 70 nm from the GaAs/Ge interface.

In order to investigate the defects near the GaAs/Si interface, STEM and NBD measurements were performed. Figure 3(a) shows the HRTEM images of GaAs layers in 65 nm trench, and the STEM images from selected areas (Figs. 3(d) and 1(e)) reveal the twin boundary and micro-twins, respectively. NBD patterns obtained from each side of twin boundary clearly show that this twin structure is constructed by (11) mirror reflection or 180^O rotation around the [111] axis. The stress distributions acquired from spots as denoted by yellow circle in Fig. 1 are plotted in Fig. 3(f). In the samples without a Ge seed layer, the graphs indicate that more compressive stress is induced in GaAs layers

along the [110] direction at the bottom of trenches due to the smaller lattice constant of Si. The compressive stress gradually decreases up to the almost relaxed state near the top level of STI oxide. In the samples with a Ge seed layer, however, the compressive stress is induced only within a Ge seed layer and it seems that the GaAs layer is fully relaxed due to the high defect density. In addition, it is considered that the remaining compressive stress in GaAs layers is resulted from the STI oxides because STI oxide could act as a pedestal retarding the strain relaxation of GaAs layers.

References

1. M. M. Heyns, M. Meuris, and M. Caymax, *ECS Trans.* 3 (2006), p. 511.

2. J. Bai, J.-S. Park, Z. Cheng, M. Curtin, B. Adekore *et al,Appl. Phys. Lett*. 90 (2007), p. 101902.

3. J. Z. Li, J. Bai, J.-S. Park, B. Adekore, K. Fox *et al,Appl. Phys. Lett*. 91 (2007), p. 021114.

4. J.-H. Yoo, S.-W. Kim, S.-M. Koo, D.-H. Ko, and H.-J. Lee, *Appl. Phys. Lett.* 98 (2011), p. 133121.

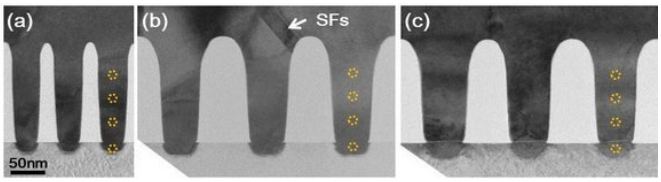

Figure1 Low magnification TEM cross-sectional images of GaAs layers in trenches of (a) 30 nm, (b) 65 nm widths, and (c) 65 nm widths with Ge seed layers.

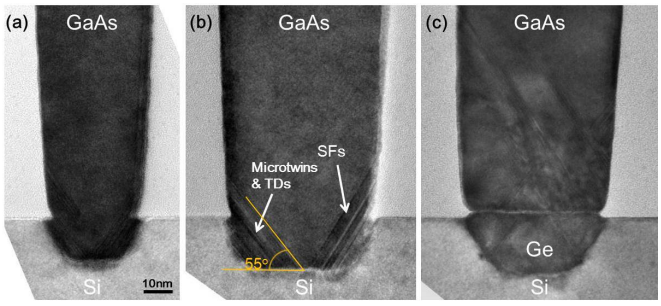

Figure2 High resolution TEM images of GaAs layers in trenches of (a) 30 nm, (b) 65 nm widths, and (c) 65 nm widths with Ge seed layers.

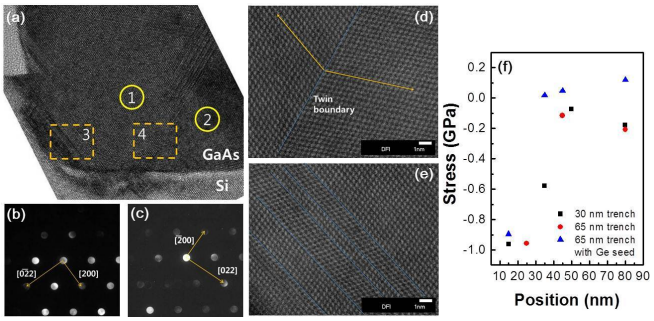

Figure 3 NBD patterns ((b), (c)), and STEM images ((d), (e)) from selected areas in (a) confirm the twin boundary and micro-twins. (f) The stress distributions acquired from spots as denoted by yellow circle in Fig. 1 using NBD method.

12:15 Oral

Strain Effect for Different Phosphorus Content of InGaAs/GaAsP Super-Lattice in GaAs p-i-n Single Junction Solar Cell.

Kentaroh Watanabe[1], Yunpeng Wang[1], Hassanet Sodabanlu[1], Masakazu Sugiyama[2], Yoshiaki Nakano[1,2]

1. *Research Center for Advanced Science and Technology, The University of Tokyo (RCAST), 4-6-1 Komaba, Meguro-ku, Tokyo 153-8904, Japan* **2.** *The University of Tokyo, 7-3-1 Hongo, Bunkyo-ku, Tokyo 113-8656, Japan*

e-mail: kentaroh@hotaka.t.u-tokyo.ac.jp

1. Introduction

A multiple quantum wells (MQWs) solar cell have an advantage of realizing higher open-circuit voltage (VOC) compared with a single junction solar cell composed by host barrier material alone [1]. Because the 1.2 eV effective band gap of optical absorber can be available with low degradation of PV performance, the InGaAs/GaAsP MQWs is one of the promised candidates as a middle cell of current-matched triple-junction solar cell [2]. Compensating a strain force on InGaAs well and GaAsP barrier layer each other during the epitaxial growth, totally minimized strain lead maximum PV performance [3]. A super-lattice (SL) consist of InGaAs well and extremely thin GaAsP barrier (~3nm) gives improved open-circuit voltage degradation at 1 SUN illumination compared to relatively thick (~10 nm) barrier thickness supported by improved carrier extraction efficiency assisted by tunneling effect through the thin barrier [4]. And also the InGaAs/GaAsP SL absorber in the i-region of GaAs p-i-n structure given better PV performance in concentrated sun irradiation by enhanced V_{OC} maintaining the its short-circuit current (J_{SC}) increment [5]. From the aspect of high-efficient correction of photo-generated carrier, both the crystal quality of SL and the carrier dynamics including a tunnel effect thorough the barrier layer is important issue for the SL solar cells. In this study, we prepared a different phosphorus content of InGaAs/GaAsP SL in GaAs p-i-n solar cells to evaluate the effect of barrier height for PV performance of SL cell.

2. Experiment

2.1.MOVPE growth of SL in p-i-n structure of GaAs

Figure 1 shows the schematic structure of GaAs p-i-n single junction solar cell with 60 periods of InGaAs/GaAsP super-lattice in the i-region. All of our samples were grown by a planetary metal-organic vapor phase epitaxy (MOVPE) system (AIXTRON, AIX2000HT) on n-type GaAs (001) substrate. A strain-compensated SL play a role of narrow bandgap photon absorber in GaAs p-i-n solar cell, should be resulted in increased current density (J_{SC}) compared to the GaAs bulk cell. During our MOVPE growth, substrate temperature was fixed to 610 ^{o}C and the inside pressure of growth chamber was controlled to 100 mbar. All of GaAs layer and the window $In_{0.5}Ga_{0.5}P$ layer were grown under the 15 of V/III ratio. As a III groups of MO source, we used the tri-methyl-gallium (TMG) and the tri-methyl-indium (TMIn), respectively. And also the tertiary-butyl-arsine (TBA) and the tertiary-butyl-phosphine (TBP) were used as a MO sources for V groups. Highly purified hydrogen was used as a carrier gas. We fabricated the SL samples with three different partial pressure of TBP by changing the source flow late. For the SL structure, the thickness of well and barrier designed as 5 nm and 3 nm, respectively. And total thickness of i-region was 800 nm for all samples. We also fabricated bulk GaAs p-i-n single junction solar cell as a reference sample whose thickness of i-region was same with SL cells. As an in-situ strain sensor, we used multi-beam stress monitor method (MOSS using the Laytech, Epicurve

System) for measuring the curvature of bowed wafer by accumulated strain during InGaAs and GaAsP growth. And during the SL growth, we applied the hydrogen purge for 1 s after InGaAs well gworth and subsequently also applied the 1sec TBP surface treatment before GaAsP barrier growth for improvement of interfacial abruptness between well and barrier [6].

After forming the backside planer and topside grid-pattern metal, mesa-etching by aqueous ammonia solution was applied for isolation each cell devices. Finally, the dual-layer of anti-reflection coatings (ARC) was applied by ZnS/SiO_2 sputtering on the top surface.

2.2.Structure evaluation

After MOVPE growth of SL samples, the high resolution x-ray diffraction (HRXRD) (004) omega-2theta scan was attempted for estimating the thickness and atomic composition for each well and barrier in SL layer. Consequently continuous wave photoluminescence (CWPL) and time-resolved photoluminescence (TRPL) was measured for each SL sample to evaluate the effective band gap energy and to observe the dynamics of photo-generated carrier at room temperature. For the measurement of CWPL, wavelength of the excitation laser diode was 784nm and varied excitation power range was attempted in the range of 1.28-12.8 mW/mm^2. The TRPL measurement was carried out by time-correlated single photon counting (TCSPC) method illuminating excitation pulsed laser with 12 pJ/pulse of energy. The excitation laser wavelength was also 784 nm and the pulse repetition frequency was 10 MHz. At the TRPL measurement, by using the monochromater, only 7nm of bandwidth of PL light was extracted at the peak wavelength obtained from the CWPL spectrum. The photon counting rate was set around 1% by regulating the number of PL photon with neutral density filter. Estimated time resolution of TRPL measurement was approximately 0.4 ns determined by instrumental response function (IRF).

2.3.Evaluation of solar cell

For obtained SL and reference bulk GaAs cells, PV performance was also evaluated. The current-voltage (I-V) characteristics was observed under AM1.5 G (100 mW/cm^2) simulated illumination to determine their short-circuit current density (J_{SC}), open-circuit voltage (V_{OC}), fill factor (FF) and power conversion efficiency (η). Spectral response of the solar cell was measured by illuminating calibrated monochromatic light for estimating the external quantum efficiency (EQE). All of the measurement for PV characterization was carried out with sample temperature fixed to 25 ^{O}C as a standard condition.

3. Result and Discussion

3.1. Detail sample structure from XRD and MOSS measurement

Figure 2 shows the result of XRD measuremnt. Sufficiently sharp satellite peaks from InGaA/GaAsP SL layer was observed, indicating high crystal quality of sample. Fitting the model to the observed XRD rocking curve, we have estimated each well and barrier composition and thickness, respectively. Table.2 shows the fitting result of each sample. Approximately 5.1nm thickness of and 11% of indium content for well InGaAs layer was fixed for the series of samples. And the barrier thickness is also similar to 3.1 nm for each sample. The gradually different phosphorus content of barrier layer was obtained corresponding to the phosphorus partial pressure difference during SL growth. For the sample of No. 788, 794 and 900, the phosphorus content was estimated as 13%, 18% and 24%, respectively. The total accumulated strain situation was clearly shown in Fig. 3. Plotting the transient of wafer curvature during the growth, each SL samples showed significant wafer bowing indicated the accumulated compressive strain direction. Because the compressive strain should be provided by InGaAs well layer on GaAs substrate in this SL system, so compensating tensile strain was insufficient for compensating total strain. Comparing the curvature transition for the sample No. 788 and No. 900, total accumulated compressive strain was reduced by increasing the phosphorus content in GaAsP barrier.

3.2. PL result

Figure 4 shows the measured CWPL spectrum of the SL cell samples of No.788, 794, 900. Each PL spectrum indicated the two individual peaks at 874 nm and around 915 nm, should be corresponding to the bulk GaAs bandgap and the SL effective bandgap energy, respectively. The PL peaks corresponding to the SL effective bandgap also shifted to shorter wavelength with increasing phosphorus content in GaAsP barrier. This result seems to be due to the increased confined energy level in the well accompanied with the higher potential barrier of increased phosphorus content in GaAsP. Relative intensity of PL peaks for each sample became stronger for the higher phosphorus content SL sample. Because the sample structure is very similar except to the barrier GaAsP composition in SL layer, this result may indicate that the reduced total compressive strain by increasing phosphorus content in barrier resulted in reduced defect density in SL layer. Figure 5 showed the excitation power dependent CWPL peak intensity at the wavelength of the bulk GaAs and the SL effective bandgap. In all SL cell samples, the SL related peak became rapidly stronger than the GaAs rerated peak. The photo-generated carriers in SL layer were forced to move to n and p GaAs region accelerated by built-in potential in the SL put in GaAs p-i-n structure. Because the case of larger number of carrier with high excitation rate resulted in the potential screening by escaped carriers in n and p region, therefore weaken effective built-in potential should provide increased carrier recombination rate in SL region. Figure 6 showed the TRPL decay curve at the GaAs and the SL effective bandgap peak of CWPL. Showing TRPL decay curve compared for two different strain condition of sample No788 and 900. The decay curve of SL related peak was almost similar to the decay curve provided from IRF. Therefore, the time-scale of photo carrier recombination in the SL layer is estimated shorter than 0.4 ns. On the other hand, the decay curve of GaAs related peak showed two different time scale; one is sufficiently faster than IRF (0.4 ns) and secondary tail of decay curve with ~1 ns of timescale. The sample structure include the flat potential region only allowing for n- or p-type GaAs layer, so the longer lifetime of PL decay is likely indicate the carrier diffusion timescale in flat-band potential of n- or p- type GaAs region.

3.3. PV performance

Finally, all of the SL cells and the reference GaAs cell evaluated as a photovoltaic performance shown in Fig. 7 and Fig. 8, and summarized in Table. 3. The SL cell samples showed similar J_{SC} around 30 mA/cm^2, ~2 mA/cm^2 larger than the reference bulk GaAs cell. Figure 7 shows the normalized EQE spectrum of different phosphorus content of SL cells and the reference bulk GaAs cell. All of samples of SL layer inserted in GaAs p-i-n structure absorbs longer wavelength photons beyond the GaAs cutoff wavelength λ=870 nm up to λ=930 nm, resulted in the increase in JSC. The shoulder of extended EQE spectrum in SL cells slightly changed by consistent to the effective bandgap energy examined by CWPL. The series of SL cells showed increased η with larger P content sample, and the best sample was No.900 with η=24.35%. The efficiency of SL cell depends on strongly on the V_{OC} clearly different with phosphorus content in SL. Figure 8 shows the I-V characteristics of each cell, showed the improvement of V_{OC} in the SL cell samples with reduced total accumulated strain. For the larger phosphorus content of barrier GaAsP should be resulted in the higher potential barrier for the electrons and holes in well InGaAs layer. In these series of SL samples, the thickness of indium content of the well is constant, so the result of larger η of SL cell with larger phosphorus content seems to be opposite tendency. Hence, we can conclude the

around 3.1 nm of barrier thickness is sufficiently thin for realize the tunneling effect through the barrier transporting carrier to n- region for electrons and p- region for holes. And we also conclude the total strain accumulation in SL layer degrade V_{OC} possibly due to the density of defects introduced not lattice-mismatch itself but by the strain accumulation in MOVPE growth.

4. Conclusion

MOVPE gown super-lattice consist of the InGaAs well and GaAsP barrier inserted in the i-region of GaAs p-i-n structure was one of the useful approach to change the effective band gap of solar cell from the 1.42 eV for bulk GaAs toward smaller remaining high-crystal quality by strain compensating. We tried approximately 3.1 nm of very thin barrier thickness of SL with different phosphorus content of GaAsP barrier by changing different partial pressure of TBP during SL growth. Actually reduced total compressive strain accumulation was examined by in-situ curvature measurement for high-phosphorus content barrier of SL. CWPL and TRPL measurement was also revealed the compressive-strain-reduced SL sample relatively strong CWPL intensity and small carrier recombination timescale in SL than 0.4 ns. The series of solar cell samples with different strain accumulated SL was evaluated their performance. The smaller compressive accumulated SL cell showed recovery of open-circuit voltage and resulted in larger power conversion efficiency in spite of taller height of barrier potential in SL layer. This result indicated that the defect related PV degradation possibly recovered by reduced total accumulated strain. And also the enhanced carrier transportation assisted by tunneling effect through the thin-barrier apparently contributed to the PV performance.

Acknowledgments

A part of this study is supported by Research and Development of Innovative solar Cell program, New Energy and Industrial Technology Development Organization (NEDO), Japan.

References

[1] K. Barnham, et al., *J. Appl. Phys*., **80**, p1201 (1996)

[2] N. J. Ekins-Daukes, et al., *Appl. Phys. Lett*., **75**, p4195 (1999)

[3] H. Sodabanlu, et al., *Jpn. J. Appl. Phys*. **51**, p10ND16 (2012)

[4] Y. Wang, et al., *IEEE J. Photovoltaics*, **2**, p387 (2012)

[5] K. Watanabe, et al., *AIP conf. Proc. of CPV8*, **1477**, p40 (2012)

[6] S. Ma, et al., J. Cryst. Growth, **352**, p245 (2012)

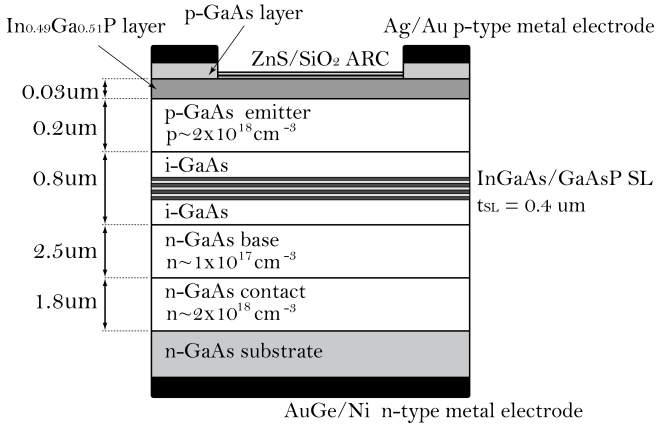

Fig.1 Schematic sample structure of GaAs p-i-n solar cell with InGaAs/GaAsP SL in the intrinsic GaAs layer.

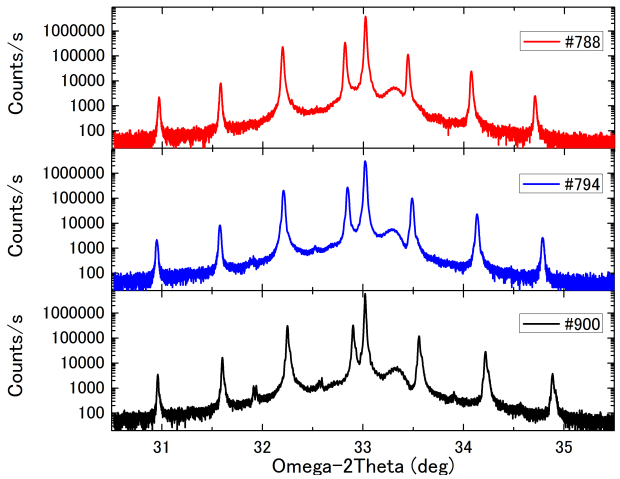

Fig.2 HRXRD (004) omega-2theta scans for each different phosphorus content of SL cells.

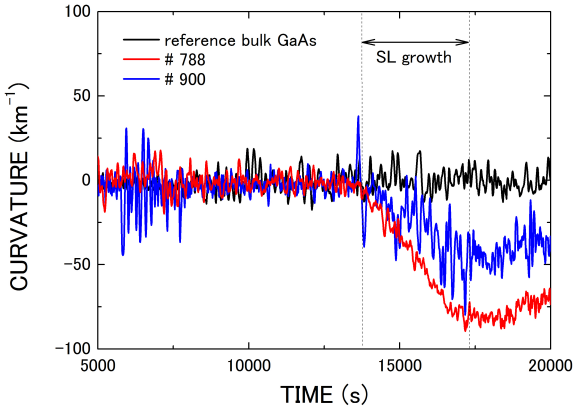

Fig.3 Time-dependent wafer curvature for the SL samples with different phosphorus partial pressure during SL growth.

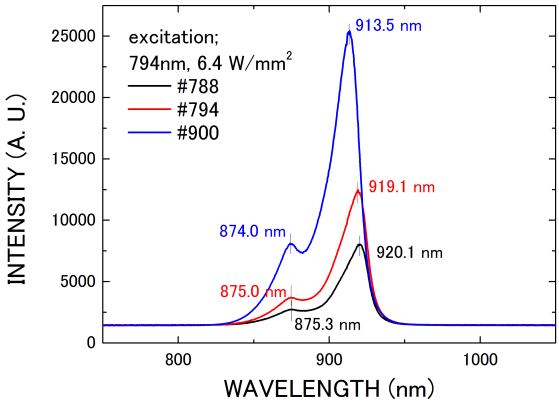

Fig.4 CWPL spectrum for the SL cell samples of No.788, 794 and 900.

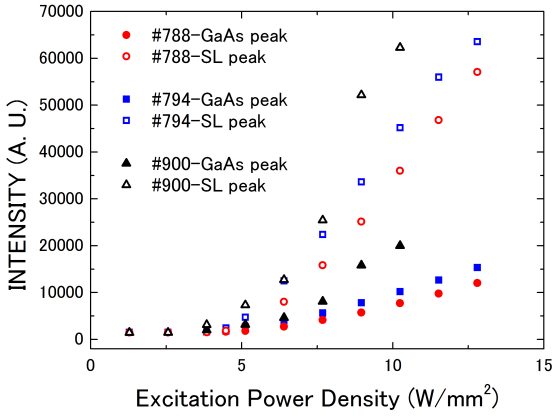

Fig.5 Excitation power dependency of the CWPL peak intensity of the SL cells at the wavelength corresponding to the GaAs bandgap (filled simbol) and the SL bandgap (blank simbol).

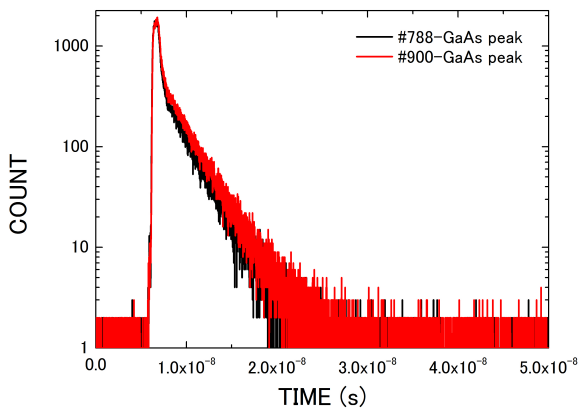

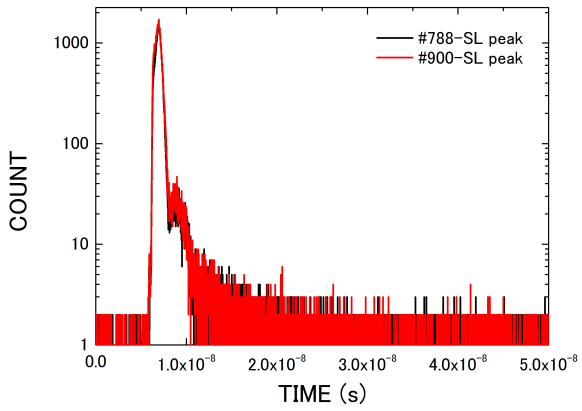

Fig.6 Time-dependent photoluminescence decay for the SL cell samples No.788 and No.900 at the wavelength corresponding to the GaAs bandgap (top) and the SL bandgap (bottom).

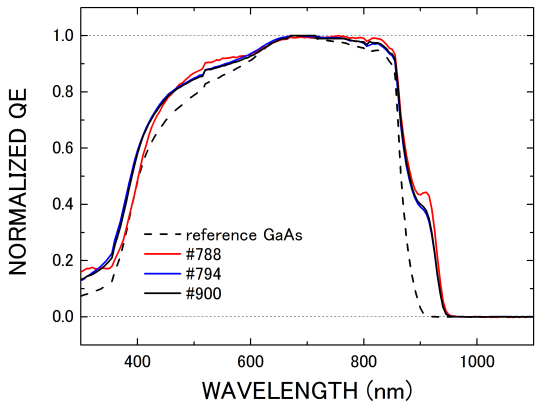

Fig.7 EQE spectrum of the SL cells and the reference GaAs bulk cell.

.

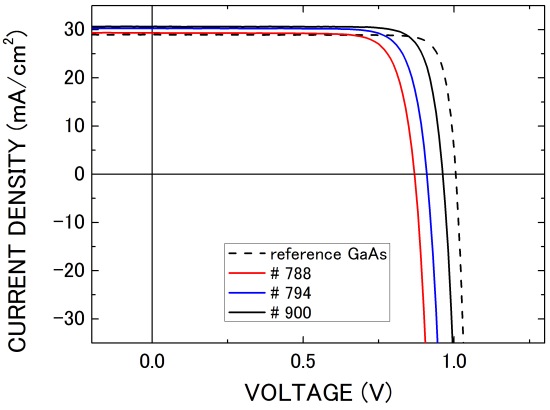

Fig.8 I-V characteristics of the SL cells and the reference GaAs bulk cell under AM 1.5 G illumination.

Table.1 Partial pressure condition of TBA and TBP for SL growth.

Sample No	Partial pressure for TBA ($\times10^{-2}$ mbar)	Partial pressure for TBP ($\times10^{-2}$ mbar)	V/III ratio
#788	4.56	7.07	39.3
#794	4.56	12.2	56.7
#900	4.56	16.2	70.0

Table.2 Thickness and composition of well and barrier estimated from XRD result.

	well		barrier	
Sample No	composition	Thickness (nm)	composition	Thickness (nm)
#788	$In_{0.11}Ga_{0.89}As$	5.1	$GaAs_{0.87}P_{0.13}$	3.2
#794	$In_{0.11}Ga_{0.89}As$	5.1	$GaAs_{0.82}P_{0.18}$	3.1
#900	$In_{0.11}Ga_{0.89}As$	5.1	$GaAs_{0.76}P_{0.24}$	3.1

Table.3 PV performance of the different phosphorus content of SL cells and the reference cell.

Sample No	J_{SC} (mA/cm^2)	V_{OC} (V)	FF	η (%)
Reference GaAs	28.98	1.005	0.8608	25.07
#788 SL	29.35	0.8689	0.7960	20.30
#794 SL	30.30	0.9099	0.8034	22.15
#900 SL	30.66	0.9624	0.8249	24.35

Closing ceremony
Friday afternoon, 16 August, 13:00

Posters

Wednesday, 14 August

WeP-T04
Wednesday afternoon, 14 August, 16:00
Room 107, Old Library

16:00 Poster We67

Nonstoichiometry and optical properties of ZnSe crystal grown from melt and vapor

Igor C. Avetissov[1], Khan Chan[1], Nikolai V. Zhavoronkov[2], Albert A. Davydov[2], Elena Mozhevitina[1], Andrew Khomykov[1], Svetlana P. Kobeleva[3], Sergei Neustroev[2]

1. *D.I.Mendeleyev University of Chemical Technology of Russia (MUCTR), Miusskaya sq. 9, Moscow 125047, Russian Federation* **2.** *Research Institute of Material Science and Technology (NIIMV), Проезд 4806, д.4, стр.2, Zelenograd Moscow 124460, Russian Federation* **3.** *National University of Science and Technology (MISIS), Leninsky prospect, 4, Moscow 119049, Russian Federation*

e-mail: igor_avetisov@mail.ru

ZnSe single crystals are of great interest as perspective materials for X-ray detectors and VIS-IR transparent windows for lasers. But till now there is no sufficient data on ZnSe homogeneity region, especially with the emphasis on wurtzite - sphalerite (3C-2H) polymorphous transformation close to the melting point. The proposed scheme of this transformation was performed in [1] based on DTA experiments.

In the present research we studied ZnSe homogeneity region by direct physical-chemical method [2] in the temperature range 765-1320 K (Fig.1). It was found out that homogeneity region of undoped ZnSe included stoichiometric composition and retrograde behavior of solidus lines both from Zn- and Se-rich sides was observed. Comparison of Zn nonstoichiometry with the of ionized defect concentrations at $S_{s\text{-}ZnSe}$-$L_{(Zn)}$ equilibrium let us say that at the above conditions the dominant point defects are electrically neutral.

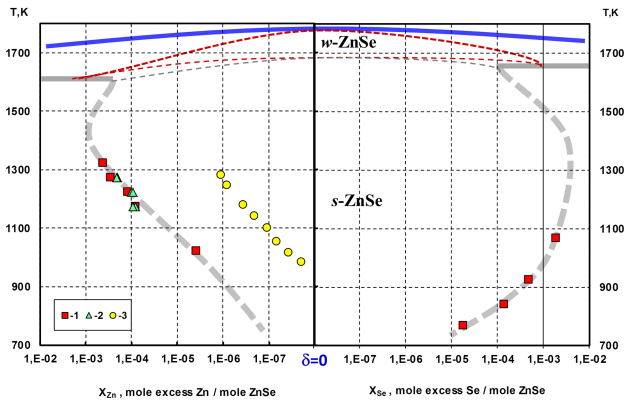

Fig.1. Homogeneity region of ZnSe with the proposed scheme of 3C-2H polymorphous transformation [1]: 1, 2- our data, 3 – calculated from free carrier concentrations [3].

In the research we studied the crystal properties produced by vapor and melt growth techniques. The vapor growth was conducted by Markov-Davydov method [4]. The crystals did not touch in contact with growth reactor walls and was grown on a sapphire substrate. As-grown crystals were 100 mm diameter and 20-25 mm height.

Other crystals were grown from the melt by directional solidification under high (100 atm) static pressure. The melt growth was conducted from graphite and glass carbon crucibles.

As a source materials we used CVD-ZnSe [5] and muli-resublimation process (4 steps) in dynamic vacuum. Due to ICP-MS analysis melt grown crystals in carbon glass crucible and vapor grown crystals were as pure as source materials. In case of a graphite crucible we observed a decrease of crystals purity.

Nonstoichiometry of all materials was examined. For the crystals the correlations between growth conditions, nonstoichiometry, luminescent properties (Fig.2) were found out.

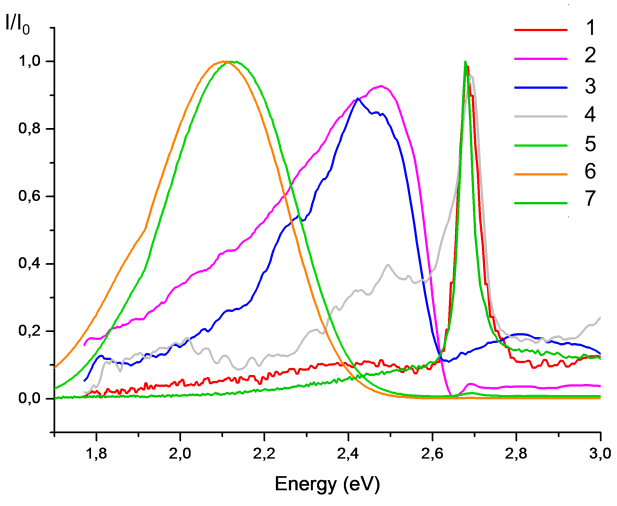

Fig.2. PL spectra of ZnSe preparations at 300 K (λ_{ext}=370 nm): 1-re-sublimated polycrystal, 2- CVD-ZnSe N1 after synthesis, 3- CVD-ZnSe N2 after synthesis, 4- CVD-ZnSe N2 (after extraction of an excess component), 5-melt grown crystals at high pressure in graphite crucible, 6- melt grown crystals at high pressure in glass-carbon crucible, 7- vapor grown crystal.

In case of vapor grown crystal (7) and resublimated ZnSe polycrystal we observed exciton peak 2.68 eV with FWHM 0.04 eV and 0.06 eV,

correspondingly. Melt grown crystals demonstrated 2.10 eV (6) and 2.13 eV (5) luminescence with FWHM 0.35 eV, which could be attributed with Se nonstoichiometric defects in ZnSe crystals. Synthesized CVD-ZnSe preparations were characterized by complex spectra but the main peaks were 2.48 eV (3) and 2.69 eV (2). According to nonstoichiometry determination these peaks were attributed with excess Zn in CVD-ZnSe preparations.

The research was supported by Ministry of Education and Science of Russia by grant N 16.513.11.3144

1. Okada H., Kawanaka T. J. Cryst. Growth. **165** (1996) 31-36.
2. I.Ch.Avetisov *Izvestia VUZov ser. Materialy Electronnoi Techniki* (*in Russian*), **3**, (2008) 68-75
3. F.T.J. Smith Solid State Communications **7**, Issue 24, (1969) 1757–1761
4. A.A.Davydov, et.al. *Neorg. Mater.* (*in Russian*), **28** (1992) 42
5. Devyatykh G.G., Gavrishuk E.M., Murskii G.L., Korshunov I.A. Patent 2046843 (RU)

16:00 Poster We68

VGF Growth of CdTe Crystal Assisted by Axial Vibration Control Technique Under Controlled Cadmium Pressure

Igor C. Avetissov, Andrey P. Sadovskiy, Mikhail Grishechkin, Vladimir Meshkov, Andrew Khomykov, Vladimir Kostikov, Ekaterina Sukhanova, Elena Mozhevitina

D.I.Mendeleyev University of Chemical Technology of Russia (MUCTR), Miusskaya sq. 9, Moscow 125047, Russian Federation

e-mail: igor_avetisov@mail.ru

Axial Vibrational Control (AVC) technique is a powerful tool for conrol of convective flows (CFs) in the melt with desirable velocity and configuration. In Czochralski and Brigdman crystal growth the AVC technique was realized by axial low-frequency harmonic oscillation of an inert baffle submerged into the melt [1, 2]. An application of low-frequency vibrations made it possible to increase in several times crystal growth rate [2], to decrease dislocation density up to unit value [3], to enhance crystal perfection [4,5]. It was experimentally established that AVC efficacy based on melt structure transformation [6]. All these open perspectives for successful invention of AVC technique to other scheme of crystal growth. Taking into account an intensive mixing of the melt and leveling of component concentrations at application of AVC technique we demonstrated the efficiency of partial pressure control at CdTe crystal growth [7].

CdTe has very low thermal conductivity and it is difficult to withdraw the crystallization (latent) heat in case of large diameter crystal growing with a fast rate. Numerical simulation showed that solid "tails" were formed at seeded VFG growth of 50 mm diameter CdTe crystals (Fig.1). AVC application with specially configured oscillating disk let us dissolved the "tails" and supported a flat interface at comparatively high growth rate (Fig.2).

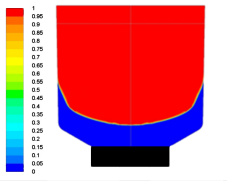

Fig.1. Numerical simuletion of crystl-melt interface position at CdTe VGF crystal growth at 5 k/cm gradient and 5 k/h crystallization rate.

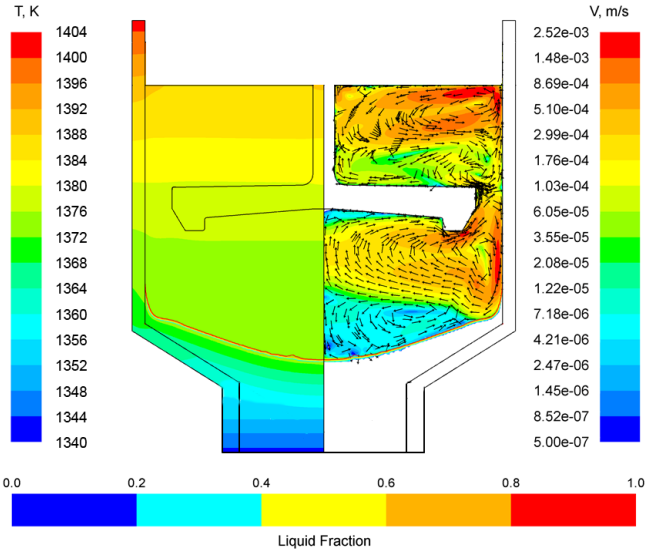

Fig.2. Mean flow velocity (right) and static temperature (left) maps at the baffle oscillation at 25 Hz frequency and 0.25 mm amplitude with solidification contours near crystal-melt interface at CdTe VGF crystal growth at 5 k/cm gradient and 5 k/h crystallization rate..

We designed and made a VGF setup assisted by AVC unit and possibility to control cadmium partial pressure using van-Doorn technique [8] (Fig.3).

CdTe crystals were grown at different Cd partial pressure and their electrical properties, structure perfection, impurities and nonstoichiometry distribution both cross-section and longitudal were analyzed. We succeeded to control the crystal type (*n,p*) by varying Cd pressure from 0,2 to 3 atm at different growth processes.

The research was supported by Ministry of Education and Science of Russia by grant N 16.552.11.7046.

[1] I. Avetissov et al. Doklady Physics, **54**, N. 9, 410 (2009)
[2] R. S. Feigelson, E. V. Zharikov, Investigation of the Crystal Growth of Dielectric Materials by the Bridgman Technique Using Vibrational Control, NASA Final Technical Report for #NAG8-1457-06, 2002
[3] I. Avetissov et al. J. Cryst. Growth **318**, 979 (2011)
[4] I. Avetissov et al. Doklady Physics **54**, N. 9, 410 (2009)
[5] Y. Zhang et al., J.Cryst.Growth **310**, 5432 (2008)
[6] I. Avetissov et al. J.Cryst.Growth (2012)
[7] I. Avetissov et al. CrystEngComm **15**, 2213 (2013),
[8] C.Z. van Doorn *Rev. Sci. Instr.,***32,** 755 (1961)

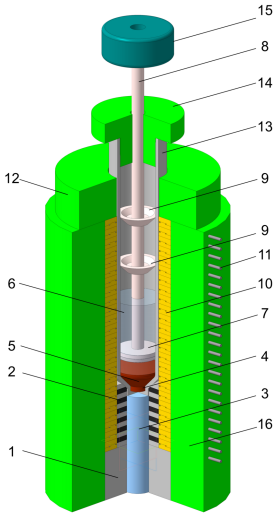

Fig.3 Scheme of CdTe VGF crystal growth setup. 1- thermo insulating stand, 2- graphte rings, 3- saphire heat removal cylynder, 4- seed, 5- crystal, 6- melt, 7- graphite vibrating baffle, 8- vibrating graphite rod, 9- Cd melt drops capture plates, 10- plate resistive heaters with ceramic, 11- heater lead-out wire, 12- thermo insulation, 13-graphite reactor, 14- thermo insulating plug, 15- vibrator

16:00 Poster We69

Investigation of morphological stability of melt/crystal interface at CZT crystal growth by the AHP method under high pressure

Svetlana V. Bykova, Vladimir D. Golyshev

CrystalsNord (CRYST), Oktiabrskaya 6 21, Aleksandrov 601654, Russian Federation

e-mail: svetlana.bykova@CrystalsNord.ru

In papers [1,2] the possibility of novel Axial Heat flux close to the Phase interface crystal growth method (AHP method) was analyzed by numerical simulation to find conditions for obtaining Zn uniform distribution in CZT. These results was used and as a results a uniform Zn distribution for all volume of CZT 2 inch ingot was obtained. Crystals of CZT were grown under high pressure of Ar without using seed. But for high-pressure (HP) AHP crystal growth there is some evaporation of Cd, the melt is concentrated by Te and the temperature of crystallization is decreased. So, morphological instability of the melt-crystal (m/c) interface can occur, it results in micro inclusions of Te. To grow CZT crystal without micro inclusions the area of morphological stability of the m/c interface was found for AHP CdZnTe crystal growth.

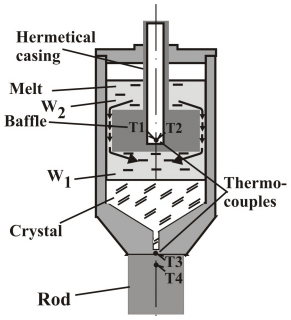

Fig.1

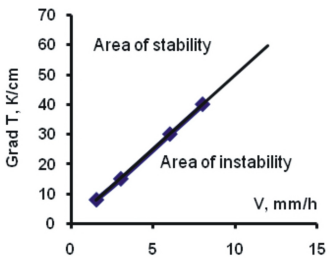

Fig.2

A set of AHP crystal growth experiments were conducted at different values of temperature gradient and crystal growth rate to find the area of morphological stability. CZT ingots were grown in 2 and 3 inches graphite crucibles using the AHP baffle as shown in Fig. 1. The thermocouples T_1 - T_4 were used to calculate axial temperature gradient in the melt, $gradT_m$. The values of $gradT_m$ were in the range of 5 – 60 K/cm. The accuracy of control of temperature was within 0.05 – 0.1 K. For obtaining a large value of *gradTm* the crystals were grown with a small distance between bottom of the AHP baffle and a melt/crystal (m/c) interface). Crystal growth rate V was in the range of 1 – 20 mm/hour.

The grown crystals were cut along the longitudinal direction and position of the m/c interface found where morphological instability took place. The crystal growth rates and values of $gradT_m$ were calculated for these m/c interface positions using a one dimensional heat transfer model, values of temperature *T1* and *T3, T4* and their temporary dependence. Thus, the set of data *Vi* and $gradT_m i$ were found which resulted in the morphological instability. The obtained data is presented in Fig. 2.

1. A. Yeckel, J. J. Derby, J. of Electronic Materials, Vol. 33, No. 6 (2004) 1-12.

2. M. Marchenko, V. Golyshev, S. Bykova, J. of Crystal Growth 303 (2007) 193–198.

16:00 Poster We70

A Comprehensive Model of the Growth of Cadmium Zinc Telluride (CZT) by the Traveling Heater Method (THM)

Jeff H. Peterson, Andrew Yeckel, Jeffrey J. Derby

University of Minnesota, Chemical Engineering and Materials Science, 421 Washington Ave. S.E., Minneapolis, MN 55455, United States

e-mail: derby@umn.edu

The traveling heater method (THM) has enjoyed particular success for the growth of cadmium telluride (CdTe) and cadmium zinc telluride (CZT). Unlike in conventional melt growth, THM material is grown via a different path on its phase diagram, notably from a liquid solvent phase that contains excess tellurium. This solvent phase is produced in a liquid zone that is moved (via a traveling heater) past a charge of CdTe or CZT. Desirable attributes of THM include lower growth temperatures and material that contains less excess tellurium than material grown from the melt. However, growth rates in THM are typically orders of magnitude less than in melt growth processes.

THM is inherently more complicated than melt growth methods, since compositional effects, including both phase equilibria and phase change kinetics, are of paramount importance. Hence, our fundamental understanding of THM is limited in comparison. In this presentation, we formulate a comprehensive mathematical model for this process, along with rigorous phase diagram information, using the framework of our prior crystal growth models that account for heat and species transfer, fluid mechanics, and moving, phase-change interfaces. We then summarize the finite element methods employed for solution of this model and present initial results.

Our objective is to study and understand THM growth characteristics, such as interface shape, thermal gradients, interfacial stability, and crystal composition (both tellurium excess and zinc distribution). In particular, we will examine parametric process sensitivity to factors such as growth rate, heater profile, and size of the melt zone. In particular, we examine phenomena that limit achievable growth rates in this system, such as constitutional supercooling, growth kinetics, and dissolution rates of the feed into the zone.

Supported in part by U.S. National Science Foundation, NSF DMR-1007885, the content of which does not necessarily reflect the position or policy of the United States Government, and no official endorsement should be inferred.

16:00 Poster We71

Modeling the Migration of Tellurium-Rich, Second-Phase Particles in Cadmium Zinc Telluride (CZT) via Temperature Gradient Zone Melting (TGZM)

Kerry Wang, Andrew Yeckel, Jeffrey J. Derby

University of Minnesota, Chemical Engineering and Materials Science, 421 Washington Ave. S.E., Minneapolis, MN 55455, United States

e-mail: derby@umn.edu

Crystals of cadmium zinc telluride (CZT) typically exhibit significant populations of large (10 micron and above) tellurium-rich particles that are deleterious to the performance of semiconductor radiation detectors. While it is well understood that melt growth of CZT can produce crystalline material that is supersaturated with tellurium, providing a thermodynamic basis for the existence of these second-phase particles, their formation mechanisms are not well understood.
As an alternative to preventing particle formation during the growth process (which may not be possible), an interesting post-growth treatment may provide a means to higher-quality crystals. Namely, these large, tellurium-enriched, secondary-phase particles can be induced to move away from a region of grown crystal and accumulate elsewhere, leaving higher-quality regions that contain far fewer particles. This accomplished by heating the sample to slightly above the eutectic temperature (the melting point of the second-phase particles) and engineering a temperature gradient across the sample. Under such conditions, the now-liquid particle dissolves on the hot side and re-solidifies on the cool side, with a net effect of migrating toward the hotter region. This process is termed "temperature gradient zone melting," or TGZM. We will present the formulation and implementation of steady-state and dynamic models that employ the Galerkin finite element method and elliptic mesh generation techniques to solve for particle migration via TGZM. Such an approach is particularly well suited for rigorous and accurate representation of geometrical and interfacial interactions in this system. We will also present initial results to verify the model and identify the dominant physical interactions involved in this process. We will also compare preliminary model results with data currently being taken on TGZM applied to CZT crystals in experiments at Brookhaven National Laboratories conducted by collaborators at Alabama A&M University.

Supported in part by U.S. Department of Homeland Security, 2012-DN-077-ARI066-02, the content which does not necessarily reflect the position or policy of the United States Government, and no official endorsement should be inferred.

16:00 Poster We72

Optical characterization of dilute nitride of InSb bulk crystals grown by vertical directional solidification technique

Manisha D. Deshpande[1], Dilip S. Maske[1], Dattatray Gadkari[1], Brij-Mohan Arora[2]

1. *Mithibai College (MITHI), Vile-Parle, Mumbai 400056, India*
2. *Tata Institute of Fundamental research (TIFR), Homi Bhbha Rd, Mumbai 400005, India*

e-mail: manishauj@gmail.com

The band gap of Indium antimonide could be substantially reduced by the doping of highly electronegative Nitrogen. Theoretically, it was expected that one percent of nitrogen should reduce the band gap by 100mev. This reduction in the band gap will make the material suitable for the far infrared detection . A lot of work is done on thin films of dilute nitrides of InSb by various researchers. in our laboratory, three bulk crystals of InSbN are grown by vertical directional solidification (VDS) technique. Through VDS technique, high quality binary compounds such as InSb and GaSb are successfully grown. For the growth of InSbN, the source materials Indium, Antimony and Indium nitride are sealed in an ampoule with tapered end on one side. The growth is carried out at 3mm/hour at reduced pressure of argon. The VDS method is advantageous for dilute nitride bulk crystals since it reduces the need for continuous flow of nitrogen or presence of nitrogen plasma. The resultant ingots were found detached from the ampoule wall. This was expected since the prior growths of InSb and GaSb bulk crystals were also found detached from the ampoule wall, resulting in high quality crystal. The physical properties were studied. The smooth appearance of the crystal, uniform diameter across the length and other studies confirm the crystal quality. EPMA was carried out for compositional analysis. The analysis confirmed the successful incorporation of nitrogen in the compound. Each ingot is about 35 mm in length and 12 mm diameter. The graph of absorption versus energy was plotted to study shift in the energy band gap with the help of FTIR. The deviation in the shift to smaller wavelength was attributed to high carrier concentration. The corresponding Moss-Burstein shift in the energy gap was calculated. The calculated values of the energy band gap due to all effects is summed up and compared with the observed values. Also the material is analyzed using Raman spectroscopy. The analysis shows change in intensity in Raman shift from LO to TO with increase in nitrogen content. The physical properties of InSbN are reported in detail.

16:00 Poster We73

The effect of charge composition on the microstructure of CdZnTe single crystals grown by sefl-seeding

Yuri Ivanov, Arsen Muslimov, Vladimir M. Kanevsky, Denis A. Zolotov, Pavel A. Prosekov, Oleg A. Kondratiev, Alexandr E. Balgov, Marina D. Pavlyuk

Institute of Crystallography, Russian Academy of Sciences, Moscow, Russian Federation

e-mail: Yurivanov@ns.crys.ras.ru

In this work, the effect of the deviation of crystal composition from stoichiometry was studied by the observation of precipitates and low-angle boundaries. Precipitates were observed using infrared microscopy and by atomic force microscope in the phase-contrast mode, and low-angle boundaries were revealed by X-ray diffraction.

16:00 Poster We74

Growth, structure and magnetic properties of $ZnCr_2Se_4$ – single crystals doped by dysprosium.

Izabela J. Jendrzejewska[1], Paweł Zajdel[2], Ewa Maciążek[1], Maria Sozańska[3]

1. *University of Silesia, Institute of Chemistry (UŚ), Szkolna 9, Katowice 40-006, Poland* **2.** *University of Silesia, Institute of Physics, Uniwersytecka 4, Katowice 40-007, Poland* **3.** *Silesian University of Technology, Department of Materials Science, Krasińskiego 8, Katowice 40-019, Poland*

e-mail: izajen@poczta.wp.pl

$ZnCr_2Se_4$ is a cubic spinel that exhibits interesting structural and magnetic properties, directly related to the presence of localized 3d electrons of the Cr^{3+} ions. The presence of magnetic dysprosium in crystal lattice causes essential changes of the physical properties of $ZnCr_2Se_4$. Growing of quaternary spinel-type chromium selenide single crystals requires a special version of the chemical transport.

The synthesis of the spinel-type selenides was carried out according to the reaction:

$$4(1–x)ZnSe + 4xDySe + (2+x)CrCl_3 = Zn_{1–x}Dy_xCr_{2+x}Se_4 + 3(1–x)ZnCl_2 + 3xDyCl_3$$

for x = 0.1÷0.2

The single crystals of $ZnCr_2Se_4$ spinel doped with dysprosium were prepared by the chemical vapour transport (CVT) in closed silica tubes using stoichiometric contents of ZnSe, DySe and $CrCl_3$ as the transporting agent. The transporting agent $CrCl_3$ dissociates to $CrCl_2$, $CrCl_4$ and Cl_2 above 773K. The transporting reactions, during which $CrCl_3$, $CrCl_4$ and Cl_2 are transporting agents were used to calculate the equilibrium coefficients in a heterogeneous system (a gas phase and some solid phases) using the computer program H.S.C. Chemistry 6.1. The ZnSe-DySe-$CrCl_3$ system fulfils conditions for the simultaneous transport of ZnSe and DySe (the same sign of enthalpy and the same value of volatility) and the crystallisation of the

$Zn_{1-x}Dy_xCr_{2+x}Se_4$ - single crystals. The plots for the dependence of the equilibrium constant vs. temperature for the transport reactions 1-9 are shown in Figure 1.

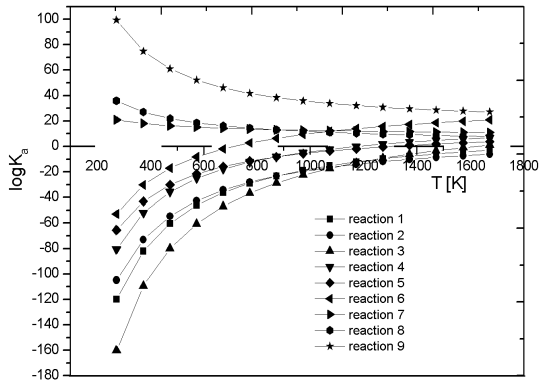

Fig. 1. Dependence of the equilibrium constant K_a on the reaction temperature T for transport with $CrCl_3$ (reactions 1-3), with $CrCl_4$ (reactions 4-6) and with Cl_2 (reactions 7-9).

The ampoules containing powdered substrates were placed in a horizontal furnace, where a melting zone temperature of 1173÷1273K and crystallization zone temperature of 1043÷1143K were used. The furnace was cooled during one day after 14 days of heating.

Chemical composition of single crystals of $Zn_{1-x}Dy_xCr_2Se_4$-system with different concentration of dysprosium was analyzed using scanning electron microscopy (Figure 2).

The single crystals were investigated at room temperature on the Oxford Diffraction Xcalibur diffractometer with Sapphire 3 CCD detector. A black piece of approx dimensions 0.04x0.12x0.12 mm was sliced from the larger octaherdon shaped crystal.

The multiscan absorption correction was done using CrysAlis package with estimated transmission in the range T(max) = 1.0, T(min) = 0.152 and data quality factors

R_{int} = 0.060/0.049, R_{sig} = 0.058/0.008. The structure refinements, taking into account site occupancy factors, indicated that Dy-ions shared octahedral sites with Cr-ions.

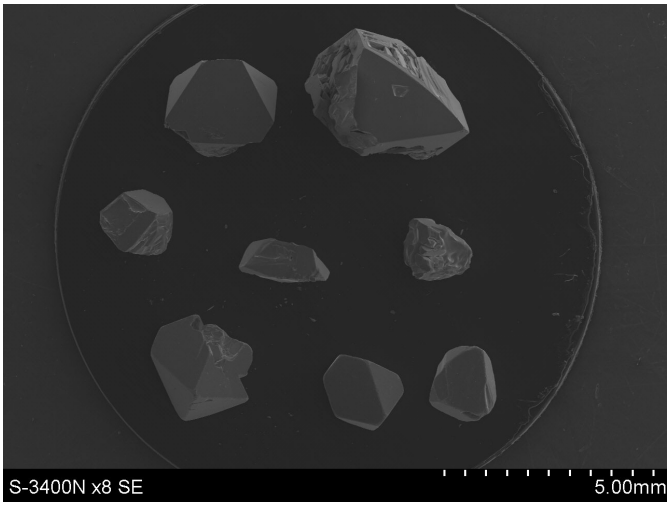

Fig.2. The single crystals of $Zn_{1-x}Dy_xCr_2Se_4$ obtained by CVT-method.

The magnetization measurements were carried out over the temperature range 2–300 K using a Quantum Design SQUID – based MPMSXL – 5-type magnetometer with magnetic field of 0.5T and found that saturation moment and transition temperature were affected by the presence of dysprosium.

Details of structural and magnetic investigations will be presented.

This work is funded from science resources for years 2011-2014 as a research project (project No. N N204 151940).

16:00 Poster We75

Microstructural and vibrational properties of PVT grown Sb_2Te_3 crystals

Konstantin A. Kokh[1,2,3], Victor Atuchin[4], Tatyana Gavrilova[4], Natalia Kuratieva[5], Natalia Pervukhina[5], Nikolai Surovtsev[6]

1. *Institute of Geology and Mineralogy SB RAS (IGM), Koptyuga ave., 3, Novosibirsk 630090, Russian Federation* **2.** *Novosibirsk State University (NSU), Pirogov 2, Novosibirsk 630090, Russian Federation* **3.** *Tomsk State University (TSU), Lenina, 36, Tomsk 634050, Russian Federation* **4.** *Institute of Semiconductor Physics SB RAS, Lavrentjeva 13, Novosibirsk 630090, Russian Federation* **5.** *Nikolaev Institute of Inorganic Chemistry SB RAS (NIIC), Acad. Lavrentiev Ave., 3, Novosibirsk 630090, Russian Federation* **6.** *Institute of Automation and Electrometry, Koptyuga ave., 1, Novosibirsk 630090, Russian Federation*

e-mail: k.a.kokh@gmail.com

Antimony telluride, Sb_2Te_3, is a well-known thermoelectric material. Besides, for several recent years Sb_2Te_3 has been of great interest because of topological insulator properties. The formation of Sb_2Te_3 crystals with high-quality structure is of prime importance for comparative diagnostics of thin films and nanostructures fabricated by epitaxial and chemical synthesis techniques. In present study the high-quality Sb_2Te_3 microcrystals have been grown by physical vapor transport (PVT) method without using a foreign transport agent. High purity (4N) elementary Sb and Te were used in the growth experiment. An element charge of 15 g weighted in stoichiometric composition Sb:Te = 2:3 was fused in a quartz ampoule sealed at residual pressure ~10^{-4} bar. After synthesis the ampoule was inclined so that the melt was located in a high temperature part of the ampoule, while opposite end was under temperature below melting point of Sb_2Te_3. Duration of experiment was around 20 hours. Resulting PVT-grown plate-like crystals were up to 1 mm in size which may suppose relatively high vapor pressure of Sb_2Te_3 melt. Micromorphology of crystals formed on the ampoule walls was observed by SEM using LEO 1430 device. The microplates are well facetted. The phase composition of grown crystals has been identified by X-ray single crystal structure analysis. The X-ray intensity data were collected on a Bruker X8Apex CCD diffractometer using standard techniques (ω- and φ-scans of narrow frames) and corrected for absorption effects (SADABS). The structure was solved by direct methods and refined by full-matrix least-squares on F^2 using the SHELX97 program set. The structure was defined in space group R-3m, a = 4.2706(1) Å, b = 30.4758(8) Å, V = 481.35(2) Å3, Z = 3 (R = 0.029). Raman microspectrometry has been used to describe the vibration parameters of Sb_2Te_3 microcrystals. Raman scattering experiment was carried out in back-scattering geometry with a triple grating spectrometer TriVista 777 under illumination by a line of λ = 488 nm of argon laser at room temperature. An achromatic lens with the focal length of 40 mm was used for focusing laser beam and collecting scattering light, at the same time. The low laser power of 15 mW was used, and it was verified that, under the conditions of our focusing system, this power does not affect the sample. The representative Raman lines observed at 82, 117 and 139 cm^{-1} are well related to known spectrum of Sb_2Te_3. Thus, the PVT growth is applicable for the preparation of high-quality stoichiometric Sb_2Te_3 microcrystals.

Acknowledgements: This study is supported by Ministry of Education and Science of the Russian Federation (Contracts 16.518.11.7091 and 2.8575.2013).

16:00 Poster We76

The growth habit, morphologies and vapor free-growth mechanism of ZnSe crystal directely grown from zinc and selenium

Huanyong Li

Northwestern Polytechnical University, Xi'an 710072, China

e-mail: lihuanyong5@gmail.com

The congruent sublimation of ZnSe compound is the negative conditional factor to ZnSe crystal vapor growth in zinc-selenium system. By replacing the homogeneous reaction between Zn(g) and Se_2(g) with non-homogenenous one, we developed a modified chemical vapor transport (CVT) method to grow ZnSe single crystals directely from zinc and selenium with the assistant of NH_4Cl transport agent, which has been recognized as the cheapest and the simplest technology to achieve ZnSe single crystals. ZnSe crystal grown free in this zinc-selenium-NH_4Cl system looks like the platelets, exhibiting a interesting growth habit rather than ZnSe bulk crystal grown by traditional CVT methods. As-grown ZnSe plate-like crystals offer us an opportunity to understand the vapor-free-growth mechanism of ZnSe crystal in closed-space CVT system, which was urgent for the effective control of ZnSe growth. Furthermore, the vapor-free-growth habit, growth orientation, micromorphologies and nucleation of as-grown ZnSe crystal were investigated using atomic force microscopy (AFM), field emission scanning electron microscope (FE-SEM) and rotating orientation x-ray diffraction (RO-XRD). The shape, number density and constituent elements ratio of growth nuclei on two surface of ZnSe crystal-flake were watched and analyzed. The studied results indicated that ZnSe crystal has (111)A face with Φ =4.64° and (111)B face with Φ=3.13°, and Φ is the angle between the (111) vicinal surface normal axle and the microface normal axle. ZnSe crystal has a sphenoid shape or growth habit. The growth nuclei formed primarily on (111)A surface, while few nuclei was found on (111)B surface. The free-growth of ZnSe crystal in zinc-selenium-NH_4Cl system was governed by three-dimension nuclei-growth mechanism on (111)B face.

16:00 Poster We77

Seebeck Coefficient and Electrical Properties of InSbBi Bulk Crystal Grown by Vertical Directional Solidification

Dilip S. Maske[1,2], Manisha Joahi[2], Dattatray Gadkari[2]

1. *D. G. Ruparel College, S B Marg, Mumbai 400016, India* **2.** *Mithibai College (MITHI), Vile-Parle, Mumbai 400056, India*

e-mail: dilip.maske@ruparel.edu

Bulk crystal of $InSb_{1-x}Bi_x$ semiconductor for x = 0.02 was grown by vertical directional solidification (VDS) Technique without seed. The source materials indium (In), antimony (Sb) and bismuth (Bi) with 6N purity were mixed in stoichiometric proportion and filled in a specially designed quartz ampoule (I.D. 12 mm). The filled ampoule was flushed ten times by argon gas to reduce contamination due to air and then it was sealed at the argon pressure 200 torr. For homogeneous melt, the mixture in the ampoule was synthesized for 11hr at temperature 800^0C and the ampoule rotation speed was 25 rpm. Growth of the crystal was carried out at the growth rate of 3mm/hr. The temperature gradient at the solid-melt interface was of the order of 18 ^{0}C/cm. The temperature of the as grown ingot was reduced slowly from 440^0C to 300^0C in 12 hr. It was detached growth, confirmed by the O.D. of the ingot and I. D. of the ampoule. The composition of the source materials (In, Sb and Bi) in the grown crystals was measured by EDAX analysis. The

wafers of the grown ingot were obtained by cutting the ingot perpendicular to the growth axis. Hall measurements had indicated that the grown ingot was n-type semiconductor with mobility 14000 cm^2/Vs. Measurement of Seebeck coefficient on the wafer in the temperature range of 32°C to 80°C, showed linear increase in the Seebeck voltage with the Seebeck coefficient 75.8 μVK^{-1}. The details results will be presented in the paper.

16:00 Poster We78

Study of p-doping profile for high-brightness AlGaInP-based light emitting diodes

Hwa Sub Oh

Korea Photonics Technology Institute, ChumDan 4-ro 5, Buk-gu, Gwangju 500-779, Korea, South

e-mail: hsoh@kopti.re.kr

We investigated high-brightness light emitting diodes (LEDs) appropriate for full color display applications in terms of their electrical and optical behaviors of devices performance according to the Mg doping profile at the p-cladding layer. As the undoped zone is inserted in the p-cladding layer, light output power was increased by 20% due to the hole spreading improvement. And, by increasing the hole concentration near at the active region, the light output power is increased by 41 % due to the enhancement of the hole injection into the active region and also to the minimization of the carrier overflowing problem. At an oversaturation of Mg doping with excess Cp_2Mg flow near at the active region, the internal quantum efficiency is started to degrade because of the decrease of hole concentration due to the oversaturated material problem.

16:00 Poster We79

Structural and Thermodynamic Properties of III-V and II-VI Ternary Semiconductor Compounds

Natalia I. Podolska[1,2,3], Alexander I. Zhmakin[1,3]

1. *Ioffe Physico-Technical Institute, RAS, Saint-Petersburg, Russian Federation* **2.** *St Petersburg Academic University, Hlopina 8/3, Saint-Petersburg 194021, Russian Federation* **3.** *Saint-Petersburg Branch of the Joint Supercomputer Center, RAS (SPBSCC), 26 Politeknicheskaya str., Saint-Petersburg 194021, Russian Federation*

e-mail: natalya@scc.ioffe.ru

III-V and II-VI compound semiconductors are basic materials for advanced micro- and nanoelectronic devices such as laser diodes, light emitting diodes, power and microwave transistors etc. To get the best performance from the device, the quality of the epitaxial layers and heterostructures should be steadily improved. To accomplish this aim, the growth methods must rely on the knowledge of the materials' structural and thermodynamic properties. While the methods of the microstructure characterization are being persistently refined, the thermodynamic parameters are extracted from indirect measurements and are not known with sufficient accuracy. The paper presents the result of the valence force field (VFF) simulation of both structural (interatomic distances in the first and second coordination spheres) and thermodynamic properties (the mixing energy, the interaction parameter, the phase diagrams) of the ternary III-V and II-VI compounds (phosphides, antimonides, arsenides, nitrides, tellurides ets.) in the complete composition range. The previously developed statistical model [1,2] is used to compute the phase diagrams.

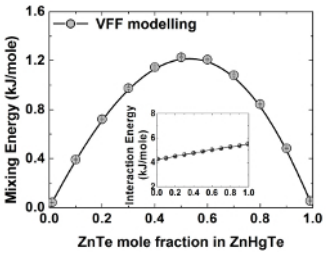

Fig.1: *Mixing energy and Interaction energy (inserted graph) as a functions of ZnTe mole fraction in ZnHgTe.*

The results are compared to both the experimental data and to the theoretical model suggested in refs. [3-5] for the interpretation of the EXAFS data as well as weakness of this the theoretical model.

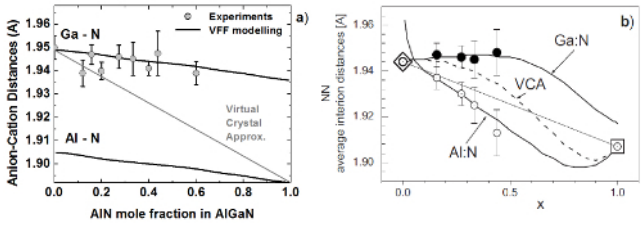

Fig.2: *Anion-Cation distances in AlxGa1-xN: VFF simulations (fig.(a)), distances predicted by the theoretical model suggested in [4] (white circles and solid lines in fig.(b)) and experimental data (gray and black circles in the both figures, consequently).*

Acknowledgments

This study was supported by the Russian Foundation for Basic Research, the Presidium of the Russian Academy of Sciences, the Presidium of the St. Petersburg Scientific Center of the Russian Academy of Sciences, and the Federal Agency for Science and Innovation.

References

[1] N.I.Podolska, "Study of thermodynamic properties of multicomponent III-V compounds by valence force field method", PhD Thesis, Ioffe Institute, Saint-Petersburg, Dec. 2011.

[2] N.I.Podolska and A.I.Zhmakin, the manuscript will be published soon.

[3] B.V.Robouch et al., Eur. Phys. J. B 84, 183-195 (2011).

[4] B.V.Robouch et al., J. of Appl. Phys. 104, 073508 (2008). [5] B.V.Robouch et al., J. of Alloys and Compounds 339, 1-17 (2002)

16:00 Poster We80

The Determination of Different Types of Conductivity Areas within Homogeneity Region of Ga Solid Solutions in PbTe films on Si-substrates

Alexander M. Samoylov[1], Sergey V. Belenko[1], Pavel V. Seredin[1], Staislav V. Ryabtsev[1], Alexandr E. Klimov[2]

1. *Voronezh State University (VGU), Universitetskaya Sq., 1, Voronezh 394006, Russian Federation* **2.** *Institute of Semiconductor Physics SB RAS, Lavrentjeva 13, Novosibirsk 630090, Russian Federation*

e-mail: samoylov@chem.vsu.ru

The thin films and single crystals of Ga-doped PbTe are the perspective materials for detecting the infrared (IR) irradiation in the middle wave range [1]. The IR sensitivity of these materials is similar to that of

$Cd_{1-x}Hg_x$ Te but processing procedures are much less demanding. Under the influence of the presence of III A group metals the energy spectrum of PbTe and its solid solutions can change significantly and depends on not only the concentration of impurity atoms but from the method of synthesizing of the investigated samples [2].

The main purpose of this work is to determine the borders of areas with different types of conductivity within homogeneity region of Ga solid solutions in PbTe/Si and PbTe/SiO_2/Si films prepared by modified HWE technique.

The chemical composition of Ga-doped PbTe/Si and PbTe/SiO_2/Si layers was analyzed by the electron probe microanalysis (EPMA) method on JEOL JCA 840 with the help of the energy dispersion (ED) and the wave dispersion (ED) spectrometers using $K\alpha_1$ - and $L\alpha_1$ - emissions. The electrical parameters of PbTe<Ga> films were evaluated from dc four-probe measurements by Van der Pauw technique and by the investigation of the *C* - *U* - curves ("Hg probe" method) also. As it is known, the oxidation process of $A^{IV}B^{VI}$ semiconductors, which intentionally or unintentionally occurs on the surface, affects the electronic properties of these materials greatly. In order to reduce this undesirable influence the silver contact pads were prepared by the thermal deposition in vacuum immediately after the plasma etching of PbTe<Ga>/Si and PbTe<Ga>/SiO_2/Si heterostructures surface through a special mask in Ar atmosphere within the same technological cycle.

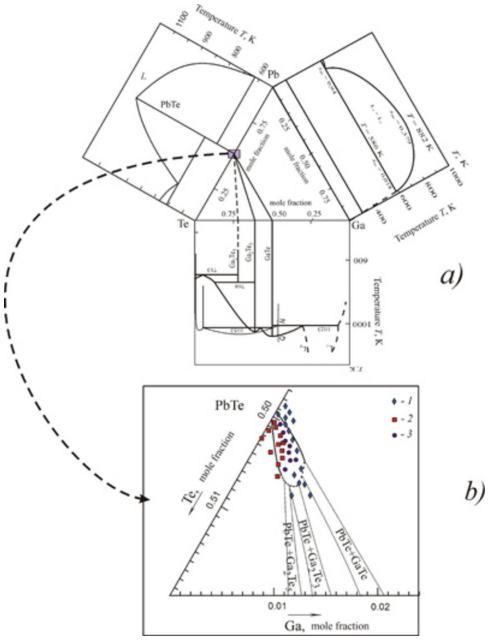

Fig. 1. The region of Ga solubility in PbTe/Si (100) and PbTe/SiO_2/Si (100) films from the point of view of the ternary Ga - Pb - Te system (*a*), and the areas with different types of conductivity within homogeneity region of Ga solid solutions (*b*); *1* - samples with *n*-type of conductivity, *2* - samples with *p*-type of conductivity, *3* - samples with semi-insolating properties.

For measurements of the electrical parameters of PbTe/Si and PbTe/SiO_2/Si heterostructures two series of samples have been prepared. The first doping procedure is based on a two-zone annealing of previously formed undoped PbTe/Si and PbTe/SiO_2/Si films in the saturated vapor which corresponds to the three-phase equilibrium L_1 - $GaTe^{(S)}$ - V in Ga - Te binary system. lead telluride samples with little excess of Te atoms have been chosen for this two stage doping procedure. These $PbTe_{1+\delta}$ films ($0.0008 < \delta < 0.006$) have usually the *p*-type of conductivity and charge carrier densities of about 10^{15} -10^{17} cm^{-3} at 77 K.

The second method of PbTe<Ga>/Si and PbTe<Ga>SiO_2/Si heterostructures preparation offers the direct one stage synthesis, in which the doping and the layer condensation processes proceed simultaneously [3]. The results of high-temperature mass-spectroscopy study have shown that at temperature interval 950 - 1300 K the saturated vapor phase over $Ga_{1-x}Pb_x$ melts is enriched by III A group metal regarding to the Raoult's law [4]. Varying the ratio of partial pressures of the metal components and the chalcogen, it is possible to synthesize $Pb_{1-z}Ga_z$ Te layers ($0.0011 < z < 0.08$), in which the tellurium content has been varied within the limits from 0.485 up to 0.525 mole fraction.

X-ray, SEM, and EPMA experimental data have demonstrated that the region of homogeneous $Pb_{1-z}Ga_z$ Te films existence was much narrow than indicated interval of Ga concentration in prepared samples [3]. It has been noted that homogeneity region of Ga - solid solutions in PbTe/Si and PbTe/SiO_2/Si is asymmetric regarding to quasibinary PbTe - GaTe cross-section (Fig. 1 *a*)

The comparison of the electrical parameters results measurements with the region of homogeneous Ga solid solutions in PbTe films existence is presented in Fig. 1 *b*. It can be seen that the areas with *n*- and *p*-types of conductivity exist within homogeneity region of Ga solid solutions in PbTe/Si and PbTe/SiO_2/Si films [5]. Besides, the samples with semi-insolating properties ([*n*], [*p*] are about 10^{13} - 10^{14} cm^{-3} at $T = 77$ K), which are perspective for fabrication of IR sensors, have been observed. It has been found that the area of existence of PbTe<Ga> films with the semi-insolated properties has the complicated shape. Along PbTe - GaTe and PbTe - Ga_2Te_3 cross-sections the maximum concentration of Ga atoms *z*Ga is approximately 0.0076 ± 0.0005.

References

1. M. Rahim, A. Khiar, M. Fill, F. Felder, H. Zogg. *Electron Lett*. **18**, 1037 (2011).

2. B.A. Volkov, L.I. Ryabova, D.R. Khohlov. *Progress in Phys. Sci. (Russ)*. 172, 875 (2002).

3. S.V. Belenko [et al]. *Journ. Surface Investig. X-ray, Synchrotron and Neutron Techn*. **4**, 170 (2010).

4. A.M. Samoylov [et al]. *Russian Journ. General Chem*. **81**, 27 (2011).

5. A.M. Samoylov, S.V. Belenko, M.K. Sharov, E.A. Dolgopolova, V.P. Zlomanov. *Journ. Cryst. Growth*. **351**, 149 (2012).

16:00 Poster We81

The Impact of Melt Temperature on Rapid in-situ Synthesis of InP

Jianye Yang, Zhiguo Liu, Ruixia Yang, Fan Yang, Shuai Li, Qingfang Huang, Xiaolan Li, Huimin Shao, Yanlei Shi, Xiuwei Tian, Wei Dai, Shujun Cai, Huisheng Liu, Tongnian Sun, Niefeng Sun

Hebei Semiconductor Research Institute, Scicence and Techonology on ASIC Laboratory, Shijiazhuang 050051, China

e-mail: niefengsun@gmail.com

Synthesis is the previous step of InP crystal growth and of vital importance to the quality of productions. 5kg of high-quality and stoichiometric InP is being rapidly synthesized and continuously grown in an improved Liquid Encapsulated Czochralski(LEC) system under an argon pressure in the range of 35 to 45 atmospheres. In this system, polycrystalline InP is produced by two double-tube injectors with in-situ injection synthesis method within 2.5 hours, the first injector loads about 550-600g red phosphorus and it takes 50-65 minutes for the phosphorus to react completely, while the second injectors loads about 500-600g red phosphorus and it takes 65-80 minutes, both of the injectors are heated by their own heater in the process of synthesis. After a series

of experiments, we find out that when the melt temperature is between 1110□ and 1090□ while using the first phophorus injector, and 1090-1070□ while using the second phosphorus injector, stoichiometric polycrystalline InP can be achieved repeatedly, the melt temperature is slowly reduced by a programme in the synthesis process. By the way, it is very difficult to measure the melt temperature accurately in such a high-pressure system by a thermocouple which is mostly used, heat radiation pyrometer is not applicable also because of the boric oxide encapsulant, while we find a convenient and effective method by counting the increase rate of a thermocouple's show value which is close to the crucible to define the melt temperature, the deviation is not more than 10□ from the truth, that is competent. The impact of melt temperature on rapid synthesis of InP is a combined action result of chemical reaction rate and chemical equilibrium, rising melt temperature can increase the rate of synthesis reaction, that is benefit on achieve rapid synthesis, and reduce the lost of red phosphorus which is not able to fully react with indium, but as the synthesis of InP is an exothermic and reversible reaction, exorbitant temperature could make the decomposition reaction too strong, and phosphorus will massively volatilize from the melt which would make phosphorus insufficient. In summary, suitable melt temperature is very important to synthesize InP, and adjusting the melt temperature based on the concentration of indium and InP in the melt is one of the key technologies to achieve rapid, stoichiometric and repeatable synthesis of InP.

16:00 Poster We82

Lattice dynamics of $CdGeAs_2$ crystal by Raman spectroscopy

Wei Huang[1], Beijun Zhao[1], Shifu Zhu[1], Zhiyu He[1], Baojun Chen[1], You Yu[2], Weijia Liu[1]

1. *College of Materials Science and Engineering, Sichuan University, ChengDu 610064, China* **2.** *College of Optoelectronic Technology, Chengdu University of Information Technology, ChengDu 610225, China*

e-mail: bjzhao@scu.edu.cn

$CdGeAs_2$ is a recent developing mid-infrared nonlinear optical material. It has high non-linear optical coefficient (d_{36} =236 pm/V), wide transparency range (2.3 ~ 18 μm), sufficient birefringence (n_e- n_o ≈ 0.09) and high thermal conductivity (about 42 - 93 mW/cm·K). These unique properties make $CdGeAs_2$ crystal a good candidate material for infrared frequency conversion applications. In this work, we have investigated in detail the low-temperature polarized-Raman-scattering spectra of $CdGeAs_2$ single crystal grown by the modified vertical Bridgman method. Comparing with the results of first-principles calculations, we identified all vibrational modes of $CdGeAs_2$ predicted from group-theory arguments. Our experimental results demonstrate that all-center modes can be grouped in three energy bands. First, within a very narrow energy range centered around 260 cm^{-1} are four modes ($1B_1$+$1B_2$+2E). Next, in an intermediate region extending from 215 to 158 cm^{-1} are five modes ($1A_1$+$1B_1$+$1B_2$+2E). And, finally, at much lower energy the dispersion of the acoustic branches gives, in the range 45-72 cm^{-1}, another series of four modes which are associated with $1B_1$+$1B_2$+2E symmetry. Calculated from the three B_2 and six E modes, the macroscopic effective charges of $CdGeAs_2$ which determine the magnitude of the LO-TO splitting (longitudinal optic-transverse optic splitting) are all quite close to the results of first-principles calculations.

Topical Session 5

Si/Ge for microelectronics and photovoltaics

Session Coordinators

Albrecht Seidl (Germany) *albrecht.seidl@schottsolar.com*

Deren Yang (China) *mseyang@zju.edu.cn*

Programme

Wednesday, 14 August

WeP-T05
Wednesday afternoon, 14 August, 16:00
Room 107, Old Library

Break
Wednesday afternoon, 14 August, 17:30

Thursday, 15 August

ThO3

T05: Si/Ge for microelectronics and photovoltaics
Thursday afternoon, 15 August, 16:30
Room A, Auditorium Maximum

16:30 Invited oral

Challenges in material improvement and cost reduction for crystalline silicon for PV application

Christian Reimann

Fraunhofer Institut IISB, Schottkystr. 10, Erlangen 91058, Germany

e-mail: christian.reimann@iisb.fraunhofer.de

At present and in the foreseeable future the dominating PV-technology is crystalline silicon, in form of multi-crystalline (mc) and mono- or quasimono crystalline material, as shown by several market surveys. Mono-crystalline silicon is at the moment mainly grown by crystal pulling (Czochralski) and multi-crystalline silicon mainly by directional solidification of large crystal ingots. As the market share of multi-crystalline silicon (47%) is significantly exceeding the market share of mono-crystalline silicon (35%), the directional solidification process can be considered as the best compromise between production costs ($) and achievable solar power (Wp) among the different crystalline silicon PV-technologies. The quasimono technology by directional solidification seems to have some potential for material improvement at low costs but still has several challenges to overcome before entering the industrial production scale.

Today crystalline silicon ingots with a weight of 240kg up to 1 000kg are industrially produced in silicon nitride coated silica crucibles with a square base of up to 1 x 1 m^2 within a few days. It has been shown that both the impurity contents (metals, carbon, oxygen etc.) and the microstructure (grain boundaries, dislocations) of the silicon material can significantly influence the production yield and the resulting solar cell efficiency. Thus, if one wants to improve these crystallization processes with respect to higher material quality (i.e. higher cell efficiency) and lower production cost, it is first necessary to clarify which crystal properties are relevant for the solar cell. Therefore, it will be briefly summarized which crystal defects in silicon crystals have a strong influence on the performance of solar cells. Then, the formation of some crystal defects is correlated to the process conditions of crystallization and examples are given for the optimization of the crystallization processes by the aid of thermal modeling and lab scale experiments. Finally, a conclusion will be given, how the crystallization of crystalline silicon might be carried out in the future.

17:00 Oral

Improvement of multi-crystalline silicon solar ingot growth by using diffusion barriers

Chung-Wen Lan, Yu-Ting Weng, Chih-Chen Hsieh

Department of Chemical Engineering, National Taiwan University, No. 1, Sec. 4, Roosevelt Road, Taipei city 10617, Taiwan

e-mail: b97504024@ntu.edu.tw

The control of impurity and nucleation is crucial to the ingot quality and yield in the directional solidification of multi-crystalline silicon for solar cells. The major impurities, such as metals, are mainly from the quartz crucible and the silicon nitride coating. The use of high-purity materials mitigates of the problem, but this increases the cost. Another way is to use diffusion barriers between silicon and these materials to reduce the incorporation of impurities. We have explored several materials and layer configurations for the diffusion barriers, and the results are promising. Both the ingot lifetime and yield have been improved. The wetting and nucleation behaviors of the diffusion barriers in contact with molten silicon are also reported and discussed.

17:15 Oral

Crystal/melt interface morphology at grain boundaries of multicrystalline silicon

Kozo Fujiwara, Masaya Ishii, Kensaku Maeda, Haruhiko Koizumi, Jun Nozawa, Satoshi Uda

Institute for Materials Research, Tohoku University, 2-1-1, Katahira, Aoba-ku, Sendai 980-8577, Japan

e-mail: kozo@imr.tohoku.ac.jp

The morphology of the crystal/melt interface during unidirectional solidifications affects the structures of materials. The generation of crystal defects, such as dislocations, twin boundaries, and grain boundaries, and the segregation of impurities are related to the morphology of crystal/melt interface. With the increasing importance of engineering metal-impurity nanodefects in multicrystalline silicon (mc-Si) to improve solar cell properties, the distributions of metal impurities in mc-Si wafers have been extensively investigated. A high metal impurity concentration has been shown to exist at grain boundaries without low coincidence site lattice (CSL) indices. However, there have been no convincing explanations why and how metal impurities segregate at grain boundaries owing to the lack of information on the effect of grain boundaries on atomic partitioning at a crystal/melt interface. In this study, we report how grain boundaries affect crystal/melt interface morphology on the basis of *in situ* observation.

We successfully observed the grain boundaries at the crystal/melt interfaces during the unidirectional solidification of mc-Si. It was clearly shown that the morphology of the crystal/melt interface at grain

boundaries is related to the grain boundary characteristics. Sharp and smooth grooves were formed at the crystal/melt interfaces at Σ 9, Σ 27 and random grain boundaries, whereas no grooves were formed at Σ 3boundaries. We explain the groove formation in mc-Si by considering the anisotropic crystal/melt interfacial energy of Si, which fully explains the reason why Σ3 boundary does not form a groove, and why the other grain boundaries form grooves at the crystal/melt interface. From these findings, we can explain why the degree of impurity segregation depends on the grain boundary characteristics by considering the impurity partitioning at the grooves at the crystal/melt interface.

17:30 Oral

Three-dimensional phase field modeling of silicon thin-film growth during directional solidification: facet formation and grain competition

Chung-Wen Lan, Hua-Kai Lin

National Taiwan University, 21 Hsu Chow Road, Taipei city 10020, Taiwan

e-mail: b93504075@ntu.edu.tw

Adaptive phase field modeling is applied to simulate directional solidification for silicon in three dimensions. Several functions are considered for the highly anisotropic interfacial energy and kinetic coefficient of silicon. The morphological evolution and the thermal field near the interface are presented and compared with experiments. The mechanisms for facet formation and grain competition are further discussed.

17:45 Oral

Modelling of unidirectional solidification of multicrystalline Si

Ronit R. Prakash[1,2], Takashi Sekiguchi[1,2], Karolin Jiptner[1], Yoshiji Miyamura[1], Jun Chen[1], Hirofumi Harada[1], Koichi Kakimoto[3]

1. *National Institute for Materials Science (NIMS), 1-1 Namiki, Tsukuba, Ibaraki, Tsukuba 305-0044, Japan* **2.** *Tsukuba Univ., Tsukuba 305-8577, Japan* **3.** *Kyushu University, Fukuoka, Japan*

e-mail: PRAKASH.Ronit@nims.go.jp

Multicrystalline (mc-) Si is the most widely used material for photovoltaic application. It should be pointed out that the efficiency of high-grade mc-Si solar cell is only 2 % lower than that of single crystal Si although the former contains a certain amount of grain boundaries (GBs) and dislocations. This small negative contribution of GBs on the solar cell efficiency may be attributed to the characteristic geometry of GBs in mc-Si. Most of the mc-Si ingots are grown by the unidirectional solidification method in the cast furnace. The ingots are cut in certain pieces and then sliced into wafers. Since the wafers are cut perpendicular to the unidirectional orientation, the GBs lie perpendicular to the wafer surface. In this study, we carefully considered geometrical effect of grain structure in unidirectional mc-Si ingots. The test ingots of 100 mm diameter were grown on the microcrystal templates [1]. After the typical growth, the ingot was vertically cut and the grain evolution behaviour was elucidated carefully. Fig. 1 shows the vertical cut image (a) and electron backscattered diffraction (EBSD) pattern of mc-Si ingot (b). The grains at the initial stage are a few hundred μm in size and start to grow until several mm in size. The grain shapes at first are rather spherical but becomes rod-like with growth. Such a change is characterized by the preference of grain growth factor. The preferential grain orientations and GB characters are also elucidated by EBSD analysis. According to the growth, the grains tend to align to lower Miller indices like [100] or [111]. The GB networks also become simpler except for a few small angle grain boundaries. Such a simplified configuration of grains gives a significant reduction of electrical activities of mc-Si.

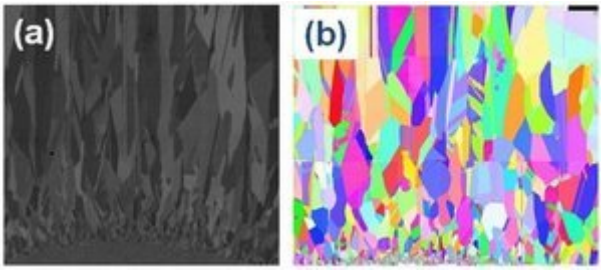

Fig. 1 (a) vertical cut image and (b) EBSD pattern of mc-Si ingot.

Acknowledgement

This work was partly supported by the New Energy and Industrial Technology Development Organization (NEDO) under the Ministry of Economy, Trade and Industry (METI).

Reference

[1] K. Arafune et al., J. Crystal Growth, 308 (2007) 5.

18:00 Oral

The Horizontal Ribbon Growth Process for Solar Silicon: Analysis of Stability and Segregation

Parthiv Daggolu, Andrew Yeckel, Jeffrey J. Derby

University of Minnesota, Chemical Engineering and Materials Science, 421 Washington Ave. S.E., Minneapolis, MN 55455, United States

e-mail: derby@umn.edu

Horizontal ribbon growth (HRG) promises the growth of crystalline silicon at rates that are orders of magnitude greater than vertical ribbon growth technologies. Unlike vertical meniscus-defined crystal growth processes, such as edge-defined film-fed growth (EFG), which are inherently stable, there are many failure modes that must be avoided in the HRG process. Thus, its successful operation will rely on a thorough understanding of system design and control.

We present a comprehensive thermal-capillary model based on finite-element methods to study the coupled phenomena of heat transfer, melt flow, segregation, and interfacial phenomena (solidification and capillarity) in the HRG process. Bifurcation analysis coupled with transient computations using this model reveals process limitations consistent with known failure modes and suggests operating windows that may allow for stable process operation. In particular, model results presented here identify failure mechanisms, including the bridging of crystal onto crucible, the spilling of melt from the crucible, and the undercooling of melt at the ribbon tip, that are consistent with prior experimental observations.

Model results also reveal interesting and potentially beneficial redistribution of impurities at the interface with inherent purging characteristics. Impurities have a tendency to accumulate towards a narrow bottom portion of the crystal leaving a majority of the crystal relatively pure. The existence of such a redistribution pattern is explained on the basis of convective flow patterns in the system, such as rotating vortices and solidification flow. High operating pull rates, impurities with low partition coefficients and low diffusivities are shown to further enhance such redistribution effects.

Supported in part by NSF CBET-075503, the content of which does not necessarily reflect the position or policy of the United States Government, and no official endorsement should be inferred.

18:15 Oral

Quality evaluation of multi-crystalline silicon ingots produced in a directional solidification furnace with different theories

Wenhan Zhao, Lijun Liu, Lei Sun, Anan Geng

School of Energy and Power Engineering, Xi'an Jiaotong University, Xi'an 710049, China

e-mail: zwh.xjtu@stu.xjtu.edu.cn

Three methods of quality evaluation based on the thermo-elastic, thermo-plastic and thermo-creep theories were established to investigate the quality of multi-crystalline silicon ingots. The thermal field in a directional solidification furnace was obtained with a 2D transient global model of heat transfer. The Von Mises stress, the accumulated plastic strain and the dislocation density were calculated to evaluate the ingot quality by the thermo-elastic, thermo-plastic and thermo-creep methods, respectively. Research was carried on in the crystal growing and the ingot annealing process. Simulation results indicate that in the crystal growing process, the low quality region distributions calculated by these methods match well with each other. The thermo-elastic method was recommended for its high computing efficiency. While in the ingot annealing process, the low quality region distributions obtained with these methods vary from each other. The real low quality region distribution in the ingot may between that calculated from the thermo-plastic and thermo-creep methods in this stage.

(a)

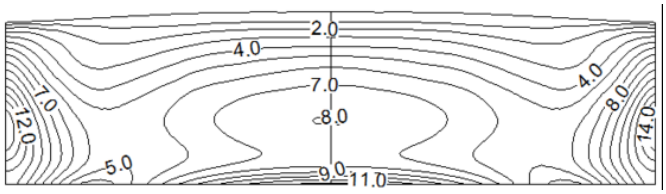

(b)

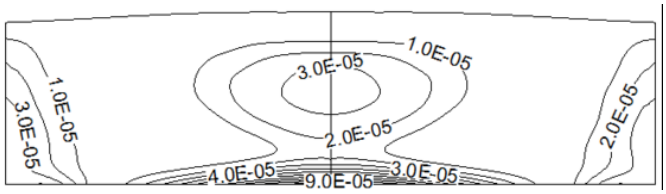

(c)

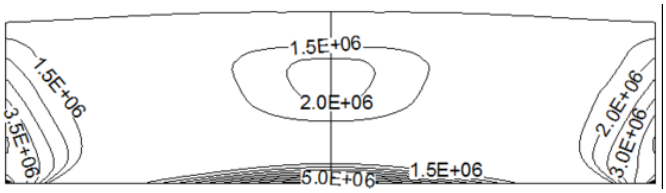

Fig. 1 Crystal quality distribution in the ingot in crystal growing process: (a) Von Mises stress calculated by thermo-elastic method (MPa), (b) accumulated plastic strain calculated by thermo-plastic method, (c) dislocation density calculated by thermo-creep method (cm^{-2}).

Break
Thursday evening, 15 August, 18:30

Friday, 16 August

FrO1

T05: Si/Ge for microelectronics and photovoltaics
Friday morning, 16 August, 8:30
Room A, Auditorium Maximum

8:30 Oral

Orientation analysis of multicrystalline silicon ingots for solar cells grown by noncontact crucible method

Kohei Morishita, Kazuo Nakajima, Ryota Murai

Graduate School of Energy Science, Kyoto University, Yoshida-honmachi, Sakyo-ku, Kyoto 606-8501, Japan

e-mail: k-morishita@energy.kyoto-u.ac.jp

Dislocations work not only as recombination sites for photogenerated carriers but also shunts of PN junctions of solar cells. Therefore, reduction of dislocation density is demanded to improve the conversion efficiency of solar cells. Crucibles used in conventional casting methods by unidirectional solidification constrain expansion of Si crystal caused by the solidification of the Si melt during whole processes of crystal growth, then, dislocations are introduced in Si crystals by stress. Once dislocations are generated, they increase in subsequent unidirectional growth process. This occurs also in the case of mono-like crystal which investigated actively these days. Recently, we proposed a noncontact crucible method [1-3], which enables reduction of stress due to constraint by crucible. In this method, nucleation occurs on the surface of a Si melt using seed crystals, and crystals grow inside the Si melt without touching the crucible walls. Then, the ingots continue to grow while being slowly pulled upward maintaining the front of crystal growth in the low-temperature region in the Si melt.

In the present study, growth morphology, defects, electrical properties and their relations in the p-type multicrystalline Si ingots grown by noncontact crucible method were studied with orientation analysis by electron back scattering diffraction patterns (EBSP), observation of etch-pit densities (EPD) and lifetime measurements. From Si ingots grown by noncontact crucible method, transverse and vertical cross-sections near Si seed were obtained. The transverse structures were radially-grown multicrystals. Such multicrystallization was thought to be aftereffects of Si_3N_4 particles which originally coated on the silica crucible. Almost grain boundaries in the transverse cross-section were Σ3 (84 % in the present sample) which should be electrically inactive. However, random grain boundaries (13 % in the present sample) caused the generation of dislocations, which increased along radial growth. On the other hand, in the case of that floating Si_3N_4 particles were not observed during growth of ingots, such ingots consisted of some large grains and dislocation density was low.

[1] K. Nakajima, R. Murai, K. Morishita, K. Kutsukake, N. Usami, J. Crystal Growth, 344, pp. 6-11, 2012.

[2] K. Nakajima, K. Morishita, R. Murai, and K. Kutsukake, J. Crystal Growth, 355, pp. 38-45, 2012.

[3] K. Nakajima, R. Murai, K. Morishita, and K. Kutsukake, J. Crystal Growth, accepted.

8:45 Oral

Growth of Si large single bulk crystals for solar cells using small crucibles with a given diameter by the Noncontact Crucible method

Kazuo Nakajima, Kohei Morishita, Ryota Murai

Graduate School of Energy Science, Kyoto University, Yoshida-honmachi, Sakyo-ku, Kyoto 606-8501, Japan

e-mail: nakasisc@energy.kyoto-u.ac.jp

We proposed the noncontact crucible method for reducing stress in Si bulk crystals [1, 2]. In this method, a Si melt has a large low-temperature region in its upper central part and a crystal grows in the region without contacting with the crucible wall. In order to confirm whether high-quality Si single bulk crystals with a large diameter can be obtained by controlling the low-temperature region, we prepared p- and n-type Si single bulk crystals using small crucibles with a given diameter. We obtained single crystals with a diameter as large as 60 % of the crucible diameter. The etch pit density of the Si single bulk crystals was 1.9 x 10^3 -1.2 x 10^4/cm^2, and the O concentration of the present ingots wasrelatively lower than that of the ingots grown by the CZ method.

1. Introduction

Generally, conventional crystal growth methods using silica crucibles cannot effectively control Si expansion due to Si melt solidification because silica crucibles have insufficient flexibility to reduce the stress. We proposed a noncontact crucible method for reducing stress in Si bulk crystals [1, 2]. In this method, a Si melt has a low-temperature region in its upper central part for natural Si crystal growth inside it. Nucleation occurs on the surface of the Si melt using a seed crystal, and a crystal grows inside the melt without touching the crucible wall. Then, the crystal continues to grow while being slowly pulled upward to ensure that the crystal growth remains in the low-temperature region. Therefore, the bottom of ingots was convex in the growth direction as shown in Fig. 1, which compares the present method with the CZ method. For the CZ growth, an ingot is grown above the surface of a Si melt and the solid-liquid interface of the ingot is generally concave in the growth direction.

Si single bulk crystals used for solar cells are mainly grown by the Czochralski (CZ) method. Generally, the diameter of the ingots grown by the CZ method was controlled within 30 % of the crucible diameter. In the present method, the crystal diameter was determined by the size of the low temperature region, and the method has a possibility of growing large ingots even using a small crucible with a given diameter. Therefore, it is very important to confirm whether a Si single crystal can be grown inside a Si melt without touching the crucible wall.

In this work, we used the noncontact crucible method to prepare p- and n-type Si single bulk crystals. The quality of the ingots was determined in terms of minoritycarrier lifetime, dislocation distribution and crystal structure. The diameter of ingots was investigated for many crucibles with and without coating Si_3N_4 particles as a function of temperature reduction.

2. Experiments

A large low-temperature region was formed in a Si melt by controlling the temperature distribution in the furnace. A Si crystal grew naturally from the seed crystal along the surface of and inside the Si melt, then continued to grow while being slowly pulled upward. The temperature reduction used for the growth was defined as the difference between the starting temperature and the final temperature. P- and n-type Si ingots were grown using silica crucibles of 30 and 33 cm diameters. The inner wall of a crucible for the growth of p-type Si multicrystals was coated with Si_3N_4 particles to prevent the oxidation of the ingots during crystal growth. The inner wall of crucibles for the growth of p- and n-type Si single bulk crystals was not coated with Si_3N_4 particles to prevent floating Si_3N_4 particles on the surface of Si melts during crystal growth.

To evaluate the quality of the ingots, minority carrier lifetime was measured by microwave photoconductive decay (PCD). The oxygen (O) and carbon (C) concentrations of the ingots were measured by Fourier transform infrared spectrometry (FTIR).

3. Results and Discussion

We can prepare an n-type Si single bulk crystal with a diameter of 20 cm even using a small crucible with a diameter of 33 cm as shown in Fig. 2. The temperature reduction used for the growth of this ingot was 45 °C. The surface structure exhibits a four-cornered pattern on its top surface. The surface orientation of the cross section was (100). The crystal diameter was as large as 60 % of the crucible diameter. For the growth of p-type Si multicrystals using crucibles with coating Si_3N_4 particles, we obtained the diameter of 26.8 cm and the crystal diameter as large as 81 % of the crucible diameter. The larger temperature reduction was required for the growth using crucibles without coating Si_3N_4 particles than for the growth using crucibles with coating Si_3N_4 particles to obtain ingots with the same diameter. The etch pit density of the n-type Si single bulk crystals was 2.0-3.2 x 10^4/cm^2 and that of the p-type Si single bulk crystals was 1.9 x 10^3 -1.2 x 10^4/cm^2 even using necking grown seeds of only 4.2-6.5 cm long. The O concentration of the present ingots was relatively lower than that of the ingots grown by the CZ method because the convection in Si melts may be suppressed by making a large low-temperature region [3]. The average minority carrier lifetime of an entire wafer cut from an n-type ingot was 83 μs (maxmum:165μs), which was much higher than that of p-type ingots [3].

4. Conclusions

It was confirmed that n- and p-type Si single bulk crystals can be grown using crucibles without coating Si_3N_4 particles by the noncontact crucible method. The surface orientation of the cross section was (100) for the ingots. Using crucibles without coating Si_3N_4, we have obtained the crystal diameter as large as 72 and 81 % of the crucible diameter for a single bulk crystal and a multicrystal, respectively. The growth of Si ingots with a larger diameter using a crucible with a given diameter is a large merit for this method. It is effective to prepare Si single bulk crystals with a large diameter by the low cost method. The distribution of minority carrier lifetime was uniform in almost the entire cross section of the single bulk crystals except in the ring-shaped region. The dislocation density was 1.9 x 10 ^{3}/cm^2 in the cross section of a single bulk crystal except at the periphery of the cross section. The average minority carrier lifetime of a wafer cut from an n-type ingot was 82.8μs for the passivated surface, which was higher than those (7.3-16.0 μs) of p-type wafers. The O and C concentrations of the present ingots which were grown using crucibles without coating Si_3N_4 particles were 2.5-8.3 x 10^{17}/cm^3 and about 1 x 10^{16}/cm^3, respectively. The O concentration is relatively lower than that of the ingots grown by the CZ method.

References

[1] K. Nakajima, R. Murai, K. Morishita, K. Kutsukake, and N. Usami, "Growth of multicrystalline Si ingots using noncontact crucible method for reduction of stress," *Journal Crystal Growth*, vol. 344, pp. 6-11, 2012.

[2] K. Nakajima, K. Morishita, R. Murai, and K. Kutsukake, "Growth of high-quality multicrystalline Si ingots using noncontact crucible method," *Journal of Crystal Growth*, vol. 355, pp. 38-45, 2012.

[3] K. Nakajima, R. Murai, K. Morishita, and K. Kutsukake, "Growth of Si single bulk crystals by the noncontact crucible method using silica crucibles without coating Si_3N_4 particles", To be submitted to J. Crystal Growth.

9:00 Oral

Silicon crystallization by Kyropoulos process for photovoltaic applications

Leslie Lhomond[1], Guy Chichignoud[1], François Lissalde[2], Kader Zaidat[1]

1. *Science et ingénierie des matériaux et des procédés, Elaboration par Procédés Magnétiques (SIMAP-EPM), 1130 rue de la Piscine, Grenoble 38402, France* **2.** *Cyberstar, 1 rue des Tropiques, Grenoble 38435, France*

e-mail: leslie.lhomond@simap.grenoble-inp.fr

Photovoltaic energy is an environmentally friendly way to produce electricity. The efficiency of photovoltaic cells based on silicon depends on the material quality and the crystalline structure. Crystalline structure depends on the crystallization process (mono-crystalline, polycrystalline and quasi-mono). Mono-crystalline silicon has a better efficient than polycrystalline cells because of fewer traps for charge carriers, so their life-time is longer. So far, the main crystallisation process used for mono-crystalline silicon is Czochralski method. Final silicon ingot obtained is cylindrical geometry, raw material has to be cut and lost to manufacture square cells. In the quasi-mono technique, multiple Si single-crystal seed crystals are arranged on the bottom surface of the crucible. The crystallized ingot is then square, matching the crucible geometry. This method is useful for reducing the number of grain boundaries by forming large single-crystal- like grains, but it has still a severe problem that polycrystalline growth from the crucible walls always occurs. The present work would deals with the adaptation of Kyropoulos process for silicon. Kyropoulos process is well known and used for sapphire. This process should be good for silicon crystallization because of the reduced stress forces applied on the material. The crystal grows naturally in the low-temperature region, then it is slowly pulled upward while ensuring that crystal growth remains in the low-temperature region. This parameter can reduce the number of dislocations. Moreover, in order to reduce the lost raw material, the final ingot should be closed like the crucible geometry (square for standard fused silica crucible). A Cyberstar furnace has been adapted for the Kyropoulos crystallization of silicon. Experimental studies were carried out to investigate favorable thermal conditions for growth from the seed. As the square geometry highly depends on the control of the radial growth, the effect of seed orientation was also considered.

9:15 Oral

Analysis of Argon Flow on Mass Transport in a CZ-Si Crystal Growth by Using Full Compressible Flow Solver

Xin Liu, Bing Gao, Koichi Kakimoto

Kyushu University, Research Institute for Applied Mechanics, Kasuga 816-8580, Japan

e-mail: liuxin@riam.kyushu-u.ac.jp

The Czochralski (CZ) method is the dominant technique to produce bulk single crystals of a wide range of electronic and photovoltaic silicon. The argon flow, acting as a protective environment, has significant effects on the generation and transportation of the impurities in the furnace. The coupled transport at the gas and melt interface then influences the levels of the main impurities in the melt and crystal, such as oxygen and carbon. Therefore, a precise simulation of the argon flow is essential to understand the relevant heat and mass transport in CZ-Si crystal growth and to improve the quality of the growing crystal.

It is well-known the argon convection is compressible flow involving low fluid speed (low Mach number) but intensive density variations because of the large temperature differences within the CZ-Si furnace. In this regime, Boussinesq approximations for incompressible flow are unsuitable because of its small temperature difference and density variation constraints. It's better to use full compressible flow solver. However, compressible flow solvers also have the stiffness problem caused by the disparity of time scales between the mean flow and the acoustic wave. To overcome these difficulties, we solve the acoustically filtered equations of viscous, low-speed compressible flow by the finite-element method for argon flow in CZ-Si crystal growth. Global simulations of coupled heat and mass transport are performed for the CZ-Si furnace. Thermal and velocity boundary conditions are fully coupled between the argon gas, silicon melt and solid parts. Transport of oxygen and carbon in argon gas and silicon melt are calculated simultaneously by considering several chemical reactions at the interfaces. The flow results show the acoustically filtered equations are reliable and easy to handle for the argon flow with a large temperature difference in CZ-Si furnace. The results of oxygen and carbon concentration also show good agreement to experimental data.

To clarify the transport mechanisms of argon flow, the effects of gas flow rate and outlet location are also investigated by a series of global simulations. It is found the amount of impurities carried away by the argon flow increases with the increase in the argon flow rate. Adjustment of the outlet location can change the purge flow pattern, and then carry out the impurities in the furnace efficiently. The present numerical model and results demonstrate a method to analyze and control the gas convection and mass transport in CZ-Si crystal growth.

9:30 Oral

Grown-in micro defects and photovoltaic characteristics of B and heavily Ge codoped CZ-Si

Mukannan Arivanandhan[1], Raira Gotoh[2], Fujiwara Kozo[2], Satoshi Uda[2], Yasuhiro Hayakawa[1], Makoto Konagai[3]

1. *Research Institute of Electronics, Shizuoka University, Johoku 3-5-1, Naka-Ku,, Hamamatsu 432-8011, Japan* **2.** *Institute for Materials Research, Tohoku University, 2-1-1, Katahira, Aoba-ku, Sendai 980-8577, Japan* **3.** *Department of Physical Electronics, Tokyo Institute of Technology, Okayama, Meguro-ku,, Tokyo 152 8552, Japan*

e-mail: arivucz@gmail.com

The quality of a Si crystal determines the cost and efficiency of a solar cell. It was found that Ge doping into Si is beneficial as it improves the quality of Si by controlling the void defects which improves the photovoltaic characteristics of B-doped CZ-Si [1]. However, Ge is obviously larger than Si and thus the addition of Ge should increase the lattice strain as the lattice mismatch between Si and Ge is about 4 %. Therefore, to explore the maximum range of Ge concentration which is beneficial for preparing high quality of Si, B and Ge codoped CZ-Si crystals with high Ge concentrations were grown and their defect and photovoltaic characteristics were studied. The experimental results show that the minority carrier lifetime (MCL) increased when the initial Ge concentration in Si melt (C_l^{Ge}) increases up to 3×10^{20} cm^{-3} and decreased drastically when the C_l^{Ge} increased beyond 3×10^{20} cm^{-3}. The etching analysis revealed that the Secco etch pit defect (SEPD) density and flow pattern defect (FPD) density decreased up to C_l^{Ge} of 3×10^{20} cm^{-3} and increased when the C_l^{Ge} increased beyond 3×10^{20} cm^{-3}, which resulted low MCL in heavily Ge codoped CZ-Si. The in-

tentional variation of growth rates (v) of heavily Ge codoped CZ-Si (to avoid the cellular growth) may be influenced on the change in type of GMDs from void defects (reveled as FPDs for the crystals grown with relatively high growth rate, 0.7 mm/min) to A/B type self interstitial defects (revealed as SEPDs in the crystals grown with relatively low growth rates, 0.4 to 0.15 mm/min). Furthermore, in the heavily Ge codoped CZ-Si, the influence of Ge concentration is relatively smaller than v of crystal on the formation of GMDs.

Reference:

1. M.Arivanandhan et al., J. Appl. Phys. **111**, 043707 (2012).

9:45 Oral

Growth of heavily tin-doped Si

Ichiro Yonenaga[1], Toshinori Taishi[2], Kaihei Inoue[1], Kentaro Kutsukake[1], Yuki Tokumoto[1], Yutaka Ohno[1]

1. *Institute for Materials Research, Tohoku University, 2-1-1, Katahira, Aoba-ku, Sendai 980-8577, Japan* **2.** *Shinshu University, 4-17-1 Wakasato, Nagano 380-8553, Japan*

e-mail: taishi@shinshu-u.ac.jp

Recently doping of isovalent substitutional impurities (Group-IV) into semiconductors have been attracted keen interests. Such impurities have almost no effects electrically but have unique interactions with harmful defects to improve the device yield and output through the local strain compensation. Particularly, Ge is effective to suppress formation of vacancy-oxygen clusters in electron-irradiated Si crystals [1]. In comparison with Ge, information on Sn is rather limited except some studies for lack of suitable crystals. These isovalent impurities are expected to affect local vibration of interstitially dissolved O_i and substitutional C_s in Si as known in SiGe alloys [2]. Here, we report the Czochralski-growth of Si crystals heavily doped with Sn and to discuss compositional variation along the growth direction of the crystals. Also, doping effects on infrared absorption spectra of O_i and C_s due to the dopant-induced elastic strain are shown.

Si single crystals heavily doped with Sn were grown by the Czochralski method with a constant pulling rate in a flowing Ar gas atmosphere. Certain amount of high purity Sn pellets was added as a dopant. [111]- or [001]-oriented Si seeds were used.

A full single crystal, as large as around 20 mm in diameter and 40 mm in length, was obtained under a pulling rate of 8 mm/h. The Sn concentration at the top part of the crystal was 1.5 x 10^{19} cm^{-3}, determined by ICP-OES and WDX, then increased along the growth direction, and reached to 4 x 10^{19} cm^{-3}, close to the solubility limit in a literature [3]. The variation of the Sn concentration well followed to a normal segregation with a coefficient 0.016 [3]. From the optical absorption peak at 1106 cm^{-1} of $O_i$measured by FT-IR, the Oi concentrations in the crystals were around 8 x 10^{17} cm^{-3}. The absorption peak shifted to the low wave number side with an increase in [Sn] along the growth direction, possibly due to the expansion of Si–Si bonds.

[1] C. A. Londos et al., J. Appl. Phys. **112**, 123517 (2012).

[2] I. Yonenaga et al., Physica B **308-310**, 539 (2001).

[3] F. A. Trumbore, Bell Syst. Techn. J. **39**, 205 (1960).

10:00 Oral

Guided gas flow as an effective mean to overcome crystal diameter limitations in FZ growth of large silicon crystals

Michael Wünscher, Helge Riemann, Hans-Joachim Rost, Robert Menzel, Sandra Haufe

Leibniz Institute for Crystal Growth (IKZ), Max-Born-Str 2, Berlin 12489, Germany

e-mail: michael.wuenscher@ikz-berlin.de

Despite the persisting demand for larger crystals, the maximum diameter of Floating Zone (FZ) silicon crystals could not increase since 2000, when a 200 mm crystal was firstly presented. We see several reasons for the stagnation in diameter evolution and focused on the contribution of the gas atmosphere.

In contrast to vacuum, the surrounding gas reduces the evaporation of silicon from the melt and is essential to grow large and long single crystals. One weakness of the commonly used argon gas is its low dielectric strength. Due to the use of inductive heating with a single turn coil, a high voltage is applied to a small gap, the main slit (thickness ~1.5mm), resulting in a high electric field. With increasing diameter more electric power and, hence, higher voltage is needed. As a consequence ionization of the gas takes place and breaks the FZ process with an arc discharge. This breakdown voltage can be increased by adding nitrogen to the atmosphere what is commonly used to grow crystals with a diameter larger than 100 mm. Another option is the increase of the gas pressure. Both, the nitrogen concentration and the gas pressure are limited during the growth of single crystals by a higher risk for generation of dislocations or crystal cracking.

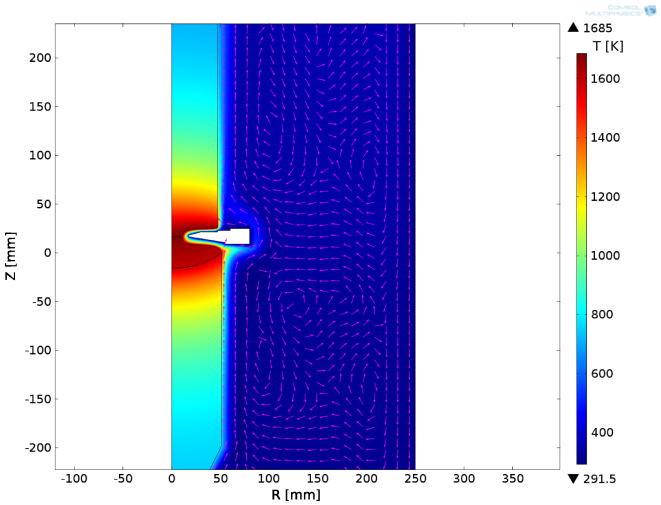

Figure 1 Numerical result of the temperature field in the crystal, melt, feed rod and gas chamber (Argon with increased viscosity) with normalized vectors of the velocity field

The breakdown voltage is inversely proportional to the gas temperature. To clarify our picture of the gas flow, we measured temperatures during growth and compared these results with our numerical calculations. The numerical investigations of the gas flow in a typical FZ machine revealed a very high gas temperature being close to melting point temperature of silicon between the melt surface and the induction coil (see fig. 1). This gave us the motivation to investigate the temperature dependency in a separate experiment, where we measured the breakdown voltage of various gases and electrode materials over the interesting temperature range. To reduce the risk of arcing we modified our standard FZ set-up to significantly lower the temperature of the

gas close to the main slit. With our standard set-up we grew several crystals and investigated the risk of arcing in the cone phase. The feed rod diameter was 100 mm. We applied an over pressure of 0.2 bar to the pure argon atmosphere without adding nitrogen. We reproducibly generated arc discharges at the main slit at cone diameters between 60 mm to 80 mm (see fig. 2). These results agree with those found in previous experiments. Under equal conditions our modification allowed to increase the diameter of the crystal up to 125 mm, before arcing happened. This modification in combination with the previously used methods can be a further step to significantly increase the crystal diameter beyond 200 mm.

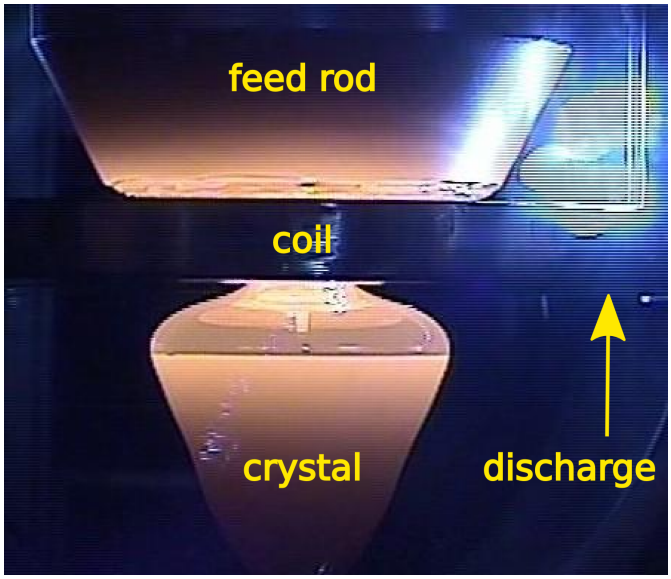

Figure 2 Arc discharge at the main slit of the induction coil during the cone phase of a growing silicon crystal (frame from our video camera)

10:15 Oral

Effect of cooling rate on the activation of slip systems in seed cast-grown monocrystalline silicon in the [001] and [111] directions

Bing Gao[1], Satoshi Nakano[1], Hirofumi Harada[2], Yoshiji Miyamura[2], Koichi Kakimoto[1]

1. *Kyushu University, Fukuoka, Japan* **2.** *National Institute for Materials Science, Tsukuba 305-0047, Japan*

e-mail: gaobing@riam.kyushu-u.ac.jp

Solar cell efficiencies are generally governed by the concentration and type of impurities, and the density and electrical activity of extended defects such as grain boundaries and dislocations [1]. Dislocations have been identified as one of the most efficiency-relevant defect centers in crystalline silicon for photovoltaic [2]. The requirement for an increase of solar cell efficiencies necessitates a reduction of the crystal dislocations. Therefore, the dislocations generated by thermal stress during crystal growth have to be effectively suppressed for the production of highly efficient solar cells.

Many optimization studies have been performed to reduce dislocations by controlling the cooling process. However, the results are not consistent. Slow cooling was suggested for obtaining low dislocation density in GaP/Si heterostructures [3] and in SiGe layers grown by liquid phase epitaxy [4]. Fast cooling was suggested for obtaining low dislocation density in Pb [5] and Si crystal growth [6] from the melt. This discrepancy shows that the effect of the cooling process on the multiplication of dislocation is complex and different for different materials, growth furnaces, and growth processes.

To better understand the relationship between the cooling rate and dislocation, it is essential to study the effect of the cooling process on the increase of dislocations from the perspective of activation of slip systems, since the generation of dislocations mainly originate from the activation of slip systems.

The results show that the cooling rate has a large effect on the activation of slip systems. In the [001] growth direction, a slow cooling rate either weakly activates 4-fold symmetric slip systems or does not activate them at all. In contrast, a fast cooling rate strongly activates the 4-fold symmetric slip systems. In the [111] growth direction, a slow cooling rate weakly activates the three 3-fold symmetric slip systems, while a fast cooling rate strongly activates the three 3-fold symmetric slip systems. The differences of the activation of the slip systems between the slow and fast cooling rates mainly cause the differences in dislocation and residual stress. Irrespective of the crystal growth direction, it is mainly the radial flux that causes the difference between the fast and slow cooling rates. Therefore, the most effective method for reducing dislocation during the cooling process is to decrease the radial flux.

References

[1] C. Häβler, G. Stollwerck,W. Koch,W. Krumbe, A. Müller, D. Franke, T. Rettelbach, Adv. Mater. 13 (23) 2001.
[2] H. El Ghitani, M. Pasquinelli and S. Martinuzzi, J. Phys. III 3 (1993) 1941.
[3] M. Tachikawa, H. Mori, J. Crystal Growth 183 (1998) 89.
[4] A.M. Sembian, F. Banhart, M. Konuma, J. Weber, S.M. Babu, P. Ramasamy, Thin Solid Films 372 (2000) 1.
[5] G.R. Blackwell, I.A. Bucklow, J. Phys. Chem. Suppl. (1967) 115.
[6] S. Nakano, X. J. Chen, B. Gao, K. Kakimoto, J. Crystal Growth 318 (2011) 280-282.

Coffee

Friday morning, 16 August, 10:30

FrO2

T05: Si/Ge for microelectronics and photovoltaics
Friday morning, 16 August, 11:00
Room A, Auditorium Maximum

11:00 Invited oral

Epitaxy of GeSi Heterostructures on Silicon Substrates

Erich Kasper, Klara Lyutovich

University of Stuttgart, Institute of Semiconductor Engineering, Pfaffenwaldring 47, Stuttgart 70569, Germany

e-mail: kasper@iht.uni-stuttgart.de

Group IV heterostructures are interesting for two reasons: Application in microelectronics, photonics, photovoltaics, and as basic material system for strained heterostructure studies.

- **Condensation and crystallization of group IV elements on Si**

Driving force of the crystalline growth is minimizing of energy because the perfect crystal is the energetically favorable solid. A requirement for epitaxy is a clean substrate surface, otherwise the information about orientation of the substrate is disordered or even destroyed and the consequences are crystalline defects up to polycrystalline or amorphous growth. Modern epitaxy techniques like molecular beam epitaxy (MBE)

or chemical vapor deposition (CVD) allow the growth of very thin crystalline silicon, silicon germanium or germanium layers with well-defined dopants by very low growth temperatures. In this temperature regime, volume diffusion is negligible. Furthermore, the critical thickness of SiGe heterostructures is increasing. However, in this low temperature growth regime surface segregation of dopant or alloy atoms has turned out to be a dominant mechanism for profile smearing.

- MBE and CVD techniques

An MBE system involves the generation of molecular beams of matrix material such as silicon, germanium or tin and doping species and their interaction with the substrate surface to form a single crystal deposit under ultrahigh vacuum (UHV) conditions. Atomic or molecular beams of the necessary species are directed toward the heated substrate and grow into epitaxial layer. The atomic or molecular fluxes of elemental constituents are evaporated or sublimated in special electron beam evaporators or in heated effusion cells. For a precise control of the beam fluxes over the substrate, all sources exhibit rapidly acting mechanical shutters and the flux of the deposition materials can be measured directly with a flux monitor, e.g. a quadrupol mass spectrometer, or indirectly over the effusion cell temperature. The formation of layers is called chemical vapor deposition (CVD) if the vapor contains chemical complexes - the precursors - which have to undergo chemical reactions to form the layer materials. CVD is a very common process in microelectronics manufacturing. The basics of silicon CVD are described in many textbooks; the reader is referred to (Chang, 1996). Rapid thermal chemical vapor deposition (RTCVD) and reduced pressure chemical vapor deposition (RPCVD) have rapidly emerged as the main production technologies for group IV alloys. Group IV based alloys, namely SiGe, SiGeC, SiC, SiSn, SiGeSn, and GeSn, are well known to be key materials for extending the capabilities of the silicon based technologies that dominate the micro-electronics industry. These alloys are fully compatible with Si technology and display advantageous electrical, optical, chemical, and mechanical properties.

- Strain and misfit dislocations: Critical thickness and metastable growth

SiGe (silicon germanium) is lattice mismatched against the Si substrate commonly used in microelectronics. The lattice mismatch *f* is nearly linear with Ge content *x* (Vegard's law: $f = 0.0417x$). Exactly, a slight parabolic bow (Dismukes law) is proven for both bulk SiGe and epitaxial SiGe.

The lattice mismatch causes strained layer SiGe growth (pseudomorphic SiGe) up to a critical thickness t_c. Thicker layers start to relax the strain by the introduction of misfit dislocation networks at the interface. By kinetic reasons (nucleation of dislocations at surface sites) the interface dislocation network is connected to the surface by threading dislocations. The onset of strain relaxation in the metastable regime is retarded by dislocation nucleation barriers and by slow motion of misfit dislocations. For clean surfaces as used in microelectronics processing, we proposed (Kasper, 2012) a metastable critical thickness band with a lower and an upper bound.

- Accommodation of lattice mismatched heterostructures: Thin virtual substrates

Structures able to adjust the strain of heterostructure layers on top of a Si substrate are called strain platforms. A universal solution to strain platforms is given by the so called virtual substrates which are composed of a thin Si substrate and an ultrathin strain relaxed buffer layer of a mismatched material system (e.g. SiGe or GeSn) offering a surface lattice constant from the underlying Si substrate. Our group (Lyutovich, 1999) managed to adjust the lattice constant in ultrathin SiGe buffers by nucleation of misfit dislocations from supersaturated point defect concentrations. Supersaturation of point defects was controlled by Si ion impact (100 eV to 1000 eV energy) or very low growth temperature intervals.

- Dopant segregation and methods to overcome it

Surface segregation during growth which is well-known from studies on dopant incorporation in Si has attracted attention for Ge/Si and Sn/Ge. Quantitatively, surface segregation is described by the segregation coefficient r_s that expresses the ratio of the impurity surface concentration n_s to the bulk concentration n. In general, r_s may not solely depend on growth parameters (temperature T and growth rate R) but also on surface coverage itself (Berbezier, 2011).

- GeSi in microelectronics, photonics and photovoltaics: Status and prospects

Heterostructure SiGe is extensively used in microelectronics circuits as stressor for PMOS channels in processors and as high frequency booster in microwave circuits (e.g. SiGe HBT for automotive radar). In future, high mobility Ge channels in CMOS will allow continuation of the anticipated performance progress. In Si photonics, integration of SOI-based waveguides with Ge detectors, modulators, and lasers is rapidly progressing. GeSn devices on Si will expand the wavelengths window from 1.2µm to beyond 2µm into the mid infrared. For photovoltaics, thick Ge buffer layers on Si are used in high efficiency tandem solar cells.

References:

C.Y. Chang and S.M. Sze, ULSI technology, McGraw-Hill (1996)

E. Kasper, N. Burle, S. Escoubas, J. Werner, M. Oehme and K. Lyutovich, "Strain relaxation of metastable SiGe/Si: Investigation with two complementary X-Ray Techniques", *J. App. Phys., 111, 063507 (2012)*

Lyutovich, K., Ernst, F., Kasper, E., Bauer, M. Oehme, M. Interaction between Point Defects and Dislocations in SiGe, Solid State Phenomena 69-70, p. 179-184 (1999)

I. Berbezier, J. P. Ayoub, A. Ronda, M. Oehme, K. Lyutovich, E. Kasper, M. Di Marino, G. Bisognin, E. Napolitani, M. Berti, "Strain engineered segregation regimes for the fabrication of thin Si1-xGex layers with abrupt n-type doping", *J. Appl. Phys. 107, 034309 (2010)*

11:30 Oral

Uniaxially strained Si/Ge heterostructures grown on selectively ion-implanted substrates

Kentarou Sawano[1], Yutarou Shoji[1], Naoki Funabashi[1], Eisuke Yonekura[1], Kiyokazu Nakagawa[2], Yasuhiro Shiraki[1]

1. *Tokyo City University, 8-15-1, Todoroki, Setagaya-ku, Tokyo 1580082, Japan* **2.** *University of Yamanashi, Takeda, Yamanashi, Yamanashi 400-8551, Japan*

e-mail: sawano@tcu.ac.jp

Strain engineering based on Si/Ge heterostructures enables us to control band structures and boost advanced device performances. Recently, the uniaxial strain has attracted attentions owing to its high potential to further widen the possibility of band engineering and consequently enhance device performances more than the biaxial one. Particularly, the uniaxial compressive stress induced along the channel length direction is highly expected to effectively increase the hole mobility. And hence, new technologies to induce the uniaxial stress are strongly required to be established. We proposed selective ion implantation technique to induce uniaxial strain into the SiGe layer [1]. In this method, strain of the SiGe is locally relaxed in the region where ions

are implanted into the Si substrate prior to the SiGe growth. Implantation induced defects play an important role in this facilitation of the strain relaxation. In proper configurations of the selective implantation, the anisotropic strain can be introduced into SiGe layers in the unimplanted regions, where the neighboring relaxed SiGe on the ion-implanted region provides the shear stress and causes the anisotropic strain to the unrelaxed SiGe in the unimplanted region. In previous works [1, 2], we obtained a SiGe (Ge: 27%) buffer layer where the strain relaxation around 40% took place only one direction and almost no relaxation did along the orthogonal direction. In this study, we examine uniaxial strain states induced in Si/Ge heterostructures with various Ge concentrations including (111) as well as (100) substrate orientation. In experimental, Ar ion implantation was performed on a Si(100), Si(111) or SiGe virtual substrate through the SiO2 mask with a stripe pattern consisting of several-mm-wide lines and spaces. After this selective ion implantation, a SiGe layer was grown and followed by thermal annealing at 900 °C for strain relaxation, where an uniaxially strained SiGe buffer layer was created. On some of the uniaxially strained SiGe buffers, SiGe layers with the higher Ge contents were grown as uniaxially strained channels. X-ray diffraction reciprocal space mapping (XRD RSM) and micro-Raman mapping measurements were carried our for evaluation of strain states of the structures. XRD RSM was performed with incident X-ray beam directions both perpendicular and parallel to the stripe line pattern direction, which can precisely determine the amount of the strain along the both direction independently. As a results we show the anisotrorpic strain states for SiGe with various Ge concentrations. Concerning the substrate orientation, it is found that the anisotropy of the strain for SiGe(111) is much smaller than that of SiGe(100). This can be explained by difference in dislocation structures. It has been shown that the uniaxial strain is realized when the misfit dislocations generated are aligned only one direction and resultantly strain is relieved along one direction. In the case of SiGe(100), dislocations are likely to be aligned perpendicular to the stripe line. By contrast in the case of SiGe(111), since intersections of (111) planes and interface create triangular shape, dislocations are not likely to be formed along one direction. It is also found that the SiGe channel layer is pseudomorphically grown on the SiGe buffer and the asymmetric strain state is realized in the channel as well as in the buffer layer. From these results it can be said that this technique is very promising for applications to the high mobility uniaxially strained Si/Ge channel MOSFETs. This work was partly supported by MEXT-Supported Program for the Strategic Research Foundation at Private Universities 2009-2013, by Grant-in-Aid for Scientific Research (Grant No. 21246003) from MEXT, Japan, by Industrial Technology Research Grant Program from NEDO, and by the Strategic Information and Communications R&D Promotion Programme (SCOPE) from MIC, Japan. References [1] K. Sawano et al., Appl. Phys. Express 1, 121401 (2008). [2] Y. Hoshi et al., Appl. Phys. Express 4, 095701 (2011).

11:45 Oral

Selective-Growth of (100)- and (111)- Ge Thin-Films on Insulator by Interfacial-Energy-Controlled Metal-Induced-Crystallization

Jong-Hyeok Park, Tsuneharu Suzuki, Akira Ooato, Masanobu Miyao, Taizoh Sadoh

Kyushu University, Fukuoka, Japan

e-mail: j_park@nano.ed.kyushu-u.ac.jp

High-quality crystalline Ge thin-films on a plastic substrate are essential to realize flexible system-in-displays, where high-speed transistors and multi-functional devices are integrated on a display panel. Ge is a promising channel material for high-speed operation, due to the higher carrier mobility compare to conventional Si devices. Furthermore, (100)- and (111)-oriented Ge films provide epitaxial templates for optical and spintronic functional materials, such as GaAs and Fe_3Si, respectively, owing to good lattice matching. Thus, selective growth technique of (100)- and (111)-oriented Ge should be developed.

Ultra-low-temperature processing (≤250°C) is another challenge for these applications to avoid softening of plastic substrates. To achieve this, we have been investigated metal-induced-crystallization techniques (MIC). In MIC methods, the catalytic effects of metals enhance the crystal nucleation and subsequent nucleus growth. In the recent study, we reported the gold-induced crystallization technique (GIC) employing a-Ge/Au stacked structures, and demonstrated crystallization of a-Ge at ultra-low-temperatures (~250°C) through the exchange of layer positions [1]. However, the grown Ge layers consist of randomly-oriented small-grains, due to the significant bulk nucleation of Ge in Au layers. To achieve orientation-control, randomly-oriented bulk nucleation should be suppressed, and instead, preferentially-oriented nucleation at Au/substrate interfaces should be dominated. This domination of interfacial nucleation can be achieved by retarding Ge atomic supply, because interfacial nucleation is energetically favorable compared to bulk nucleation. Here, (100)- or (111)-oriented interface nucleation can be obtained by employing Al_2O_3 or SiO_2 substrates, respectively, due to the lowest interfacial energy [2,3]. Based on these ideas, the present study demonstrates selective growth of (100)- and (111)- Ge by controlling interfacial energy in the nucleation process of GIC.

The sample structure is schematically shown in Fig. 1. Quartz (SiO_2) substrates and Al2O3 covered (30 nm) quartz substrates were employed. On these substrates, a-Ge/Au stacked structures (thickness: 100 nm, respectively) having the diffusion barriers [thin Al2O3 layers (0-10 nm)] at the a-Ge/Au interfaces were formed. These samples were annealed (250°C) in dry N_2 ambient.

For samples with diffusion-barrier thickness of 0-7 nm, randomly-oriented small-grain Ge (1-2 μm) was obtained. This indicates the bulk nucleation cannot be suppressed by such thin diffusion barriers. Interestingly, for diffusion-barrier thickness of 8 nm, (100)- or (111)-oriented large-grains (20-50 μm) were achieved on quartz (SiO_2) and Al_2O_3 covered substrates, respectively [Fig. 2. (a, b)]. Further increase of diffusion-barrier thicknesses resulted in significant retardation of growth. These results show that random bulk nucleation is effectively suppressed and thus interface nucleation is dominated by using diffusion barrier of ~8 nm thickness. Consequently, selective-growth of (100)- and (111)-oriented Ge becomes possible through the interfacial energy modulation by employing SiO_2 and Al_2O_3 substrates, respectively.

In summary, interfacial-energy-controlled GIC process has been developed, which enables the selective formation of (100)- or (111)-oriented Ge crystals on insulators at an ultra-low-temperature (250°C). This technique is very useful to realize advanced new-functional flexible devices.

[1] J. H. Park, et al.: Thin Solid Films 520 (2012) 3293.
[2] J. Schneider, et al.: J. Cryst. Growth 287 (2006) 423.
[3] R. Jaccodine: J. Electrochem. Soc. 110 (1963) 524.

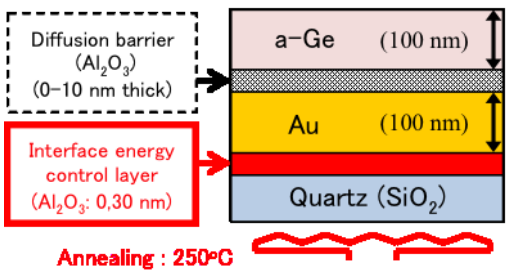

Fig. 1 Schematic sample structure.

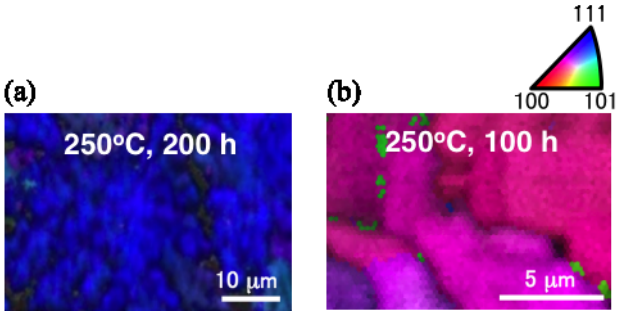

Fig. 2 EBSD images of grown layer of the samples on quartz (SiO2) (a) and Al2O3-covered substrate (b).

12:00 Oral

SiGe crystal growth in the absence of the crucible

Simona Binetti[1], Arne Croell[2], Michael A. Gonik[3,4], Amalia C. Wagner[5]

1. *University of Milano-Bicocca (UNIMIB), Piazza della Scienza, 1, MILANO 20126, Italy* **2.** *Kristallographie, Universität Freiburg (KI), Hermann-Herder-Str. 5, Freiburg 79104, Germany* **3.** *Centre for Material Researches (PHOTON), Cheska-Lipa, 10, Aleksandrov 601655, Russian Federation* **4.** *Centre for Thermophysical Researches (THERMO), Institutskaya, 1, Aleksandrov 601650, Russian Federation* **5.** *Institute of Inorganic and Analytical Chemistry, Albertstraße 21, Freiburg D-79104, Germany*

e-mail: Thermo.ltd@relcom.ru

Crystal growth of Si-Ge alloys [1] without contact to container walls by the so called “detached Bridgman” technique was found to have considerable improvements in crystalline quality being ascribed to a reduced radial temperature gradient during solidification under detached conditions which, in turn, is associated with a lower thermal shear stress at the interface. The progress under microgravity conditions encouraged our ground-based experiments to grow Si-Ge crystals in the absence of the crucible. Besides, Si-rich Si_xGe_{1-x} compounds (x>70-80%), like silicon itself for the purposes of electronics, seem to be practically impossible to grow in containers. However, it is very difficult to apply the detached technique on the ground especially for Si-Ge system because of instability of the process leading to breakage of the conditions of the crucibleless growth. Thus, the Floating Zone (FZ) technique was taken as a basis.

Crystal growth was carried out in a laboratory double-ellipsoid mirror FZ furnace in which two light beams of 10 mm in a height were focused at the centerline of the setup. The Si single crystal of 8 mm diameter was used as a seed; while a 20 mm high cylinder of a uniform Si-20%atGe compound was specially prepared as a feeding material. Solidification of the Si-Ge crystals was conducted at the pulling rates of 0.2-0.4 mm/min to prevent the occurrence of morphological instabilities due to the constitutional supercooling.

Along with the conventional process of the crystal growth, the modified FZ technique was applied. An additional heater enabling the realization of the Axial Heating Process (AHP) was used with the end purpose to control the both shape of the melt/crystal interface and thermal conditions over it during all the run. A crystal grows from the thin melt layer under conditions of weak melt flows similar to those established for conventional methods under microgravity conditions.

The graphite casing of the AHP heater of 15 mm in a diameter and 8 mm high was coated with SiC of a special nanostructure to protect it against the Si melt attack. The melt on both the top and bottom surfaces of the AHP heater was suspended by forces of surface tension. During the growth process, the melt layer at the top side of the heater was held within 2-3 mm, while the height of the melt layer under the heater was varied from 2 to 8 mm.

To examine the technique, a set of growth experiments with Si as a model material was conducted [2]. Crystals in a wide diameter range - relative to the diameter of the AHP heater - were grown: from 2-3 mm up to 20 mm, twice exceeding the diameter of the feed rod. Thus the complete procedure beginning from necking and then passing to the solidification of the large-scale crystal can be realized. Special experiments were conducted to examine the design of the AHP heater allowing to maintain the different temperatures at its top and bottom faces taking in account 1360°C and 1280°C as liquidus and solidus temperatures, respectively, of the Si-20%at Ge compound.

A number of Si and its alloy with Ge crystals were obtained, sliced along the axis, polished and etched. The microscope images of the grown Si-Ge crystals are presented in Fig. 1.

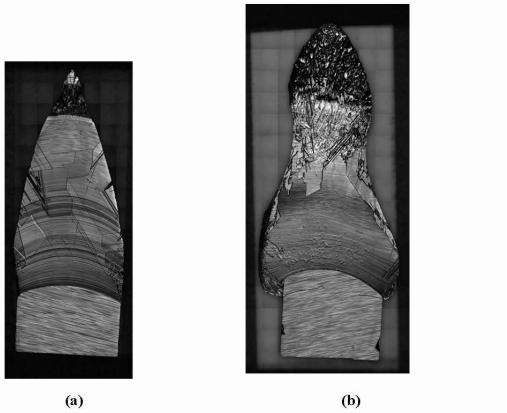

Figure 1. Microscope images of the grown Si-Ge crystals by conventional (a) and modified (b) FZ technique

The crystallinity of the grown silicon and silicon-germanium crystals, as well as interstitial defects in bulk of the material were investigated by means of microprobe/EDX measurements, SEM, NDIC and high resolution XRD are discussed. In order to determine the effects of different growth conditions on the main physico-chemical properties, to reveal the presence of SiC together with products of its decomposition and to get the nature of inclusions available, structural chemical, electrical and spectroscopic characterization were done.

The presence of the main deleterious impurities through electrical measurements and spectroscopic tools, as well as the density and distribution of dislocations and grain boundaries along the ingot are determined. Both the longitudinal and lateral distributions of the second component in Si-Ge crystals are presented.

1. Croell A., Mitric A., Senchenkov A. Abstracts in ICASP-2, Seggau, Austria, (2008).

2. M. Gonik, A.Croell. CrystEngComm 15(12) (2013) 2287-2293.

12:15 Oral

The low thermal gradient Cz technique as a way of growing of dislocation-free germanium crystals

Vitaly A. Moskovskih[1], Pavel V. Kasimkin[1], Vladimir N. Shlegel[2], Yan V. Vasiliev[2], Viktor A. Gridchin[1], Oleg I. Podkopaev[3]

1. *Novosibirsk State Technical University (NSTU), K. Marx av., 20, Novosibirsk 630092, Russian Federation* **2.** *Institute of Inorganic Chemistry of RAS, Novosibirsk 630090, Russian Federation* **3.** *OJSC Germanium, Krasnoyarsk 660027, Russian Federation*

e-mail: v.moskovskih@gmail.com

Germanium is commonly used as a semiconductor material for opto-electronic and electronic applications. One of modern applications of Ge is a substrate for GaAs/Ge solar cells with high conversion efficiency more than 41% [1]. For use as a substrate, material has to be dislocation-free or very low density of dislocations to avoid the negative impact of crystal defects on the quality of the growing epitaxial layers [2].

The obtaining of dislocation-free germanium single crystals is difficult. Formation of crystal defects, caused by thermoelastic stresses, is determined by the temperature field during the growth and cooling of the crystal. It is known that to decrease dislocation density it is necessary to reduce temperature gradients.

The aim of the work was a check of ability to grow single crystals of germanium with a low dislocation density by the low-thermal-gradient Czochralski technique (LTG Cz), which has been successfully used for the growth of oxide crystals [3]. The use of conventional weighing control for the growth of semiconductors, in particular germanium, silicon and gallium arsenide, by the method LTG Cz is somewhat difficult because of so-called "anomalous" behavior of the weighted signal [4]. For automatic control of the germanium crystals growth processes by LTG Cz we developed a method of obtaining information on the value of cross-sectional area of growing crystal based on modulation of pulling rate by the fast small measuring movements of the pulling rod, which cause weighing signal modulation by buoyancy forces.

Results of experiments on growing germanium crystals with a diameter of 45 mm from the graphite crucibles are presented. The crystals were grown in the directions [111], [100], [211] with growth rate from 3.5 to 10 mm/h. Simulation of Cz by CGSim commercial package let estimate that the temperature gradients during growth process did not exceed 1.5 K/cm. Single crystals were grown with a dislocation density of Nd = 100-200 cm-2. Grown crystals are partially faceted, their cross-sections differ from the round.

1. W. Guter, J. Schone, S.P. Philipps, et al, Appl.Phys.Lett. 94 (2009)

2. T. Taishi, Y. Ohno, I. Yonenaga, J. Cryst. Growth 311 (2009) 4615.

3. Ya.V. Vasiliev, Yu.A. Borovlev, E.N. Galashov, et al. Stcintilliatcionnye materialy. Inzheneriya, ustroistva, primenenie. Kharkiv: ISMA (2011) pp. 119–180.

4. W. Bardsley, D.T.J. Hurle, G.C. Joyce, J. Cryst. Growth 40 (1977) 13.

12:30 Oral

New improvements in industrial growth of silicon mono crystals for solar application by using Magnetic-Cz

Alexander Molchanov[1], Frank Mosel[1], Alexey V. Denisov[1], Albrecht Seidl[2]

1. *PVA TePla AG, Im Westpark 10-12, Wettenberg 35435, Germany* **2.** *Schott Technology Center Crystals, Ilmstr. 8, Jena 07749, Germany*

e-mail: alexander.molchanov@pvatepla.com

Solar industry requires further increasing of solar cell efficiency and reduction of production costs.

The quest for the improvement of solar cell efficiency is the intention for the Magnetic Czochralski (MCZ) growth of mono crystals for the PV industry. It is established that a steady magnetic field damps the convective melt flow and hence affects the oxygen concentration in the crystal which influences the cell efficiency.

A superconducting magnet in a CUSP configuration was installed on a Czochralski puller for the growth of silicon mono crystals. For investigation several boron-doped silicon crystals were grown. Different field configurations with respect to the field strength and the position of the symmetry line of the cusp field were applied. Additionally other growth parameters which affect the crystal quality were modified in order to find the best interaction of all these parameters for the production of high efficiency solar cells. Also importance was attached to high growth productivity.

We report in detail about the equipment configuration and the process parameters which were successfully applied resulting in high quality crystals. Complete characterisation of the ingots especially with respect to the oxygen distribution and finally to the cell efficiency is presented.

High quality crystals for the production of high efficiency cells can be grown by the application of a cusp magnetic field. It is shown that the additional investment and the operation costs of the superconducting magnet can be compensated by improved operational conditions and a high quality of the substrate material.

Further approaches and special tools to increase the productivity and to reduce the production costs of Cz-Si for PV will be presented and discussed.

Closing ceremony
Friday afternoon, 16 August, 13:00

Posters

Wednesday, 14 August

WeP-T05
Wednesday afternoon, 14 August, 16:00
Room 107, Old Library

16:00 Poster We84

Effects of Crucible Coating on the Quality of Multi-crystalline Silicon Grown by a Bridgman Technique

Vasile Pupazan, Radu-Andrei Negrila, Marius Stef, Madalin O. Bunoiu, Irina Nicoara, Daniel Vizman

West University of Timisoara (UVT), Bd.V. Parvan nr.4, Timisoara 300223, Romania

e-mail: madalin.bunoiu@rectorat.uvt.ro

Because of its low costs and its similarities with directional solidification, Bridgman growth of small diameter (max. 3cm) multi-crystalline silicon is a suitable technique for a fundamental study of the influence of growth parameters (like growth rate, temperature gradients, crucible coating) on the interface shape, grains size and impurity distribution (carbon, oxygen), which are important parameters for the photovoltaic applications. In order to study the influence of the crucible material and of the coating on the crystals quality, different growth experiments using a Bridgman set-up were performed. In this respect crucibles made in graphite and quartz were used as well as two coating materials ($Si_3N_4$and $CaCl_2$).

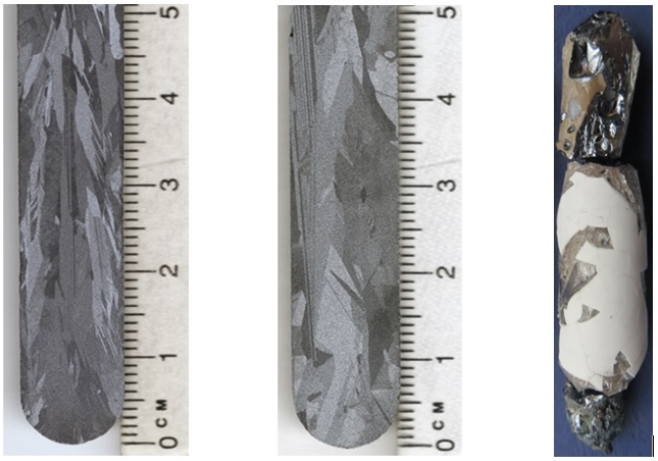

(a) (b) (c)

Fig.1. Crystals grown in quartz crucible with different coating materials: a) Si_3N_4. b) $CaCl_2$. c) no coating.

Because thecoating material can have different effects on crucibles made in different materials, the use of a $CaCl_2$ as an alternative coating material was revisited (see [1]) in the case of quartz crucibles and tested for graphite ones. Because of acting as a liquid encapsulant, calcium chloride allows the release of the silicon ingot and suppresses nucleation simultaneously, thus allowing large grain growth [1].

The first studies were devoted to observe the influence of the use of different coatings materials in order to avoid the adhesion of the Si crystal to the quartz crucible for the same set of growth conditions. It was observed that the silicon crystal was very easily released from the crucible and the grain size is higher in the case of $CaCl_2$ coating (fig. 1.b) then in the case of Si_3N_4 coating (fig. 1a). The same results were obtained also by Ravishankar [1].

In the case of the graphite crucible, although the grains were also larger, the crystal could not be removed from the crucible. FT-IR spectroscopy was used in order to analyze the oxygen and carbon concentration for both cases.

The study has given some clear indications about the possible benefits when a coating material is used but also on the specific problems that arose for each new type of coating-crucible combination investigated and lays the way for new investigations regarding a novel coating-crucible combination that could be of benefit for the PV industry in the future.

[1] P. S. Ravishankar, Journal of Crystal Growth, 94 (1989) 62-68

16:00 Poster We85

Material development for directional solidification of multicrystalline silicon by AHP method

Michael A. Gonik[1,2], Stephan Riepe[3], Claudia Schmid[3], Andrey Smirnov[4]

1. *Centre for Material Researches (PHOTON), Cheska-Lipa, 10, Aleksandrov 601655, Russian Federation* **2.** *Centre for Thermophysical Researches (THERMO), Institutskaya, 1, Aleksandrov 601650, Russian Federation* **3.** *Fraunhofer Institut for Solar Energy Systems (ISE), Heidenhofstraße 2, Freiburg 79110, Germany* **4.** *STR Group Ltd., Engels av. 27, Saint-Petersburg 194156, Russian Federation*

e-mail: Thermo.ltd@relcom.ru

The Axial Heating Process (AHP) technique has proven its capability for directional solidification processes [1]. In order to make use of this technique for silicon, suitable material systems for the submerged heating device have to be identified. Due to the prolonged contact of the device with liquid silicon, the material system has to be mechanically and chemically stable without introducing high amounts of impurities into the silicon material.

For the following investigations, a graphite material encapsulated by a high quality SiC layer has been used. At this stage of the AHP development, we have conducted a growth experiment in a G1 size quartz crucible coated with silicon nitride, in which the melt surface was almost entirely covered by a plate as a model of the AHP heater being on the float. The plate had dimensions allowing a gap with the crucible walls of about 15 mm for SiO and CO gas transport through the melt surface. High quality silicon feedstock was filled inside the quartz crucible and doped with boron. In order to prevent a reaction of the plate with the crucible material, the plate was placed on two spacers at the crucible bottom, which were made out of silicon nitride material. Multicrystalline silicon was grown under standard growth conditions for directional solidification.

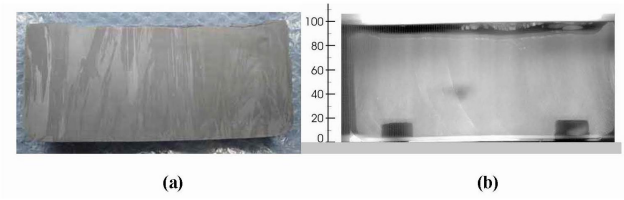

(a) (b)

Fig. 1. Crystal structure (a) and infrared transmission (b) of the Si ingot obtained

After solidification, the top part of the silicon block with the grown in graphite plate was removed by sawing for further investigation. Crystal structure visible at side cut of the solidified G1 block (see Fig. 1a) shows columnar growth with a sufficient grain size. Infrared transmission of Si below the graphite plate is presented in Fig. 1b. Only minor inclusions (probably SiC) at 40 mm height in the middle of the silicon block are observed. The two dark objects visible at the bottom of the material are the silicon nitride spacers.

The desired range of resistivity between 1.3 and 1.0 Ωcm was achieved (see Fig. 2a), as well as acceptable μPCD-lifetime of the minority carriers (see Fig. 2b) being half as less again as the characteristics for

standard blocks with high quality material. Besides probable introduction of impurities originated from the AHP model, the process was not adapted to using a floating plate.

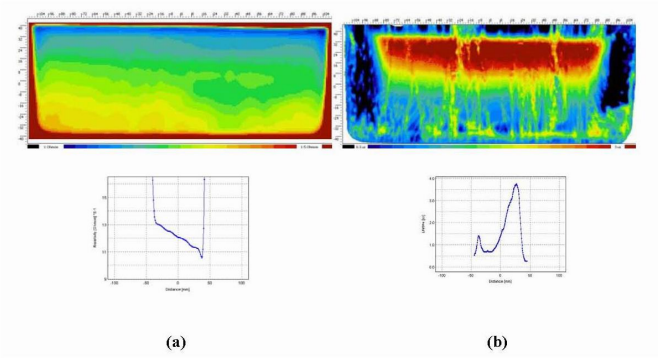

Fig. 2. Resistivity (a) and μPCD-lifetime (b) at cross section of the Si ingot. Bottom curves correspond to the centerline distribution of the parameter

FTIR and ICP-MS/NAA are correspondently applied to measure carbon and oxygen, as well as to analyze impurities in Si. Computer modeling has been applied for description of the thermal, convective and chemical transport processes during the growth run. The use of silica free crucibles is under discussion. The Si growth under these conditions may drastically change physical-chemical phenomena resulting in essential reduction of oxygen in silicon.

1. M.A. Gonik, A.I. Nepomnyaschih, V.V. Kalaev, A.D. Smirnov. Application of the Submerged AHP Heater for the Growing of the Multi-crystalline Silicon. Abstracts of the ACCGE-17 Conference, Lake Jeneva, Wisconsin, 2009.

16:00 Poster We86

Growth of Spherical Si Crystals on Porous Si_3N_4 Substrate that Repels Si Melt

Hironori Itoh, Hideyuki Okamura, Chihiro Nakamura, Takashi Abe, Masaharu Nakayama, Ryuichi Komatsu

Yamaguchi University, 2-16-1 Tokiwadai, Ube 755-8611, Japan

e-mail: ito-hrnr@yamaguchi-u.ac.jp

Almost 90% of solar cells currently on the PV market use crystalline Si as the main material [1]. Cutting loss of grown Si ingot to wafers during the conventional manufacturing process of crystalline Si solar cells is up to 60% of the initial weight of grown Si crystals [2], which is considered to be one of the main obstacles of the cost reduction of solar cells. Therefore, direct growth technique of shaped Si crystals without cutting process has been remarkably investigated to fabricate low-cost Si solar cells [3-5]. We have also been investigated to develop a novel growth technique of shaped Si crystals using the Si_3N_4 porous ceramic substrate [6]. The solar cells consist of spherical Si crystals are on the market recently. These spherical Si crystals have been fabricated by the drop tower method [7]. In this method, droplets of Si melt are crystallized during free-fall within a few seconds and most of the fabricated spherical Si becomes fine multicrystalline because of the high cooling rate of Si melt. These multicrystalline spherical Si need further re-melting and re-crystallizing process at slow cooling rate to improve crystalline quality for use as solar cells [8]. In this study, we report successful results of growth of high quality spherical Si crystals with slow cooling on the developed porous substrate.

Powders of Si_3N_4, SiO_2 and PMMA particles (5μm in diameter) were mixed and pressed into pellet. The porous ceramic film with same composition was also prepared on AlN board by spin coating method. These substrates were degreased under air at 873-1373 K and then fired under N_2 atmosphere at 1873 K. Porous structure was obtained by the thermal decomposition of mixed PMMA particles (Fig. 1). Spherical Si crystals were grown on the porous substrate in the horizontal tube furnace. Multiple pieces of semiconductor grade Si material (10 mg) was melted on the substrate at a temperature of 1753 K for 6 minutes with the heating rate set to 200 K/h and the cooling rate to 150 K/h.

Spherical Si crystals with diameters of up to 2 mm were successfully grown on the porous substrate with good reproducibility (Fig. 2a). The degree of undercooling of Si melt at crystallization of spherical Si was estimated to be less than 70 K, based on the difference between the heater temperature at melting of Si and that at crystallization of Si. Grown spherical Si crystals show metallic luster and most of them consist of single grain or only 2-3 grains with twinning planes observed from their etched cross sections (Fig. 2b). This confirmed that spherical Si crystals close to single crystals in their properties can be obtained stably by crystallizing Si on the porous substrate with a sufficiently low cooling rate without additional re-melting and re-crystallizing process of grown Si. The concentration of carbon and oxygen atoms in the grown Si crystals (C: 6 ppm, O: 5 ppm) analyzed by SIMS satisfies the specification of solar grade Si (C: 10 ppm, O: 20 ppm) [9]. Neither sticking nor infiltration of Si against the porous substrate was observed and the contact angle of Si against porous substrate was not changed through growth of spherical Si crystals on the same substrate with multiple times. Thus, the developed porous substrate is continuously reusable for the growth of high quality spherical Si crystals.

This study is supported by Regional Innovation Cluster Program (Global Type) by Ministry of Education, Culture, Sports, Science and Technology; Yamaguchi Green Materials Cluster (2009-2013).

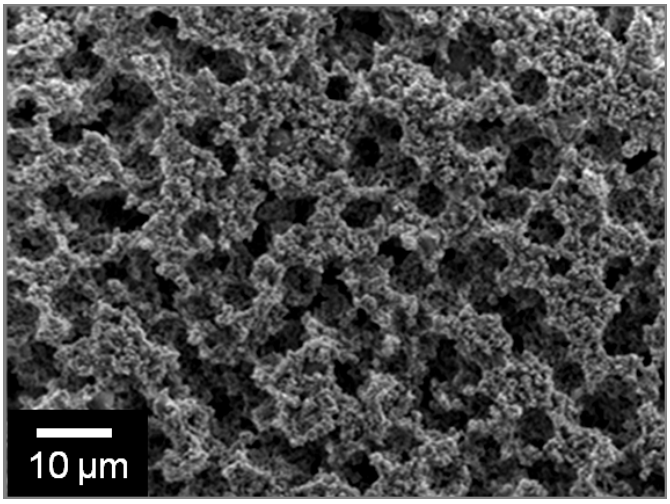

Figure 1. SEM micrograph of surface of the fabricated Si_3N_4 porous ceramic substrate. Holes formed by thermal decomposition of mixed PMMA particles were connected to each other.

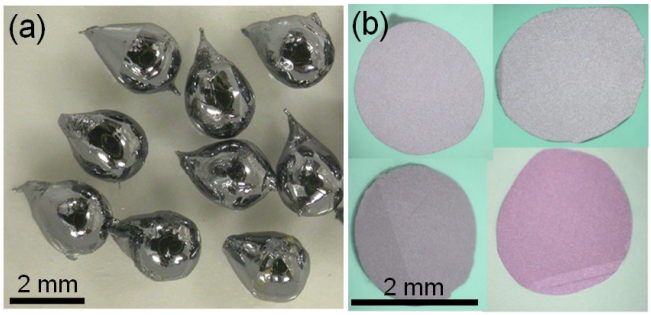

Figure 2. (a) As-grown spherical Si crystals and (b) their cross sections after polishing and NaOHaq etching. They are composed of single grain or only 2-3 grains with twinning planes.

References

[1] W.G.J.H.M. van Sark *et al*., Energy Policy 35 (2007) 3121-3125. [2] D. Sarti and R. Einhaus, Sol. Energy Mater. Sol. Cells 72 (2002) 27-40. [3] I. Hide *et al*., J. Cryst. Growth 79 (1986) 583-589. [4] G. H. Lee and Z. H. Lee, J. Cryst. Growth 233 (2001) 45-51. [5] S. Sakuragi *et al*., Proc. 14th Workshop on Crystalline Silicon Solar Cells & Modules – NREL (2004) 188-191. [6] H. Itoh *et al*., J. Ceram. Soc. Jpn. (2013) in press. [7] K. Nagashio *et al*., Jpn. J Appl. Phys. 45 (2006) L623-626. [8] Z. Liu, A. Masuda and M. Kondo, J. Cryst. Growth 311(2009) 4116-4122. [9] M.G. Mauk *et al*., Proc. 3rd World Conf. Photovolt. Energy Convers. (2003) 939-942.

16:00 Poster We87

Grain Control by Patterned Layers in Multi-crystalline Silicon Growth by Directional Solidification

Chung-Wen Lan, Yu-Ting Wong, Chih-Chen Hsieh

Department of Chemical Engineering, National Taiwan University, No. 1, Sec. 4, Roosevelt Road, Taipei city 10617, Taiwan

e-mail: cwlan@ntu.edu.tw

The grain control in multi-crystalline silicon directional solidification is crucial to crystal quality and thus their photoelectric conversion efficiency. To control the grain structures, the initial grain layer is crucial. In this study, we considered different layers for the initial growth either from holes or notches for this purpose. It was found that the grain structures could be better controlled. The growth from the patterned layer had a higher percentage of non-coherent grain boundaries and a more uniform grain structure. The grain orientation and structures were determined by electron back scattering diffraction (EBSD) and the defect density and photo luminance (PL) mappings were carried out. The relationship between the grain structures and the defects was further discussed.

16:00 Poster We88

Development of grain structures of multi-crystalline silicon in directional solidification

Chung-Wen Lan[1], Yu-Ting Weng[1], Wen-Ching Hsu[2], Michael Yang[2]

1. *Department of Chemical Engineering, National Taiwan University, No. 1, Sec. 4, Roosevelt Road, Taipei city 10617, Taiwan* **2.** *Sino-American Silicon Products Inc., Hsinchu 30075, Taiwan*

e-mail: cwlan@ntu.edu.tw

Development of grain structures of multi-crystalline silicon from small spherical seeds with random orientations in directional solidification was investigated. The electron backscattered diffraction (EBSD) analyses of the grains at different pulling rates, i.e., 10, 50, and 200 mm/h, were carried out. It was found that the {112} orientation was dominant at the low crucible pulling speed, while {111} at the high pulling speeds. The percentage of {100} grains was found very low near the top of the ingots. The percentage of non-S grain boundaries was around 70% at the beginning and decreased with the solidification distance, while S3 grain boundaries or twins increased indicating the importance of twining in the development of grain structures.

16:00 Poster We89

Cooling-Rate-Controlled Rapid-Melting-Growth for Giant-Single-Crystal SiGe on Insulator

Ryo Matsumura, Ryusuke Kato, Yuki Tojo, Taizoh Sadoh, Masanobu Miyao

Kyushu University, Fukuoka, Japan

e-mail: r_matsumura@nano.ed.kyushu-u.ac.jp

1. Introduction

To break through the scaling limit of LSIs, multi-functional devices should be integrated on Si platform. SiGe-on-insulator (SGOI) structures are essential for this purpose. They provides advanced channels for high-speed transistors. In addition, SiGe are ideal epitaxial template for various optical- and spintronic-materials with different lattice constants. Recently, we proposed the Si-seeded rapid-melting growth (RMG) of a-SiGe [1,2] and realized laterally graded SiGe on insulator (SGOI) [3]. To expand the application fields, SGOI with uniform Si concentration profile should be developed.

In this study, rapid-melting growth of SiGe is investigated with seed-free processing. Large SGOI with uniform Si concentration through segregation-free RMG is realized by optimizing the cooling rate.

2. Experimental Procedure

Si(100) wafers covered with Si_3N_4 films were employed. After a-Si_xGe_{1-x} ($0.07 \leq x \leq 0.2$) films (thickness: 100 nm) were deposited, the SiGe films were patterned into strips (width: 5 mm, length: 400 mm). After deposition of SiO_2 capping layers (thickness: 800 nm), the samples were heat-treated by RTA (1150^{o}C, 1 sec) [Fig.1(a)]. The cooling rate after RTA was controlled in a wide range of 2-17^{o}C/sec.

As shown in Fig.1(b), for the slow cooling rate (i), Si-rich nuclei will be generated in the molten region, when the temperature approaches the solidus curve. Growth initiated at the nuclei follows the solidus curve, which results in SiGe segregation. However, for the fast cooling rate (iii), nucleation occurs at temperatures far below the solidus curve. This is because incubation time for nucleation cannot be secured above the solidus curve. Such super cooling will result in poly-crystallization without segregation. On the other hand, for the medium cooling rate (iii), the nucleation will occur at temperatures in the vicinity of the solidus curve. Such “mild” super cooling will generate a limited number of nuclei and thus, result in a large single-crystal SiGe without segregation.

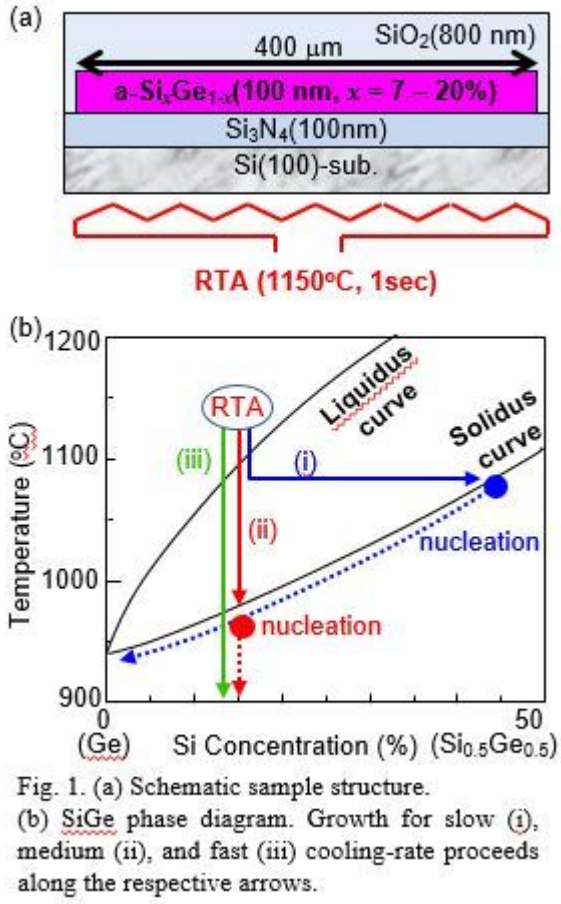

Fig. 1. (a) Schematic sample structure. (b) SiGe phase diagram. Growth for slow (i), medium (ii), and fast (iii) cooling-rate proceeds along the respective arrows.

3. Results and Discussion

Growth features of samples with various initial Si concentrations grown under various cooling rates are summarized in Fig.2. Typical EBSD images and Si concentration profiles for $Si_{0.1}Ge_{0.9}$ samples are also shown in Fig. 2. As we expected, for the fast cooling (triangles), the EBSD image indicates poly-crystallization (grain size: 5-10 μm). For the slow cooling (squares), the EBSD image indicates formation of a giant crystal grain (~400 mm). However, the Si concentration shows a laterally graded profile indicating segregation during melt-back process [3]. Interestingly, a large SiGe crystal with uniform Si concentration is achieved under medium cooling rate (circles), where the concentration is identical to the initial value.

As shown by the circles in Fig.2, giant single-crystal SiGe grains with uniform Si profiles are obtained in a wide range of Si concentrations by selecting the cooling rate.

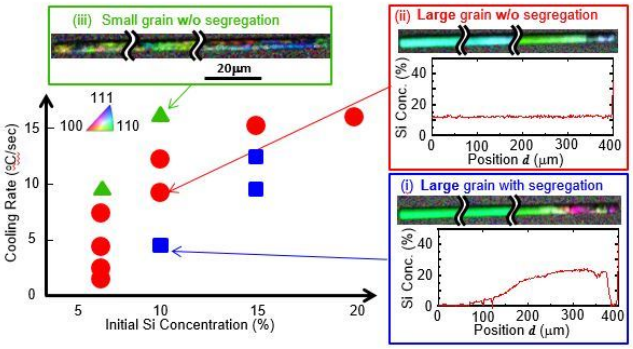

Fig.2 Summary of SiGe growth features as a function of Si concentration and cooling rate.

4. Conclusions

Seedless rapid-melting growth of SiGe has been investigated. By controlling the cooling rate, segregation-free giant SGOI is achieved for a wide range of the Si concentrations. These results open up the possibility of integration of advanced functional devices on Si platform.

Reference

[1] M.Miyao et al., APEX 2, 045503 (2009).

[2] T.Tanaka et al., APEX, 3, 031301 (2010).
[3] R.Matsumura et al., APL 101, 241904 (2012).

16:00 Poster We90

Crystal growth of MCZ silicon with ultra low carbon concentration

Yuta Nagai, Satoko Nakagawa, Kazuhiko Kashima

Global Wafers Japan Co., Ltd. (GWJ), 30 Soya, Hadano-shi, Kanagawa 257-8566, Japan

e-mail: Yuta_Nagai@sas-globalwafers.co.jp

Introduction:

Generally, Floating Zone (FZ)-grown silicon (Si) is used in high power devices that require long carrier lifetime. FZ Si has longer lifetime than magnetic-field-induced Czochralski (MCZ) Si, because FZ Si has little oxygen precipitate nuclei that act as the recombination center of the carrier. However, the application of FZ Si for the mass production might not be possible, because FZ Si is difficult to make enlargement in diameter. Therefore, in order to support the rapidly increasing volume of high power devices, we have started the development of high quality MCZ Si with a longer lifetime by reducing carbon impurities that act as heterogeneous nucleation sites for oxygen precipitates. In general, MCZ Si has more carbon incorporation than FZ Si, because many graphite parts and a silica crucible are used in a CZ furnace. The pathway for carbon incorporation into a crystal is schematically shown in Fig. 1[1]. The main factor of carbon incorporation is the back-diffusion of carbon mono-oxide (CO) from the hot graphite parts, where CO is formed by the reaction of silicon mono-oxide (SiO) with graphite, to the melt. Therefore, in order to grow MCZ Si with lower carbon concentration than FZ Si, it is necessary to prevent CO back-diffusion. Furthermore, in order to achieve ultra low carbon concentration such as less than 10^{14} atoms/cm^3, carbon impurities that originate from the poly-Si starting material must be reduced. For achieving this, one applicable method is to evaporate carbon impurities from the Si melt. Endo *et al.*[2] suggested that carbon

impurities in the Si melt evaporate as CO in accordance with following reaction (1).

$$C\ (diss) + O\ (diss) \leftrightarrow CO\ (gas) \qquad (1)$$

In this study, we demonstrate how to prevent CO back-diffusion and to promote CO evaporation in order to grow MCZ Si with ultra low carbon concentration.

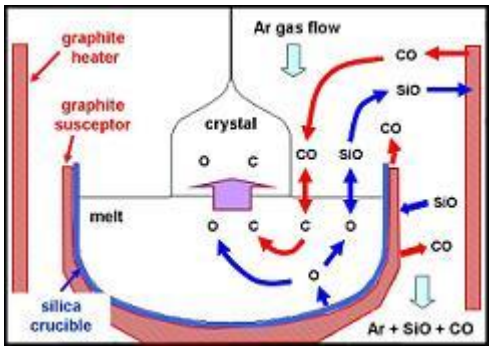

Fig. 1. Pathway for carbon incorporation into a crystal.

Experimental and results:

In this study, CZ puller for 3 inches Si crystal in diameter was used. Carbon concentration was evaluated by Photoluminescence (PL) spectroscopy with a detection limit of 10^{13} atoms/cm^{3}[3]. First, the flow path of argon (Ar) gas in a CZ furnace and growth parameters (Ar gas flow rate, heater power, etc.) were adjusted to reduce CO back-diffusion, and CZ Si with lower carbon concentration than FZ Si (<10^{15} atoms/cm^3) was grown. Next, the effect of CO evaporation on the carbon concentration in CZ Si was investigated by increasing the Ar gas flow rate. The results confirmed that the carbon concentration was markedly reduced to below 10^{14} atoms/cm^3. This indicates that the reaction (1) proceeded to the right side with a reduction in the CO concentration just above the melt surface. On the basis of the results, it is possible to grow CZ Si with lower carbon concentration (<10^{14} atoms/cm^3) than FZ Si by the reduction of CO back-diffusion and the promotion of CO evaporation from the melt.

References:

1) D. E. Bornside, R. A. Brown, J. Electrochem. Soc. **142** (1995) 2790

2) Y. Endo, Y. Yatsurugi, Y. Terai, T. Nozaki, J. Electrochem. Soc. **126** (1979) 1442

3) S. Nakagawa, K. Kashima, M. Tajima, Proceedings of the Forum on the Science and Technology of Silicon Materials 2010 (2010) 326

Acknowledgments:

This work was partly supported by the New Energy and Industrial Technology Development Organization (NEDO) under the Ministry of Economy, Trade and Industry (METI) of Japan.

16:00 Poster We91

Study of resistivity and lifetime profiles in highly polluted multi-crystalline silicon grown in a graphite crucible by a Bridgman technique

Radu-Andrei Negrila, Vasile Pupazan, Madalin O. Bunoiu, Daniel Vizman

West University of Timisoara (UVT), Bd.V. Parvan nr.4, Timisoara 300223, Romania

e-mail: negrila.andrei.radu@gmail.com

A small diameter Bridgman equipment was used to grow multi-crystalline silicon of 3 cm diameter in a graphite crucible. The purpose of the work is to study the influence of process parameters on the resistivity and lifetime profiles and to understand the relation between melt convection and impurity distribution.

According to the literature [1], a convective dissolution rate of a crucible leads to a higher impurity concentration in the melt. In the studied crystals a very high neutral impurity (C and O) concentration has been found. These impurities have largely entered the molten silicon through the liquid phase diffusion, aided by convective transport. Therefore the carbon concentration in the melt is strongly related with the time duration in which the silicon was in the molten phase. In order to study the influence of the carbon concentration on the resistivity distribution, first two experiments were performed: one with a shorter time in molten phase (fig.1.a) – probe A– and one with a longer time in molten phase (fig.1c) – probe B. It was observed that the resistivity pattern changed from a w-shape in radial direction for A (fig.1.b) to a v-shape for B (fig1.d). In the paper this behaviour in relation with the interface shape, melt convection and mobility limitation through scattering on neutral impurity centres (C and O) [2] will be explained.

Furthermore, we analyse the incorporation of impurities, their distribution and precipitation in relation with the multi-crystalline growth, through the lifetime and resistivity scans for other samples grown at different process parameters.

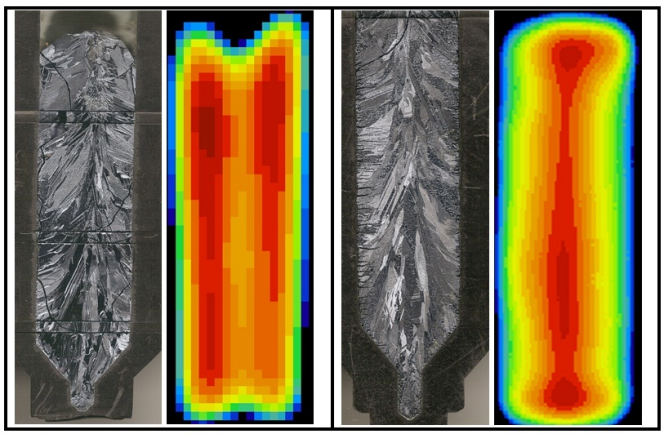

Figure1. Probe A:(a)Optical scan; (b)Resistivity scan. **Probe B**:(c)Optical scan; (d)Resistivity scan

[1] A. Popescu, D. Vizman - International Journal of Heat and Mass Transfer 54 (2011), 5540-5544

[2] P. S. Kireev, Semiconductor Physics, Mir Publishers 1978.

16:00 Poster We92

Modelling of 3D features of molten zone in FZ silicon crystal growth

Matīss Plāte, Armands Krauze, Andris Muiznieks

Faculty of Physics and Mathematics, University of Latvia, Zellu Street 8, Riga LV-1002, Latvia

e-mail: matiss.plate@lu.lv

Nowadays there is an ever growing demand for a continuous development of the industrial silicon single crystal growth techniques. Complexity of the processes and high experimental costs is the motivating factor for advancing the mathematical modelling. We present our general approach for the modelling of industrial floating zone (FZ)

process considering 3D features of molten zone shape and heat exchange there.

Considering the partly axisymmetric characteristics of the FZ system, axisymmetric phase boundary shapes, temperature field and radiation heat exchange (view factor method) in a quasi-stationary state are obtained by iteratively coupled calculations with program FZone [1]. The high frequency (≈3MHz) EM field is essentially asymmetric due to the asymmetry of the single turn inductor and therefore is modelled using 3D boundary element method [2]. Since the crystals are rotated, a reasonable assumption is to azimuthally average the obtained current density distributions for boundary conditions of the axisymmetric calculations. Illustrative calculation results as temperature field and shapes of phase boundaries for a typical 4” FZ crystal (process data from IKZ, Berlin) are depicted in Fig. 1.

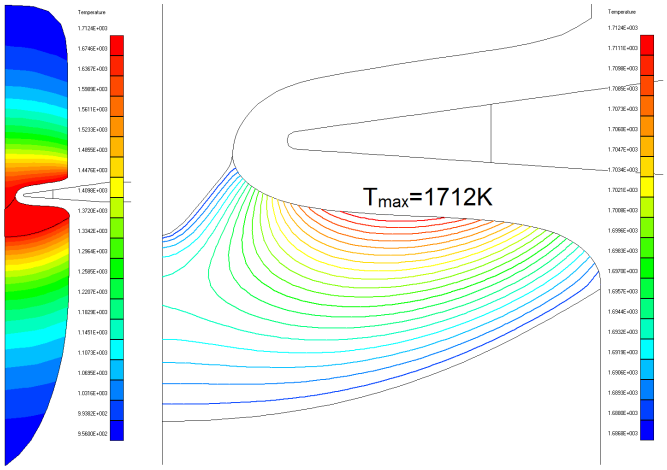

Figure 1. Calculation results obtained with program FZone. Axisymmetric temperature field in feed rod, melt and crystal (left), isotherms in melt (right).

Nevertheless due to a pronounced asymmetry of the EM field for a more detailed considering of the molten zone, the influence of induced power density and EM pressure on silicon free melt surface cannot be regarded as axisymmetric. E.g., there are distinct maxima of induced power density on the free melt surface below the slits of inductor (Fig. 2) and therefore temperature field in the molten zone will be asymmetric. The maxima of electromagnetic pressure correspond to the maxima of the induced power density and will lead to asymmetry of the shape of the free melt surface.

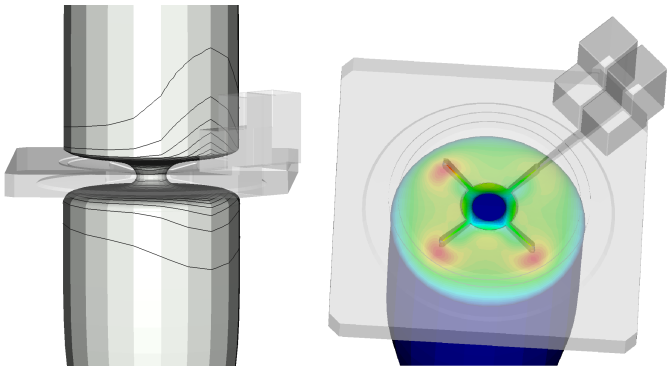

Figure 2. Calculation results with program FZone. Induced current lines on silicon surfaces (left) and induced power density on the free melt surface (right).

We have developed a calculation algorithm for solving the equilibrium shape of free melt surface. The approach of our model is similar to that of the program Surface Evolver with energy functional minimization, i.e., finding equilibrium of gravity, surface tension, hydrostatic and EM forces which all are acting on the free surface. Triple point line (TPL) positions are fixed. Grid vertices are shifted in normal direction proportionally to the total force exerted on the vertex. Hydrostatic pressure p0 is chosen such that the average meniscus angle of the free surface at the crystal TPL is equal to the silicon growth angle. Since free melt surface shape affects the EM pressure distribution, solving both the EM and the free surface shape equations is iteratively coupled. Obtained calculation results for the shape of free melt surface, including comparison of azimuthal distributions of meniscus angle for 4” and 6” processes, is shown in Fig. 3.

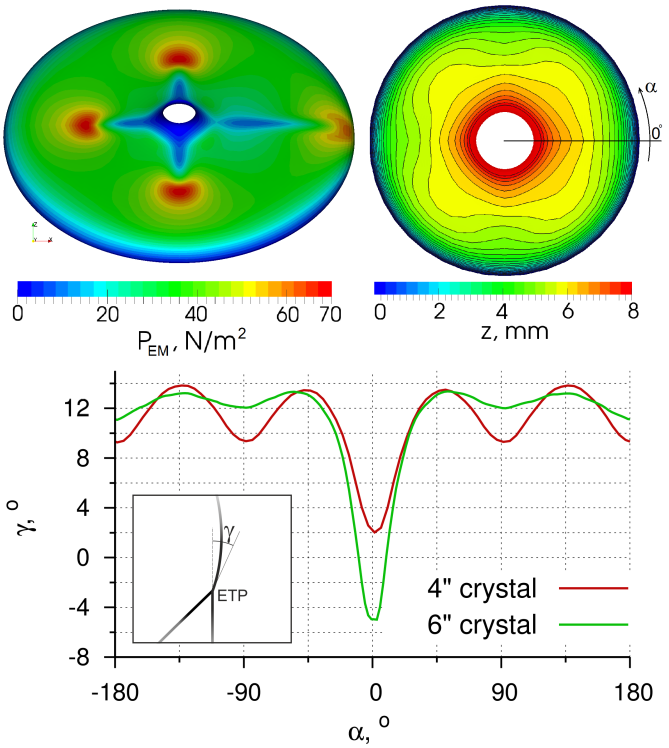

Figure 3. EM pressure distribution (top left), isolines of vertical coordinate (top right) on the free surface of 4” crystal and azimuthal distribution of meniscus angle for 4” and 6” processes (bottom).

The asymmetry of induced power density creates asymmetric temperature field in the melt, which might affect the crystallization interface. The model for heat transfer in the molten zone is modelled as steady state heat diffusion, where temperature distribution is determined by Laplace equation with constant temperature boundary conditions on the crystallization and melting interfaces and given heat flux density on free melt surface. Direct boundary element method is used to solve the Laplace equation. Temperature values on the free surface and temperature normal derivatives on the crystallization interfaces are used as unknowns. The heat flux density on the free melt surface, which is used to formulate the boundary conditions, depends on the distributions of the EM power density, absorbed radiation heat flux density, and surface temperature. Due to the temperature dependence of the boundary conditions, the temperature equations are solved repeatedly, each time updating the boundary conditions until a steady solution is obtained. Results of the 3D heat exchange program are shown in Fig. 4.

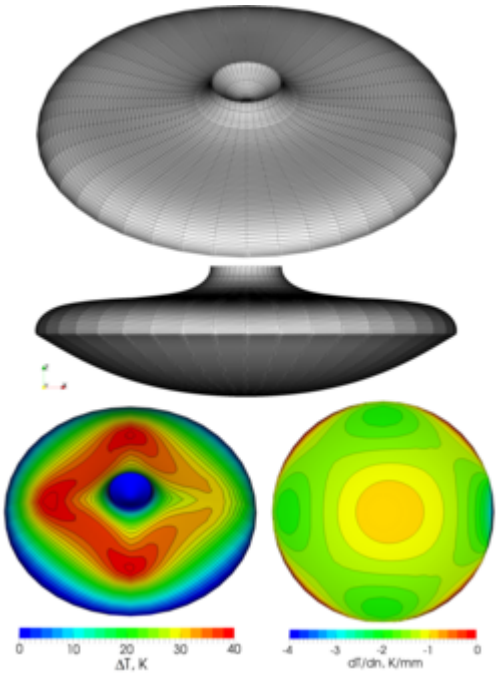

Figure 4. View of the molten zone with boundary element mesh (top and centre), temperature distribution on free melt surface (bottom left) and temperature normal derivative on crystallization interface (bottom right).

The described mathematical models and respective programs have been incorporated into a calculation cycle with program FZone. The converged quasi-stationary axisymmetric solution obtained by FZone is used to generate a 3D mesh for iterative 3D EM field and free surface calculations. The calculated 3D free surface shape and EM power distribution on it are used to run 3D temperature calculations in the molten zone. The EM power distribution and absorbed radiated heat is used to formulate the boundary conditions for the free melt surface. The result of the 3D BEM heat transfer calculations is heat flux density distributions on the crystallization and melting interfaces. These distributions are azimuthally averaged and supplied to the FZone program for the use in 2D axisymmetric phase boundary calculations. The cycle is repeated until the necessary precision is reached.

Acknowledgements

The present work is carried out at the University of Latvia and has been supported by the European Regional Development Fund, project contract No. 2011/0002/2DP/2.1.1.1.0/10/APIA/VIAA/085.

References

[1] G. Ratnieks et al., Modelling of phase boundaries for large industrial FZ silicon crystal growth with the needle-eye technique, JCG, 255, 227-240 (2003)

[2] A. Muižnieks et al., Development of numerical calculation of electromagnetic fields in FZ crystal growth process, MHD, 46, 475-486 (2010)

16:00 Poster We93

Impurities, precipitates, and dislocations in multicrystalline silicon grown from well-mixed and poorly mixed melts

Claudia Funke[2], Ekaterina Schmid[1], Anna Poklad[1], Günter Gärtner[2], Vladimir Galindo[3], Lutz Raabe[4], Olf Pätzold[2]

1. *TU Bergakademie Freiberg, Institute of Nonferrous Metallurgy and Purest Materials, Leipziger Str. 34, Freiberg 09599, Germany* **2.** *TU Bergakademie Freiberg, Institute of Experimental Physics, Leipziger Str. 23, Freiberg 09599, Germany* **3.** *Helmholz-Zentrum Dresden-Rossendorf, Institute of Fluid Dynamics, P. O. Box 510119, Dresden 01314, Germany* **4.** *Muldenhütten Recycling und Umwelttechnik GmbH, Freiberg 09599, Germany*

e-mail: Anna.Poklad@inemet.tu-freiberg.de

Multicrystalline silicon (mc-Si) is one of the most important substrate materials for solar cells. The efficiency of the processed cells depends strongly on the concentration of impurities and structural defects in the material. A detailed understanding of defect-related phenomena is necessary to control and reduce the concentration of defects in mc-Si crystals, which is the major challenge crystal growers are faced with. For a successful defect engineering, however, still too little is known about the mutual interaction between impurities, precipitates and dislocations during crystal growth as well as about the correlation between the formation of defects and growth conditions.

This paper presents results on the correlations between impurities, precipitates, and dislocations in mc-Si crystals grown from well-mixed and poorly mixed melts. The crystals were grown in a high-vacuum induction furnace by the vertical Bridgman method. The melt mixing was modified by changing the growth rate and the intensity of the melt flow. The crystals were sliced into vertical and horizontal samples, which were polished and etched to detect impurities, precipitates and dislocations. The impurity concentration was measured by FTIR spectroscopy. Precipitates and dislocations were analyzed by reflected light and IR-transmission microscopy. SEM and EDX were used to detect the morphology and composition of precipitates.

The results show that the formation of precipitates can be completely suppressed in growth from a well-mixed melt, whereas extended precipitated areas are observed in crystals grown from a poorly mixed melt. Mainly SiC and Si_3N_4 precipitates are found. Apparently, they are formed when the melt becomes supersaturated by carbon and nitrogen in front of the interface due to axial segregation during growth under poor mixing conditions. Within precipitated areas the dislocation density is increased, too. Often, a high dislocation density was detected in the direct neighborhood of a precipitate. This demonstrates that precipitates are an important source of dislocations in mc-Si.

16:00 Poster We94

Fabrication of large-area Si-based photonic nanostructures coupled with Ge quantum dots and their application to solar cells

Noritaka Usami[1], Yusuke Hoshi[1], Takanori Kiguchi[2], Kazufumi Ooi[3], Takeshi Tayagaki[3]

1. *Graduate School of Engineering, Nagoya University, Furo-cho, Chikusa-ku, Nagoya 464-8603, Japan* **2.** *Institute for Materials Research, Tohoku University, 2-1-1, Katahira, Aoba-ku, Sendai 980-8577, Japan* **3.** *Institute for Chemical Research, Kyoto University, Kyoto 611-0011, Japan*

e-mail: usa@numse.nagoya-u.ac.jp

Photonic crystals or nanostructures are regarded as promising in the field of optoelectronics since they could control and manipulate photons. Management of photons is of great importance also in solar cells. However, application of photonic nanostructures to solar cells has been considered to be not feasible. This is due to the fact that fabrication of photonic nanostructures generally requires advanced lithography techniques and is limited to a small-area. It would be ideal if one could fabricate large-area photonic nanostructures without any lithography techniques so that one can implement photonic nanostructures to solar cells.

We show that lateral modulation in strain in vertically aligned Ge quantum dots leads to modulation in the etching rate against a chemical solution. This could be utilized for fabrication of Si-based large-area photonic nanostructures coupled with Ge quantum dots without any lithography techniques.

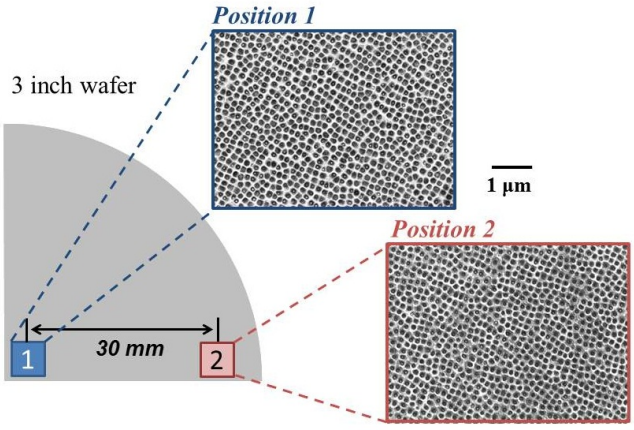

We have grown 15-50 multiple layers of Ge/Si on Si(100) by gas-source molecular beam epitaxy. The amount of Ge was chosen as ~8 monolayers (ML) to exceed the critical coverage of the growth mode changeover. The Si spacer thickness was carefully chosen so that Ge dots can be vertically aligned. Scanning electron microscopy and atomic force microscopy clarified that photonic nanostructures can be formed by a simple wet etching of the vertically aligned Ge quantum dots. The surface dip depth formed by the wet etching increases with decreasing Si spacer thickness. Furthermore, spatial uniformity of the nanostructures was found to be affected by the Si spacer thickness. By changing with the etchant, the geometry of the nanostructures can be widely changed.

The photonic nanostructures could change optical properties. In fact, we observed that photoluminescence intensity of Ge quantum dots is drastically increased by the presence of the photonic nanostructures. Furthermore, the conversion efficiency of the solar cell with photonic nanostructures was found to be slightly higher than that of the control Si solar cell with a flat surface.
It is therefore concluded that photonic nanostructures formed by our unique technology are promising for management of photons in large-area optical devices such as solar cells.

Topical Session 6

Oxides and halides including laser and nonlinear optical applications

Session Coordinators

Hanna Dabkowska (Canada) *dabkoh@mcmaster.ca*

Vyacheslav Puzikov (Ukraine) *puzikov@isc.kharkov.ua*

Programme

Monday, 12 August

MoO1

T06: Michael Schieber Symposium
Monday morning, 12 August, 11:00
Mickiewicz Hall, Auditorium Maximum

11:00 Invited oral

Cadmium Zinc Telluride X- and Gamma-Ray Detectors - Past, Present and Future

Ralph B. James[1], A. E. Bolotnikov[1], G. Camarda[1], Yonggang Cui[1], Anwar Hossain[1], Ki Hyun Kim[2], Utpal Roy[1], Ge Yang[1]

1. *Brookhaven National Laboratory (BNL), Upton, NY 11973, United States* **2.** *Korea University, Department of Radiologic Science, 161 JeongNeung3-dong Seongbuk-gu, Seoul 136-703, Korea, South*

e-mail: rjames@bnl.gov

Cadmium zinc telluride (CZT) is one of the most promising materials for the production of large-volume X-ray and gamma-ray spectrometers and imaging arrays operable at room temperature. The performance of CZT devices, the global capacity for growth of detector-grade crystals, and the size of the commercial market have progressed steadily over the past 10 years. Because of deficiencies in the quality of the material, commercial high-resolution CZT spectrometers are still limited to relatively small dimensions (< 5 cm^3), which makes them inefficient at detecting high photon energies (> 1 MeV) and somewhat ineffective for weak radiation signals except in proximity to the source. The detectors are very attractive for a much broader potential range of spectroscopic and imaging applications; however, increases in their efficiency are needed without sacrificing the ability to spectrally resolve gamma-ray energies. To increase the detector efficiency for medical and space applications, the most common method has been to tile separate high-energy-resolution CZT detectors into a suitable mosaic array, although this approach comes at the expense of system cost and complexity. Achieving the goal of low-cost, efficient CZT detectors requires progress in the following areas: better uniformity of detector response, growth of large uniform single crystals, and improved device fabrication procedures. For some medical applications such as digital X-ray radiography, it will also be necessary to understand and reduce the detrimental effects of device polarization, which is present only under high-excitation conditions. Despite the current material constraints, several types of electron-transport-only detectors have been developed: pixel, coplanar-grid, cross-strip, drift-strip, orthogonal coplanar strip, and virtual Frisch-grid, some of which are poised to address important applications. This talk summarizes the factors limiting the performance of CZT detectors, and it relates the defects observed in the crystals to growth and doping processes. It provides new insight into the critical role of small-scale defects on the energy resolution and efficiency of detectors. One of the main tools in these material and device characterizations is collimated synchrotron X-ray radiation provided by the National Synchrotron Light Source (NSLS). Data from the NSLS has helped to elucidate, in detail, the roles of non-uniformity and extended defects on the performance of CZT detectors, as well as the root cause of device polarization during exposure to a high flux of incident X-rays. Measurements of carrier traps within different detectors will be reported, including their nature and relationships to four growth methods (conventional vertical Bridgman, high-pressure Bridgman, traveling heater, and floating zone methods) and post-growth thermal processing. Most findings will be correlated with the performance of spectrometer-grade CdZnTe X-ray and gamma detectors, and new directions to resolve the material deficiencies will be offered.

Brief Summary (Invited – Michael Schieber Session): This presentation will summarize recent progress to understand the factors limiting the performance of current cadmium zinc telluride (CZT) gamma-ray detectors and discuss ways to overcome the material defects through appropriate corrections in the growth and post-growth thermal annealing processes.

11:40 Invited oral

Composite boron nitride neutron detectors

Michael L. Roth, Oleg KhaKhan, Evgeny Mojaev, Alon Fleider, Evgeny Dul'kin, Michael Schieber

The Hebrew University of Jerusalem (HUJI), Givat Ram, Jerusalem 91904, Israel

e-mail: mroth@vms.huji.ac.il

Single phase polycrystalline hexagonal boron nitride (BN) or mixed with boron carbide (B_xC) and/or polycrystalline cubic lithium fluoride (LiF) have been embedded in an insulating polymeric matrix acting as a binder and forming a composite material. Such materials have been tested as thermal neutron converters in a multilayer thermal neutron detector design. Metal sheet electrodes were covered with 20 - 50 microns thick layers of composite material and assembled in a multi-layer sandwich configuration. High voltage was applied to the metal electrodes to create in an interspacing electric field. The spacing volume could be filled with air, nitrogen or argon. Thermal neutrons were captured in converter layers due to the presence of the ^{10}B isotope. The resulting nuclear reaction produced a-particles and ^{7}Li ions which ionized the gas in the spacing volume. Electron ion pairs were collected by the field to create an electrical signal proportional to the intensity of the neutron source. Pixel structures of such neutron detectors necessary for imaging applications will be discussed as well.

12:20 Invited oral

(Cd, Mn)Te Crystals for X and Gamma Radiation Detectors - an Alternative Material to CdTe and (Cd,Zn)Te.

Andrzej Mycielski[1], Dominika M. Kochanowska[1], Marta Witkowska-Baran[1], Marcin Rasiński[2], Malgorzata Lewandowska[2], Rafał Jakieła[1], Piotr Nowakowski[1], A. Suchocki[1], Wojciech Knoff[1], Aleksander Wittlin[1], Krzysztof P. Korona[3]

1. *Institute of Physics, Polish Academy of Sciences, Warsaw 02-668, Poland* **2.** *Warsaw University of Technology, Faculty of Materials Science and Engineering, Woloska 141, Warsaw 02-507, Poland* **3.** *Warsaw University, Institute of Experimental Physics (IEP UW), Hoża 69, Warszawa 00-681, Poland*

e-mail: mycie@ifpan.edu.pl

Merits and demerits of (Cd,Mn)Te crystals will be compared with those, well known, of Cd,Te and (Cd,Zn)Te, and the differences in the crystal growth technologies, suitable for each type of crystals, will be discussed.

It is known that the presence of grain boundaries and twinning planes plagues the CdTe and (Cd,Zn)Te crystals. For (Cd,Mn)Te the tendency to form those defects is significantly smaller and large (e.g. $40 \times 40 \times 3$ mm^3), monocrystalline plates can be obtained.

In the (Cd,Zn)Te crystals the segregation of Zn occures for all the growth methods. While the segregation of Mn does occur during the growth of (Cd,Mn)Te by the travelling heater method (THM), it does NOT occur for the Bridgman method.

All types of crystals - (Cd, Mn)Te, CdTe and (Cd,Zn)Te always contain tellurium precipitates (the size below 1 μm) and inclusions (the size between 1μm and 50μm). Analyses show that inside those objects the concentrations of intentional and unintentional impurities are larger than in the surrounding crystal.

Removal of a significant part of precipitates and inclusions is performed by various annealings, which are applied to the crystals, also in order to lower (annealing in the cadmium vapours) the concentration of the cadmium vacancies, which are present, especially in the crystals grown by low-pressure Bridgman method. The cadmium vacancies act as double acceptors with small and medium first and second ionization energy of holes, respectively. Thus, to obtain semiinsulating crystals for detector applications we have to eliminate cadmium vacancies, and, as this is not enough, to add compensating dopants. Usually chlorine, indium, gal, or the transition metal - vanadium are used.

To characterize the manufactured (Cd, Mn)Te crystals from the point of view of the detector applications, and to confront the results with those for CdTe and (Cd,Zn)Te, the following investigations were performed:

- contactless mapping of the resistivity and μτ product
- microscopic visual observation of the precipitates and inclusions with infra-red and visible light
- investigating the surface with scanning electron microscope (SEM)
- measurements of the concentrations of impurities (both intentional and unintentional) with secondary ions mass spectroscopy (SIMS)

- low-temperature photoluminescence (PL) measurements
- low-temperature paramagnetic resonans (EPR) measurements
- low-temperature time-resolved photoluminescence (TRPL) measurements

The results will be shown and discussed.

Lunch (JCG Editors meeting)

Monday afternoon, 12 August, 13:00

MoO2

T06: Oxides and halides including laser and nonlinear optical applications

Monday afternoon, 12 August, 15:00

Mickiewicz Hall, Auditorium Maximum

15:00 Invited oral

Discovery and Crystal Growth of New Scintillators

Edith Bourret

Lawrence Berkeley National Laboratory (LBNL), 1, Cyclotron Rd, Berkeley 94720, United States

e-mail: EDBourret@lbl.gov

Scintillator materials with better performance are in high demand for many applications: better resolution for medical imaging, better stopping power and resolution for national security. This is driving a large effort to discover new scintillating crystals and the establishment of a unique crystal growth laboratory at the Lawrence Berkeley National Laboratory. The search has lead to the discovery of numerous new materials. A number of alkali-earth halides materials activated with Eu^{2+} are receiving much attention due to their high luminosity close to the theoretical limit and very good energy resolution. Other materials activated by Ce^{3+} and Tl^{+} have also been discovered and are now under development. In parallel, fundamental studies of scintillation are guiding the growth of known scintillators with improved performance. Large deployment of crystals in devices for national security adds an other challenge for the crystal growth community, as the improved scintillators must be produced at very low cost. We will present progress achieved in the synthesis, growth and performance of these new scintillators and highlight our approach to screen materials prior to their study as single crystals.

This work was supported in part by the U.S. Department of Energy/NNSA/NA22 and carried out at Lawrence Berkeley National Laboratory under Contract NO. AC02-05CH11231 and in part bythe US Department of Homeland Security, Domestic Nuclear Detection Office, under competitively awarded contract/IAA HSHQDC-07-X-00170. This support do not constitute an express or implied endorsement on the part of the Government.

References

1. E. D. Bourret-Courchesne et al, BaBrI:Eu^{2+}, a new bright scintillator, Nucl. Instr. Meth. Phys. Res. A, 613, (2010), 95-97.

2. E. D. Bourret-Courchesne et al, Eu^{2+}-doped Ba(2)CsI(5), a new high-performance scintillator, Nucl. Instr. Meth. Phys. Res. A, 612, (2009), 138-142.

3. Gregory Bizarri, Edith D. Bourret-Courchesne, Zewu Yan, and Steve E. Derenzo,Scintillation and Optical Properties of BaBrI and Cs_2BaI_5, IEEE Trans. Nuc. Sc., Vol.58, No6, December 2011, 3403.

4. Zewu Yan, Gregory Bizarri, Edith Bourret-Courchesne,"Scintillation properties of improved 5%Eu^{2+}-doped $BaCl_2$ single crystal for X-ray and gamma-ray detection" Nuclear Instruments and Methods in Physics Research A 698 (2013) 7-10.

15:30 Oral

Growth, spectroscopic and laser properties of $(Er^{3+},Yb^{3+}):GdAl_3(BO_3)_4$ crystals

Victor Maltsev[1], Elizaveta V. Koporulina[1], Nikolay I. Leonyuk[1], Konstantin N. Gorbachenya[2], Victor E. Kisel[2], Anatoliy S. Yasukevich[2], Nikolay V. Kuleshov[2]

1. *M.V. Lomonosov Moscow State University, Vorobyevy gory, Moscow 119992, Russian Federation* **2.** *Belarussian National Technical University (BNTU), F. Skariny, 65, Minsk 220027, Belarus*

e-mail: maltsev@geol.msu.ru

Borate crystals with the general formula $RAl_3(BO_3)_4$ (R=Y; Pr–Lu) have good mechanical, thermal properties, and their possibility of wide isomorphous substitutions in R-positions is favorable as one of the most ideal laser host materials. Recently, flux growth technology has been developed for single crystals $YAl_3(BO_3)_4$ (YAB) co-doped with Er^{3+} and Yb^{3+} as highly efficient CW, Q-switched and ultra-fast diode-pumped solid-state and wave-guide lasers emitting in the eye-save 1.5-1.6 mm spectral range [1,2]. Their power levels demonstrate several times higher that those of lasers developed earlier for the spectral NIR range around 1.5 mm. These eye-save crystalline laser materials are found to be of particular importance for applications in ultra-high speed data-communications as well as in medicine, environmental sensing and range-finding. Spectroscopic properties and efficient laser operation at 1.5–1.6 m of $(Yb^{3+},Er^{3+}):GdAl_3(BO_3)_4$ (Er:Yb:GdAB) crystal are also reported [3]. In this paper, recent investigations of crystal growth conditions, spectroscopic and laser properties of both these materials has been discussed.

Phase relationships and $Er:Yb_xGd_{1-x}Al_3(BO_3)_4$ solubility in the $K_2Mo_3O_{10}$-B_2O_3-$(Gd,Er,Yb)_2O_3$ complex fluxes have been refined in the temperature range of 1150-800°C. In this case, the x value was varying from 0 to 0.2, but the Er admixture was up to 1 at.%. Additions of ytterbium and erbium to the system leads to increasing saturation temperature of high-temherature solutions (about 5-10°C, depending on the flux composition). Solubility diagrams of $Yb_xGd_{1-x}Al_3(BO_3)_4$ were studied in the range of x = 0.05–0.15. The main attention is focused on comparison of primary fields of YAB and GdAB crystallization, and their solubilities depending on the flux composition. Since the regions of single-phase YAB and GdAB crystallization do not exist at their concentration above 20 wt % in the temperature range of 1150-1050°C, these crystals can be grown only at lower nutrient concentrations. As a result, (Er,Yb):GdAB single crystals with optical quality and the size up to 20x10x10 mm^3 have been grown on the seeds. Also, an attempt is made to compare the data obtained with earlier results on crystal growth of other $RAl_3(BO_3)_4$. The segregation coefficients of the Er and Yb are close to unit as a consequence of minor difference in the sizes of R-cations.

The absorption spectra of (Er,Yb):GdAB crystal were measured using Cary-500 spectrophotometer with spectral resolution 0.4 nm. An optical parametric oscillator LOTIS LT-2214OPO pumped by Nd:YAG laser was used as an excitation source for lifetime measurements.

The polarized absorption spectra of (Er,Yb):GdAB crystal around 980 nm at room-temperature are shown in Fig. 1. A strong absorption band corresponding to the transition $^2F_{7/2}\rightarrow{}^2F_{5/2}$ of Yb^{3+} ions is centered at 976 nm in σ polarization, with a maximum absorption cross-section of about 2.5×10^{-20} cm^2 and bandwidth of 18 nm (FWHM). The absorption and emission spectra of (Er,Yb):GdAB and (Er,Yb):YAB are similar.

The decay curve of $^4I_{13/2}$ level of Er^{3+} was single exponential, and the decay time was measured to be about 350 μs. Luminescence decay from the $^2F_{5/2}$ level of Yb^{3+} was measured in Yb single-doped GdAB as well as in Er,Yb:GdAB. To prevent radiation trapping (reabsorption) caused by significant overlap of the absorption and emission bands, a fine powder of crystals immerced in glycerin was used [4]. The lifetime of Yb^{3+} ion in Yb(1 at.%):GdAB crystal was measured to be 450 μs, whereas in Er(1.5 at.%),Yb(11 at.%):GdAB it shortens to 75 μs. The energy transfer efficiency was obtained to be of about 83%.

The CW laser experiments were carried out with the four-mirrors cavity. As a pump source a 7 W fiber-coupled (Ø=105 μm, NA=0.22) laser diode emitting near 976 nm was used. The 1.5-mm-thick Er(1.5at.%),Yb(11at.%):GdAB crystal was kept at 18 °C by the thermoelectrically-cooled heatsink. The cavity-mode diameter at the active element was close to the pump beam waist. CW diode-pumped Er,Yb:GdAB laser was realized for the first time to our knowledge. The laser threshold was measured to be about 1 W of absorbed pump power. The maximum CW output power of 750 mW with slope efficiency near 26 % was obtained at 1531 nm at about 4 W of absorbed pump power.

This research was supported in part by the RFBR grants 12-05-90010-Bel_a, 12-05-00912_and BRFFR 12P-183.

1. N. I. Leonyuk, Crystallography Reports **53** (2008) 511.

2. N.A. Tolstik, S.V.Kurilchik, V.E. Kisel, et al., Optics Letters **32** (2007) 3222.

3. Y. Chen, Y. Lin, X. Gong, et al., IEEE J. Quantum Electron. **43(**2007) 950.

4. V.E. Kisel, A.E. Troshin, N.A. Tolstik, et. al., Optics Letters **29** (2004) 2491.

15:45 Oral

A promising nonlinear crystal for third harmonic generation in UV: $Ca_5(BO_3)_3F$

Simon Ilas[1], Loïc Deyra[2], Alexandra Szemjonov[1], Pascal Loiseau[1], Gérard Aka[1], François Balembois[2], Patrick Georges[2], François Salin[3]

1. *Ecole Nationale Supérieure de chimie de Paris (ENSCP), 11 rue P. et M. Curie, Paris 75005, France* **2.** *Laboratoire Charles Fabry, Institut d'optique, CNRS, Univ Paris-Sud, Palaiseau 91127, France* **3.** *Eolite systems, Pessac 33600, France*

e-mail: pascal-loiseau@chimie-paristech.fr

CBF is a potential nonlinear material for third harmonic generation. CBF single crystals were grown using LiF as a flux. 300 mW average power at 343 nm by frequency tripling were obtained. d_{eff} were estimated as from conversion efficiency measurements. We present here studies of new flux to growth CBF such as: LiF-B_2O_3, LiF-NaF, LiF-CaF_2, CaF_2, NaF. Diffferentiel thermal analysis (DTA), spontaneous crystallization and crystal growth using these flux will be presented.

1. Introduction

The calcium fluoroborate, $Ca_5(BO_3)_3F$ is an interesting and new nonlinear optical material for UV applications. This material crystallizes in the same acentric space group Cm (Z=2) as $YCa_4O(BO_3)_3$ (YCOB) but with extented properties towards UV. CBF can be grown by flux method, using LiF as a flux [1][2]. Its structure is built from $[BO_3]^{3-}$ anionic groups, which are the most suitable for the design of nonlinear crystals aimed to have UV applications. CBF can be considered as derived from YCOB since Y^{3+} is replaced by Ca^{2+} and O^{2-} is substituted by F^- to preserve the electroneutrality of its structure. The CBF crystals are chemically stable and are not hygroscopic. The UV absorp-

tion edge of CBF is around 190nm. The nonlinear optical properties was determined by Xu et al [3].

2. Third harmonic generation in CBF (λ=343 nm)

A CBF crystal with a large size (diameter = 17 mm and length = 35 mm) has been obtained by using 20wt% LiF as flux in air (Fig. 1). The CBF boule was cut in two different planes corresponding to the two possible type-II THG phase matching directions for 1030 nm: two crystals of dimensions 3x3x3 mm^3 were cut in the YZ plane, with θ=57.7° and a third crystal of dimension 3x3x5 mm3 was cut in the XY plane with φ=72.6°. We used for the experiment an infrared source emitting 20 W at 1030 nm at a repetition rate of 30 kHz with pulse width of 15 ns. A 20 mm long, type-I LBO was used in NCPM configuration to obtain 12 W of green power. Both XY and YZ principal planes of the type II-CBF crystals were tested and the UV output power was measured. 300 mW average power was obtained in the XY plane and 130 mW average power in the YZ plane. d_{eff} were estimated as from conversion efficiency measurements: 0,48 pm/V in the XY plane and 0,35 pm/V in the YZ plane.

Fig. 1: CBF single crystal grown using LiF as a flux

3. Study of new flux

The usual flux to growth CBF is LiF. The prominent drawback of LiF is its volatility. Moreover, single crystals of CBF often contain inclusions of LiF. That is why an optimization of the flux has to be done. We have studied the influence of LiF-B_2O_3, LiF-NaF, LiF-CaF_2, CaF_2, NaF on thermal properties and growth of CBF. The crystallization temperature of CBF for the ratio 20 CBF / 80 LiF (% mol) is around 1000 °C. We studied the system 20 CBF - (80 - x) LiF - x B_2O_3. The addition of B_2O_3 to LiF allows to reduce the crystallization temperature of CBF to 950 °C for the composition 20 CBF - 75 LiF - 5 B_2O_3. This is interesting concerning the volatility of the melt. With NaF as a flux, CBF crystallize at 1000 °C too but X-ray diffraction analysis reveals $Ca_3B_2O_6$ phase. The ratio CBF/NaF has to be adjusted to see if NaF can be a suitable flux for CBF. The DTA study of the system 20 CBF – (80-x) LiF – x CaF2 (% mol) is represented on Figure 2.

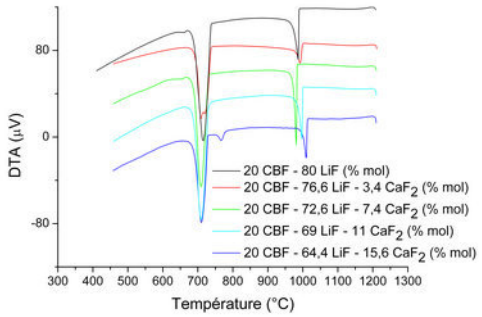

Fig. 2: differential thermal analysis cooling curves of the system 20 CBF - (80-x) LiF - x CaF_2

The use of CaF_2 is interesting because the thermal properties of the system are not changed while reducing the quantity of LiF. The other advantage is that CaF_2 is one of the reagent in the synthesis of CBF so it does not disturb the system by introducing foreign elements. Spontaneous crystallization and growth of single crystals using flux mentioned above will be presented at the conference.

[1]G. Chen et al, Journal of Crystal Growth, 292, 449–453 (2006).

[2]Xu et al, Crystal Growth & Design, 9, 2235-2239 (2009)

[3]Xu et al, Optics Express, 16, (2008)

16:00 Oral

Analysis of Scintillator Crystal Production via the Edge-Defined Film-Fed Growth Method

Andrew Yeckel[1], Robert S. Feigelson[2], Jeffrey J. Derby[1]

1. *University of Minnesota, Chemical Engineering and Materials Science, 421 Washington Ave. S.E., Minneapolis, MN 55455, United States* **2.** *Materials Sceince and Engineering, Stanford University, Stanford, CA 94305, United States*

e-mail: derby@umn.edu

A model of edge-defined film-fed crystal growth (EFG) is developed to study melt growth of cylinders of the scintillator crystal cesium iodide (CsI). The model, which includes fluid flow, heat transfer, and gravitational effects, is solved numerically by the finite element method to predict crystal diameter as a function of growth rate and die geometry. The model computes the location and shape of the crystal-melt interface and the meniscus to satisfy a self-consistent formulation of phase change and capillary dynamics. A sharp interface formulation solved on a deforming finite element mesh ensures accurate conservation of mass, energy, and momentum at the interfaces.

This system is characterized by strongly nonlinear interactions of heat transfer, capillarity, and die geometry that give rise to multiple stationary solution states under a single set of operating conditions. We use bifurcation theory and parameter continuation techniques to identify these solution states and characterize their stability.

Purely capillary instabilities are identified that result from the interaction of surface tension with gravity, and also the interaction of in-plane and out-of-plane (hoop stress) curvatures of the meniscus. These give rise to two solution families distinguished by a difference in gap width between die face and growth interface. The narrow gap solutions are shape stable, and the wide gap solutions are shape unstable, though these can be stabilized by heat transfer in a manner similar to Czochralski growth.

Additionally we identify several instabilities of convective heat transfer, which generally are of two types. One type is mostly convective in nature and largely independent of the interface or meniscus shapes. In this type the solution families are distinguished by different flow structures within the capillary bore. The other type is characterized by a strong interaction of convection with the geometry of the growth interface. Stronger convection moves the interface to a higher position, forming a larger gap. The larger gap allows a stronger flow to form, which enhances convection. This reinforcing behavior enables a family of solutions to exist in which the growth interface shape is concave in the central region, though it is convex elsewhere. Finally, we address the possible mechanism leading to the formation of longitudinal pores of cylindrical shape observed in crystals grown by experiment.

Supported in part by U.S. Department of Homeland Security, HSHQDC-11-C-00094, the content of which does not necessarily reflect the position or policy of the United States Government, and no official endorsement should be inferred.

16:15 Oral

Crystal growth and scintillation properties of selected fluoride crystals for VUV scintillators

Jan Pejchal[1,2], Kentaro Fukuda[3], Yuui Yokota[1,4], Shunsuke Kurosawa[1,4], Robert Kral[2], Martin Nikl[2], Vladimir Babin[2], Akira Yoshikawa[1,4]

1. *Institute for Materials Research, Tohoku University (IMR), Sendai 980-8577, Japan* **2.** *Czech Academy of Sciences, Institute of Physics, Cukrovarnicka 10, Prague 16253, Czech Republic* **3.** *Tokuyama Corporation, Tokyo 150-8383, Japan* **4.** *New Industry Creation Hatchery Center, Tohoku University, Aoba-yama 6-6-10, Aoba-ku, Sendai, Miyagi, Sendai 980-8579, Japan*

e-mail: pejchalj@imr.tohoku.ac.jp

The possibility of development of new X-ray or gamma ray radiation detection systems based on the vacuum ultraviolet (VUV) scintillators have attracted attention some years ago [1]. One of the candidates for the VUV scintillator can be the Nd-doped materials based on monoclinic BaY_2F_8. The fast VUV emission around 185 nm with a decay time of several nanoseconds is due to the allowed 5d-4f transition of the Nd^{3+} ion.

Recently, we tried to improve the scintillation properties by Tm-codoping [2] or Lu admixture to replace the Y in the BaY_2F_8 matrix using this method. The Lu admixture increased the material density, which is favorable for increasing the high-energy photon stopping power.

We used the micro-pulling-down method which is a fast and promising crystal growth method suitable for material research and composition screening [3]. The micro-pulling-down setup was modified for the crystal growth of fluorides using carbon hot-zone and argon atmosphere with admixture of CF_4 which acted as moisture scavenger gas.

Obviously, it would be interesting to increase the Lu-content as much as possible and preferably reach the $BaLu_2F_8$ composition. However, this is very difficult due to $BaLu_2F_8$ phase transition from orthorhombic to monoclinic phase occurring around 50°C below the melting point, which is around 945°C. Finally, the monoclinic $BaLu_2F_8$ single crystals of reasonable optical quality were grown by the micro-pulling-down method employing the melt-supercooling procedure with the help of LiF flux. From the point of view of luminescence, also the high-temperature orthorhombic modification of $BaLu_2F_8$ single crystal might be interesting due to two non-equivalent Lu sites [4]. Better energy transfer from the matrix or between the rare-earth ions can be expected. This modification was prepared by the micro-pulling-down-method using a quenching procedure with specially modified hot-zone. The hot zone was arranged to reach very shallow gradient near the crucible nozzle so that the grown crystal was still kept above the phase transition temperature. Then the crystal was rapidly cooled preventing the phase transition to take place. The micro-pulling-down crystal growth, luminescence and scintillation properties of rare-earth-doped monoclinic and orthorhombic $BaLu_2F_8$ VUV scintillation crystals will be compared and discussed. It will be also shown that despite the relatively efficient energy transfer between some rare-earth ions in the orthorhombic $BaLu_2F_8$ matrix, the energy transfer from the matrix to the rare-earth ions is hampered due to preferential energy transfer to the lattice defect states.

Another candidate for VUV scintillator can be the ErF_3 single crystal. Again, its crystal growth is complicated by a phase transition from hexagonal to tetragonal modification occurring some 20°C below the melting point, which is at 1140°C. However, the melt has a strong tendency for supercooling and in the past some successful attempts of crystal growth have been reported [5]. However, when we tried to prepare the crystal using the micro-pulling-down method, supercooling was not sufficient and phase transition seriously degraded the quality of the crystal, which was not then applicable for any optical characterizations. These difficulties have been overcome with LiF flux to slightly lower the melting point and modified hot-zone to reach extremely steep gradient at the crucible nozzle. Then, high-quality crystals have been prepared. In some cases, Nd^{3+} ion has been introduced as a luminescence center. In some hosts, the Er^{3+} 5d-4f emission spectrum coincides with the Nd 4f-5d absorption band and thus the energy could migrate over the Er^{3+} 5d levels to the Nd^{3+} ones [6]. Similar mechanism is expected in the ErF_3:Nd. This concept is similar to that reported for PrF_3:Ce scintillator, where an efficient energy transfer from the $Pr^{3+1}S_0$ 4f-level to the 5d-levels of Ce^{3+}[3]. On the other hand, we may expect strong energy migration over the Er^{3+} levels and resulting luminescence quenching. Admixture of other rare-earth-ions might be a solution. Besides the crystal growth, basic photoluminescence and scintillation characteristics of ErF_3 admixed with other rare-earth ions will be presented and discussed.

1. C. W.E. van Eijk, P. Dorenbos, R. Visser, IEEE Trans. Nucl.Sci. 41 (1994) 738
2. J. Pejchal, M. Nikl, F. Moretti, et al., IOP Conf. Ser.: Mater. Sci. Eng. 15 (2010) 012018
3. A. Yoshikawa et al., J. Cryst. Growth 270 (2004) 427
4. A. A. Kaminskii et al., Journal of Alloys and Compounds 275–277 (1998) 442
5. B. P. Sobolev et al., Materials Research Bulletin 11 (1976) 999
6. J. Pejchal et al., Rad. Meas. 45 (2010) 265

16:30 Oral

Light yield behavior in mixed oxide scintillation crystals

Oleg Sidletskiy[1], Alexander Gektin[1], Boris Grinyov[1], Andrei Belsky[2]

1. *Institute for scintillation materials of NAS of Ukraine (ISMA), Lenin avenue, 60, Kharkov 61158, Ukraine* **2.** *Universite de Lyon, CNRS, Institut Lumiere Matiere, Villeurbanne 69622, France*

e-mail: sidletskiy@isma.kharkov.ua

A large variety of mixed scintillation crystals based on isovalent substitution of host atoms has been developed for a range of applications. Multicomponent crystals are usually avoided by technologists owing to complex character of components segregation leading to crystal inhomogeneity and, in many cases, to formation of cracks. Nevertheless, in some cases a variation of crystal host composition is a chance to modify functional properties of crystal and/or to simplify growth procedure. The current report is focused at development of fast, dense and bright new mixed oxide crystals doped with Ce^{3+}. Primarily this trend of studies was pointed at simplification of crystal growth process ($Lu_{2x}Y_{2-2x}SiO_5$ (LYSO) instead of Lu_2SiO_5 (LSO)) by lowering of crystallization temperature and higher crystal production yield; no significant improvement in scintillation parameters was achieved. Later, it has been discovered that in many Ce-doped mixed crystals the behavior of light yield and other scintillation parameters is non-additive in respect to their constituents. For example, substantial improvement of light yield was achieved in $Lu_{1-x}Y_xAlO_3$:Ce [1], $Lu_{1-x}Sc_xBO_3$:Ce [2], $Lu_{2x}Gd_{2-2x}SiO_5$ (LGSO:Ce) [3], $RE_3(Al_{1-x}Ga_x)_5O_{12}$:Ce (RE=Y, Lu, or Gd) [4, 5]. All mentioned systems exhibit maximal light yield at x = 0.4 – 0.6, i.e., at component ratio near 1:1.

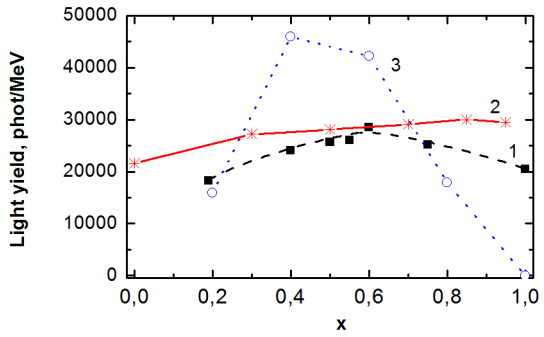

Fig. 1. Light yield in Ce-doped $Lu_{2x}Gd_{2-2x}SiO_5$ (1), $Lu_{2x}Y_{2-2x}SiO_5$ (2), $Gd_3(Al_{1-x}Ga_x)_5O_{12}$ (3), in accordance with [3, 4, 6]. Horizontal axis denotes formula units (*x*).

Mechanisms of the observed phenomenon may relate to different stages of scintillation process. In the present report we illustrate them on example of LGSO:Ce and YAGG:Ce crystals obtained by the Czochralski method and compared with the analogues. In garnet scintillators, substitution of lanthanide cation or Al/Ga is accompanied by the bandgap change and shift of Ce^{3+} energy levels in crystal field [4]. Thereby tuning of the cation ratio provides choice of proper position of activator energy levels in the forbidden band and suppression of shallow electron traps which believed to dump carrier transport to activator. However, in the rest of mentioned systems, no evidences of energy structure modification were obtained. Crystalline structure in these solid solutions in long-range scale is linear dependent on component ratio in accordance with the Vegard's law. In short-range scale, arising fluctuations of substituting atoms content influence electronic processes, for ex., conductivity, or magnetic properties. In case of scintillatorsthe increase in light yield can be called by limitation of electron-hole separation length due to interaction of thermalized carriers with charge fluctuations on defects called by inhomogeneities in mixed crystal [3]. The inhomogeneity in the component ratio near 1:1 is supported by surprisingly high Ce^{3+} segregation coefficients, and variation of luminescent characteristics across LGSO:Ce crystal obtained by confocal microscopy. Besides this, shape of Ce^{3+} luminescence excitation spectra demonstrate increase in carrier multiplication efficiency in the same concentration range.

Feasibility of the mentioned mechanisms for certain mixed crystals is discussed. The effect of energy structure modification is more pronounced in crystals with strong crystal field such as rare-earth garnets, where splitting of Ce^{3+} 5d levels substantially depends on cation environment. A degree of inhomogeneity in crystal should increase with the difference between ionic radii of substituting cations. Maximal improvement in light yield evidently can be reached when different mechanisms are involved simultaneously.

The presented examples demonstrate the potential for significant improvement of scintillator parameters. This methodology can serve as the basis at engineering of new mixed crystals with optimized properties for optics and electronics.

The work is partially supported by the Project FP7-INCO-2011-6 ("SUCCESS").

1. A. N. Belsky, E. Auffray, P. Lecoq et al. IEEE Trans. Nucl. Sci., **48**, 1095 (2001).

2. Y. Wu, D. Ding, S. Pan et al,Journ Alloys Comp. **509**, 366 (2011).

3. O. Sidletskiy, A. Belsky, A. Gektin et al. Cryst. Growth Des. **12,** 4411 (2012).

4. K. Kamada, T. Endo, K. Tsutumi et al. Cryst. Growth Des. **11**, 4484 (2011).

5. O. Sidletskiy, V. Kononets, K. Lebbou et al. Mater. Res. Bull. **47**, 3249 (2012).

6. J.Chen, L. Zhang, R.-Y. Zhu. IEEE Trans. Nucl. Sci., **52**, 3133 (2005).

16:45 Oral

Crystal growth of Pr:$(Lu,Gd,Y)_3(Al,Ga)_5O_{12}$ by micro pulling down method and their scintillation properties

Akira Yoshikawa[1,2], Kei Kamada[2], Yasuhiro Shoji[1], Shunsuke Kurosawa[1,2], Yuui Yokota[2], Petr Prusa[3], Martin Nikl[1,3]

1. *Institute for Materials Research, Tohoku University, 2-1-1, Katahira, Aoba-ku, Sendai 980-8577, Japan* **2.** *New Industry Creation Hatchery Center, Tohoku University, Aoba-yama 6-6-10, Aoba-ku, Sendai, Miyagi, Sendai 980-8579, Japan* **3.** *Czech Academy of Sciences, Institute of Physics, Cukrovarnicka 10, Prague 16253, Czech Republic*

e-mail: yoshikawa@imr.tohoku.ac.jp

Praseodymium ion Pr3+ exhibits fast 5d-4f emission in several host materials; such systems can be applied to obtain crystal scintillators with high figures of merit. Recently, our group intensively examined the scintillation properties of several Pr-doped compounds. Among those materials, Pr:Lu3Al5O12(Pr:LuAG) was found with the highest figure of merit due to high density (6.7g/cm3), high light yield (approximately 20000 photon/MeV by using PMT), good energy resolution, and a very fast 5d-4f emission decay time (20 ns)[1]. On the other hand, aluminum garnet hosts such as Y3Al5O12 (YAG) and LuAG have electron traps related to anti-site defects. A thermoluminescence (TSL) measurement in LuAG:Ce has identified electron traps associated with LuAl3+ defects, which are responsible for glow curve peaks within 120–200K. Such shallow trapping states in the LuAG host slow down scintillation decay kinetics, and considerable amount of slower decay components was found[2]. To optimize the performance of LuAG-based scintillator towards its intrinsic limits, understanding and control of such kind of defects through manufacturing technology are of crucial importance. Recently, Our group reported that Ga substitution of the Al site and Y substitution of the Lu site in Pr:LuAG suppress such defect and reduce slower decay components. In this study, Pr:(Lu,Y,Gd)3(Ga,Al)5O12 single crystals were grown by the micro-pulling down (μ-PD) method. Example photographs are shown in Fig.1. Luminescence and scintillation properties were measured. The substitution phenomenon in the Lu3+ sites with Y3+ and Gd3+, and Al3+ sites with Ga3+ + in garnet structure has been studied. In the case of Pr: (Lu,Y)3(Ga,Al)5O12 series, Pr3+5d-4f emission within 300-400nm accompanied by weak Pr3+ 4f-4f emission in 480-650nm are observed in Ga 0-60 at.% substituted samples(Fig.2). Ga 80 at.% substituted sample shows only Pr3+ 4f-4f emission. In the case of Pr: (Lu,Gd)3(Ga,Al,Sc)5O12 series, strong Pr3+ 4f-4f emission in 480-650nm are observed accompanied by weak Pr3+5d-4f emission within 300-400nm and Gd3+4f-4f emission in 312nm. (Lu,Y)3(Ga,Al)5O12 series shows higher light output than that of Pr: (Lu,Gd)3(Ga,Al)5O12 and Pr: (Y,Gd)3(Ga,Al)5O12series. The light output of Pr1%:Lu1Y2Ga2Al2O12 sample was almost same as that of Cz grown Pr:LuAG standard. Two-component scintillation decay shows 16.9ns (90%) and 88.0ns (10%) using the PMT and digital oscilloscope. Details will be reported in the presentation.

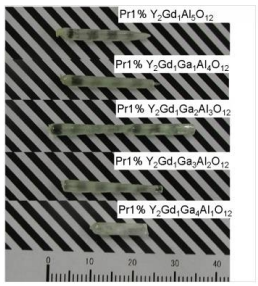

Fig1. Example photographs of Pr: $(Lu,Y,Gd)_3(Ga,Al)_5O_{12}$ crystals grown by the μ-PD method

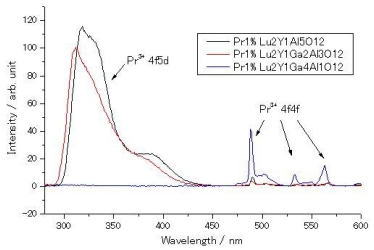

Fig. 2 Radioluminecensce spectra of Pr: $(Lu,Y)_3(Ga,Al)_5O_{12}$

[1] K. Kamada , T. Yanagida, K. Tsutsumi, Y. Usuki, M. Sato, H. Ogino, A. Yoshikawa, et al., IEEE Trans. Nucl. Sci., 2009, Volume 56, Issue 3, pp. 570 – 573, Jun, 2009 [2] M. Nikl, Yoshikawa, et al., Phys.StatusSolidi(a)202, pp.201-207, Jan. 2005

MoPo-T06
Monday afternoon, 12 August, 17:00
Rooms 207, 211, Old Library

Break
Monday evening, 12 August, 18:30

Tuesday, 13 August

TuO1

T06: Oxides and halides including laser and nonlinear optical applications
Tuesday morning, 13 August, 10:20
Mickiewicz Hall, Auditorium Maximum

10:20 Invited oral

Crystal growth of novel single crystals for electro-optical applications

Kiyoshi Shimamura[1,2], Encarnacion Garcia Villora[1]

1. *National Institute for Materials Science (NIMS), Tsukuba 305-0044, Japan* **2.** *Waseda University, Tokyo 169-8555, Japan*

e-mail: SHIMAMURA.Kiyoshi@nims.go.jp

Recently, optical technology progress in a wide range of applications, and still demands the further development. Since conventional crystal materials face some of the limitations, these issues require new optical single crystals. Here, novel single crystals, which have advantageous characteristics toward the above demands, will be introduced.

β-Ga_2O_3 exhibits the largest band gap (*Eg* = 4.8 eV) among the transparent conductive oxides (TCOs). 1 and 2 inch size β-Ga_2O_3 single crystals were grown by the FZ and EFG techniques, respectively. Epitaxial growth of *c*-plane wurtzite InGaN-MQW on *a*-plane β-Ga_2O_3 was realized by the MOCVD technique. Vertical structured blue LEDs on β-Ga_2O_3 with different packaging styles were demonstrated.

$Tb_3(Sc_{1-x}Lu_x)_2Al_3O_{12}$ (TSLAG) single crystals with 1 inch in diameter have been designed and grown for high-power laser machinery. TSLAG showed a higher visible transparency and a larger Faraday rotation than $Tb_3Ga_5O_{12}$. TSLAG is therefore very promising material in particular for new magneto-optical isolator applications in the VIS-NIR wavelength.

High-brightness LEDs (HB-LEDs) are facing several difficulties such as temperature- and photo-degradation of Ce:YAG powder phosphor and epoxy dome containing them. A new concept of white LEDs based on Ce,Gd:YAG single crystal phosphor plates (SCPPs), which are able to overcome the above issues, is proposed. SCPPs demonstrated excellent thermal stability with no temperature quenching, high values of luminous efficacy and increased quantum efficiency.

Acknowledgements: Authors would like to thanks to Mr. K. Aoki of Koha Co., Ltd., Dr. D. Inomata of Tamura Corp., and Mr. T. Hatanaka, Mr. A. Funaki, Mr. T. Kizaki and Mr. K. Naoe of Fujikura Ltd., for the collaboration.

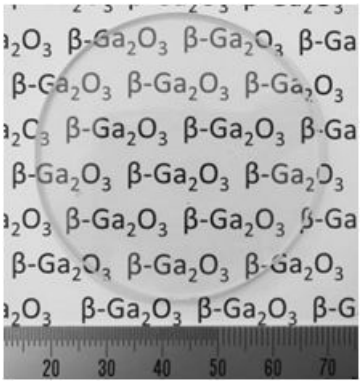

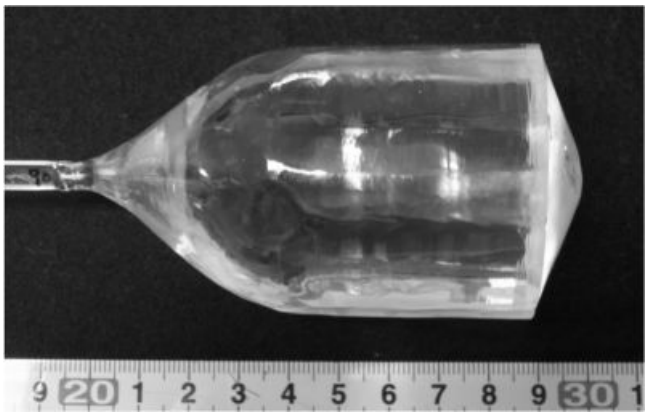

Fig.: 2-inch size β-Ga_2O_3 single crystal wafer grown by the EFG technique (left) and magneto-optical $Tb_3(Sc_{1-x}Lu_x)_2Al_3O_{12}$ single crystal grown by the Czochralski technique (right).

10:50 Oral

Cuprate spin ladder crystals grown by floating zone method under elevated oxygen pressure

Guochu Deng[1,2], Kazimierz Conder[1], Ekaterina Pomjakushina[1]

1. *Paul Scherrer Institut (PSI), WLGA, Villigen PSI 5232, Switzerland* **2.** *Bragg Institute,, New Illawarra Road, Lucas Height, New South Wales 2233, Austria*

e-mail: kazimierz.conder@psi.ch

Quasi-one-dimensional cuprates $Sr_{14-x}Ca_xCu_{24}O_{41}$, have attracted much attention, mainly because they represent an unique class of superconducting copper oxides with a non-square copper oxide layers. For the first time superconductivity with $T_C \approx 12$ K was observed for highly Ca-doped samples ($x \approx 13.6$) under high hydrostatic pressure of 3-4.5GPa [1]. In spite this system is investigated since years it looks

that many discrepancies could be clarified if high quality, large size, highly Ca doped single crystals would be available. Such crystals with Ca-content close to x=12 were grown by Travelling Solvent Floating Zone (TSFZ) method under oxygen pressure of 12bar [2], already slightly exceeding a pressure limit of the commercially available mirror furnaces. In this work for the crystal growth of $Sr_{14-x}Ca_xCu_{24}O_{41}$ with high Ca content (x>12), we have modified the mirror furnace to provide a stable crystal growth at oxygen pressure up to 35bar [3]. The grown crystals were found to be of high quality as studied by microscopy, micro X-ray fluorescence elemental analysis and X-ray diffraction. Incommensurate crystal structures of the series $Sr_{14-x}Ca_xCu_{24}O_{41}$ (x=3, 7, 11, 12.2) were characterized by powder neutron scattering method. The Ca doping effects on the lattice parameters, atomic displacement, Cu-O distances, Cu-O bond angles and Cu bond valence sum were studied [4]. Measurements of superconducting and magnetic properties under hydrostatic [5] and uniaxial pressure will be also presented.

[1] M. Uehara et al., *J Phys Soc Jpn.,* 65 (1996) 2764

[2] S. Vanishri et al., *J. Cryst. Growth,* 311 (2009) 3830

[3] G. Deng et al., *J. Cryst. Growth,* 327 (2011) 182

[4] G. Deng et al., *Phys. Rev. B*, 84 (2011) 144111

[5] A. Hisada et al., *Phys. Rev. B*, submitted

11:05 Oral

Investigation of $Ga_{2-x}Fe_xO_3$ single crystals grown by floating zone method

Srimathy Balasubramanian[1], Indranil Bhaumik[2], Ganesamoorthy Sarveswaran[3], Rajeev Bhatt[2], Karnal Ak[2], Kumar Janakiraman[1]

1. *Crystal Growth Centre, Anna University, Chennai, Chennai 600025, India* **2.** *Laser Materials Development and Devices Division, Raja Ramanna Centre for Advanced Technology (RRCAT), Indore 452013, India* **3.** *X ray Scattering and Crystal Growth Section, Condensed Matter Physics Division, Material Science Group, IGCAR, Kalpakkam, Chennai 603102, India*

e-mail: marsjk@annauniv.edu

Gallium iron oxide ($Ga_{2-x}Fe_xO_3$, $0.7 \leq x \leq 1.4$) is a piezoelectric ferromagnetic compound exhibiting large magnetoelectric (ME) effect. These kind of magnetoelectric materials find applications in new kind of multistate non-volatile memories such as magnetically tunable ferroelectric random access memories, electrically tunable magnetic random access memories and high frequency filters, etc. Single crystals of $Ga_{2-x}Fe_xO_3$ with x = 0.8, 1 and 1.2 were successfully grown by a Optical Floating Zone (OFZ) method under a high oxygen pressure of 9–10 atm. Figure 1 shows the picture of as grown $GaFeO_3$ single crystal. From the powder X-ray diffraction measurements, it was confirmed that the grown crystals are in single phase. All the peaks were indexed by the *Pc*21*n* orthorhombic unit cell of $Ga_{2-x}Fe_xO_3$. Lattice parameters were obtained by Rietveld refinement. The chemical compositions of the crystals were determined by energy dispersive X-ray spectrum (EDAX). Uniform growth steps were seen on the surface of the crystal along the growth direction. Etching studies were carried out at various temperatures with H_3PO_4 and mixture of H_3PO_4 and HNO_3 as etchants. Etch pit rows were observed to be circular and shallow. With increase in temperature of the etchant, the time to nucleate an etch pit decreased. Figure 2 shows the variation of dielectric constant (ε') and dielectric loss factor (tan δ) with temperature at different frequencies for $GaFeO_3$. ε' clearly showed a Debye-like relaxation and enhancement of hopping conduction. With increase in x for $Ga_{2-x}Fe_xO_3$, ε' and tan δ increases considerably. Magnetization showed a well saturated hysteresis loop at room temperature for the single crystals which are investigated in detail.

Fig.1 As grown $GaFeO_3$ single crystal

Fig.2 Variation of ε' and tan δ with temperature at different frequencies

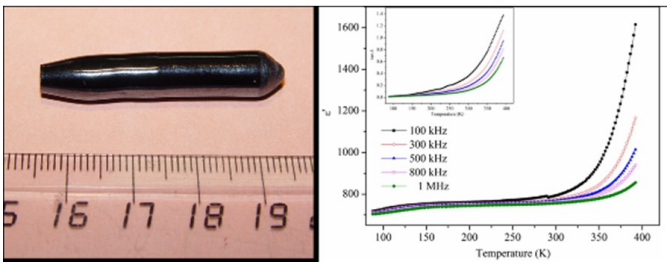

11:20 Oral

Growth of high-quality hexagonal $ErMnO_3$ single-crystals with intriguing electronic domain wall properties

Zewu Yan[1], Dennis Meier[2,3], Ramamoorthy Ramesh[2,3], Edith Bourret[1]

1. *Materials Sciences Division, Lawrence Berkeley National Laboratory, Berkeley, CA 94720, United States* **2.** *Department of Physics, University of California, Berkeley, California, Berkeley, CA 94720, United States* **3.** *Department of Materials Science and Engineering, University of California, Berkeley, CA 94720, United States*

e-mail: zyan@lbl.gov

Multiferroic domain walls may play an important role in electronic devices in the near future due to strong interactions between charges, spin, low symmetry, unique electrostatics and strain. The domain and domain wall structures in the multiferroic hexagonal manganites, h-$RMnO_3$ (R -Sc, Y, Dy-Lu), currently attract tremendous attentions, motivated in part by the observation of stable charged domain walls with exotic electronic conduction properties. At the current stage, however, our understanding of the complex underlying physics remains fragmentary as only structure and transport properties are analyzed in detail. Comprehensive experimental investigations in high quality single crystals of prototypical model systems are highly desirable. In order to access the so far unexplored electrostatic domain wall properties and facilitate experiments in terms of high-resolution low-energy electron microscopy (LEEM) we synthesized large-size and high-quality hexagonal $ErMnO_3$ single crystals using the floating-zone technique. We managed to grow a-orientation crystals with a size up to Ø 5.4 mm × 60 mm by optimizing the growth parameters under different protective atmospheres and different pressures. The details of the growth process will be presented along with spatially resolved LEEM data taken on a- and c-oriented $ErMnO_3$ specimens. Our data reveals electrostatic potential variations associated to the domain walls in $ErMnO_3$ and helps understanding the connection between structural and electronic domain wall properties.

11:35 Oral

Floating-zone growth and physical properties of $Ca_xBa_{1-x}Nb_2O_6$ single crystals

Yunfeng Ma[1], Yijian Jiang[1], Yue Wang[2], Guoqing Liu[2]

1. *Beijing University of Technology, Institute of Laser Engineering, Beijing 100124, China* **2.** *Beijing University of Technology, College of Applied Sciences, Beijing 100124, China*

e-mail: mayunfeng@emails.bjut.edu.cn

In this presentation, the growth of single crystals of calcium barium niobate ($Ca_xBa_{1-x}Nb_2O_6$, $0.22 \leq x \leq 0.37$) with using the optical floating zone method was reported. The relationship between crystal quality and growth condition was studied and the optimum technological condition was obtained. At a growth rate of 1-5 mm/h and a rotation rate of 20-40 min^{-1}, the grown crystals with 6-8 mm in diameter and 70-115 mm in length exhibit pale yellow and transparent after annealing in the O_2 , showed no macroscopic defects such as second phase precipitates and cellular growth. The compositional profile in the rod-like crystals was measured by electron probe micro-analyzer (EPMA). In the case of sample CBN-35.1, the radial deviation of composition could be neglected. However, the composition x at the upper, middle and end region were 0.337, 0.351, 0.366 respectively. The result may be due to the changing composition in the melting zone and Segregation effect. X-ray powder diffraction experiment indicated that only the c_0 lattice parameter offers a clearly marked dependence from the composition while the a_0 lattice constant is nearly constant. We can explain it on the basis of the general crystal structure of the TTB. Which also provide for CBN crystals with excellent piezoelectric, dielectric, ferroelectric, electro-optic and photorefractive properties. In addition, X-ray densities calculated from lattice parameter and actual densities measured by buoyancy method agree very well, they all decrease linearly with increasing Ca proportion x from 0.224 to 0.366. The rocking curves on (001) and (100) crystal planes showed that the symmetry of the diffraction peak is very well. The full-width at half-maximum (FWHM) value was measured to be approximately 0.1°. Which indicate that the as-grown single crystals have medium crystalline quality. The flake XRD patterns of the CBN-24.6, 32.5, 35.1, 36.6 showed that the direction of crystal growth is along *c*-axis. The transmittance spectra of *Z*-cut plates were recorded on a UV-3600 spectrophotometer at room temperature in the range of 190-2500 nm, the cut-off wavelength is 361-370 nm depending on the actual composition, which was shorter than that of SBN crystal (400 nm). CBN crystals have high optical transmittance above 80% for wavelength above 500 nm and wide transparency range covering visible and near-infrared lights. Micro-Raman spectrum was measured at room temperature for *X*-cut plates of CBN crystals. We can see that with x increased, two Raman characteristic peaks v_2, v_5 broaden and move to the low wave number direction, the FWHM of Raman peak is related to the NbO_6 octahedral distortion and the relative intensity of v_5 peak relative to v_2 peak increase gradually. That is because the degree of disorder increases in the crystal cell structure. In order to characterize the vibration modes, we measured the Raman spectrum for CBN-22.4 crystal in different polarizations. The result of the single crystal X-ray structure analysis showed no miscellaneous points in the projection map of lattice structure along [001], [010],[100]-orientation, indicate good microcosmic crystalline quality. At room temperature and 1MHz, with increasing crystal composition x from 0.224 to 0.366, ε_{33} and ε_{11} increase linearly up to 468.1 and 342.0 respectively. The measured dependence of dielectric constants on temperature showed the Curie temperature of the CBN-22.4 crystal has maximum 347 °C, which is about 270 °C higher than SBN-60, as a main advantage, makes CBN potentially attractive for applications to high temperature devices. There is a clear linear correlation between actual composition x and the values of piezoelectric constants d_{33}, d_{15}, d_{31}. The optimum values d_{33}, d_{31} of CBN-36.6 and d_{15} of CBN-22.4 were 90.0, -54.7, 89.2 p C/N respectively. Typical *P-E* hysteresis loops were measured at room temperature and 1 Hz for (0 0 1) surface of CBN crystals, the remnant polarization of CBN-28 was 31.7 μC/cm^2, which was a little smaller than the first-best result of 32.2 μC/cm^2, but the coercive field (E_c) was 16.9 kV/cm, better than informational 38.1 kV/cm. The spontaneous polarization, remnant polarization and coercive field of CBN-36.6 crystal were 27.4μC/cm^2, 25.5μC/cm^2 and 14.4 kV/cm, and E_c decreased with increasing actual composition x. In conclusion, the mechanism of electrical property modulation by actual composition x for CBN crystals can be investigated on the basis of the composition-structure-property relationship.

11:50 Oral

A route to characterize the $LiCoPO_4$ crystals grown by Floating Zone technique

Kunpeng Wang

Universität Heidelberg, Im Neuenheimer Feld 253, Heidelberg 69120, Germany

e-mail: kunpeng.wang@kip.uni-heidelberg.de

Cathode material $LiCoPO_4$ has been grown using $Co(NO_3)_2.6H_2O$ and CoO as the precursor materials, abbreviated as LCP_N and LCP_O respectively, by the travelling-solvent floating-zone method at low Argon pressure. We presented a route to characterize both of the crystal boules including chemical analysis, phase purity analysis, Laue back scattering, polarization images, as well as the orientation determination of the single crystalline grains. Besides, we defined the development factor (V) to evaluate the growth rate of the grains, and defined the orientation deviation factor (δ) to evaluate the quality of the as-grown crystal boules. The calculated V for LCP_N and LCP_O are 0.05 and 0.09, respectively, indicating that the grains of LCP_O develop faster than that of LCP_N. The calculated total δ for LCP_N and LCP_O are 0.7723 and 1.9972, respectively, indicating that the grown LCP_N has a better quality than that of LCP_O. The results show that the grains containing in the as-grown LCP_O crystal boule develop faster than that in LCP_N, and the LCP_N boule has a better quality than that of LCP_O.

12:05 Oral

Study on Flux Growth of KBBF Crystals in Rotary Temperature Field by Rotating Chamber Furnace

Xiaoyang Wang[1], Lijuan Liu[1], Xiaoshan Wang[1,2], Tao Xu[1,2], Xiaolong Wang[1,2], Chuangtian Chen[1]

1. *Institute of Physics and Chemistry, Chinese Academy of Sciences, Beijing 100190, China* **2.** *Graduate University of Chinese Academy of Sciences, beijing 100049, China*

e-mail: xywang@mail.ipc.ac.cn

KBBF and RBBF are the only two deep-UV nonlinear optical crystals that can generate coherent radiation below 200 nm by direct second harmonic. The common technique used to grow these two kinds of crystals is spontaneous nucleation by flux method. In this paper, we modified the growth method by applying a rotating temperature field during the crystallization process. The rotary temperature field was realized by rotating the heating chamber while the crucible and crystal were immobilized. It enhances the mass and heat transport during a non-seeded growth process in the absence of convective flow. The in-

clusions enveloped in crystals were reduced and the growth rate of KBBF crystal was increased. By studying the mass and heat transfer within the melt and subsequently optimizing the growth parameters in rotating temperature field, we were able to obtain high quality KBBF crystals. The prospect of this new crystal growth method was evaluated.

Lunch (IOCG Exec. Com. meeting)

Tuesday afternoon, 13 August, 12:20

TuO2

T06: Oxides and halides including laser and nonlinear optical applications
Tuesday afternoon, 13 August, 14:00
Mickiewicz Hall, Auditorium Maximum

14:00 Oral

Growth and characterization of garnet laser crystals

Haohai Yu, Huaijin Zhang, Jiyang Wang

State Key Laboratory of Crystal Materials, Shandong University, Jinan 250100, China

e-mail: haohaiyu@sdu.edu.cn

Garnet laser crystals including neodymium doped YAG, YGG, CNGG and $Lu_3Sc_xGa_{5-x}O_{12}$ ($0 < x < 2$) are investigated including their growth and characterizations. By the Czochralski and optical floating zone methods, the garnet laser crystals were grown. Their structural, thermal and continuous-wave laser performance was studied and compared with each other. The passively Q-switched and mode-locked fetomsecond lasers were obtained. All the results presented here show that the garnet laser crystals are a series of important laser gain materials for the generation of pulsed lasers.

14:15 Oral

Development of new nonlinear optical crystals for the design of laser devices emitting in the visible and ultraviolet

Lucian Gheorghe[1], Alexandru Achim[1], George Stanciu[1], Flavius Voicu[1], Pascal Loiseau[2], Gérard Aka[2]

1. *National Institute for Lasers, Plasma and Radiation Physics, 111 Atomistilor Street, Bucharest- Magurele 77125, Romania* **2.** *Ecole Nationale Supérieure de chimie de Paris (ENSCP), 11 rue P. et M. Curie, Paris 75005, France*

e-mail: lucian.gheorghe@inflpr.ro

In recent years, there has been a growing demand for specific visible and ultraviolet laser sources in medicine, industrial processing, remote sensing, laser printing, optical displays, and other areas. At this time, the availability of laser frequencies in the visible and UV is limited by laser materials and pump sources. Frequency conversion of solid-state lasers operating in the near infrared range by nonlinear optical (NLO) crystals has become the most available method to obtain shorter wavelength lasers with high beam stability, low cost and compactness. Thus, the reliance on nonlinear methods of frequency generation demonstrates the need for new nonlinear harmonic crystals with the ability to frequency convert a wide variety of laser wavelengths.

$YCa_4O(BO_3)_3$ (YCOB) has attracted great attention as a new NLO crystal for frequency generation since its earliest development [1]. YCOB is a congruent melting non linear material allowing the growth of large dimensions and high optical quality crystals to be used as frequency converters in solid-state laser systems [1-4]. Our previous researches [5-7] showed that in YCOB crystal, the Y^{3+} ions can be partially substituted by smaller radius ions Sc^{3+} or Lu^{3+} in order to tune the chemical composition of the crystal. By changing the compositional parameter x of $Y_{1-x}R_xCa_4O(BO_3)_3$ (R = Lu, Sc) crystals, their optical birefringence can be controlled in order to perform non critical phase matching (NCPM) second harmonic generation (SHG) of specific near infrared laser emission wavelengths shorter than phase matching cutoff wavelength of YCOB crystal (724 nm along Y axis and 832 nm along Z axis at room temperature [8]).

For biaxial crystals like YCOB family compounds, NCPM is the phase matching along one principal axis of the crystal, and for frequency conversion applications, NCPM is advantageous because of its large angular acceptance and because it eliminates walk-off between fundamental and harmonic radiations which leads to the highest efficiency.

Since NCPM is determined by the optical birefringence and is accomplished to an unique wavelength for each NLO process, the objective of this work is to evaluate the potential of $Y_{1-x}R_xCa_4O(BO_3)_3$ crystals as frequency converters for the laser emissions around 800 nm (AlGaAs laser diodes and the strongest emission of Ti: Sapphire laser) and about 700 nm (red laser diodes) in order to obtain visible or near-UV laser radiations by type-I NCPM SHG processes at room temperature. In this aim, crystal growth and NCPM frequency conversion properties of $Y_{1-x}R_xCa_4O(BO_3)_3$ new nonlinear crystals are reported.

Five new NLO crystals of $Y_{1-x}Lu_xCa_4O(BO_3)_3$ and $Y_{1-x}Sc_xCa_4O(BO_3)_3$, with x = 0.19, 0.29, 0.39 and x = 0.07, 0.11, respectively, of good quality with no cracks and bubbles have been grown by Czochralski method, and their NCPM properties were investigated. It was demonstrated that efficient room temperature type-I NCMP SHG of any wavelength from 692.6 - 724 nm and 791.4 - 832 nm spectral ranges, can be achieved in $Y_{1-x}R_xCa_4O(BO_3)_3$ crystals by tuning the composition. These results have very important implications for many of today's tunable solid-state lasers (Ti: Sapphire, Cr: LiSAF, Cr: LiCAF, Alexandrite) and laser diodes (AlGaAs, AlGaInP) with emission in these spectral ranges, in order to obtain specific blue and/or near-UV laser emissions.

References:

[1] M. Iwai, T. Kobayshi, H. Furuya, Y. Mori, T. Sasaki, Jpn. J. Appl. Phys. 36, L276 (1997).
[2] Q. Ye, B.H.T. Chai, J. Cryst. Growth 197, 228 (1999).
[3] D. Vivien, G. Aka, A. Kahn-Harari, A. Aron, F. Mougel, J.M. Bénitez, B. Ferrand, R. Klein, G. Kugel, N. Le Nain, M. Jacquet, J. Cryst. Growth 237-239, 621 (2002).
[4] Y. Fei, B.H.T. Chai, C.A. Ebbers, Z.M. Liao, K.I. Schaffers, P. Thelin, J. Cryst. Growth 290, 301 (2006).
[5] L. Gheorghe, A. Achim, F. Voicu, C. Ghica, J. Optoelectron. Adv. Mater. 12, 1680 (2010).
[6]. L. Gheorghe, A. Achim, B. Sbarcea, S. Mitrea, Optoelectron. Adv. Mater.-Rapid Commun. 4, 318 (2010).
[7]. A. Achim, L. Gheorghe, S. Georgescu, F. Voicu, Optoelectron. Adv. Mater.-Rapid Commun. 4, 1977 (2010).
[8] N. Umemura, K. Yoshida, H. Nakao, H. Furuya, M. Yoshimura, Y. Mori, T. Sasaki, K. Kato, Jpn. J. Appl. Phys. 40, 596 (2001).

14:30 Oral

Growth and Optical properties studies of UV NLO Crystals: $ReAl_3(BO_3)_4$(Re=Y,Gd)

Yinchao Yue, Zhanggui Hu, Yuan Lin, Ying Zhao, Heng Tu, Lei Yang

Institute of Physics and Chemistry, Chinese Academy of Sciences, Beijing 100190, China

e-mail: ycyue@mail.ipc.ac.cn

In recent years, research of $ReAl_3(BO_3)_4$(Re=Y, Gd) crystals as ultraviolet nonlinear optical crystal has attracted more and more attention. [1, 2] reported that $YAl_3(BO_3)_4$(YAB) crystal presents good nonlinear optical properties, especially for the fourth harmonic generation of Nd-based lasers at 266 nm. However, it is difficult to grow high-quality YAB single crystals due to high growth temperature and large viscosity. In addition, impurity ions such as Fe3+ etc. in YAB lead intense non-intrinsic absorption around 266nm wavelength. In this study, using top-seeded solution growth method, a high-quality YAB crystal with the dimensions of 20×20×18mm3 was obtained from B_2O_3-Li_2O flux system (Fig. 1). The fourth harmonic generation of a frequency doubled Nd:YAG laser, from 532 to 266 nm, was carried out with four different lengths of YAB crystal elements which show obvious UV absorption. The results show that the conversion efficiency from 532 to 266 nm is inversely proportional to the length of the crystal elements. Therefore, UV absorption of YAB crystal seriously affects its fourth harmonic laser output properties. To overcome the shortcoming, we grew an eliminating the UV absorption of YAB crystal using a special equipment in oxygen-free atmosphere (the UV transmittance spectrum shown in Fig. 2). Further investigations in the fourth harmonic laser output of free UV absorption of YAB crystal are in progress.

$GdAl_3(BO_3)_4$(GAB) crystal belong to the same structure type as YAB. We explore a metal oxide-B_2O_3-fluoride flux system for GAB crystal growth. Base on lower growth temperature and viscosity of the system, it is easier to grow large-size GAB crystals. In this paper, GAB crystals grown successfully by top-seeded solution growth method. The transmittance spectrum indicates that the UV cut-off edge of GAB crystal is 175nm. Powder SHG test on ground crystals reveals that GAB is phase-matchable material with SHG intensity approximately as large as 3.5 times that of KDP standard. The refractive indices of GAB crystals were precisely measured. The SHG phase-matching angles were calculated based on the Sellmeier equations. The shortest wavelength that can be achieved by type-I phase-matching is down to 248nm.

These results show that $ReAl_3(BO_3)_4$ (Re=Y, Gd) are promising fourth harmonic generation materials.

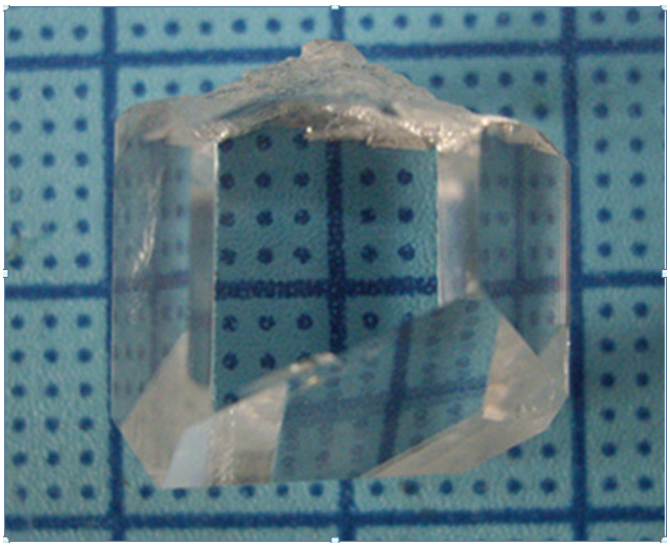

Fig. 1. YAB crystals grown with the dimensions of $20\times20\times18mm^3$

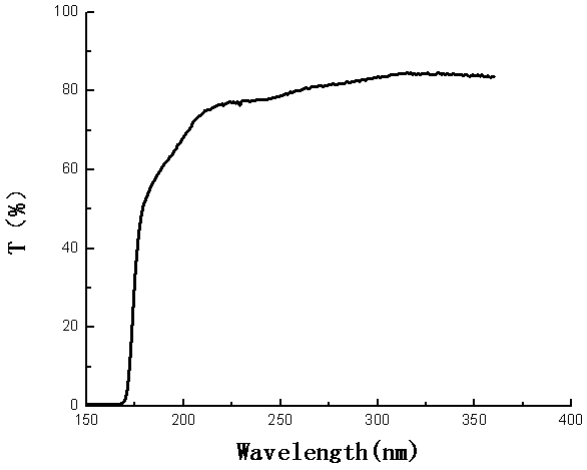

Fig. 2. UV transmittance spectrum of YAB crystal grown in non-oxygen atmosphere

References:

[1] Xuesong Yu, YinchaoYue, Zhang-gui Hu, J.Crystal Growth. 312 (2010) 3029-3033.

[2] Qiang Liu, Ning Ye, etc. Optics Letters. 36(2011) 2653-2655.

14:45 Oral

New type Anti-Stokes laser cooling materials: Yb:$LiLuF_4$ crystal

Jigang Yin, Guangzhu Chen, Zhe Chen, Yin Hang, Kaijie Ning, Xiangyong Wang, LianHan Zhang, Peixiong Zhang

Shanghai Institute of Optics and Fine Mechanics China Academy of Sciences, Shanghai 201800, China

e-mail: yjg@siom.ac.cn

Optical irradiation accompanied by spontaneous anti-Stokes emission can lead to cooling of matter, in a phenomenon known as laser cooling, or optical refrigeration, which was proposed by Pringsheim in 1929. Recently, cooling of a high-density gas through collision redistribution

of radiation has been demonstrated. In laser cooling of solids, heat is removed through the annihilation of lattice vibrations in the process of anti-Stokes fluorescence. Since its initial observation in 1995, research has led to achieving a temperature of 208 K in ytterbium-doped glass. In this Letter, we report Anti- Stokes laser cooling in ytterbium-doped $LiLuF_4$ single crystals grown using the Czochralski technique. The spectroscopic characterization of the crystals has been used to evaluate the laser cooling performance of the samples. Cooling by 6 degrees below ambient temperature is obtained.

15:00 Oral

Simulation of facet formation during Czochralski growth of YAG and GGG

Vasif Mamedov, Andrey Smirnov

STR Group, Inc., Engels av. 27, P.O. Box 89, St-Petersburg 194156, Russian Federation

e-mail: vasifm@mail.ru

Faceting of the melt-crystal interface is an important phenomenon affecting crystal quality. It is related with generation of many defects. For example strained core of YAG is assumed to be produced by the faceting of the interface [1]. The localization of the core along the axis of the crystal correlates with facets arising on the peak of conical interface. Another example is a spot-like defect structure with symmetry by 120 degrees rotation around the crystal axis which is observed in garnets grown in <111> direction. This 3-fold symmetry also can be explained by the faceting of the interface. Faceting affects the crystal quality by stress generation, by different segregation at the facets and at rough surface or by some other way. Anyway regardless to the mechanism of defect generation the control of facet formation allows to improve the crystal quality. To investigate possible ways of controlling crystal facets, computer modeling of Cz growth of YAG and GGG has been performed by CGSim software package [2]. This software allows to take into account heating, crystallization, convection and radiation inside the whole furnace in axisymmetric approximation. It should be noted that despite of the three-dimensional shape of faceted crystal the axisymmetric simulation is quite reasonable for the aim to avoid faceting (because of axysymmetric shape of non-faceted melt-crystal interface). Facet formation has been modeled by taking into account the anisotropy of interface undercooling. The interface of growing crystal is colder than the melting temperature. The value of undercooling affects the local crystallization rate in different extent for rough and faceted growth. CGSim computes undercooling anisotropy using the model of Weinstein and Brandon [3, 4]. This model suggests the crystallization rate to be proportional to the undercooling on the rough part of interface. Crystallization rate on the faceted part is assumed to be depending not only on undercooling but also on the angle of misorientation between facet direction and normal to the interface. Obtained results are verified using available experimental data.

1. C.W. Lan,C.Y. Tu, J. Cryst. Growth 233, 523 (2001)
2. www.str-soft.com
3. O. Weinstein, S. Brandon, J. Cryst. Growth 268, 299 (2004)
4. O. Weinstein, S. Brandon, J. Cryst. Growth 268, 232 (2004)

15:15 Oral

Crystal growth and characterization of 4 inches $YCa_4O(BO_3)_3$ crystal

Xiaoniu Tu, Yanqing Zheng, Kainan Xiong, Yifan Tu, Erwei Shi

Shanghai Institute of Ceramics, Chinese Academy of Sciences, 1295 Dingxi Road, Shanghai 200050, China

e-mail: xiaoniu_tu@mail.sic.ac.cn

Rare earth calcium oxybrorate single crystals $ReCa_4O(BO_3)_3$ (Re- rare earth elements such as Gd, La, Y, Sm, and so on) were studied for second-harmonic generation (SHG) in the past two decades because of several advantages, such as, easy to grow, not hygroscopic, significant effective NLO coeffient, and small birefringence [1,2]. Among this series of crystals, $YCa_4O(BO_3)_3$ (YCOB) crystal has attracted more and more attention in the past few years. Due to their nonlinear-effect, thermo-optic effect, mechanical characteristic, large aperture and low cost, YCOB can be used for both high-peak and high-average power pulse genaration in high-energy and high-power ultra-short laser systems [3]. Besides, their excellent high temperature piezoelectric property enables YCOB to be used in automotive and aerospace industries [4].

For high-power laser system and high temperature piezoelectric applications, large aperture and high qanlity YCOB crystal is required. In this work, 4 inches in diameter and 4 inches in length YCOB crystals were grown by Czochralski method. The high quality crystals without inclusions, cleavages and spiral growth were abttained through optimizing the growth system by Czochralski crystal growth modeling. The cleavage property of YCOB was discussed from three aspects, thermal expansion, excess stress and growth technology. The high resolution X-ray diffraction, specific heat and thermal diffusion coefficient of the as-growth crystal were measured. The thermal conductivity and thermal expansion coefficient along X, Y, Z and two cleavage planes (010) and (-201) were also measured. The optical homogeneity and anti-laser damage threshold were tested. All the results show that the large aperture YCOB crystal can satisfy the requirements of high-energy and high-power ultra-short laser systems .

reference

[1] F. Mougel, G. Aka, F. Salin, D. Pelenc, B. Ferrand, A. Kanh-Harari, D. Vivien, Advanced Solid-State Lasers, 26(1999), PP. 709-714

[2] T. Sasaki, Y. Mori, M. Yoshimura, Y. K. Yap, T. Kamimura, Materials Science and Engineering, 30(2000), pp. 1-54

[3] L. H. Yu, X. Y. Liang, J. F. Li, A. H. Wu, Y. Q. Zheng, X. M. Lu, Ch. Wang, Y. X. Leng, J. Xu, R. X. Li, ZH. Zh. Xu, Optics Letters, 37(2012), pp. 1712-1714

[4] Sh. J. Zhang, Y. T. Fei, E. Frantz, D. Snyder, Bruce H. T. Chai, T. R. Shrout, IEEE Transaction on Ultrasonics, Ferroelectrics, and Frequency Control, 55(2008), pp. 2703-2708

Break
Tuesday afternoon, 13 August, 15:30

Wednesday, 14 August

WeO1

T06: Oxides and halides including laser and nonlinear optical applications
Wednesday morning, 14 August, 10:20
Mickiewicz Hall, Auditorium Maximum

10:20 Invited oral

Improved performances of relaxor-based single crystals for sensor applications

Haosu Luo, Xiangyong Zhao, Xiaobing Li

Shanghai Institute of Ceramics, Chinese Academy of Sciences, 1295 Dingxi Road, Shanghai 200050, China

e-mail: hsluo@mail.sic.ac.cn

Large size and high quality of relaxor-based single crystals have grown by the modified Bridgman technique in SICCAS. These crystals exhibit not only extra high piezoelectric performances but also high optoelectric and pyroelectric performances. They could be widely used in various fields such as ultrasound transducers, actuators, and infrared detectors etc. However, for a few piezoelectric device applications, PMNT single crystals, the first generation of generation of relaxor-based single crystals, needs to increase their Tc, Trt, and Ec further. Thus PIMNT single crystals, as the second generation of relaxor-based single crystals, have been grown in the same technique, and they exhibit higher Tc, Trt, and Ec, but more serious issue of compositional segregation. For some sensor applications, PMNT and PIMNT doped transition elements, as the third generation of relaxor-based single crystals, have been grown to improve their ferroelectric and dielectric performances.

After investigated the dielectric, piezoelectric and pyroelectric performances, Mn-doped PMNT and PIMNT could reduce their dielectric loss tandsignificantly, and increase their coercive field E_c. For example, the dielectric loss could be significantly reduced from 0.3% undoepd PMNT to 0.05%. Dipole defect $Mn_{Ti}^{''}$-$V_O^{\times\times}$is suggested upon on the XAFS and EPR results, where Mn^{2+} is in B-site of perovskite ABO3 structure. These dipole defect $Mn_{Ti}^{''}$-$V_O^{\times\times}$produce an inner electric field, and pin the movement of domain wall, in the result of lower dielectric loss and higher the coercive field Ec.

By using the third generation of relaxor-based single crystals, high performances of infrared detectors and magnetic sensors have been fabricated to reduce their intrinsic dielectric noise and increase the ratio of signal and noise.

10:50 Oral

$SrMgF_4$ crystal as a new perspective nonlinear ferroelectric material.

Alina A. Goloshumova[1], Alexander P. Yelisseyev[1], Sergey I. Lobanov[1], Dmitry Y. Naumov[2], Svetlana V. Melnikova[3], Igor N. Ogorodnikov[4], Lyudmila I. Isaenko[1]

1. *Institute of Geology and Mineralogy SB RAS (IGM), Koptyuga ave., 3, Novosibirsk 630090, Russian Federation* **2.** *Nikolaev Institute of Inorganic Chemistry SB RAS (NIIC), Acad. Lavrentiev Ave., 3, Novosibirsk 630090, Russian Federation* **3.** *L.V.Kirensky Institute of Physics Siberian Branch of the Russian Academy of Science (IPH SB RAS), Academgorodok, 50, Krasnoyarsk 660036, Russian Federation* **4.** *Ural Federal University, Mira Street, 19, Ekaterinburg 620002, Russian Federation*

e-mail: alingol-nsk@yandex.ru

Inorganic fluoride crystals are of particular interest to researchers as promising optical materials. In addition, they may be considered as a host matrix for rare earth ions. $SrMgF_4$ crystals have been attracted attention recently. They were theoretically supposed to have ferroelectricity [1], but still there are no practical proofs. The goal of this work was to grow $SrMgF_4$ crystals of a good quality, to study their crystal structure and physical properties to check the presence of ferroelectric nature.

$SrMgF_4$ crystals were grown via vertical Bridgman method. Powders of MgF_2(99.99%) and SrF_2(99.99%) were used as starting materials. To remove oxygenic impurities, adsorbed from the atmosphere, the synthesized mixture was ignited at 1000˚C and the vacuum of 10^{-1} Pa in 24 hours. Then the purified material was melted and held stirring up during an hour. The crystals of $SrMgF_4$ were grown in a two-zone furnace with a temperature in a hot zone of 1200˚C. The pulling speed and the temperature gradient in a growth region were 1 mm/h and 10-20˚C/cm, respectively. The size of grown crystals was 10×10×5 mm. To study the structure of grown crystals single crystal and powder X-ray analyses were carried out. $SrMgF_4$ has noncentrosymmetrical monoclinic structure, space group $P2_1$. All crystallographic parameters were determined. Coordination numbers of Sr ions were estimated. Altogether the structure can be described as a laminated one. Layers, oriented along c axis, are composed of chains, which are drawn along b axis and consist of irregular corner-sharing MgF_6 octahedra, rotated relative to each other (Fig.1). Obtained results are in good agreement with those published earlier [2].

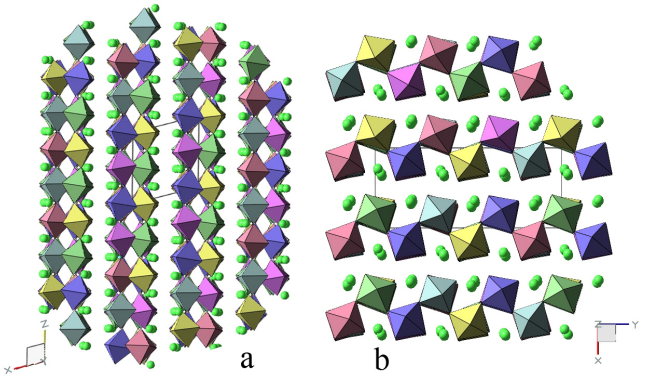

Figure 1. Crystal stucture of $SrMgF_4$ progected among c axis (a) and b axis (b).

Emission, excitation and reflection spectra were obtained. The value of E_g was estimated and spectroscopic features were studied carefully. Polarization-optical study showed the presence of phase transition at 170-200ºC. Also pyroelectric properties were detected at nearly the

same temperature region. To assign the high-temperature phase powder X-Ray diffraction at the temperature of 300ºC was performed. According to obtained results $SrMgF_4$ crystals are promising nonlinear material indeed and more detailed study should be carried out.

[1] S.C. Abrahams, Acta Crystallogr. B58 (2002) 34.
[2] N. Ishizawa, K. Suda, B. Etschmann, T. Oya, N. Kodama, Acta Crystallogr. C57 (2001) 784.

11:05 Oral

Growth and characterization of undoped and Mn-doped lead-free piezoelectric single crystals $0.80Na_{0.5}Bi_{0.5}TiO_3$-$0.20K_{0.5}Bi_{0.5}TiO_3$

Anandha Babu Govindan[1], Indranil Bhaumik[2], Ganesamoorthy Sarveswaran[3], Ramasamy Perumalsamy[1], Gupta P K[2], Muthu Raja Arumugam[1]

1. *SSN College Of Engineering (SSNCE), Kalavakkam, chennai 603110, India* **2.** *Laser Materials Development and Devices Division, Raja Ramanna Centre for Advanced Technology (RRCAT), Indore 452013, India* **3.** *X ray Crystallography and Crystal Growth Section, Condensed Matter Physics Division, Material Science Group, IGCAR (IGCAR), Kalpakkam, Tamil Nadu, Chennai 603 102, India*

e-mail: anandcgc@gmail.com

Sodium bismuth titanate, $Na_{0.5}Bi_{0.5}TiO_3$ (NBT)-based solid solutions are considered to be an excellent candidate as lead-free piezoelectric materials, as they have strong room temperature ferroelectricity with high Curie temperature. For unmodified NBT a great deal of difficulties have been experienced in poling because of its high coercive field (E_c=73 kV/cm).

Recently, some modifications of NBT ceramics by forming solid solution with $BaTiO_3$, $SrTiO_3$, $NaNbO_3$, $BiFeO_3$, La_2O_3, and $K_{0.5}Bi_{0.5}TiO_3$(KBT) have been found to be helpful in the poling process. (1-x)NBT–xKBT system exhibits rhombohedral–tetragonal morphotropic phase boundary (MPB) in the vicinity of x =0.16-0.20. Also, introducing small amount of dopants, such as MnO_2, Sb_2O_3 and Nb_2O_5 into (1-x)NBT–xKBT based ceramics can greatly improve the piezoelectric properties. However, no investigation has been carried out on doped (1-x)NBT–xKBT single crystals yet. So it is of interest to investigate the effects of doping in $0.80Na_{0.5}Bi_{0.5}TiO_3$–$0.20K_{0.5}Bi_{0.5}TiO_3$ (0.80NBT-0.20KBT) single crystal for seeking high preference lead-free piezoelectric materials. Pure $0.80Na_{0.5}Bi_{0.5}TiO_3$–$0.20K_{0.5}Bi_{0.5}TiO_3$ and 1 wt.% Mn-doped 0.80NBT-0.20KBT lead-free piezoelectric single crystals with tetragonal structure were grown by the flux growth method. The crystal structure and lattice parameter of the grown crystal was assessed by Powder X–ray diffraction (PXRD) and the lattice strain (η) has been calculated by using Hall-Williamson relation. The temperature dependence of dielectric constant and loss were investigated in the grown crystals. Two dielectric peaks corresponding to depolarization temperature (T_d) and transition temperature (T_c) appeared in curves of dielectric permittivity vs. temperature for the pure 0.80NBT-0.20KBT single crystal. Compared to pure 0.80NBT-0.20KBT single crystal, Mn-doping restrained the transition of ferroelectric phase to antiferroelectric phase. Fitting of the experimental data to a modified Curie-Weiss equation indicates the occurrence of relaxor likes phase transition in grown crystals. The impedance studies have been carried out on Mn doped 0.80NBT-0.20KBT single crystal.

11:20 Oral

Fabrication of quasi-phase-matching structure in lithium tetraborate

Kensaku Maeda, Kozo Fujiwara, Satoshi Uda

Tohoku University, Institute for Materials Research (IMR), 2-1-1, Katahira, Aoba-ku, Sendai 980-8577, Japan

e-mail: kensaku@imr.tohoku.ac.jp

The development of an all-solid-state vacuum-UV light source is essential for achieving ultrafine laser processing. Such an all-solid-state light source must be both inexpensive and maintenance free. Devices with QPM (quasi-phase-matching) structure can reduce the incoming wavelength by half. It can be achieved in structures in which the sign of the nonlinear optical coefficient is periodically reversed. This QPM structures can be formed in ferroelectric materials such as $LiNbO_3$ and $LiTaO_3$ by applying an external electric field. However, the converted light with vacuum-UV cannot pass through ferroelectric materials since they are opaque to vacuum-UV (wavelength: < 300 nm).

Lithium tetraborate ($Li_2B_4O_7$; LB4) has a high nonlinear optical coefficient (d_{33} = 0.93 pm/V), and transparent to light with wavelengths down to 160 nm. However, LB4 is not ferroelectric and thus polarization methods cannot apply to the formation of QPM in LB4. Thus, to realize a QPM structure in LB4, we propose to make a crystal with periodically inverted *c*-axis twin structure.

We investigate the relationship between crystal growth directions and twin boundary orientations in LB4. When the growth direction was between <100> and <110>, (010) twin boundaries formed. In contrast, when the growth direction was between <110> and <010>, (100) twin boundaries formed. We developed a twin boundary control method based on the above relationship. The intervals of the twin boundaries are dependent on the fineness of heating method. A fabricated crystal includes 100 μm interval periodic twin boundaries and can function as a 5th-ordered QPM structure for a second-harmonic-generation of Nd:YAG laser (1064 nm). A finer periodically twinned crystal would be required to tune in shorter phase-matching wavelengths.

11:35 Oral

Flux Growth and characterization of lead-free Sodium Bismuth Titanate -Barium Titanate (NBBT) at composition near the morphotropic phase boundary

Aravinth Karuppanan, Anandha Babu Govindan, Ramasamy Perumalsamy

Centre for Crystal Growth,SSN College of Engineering,Kalavakkam,Chennai, Chennai 603110, India

e-mail: phyaravinth@gmail.com

In recent years, growing attention has been given to the research for improving piezoelectric properties of lead-free piezoelectric materials, which are viewed as possible substitutes for lead-based piezoelectric materials from the viewpoint of environmental protection. Among these NBT-based solid solutions, $Na_{1/2}Bi_{1/2}TiO_3$–$BaTiO_3$ (NBBT) system is most attractive due to their excellent piezoelectric properties, which exists as morphotropic phase boundary (MPB) between the rhombohedral phase (NBT) and the tetragonal phase (BT). The improved electromechanical properties can be generally achieved in single crystals based on engineering domain configuration. So it is expected that the superior piezoelectric properties could be achieved in NBBT94/6 single crystal. 0.94NBT-0.06BT single crystal with reasonable size has been successfully grown by flux growth method. Single

crystal X-ray diffraction (SXRD) was used to confirm the crystal system of the grown NBBT94/6 crystal. The Energy Dispersive X-Ray analysis method was used to measure the concentrations of Ba, Bi, Ti and Na elements in the as-grown crystal. The temperature dependence of dielectric constant for various frequencies (100 Hz–2 MHz) has been determined. Two dielectric anomalies are observed at 159^{o}C and 310^{o}C, corresponding to the depolarization temperature (T_d) and Curie temperature (T_m). The dielectric data fitted with Curie-Weiss law shows that the gamma value of the as-grown crystal is 1.46, which also confirms the better relaxor behavior.

11:50 Oral

Noncentrosymmetric halide borate: $K_3B_6O_{10}Cl$

Shilie Pan

Xinjiang Technical Institute of Physics and Chemistry Chinese Academy of Sciences(Urumuqi)830011 P.R.China, Beijing south road 40# add 1#, urumuqi 830011, China

e-mail: slpan@ms.xjb.ac.cn

A perovskite-like phase, $K_3B_6O_{10}Cl$ exhibits a large second harmonic response about four times that of KH_2PO_4 (KDP) and is transparent from the deep UV (180 nm) to middle-IR region. A high quality single crystal of $K_3B_6O_{10}Cl$ with dimensions up to 30 × 15 × 7 mm^3 was successfully grown by the top-seeded solution growth method. Crystal morphologies and growth habits of $K_3B_6O_{10}Cl$ grown with seeds oriented along [101] and [211] were studied, and the best growth direction was obtained., The refractive indices of the crystal were measured by the minimum deviation technique and fitted to the Sellmeier equations[1].The nonlinear optical coefficients have been determined by the method of Maker fringes at λ=1064 nm. The suitable nonlinear optical coefficients as well as comparatively easy crystal growth make the $K_3B_6O_{10}Cl$ crystal a promising candidate for NLO materials[2-9].

1. Born, M.; Wolf, E.; *Principles of Optics*, Pergamon, Oxford, **1975**.

2. Chen, C. T.; Wu, B. C.; Jiang, A. D., etc. *Sci. Sin. B***1985**, *28*, 235.

3. Chen, C. T.; Wu, Y. C.; Jiang, A. D., etc. *J. Opt. Soc. Am.B***1989**, *6*, 616.

4. Wu, B. C.; Tang, D. Y.; Ye, N.; Chen, C. T. *Opt.Mater.***1996**, *5*, 105.

5. David, C. *Nature***2009**, *457*. 953.

6. Wu, H. P.; Yu, H. W.; Pan, S. L.,* ect. *Angew. Chem. Int. Ed.*, **2013,***52*, 3406.

7. Yang, Y.; Pan, S. L.;* Han, J., *Cryst. Growth Des.*, **2011**, *11*, 3912.

8. Yu, H. W.; Wu, H. P.; Pan, S. L.,* ect. *J. Mater. Chem.,***2012**, *22*, 9665.

9. Yang, Y.; Pan, S. L.;* Hou, X. L., ect. *J. Mater. Chem.*, **2011**, *21*, 2890.

Lunch (IOCG Council meeting)

Wednesday afternoon, 14 August, 12:20

WeO2

T06: Oxides and halides including laser and nonlinear optical applications
Wednesday afternoon, 14 August, 14:00
Mickiewicz Hall, Auditorium Maximum

14:00 Invited oral

Constructional and optical sapphire for application in medicine

Lytvynov Leonid

Institute for Single Crystals NAS of Ukraine (ISC), 60 Lenin Ave., Kharkov 61001, Ukraine

e-mail: lytvynov@isc.kharkov.ua

Unique inertness, including electrolytic passiveness, biocompatibility, corrosion resistance, andhardness characteristic of sapphire, define its main fields of application in medicine: implants,medical instrument and devices making.

Medical-biological investigations have shown that sapphire is not toxic for humans and does notcause changes in the functions of the central nervous system, liver, kidneys, protein and fatmetabolism, and general reactivity. It does not possess carcinogenic, mutagenic, embryotrophic,or other types of remote effects. Collagen fibrillar capsule growing on the implant passes intobone and muscular tissue, which preserves the normal structure. In contrast to titanium,electrically neutral sapphire is not carried by electrochemical reactions into lymph nodes andother parts of the body, does not cause immunodepressions and other changes in the immunesystem, and does not lead to demineralization of adjacent bone tissue.

Crystallographic aspects. Beyond other conditions, the rate of implant adaptation in the patientdepends on the crystallographic conformity between the structures of the implant and the mineralcomponent of the bone tissue (crystalline fibers contained in microfibrils). The mineralcomponent is essential and it is necessary to take into account the crystallographic interactionbetween the crystals of the bone tissue and the lattice of the implant. Such considerations aresimilar to heteroepitaxy and intergrowth of crystals. Biochemical and biomechanical testing ofimplants made from crystals with different syngony and lattice parameters showed theadvantages of sapphire.

Functional merits of the sapphire are clearly seen in the comparison of their basic, functionalproperties with those of the widely used titanium analogs.

It is known that immunologic disturbances are defined by the implant material. The resistance ofsapphire to any acid and alkali is immensely higher than that of metals and even ofpolycrystalline aluminum oxide. This likely explains the fact that sapphire does not change theimmunological status of patients. At the same time, 73% of the cases involving metallic implantinsertion are followed by immunodepression, changes of immunoreactivity, and otherimmunologic disturbances (especially for male patients). All these manifestations raise theprobability of postoperative complications.

It is well-known that the nickel and chromium contained in some implants are carcinogenic,possess cytotoxic effects, and may affect allergies. Approximately 15% of people are especiallysensitive to nickel, and 8% to chromium. Survival tests for L-132 cells (RPE, relative platingefficiency) placed in media of different implant materials for a long period of time show thataluminum oxide, platinum, and $TiAl_6V_4$ alloy possess a level of survival close to 100%. For Ni—Cr—Co alloy this characteristic is on the order of 23%, while for Ni—Cr—Mo alloy it is evenlower. The sapphire is especially suitable for those patients who suffer from intolerance tometals, or already have metallic implants inserted.

The use of sapphire in friction pairs is of particular interest. As a rule, orthopedic implants areof large size and, therefore, an essential amount of metal is introduced into the patient duringtraditional implantation. For instance, a hip joint endoprosthes contains 300–350 g of titaniumand alloyed steel (the latter being even less physiological). The metal corrosion productspenetrate into the bone and may lead to trau-

matic osteomyelitis. The service life of the widelyused metal-plastic hinges on hip joint prostheses is insufficient (5–7 years) due to the highfriction coefficient of the metal-polyethylene pair, which increases over time with use. Theservice life of joint prostheses depends on the quality of spherical surface polishing. Metallicand ceramic surfaces cannot maintain a high finish class because of the presence of disorientedgrains and intergranular boundaries with different physical and mechanical characteristics thanthose of the grains. Different rates of wear of this microstructure raise the friction coefficient ofthe pair and lead to elevated wear of the mating component. The rough surface which is goodfor conventional intraosteal implants is undesirable for friction pairs. The probability ofadherence of organic molecules to such a surface increases, thus deteriorating the performance ofthe friction pairs. Sapphire not containing block (grain) boundaries allows surfaces with a highpolish quality to be obtained (possessing a slight roughness and containing practically noscratches and pits). Moreover, sapphire is one of the most wear-resistant materials (this fact ledto its wide employment in the friction pairs of watches and other devices). The frictioncoefficient of polished sapphire pairs actually decreases over the life of their operation; the wear index approaches the corresponding value of natural jointsThe wear of the polyethylene component of polyethylene – alumina ceramic pairs (even if thelatter is of low quality) is less than with polyethylene – zirconium dioxide pairs . It is natural thatfor polyethylene coupled with sapphire this characteristic is much better compared to the ceramicmaterials.

14:30 Oral

Czochralski growth and characterization of $MgAl_2O_4$ single crystals

Andrzej L. Bajor, Marcin Chmielewski, Ryszard Diduszko, Jaroslaw Kisielewski, Tadeusz Łukasiewicz, Krzysztof P. Orliński, Wlodzimierz Szyrski

Institute of Electronic Materials Technology (ITME), Warszawa 01919, Poland

e-mail: Andrzej.Bajor@itme.edu.pl

Introduction

Although $MgAl_2O_4$ (MALO) spinel belongs to highest (m3m) symmetry group, and, therefore, not much effort is required to cut properly oriented seeds for pulling these crystals by Czochralski method, by no means this is easy to be grown due to its high melting point (2105°C [1] to 2130°C [2]). Therefore, only a limited number of papers exist on growing these crystals. Basically, some details on Czochralski growth were only provided in a few earlier works (e.g. [3]). However, many researchers has paid considerable attention to MALO (also grown by other techniques (e.g. micro-pulling down [4]), since this is an interesting material to be used in many applications, including saturable absorbers in laser heads. However, the researchers usually buy this crystal from different manufacturers, and they usually neither pay much attention to growth conditions, nor to real parameters of the crystals themselves, which as a standard procedure are taken from the manufacturers' catalogues.

We grew undoped and Co-doped MALO by classical Czochralski method from iridium crucible. Optical quality of crystals was verified by conoscopic and polariscopic methods. Although we made a couple of other experiments, our major efforts were concentrated upon investigation of thermal properties of this crystal, because they are very important in laser technique, and to our knowledge they haven't been yet well verified by other investigators.

State of the art, crystal growth and investigations

Although there has been nothing odd about growing MALO by the Czochralski method, one has to be careful about the process itself, since in temperatures exceeding 2100°C a certain deformation as well as a certain evaporation of the crucible material (iridium) can be observed. Especially then a suitable thermal isolation of the crucible is needed. Another problem is doping of MALO with Co^{+2} ions, which makes the crystal to work as a saturable absorber in laser heads. Apart of the mentioned work by Volk et al. [1],as said only a few reports have been presented on making single crystals. More detailed studies of alumina-rich MALO were conducted by Tang et al. [5-7]. There have been also a couple of investigations on powdered MALO [e.g. 8-9]. A very nice example of using MALO as saturable absorber at eye-safe wavelength of 1.5 μm was given by Mlynczak et al. [10].

Since we expect several kW of absorbed pumping powers, as well as ab. 2-5 KW of the output powers from miniature laser structures (it's expected that MALO will be thermally bonded to the host material (e.g. Er,Yb glass)) it is important to know basic thermal parameters of the absorber that can be later compared to this of the host. Since we expected that these parameters may depend on Co concentration, we grew crystals doped with Co between 0.06 and 0.21 at. %.

Since at the beginning we had no seeds, we grew two undoped MALO using iridium wire. By X-ray method it was found that the both crystals were pulled in <111> direction. Next we grew Co-doped MALO using regular seeds that were cut out from the undoped crystals. All of the crystals were checked by XRD (powder) technique for eventual admixtures of different crystallographic phases. After cutting off the conical and tail parts, the end faces of remaining boules were polished for optical investigations.

By conoscopic, polarimetric, plane- and circular-polariscopic methods it was found that the majority of crystals were grown without core in their central parts, which, on the contrary, is a typical case in e.g. <111> YAG crystals which also grow, like MALO, with convex front of crystallization (to the melt), as well as they also belong to m3m symmetry group. Although it's rather a well know fact that the core "consumes" practically all of so-called residual stresses (the core is avoided when cutting the samples for practical use), a minor residual stresses in these crystals were, generally, a good news from the point of view of MALO's further applications. After measuring refractive indices and their optical dispersion in all crystals, we also cut a certain number of wafers and other elements for spectral and thermal investigations. So, we examined undoped and Co-doped crystals for linear expansion coefficient, specific heat, thermal diffusivity and thermal conductivity. Although from general theories (e.g. [11]) it follows that the thermal properties are (or should be) isotropic in cubic crystals, we also cut a certain number of <100> oriented samples for these investigations. In the future we are planning researches of laser parameters of these crystals as saturable absorbers. There is no room for futher discussion of this problem here, but, however, there is a need for checking whether a couple of these parameters are either orientation dependent, or they depend on the plane of polarization of the incident radiation.

References

[1] Y. V. Volk, A. M. Malyarevich, K. V. Yumashev, V. N. Matrosov, T. A. Matrosova and M. I. Kupchenko, "Anisotropy of nonlinear absorption in Co^{2+}:$MgAl_2O_4$ crystal", Appl. Phys. **B88**, 443-447 (2007).

[2] Products catalogue of MTI Corp. www.mtixtl.com

[3] E. Kasper, P. Korczak and H. Henkel, "X-ray topographic analysis of dislocations in Czochralski-grown stoichiometric $MgAl_2O_4$ spinel single crystals", J.Mater. Sci. **9**, 1699-1700 (1974).

[4] A. Jouni, A. Yoshikawa, T. Fukuda and G. Boulon, "Growth and characterization of Mn^{2+}-Activated magnesium aluminate spinel single crystals", J. Cryst. Growth **293**, 517-521 (2006).

[5] H. Tang, J. Xu, Y. Dong and F. Wu, "Growth and annealing properties of $Mg_{0.4}Al_{2.4}O_4$ crystal", J. Alloys Comp. **470**, L29-L32 (2009).

[6] H. Tang, J. Xu, H. Li, Y. Dong, F. Wu and M. Chen, "Structure, thermal expansion and optical property of alumina-rich spinel substrate", J. Alloys Comp. 479, L26-L29 (2009).

[7] H. Tang, J. Xu, H. Li, Y. Dong, F. Wu and X. Yang, "Thermal and mechanical properties of novel substrate crystal $Mg_{0.4}Al_{2.4}O_4$", Mater. Lett. **63**, 1800-1802 (2009).

[8] I. Ganesh, R. Johnson, G.V. N. Rao, Y. R. Mahajan, S. S. Madavendra and B. M. Reddy, "Microwave-assisted combustion synthesis of nanocrystalline $MgAl_2O_4$ spinel powder", Ceramics Int. **33**, 67-74 (2005).

[9] V. Singh, M. Haque and D. K. Kim, "Investigation of a new red-emitting, Eu^{3+}-activated $MgAl_2O_4$ phosphor", Bull. Korean Chem. Soc. **28**, 2477-2480 (2007).

[10] J. Mlynczak, K. Kopczynki, Z. Mierczyk, M. Malinowska and P. Osiwianski, „Pulse generation at 1.5 μm wavelength In New EAT14glasses moped with Er^{3+} and Yb^{3+} ions", Opto-Electron. Rev. **20**, 14-17 (2012).

[11] J. F. Nye, "Physical properties of crystals", Clarendon, Oxford 1957.

14:45 Oral

Crystal growth of Bi_2TeO_5 by a double crucible Czochralski method

Jesiel F. Carvalho[1], Zanine V. Fabris[1], Ivan de Oliveira[2], Jaime Frejlich[3]

1. *Universidade Federal de Goiás (UFG), Campus Universitário Samambaia, Goiânia 74690900, Brazil* **2.** *Faculdade de Tecnologia da Unicamp, Limeira 13484-332, Brazil* **3.** *Instituto de Física, Unicamp, Campinas 13083-859, Brazil*

e-mail: carvalho@if.ufg.br

Abstract

Single crystals of bismuth tellurite (Bi_2TeO_5) were grown by a double crucible Czochralski method at different pulling and rotation rates, ranging from 0.1 mm/h to 0.8 mm/h and from 5 to 20 rpm, respectively. Growth conditions were studied and the crystallized phase was verified by X-ray diffraction. Crystals were oriented by X-ray back-reflection Laue photographs and good crystalline samples were cut and polished, presenting uniform pale yellow coloration. They were investigated by optical transmission and holographic recording.

1. Introduction

Bismuth tellurite (Bi_2TeO_5), here labeled BTeO, shows interesting linear and nonlinear optical and electro-optical properties, being a promising photorefractive crystal [1-3]. Bi_2TeO_5 was firstly synthesized in 1971 by Frit et al. [4], but just in 1990 the first detailed report on bulk single crystal growth using Czochralski method was published by Földvári et al. [5]. Since then, other methods like floating zone [6] and Bridgman [7], in addition to Czochralski [8, 9], were also used to grow pure and doped BTeO crystals.

Bi_2TeO_5 crystallizes in an orthorhombic structure, with non-centrosymmetric space group *Abm2*, and unit cell parameters a =11.602(2) Å, b = 16.461(3) Å and c = 5.523(1) Å [2, 10]. It is a biaxial negative crystal with refractive indices n_1=2.3203(3), n_2=2.3678(3) and n_3 = 2.4022(3), at λ=632.8 nm [3]. The (100) crystallographic plane is easily cleavable producing mirror-like surfaces [5].

The high vapor pressure of TeO_2 at the melting point of Bi_2TeO_5 and the easy cleavage through (100) plane impose some additional difficulties for crystal growth of BTeO. In this work we adopted a double crucible Czochralski method to overcome the trouble of TeO_2 evaporation, and a low rotation speed combined with an appropriate crystal seed orientation was used to minimize the risk of cleavage during growth. Homogeneous and pale yellow in color single crystals of Bi_2TeO_5 were grown and preliminarily characterized by optical and structural techniques.

2. Experimental

2.1. Crystal growth

Bismuth oxide (Bi_2O_3, Sigma-Aldrich, 99,999%) and tellurium oxide (TeO_2, Sigma-Aldrich, 99,99%) were used as starting materials. They were mixed in the molar ratio of $1Bi_2O_3$:$1.1TeO_2$ and pre-synthesized by solid-state reaction, in order to minimize the partial loss of TeO_2 during the melt. The synthesis was carried out in two steps, the first at 650°C and the second at 750°C, both during 24 hours, being the result monitored by X-ray powder diffraction.

A double crucible system consisting of two concentric cylindrical crucibles (platinum-5% gold) whose walls were separated by about 4 mm was used. The inner crucible was filled with the previously synthesized precursor powder, and the space between them was filled with a lower melting point powder with composition $3Bi_2O_3$:$7TeO_2$, richer in TeO_2. At the growth temperature, the evaporation of tellurium oxide is higher in the outer crucible, producing a saturated atmosphere of TeO_2 near the liquid surface from which the crystal is grown. The resulting condition of dynamic equilibrium between the vapor and liquid phases prevents high deviations in the melt stoichiometry, sustaining the crystal growth for a long time.

Crystal growth was performed on seeds oriented along [001] direction, keeping the cleavage plane in the vertical to prevent breaking during growing. Oriented seeds were obtained by nucleation on platinum wire, followed by crystallographic orientation and cutting. A resistive furnace equipped with a 2416 Eurotherm microprocessor-based digital temperature controller unit attached to a Pt-Pt10%Rh thermocouple was used, presenting temperature stability better than 0.2 °C and axial temperature gradient above the melt of about 30 °C/cm. The growth system is equipped with a pure platinum seed holder controlled by an accurate pulling and rotation system. All runs were carried out in air and the pulling and rotation rates were kept constant in each experiment during the entire process, being the furnace temperature adjusted to control the crystal diameter.

2.2. Characterization

X-ray diffraction (XRD) analyses were carried out on a Shimadzu XRD-6000 diffractometer using CuK radiation (step size 0.02° and 5 s counting time), and for Rietveld refinement the software GSAS [11] was used. Differential thermal analysis (DTA) and thermogravimetric analysis (TG) were performed in a Shimadzu DTG-60H. Optical transmission spectra were measured in a PerkinElmer Lambda 1050 spectrophotometer. Electron micrograph and microanalysis were carried out on a Jeol JSM-6610 scanning electron microscope (SEM) equipped with an energy dispersive X-ray spectrometer (EDS). Holograms were recorded using direct λ = 532 nm laser beams in the experimental setup schematically shown in Fig.1.

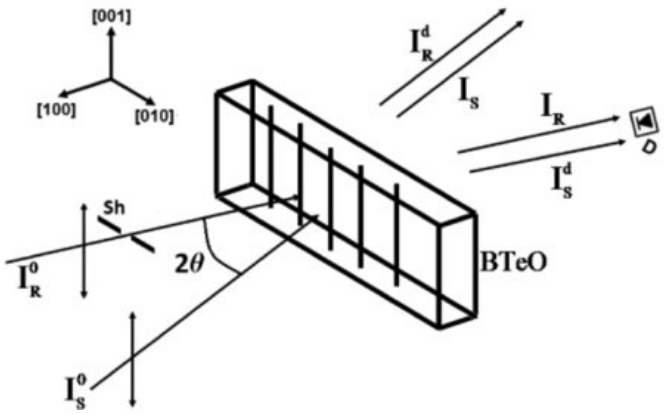

Figure 1 - Schematic illustration of the recording setup: BTeO is the crystal, I_S^0 and I_R^0 are the two recording beams, the former one referred to as the "signal beam" and the latter as the "reference beam", I_S^d is the diffracted signal beam that is measured using the photodetector *D*, once the incident reference beam is cut off using the shutter *Sh*.

3. Results

Using the experimental conditions described above crystals were grown at different pulling and rotation rates, ranging from 0.1 mm/h to 0.8 mm/h and from 5 to 20 rpm, respectively. The use of the lower pulling rates proved unsuitable because of the long time required for crystal growth and the resulting problems in maintaining the melt composition. On the other side, the use of the higher rates favored the occurrence of defects like voids and inclusions. Such defects can originate from constitutional supercooling effects close to liquid/crystal interface because the differences in melt and crystal compositions, the first is richer in TeO_2, and the low axial thermal gradient. An intermediate pulling rate of 0.3 mm/h showed the best results.

In order to minimize the probability of cleavage during crystal growth, it was tried the use of low rotation rates. But rates less than 10 rpm was not sufficient to ensure liquid homogeneity close to the surface, unlike a stagnant layer with composition deficient in TeO_2 was formed. This layer enveloped the crystal as it grew, solidifying as a polycrystalline cape around it, as shown in Figure 2. The black drawn lines in that figure separate the bulk of crystal and the cape, whose microstructure shows the grain boundaries typical of polycrystalline ceramics, as can be seen by the SEM micrograph in the insert. The Te/Bi ratio measured by SEM/EDS is 0.33 in the cape, below the value of 0.50 for the crystal. The formation of an opaque layer at the outer surface of BTeO crystal, maybe with a similar origin, was also reported in ref. [8]. In our case the combination of double crucible to minimize the loss of TeO_2, and a 15 rpm rotation rate was effective to suppresses this defect.

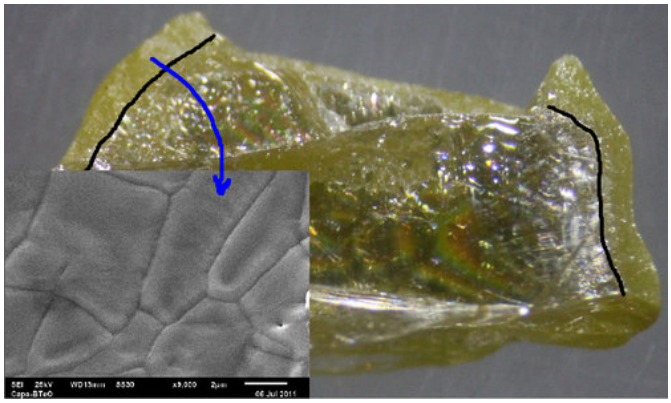

Figure 2 - Image of cleaved BTeO crystal showing the formation of polycrystalline cape due stagnant layer deficient in TeO_2. The ratio of Te/Bi in that layer is 0.33 as measured by SEM/EDS, below the expected value of 0.50 for the crystal. Insert: micrograph of the cap revealing the microstructure characteristic of ceramics grain boundaries.

The furnace with low axial temperature gradient was preferred in order to perform the crystals growth closer to the equilibrium condition, favoring their structural perfection, and reducing the chance of damage due thermal stresses. The use of double crucible system proved to be effective in maintaining the melt composition near the stoichiometric one, enabling the growth of crystals at low pulling rates up to 10 days. Single crystal grown by the double crucible method using pulling rate of 0.3mm/h and 15 rpm rotation speed is shown in Figure 3(a), as-grown, presenting a very uniform pale yellow color. Figure 3(b) shows polished samples used for the optical measurements; they are free of macroscopic defects like voids, inclusions or sources of stress birefringence. X-ray powder diffraction combined with Rietveld refining confirmed the orthorhombic structure of crystals, see Figure 4, with calculated cell parameters a = 11,582(1) Å, b = 16,450(1) Å, and c = 5,522(1) Å, in good agreement with refs. [2, 10]. DTA/TG analyses show no occurrence of phase transition in the interval from room temperature to melting point, and confirmed the melting temperature as being T_m= 905 ± 5 °C. Thermogravimetric curve shows a strong loss of mass associated to evaporation of TeO_2 above the melting point. In ref. [5] is pointed out that BTeO crystals present a wide range of optical transparency. This was confirmed by our optical transmission measurements carried out in a crystal with 0.4 mm thickness in the [100] direction, which showed a transmittance greater than 50% in the range of 450 nm to 2500 nm. The optical band gap of BTeO was calculated from the plot of $(\alpha hv)^2$ *versus* hv being E_g = 3.1 eV.

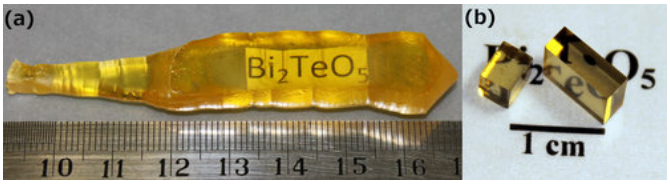

Figure 3 -(a) As-grown BTeO crystal using de double crucible method; (b) Polished samples used for the optical measurements.

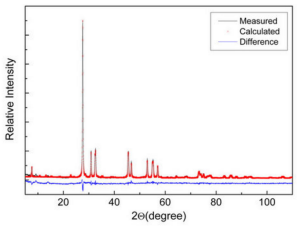

Figure 4 - X-ray powder diffraction of BTeO crystal with Rietveld refining.

The grown BTeO crystal was shown to exhibit excellent properties as optical recording material. Holograms were recorded for 2 min with different total intensity beams (both recording beams of roughly similar intensity) and then erased using one of the recording beams. Hologram erasure curves displayed in Figure 5 show the typical behavior of hole-electron competition with holes and electrons being photoexcited from different photoactive centers in the crystal. The first fast growing part of the curves represents the erasure of the fast (presumably electron-based) hologram that puts into evidence the presence of the slower (presumably hole-based) hologram, where the maximum shows the point where the faster hologram has been completely erased and the erasure of the slower one, at a much slower rate, becomes evident. The peak in these curves approximately represents the maximum diffraction efficiency of the recorded slower hologram, that is roughly the same

than that of the faster one in this case, once both seem to be roughly compensated (that is, of similar value) at starting of erasure.

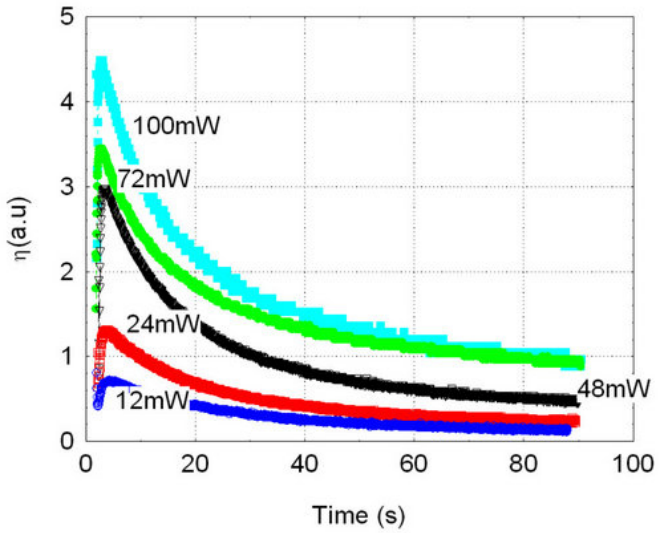

Figure 5 - Erasure, using one of the recording beams, of holograms being recorded with two λ = 532 nm beams of roughly similar intensities during 2 min, with different total beams intensities, always with a grating vector value K = 13 μm^{-1}. The peak of the curve with the highest laser intensity roughly represents a diffraction efficiency η ≈ 50% and that for the lowest intensity is η ≈ 30%.

4. Conclusion

In this work we successfully demonstrated that the use a double crucible approach, with tellurium oxide excess in the outer one, is adequate to minimize the effects of TeO_2 evaporation during the crystal growth of BTeO. This was combined with the use of a furnace with low axial thermal gradient, in searching for a good compromise between low crystal pulling rates, to improve the structural quality of the crystals, and reduced rotation rate, to minimize the risk of crystal crack during growth. By this way, homogeneous and defect free crystalline samples were obtained and our results confirmed its adequacy for holographic recording.

Acknowledgments.

We acknowledge the financial support from Conselho Nacional de Desenvolvimento Científico e Tecnológico (CNPq), the Coordenação de Aperfeiçoamento de Pessoal de Ensino Superior (CAPES), the Fundação de Amparo à Pesquisa do Estado de Goiás (FAPEG), Fundação de Amparo à Pesquisa do Estado de São Paulo (FAPESP), and Fundo de Apoio ao Ensino, Pesquisa e Extensão da Universidade Estadual de Campinas (FAEPEX).

Bibliography

[1] W. Horn, I. Földvári and C. Denz, Journal of Physics D: Applied Physics 41 (2008) 224006.
[2] Kang Min Ok, N. S. P. Bhuvanesh, P. Shiv Halasyamani, Inorganic Chemistry 40 (2001) 1978.
[3] G. Mandula, L. Kovács, Á. Péter and E. Hartmann, Optical Materials 1 (1992) 161.
[4] B. Frit, M. Jaymes, G. Perez, P. Hagenmuller, Revue de Chimie Minérale 8 (1971) 453.
[5] I. Földvári, Á. Péter, R. Voszka, Journal of Crystal Growth 100 (1990) 75.
[6] Senlin Fu, Hiroyuki Ozoe, Journal of Materials Processing & Manufacturing Science 10 (2001) 107.
[7] Hongbing Chen, Rongsheng Li, Congxin Ge, Xiang Ge, Wei Xu, Journal of Crystal Growth 281 (2005) 303.
[8] S. Kumaragurubaran, D. Krishnamurthy, C. Subramanian, P. Ramasamy, Journal of Crystal Growth 209 (2000) 855.
[9] Á. Péter, O. Szakács, I. Földvári, L. Bencs, A. Munoz F, Materials Research Bulletin 31 (1996) 1067.
[10] D. Mercurio, M. El Farissi, B. Frit, P. Goursat, Materials Chemistry and Physics 9 (1983) 467.
[11] A.C. Larson, R.B. Von Dreele, General Structure Analysis System (GSAS), Los Alamos National Laboratory Report LAUR 86-748 (2000).

15:00 Oral

Magnetic and optical properties of $Li_{0.28}Na_{1.72}Ge_4O_9$:Cr, Mn (0.1mol%) single crystals

Slawomir M. Kaczmarek[1], Taiju Tsuboi[3], Yoshio Nakai[3], Marek Berkowski[2], Grzegorz Leniec[1], Anna Leniec[1]

1. *West Pomeranian University of Technology, Szczecin (ZUT), Szczecin 70-310, Poland* **2.** *Polish Academy of Sciences, Institute of Physics, al. Lotników 32/46, Warszawa 02-668, Poland* **3.** *Department of Materials Science and Engineering, Kyoto University, Kyoto 606-8501, Japan*

e-mail: skaczmarek@zut.edu.pl

$Li_{0.28}Na_{1.72}Ge_4O_9$:Cr (0.1mol.%) and $Li_{0.28}Na_{1.72}Ge_4O_9$:Cr, Mn (0.1mol%, 0.1mol.%) (LNG) single crystals have been prepared by Czochralski method. They were investigated by electron paramagnetic resonance (EPR) and photoluminescence (PL) in a temperature range of 3-300 K. EPR signal from Cr^{3+} ions shows at least two magnetically nonequivalent centers and some features characteristic of dissimilar ion pairs transitions (chromium and sodium), that are found from roadmap at high magnetic fields (over 4000 Gs) in limited range of angles. Manganese ion enters as divalent ion and reveals different locations. The area in roadmap where dissimilar pairs transitions are located is split in a case of Mn codoped crystal.

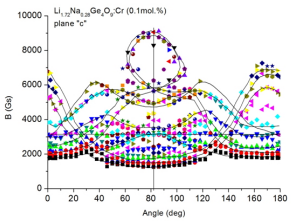

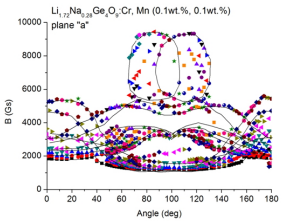

PL spectra show two bands centered at about 425 nm and 695 nm, which are attributable to chromium ions in disordered matrices. Co-doping with Mn^{2+} leads to energy transfer to chromium ions. The maximum of PL for LNG:Cr, Mn is about 20 times higher than that for chromium only doped crystal.

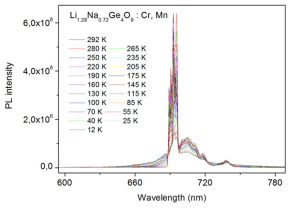

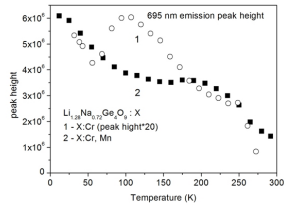

15:15 Oral

New $Ca_{10}Li(VO_4)_7$ laser host: growth and properties

Alexey N. Shekhovtsov[1], Myron B. Kosmyna[1], Viacheslav M. Puzikov[1], Boris N. Nazarenko[1], Wojciech Paszkowicz[2], Akram Behrooz[2], Przemysław Romanowski[2], Anatoliy S. Yasukevich[3], Nikolay V. Kuleshov[3], Maxim P. Demesh[3], Wojciech Wierzchowski[4], Krzysztof Wieteska[5], Carsten Paulmann[6]

1. *Institute for Single Crystals NAS of Ukraine (ISC), 60 Lenin Ave., Kharkov 61001, Ukraine* **2.** *Polish Academy of Sciences, Institute of Physics, al. Lotników 32/46, Warszawa 02-668, Poland* **3.** *Belarussian National Technical University (BNTU), F. Skariny, 65, Minsk 220027, Belarus* **4.** *Institute of Electronic Materials Technology (ITME), Wólczyńska 133, Warszawa 01-919, Poland* **5.** *National Centre for Nuclear Research, Radioisotope Centre POLATOM (NCNR), Andrzeja Soltana 7, Otwock-Świerk 05-400, Poland* **6.** *HASYLAB at DESY, Notkestr., Hamburg 22607, Germany*

e-mail: shekhov@isc.kharkov.ua

The unique combination of physical-chemical properties of the vanadate crystals makes them promising hosts for active elements of diode-pumped high-efficient CW, Q-switched and mode-locked lasers. The particular advantages of these materials are high thermal conductivity, chemical stability, low lasing threshold, and high lasing efficiency. The stimulated emission cross section of Nd^{3+} is much larger than that of YAG:Nd crystal.

Disordered calcium vanadates with trigonal structure are attractive materials for non linear optics because of efficient second harmonic generation [1]. Moreover disordered calcium vanadates are promising hosts for diode pumping lasers. The $Ca_{10}Li(VO_4)_7$ vanadate was chosen for investigations of crystal growth and laser application abilities.

A solid state synthesis was carried out to produce $Ca_{10}Li(VO_4)_7$ compound. For the growth process, an automatic "Analog" puller equipped with a weight control system was used. Cylindrical crystals of diameter up to 25 mm and length up to 50 mm were grown from a [001] oriented seed by the Czochralski technique. The pure crystals were of yellow colour, whereas Nd doped crystals were lilac.

The crystal structure of $Ca_{10}Li(VO_4)_7$ single crystal was determined by the powder diffraction method. Defect structure of crystal was studied with the use of both, high-resolution diffraction using a laboratory instrument and X-ray topographic techniques employing synchrotron radiation at the Hasylab laboratory (Hamburg).
Polarized absorption and luminescence spectra of Nd doped $Ca_{10}Li(VO_4)_7$ crystal were investigated in details. Spectral and temporal characteristics of Nd^{3+} luminescence associated with $^4F_{3/2} \rightarrow {}^4I_{9/2}$, $^4I_{11/2}$ and $^4I_{13/2}$ transitions were studied. At Nd^{3+} doping the laser oscillation was obtained under flash lamp pumping. The slope efficiency of 0.87% was achieved in the free-running mode. The ways of lasing efficiency increasing are discussed.

15:30 Oral

Growth and piezoelectric properties of gallium-free langasite structure crystal $Ca_3NbAl_3Si_2O_{14}$

Yanqing Zheng, Jun Xin, Kainan Xiong, Xiaoniu Tu, Haikuan Kong, Erwei Shi

Shanghai Institute of Ceramics, Chinese Academy of Sciences, 1295 Dingxi Road, Shanghai 200050, China

e-mail: zyq@mail.sic.ac.cn

Piezoelectric crystals with langasite structure were broadly used in high temperature sensors in recent years. The high content of gallium made these crystals much more expensive compared than quartz. A bulk single crystal of gallium-free compound $Ca_3NbAl_3Si_2O_{14}$ (CNAS) with langasite structure was successfully grown by Czochralski technique. The CNAS was in strong growth habits with the dimensions of 10 mm in thickness, 25 mm in width and 45 mm in length. The piezoelectric properties of CNAS were forecasted by first-principle calculation. The density measure by Archimedes method is 3.28 kg/m^3. High-resolution X-ray diffraction (HRXRD) results indicate that CTAS crystals are free of low-angle boundaries. The whole set of piezoelectric, elastic and dielectric tensors were tested by the resonance method. The piezoelectric constant d_{11} is -4.69 pC/N and d_{14} is 3.57 pC/N. The dielectric constant ε_{11} is 13.28 and ε_{33} is 17.7. The electromechanical coefficient k_{12} is 14.7% and k_{26} is 17.2%. The comparison of experimental and theoretical results shown that the first-principles is a good tool for searching novel piezoelectric crystals. Combined with the properties of the high resistivity under high temperature, CNAS is a good candidate for high temperature application.

15:45 Oral

Bulk Growth $ZnGeP_2$ crystals and their Study by X-Ray Topography

Galina A. Verozubova[1], Alexey Okunev[2], Chunhui Yang[3], Andrey Y. Trofimov[1]

1. *Insitute of Climatic and Ecological Systems of SB RAS (IMCES), 10/3 ave Akademicheskii, Tomsk 634055, Russian Federation* **2.** *Novgorod State University, ul. B. St. Petersburgskaya, 41, Veliky Novgorod 173003, Russian Federation* **3.** *Harbin Institute of Technology (HIT), No.92, West Da-Zhi Street,Harbin, Heilongjiang, Harbin 150001, China*

e-mail: verozubova@mail.tomsknet.ru

$ZnGeP_2$ (ZGP) crystals are used as a high effective nonlinear optical medium for laser radiation frequency conversion in the middle IR. They are also promising for creation of tunable terahertz radiation sources. Application in nonlinear optical devices demands from crystals a high structural perfection and uniformity of properties. A presence of two volatile components, Zn and P, in $ZnGeP_2$ structure makes difficult it's high-yield synthesis and causes deviations of the melt composition from stoichiometry during synthesis and growth, what leads to emergence of point and other growth defects.

The aim of this contribution is to present results of our studies on synthesis, growth and structural defects in ZGP crystals, revealed by X-Ray transmission topography based on Borrmann effect and other methods.

ZGP compound was synthesized from elements by two-temperature method. Vertical Bridgman method was used to grow the single crystals 24-45 mm in diameter. Typical broadening of the rocking curves (FWHM) is 13-35 seconds of arc what shows a high crystal structural perfection. At that FWHM is larger in the center of the cross-section of crystals than that on periphery, what is apparently related with concave interface during growth. Presumably, the defects are accumulated in the center because of the interface concavity as it was demonstrated by K. Sangwal and K.W. Benz.

X-Ray topography reveals edge and screw dislocations, inclusions of second phases of different types and composition. Some of the inclusions (so-called solute trails) give dislocations with powerful impurity atmospheres. But, as a rule, coherent microdefects of second phases are the primary in our ZGP. Their density is varied from $1x10^2$ cm^{-2} ($1.4 x10^3$ cm^{-3}) to $5x10^2$cm^{-2} ($7x10^3$ cm^{-3}). The inclusions of vacancy

type are met in 8 times more often than the inclusions of interstitial type. Such microdefects as dislocation loops amount less than 2% from the total ones. In all studied crystals growth striae, having concave shape (type I), are observed. A contrastive analysis of optical transmission microscopy and X-Ray topographs allows to assume that striae are related to variations of Zn vacancy concentration, giving a high absorption in ZGP near fundamental absorption edge (~0.65 mkm), as it was shown by American scientists. With perpendicular directions of diffraction vector **g** (the reflection planes are parallel to growth axis (case 1) or reflection from planes, perpendicular to growth axis (case 2)) the X-Ray topographs from the same sample are different. In the first case the striation is not seen, but rectilinear dislocations inclined or located along the growth axis and microdefects are seen. For the second case (**g** is parallel to growth axis) conditions of observation of growth striae are realized with maximal contrast. Here the dislocations are also seen. However, a washout of dislocation images in so- called "special position" and absence of dislocation images in case 2, seen on the topograph, obtained with perpendicular direction of diffraction vector **g** (case 1) are strange. This can be related to features of chalcopyrite lattice of ZGP. The center of cross cuts of single crystals contains dislocations with big edge component of the Burgers vector and their rows, they are perpendicular to the sample surface. The periphery of the cross plates has dislocations, giving a black and white contrasts, with a big screw component of the Burgers vector and crossing the samples approximately orthogonally. The dislocation density is decreased from the origin of the ingot to it's end from $2x10^3$ cm^{-2} to $2.5x10^2$ cm^{-2} on average.

Thermal annealing and electron irradiation allows us to decrease the optical absorption at 2.06 mkm (the main wavelength for optical parametric oscillation from ZGP) from 0.5 to 0.02 cm^{-1} that allows to use our ZGP in powerful optical systems.

Posters WePo
Wednesday afternoon, 14 August, 16:00

Break
Wednesday afternoon, 14 August, 17:30

Thursday, 15 August

ThO1

T06: Oxides and halides including laser and nonlinear optical applications
Thursday morning, 15 August, 10:20
Mickiewicz Hall, Auditorium Maximum

10:20 Invited oral

Flux growth and characterization of PLZST relaxor antiferroelectric single crystal with MPB composition

Qiang Li[1], Yuanyuan Li[1], Yiling Zhang[2], Jinghan Gao[1], Fangping Zhuo[1], Qingfeng Yan[1], Xiaoqing Xi[2], Xiangcheng Chu[2]

1. *Department of Chemistry, Tsinghua University, Beijing 100084, China* **2.** *State Key Laboratory of New Ceramics and Fine Processing, Tsinghua University, Beijing 100084, China*

e-mail: qiangli@mail.tsinghua.edu.cn

The Pb (Zr, Sn, Ti)O_3 family of perovskite antiferroelectrics, modified with La, has attracted much attention in recent years because of its high electric-field-induced longitudinal and volume strains close to the morphotropic phase boundary (MPB) between the antiferroelectric tetragonal [AFE] and ferroelectric rhombohedral [FE] phases.[1,2] However seldom learned its electrical and optical properties while polarized from AFE to FE phase. In order to understand the influence of phase structure and domain on the transition and polarization behaviors, La doped antiferroelectric Pb(Zr, Sn, Ti)O_3 (PLZST) single crystals with MPB composition have been grown by an optimized flux method in our lab.[3] PbO-PbF_2-B_2O_3 is proved more effective for growing lead-based perovskite crystals than formal PbO-B_2O_3 flux. PbF_2-evaporation-dependent was considered as the result of larger size PLZST single crystal growth in PbO-PbF_2-B_2O_3 flux system. Mass loss and growth produces investigations indicate that the compositions of as-grown crystals are strongly influenced, but can be adjusted by changing the ratio of starting materials. Domain structure of PLZST single crystal, with MPB composition, is studied by in situ polarized light microscope (PLM) at various P/A & different temperature. Wavelength-dependent optical transmission spectrum analysis, from 0.2 to 12.0 μm, indicates that as-grown PLZST single crystal exhibits a higher optical transmittance from the ultraviolet to near infrared region. The broader optical transparency region in PLZST crystal suggests that it can be introduced as a promising optical crystal in antiferroelectric devices.

Reference

1. 1.Nengneng Luo, Yuanyuan Li, Zhiguo Xia and Qiang Li, ***CrystEngComm***, 14(2012), 4547–4556.

2.Yuanyuan Li, Qiang Li, Qingfeng Yan, Yiling Zhang, Xiaoqing Xi, Xiangcheng Chu and Wenwu Cao**,Appl. Phys. Lett.**, 101 (2012), 132904152.

3.Zi Yang, Qiang Li, Yuanyuan Li, Shaofeng Zhang and Lin Wang, **J. Mater. Sci.,** 47(2012), 8007-8012

10:50 Oral

Flux growth of highly Yb^{3+}-doped cubic Gd_2O_3 laser crystals

Matias Velazquez[1], Philippe Veber[1], Gabriel Buse[1], Emmanuel Véron[2], Daniel Rytz[3], Frédéric Druon[4], Sylvie Janicot[4], Stanislav Péchev[1], Oudomsack Viraphong[1], Marwan Abdou-Ahmed[5], Thomas Graf[5], Patrick Georges[4]

1. *Institut de Chimie de la Matiere Condensée de Bordeaux, ICMCB - CNRS, 87 avenue du Dr Albert Schweitzer, Pessac 33608, France* **2.** *CEMHTI, 1D avenue de la Recherche Scientifique, Orléans 45071, France* **3.** *Fee-GmbH, Struthstrasse 2, Idar-Oberstein 55743, Germany* **4.** *Laboratoire Charles Fabry de l'Institut d'Optique (LCFIO), Univ. Paris Sud, 2, Avenue Augustin Fresnel, Orsay 91127, France* **5.** *Institut für Strahlwerkzeuge (IFSW), Universität Stuttgart, Pfaffenwaldring 43, Stuttgart 70569, Germany*

e-mail: matias.velazquez@icmcb-bordeaux.cnrs.fr

Developing large laser grade cubic rare-earth sesquioxides (RE_2O_3, RE=Sc,Y,Lu) single crystals doped with Yb^{3+} ions stands as one of the most challenging endeavours of today's crystal growth [1,2], essentially because of the high melting point of these compounds (~2400-2500 °C) and, in some of them, a series of structural phase transitions occurring upon cooling. Recent studies on cubic RE_2O_3 single crystals have demonstrated the laser potential of these materials and highlighted the extreme thermodynamic conditions in which their growth takes place [1-3]. In 2010, a successful power scaling of a passively mode-

locked femtosecond thin-disk laser was achieved with $Lu_2O_3:Yb^{3+}$ crystals which delivered an average power of 141 W under diode pumping at 976 nm [4]. In 2011, it is an impressive 670 W output power that was obtained in CW regime also using thin disk technology [5]. Several methods have been put forward these last three years to grow pure and RE'^{3+}-doped (RE'=Tm, Er or Yb) cubic RE_2O_3 (RE=Y, Lu or Sc) single crystals [2,6-8]. In this work, we will present Yb^{3+}-doped Gd_2O_3 single crystals of the cubic phase, with dimensions 6X5X1.4 mm^3, which were recently grown by a newly designed high-temperature solution growth method [6] and characterized by means of X-ray diffraction, Fourier transformed infrared (FTIR) spectroscopy, electron probe microanalysis (EPMA) coupled with wavelength dispersive spectroscopy (WDS). Our method uses an original and nontoxic solvent with a growth setup design operating in air and at half the melting temperature of rare-earth sesquioxides. The high-temperature solution growth conditions will be discussed. Because of the closeness of the sursaturation temperature of the new solvent used for the growth and that of the monoclinic-cubic phase transition temperature, the latter was completely revisited by means of high-temperature powder X-Ray diffraction. Our data evidence the temperature spreading from ~1200 to 1300°C as well as the strongly hysteretic nature of this first-order phase transition. They illustrate the benefit of using the $Li_6Gd(BO_3)_3$-based solvent in order to stabilize directly the cubic polymorph of Gd_2O_3. Indeed, cubic Gd_2O_3 contracts isotropically and less than its metastable monoclinic polymorph, the thermal contraction of which remains anisotropic from 1250°C to room temperature. The case of cubic $Gd_2O_3:Yb^{3+}$ is particularly interesting since its basic spectroscopic and laser properties have never been detailed and we were capable of achieving doping levels as high as 14 % (=$Gd_{1.72}Yb_{0.28}O_3$, that is, an Yb^{3+} concentration of 3.6 10^{21} cm^{-3}). Such a concentration proves to be much more off the experimental lifetime optimum resulting from the antagonistic effects of self-trapping and concentration quenching but it will permit to reduce the thickness of the crystal down to a few hundred microns, allowing for an efficient cooling while maintaining a high absorption yield under thin-disk laser operation. In this presentation, we will emphasize that this flux growth process allows for achieving optimal doping for high-power laser applications, impedes the dissolution of OH^- groups in the crystals, avoids the reduction of Yb^{3+} ions into Yb^{2+} ones (and its resulting absorption bands around 600, 520 and 480 nm [9]), favours broader absorption and emission bands. Such an inhomogeneous broadening, as well as anti-Stokes emission spectra, will be discussed within the scope of an exhaustive and complete chemical analysis of the samples by GDMS. We will highlight the fact that the 5-4 transition peaks at 1074 nm in the cubic form of Gd_2O_3, hence reducing the quantum defect with respect to the classical monoclinic Gd_2O_3 crystals, in which this transition is shifted at ~1105 nm [10]. Finally, these uncoated new Yb^{3+}-doped cubic Gd_2O_3 crystals have been succesfully tested in different laser cavities under Ti:sapphire and diode pumping. Under diode pumping at 977 nm, the maximum achieved laser power is 1.4 W in Qcw regime and 0.27 W in cw regime. For this high doping level, the laser emission was at 1076 nm.

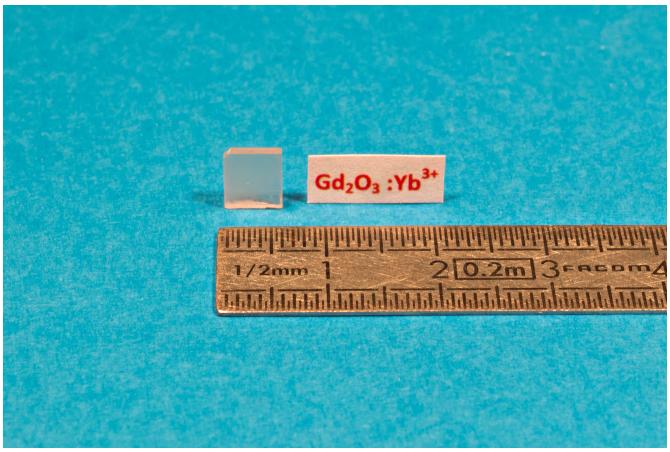

Figure 1 : a typical cubic $Gd_{1.72}Yb_{0.28}O_3$ single crystal grown by our new flux method.

[1] A. Yoshikawa and V. Chani, MRS Bulletin, 34 (2009) 266.

[2] A. Fukabori, V. Chani, K. Kamada, F. Moretti and A. Yoshikawa, Cryst. Growth & Des., 11 (2011) 2404.

[3] R. Peters, C. Kränkel, K. Petermann and G. Huber, J. Cryst. Growth, 310 (2008) 1934.

[4] C. Baer, C. Kränkel, C. J. Saraceno, O. H. Heckl, M. Golling, R. Peters, K. Petermann, T. Südmeyer, G. Huber and U. Keller, Opt. Lett., 35 (13) (2010) 2302.

[5] B. Weichelt, K. Wentsch, A. Voss, M. Abdou Ahmed, Th. Graf, Laser Phys. Lett., (2012) 110–115.

[6] Ph. Veber, M. Velázquez, V. Jubera, S. Pechev and O. Viraphong, Cryst. Eng. Comm. 13 (16) (2011) 5220.

[7] C. McMillen, D. Thomson, T. Tritt and J. Kolis, Cryst. Growth & Des., 11 (10) (2011) 4386.

[8] A. Fukabori, V. Chani, K. Kamada, A. Yoshikawa, J. Cryst. Growth, 352 (2012) 124.

[9] V. Peters, *Growth and spectroscopy of Ytterbium-doped sesquioxides*, PhD thesis, University of Hamburg, Germany, (2001).

[10] L. Laversenne, Y. Guyot, C. Goutaudier, M.-Th. Cohen-Adad, G. Boulon, Opt. Mater., 16 (2001) 475.

11:05 Oral

Growth and characterization of $YAl_3(BO_3)_4$ single crystal

Simon Ilas[1], Alexandra Szemjonov[1], Pascal Loiseau[1], Gérard Aka[1], Takunori Taira[2]

1. *Ecole Nationale Supérieure de chimie de Paris (ENSCP), 11 rue P. et M. Curie, Paris 75005, France* **2.** *Institute for Molecular Science (IMS), 38 Nishigonaka, Myodaiji, Okazaki 444-8585, Japan*

e-mail: simon.ilas@gmail.com

Yttrium aluminum borate (YAB) is a potential candidate for UV applications especially at 266 nm. Many flux can be used to growth YAB: Li_2O-B_2O_3, Li_2O-B_2O_3-Al_2O_3, Li_2WO_4-B_2O_3. Here the flux La_2O_3-B_2O_3 is presented. Several undoped and Yb doped single crystals were grown. Physical parameters such as: thermal coefficients, absorption coefficent, refractive index and phase matching angles were determined. Moreover 14 % conversion efficiency from 532 to 266 nm were obtained using a YAB single crystal of 3 mm length.

The yttrium aluminum borate $YAl_3(BO_3)_4$ (YAB) is a very promising nonlinear material for UV applications. YAB crystallizes in the space group R_{32}. Its structure is built from $[BO_3]^{3-}$ anionic groups. This material is currently widely studied because of its great potential for UV generation. In fact, it has a lot of good properties such as large NLO coefficient, moderate birefringence and good physical and chemical stability. The intrinsic UV cut-off wavelength was reported to be 160 nm. Nevertheless, one of the drawbacks is the hindered transparency of YAB crystals below 300 nm. Fe^{3+} ions can enter in the structure in substitution of Al^{3+} and cause some very efficient charge-transfer transitions between 300 and 200 nm. Moreover, the crystal growth is not well mastered yet. Because of its non-congruent melting, YAB crystals have to be grown using a flux. Many flux can be used: Li_2O-B_2O_3 [1], Al_2O_3-Li_2O-B_2O_3 [2], Li_2WO_4-B_2O_3 [3].
We present here the study of the flux La_2O-B_2O_3. Several undoped and Yb doped crystals with weight of 15-20 g were obtained by cooling under air the melt in the temperature range: 1150 °C - 1100 °C. The average thermal expansion coefficients were determined: $\alpha_1 = 4{,}3.10^{-6}\ K^{-1}$ and $\alpha_3 = 1{,}23.10^{-6}\ K^{-1}$. The absorption coefficient at $\lambda =$ 266 nm is $\alpha \cong 2{,}9\ cm^{-1}$. Measurement of refractive index and phase matching angle were determined. The environement of Yb^{3+} is studied by EPR and FTIR spectroscopy to evaluate the crystal quality. Moreover, crystals were cut in ZX plane for Type I SHG (532 --> 266 nm) (Fig. 1). 14 % conversion efficiency was obtained using a YAB single crystal of 3 mm length. The infrared source emits 1,6 mJ/pulse with a pulse duration of 500 ps at a frequency of 100 Hz. A 10 mm long type-I LiB_3O_5 (LBO) was used to obtain green power.

Fig. 1: YAB single crystal cut in the ZX plane for 266 nm generation

[1]X. Yu et al, Journal of Crystal Growth, 312, 3029–3033 (2010)
[2]J. Yu et al, Journal of Crystal Growth, 341, 61-65 (2012)
[3]H. Liu et al, Materials Research Innovations, 15, 102-106 (2011)

11:20 Oral

Impurity control of $CsLiB_6O_{10}$ for improving UV-induced damage tolerance

Kei Takachiho[1,2], Masashi Yoshimura[1,2], Kazuki Masuda[1,2], Yoshinori Takahashi[1,2], Mamoru Imade[1], Takatomo Sasaki[1,2], Yusuke Mori[1,2]

1. *Osaka UNIV., Yamadaoka 2-1, Suita 565-0871, Japan* **2.** *Core Research for Evolutional Science and Technology, Japan Science and Technology Agency (CREST-JST), Chiyoda-ku, Tokyo 102-0075, Japan*

e-mail: takachiho@cryst.eei.eng.osaka-u.ac.jp

$CsLiB_6O_{10}$ (CLBO) is an excellent nonlinear optical crystal for generating high-power UV output with wavelengths below 300 nm. The deep-UV sources employed on CLBO have been prevalent for high-resolution inspection in the semiconductor manufacturing process. Laser-induced damage of crystals is one of critical issues for scaling the UV power. We confirmed that UV output degradation and beam distortion in CLBO occurred at a lower peak power density than the bulk laser-induced damage threshold (LIDT) [1]. In this study, we report on impurity control of CLBO for improving UV-induced degradation resistance.

Al-doped CLBO crystals were grown from 0.5 mol% Al_2O_3- and 10 mol% LiF-added stoichiometric melt by the solution-stirring top-seeded solution growth method. The addition of a fluoride component was used to decrease the solution viscosity. High-quality single crystal with the size of $79\times36\times22\ mm^3$ was obtained by the LiF flux solution. The concentration of Al incorporated into the crystal was about 10 wt ppm. On the other hand, the water impurities in a CLBO sample significantly degrade its UV optical properties and the bulk LIDT [2]. Therefore, prior to experiment, the water impurities in Al-doped and undoped CLBO samples were reduced by post-growth heat treatment at 150 ^oC in ambient and dry atmosphere.

We evaluated UV-induced degradation in CLBO. Figure 1 shows a schematic of the experimental setup for measuring degradation induced by UV pulses. UV beam (wavelength: 266 nm; peak power density at the focal point: $56\ MW/cm^2$) was tightly focused at the center of CLBO sample to observe the degradation behavior in a short time. The transmitted power through the aperture after the sample was measured to detect the UV-induced degradation that occurred near the focal point in CLBO. Figure 2 shows a typical result obtained for undoped and Al-doped CLBO samples. Pattern distortion occurred after UV illumination for a while, and the transmitted power then decreased gradually. As is the case with the bulk LIDT [2], the UV-induced degradation resistance was significantly improved by eliminating water impurities from the crystal. The more important result is that Al-doping of CLBO can slow down UV-induced degradation. We will discuss about properties of Al-doped crystals and the degradation phenomena in detail.

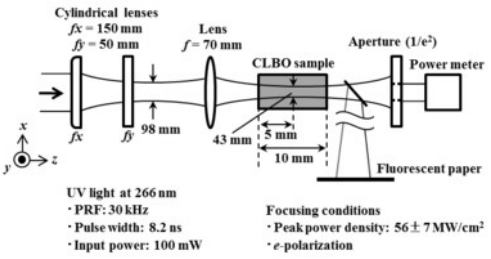

Fig. 1. Schematic of the experimental setup for measuring degradation induced by UV pulses.

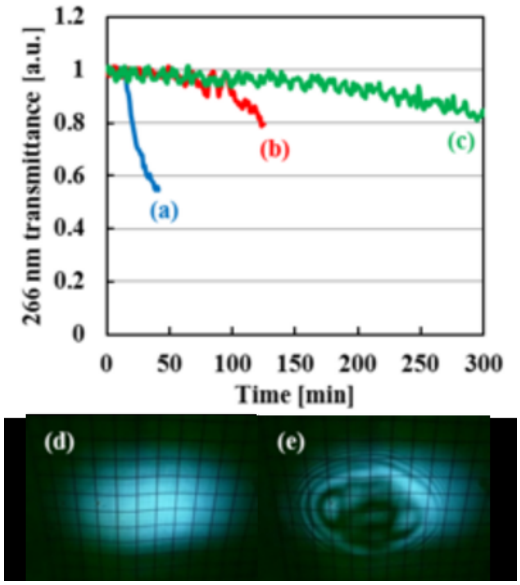

Fig. 2. Top: 266 nm transmitted power degradation through CLBO sample at 150 °C and aperture. (a) Undoped CLBO before dehydration, (b) undoped CLBO after dehydration, and (c) Al-doped CLBO after dehydration. Bottom: (d) Initial and (e) distorted transmitted UV beam through CLBO. The images were observed on fluorescent paper in the far-field.

Rererences

[1] K. Takachiho, M. Yoshimura, Y. Fukushima, Y. Takahashi, M. Imade, T. Sasaki, and Y. Mori, Appl. Phys. Express **6** (2013) 022701.

[2] T. Kawamura, M. Yoshimura, Y. Honda, M. Nishioka, Y. Shimizu, Y. Kitaoka, Y. Mori, and T. Sasaki, Appl. Opt. **48** (2009) 1658.

11:35 Oral

Growth and Characterization of $(Bi_{0.5}Na_{0.5})_{1-x}Ba_xTiO_3$ ($x \leq 0.1$) single crystals

Michael Woll[1], Manfred Burianek[1], Detlef Klimm[2], Semen Gorfman[3], Manfred Muehlberg[1]

1. *University of Cologne, Institute of Crystallography, Greinstr. 6, Köln 50939, Germany* **2.** *Leibniz Institute for Crystal Growth (IKZ), Max-Born-Str 2, Berlin 12489, Germany* **3.** *Universität Siegen, Adolf-Reichwein Str., Siegen 57068, Germany*

e-mail: michael.woll@uni-koeln.de

$Bi_{0.5}Na_{0.5}TiO_3$ (BNT) and $(Bi_{0.5}Na_{0.5})_{1-x}Ba_xTiO_3$ (BNBT) belong to the group of actively investigated materials, which crystallize in a perovskite-type structure and show a number of interesting physical properties.

One of the most interesting features of BNBT is the morphotropic phase boundary (MPB) in the range of about x=0.055 where both ferroelectric and piezoelectric properties are strongly enhanced. Therefore BNBT is a potential candidate to replace lead containing perovskites such as PZT, PZN-PT, PMN-PT, etc.

BNT crystallizes at T=1290°C. The high-temperature phase BNT is described by the structure of a cubic symmetry (space group). Upon cooling BNT undergoes two phase transitions at ~580°C to the tetragonal (P4bm) phase and at ~320°C to the rhombohedral R3c (now discussed to be monoclinic Cc [1]).

Inside the binary systems Bi_2O_3-TiO_2 and Na_2O-TiO_2 there are a lot of different compounds, so that a very complex three-component BNT system can be expected. The knowledge about the phase diagram of BNT is essential for the synthesis of large and defect reduced crystals. The phase diagram is largely unexplored in BNT and BNBT, therefore first thermoanalytical data was gathered with DSC/TG-measurements. Both BNT and BNBT show a congruent melting behavior according to DSC-data, so a decreasing liquidus curve in the direction of higher Bi_2O_3 and Na_2O content can be expected.

BNBT single crystals of different compositions (x=0.055, x=0.07 and x=0.1) were grown by Top Seeded Solution Growth (TSSG) method in dimensions up to 16x16x4 mm^3 using congruent melt composition. The growth process was initiated by supercooling of approximately 5K. This near equilibrium crystal growth led to crystals with a {100} habitus. The crystals chemical compositions were determined by electron microprobe analysis showing significantly lower Ba-content than melt content.

Contrary to BNBT, BNT single crystals were obtained using a flux composition with an excess of 10 wt%. of Na_2O and Bi_2O_3, lowering the melt temperature about 15K.

Both BNT and BNBT crystals were also obtained using µ-PD-method for the first time.

The phase transition sequence was investigated using heating cooling microscopy and optical birefringence microscopy. The deviations of the results from the literature data will be discussed in the poster.
Citations

[1] Gorfman, S., Glazer, A. M., Noguchi, Y., Miyayama, M., Luo, H., & Thomas, P. (2012). Observation of a low-symmetry phase in Na0.5Bi0.5TiO3 crystals by optical birefringence microscopy. *J. Appl. Cryst. 45* , pp. 444-445.

11:50 Oral

Morphology of a polar twin structure in Czochralski grown α-SrB_4O_7 crystals

Alexandre I. Zaitsev[1,2], Aleksandre V. Cherepakhin[1,2], Nikita V. Radionov[1], Anatolii V. Zamkov[1]

1. *L.V.Kirensky Institute of Physics Siberian Branch of the Russian Academy of Science (IPH SB RAS), Academgorodok, 50, Krasnoyarsk 660036, Russian Federation* **2.** *Siberian Federal University (SFU), 79 Svobodny Prospect, Krasnoyarsk 660041, Russian Federation*

e-mail: az@iph.krasn.ru

In the last years a number of investigations devoted to the creation of a regular polar twin structure in nonferroelectric crystals have appeared [1, 2]. The abilities of the structures for obtaining deep UV region optical radiation by the second harmonic generation (SHG) with quasi-phase-matching (QPM) in quartz and $Li_2B_4O_7$ have been shown. Orthorhombic α-SrB_4O_7 crystals with a short fundamental edge close to 120 nm, high damage resistivity and chemical stability, as well as sufficiently high optical nonlinearity [3, 4, 5] have been shown to be attractive candidates for the same role [6,7].

The arrangement of a polar twin structure in Czochralski grown α-SrB_4O_7 crystals has been investigated by the preparation of several cross-sections and subsequent etching in a nitric acid solution.

The crystals have been growing mainly with the seeds oriented in [100] direction (space group being $Pmn2_1$). The formation of the twin structure has been observed to be located exceptionally on one side away from the seed in the direction of the polar axis [001]. This direction is conditionally named “minus” direction because the plane (001)

on this side is robust for etching unlike the analogous plane from the other side which has the etching rate which is two orders of magnitude higher. It is established that a complicated structure of microtwins appeared in the growth pyramids (101) growing in the "minus direction" (see Fig 1).

The microtwins appear as uneven, wavelike sheets parallel to the plane (010) (see Fig 2). The observations of several crystals show that their average extensions along the axes [100] and [001] are up to 20 μm and 200 μm correspondingly, while their extension along the axis [010] is quite uniform and comprises about 1 μm.

It is also seen that if a microtwin happens to run across the boundary between the growth pyramids (101) and (100), its subsequent shape drastically alters. From its intersection point, this twin expands infinitely into the growth pyramids (100) and (101) along the axes [101] and [100] respectively, forming a plain layer (henceforth "plain twin") with a constant extension along the axis [010]. Such multiple plain twins compose a laminated structure with twin boundaries parallel to the plane (010). As opposed to the original microtwins, the plain twins can extend along the axis [010] from sub-micron values to several hundreds of microns. The dimensions, planarity and thickness stability of each individual plain twin are the features favorable for organizing QPM conditions for NLO doubling of high aperture beams.

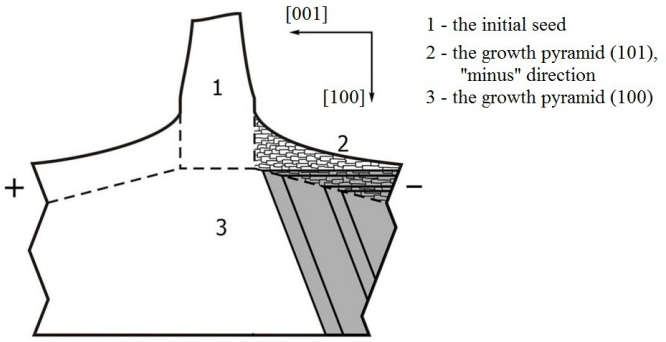

Fig. 1. The arrangement of a polar twin structure in α-SrB_4O_7 crystal. View direction is [010].

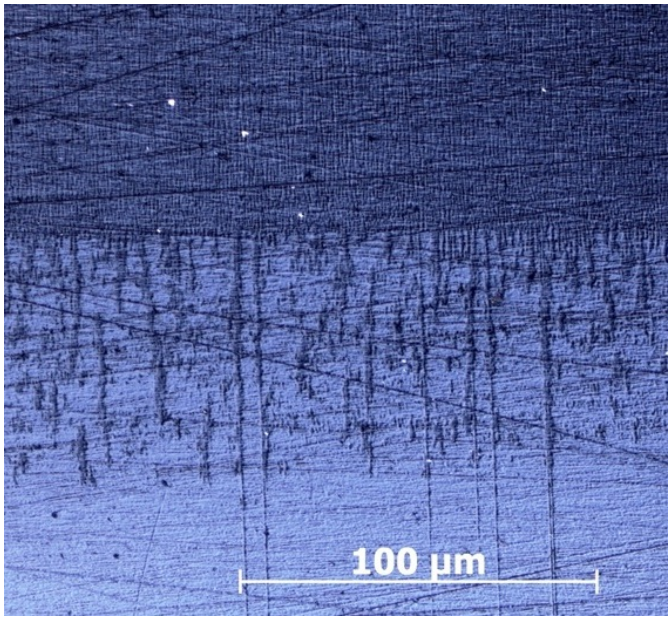

Fig. 2. The "minus" (001) cross-section. Boundary between the growth pyramids (101) with the microtwins and (100) with a few plain twins.

Acknowledgements: This study is supported by PSB RAS Project 2.5.2, by Grant of the President of the Russian Federation for the support of leading scientific schools SS-4828.2012.2 and by RFBR Grant 11-02-00596-a.

References

1. S. Kurimura, M. Harada, K. Muramatsu, M. Ueda, M. Adachi, T. Yamada, and T. Ueno. Quartz revisits nonlinear optics: twinned crystal for quasi-phase matching // Optical Materials Express. – 2011. - V. 1, No. 7. – pp. 1367-1375.

2. Kensaku Maeda, Satoshi Uda, Kozo Fujiwara, Jun Nozawa, Haruhiko Koizumi, Shun-ichi Sato, Yuichi Kozawa, and Takahiro Nakamura. Fabrication of quasi-phase-matching structure during paraelectric borate crystal growth // Applied Physics Express – 2013. - No.6. - pp. 015501-1 - 015501-3.

3. Oseledchik Yu.S., Prosvirnin A.L., Pisarevskiy A.I., et al. New nonlinear optic crystals: strontium and lead tetraborates // Optical Materials. – 1995. – V. 4. – pp. 669-674.

4. Petrov V., Noack F., Shen D., Pan F., Shen G., Wang X., Komatsu R., Alex V.. Application of the nonlinear crystal SrB_4O_7 for ultrafast diagnostics converting to wavelengths as short as 125 nm // Optical Letters. – 2003. –V. 29, No. 4. – pp. 373-375

5. Zaitsev A.I., Aleksandrovskii A.S., Zamkov A.V., Sysoev A.M.. Nonlinear optical, piezoelectric, and acoustic properties of SrB_4O_7 // Inorganic Materials. – 2006. – V. 42, No. 12. – pp. 1360-1362

6. Aleksandrovsky A.S., Vyunishev A.M, Zaitsev A.I., and Slabko V. V. Random quasi-phase-matched conversion of broadband radiation in a nonlinear photonic crystal // Phys. Rev. A – 2010. – V. **82. –** p. 055806.

7. Aleksandrovsky A.S., Vyunishev A.M., Zaitsev A.I. Applications of random nonlinear photonic crystals based on strontium tetraborate // Crystals. – 2012. - V.2., No.4. – pp.1393 - 1409.

12:05 Oral

Impact of incorporation of TiO_2 and Al_2O_3•nH_2O metal oxide nanoparticles on bulk properties of KDP crystals

Igor M. Prytula[1], Marina I. Kolybaeva[1], Anna Kosinova[1], Olga N. Bezkrovnaya[1], Viacheslav M. Puzikov[1], Valentin Tkachenko[1], Maksim Kopylovsky[2], Mykhaylo Brodyn[2], Vladimir Gayvoronsky[2]

1. *Institute for Single Crystals NAS of Ukraine (ISC), 60 Lenin Ave., Kharkov 61001, Ukraine* **2.** *Institute of Physics NAS of Ukraine, pr. Nauki 46, Kiev 03680, Ukraine*

e-mail: pritula@isc.kharkov.ua

Ferroelectric single crystals (SCs) of the KDP family are characterized by a unique set of properties, such as a wide range of optical transparency, nonlinear, electrooptical and piezoelectric effects. However, one of the main shortcomings of KDP SCs is its relatively low quadratic susceptibility. A possible way to increase this susceptibility and, subsequently, the efficiency of the three-wave processes is by altering its structure through a formation of nanocomposite medium. Nanoparticles (NPs) incorporation into the KDP matrix was realized in order to design novel lasing media.

In the present work, the impact of titanium dioxide (anatase, TiO_2) and aluminium oxyhydroxide (Al_2O_3•nH_2O, NOA) metal oxide NPs on growth process, optical and structural properties of KDP single crystal was was determined by several complementary methods: transmission and scanning electron microscopy, Uv-vis-IR spectroscopy, EDAX, FTIR, measurements of nonlinear optical (NLO) response.

It is found that the incorporation of TiO_2 NPs (C = 10^{-5} –10^{-3} wt.%) into the crystal matrix is accompanied with insignificant lowering of the growth rate. X-ray diffraction analysis shows that TiO_2 NPs are captured preferentially by the pyramidal face. For KDP:TiO_2 crystals there was found a relative change of the crystal lattice parameter caused by incorporation of TiO_2 into the boundaries of the growth layers. It leads to formation of two-dimensional layered macroscopic structure KDP:TiO_2:KDP with spatial period 15-20 μm. High optical quality of the KDP:TiO_2 SCs was shown experimentally [1,2]. The effect of the NOA NPs on the growth kinetics of the crystal faces is investigated. The predominating interaction of the NPs with the {100} crystal faces is established. This is confirmed by an elevated NPs concentration in the {100} growth sector, the increase of the dead zone and the halfwidth of DRC exceeding the one of the {101} faces. The capture of the NPs by the {100} faces is shown to be realized through the formation of hydrogen bonds.

The presence of the metal oxide NPs in the crystal matrix caused the enhancement of the cubic NLO response and the sign change of the nonlinear refraction index of the composite system at picosecond pulses excitation at 1064 nm. The effect has been explained by giant NLO response of the anatase NPs due to the resonant excitation of their surface defect states under picosecond laser pulses. The enhancement of frequency conversion efficiency (~70%) was obtained in KDP:TiO_2 versus KDP SCs due to the internal self-focusing effect of the pumping beam caused by the giant cubic NLO response of the embedded NPs [3].

For the KDP:NOA SCs demonstrated the sign inversion and enhancement of the refractive nonlinear optical response relatively to nominally pure KDP matrix at the self-action of pulsed laser radiation of picosecond range (λ=1064 nm).

[1] I Pritula et al. Optical Materials 33 (2011) 623
[2] V Grachev et al. J. Appl. Phys.112 (2012) 014315I
[3] V Ya Gayvoronsky et al. Laser Phys. Lett. 10 (2013) 035401

Lunch (EMCG meeting)
Thursday afternoon, 15 August, 12:20

Posters

Monday, 12 August

MoPo-T06
Monday afternoon, 12 August, 17:00
Rooms 207, 211, Old Library

17:00 Poster Mo142

Features of YAG crystal obtaining by Czochralski method using Mo crucibles

Pavel Arhipov, Sergey Tkachenko, Mikhail Biatov, Oleg Sidletskiy, Sergey Vasyukov

Institute for scintillation materials of NAS of Ukraine (ISMA), Lenin avenue, 60, Kharkov 61158, Ukraine

e-mail: pavlentich@yandex.ru

Rare-earth doped $Y_3Al_5O_{12}$ (YAG) crystals are widely used as laser elements, scintillators, phosphors, etc. Ir crucibles and equipment is a substantial component of crystal cost at growth of high melting point crystals, for ex. by the Czochralski method. Obtaining of high-quality YAG crystals without using Ir is a relevant task. There are some experiments on YAG growth from Mo crucibles described in literature, however, characteristics of the obtained crystals are not so high owing to presence of admixtures and formation of coloration centers.

This work is devoted to possibility estimation of high-quality YAG crystal growth by the Czochralski method using Mo crucible, graphite-based heat insulation, and induction heating in Ar growth atmosphere. It is shown that YAG quality depends on quantity of admixtures and structure defects, which, in turn, are determined by growth conditions and atmosphere. Mechanism of Mo admixture trapping into melt and its impact on optical characteristics are determined; methods decreasing its concentration in crystals are elaborated. Carbon influence at melt stoichiometry and formation of coloration centers is estimated, and solutions providing decrease of its concentration are proposed.

YAG crystals with 30mm diameter and 150 mm length were grown, and their optical and luminescent characteristics (transmission, X-ray luminescence, photoluminescence spectra, thermoluminescence curves) were studied. Optimized conditions of post-growth annealing suppress formation coloration centers and provide crystal absorption ~2 cm^{-1} in visible band and < 5 $см^{-1}$ in UV band. These parameters are not worse than those in crystals grown using Ir crucibles. The obtained results show a possibility to obtain high-quality YAG-based crystals by Czochralski method without using high-cost Ir.

17:00 Poster Mo143

The effect of pure and mixed solvents on solute-solvent interactions, solubility and growth aspects of 4-aminobenzophenone

Veerabagu Natarajan[1], Mukannan Arivanandhan[2], Yasuhiro Hayakawa[2]

1. *Department of Physics, Aditanar College of Arts and Science,, Tiruchendur 628216, India* **2.** *Research Institute of Electronics, Shizuoka University, Johoku 3-5-1, Naka-Ku,, Hamamatsu 432-8011, Japan*

e-mail: arivucz@gmail.com

The NLO materials are playing an important role in generating the green and blue lasers by second harmonic generation (SHG) of frequency doubling of low frequency laser radiations. Organic nonlinear optical crystals are the current interest because of their high NLO efficiency and fast response than the inorganic NLO materials. Benzophenone and its derivatives are potential organic NLO material with good optical, mechanical properties, and non hygroscopic nature is a best alternate material for urea. Although 4-amino benzophenone (4-ABP) is one of the best derivatives of benzophenone with the SHG efficiency of 360 times larger than that of ADP, growth of high quality bulk crystal still remains as a difficult task. In this scenario, the effect of pure and mixed solvents on the growth aspects of 4-ABP was investigated to grow 4-ABP bulk crystals. Ethyl acetate, ethanol and acetone were chosen as solvents for the present investigation. Single crystals of 4-ABP were grown by slow evaporation method using the above solvents. In addition with the above solvents, ethanol and acetone (1:1) mixed solvent was used for the growth of 4-ABP crystal to study the effect of mixed solvent. Solvent inclusions were observed in particular growth faces which have relatively high growth rates. The structural, mechanical and optical properties of the grown 4-ABP were analyzed. The optical transmission study shows that the 4-ABP crystal has about 70 % transparency in the visible region and it has the cut off wavelength of 400 nm. The 4-ABP sample exhibits the SHG efficiency of 161 times larger than that of KDP.

17:00 Poster Mo144

Peculiarities of the crystal growth in the system of hexaferrites $Sr_3Co_2Fe_{24}O_{41}$ and $SrCo_xTi_xFe_{12-x}O_{19}$ by floating zone melting

Anatoly M. Balbashov[1], Marya E. Voronchikhina[1], Alexander A. Mukhin[2], Vsevolod Y. Ivanov[2], Ludmila D. Iskhakova[3]

1. *Moscow power engineering institute (MPEI), Moscow 111250, Russian Federation* **2.** *A.M. Prokhorov General Physics Institute of Russian Academy of Sciences (GPI), Vavilov Str. 38, Moscow 119991, Russian Federation* **3.** *Fiber Optics Research Center of Russian Academy of Sciences, Vavilov Str. 38, Moscow 119991, Russian Federation*

e-mail: balbashovam@mpei.ru

Hexaferrites with a cone magnetic structure attract recently a significant attention as new high (room) temperature magnetoelectric (ME) materials [1, 2]. We have attempted to grow single crystals of $Sr_3Co_2Fe_{24}O_{41}$ (Z-type) and $SrCo_xTi_xFe_{12-x}O_{19}$, x =1.5- 2 (M-type) hexaferrites.

The single crystals have been grown by floating zone (FZ) melting with light heating [3] from feed rods of stoichiometric compositions. All crystal growth processes were performed in pure oxygen under high pressure up to 80 atm in order to (a) prevent of Fe^{2+} ions arising due to high melting points of these compositions and (b) suppress of peritectic phase transformation [4]. Typical growth speed was 5 mm/h. Investigations of chemical composition were carried out by scanning electron microscope JSM 5910-LV (JEOL) with INCA ENERGY (Oxford Instruments). The XRD measurements were carried out using DRON-4-13 diffractometer (CuK_α-radiation, graphite monochromator).

Obtained crystals are the cylindrical rods about 6 mm in diameter and up to 60 mm in length. The true phase diagram of these compositions is not known, but one can assume the congruent melting and freezing are not take place. Therefore the seed crystallization is possible from float zone melt composition conformed to crystallization field of needed compounds. Really mentioned hexaferrites were grown using polycrystalline seeds, however, after beginning of crystal growth process the change of the melt composition occurred. Then the crystal growth of stoichiometric composition started as the growth from a high temperature solution like that for iron garnets grown by FZ [3]. After growth of initial part (~10 mm) of the crystal concurrent crystal blocks disappear and only single block crystal survives with hexagonal plane oriented along of growth axis.

Digital X-ray Laue analysis confirmed the good crystal quality of SrCoTi M-hexaferrite and X-ray microprobe did not reveal any other phases. The magnetic measurements revealed a strong anisotropy of magnetization along and perpendicular hexagonal c-axis and change of the easy direction from the c-axis to the basal plane with increasing x from 1.5 to 2.

For SrCo Z-hexaferrite the picture is different. On the microprobe image it was observed two phase structures: the composition of the main (dark) phase was identified close to $SrCoFe_{11}O_{19}$ and the minor number of precipitations of second (white) phase was identified as $Sr_4Fe_6O_{13}$. The main phase had the shape of rather large single crystalline platelets with a mirror surface looked on the boule cleavage. The platelets were directed along boule axis. Laue X-ray measurements revealed the hexagonal structure of the platelets with c-axis perpendicular to plane of platelets. A noticeable magnetic anisotropy confirmed the anisotropic contribution of the M - hexaferrite. The growth of these crystals evidently proceeds from the melt of non- stoichiometric composition. Therefore the crystal growth of this material on the crystalline seed is difficult and requires of a small growth speed.

1. Y. Kitagawa, et al., Nature Mater. **9**, 797 (2010).

2. L. Wang, et al., Sci. Rep. **2**, 223 (2012).

3. A.M. Balbashov, S.K. Egorov, J. Cryst. Growth, **52,** 498-504 (1981).

4. H.J. Van Hook, J.Am.Ceram. Soc. **47,** 579 (1964).

17:00 Poster Mo145

Studies on growth, characterization, thermal and dielectric properties of yttrium doped dysprosium phosphate crystal

Krishan K. Bamzai, Nidhi Kuchroo, Vishal Singh, Shivani Suri

CGMR Lab, Department of Physics, University of Jammu, Jammu 180006, India

e-mail: kkbamz@yahoo.com

Yttrium doped dysprosium phosphate with zircon structure was synthesized as single crystal at ambient temperature from aqueous solution using rare earth chloride, phosphoric acid and traces of ammonium hydroxides. The yttrium doping in dysprosium phosphate was about 2%. The prepared crystal was then anlaysed for their structural investigations using X-ray diffraction (XRD), energy dispersive X-ray anlysis (EDAX) and scanning electron microscopic (SEM) studies. X-ray studies establishes crystal belonging to tetragonal system with cell parameters as: a = b = 7.1208 Å, c = 6.8257 Å and $\alpha = \beta = \gamma = 89.99^0$. EDAX establishes all the constituent elements like yttrium, dysprosium, phosphorous and oxygen in the proportion as was expected for this composition. The theoretical atomic and weight percentage calculated on the basis of the formula $Y_{0.02}Dy_{0.98}PO_4xH_2O$ fits very well with the experimentally calculated values. SEM studies shows growth in the form of fibres. The spectroscopic investigations were done using Fourier tansformed infra-red spectroscopy which shows presence of various functional groups including the water molecules. Thermal behaviour was studied using thermo-gravimetric techniques like thermo-gravemtric analysis (TGA), differential thermal analysis (DTA) and differential scanning calorimetry (DSC). TGA shows that this material is thermally stable up to a temperature of 200^0C and then decomposition begins. The decomposition takes place in two different stages where in the phosphate gets converted in oxides. Solid state reaction kinetics for the two stages of the decomposition was studied using three models viz., Horowitz - Metzger, Coats - Redfern and Piloyan - Novikova. Using these three models various values like energy of activation (E), order of reaction (n) and frequency factor (Z) were calculated. The activation energy for the first stage of decomposition is higher as compared to the second stage, thus suggesting that the formation of by product in this stage is hard reaction. Electrical property in the form of dielectric constant (ϵ') was calculated for different temperature ranging of 40 - 500^0C in the frequency range of 10^2 - 10^3 kHz. The maximum value of ϵ' was found to 432 for 10 kHz at a temperature of 500^0C. The detailed results will be presented and discussed.

17:00 Poster Mo146

Growth and spectroscopic characteristics of 2.7-3 μm Er:GYSGG laser crystal

Jiakang Chen, Dunlu Sun, Renqin Dou, Jianqiao Luo

Anhui Institute of Optics and Fine Mechanics, Chinese Academy Sciences, Hefei 230031, China

e-mail: chenjiakang001@126.com

The high optical quality crystal of Er:GYSGG with a size up to Φ 30×100 mm was first successfully grown by the Czochralski method. The lattice parameter of Er:GYSGG is 12.5073Å and the Sellmeier

coefficients were fitted to be A=3.78681, B=0.01579 μm^2, C=2.72454 μm^2, D=0.08204 $(\mu m^2)^{-1}$, respectively. The absorption and fluorescence spectra of Er:GYSGG before and after 100 Mrad gamma-ray radiation have no obviously changed, and the irradiated crystal has a shorter lifetime of lower energy level than the crystal with no radiation. All the results suggest that Er:GYSGG is a promising material for 2.7-3μm wavelength laser gaining and its excellent ability of radiation resistance indicated that it can be used in radiant environments such as outer space

17:00 Poster Mo147

Growth and Characterization of $RbTiOPO_4$ Crystals for Electro-Optic Application

Jianrong Chen, Cunxin Huang

Research Institute of Synthetic Crystals, Beijing 100018, China
Beijing Sinoma Synthetic Crystals Co., Ltd., Beijing 100018, China

e-mail: chenjianrong@gmail.com

Electro-optic crystals have a wide variety of applications in modern optoelectronics and lasers technology, such as modulators, Q-switches, pulse-pickers, electro-optic deflectors so on. In comparison with other DKDP, $LiNbO_3$ and BBO crystals, Rubidium titanyl phosphate ($RbTiOPO_4$, RTP) is considered as a promising material, mainly due to large effective electro-optic coefficients, high optical damage threshold, very low Piezoelectric Ringing, which makes it especially suitable for the high repetition rate lasers.

In this paper, high resistivity 10^{11}-10^{12} W×cm RTP crystals with dimension up to 40´40´30mm were obtained using an optimized high [Rb]/[P] molar ration flux composition and concentration by improved TSSG method. In our opinion, the detrimental electrochromism, optical homogeneity and monodomain determine the performance for RTP electro-optic application. The detrimental electrochromism was not observed under a continuous 2500V/mm Z-directed electric field over more than 1000 hours. The experimental homogeneity and d33 coefficient measurement indicated that optical property and monodomain have the excellent results.

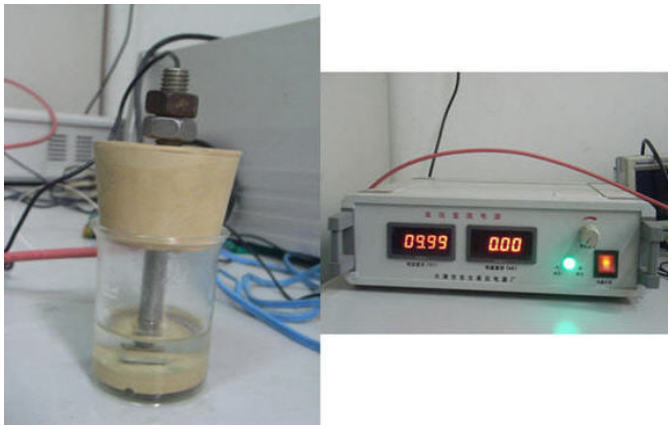

Fig 1. The 10000V/4mm electrochromic damage experiment for RTP crystal

The RTP Q-switch was built utilizing thermally compensated double-crystal designs. A series of electro-optic experiments, including half-wave voltage, contrast ratio, insertion loss, thermal stability, high repetition rate and so on, were extensively investigated. The results have proved that RTP crystals can be the good choice for the majority of Q-switching applications.

References

[1] E. Lebiush, R. Lavi, Y. Tsuk, N. Angert, A. Gachechiladze, M. Tseitlin, A. Zharov and M. Roth, Proc. of ASSL (Advanced Solid State Lasers), TOPS Vol. 34 (2000) 63.

[2] Tseitlin, E. Mojaev and M. Roth. Growth of high resistivity RbTiOPO4crystals.J. Cryst. Growth 310 (2008) 1929.

17:00 Poster Mo148

Growth and spectral properties of 5at%Yb :$GdNbO_4$ Crystal

Renqin Dou

Anhui Institute of Optics and Fine Mechanics, Chinese Academy Sciences, Hefei 230031, China

e-mail: drq0564@mail.ustc.edu.cn

A new Yb-doped niobate, 5at%Yb :$GdNbO_4$, has been grown by Czochralski method. The structures of Yb: $GdNbO_4$were determined by Retvield refine to their X-ray powder diffraction. Their diffuse reflection spectra, photo-luminescence spectra and lifetime at room temperature were measured and the corresponding energy level transitions were assigned, respectively. Then spectroscopic parameters of Yb: $GdNbO_4$ were calculated and compared with Yb: $YNbO_4$, Yb: $GdTaO_4$ and Yb:YAG. Results indicated that Yb: $GdNbO_4$ crystal is advantageous for tunable and ultrafast pulse laser output and will be a new promising Yb laser material pumed by LD.

17:00 Poster Mo149

Experimental investigation and crystal-field modeling of Er^{3+} energy levels in GSGG crystal

Jinyun Gao, Qingli Zhang, Dunlu Sun, Shaotang Yin

Anhui Institute of Optics and Fine Mechanics, Chinese Academy Sciences, Hefei 230031, China

e-mail: jygao1985@gmail.com

The Er^{3+}-doped $Gd_3Sc_2Ga_3O_{12}$ (Er^{3+}:GSGG) single crystal, a excellent medium of the mid-infrared and anti-radiation solid state laser pumped by laser diode, was grown by Czochralski method successfully. The absorption spectra was measured and analyzed in a wider spectral wavelength range of 350-1700 nm with different temperature points from low to room temperature (7.6 K, 77 K, 200 K and 300 K). The free-ions and crystal-field parameters were fitted to the experimental energy levels with the root mean square deviation of 8.69 cm^{-1}. According to the crystal-field calculations, 52 Stark energy levels of Er^{3+} in GSGG host crystals were assigned. The fitting results of free-ions and crystal-field parameters were compared with those already reported of Er^{3+}:YSGG. The results indicated that the free-ions parameters are similar to those of the Er^{3+} in GSGG and YSGG crystals, and the crystal-field interaction of GSGG is weaker than that of YSGG, which may result in the better laser characterization of Er^{3+}:GSGG crystal.

17:00 Poster Mo150

Obtaining of Inorganic Halids for Growing Single Crystals

Akhmedali Gasanov[1], Vasiliy Ancudinov[2], Elena Chuvilina[3]

1. *State Institute of Rare Metals (GIREDMET), B. Tolmachevsky per., Moscow 119017, Russian Federation* **2.** *Moscov Pover Engineering Institute, Krasnokasarmennaya 14, Moscow 11250, Russian Federation* **3.** *Lanhit-Ltd, B.Tolmachevskiy per 5, Moscow 119017, Russian Federation*

e-mail: gasanov@giredmet.ru

Anhydrous inorganic halides - chlorides, bromides, iodides - are widely used for growing single crystals for laser and scintillation technology. These compounds have high demands on purity despite the absence of the valid data on the dependence of the optical characteristics of materials obtained from the concentration of certain impurities in them are missing. Specialists in crystal growth for the most part cannot approach the task of content of specific "dangerous" elements, therefore, they formulate common requirements as "material 99,99% of metal (or rare earth) impurities". A separate problem is a difficult purification from carbon impurities, which is not defined in the analysis of the material, but makes the crystals opaque.

Using your own design or using certain specially improved the way we produce halides over 200 titles not in preparative quantities, and kilograms and tens of kilograms. To purify the resulting compounds, especially in cases of separation of pairs of similar properties halides, we use methods of distillation, sublimation, high-temperature distillation, directional solidification, zone melting.

Particular attention is paid to the interaction of inorganic halides with the air moisture. As s rule, the consumers tend to impose very strict requirements on the content of water, hydroxyl groups and oxygen, as the presence of oxyhalide phases are unacceptable. A majority of halides turn to stepped and irreversible hydrolysis in the presence of moisture. In addition, nearly all halides - hygroscopic substances, so besides the problem of **obtaining high-purity halides** must be addressed as the tasks of **delivering these substances to the consumer and the convenience of the practical use.**

Now we produce anhydrous halides in the form of nearly monodispersed fused spherical granules (beads). In our view, this type of material has clear benefits for the consumers: halides undergo stages of melting and filtering to prevent the ingress of solid particles of oxyhalide phases in the product, spherical shape minimizes the surface contact with the possible pairs of moisture during further using of the material; monodimension particles may easily and quickly be dosed. In particular, monodisperse granules metal halides can be effectively used in growing single crystals by the Czochralski method with the fueling of the material into the zone melting. We use the author's technique and equipment for granules.

The resulting overall purities of produced halides are between 99.9 and 99.9999%; organic impurities - less than 0,1-1 ppm; content of hydrolysis products, OH-group and water in “anhydrous” products is about 0,2-0,3%, in “ultra dry” products - 10-30 ppm.

17:00 Poster Mo151

Phase and Hydrothermal Growth of $Bi_4Si_3O_{12}$ Crystals

Xiaoling He, Hande Huo, Haitao Zhou, Mengde Ren, Changlong Zhang, Yanbin Zuo, Jinliang Wang

China Nonferrous Metal Guilin Geology And Mining Co., Ltd. (CNMC), Guilin 541004, China

e-mail: hxlpl@hotmail.com

Bi4Si3O12 (BSO) is an excellent scintillation crystal having heterogeneous isomorphism with the famous Bi4Ge3O12 (BGO) crystal[1]. BSO has three times as fast fast response time and better radiation hardness than BGO, apart from so better scintillaion properties, the cost of BSO crystal is lower than BGO because the cost of high purity GeO2 is higher than SiO2. In the past twenty years, BSO crystals’ growth was mainly researched by the Bridgman and the Czochralski methods. However, due to the much difference of the density and the melting point of Bi2O3 and SiO2, furthermore, the complicated phase relation of Bi2O3-SiO2, the growth process is difficult to control.

The hydrothermal method could result in a good optical uniformity and lower thermal stress in grown BSO because of its free growth environment and lower growth temperature, but there is no much effort made to grow BSO by hydrothermal method. To date, only a few reports about powder or aggregating BSO growth were made[2]. In this paper, the growth of BSO single crystal was studied by the hydrothermal method under the condition of sintered 2Bi2O3:3SiO2 as nutrient, NaOH aqueous as mineralizer. In this system, the phase diagram was studied firstly and the results show that there always exist two different phase (Bi4Si3O12 and Bi12SiO20) when the growth temperature between 380□ and 500□ and the concentration of NaOH aqueous between 1.5M and 4M. The single BSO phase was obtained through studying the influence of additional SiO2 doped in the mineralizer. BSO crystals with size larger than 8mm were produced. The FWHM of the X-ray rocking curve was 25 arcsec, and the absorption edge was 284nm. From the above results, it is proposed that high quality BSO crystals can be grown by hydrothermal method. Acknowledgement:This work was supported by Guangxi Natural Science Foundation (2012GXNSFAA053215).

* corresponding author e-mail: chnhhd@sina.com

References:

1. M. Kobayashi, K. Harada, Y. Hirose, M. Ishii, I. Yamaga. Large-size bismuth silicate (Bi4Si3O12) scintillating crystals of good quality, Nuclear Instruments and Methods in Physics Research. A 400, 392 (1997) 2. D. E. Kozhbakhteeva, N. I. Leonyuk. Hydrothermal synthesis and morphology of eulytite-like single crystals, Journal of Optoelectronics and Advanced Materials. 5, 621 (2003)

17:00 Poster Mo152

Float zone growth and spectral properties of Cr,Nd:YVO_4 single crystals for potential use in solar-pumped solid state lasers

Mikio Higuchi[1], Kazuki Kiyohara[1], Sho Namiki[2], Takayo Ogawa[2], Satoshi Wada[2]

1. *Hokkaido University, Sapporo 060-8628, Japan* **2.** *RIKEN, Wako 351-0198, Japan*

e-mail: hig@eng.hokudai.ac.jp

Solar-pumped solid state lasers are one of the promising systems to utilize the solar energy. In previous studies, Cr,Nd:YAG has been used as a gain medium; however, its spectral properties are not sufficient for efficient energy conversion. Nd:YVO_4 is known as an excellent gain medium for Nd-lasers because of excellent optical properties. In this study, we grew Cr,Nd:YVO_4 single crystals by the floating zone method and investigated their spectral properties.

A ceramic feed rod was prepared with a composition of $Y_{1-x-y}Cr_xNd_yVO_4$ where x=0.005-0.02 and Y=0.25-2. Single crystals were grown under conditions of growth rate: 10-20 mm/h, seed orientation: [110], atmosphere: air or O_2/N_2 mixed gas.

When the growth rate was 20 mm/h, the grown crystals showed green gradation parallel to the growth direction. Little gradation was observed for the crystal grown at 10 mm/h, but the green color was not so deep. These results imply that segregation and evaporation of Cr-component simultaneously occur during crystal growth. The most effective way to obtain a crystal with homogeneous Cr-concentration was to prolong the growth length more than 40 mm.

Cr,Nd:YVO_4 showed strong absorption in the wavelength region of 350-500 nm. Although the peak wavelength of 400 nm does not correspond to the solar radiation peak, the absorption coefficient of Cr,Nd:YVO_4 is significantly large in despite of relatively low Cr-concentration of less than 1 at%. The absorption cross section of Cr,Nd:YVO_4 at 430 nm, where Cr,Nd:YAG has the maximum absorption is about $33'10^{-20}$ cm^2, which is 4.7 times as large as that of Cr,Nd:YAG. By pumping at 400 nm, Cr,Nd:YVO_4 showed strong fluorescence band around 900 nm and 1060 nm by Nd^{3+}. No fluorescence band of Cr^{3+} was observed in the visible region, which implies that most of the energy absorbed by Cr^{3+} is effectively transferred to Nd^{3+}. These results demonstrate that Cr,Nd:YVO_4 single crystals are one of the promising materials for solar-pumped solid state laser systems.

17:00 Poster Mo153

Crystal growth of $CaGdAlO_4$ by Cz method

Qiangqiang Hu, Zhitai Jia, Xiuwei Fu, Yanru Yin, Jun Shu, Xutang Tao

e-mail: hqq514@yahoo.cn

$CaGdAlO_4$ (CGA) crystal with dimensions of Φ 30 × 30 mm^3 was successfully grown by the Czochralski (CZ) method. The $CaGdAlO_4$ crystal belongs to an isostructural family of crystals with the general formula $ABCO_4$, where A denotes Ca or Sr, B represents rare-earth ion, C is Al or Ga. In this structure, the C exists in slightly distorted octahedral sites stacked in layers perpendicular to the c-direction. In the layers, the divalent A and trivalent B cations reside in ninefold coordinated sites which have distorted C_{4v} Symmetry due to the random occupation of neighbouring sites by Ca^{2+} and Gd^{3+}[1]. It is a promising host material for ultrafast laser due to its disorder structure and high thermal conductivity.

The crystal growth was carried out in State Key Laboratory of Crystal Materials, Shandong University. The raw materials, including $CaCO_3$ and Gd_2O_3, and Al_2O_3, were accurately weighed according to charges of stoichiometric composition and adequately mixed, and then pressed into tablets with dimensions of Φ 50 × 60 mm^3. Afterwards, the tablets were sintered in air at 1350 °C for 45h before they were melted in an Ir crucible with a diameter of 60 mm and a height of 60 mm. An inert atmosphere of argon gas was adopted in order to prevent oxidation of the iridium crucible. After the crystal growth, a high quality CGA crystal along c-direction was grown.

Single crystal X-ray analysis was carried out on a Bruker SMART APEX-II equipped with CCD area-detector diffractometer at 296 K using graphite-monochromated Mo Kα radiation (λ = 0.71073 Å) with the f and w scans method. In addition, thermal properties including thermal expansion, specific heat, thermal diffusivity and thermal conductivity were investigated as a function of temperature. The transmission spectra and refractive indices were also measured.

References:

[1] Jon-Paul R Wells, Mitsuo Yamaga Nobuhiro Kodama andThomas P J Han

17:00 Poster Mo154

EPR and optical properties of $PbMoO_4$:Co single crystals

Slawomir M. Kaczmarek[1], Taiju Tsuboi[3], Yoshio Nakai[3], Marek Berkowski[2], Tomasz Skibiński[1], Grzegorz Leniec[1], Zbigniew Kowalski[1]

1. *West Pomeranian University of Technology, Szczecin (ZUT), Szczecin 70-310, Poland* **2.** *Polish Academy of Sciences, Institute of Physics, al. Lotników 32/46, Warszawa 02-668, Poland* **3.** *Department of Materials Science and Engineering, Kyoto University, Kyoto 606-8501, Japan*

e-mail: skaczmarek@zut.edu.pl

$PbMoO_4$:Co (0.2 mol. %, 0.5 mol.% and 1 mol.%) single crystals have been prepared by Czochralski method. They were investigated by electron paramagnetic resonance (EPR)and photoluminescence (PL) in a wide temperature range of 3-300 K. EPR investigations of oriented single crystal samples show clear signals with hyperfine structure due to Co^{2+} ions with a spin S=3/2, vanishing over 35 K. Temperature dependence of double integral of EPR signal obeys the Curie-Weiss law. Some discrepancies, however, are observed above5 K, suggesting the presence of internal magnetic fields due to e.g. clusters. It reveals low ferromagnetic interactions with Curie-Weiss temperature estimated as 1.8 and 2.8 K at 0.2 and 0.5 mol % Co up to 10K, respectively. Above 10K the magnetic phase changes to antiferromagnetic phasewith Curie-Weiss temperature of about -12 K.

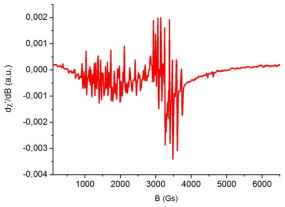

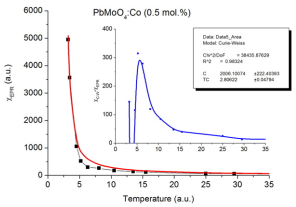

The PL spectra show a broad band in a range from 400 to 700 nm.

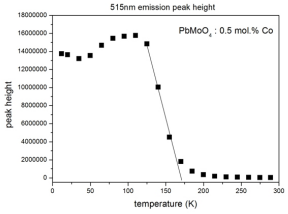

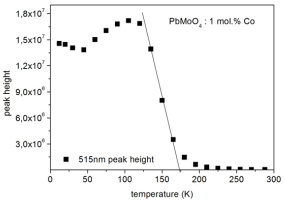

We observed blue PL emission due to electronic transitions within the isolated $[MoO_4]$ tetrahedron groups and green emission due to extrinsic transitions caused by the defects or impurities. Temperature dependence of PL spectrum shows ananomaly in a range of 100-200 K, indicating a structural phase transition at about 175 K.

17:00 Poster Mo155

Temperature dependence of PL and EPR spectra of $Sr_{0.33}Ba_{0.67}Nb_2O_6$:Cr (0.02mol.%) single crystals

Slawomir M. Kaczmarek[1], Taiju Tsuboi[3], Yoshio Nakai[3], Marek Berkowski[2], Grzegorz Leniec[1], Anna Leniec[1]

1. *West Pomeranian University of Technology, Szczecin (ZUT), Szczecin 70-310, Poland* **2.** *Polish Academy of Sciences, Institute of Physics, al. Lotników 32/46, Warszawa 02-668, Poland* **3.** *Department of Materials Science and Engineering, Kyoto University, Kyoto 606-8501, Japan*

e-mail: skaczmarek@zut.edu.pl

$Sr_{0.33}Ba_{0.67}Nb_2O_6$:Cr (0.02mol.%) single crystals have been prepared by Czochralski method. They were investigated by electron paramagnetic resonance (EPR) and photoluminescence (PL) in a temperature range of 3-300 K. EPR signal shows at least two magnetically nonequivalent centers and some features characteristic of dissimilar ion pairs transitions, that are found from EPR roadmap at high magnetic fields (over 4000 Gs).

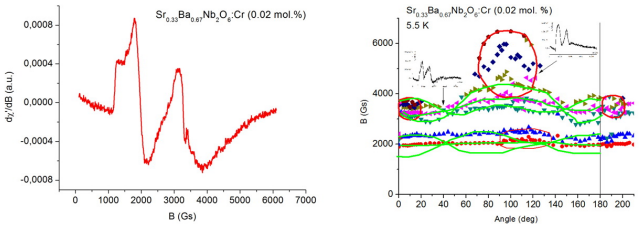

PL spectra reveal two separated bands centered at 544 and 766 nm, that are due to chromium ions in disordered matrices. The 544 nm broad band shows a little temperature dependence and has several sharp lines at high-energy side. The 766 nm band is sharp and the intensity dramatically decreases with increasing temperature up to 100 K.

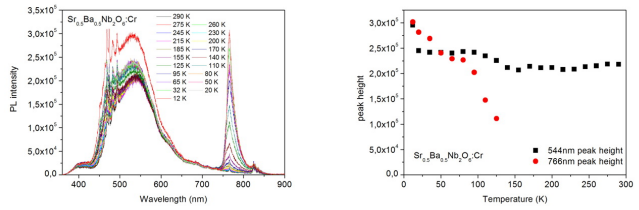

17:00 Poster Mo156

Growth and characterization of new nonlinear-optical crystal $Nd_xY_ySc_z(BO_3)_4$ (x+y+z=4)

Alexander E. Kokh[1], Nadegda G. Kononova[1], Mariya V. Fedorova[1], Dmitry Kokh[1], Alain Maillard[2], Regine Maillard[2]

1. *Institute of Geology and Mineralogy SB RAS (IGM), Koptyuga ave., 3, Novosibirsk 630090, Russian Federation* **2.** *LMOPS Lorraine Universit, Supelec, Metz 57070, France*

e-mail: a.e.kokh@gmail.com

Simple and complex rare-earth borates have been actively studied for the last few decades as possible active and nonlinear-optical media or as both in one crystal. Among the great number of published works we want to mention [1, 2], which consider the growth and study of yttrium-lanthanum-scandium borate with the chemical formula $Y_{0.57}La_{0.72}Sc_{2.71}(BO_3)_4$ – (LYSB). The authors report that they have found the composition at which stabilization of huntite – like non-centrosymmetrical structure with space group **R32** takes place. They had grown relatively large crystals from which samples for the analysis of quality and second-harmonic generation were made. The major problem they faced was the impossibility to grow a crystal of this composition with a high optical quality [3]. Therefore, its practical application is doubtful.

In the Institute of Geology and Mineralogy, Siberian Branch of the RAS, a procedure of solid-phase synthesis was used to synthesize compounds of similar composition and with identical X-ray patterns, replacing La cations by Ce, Pr, or Nd [4]. Spontaneous crystals containing Pr & Nd were grown using $LiBO_2$-LiF flux as a solvent. We did not succeed in growing Ce-bearing spontaneous crystals. In this paper we report on the progress in the growth of bulk Nd-bearing (NdYSB) crystals and study of their optical and nonlinear-optical properties. We can suppose that the chemical composition of NdYSB is similar to LYSB formula: $Y_{0.57}Nd_{0.72}Sc_{2.71}(BO_3)_4$.

To grow bulk crystals, we used the eutectic composition of the $LiBO_2$–LiF system with 59 mol.% $LiBO_2$ and eutectic temperature T=725ºC. The search for a flux was carried out among the studied diagrams of melting ability of systems based on borates and fluorides of alkali metals. The selected eutectic composition has a low viscosity, as LiF promotes the rupture of spatial bonds between borate groupings.

A crystal weighing 5.3 g was grown by the Kyropoulos procedure. The temperatuure interval of growth was 17 degrees, beginning from 900°C. The crystal distinctly displays the faces of rhombohedron and hexagonal prism. The grown crystals have a perfect cleavage on rhombohedron. The hardness of crystals is about 6 on the Mohs scale.

A 3.05 mm thick plate was cut and polished from the grown crystal with orientation 31 degrees to the optical axis on the assumption that the SHG (second harmonic generation) angle must be close to the angle of phase matching for LYSB (for which θ= 33.48 degrees, φ=0) [2]. The plate has transparent windows which are big enough for analyzing the optical quality and efficiency of SHG. The optical quality of the studied sample was higher than that of LYSB crystal. It was confirmed by the Schlieren method.

The SHG experiments evidence that the θ angle for type I phase matching is 34.8°. In continuous mode with a focused Gaussian beam we obtained P(ω)/P(2ω) = 1.9W/810 nW and 2W/460 nW for 43μm and 92μm waist size, respectively. That corresponds to calculated d_{eff} I (pm/V) 0.24 and 0.23, respectively without taking the absorption into account. In pulsed mode (repetition rate 1kHz, pulse width 90ns), we obtained 0.6W/614μW and 0.56W/310μW for the same beam waist sizes. The calculated transformation efficiency of the sample was found to be rather low, about 0.1%. At the same time, the qualitative pattern of transformation evidences the opposite: we observed intense green spots at the output.

NdYSB transmission measurements were conducted on the Perkin Elmer Lambda 900 device in the range of wavelength from 190 nm to 3200 nm. It is a typical Nd spectrum with a lot of absorption peaks in the 250-900 nm range. Transmission coefficient at 532 nm was only about 0.06. Transmission measurement on this sample in the experimental conditions of SHG yielded still lower transmission coefficient at 532 nm – 0.009.

As a next step we have decreased the thickness of example from 3.05mm to 0.88mm and repeated SHG experiment by 43μm waist size. In continuous mode we obtained P(ω)/P(2ω) = 2.75W/3.42μW. That

corresponds to calculated d_{eff} I = 0.91 pm/V without taking the absorption into account. This value increases to 2.5 pm/V if we take into account the 21cm^{-1} at 532nm and 0.2cm^{-1} at 1064nm absorption calculated with the differential transmission spectrum of two samples of 0.88 and 1.76mm.

Measurements have also been performed in a pulsed mode. For the maximum incident power 0.82W corresponding to the density of 156MW/cm^2 we have obtained about 0.5% efficiency. Apparently higher transformation efficiency can be achieved at a higher incident power. We can also predict an increase in the efficiency by thinning the sample thickness.

The laser properties of this crystal is under investigation.

References

1. N.Ye, J.L.Stone-Sundberg, M.A.Hruschka, G.Aka, W.Kong, and D.A.Keszler. Nonlinear optical crystal $Y_xLa_ySc_z(BO_3)_4$ (x+y+z=4). - Chem. Mater. 17(10), 2687–2692 (2005).
2. N.Ye, Y.Zhang, W.Chen, D.A.Keszler, and G.Aka. Growth of nonlinear optical crystal $Y_{0.57}La_{0.72}Sc_{2.71}(BO_3)_4$. - J. Cryst. Growth 292(2), 464–467 (2006).
3. M.Bourezzou, A.Maillard, R.Maillard, Ph.Villeval, G.Aka, J.Lejay, P.Loiseau, and D.Rytz. Crystal defects revealed by Schlieren photography and chemical etching in nonlinear single crystal LYSB – Optical materials express, 2011, Vol. 1, No. 8, pp. 1569-1576.
4. A.E.Kokh, N.G.Kononova, M.V.Fedorova, P.P.Fedorov, and M.N.Mayakova. New nonlinear optical crystals of the $M_{1-x}Sc_{3-y}Y_{x+y}(BO_3)_4$ (M=Ce, Pr, or Nd) family. – Doklady Physics, 2012, Vol. 57, No. 4, pp. 148-150.

The work was partly supported by grants 12-05-31028-mol and 12-02-01116-a from the Russian Foundation for Basic Research

17:00 Poster Mo157

Growth, optical and microstructural properties of PbB_4O_7 plate crystals

Alexandre I. Zaitsev[1,5], Alexander Aleksandrovsky[1], Lev Pokrovsky[2], Victor Atuchin[2], Konstantin A. Kokh[3,4]

1. *L.V.Kirensky Institute of Physics Siberian Branch of the Russian Academy of Science (IPH SB RAS), Academgorodok, 50, Krasnoyarsk 660036, Russian Federation* **2.** *Institute of Semiconductor Physics SB RAS, Lavrentjeva 13, Novosibirsk 630090, Russian Federation* **3.** *Institute of Geology and Mineralogy SB RAS (IGM), Koptyuga ave., 3, Novosibirsk 630090, Russian Federation* **4.** *Novosibirsk State University (NSU), Pirogov 2, Novosibirsk 630090, Russian Federation* **5.** *Siberian Federal University (SFU), 79 Svobodny Prospect, Krasnoyarsk 660041, Russian Federation*

e-mail: k.a.kokh@gmail.com

The noncentrosymmetric optical borate crystals are the basic materials of modern high-power laser systems because of appropriate nonlinear optical (NLO) coefficients, wide transparency window including visible and UV ranges and high optical damage thresholds. Orthorhombic lead tetraborate PbB_4O_7 (PBO) was discovered in binary system PbO-B_2O_3 many years ago. The crystal structure of PBO belongs to mm2 point group, space group being $Pmn2_1$. The PBO structure is formed by the rigid three-dimensional network of corner-linked BO4 tetrahedrons, and lead atoms occupy the large cages of the structure and are coordinated by nine oxygen atoms. PBO is a nonlinear crystal with rather large nonlinearity of the second order and large Raman-type nonlinearity of the third order.

The PbB_4O_7 single crystal has been grown from the melt by Czochralski method. The charge has been prepared from $2PbCO_3$•$Pb(OH)_2$ and H_3BO_3 taken with stoichiometric ratio. Crystal growth was performed in the air from a platinum crucible 50 mm in diameter and 70 mm in high with 300 grams of the charge. The seed oriented in [100] direction was used. The plate-like transparent, colorless PbB_4O_7 single crystal with dimensions 2×22×38 mm along [100], [010] and [001] directions correspondingly was grown after three days. The growth process included starting growth without pulling (the rotation rate was 8 rpm) during two days and growth with pulling rate 1.2 mm/day during one day. This crystal had several rather well developed facets; especially pronounced were the facets corresponding to the planes [100], [010] and [101]. From as grown crystal was cut off the sample which was subjected to etching in diluted nitric acid (5 weight %) at the temperature of 90°C during 10 minutes. A system of defects has been revealed by optical microscopy. Growth steps and boundaries of polar growth twins can be observed on as-grown surfaces. Etching of as-grown (100) surface revealed etching pits, being the dislocations outcrop onto the surface. The etching patterns observed on this surface reveal the stripes of different etching behavior that means the existence of twins, despite (100) is not a polar surface. Twin boundaries probably correspond to (010) planes, in accordance with isostructural crystal SBO. The twin boundary nature of observed stripes is admitted by the difference of etching pits symmetry in twin-free regions and twin boundaries.

Structural properties and micromorphology of etched PbB4O7(100) surface have been observed by RHEED using EFZ4 device at electron energy of 50 keV and AFM measurements performed with Solver P-47H device in noncontact mode, respectively. A system of Kikuchi lines has been recorded from PbB_4O_7 (100) surface.

Acknowledgements: This study is supported by SB RAS, Projects 28.13 and 43.12, and by PSB RAS Grant 2.5.2.

17:00 Poster Mo158

Growth and characterization of $KNbO_3$ plate crystal from liquid with stoichiometric composition by the μ-PD method

Ryuichi Komatsu[1], Naoki Masuda[1], Maki Ueda[1], Hironori Itoh[1], Kuniyuki Akishige[2]

1. *Yamaguchi University, 2-16-1 Tokiwadai, Ube 755-8611, Japan*
2. *Department of Materials Science, Shimane University, Matsue, Shimane, Japan, Matsue 690-8504, Japan*

e-mail: r-komats@yamaguchi-u.ac.jp

Potassium niobate ($KNbO_3$; KN) is a well-known ferroelectric material with a perovskite structure, discovered in 1949. There are reports of its physical properties, crystal growth, crystal structure, and other characteristics [1]. In addition, recently these crystals were found to have a high electromechanical coupling coefficient for surface acoustic waves (SAWs), which makes potassium niobate a promising material for next-generation elastic wave elements [2]. KN also has become a very promising candidate as a lead-free piezoelectric material since it was found that the coupling factors in the bulk acoustic wave (BAW) have very high values at optimum cuts [3]. This crystal has thus drawn much attention as an environmentally friendly material useable in SAW and BAW devices.

Potassium niobate is an incongruent melting compound in which $KNbO_3$ solid phase cannot coexist in equilibrium with liquid phase. Therefore, these crystals cannot be grown by the Czochralski (CZ) method used for lithium niobate and lithium tantalate. Instead, TSSG (Top-Seeded Solution Growth) using a liquid phase of $KNbO_3$ with excess addition of K_2O, or the Bridgman method are employed. However, these methods have problems such as contamination of the

crystal with flux, and cannot be used for mass production of large crystals. In addition, potassium niobate transitions from cubic crystals to tetragonal crystals at 435 °C, and to orthorhombic crystals at 225 °C. Because of these two phase transitions, single-domain processing after cooling is not easy, and multiple operations are required. Cracks and other problems occur in single-domain processing. As a result, single-domain processing of asgrown bulk crystals is presently difficult, even though large crystals could be grown at low cost. Thus, there are a number of problems to be solved for the growth of large $KNbO_3$ crystals.

There is another melt growth method in addition to CZ and TSSG, namely, fiber growth. In particular, the main methods of growing oxide crystal fibers are the laser heated pedestal growth (LHPG) method of Feigelson [4] and the micro-Czochralski method developed by Ohnishi and Yao [5]. Pulling-down offers better crystal quality and other characteristics than pulling-up, and thus the micro-pulling-down (μ-PD) method was developed. Many oxide crystal fibers have been grown by this method [6]. Chani et al. first reported the growth of potassium niobate crystal fibers from various liquid compositions by the μ-PD method [7]. Their study is noteworthy because it showed the possibility of growing potassium niobate single-phase fibers from a liquid with stoichiometric composition. However, the report does not include growth conditions and other details. It is very important to clear the growth conditions of KN fiber crystals from KN liquid by μ-PD method.

On the other hands, the cutting loss for the manufacturing devices is normally up to 60% of the initial weight of grown crystals by CZ method, and thus it may be remarkably useful to develop new method to grow crystals with rectangular plate with similar to the width and thickness of devices for the reduction of production cost. There also is a serious challenge for crystal growers to develop so-called shaped growth techniques offering ready-to use crystals with form similar to the devices dimensions.

Therefore, we have been investigating the growth of KN plate crystals with rectangular shape, similar to the device dimensions, from the melt with a stoichiometric composition. In this paper, we describe growth of plate-shaped KN crystal form by the μ-PD method from several liquid composition including a stoichiometric composition, and also characterization of grown plate KN crystals.

The μ-PD furnace used in this study is shown in Fig.1, and the platinum crucible with a rectangular nozzle at the bottom is shown in Fig. 2. We used a cylindrical platinum crucible with rectangular nozzle (5mm×1mm, height 2mm and 0.4 mm hole at a center), stabilizing the solid-liquid interface during the growth in order to keep the crystal shape uniformly. The growth furnace is of the resistance heating type. A voltage is applied to heat the platinum crucible (Fig. 2). KN crystal powder was used as the starting materials. The staring materials were melted in a crucible. A seed crystal was brought into contact with the melt drop at the nozzle and was then pulled down. The grown plate crystal was about 35mm long, about 1.5 mm thickness and about 4 mm width; it was colorless and striation was often observed. $K_4Nb_6O_{17}$ phase in grown crystals was also detected as the second phase in a high-temperature gradient. For a lower temperature gradient, a single-phase KN plate crystal was obtained as shown in Fig.3. Plate shaped KN crystal has been successfully grown form a stoichiometric melt.

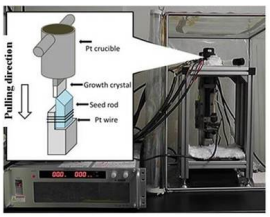

Fig. 1 Micro-PD furnace

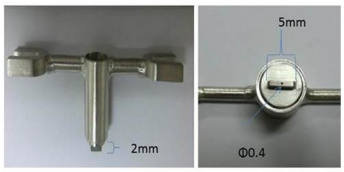

Fig.2 Pt crucible with rectangular nozzle

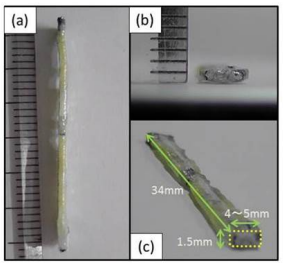

Fig.3 Grown plate KN crystal

According to the phase diagram of KN, potassium niobate should not deposit from a stoichiometric melt. The decomposition temperature of potassium niobate is, however, very close to the temperature at which all of its components melt, and thus it may be considered that potassium niobate may grow as a primary crystal from KN melt under strong supercooling in a lower temperature gradient. Large supercooling may be absolutely necessary for this crystal growth; in the case of the μ-PD method, the degree of supercooling can be set easily higher than in the CZ method and other conventional methods. Therefore, it appears possible that single-phase potassium niobate plate crystals could be grown from a stoi-chiometric melt using potassium niobate crystals as seed crystals by this method. This single-phase KN plate crystal also showed clear periodical striations. This periodic striations may be due to the periodical change of growth rate.

The temperature and frequency dependences of the permittivity and dielectric loss (during tempera-ture descent) are also measured. At temperatures below about 400°C, there is no variation in the measured temperature range, and tanδ is smaller than 0.1. When the temperature exceeds 400 °C, tanδ increases, and dielectric dispersion occurs. In addition, sharp increases in permittivity during temperature rise at 225 and 430 °C was observed, indicating phase transitions. The phase transition temperatures of KN crystals grown by Matthias and Remeika using the flux method [8] were 224 and 434 °C, respec-tively, which are close to the results of this study. The dielectric loss too is close to that of other bulk crystals.

In conclusions, the results of this study are summarized as follows.

(1) Single-phase KN plate crystal was successfully grown from KN liquid phase by the μ-PD method. Providing a lower temperature gradient and the large supercooling beneath the nozzle is necessary for reproducible crystal growth.

(2) The phase transition temperatures of the grown KN plate crystals agreed well with previously report-ed data, and sharp transitions were observed.

(3) In addition, domains structure in grown crystal and other issues of domain control will be also dis-cussed.

Reference

1. Matthias BT, Remeika JP. Phys Rev 1949;76:1886.
2. Yamanouchi et al., Electron Lett 1997;33:193–194.
3. Nakamuraet al., IEEE Trans Ultrason Ferroelect Freq Control 2000;47:750–755.
4. Feigelson RS. J Crystal Growth 1986;79:669–680.
5. Ohnishi N, Yao T., Jpn J Appl Phys 1989;28:L278–280.
6. Yoon DH, Fukuda T., J. Crystal Growth 1994;144:201–206.
7. Chani VI et al., Crystal Res Tech 1999;34:519–525.
8. Matthias BT, Remeika JP. Phys Rev 1951;82:727–729.

17:00 Poster Mo159

Analysis of dielectric properties of $PbMoO_4$:Nd and $PbWO_4$:Nd single crystals

Yuriy N. Gorobets, Myron B. Kosmyna, Boris N. Nazarenko, Viacheslav M. Puzikov, Alexey N. Shekhovtsov

Institute for Single Crystals NAS of Ukraine (ISC), 60 Lenin Ave., Kharkov 61001, Ukraine

e-mail: kosmyna@isc.kharkov.ua

Currently, $PbMoO_4$:Ndand $PbWO_4$:Nd single crystals are considered to be promising active media for Raman lasers, which combine lasing and conversion functions due to stimulated Raman scattering (SRS). Efficient SRS conversion calls for high pump densities. This circumstance imposes stringent requirements on the radiation resistance of SRS materials. The dependence of the optical breakdown of $PbMoO_4$:Nd and $PbWO_4$:Nd crystals on the neodymium concentration and the doping scheme was studied. It was established, that dielectric relaxation phenomenon in $PbMoO_4$:Nd and $PbWO_4$:Nd crystals depend on neodymium concentration and the doping scheme [1].

The $PbWO_4$:Nd and $PbMoO_4$:Nd single crystals were grown by the Czochralski method by the use of different doping scheme. Dielectric properties have been studied in the temperature range of 20–550°C at frequencies from 25 to 10^6 Hz. The activation energies of dielectric relaxation processes are determined for all crystals. The frequency dependence of tan δ for the $PbWO_4$:Nd and $PbMoO_4$:Nd crystals was analyzed in the frame of computer model for the substitution of the insulator under study using the equivalent electric scheme. The parameters of the substitution electric scheme for different temperatures were defined and analyzed. The doping mechanism of $PbWO_4$:Nd^{3+} and $PbMoO_4$:Nd^{3+} crystals was discussed too.

1. Yu.N.Gorobets, M.B.Kosmyna, A.P.Luchechko et. al. // Crystallography Reports, 2012, V.57, #7, p.962.

17:00 Poster Mo160

Segregation study of titanium ions in sapphire single crystal fibers grown by the µ-PD technique

Abdallah Laidoune[1], Abdeldjalil Nehari[2], Kheirreddine Lebbou[2], Derradji Bahloul[1]

1. *Département de Science de la Matière, Faculté des Sciences, Université Hadj Lakhdar de Batna, 1 Avenue Boukhlouf Mohamed El Hadi, Batna 05000, Algeria* **2.** *LPCML Université de Lyon I, Villeurbanne, Lyon 69100, France*

e-mail: aballah_laidoune@yahoo.fr

We have been able to grow, under steady state conditions, titanium doped sapphire single crystal fibers using the micro pulling down technique. The Ti:Sapphire obtained fibers have good morphological and optical quality. The x-ray diffraction confirms that we obtained a monocrystalline structure of Al_2O_3 in the phase Alumin-a and free from defects. The growing conditions are very stable for fibers of different diameters and at different pulling rates. The obtained fibers are homogeneous and have stable diameter. The minimization of segregation of titanium is realized through the optimization of the growing conditions (drawing rate, the heating power and the titanium concentration). In fact the segregation has been minimized using high pulling rates. The optical characterization of the drawn fibers shows that they have good transparency and they have a homogeneous radial and longitudinal distribution of Ti^{3+}. Furthermore the small size diameters minimize the segregation of titanium ions Ti^{3+} in the sapphire host. The decay curves shows a life time of the order of 3 µs which is conform to the standard laser applications requirements. This study shows that the micro pulling down µ-PD technique helps to avoid many of crystal deficiencies and allows growing high quality crystals. This work confirms the importance of crystalline fibers as good candidates in the design of new photonic devices for laser application.

17:00 Poster Mo161

A High-power Generation in Mid-Infrared Region Based on $ZnGeP_2$ Optical Parametric Oscillation

Zuotao Lei, Chong-Qiang Zhu, Chao Xu, Chunhui Yang

Harbin Institute of Technology (HIT), No.92, West Da-Zhi Street,Harbin, Heilongjiang, Harbin 150001, China

e-mail: leizuotao@hit.edu.cn

Zinc germanium phosphide ($ZnGeP_2$, ZGP) is known as one of the most promising materials for nonlinear optical applications due to large nonlinear coefficient and high laser damage threshold. A high optical quality $ZnGeP_2$ single crystal of 50 mm in diameter was successfully grown by the vertical Bridgman technique. The OPO devices were fabricated from ZGP crystal as shown in Fig.1. The absorption coefficient of ZGP OPO devices for *o*-polarized 2 µm light incidence was significantly reduced to 0.02 cm^{-1} by thermal annealing and high energy electron irradiation (Fig2.). Moreover, improvement to the polishing of ZGP OPO devices (Fig.3) resulted in an increased laser-induced damage threshold. The value was increased to 2.0 J/cm^2 at 2.05 µm and 10 kHz pulse rate frequency. As a result, the maximum output of 20.5 W was obtained by high pulse repetition frequency Ho:YAG laser emitting at 2.09 µm under a pump power of 46W. The corresponding slope efficiency was 68.7% and the conversion efficiency was 44.3% (Fig.4). These results manifested the large crystals with high optical quality are acceptable for the fabrication of the infrared nonlinear OPO devices.

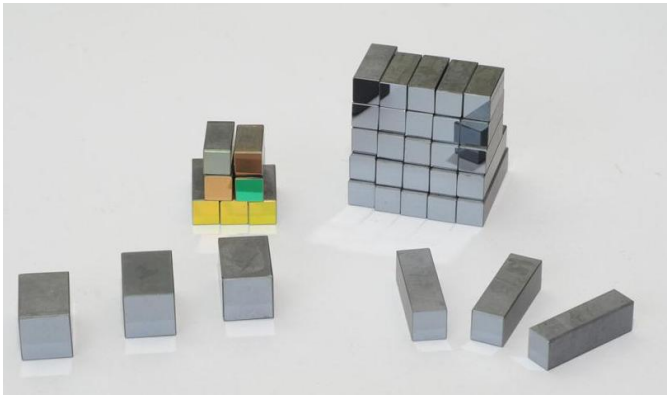

Fig. 1 ZGP-OPO devices

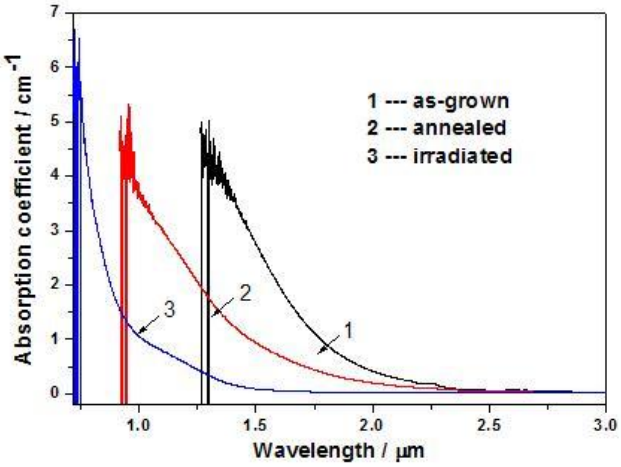

Fig.2 Optical absorption coefficient for o-light

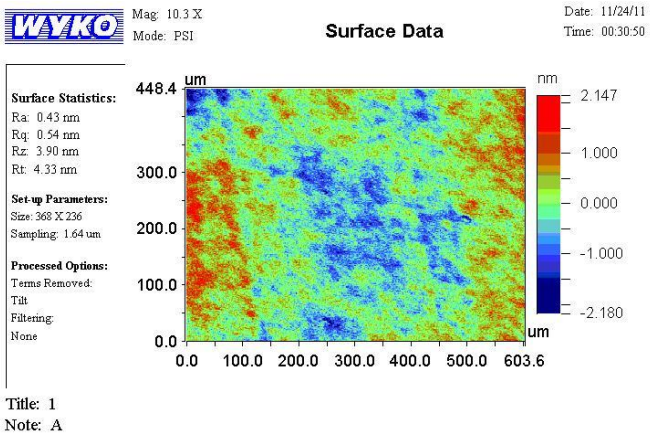

Fig.3 Patterns of roughness and flatness

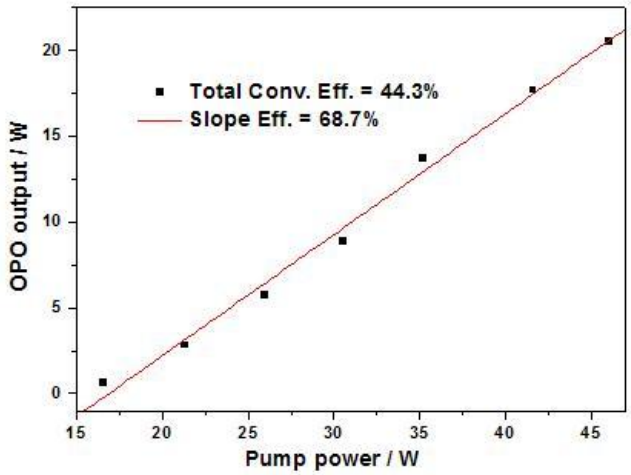

Fig.4 Output power and slope efficiency

17:00 Poster Mo162

Crystal growth of scheelite-like double tungstates and molybdates

Denis Lis[1], Kirill A. Subbotin[1], Evgeny V. Zharikov[1,2]

1. *A.M. Prokhorov General Physics Institute of Russian Academy of Sciences (GPI), Vavilov Str. 38, Moscow 119991, Russian Federation* **2.** *D.I.Mendeleyev University of Chemical Technology of Russia (MUCTR), Miusskaya sq. 9, Moscow 125047, Russian Federation*

e-mail: lisdenis@lsk.gpi.ru

In the scheelite ($CaWO_4$) structure (sp. gr. I41/a), Ca^{2+} locates in a somewhat distorted dodecahedral oxygen coordination, with two sets of bond distances: coordination number (CN) = 4 + 4. Each CaO_8 polyhedron share edges with four analogous dodecahedra. W locates in a slightly distorted tetrahedral coordination, with identical W–O bond distances (CN = 4), but different bond angles. In the $NaR(TO_4)_2$ (where R = Ln^{3+}, Y^{3+}, or Bi^{3+}; and T = W^{6+} or Mo^{6+} scheelite-like double tungstates and molybdates phases, the Na^+ and R^{3+} cations distribution on the dodecahedral (calcium) sites of the scheelite structure may be random (strictly statistical) or partially ordered. A strictly statistical distribution of the Na^+ and R^{3+} ions does not change the symmetry of the crystal. A partially ordered cation distribution, as a rule, distorts symmetry of the crystal, and reduces it`s space group.

Na^+ and R^{3+} cations, lie between the [TO_4] tetrahedra along the fourth-order crystallographic axis and are more or less randomly distributed over the crystallographic sites. Thus, the dopant R_1^{3+} ions substituting the host R^{3+} ions are affected by an infinitely large set of crystal fields with an infinitely small difference between each other. Therefore, the absorption and luminescence lines of R^{3+} ions in scheelite-like crystals demonstrate pronounced inhomogeneous broadening, which, along with the large number of Stark components of low-lying energy levels (for example, the $^3H_6$ level of Tm^{3+} ions has 13 Stark components) and comparatively small energy spacings between them gives rise to broad and rather smooth luminescence bands. This makes it possible to obtain easily continuous tuning of the wavelength of the laser oscillation [1] and to obtain subpicosecond laser pulses in the mode-locking regime. Furthermore, since the absorption bands are smooth and inhomogeneously broadened, possible temperature fluctuations of the emission wavelength of the pumping diode have not as drastic influence on the laser efficiency, as in case of ordered laser hosts like YAG. The advantages of the use of structurally disordered crystals as active media for solid-state lasers were considered more detail in [2].

The further disorder of scheelite structure may be accomplished by the simultaneous usage of different cations in R^{3+} and T^{6+} positions. One example of the first option was given in [3]. The crystals of mixed scheelite-like tungstates Tm^{3+}: $NaLa_xGd_{1-x}(WO_4)_2$ with a variable La-Gd composition occupy an intermediate position between the lanthanum and gadolinium tungstates. The efficient tuning of laser wavelength was demonstrated at this crystal [4].

Another advantage of scheelite-like crystals is very high probabilities of the electro-dipole transitions within f-electronic shell of Ln^{3+} laser dopants. It leads to high specific intensities of the optical absorption and luminescence bands of the doped crystals. Recently we found [5] that the main reason for such high probabilities is high distorsions of the local Ln^{3+} environment in the scheelite structure.

Over the last 10 years our team has made a large number of studies on the structure, spectral and lasing properties of crystals of double tungstates and molybdates [4,6-8]. A necessity to obtain the samples of

high optical quality demanded to make a number of improvements in the standard Czochralski method.

The main problem in the growth of crystals of this type is their tendency to cracking predominantly in the <001> cleavage plane (perpendicularly to the optical axis) [9]. Cracking may happen during the growth process and upon the cooling of as-grown crystal to room temperature. This phenomenon is caused by large thermoelastic stresses, developing under the influence of the temperature gradient, and on the other hand, by relatively low mechanical durability of scheelite-like crystals. Besides that, significant anisotropy of thermal expansion coefficients is typical for scheelite-like crystals. In order to prevent such a cracking we used the growth directions parallel to the cleavage plane <001>, optimized the configuration of heat shields. In particular, significant increase of thermal gradients is related with the presence of a through hole in the radial direction, which served as a window. This inspection window makes a significant distortion in the shape of the temperature field, making it dramatically asymmetrical in the radial direction (see fig.1). We tested several variants of smoothing these distortions. Especially nice results gave the coverage of inspection window, made in ceramic heat-shields, by plate of transparent material (e.g. quartz). In this case, the inspection window is no longer straight-through, which sharply reduces the heat transfer through it and substantially smooth out the shape of the temperature field. The insertion of a transparent cylindrical ring to the inside of ceramic heat-shields with a close location to the melt leads to quite rapid loss of transparency of the silica glass ring due to the condensation of the melt vapor on the surface of the window. Therefore, as a next step we start using a transparent ring, located in the outer layer of heat-shields. In this case, the inspection window maintains the acceptable transparency throughout the entire growth process, and the effect of lowering the thermal gradients does not reduce. Modification of the heat-shields allowed us to avoid the problem of cracking of crystals on the stage of crystal growth. However, the crystals continued to crack at the stage of postgrowth cooling to room temperature. Therefore, we have made additional improvements to the configuration of heat shields, e.g. introduced the resistive annealing furnace instead of the inner heat shield. The furnace was controlled with a programmable thermocontroller. After tear off the crystal from the melt, it is raised to a level to be approximately in the middle of the temperature field resistive furnace. Then the RF-coil heating was reduced to zero during a short time (2-3 hours), and the furnace was programmed to reduce the temperature at ~10 degrees per hour. This improvement allowed on the one hand to substantially smoothen the temperature gradients above the crucible, and on the other hand, to reduce the cooling rate. As a result, the problem of cracking of crystals was practically resolved. Moreover, additional annealing of crystals in a muffle furnace is generally not required after the introduction of this improvement. One can see from the fig.1 that the changes made in the design of heat-shields, have made nearly uniform axial temperature gradient (~9 K/mm) along the crystal growth axis and greatly reduce the asymmetry of the thermal field caused by a viewing window.

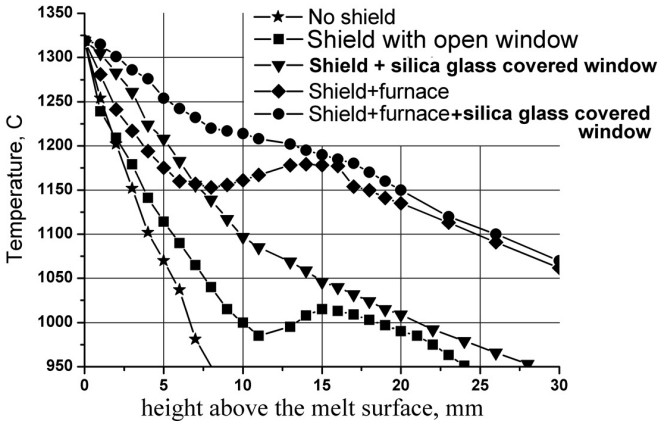

Fig.1. The temperature distribution above the melt surface

REFERENCES

1. X. Mateos, V. Petrov, J. Liu, et al., IEEE J. Quantum Electron. 42, 1008 (2006).

2. Yu.K.Voron'ko, K.A.Subbotin, V.E.Shukshin, D.A.Lis, S.N.Ushakov, A.V.Popov, E.V.Zharikov. Optical Materials, 2006, vol. 29, p. 246-252

3. F.A. Bol'shchikov, E.V. Zharikov, N.G. Zakharov, D.A. Lis, P.A. Ryabochkina, K.A. Subbotin, O.L. Antipov. Quantum Electronics, 2010, Vol.40 (2) p. 101-102

4. F.A. Bol'shchikov, E.V. Zharikov, D.A. Lis, N.G. Zakharov, P.A. Ryabochkina, K.A. Subbotin, O.L. Antipov, QUANTUM ELECTRON, 2010, 40 (10), 847–850.

5. P.A. Ryabochkina, S.A. Antoshkina, S.A. Klimin, D.A. Lis, K.A. Subbotin, S.N. Ushakov, E.V. Zharikov. Journal of Luminescence, Volume 138, 2013, p.32–38

6. F.Cornacchia, A.Toncelli, M.Tonelli, E.Favilla, K.A.Subbotin, V.A.Smirnov, D.A.Lis, E.V.Zharikov. J. Appl. Phys. 101, p. 123113 1-7, (2007)

7. F.A. Bolschikov, G.M.Kuz'micheva, D.A.Lis, Yu.M.Papin, A.V.Popov, P.A.Ryabochkina, V.B.Rybakov, V.G.Senin, V.A.Smirnov, K.A.Subbotin, Yu.K.Voron'ko, V.V.Voronov, E.V.Zharikov. Journal of Crystal Growth v. 311 iss. 17 (2009) p. 4171–4178

8. G.M. Kuzmicheva, V.B. Rybakov, K.A. Subbotin, E.V. Zharikov, D.A. Lis, O.Zaharko, D.A. Nikolaev, V.G. Senin. Russian Journal of Inorganic Chemistry, Vol. 57, No. 8, 2012, p. 1128

9. D. A. Lis, K. A. Soubbotin, E. V. Zharikov, et al., in Proceedings (Technical Digest) of 18th Topical Meetings on Advanced Solid State Photonics, San-Antonio, USA, 2003 (San-Antonio, 2003).

17:00 Poster Mo163

Defect comparison and analysis of flux and hydrothermally grown $KBe_2BO_3F_2$ crystals

Lijuan Liu[1], Tao Xu[1,2], Xiaolong Wang[1,2], Xiaoyang Wang[1], Chuangtian Chen[1]

1. *Institute of Physics and Chemistry, Chinese Academy of Sciences, Beijing 100190, China* **2.** *Graduate university of Chinese Academy of Sciences, Beijing 100049, China*

e-mail: llj@mail.ipc.ac.cn

It is very interesting that the $KBe_2BO_3F_2$ (KBBF) crystals are grown both by flux and hydrothermal method. In this paper, defects of KBBF crystals grown by these two methods were examined by the optical microscope. The main defects of flux grown KBBF crystals were etch pits and twin boundaries, which were also observed in the hydrothermally grown ones. The composition and morphologies of these defects were analyzed. Some formation mechanisms and the methods of eliminating these defects were also discussed. While the main defect for the hydrothermally grown KBBF is inhomogeneous with two structures R32 and R-3c mixing that is never discovered in the flux grown ones. It is very difficult to overcome up to date. Up to now the high power sixth harmonic generation of Nd:YAG laser at 177.3nm have all been produced by the flux grown KBBF crystals and we suspect that the hydrothermal method is not practical for KBBF crystal growth and applications.

17:00 Poster Mo164

Thermo- and Optically- Stimulated Luminescence of Crystals Grown by Micro-Pulling-Down Method

Barbara Marczewska, Paweł Bilski, Wojciech Gieszczyk, Mariusz Kłosowski, Anna Piaskowska, Michal Sądel, Anna Twardak, Dagmara Wróbel

Institut of Nuclear Physics Polish Academy of Science (IFJPAN), Radzikowskieg 152, Kraków 31-342, Poland

e-mail: Barbara.Marczewska@ifj.edu.pl

Micro-Pulling-Down Method (MPD) can be applied for the relatively fast growth of fluorides and oxides crystals, working as detectors of ionizing radiation. The aim of the work was to measure the thermo- and optically- stimulated luminescent (TL and OSL) properties of radiation sensitive fluorides and oxides, such as LiF, CaF_2 and Al_2O_3, in a pure and in doped state.

Crystals of fluorides and oxides grown in MPD system at the Institute of Nuclear Physics (IFJ PAN) in Krakow in the form of rods with a diameter up to 3mm were tested regarding their TL and OSL properties. After growing in MPD system, consisting of an induction furnace and 20kW generator, the crystals were cut to a smaller slides. Irradiation was performed using ^{137}Cs photons and ^{241}Am 5.49 MeV alpha particles. The measurements were carried out using conventional TL and OSL readers with a blue and green light for stimulation of the signal and a set of interferential filters for stimulation and excitation light control. The measurement results were referred to the substrate powder or standard detectors. The single crystals "as grown" longer than 1cm before cutting were additionally irradiated and read out in 2-dimensional TL reader equipped with a CCD camera to investigate the sensitivity of the particular parts of the crystals and unhomogenity of dopants distribution in the crystal structures. The crystal structure was analysed by x-ray diffraction.

The preliminary results showed that MPD method is a very useful tool for the laboratory research on TL and OSL detector doping due to the relatively fast growth of single crystals of fluorides and oxides.

Acknowledgments: This work was supported by the National Science Centre (Contract No. DEC-2012/05/B/ST5/00720).

17:00 Poster Mo165

Growth of organic Non-linear optical crystal of p-aminoazobenzene (4- aminoazobenzene) by slow evaporation method

Srinivasan Padmanabhan, Nagalakshmi Srinivasan, Etelvina Demitos gomes, Rajesh Ponraj

AnnaUniversity (AU), Sardar Patel Road, Guindy, Chennai 600025, India Anna University of Technology Tiruchirappalli, Department of Physics, Anna University of Technology Tiruchirappalli, Trichy, Tiruchirappalli 624024, India

e-mail: sril35@gmail.com

Non-linear optical (NLO) crystal of *p*-Aminoazobenzene (*p*-AAZB) (or 4- aminoazobenzene) has been grown by slow evaporation solution technique using acetone as a solvent. The 0.1M of *p*-Aminoazobenzene (*p*-AAZB) was dissolved in 20ml of acetone and the beaker containing the solution was kept in a magnetic stirrer for 5 minutes. Then the beaker was taken from the magnetic stirrer and solution has been allowed for slow evaporation. A good quality optical crystal can be obtained after 10 days. The structural properties of the as grown title crystal were studied using X-Ray diffraction. The mechanical property of the crystal was examined by Vicker's microhardness tester. Thermal properties and Dielectric properties were also been studied for grown crystal.

17:00 Poster Mo166

Growth,thermal properties and laser operation of a new disordered Yb:$Ca_3La_2(BO_3)_4$ laser crystal

Zhongben Pan, Huaijin Zhang

State Key Laboratory of Crystal Materials Institute ofCrystal MAterials Shandong University, Jinan 250100, China

e-mail: pzb8625@126.com

A high quality Yb:$Ca_3La_2(BO_3)_4$ disordered laser crystal has been successfully grown by the Czochralski method. The complete set of anisotropic thermal properties were systematically studied for the first time. In addition to, continuous-wave and passively *Q*-switched laser operation of the disordered Yb:$Ca_3La_2(BO_3)_4$ has been demonstrated under diode pumping. The most efficient cw output power of 1.83W was obtained along the a-cut with an optical-to-optical efficiency of 23.9%. The slope efficiency in the whole range was 27.6%. Passively *Q*-switched by a Cr^{4+}: YAG saturable absorber, the laser yielded an average output power of 0.47W with a slope efficiency of 7.6%. The generated pulse energy, duration, and peak power were 94 μJ, 33ns, and 2.85KW, respectively. We believe that the reliability and stability of these lasers makes the Yb:$Ca_3La_2(BO_3)_4$ disordered crystal of considerable interest for applications.

17:00 Poster Mo167

Progress in growth of large CdWO4 and ZnWO4 crystals by the Low-thermal-gradient CZ technique

Alexander P. Chubarev[1], Anna G. Postupaeva[1], Vasily N. Zhdankov[1], Yuri A. Borovlev[2], Olga E. Safonofa[2]

1. *Crystal Manufacturing Lab (CML), Lavrentev 3, Novosibirsk 630090, Russian Federation* **2.** *Institute of Geology and Mineralogy SB RAS (IGM), Koptyuga ave., 3, Novosibirsk 630090, Russian Federation*

e-mail: crysmalab@gmail.com

Cadmium tungstate CdWO4 (CWO) is scintillator widely studied and used in spectrometric and radiometric devices, X-ray computed tomography and cargo inspection. Zinc tungstate ZnWO4 (ZWO) is similar to CWO but is non-toxic while CWO is. Though ZWO has smaller light output, it may replace CWO in some cases applications. A wide using of ZWO is limited because it is not produced on an industrial scale. The main problem complicating the growing of ZWO is its tendency to cracking [1].

The largest of the previously created CWO single crystals with the weight up to 10 kg, size up to 80 mm in diameter and height 200 mm were grown along [001] direction in the Nikolaev Institute of Inorganic Chemistry SB RAS (NIIC) by the Low thermal gradient Czochralski technique (LTG CZ). Research and development puller HX620 with crucible 140 mm in diameter and height 300 mm were used [2].

The aim of this work is further development of LTG CZ method capability and increasing of CWO and ZWO single crystals sizes. For growing of large CWO and ZWO crystals by the LTG CZ production puller GRAN-4/140 was developed. As a prototype puller HX780 [2] designed at NIIC was used and adopted for working with toxic charge. The GRAN-4/140 puller has doorless lift opening camera. Auxiliary upper chamber is used to separate the crystal from the seed after the process. The three zone resistive heater enables using of crucibles up to 140 mm in diameter. The puller GRAN-4/140 is supplied with the crucible weighing cell DSHT-026 having maximal load 50 kg and weighing range 25 kg. Input signal processing and control actions are provided by PLK100 controller (ARIES). Software package InduSoft Web Studio™ is used as HMI/SCADA system.

In the development of the process of obtaining of isotopically enriched CWO crystals [3, 4] growth along the [010], has been successfully implemented. This experience was applied to the growth of large ZWO and CWO crystals. The influence of growth conditions on crystal morphology and quality for both types of crystals and different growth directions is discussed. High quality single crystals free of inclusions were grown with a fully rounded interface or flat interface formed by [010] face. Melt losses due to evaporation were less then 0.5 wt%. The utilization of the charge was better then 80%.

Optical and scintillation characteristics of grown crystals are reported.

[1] Sangeeta, S.C. Sabharwal. J. Crystal Growth **310** (2008) p. 2899

[2] A.A. Pavlyuk, Yu.G. Stenin. SCINT-1999. Abstracts book, p. 147.

[3] Ya.V. Vasiliev, Yu.A. Borovlev, E.N. Galashov, et al. Stcintilliatcionnye materialy. Inzheneriya, ustroistva, primenenie. Kharkiv: ISMA (2011) pp. 119–180.

[4] E.N. Galashov, V.A. Gusev, V.N. Shlegel et al. Crystallography Reports **54**, (2009) p. 689.

17:00 Poster Mo168

Transition-metal monoxide single crystal growth by the floating-zone technique

Dharmalingam Prabhakaran, Andrew T. Boothroyd

University of Oxford, Department of Physics, The Clarendon Laboratory, Parks Road, Oxford OX13PU, United Kingdom

e-mail: d.prabhakaran@physics.ox.ac.uk

Exciting phenomenon in physics such as high Tc superconductivity, Colossal magnetoresistance (CMR) and multiferroic have been discovered in many different families of compounds containing some magnetic elements such as Mn, Fe, Co and Ni. One way of understanding the basic mechanism of these complicated systems is to study the simple monoxides in detail. Neutron and X-ray scattering studies are particularly desirable to probe the spin and charge states and both need large size single crystals. However, growing a phase pure monoxide single crystal is quite a challenging task due to the mixed valency states.

The phase pure MnO, FeO, CoO and NiO have been obtained by annealing the powder in a reduced atmosphere. We have employed the floating-zone method to grow large size single crystals. Crack-free single crystals have been grown successfully. The purity of the material was confirmed both before and after the crystal growth process. We have studied the variation in the physical properties of the grown crystals. We will discuss the growth conditions, crystal quality and magnetic properties of the monoxide crystals.

References:

1. Z.Yamani, W.J.L. Buyers, R.A. Cowley and D. Prabhakaran Canadian journal of Physics 88 (2010) 729.

2. M. Massot, A. Oleaga, A. Salazar, D. Prabhakaran, M. Martin, P. Berthet and G. Dhalenne, Physical Review 77 (2008) 134438

17:00 Poster Mo169

Comparison of RE ion luminescence in zirconia nanocrystals and Single crystals

Krisjanis Smits[1], Jiayue Xu[2], Janis Grabis[3], Donats Millers[1], Larisa Grigorjeva[1]

1. *Institute of Solid State Physics, University of Latvia, 8 Kengaraga, Riga LV-1063, Latvia* **2.** *Shanghai Institute of Technology (SIT), Haiquan Road, Fengxian, Shanghai 201418, China* **3.** *Riga Technical University, Miera 34, Riga, Latvia*

e-mail: smits@cfi.lu.lv

The study of time-resolved luminescence of Y stabilized as well as RE ion activated zirconia single crystals and free standing nanocrystals (with the same contamination) was carried out. Zirconis single crystals were growth by skull melting process, the nanocrystals were synthesized with the same contamination of activators by Sol- Gel and microwave driven hydrothermal methods.

The different excitation sources (e-beam, x-ray, lasers 6,42eV, 4.66eV and 3.67eV) were used in experiments. The previous research shows that intrinsic defects in nanocrystals and in single crystal are the same, however the defect concentration and distribution is various [1]. The comparison of RE doped nanocrystals and single crystals gives additional information about the defect type and distribution. The RE ions

are used as luminescent probes to analyze the local symmetry and energy transfer.

The intrinsic defects related and activator luminescence bands were observed. The luminescence dependence on activators concentration in zirconia nanocrystals is shown.

The excitations in zirconia are mobile, so with increasing of activator concentration the intrinsic defects related luminescence band intensity decreases and activator luminescence intensity increases until it reaches the saturation.

The RE ion luminescence showed that this luminescence decay kinetics depends on both activator and intrinsic defects concentration in nanocrystals.

The use of different excitation sources allow to determine role of direct excitation of luminescence centers, energy transfer by excitons to these centers and band carriers trapping involved in the creation of excited states of luminescence centers. The mechanisms of excited state creation and the possible models of luminescence centers in the nanocrystals will be discussed.

[1] Smits, K., Grigorjeva, L., Millers, D., Sarakovskis, A., Grabis, J., Lojkowski, W. Intrinsic defect related luminescence in ZrO 2, (2011) Journal of Luminescence, 131 (10), pp. 2058-2062.

17:00 Poster Mo170

Influence of Na^+ and Pb^{2+} ions on the optical properties of Yb^{2+} ions in YbF_3 doped CaF_2 crystals

Marius Stef, Irina Nicoara

West University of Timisoara (UVT), Bd.V. Parvan nr.4, Timisoara 300223, Romania

e-mail: stef@physics.uvt.ro

The rare-earth ions can be stabilized in the divalent state in CaF_2 lattice, besides the trivalent state, with which can coexist. It is known that certain fraction of Yb^{3+} ions can be reduced to divalent state by various methods [1] or directly in the as-grown crystals using high deoxidization growth conditions [2]. The spectroscopic properties of the Yb^{2+} ions have been less investigated, mainly only for its intense and broad yellow-green luminescence [2].

The purpose of this work is to study the influence of Na^+ and Pb^{2+} ions on the absorption and emission spectra of YbF_3-doped CaF_2 crystals with high divalent ytterbium content in the as-grown crystals.

NaF and PbF_2 codoped $Ca_{1-x}Yb_x F_{2+x}$ (x = 0.0007, 0.0017, 0.007, 0.0116) crystals have been grown using the conventional Bridgman technique [3]. In order to obtain high Yb^{3+} - Yb^{2+} conversion a special procedure has been developed [4]. Room temperature optical absorption spectra reveal the characteristic UV absorption bands of the Yb^{2+} ions. The presence of the Na^+ ions drastically decrease the absorption intensity of the characteristic UV peaks of Yb^{2+} ions. The absorption peaks of the Pb^{2+} ions are in UV domain; the influence of these ions on the various Yb^{2+} ion peaks depends on the YbF_3 concentration in CaF_2. For low YbF_3 concentrations the peaks intensity increases, for high concentrations decreases. The luminescence studies reveal a strong YbF_3 concentration and codopant dependence of the near-UV emission bands. Besides the reported yellow-green luminescence, new emission bands have been observed in the near-UV spectral region. The Na^+ ions drastically decrease the emission intensity of the characteristic UV peaks observed for the CaF_2:YbF_3 samples. The Na^+ ions influence on the emission intensity depend on the $\lambda_{excitation}$ and on the NaF and YbF_3 concentration. For the crystals codoped with Pb^{2+} ions the emission intensity increases in comparison with the CaF_2:YbF_3 samples. This effect depends on the YbF_3 concentration and on the $\lambda_{excitation}$. The observed emissions in the visible domain are attributed to the anomalous luminescence [5].

References

[1] Kaczmarek S M, Tsuboi T, Ito M, Boulon G and Leniec G *J. Phys.: Condens. Mater.***17** (2005) 3771

[2] Feofilov P P *Opt. Spectrosc.***1** (1956) 992

[3] D. Nicoara and I. Nicoara, Mater. Sci. Eng. A 102 (1988) L1

[4] I. Nicoara, M. Stef, A. Pruna *J. ofCrystalGrowth***310** (2008) 1470

[5] P. Dorenbos, J. Phys.: Condens. Matter 15 (2003) 2645.

17:00 Poster Mo171

Synthesis of the promising laser material Cr^{4+} doped $LiGaSiO_4$ nano-glass-ceramics

Kirill A. Subbotin[1], Valerii V. Voronov[1], Yulia N. Osipova[2], Evgenii V. Vrublevskii, Evgeny V. Zharikov[2]

1. *A.M. Prokhorov General Physics Institute of Russian Academy of Sciences (GPI), Vavilov Str. 38, Moscow 119991, Russian Federation* **2.** *D.I.Mendeleyev University of Chemical Technology of Russia (MUCTR), Miusskaya sq. 9, Moscow 125047, Russian Federation*

e-mail: soubbot@lsk.gpi.ru

Cr^{4+} doped oxide materials attract a substantial attention of researchers as the active media of tunable and femtosecond solid-state lasers operating in the spectral range of 1,1-1,6 mm. Such lasers can be used in fiber optics communications, ophthalmology, laser ranging, etc. However, the wide application of these lasers is suppressed by absence of the efficient hosts for this ion. Cr^{4+}:$Y_3Al_5O_{12}$ and Cr^{4+}:Mg_2SiO_4 single crystals, used in practice, have rather low fluorescence quantum yield and short excited state lifetime of Cr^{4+}. Another problem is low available concentrations of Cr^{4+} and presence of the parasitic oxidation states of chromium in above crystals.

The search for new, more efficient laser hosts for Cr^{4+} ion is the actual problem. The attempts to find such a host among single crystals and glasses, continued during the last 25 years, had no great success: there were found some crystals, very promising from the point of view of their spectroscopic characteristics, and having good admittance for Cr^{4+}. However, these crystals cannot be grown from melt as the samples of laser quality, because of sub-solidus polymorph transitions, and/or because of strongly incongruent melting, and/or because of very high selective evaporation of the melt components.

That is why, at the last decade researchers pay much attention to another kind of optical materials, ultra-transparent nano-glass-ceramics as to the alternative hosts for Cr^{4+}. These materials reproduce the valuable spectroscopic properties of the corresponding single crystals in substantial extent. On the other hand, nano-glass-ceramics can be rather easily obtained as high-quality bulk samples of any shape (including single mode optical fiber) with high concentrations and uniform distribution of a dopant over the sample.

Erlier, we studied Cr^{4+}:$LiGaSiO_4$ single crystals for the first time. Cr^{4+} possess the attractive spectroscopic properties in this crystal. Its structure is favorable for Cr^{4+} formation, and unfavorable for the formation of the parasitic Cr^{2+} and Cr^{3+} ions. However, the incongruent melting of the compound prevents the possibility to grow the high-quality Cr:$LiGaSiO_4$ single crystals from melt. Meanwhile, an ultra-transparent Cr:$LiGaSiO_4$ nano-glass-ceramics looks very promising, and that was the subject of our studies in Refs. [1, 2, 3]. In this talk we

present the studies of different crystalline phases formation in the parent Cr-Li-Ga-Si-O glass depending on the temperature and duration of crystallization, as well as on the particular composition of the parent glass.

The samples of a parent glass (vitreous precursors) were sintered by melting the charge in air or in pure argon, and keeping the melt above the liquidus temperature (~ 1350 ^{o}C), with stirring during 0,5 to 50 hours, until the melt become completely transparent. For different charge compositions the temperature and duration of melting, necessary for the synthesis, varied in considerable ranges. In particular, heavily chromium doped compositions required extremely long melting exposure (several tens of hours), whereas chromium-free and silica-enriched charges became transparent just after several minutes of melting. The charges containing TiO_2, ZrO_2 or WO_3 required considerably increased temperatures for a complete dissolution of all the solid particles, flowing in the melt, whereas the addition of Li_2O, BaO or B_2O_3, on the contrary, reduced the melting temperature.

After the melt achieved complete transparency, and after the complete dissolution of all the solid inclusions happened, they were quenched by removing from a hot zone. High quality transparent glass samples were obtained. The colour of the samples was yellowish-green, except chromium-free samples, which were colourless. Our attempts to quench the opaque Cr-Li-Ga-Si-O melts (even without visible solid inclusions) resulted in obtaining of opaque, partially crystallized samples.

The controlled crystallization of the glass samples was performed by their heat treatment using different thermal-temporal regimes. The crystalline phases formed in the samples were monitored by XRD analysis.

Several different crystalline phases were observed in the studied glass-ceramic samples. Not taking into the consideration well-known phases observed in the samples with very specific initial compositions (like spodumene-related phases in the heavily SiO_2-enriched samples), we will discuss four different phases, observed in the most part of the studied samples. They are:

1. Well-known stable eucryptite-like α-$LiGaSiO_4$ polymorph modification. This is the most attractive laser host for Cr^{4+}, hence its formation is the most desirable;

2. The metastable γ-$LiGaSiO_4$ modification. The particular structure of this crystalline polymorph has not been studied, because of difficulties in obtaining the macroscopic single crystals of γ-$LiGaSiO_4$, and to study it by single-crystalline X-ray diffraction methods, although some similarities between the structures of α- and γ- $LiGaSiO_4$ do, obviously, exist, because the most part of the α- $LiGaSiO_4$ and γ-$LiGaSiO_4$ XRD-peaks are very close to each other. γ-$LiGaSiO_4$ is not as attractive laser host for Cr^{4+}, as α- $LiGaSiO_4$. However, Cr^{4+} doped nano-glass-ceramic containing γ-$LiGaSiO_4$ crystallites also has rather strong fluorescence in the range 1,2-1,5 μm;

The rest two crystalline phases are very specific ones, they were not observed earlier anywhere, to our knowledge, and are absent in XRD-catalogues. Both these phases have no Cr^{4+} fluorescence, but can cause the scattering in the samples. Therefore, their presence in laser Cr:$LiGaSiO_4$ nano-glass-ceramics is strongly non-desirable. Both these phases are, obviously partially ordered, each of them have just two very strong XRD-peaks.

3. First of them is the phase, which we have titled as X-phase. It has XRD peaks at 2Q ~ 22^{o}, and less intensive peak at 2Q ~ 45^{o}. The latter peak corresponds to the inter-plane spacing of 2,0Å that fits very well the typical height of [SiO_4] tetrahedron, whereas the former peak corresponds to the inter-plane space of 4,0Å that fits very well to the double typical height of [SiO_4] tetrahedron, or to the typical lengths of [Si_2O_7] doubled tetrahedron.

4. The phase, which we have titled as Y-phase. It has two XRD peaks of comparable intensities at 2Q ~ 27^{o}, and at 2Q ~ 56^{o}. The former peak corresponds to the inter-plane spacing of 3,3Å that fits very well the interatomic Li-Li distance in the cubic Li_2O crystalline phase.

The content of these crystalline phases depend on the temperatures and duration of crystallization, as well as on the parent glass compositions. These dependencies, as well as some our versions about the structures and compositions of the X- and Y-phases are presented and discussed in the talk.

References

[1] K.A.Subbotin, V.A.Smirnov, E.V.Zharikov, L.D.Iskhakova, V.G.Senin V.V.Voronov, I.A.Shcherbakov. - *Optical Materials*, v.32 iss. 9, (2010) p. 896–902.

[2] K.A.Subbotin, S.M.Arakelian, V.V.Voronov, V.G.Senin, M.N.Gerke, V.A.Smirnov, D.A.Nikolaev, E.V.Zharikov, I.A.Shcherbakov.– *J. Crystal Growth*, v.328 iss. 1, (2011) p. 95–101.

[3] K.A.Subbotin, A.A.Veber, D.A.Nikolaev, V.G.Senin, V.A.Smirnov, Yu.N.Osipova, E.V.Zharikov, I.A.Shcherbakov.– Optics and Spectroscopy v. 114, iss. 5, pp. 71– 75

17:00 Poster Mo172

Growth, morphology, thermal characteristic and spectroscopic properties of Nd^{3+} doped $KGdP_4O_{12}$ crystal, a new promising laser material

Tongqing Sun, Yu Zhang, Shaolin Chen, Yongfa Kong, Jingjun Xu

Nankai University, Tianjin 300071, China

e-mail: suntq@nankai.edu.cn

With the development of the diode pumped all solid state lasers based on neodymium doped crystals, research on new laser host materials has gained much interest. Since the emission wavelength of AlGaAs diode laser (λ= 808 nm) is increased at a rate of 0.2–0.3 nm/°C with the operating temperature of the laser device, the temperature stability of the output wavelength of the diode laser needs to be crucially controlled. Therefore, it is necessary to explore new more efficient crystal materials whose absorption band should have a large full-width at half-maximum (FWHM) near the output wavelength of AlGaAs.

Host crystals with low symmetry present strong anisotropy of physical properties which maybe rich the spectroscopic properties of doped active ions. Double tetra-metaphosphates of potassium and gadolinium have a low symmetry (monoclinic system), including three structural types: type III ($P2_1$) and IV ($P2_1/n$) $KGd(PO_3)_4$, both of which have a PO_4 long chain geometry, and type A $KGdP_4O_{12}$, which has a $[P_4O_{12}]^{4-}$ cycling geometry. Compared with the former two types, $KGdP_4O_{12}$ crystal is not easy to cleavage from the point of view of bonding and structure. So we studied the growth, thermal and spectral properties of Nd^{3+} doped $KGdP_4O_{12}$ crystal.

Nd^{3+}:$KGdP_4O_{12}$ crystal has been grown successfully by the top seeded solution growth (TSSG) technique using Nd_2O_3, Gd_2O_3, K_2CO_3 and $NH_4H_2PO_4$ as starting materials. It crystallizes in space group $C2/c$ with cell parameters a = 7.812(2) Å, b = 12.307(3) Å, c = 10.474(2) Å, β = 110.84(3)° and Z = 4. The IR and Raman spectra also testified that the phosphoric polyhedra of Nd:$KGdP_4O_{12}$ has a cycling symmetry. The chemical compositions of the as-grown crystal were analyzed, and the distribution coefficient of Nd^{3+} was calculated. The as-grown crystal was made up of the crystalline forms {001}, {010},

{110}, {021}, which were consistent with the simulated results of the morphology.

The TG-DSC analytical result shows that $KGdP_4O_{12}$ crystal has a good thermal stability and decomposes at 920°C. The specific heat of the $Nd:KGdP_4O_{12}$ crystal increases almost linearly from 0.485 $J{\cdot}g^{-1}{\cdot}K^{-1}$ to 0.799 $J{\cdot}g^{-1}{\cdot}K^{-1}$ with the temperature increase from -10°C to 510 °C, which means that the $Nd:KGdP_4O_{12}$ crystal can tolerate more thermal energy at high temperature. The thermal diffusion coefficient was also measured and then the thermal conductivity was calculated (1.66 W/m·K along the *c** direction). This implies that $Nd:KGdP_4O_{12}$ crystal has a moderate thermal conductivity.

The spectroscopic properties of the $Nd:KGdP_4O_{12}$ crystal were studied in detail. Theunpolarized absorption spectrum [Fig. 1(a)] of the 5at% Nd^{3+}-doped $KGdP_4O_{12}$ crystal was measured at room temperature. The absorption band around 798 nm has an FWHM of 14.7 nm. The Judd-Ofelt theory was applied to calculate the optical parameters. The excitation fluorescence spectrum [Fig. 1(b)] shows that $Nd:KGdP_4O_{12}$ crystal can be effectively pumped by AlGaAs in a very broad range (FWHM = 39 nm), which implies that stringent control of the diode laser temperature would be unnecessary in laser action. The emission spectrum at room temperature excited at 808nm wavelength was shown in Fig. 1(c). The FWHM of the emission peak and the emission cross section for the transition $^4F_{3/2} \rightarrow {}^4I_{11/2}$ were 14.5 nm and $6.25\times10^{-20}cm^2$, respectively. The fluorescence lifetime of the $^4F_{3/2}$ energy level of Nd^{3+} was determined to be 300μs. The higher value should be contributed to the structural characteristic of isolated GdO_8 polyhedra and would be beneficial to high energy storage in laser operation. In addition, the higher doping concentration of Nd^{3+} and the bigger fluorescence lifetime will also be useful in increasing the quality factor of laser materials. The fluorescent quantum efficiency was about 96%. All the results indicate that $Nd:KGdP_4O_{12}$ crystal can be considered as a very promising material for solid-state laser application.

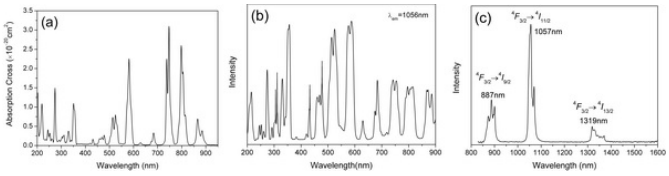

Fig. 1. The absorption spectrum (a), the excitation (b) and emission (c) fluorescence spectra of the 5at%Nd^{3+} doped $KGdP_4O_{12}$ crystal at room temperature.

References:

[1] Kaminskii A.A. Laser & Photon. Rev. 2007, 1(2): 93-177.

[2] Ettis H., Naïli H., Mhiri T. Cryst. Growth & Des., 2003, 3(4): 599-602.

[3] Rekik W., Naïli H., Mhiri T. Acta Crystallogr. Sect. C 2004, 60: i50-i52.

[4] Parreu I., Solé R., Gavaldà J., et al. Chem. Mater. 2005, 17(4): 822-828.

17:00 Poster Mo173

Electronic structure and magnetic properties of nano and single crystals $SrLaAlO_4$: Mn

Ewa Talik[1], Anna Pajaczkowska[2], Adam Guzik[1], Paweł Zajdel[1], Joachim Kusz[1], Agnieszka Szysiak[2]

1. *University of Silesia, Institute of Physics, Uniwersytecka 4, Katowice 40-007, Poland* **2.** *Institute of Electronic Materials Technology (ITME), Wólczyńska 133, Warszawa 01-919, Poland*

e-mail: talik@us.edu.pl

$SrLaAlO_4$ (SLA) compound belongs to the group of compounds with the chemical formula $ABCO_4$, where A = Ca, Sr or Ba, B = Y or some other rare earth metal, and C = Al, Ga or some transition metal [1]. These compounds belong to the tetragonal K_2NiF_4 structure type with space group *I4/mmm*. Basic building elements of $LaSrAlO_4$ structure are double planes of randomly distributed La/Sr ions in corrugated layers, placed between single flat square lattices of AlO_2. These layered perovskite-related compounds have been intensively studied previously from the point of view of their possible applications as substrate material for high-temperature superconductors (HTSC) as well as host material for laser media and phosphors [1-4].

Single crystals of $SrLaAlO_4$ doped by Mn ions were obtained by the Czochralski method. The crystals were grown from the nonstoichiometric melts of $SrLa_{1,03}Al_{0,97}O_4$. This composition was reported earlier for obtaining of good quality SLA single crystal [1]. Thermal isolation of the system contains a ceramic disc between the crucible and the passive afterheater to ensure proper temperature gradient across the surface of the melt. Crystals were grown from iridium crucible of 50 mm in diameter. Crystal growth was conducted in pure nitrogen.

Manganese dopant was introduced into the melt in the form of MnO_2 oxide and was added to the above mentioned SLA compound. The assumed concentration of dopants in the melt was equal to 0, 02 and 0, 1 wt%. The pulling rate in the case of lower doping level was 1 mm/h and rotation rate was equal to 17 rpm. Good quality single crystals of 18 mm in diameter and 35 mm in length were grown using <100> seed orientated. Single crystals doped with 0.1 wt% of Mn were easily cracked, even when the pulling rate was reduced up to 0.7 mm/h. However, an inside some parts of crystal were good quality not cracked and were used in further investigations.

SLA doped with Mn^{2+} ions (0,02 mol%) was synthesized by modified sol-gel (Pechini) method as follows: lanthanum oxide was dissolved in solution of acetic acid, then strontium carbonate, aluminum nitrate, solution of nitric acid and manganese acetate were added. After two hours of stirring the ethylene glycol as polymerizing agent was used. Subsequently the solvent was evaporated and the xerogel was dried at 150°C for 12 hours, grinded in an agate mortar to obtain fine powder, next annealed at 1450ºC in furnace for 4 hours. The diffraction patern shows the one phase compound of SLA structure.

The purpose of the present work was to study electronic structure and magnetic properties of manganese ions in $SrLaAlO_4$ host.

Magnetic susceptibility was measured using a Quantum Design MPMS–XL–7AC SQUID magnetometer in the temperature range 1.9 – 400 K.

The XPS spectra were obtained using a PHI 5700/660 Physical Electronics Photoelectron Spectrometer with monochromatized Al K_α X–ray radiation (1486.6 eV).

The microstructural observations of the nanopowders as well as the microcompositional analysis were conducted on a JEOL–7600F scan-

ning electron microscopy equipped with the Oxford X–ray energy dispersive spectroscope EDS.

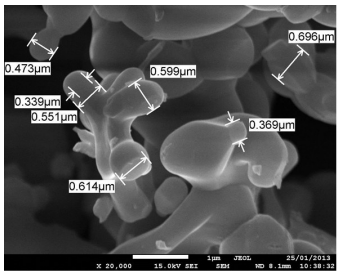

Fig. 1. SEM image of SLA: 0.02Mn.

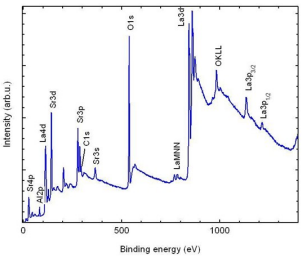

Fig.2. XPS overview of SLA:0.02 Mn single crystal

sample SLA	χ_0 (emu/mol)	μ_{eff} (μ_B)	Θ (K)
undoped	$-6.67*10^{-5}$	0.04	-4.0
nano / 0.02 Mn	$-55.63*10^{-5}$	0.14	-4.4
yellow / 0.02 Mn	$-7.09*10^{-5}$	0.21	-5.0
dark / 0.1 Mn	$-2.87*10^{-5}$	0.40	-1.9

Table 1. Magnetic measurements results.

Electronic structure measurements showed a decomposition of the surface of the nanocrystals SLA. Magnetic measurements confirmed the presence of Mn^{4+} in the measured doped samples what is essential for spectroscopic properties of such crystals.

Acknowledgements

This work was partially financed by the Polish National Science Centre under grant no. NN 515 500 440.

1. A. Pajaczkowska, A. Gloubokov, Synthesis, growth and characterization of tetragonal $ABCO_4$crystals, *Prog. Crystal Growth and Charact.* 36 (1998) 123–162.

2. W. Ryba-Romanowski, S. Gołąb, A. Gloubokov, A. Pajączkowska, Spectroscopic properties of chromium-doped $SrLaAlO_4$ single crystals, *Opt. Mater.* 4 (1995) 515–519.

3. W. Ryba-Romanowski, S. Gołąb, I. Sokólska, W.A. Pisarski, G. Dominiak-Dzik, A. Pajączkowska, M. Berkowski, Anisotropy of optical properties of $SrLaAlO_4$ and $SrLaAlO_4$:Nd, *J. Alloys Comp.* 217 (1995) 263–267.

4. L. Vasylechko, N. Kodama, A. Matkovskii, Ya. Zhydachevskii, Crystal structure and optical spectroscopy of $CaGdAlO_4$:Er single crystal, *J. Alloys Comp.*300-301 (2000) 475–478.

5. Ya. Zhydachevskii, A. Suchocki, D. Sugak, A. Luchechko, M. Berkowski, S. Warchol, R. Jakiela, Optical observation of the recharging processes of manganese ions in YAlO3:Mn crystals under radiation and thermal treatments. J. Phys.: Condens. Matter 18 (2006) 5389–5403.

6. Ya. Zhydachevskii A. Suchocki, M. Berkowski, D. Sugak, A. Luchechko, S. Warchol, Technological approaches for improving thermoluminescent properties of the Czochralski-grown$YAlO_3$:Mn crystals. J.Cryst.Growth 310(2008) 3219–3232.

17:00 Poster Mo174

Float zone growth and spectral properties of Cr,Nd:CaREAlO$_4$ (RE=Y, Gd) single crystals for potential use in solar-pumped solid state lasers

Aki Ueda[1], Mikio Higuchi[1], Daiki Yamada[1], Sho Namiki[2], Takayo Ogawa[2], Satoshi Wada[2]

1. *Hokkaido University, Sapporo 060-8628, Japan* **2.** *RIKEN, Wako 351-0198, Japan*

e-mail: septaky.18-i.wlam@frontier.hokudai.ac.jp

Solar-pumped lasers have recently been attracted much attention from the viewpoint of suitable energy development. In previous studies, Cr,Nd:Ca*RE*AlO$_4$was developed as a host crystal for the Nd-lasers, but there have no reports on the crystal growth and spectral properties of Cr- and Nd-codoped Ca*RE*AlO$_4$. Since Ca*RE*AlO$_4$ does not have any tetrahedral site, spectral drawbacks found in YAG may be improved. In this study, we grew Cr,Nd:Ca*RE*AlO$_4$(*RE*=Y, Gd) single crystals by the floating zone method and investigated their spectral properties.

A ceramic feed rod with a composition of $CaRE_{1-x}Nd_xAl_{0.999}Cr_{0.001}O_4$where x=0-0.01 was used for the single crystal growth by the floating zone method. Crystals were grown with conditions of growth rate: 2.5-5mm/h, atmosphere: air, CO_2 or O_2, rotation rate: 30-60 rpm.

The grown single crystals were transparent and deep red in whole. A lower growth rate of 2.5 mm/h and a higher rotation rate of 60 rpm were effective to suppress the formation of voids.

Cr,Nd:$CaYAlO_4$showed strong absorption in the wavelength region of 320-600 nm. The absorption cross section of σ-polarization at 430 nm, where Cr,Nd:YAG has the maximum absorption, is about 862 $\times 10^{-20}$ cm^2, which is 120 times as large as that of Cr,Nd:YAG. Cr,Nd:$CaGdAlO_4$ also showed strong absorption in the wavelength region of 340-600 nm. Although the absorption cross section of Cr,Nd:$CaGdAlO_4$ was less than that of Cr,Nd:$CaYAlO_4$, the absorption peak was shifted to the longer wavelength of 470 nm. By pumping at 400 nm, Cr,Nd:$CaYAlO_4$ showed strong fluorescence bands around 900 nm and 1080 nm by Nd^{3+}. This result indicates that the energy absorbed by Cr^{3+} is effectively transferred for Nd^{3+}in these crystals, and Cr,Nd:Ca*RE*AlO$_4$single crystals are therefore one of the promising materials for solar-pumped solid state laser systems.

17:00 Poster Mo175

Explorations of deep-ultraviolet nonlinear optical borates: approaching to the end

Wenjiao Yao[1,2], Ran He[1,2], Zheshuai Lin[1], Chuangtian Chen[1]

1. *Institute of Physics and Chemistry, Chinese Academy of Sciences, Beijing 100190, China* **2.** *University of Chinese Academy of Sciences (UCAS), Beijing 100080, China*

e-mail: yaowenjiao09@mails.ucas.ac.cn

The rapid development of deep-UV (DUV) all-solid-state laser sources greatly depends on the nonlinear optical (NLO) crystals with good performances. In this work, from the point of view of the structure-property relationship we comprehensively investigate the developing spaces of the NLO borates that are the sole NLO crystals used to produce harmonic generation in the UV and DUV spectral regions. The microscopic structural units, energy band gaps, linear and nonlinear

optical properties of numerous borate compounds with diverse structural features are compared and summarized. The results clearly demonstrate that the $KBe_2BO_3F_2$ (KBBF) crystal almost achieves the theoretical limits of DUV NLO borates. It is anticipated that any other borate that can match KBBF would be hardly discovered for producing the coherent light output below the wavelength of 190nm only with Second Harmonic Generation (SHG) method. The future prospect of exploring new DUV NLO borates is not optimistic.

17:00 Poster Mo176

Fabrication and characterization of highly-concentrated Nd-doped YAG laser ceramics

Roman P. Yavetskiy[1], Denis Y. Kosyanov[1], Alexander V. Tolmachev[1], Yurii Kopylov[2], Valery Kravchenko[2], Sergey V. Frolov[3], Viktor B. Taranenko[3], Vladimir L. Vozniy[4]

1. *Institute for Single Crystals NAS of Ukraine (ISC), 60 Lenin Ave., Kharkov 61001, Ukraine* **2.** *Fryazino Institute of radioengineering and electronics Russian Academy of Sciences (FIRE RAS), Vvedenskogo sq., Fryazino 141190, Russian Federation* **3.** *IC Institute of Applied Optics, Kiev 04053, Ukraine* **4.** *EDAPS-Laser, Kyiv 02088, Ukraine*

e-mail: yavetskiy@isc.kharkov.ua

Optical ceramics are promising materials for utilization as phosphors, transparent armor, lamp envelopes, scintillation detectors, etc. Laser ceramics possess several advantages over traditional materials among which there are improved processability, lower cost of fabrication, wider range of compositions, higher doping concentration, and larger size of samples. Nd:$Y_3Al_5O_{12}$ (Nd:YAG) optical ceramics doped by trivalent rare earth ions is considered as promising material for high-power and ultrafast solid state laser, microchip lasers, etc. In this paper we present results of fabrication of highly-concentrated Nd:YAG transparent ceramic and characterization of its optical and laser properties.

Highly-concentrated Nd:YAG (1-4 at. %) optical ceramics has been produced by solid-state reactive sintering of fine oxide powders at the temperatures of 1600-1800 °C and vacuum of 10^{-3}-10^{-5} Pa. Submicron Y_2O_3, Al_2O_3 and Nd_2O_3 powders were used as starting materials. The structural and phase state of laser ceramics depending fabrication conditions has been studied. The sintering trajectory of submicron powders will be presented. Influence of neodymium ions concentration on density, average grain size and lattice parameter will be discussed. The optical and luminescence properties, laser characteristics of sintered ceramics depending on neodymium ions concentration will be presented. The quasi-continuous laser operation of highly-concentrated Nd:YAG (1-4 at. %) ceramics will be presented. We will discuss the ways to improve the optical quality and lasing efficiency of the Nd:YAG ceramics samples.

17:00 Poster Mo177

Growth of Al doped $Ca_3TaGa_3Si_2O_{14}$ piezoelectric single crystals with various Al concentrations and their physical properties

Yuui Yokota[1], Tetsuo Kudo[2], Masato Sato[3], Kazushige Toota[3], Ko Onodera[2,3], Shunsuke Kurosawa[1,2], Kei Kamada[1], Akira Yoshikawa[1,2,4]

1. *New Industry Creation Hatchery Center, Tohoku University, Aoba-yama 6-6-10, Aoba-ku, Sendai, Miyagi, Sendai 980-8579, Japan* **2.** *Institute for Materials Research, Tohoku University (IMR), Sendai 980-8577, Japan* **3.** *TDK Corporation, Akita 018-0147, Japan* **4.** *C and A corporation, Sendai 980-8579, Japan*

e-mail: yokota@imr.tohoku.ac.jp

Langasite-type single crystals have been energetically investigated as a piezoelectric material due to the high piezoelectric constant and electromechanical coupling factor at high temperature. Therefore, the langasite-type crystals have been expected to be applied for various sensor devices at high temperature such as the combustion pressure sensor and temperature sensor. Recently, rare-earth (RE) free langasite-type crystals such as $Ca_3TaGa_3Si_2O_{14}$ (CTGS) and $Ca_3NbGa_3Si_2O_{14}$ (CNGS) have been developed and they are playing the role of an engine for recent researches of langasite-type crystals because their electrical resistivity at high temperature is higher than the langasite-type containing RE such as $La_3Ta_{0.5}Ga_{5.5}O_{14}$ and $La_3Ga_5SiO_{14}$. In addition, the manufacturing cost would be decreased due to the change from crystals with RE ion (La ion) to RE free crystal. However, the RE free langasite-type crystals still contain the Ga ion which is relatively high cost of starting materials and the manufacturing cost of langasite-type crystals are more than ten times higher than quartz element. If the mount of Ga ion in the crystal would be decreased, the manufacturing cost would be decrease. In the previous reports about the langasite-type containing RE ion, the 20% Ga site in the crystal could be substituted by the Al ion. In this study, we grew the Al doped CTGS single crystals with various Al concentrations to decrease the amount of Ga ion in the crystals and their physical properties were investigated.

Al doped $Ca_3TaGa_3Si_2O_{14}$ crystals were grown by the μ-PD method using the Pt-Rh crucible as nominal compositions of $Ca_3Ta(Ga_{1-x}Al_x)_3Si_2O_{14}$ [CTGAS] x = 0, 0.2, 0.4, 0.6, 0.8 and 1. The mixed powders were prepared using $CaCO_3$, Ta_2O_5, Ga_2O_3, Al_2O_3, SiO_2 and the mixed powders were sintered at 1200°C 12 hours in air several times. The sintered powder was set in the crucible and the crucible was put in the center of the high-frequency induction coil. The crucible was heated in air up to the melting point of by the CTGAS by the coil and the melt was pulled down by the seed crystal with a-axis along to the growth direction. During the crystal growth, the liquid-solid interface was observed by the CCD camera. The structural phases of grown crystals were identified by the powder X-ray diffraction (XRD) measurement. The plate crystals were cut from the grown crystals and they were polished for the measurements of crystallinity, chemical composition, local observation, piezoelectric constant and electrical resistivity.

The Al20% doped CTGS crystal was grown by the μ-PD method and the liquid-solid interface during crystal growth is shown in Fig.1(a). The meniscus was limited by the plate-shaped die of crucible and plate-shaped Al doped CTGS crystal was obtained (Fig.1(b)). The obtained crystal had high transparency and there is no visible cracks in the crystal.

The XRD patterns of undoped and Al20% doped CTGS crystals are indicated in Fig.2. The results showed that both undoped and Al20% doped CTGS crystals had a single phase of langasite-type structure

(trigonal, P321). The lattice parameters were calculated from the XRD patterns and the a- and c-axes of Al20% doepd crystal were smaller than those of undoped crystal (Fig.2). The decrease of lattice parameters suggests the Ga sites in CTGS crystal were substituted by the Al ions with smaller ionic radius than Ga ion. The crystal growth, actual chemical compositions and other physical properties of Al doped CTGS crystals with various Al concentrations will be reported.

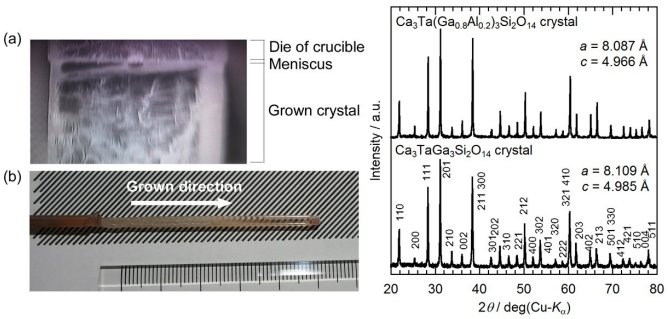

17:00	Poster	Mo178

Growth of Ce:doped $Lu_2Gd_1Al_2Ga_3O_{12}$ single crystal by the Czhocralski method and their scintillation properties

Akira Yoshikawa[1,2], Kei Kamada[2], Yasuhiro Shoji[1], Shunsuke Kurosawa[1,2], Yuui Yokota[2], Petr Prusa[3], Martin Nikl[1,3]

1. *Institute for Materials Research, Tohoku University, 2-1-1, Katahira, Aoba-ku, Sendai 980-8577, Japan* **2.** *New Industry Creation Hatchery Center, Tohoku University, Aoba-yama 6-6-10, Aoba-ku, Sendai, Miyagi, Sendai 980-8579, Japan* **3.** *Czech Academy of Sciences, Institute of Physics, Cukrovarnicka 10, Prague 16253, Czech Republic*

e-mail: yoshikawa@imr.tohoku.ac.jp

Scintillator materials combined with photodetectors are used to detect high energy photons and particles in X-ray computed tomography (CT), positron emission tomography (PET) and other medical imaging techniques, high energy and nuclear physics detectors, etc. In the last two decades, great effort was made to develop more efficient and faster scintillators in order to detect ionizing radiation. This effort resulted in development of Ce-doped orthosilicates, namely the Gd_2SiO_5 (GSO), Lu_2SiO_5 (LSO), $(Lu_{1-x}Y_x)_2SiO_5$ (LYSO), pyrosilicates based on $RE_2Si_2O_7$ (RE=Lu, Y,Gd) and most recently LaX_3 (X=Cl,Br) single crystal hosts. The best combination of stopping power, decay time, and light yield is currently achieved by Ce-activated materials. Nevertheless, there is still a continuous demand for new scintillator materials with even better properties. Oxide materials based on garnet structure are promising candidates for scintillator applications because of well mastered technology developed for laser hosts and other applications, optical transparency and easy doping by rare-earth elements. The Ce-doped $Lu_3Al_5O_{12}$ (Ce:LuAG) single crystal showed to be a prospective scintillator material with relatively high density of 6.7 g/cm^3, fast scintillation response of about 60–80 ns (due to the 5d1-4f radiative transition of Ce^{3+} providing the emission around 500–550 nm), and light yield of about 12–14,000 photon/MeV [1]. Recently, Ce:$(Lu_{y}Gd_{1-y})_3(GaxAl_{1-x})_5O_{12}$ scintillator grown by μ-PD method were investigated and $Lu_2Gd_1Ga_3Al_2O_{12}$ showed light yield of about 21000photon/MeV decay time of 46ns and density of 7.13 g/cm^3[2]. In this study, 1 and 2inch size $Lu_2Gd_1Ga_3Al_2O_{12}$ (LGGAG) single crystals were grown by the Czhocralski (Cz) method using an RF heating system. The rotation rate was 4–10 rpm and the growth rate was 1.0 mm/h. An automatic diameter control system using crystal weighing was applied to control the growth parameters. Crystals were grown from a 100mm diameter Ir crucible under Ar with adding CO_2 atmosphere to prevent evaporation of gallium oxide. The seed crystal was a [100] oriented LuAG crystal. The LGGAG crystals with a diameter of 50mm and length of 150 mm were grown. Powder X-ray diffraction and Electron Probe Micro Analyzer were performed to observe crystal phase and chemical composition of grown crystals. Scintillation properties such as light yield and decay time were also evaluated. The light yield of 2 inch size LGGAG was around 25,000photon/MeV. Effect of growth atmosphere, evaporation of gallium oxide and growth scale on scintillation properties will be discussed in the presentation.

Fig.1 Photograph of Cz grown LGGAG single crystal

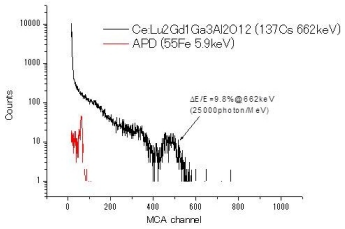

Fig.2 Energy spectra of LGGAG using APD S8664-55 at 20°C excited by ^{137}Cs

[1] Nikl, M.; Mihokova, E.; Mares, J. A.; et al. Phys. Stat. Sol. 2000, B 181, R10-R12 [2] K. Kamada, T. Yanagida J. Pejchal, M. Nikl, T. Endo, K. Tsutumi, Y. Fujimoto, A. Fukabori and A. Yoshikawa, Crystal Growth and Design, 11 (2011) 4484–4490

17:00	Poster	Mo179

Optical birefringence of β-SrB_4O_7 crystals with strontium substitutions

Alexandre I. Zaitsev[1,2], Maxim S. Molokeev[1], Aleksandre V. Cherepakhin[1,2], Nikita V. Radionov[1], Anatolii V. Zamkov[1]

1. *L.V.Kirensky Institute of Physics Siberian Branch of the Russian Academy of Science (IPH SB RAS), Academgorodok, 50, Krasnoyarsk 660036, Russian Federation* **2.** *Siberian Federal University (SFU), 79 Svobodny Prospect, Krasnoyarsk 660041, Russian Federation*

e-mail: az@iph.krasn.ru

Borate compounds with the noncentrosymmetric crystal structure are attractive materials for nonlinear optical (NLO) applications, especially in the UV region [1]. Orthorhombic α-SrB_4O_7 (α-SBO) crystals have been established to possess high NLO coefficients and a very short absorption edge but they have not sufficient birefringence for the existence of the second harmonic generation (SHG) phase matching conditions [2, 3, 4]. Recently, strontium tetraborate crystals have been obtained with another structure modification and their structure has been established. The structure of this β-SrB_4O_7 (β-SBO) with the trigonal symmetry belongs to the noncentrosymmetric P3 space group, the unit cell parameters being: a = 17.145 (1) Å, c = 4.2527 (5) Å [5]. The dispersion dependence of the refraction indexes β-SBO has been investigated and SHG phase matching conditions have been calculated [6]. According to [6] β-SBO crystals can be used in Type I SHG process down to 672 nm of the fundamental wavelength. Though the NLO coefficients of β-SBO haven't been measured yet, some attempts to extend investigations on the solid solution β-SBO:Pb have already been made [7].

Small single crystals of the solid solutions β-SBO:Ba and β-SBO:Pb have been obtained and main optical birefringence of these crystals has been measured.

β-SBO itself is a metastable crystal modification of this compound [8], so β-SBO crystals cannot be obtained with a temperature higher than ~ 780°C (the stable α-SBO melting temperature is 1000°C). Solid solution crystals β-SBO:Ba have been grown from a supercooled melt of the compositions (1-x)SrB_4O_7 × xBaB_4O_7 with x = 0.05; 0.1; 0.3 at about 700 – 720°C. β-SBO:Pb has been grown at 680°C from the melt with 15 mol % of PbB_4O_7.

Single crystal X-ray diffraction data on the obtained solid solution crystals were collected using diffractometer SMART APEX II (Bruker) with CCD detector.

The birefringence of the crystals has been measured by the compensation method with a Karl ZEISS AxioScop 40 polarized light microscope and a Berek compensator. The birefringence temperature dependence has been measured with a Lincam LTS 350 temperature controlled stage in the range from – 150 to +150°C.

The results are presented in Table 1.

One can see the solid solution birefringence increase with the increase of barium concentration. The effect of lead in the solid solution on the β-SBO birefringence is much higher, so the β-SBO:Pb birefringence is slightly higher than that for β-SBO:Ba with the dopant concentration being twice higher.

The birefringence temperature dependence has a sufficiently weak linear character for all the crystals with the temperature coefficient in range 1.5-3×10^{-6} $grad^{-1.}$

Barium substitutes strontium in the β-SBO structure only in three from five nonequivalent positions, though lead is distributed between all the positions.

Table 1.

Crystals of the β-SBO grown from the melt composition	Δn
SBO	0.031
SBO:5 % Ba	0.032
SBO:10 % Ba	0.034
SBO:30 % Ba	0.039
SBO:15 % Pb	0.040

Acknowledgements:

This study is supported by SB RAS Project 103, by Grant of the President of the Russian Federation for the support of leading scientific schools SS-4828.2012.2 and by RFBR Grant 11-02-00596-a.

References

1. Chuangtian Chen, Takatomo Sasaki et al. Nonlinear Optical Borate Crystals // WILEY-VCH, 2012, 388 P.

2. Oseledchik Yu.S., Prosvirnin A.L., Pisarevskiy A.I., et al. New nonlinear optic crystals: strontium and lead tetraborates // Optical Materials. – 1995. – Vol. 4. – pp. 669-674.

3. Zaitsev A.I., Aleksandrovskii A.S., Zamkov A.V., Sysoev A.M. Nonlinear optical, piezoelectric, and acoustic properties of SrB_4O_7 // Inorganic Materials. – 2006. – V. 42, No. 12. – pp. 1360-1362.

4. Petrov V., Noack F., Shen D., Pan F., Shen G., Wang X., Komatsu R., Alex V. Application of the nonlinear crystal SrB_4O_7 for ultrafast diagnostics converting to wavelengths as short as 125 nm // Optical Letters. – 2003. –V. 29, No. 4. – pp. 373-375.

5. Vasiliev A.D., Cherepakhin A.V., Zaitsev A.I. Trigonal crystal phase of strontium tetraborate, β-SrB_4O_7 // Acta Cryst. E. – 2010. – V. 66. – pp. 48-65.

6. Cherepakhin A.V. Obtainig, optical and nonllinear-optical properties of the α-, β- SrB_4O_7 and δ- BiB_3O_6. // DSc. Thesis, L.V. Kirensky Institute of Physics. - Krasnoyarsk. - 2011. - URL: http://www.kirensky.ru/zdoc/chav.pdf (in Russian).

7. Oseledchik Yu.S., Prosvirnin A.L., Lutsenko V.Yu. Nonlinear-optical phases in strontium tetraborate-lead tetraborate system // Functional materials. - V.19, No.1. - 2012. - pp 116-120.

8. Zaitsev A.I., Zamkov A.V., Koroleva N.S., Molokeev M.S., Cherepakhin A.V. Phase formation upon crystallization of $SrO{\cdot}2B_2O_3$ glasses // Crystallography Reports. - 2011. - V. 56, No. 1. - pp. 44–51.

17:00 Poster Mo180

Influence of the prolonged oxidizing annealing onto the spectroscopic properties of Cr:Mg_2SiO_4 crystals

Olga N. Zaytseva[1], Kirill A. Subbotin[1], Denis Lis[1], Anatoliy A. Ivanov[2], Evgeny V. Zharikov[1]

1. *A.M. Prokhorov General Physics Institute of Russian Academy of Sciences (GPI), Vavilov Str. 38, Moscow 119991, Russian Federation* **2.** *Photochemistry Center, Russian Academy of Sciences, Novatorov str. 7a, Moscow, Moscow 117421, Russian Federation*

e-mail: ozaytceva@mail.ru

Chromium doped forsterite Cr:Mg_2SiO_4 is well-known crystal for a tunable and femtosecond solid-state lasers emitting in the near infrared range (1.17-1.37 μm). It is using both in the optical communication and in biomedical field [1]. However, the wide usage of Cr: forsterite lasers is restrained by the parasitic absorption of Cr^{2+} ions. Earlier, in Refs [2, 3] there was reported that oxidizing annealing can, in principle, reduce the concentration of divalent chromium ions and at the same time the content of tetravalent chromium ions increases. The results of our attempts to optimize the characteristics of Cr:Mg_2SiO_4 laser crystals by the prolonged oxidizing annealing are presented in this talk. The dynamics of evolution of chromium content in different oxidation states during the series of prolonged oxidizing annealings of forsterite single crystals grown in different conditions and having initially different ratios of Cr^{2+}: Cr^{3+}: Cr^{4+} concentrations were studied. Forsterite single crystals were grown by the Czochralski technique [4] using iridium crucibles on seeds cut along the **a** crystallographic axis (P*bnm* notation). The pulling and rotation rates of the crystals were 3 mm/h and 12 rpm, respectively. The stoichiometric mixture of oxides MgO and SiO_2 with 4N qualification was used as the charge. Chromium concentrations in the melt were 0.13 - 0.14 wt %. The growth atmosphere was extra-pure argon or a mixture of argon with oxygen (the partial oxygen pressure 2.2 kPa). This parameter was controlled in real time using the oxygen analyzer AKPM-01. Samples shaped as cube (5x5x5 mm^3) were cut from single crystals and oriented using a DRON-4-13 X-ray diffractometer. The series of annealings of the samples in air was performed at 1573 K during 240 hours each treatment. Room-temperature polarized absorption spectra were measured before treatment and after each subsequent annealing by a Shimadzu UV-VIS-NIR scanning spectrophotometer. The obtained absorption spectra were approximated by sums of elementary Gaussians corresponding to elementary transistions between spin-orbital components of the ground and excited states of chromium ions of different oxidation states (Cr^{4+}, Cr^{3+} and Cr^{2+}). The spectra of the samples, in which the elementary band of the particular type is the best resolved, had been used to determine the peak position ν^c_i and half-width w_i for the corresponding Gaussian. Then, using the set of Gaussians with determined

in such a way fixed ν^c_i and w_i values, we calculated the Gaussian amplitudes A_i and background levels y_0 for each spectrum, which provided the best approximation of the experimental curve. It was found, that the prolonged oxidizing annealing of $Cr:Mg_2SiO_4$ crystals leads to the fast decrease of the Cr^{2+} ion concentration and slow monotonic increase of Cr^{4+} ion concentration. The dynamics of both processes were studied and discussed.

REFERENCES:

1. A. A. Ivanov, M. V. Alfimov, and A. M. Zheltikov // Physics-Uspekhi, 2004, Vol. 47, No. 7, P. 687-704.

2. Y. Yamaguchi, K. Yamagishi, A. Sugimoto, Y. Nobe // OSA Proceedings on Advanced Solid-State Lasers. 1991, Vol. 10. P. 52-56.

3. W. Chen, G. Boulon // Optical Materials. 2003. Vol. 24. P. 163–168.

4. E.V. Zharikov, A.V. Gaister, V.B. Dudnikova, and V.S. Urusov // J. Cryst. Growth, 2005, Vol. 275, No 1-2, P. e871-e875.

17:00 Poster Mo181

Research Advancement of Nonlinear Optical Crystal CsB3O5

Guochun Zhang, Shanshan Liu, Yicheng Wu

Center for Crystal Research and Development, Key Laboratory of Functional Crystals and Laser Technology, Technical Institute of Physics and Chemistry, Baoding 100190, China

e-mail: gczhang@mail.ipc.ac.cn

CsB_3O_5 (CBO) crystal possesses a relatively large effective nonlinear optical coefficients, a high laser damage threshold (26 GW/cm^2 for 1.0 ns pulses at 1053 nm), and a wide optical transparency range (167-3400 nm). CBO crystal can be expected to generate more efficient and high power ultraviolet light by frequency conversion of Nd:YAG laser radiation than LiB_3O_5 (LBO) crystals. This work presents the progress of CBO crystal on growth, properties, as well as output of ultraviolet laser.

A free of scattering centers CBO crystal, up to 47×45×41 mm^3 in size and 221 g in weight, has been grown by the top-seeded solution growth (TSSG) method from Cs_2O-B_2O_3-MoO_3 system. The suitable region for CBO crystal growth was investigated by the growth experiments, viscosity and volatility measurements, which confirmed that the optimal molar ratio of Cs_2O: B_2O_3: MoO_3 was 2:3:2.5. The grown CBO crystals possess high optical quality. The full-width at half-maximum (FWHM) of the rocking curve is 0.0057 º, and the optical homogeneity is at the level of 10-6 cm^{-1}. The optical absorption at the critical wavelengths of 1064 and 532 nm was measured to be 200 and 60 ppm cm^{-1}, respectively. The laser-induced damage threshold (LIDT) at λ=1.064 nm and τ=5.0 ns is about 4.50 GW cm^{-2}.

Thermophysical properties including the specific heat, thermal diffusion, thermal conductivity, and thermal expansion were systemically investigated for the first time. The specific heat was measured to be 0.512-0.796 J·g^{-1}·K^{-1} in the temperature range from 25 to 300°C. According to the measured thermal diffusion coefficients, the thermal conductivities along the *a*-, *b*-, and *c*-axis at 30°C were calculated to be κ_a =1.43 W·m^{-1}·K^{-1}, κ_b =2.50 W·m^{-1}·K^{-1}, and κ_c =1.51W·m^{-1}·K^{-1}, respectively. CBO exhibits strongly anisotropic thermal expansion behavior, and the mean thermal expansion coefficients in the temperature range from 25 to 500 °C are α_a=46.77×10^{-6}/°C, α_b=18.39×10^{-6}/°C, and α_c= -3.80×10^{-6}/°C.

Principal refractive indices of crystal CsB_3O_5 (CBO) at the wavelengths of 0.266, 0.355, 0.532, 0.473, 0.633, 1.064, and 1.338μm were accurately measured by using auto-collimation method within the temperature range from 40 to 190ºC. Equations of thermal refractive index coefficients as a function of wavelength were derived and reported for the first time, which could be used to calculate the principal thermal refractive indices at different wavelengths. Sellmeier equations at different temperatures were derived and used to calculate the phase-matching (PM) angles for the third-harmonic generation (THG) and the fourth-harmonic generation (FHG) of CBO crystal at different temperatures.

In addition, a high-power 278 nm ultraviolet (UV) laser through fourth harmonic generation (FOHG) of a diode-pumped 1112 nm Nd:YAG laser has been demonstrated in CBO crystal for the first time. The maximum average output power of the 278 nm laser is up to 1.5 W. The results demonstrated that CBO crystal is a promising NLO material for UV high-power lasers below 300 nm.

Key words: CsB_3O_5; nonlinear optical crystal; thermophysical property; thermal refractive index coefficient

References

[1] Y. C. Wu, T. Sasaki, N. Nakai, A. Yokotani, H. G. Tang and C. T. Chen, *Appl.Phys. Lett.,62* (21) (1993)2614-2615.

[2] Y. C. Wu, P. Z. Fu, J. X. Wang, Z. Y. Xu, L. Zhang, Y. F. Kong and C. T. Chen, *Opt. Lett.,* 22 (24) (1997) 1840-1842.

[3] N. A. Pylneva, L. L. Pylneva, A. B. Meshalkin, V. I. Kosyakov and A. B. Kaplun, The 16th international conference on crystal growth (ICCG16), Beijing, China, August 8-13, 2010.

[4] H. Y. Shen, D. Y. Zhang, W. Liu, W. Z. Chen, G. F. Zhang, G. Zhang, and W. X. Lin, *Applied Optics*, 38 (1999) 987-990.

17:00 Poster Mo182

Single crystal growth, characterization, and properties of multifunctional materials $LiMP_2O_7$ (M = Fe, Cr)

Weiguo Zhang[1], Elise Pachoud[2], Kao-Chen Liang[3], Bernd Lorenz[3], Shiv Halasyamani[1], Paul Chu[3,4]

1. *Aalto University, Espoo FI-00076, Finland* **2.** *University of Houston, Chemistry Dept., Houston, TX 77204, United States* **3.** *University of Houston, Texas Center for Superconductivity and Advanced Materials, Houston, TX 77204, United States* **4.** *Lawrence Berkeley National Laboratory (LBNL), 1 Cyclotron Road, Berkeley, CA 94720, United States*

e-mail: wgzhang82@gmail.com

Multifuctional materials, especially multiferroics, have attracted much attention attributable to their coexistence and mutual interaction of magnetic and electric orders. However, ferroelectricity and magnetic ordering are often mutually exclusive, which leads to the rarity of materials exhibiting both properties. On the other hand, large single crystals of advanced functional materials are necessary for detailed physical property measurements. This is particularly true with low symmetric systems, such as polar oxides. $LiFeP_2O_7$ and $LiCrP_2O_7$, both crystallize in polar structures with the monoclinic space group $P2_1$ (No. 4). Meanwhile, Fe^{3+} and Cr^{3+} are magnetic ions. The coexistence of the magnetic order with the electrical polarization makes $LiFeP_2O_7$ and $LiCrP_2O_7$ interesting candidates for studying the magnetoelectric coupling in electrically polarized materials. Using a flux growth method, we have grown centimeter size crystals of new polar materials - $LiFeP_2O_7$ (Figure 1), and $LiCrP_2O_7$. SHG, piezoelectricity, and polarization were measured. In addition, the magnetic, thermodynamic, and pyroelectric properties of oriented single crystals are investigated. Crystal growth details and functional property measurements will be described.

Figure 1. $LiFeP_2O_7$ single crystal

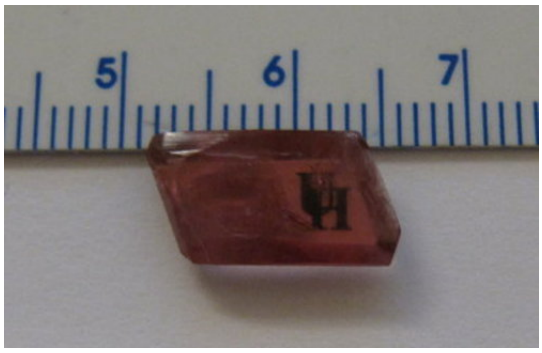

17:00 Poster Mo183

Growth and high temperature properties of langasite structure crystal $Ca_3Ta(Al_{0.9}Ga_{0.1})_3Si_2O_{14}$

Kainan Xiong[2], Yanqing Zheng[1], Xiaoniu Tu[2], Shujun Zhang[3], Haikuan Kong[2], Erwei Shi[2]

1. *Shanghai Institute of Ceramics, Chinese Academy of Sciences, 1295 Dingxi Road, Shanghai 200050, China* **2.** *Shanghai institute of ceramics, Chinese academy of sciences, Shanghai 201800, China* **3.** *Penn State University, State College, PA 16802, United States*

e-mail: zyq@mail.sic.ac.cn

Piezoelectric crystals of langasite, langatate and $Ca_3TaGa_3Si_2O_{14}$ (CTGS) with langasite structure were broadly used in high temperature sensors in recent years. The high content of gallium made these crystals much more expensive compared than quartz. A bulk single crystal $Ca_3Ta(Al_{0.9}Ga_{0.1})_3Si_2O_{14}$ (CTAGS) of langasite structure in which 90% percent of gallium was replaced by aluminum was successfully grown by Czochralski technique. The as-grown CTAGS crystal has similar growth habits of CTGS with the dimensions of 20 mm in thickness, 70 mm in width and 80 mm in length. The piezoelectric constant d_{11}, the dielectric constant ε_{11}, the electromechanical coupling coefficient k_{12}, the mechanical quality factor Q, the electric resistivity, and dielectric loss of x-cut plate of CTAGS were measured under different temperatures from room temperature up to 900ºC. The d_{11} rise from 3.99 pC/N to 5.67 pC/N while rise from 13.7% to 15.4%. Compared with reported data, it is found that at temperature below 600ºC, CTAGS crystal has highest resistivity among langasite structure crystals. The advantages of low cost of raw material, easy to grow bulk crystal, combined with the properties of the high resistivity make CTAGS a potential materials for high temperature application.

Wednesday, 14 August

Posters WePo
Wednesday afternoon, 14 August, 16:00

Topical Session 7

Novel materials and structures

Session Coordinators

Jacek Baranowski (Poland) *Jacek.Baranowski@fuw.edu.pl*

Jacek Majewski (Poland) *jacek.majewski@fuw.edu.pl*

Sudhir B. Trivedi (USA) *strivedi@brimrose.com*

Programme

Wednesday, 14 August

WeP-T07
Wednesday afternoon, 14 August, 16:00
Room 106, Old Library

Break
Wednesday afternoon, 14 August, 17:30

Thursday, 15 August

ThO3

T07: Novel materials and structures
Thursday afternoon, 15 August, 16:30
Room B, Auditorium Maximum

16:30 Invited oral

CVD of graphene on SiC

Wlodek Strupinski

Institute of Electronic Materials Technology (ITME), Wólczyńska 133, Warszawa 01-919, Poland

e-mail: wlodek.strupinski@itme.edu.pl

Graphene, the first available to us two-dimensional (2D) atomic crystal is a new material composed of one or more sheets of carbon atoms in which each carbon atom is covalently bound to its 3 neighbors (sp^2 bonds) to form the honeycomb structure. For discovery of this material the Nobel Prize in Physics 2010 was awarded. The particular arrangement of the graphene layers called the Bernal stacking and the exceptional properties of the strong bonds sp^2 which are stronger than carbon bonds in diamond greatly affects the electronic, mechanical and thermal properties of this material and its applications (e.g. RT mobility >200000cm^2/Vs). The properties of epitaxial graphene are so compelling that it is currently recognized by the electronics industry as a possible alternative or even the successor to silicon for large scale integrated electronics and also suggest that graphene could be applied in other innovative devices or composites replacing traditional materials. Additionally, these extreme properties combined in one material could also enable development of new technologies as flexible electronics, transparent protective coatings and barrier films.

However, the true scientific and technological potential of graphene may not be known until very high quality material are created. This can only be achieved by facing such challenges as a graphitization with one atomic layer resolution and characterization of graphene morphology and electrical features in nano-technology, physics, chemistry and material science.

In order to improve graphene structure, in particular to increase the graphene flakes and thickness uniformity various growth directions were explored to obtain graphene growth conditions that retain essential features of a single graphene layer regardless of their number. The optimization of the growth conditions enabled to achieve atomic layer-by-layer control on the graphene growth. A principle issue in any future studies of the electrical properties of 2D graphite sheets is a precise measurement of the film thickness, defects (cracks, flakes borders, "puckers") and strains.

Graphene deposited on a SiC has great potential for electronics applications, however, a major factor hindering the development of technology for the large-scale production of graphene-based nano-electronic devices is the lack of access to high-quality uniform graphene layers grown on large SiC substrates. Graphene produced by sublimating Si from SiC heated to high temperatures (1200-2000^oC) is sensitive to the surface quality of the SiC substrates. Concurrently, the CVD epitaxial growth of graphene on metal substrates has lately received much attention. Unfortunately, epitaxial growth on metals suffers from the disadvantage that electronic applications require graphene on an insulating substrate, and although wafer-scale transfer is possible, it is a difficult process. A fundamental question thus arises: how can one reduce the dependence of graphene growth on substrate quality and simultaneously improve graphene layer uniformity? The differences between epitaxial graphene layers on 4H-SiC(0001) obtained by two different growing techniques have been investigated. The first method, commonly used is based on sublimation of Si from SiC(0001) surface at high temperature (S-EG). The second method has been developed by chemical vapor deposition technique (CVD-EG). In this paper, we report the CVD of epitaxial graphene (CVD-EG) on SiC substrates using propane gas as the carbon precursor. Graphene layers were grown using a commercially available horizontal CVD hot-wall reactor (Aixtron VP508), which is inductively heated with an rf generator. The epitaxial CVD of graphene relies critically on the creation of dynamic flow conditions in the reactor that simultaneously stop Si sublimation and enable the mass transport of propane to the SiC substrate. While protecting against Si sublimation, C deposition was enabled with one monolayer resolution by taking advantage of the high efficiency of kinetic processes at high *T* and low *P*.

The CVD-EG approach offers numerous potential benefits in comparison to S-EG, including the reduction of substrate surface influence on graphene thickness uniformity and the application of well-developed commercial epi-systems for SiC epitaxy. The proposed method permits the growth rate of graphene on the C-face of SiC(000-1) to be considerably lowered enabling the growth of 1ML, which is extremely difficult in the case of S-EG. Additionally, FLG can be grown on the Si-face SiC(0001) which, in comparison to max 2-3 ML of S-EG, creates greater research opportunities. Our approach also enables precise growth rate control by adjusting the mass transport of the carbon precursor in a similar way to the method used in MOCVD/CVD, as well as the passivation of the SiC substrate by any substances prior to graphene growth. Moreover, one can tune the reactor conditions to grow both CVD-EG and S-EG in the same system.

The growth mechanism is discussed and the hydrogen intercalation results are presented. To provide information at the atomic scale, samples were characterized by scanning tunneling microscopy (STM), micro-Raman spectroscopy, LEEM, LEED and transmission electron

microscopy (TEM). The thickness of the graphene films were estimated also by ellipsometry, the position of the s and p electronic energy bands were evaluated by angle-resolved photo-emission spectroscopy (ARPES). ARPES data clearly show the expected linear dispersion for relativistic electrons near Dirac point. The transport parameters of the graphene samples were measured with the van der Pauw method and microwave resonance technique at room temperature. The electron density in several 1-2 ML graphene films grown in subsequent processes was typically 2-4x10^{12} cm^{-2}, with a macroscopically averaged electron mobility inferred from Hall voltage in the range 1200-1800 cm^2/Vs, demonstrating the high electronic quality of the CVD-EG layers on the wafer scale. The micro Raman maps have been created with 3mm light spot using 530 points measured on 2,3 x 2,3 mm^2 area in the center of the sample. Histograms reveal that CVD growth of graphene produces less strained layers in comparison with S-EG.

17:00 Invited oral

Structural controllability of C clusters by template effect of SiC step

Masato Inoue[1], Yoshihiro Kangawa[1,2], Hiroyuki Kageshima[3], Koichi Kakimoto[1,2]

1. *Kyushu University, Department of Aeronautics and Astronautics, Fukuoka 819-0395, Japan* **2.** *Kyushu University, Research Institute for Applied Mechanics, Kasuga 816-8580, Japan* **3.** *NTT Basic Research Laboratories, Atsugi 243-0198, Japan*

e-mail: minoue@riam.kyushu-u.ac.jp

The thermal decomposition of SiC(0001) surface is a promising industrial-scale graphene growth method; however, the crystalline quality of graphene still has considerable scope for improvement, for which it is essential to understand the growth process and clarify governing factors. In this study, we dedicated ourselves in theoretically investigating the C clustering (nucleation) process, with an aim to clarify the template effect of the SiC(0001) surface for the initial stage of graphene growth.

We studied the C clustering process at a single-bilayer SiC step tilting towards the [11$\underline{2}$0] or [1$\underline{1}$00] direction via the tight-binding total-energy calculation [1]. The clustering process was determined as follows: 1) a hexagonal C cluster with the lowest energy was placed on the SiC(0001) surface. 2) C atoms were added one-by-one to various sites around the cluster. 3) The most stable structure of the C cluster up to C_{30} was determined.

Our numerical analysis revealed that penta-heptagonal/purely hexagonal structures appear at the C-terminated [1$\underline{1}$00] (C-[1$\underline{1}$00]) step or at the [11$\underline{2}$0] and Si-[1$\underline{1}$00] step. At the [11$\underline{2}$0] and Si-[1$\underline{1}$00] steps, C clusters bonded with the step edge and formed a 3D round structure, while those at the C-[1$\underline{1}$00] step extended to the terrace and formed the 2D island structure.

C clusters on the terrace exhibit penta-heptagonal structure so that they can relax the lattice mismatch between graphene and SiC(0001) surface [2]. This result on the terrace analogously explains the appearance of 2D penta-heptagonal structures at the C-[1$\underline{1}$00] step. In addition, the purely hexagonal configuration can be attributed to the 3D structure because the 3D structure is partly apart from the surface and free from the lattice mismatch. The dimension of the cluster (2D or 3D) is subject to the edge decollation by C clusters. This trend is determined by the SiC step structure, i.e. dangling bonds on the step edge. Hence, we revealed the structural controllability of C clusters by the template effect of SiC steps.

Acknowledgments

This work was partially supported by a Grant-in-Aid for JSPS Fellows (40-7700). We thank Prof. S. Tanaka of Kyushu University for useful discussions and comments.

References

[1] M. Yu et al., Physica E 42 (2009) 1-16.

[2] M. Inoue et al., Physical Review B 86 (2012) 085417-1-7.

17:30 Oral

A simple model of epitaxial graphene growth on SiC substrates

Rafał Bombolewski, Piotr Szymczak

Faculty of Physics, University of Warsaw, Hoża 69, Warszawa 00-681, Poland

e-mail: rbomb@fuw.edu.pl

Graphene, an atom-thick, two-dimensional carbon sheet holds great promise for future application in high-speed electronics. One of the most important challenges for researchers since its discovery has been manufacturing graphene sheets of high quality and controlling the growth kinetics. In our work, we present a theoretical model of growth of graphene on (0001) face of 6H-SiC . The model is an extension of the kinetic MC model of graphene growth proposed by Ming & Zangwill (PR B 84, 115459 (2011)).

We show that if the growth is stable and nucleation of graphene layers on terraces is faster than their propagation, kinetic equations describing evolution of the system in time simplify considerably. The growth dynamics is then characterized by a number of linear growth regimes, in each of which the growth rate remains constant. We will show that model is self-consistent by comparing its predictions with KMC numerical data. Different methods of extracting model's parameters from experimental data will be discussed.

17:45 Oral

An influence of parallel electric field on the dispersion relation of graphene – a new route to Dirac logics

Jakub Sołtys[1], Stanisław Krukowski[2], Jolanta Borysiuk[3,4], Jacek Piechota[5]

1. *University of Warsaw, Interdisciplinary Centre for Mathematical and Computational Modelling (ICM), Pawinskiego 5a, Warsaw 02-106, Poland* **2.** *Polish Academy of Sciences, Institute of High Pressure Physics (UNIPRESS), Sokolowska 29/37, Warszawa 01-142, Poland* **3.** *Polish Academy of Sciences, Institute of Physics, al. Lotników 32/46, Warszawa 02-668, Poland* **4.** *Instytut Fizyki PAN, Al. Lotnikow 32/46, Warszawa 02668, Poland* **5.** *Interdisciplinary Centre for Mathematical and Compuerial Modelling, University of Warsaw (ICM), ul. Pawinskiego 5a, Warszawa 02-106, Poland*

e-mail: qba@icm.edu.pl

Ab initio density functional theory (DFT) simulations were used to investigate an influence of electric field, parallel to single and multilayer graphene on its electron dispersion relations close to K point. It was shown that for both single layer and AAAA stacking multilayer graphene under influence of parallel field the dispersion relations transform to nonlinear, i.e. emergence of mass. The effect, associated with the hexagonal symmetry breaking, opens new route to high speed transistors and logical devices working in Dirac regime. The implementation of such device is presented.

18:00 Oral

Formation of p/n junction in some tetradymite-type topological insulators

Konstantin A. Kokh[1,2,3], Oleg Tereshchenko[2,3,4], Sergey Makarenko[2,4], Vladimir Golyashov[2,4]

1. *Institute of Geology and Mineralogy SB RAS (IGM), Koptyuga ave., 3, Novosibirsk 630090, Russian Federation* **2.** *Novosibirsk State University (NSU), Pirogov 2, Novosibirsk 630090, Russian Federation* **3.** *Tomsk State University (TSU), Lenina, 36, Tomsk 634050, Russian Federation* **4.** *Institute of Semiconductor Physics SB RAS, Lavrentjeva 13, Novosibirsk 630090, Russian Federation*

e-mail: k.a.kokh@gmail.com

Layered compounds with the structure of tetradymite mineral were considered as the cost-effective thermoelectric materials. But recently they have attracted more attention due to discovery of new physical properties - topological insulating [1]. It means that they have specific spin-split surface states which provide unobstructed motion of electrons in the surface layer while the bulk conductivity theoretically tends to zero. However these materials are hard to be bulk grown with stoichiometric composition. Therefore they exhibit metallic behavior due to intrinsic carriers which in turn hamper the study and application of the specific surface states.

Sidestepping of this problem may be done by means of p-n transition which should result in the compensation of intrinsic carriers [2]. Experimental attempts concerning bulk crystals were reported only for the system Bi-Te-Se up to date. The first work has shown positive to negative transition of Hall coefficient with temperature in the Bridgman solidified $Bi_2Te_2Se_{0.995}$ melt [3], while another team has correlated a presence of p- and n- type phases in room-temperature Bi_2Te_2Se crystal with the decay of solid solution [4].

In order to obtain p-n transition in the as-grown crystals of topological insulators it is proposed to use natural segregation of the components during quazi-equilibrium crystallization of solid solution. According to this approach we report the procedure and theoretical explanation of reproducible growth of Bi_2Te_3 single crystals with p- and n- conductivity in the beginning and final parts, correspondingly. Due to orientation of cleavage plane {0001} along the growth axis the samples with p/n junctions were obtained. The electrophysic measurements have shown high charge mobility for this region – more than 6×104 cm^2/Vs at T=4 K.

Also, a possibility of creating p/n transitions in ternary compounds $Bi_2(Te,Se)_3$ and $(Bi,Sb)_2Te_3$will be discussed.

Acknowledgments to RFBR project #12-02-00226-a.

References:

1. Zhang H., Liu C.-X., Qi X.-L., Dai X., Fang Z., Zhang S.-C. Topological insulators in Bi_2Se_3, Bi_2Te_3 and Sb_2Te_3 with a single Dirac cone on the surface // Nature Physics 2009, 5, 438-442.

2. J. Wang, X. Chen, B.-F. Zhu, and S.-C. Zhang. Topological p-n junction // Phys. Rev. B 2012, 85, 235131(4).

3. Sh. Jia, H. Ji, E. Climent-Pascual, M.K. Fuccillo, M.E. Charles, J. Xiong, N.P. Ong, R.J. Cava. Low-carrier-concentration crystals of the topological insulator Bi_2Te_2Se // Phys. Rev. B 2011, V.84, 235206(6).

4. J.-Li Mi, M. Bremholm, M. Bianchi, K. Borup, S. Johnsen, M. Sodergaard, D. Guan, R.C. Hatch, P. Hofmann, Bo B. Iversen. Phase separation and bulk p-n transition in single crystals of Bi_2Te_2Se topological insulator // Advanced materials 2013, 25, 889-893.

18:15 Oral

Exploratory investigation of new IR NLO materials

Jiyong Yao, Wenlong Yin, Kai Feng, Yicheng Wu, Chuangtian Chen

e-mail: jyao@mail.ipc.ac.cn

The search for new IR nonlinear optical (NLO) materials is a very active field in modern Inorganic Materials Chemistry. By applying a research strategy that combines "structural design" with "exploratory synthesis", we have discovered a number of new IR NLO materials, namely the $BaGa_4Se_7$, $LiGaGe_2Se_6$, $Li_2In_2MQ_6$ (M=Si,Ge; Q = S,Se), and $BaGa_2MQ_6$(M = Si,Ge;Q = S,Se) compounds. They possess not only large NLO responses and large band gaps but also the valuable thermal behavior of congruent-melting, which makes it feasible to grow high quality bulk crystals needed for thorough evaluation and practical application. We have obtained high quality $BaGa_4Se_7$ single crystal in centimeter size and measured many important physical properties incluing the refractive index, the NLO coeffecient, and the laser damage threshold. The results indicate that $BaGa_4Se_7$ is a promising new IR NLO material with good overall properties.

Break
Thursday evening, 15 August, 18:30

Friday, 16 August

FrO1

T07: Novel materials and structures
Friday morning, 16 August, 8:30
Room B, Auditorium Maximum

8:30 Invited oral

The Weak Bonds in the Growth of Low-Dimensional Crystals

Christian Kloc

Nanyang Technological University, Singapore, Singapore

e-mail: ckloc@ntu.edu.sg

Widely used metals, semiconductors or insulators contain well defined elements or compounds like semiconductors, Si or GaAs, where all chemical bonds between individual atoms are the same. The covalent bonds between silicon atoms in silicon crystal or covalent bonds between gallium and arsenic atoms in GaAs crystal make such single crystal similar to one very large molecule. In many substances, not all bonds are the same. In some, additionally to the covalent bonds, the weak Van der Waals bonds appear and may be nice oriented in parallel layers. These types of crystals are oft labeled as two dimensional crystals. As examples, graphene and transition metal dichalcogenides can be named. Specific 2D properties and new defects emerge and specify behavior of low dimensional structures. If the weak bonds are oriented in two non-parallel layers, the strong covalent bonds prevail only in one direction and one-dimensional crystals are formed. Needles made from $NbSe_3$ may be an example of such 1D crystal. However, the largest group of crystals, with weak bonds, is this where elements or molecules are weak bonded like in crystals made from noble gases, or crystals made from molecules. In the last the group, atoms forming molecule are bond by strong intra-molecular covalent bonds and mo-

lecules with each other are bonded by weak Van der Waals bonds. Millions of organic molecular crystals show such behavior. If the molecules in molecular crystals are not all the same, assume two different types of molecules, one type may behave as a charge acceptor or the other as a charge donator than new type of compounds, resembling binary compounds, may be formed. One of such group is classified as organic binary compounds or charge transfer salts. Whereas inorganic binary compounds are well represented in binary phase diagrams, binary phase diagrams composed of organic weak bonded compounds are practically non-existing, in spite that individual binary compounds are well defined and intensively studied. For example, Tetrathiafulvalene and 7,7,8,8-Tetracyanoquinodimethane (TTF-TCNQ) in the relation 1:1 are famous for excellent electrical conductivity reaching those of metals. B'-(BEDT-TTF)-ICl2 in stoichiometry 1:1:2 is an organic superconductor with critical temperature as high as 14.2 K. One may ask, what are the properties of other compounds with stoichiometry 1:2, 2:3, 3:2 or do such compounds exist? Because the phase diagrams are not known this question cannot be simple answered and the computer simulations deliver only vague indications. Also the questions how to crystallize binary weak bonded compounds when even the existence of compounds is guessed is ambiguous. A weak bonded binary system, where phase diagram is not known but two binary compounds are already detected, is the system perylene –TCNQ . Compounds P1T1 and P3T1 have been reported in literature. One more, P2T1 has been found by authors and reported in this talk. The phase relation, crystal growth of binary compounds between perylene and TCNQ in relation to the general problem of crystallization and structure – properties relations in weak bonded systems is discussed. Single crystal of organic binary compounds of (perylene)1-TCNQ1 (P1T1), (perylene)2-TCNQ1 (P2T1) and (perylene)3-TCNQ1 (P3T1) were synthesized and grown in one process. Due to the weak bonds, both the solution and the physical vapor transport methods have been applied. Needle and plate-like single crystals were used for X-ray structure determination and for electrical measurement. Depends on stoichiometry, n-type, p-type and ambipolar behavior have ben measuring. This example illustrate that forming weak bonded binary or more complex compounds leads to new properties unavailable in simple monocomponent crystals.

9:00 Invited oral

High pressure growth of new multiferroics materials

Edmondo Gilioli

IMEM- CNR (IMEM), Parma, Italy

e-mail: edi@imem.cnr.it

Multiferroics are defined as materials exhibiting simultaneously more than one primary ferroic order parameter among ferromagnetism, ferroelectricity, ferroelasticity and ferrotoroidicity.

Beside the fundamental research at the frontline of the material science, multiferroics are gaining increasingly interest for their potential applications in the field of sensors, electronic devices or whenever the electrical/magnetic properties can be mutually controlled.

However, these compounds are rare in nature and the coupling (between ferromagnetism and ferroelectricity in the most common case) is typically weak for practical use.

The synthesis under high pressure/high temperature (HP/HT) is a powerful tool to obtain new materials; moreover, the application of external pressure induces structural changes, which are often responsible of peculiar properties.

In this presentation, a selection of bulk multiferroic materials with perovskite-based compounds synthesized by HP/HT techniques at IMEM-CNR will be reviewed. The perovskite structure is a model system, for its ability to accommodate pressure-induced distortions in different ways, giving rise to metastable phases.

Increasing the structural complexity, from conventional-perovskite compound (BiMnO3) to double- (Bi2FeMnO6, PbFeMoO6) and quadruple-perovskite (BiMn7O12), the fundamental role of high pressure on the structural and the magneto-electric properties originated by the multiferroic coupling will be discussed.

9:30 Oral

Synthesis of novel aluminum-based alloy hydrides under high pressure and high temperature

Hiroyuki Saitoh[1], Naruki Endo[1], Akihiko Machida[1], Yoshinori Katayama[1], Katsutoshi Aoki[2]

1. *Japan Atomic Energy Agency (JAEA), 1-1-1 Kouto, Sayo-cho,Sayo-gun, Hyogo 679-5148, Japan* **2.** *Institute for Materials Research, Tohoku University, 2-1-1, Katahira, Aoba-ku, Sendai 980-8577, Japan*

e-mail: cyto@spring8.or.jp

Aluminum-based alloy hydrides have been explored as lightweight hydrogen storage materials. A few aluminum-based alloys have been reported. For example, F. Gingle et al. have reported $SrAl_2H_2$ Zintl phase hydride [1]. $Y_3Al_2H_{6.5}$ has been synthesized by hydrogenating Y_3Al_2 alloy [2]. These hydrides have been synthesized near ambient pressure. Novel aluminum-alloy hydrides are expected to be synthesized under high pressure and high temperature in which conditions hydrogen becomes extremely reactive and it can reacts with passivated aluminum [3]. In the present study, hydrogenation reactions of aluminum-based alloys were investigated under high pressure and high temperature. The reactions were monitored by *in-situ* synchrotron radiation x-ray diffraction measurements to clarify its reaction process and to optimize its synthetic conditions.

High-pressure and high-temperature conditions were generated using a cubic-anvil-type multi-anvil high pressure apparatus. Aluminum-based intermetallic alloys were pressurized and immersed in hydrogen fluid at high temperatures to form their hydrides. Hydrogenation reactions were monitored by an *in-situ* measurement system installed in the beamline BL14B1 at SPring-8.

It was clarified that Al_3Ti intermetallic alloy was hydrogenated to form Al_3TiH_x (x~0.4) interstitial hydride at 10 GPa and 625°C. While Al_3Ti alloy was successfully hydrogenated, other aluminum-based alloys such as Al-Ga, Al-Si and Al-Mg were not hydrogenated. In the case of these alloys, pure AlH3 was formed by the high-pressure and high-temperature treatment. The formation mechanism of aluminum-base alloy hydride are being investigated using the *in-situ* measurement system to explore other novel aluminum-based alloy hydrides.

Part of this work was supported by New Energy and Industrial Technology Development Organization (NEDO), "Advanced Fundamental Research Project on Hydrogen Storage Materials" and "Feasibility Study on Advanced Hydrogen Storage Materials for Automotive Applications (2012)."

9:45 Oral

The forming of thermoelectric compound by hot extrusion: numerical simulation and microstructure control

Anatoly I. Prostomolotov[1], Mikhail V. Mezhennyi[2], Mikhail G. Lavrentev[3], Vladimir B. Osvenskyi[3]

1. *Institute for Problems in Mechanics of RAS (IPMECH), Vernadskogo prospect 101, bl. 1, Moscow 119526, Russian Federation*
2. *Technological Institute for Superhard and Novel Carbon Materials (TISNCM), Centralnaya, 7a, Moscow 142190, Russian Federation*
3. *State Institute of Rare Metals (GIREDMET), B. Tolmachevsky per., Moscow 119017, Russian Federation*

e-mail: prosto@ipmnet.ru

The most widespread methods for producing thermoelectric materials are directional solidification techniques: Czochralski, Bridgman methods and zone melting. The other group of methods belongs to a powder metallurgy. However, the powder compressed samples include the disoriented grains, which impair their thermoelectric properties. The more efficient method is the hot extrusion (HE) [1,2]. Its advantages in comparison of crystallization methods are following: the high mechanical strength and uniformity of extruded rod, the possibility of variation of its shape and cross-section, the high productivity and lower costs.

During HE process a pressed cylindrical billet (with diameter D and height L) is forced by a punch through a die at temperature T ~ 400 °C in according to the scheme shown in Fig. 1. The geometrical parameters of this die and the punch rate have the decisive impact on a product quality and process productivity.

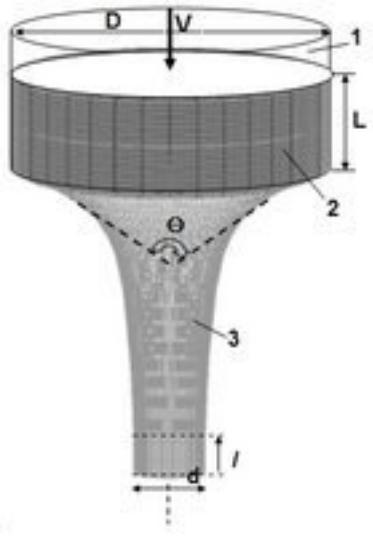

Fig. 1. Scheme of hot extrusion for thermoelectric composite *Bi*0.4*Sb*1.6*Te*3: 1 – ram, 2 – pressed billet, 3 – forming die (θ – angle of curvature, d – diameter, l – length of cylindrical outlet). V is the punch rate.

This work presents the numerical simulation of HE process for thermoelectric compound *Bi*0.4*Sb*1.6*Te*3, on the basis of which the evolution of its stress-strain state was investigated at different stages of this process. The numerical model is based on joint elastic-plastic approach. The numerical method uses the finite-element approximation on Lagrangian time-dependent grid, which changes with taking into account of a forming die. Calculations have been carried out by means of MSC Marc^{Ò} code [3].

The influence of die geometric parameters was investigated for its following variation: d= 20, 30 mm at l = 10 mm and θ = 100 and 120^{o}. Mechanical parameters of the material were set as the following: Young's modulus E = 40 GPa, Poisson's ratio ν = 0.3. The critical stress of elastic-plastic transition was set in accordance with the measured «stress-deformation» dependence as σ_o = 102 MPa.

The transverse and longitudinal changes in a composition structure of extruded samples have been investigated by x-ray diffraction measurement, optical and electronic microscopy [4]. In accordance with these experimental data the regions were established, which were responsible for the composition formation and microstructure of these samples. Their comparison with the data of numerical simulation has showed that these regions correspond to a plastic deformation at distance ~ 4 cm from the upper edge of die, where stresses reach the maximum values.

Acknowledgments

This investigation was supported by JSC "ROSATOM" (the state contract:H.4б.44.90.13.1050), and Russian Foundation for Basic Research (the grants: 11-08-00966, 12-02-01126*).*

References

[1] Sabo Ye.P. // J. Thermoelectricity. 2005. V. 3. P. 52-68.

[2] Yang J., Chen R., Fan X. et al. // J. Allows&Compounds. 2007. V. 429. P. 156-162.

[3] License certificate of MSC Marc^{Ò}: RE007990PCS. 2008.

[4] Lavrentev M.G., Osvenskii V.B., Mezhennii M.V. et al. // J. Thermoelectricity. 2012. V. 4. P. 36-42.

10:15 Oral

Improved Chemical Vapour Transport Growth of Transition Metal Dichalcogenides

Alberto Ubaldini, Enrico Giannini, Dirk Van Der Marel

DPMC, University of Geneva, 24 quai Ernest-Ansermet, Geneva 1211, Switzerland

e-mail: Alberto.Ubaldini@unige.ch

Layered transition metal chalcogenides, MX_2 (X = S, Se or Te) are long known and include a variety of compounds with a wide spectrum of electronic properties (semiconducting, semimetals, superconductivity and charge ordering). Recent studies on exfoliated semiconducting MoS_2 mono-layers have roused a growing interest in this class of materials, as being promising candidates for novel electronics, complementary to graphene. Tunability of the electronic structure in $TiSe_2$ and superconducting Cu-intercalated $TiSe_2$ has motivated investigations on the interplay between superconductivity and charge ordering. Despite of long standing reports on the crystal growth of MX_2 and wide growing interest in this materials, many details of the growth process (in most of the case, the crystals are prepared by Chemical Vapour Transport, CVT) and optimum experimental conditions still remain overlooked. In this work, we report the results of a systematic investigation of the effects of various parameters, like temperature, thermal gradient, nominal composition, total pressure, concentration of the transport agent and its nature, and annealing time on the crystal growth of semi-metallic $TiSe_2$, superconducting Cu_xTiSe_2 and semiconducting TaX_2 and MoX_2 (X = S, Se, Te). By optimizing the temperature, the temperature gradient and the initial concentration of I_2, very large crystals of about 1 cm^2 were grown within one day, instead of several days as usually reported. The effect of the I_2-M ratio has been better clarified, highlighting that the transport and growth mechanism occur via the formation of highly volatile iodides, like TiI_4, that determines

the nucleation rate. The growth kinetic is very fast at the beginning of the process and, depending on the temperature, mm^2 sized crystals can grow in few hours. Copper intercalated crystals could be grown either directly from a mixture of Cu, Ti, Se, using iodine, or by intercalating Cu atoms in already grown $TiSe_2$ crystals. In both cases, the copper content can be controlled and superconducting crystals are obtained. The effects of the nominal starting composition, in additions to the others factors, is discussed Interestingly, iodine is proven not to be the most effective transport agent for the heavy transition metals, like Mo and Ta. For this reason, a new growth route, starting from mixtures of chlorides, $MoCl_3$, $MoCl_5$ or $TaCl_5$, and their metals, was successfully gone through. In this case, the upper temperature was found to be the most critical parameter must be tuned as a function of the chalcogen element. The morphology of the crystals depends on the starting chlorine concentration and whiskers of $TaSe_2$ as thin as few μm and several mm long were found to grow when the Cl/Ta is too high.

Coffee

Friday morning, 16 August, 10:30

FrO2

T07: Novel materials and structures
Friday morning, 16 August, 11:00
Room B, Auditorium Maximum

11:00 Oral

Ceramic material ZnSe(Te) fabricated by nanopowder technology. Fabrication, phase transformations and photoluminescence.

Elena Borisenko, Nikolai Kolesnikov, Dmitrii Borisenko, I. I. Zverkova, Aleksei Tereschenko, Anna Timonina

Institute of Solid State Physics Russian Academy of Sciences, Akademika Osip'yana 2, Chernogolovka 142432, Russian Federation

e-mail: borisenk@issp.ac.ru

Zinc selenide is used in optics due to wide transmission range, low absorbtion coefficient. Doping with some activators increases photoluminescence properties of ZnSe crystals [1]. Studies of emitting properties of tellurium doped ZnSe crystals have shown that they can be efficiently used as scintillators in dosimeters and x-ray radiation detectors [2]. It is non-hygroscopic, which is one more advantage for usage in detectors. The most widely used method of production ZnSe and ZnSe(Te) materials is melt growth [1, 3]. This technique requires a complicated equipment to supply the growth process with high pressure of inert gas and to maintain high temperature. A serious drawback of a grown crystal is non-uniform distribution of components along a boule. Among other methods of fabrication of bulk ZnSe and tellurium-doped zinc selenide is recently developed hot pressing [4]. This method provides dense ceramics for optical applications. However, its implementation has some drawbacks: it is attributed to high isostatic pressure and melting temperatures, the fabricated material is carbon contaminated because of usage of protecting foil, and contains traces of lubricants. Production of II-VI ceramics from micropowders by cold compression failed, because of low density of produced materials (no better than 60 % of crystallographic density).

Choice of nanopowder as a precursor for ceramic production gives a unique possibility for fabrication of dense ceramics by powder technology. The CdTe and Cd-Zn-Te ceramics (95 % of crystallographic density) produced by cold compaction [5] proves to be less expensive than crystal growth by Bridgman technique, and, contrary to hot isostatic compression, does not entail contamination of the produced ceramics. The produced material is competitive in applications for optic filters and ionizing radiation detectors [6]. That was the reason to develop new ZnSe(Te) ceramics by nanopowder compaction, which we have recently begun [7].

The aim of this work is fabrication of new bulk material, Te-doped ZnSe ceramics and studying of the effect of compaction and heat treatment on its phase composition, structure and luminescent properties.

Pure and doped II-VI nanopowders were obtained by vapor deposition on the set up designed in our laboratory [6]. Crumble of ZnSe polycrystal doped with 0.5 at % Te (the precursor purity of the components for crystal growth was ZnSe (99.999 %) and synthesized ZnTe from Zn (99.999 %) and Te(99.9995 %) was put in a plate loaded in the quartz reactor. Nanopartices deposited on cold walls of the quartz reactor. Partly nanoparticles were transported by helium flow and trapped in the bubbler. The deposition zone is conditionally divided into three zones: hot zone III (T = 200ºC), intermediate zone II (100<T<200ºC), cold zone I (T ≤ 100ºC).

The nanopowders were compacted on a TT-CM-L Instron machine under pressure 650 MN/m^2 at room temperature in a steel matrix of 10^{-2} m in diameter without bindings or lubricants. X-ray diffraction (XRD) patterns were taken on a Siemens D500 diffractometer under CoK_α or CuK_α radiation, at the angle range from 20 to 120 degrees. Phase analysis, calculation of unit cell parameter, and estimation of grain size were done using PowderCell (Werner Kraus & Gert Nolze, BAM Berlin). Accuracy of the unit cell measurements was 0.003Å. Photoluminescence (PL) of the nanopowders and ceramics was measured at room temperature. He-Cd laser with the wavelength 325 nm and the pump power 0.5 W/cm^2 was used for excitation of PL. Electron probe microanalysis (EPMA) was performed on a Supra 50VP scanning electron microscope (SEM) equipped with INCA Energy+ add-in. Samples were annealed in a furnace separately in sealed tubes under pressure 1.3 N/m^2. The samples were put in the furnace at the annealing temperature, which was measured by a chromel-alumel thermocouple. The samples were cooled with the furnace to room temperature at the rate 10^{-2} deg/s.

According to XRD and EPMA data, there are three different nanopowders whose content and phase composition depends on temperature of the deposition zone. Nanopowder from zone I, in which Tdep ≤ 100ºC, consists of 35 vol % of sphalerite and 65 vol % of wurzite. The unit cell parameters of cubic and hexagonal phases are the same as the respective database parameters for pure ZnSe: a_{cub} = 5.669Å, F-43m (216) (№ 37-1463 JCPDS), a_{hex} = 3.996Å, c_{hex} = 6.55Å, P63mc (186) (№ 15-0105 JCPDS). The XRD data show that the deposited nanopowder from zone I contains no tellurium. The microanalysis data show that Te content in the nanopowder in this case does not exceed 0.5 at %. This agrees with the result of X-ray phase analysis. Grain size estimated by FWHM from X-ray diffraction patterns is 16 nm in the cubic phase and 11 nm in the hexagonal phase.

Phase analysis of the nanopowder from zone II shows that the ratio between sphalerite and wurzite is approximately 1:1. Besides, in the zone II nanopowder traces of free Te (№ 36-1452 JCPDS) appear in diffraction patterns. Unit cell parameters of the hexagonal lattice are the same as in the previous case, while the unit cell parameter of the cubic phase calculated from XRD patterns is a_{cub} = 5.671Å. Grain sizes are 26 and 13 nm in the cubic and hexagonal phase, respectively. Nanopowder from hot zone III also consists of cubic and hexagonal phases, but fraction of hexagonal phase decreases as compared with the previous two cases: nanopowders from I and II zones. There is 23 vol % of wurzite and the rest is cubic phase. Grains are coarser than in the previous cases, the nanopowders consist of grains of 35-40 nm. So, it can be concluded from the experiment that the higher the temper-

ature in the deposition zone, the greater is fraction of the cubic phase, and nanopowder grains are coarser, while they size distribution is more homogeneous. Compaction of the nanopowders II and III did not lead to significant changes in phase composition of respective ceramic materials.

The ceramics made of tellurium doped ZnSe nanopowder from zones II and III were annealed at T = 700°C for t = 0.5 h. This treatment brought to phase transition from hexagonal to cubic phase, which was not completed in either of powders. The repeated annealing under the same conditions brought to complete phase transition to the cubic phase in the ceramics III, while in the ceramics II just several percents (~3-5 vol %) of the hexagonal phase remain. The unit cell parameters after the second annealing were a_{cub} = 5.676Å and a_{cub} = 5.680Å for II and III ceramics, respectively. It is known that the ZnSe-ZnTe pseudo-binary system forms a continuous range of solid solutions. According to Vegard law, increase in the unit cell parameter shows formation of ZnSe(Te) solid solution, containing 1.6 and 2.5 at % Te in II and III ceramics, respectively. The results of EPMA show that after double annealing Te enters solid solutions entirely without any loss during annealing. The Te content corresponds to that of nanopowders from respective deposition zones.

Figure 1 shows SEM images of microstructure of ceramics III. Average grain size measured from these micrographs is 50 nm, which agrees well with the grain size estimated from the diffraction patterns.

Figure 2 shows PL spectra of the ZnSe(Te) nanopowders from zones II and III and the ceramics after annealing. PL spectra of the ZnSe(Te) nanopowders and the ceramics after annealing show that intensity of photoluminescence increases as Te concentration increases. The main peak is at about 625 nm, which is typical for ZnSe(Te) self-activating photoluminescence [8]. Additional lines at 708 nm appear in both nanopowders from II and III zones and weaken in the ceramics III after annealing. According to [8], these lines are associated with selenium vacancies $\{V_{Se+}\}$, which probably, disappear during annealing as they are substituted by $\{Te_{Se0}\}$ in the cubic lattice of the more saturated solid solution. Self-activating PL intensity increases (line 4) after annealing, which may be due to increase in concentration of recombination centers $\{V_{Zn-} + Te_{Se0}\}$. The results of the experiments allow considering ZnSe(Te) ceramics produced by nanopowder technology as promising materials for dosimeters and scintillating materials in X-ray and gamma ray detectors.

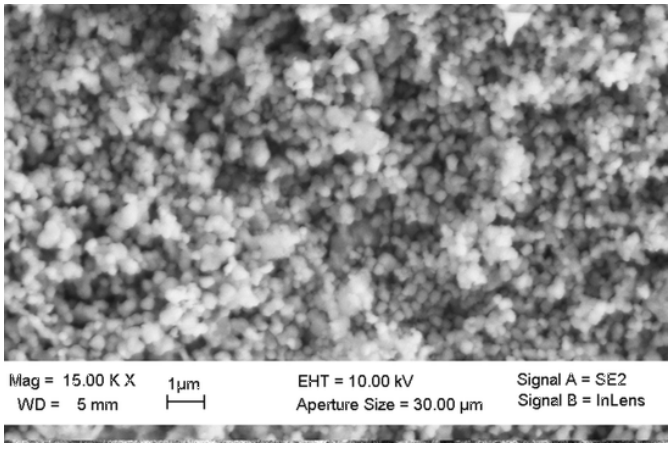

Fig. 1. Microstructure of ZnSe(Te) ceramics

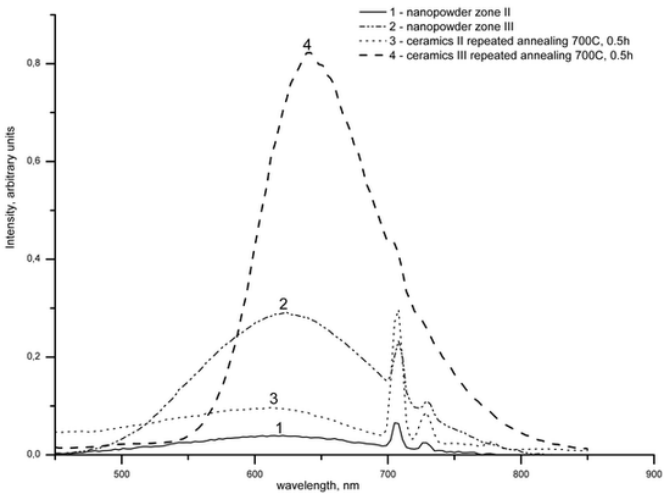

Fig. 2. PL spectra of ZnSe(Te) nanopowders and ceramics

REFERENCES

[1] W. G. Lee, Y. K. Kim, J. K. Kim, N. Starzhinskiy, V. Ryzhikov, B. Grinyov, Growth and properties of new ZnSe(Al, O, Te) semiconductor scintillator, Radiation Measurements, (2008) v. 43, 502-505;

[2] V. D. Ryzhikov, N. Starzhinskiy, L. Gal'chinetskii, P. Gashin, D. Kozin, E. Danshin, IEEE Transaction on Nuclear Science (2001)b, v. 48, 356-359;

[3] N. N. Kolesnikov, R. B. James, N. S. Berzigiarova, M. P. Kulakov, HPVB and HPZM shaped growth of CdZnTe, CdSe, and ZnSe crystals, in: R. B. James, L. A. Frank, A Burger, E. M. Westbrook, R. D. Dust (Eds.) Proceeding of SPIE: X-ray and Gamma-ray detectors and Applications IV, San Diego, (2002) v. 4784, 93-104;

[4] S. Cool, S. Miller, C. Brecher, H. Lingertat, V. Sarin, K. Riley, S. Mashl, P. Tylus, V. Nagarkar, Fabrication of ZnSe:Te by Hot Pressing Techniques, IEEE Transactions on Nuclear Science, (2010) v. 57 (3), 944-950;

[5] N. N. Kolesnikov, E. B. Borisenko, D. N. Borisenko, B. A. Gnesin, Ceramic materials made of CdTe and Cd-Zn-Te nanocrystalline powders, Cent. Eur. J. Chem. (2011), v. 9, (4), 619-623;

[6] N. N. Kolesnikov, E. B. Borisenko, V. V. Kveder, D. N. Borisenko, A. V. Timonina, B. A. Gnesin, Semiconductor ceramic materials, in: E. I. Pertsov (Ed.) Nanomaterials: New Research and Development (Nova Science Publishers: New York, 2008);

[7] N. N. Kolesnikov, E. B. Borisenko, D. N. Borisenko, I. I. Zverkova, A. V. Timonina, The effect of compaction and heat treatment on phase Transitions of ZnSe(Te) bulk material made of nanopowder, J. of Crystal Growth, (2012), v. 347, 11-14;

[8] R. Baltramiejunas, V. D. Ryzhikov, V. Gavryushin, A. Kazlauskas, G. Raciukaitis, V. I. Silin, D. Juodzbalis, V. Stepankevicius, Luminescent and nonlinear spectroscopy of recombination centers in isovalent doped ZnSe:Te crystals, Journal of Luminescence, (1992) v. 52, 71-81.

11:15 Oral

Preparation of fluoride laser ceramics

Maxim E. Doroshenko[1], Pavel Fedorov[1], Eugene A. Garibin[2], Sergey V. Kuznetsov[1], Vjatcheslav V. Osiko[1]

1. *General Physics Institute, Vavilov Str. 38, Moscow 117942, Russian Federation* **2.** *INCROM Ltd (INCROM), Babushkina, str.36, b.1, Saint-Petersburg 192029, Russian Federation*

e-mail: kouznetzovsv@gmail.com

The history of fluoride laser ceramics begins in 1964 [1], but it was the preparation of fluoride laser ceramics via the hot forming technique that provided a tremendous boost in this area of research and manufacturing. This method is based on the plastic deformation of the single crystals at high temperatures [2-4]. Application of this technique allowed to obtain lasing in fluoride ceramics of CaF_2, SrF_2, $(Ca,Sr)F_2$, $(Sr,Ba)F_2$ doped with a number of RE^{3+} ions such as Yb^{3+}, Nd^{3+}, Pr^{3+}, Tm^{3+}, and Er^{3+} [2-9] (example of CaF_2:Yb ceramics is shown in Fig.1). The investigated ceramic samples have demonstrated spectral and laser properties similar to that of single crystals. At the same time, the use of an alternative classic technique of powder precursors hot pressing resulted in significant improvement of the mechanical properties of prepared laser ceramics, while maintaining nearly the same optical and lasing properties [8], as well as thermal conductivity, thermal expansion, heat capacity, microstructure, etc. [4,9-11] as hot formed laser ceramics.

Fig.1. CaF2:Yb laser ceramics

References

1. S. E. Hatch, W. F. Parsons, and R. J. Weagley, Appl. Phys. Lett., 1964.**5**(8), 153-154.

2. T.T. Basiev, M.E. Doroshenko, V.A. Konuyshkin, V.V. Osiko, L.I. Ivanov, and S.V. Simakov, Quantum Electron., 2007, **37**(11), 989-990.

3. T.T. Basiev, M. E. Doroshenko, P P. Fedorov, et all., Optics Letters, 2008, **33**(5), 521-523.

4. P.P. Fedorov, Fluoride laser ceramics. In: Handbook on solid-state lasers: materials, systems and applications. Woodhead Publishing. Cambridge UK. 2013.

5. T.T.Basiev, M.E. Doroshenko, V.A. Konyushkin, and V.V. Osiko, Optic. Letters., 2010, 35 (23), 4009-4011.

6. T.T. Basiev, V.A. Konyushkin, D.V. Konyushkin, M.E. Doroshenko, et all, Optical Materials Express, 2011, **1**(8), 1511-1514.

7. P.A. Ryabochkina, A.A. Lyapin, V.V. Osiko, P.P. Fedorov, et all, Quantum Electron., 2012, **42(**9), 853-857.

8. M. Akchurin, T. Basiev, A. Demidenko , M. Doroshenko, et al., Optical Materials, 2013, **35**, p.444-450.

9. M.E. Doroshenko, A.A. Demidenko, P.P. Fedorov, et al., physica status solidi, in press.

10. M. Sh.Akchurin, R. V. Gainutdinov, E. A. Garibin, Yu. I. Golovin, et all, Inorg. Mater.: Applied Research, **2**(2) (2011) 97-103.

11. P.A. Popov, P.P. Fedorov, S.V. Kuznetsov, et all, Dokl. Phys., **53** (4) (2008) 198 – 200.

11:30 Oral

Growth and Electrical Properties of Ternary ZrSTe Crystals

Abhay K. Dasadia, Brinda B. Nariya, Ashvinkumar R. Jani

e-mail: abhi2physix@gmail.com

We reports new ternary ZrSTe crystals gown by chemical vapour transport method. Vapor transport experiments with iodine were performed on the system ZrSTe to define optimum growth conditions in terms of crystal size and surface perfection. Confirmation of stoichiometric proportion of constituent elements of grown crystals was done by Energy Dispersive Analysis of X-rays (EDAX) . To find out resistivity we have performed two probe resistivity measurements and Hall coefficient, mobility as well as carrier concentration are obtained by Hall effect measurements along the cleavage plane of as grown ZrSTe crystals. Preliminary electrical resistivity measurements show a decrease of the resistance with temperature which suggests a semiconducting nature of ZrSTe. We also report thermoelectric power of ZrSTe crystals in temperature range 313K-573K. Data of Hall coefficient and thermo electric power have good agreement with available data and confirms the semiconducting behavior as well as n-type nature of ZrSTe crystals. This finding will inspire the search for similar materials and promote an in-depth investigation of the detailed operating mechanism.

11:45 Oral

New polymer–drug conjugate as template for biomimetic $CaCO_3$ mineralization

Marcela Mihai[1], Dana Damaceanu[1], Simona Schwarz[2]

1. *Petru Poni Institute of Macromolecular Chemistry of the Romanian Academy, Aleea Grigore Ghica Voda 41A, Iasi, Romania*
2. *Leibniz Institute of Polymer Research Dresden, Dresden 01069, Germany*

e-mail: marcelas@icmpp.ro

The mineralization process in the biological system has attracted many scientists to biomimetically synthesize inorganic/organic materials. An important method of biomimetic synthesis is to use a soft organic template and to control the morphogenesis of inorganic materials with complex forms. The copolymer was obtained by Yamazaki-Higashi method, involving carboxylic groups of the copolymer and the amine group of the oxadiazole derivative. The oxadiazole derivative contents relative to maleic comonomer units was estimated to be 29%. The crystallization of $CaCO_3$ particles from aqueous solutions, in the absence and presence of a polymer–drug conjugate based on N-vinylpyrrolidone with maleic anhydride P(NVP-MA) as support and 2-amino-5-(4-methoxy-phenyl)-1,3,4-oxadiazole is followed in this study. P(NVP-MA) is biocompatible, with low toxicity and carriers of biologically active compounds, gradually releasing native drugs from their conjugates in response to changes in pH. The influence of polymer concentration and the initial supersaturation on the nucleation and growth of calcium carbonate has been deeply investigated, showing a strong effect on the morphology of the formed composite materials [1,2]. The new materials were characterized by scanning electron microscopy, polarized optical microscopy, X-ray diffraction, particles charge density, and electrophoresis. Smaller, more circular particles, and less porous were obtained for $CaCO_3$/copolymer sample. Due to the presence of the copolymer as template in $CaCO_3$ mineralization process, the particles stability increased up to pH = 3.4. The adsorption

capacity of the microparticles as a function of their characteristics was tested using methylene blue.

1. M.-D. Damaceanu, M. Mihai, I. Popescu, M. Bruma, S. Schwarz, React Funct Polym 2012, 72, 635.

2. M. Mihai, M.-D. Damaceanu, S. Schwarz, Cryst Growth Des 2012, 12, 4479.

Acknowledgment: *The research leading to these results has received funding from the European Union's Seventh Framework Programme (FP7/2007-2013) under grant agreement n°264115 - STREAM.*

12:00 Oral

Complex anionic isomorphism in new non-centrosymmetric fluoride borates

Tatyana Bekker[1], Sergey Rashchenko, Vladimir Bakakin, Yurii Seryotkin, Pavel Fedorov[2], Alexander Yelisseyev, Alexander E. Kokh[1]

1. *Institute of Geology and Mineralogy SB RAS (IGM), Koptyuga ave., 3, Novosibirsk 630090, Russian Federation* **2.** *General Physics Institute, Vavilov Str. 38, Moscow 117942, Russian Federation*

e-mail: tatyana_bekker@mail.ru

Isomorphic substitution is a very powerful and flexible tool to control the properties of materials, stabilize their desired crystal structure and optimize the conditions of their synthesis. This phenomenon exists in various forms, such as isovalent/heterovalent isomorphism as well as cationic/anionic and combined cationic-anionic isomorphism, that are well represented among natural and man-made materials. Anionic, specifically heterovalent anionic isomorphism, with a change in the number of ions in the unit cell (e.g., heterovalent inclusion of oxygen in tysonite lattices in LnF_3-Ln_2O_3 systems, where Ln = rare earth element [Fedorov P. P. *Russ. J. Inorg. Chem.* 45 (Suppl. 3), S268-S291 (2000)]) is a much rarer phenomenon than the other types of isomorphism.

Inorganic borates are quite famous for their nonlinear optical properties and transparency in the UV range of the electromagnetic spectrum. Fluoride borates stand out amongst other borates, as they possess much broader areas of transparency with the cut-off edges shifted further in the aforementioned UV range [Wu, B. C., Tang, D. I., Ye, N.and Chen, C. T. *Opt. Mater*. **5**, 105–109 (1996)].

We prepared a new $Ba_{4-x}Sr_{3+x}(BO_3)_{4-y}F_{2+3y}$ phase (space group $P6_3mc$) and grew its single crystals in $BaSrBO_3F$–NaF system [Rashchenko S.V., Bekker T.B., Bakakin V.V., Seryotkin Yu.V., Shevchenko V.S., Kokh A.E., Stonoga S.Yu. Cryst. Growth & Design. 2012, 12, 2955-2960]. The distinguishing feature of its structure is the simultaneous $Ba^{2+} \leftrightarrow Sr^{2+}$ cationic and $(BO3)^{3-} \leftrightarrow 3F^-$ anionic isomorphism. No stoichiometric $Ba_3Sr_4(BO_3)_3F_5$ compound has been found: its existence is not supported by experimental data. Another new $Ba_7(BO_3)_{4-y}F_{2+3y}$ solid solution with similar $(BO_3)^{3-} \leftrightarrow 3F^-$ anionic isomorphism has been found in BaB_2O_4–BaF_2–BaO ternary system ($0.21<y<0.65$, $Ba_7(BO_3)_{3.35}F_{3.95}$ to $Ba_7(BO_3)_{3.79}F_{2.63}$ area of homogeneity, for y = 0.49, $Ba_7(BO_3)_{3.51}F_{3.47}$, a=11.18241(11) Å, c=7.23720(8) Å, space group $P6_3$) [Bekker T.B., Rashchenko S.V., Bakakin V.V., Seryotkin Yu.V., Fedorov P.P., Kokh A.E., Stonoga S.Yu. CrystEngComm. 2012, 14, 6910-6915].

Both $Ba_{4-x}Sr_{3+x}(BO_3)_{4-y}F_{2+3y}$ and $Ba_7(BO_3)_{4-y}F_{2+3y}$ structures present a previously-unknown mechanism of $(BO_3)^{3-} \leftrightarrow 3F^-$ heterovalent anionic substitution in fluoride borates via $[(BO_3)F]^{4-} \leftrightarrow 4F^-$ replacement, where the fourth fluorine atom in these fragments play a crucial role in the replacement of three fluoride ions by the orthoborate ion.

Variation of $Ba_{4-x}Sr_{3+x}(BO_3)_{4-y}F_{2+3y}$ and $Ba_7(BO_3)_{4-y}F_{2+3y}$ compositions allows controlling their optical properties.

Closing ceremony
Friday afternoon, 16 August, 13:00

Posters

Wednesday, 14 August

WeP-T07
Wednesday afternoon, 14 August, 16:00
Room 106, Old Library

16:00 Poster We40

The effect of hippuric acid on crystal growth, structural and optical properties of ZTS single crystals

Anbazhagan Kumaresh[1], Raman Arun Kumar[1], Mukannan Arivanandhan[2], Yasuhiro Hayakawa[2]

1. *PSG College of Technology, Department of Basic Sciences, Coimbatore 641004, India* **2.** *Research Institute of Electronics, Shizuoka University, Johoku 3-5-1, Naka-Ku,, Hamamatsu 432-8011, Japan*

e-mail: arivucz@gmail.com

Zinc tris thiourea sulphate (ZTS) is one of the promising semiorganic crystals useful for nonlinear optical application. The effect of hippuric acid doping on the growth aspects, structural and optical properties of ZTS crystal was investigated. In the present work, slow evaporation technique was employed to grow pure and 1 mol% hippuric acid doped ZTS (HAZTS) single crystals. The grown crystals were obtained in a period of 23 days. Powder XRD analysis reveals the crystalline nature of the grown crystals. Both the crystals exhibit orthorhombic crystal structure. The lattice parameters of the grown crystals are: a = 11.0466 Å, b = 7.6949 Å and c = 15.6393 Å (for pure ZTS); a = 11.1302 Å, b = 7.7081 Å and c = 15.5033 Å (for HAZTS). The UV-Vis-NIR spectral analysis was carried out to study the effect of doping on the optical characteristics of the grown crystals. The crystal is transparent over the entire visible region. The bonding structure and molecular associations were analyzed by FTIR spectroscopy.The results of powder SHG test, HRXRD analysis will also be presented and discussed in detail.

16:00 Poster We41

Sol-gel Synthesis and Luminescence studies on Dy^{3+} Doped $NaGd(WO_4)_2$ Yellow Phosphor for Solid State Light Applications

Durairajan Arulmozhi[1], Balaji Devakumar[2], Kavirasu Kallimuthu, Moorthy Babu Sridharan

1. *Anna university, chennai 600025, India* **2.** *Crystal Growth Centre, Anna University, Chennai, Chennai 600025, India*

e-mail: durairajan.a@gmail.com

Concentrated efforts were made towards the synthesis of rare-earth activated inorganic oxides based materials for potential applications like solid state lighting (SSL), displays, sensing device and so on. Materials now used in SSL applications like Ce:YAG (excited by blue LED) and tricolour phosphors (excited by UV LED) have their own drawbacks. In this regard as a complimentary materials, $NaGd_{1-x}Dy_x(WO_4)_2$ (Dy:NGW) were prepared in sol-gel methods for possible application in SSL devices. Dy:NGW have two principle emission schemes in blue and yellow region corresponding to transitions of $^4F_{9/2}$-$^6H_{15/2}$ and $^4F_{9/2}$-$^6H_{13/2}$ at specific wavelengths, 480 and 574 nm. Sol-gel synthesised Dy:NGW powders were characterized by X-ray diffraction (XRD), scanning electron microscope (SEM), Fourier transform infra-red spectroscopy (FT-IR), Raman and spectroflorimeter analysis. The disordered NGW scheelite structure was confirmed by XRD results. SEM images clearly show the surface morphology and size of particles. The formation of tungstate tetrahedral and its corresponding vibration were analyzed with FT-IR and Raman studies. The combined charge transfer band (CTB) of O^{2-}-W and O^{2-}-Dy^{3+} were obtained in excitation spectrum. The CTB observed in the region of 230 to 310 nm and high absorption centered at 270 nm and above 310 nm ascribe the various f-f transitions of Dy^{3+} ions. Compared to CTB at 270 nm the f-f transition at 353 nm has high absorption intensity as observed in the emission spectrum. The concentration and excitation wavelength dependent luminescence property were analyzed through emission spectrum. Three lines were observed at 480, 575 and 665 nm in blue, yellow and red region corresponding to the transitions of $^4F_9$ to^6H_J (J = 15/2, 13/2 and 11/2) in the emission spectrum. Based on the results, the optimum dopant concentration of Dy^{3+} ions in NGW has been found to be 7 at% .

16:00 Poster We42

Czochralski grown large diameter Li_2MoO_4 single crystals

Olga Barinova, Svetlana Kirsanova, Andrey P. Sadovskiy, Igor C. Avetissov

D.I.Mendeleyev University of Chemical Technology of Russia (MUCTR), Miusskaya sq. 9, Moscow 125047, Russian Federation

e-mail: igor_avetisov@mail.ru

Molybdenum containing crystals are known as effective materials for cryogenic phonon-scintillating detectors and widely used for ^{100}Mo 2β decay investigations and dark matter search [1]. The most perspective detectors so called «active» detectors allow realizing the generation of rare nuclear event and its registration in the same crystal. Materials for them have predominantly scheelite-type structure ($CaMoO_4$, $CdMoO_4$), high light yield at the low temperature, but all of them have long-lived radioactive isotopes (^{48}Ca,^{116}Cd) entangles neutrinoless 2β decay searches.

Recent observation of possible molybdenum containing materials for cryogenic phonon-scintillating detectors gets clear applicability of Li_2MoO_4 crystals: they had absence of long-lived lithium isotopes, adequate light yield at low temperatures, high intrinsic radiopurity [2, 3], rather low melting point, but were not large and had a lot of intrinsic impurities and defects. More over the question of existence of phase transitions at atmospheric pressure wasn't clear [4, 5]

In the present research large transparent Li_2MoO_4 crystals were grown by Czochralski technique, their structure were investigated by XRD, Raman and IR- spectra, by chemical etching.

Li_2MoO_4 was obtained from stoichiometric mixture Li_2CO_3 and MoO_3 by solid-state synthesis technique with subsequent recrystallization from aqueous solutions. Synthesis was carried out at 723 K for 2 h and at 893 K for 4 h. It was noticed that applying of Al_2O_3 crucible due to interaction between Al_2O_3 and MoO_3 leads to contamination of Li_2MoO_4 powder by orange inclusions of $LiAl(MoO_4)_2$. Transparent crystals with up to Ø25x60 dimensions were grown by the Czochralski technique with 4 mm/h pooling rate (Fig.1).

Fig.1. Li_2MoO_4 single crystal grown by Czochralski technique and Ø25x1 mm plate cut from the crystal

The crystals corresponded to R3 (phenacite-type structure) space group: a=14,32±0,02 Å , c=9,56±0,03 Å / The crystal density derived from XRD data (3.06± 0.01g/cm^3) was slightly different from the hydrostatic density (3.03± 0.01g/cm^3). It was found out that Li_2MoO_4 crystals had no MoO_4^{2-}complexes distortion. Raman spectra had shown differences for || c oriented and ⊥c oriented crystal spectra (Fig.2).

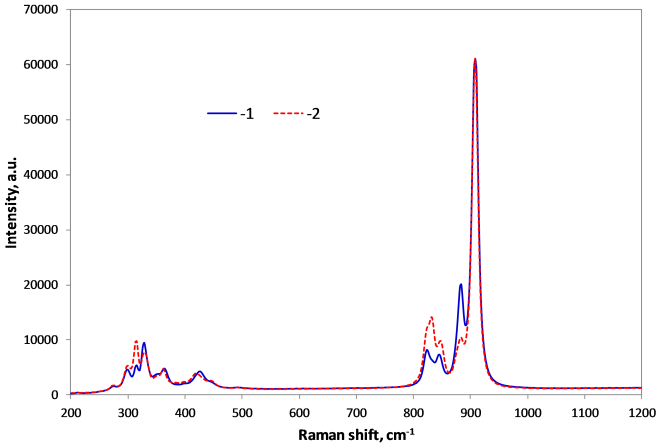

Fig.2. Raman spectra of Li_2MoO_4 single crystals cut along: 1 - ⊥c, 2- || c

[1] V.B.Mikhailik, H.Kraus. J.Phys.D: Appl.Phys. 39 (2006) 1181-1191

[2] O.P.Barinova, F.Capella, R.Cerulli, F.A.Danevich, S.V.Kirsanova, V.V.Kobychev, M.Laubenstein, S.S.Nagorny, F.Nozzoi, V.I.Tretyak. Nucl. Instr. And Meth. A607 (2009) 573–575

[3] O.P.Barinova, F.A.Danevich, V.Ya.Degoda, S.V.Kirsanova, V.M.Kudovbenko, S.Pirro, V.I.Tretyak. Nucl. Instr. And Meth. A613 (2010) 54–57

[4] U. Kolitsch. Zeit. für Kristal.. 216, №8 (2001) 449-454 [5] S. Sharma; R. N. P. Choudhary. J. of Mat. Sci. Lett. 18, № 9 (1999), 669-672

16:00 Poster We43

Single crystals growth and Pechini synthesis of δ-BiB_3O_6:Pr^{3+}

Maciej J. Chrunik[1], Andrzej Majchrowski[1], Edward Michalski[2], Przemysław Morawiak[1], Józef Żmija[2], Ivan V. Kityk[3]

1. *Military University of Technology, Institute of Applied Physics, ul. Kaliskiego 2, Warszawa 00-908, Poland* **2.** *Military University of Technology, Institute of Optoelectronics (IOE), Kaliskiego 2, Warszawa 00-908, Poland* **3.** *Czestochowa University of Technology, Electrical Engineering Department, Armii Krajowej 13/15, Częstochowa 42201, Poland*

e-mail: mchrunik@wat.edu.pl

Monoclinic α-BiB_3O_6 (α–BIBO) single crystals have excellent nonlinear optical (NLO) properties. They find numerous applications in second harmonic generators (SHG), optical parametric oscillators (OPO) and other NLO devices [1]. In the past there were taken efforts to dope α-BIBO with rare earths (RE) active ions (Nd^{3+}, Yb^{3+}) to create a material joining both NLO and lasing properties. It would lead to self frequency doubling (SFD) applications. Unfortunately it was shown that the level of RE doping of α phase is insufficient [2]. According to Aleksandrovsky et al. [3] another BiB_3O_6 NLO phase, namely orthorhombic δ-BIBO, can be also crystallized from the stoichiometric melts. Moreover it was shown recently that the δ phase, despite its higher density than in case of α phase, can be efficiently doped with some RE ions such as Nd^{3+} [4]. It was proved that some RE dopants can stabilize the orthorhombic δ-BIBO phase, probably due to the fact that it is isostructural to REB_3O_6 [5]. This distinctive feature of δ-BIBO allows to obtain significantly high doping level of some RE^{3+} cations, reaching up to 15 at.% for La, Pr, Ce and Nd.

Our investigations were devoted to synthesis of δ-BIBO phase doped with Pr^{3+} ions as a material for photoinduced SHG experiments. To obtain δ-BIBO:Pr^{3+} samples two approaches were used. Single crystal growth was carried out by Kyropoulos technique from stoichiometric melts under conditions of low temperature gradients, while δ-BIBO powders were synthesized by means of sol-gel Pechini method by citric way [6]. In current work we describe the details of δ-$Bi_{1-x}Pr_xB_3O_6$ samples synthesis (x = 0.025 and 0.075) and their XRD characterization, determining precise lattice parameters of orthorhombic phase using Cohen method [7]. Samples obtained by Pechini method were also characterized by calculating crystallite size and lattice strain using Williamson-Hall method [8] comprised to Scherrer formula. Photoinduced SHG of YAG: Nd^{3+} 1.064 μm laser radiation in obtained δ-BIBO:Pr^{3+} samples was investigated similarly to the method described in Ref [9]. Obtained results show that Pr^{3+} doping increases NLO properties of δ-BIBO.

REFERENCES

1. V. Petrov, M. Ghotbi, O. Kokabee, A. Esteban-Martin, F. Noack, A. Gaydardzhiev, I. Nikolov, P. Tzankov, I. Buchvarov, K. Miyata, A. Majchrowski, I.V. Kityk, F. Rotermund, E. Michalski, M. Ebrahim-Zadeh, Laser and Photonic Reviews, **4** (2010) 53.

2. A. Brenier, I.V. Kityk, A. Majchrowski, Opt. Commun., **203** (2002) 125.

3. A.S. Aleksandrovsky, A.D. Vasiliev, A.I. Zaitsev, A.V. Zamkov, J. Cryst. Growth, **310** (2008) 4027.

4. D.A. Ikonnikov, A.V. Malakhovskii, A.L. Sukhachev, A.I. Zaitsev, A.S. Aleksandrovsky, V. Jubera, Opt. Mater., **34** (2012) 1839.

5. R. Cong, T. Yang, Z. Lin, L. Bai, J. Ju, F. Lian, Y. Wang, J. Lin, J. Mater. Chem., **22** (2012) 17934.

6. M.P. Pechini, Method of preparing lead and alkaline earth titanates and niobates and coating method using the same to form a capacitor, United States Patent Office, USA 1967.

7. M. U. Cohen, Rev. Sci. Instrum. **6** (1935) 68.

8. G.K. Williamson, W.H. Hall, Acta Metallurgica, **1** (1953) 22.

9. A. Majchrowski, J. Ebothe, E. Gondek, K. Ozga, I.V. Kityk, A.H. Reshak, T. Lukasiewicz, J. Alloys Compounds, **485** (2009) 29.

16:00 Poster We44

Non-equilibrium Growth of Nanostructured Electrodeposits and Conducting Polymers

Ishwar Das

DDU Gorakhpur University, Civil Lines, Gorakhpur 273009, India

e-mail: ishwar_das@rediffmail.com

Metal electro-deposition and electropolymerization at an air liquid interface have attracted a great deal of attention from the point of view of their morphologies, electrical conductivity and oscillation in potential. Conducting polymers with large Π –conjugation structure have received considerable attention due to their applications in science and technology. Various electrodeposits and nano-structured conducting polymers have been synthesized and characterized by various techniques. Potential oscillations were also monitored as a function of time during their electro-synthesis and results were interpreted.

16:00 Poster We45

Luminescent properties of Tb^{3+} activated $CsLa(WO_4)_2$ green phosphors from polymeric sol-gel method

Balaji Devakumar, Durairajan Arulmozhi, Kavirasu Kallimuthu, Moorthy Babu Sridharan

Crystal Growth Centre, Anna University, Chennai, Chennai 600025, India

e-mail: balajidevakumarcgc@gmail.com

Rare earth activated inorganic materials are still attracting much attention due to its potential application in various optoelectronic devices such as field emission displays (FEDs), plasma display panels (PDPs), cathode-ray tubes (CRTs) and fabrication of white light-emitting diodes (WLEDs). White light can be generated by the following approaches, combining GaN based LED (465nm blue light) with Ce^{3+}: YAG phosphor (yellow) which has two drawbacks such as lower colour-rendering index (CRI), low colour reproducibility, and poor luminous efficiency. Rare Earth tungstates are of great interest as a host lattice for luminescent ions, due to their excellent properties such as strong covalent interaction, high stability and strong visible luminescence. They have broad and intense charge-transfer (C-T) absorption bands in near UV region and capable of transferring energy to the activators by non-radiative mechanism. In this present work, Tb^{3+} activated $CsLa(WO_4)_2$ was synthesized by polymeric sol-gel process using nitrates, water soluble para tungstates, citric acid (as chelating agent) and ethylene glycol (as binding agent) as precursors. The effect of calcination, crystallanity, surface morphology, tungstate chain formation and luminescence properties were studied. Phase purity has been confirmed by powder XRD. Formation of metal citrate with ethylene glycol resin was confirmed by FT-IR spectrum and the liberation of organics from gel at higher calcination temperature was also analyzed. Raman bands reveal the formation of tungstate chains at higher frequency region. The excitation spectra consist of broad bands due to $4f^8 \rightarrow 4f^7 5d^1$ transition and some sharp peaks due to f→f transition

within Tb^{3+} $4f^8$ configuration. The emission spectra consists of two visible emissions (i.e.) blue ($^5D_3 \rightarrow {}^7F_J$) and green ($^5D_4 \rightarrow {}^7F_J$). The role of different concentration of Tb in CsLW and different synthesis processes on physical and luminescence properties were evaluated. The results will be discussed in detail.

16:00 Poster We46

Synthesis and structural study of Graphene nano particles and their application in gas sensing

Kashinath Lellala[1], Murugan Ramachandran[1], Senthilkumar Rajamanickam[1], Hayakawa Yasuhiro[2], Ravi Ganesan[1]

1. *Department of Physics, Alagappa University,, Karaikudi 630 003, India* **2.** *Shizuoka University, Hamamatsu 432-8011, Japan*

e-mail: gravicrc@gmail.com

Graphene, is one-atom-thick planar sheet of carbon atoms densely packed in a honey comb structure is the first stable two-dimensional crystal lattice in nature, has grabbed appreciable attention due to its exceptional electronic, mechanical, electrical, optical, thermal and opto-electronic properties. Advancement of research in graphene, in the area of synthesis, properties and applications due to its wide range of applications in gas sensor, touch screen, magnetic, catalyst and electronic devices enhanced the research. Synthesis of graphene is done in many ways in physical and chemical approach, in this present paper, we report on the synthesis of graphene oxide and graphene by a simple hydrothermal chemical co-precipitation (modified Hummers) method and its application in gas sensors. Graphene oxide (GO) was effectively prepared by Hummers and Offeman method and it possesses different types of oxygen functionalities which allows GO to interact with organic and inorganic materials in covalent, non covalent or ionic manner. The GO was reduced by hydrazine hydrate as reducing agent to obtain graphene as end product. The prepared samples were characterized by X-ray diffraction (XRD), Raman, FT-IR, UV, PL, scanning electron microscopy (SEM), Energy dispersive X-ray (EDX) analysis and transmission electron microscopy (TEM). The prepared sample is used to detect the presence of ethanol at room temperature conditions.

References:

1. Jiayu Dai, Jianmin Yuan and Paolo Giannozzi , Applied Physics Letters, 95 (2009) 232105.

2. Daniela C. Marcano, Dmitry V. Kosynkin Jacob M. Berlin, Alexander Sinitskii, Zhengzong Sun,Alexander Slesarev, Lawrence B. Alemany, Wei Lu and James M. Tour, ACS Nano, 4 (2010) 8.

3. Son Truong Nguyena, Hoa Tien Nguyen , Ali Rinaldi , Nam P.V. Nguyen, Zeng Fan , Hai Minh Duong, Colloids and Surfaces A: Physicochemical and Engineering Aspects 414 (2010) 352

4. Tian-you zhangand Dong zhang,Bull. Matter. Sci., 34 (2011) 25.

5. Ming-Liang Chen, Chong-Yeon Park, Jong-Geun Choi and Won-Chun Oh , Journal of Koran chemistry , 48 (2011) 147.

16:00 Poster We47

New chemical analogs of triglycine sulfate

Vahram V. Ghazaryan[1], Michel Fleck[2], Aram M. Petrosyan[1]

1. *Institute of Applied Problems of Physics, Yerevan 0014, Armenia*
2. *Institute of Mineralogy and Crystallography, Althanstraße 14, Wien 1090, Austria*

e-mail: vahram_ghazaryan@yahoo.com

Triglycine sulfate (TGS), known since 1956 [1], is a technologically very important ferroelectric crystal. Two more its analogs, triglycine selenate (TGSe) [1] and triglycine tetrafluoroberyllate (TGBeF$_4$) [2] are known too. Their molecular structure can be presented as AH(A···AH)Y, where A is amino acid (in present case glycine) in zwitter-ionic form, AH is protonated cationic amino acid, (A···AH) is dimeric cation, where A and AH are connected by short hydrogen bond, and Y is divalent (SO_4^{2-}, SeO_4^{2-}, BeF_4^{2-}) anion. Later new analogs of TGS, namely tri-*L*-valine sulfate [3] and tri-*L*-valine selenate [4], were discovered.

Recently we started a systematic investigation of salts of amino acids with hexafluorosilicate anion (SiF_6^{2-}) [5]. In the course of this work we discovered four more new analogs of TGS formed by the same mechanism: GlyH(Gly···GlyH)SiF_6 (I), SarH(Sar···SarH)$SiF_6 \cdot 2H_2O$ (II), *L*-AlaH(*L*-Ala···AlaH)$SiF_6 \cdot H_2O$ (III) and *L*-ProH(*L*-Pro···*L*-ProH)$SiF_6 \cdot H_2O$ (IV). Our results on the investigation of crystals of salts of *L*-alanine (III) and sarcosine (II) were recently published [6,7]. In the present work we report our results on the investigation of crystals of salts of glycine (I) and *L*-proline (IV) in comparison with salts of sarcosine (II), *L*-alanine (III) and TGS.

The molecular structures of (I) and (IV) are shown in Fig. 1

Table 1. *Some crystallographic data of GlyH(Gly···GlyH)SiF_6 (I), SarH(Sar···SarH)$SiF_6 \cdot 2H_2O$ (II), L-AlaH(L-Ala···AlaH)$SiF_6 \cdot H_2O$ (III) and L-ProH(L-Pro···L-ProH)$SiF_6 \cdot H_2O$ (IV).*

Crystal	(I)	(II)	(III)	(IV)
Crystal system	Monoclinic	Orthorhombic	Monoclinic	Orthorhombic
Space group	$P2_1/n$	*P*nma	$P2_1$	$P2_12_12_1$
a (Å)	5.6134(11)	11.705(2)	11.3321(5)	5.7740(2)
b (Å)	12.900(3)	14.709(3)	5.8734(3)	10.0468(3)
c (Å)	19.554(4)	11.113(2)	13.9471(6)	38.3966(12)
α (°)	90	90	90	90
β (°)	91.31(3)	90	90.806(1)	90
γ (°)	90	90	90	90
Z	4	4	2	4
O···O distance, Å	2.458(3)	2.466(2)	2.553(2)	2.420(4)

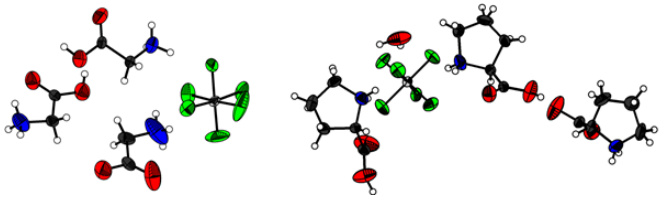

Fig.1. *Molecular structure of GlyH(Gly···GlyH)SiF_6 (I, left) and L-ProH(L-Pro···L-ProH)$SiF_6 \cdot H_2O$ (IV, right). Probability ellipsoids are shown at the 50% level.*

Crystals of salts of optically active amino acids (III, IV) necessarily crystallize in noncentrosymmetric structures (species III has even polar symmetry), while crystals of salts of achiral amino acids (I, II) often crystallize in centrosymmetric structures (see Table 1). The O···O distances in the structures of (I, II, III) are close to the respective distance

in TGS (2.470(9) Å) [8], while in the case of (IV) this distance is significantly shorter (see Table 1). As observed for TGS, TGSe and TG-BeF_4, phase transitions are possible in related crystals as well. A phase transition was observed in the structure of tri-*L*-valine selenate at 138K [4], also a structural centrosymmetric-noncentrosymmetric phase transition was observed in (II) near 180K. The work in this direction is in progress. Crystallization conditions of all four crystals (I-IV) will be discussed as well as their infrared and Raman spectra.

References

[1] B.T. Matthias, C.E. Miller, J.P. Remeika, Ferroelectricity of glycine sulfate. Phys. Rev. 104(3), 849-850(1956).

[2] S. Hoshino, T. Mitsui, F. Jona, R. Pepinsky, Dielectric and thermal study of tri-glycine sulfate and tri-glycine fluoberyllate. Phys. Rev. 107(5), 1255-1258(1957).

[3] I. Němec, Preparation and Study of Addition Compounds of Aminoacids with Inorganic Oxyacids. PhD thesis, Charles University in Prague, Faculty of Science (1998).

[4] I. Němec, Z. Mička, Tri-*L*-valine selenate-study of vibrational spectra and structural phase transition, J. Molecular Structure 563-564, 289-294(2001).

[5] V.V. Ghazaryan, M. Fleck, A.M. Petrosyan, Salts of amino acids with hexafluorosilicate anion, J. Crystal Growth 362, 162-166(2013).

[6] V.V. Ghazaryan, M. Fleck, A.M. Petrosyan, Hexafluorosilicates of alanine, Z. Kristallographie 227(9) 646-655(2012).

[7] M. Fleck, V.V. Ghazaryan, A.M. Petrosyan, Hexafluorosilicates of sarcosine, Solid State Sciences 14, 952-963(2012).

[8] R.R. Choudhury, R. Chitra, Single crystal neutron diffraction study of triglycine sulphate revisited. PRAMANA-journal of physics 71(5), 911-915(2008).

16:00 Poster We48

Formation features of stabilized Y_2O_3 nanopowders with controlled structural and morphological characteristics

Denis Y. Kosyanov, Andrey G. Doroshenko, Neonila A. Matveevskaya, Alexander V. Tolmachev, Oleg M. Vovk, Roman P. Yavetskiy

Institute for Single Crystals NAS of Ukraine (ISC), 60 Lenin Ave., Kharkov 61001, Ukraine

e-mail: Kosyanov@isc.kharkov.ua

Control of structure and morphology of starting nanopowders is an important technological task in formation of novel consolidated materials for functional applications. In particular, obtaining of low agglomerated nanopowders of rare earth oxides with controlled morphology is of significant interest for the development of laser ceramics for the new generation of solid-state lasers.

One of the ways of solving this problem in the framework of the traditional method of chemical precipitation is an introduction of some additives into the reaction mixture which modifies in some way the charge state of synthesized particle surfaces. The purpose of such modification is to provide formation of double charged layer onto the surface of each particle and, consequently, to increase the repulsion forces between the particles and prevent their agglomeration during thermolysis of the precursor. It was recently reported that sulfate ions promote formation of monodisperse quasy-spherical nanosized oxide powders and hinder their agglomeration. We have previously shown that introduction of sulfate ions into reaction mixture allows one to produce low agglomerated $Y_3Al_5O_{12}$ nanopowders with quasy-spherical morphology of particles [1]. Despite some reports on improving the morphology, particle size, and agglomeration degree of precipitated Y_2O_3 nanopowders via sulfate ions introduction, the role of sulfate ions is not well understood. The purpose of this work is to study the effect of sulfate ions on the structural and morphological characteristics of precipitated Y_2O_3 nanopowders, a promising material to be used as structural elements of yttrium aluminum garnet laser ceramics.

Sulfate-stabilized Y_2O_3 nanopowders were produced by chemical precipitation. The evolution of phase composition, specific surface area, crystallite size and morphology of Y_2O_3 nanopowders during thermal annealing of the precursor in the 600-1300°C temperature range has been studied by means of XRD, DTA-TG, BET methods and FT-IR spectroscopy. It has been found that the presence of residual SO_4^{2-}-ions on the surface of the particles provide nearly equal growth rate of different crystallographic planes of Y_2O_3, resulting in a nearly spherical particle morphology and prevents their agglomeration at the stage of thermal annealing of the precursor up to 1200°C. It has been shown that Y_2O_3 stabilized nanopowders have a higher sinterability than non-stabilized ones, which allow one to consider them as a prospective component for obtaining of YAG laser ceramics by reaction sintering.

References:

[1] T.G. Deineka et al., *J. Alloys Compd.*, **508**, 200-205 (2010).

16:00 Poster We49

Synthesis, Crystal Structure, Characterization and Luminescent Properties of $KBaTbB_2O_6$

Zhipeng Lian, Jianfeng Sun, Lijing Zhang, Dezhong Shen, Guangqiu Shen, Qingfeng Yan, Xiaoqing Wang

Department of Chemistry, Tsinghua University, Beijing 100084, China

e-mail: lianzperic@gmail.com

Rare-earth borates have attracted considerable attention due to the practical applications in various areas such as solid-state lasers, nonlinear optical (NLO) crystal, plasma display panel (PDP), and LED.[1-4] To date, extensive research efforts have been devoted to develop fluorescent materials doped with rare earth (RE^{3+}) ions.

In this work, novel rare-earth borate $KBaTbB_2O_6$ (KBT)was synthesized using a conventional solid-state reaction method. The crystal structure of KBT has been determined by the Rietveld analysis performed with the General Structure Analysis System (GSAS) software,[5] as shown in Figure 1, and the single crystal growth is still under investigation. The Rietveld refinement demonstrates that KBT is isomorphous with $KBaY(BO_3)_2$[6] and crystallizes in the planar trigonal $[BO_3]^{3-}$ group R-3m with lattice parameters of a = 5.45623(6) Å, c = 17.8629(2) Å, and Z = 3. Crystal structure data are listed in Table 1.

Since Tb^{3+} is introduced into $[BO_3]^{3-}$ net of the structures, the host sensitization of Tb^{3+} would occur, which gives rise to an efficient luminescence from the Tb^{3+}.[7] By doping rare earth ions such as Eu^{3+} and Ce^{3+} into KBT, the light emitting ions can be enhanced or quenched via the energy transfer process. In this study, a series of novel emission-tunable Ce^{3+}/Eu^{3+} solely doped KBT samples were synthesized in form of highly crystalline powders. The photoluminescence properties and energy transfer mechanism are investigated in detail. The weak green emission from Tb^{3+} was enhanced significantly by introduction of sensitizer Ce^{3+} ions, owing to an efficient resonant-type energy transfer from Ce^{3+} to Tb^{3+}. Energy transfer also occurred from Tb^{3+}

to Eu^{3+} for KBT: Eu^{3+} and tunable emission was obtained by changing the doping concentration of Eu^{3+}. The critical energy transfer distance was calculated by the concentration quenching theory. Our investigation has demonstrated that KBT can act as a potential luminescent material for the application of PDP and n-UV LED.

Keywords: $KBaTbB_2O_6$, Rietveld analysis, luminescence, energy transfer

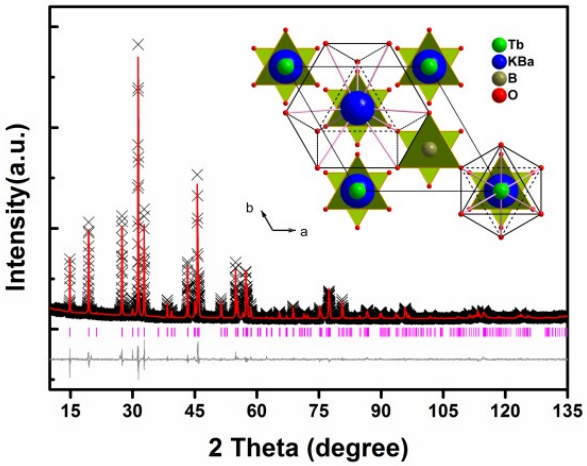

Figure 1. Experimental (crosses) and calculated (red solid line) XRD patterns and their difference (blue solid line) for the Rietveld fit of KBT XRD pattern by GSAS program. The short vertical lines show the position of Bragg reflections of the calculated pattern. The inset shows the crystal structure of KBT along the c-axis direction.

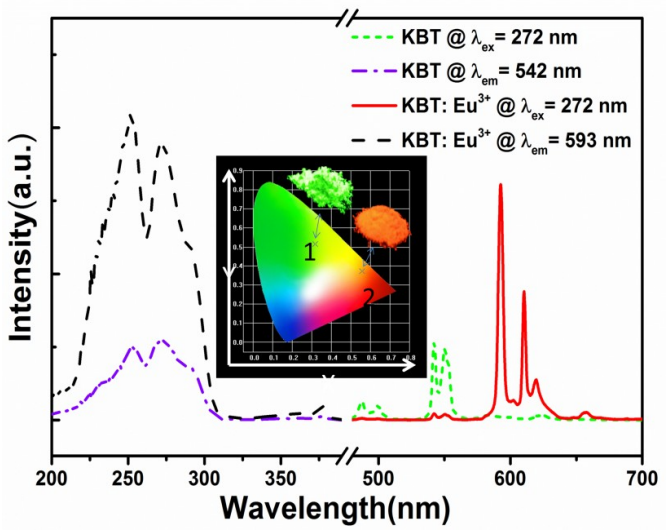

Figure 2. PL and PLE spectra of KBT, KBT: Eu^{3+} and KBT: Ce^{3+}.The insets show the CIE chromaticity coordinates for KBT, KBT: Eu^{3+} and KBT: Ce^{3+} (from No.1 to No.3)and the corresponding samples under a UV lamp box (254 nm for No.1 and No.2, and 365 nm for No.3).

Table 1. Basic crystallographic and experimental data of KBT based on Rietveld refinement.

Formula sum	$K_{0.93}Ba_{1.07}TbB_2O_6$
Formula weight	460.06 g/mol
Crystal system	trigonal
Space-group	R-3m (166)
Cell parameters	a = 5.4562(1) Å c = 17.8629(2) Å
Cell volume	460.54(1) $Å^3$
Z	3
Calc. density	4.97611 g/cm^3
Diffractometer	Panalytical X'pert diffractometer with Cu Kα radiation at 40 kV and 40 mA
Refinement method	Rietveld method based on GSAS program
Rwp(%)	4.77%
Rp(%)	3.25%
χ^2	3.169

References

(1) Guo, R.; Wu, Y.; Fu, P.; Jing, F. *Opt. Commun.***2005**, *244*, 321-325.

(2) Mills, A. *Inorg. Chem.***1962**, *1*, 960-961.

(3) Zeng, X.; Im, S.-J.; Jang, S.-H.; Kim, Y.-M.; Park, H.-B.; Son, S.-H.; Hatanaka, H.; Kim, G.-Y.; Kim, S.-G. *J. Lumin.***2006**, *121*, 1-6.

(4) Xia, Z. G.; Zhuang, J.; Liao, L. *Inorg. Chem.***2012**, *51*, 7202-7209.

(5) Larson, A. C.; Von Dreele, R. B. *GSAS Generalized Structure Analysis System, Laur, 86-748*, Los Alamos National Laboratory: Los Alamos, NM, **1994**.

(6) Gao, J. H.; Song, L. M.; Hu, X. Y.; Zhang, D. K. *Solid State Sci.***2011**, *13*, 115-119.

(7) Han, L.; Wang, Y.; Wang, Y.; Zhang, J.; Tao, Y. *J. Alloy. Compd.***2012**, *551*, 485-489.

16:00 Poster We50

Physical characterizations of Li_3PO_4 single crystal grown by the flux method

Jing Li, Jiyang Wang, Yang Zhang, Tianzhen Zhang

State Key Laboratory of Crystal Materials, Shandong University, Jinan 250100, China

e-mail: jingli@sdu.edu.cn

Recently, solid-state lithium ion electrolytes materials have been attracted intensive interests for their wide applications in batteries and related technologies. Li_3PO_4 crystal was important materials with possible applications to fast ion conductors because of its super ionic conductivity effect.

Li_3PO_4 crystal has three forms: α, β, λ, at past, they can be obtained by solid-state reaction. In this paper, we report the details of Li_3PO_4 crystals growth using flux system and the results of various characterizations of the grown crystals.

Transparent single crystals, Li_3PO_4 have been grown by flux method. We analyze the phase transition temperature of Li_3PO_4 crystals, the results indicate that we can obtain two different system β, λ by using two different fluxes.

The as-grown crystals were characterized by single-crystal X-ray diffraction, differential thermal analysis (DTA) and thermo-gravimetric analysis (TGA) techniques. The results show that the as-grown crystals were well crystallized and indexed in a hexagonal crystal system with space group Pnma. The crystal is stable in the measurement temperature

range of 25–1130°C, and the frequencies of the vibration modes of the crystal were also obtained from measurements of the infrared spectrum. X-ray photoelectron spectroscopy (XPS) was employed to measure the chemical or electronic state of each element.

The results prove that Li_3PO_4 crystals grown by flux method have better characteristic.

16:00 Poster We51

Effect of double hydrophilic copolymer presence, pH and supersaturation on the morphology, size, and pH stability of $CaCO_3$ composite microparticles

Marcela Mihai[1], Grigoris Mountrichas[2], Stergios Pispas[2]

1. *Petru Poni Institute of Macromolecular Chemistry of the Romanian Academy, Aleea Grigore Ghica Voda 41A, Iasi, Romania* **2.** *National Hellenic Research Foundation, Theoretical and Physical Chemistry Institute, Vass. Constantinou Ave., Athens 116 35, Greece*

e-mail: marcelas@icmpp.ro

The crystallization characteristics of calcium carbonate microparticles from supersaturated aqueous solutions in the presence of a double hydrophilic block copolymer poly(p-hydroxystyrene – b- methacrylic acid), PHOS-PMAA, have been investigated. The studies aim to highlight both the possibilities and the limitations of $CaCO_3$/PHOS-b-PMAA microparticles formation under different conditions: initial solution supersaturation and the relative inorganic/polymer ratio, solutions pH, and polymer concentration. Scanning electron microscopy (SEM) and atomic force microscopy (AFM) were used to provide high resolution of the particles morphology, flow particle image analysis (FPIA) to evidence their mean size and circularity, whereas X-ray diffraction and Raman spectroscopy were used to determine the polymorphs type and crystallites characteristics. The polymer presence into the composite particles was evidenced by thermogravimetric analysis (TGA), particles charge density and zeta potential. The pH stability of the new composites, given by the polymer presence, as weak polyanion, has been followed by streaming potential variation.

Acknowledgment: *The research leading to these results has received funding from the European Union's Seventh Framework Programme (FP7/2007-2013) under grant agreement n°264115 - STREAM.*

16:00 Poster We52

Two crystalline forms of sarcosine sarcosinium hydrogen L-tartrate

Michel Fleck[1], Vahram V. Ghazaryan[2], Aram M. Petrosyan[2]

1. *Institute of Mineralogy and Crystallography, Althanstraße 14, Wien 1090, Austria* **2.** *Institute of Applied Problems of Physics, Yerevan 0014, Armenia*

e-mail: aram.m.petrosyan@gmail.com

In continuation of our work on salts of amino acids with dimeric cations [1] we have investigated some new crystalline salts of sarcosine with sarcosine sarcosinium dimeric cation: (Sar···Sar$^+$)Cl$^-$, (Sar···Sar$^+$)Br$^-$[2], (Sar···Sar$^+$)I$^-$ [3], (Sar···Sar$^+$)BF_4^-, (Sar···Sar$^+$)ClO_4^- [4], (Sar···Sar$^+$)NO_3^- [5]. With this contribution, we present our results on the system sarcosine + *L*-tartaric acid + H_2O. In particular, we wanted to find out if salts with dimeric cation of the type Sar···Sar$^+$ (as have been established in other sarcosine salts [2-5]) could be found in this system.

In addition to the previously reported crystal sarcosinium hydrogen *L*-tartrate (I) [6], we have identified two new phases (II) and (III), which turned out to be polymorphs of sarcosine sarcosinium hydrogen *L*-tartrate (Table 1). Both phases were investigated by means of single crystal XRD and vibrational spectroscopy, and found to contain a zwitter-ionic sarcosine, a sarcosinium cation, and a hydrogen *L*-tartrate anion in the asymmetric unit, i.e., they represent a 2:1 ratio of constituents. It is worth noticing that both species crystallize in the same symmetry, *viz*. the orthorhombic space group $P2_12_12_1$, but have a different arrangement of building units.

The expected dimeric Sar···Sar$^+$ cation was found in phase (III) only, whereas in (II) the sarcosinium cation forms a strong O–H···O hydrogen with the carboxylate group of the hydrogen *L*-tartrate anion bond (O···O distance of 2.4553(15) Å). The carboxyl group of the anion forms in turn an O–H···O bond towards the carboxylate group of the third molecule in the asymmetric unit, *viz*. the sarcosine zwitter-ion (O···O distance of 2.5065(14) Å, Fig. 1). In contrast, the building unit in (III) are said dimeric sarcosine sarcosinium cations (O···O distance of to 2.512(3) Å) as well as the hydrogen *L*-tartrate anions, forming hydrogen bonded infinite

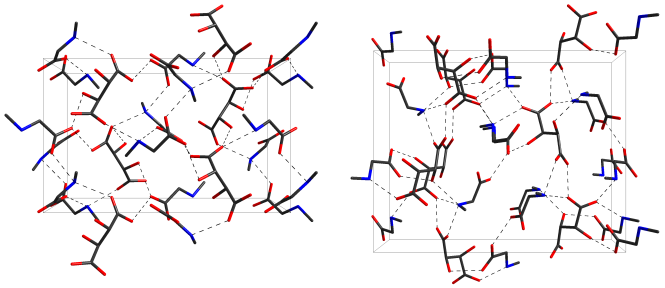

Fig. 1.*Crystal structures of forms (II, left) and (III, right) of sarcosine sarcosinium hydrogen L-tartrate. Note the differences in arrangement and conformation.*

chains (O···O distances between carboxyl and carboxylate groups of to 2.510(2) Å). In addition, one more phase (IV) was identified by its infrared spectrum without structure determination.

Concluding, we found that the system sarcosine + *L*-tartaric acid + H_2O contains at least four phases, three of which have been characterized structurally. In addition to the previously known species (I) Sar$^+$·*L*-tartrate$^-$, two 2:1 compounds were found, which have the same symmetry but different arrangements of constituents, i.e., Sar$^+$···*L*-tartrate$^-$···Sar (II) and (Sar···Sar$^+$)·*L*-tartrate$^-$ (III). This pair of crystals represents an example of dimorphism where both structures have the same space group and comparable unit cell size (as can be seen by the value of *Z*). Such examples are rare, but have been found before (e.g. [7, 8]).

Table 1.*Crystal data for two forms (II and III) of sarcosine sarcosinium hydrogen L-tartrate, compared with sarcosinium hydrogen L-tartrate (I) [6]. All sets measured at ambient conditions.*

Phase	(I)	(II)	(III)
Empirical formula	$C_7H_{13}NO_8$	$C_{10}H_{20}N_2O_{10}$	$C_{10}H_{20}N_2O_{10}$
Crystal system	Triclinic	Orthorhombic	Orthorhombic
Space group	*P*1	$P2_12_12_1$	$P2_12_12_1$
a (Å)	5.0038(15)	9.581(2)	6.0518(5)

b (Å)	6.442(2)	9.809(2)	13.8637(11)
c (Å)	8.3179(11)	15.811(3)	17.4678(12)
α (°)	78.60(2)	90	90
β (°)	80.62(2)	90	90
γ (°)	79.80(2)	90	90
V (Å^3)	256.4(11)	1486.0(5)	1465.6(2)
Z	1	4	4

References

[1] V. V. Ghazaryan, M. Fleck, A. M. Petrosyan, New salts of amino acids with dimeric cations. Proc. SPIE 7998 (2011) 79980F.

[2] V.V. Ghazaryan, M. Fleck, A.M. Petrosyan, Sarcosine sarcosinium chloride and sarcosine sarcosinium bromide, J. Mol. Struct. 1020, 160-166(2012).

[3] V.V. Ghazaryan, M. Fleck, A.M. Petrosyan, Iodides of sarcosine. J. Mol. Struct. 1032, 35-40(2013).

[4] V.V. Ghazaryan, M. Fleck, A.M. Petrosyan, Sarcosine sarcosinium tetrafluoroborate and sarcosine sarcosinium perchlorate: synthesis, structure and vibrational spectra, J. Mol. Struct. 1021, 130-137(2012).

[5] M. Fleck, V.V. Ghazaryan, A.M. Petrosyan, Crystal structure at 296 and 150K, vibrational spectra and thermal behaviour of sarcosine sarcosinium nitrate. Z. Kristallographie 227(12), 819-824(2012).

[6] R.V. Krishnakumar, M. Subha Nandhini, S. Natarajan, Sarcosinium tartrate. Acta Crystallogr. C57 (2001) 165-166.

[7] N. Nagel, H. Bock, P. Eller, Dimorphism and inclusion compounds of N,N'-di(benzenesulfonyl)-p-phenylenediamine. Acta Crystallogr. B56 (2000) 234-244.

[8] J.P. Jasinski, R.J. Butcher, K. Veena, B. Narayana, H.S. Yathirajan, A second polymorph of (2E)-1-(4-fluorophenyl)-3-(3,4,5-trimethoxyphenyl)prop-2-en-1-one. Acta Crystallogr. E65 (2009) o1965-o1966.

16:00 Poster We53

New mixed salts of L-histidinium(2+) comprising hexafluorosilicate anions

Aram M. Petrosyan[1], Michel Fleck[2], Vahram V. Ghazaryan[1]

1. *Institute of Applied Problems of Physics, Yerevan 0014, Armenia*
2. *Institute of Mineralogy and Crystallography, Althanstraße 14, Wien 1090, Austria*

e-mail: aram.m.petrosyan@gmail.com

In our previous works we have shown that the search and investigation of crystalline mixed salts of amino acids with different anions is a promising direction for the discovery new materials (see [1] and references therein).

Recently we started a systematic investigation of salts of amino acids with the hexafluorosilicate anion (SiF_6^{2-}) [2]. In addition to simple salts comprising hexafluorosilicate anions, a mixed salt with different anions, namely 2*L*-His^{2+}.2BF_4^-.SiF_6^{2-}.2H_2O (I), has been obtained. Continuing this work we obtained four more mixed crystalline salts: orthorhombic 2*L*-His^{2+}.2ClO_4^-.SiF_6^{2-}.2H_2O (II) (space group $P2_12_12$, Z=2, a=10.1549(8) Å, b=14.847(1) Å, c=8.7536(7) Å, which is isostructural with (I)), monoclinic 2*L*-His^{2+}.2Cl^-.SiF_6^{2-} (III) and isostructural 2*L*-His^{2+}.2Br^-.SiF_6^{2-} (IV) (space group $C2$, Z=2, a=27.063(6) Å, b=7.1013(17) Å, c=5.5076(11) Å, β=92.141(11)°), as well as triclinic 2*L*-His^{2+}.SO_4^{2-}.SiF_6^{2-}.3H_2O (V) (space group $P1$, Z=1, a=8.5005(17) Å, b=8.7896(18) Å, c=9.7286(19) Å, α=71.49(3)°, β=92.141(11)°, γ=86.17(3)°).

In the present work we will provide crystallization conditions of single crystals of these salts, their crystal and molecular structures as well as vibrational (infrared and Raman) spectra.

Apart from possible applications as materials with interesting physical properties (as many amino acid salts possess), the salts of amino acids with hexafluorosilicate anions may be used in stomatology as preparations having anti-caries activity [3].

References

[1] V.V. Ghazaryan, M. Fleck, A.M. Petrosyan, Mixed salts of amino acids with different anions, J. Crystal Growth 362, 182-188(2013).

[2] V.V. Ghazaryan, M. Fleck, A.M. Petrosyan, Salts of amino acids with hexafluorosilicate anion, J. Crystal Growth 362, 162-166(2013).

[3] Petrosyan A.M., Ghazaryan V.V., Fleck M., Harutyunyan A.V., Andriasyan L.H., Brsikyan N.A., Hexafluorosilicates of amino acids having anti-caries activity, Armenian patent #2695 (2012).

16:00 Poster We54

Synthesis, Crystal structure, Crystal growth and Characterization of 2-Amino-4-picolinium-4-chlorobenzoate

Subramaniyan Raja Ramakrishnan, Anandha Babu Govindan, Ramasamy Perumalsamy

Centre for Crystal Growth,SSN College of Engineering,Kalavakkam,Chennai, Chennai 603110, India

e-mail: maheraja88@gmail.com

2-Amino-4-picolinium-4-chlorobenzoate (2A4P4CB) has been synthesized by dissolving 2-amino-4-picoline (2-amino-4-methyl pyridine) and 4-chlorobenzoic acid in methanol in 1:1 molar ratio. Solubility studies were carried out in various solvents such as acetone, methanol, ethanol and mixed solvents to choose a suitable solvent for crystal growth. It is observed that 2A4P4CB has maximum solubility in acetone-methanol (1:1) solvent mixture when compared to other solvents. Single crystals of 2A4P4CB were successfully grown from the saturated solution by slow evaporation solution growth technique at the room temperature. Single crystal X-ray diffraction studies were carried out on the grown crystal to determine the crystal structure. 2A4P4CB crystallizes in monoclinic system with space group $P2_1/c$. The unit cell parameters are a = 9.520(5)Å , b = 11.499(5)Å, c = 11.445(5)Å, α = γ = 90º, β = 98.788º(5) and V = 1238.2(10)Å^3 . Fourier transform infrared (FTIR) spectrum of 2A4P4CB was recorded in the region 400-4000 cm^{-1} to identify the functional groups. The optical transmittance and the lower cut off wavelength of 2A4P4CB have been identified by UV-Vis-NIR spectral analysis. These studies were carried out without any antireflection coatings. The lower cut off wavelength is found to be 367 nm. The thermal properties of 2A4P4CB have been identified from the TG/DTA studies. Microhardness studies were carried out on the grown crystal to measure the load dependant hardness. Indentation time is 5s. It is observed that the hardness number increases with the load which indicates that the reverse indentation size effect occurs in 2A4P4CB crystals

16:00 Poster We55

Structural Aspects and Second Harmonic Generation Response of Novel Chiral Phthalimides

Brijesh Rathi

University of Delhi, Delhi 110007, India

e-mail: brathi@svc.ac.in

Design and synthesis of organic molecules possessing significant second harmonic generation response is of great interest owing to their versatile applications in the field of existing and future technologies. Organic materials are always preferred in material science due to their easy tailoring and high solubility over pure inorganic materials. A series of small chiral phthalimides have been designed and synthesized with the aim to explore their structural features and their nonlinear optical properties. The composition of newly prepared molecules was confirmed by analytical and spectroscopic techniques and also by single crystal X-ray diffraction technique. The interesting and enthusing results are observed and will be presented.

16:00 Poster We56

Synthesis and luminescence properties of Sm^{3+}-doped $Sr_3B_2SiO_8$ phosphors for near-UV pumped light-emitting diodes

Jianfeng Sun, Guangqiu Shen, Dezhong Shen

Tsinghua University, Tsinghua Garden, Beijing 100084, China

e-mail: sunjf_0_0@sina.com

GaN-based white light-emitting diodes (LEDs), the so-called next generation solid-state lighting (SSL) technology, have attracted substantial attention for lighting, display, and scintillation applications because of their merits of high energy efficiencies, long operation lifetimes, lower power consumptions, and ecofriendly constituents.[1,2] White LEDs, therefore, are promising candidates to replace the conventional SSL sources in the coming future. However, there is still a trade-off between higher color rendering index (CRI) and higher luminance among these phosphors. Until now, the task of searching for efficient inorganic rare-earth phosphors with strong absorptions in the near-UV spectral region is still urgent and attractive.

In this abstract, we reported the $Sr_3B_2SiO_8$: $x$$Sm^{3+}$, $x$$Na^+$ (SBSO: $x$$Sm^{3+}$, $x$$Na^+$)phosphor system with *Pnma* space group by using high-temperature solid-state reactions. The crystal structure and overall luminescence performance (i.e., PL intensity, quantum efficiency, thermal-quenching behavior, and CIE coordinates) of the as-prepared phosphors were investigated for the first time. The results indicated that SBSO: $x$$Sm^{3+}$, $x$$Na^+$ phosphors could be efficiently excited by the near-ultraviolet light (400 nm) to realize three novel emission bands peaking at 561, 600, and 648 nm, respectively, corresponding to the characteristic emission transitions of $^4G_{5/2}$-^6H_J (J = 5/2, 7/2, and 9/2) of Sm^{3+} ions in the SBSO host. Based on the theoretical calculation, the dipole-dipole interaction was dominantly involved in the mechanism of concentration quenching of Sm^{3+} in the phosphors, and the critical distance (R_C) as well as the activation energy for thermal quenching (ΔE) were determined to be 16.12 Å and 0.21 eV, respectively. In addition, the effects of charge compensation on the luminescence behaviors of SBSO: $x$$Sm^{3+}$, $x$$M^+$), where M^+ represented a monovalent cation like Li^+, Na^+, or K^+ acting as a charge compensator, were also investigated in detail. In view of their strong absorption in the near-ultraviolet, the intense visible emitting light, as well as the relatively low thermal quenching, the Sm^{3+}-doped SBSO phosphors can serve as potential new materials for phosphor-converted LEDs.

Keywords: Borosilicate phosphor; $Sr_3B_2SiO_8$: Sm^{3+}; Luminescence; White LEDs

References

(1) Hashimoto, T.; Wu, F.; Speck, J. S.; Nakamura, S. *Nat. Mater.***2007**, *6*, 568.

(2) Lin, C. C.; Xiao, Z. R.; Guo, G. Y.; Chan, T. S.; Liu, R. S. *J. Am. Chem. Soc.***2010**, *132*, 3020.

(3) Sun, J. F.; Zhang, W. L.; Shen, D, Z.; Sun, J. Y. *J. Electrochem. Soc.***2012**, *159*, J107.

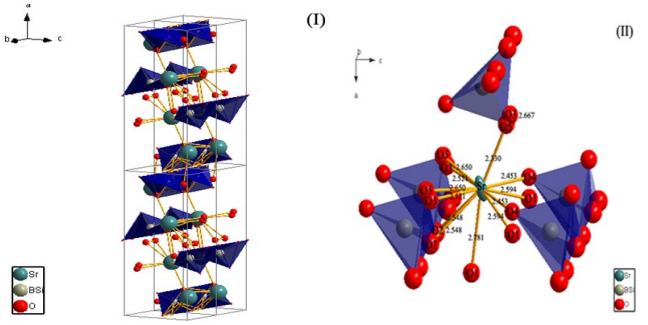

Figure 1 The sketch map of $Sr_3B_2SiO_8$ crystal structure (I), and coordinate environment around Sr atom (II) drawn by referring the crystallographic data in Ref. 3. Green, gray, and red spherical balls represent Sr, B/Si, and O atoms, respectively.

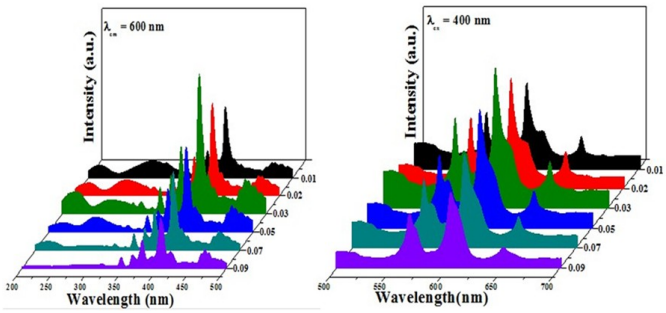

Figure 2 The PLE and PL spectra of SBSO: $x$$Sm^{3+}$, $x$$Na^+$ (x = 0.01-0.09, λ_{ex} = 600 nm, and λ_{em} = 400 nm.)

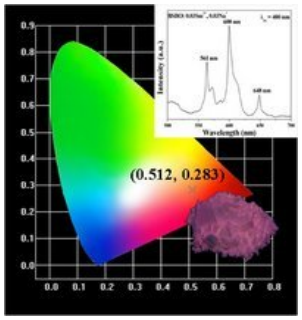

Figure 3 CIE chromaticity diagram from PL spectra of the SBSO: 0.03Sm^{3+}, 0.03Na^+ phosphor excited at 400 nm. The inset below shows the image of the SBSO: 0.03Sm^{3+}, 0.03Na^+ phosphor taken in the daylight and irradiated under 365 nm UV lamp box.

16:00 Poster We57

Ammonothermal synthesis of $LaTaON_2$ for Photocatalytic Materials

Tomoaki Watanabe, Kazuhisa Kishida, Chihiro Izawa

Meiji University, Kawasaki 2148571, Japan

e-mail: tomowata@meiji.ac.jp

Transition metal oxynitrides have received much attention owing to various applications in electronic devices because of their unusual dielectric and optical properties and ionic conductivity as well as their catalytic activity, and show particular potential as photocatalysts for the splitting of water. They have a number of other intriguing properties as well. Particularly intriguing are the recent findings that some Ta-based oxynitrides can serve as visible-light-driven photocatalysts because of their narrow band gaps. For example, Domen et al. reported recently that Ta-based oxynitrides such as TaON, Ta3N5[1], and $LaTaON_2$ show high activity for water reduction and oxidation in aqueous solutions containing sacrificial reagents under visible-light irradiation. Despite these promising findings, transition metal oxynitrides have been much less investigated in terms of syntheses, properties, and applications, than have the corresponding oxides. For example, transition metal oxynitrides are still generally synthesized by the conventional but rather difficult routes of calcining oxide or reactive oxide precursors with flowing ammonia at high temperatures. However, the products so obtained rarely exhibit the expected properties, but rather tend to exhibit low crystallinity, slow reaction rates, and significant structural defects because of the long duration and high temperature of calcination.Among the new methods for synthesizing oxynitrides, the use of supercritical ammonia shows promise. Important advantages of this method compared with the conventional methods are that it gives well-crystallized nitrides such as GaN[2], $CaAlSiN_3$[3], $SrAlSiN_3$[4] ,$LaTaON_2$[5] at relatively low temperatures and it suppresses defect formation because the reaction scheme is not so much a solid-state reaction as it is a liquid-state reaction. However, there are a few reports about the synthesis of transition metal oxynitrides in supercritical ammonia. Thus, in the present poster ,we will demonstrate the synthesis of well-crystallized $LaTaON_2$ at 873 K by reacting metal precursors in ammonia under supercritical conditions.

1. Yanbo Li , Tsuyoshi Takata , Dongkyu Cha , Kazuhiro Takanabe , Tsutomu Minegishi ,Jun Kubota , and Kazunari Domen, Adv. Mater., 25, 125–131 (2013)

2. G. G. D. Ehrentraut, Y. Kagamitani, T. Fukuda, F. Orito, S. Kawabata, K. Katano, S. Terada, J. Crystal Growth 310(17), 3902(2008)

3. J.W. Li, T. Watanabe, H. Wada, T. Setoyama, M. Yoshimura, Chemstry of Materials, 19, 3592 (2007)

4. Tomoaki Watanabe, Kazumichi Nonaka, Jin Wang Li, Kazuhisa Kishida and Masahiro Yoshimura, J. Ceramic Society of Japan 120 [11] 500-502 (2012)

5. Tomoaki Watanabe, K. Tajima, J.W. Li, N. Matsushita, M. Yoshimura, Chem. Lett. 40 1101 (2011)

16:00 Poster We58

Microstructure of Diphase Dendrite in Al-35%La Alloy During Directional Solidification

Ya-Hong Zheng[1], Zi-Dong Wang[2], Ming-Wen Chen[3]

1. *Wuxi Radio and Television University, Guangrui Road No.390, Wuxi, Jiangsu 214011, China* **2.** *University of Science and Technology Beijing, Xueyuan Road No.30, Haidian District, beijing 100083, China* **3.** *University of Science and Technology Beijing, Lihua Building 214, Xueyuan Rd 30, haidian district, Beijing, Beijing 100083, China*

e-mail: zhengyh1963@163.com

The samples of Al-35%La alloy with different directional solidification velocities (0.05 ~ 4mm.s^{-1}) were prepared by adopting directional solidification method. The feature of the dendrite structure of these samples was studied. It is found that, when the directional solidification velocity was 0.05mm.s^{-1} during directional solidification, the samples have obvious directionality and have a periodic diphase dendrite structure; when the directional solidification velocity were 0.2 ~ 1 mm.s^{-1}, the dendrite growth direction clutters without a certain direction, the periodic diphase dendrite structure are shown, and it is difficult to obtain the directional solidification structure; when the directional solidification velocity was 3 mm.s^{-1}, the structure feature of directional solidification periodic diphase dendrite was more obvious, as shown in Figure 1. The results show that the microstructure and morphology of the periodic diphase dendrite of Al-35%La is closely related with its growth rate to the directional solidification conditions. It was periodic diphase dendrite structure along the growth direction, and dendrite growth direction perpendicular to the direction of the faster growing, forming a box-shaped periodic diphase dendrite structure.

Topical Session 8

External fields, microgravity

Session Coordinators

Arne Cröll (Germany) *arne.croell@krist.uni-freiburg.de*

Alexandar Ostrogrosky (USA) *aostrogo@iit.edu*

Programme

Wednesday, 14 August

WeP-T08
Wednesday afternoon, 14 August, 16:00
Room 215, Old Library

Break
Wednesday afternoon, 14 August, 17:30

Thursday, 15 August

ThO1

T08: External fields, microgravity
Thursday morning, 15 August, 10:20
Room A, Auditorium Maximum

10:20 Invited oral

Analysis of the Nonlinear Behavior of Detached Bridgman Growth in Microgravity

Andrew Yeckel, Jeffrey J. Derby

University of Minnesota, Chemical Engineering and Materials Science, 421 Washington Ave. S.E., Minneapolis, MN 55455, United States

e-mail: derby@umn.edu

Detached growth represents a radical change from classical Bridgman crystal growth. In this process, first observed in space-based growth experiments, the melt dewets the ampoule wall, allowing the crystal to pull away from it. Detached growth eliminates deleterious interactions between the growing crystal and the ampoule, dramatically improving crystal quality. However, the promising early results of microgravity experiments have been difficult to advance in terrestrial growth systems due to a number of instabilities that can be manifest during growth.

As a basis for better understanding the physics underpinning this process, we develop and apply a thermocapillary model to study the existence, stability, and nonlinear dynamics of detached melt crystal growth in a vertical Bridgman system under zero gravity conditions. The model incorporates time-dependent heat, mass, and momentum transport, and accounts for temperature-dependent surface tension effects at the meniscuses bounding the melt. The positions of the meniscus and phase-change boundary are computed to satisfy the conservation laws rigorously. In addition, we examine the capability of a capillary statics model developed by Duffar et al. for explaining shape stability in this system.

A rich bifurcation structure in gap width versus pressure difference is uncovered, demarcating conditions under which growth with a stable gap is feasible. Thermal effects shift the bifurcation diagram to a slightly different pressure range, but do not alter its general structure. Necking and freeze-off are shown to be two different manifestations of the same instability mechanism. Supercooling of melt at the meniscus and low thermal gradients in the melt ahead of the crystal-melt-gas trijunction, either of which may be destabilizing, are both observed under some conditions. The role of wetting and growth angles in dynamic stability is clarified.

We also discuss the dynamics, operability limits, and tuning of several feedback controllers to stabilize detached vertical Bridgman crystal growth. Proportional and proportional-integral control can stabilize unstable growth, but only within tight operability limits imposed by the narrow range of allowed meniscus shapes. Substantially better performance is shown to arise from a nonlinear, model-based control.

Supported in part by DOE/NNSA, DE-FG52-08NA28768, the content of which does not necessarily reflect the position or policy of the United States Government, and no official endorsement should be inferred.

10:50 Oral

Stability of Menisci in Detached Bridgman Growth

Konstanty Mazuruk[1], Martin Volz[2]

1. *University of Alabama in Huntsville (UAH), 302 Sparkman Dr., Huntsville, AL 35899, United States* **2.** *NASA Marshall Space Flight Center (MSFC), EM31, Huntsville, AL 35812, United States*

e-mail: mazuruk@uah.edu

Detached growth, also referred to as dewetted growth, is a Bridgman crystal growth process in which the melt is in contact with the crucible wall but the crystal is not. A meniscus bridges the gap between the top of the crystal and the crucible wall. The meniscus shape depends on the contact angle of the melt with the crucible wall, the growth angle of the melt with respect to the solidifying crystal, the gas pressure differential, the Weber number describing the rotation rate of the crucible, and the Bond number. Only some of the meniscus shapes are stable and the stability criterion is the sign of the second variation of the potential energy upon admissible meniscus shape perturbations. The effects of confined gas volumes above and below the melt and crucible rotation are evaluated. The analysis is applicable to the non-stationary case where the crystal radius changes during growth. Static stability maps (crystal radius versus pressure differential) are obtained for a series of Bond numbers, growth angles and Weber numbers. Also, the specific cases of Ge and InSb, in both terrestrial and microgravity conditions, are analyzed. Stability was found to depend significantly on whether the interior surface was considered to be microscopically rough or smooth, corresponding to pinned or unpinned states. It was also found that all meniscus shapes are statically stable in a microgravity environment.

11:05 Oral

Crystal shape evolution in detached Bridgman growth

Martin Volz, Konstanty Mazuruk

NASA Marshall Space Flight Center (MSFC), EM31, Huntsville, AL 35812, United States

e-mail: Martin.Volz@nasa.gov

Detached (or dewetted) Bridgman crystal growth defines that process in which a gap exists between a growing crystal and the crucible wall. Existence of the gap provides several advantages, including no sticking of the crystal to the crucible wall, reduced thermal and mechanical stresses, reduced dislocations, and no heterogeneous nucleation by the crucible. Numerical calculations are used to determine the conditions in which a gap can exist. According to crystal shape stability theory, only some of these gap widths will be dynamically stable. Beginning with a crystal diameter that differs from stable conditions, the transient crystal growth process is analyzed. In microgravity, dynamic stability depends only on capillary effects and is decoupled from heat transfer. Depending on the initial conditions and growth parameters, the crystal shape will evolve towards the crucible wall, towards a stable gap width, or towards the center of the crucible, collapsing the meniscus. The effect of a tapered crucible on dynamic stability is also described.

11:20 Oral

Nucleation experiment in vapor phase under microgravity using the sounding rocket S-520-28

Yuki Kimura[1], Kyoko K. Tanaka[2], Katsuo Tsukamoto[1], Shinsuke Takeuchi[3], Yuko Inatomi[3]

1. *Graduate school of Scienece, Tohoku University, Sendai 980-8578, Japan* **2.** *Hokkaido University, Institute of low temperature science, N19-W8, Kita-ku, Sapporo 011-0819, Japan* **3.** *Institute of Space and Astronautical Science (JAXA), Yoshinodai, Sagamihara 229-8510, Japan*

e-mail: ykimura@m.tohoku.ac.jp

Nucleation is a fundamental event to determine character, such as size, number density and morphology, of produced crystals [1]. Therefore, understanding and control of nucleation process are crucial in various fields. Nucleation theories have been used to understand the nucleation temperature, number density and size of produced particles. However, it has been well known that nucleation rates obtained by classical nucleation theory (CNT) and by experiments have a large difference. The semi-phenomenological (SP) nucleation theory proposed by Dillmann and Meier (1991) [2] explains some results of laboratory experiments and agree well with results from numerical approaches based on molecular dynamics (MD) simulations of homogeneous nucleation over a wide range of temperatures for liquids and solids [3,4]. However, SP model also has a limitation; nucleation rates in experiments of relatively complex molecules [5,6] and in a system of larger size of critical nuclei [7] cannot be explained.

Recently, we started a new project to determine the physical parameters of nanometer sized particles and evaluate nucleation theories by homogeneous nucleation experiments in vapor phase. Nanoparticles were formed from a highly supersaturated vapor, supersaturation ratio was as high as ~5×10^4, after evaporation by electrical heating in a gas atmosphere. The temperature and concentration at the nucleation sites were obtained by an in-situ observation system using interferometry. We succeeded to determine surface free energy and sticking probability of manganese nanoparticle from condensation temperature and size of produced particles, which was determined by transmission electron microscopy, based on nucleation theories [8]. The surface free energy and sticking coefficient of Mn at1106 ± 50 K were 1.55 ± 0.10 J/m^2 and 0.39 (+0.39, -0.2), respectively, by CNT and 1.57 ± 0.35 J/m^2 and 0.42 (+0.42, -0.21), respectively, by a SP model.

In this laboratory experiment, hot evaporation source generates heterogeneity of nucleation temperature and concentration caused by strong convection of gas atmosphere. In addition, there is a possibility of that produced nuclei collides and then fused together to be a larger particle and decreasing number density after a stage of nucleation, which called fusion growth in nanoparticles [9]. This phenomenon might be a reason of large differences of nucleation rates between experiments and theories and of very small sticking coefficient of zinc, ~10^{-5}, obtained by microgravity experiment [10]. If there is no convection, evaporated vapor diffuses uniformly and the temperature profile becomes concentric around the evaporation source. As the result, nucleation will occur at the same condition. Then, we can obtain physical properties with relatively smaller error bars and then we may be able to evaluate nucleation theories more precisely. Therefore, we performed a microgravity experiment using the sounding rocket S-520-28 launched on December 17th, 2012.

We prepared specially designed double wavelength Mach–Zehnder-type interferometers with an evaporation chamber and camera recording systems to fit the space and weight limitations of the rocket. Three systems, named DUST 1 to 3, with same configuration except evaporation source and gas pressure in the chamber were installed into the nosecone of the rocket. The evaporation source and gas atmosphere were tungsten and gas mixture of oxygen (4.0×10^3 Pa) and argon (3.6×10^4 Pa) for DUST 1, iron and argon (2.0×10^4 Pa) for DUST 2, and iron and argon (4.0×10^4 Pa) for DUST 3. The experiments were run sequentially and automatically started from 100 s after launch of the rocket. The evaporation source was electrically heated under microgravity. Evaporated vapor was concentrically diffused uniformly, cooled and condensed in the gas atmosphere. The temperature and concentration at the nucleation site were determined from the movements of the fringes in the interferogram. The nucleation occurred very far from the thermal equilibrium and the supersaturation ratio was extremely high, more than 10^{10}. Here, we will show the first results of the homogeneous nucleation in vapor phase under microgravity.

[1] e.g., Vekilov, P. G. *Cryst. Growth Des.***2010**, 10, 5007-5019.
[2] Dillmann, A.; Meier, G. E. A. *J. Chem. Phys.***1991**, 94, 3872-3884.
[3] Tanaka, K. K.; Tanaka, H.; Kawamura, K.; Nakazawa, K. *J. Chem. Phys.***2005**, 122, 184514.
[4] Tanaka, K. K.; Tanaka, H.; Yamamoto, T.; Kawamura, K. *J. Chem. Phys.***2011**, 134, 204313.
[5] Hämeri, K., Kulmala, M. *J. Chem. Phys.***1996**, 105, 7696.
[6] Anisimov, M. P. et al. *J. Chem. Phys.***2001**, 115, 810.
[7] Tanaka, K. K et al. To be submitted.
[8] Kimura, Y.; Tanaka, K. K.; Miura, H.; Tsukamoto, K. *Cryst. Growth Des.***2012**, 12, 3278-3284.
[9] Kimura, Y.; Miura, H.; Tsukamoto, K.; Li, C.; Maki, T. *J. Cryst. Growth***2011**, 316, 196−200.
[10] Michael, B. P., Nuth III, J. A., Lilleleht, L. U. *Astrophys. J.***2003**, 590, 579-585.

11:35 Oral

Effective Segregation Coefficient for Segregation in Microgravity

Aleksandar G. Ostrogorsky

Illinois Institute of Technology, 10 West 33rd Street, Chicago, Il 60616, United States

e-mail: AOstrogo@IIT.edu

A new model for effective segregation coefficient in microgravity is proposed. Natural convection is quantified using Nusselt numbers, so that solute film thickness δ does not need to be known. A "Combined-Convection" Nusselt number, Nu_{CC} is derived for the solid-liquid interface, which accounts for buoyancy-driven flow, and the cross-flow velocity f, entering the interface. Nu_{CC} is used to calculate the effective

segregation coefficient, k_{eff} at low levels of natural convection, occurring in space laboratories.

11:50 Oral

Crystallization and annealing of colloidal crystals under gravitational fields

Yoshihisa Suzuki[1], Jin Endoh[2], Yohei Hamada[2], Atsushi Mori[1], Masahide Sato[3], Hiroyasu Katsuno[4]

1. *Institute of Technology and Science, The University of Tokushima, 2-1 Minamijosanjima, Tokushima, Tokushima 770-8506, Japan* **2.** *Department of Chemical Science and Technology, The University of Tokushima, 2-1 Minamijosanjima, Tokushima, Tokushima 770-8506, Japan* **3.** *Kanazawa University, Kakuma-machi, Kanazawa 9201192, Japan* **4.** *Gakushuin University, 1-5-1 Mejiro,Toshima-ku, Tokyo 171-8588, Japan*

e-mail: suzuki@chem.tokushima-u.ac.jp

A three-dimensionally (3D) large and close-packed face-centered cubic colloidal crystal is useful as a template for inverse opals with perfect three-dimensional photonic bandgap [1]. Although bulk close-packed colloidal polycrystals are easily fabricated by drying highly-concentrated colloidal crystals [2], controlled fabrication of the highly-concentrated colloidal crystals with sufficiently large and high quality grains for device applications is still difficult.

We developed effective enlargement [3] and annealing [4] methods to obtain such a colloidal crystal grain by applying a gravitational field.

For enlargement studies, a highly concentrated and 3D large colloidal crystal grain was obtained by centrifugation of polystyrene particles (Duke Scientific, diameter d = 200 nm, volume fraction of the dispersion φ = 0.1) at 21G with the control of the angle of substrates (walls of growth cell). We adjusted the angle of an optical cell with a rid using a specially-designed cell holder.

For annealing studies, a highly concentrated colloidal crystal was obtained by centrifugation of silica particles (Nippon Shokubai Seahoster KE-W10, d = 110 nm, φ = 0.0968) at 9 G for 2 days. Polarized transmission image of a grain in the crystal showed some striations in the grain. The striations show the stacking disorders in the grain [5]. After the first observation, the crystal was centrifuged again at 50 G for 5 days. The number of the striations seemed to decrease after the additional centrifugation. The decrease shows the shrinkage of the stacking disorders under high gravity [4].

[1] A. Blanco, et al., *Nature*, **405**, 437-440 (2001). [2] Y. Suzuki, et al., *J. Cryst. Growth*, **322**, 109-113 (2011). [3] Y. Suzuki, et al., *J. Cryst. Growth*, **318**, 780-783 (2011). [4] Y. Suzuki, et al., *Defect & Diffusion Forum*, **323-325**, 555-558 (2012). [5] Y. Monovoukas, et al., *Phase Transitions*, **21**, 183-195 (1990).

12:05 Oral

Interaction of Foreign phase particles with moving solid-liquid interface during directional solidification of silicon for photovoltaics

Maral Azizi[1], Christian Reimann[1], Jochen Friedrich[1], Arne Croell[2], Tina Sorgenfrei[2], Thomas Jauss[2], Heike Emmerich[3], Henning Hoerstermann[3], Julia Kundin[3]

1. *Fraunhofer Institute of Integrated Systems and Device Technology (IISB), Schottkystraße 10, Erlangen 91058, Germany* **2.** *Univ.Freiburg, Freiburg, Germany* **3.** *Universität Bayreuth, Universitätsstr. 30, Bayreuth 95440, Germany*

e-mail: maral.azizi@iisb.fraunhofer.de

During the crystallization of multi-crystalline silicon the melt is contaminated by nitrogen, from the crucible coating as well as by carbon already present in the initial feedstock or transported via the gas atmosphere to the melt surface, where it is then dissolved. When the solubility limit is exceeded, SiC and Si_3N_4 particles are formed. Such particles cause problems during the wire sawing process due to their hardness. They can also influence the grain growth and size negatively, leading to the small grain "grit" structure and the formation of dislocations. Finally, SiC-precipitates can act as shunts reducing the performance of the solar cells. Therefore, the incorporation of such deleterious particles has to be avoided.

The occurrence of such foreign phases in the solid silicon can be correlated to melt convection. However, the interaction of such particles with the moving crystallization front and their incorporation into solid silicon are not fully understood today. Under the assumption that the particle would form in the melt, a critical growth velocity vcr should exist depending on the density, size and morphology of the particles. Below vcr a particle will be pushed in front of the growth interface, whereas above vcr, the particle will be captured and frozen into the growing crystal. This particle engulfment depends on the so-called interface-, drag-, lift-, and gravity-forces acting on the particle in the vicinity of the interface. It has been theoretically shown that only mm-sized particles should be captured for typical growth velocities used in crystallization of multi-crystalline silicon if only drag and interface forces are considered. This result is in full contradiction to the experimental observations that the particles detected in silicon are µm-sized. Preliminary investigations where SiC-particles were added to the melt have shown that gravity and lift forces (due to melt convection) are most likely determining the transport of the particles under terrestrial conditions. Depending on the size and density of the particles and on the convection intensity they can either sink to the bottom of the melt or float on the melt surface. Since gravity affects melt movement, solute distribution, and sedimentation of the particles, microgravity offers the unique opportunity to study particle nucleation, transport, and incorporation under purely diffusive conditions.

Therefore, it is one of the major goals of the ParSiWal-project to understand in detail the interaction of foreign phase particles with the moving solid-liquid interface during directional solidification of silicon under diffusion controlled growth conditions in the ELLI furnace during the TEXUS 51 mission scheduled for April 2013.

In the presentation the results of terrestric experiments and first results of the flight experiment will be shown. During all experiments single crystalline silicon rods with 8mm diameter containing a reservoir of SiC particles with particle size varying from 7µm to 300µm will be zone melted at different growth rates of 0.2-10 mm/min. In order to avoid Marangoni convection the rods are covered by a 5 µm thick oxide skin. Terrestric experiments with and without magnetic stirring before and during crystallization were done. The samples were analyzed by

infrared transmission microscopy to determine the distribution of the particles in the silicon after processing, to gain information about the particle incorporation depending on the growth rate.

Lunch (EMCG meeting)

Thursday afternoon, 15 August, 12:20

ThO2

T08: External fields, microgravity
Thursday afternoon, 15 August, 14:00
Room A, Auditorium Maximum

14:00 Invited oral

The Effect of an External Electric Field on Phase Equilibria, Nucleation and Growth

Satoshi Uda

Tohoku University, Institute for Materials Research (IMR), 2-1-1, Katahira, Aoba-ku, Sendai 980-8577, Japan

e-mail: uda@imr.tohoku.ac.jp

Regarding a new growth method, it may be differentiated into two classes. One is associated with a simply technological improvement and the other is a fundamental reform of crystal growth. The former includes, for the case of melt growth via the Czochralski technique, the optimization of temperature distribution and gas flow in a furnace, rotation and pulling rate, etc., which I would say is a simple manipulation of growth conditions. In contrast the latter could bring a radical change of crystal growth based on scientific principles, which would be more interesting.

Applying an external electric field to the growth system is one of the latter cases and leads to a completely new growth approach since it creates one more freedom in terms of Gibbs phase rule, which would allow us to move from *invariant* to *univariant* or *univariant* to *divariant*, etc. Such an increase of freedom enables us to change equilibrium phase relationship, that is, the conversion of incongruency to congruency of a compound.

There may be two ways to apply an electric field to the growth system. One is concerned with an electrostatic field applying through the inert gas that is an electrically -insulating phase [1,2]. Because oxide melts or protein solutions show high ionic conductivity, the electric potential distribution is nearly flat in them even if an electric field as large as several-hundred V/cm is electrostatically applied. However, the imposition of such an external electric field would form an *electric double layer* (EDL) of ~nm width between two different substances, i.e., crystal and melt or solution. This is the place where a large electric field of 10^4 to 10^5 V/cm could be sustained, which modifies phase relationship, nucleation and growth [3].

The other is a direct injection of an electric current to the solid-interface-liquid [4]. Because of the resistivity of the melt or solution, the injected current generates an electrical potential distribution leading to an electric field with the order of ~ 1 V/cm. It should be noted that the current injection also induces the adsorption or rejection of ionic solute at the interface, which would make solute behavior at the interface a little more complicated.

Application of an external electric field on the crystallization process modifies the chemical potentials of associated phases leading to two distinct consequences: (i) thermodynamic effect and (ii) growth-dynamic effect. The former pertains to the macroscopic picture and changes the equilibrium phase relationship, while the latter is on a microscopic scale and modifies the solute transport, nucleation, growth kinetics, surface creation and defect generation related to crystal growth.

We demonstrate the former case that the electric field converted the incongruent-melting state of langasite (LGS: $La_3Ga_5SiO_{14}$) into congruent-melting state [1] and the latter case that the electric field changed the critical nucleation energy resulting in the control of nucleation rates of the hen-egg white lysozyme [2]. It should be also noted that such an energy shift is dominated by the magnitude of electrical permittivities of solid and liquid phases and their compositional dependence. By varying frequency of an applied field, we see that these dominant parameters could change the nucleation of lysozyme [2].

The current injection to the interface of growing Mn:$LiNbO_3$ controls Mn distribution in the grown crystal for which the equilibrium partition coefficient, k_0 of Mn into $LiNbO_3$ crystal should be replaced with the field-modified partition coefficient, k_{E0}.

[1] S. Uda, X. Huang and S. Koh, *J. Cryst. Growth***281** (2005) 481.

[2] H. Koizumi, S. Uda, K. Fujiwara and J. Nozawa, *Langmuir***27** (2011) 8333.

[3] S. Uda, S. Koh and X. Huang, *J. Cryst. Growth***292** (2006) 1.

[4] S. Uda and T. Tsubota, *J. Cryst. Growth***312** (2010) 3650.

14:30 Oral

Improvement of crystal quality for tetragonal hen egg white lysozyme crystals under application of an external alternating current electric field

Haruhiko Koizumi[1], Satoshi Uda[1], Kozo Fujiwara[1], Masaru Tachibana[2], Kenichi Kojima[3], Jun Nozawa[1]

1. *Institute for Materials Research, Tohoku University, 2-1-1, Katahira, Aoba-ku, Sendai 980-8577, Japan* **2.** *Graduate School of Nanobioscience, Yokohama City University, 22-2 Seto, Kanazawa-ku, Yokohama 236-0027, Japan* **3.** *Department of Education, Yokohama Soei University, 1 Miho-tyou, Midori-ku, Yokohama 226-0015, Japan*

e-mail: h_koizumi@imr.tohoku.ac.jp

High-quality single crystals of proteins are required for studies related to structure-guided drug design and controlled drug delivery, because the crystal quality governs the refinement of the three-dimensional structure of protein molecules obtained from X-ray structure analysis. However, it is quite difficult to obtain high-quality single crystals of proteins. In addition, the crystallization of proteins is also difficult, and therefore the establishment of a crystallization technique that can obtain high-quality single crystals of proteins and control the nucleation of proteins is required.

Previously, we have successfully achieved both an increase and a decrease in the nucleation rate of protein crystals by applying an external alternating current (AC) electric field, by focusing on the magnitude of the electrostatic energy added to the chemical potentials of the liquid and solid phases [1),2)]. It is considered that such effect of the electrostatic energy is added to not only the chemical potential but also entropy. Thus, we demonstrate the improvement of the crystal quality of protein crystals by applying an external AC electric field.

The FWHMs obtained from crystals prepared without an external electric field increased for diffraction peaks with order higher than the

440 reflection. In contrast, for crystal growth with an external electric field at 1 MHz, the FWHMs were smaller than those for crystals grown without. This suggests that the crystal quality be improved by applying an external AC electric field. In this presentation, the improvement of the crystal quality is discussed in the light of the change in entropy of the solid.

Reference

1) H. Koizumi, K. Fujiwara, and S. Uda, *Cryst. Growth Des.***9**, 2420-2424 (2009).
2) H. Koizumi, Y. Tomita, S. Uda, K. Fujiwara and J. Nozawa, *J. Crystal Growth***352**, 155-157 (2012).

14:45 Oral

Study of thermal stratification in EM force driven turbulent flow in square-shaped crucible for directional solidification method

Vadims Geza[1,2], Bernard Nacke[1], Egbert Baake[1], Andris Jakovics[2]

1. *Leibniz Universitaet Hannover, Institute of Electrotechnology (ETP), Wilhelm-Busch-Str. 4, Hannover 30167, Germany* **2.** *Faculty of Physics and Mathematics, University of Latvia, Zellu Street 8, Riga LV-1002, Latvia*

e-mail: geza@etp.uni-hannover.de

As fossil energy resources are getting exhausted, demand for alternative energy sources is growing. For example, in 2011 in Germany the renewable energy part was 12.5%, and it is almost doubled during last 6 years [1]. Directional solidification (DS) is widely used for the production of photovoltaic materials in crucibles, usually square-shaped for convenient and material-loss effective wafer production. These ingots are produced in different sizes which are still growing to fit growing demand for solar cells. The quality of such ingot depends primarily on the feedstock. However, the success of each production step, two of which – melting and solidification – include the liquid phase, is also crucial for such parameters as polycrystalline grain size, concentration of incorporation, dislocation and other defects. Understanding and controlling of the melt flow during solidification phase is important for the reduction of N, C and O incorporations and precipitation formations [2], [3], [4].

This study is devoted to the numerical and experimental investigation of the turbulent melt motion in a square crucible where the flow is created by Lorentz forces generated by external AC magnetic field through. As a strong vertical thermal gradient is present in DS method in melt, stratification effect takes place and motion in vertical direction is damped by buoyancy forces.

Governing processes

Incompressible fluid flow is described by Navier-Stokes equation, which in dimensionless form includes few parameters - Reynolds number Re, electromagnetic interaction parameter F_0, Richardson number Ri. All these parameters define the flow regime. The Richardson number is a ratio of buoyancy forces to inertial forces. In case of Ri below unity, the inertial forces dominate and buoyancy forces are not sufficient to prevent turbulent mixing. In the opposite case, Ri much above unity, buoyancy damps the turbulent pulsations in z directions. Typical Ri for directional solidification devices is of the order of magnitude 10.

Numerical research of melt motion problem in crucible implies the solution of fluid flow and heat transfer, and electromagnetic (EM) equations when EM stirring is present. However, if the flow is turbulent, a modelling approach has to be used to obtain solution in reasonable time – DNS method, which resolves all turbulent scales down to Kolmogorov scales, is very time and resource demanding and is not able to solve turbulent for high Reynolds numbers. Two most well known approaches for turbulence modelling are Reynolds Averaged Navier-Stokes (RANS) and Large Eddy Simulation (LES), widely used also in modelling of melt flow in DS method. The numerical results show that turbulent heat flux in vertical direction in overestimated in RANS models, especially at high Ri numbers. The main reason for this is assumption of isotropic turbulence. However, LES models with significant spatial resolution is able to capture anisotropy effect.

Experimental Measurements

Physical model experimental device (Figure 1) was built, using eutectic Wood's alloy (50% Bi, 25% Pb, 12.5% Sn, 12.5% Cd, melting temperature 72°C) as working liquid. The set-up consists of square-shaped crucible with side length 420 mm, and height 270 mm, filled with Wood's alloy to level H=120mm. The crucible has stainless steel walls with thickness 1.5 mm. The crucible is placed on water heated (T=80°C) aluminium plate. The radiation heater is used as lid on the crucible, which allows achieving vertical temperature gradient in the alloy. However, the emissivity of the Wood's alloy is very low (~0.15) and therefore radiative heat flux on the free surface is low, thus major heat flux on the free surface is ensured by the heated air in the space between alloy and lid. In this set-up steady temperature difference between top and bottom surface up to 80°C was obtained without EM mixing.

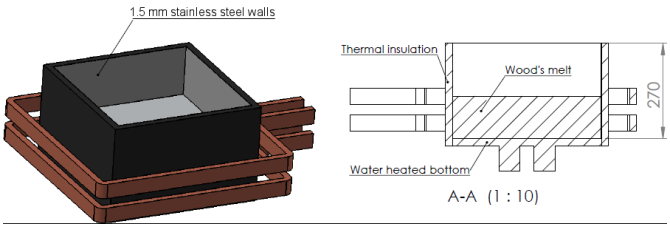

Fig 1. Sketch of experimental set-up. Left - 3D view. Right - vertical middle cross section.

Ultrasound Doppler Velocimetry (UDV) allows to measure the velocity profile along the ultrasound beam and is able to obtain signal even through wall [5]. For this reason UDV technique (device Signal Processing DOP 3000) was chosen for current set-up. Vertical temperature profile was measured with 6 thermocouples with vertical spacing 20 mm starting from 10 mm above bottom.

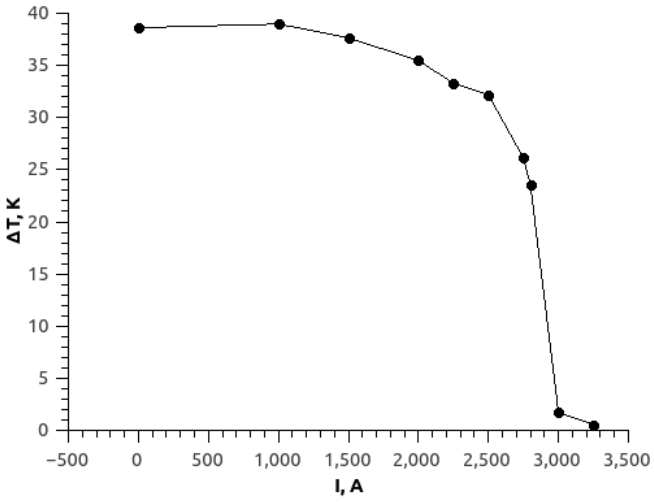

Fig 2. Vertical temperature gradient dependence on total inductor current.

The important effect of stratification is the damping of vertical motion including vertical turbulent pulsations. Figure 2 shows vertical temperature difference in dependence on total current I in the inductors. In developed turbulent regime Ri~$1/I^2$ dependence is expected. Then it is also clear, that some critical current I_{CR} exists, when Ri becomes smaller than unity and turbulent mixing prevail, thus change of flow structure is possible. Slight decrease of vertical temperature difference with growth of I which is observed also below I_{CR} (0-2,500A), this can be explained with increase of turbulent pulsations and thus turbulent heat conductivity. At the I_{CR} vertical temperature displacement due to turbulence become so large that fluid particle displaced from thermal equilibrium buoyancy forces are unable to return to initial level. Here flow structure changes from stratified quasi-two dimensional layered structure to three dimensional.

Summary

In current work numerical models in case of stratified EM driven flow were tested and compared with experimental results, which are obtained with physical model. Existing physical model allows to measure velocity and temperature field in stratified flows. Using obtained results, main features of stratified flows were obtained, including two dimensionality of mean flow and damping of vertical turbulent pulsations.

References

[1] D. Bohme. Entwicklung der erneuerbaren Energien in Deutschland im Jahr 2011. http://www.erneuerbare-energien.de.
[2] C. Reimann, M. Trempa, T. Jung, J. Friedrich, G. Muller. Journal of Crystal Growth.(2010) Vol 312. pp. 878.
[3] H.J. Moller, L. Long, M. Werner, D. Yang. Phys. Stat. Sol. (1999) Vol 171. pp. 175.
[4] G. Du, N. Chen, P. Rossetto. Sol. Energy Mater. Sol. Cells (2008) Vol 92. pp. 1059.
[5] S. Eckert , G. Gerbeth. Experiments in Fluids 32 (2002) 5, p. 542-546

15:00 Oral

Heat transfer in the whole directional solidification process for multi-crystalline silicon ingots under traveling magnetic fields

Qinghua Yu, Lijun Liu, Zaoyang Li, Peng Su

School of Energy and Power Engineering, Xi'an Jiaotong University, Xi'an 710049, China

e-mail: yqh.2010@stu.xjtu.edu.cn

Multi-crystalline silicon (mc-Si) produced by the directional solidification (DS) method has been the main material for solar cells due to low manufacturing cost. However, solar cells made from mc-Si have disadvantages in photoelectric conversion efficiency. This is because a grown mc-Si ingot incorporates impurities, precipitates and structural defects, of which generation and distribution are determined mainly in the DS process. In order to improve ingot quality and therewith cell efficiency, it is vital to control and optimize the DS process. During the DS process, silicon melt convection, acting as an important carrier of heat and mass transfer, could significantly affect the temperature distribution, impurities transport and crystallization interface shape. Therefore, precise control of melt flow pattern is crucial to optimizing the DS process and improving ingot quality. In the conventional DS system, the melt flow is driven mainly by buoyant force resulting from horizontal temperature gradient. Control ability of this driving manner for melt flow pattern is limited. A more effective manner is the use of traveling magnetic fields (TMFs). Detailed understanding of heat transfer in the whole DS process under TMFs is the key to adopt TMFs to optimize the DS process. However, few studies have been conducted on the whole DS process under TMFs.

The DS process is a highly coupled nonlinear thermal process with complex thermal interaction among the melt convection, argon flow and different solid components. It is therefore necessary to employ global modeling, which takes into account thermal convection, conduction, radiation and phase change, to reproduce the whole DS process under TMFs. During the DS process, the crystallization interface is continuously moving and a steady-state position of the interface physically does not exist, i.e. the melt height is changing. This requires the incessant recalculation of the Lorentz force distribution during the DS process. The coupling effect between the melt height and the Lorentz force distribution makes the numerical modeling of the whole DS process under TMFs more complicated.

In this study, we developed a fully coupled transient global model for the whole DS process under TMFs. On the basis of this model, the evolutions of Lorentz force distribution, thermal field, melt flow and crystallization interface shape were predicted during the whole DS process. Special attention was paid to comparisons of the melt flow pattern and crystallization interface shape as well as their evolutions under different cases without TMFs, with downward directed TMFs and with upward directed TMFs. These results can provide essential knowledge for optimizing the DS process of mc-Si via TMFs.

15:15 Oral

Analysis of a Traveling Magnetic Field (TMF) on Bridgman Crystal Growth of Cadmium Zinc Telluride (CZT)

Andrew Yeckel, Jeffrey J. Derby

University of Minnesota, Chemical Engineering and Materials Science, 421 Washington Ave. S.E., Minneapolis, MN 55455, United States

e-mail: derby@umn.edu

Large, single crystals of cadmium zinc telluride (CZT) are needed for portable, low-cost, and sensitive devices to detect radioactive materials. However, CZT is a particularly difficult material to grow, and advances in growth methods are needed.

Recently, the application of traveling magnetic fields (TMF) has garnered attention for its promising outcomes in many semiconductor melt growth systems. The application of TMF produces Lorentz forces through the molten phase, and these forces can be tuned in magnitude and spatial orientation to profoundly impact melt flows. In turn, these flows modify heat and mass transfer, influencing the shape of the melt-solid interface and segregation along the interface. Since the applied TMF can be instantaneously changed, it provides for a potentially ideal control action, if its complicated effects can be predicted and understood.

In this presentation, we employ fundamental mathematical models solved via finite element methods to assess the impact of TMF applied to Bridgman crystal growth processes. In particular, we aim to assess the potential of TMF to improve CZT growth. We discuss the mathematical formulation of our TMF analysis and, more importantly, our initial results on the effects of TMF applied to a prototypical CZT growth system.

Supported in part by DOE/NNSA, DE-FG52-08NA28768, the content of which does not necessarily reflect the position or policy of the United States Government, and no official endorsement should be inferred.

15:30 Oral

Model experiment on a special type of electromagnetical stirring in a GaInSn melt

Radu-Andrei Negrila, Marius Paulescu, Alexandra Popescu, Daniel Vizman

West University of Timisoara (UVT), Bd.V. Parvan nr.4, Timisoara 300223, Romania

e-mail: vizman@physics.uvt.ro

One of the key issues in the technology development os directional solidification (DS) for multicrystalline silicon ingots for photovoltaic applications is to control the impurities distribution in the mould, which can influence important parameters related to the solar cell efficiency.It is well known that melt convection plays an important role in the impurities distribution. Therefore, a better control of melt convection will improve the quality and yield of the solidification process by influencing the interface shape and dopant and impurities distribution in a beneficial way. Based on the idea of melt stirring from Electromagnetic Czochralski method [1] and on a similar idea with one electrode for DS [2], a new configuration with two electrodes is proposed for a DS melt placed in a vertical low intensity magnetic field. The two electrodes are in contact with the free melt surface and an electrical DC current passes through the electrodes.

In order to show the potential of this method, both numerical and experimental investigations have been carried out. The experimental set-up consists of a square-shaped crucible ($7x7x7cm^3$), which contains a GaInSn alloy placed in a vertical magnetic field(fig.1). This eutectic alloy is suitable for such room temperature model experiments, because it is liquid above 11 degrees Celsius. The electrical current passes the melt through two electrodes (fig.1). The melt velocity is measured using an Ultrasound Doppler Velocimeter.

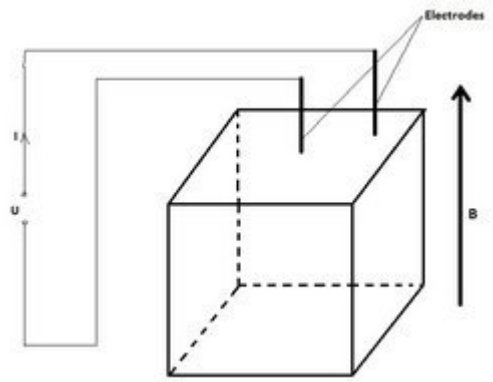

Fig.1. Geometry of melt and the electromagnetic set-up

STHAMAS3D software was used to performed numerical simulations. The melt is modeled as a Boussinesq fluid and the transient Navier–Stokes equations are solved simultaneously with the transient heat equation. The influence of the steady magnetic field on the melt flow is considered by the Lorentz force density in the Navier-Stokes equations. For the calculation of the Lorentz force, the electric current density is computed using a scalar electrical potential, which is obtained by solving an additional equation.

It was found that even a small magnetic field (10 mT) and an electrical current in the electrodes of maximum 10 A can produce a significant stirring effect. The rotation rate increases with the increase of the intensity of electrical current and the flow structure depends on the electrodes position. The numerical results for the melt convection (intensity and flow patterns) support the experimental findings.

The main contribution of this idea is to provide some additional growth parameters (like intensity of electrical current and position of the electrodes) easy to be adjusted in order to control the melt flow and interface shape. It is also clear that the electrodes design is a crucial issue before to apply this idea in a real growth facility, mainly because the electrodes should passed the hot zone and can bring more impurities in the melt.

The results prove that a combination of a low intensity vertical magnetic field and electrical current (EMF) has the potential to control the melt flow and interface shape and can lead to a homogeneous impurities distribution through the melt stirring effect.

[1] W.Wang, et.al., Jpn.J.Appl.Phys. Vol 39(2000), pp.372-377

[2] C. Tanasie, D. Vizman, J. Friedrich, J. Cryst. Growth 318 (2011) 293-297

15:45 Oral

Features of semiconductor crystal growth in ultrasonic fields by Czochralski method

Gennadiy N. Kozhemyakin

Volodymyr Dahl East Ukrainian National University, Luhansk 91050, Ukraine

e-mail: genakozhemyakin@mail.ru

Growth striations are a major problem in growth crystal, which limits the application of semiconductor single crystals in nanoelectronics. External fields such as microgravity, magnetic fields, and ultrasound can create crystal growth conditions for homogeneous component distribution in semiconductor single crystals. Our group has been studying the effect of high frequency ultrasound on the growth of semiconductor crystals by the Czochralski method for the past 28 years and demonstrated the potential of this method for the striation decrease. Experimental results of GaAs, InSb, Bi_xSb_{1-x}, and $Ga_xIn_{1-x}Sb$ solid solution growth are unclear, depending on their physical and chemical properties.

The direction of ultrasonic waves was parallel to the pulling axis in the first series of our experiments. InSb, Bi_xSb_{1-x}, and $Ga_xIn_{1-x}Sb$ single crystals with 10 mm diameter were grown with rotation rates of < 10 rpm from 150 g melt, without crucible rotation. The crystals were pulled in the atmosphere of high purity Ar at pressures 0.2÷2 atm. The ultrasound was introduced into the melt from a piezotransducer through a fused silica waveguide with 10 mm diameter and 300 mm length, fused to the bottom of the silica crucible. Each single crystal had regions, which were pulled with and without ultrasound. The pulled single crystals were cut parallel to the growth direction, ground, polished and etched in order to reveal the growth striations under an optical microscope and an electronic microscope “Nanolab-2100”.

Sb striations in Bi_xSb_{1-x} single crystals (x = 0.03÷0.15) with separations of 7 to 400 μm were located mainly parallel to or at an angle of 60° with the solid-liquid (S/L) interface, and were observed in each region grown without ultrasound. The introduction of ultrasound at frequencies of 0.65, 2.5, or 5 MHz into the melt eliminated Sb striations in Bi_xSb_{1-x} single crystals grown with constant diameter and in the central part of the crystals with changing diameter. It was found that for constant diameter growth, after “processing” the melt with ultrasound, the striations did not reappear until 2 hours have passed.

InSb:Te single crystals were grown in the <111> direction. The effect of ultrasonic field at frequencies 0.25, 0.6, 1.2, 2.5, 5, or 10 MHz eliminated the striations with width of 5 to 15 μm in the facet growth

region. However, striations with smaller periodicity remained. A similar result of incomplete striation removal was observed in $Ga_{0.03}In_{0.97}Sb$ single crystals grown with ultrasound at frequencies 0.72 and 1.44 MHz.

GaAs single crystals with 50 mm diameter were pulled from 1.5 kg of the melt containing Cr impurity at a concentration of 10^{16} cm^{-3} using B_2O_3 as an encapsulant. The seed rotation rate was 4–5 rpm, and the crucible rotation rate was 16–18 rpm, in opposite directions. An investigation of As distribution was carried out in GaAs single crystals pulled in the presence of ultrasound at a frequency of 0.15 MHz. Striations with separations of 25 to 140 μm were located parallel to the (S/L) interface. In the region where the diameter of the crystal was changed, the ultrasound did not decrease the As inhomogeneity. There was a decrease of As inhomogeneity in the region of the crystal grown with constant diameter. However, striations reappeared again when the ultrasound was interrupted for a short duration. Additionally, it was found that the ultrasound did not affect striations in 3 kg melt, when the melt depth increased from 30 mm to 60 mm in a 90 mm diameter crucible.

We also studied the influence of ultrasound in two orthogonal directions, and the effect of the S/L interface shape to eliminate striations with smaller periodicity in InSb single crystals, pulled by the Czochralski method. The ultrasound at frequencies from 1.25 to 2 MHz introduced into the melt in a direction perpendicular to the pulling axis did not eliminate striations in the grown crystals. However, the introduction of ultrasound simultaneously in two orthogonal directions at frequencies different by a factor of 2 totally eliminated striations in grown crystals with convex S/L interface. This was a result of complex oscillations of melt particles in ultrasonic standing waves, which damped convection under the S/L interface.

We also investigated the influence of ultrasound at a frequency of 3 MHz on the growth of GaAs layers by liquid-phase epitaxy (LPE). The introduction of ultrasonic waves in Ga solution promoted the conditions for LPE growth with flat shape of the S/L interface. Ultrasonic waves in Ga solution changed the macrostep morphology within a few minutes after switching on the ultrasound. In these experiments, we observed LPE growth with one macrostep. However, the macrostep growth converted into an ordinary growth with a few macrosteps within 2 minutes after switching off the ultrasound.

We modeled the growth conditions and the ultrasound effect using the light cut method. It was found that a standing wave channel formed between the S/L interface and a waveguide. The standing waves damped the convective flow under the S/L interface, and as expected, the component inhomogeneity in grown single crystals decreased. The ultrasonic standing waves induced a stationary convection at a Raleigh number less than $Ra < 10^5$ in studied melts and solutions.

However, the melt depth continuously decreases during the growth by the Czochralski method. Maintaining a stable standing wave channel in the melt during the growth process is an important circumstance for the method application. Therefore, we investigated the effect of changing melt level on the behavior of ultrasonic standing waves. We saw that the standing wave channel did not disappear during a decrease or increase of the liquid depth. We found that ultrasonic standing waves can form and stay in a liquid even when the distance between the ultrasonic transducer and reflector is not equal to a multiple of the total number of half wavelengths. The standing wave channel remained in the liquid above the ultrasonic transducer, and any change of the liquid level leap-changed its height by the multiple of one antinode.

From these experimental results, we can say that it is possible to solve the striation problem in Czochralski crystal growth using the ultrasound. The potential virtue of ultrasound is that it can form standing waves to dump convective flow and eliminate striations as a result. Ultrasonic fields can be implemented at a reasonable cost in industrial crystal growth of semiconductor single crystals to improve growth conditions of striation-free crystals. Therefore, we recommend this technique for commercial application.

Coffee
Thursday afternoon, 15 August, 16:00

Posters

Wednesday, 14 August

WeP-T08
Wednesday afternoon, 14 August, 16:00
Room 215, Old Library

16:00 Poster We208

Numerical simulations of heat and mass transfer in traveling liquidus-zone crystal growth process of SiGe under microgravity

Keita Abe[1], Sara Sumioka[1], Ken-ichi Sugioka[1], Masaki Kubo[1], Takao Tsukada[1], Kyoichi Kinoshita[2], Yasutomo Arai[2], Yuko Inatomi[2]

1. *Department of Chemical Engineering, Tohoku University, 6-6-07 Aramaki, Aoba-ku, Sendai 980-8579, Japan* **2.** *Institute of Space and Astronautical Science, Japan Aerospace Exploration Agency (JAXA), 2-1-1 Sengen, Tsukuba, Ibaraki 305-8505, Japan*

e-mail: k.abe@pcel.che.tohoku.ac.jp

Single crystals of SiGe, especially $Si_{0.5}Ge_{0.5}$, attract the attentions as the post Si semiconductor substrates, and enable to produce high-speed and low energy devices, because both strained Si and Ge films grown on SiGe substrates have higher mobility than intrinsic Si and Ge substrates. For the production of homogeneous SiGe bulk single crystals, a lot of growth techniques have been developed. Recently, Kinoshita et al. [for instance, *Journal of Crystal Growth*, **349**, 50(2012)] have developed the travelling liquidus-zone (TLZ) method to grow homogeneous SiGe crystals. In the TLZ method, Ge which is sandwiched by a Si seed and a Si feed is melted at around 1100°C above the melting point of Ge and at relatively low temperature gradients (5-15°C/cm) as shown in Figure 1. Since the solute Si is almost saturated throughout the molten zone in this method, the concentration profile coincides with that on liquidus line, and consequently, is uniquely determined following the temperature gradient in the zone. The crystal growth of SiGe occurs spontaneously due to interdiffusion of Si and Ge following their concentration gradients through the molten zone.

Although homogeneous SiGe single crystals with a diameter of 2 mm were successfully grown by the TLZ method, the growth of larger diameter crystals was not succeeded yet, because free convection induced by the temperature and concentration gradients in the melt strongly affects the homogeneity of the crystals on the ground. In order to clarify the effect of free convection on the TLZ crystal growth of SiGe, therefore, the crystal growth experiments under a microgravity environment in International Space Station (ISS) have been planned and are being performed this year by JAXA.

In this work, to understand transport phenomena in the TLZ crystal growth process of SiGe under microgravity in detail, a mathematical

model for the crystal growth process of SiGe by the TLZ method has been developed, where the velocity field in the melt, the thermal field in the furnace, Si concentration field in the melt and crystal, and the melt/crystal interface shapes can be predicted numerically. Figure 2 shows the numerical results of temperature filed in the furnace (left side) and Si composition field in the molten zone (right side) during dissolution and crystal growth. The crystal diameter, temperature gradient of furnace and its moving speed are 10.2 mm, 9ºC/cm and 0.082 mm/h respectively. Firstly, the molten Ge dissolved the Si feed and seed, and consequently, the molten zone became longer (Figure 2(b)). At 400 min, the crystal began to grow (Figure 2(b)), and at 8000 min, grew up to 10.7 mm in length (Figure 2(d)). In this work, we investigated the effects of operational conditions, e.g., moving speed of furnace, thermophysical properties of crucible and crystal radius, on the spatial homogeneity of grown single crystals and the melt/crystal interface shapes which are macroscopic characteristics related to crystal quality.

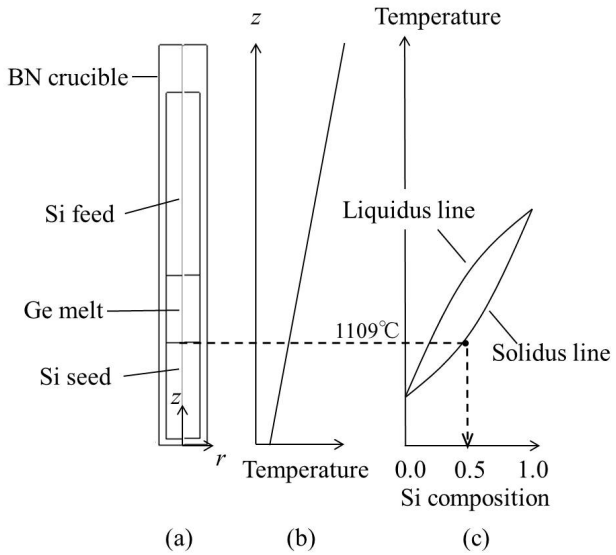

Figure 1 Schematic of the TLZ process.

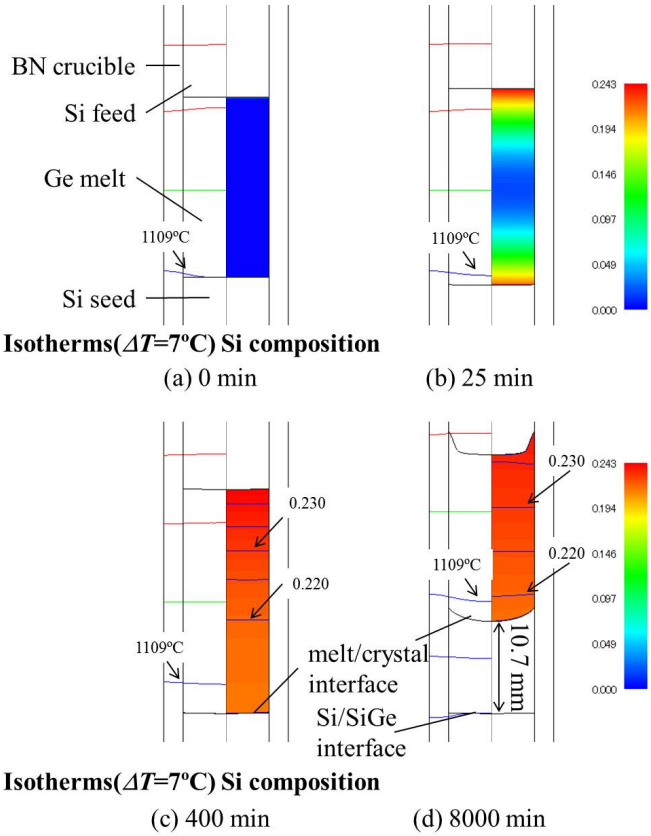

Figure 2 Numerical results of temperature filed in the furnace (left side) and Si composition field in the molten zone (right side) during dissolution and crystal growth.

16:00 Poster We209

Czochralski growth of $NaNO_3$-$LiNO_3$ solid solution single crystals using axial vibrational control technique

Evgeny V. Zharikov, Stanislav Belov, Chan Kong Khan, Elena Mozhevitina, Andrey P. Sadovskiy, Igor C. Avetissov

Mendeleyev University of Chemical Technology of Russia, Moscow 123480, Russian Federation

e-mail: igor_avetisov@mail.ru

Axial vibration control (AVC) technique is powerful tool for melt activation by low-frequency oscillation of inert baffle submerged into melt [1]. It was demonstrated that AVC grown crystals strongly differs in many properties comparing with the crystals grown by conventional directional solidification methods both Bridgman [2] and Czochralski [3] techniques.

Single crystals of $LiNO_3$-$NaNO_3$ solid solutions were grown by AVC-CZ technique [3] using 0.3 mm amplitude and 0-25 Hz frequency oscillations of an inert aluminum disk in the melt. The crystal diameter was 30-35 mm with 30-35 mm length of every part grown at fixed AVC parameters. To analyze impurities distributions in crystals we cut them along. then cut a slice perpendicular to the growth axis [006], and then cut into small pieces 3x3x2 mm. Every piece was dissolved and analyzed using ICP-MS technique (NexION 300 D, Perkin Elmer). Thus, we got a distribution of all impurities in the crystal.

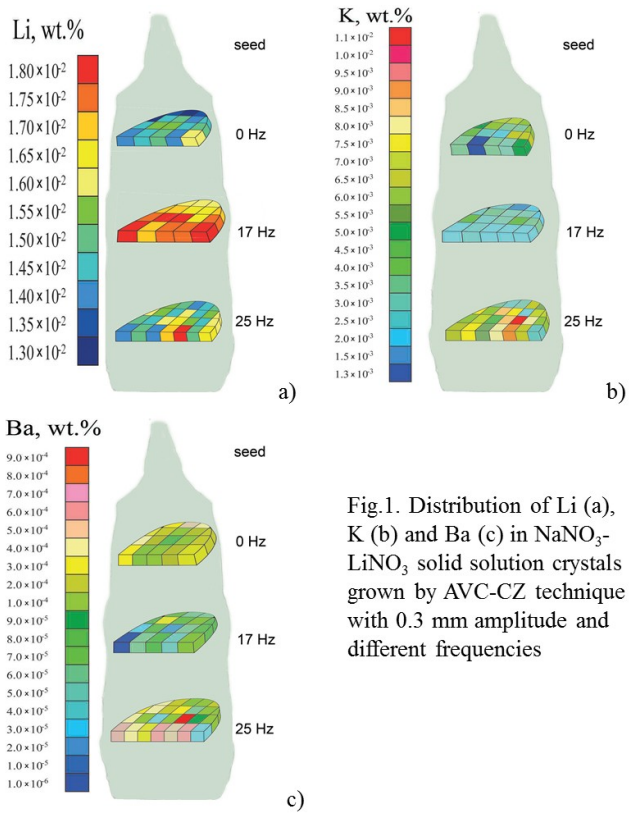

Fig.1. Distribution of Li (a), K (b) and Ba (c) in $NaNO_3$-$LiNO_3$ solid solution crystals grown by AVC-CZ technique with 0.3 mm amplitude and different frequencies

We found out that application of AVC-CZ technique resulted in sufficient changes of Li effective distribution coefficient up to 40 % relative to the conventional CZ growth.

The problem of different molecular weight impuirities distribution at crystal growth is very important for homogeneous doping. AVC technique produces vibrational flows in the melt could strongly change the impurity distribution pattern. We observed that various impurities acted differently at AVC application. Light molecular weight impurities (presented by Li) demonstrated significant leveling of concentration inside the crystal volume simultaneously with an increase of segregation coefficients (fig.1a). The similar leveling was observed for middle molecular weight impurities (presented by K) but their segregation coefficients changed insufficient (fig.1b). In case of heavy molecular weight impurities (presented by Ba) we also observed their concentration leveling (fig.1c) but segregation coefficients were nearly the same as for the conventional CZ grown crystals.

Effect of vibrational intensity ($I=A\times f^2$) on vibrone and optical characteristics, microhardness, dislocation density of AVC-CZ $LiNO_3$-$NaNO_3$single crystals was studied. In case of AVC-CZ crystals we observed a decrease of dislocation density up to single values, an increase of microhardness up to 10 rel.% (fig.2), an increase of optical transmission up to 10 rel.% (fig. 3).

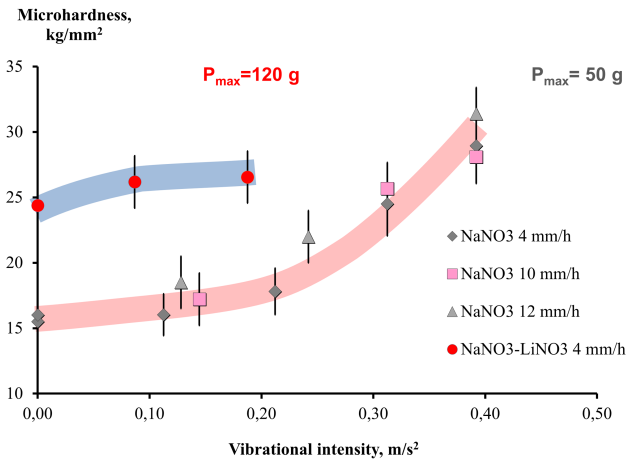

Fig.2 Microhardness *vs* vibrational intensity of AVC-CZ grown $(LiNO_3)_{0,01}$ $(NaNO_3)_{0,99}$ crystals

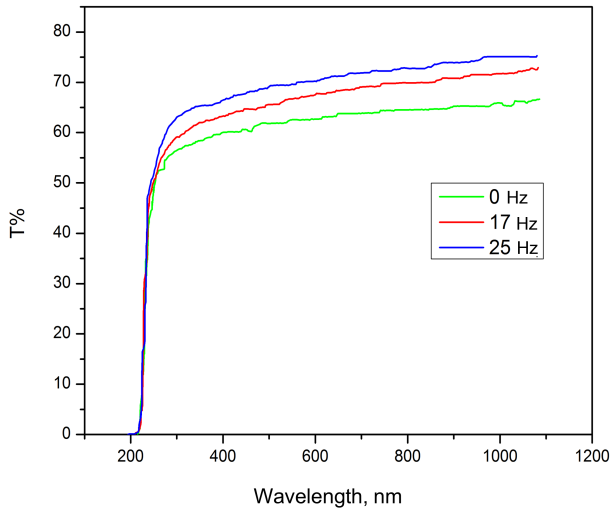

Fig. 3. Transmission of AVC-CZ $(LiNO_3)_{0,01}(NaNO_3)_{0,99}$ crystals grown at different frequencies and 0.3 mm amplitude

We also observed an oscillation leveling of different vibron modes analyzed from Raman spectra, which indicated on a decrease of structure defects in crystal.

Vibrational frequency, Hz	ν_1=726.1 cm^{-1}		ν_2=1068.7 cm^{-1}		Ratio	
	$FWHM_1$	**I_1**	**$FWHM_2$**	**I_2**	**$FWHM_2/FWHM_1$**	**I_2/I_1**
0	8.383	505	6.910	4931	0.824	9.764
17	8.931	360	7.077	3468	0.792	9.633
25	9.415	265	6.985	2027	0.742	7.649

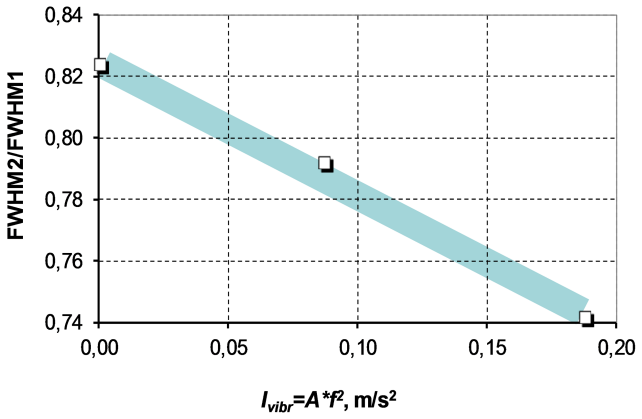

Fig.4. Ratio of $FWHM_2/FWHM_1$ of different vibron modes *vs* vibrational intensity of AVC-CZ grown $(LiNO_3)_{0,01}(NaNO_3)_{0,99}$ crystals

The research was financially supported by Ministry of Education and Science of Russia by grant N 16.552.11.7046

[1] E.V. Zharikov In Crystal Growth Technology. Semiconductors and Dielectrics
(eds P. Capper and P. Rudolph), Wiley-VCH Verlag, Weinheim, 2010, 41-64
[2] Avetisov I. Kh., Mel'kov A. Yu., Zinov'ev A. Yu., Zharikov E. V. Crystallography Reports. 2005. V. 50. Suppl. 1. P. 124-129.
[3] I. Ch. Avetissov, A.P. Sadovskiy, E.A. Sukhanova, G.Yu. Orlova, I.A. Belogorokhov, E.V. Zharikov J. Cryst. Growth, 2012, 360, 167

16:00 Poster We210

Optimization of vibrating baffle configuration at AVC-CZ crystal growth

Igor C. Avetissov[1], Andrey P. Sadovskiy[2], Stanislav Belov[1], Chan Kong Khan[1], Ekaterina Sukhanova[1], Evgeny V. Zharikov[1]

1. *D.I.Mendeleyev University of Chemical Technology of Russia (MUCTR), Miusskaya sq. 9, Moscow 125047, Russian Federation*
2. *NTO IRE-Polus (IPG), pl. Academika B.A. Vvedenskogo, 1, bld. 3, Fryazino 141190, Russian Federation*

e-mail: igor_avetisov@mail.ru

Axial vibrational control (AVC) is a powerful method to govern the heat and mass transfer and growth kinetics during crystallization from liquid phase [1]. It is realized by low-frequency oscillation of inert baffle submerged into melt. The investigations of AVC efficacy technique were carried out using $NaNO_3$ as a model transparent low melting substance. The AVC-Bridgman and AVC-CZ grown crystals had low dislocation density [2] and high structure perfection [3]. In all experiments the oscillating baffle was made in form of a cylindrical disk with sharp edges. The optimal relation between disk thickness and edge rounding was found out [3].

For many practically important materials (e.g. laser materials) the CZ growth process is conducted in Pt or Ir crucible. In case of AVC technique application to these processes the oscillating disk could be not easy and expensive. We studied the problem of optimization of oscillating baffle configuration in AVC process with the emphasis on

- construction mass,
- intensity and direction of produced vibrating flows,
- construction rigidity,
- possibility of baffle production from Pt (Ir, etc.) with assigned allowance.

In the research we combined numerical and physical modeling for disk optimization. The details of numerical modeling using FULENT software is described in [3]

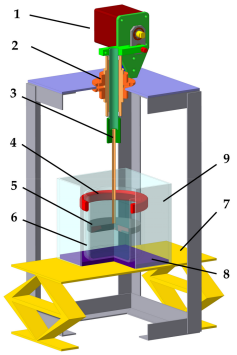

Fig. 1. Scheme and 3D model of physical modeling setup. 1- low-frequency generator (commutatorless motor FL86BLS98 with control unit 48ZWSK with eccentric) 2 – damping system; 3 – axis with a muff; 4 – upper heater; 5 – oscillating baffle; 6 – crucible with water-glycertol solution; 7 – vertical translating mechanism; 8 – bottom cooler; 9 – transparent vessel with flat walls

The setup for physical modeling of AVC process in shown on Fig. 1. To analyze the heat-mass transfer process at AVC action we used water–glycerol solutions with different viscosity (1–400 cPz). Cylindrical container made from quartz glass was used as a model crucible. To avoid cylindical distorsions the square rounded external vessel from glass was used. The vessel volume was filled with distilled water. A temperature gradient along the model crucible was organized by heating the upper part of the quartz glass by means of hot water, which was circulated on silicon hose.

Structure and velocity of convective flows were recorded by digital camcoder Panasonic NV-GS 400 and digital camera Canon EOS350D. The "light knife" was produced by diode laser S-11 (λ= 532 nm) with a plane 3 mm thickness beam. To visualize melt flows a fixed amount of polymer particles Pliolite VTLTM (1.01 g/cm^3 density, 10-100 micron diameter) was put into the melt.

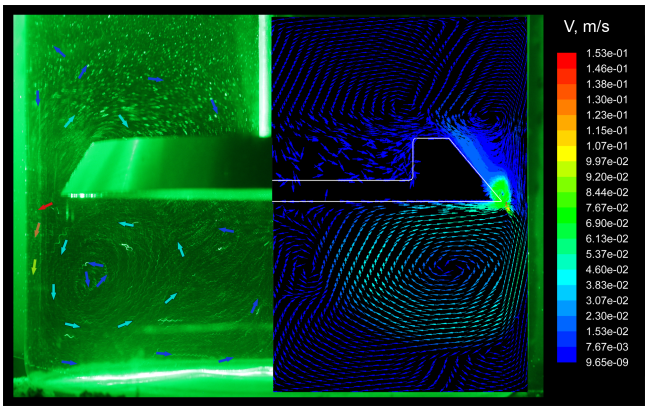

Fig. 2. Experimental (left) and calculated (right) mean velocity magnitude (m/s) of flows in water-glycerol solution at the disk oscillating with 0.3 mm amplitude and 20 Hz frequency

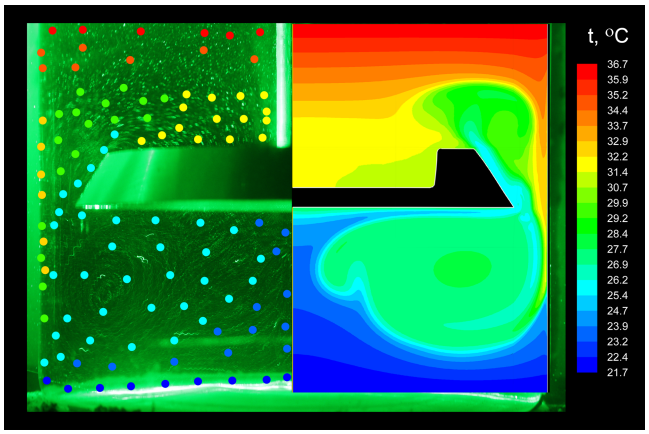

Fig. 3. Experimental (left) and calculated (right) map of static temperature (°C) in water-glycerol solution at the disk oscillating with 0.3 mm amplitude and 20 Hz frequency.

Comparison of numerical simulation with physical modeling results (Fig.2,3) showed that we produced an adequate model of the AVC process.

Modeling of different disk configurations with varying of generatrix slashing, baffle thickness, chasing dimension allowed to produce an optimal baffle configuration, which met the requirements. Taking into account the symmetry of CZ configuration we produced the baffle shown on Fig.4.

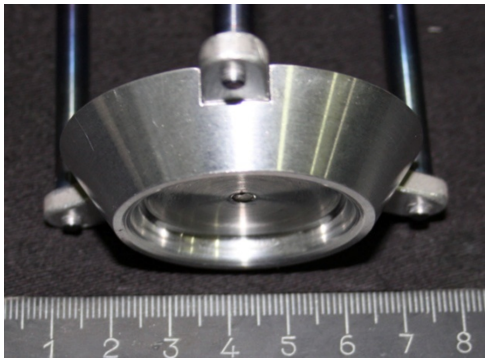

Fig.4. Aluminum vibrating baffle for AVC-CZ $NaNO_3$ crystal growth with decreased mass and vertical support rods for $NaNO_3$ crystal growth.

We succeeded to reduce the baffle mass in 3 times keeping the vibrational flow intensity the same as for the initial cylindrical disk [3].Using the optimized baffle for AVC-CZ growth of $NaNO_3$ crystal from 100 mm diameter crucible showed the high crystal perfection according to rocking curves measurements. Analyzing dislocation density, we failed to detect any etch pits in AVC-CZ grown crystals.

1. E.V. Zharikov Advanced Technologies of Crystal Growth from Melt Using Vibrational Influence. In: “Crystal Growth Technology. Semiconductors and Dielectrics”. Ed. by P. Capper and P. Rudolph. WILEY-VCH Verlag, Weinheim, 2010, 41-64

2. 2.I.Ch. Avetissov, A.P. Sadovskii, E.A. Sukhanova, E.V. Zharikov, A.I. Belogorokhov, B.N. Levonovich Czochralski crystal growth assisted by axial vibrational control technique. Journal of Crystal Growth **312** (2010) 1104–1108

3. I.Ch. Avetissov, A.P. Sadovskiy, E.A. Sukhanova, G.Yu. Orlova, I.A. Belogorokhov, E.V. Zharikov Perfection of $NaNO_3$ single crystals grown by axial vibrational control technique in Czochralski configuration. Journal of Crystal Growth **360** (2012) 167–171

16:00 Poster We211

Directional solidification of Silicon under the influence of traveling magnetic field

Mircea Cablea, Kader Zaidat, Annie Gagnoud, Abdallah Nouri, Yves Delannoy

Science et ingénierie des matériaux et des procédés, Elaboration par Procédés Magnétiques (SIMAP-EPM), 1130 rue de la Piscine, Grenoble 38402, France

e-mail: mircea.cablea@simap.grenoble-inp.fr

Silicon is the most widely used semiconductor for photovoltaic solar cells, and also the most extensively studied. The need for cost reduction lead solar cell producers to look for cheaper raw silicon, allowing a higher impurity content in the charge used as input for crystallization and making it very different from the extensively studied electronic-grade silicon. In order to keep a good efficiency of the solar cells, the impurities that have a huge impact over the electrical properties of the material should be removed from the final ingot. Controlling the segregation of impurities during the solidification is therefore mandatory. A study of the solidification of metallurgical grade silicon under controlled solidification parameters such as growth rate, thermal gradient and forced convection flow was conducted in a Bridgman set-up. Forced convection was induced by a travelling magnetic field (TMF) during the solidification, and resulted in a mixing of excess impurities in the liquid, removing them from the vicinity of the solidification front. As a result the purity of the final ingot is increased. The impact of the forced convection on the segregation of metallic impurities and on the orientation of grain boundaries during the silicon solidification is presented in this paper.

16:00 Poster We212

Numerical Simulation of Oxygen Transport during the Czochralski Silicon Crystal Growth with a Cusp Magnetic Field

Jyh-Chen Chen[1], Wen-Chung Guo[1], Ching-Hsin Chang[1], Ying-Yang Teng[2], Chuck Hsu[3]

1. *National Central Univercity, Department of Mechanical Engineering, Taoyuan 32001, Taiwan* **2.** *Chung Shan Institute of Science and Technology, Taoyuan 32546, Taiwan* **3.** *Sino-American Silicon Products Inc., Hsinchu 30075, Taiwan*

e-mail: jcchen@ncu.edu.tw

The numerical simulation has been performed to investigate the effect of a cusp magnetic field on the melt flow, thermal field and oxygen concentration during the Czochralski silicon crystal growth. The results show that the oxygen concentration is decreased by the size reduction of the secondary flow cell formed between the Taylor–Proudman vortex and the buoyancy-driven one. The size of the secondary flow cell is significantly reduced when the magnetic field is applied. Therefore, the oxygen concentration along the melt-crystal surface decreases significantly for higher strength of magnetic field. The oxygen concentration is very sensitive to the crucible rotation. There is an optimum combination of crucible and crystal rotation for obtaining the lowest oxygen concentration. The oxygen concentration is higher for lower argon flow rate. The oxygen concentration decreases as zero-Gauss plane (ZGP) is moved from the free surface towards crucible bottom. The secondary flow cell gets bigger when

the ZGP is far from the free surface. Therefore, there is an optimum position of the ZGP for getting the lowest the oxygen concentration.

16:00 Poster We213

Three-dimensional numerical simulation of flow, thermal and oxygen distributions for a Czochralski silicon growth with in a transverse magnetic field

Jyh-Chen Chen[1], Ying-Yang Teng[2], Pei-Yi Chiang[1], Chun-Hung Chen[1], Ching-Hsin Chang[1], Chien-Cheng Liu[3]

1. *National Central Univercity, Department of Mechanical Engineering, Taoyuan 32001, Taiwan* **2.** *Chung Shan Institute of Science and Technology, Taoyuan 32546, Taiwan* **3.** *Sino-American Silicon Products Inc., Hsinchu 30075, Taiwan*

e-mail: jcchen@ncu.edu.tw

A three-dimensional numerical simulation has been performed to understand the motion of the melt flow during the Czochralski silicon single crystal growth process under the influence of a transverse magnetic field. With the application of a transverse magnetic, the velocity, temperature and oxygen distributions in the melt become three-dimensional and asymmetric. A stronger spiral vortex motion is formed under the crystal-melt interface. The temperature is higher at the crucible wall due to the stronger downward flow motion near the crucible center and the weaker flow motion near the sidewall. This increases the dissolution rate of oxygen from the quartz crucible. However, the stronger spiral motion can prevent the transfer of oxygen impurities towards the crystal-melt interface. This may explain why the presence of a transverse magnetic field decreases the incorporation of oxygen. The effect of crucible rotation on the oxygen concentration and distribution is investigated. In the transverse magnetic field, the results show that the oxygen concentration decrease with the crucible rotation rate decreased. For larger size of the silicon crystal, the results also display this tendency.

16:00 Poster We214

Detached Growth: Unfolding the four decades growth mystery in vertical directional solidification technique on Earth

Dattatray Gadkari

Mithibai College (MITHI), Vile-Parle, Mumbai 400056, India

e-mail: dr_gadkari@yahoo.com

Modeling of detachment of the bulk crystal growth and its mechanism to achieve it on terrestrial laboratory is recommended. Experimental evidence of the repeatable detached growth of entire crystal and perfection in physical properties is yet mystery!

Since 1993, the goal of research was to determine the influence of favorable operating conditions to achieve detached solidification. The vertical directional solidification (VDS) technique has shown experimental evidences as bulk crystal growth process for the entire detached growth of InSb/GaSb ingot grown- without seed, without wall contact, without coating and without external pressure in our laboratory. A furnace was constructed with the temperature increasing with height for the transport of dissolved gases into the gap. The ends of the ampoule were sealed and it was added factors favoring detachment with a high Young's contact angle and a low gas-melt surface tension. The detached growth and apparition of the gap perform spontaneous tricks to the entire ingots by the self detached growth and self pressure difference. The sufficient growth parameters and conditions necessary such as ampoule cone geometry, filled argon pressure, self stabilization pressure difference across the meniscus, concave interface shape of the melt, Young's thermal contact angle, thin oxide layer, capillarity effect, thermal field, thermocapillary effect. In VDS, 80% ingots slide out easily, 15% ingots entrapped in conical region, and 5% ingots attached to wall of ampoule. Three types of detached growth are investigated, gap constant, gap increases, and gap decreases. Experimental statistical analysis showed that it is repeatable and reproducible growth. Unfortunately, none of the models cited concur with the correlation to VDS published experimental results.

On the basis of our experimental analysis and qualitative knowledge, detached growth is predicted in VDS and it shows significant enhancement into the crystalline quality. The meniscus conversion from concave to convex and concave crystal-melt interface shape is predicted from the strong evidence of the analysis of experimental results. It is predicted that plane or slightly concave meniscus shapes and concave interface shape are shown largest crystalline quality, and it is highest for the crystal grown ever. Statistics of experimental measurement for the detached growth, its mystery of the four decades reveal in VDS grown ingots. Physics behind detached growth is discussed on the basis of "A steady and stable meniscus and interface model. Its qualitative physical model is proposed on the basis of the experimental statistics as "A new crystal growth process".

16:00 Poster We215

Calcite nucleation in microgravity of a sounding rocket experiment

Arnold Gucsik[1], Katsuo Tsukamoto[1], Seiji Kosumi[1], Yuki Kimura[1], Yuko Inatomi[2], Takashi Itoh[3]

1. *Earth and Planetary Science, Department of Science, Tohoku University, Sendai 984-0065, Japan* **2.** *Japan Aerospace Exploration Agency (JAXA), 3-1-1 Yoshinodai, Chuo-ku, Sagamihara, Tokyo 252-5210, Japan* **3.** *Tohoku University, Sendai, Japan*

e-mail: argu1986@hotmail.com

Here, we present preliminary results of impedance and light scattering investigations of $CaCO_3$ crystallization under a sounding rocket experiment. In addition, we discuss phase transition of crystalline and amorphous states of calcium carbonates after homogeneous nucleation by ground-based Macro-Raman spectroscopical measurements.

Compared to ground-based data obtained, rapid crystallization (around 2 sec induction) occurs at a relatively high concentration of 5 mM solution of the rocket experiment, which might be due to a presence of a bubble within the solution at high G conditions. Other cells (at medium or low concentrations) show relatively long induction time such as: 3 mM-132 sec, 3.8 mM-49 sec, 4 mM-23 sec and 4.5 mM-14 sec.

In the medium spectral range, there are two typical carbonate-related Raman bands, which centered at around 1085 cm^{-1} (CO_3-bending in calcite) (Urmos et al., 1991) and 1650 cm^{-1} (H_2O-bending). H_2O-related antisymmetric and symmetric stretching vibrational modes at 3250 and 3450 cm^{-1} are dominant (Tlili et al., 2001). An additional peak appears at around 540 cm^{-1} (in most cases at 544 cm^{-1}) at 2, 3.6, 4.5 and 50 mM, however, this peak is an absent one from 4 and 5 mM solutions, which may be related to the lattice H_2O libration or translation in the hexahydrate carbonate ($CaCO_3xH_2O$) (Gauldie et al., 1997).

Consequently, high concentrations show rapid crystallization under the microgravity conditions, whereas medium or low concentrations represent relatively slow processes as same as under the gravity. Macro-Raman spectral investigations were not conclusive in terms of the

phase determination, however, further systematic analyses must be done.

References

Gauldie, W.R., Sharma, K.S. and Volk, E. (1997) Comp.Biochem.Physiol. 118A, 753-757

Tlili, M.M., Ben Amor, M., Gabrielli, C., Joiret, S., Maurin, G. and Rousseau, P. (2001) J. Raman Spectroscopy 33, 10-16.

Urmos, J., Sharma, S.K., Mackenzie, F.T. (1991) American Mineralogist 76, 641-646.

16:00 Poster We216

Behaviour of Particle Depots in Molten Silicon Under Terrestrial And Microgravity Conditions

Thomas Jauß[1], Arne Croell[1], Tina Sorgenfrei[1], Maral Azizi[2], Christian Reimann[2], Jochen Friedrich[2], Henning Hoerstermann[3], Julia Kundin[3], Juliane Böhm[3], Heike Emmerich[3]

1. *Kristallographie, Universität Freiburg (KI), Hermann-Herder-Str. 5, Freiburg 79104, Germany* **2.** *Fraunhofer Institut IISB, Schottkystr. 10, Erlangen 91058, Germany* **3.** *Universität Bayreuth, Universitätsstr. 30, Bayreuth 95440, Germany*

e-mail: thomas.jauss@fmf.uni-freiburg.de

Multi crystalline solar cells made of silicon provide the largest market share in the photovoltaics industry. The silicon for these cells is grown by directional solidification. During the growth process, carbon monoxide from the furnace atmosphere and silicon nitride from the crucible coating are dissolved by the silicon melt in addition to the carbon already present in the silicon feedstock. At later stages of the growth the melt supersaturates with respect to carbon and nitrogen, so SiC and Si_3N_4 particles are precipitated. These particles can grow up to several hundred micrometers in diameter and lead to severe problems during the wire sawing process for wafering the ingots. Furthermore particles may act as nucleation sources for silicon grains, leading to a grit structure of small grains, or act as sources for dislocations. If the SiC is doped with nitrogen from the dissolved crucible coating, it becomes semiconducting and may act as a shunt, short circuiting parts of the solar cell. For these reasons, the incorporation of such particles needs to be avoided.

Under terrestrial conditions, the transport of particles in the melt is dominated by convection and gravitational sedimentation. During the TEXUS 51 sounding rocket mission (April 2013), a silicon crystal of 8mm diameter, with an oxide layer of approximately 5µm thickness on the surface to eliminate Marangoni convection, will be processed. Microgravity provides a purely diffusion dominated regime for the crystal growth, as shown in an older experiment on TEXUS 12, which offers the opportunity to investigate particle transport and incorporation only as a function of growth rate and particle size to serve as a baseline for ground –based processes. For a better understanding of particle behavior during the growth of solar silicon, SiC particles of variable size and shape are placed in single crystal silicon rods. This is achieved by drilling a hole of 2mm diameter, filling in the particles and closing the hole by melting the surface of the rod until a film of silicon covers the hole. The samples are processed under a vacuum of $1*10^{-5}$ mbar or better, to prevent gas inclusions. On the ground, during the float-zone growth the particles are expected to distribute in the melt, due to thermal convection. In dependence of the growth rate, particles of a given size should be incorporated or pushed by the solid-liquid-interface. Experiments have shown that in contrast to the expectations the particles stay agglomerated in the cylindrical shape of the former depot. Furthermore these depots sink to the lower phase boundary and are incorporated at the interface for particle sizes of 60µm and larger, but get pushed along in the case of a particle size of 7µm, despite the fact that the mass is roughly the same. Pötschke [1] observed that particles in the melt coagulate if convection is present, and depending on their density, they sink or float in the melt. Despite the general idea given by this observation it is unclear why the depots behave differently if the only significant difference is the size of the particles forming them. However, further experiments have shown that either slow growth rates of 0.2mm/min or the application of a rotating magnetic field lead to the desired distribution of the particles and the depots were scattered.

[1] Pötschke, J.: Metall-Oxydispersion, TEXUS 1-10 Abschlussbericht, S.59-61

16:00 Poster We217

Simulation of ultrasound influence on melt convection for the growth of striation-free $Ga_xIn_{1-x}Sb$ and Si single crystals by the Czochralski method

Gennadiy N. Kozhemyakin, Ludmila V. Nemets, Ann Bulankina

Volodymyr Dahl East Ukrainian National University, Luhansk 91050, Ukraine

e-mail: genakozhemyakin@mail.ru

It has been shown previously that the presence of ultrasound parallel to the pulling axis in the melt decreased growth striations in semiconductor single crystals grown by the Czochralski method. The effect of ultrasound on striations, which decrease in number and disappear in the central part of InSb, GaAs, Bi_xSb_{1-x} and $Ga_xIn_{1-x}Sb$ solid solutions pulled single crystals, was studied and reported in several publications of our group [1-4]. We showed experimentally that ultrasonic waves at frequencies from 0.15 to 5 MHz can be used for damping of convection in the melt during crystal growth. The damping of convection is attributed to forming of ultrasonic standing waves under the sold-liquid (S/L) interface. However, the behavior of convective flow under the effect of ultrasound was not studied.

In the present study, we modeled convection at the growth conditions of small $Ga_xIn_{1-x}Sb$ and large Si single crystals. The flow simulation for $Ga_xIn_{1-x}Sb$ and Si melts was conducted for quasi-steady conditions, when Raleigh number was less than 10^5. For these conditions applied to $Ga_{0.03}In_{0.97}Sb$ and Si single crystals, the growth parameters have the values listed in Table 1.

Table 1. Parameters of the growth crystals

Variable	Symbol	Crystal	
		$Ga_{0.03}In_{0.97}Sb$	Si
Crystal radius, mm	r	5	75
Crucible radius, mm	R_c	15	150
Melt height, mm	h	23	40
Crystal rotation rate, rpm	Ω	1 – 20	5 – 10
Maximum velocity of flow, cm/s	V	0.047–0.9	12.6 – 28
Particle radius, nm	r_p	5	5
Particle mass, kg	P_p	3×10^{-21}	$1{,}3\times10^{-21}$

To formulate the mixed convection problem these melts, a viscous incompressible flow in a cylindrical crucible was considered. The growing crystals were pulled very slowly from the center of the stationary crucible, and the vertical motion of the crystals was assumed to be

negligible. The temperature of crucible walls and bottom surfaces was fixed at a constant value. The Navier-Stokes equation was used for the calculations of convective flow velocity in $Ga_xIn_{1-x}Sb$ and silicon melts for quasi-steady conditions. The flow was assumed to remain laminar and incompressible, with constant fluid properties.

The radial and axial distributions of flow in $Ga_xIn_{1-x}Sb$ and silicon melts were calculated. The radial velocity distribution of flow increases from the center to $R_c/2$ in both crucibles, and then decreases. The maximum velocity of axial flow was under the S/L interface at the axis of the crucibles. However, summary values of the radial and axial flow velocities had maximum values under the S/L interface near periphery of the crystals. The maximum velocities were 0.9 cm/s and 28 cm/s for $Ga_xIn_{1-x}Sb$ and silicon melts, respectively.

The maximum calculated flow velocity was used for the calculation of the force F_c acting on Si particles in the melt. Particles of 5 nm radius and different mass for these melts were accepted for our calculations. Then, the maximal force F_C acting on the particle in convective flow was $3\cdot10^{-21}$ N and $1.2\cdot10^{-21}$ N for $Ga_xIn_{1-x}Sb$ and Si melts, respectively.

It is established that introduction of ultrasound into the liquid forms a standing wave channel under the S/L interface. The force F_{US} acting on the melt particle in ultrasonic standing waves was calculated according to the equation in [4]. The ultrasonic field parameters for a given system were selected at frequencies of 0.1 – 4.0 MHz. The force F_{US} increases with increase of the frequency in $Ga_xIn_{1-x}Sb$ and Si melts from $1\cdot10^{-20}$ N to $7\cdot10^{-19}$ N and $6.3\cdot10^{-23}$ N to 4.0×10^{-18} N, respectively.

The results of these calculations have shown that the ultrasound at frequencies over 0.1 MHz can be used for reduction of striations in pulled $Ga_xIn_{1-x}Sb$ single crystals, since the force F_{US} is larger than the convective force F_C by a factor of 3 – 600 in this melt. However, for striation-free Si single crystals, the ultrasound frequencies must be larger than 0.5 MHz, according to our calculations.

Therefore, we believe that ultrasound at a high frequency can be used for reduction of convection in Czochralski growth of $Ga_xIn_{1-x}Sb$ solid solutions and Si single crystals. The strong reduction of flow motion is associated with the formation of a standing wave channel between the S/L interface and the crucible bottom. This modeling has shown the potential of using ultrasound to damp convection in the melt and decrease striations in semiconductor single crystals.

References

[1] G.N. Kozhemyakin,V.G. Kosushkin, S.Y. Kurochkin, J. Crystal Growth. **121**, 240 (1992).

[2] G.N. Kozhemyakin,L.G. Kolodyazhnaya, J. Crystal Growth. **147**, 200 (1995).

[3] G.N. Kozhemyakin, J. Crystal Growth. **149**, 266 (1995).

[4] G.N. Kozhemyakin, J. Crystal Growth. **257**, 237 (2003).

16:00 Poster We218

Energy efficiency and adaptability of the AVC technique

Andrey P. Sadovskiy

Armoled Ltd., 9 Miusskaya square, Moscow 125047, Russian Federation

e-mail: sapruss@gmail.com

The development of equipment and technology of crystal growth is traditionally based on the new ways of producing pure mixtures and on improving the growth equipment. The technology of crystal growth is the complex multi-parametric process. Experts point out ten or more growth parameters should be adjusted for the successful crystal growth setup. It is generally agreed today that control and stabilization of heat and mass transfer processes in liquid have a primary influence on the quality and properties of the grown crystals [1]. Attempts to control heat and mass transfer in liquid take place regularly. Some positive results have been achieved. Usually, heat and mass transfer control is carried out by applying some additional external force to the growth system.

Additional forces are applied to accelerate the crystalgrowth and to growth crystals with some unique properties. Number of additional forces continuously increases mainly due to the symbiosis of various fields techniques actions: submerged inert body [2, 3]; RMF, PMF, TMF [4-8]; electromagnetic field [9, 10]; centrifugal force [11, 12];additional heater [3, 13, 14, 15]; different vibration effects: ACRT (AVT) [16- 21], CVS [22, 23], ultrasound [24- 27], LFV [28, 29] and etc.

One cannot deny that the vibration effects is the most energy efficient of additional external force to the growth system.

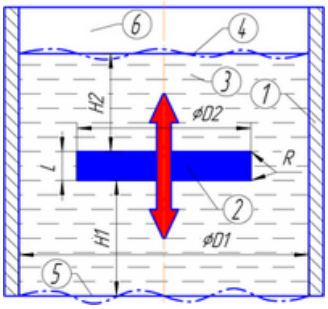

Fig. 1. The AVC technique scheme:1 –crucible wall, 2 – vibrating inert baffle, 3 – liquid, 4 - liquid- gas interface, 5 - solid-liquid interface, 6 – gas or liquid with density lower than 3, ∅D1 - inner diameter of the ampoule/crucible, ∅D2 - baffle diameter, L – baffle height, R - curvature radius of the baffle's edges of the baffle, H1 – distance between the baffle and liquid-gas interface, H2 – distance between the baffle and liquid-solid interfaces.

The AVC technique [30] in general is: axial low-frequency harmonic oscillation of an inert baffle submerged into liquid (melt) at a fixed distance from the solid-liquid and / or liquid-gas interface [31, 36] (fig. 1). AVC is the additional external action force in liquid (melt) during the crystal growth set up. The first thing that needs to be said is very high efficiency of energy transfer coefficient by AVC. Electricity consumption at AVC technique application does not exceed 100 watts per 1.5 liter melt.

AVC technique, like many others methods of influence on liquid during manufacturing operations, finds its application in other areas, such as metallurgy [34, 35]. Low-frequency vibrations after some adaptation demonstrate the possibility to achieve unique properties of steel alloys. Unfortunately, metallurgists do not explain observed phenomena.

It should be also pointed out that there is an adequate thermodynamic efficiency explanation of AVC technique for crystal growth application [31]. It has been experimentally proved that AVC technique efficacy is based on melt structure transformation (change the component composition) in liquid (melt). The AVC technique results in increase of crystal growth rate [36], a decrease of dislocation density [37], an enhancement of crystal perfection [30, 37].

The AVC technique has a very good possibility (to be scaled and applied) for scaling and relevance to many crystal growth configurations (fig. 2).

The arguments we have presented indicate that AVC technique is a very promising method both for crystal growth equipment modernization and research area.

The research was supported by Ministry of Education and Science of Russia by grant N 16.552.11.7046.

1. V. R. Ren'yan, Technology of Semiconductor Silicon [in Russian], Moscow (1969).
2. Brandle C.D. et al. J. Cryst. Growth 400, V.42 (1977).
3. Haisheng Fang et al. Crystal Growth & Design 1840, Vol. 8., No. 6., (2008).
4. Von Ammon W. Proc. Joint 15th Riga and 6th Pamir intern. conf. Fundamental and applied MHD, Riga, Jurmala, Latvia, June 27 – July 1. 2005., pp. 41-54.
5. Dold P. Progr. Crystal. Growth Charac. Mater. 39, Vol. 38., Issue 1-4., (1999).
6. Feonychev A. I. et al. J. Eng. Physics and Thermophysics. 731, Vol. 77., No. 4., (2004).
7. Willers B. et al. Metallurgical and Materials Transactions B. 304, v. 39b., (2008).
8. Rudolph P. J. Cryst. Growth. 1298, Vol. 310., Is 7-9., (2008).
9. Nassau K. et al. J. Phys. Chem. Solids. 989, Vol. 27., Is. 6-7., (1966).
10. Budevski E. Electrochim. Acta. 2559, Vol. 45., Is. 15-16., (2000).
11. Rodot H. J. Cryst. Growth. 77, Vol. 79., Is 1-3., (1986).
12. Friedrich J. J. Cryst. Growth. 45, Vol. 167., Is 1-2, (1996).
13. Ostrogorsky A.G. et al. J. Crystal Growth. 950,. V.110. (1991).
14. Gonik M. A. et al. Inorganic Materials. 1263, V. 43., N. 11., (2007).
15. Ostrogorsky A.G. J. Crystal Growth. 64, V. 137., (1994).
16. Scheel H.J. et al. J. Cryst. Growth. 304, Vol. 8., Is. 3., (1971).
17. Scheel H.J. et al. WILEY-VCH Verlag GmbH & Co. KGaA, Weinheim 505, (2008).
18. Kobayashi N. et al. J.Cryst Growth. 419, Vol. 49., N. 3., (1980).
19. Turner C.E.,. et al. Journal of Crystal Growth 234, Vol. 35., Is. 2., (1976).
20. Horowitz A., et al. J. Crystal Growth 323, V.61., (1983).
21. Zhou J., et al. J. Crystal Growth 173, V. 128., Is. 1-4., (1993).
22. Kevin T. Zawilski et al. J. Crystal Growth 236, Vol. 282., (2005).
23. Kevin T. Zawilski et al. 196., (2003).
24. Kozhemyakin G.N. et al. J. Crystal Growth 240, Vol. 121., Is. 1-2., (1992).
25. Kozhemyakin G.N. et al. J. Crystal Growth 237, Vol. 257., Is. 3-4., (2003).
26. Kozhemyakin G.N. et al. J. Crystal Growth 1466, Vol. 311., Is. 6., (2009).
27. Kozhemyakin G.N. et al. Crystallography Reports 318, Vol. 49., №2, (2004).
28. Zhang Y. et al. J. Crystal Growth 5432, Vol. 310., (2008).
29. Zhang Y. et al. Cryst. Res. Technol. 248, Vol. 44., No. 3., (2009).
30. I. Avetissov et al. Doklady Physics, 54, N. 9, 410, (2009).
31. I. Avetissov et al. Materialy Elektonnoi Tekhniki 45, N1., (2012).
32. I. Avetissov et al. CrystEngComm 2213, 15, (2013).
33. I. Avetissov et al. J. Crystal Growth 1104, 312, (2010).
34. Y. Konsevoiy et al. Metallurgy 55, Vol. 10, (2007).
35. I. Ignatev et al.Melts 3, Vol. 5, (2010).
36. R.S. Feigelson NASA Final technical report for #NAG8-1457-06, (2002).
37. I. Avetissov et al. J. Crystal Growth 318, 979, (2011).

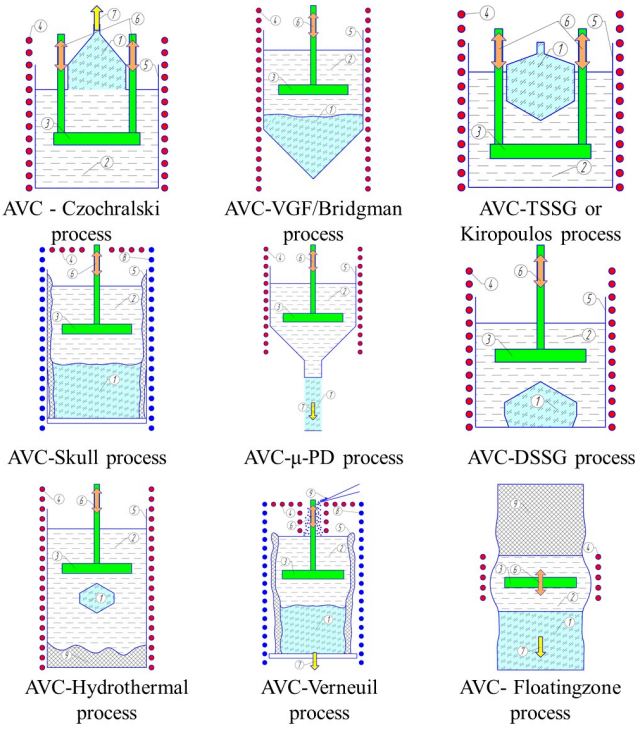

Fig. 2. AVC technique applications.

1 – monocrystal, 2 – melt/solution, 3 – disk, 4 – heater, 5 – crucible or skull, 6 – vibration direction, 7 – crystal growth transport direction, 8 – cooler, 9 – initial mixture.

16:00 Poster We219

Revision of one-dimensional analytical models of effective segregation coefficient and their application for recovering the crystal growth conditions of space grown GaSb:Te

Alexey E. Voloshin[1], Anatoly I. Prostomolotov[2], Nataliya A. Verezub[3], Tatau Nishinaga[4]

1. *A.V.Shubnikov Institute of Crystallography The Russian Academy of Sciences, Moscow, Russian Federation* **2.** *Institute for Problems in Mechanics of RAS (IPMECH), Vernadskogo prospect 101, bl. 1, Moscow 119526, Russian Federation* **3.** *Institute for Problems in Mechanics RAS (IPMECH), Vernadskii prospect 101, bl. 1, Moscow 119526, Russian Federation* **4.** *The University of Tokyo, Bunkyo-ku, Tokyo 113-8655, Japan*

e-mail: labsol@yandex.ru

The well known Burton-Prim-Slichter (BPS) [1] and Ostrogorsky-Muller (OM) [2] 1D analytical models describe in a simple form the dependence of impurity effective segregation coefficient on the crystal growth parameters such as crystal growth rate and melt convective velocity. By this reason they are frequently used for the estimation of actual conditions in realized space crystal growth experiments basing on the impurity concentration profile in the crystal sample. Unfortunately, their adequate trial still was not done. Therefore their validity is not completely clear.

A careful comparison of both BPS and OM models with the results of 2D numerical simulation carried out by means of widespread Ansys Fluent code [3] has been done in this work for Bridgman growth technique. A wide range of growth cell dimensions and physical parameters (diffusion coefficient, viscosity, crystal growth rate) was tested. For the calculations by BPS model the well known formula for

the diffusion layer thickness based on the "flat plate solution" was applied

$$\delta = 5(\nu L / V_\infty)^{1/2}(D/\nu)^{1/2} \quad (1)$$

Here ν is the melt kinematic viscosity, L is the characteristic interface size (growth cell diameter), V_∞ is the convective flow velocity beyond the boundary layer, D is the impurity diffusion coefficient in the liquid phase.

A correspondence between 1D and 2D models was analyzed in terms "mean impurity concentration Cmean" – "maximal Vmax (or mean Vmean) convective velocity". Both BPS and OM models show a good agreement with 2D calculations (Fig. 1): the misfit did not exceed several percents.

It was found that from above some cell dimension (L>1.5 cm in the case of material parameters indicated in Fig.1) the agreement is drastically decreases. 2D simulation shows that the melt flow becomes sufficiently two-dimensional and another formula for δ is required. The good result is obtained with

$$\delta = 8(\nu L D / V_\infty^2)^{1/3} \quad (2)$$

The criterion for application of eq. (1) or (2) is discussed.

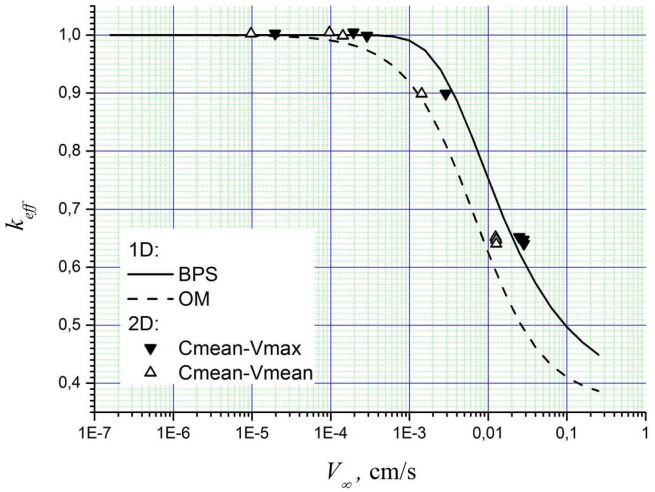

Fig.1 Comparison of 1D and 2D models for the parameters: L=0.6 cm, D=5*10^{-5} cm^2/s, ν=3.75*10^{-3} cm^2/s, k=0.37 (equilibrium segregation coefficient), R=3*10^{-4} cm/s (crystal growth rate).

Despite of the good agreement between 1D and 2D calculations, no one of BPS and OM steady state models allow to determine the crystal growth and convective rates simultaneously providing just R/V_∞ ratio. We show that study of initial transient regime is required. The expressions for initial transient regime were derived for both BPS and OM models. While C_0 is the impurity concentration in the melt beyond the boundary layer, the complete profile of its concentration in the crystal C_S is described as

$$C_S(x) = C_0(k_{eff} - (k_{eff} - k)e^{-\alpha x}), \quad \text{here}$$

$$k_{eff} = \frac{k}{k + (1-k)e^{-\Delta}}, \quad \Delta = \frac{R\delta}{D}, \quad \alpha = \frac{R}{D}\frac{k}{k_{eff}}\frac{1}{1-(1+\Delta)e^{-\Delta}} \quad \text{in BPS model}$$

$$k_{eff} = \frac{1+\eta}{1+\eta/k}, \quad \eta = \frac{V_\infty D}{R^2 L}(1-e^{-4.6D/\nu}), \quad \alpha = \frac{R}{D}\frac{k_0(1-k_0)}{(k_{eff}-k_0)} \quad \text{in OM model.}$$

The obtained results were applied to recovering the growth conditions of space grown GaSb:Te, the study of which was reported earlier in [4]. The crystal contains the areas grown by the atomically rough (rounded) interface as well as by the faceted one. The map of Te distribution obtained by quantitative X-ray topography was performed in [3]. It gives the data for recovering the growth conditions in the sample. We succeeded in estimating crystal growth and convective rates, axial and radial thermal gradients, facet supercooling. It was shown that the facet grew by spiral dislocation mechanism. It is demonstrated that even weak temperature variations (~0.1 K) could result in perceptible composition inhomogeneity.

The possible optimization of space growth conditions based on the carried out estimations is discussed.

The work is supported by the Russian Foundation for Basic Research (grant No. 12-02-01126).

[1] J. A. Burton, R. C. Prim, W. P. Slichter. J. Chem. Phys., 21 (1953) 1987-1991.

[2] A.G. Ostrogorsky, G. Muller. J. Cryst. Growth, 128 (1993) 207-212.

[3] Ansys CFD // Lisence of IPMECH RAS, No. 659778-23-Aug-2011.

[4] A.E. Voloshin, T. Nishinaga, P. Ge, C. Huo. J. Cryst. Growth, 234 (2002) 12–24.

16:00 Poster We220

The influence of melt flow on grain growth during ultrafast quenching from the melt

Olga Gusakova[1,2], Vasiliy Shepelevich[2]

1. *International Sakharov Environmental University (ISEU), 23 Dolgobrodskaya Street, Minsk 220070, Belarus* **2.** *Belarusian State University (BSU), F. Skaryna av. 4, Minsk 220050, Belarus*

e-mail: ol.gusakova@gmail.com

The classical methods to improve materials mechanical properties have already been well studied. Currently intense research work of the materials production in non-equilibrium solidification conditions is conducted. Strongly nonequilibrium crystallization conditions are implemented in such techniques as: melt spinning technique, ultrafast quenching from the melt; laser, ion-plasma, compression-plasma surface treatment. These techniques allow the purposeful influence on the functional material properties. In these processes, the cooling rate of the melt reached 10^4 ... 10^7 K/s. Solidification begins at deep undercooling and proceeds with a high liquid – solid interface velocity in the range 1 - 10 m /s [1]. In this case, the melt at the interface is not fixed and moves directly. Thus, at ultra-fast quenching melt velocity is comparable to the linear crystallizer velocity and is a few meters per second [2]. It is known that the viscosity of the melt decrease when its temperature increases, rising by fifteen orders from the melting point to the glass transition temperature. The directional movement of the viscous supercooled melt cause the shear stress on the surface of the solidified layer, lead to the material deformation and the microstrain arise in the grain volume i.e. strain hardening. In the present study were investigated grain structure of foils of tin and and its alloys, obtained by ultrafast quenching from the melt.

Foils were prepared by splashing of melt drops of mass 0.2-0.3 g on a polished inner surface of a rotating hollow copper cylinder (mold). Studies of the grain structure and texture of the foils were performed by the electron backscatter diffraction technique (EBSD), which was implemented using the phase analysis attachment «HKL CHANNEL 5» to the scanning electron microscope LEO 1455 VP.

It was obtained that grains size and shape varies along the foil length. equiaxial relatively small grains formed in the first part of the foil. In the central part of the foil the grains of two types are formed:

large grains elongated in the direction of foil spreading and fine equiaxed grains localized on the border of the large ones. The Fig. 1 shows the grain structure of the central part of the foil.

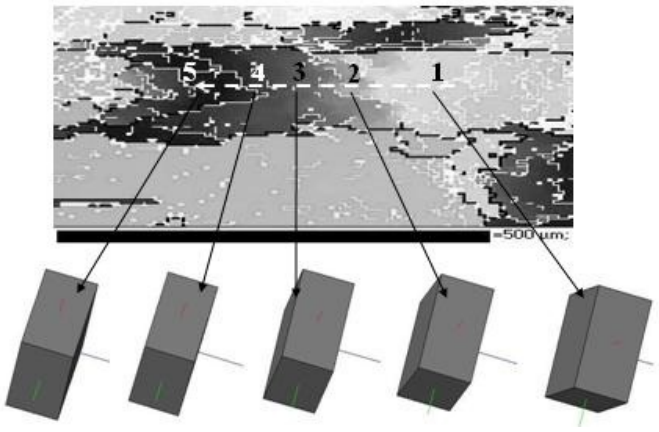

Fig. 1. The orientation changes in the B type grain

High-angle grain boundaries (the angle between the grains orientation of more than 10 degrees) outlined by black lines. Elongated grains are two types of coloration: uniform (grain type A) and non-uniform (grain type B). Uniform coloration of B type grains means that the crystal orientation is changed within the same grain. It was found that the A type grains grow in the case where the (100) plain parallel to the surface of the foil, and the axis C_4 parallel to the direction of foil spreading.The subgrain structure of large elongated grains depends on the nucleation center crystallographic orientation. If the nucleation center oriented so that the (100) plane parallel to the foil surface or rejected by a small angle and the C_4 axis deviated from to the spreading direction by any angle, the lattice orientation monotonically changes during the growth process. A sequence of low-angle boundaries (outlined by white lines) is revealed in the grains of type B by the EBSD technique. The lattice orientation change at the points 1, 2, 3, 4 and 5 of the B type grain showed at the Fig. 1. It was found that the crystal orientation changes in a way that it is "turn" around the C_4 axis. The C_4 axis deviates from the initial position so long until (110) plane becomes parallel to the foil surface.

It can be assumed that the reason for the change of the B type grains crystallographic orientation is the deformation of solidified material by the viscosity force of undercooled melt which moves above the crystallization front in the direction of the foil spreading. The easy slip systems of tin are (110) [111] and (110) [001] [3]. Therefore, if a grain is positioned so that the projection of the shear stress on the plane (110) has a component along the [111] and [001] directions, the crystal rotates until the sliding direction is parallel the foil spreading direction. Shear deformation is so long until the shear stress is not zero, that is, until the (110) plane is parallel to the melt flow direction.

References

1. S.L. Sobolev Effect of local equilibrium for high-speed binary alloy solidification. The Journal of Physical Chemistry. - 1998. - T 68, № 3. - P. 45-52.
2. I.S. Miroshnichenko Quenching from the liquid. - Moscow, Metallurgy, 1982. - 168 p.
3. Fuqian Yang, J. C. M. Li Deformation behavior of tin and some tin alloys. J Mater Sci: Mater Electron, 2007, V. 18, P. 191–210

Topical Session 9

Late news session

Session Coordinators

Zbigniew R. Zytkiewicz (Poland) *zytkie@ifpan.edu.pl*

Jochen Friedrich (Germany) *Jochen.Friedrich@iisb.fraunhofer.de*

Programme

Wednesday, 14 August

WeP-T09
Wednesday afternoon, 14 August, 16:00
Room 215, Old Library

Break
Wednesday afternoon, 14 August, 17:30

Posters

Wednesday, 14 August

WeP-T09
Wednesday afternoon, 14 August, 16:00
Room 215, Old Library

16:00 Poster We222

Temperature dependence of the electrical conductivity and Hall effect of thallium gallium disulphide single crystal

Sabah E. Algarni

King Abdulaziz University-Physics Department, Jeddah 23534, Saudi Arabia

e-mail: seef73@gmail.com

Single crystal of the layered compound $TlGaS_2$ were grown by direct synthesis of their constituents. Their electrical conductivity and Hall effect was studied as a function of the temperature, perpendicularly and parallel to the layer planes and it proved to be highly anisotropic. The Hall effect measurements revealed the extrinsic p-type conduction with an acceptor impurity level located at 0.586 eV for $\sigma_{\perp}$ and 0.43 eV for $\sigma_{//}$ above the valence band maximum. The variation of the Hall mobility as well as the carrier concentration with temperature was investigated. The scattering mechanism of the carrier in the whole temperature range of investigation was checked. The anisotropic factor was also estimated and its temperature dependence was illustrated.

16:00 Poster We223

Exploring the multiferroic property and structural stability in n-$LaFeO_3$, n-$SrTiO_3$- and n-$BiFeO_3$, -$Bi_4Ti_3O_{12}$ thin films with Aurivillius structure

Yanbin Chen

National Laboratory of Solid State Microstructures, Department of Physics, Nanjing University (NJU), Hankou Road 22#, Nanjing 210093, China

e-mail: ybchen@nju.edu.cn

Exploring single phase with ferroelectric and ferromagnetic/ferromagnetic properties simultaneously at ambient temperature is one of the key problems in the research of multiferroic materials. It is also a prerequisite for the study of coupling mechanism between ferroelectric and magnetic orderings. In this work, we explore the multiferroic property in n-$LaFeO_3$-$Bi_4Ti_3O_{12}$, n-$BiFeO_3$-$Bi_4Ti_3O_{12}$ thin films. The c-axis epitaxially 0.5-$LaFeO_3$-$Bi_4Ti_3O_{12}$, 1.0-$LaFeO_3$-$Bi_4Ti_3O_{12}$ and 1.5-$LaFeO_3$-$Bi_4Ti_3O_{12}$, 2.0-$LaFeO_3$-$Bi_4Ti_3O_{12}$ and 2.5-$LaFeO_3$-$Bi_4Ti_3O_{12}$ thin films were successfully synthesized by pulsed laser deposition. X-ray diffraction, atomic-force-microscopy and transmission-electron-microscopy (TEM) characterization substantiate that all of these films have good crystalline quality. The temperature-dependence of magnetization under zero-field and field-cooling conditions show that there is anti-ferromagnetic interaction in these films. But for 0.5-$LaFeO_3$ and 1.5-$LaFeO_3$-$Bi_4Ti_3O_{12}$, magnetic hysteresis loop measurement proves that these films do have *ferrimagnetic* property. Based on the crystal structure of n-$LaFeO_3$-$Bi_4Ti_3O_{12}$, the observed ferrimagnetic property is discussed qualitatively. At the same time, the ferroelectric hysteresis loop measurement proves that there is ferroelectric property along the c-axis at ambient temperature. Thus, these films (0.5-$LaFeO_3$-$Bi_4Ti_3O_{12}$ and 1.5-$LaFeO_3$-$Bi_4Ti_3O_{12}$) have multiferroic property at the ambient temperature. But in n-$BiFeO_3$-$Bi_4Ti_3O_{12}$ series, highly leakage current and quite weak magnetism are observed. By means of TEM, the structural stability of n-$LaFeO_3$, n-$BiFeO_3$ and n-$SrTiO_3$ were characterized. It shows that n being as high as 3, there is high intergrowth density in n-$SrTiO_3$-$Bi_4Ti_3O_{12}$, while n-$BiFeO_3$-$Bi_4Ti_3O_{12}$ still keeps intact structure. Structure of n-$LaFeO_3$-$Bi_4Ti_3O_{12}$ is the most un-stable, it has collapsed Aurivillius structure when n is equal to 2.5. The feature of structure stability can be captured by the first principle calculations. This work provides a novel material system for exploring the devices based on multiferroic materials and studying the coupling mechanism between ferroelectric and ferromagnetic orderings.

16:00 Poster We224

Directionally solidified $MnTiO_3$ –TiO_2 eutectic as a potential material for photoelectrochemistry

Katarzyna B. Kołodziejak[1], Piotr Barczuk[3], Bruce Alexander[2], Dorota A. Pawlak[1]

1. *Institute of Electronic Materials Technology (ITME), Wólczyńska 133, Warszawa 01-919, Poland* **2.** *University of Greenwitch, School of Science, Central Avenue, Kent ME4 4TB, United Kingdom* **3.** *University of Warsaw, Department of Chemistry, Pasteura 1, Warsaw, Warszawa 02-093, Poland*

e-mail: katarzyna.kolodziejak@itme.edu.pl

Eutectic materials are two or multiphase materials formed during cooling of a mixable melt with a eutectic composition. The possibility of considering versatile combinations of various component materials

in eutectics provides a broad palette for many applications.[1],[2],[3] Eutectics also seem to be very attractive as energy-generating materials. This possible application of eutectics has been preliminarily studied, including solid-oxide fuel cells[4],[5],[6], thermoelectric materials[7],[8], and recently photoelectrochemical cells (using an $SrTiO_3$-TiO_2 eutectic system).[9] In the case of photoelectrochemical cells, eutectics made of photoactive phases could be very attractive due to their multiphase character and potential broadband absorption, high crystallinity, and high fraction of interfaces (clean and atomically sharp) which may enable better charge transport.

A manganese titanate-titanium dioxide, $MnTiO_3$–TiO_2, eutectic is a new composite material obtained by the self-organization mechanism, which is easily available in millimeter-scale pieces. The TiO_2 phase forms the interconnected precipitate-pattern and the $MnTiO_3$ is the matrix phase. The microstructure is in the form of 3D-oval TiO_2 inclusions/particles interconnected with each other by thin TiO_2 layers/plates and this interconnected structure is embedded in the $MnTiO_3$ phase (Fig.1).

Such mixed materials made of two semiconducting phases with bandgaps enabling absorption of UV-Vis wavelengths and with both phases extending in a connected way across the whole sample may be promising for photoelectrochemical applications. For this application, materials including such phases as TiO_2 – a photoactive material under UV-light and, after proper doping, under visible light – would be particularly interesting.[10] TiO_2 is a wide band gap semiconductor thus enabling UV absorption. On the other hand, $MnTiO_3$ has not been considered as material for photoelectrochemical applications yet, though the recently-reported band gap for this material of 2.4 eV [11], or 1.8 eV [12] should provide absorption in the visible range of the solar spectrum. So such a mixed composite could potentially be interesting for photoelectrochemical applications.

The growth and characterization of the eutectic microstructure from a TiO_2-MnO (57% - 43%) system, via directional solidification by the micro-pulling down method will be presented. The preliminary results of the measurements performed with manufactured by us $MnTiO_3$-TiO_2 photo anode will be also discussed.

Acknowledgements: The research has been supported by a grant from Switzerland through the Swiss Contribution to the enlarged European Union.

(1) D. A. Pawlak, K. Kolodziejak, S. Turczynski, J. Kisielewski, K. Rozniatowski, R. Diduszko, M. Kaczkan, M. Malinowski, Chem. Mater., 2006, 18, 2450-2457.
(2) D. A. Pawlak, Self-organized structures for metamaterials in Applications of Metamaterials (Metamaterials Handbook), 2009, Capolino F., Ed.; CRC Press, Vol II, Chapter 31.
(3) D. A. Pawlak, S. Turczynski, M. Gajc, K. Kolodziejak, R. Diduszko, K. Rozniatowski, J. Smalc and I. Vendik, Adv.Funct. Mat., 2010, 20, 116-1124.
(4) M. A. Laguna-Bercero, A. Larrea, R. I. Merino, J. I. Pen and V. M. Orera, J. Am. Ceram. Soc., 2005, 88, 3215-3217.
(5) M. A. Laguna-Bercero, A. Larrea, J. I. Peña, R. I. Merino, V. M. Orera, J. Europ. Ceram. Soc. 2005, 25, 1455-1462.
(6)R. I. Merino, J. I. Pena and V. M. Orera, J. Europ. Ceram. Soc., 2010, 30, 147-152.
(7) G. J. Snyder and E. S. Toberer, Nature Materials, 2008, 7, 105-114.
(8) M. I. Aliev, A. A. Khalilova, D. G. Arsaly, R. N. Ragimov and M. Tanogly, Inorg. Mater., 2004, 40, 331– 335.
(9) K. Bienkowski, S. Turczynski, R. Diduszko, M. Gajc, E. Gorecka, D. A. Pawlak, Cryst. Growth & Design, 2011, 11, 3935–3940.
(10) Grimes C. A.; Varghese, O. K.; Ranjan, S. In Light, water, hydrogen; Springer 2007, Chapter 4.
(11) Agui, A.; Mizumaki, M. J. Electr. Spectr. Rel. Phenom. 2011, 184, 463– 467.
(12)Szubka, M.; Talik, E.; Kołodziejak, K.; Pawlak, D. A. Journal of Physics: Conference Series 2011, 200, 072097-072100.

???

16:00 Poster We225

Fast synthesis of TaC under high energy conditions

Andrzej Huczko[2], Olga M. Łabędź[1], Jakub Nowiński

1. *Uniwersytet Warszawski, Wydział Chemii, Warszawa, Poland*
2. *Warsaw University, Faculty of Chemistry, Pasteura 1, Warszawa 02-093, Poland*

e-mail: olabedz@chem.uw.edu.pl

Among the high-melting carbides, tantalum carbide is an industrially significant and attractive candidate because of its exceptional high hardness, thermal and high corrosion resistance, and catalytic properties [1]. Classical chemical procedures to synthesize TaC involve reactions of metal, metal oxide or any suitable Ta precursor with carbon sources. The long-lasting process is always performed at high temperature (from 1000 ^oC up to 2000 ^oC). It is well known, however, that TaC is a difficult material to make using conventional techniques [2]. We propose here fast one-step formation of TaC under high energetic conditions, i.e. using either (i) **plasma** or (ii) **combustion** activation of reactants. The microstucture of the products was examined using SEM and TEM, while phase composition was determined via X-ray diffraction.

Regarding the **plasma synthesis** of TaC, the DC arc system generating carbon vapors commonly used to produce fullerenes, carbon nanotubes and encapsulates was used [3, 4]. Two types of arc sublimated anodes were used: heterogeneous and homogeneous. To prepare the first type, graphite rods were drilled and filled with mixtures of fine graphite and Ta powders with two different ratios (5 and 55 wt % of Ta in respect to the total graphite). The homogenous anodes used for the experiments were also prepared using the same Ta/C ratio and also Ta_2O_5/C composition (Ta content 45 wt%). A tar pitch was added as a binding agent. The as prepared mixtures were then pressed under 2 MPa pressure to form rods of 8 mm in diameter and 30 mm in length. Next, the rods were calcinated under Ar atmosphere at 1000□C for 10 hours to ensure the complete removal of all organic components of the tar pitch.

The arcing was carried out in He atmosphere, at a current value of 80-120 A in the case of heterogeneous electrodes, and 70-80 A while using the homogenous ones. The pressure in the reactor was kept at a constant value of 10 or 80 kPa. In all runs the rubbery sooth was collected from the lid and walls of the water-cooled reactor. For the experiments where Ta_2O_5 was used, the product had a web-like structure (formerly found in case of a high content of 1D carbon nanostructures).

In the last two decades the method known as self-propagating high-temperature synthesis (SHS), or **combustion synthesis**, has become an attractive method of producing advanced materials [5]. This high-temperature redox technique, when compared to traditional processing routes has the advantages of being extremely time- and energy- efficient. SHS was also successfully applied for one-step synthesizing SiC nanofibers [6]. The following Ta-containing compositions were combusted: $TaSi_2$/PTFE, Ta/PTFE, $TaCl_5/C_{10}H_8$, and $TaCl_5/C_{14}H_{10}$. All experiments were performed in high-pressure stainless-steel reactor. A green stoichiometric mixture of the reactants was homogenized in an agate mortar. After the reactants were placed in the reactor and the desired pressure (0,1 MPa) of Ar atmosphere was obtained in the combustion chamber, the reaction was initiated using the carbon filament. The combustion was completed usually within the fraction of a second. All compositions were successfully combusted yielding black fine powders.

16:00 Poster We226

Growth and structure of the $CdCr_2Se_4$ and $CuCr_2Se_4$ single crystals doped with niobium

Ewa M. Maciazek[1], Anna B. Gągor[2], Paweł Ł. Zajdel[4], Izabela J. Jendrzejewska[1], Maria Sozańska[3]

1. *University of Silesia, Institute of Chemistry (UŚ), Szkolna 9, Katowice 40-006, Poland* **2.** *Institue of Low Temperature and Structure Research, Polish Academy of Sciences (INTIBS-PAN), P.Nr 1410, Wrocław 50-950, Poland* **3.** *Silesian University of Technology, Department of Materials Science, Krasińskiego 8, Katowice 40-019, Poland* **4.** *University of Silesia, August Chełkowski Institute of Physics, Department of Physics of Crystals, Uniwersytecka 4, Katowice 40-007, Poland*

e-mail: ewa.maciazek@us.edu.pl

Chemical vapor transport method was applied in order to obtain $CdCr_2Se_4$ and $CuCr_2Se_4$ single crystals doped with niobium. Binary selenides: Nb_2Se_3 and CdSe or CuSe, respectively, were used as a starting material. Anhydrous chromium chloride was used as a transport agent. Taking into account the site preference energy and cation valency it was assumed that niobium would substitute chromium and proper amounts of substrates were calculated according to the reaction:

$$4\,CdSe + (2\text{-}x)\,CrCl_{3(g)} + Nb_2Se_3 \rightarrow Cd[Cr_{2-x}Nb_x]Se_4 + 3\,CdCl_{2(g)} + 2\,NbCl_{3(g)} + 2\,Se_{3(g)} \quad \text{for } x=0.1;\ 0.25;\ 0.5$$

or

$$4\,CuSe + (2\text{-}x)\,CrCl_{3(g)} + Nb_2Se_3 \rightarrow Cu[Cr_{2-x}Nb_x]Se_4 + 3\,CdCl_{2(g)} + 2\,NbCl_{3(g)} + 2\,Se_{3(g)} \quad \text{for } x=0.1;\ 0.25;\ 0.5$$

The crystallization process was carried out in evacuated quartz ampoules put to the horizontal zone temperature furnace. In case of $CdCr_{2-x}Nb_xSe_4$ two different temperature gradients were applied: ΔT=10K or ΔT=100K. In both cases two types of single crystals were obtained: pellets and needles. Single crystals of $CuCr_{2-x}Nb_xSe_4$ had a shape of regular octahedral. In both cases the crystallization process was successful only for x=0.25.

The chemical composition was verified using scanning electron microscope.

Single crystals of different type of shape were chosen for X-ray diffraction measurements on a four – circle diffractometer X-calibur/CCD Oxford Diffraction using graphite monochromated MoKα radiation. The structure refinement was performed using the SHELXL-97 program package.

This work is funded from science resources for years 2011-2014 as a research project No N N204 151940.

Chemical vapor transport method was applied in order to obtain $CdCr_2Se_4$ and $CuCr_2Se_4$ single crystals doped with niobium. Binary selenides: Nb_2Se_3 and CdSe or CuSe, respectively, were used as a starting material. Anhydrous chromium chloride was used as a transport agent. Taking into account the site preference energy and cation valency it was assumed that niobium would substitute chromium and proper amounts of substrates were calculated according to the reaction:

$$4CdSe + (2\text{-}x)CrCl_{3(g)} + (2+x)/2\,Nb_2Se_3 \rightarrow Cd[Cr_{2-x}Nb_x]Se_4 + 3CdCl_{2(g)} + 2\,NbCl_{3(g)} + 2\,Se_{3(g)} \quad \text{for } x=0.1;\ 0.25;\ 0.5$$

or

$$4\,CuSe + (2\text{-}x)CrCl_{3(g)} + (2+x)/2\,Nb_2Se_3 \rightarrow Cu[Cr_{2-x}Nb_x]Se_4 + 3CdCl_{2(g)} + 2\,NbCl_{3(g)} + 2\,Se_{3(g)} \quad \text{for } x=0.1;\ 0.25;\ 0.5$$

The crystallization process was carried out in evacuated quartz ampoules put to the horizontal zone temperature furnace. In case of $CdCr_{2-x}Nb_xSe_4$ two different temperature gradients were applied: ΔT=10K or ΔT=100K. In both cases two types of single crystals were obtained: pellets and needles. Single crystals of $CuCr_{2-x}Nb_xSe_4$ had a shape of regular octahedral. In both cases the crystallization process was successful only for x=0.25.

The chemical composition was verified using scanning electron microscope.

Single crystals of different type of shape were chosen for X-ray diffraction measurements on a four – circle diffractometer X-calibur/CCD Oxford Diffraction using graphite monochromated MoKα radiation. The structure refinement was performed using the SHELXL-97 program package.

This work is funded from science resources for years 2011-2014 as a research project No N N204 151940.

16:00 Poster We227

A photoconductive approach to negative refraction

Krzysztof P. Orliński[1], Maria Massaouti[2], Maria Kafesaki[2], Stelios Tzortzakis[2], Dorota A. Pawlak[1]

1. *Institute of Electronic Materials Technology (ITME), Wólczyńska 133, Warszawa 01-919, Poland* **2.** *Institute of Electronic Structure and Laser, FORTH,, P.O. Box 1527, Vassilika Vouton, Heraklion 71110, Greece*

e-mail: krzysztof.orlinski@itme.edu.pl

Almost half a century has passed since Victor Veselago published his work [1] on negative refractive index. The idea grew, following the experiments of Smith [2], Hoffman [3], Yao [4] and many more to establish the field of optical metamaterials. Negative refractive index was originally demonstrated on various metallodielectric materials, such as split-ring resonators [5], pairs of metallic wires, or a fishnet structure. Only later negative refraction has been demonstrated in the materials with hyperbolic dispersion, which are structurally anisotropic materials with anisotropic distribution of permittivity,e.g. silver rods embedded in alumina matrix[4]. Directional solidification of eutectics provides possibilities of manufacturing materials with various geometries such unusual as split-rings [6] as well as so usual as rods of one phases embedded in another phase [7]. That is why in this paper we will utilize the eutectic materials.

We propose a different approach to manufacturing a switchable metamaterial, suggested by S. Tzortzakis. A fibrous structure in the form of a ceramic eutectic is composed of two materials, each with a different bandgap. The matrix material is chosen as to have a big energy bandgap (e.g. 5eV), whereas the fibre material should have at least 2eV lowerbandgap. The idea is to transform the rods into the conductive state with a strong laser pulse. That way the material can be switched "on" and "off" according to the will of the user.

We present results obtained for a $GdCrO_3$-$Gd2O_3$ eutectic fabricated by the micro-pulling down method. The single phase materials were synthesized in the form of powders via sol-gel combustion method. The THz time-domain spectroscopy was performed on all three types of samples and dielectric permittivitiesof the component phases ($GdCrO_3$, Gd_2O_3) were utilized to perform the modeling of the electromagnetic properties of the eutectic composite.The first results reveal resonant

[1] „The electrodynamics of substances with simultaneously negative values of ε and μ" – Veselago V., Soviet Physics USPEKHI 10 (509) 1968

[2] "Composite Medium with Simultaneously Negative Permeability and Permittivity" - Smith, D. R.; Padilla, WJ; Vier, DC; Nemat-Nasser, SC; Schultz, S.; Physical Review Letters 84 (18) 2000, pp. 1484-1487

[3] „Negative refraction in semiconductor metamaterials" – Hoffman, A. J.; Alekseyev, L.; Howard, S. S.; Franz, K. J.; Wasserman, D.; Podolskiy, V. A.; Narimanov, E. E.; Sivco, D. L.; Gmachl, C.; Nature Materials 6, 2007

[4] „Optical negative refraction in bulk metamaterials of nanowires" – Yao, J.; Liu, Zh.; Liu, Y.; Wang, Y.; Sun, Ch.; Bartal, G.; Stacy, A. M.; Zhang, X.; Science 321, 2008

[5] „Reversing light: Negative refraction" – Smith, D.R., Pendry, J.B.; Physics Today 57(6) 2003

[6] "How far are we from making metamaterials by self-organization? The microstructure of highly anisotropic particles with an SRR-like geometry" – Pawlak, D.A., Turczynski, S., Gajc, M., et al., **Advanced Functional Materials** 20, 1116, (2010)

[7] *„PrAlO3-PrAl11O18 eutectic: Its microstructure and spectroscopic properties"*- Pawlak, D.A., Kolodziejak, K.,Turczynski, S., Kisielewski, J., Rozniatowski, K., Diduszko, R., Kaczkan, M., Malinowski, M., Chemistry of Materials 18, 2006, pp. 2450-2457 .

16:00 Poster We228

Fabrication of zinc oxide nanorods via solution method on conductive substrates

Lesya V. Podrezova[1], Valentina Cauda[2], Stefano Stassi[2,3], Giancarlo Cicero[3], Khabibulla A. Abdullin[4], Balausa E. Alpysbayeva[4]

1. *Kazakh National Technical University n.a. K.I.Satpaev, Department of General and Theoretical Physics (KAZNTU), Satpaev str., 22, Almaty 050013, Kazakhstan* **2.** *Center for Space Human Robotics, Istituto Italiano di Tecnologia (IIT), Corso Trento 21, Torino 10129, Italy* **3.** *Department of Applied Science and Technology, Politecnico di Torino, Corso Duca degli Abruzzi, 24, Torino 10129, Italy* **4.** *National Nanotechnology Open Laboratory, Kazakh National University, 71 Al-Farabi Ave., Almaty 050000, Kazakhstan*

e-mail: podrezova_lv@mail.ru

Zinc oxide nanorods were synthesized via simple hydrothermal synthesis process, using water solution of 30 mM zinc nitrate hexahydrate $Zn(NO_3)_2 \cdot 6H_2O$, 60 mM hexamethylenetetramine $C_6H_{12}N_4$, ammonium hydroxide as catalyzer and polyethylenimine (PEI), as cappingagent. We studied the influence of different metal sputtered layers, such as Ni, Cu, Au, Ag, Pt on silicon substrates and F-doped SnO_2 coated-glass wafers (FTO) on the morphology of the final ZnO nanorods (NRs). In addition we also evaluated the influence of the seed-layer concentration on the final ZnO nanorods. The samples were studied by scanning electron microscopy (Fig.1), X-ray diffraction (XRD) and current-voltage (I – V) characteristics. We obtained vertically aligned ZnO nanorod arrays on the all used substrates, proving how ease and reproducible is the growth of ZnO nanorods on different substrates. Depending on the deposited conductive material as bottom layer, we obtained different morphologies and electrical features.

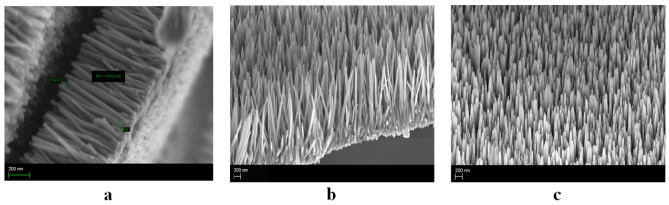

a b c

Fig.1 Morphology of ZnO nanorods grown by hydrothermal route on Si substrates with sputtered layer of a – Cu, b – Ni, c – Au substrates.

References:

[1] Zhong Lin Wang, J. Phys.: Condens. Matter, 16, 2004, pp. 829–858.
[2] Y.W. Heo, et al., Mater. Sci. Eng. R, 2004, 47, issue 1, pp.1-47.

[3] Özgür Ü., Alivov Ya.I et al., J. Appl. Phys. Rev., 041301, 2005, 98, 103 pages.

16:00 Poster We229

Self-organized metallodielectric eutectic nanoparticle based composite material: manufacturing and properties

Katarzyna Sadecka, Marcin Gajc, Andrzej Kłos, Barbara Surma, Dorota A. Pawlak

Institute of Electronic Materials Technology (ITME), Warszawa 01919, Poland

e-mail: katarzyna.sadecka@itme.edu.pl

Metallodielectric composites are very interesting from the point of view of metamaterials and plasmonics. Bottom-up methods, like self-organization and other chemical methods are potential future manufacturing techniques which could be suitable for large scale fabrication [1, 2, 3, 4].

The main idea of the work is to utilize the self-organization mechanism of metallodielectric eutectic materials to create plasmonic nanocomposites trough directional solidification.

In this work Bi_2O_3-Ag eutectic directionally solidified by the micro-pulling down method has been studied. The composite exhibits three-dimensional silver multiscale structure embedded in the bismuth oxide matrix. After applied annealing procedure in the Bi_2O_3-Ag composite the metallic nanoparticles are formed and material exhibits a localized surface plasmon resonance (LSPR) at around 590nm, which has been confirmed by the UV-VIS transmission spectra. This is the first demonstration of plasmonic behaviour in a eutectic which has been engineered specifically for this purpose using the self-organization mechanism.

The study of an influence of annealing temperature of the composite on the resonance properties in comparison with the pure bismuth oxide phase, together with micro/nano-structural investigation (XRD, SEM, TEM) will be presented. Additionally after doping the material with erbium ions, the enhancement of the luminescence at the telecommunication wavelength is observed.

References

[1] D. A. Pawlak, S. Turczynski, M. Gajc, et al., How far are we from making metamaterials by self-organization? The microstructure of highly anisotropic particles with an SRR-like geometry. **Adv. Funct. Mat.** 20, 1116, (2010).

[2] M. Gajc, B. H. Surma, A. Klos, K. Sadecka, K. Orlinski, A. E. Nikolaenko, K. Zdunek, D. A. Pawlak, Nanoparticle Direct Doping: novel method for manufacturing three-dimensional bulk plasmonic nanocomposites. **Adv. Funct. Mat.** 10.1002/adfm.201203116 (2013)

[3] C. Rockstuhl, T. Scharf, A metamaterial based on coupled metallic nanoparticles and its band-gap property, **J. Microsc**, 229, 2, 281, (2008).

[4] N.I. Zheludev, The Road Ahead for Metamaterials, **Science**, 328, 582, (2010).

16:00 Poster We230

Improvement of the quality of polished SiC wafers using chemical oxidation and heat treatment

Halina Sakowska[1], Krystyna Mazur[1], Dominika N. Teklińska[1,2], Maciej Gała[1]

1. *Institute of Electronic Materials Technology (ITME), Wólczyńska 133, Warszawa 01-919, Poland* **2.** *Warsaw University of Technology, Faculty of Materials Science and Engineering, Woloska 141, Warsaw 02-507, Poland*

e-mail: sakowska@itme.edu.pl

Silicon carbide (SiC) is categorized as hard-to-process material. Usually, standard wafers manufacturing like chemical-mechanical polishing (CMP) with SiO_2 or diamond abrasive is used [1]. Such processing does not guarantee perfect surface which is expected to grown epitaxial films on them or to use it as a substrate. Because of physical hardness and chemical inertness is difficult to obtain atomic level surface flatness without subsurface damage [2, 3].

The efforts of finding extra process which could be applied after standard polishing of SiC wafers are demonstrated.

Two methods of improvement of the quality of the polished surface have been presented:

1. chemical oxidation using Fenton process,

2. thermal annealing with assorted conditions.

According to Fenton reaction, ($OH^{\bullet}$) radicals which is are an oxidizing agent, are generated during the decomposition of a hydrogen peroxide (H_2O_2) solution in the presence of ion Fe^{2+} as a catalyst.

$$Fe^{2+} + H_2O_2 \rightarrow Fe^{3+} + OH^{\bullet} + OH^{-}$$

In the second step, SiC surface is oxidizing as follows:

$$SiC + 4OH^{\bullet} + O_2 = SiO_2 + 2H_2O + CO_2^{\uparrow}$$

Thin film of SiO_2 is dissolved in HF solution or removed by polishing. As a result, the quality of the surface roughness parameters was improved ($R_a \approx 0.39$ nm).

The thermal annealing in vacuum, $T = 900$ ºC caused very smooth surface with $R_a \leq 0.10$ nm and significantly reduced subsurface damaged layers [4].

To check the effectiveness of this improvement, two silicon carbide wafers were prepared as substrates for new grown process of SiC crystals: one of them following standard technique and another one using chemical oxidation. The surface smoothness before and after processing was measured using atomic force microscope (AFM) and optical microscope.

To compare crystallographic quality of new SiC crystals the X-ray methods were used.

Acknowledgements: This work was supported by the SICMAT Project co-financed by the European Regional Development Fund under the Operational Programme Innovative Economy (Contract No. UDA-POIG.01.03.01-14-155/09).

References:

[1] H. Aida, T. Doi, H. Takeda, H. Kakatura, S.-W. Kim, K. Koyama, T. Yamazaki,
M. Uneda, Current Applied Physics **12** (2012) S41-S46.

[2] A. N. Hattori, T. Okamoto, S. Sadakuni, J. Murata, K. Arima, Y. Sano, K. Hattori,
H. Daimon, K. Endo, K. Yamauchi, Surface Science **605** (2011) 597-605.

[3] L. Zhou, V. Audurier, P. Piruoz, J.A. Powell, Journal of Electrochemical Society **144** (6) (1997) L 161-163.

[4] C. Richtarch: Method of preparing a surface of a semiconductor wafer to make it epiready, United States Patent: US 7,060, 620, B2, 2006.

16:00 Poster We231

The influence of pressure on growth of 3C-SiC heteroepitaxial layers on silicon substrates

Dominika N. Teklińska[1,2], Iwona Jóźwik-Biała[1], Kacper Grodecki[1,3], Piotr Caban[1], A. Olszyna[2], Wlodek Strupinski[1]

1. *Institute of Electronic Materials Technology (ITME), Wólczyńska 133, Warszawa 01-919, Poland* **2.** *Warsaw University of Technology, Faculty of Materials Science and Engineering (InMat), Wołoska 141, Warszawa 02-507, Poland* **3.** *Uniwersytet Warszawski, Wydział Fizyki, Instytut Fizyki Doświadczalnej, Hoża 69, Warszawa 00-681, Poland*

e-mail: dteklinska@gmail.com

Epitaxial growth of cubic silicon carbide on silicon is a promising alternative, which provides low-cost substrates for growth of other wide band gap materials (GaN, graphene, etc.) for electronic applications. The main factors preventing a large scale development of 3C-SiC/Si technology are the lattice mismatch (~20%) and the difference in thermal expansion coefficients (~23% at a deposition temperature) between 3C-SiC layers and a Si substrate.

The top method to improve the crystalline quality of 3C-SiC is to grow a buffer layer prior to crystal growth because it helps to accommodate mismatches between SiC and Si. We observed that a carbonization layer was formed while silicon atoms, which out-diffused from the substrate, reacted with carbon atoms (precursor – propane). The thin 3C-SiC layer obtained in the carbonization process strongly affected the crystalline quality of subsequent 3C-SiC epilayers.

This mechanism led to generation of voids, which are a common interfacial defect associated with heteroepitaxial growth of 3C-SiC on Si. These defects were formed due to silicon out-diffusion, which resulted in coalescence of Si vacancies. The voids were formed at a different depth of the substrate. Moreover, the most common surface defects connected with growth of 3C-SiC on silicon were carbon inclusions.

The used samples were grown in a resistively heated horizontal hot-wall Chemical Vapor Deposition reactor. Epitaxial layers were grown on on-axis silicon substrates. The predominant goal was to analyze the relationship between the pressure used during growth and the crystalline quality of the obtained layers. Special attention was paid to homogeneity of the 3C-SiC layers obtained on silicon substrates. The morphology of the 3C-SiC buffer layer was investigated by scanning electron, atomic force and optical microscopies as well as Raman Spectroscopy.

Based on the results gathered in this work, it can be concluded that 20 mbar is the optimum process pressure. While using such growth conditions for 3C-SiC on silicon substrates, we can obtain a homogeneous layer without any carbon inclusions. Moreover, process pressure has influence on the crystalline quality of obtained 3C-SiC, which can be analyzed using AFM. The lowest roughness was obtained when using the appropriate value of pressure during growth. This proves that the 3C-SiC carbonization layer has much less stress in the interface

between 3C-SiC and Si, which means the structure of the carbonization layer will have a better match to the substrate.

Acknowledgments: This work was supported by the SICMAT Project co-financed by the European Regional Development Fund under the Operational Programme Innovative Economy (Contract No. UDA-POIG.01.03.01-14-155/09).

16:00 Poster We232

Modeling the Migration of Tellurium-Rich, Second-Phase Particles in Cadmium Zinc Telluride (CZT) via Temperature Gradient Zone Melting (TGZM)

Kerry P. Wang, Andrew Yeckel, Jeffrey J. Derby

University of Minnesota, Chemical Engineering and Materials Science, 421 Washington Ave. S.E., Minneapolis, MN 55455, United States

e-mail: wang3790@umn.edu

Crystals of cadmium zinc telluride (CZT) typically exhibit significant populations of large (10 micron and above) tellurium-rich particles that are deleterious to the performance of semiconductor radiation detectors. While it is well understood that melt growth of CZT can produce crystalline material that is supersaturated with tellurium, providing a thermodynamic basis for the existence of these second-phase particles, their formation mechanisms are not well understood. As an alternative to preventing particle formation during the growth process (which may not be possible), an interesting post-growth treatment may provide a means to higher-quality crystals. Namely, these large, tellurium-enriched, secondary-phase particles can be induced to move away from a region of grown crystal and accumulate elsewhere, leaving higher-quality regions that contain far fewer particles. This accomplished by heating the sample to slightly above the eutectic temperature (the melting point of the second-phase particles) and engineering a temperature gradient across the sample. Under such conditions, the now-liquid particle dissolves on the hot side and re-solidifies on the cool side, with a net effect of migrating toward the hotter region. This process is termed "temperature gradient zone melting," or TGZM. We will present the formulation and implementation of steady-state and dynamic models that employ the Galerkin finite element method and elliptic mesh generation techniques to solve for particle migration via TGZM. Such an approach is particularly well suited for rigorous and accurate representation of geometrical and interfacial interactions in this system. We will also present initial results to verify the model and identify the dominant physical interactions involved in this process. We will also compare preliminary model results with data currently being taken on TGZM applied to CZT crystals in experiments at Brookhaven National Laboratories conducted by collaborators at Alabama A&M University.

Supported in part by U.S. Department of Homeland Security, 2012-DN-077-ARI066-02, the content which does not necessarily reflect the position or policy of the United States Government, and no official endorsement should be inferred.

16:00 Poster We233

Growth, structure and dielectric properties of two dimensional $La_{2-x}Sr_xCoO_4$ crystals

Shuhua Yao[1], Ning Sun[1], Binbin Zhang[1], Songtao Dong[1], Yanbin Chen[2]

1. *Department of Materials Science and Engineering, Nanjing University (NJU), Nanjing 210093, China* **2.** *National Laboratory of Solid State Microstructures, Department of Physics, Nanjing University (NJU), Hankou Road 22#, Nanjing 210093, China*

e-mail: shyao@nju.edu.cn

$La_{2-x}Sr_xCoO_4$ (x = 0.4, 0.5, 0.6) crystals with Ruddlesden-Popper K_2NiF_4-type structure have been investigated as potential dielectric application. In this report, $La_{2-x}Sr_xCoO_{4-\delta}$ crystals have been grown by Floating Zone. Rietveld refinement revealed that these compounds are crystallized in K_2NiF_4-type structures with space group I4/mmm. It was found that the lattice parameter c decreases as x increases. The phonon spectra of $La_{2-x}Sr_xCoO_4$ have been investigated by Raman spectroscopy. Dielectric properties of La2-xSrxCoO4 crystals were studied in a broad frequency and temperature range. The dielectric relaxation should be attributed to the non-adiabatic small polaroic hopping. There was one obvious dielectric relaxation around room temperature. This dielectric relaxation was a thermal-activated process. It should be attributed to the mixed-valence structure (Co^{2+}/Co^{3+}) since its activation energy was similar to that of small polaronic hopping process.

16:00 Poster We234

Effects of reaction temperature on the synthesis of high purity SiC powder

Wang Yingmin

The Second Research Institute of China Electronics Technology Group Corporation (CETC2), No.115 Heping South Street,Taiyuan,Shanxi,China, Taiyuan 030024, China

e-mail: xiaoxun19840@163.com

Abstract: High purity silicon carbide (SiC) powder for growing semi-insulating SiC single crystal was synthesized using the chemical reaction between high purity carbon and silicon powder. The effects of reaction temperature on the phase composition, particle size, and yield of products were discussed. The phase composition, particle size, morphology of the products were investigated by X-ray diffraction (XRD), Malvern laser particle analyzer (MS2000) and scanning electron microscopy (SEM), respectively. The yield of products was calculated by removing the residual carbon and silicon. The results shown that with the increase of reaction temperature, the phase transition of production from βtoαwas found. Moreover, the particle size and the yield of production firstly increased with increasing the temperature and than decreased when the temperature was higher. The results of glow discharge mass spectroscopy (GDMS) indicated that the synthesized products can meet the requirement for semi-insulating SiC single crystal growth. Finally, the semi-insulating 4H-SiC single crystal were grown using SiC powder which was synthesized in our lab.

16:00 Poster We235

Preparation and characterization of anhydrous $LaBr_3$ and $CeBr_3$ for scintillation crystal growth

Jinqiu Yu, Lei Cui, Huaqiang He, Shihong Yan, Yunsheng Hu, Hao Wu

General Research Institue for Nonferrous Metals, Xinjiekouwai No.2 street, Beijing 100088, China

e-mail: yujinqiu@mail.ipc.ac.cn

$LaBr_3:Ce^{3+}$ is a superior scintillation crystal with incomparable scintillation properties. However, the high cost of crystal manufacturing blocks its wide applications. A costless method for mass production of high purity anhydrous $LaBr_3$ and $CeBr_3$, which are essential raw materials for crystal growth but extremely hygroscopic, is critical to the future development of $LaBr_3:Ce^{3+}$ crystal. In this paper, we presented our recent work on the preparation of high purity anhydrous $LaBr_3$ and $CeBr_3$ by the ammonium-bromide route. Using La_2O_3, $Ce_2(CO_3)_3$, NH_4Br and HBr acid as raw materials, high purity anhydrous $LaBr_3$ and $CeBr_3$ were successfully obtained. The detailed preparation conditions,including the optimum formula of the raw materials in use and the detailed dehydration procedures, were introduced. The as-prepared anhydrous products were characterized by X-ray diffraction and Raman spectroscopy. The purity of them was evaluated by measurements of impurities such as water, oxygen and other trace metals. Results show that the purity of the as-prepared $LaBr_3$ and $CeBr_3$ is above 99.99% and 99.95%, respectively. The ammonium-bromide method shows great potential for low-cost industrial production of these anhydrous bromides.

16:00 Poster We236

influence of helium flow on sapphire crystal growth by HEM method

Lili Zhao, Tiezheng Lu, Hui Liu, Lijun Liu, Yang Yang

Harbin Institute of Technology (HIT), No.92, West Da-Zhi Street,Harbin, Heilongjiang, Harbin 150001, China

e-mail: zhaolili@hit.edu.cn

We carried out transient global simulations of heat transfer in an industrial heat exchanger method (HEM) furnace for sapphire crystal to investigate the helium flow effect on the melt convection, growth rate and melt-crystal (m-c) interface shape during the growth process. We found that an m-c interface reversal due to crystal internal radiation occurred in the growth process, which is easy to cause high thermal stress and the formation of grain boundary. Smaller helium flow rate has influence on reducing the growth rate at the time of interface reversal, which is conductive to improve the crystal quality. At the middle stage of growth process, the melt convection increases as helium flow rate increases, while the temperature difference between the m-c interface and melt free surface has no change due to the minor cooling helium gas effect on the melt. When the whole melt is solidified, helium flow rate has a significant effect on the axial temperature gradient at the bottom region of crystal, while in other regions of crystal, the impact is slight.

16:00 Poster We237

Multi-scale molecular dynamics simulations of propane, benzene, and graphene flakes adsorption on (0001) Si-terminated 4H-SiC surface

Kamil Tokar[1,2], Przemyslaw Tredak[1], Jacek A. Majewski[1]

1. *Faculty of Physics, University of Warsaw, Hoża 69, Warszawa 00-681, Poland* **2.** *Slovak Academy of Sciences, Institute of Physics, Dúbravská cesta 9, Bratislava 84511, Slovakia (Slovak Rep.)*

e-mail: jacek.majewski@fuw.edu.pl

The growth of epitaxial layers of graphene on silicon carbide substrate is a technologically very important process, however, the physics and chemistry of this process are still far from being well understood. In this work we study first stages of formation of buffer hydrocarbon structures on the (0001) Si-terminated surface of the 4H-SiC, which occur during the deposition of propane (C_3H_8) and benzene (C_6H_6) under thermal conditions corresponding to the growth in a chemical vapor deposition (CVD) reactor [1]. Our studies of the first stages of graphene growth through deposition of propane (benzene) precursor are performed by *ab initio* and classical molecular dynamics.

First, the mechanisms of C_3H_8 and C_6H_6 chemisorption were studied by means of DFT+GGA molecular dynamics (MD) with Nose–Hoover thermostat approximation. We performed calculations for a slab containing surface layers with lateral 3 x 3 surface unit cell and adsorbed molecules employing the SIESTA DFT-based package. The thermostat temperature was set close to the growth temperature of 1500 – 1800 K, and the time evolution of the system was followed up to 500 fs. Various starting positions of the C_3H_8 and C_6H_6 precursors were considered.

Performed MD simulations shed light on characteristic features of the hydrocarbon molecule adsorptive interactions with the 4H–SiC Si–terminated surface. In the case of propane, the following picture of the early growth stages emerges. At first, one of the C-H bonds in the propane molecule brakes owing to the interaction with a Si-site and one hydrogen atom is released, which neither binds with the substrate atoms nor with the propane molecule (owing to the access of the kinetic energy). The propane's C atom in terminal or central position forms chemical bond to the surface Si–site. Then, adsorbed C_3H_7 moiety configuration behaves as dynamically stable evolving its vibrational states and stays chemically bonded to the surface. In the case of C_6H_6 precursor, we observe that thermal energy at the 1800K is large enough to cause braking of the stable benzene core at certain C atom site of the benzene ring. The resulting system: CH2=C=CH–CH=C=CH2 has linear molecular chain configuration and possess further dynamical stability during MD simulation. From the other side, the same chain molecule can be obtained from $C_3H_3+C_3H_3$ reaction between resonance-stabilized radicals [2]. The resulting chain includes all H atoms, which originally belonged to the benzene ring and created no bonding with the Si–clean 4H–SiC surface.

These MD simulations of the precursor adsorption, as well as the previous static DFT calculations [3], allow for tuning of the parameters in the empirical potentials employed in the classical MD [4]. Further, simulations of the growth process are performed within the classical MD and provide physical insight on larger length and time scales.

[1] W. Strupinski *et al*., *Nano Lett*. **11**, 1786 (2011).

[2] Y. Georgievskii *et al.,Phys. Chem. Chem. Phys*. **9**, 4259 (2007).

[3] K. Tokar and J.A. Majewski, *Acta Physica Polonica* A **122**, 1049 (2012).

[4] J. Tersoff, *Phys. Rev*. B **37**, 6991 (1988); D. W. Brenner, *Phys. Rev*. B **42**, 9458 (1990) and erratum *Phys. Rev*. B **46**, 220 (1992).

16:00 Poster We238

Ab initio studies of early stages of nitride growth process on silicon carbide

Elwira Wachowicz[1], Malgorzata Sznajder[2], Jacek A. Majewski[3]

1. *Wrocław University, Institute of Experimental Physics (IFDUWr), plac M.Borna 9, Wrocław 50-204, Poland* **2.** *University of Rzeszow, Institute of Physics, Rejtana 16, Rzeszów 35-310, Poland* **3.** *Faculty of Physics, University of Warsaw, Hoża 69, Warszawa 00-681, Poland*

e-mail: jacek.majewski@fuw.edu.pl

Thin nitride films are still attracting much interest because of their potential applications in opto- and microelectronics. An important substrate for epitaxial growth of AlN and GaN layers is SiC, since it is nearly lattice matched with AlN and has relatively low misfit with GaN. Nitride heterostructures are mainly grown on the 4H- and 6H-SiC with the growth direction along the hexagonal *c*-axis. Such heterovalent heterostructures exhibit the built-in macroscopic electric fields [1] that originate from (i) the heterovalent character of the interface, and (ii) piezo- and pyroelectric character of the constituent bulk materials. In spite of considerable experimental [1,2] and theoretical efforts [3-5], the physical understanding of these intriguing interfaces is still incomplete.

In this paper, we present results of *ab initio* density functional theory calculations of formation of Al, Ga, and N layers on 4H and 6H silicon carbide surfaces. These studies provide us physical insight in the first stages of the formation of AlN and GaN layers on hexagonal SiC. We use slab geometry consisting of 12 layers with the 'bulk' end of the slab saturated with hydrogen atoms and employ SIESTA package. We consider ideal as well as reconstructed surfaces of SiC with Al, Ga, N coverages of 0.25, 0.33, 0.5, and 1 mono layer (ML) with adatoms placed originally into all possible localizations at the surface. The full relaxation of the geometry is performed for the upper layers (the lowest one are kept rigid to simulate bulk region) and the energetically favorable positions of the adatoms are determined. Further, the formation enthalpies, charge distribution around the adatoms, and macroscopically averaged charge and potentials are computed. For some cases, we have also calculated the potential path of the adatom for the move from the one adsorption position to the other. Interestingly, we find out that for the Ga layer on the Si terminated 4H-SiC surface, the adsorption energy diminishes with the growing coverage (from -5.39 to -8.95 ev/atom), however, Al layer generally does not follow this trend. Our study indicate that ideal single Ga (or Al) layer can be stable on top of Si one, whereas some kind of the intermixing must occur to stabilize such interface in the bulk material [5].

References:

[1] A. Rizzi, R. Lantier, and H. Luth, phys. stat. sol. (a) **177**, 165 (2000).

[2] S.W. King, R.F. Davis, C.Ronning, M.C. Benjamin, and R.J. Nemanich,

J. Appl. Phys. **86**, 4483 (1999).

[3] R.B. Capaz, H. Lim, and J.D. Joannopoulos, Phys. Rev. B **51**, 17755 (1995); F.A. Ponce, C.G. Van de Walle, and J.E. Northrup, Phys. Rev. B **53**, 7473 (1996); R. Di Felice, J.E. Northrup, and J. Neugebauer, Phys. Rev. B **54**, R17351 (1996); P. Ferrara, N. Binggeli, and A. Baldereschi, Phys. Rev. B **55**, R7418 (1997).

[4] M. Staedele, J. A. Majewski, and P. Vogl, Phys. Rev. B **56**, 6911 (1997).

[5] M. Rouhani Laridjani, P. Masri, and J. A. Majewski, Mat.Res.Soc.Symp.Proc. Vol. **639**, G11.34 (2001).

16:00 Poster We239

Cu Doped SnO_2 Nanowire for H_2S Gas Sensing Application

Gyanendra P. Shukla

Indian Institute of Technology Delhi (I.I.T Delhi), hauz Khas, New Delhi, Delhi 110016, India

e-mail: gyanendrashukla86@gmail.com

There are many techniques to synthesized nano material, one of the versatile methods for synthesis of nonmaterial utilizing bottom up approach of nanotechnology. It involves heating of source material in a tubular furnace at high temperature in presence of some carrier gas flow, so that nanosized particles of source material are allowed to condense over substrate surface placed at some distance away from the source in downward flow direction. The nanostructure formed over the substrate surface strongly depends on temperature of the substrate and nature of the substrate. The pressure inside the tube, carrier gas, rate of flow of carrier gas, distance between source and substrate can also affect the microstructure of the products. Cu doped tin oxide nanowire has been successfully synthesized by thermal evaporation method.H_2S Gas sensing has been investigated by this Cu doped tin oxide. In this study, Cu doped SnO_2 nanowire has been grown on silicon substrate by thermal evaporation process. The morphological, structural properties of nanowire have been investigated systematically using scanning electron microscopy, x-ray diffraction.

16:00 Poster We240

GaN/AlN junctions - density functional study

Jacek Piechota[1], Jakub Sołtys[1], Stanisław Krukowski[1,2]

1. *University of Warsaw, Interdisciplinary Centre for Mathematical and Computational Modelling (ICM), Pawinskiego 5a, Warsaw 02-106, Poland* **2.** *Polish Academy of Sciences, Institute of High Pressure Physics (UNIPRESS), Sokolowska 29/37, Warszawa 01-142, Poland*

e-mail: qba@icm.edu.pl

GaN is a promising material because of its properties: it can be used in high-temperature, highfrequency and high-power device applications. The study of GaN-based junctions is very important for these applications. GaN/AlGaN junctions have been widely used as high electron mobility transistors [1] or sensors [2]. However it has been shown that for the GaN/AlN/GaN junction with ultra-thin AlN layer significant improvement over GaN/AlGaN is attained [3]. In this work we show results of density functional study of the GaN/AlN junction. We have shown crystallographic structure of such device as well as electric potential profile within the slab. Moreover, we have modelled properties of 2D electron gas at the GaN/AlN interface. We have evaluated dependence of properties of such system with varying thickness of the AlN layer.

[1] B.S. Kang et. al. Appl. Phys. Lett. 89, 122102 (2006)

[2] B.H. Chu et. al. Appl. Phys. Lett. 93, 042114 (2008)

[3] A. Bengoechea Encaboa et. al. Sensors and Actuators B: Chemical 142, 304 (2009)

16:00 Poster We241

Making attempts to obtain semiconductor compounds for applications in advanced thermoelectric generators and further investigating

Aleksandra K. Królicka

Instytut Technologii Materiałów Elektronicznych (ITME), Wólczyńska, Warszawa 01-919, Poland

e-mail: aleksandra.krolicka@itme.edu.pl

Since the 1950s, increased interest in thermoelectric materials has been observed. But the discovery of new phenomena and innovative methods of production at the beginning of the 21st century has led to significant growth in the field of thermoelectric materials and their applications. The mentioned progress is inextricably connected with new requirements for energy production as a result of fossil fuel depletion and global efforts to overcome this problem by developing and implementing renewable energy sources.

The aim of this study was to obtain thermoelectric material based on lead telluride with the highest values of thermoelectric parameters and the subsequent manufacturing the thermoelectric generator based on this material.

Thermoelectric generators are devices that use the Seebeck effect to convert thermal energy into electricity. So they can be used for example to power satellites and spacecrafts, to power or charge variety of small devices, such as flashlights, cameras, night vision goggles, watches, cell phones, etc. One of the recent interests is a thermoelectric generator which could convert recovered heat into electricity in car exhaust systems. As it was already said, this last use makes thermoelectric materials an attractive source of renewable energy, and thus an interesting alternative to traditional sources of energy derived mostly from fossil fuels.

As part of work, we prepared a few crystals of lead telluride: undoped, doped with Cr, I and doped both with Cr and I by the Bridgman method. Then the following tests were carried out to allow for calculation of their electric and thermoelectric parameters: the Hall measurements: type of conductivity, carrier mobility, concentration, resistance (from which then electrical conductivity was determined), thermal conductivity and the Seebeck coefficient. Then, based on these measurements, the thermoelectric figure of merit (ZT) of these materials was determined. ZT is a factor which determines the quality of the thermoelectric material.

XRD and SEM studies of selected samples were also carried out.

In the further works we will subject the obtained crystals to "mechanical alloying" method and subsequent pressing and sintering of the material, in order to obtain material with even better thermoelectric performance.

It is believed that achieving figure of merit ≥ 3 will enable the construction of cost-effective thermogenerators of high performance. Therefore, materials with improved electrical properties and materials with low thermal conductivity coefficient are systematically explored.

State-of-the-art methods to achieve these goals include mechanical alloying - one of the nanostructure manufacturing techniques, which is based on two processes: mechanical grinding of powders and sintering of cold shredded pieces, hot pressing and its variants such as hot isostatic pressing, melt spinning method, which consists of casting molten stream on rapidly rotating metal drum and the rapid cooling from the liquid by centrifugation, and spark plasma sintering method.

16:00 Poster We242

Calcium carbonate scale precipitation and deposition kinetics in oil and gas pipelines

Miriam Barber, Kevin J. Roberts

University of Leeds (SPEME), Leeds LS2-9JT, United Kingdom

e-mail: pre5m2b@leeds.ac.uk

The oil and gas industry has been facing the challenge of minimising and optimising the control of inorganic scale formed within their facilities. Due to environmental, safety and economic reasons, it is essential to improve the current inhibition strategies. Hence, the need to understand fundaments behind mineral scale formation and deposition to surfaces.

This study focused on both crystallization mechanisms: nucleation and growth in order to assess kinetics associated to calcium carbonate ($CaCO_3$) scale encountered in oil and gas pipelines.

Managing $CaCO_3$ formation depends on chemistry of the scale, equipment design and use of appropriate techniques which enable an in-situ monitoring of the crystallization process. This highlights the need to understand both bulk and surface crystallization in order to detect the early stages of precipitation within flowing pipes. Parameters such as concentration, temperature, pressure and time were considered throughout our studies. Furthermore, a range of analytical techniques were used in-situ to detect both nucleation and growth stages of $CaCO_3$ formation in the bulk and surface at real time and at temperatures varying from 25°C to 80°C. Experiments were conducted in batch crystallization reactors and using a rotating cylinder electrode (RCE) with mixing rate of $0.01 dm^3/s$.

Results showed that bulk induction times increased with decrease in Supersaturation and in turn decreased with increase in temperature. This certified that $CaCO_3$ tends to get less soluble in water as the temperature increases. Surface induction times were faster due to the fact that nucleation was heterogeneous only – whilst bulk displayed both homogeneous (high σ) and heterogeneous (low σ). Bulk interfacial energies increased with increase in temperature but ranged from 8 – $260 mJ/m^2$ were identical to prediction done in the past by Mullin.

Finally, bulk crystal's development showed some ACC particles at very initial stages of crystallization moving then to more organized forms such as vaterite and calcite/aragonite – this has been explained in literature by the non-classical aggregation mechanism. Surface polymorphic precursor was vaterite due to the interface instability in turbulent flow.

Understanding the shape and size evolution gave a quantification of in-situ Supersaturation and possible mechanisms driving those changes. Kinetic parameters linked to nucleation and growth mechanisms are very important to create a prediction model for $CaCO_3$.

Exhibitions

Index

A

B

C

D

E

F

G

H

I

J

K

L

M

N

O

P

Q

R

S

T

U

V

W

X

Y

Z